

Inter-University Electronics Series, Vol. 7

ANTENNA THEORY

part 1

Robert E. Collin

Division of Electrical Sciences and Applied Physics

Case Western Reserve University

Cleveland, Ohio

Francis J. Zucker

Air Force Cambridge Research Laboratories

L. G. Hanscom Field

Bedford, Massachusetts

McGraw-Hill Book Company

New York St. Louis San Francisco London Sydney Toronto Mexico Panama

PROPERTY

ANTENNA THEORY, PART 1

Copyright © 1969 by McGraw-Hill, Inc. All rights reserved. Printed in the United States of America. No part of this publication may be reproduced, stored in a retrieval system, or transmitted, in any form or by any means, electronic, mechanical, photocopying, recording, or otherwise, without the prior written permission of the publisher.

Library of Congress Catalog Card Number 68-8031

11799

1 2 3 4 5 6 7 8 9 0 MAMM 7 6 5 4 3 2 1 0 6 9

INTER-UNIVERSITY ELECTRONICS SERIES

Series Purpose

The explosive rate at which knowledge in electronics has expanded in recent years has produced the need for unified state-of-the-art presentations that give authoritative pictures of individual fields of electronics.

The Inter-University Electronics Series is designed to meet this need by providing volumes that deal with particular areas of electronics where up-to-date reference material is either inadequate or is not conveniently organized. Each volume covers an individual area, or a series of related areas. Emphasis is upon providing timely and comprehensive coverage that stresses general principles, and integrates the newer developments into the overall picture. Each volume is edited by an authority in the field and is written by several coauthors, who are active participants in research or in educational programs dealing with the subject matter involved.

The volumes are written with a viewpoint and at a level that makes them suitable for reference use by research and development engineers and scientists in industry and by workers in governmental and university laboratories. They are also suitable for use as textbooks in specialized courses at graduate levels. The complete series of volumes will provide a reference library that should serve a wide spectrum of electronics engineers and scientists.

The organization and planning of the Series is being carried out with the aid of a Steering Committee, which operates with the counsel of an Advisory Committee. The Steering Committee concerns itself with the scope of the individual volumes and aids in the selection of editors for the different volumes. Each editor is in turn responsible for selecting his coauthors and deciding upon the detailed scope and content of his particular volume. Overall management of the Series is in the hands of the Consulting Editor.

Frederick Emmons Terman

PREFACE

When we first agreed to undertake the development of a book on antennas for the Inter-University Electronics Series, the plan called for a rather modest effort devoted mostly to recent advances in this field. Subsequent discussions led to the conclusion that there was a real need for a more complete treatise dealing with all aspects of antenna theory. We therefore agreed to join forces as coeditors to carry out this rather ambitious plan.

Twenty years have passed since the publication of Silver's classical work on antennas in the M.I.T. Radiation Laboratory Series.[†] Considering the importance of antennas in modern communications technology, the number of antenna books published since then is surprisingly small (see Bibliography). Also, most of these books were written more than a decade ago and do not reflect the present state of development in the antenna field. Consequently, we made plans for a book that would develop the underlying theory from basic principles, would apply it to the many varieties of radiating structures that we call antennas, and would emphasize the more recent developments in this field.

We also recognized the intimate relationships between the performance of an antenna and its environment, and we have therefore included chapters on the behavior of an antenna immersed in lossy media or plasmas or located on a lossy earth. The demands on antenna systems in the current era can often be met only by overall system optimization, and this made it essential to also include chapters dealing with the signal-processing and spatial-filtering aspects of antennas.

The first seven chapters cover the general theory of antennas without reference to any particular type of structure except by way of illustration. Much of this material may be regarded as classical antenna theory. However, the development has been carried far enough to include topics that have become important in more recent years. For example, in the chapter on receiving antennas, quasi-monochromatic and partially polarized waves are dealt with. A whole chapter is devoted to large non-uniformly spaced arrays, and another chapter brings together and assesses the large number of pattern synthesis schemes that have been proposed over the years.

The next three chapters (Chapters 8 to 10) present the latest developments in the theory of cylindrical antennas. Significant portions of these chapters are new contributions to the field and have not appeared elsewhere before. The remaining five chapters of Part 1 cover the older classical radiating structures such as loop antennas, conical and spheroidal antennas, slot antennas,

[†]S. Silver (ed.), "Microwave Antenna Theory and Design," M.I.T. Radiation Laboratory Series, vol. 12, McGraw-Hill Book Company, New York, 1949.

and open waveguides and horns. The reader will find that these chapters bring together in a single place a rather complete overall view and the relevant references to the literature on these types of radiators.

The first three chapters of Part 2 are a coordinated sequence covering large-aperture antennas such as reflectors and lenses, preceded by an account of ray optics fundamentals that are basic in their analysis and design. These are followed by four extensive chapters on traveling-wave antennas. Leaky-wave and surface-wave antennas are of more recent origin, and the underlying theory given here is the most extensive and up-to-date treatment available. The fourth chapter in this sequence deals with the very important "frequency-independent" structures known as log periodic antennas; their theory has many features in common with other traveling-wave antennas, and it was therefore included here. The remaining six chapters of Part 2 are devoted to environmental and systems aspects; their contents were briefly mentioned earlier.

We originally planned to devote a chapter to mutual impedance coupling effects in large arrays and to other problems associated with the electronic scanning of such arrays, but a three-volume series devoted to microwave scanning antennas was recently published.[†] To avoid duplication, we decided to omit this topic; it is the only major aspect of antenna theory not included in these volumes.

As editors, we strove for a reasonably uniform notation, but because of the wide diversity of topics, complete uniformity was not possible. That the same symbol often means different things in different chapters should not, when taken in context, be confusing. A major point of departure from convention is the use of both $e^{j\omega t}$ and $e^{-i\omega t}$ (in separate chapters) to represent the time dependence of steady-state monochromatic fields. The former is standard among electrical engineers; the latter is preferred by physicists and applied mathematicians. We did not take a firm stand on this point, but instead let individual authors follow their own preferences. The use of j or i as the imaginary unit $\sqrt{-1}$ will alert the reader to which convention is adopted in each chapter. Since the contemporary literature is about evenly divided in the use of the two conventions, and since it is as impossible to talk an electrical engineer into writing an inductive impedance in the form $Z = R - i\omega L$ as it is to convince an applied mathematician an outgoing attenuating wave should be represented in the fourth quadrant of the complex-wave-number plane, we did not feel it desirable to legislate against either.

The two parts offer a number of possibilities as texts for antenna courses. A complete course on antennas cannot be offered in a single semester on the basis of three lectures per week, so there must be a selection of topics, usually according to the interests of the instructor and the class. For a basic short

[†]R. C. Hansen (ed.), "Microwave Scanning Antennas," Academic Press Inc., vol. I, 1964, vols. II and III, 1966.

course Chapters 1 to 5, selected parts of Chapters 6 and 7, Chapter 9, and topics from Chapters 12 to 15 would provide a good coverage of classical antenna theory. A course in which aperture antennas are emphasized would include Chapters 16 to 18, while Chapters 19 to 22 covering traveling-wave antennas, Chapters 23 to 25 for environmental effects, and Chapters 26 and 27 for systems aspects would be included in courses designed to emphasize those topics. A number of problems and exercises, dispersed throughout the various chapters, have been included to enhance the usefulness of the books in antenna courses.

We have been very fortunate in obtaining chapter contributions from truly outstanding antenna specialists. To the contributing authors we also owe a great deal for their wise counsel and enduring patience with a project that has extended over several years. Any remaining shortcomings must be blamed on the editors.

The work described in these two volumes is that of a great many engineers and physicists. A reasonable effort was made to ensure proper references and credits. To those whose work is not properly referenced, we offer our apologies. The lack of credit is not intentional; it was caused by the difficulty of tracing the history of any particular topic back to its originators.

Finally, as editors, we would appreciate having misprints and errors called to our attention so that future printings may be corrected.

The editors express their sincere appreciation to the following organizations for their kind permission to use a number of figures from their various publications:

The Institute of Electrical and Electronic Engineers, Inc.
345 East 47th Street
New York, N.Y. 10017

American Institute of Physics
335 East 45th Street
New York, N.Y. 10017

The Institution of Electrical Engineers
Savoy Place
London W.C.2, England

Institution of Electronic and Radio Engineers
8-9 Bedford Square
London W.C.1, England

National Research Council of Canada
Ottawa 7
Ontario, Canada

Robert E. Collin
Francis J. Zucker

CONTENTS

Foreword	v
Preface	vii

CHAPTER 1

ELECTROMAGNETIC FIELDS

R. E. Collin

1.1	<i>Introduction</i>	1
1.2	<i>Maxwell's Equations</i>	2
1.3	<i>Energy and Power</i>	6
1.4	<i>Some Properties of the Constitutive Parameters</i>	8
1.5	<i>Wave Equation</i>	10
1.6	<i>Group and Energy Flow Velocities</i>	13
1.7	<i>Boundary Conditions</i>	16
1.8	<i>Potential Theory</i>	22
1.9	<i>Reciprocity</i>	24
	Problems	26
	References	27

CHAPTER 2

RADIATION FROM SIMPLE SOURCES

R. E. Collin

2.1	<i>Introduction</i>	29
2.2	<i>Radiation from a Current Element</i>	29
2.3	<i>Basic Antenna Parameters</i>	32
2.4	<i>Magnetic Dipole Radiation</i>	36
2.5	<i>Radiation from Arbitrary Current Distributions</i>	37
2.6	<i>Free Space Dyadic Green's Functions</i>	41
2.7	<i>Radiation from Thin Wire Antennas</i>	43
2.8	<i>Radiation from a Traveling-wave Source</i>	47
2.9	<i>Antenna Input Impedance</i>	48
	Problems	57
	References	59

CHAPTER 3

RADIATION FROM APERTURES

R. E. Collin

3.1	<i>Aperture-type Antennas</i>	61
3.2	<i>Aperture in an Infinite Conducting Plane</i>	62
3.3	<i>Field Equivalence Principles</i>	69
3.4	<i>Radiation from Aperture Fields</i>	71
3.5	<i>Radiation Patterns from Typical Aperture Fields</i>	74
3.6	<i>General Formulas for Scattering and Diffraction</i>	79
3.7	<i>The Focused Aperture</i>	86
	Problems	89
	References	91

CHAPTER 4

THE RECEIVING ANTENNA

R. E. Collin

4.1	<i>Introduction</i>	93
4.2	<i>Reciprocity for Antennas</i>	94
4.3	<i>Directional Properties of a Receiving Antenna</i>	98
4.4	<i>Antenna Receiving Cross Section</i>	100
4.5	<i>Reception of Completely Polarized Waves</i>	103
4.6	<i>Reception of Partially Polarized Waves</i>	109
4.7	<i>Radiation from Distributed Sources</i>	114
4.8	<i>Noise in Antenna Systems</i>	119
4.9	<i>Scattering Properties of an Antenna</i>	123
	Problems	133
	References	135

CHAPTER 5

UNIFORMLY SPACED ARRAYS

H. Bach and J. E. Hansen

5.1	<i>Introduction</i>	138
	Analysis of Arrays	139
5.2	<i>Radiation from an Array. Factorization</i>	139
5.3	<i>Basic Array Parameters</i>	142
5.4	<i>Linear Arrays with Uniform Current Distribution</i>	145
5.5	<i>Linear Arrays with Tapered Current Distribution</i>	158
5.6	<i>Circular Arrays</i>	163
5.7	<i>Array of Arrays</i>	172
5.8	<i>Excitation of an Array</i>	176
	Synthesis of Arrays	184
5.9	<i>Synthesis of Array Patterns</i>	184
5.10	<i>Optimization of Array Patterns (Dolph-Chebyshev Arrays)</i>	186
5.11	<i>Optimization of Performance Indices</i>	194
	Problems	201
	References	203

CHAPTER 6

NONUNIFORM ARRAYS

Merrill I. Skolnik

6.1	<i>Introduction</i>	207
6.2	<i>Synthesis with Unequally Spaced Arrays</i>	210
6.3	<i>Density Taper — Deterministic</i>	212
6.4	<i>Density Taper — Statistical</i>	219
6.5	<i>Missing Elements in Equally Spaced Arrays</i>	225
6.6	<i>Random Errors in Arrays</i>	227

Problems	233
References	234

CHAPTER 7

ANTENNA PATTERN SYNTHESIS

A. C. Schell and A. Ishimaru

7.1	<i>Introduction</i>	235
7.2	<i>Gaussian Error — Rectangular Array</i>	238
7.3	<i>Gaussian Error — Rectangular Aperture</i>	244
7.4	<i>An Equivalence between Arrays and Apertures</i>	246
7.5	<i>Gaussian Error — Circular Array</i>	248
7.6	<i>Gaussian Error — Circular Aperture</i>	250
7.7	<i>The Reactive Power Constraint</i>	257
7.8	<i>Methods Suited to the Production of Narrow-beam, Low-side-lobe Patterns</i>	260
7.9	<i>Non-uniformly Spaced Array Pattern Synthesis</i>	265
7.10	<i>The Phase Constraint: Power-pattern Synthesis</i>	270
7.11	<i>Other Synthesis Techniques</i>	288
	Problems	299
	References	300
	Additional References	302

CHAPTER 8

INTRODUCTION TO LINEAR ANTENNAS

Tai Tsun Wu

8.1	<i>Maxwell's Equations</i>	306
8.2	<i>Green's Functions and Radiation Conditions</i>	309
8.3	<i>Preliminary Formulation of the Problem of Linear Antennas</i>	311
8.4	<i>The Circular Tubular Antenna</i>	314
8.5	<i>Integral Equations for the Current Distributions</i>	320
8.6	<i>Iterative Solutions for the Current Distributions</i>	324
8.7	<i>Comparison of the Iterative Solutions</i>	329
8.8	<i>The Circular Tubular Antenna (Continued)</i>	332
8.9	<i>Integral Equations for the Current Distributions (Continued)</i>	336
8.10	<i>A More General Case</i>	339
8.11	<i>Conclusions</i>	346
8.12	<i>Transient Response of a Dipole Antenna</i>	347
	References	351

CHAPTER 9

CYLINDRICAL ANTENNAS AND ARRAYS

Ronold W. P. King

9.1	<i>Introduction</i>	352
9.2	<i>The Internal Impedance and the Vector Potential of a Transmitting Antenna</i>	352

9.3	<i>Integral Equation for the Current and Its Approximate Solution</i>	356
9.4	<i>Distributions of Current and Charge; Admittance</i>	360
9.5	<i>The Electromagnetic Field near a Cylindrical Antenna</i>	367
9.6	<i>The Radiation Field of a Cylindrical Antenna</i>	371
9.7	<i>Distributions of Current and Charge in a Center-loaded Receiving Antenna</i>	374
9.8	<i>Effective Length and Directivity of a Center-loaded Receiving Antenna</i>	378
9.9	<i>The Electromagnetic Field near a Thin Scattering Cylinder</i>	379
9.10	<i>The Simultaneous Integral Equations for the Parallel Array</i>	381
9.11	<i>The Circular Array — Phase-sequence Currents</i>	384
9.12	<i>Arbitrarily Driven Circular Array</i>	387
9.13	<i>The Curtain Array</i>	392
9.14	<i>Parasitic Arrays</i>	402
9.15	<i>More General Curtain Arrays</i>	406
9.16	<i>Arrays with Collinear and Staggered Elements</i>	409
9.17	<i>Dipole Coupled to an Open-wire Line</i>	410
9.18	<i>Arrays of Dipoles Coupled to an Open-wire Line</i>	417
	Problems	419
	References	419

CHAPTER 10

THEORY OF THE LONG DIPOLE ANTENNA

Chin-Lin Chen and Tai Tsun Wu

10.1	<i>Introduction</i>	421
10.2	<i>The Infinitely Long Dipole Antenna Driven from a Coaxial Line</i>	422
10.3	<i>Discussion of the Existing Solutions for Short Dipole Antennas</i>	430
10.4	<i>Plan for the Wiener-Hopf Approach</i>	432
10.5	<i>Integral Condition</i>	434
10.6	<i>Finite Dipole Antennas</i>	438
10.7	<i>Summary of Results and Their Restrictions</i>	444
10.8	<i>Discussion</i>	447
	References	456

CHAPTER 11

THE LOOP ANTENNA FOR TRANSMISSION AND RECEPTION

Ronold W. P. King

11.1	<i>Description and Application of the Loop</i>	458
11.2	<i>Integral Equation for the Circular Transmitting Loop and Its Solution</i>	458
11.3	<i>Evaluation of Coefficients</i>	461
11.4	<i>The Admittance of and Current in a Circular Loop in Air and in a Dissipative Medium</i>	463
11.5	<i>The Radiation Field of a Loop Antenna</i>	470
11.6	<i>The Electrically Small Transmitting Loop</i>	472
11.7	<i>The Electrically Small Receiving Loop</i>	474
11.8	<i>The Shielded Loop</i>	478

11.9	<i>Loop Antennas Coupled to Open-wire Lines</i>	480
	Problems	481
	References	482

CHAPTER 12

ELECTROMAGNETIC RADIATION FROM
CONICAL STRUCTURES

James R. Wait

12.1	<i>Introduction</i>	483
12.2	<i>General Equations for Biconical Structures</i>	484
12.3	<i>The Formal Solution of the Biconical Antenna Problem</i>	488
12.4	<i>Spherical Antenna as a Limiting Case</i>	491
12.5	<i>Thin Wire Antenna as a Limiting Case</i>	492
12.6	<i>Variational Treatment of Biconical Antennas</i>	494
12.7	<i>Some Extensions of Biconical Antenna Theory</i>	499
12.8	<i>General Formulation for Biconical Antenna in Inhomogeneous Dissipative Media</i>	499
12.9	<i>Biconical Antenna with Dielectric Loading</i>	502
12.10	<i>Dielectric-loaded Biconical Antenna Immersed in a Conducting Medium</i>	503
12.11	<i>Dielectric-loaded Biconical Antenna Immersed in a Plasma</i>	506
12.12	<i>Asymmetric Biconical Structures</i>	506
12.13	<i>Radiation from a Single Infinite Cone</i>	508
12.14	<i>Radiation from a Dielectric-coated Conical Structure</i>	510
12.15	<i>Radiation from a Dipole with a Conical Sheath</i>	513
	Appendix: A Modified Iterative Approach for a Biconical Antenna	519
	References	520
	Additional References	522

CHAPTER 13

ELECTROMAGNETIC RADIATION FROM
SPHEROIDAL STRUCTURES

James R. Wait

13.1	<i>Introduction</i>	523
13.2	<i>Prolate Spheroid Coordinates</i>	523
13.3	<i>Prolate Spheroidal Wave Functions</i>	525
13.4	<i>Prolate Spheroidal Antenna in Free Space</i>	527
13.5	<i>Prolate Spheroidal Antenna with a Confocal Sheath</i>	533
13.6	<i>A Note on the Spheroid Excited by an Azimuthally Directed Electric Field</i>	540
13.7	<i>Excitation of Spheroid by External Sources</i>	540
13.8	<i>Excitation of Spheroid System by a Ring Magnetic Current</i>	545
13.9	<i>The Green's Function in Spheroidal Coordinates</i>	548
13.10	<i>Application of Scalar Green's Function to Dipole Scattering</i>	550
13.11	<i>Extension to Oblate Spheroid</i>	551
13.12	<i>Excitation of Oblate Spheroid by Axial Dipole</i>	553
13.13	<i>Fields of a Horizontal Dipole over a Disk</i>	554
	References	557
	Additional References	558

CHAPTER 14

SLOT ANTENNAS

R. T. Compton, Jr., and R. E. Collin

14.1	<i>Introduction</i>	560
14.2	<i>The Slot Antenna in a Ground Plane</i>	560
14.3	<i>Slots on Cylinders — Formal Solution</i>	567
14.4	<i>The Uniformly Excited Circumferential Slot</i>	573
14.5	<i>The Circumferential Slot of Finite Width</i>	574
14.6	<i>Half-wave Axial Slot</i>	581
14.7	<i>Slots on Spheres</i>	584
14.8	<i>Slotted Waveguide Arrays</i>	587
14.9	<i>Impedance of Slots in Rectangular Waveguides</i>	602
14.10	<i>Variational Method for Slot Impedance</i>	611
	Problems	616
	References	617

CHAPTER 15

OPEN WAVEGUIDES AND SMALL HORNS

R. T. Compton, Jr., and R. E. Collin

15.1	<i>Introduction</i>	621
15.2	<i>Radiation from a Parallel-plate Guide</i>	621
15.3	<i>Radiation from Circular Waveguides</i>	631
15.4	<i>Horn Antennas</i>	632
15.5	<i>Lens-corrected Horns</i>	646
	Problems	653
	References	654
	Bibliography	657
	Index	659

CHAPTER 1

ELECTROMAGNETIC FIELDS

R. E. Collin

1.1 Introduction

This book† deals with the theory of antennas which are used to radiate and receive electromagnetic energy. Since antenna theory is based on classical electromagnetic theory as described by Maxwell's equations, it is appropriate to begin a book on antennas with a review of that portion of classical electromagnetic phenomena which finds extensive and repeated use in the chapters to follow. We shall assume that the reader is familiar with the more elementary aspects of electromagnetic fields and their properties so that detailed derivations of all the results we shall need will not be required. (Typical introductory texts are those by Jordan,¹ Kraus,² King,³ Plonsey and Collin,⁴ Ramo, Whinnery, and Van Duzer,⁵ Schelkunoff,⁶ and Toraldo di Francia⁷.) Another purpose of this introductory chapter is to acquaint the reader with the terminology and symbols that will be used throughout the book. Only the rationalized mks system of units is employed.

The electric and magnetic fields are vector fields dependent on spatial coordinates, such as rectangular coordinates x , y , z , and time t . When an arbitrary time dependence is implied, the field vectors will be represented by boldface script letters, for example, $\mathfrak{E}(x, y, z, t)$, or more briefly simply \mathfrak{E} . However, the major portion of the theory will deal with pure monochromatic fields, i.e., fields having a simple sinusoidal time dependence under steady-state conditions. As is customary in electrical engineering texts, a time dependence of $e^{j\omega t}$ is assumed in most of the book. All time derivatives may then be replaced by $j\omega$. The field vectors are now complex phasors depending on the spatial coordinates (and ω) only and will be represented by boldface roman type, for example, $\mathbf{E}(x, y, z, \omega)$ or simply \mathbf{E} . When it is desired to emphasize that a quantity is complex, it will be underscored by a wavy line, for example, $\underline{\mathbf{E}}$. The alternative choice of $e^{-i\omega t}$, which is favored by physicists, is used in Chaps. 8, 10, 19, 20, and 21.‡

Unit vectors along coordinate axis will be designated by the coordinate variable in boldface type with a circumflex, for example, $\hat{\mathbf{x}}$, $\hat{\mathbf{y}}$, $\hat{\mathbf{z}}$, or $\hat{\mathbf{r}}$, $\hat{\boldsymbol{\theta}}$, $\hat{\boldsymbol{\phi}}$. Other arbitrary unit vectors will be represented in a similar way, e.g., propagation vector $\mathbf{k} = k\hat{\mathbf{k}} = k_x\hat{\mathbf{x}} + k_y\hat{\mathbf{y}} + k_z\hat{\mathbf{z}}$.

†Please note that this book consists of two separate volumes; Part 1 contains Chaps. 1 to 15 and Part 2, Chaps. 16 to 28.

‡Both notations are standard ones, and the authors have followed their own preferences.

Coordinates designating an arbitrary point at which the field is evaluated are represented by the usual symbols such as x, y, z ; r, ϕ, z ; and r, θ, ϕ in rectangular, cylindrical, and spherical coordinates, respectively. For brevity the position vector \mathbf{r} will also be used to designate an arbitrary point. Coordinates describing a source distribution will be identified by primed variables, and a corresponding position vector \mathbf{r}' will be used for brevity. The scalar distance between a field point (x, y, z) and a source point (x', y', z') is $|\mathbf{r} - \mathbf{r}'|$ and will, for brevity, be often represented by the symbol $R = [(x - x')^2 + (y - y')^2 + (z - z')^2]^{1/2}$.

Dirac delta functions of appropriate dimensions will be used to represent a unit source. In an orthogonal curvilinear coordinate frame with coordinate variables u_1, u_2, u_3 and with metric coefficients h_1, h_2 , and h_3 the three-dimensional delta function is given by

$$\frac{\delta(u_1 - u'_1)\delta(u_2 - u'_2)\delta(u_3 - u'_3)}{h_1 h_2 h_3} = \delta(\mathbf{r} - \mathbf{r}')$$

where $\delta(\mathbf{r} - \mathbf{r}')$ is a condensed notation. The essential properties of the unit source function $\delta(\mathbf{r} - \mathbf{r}')$ that are employed are:

1. $\delta(\mathbf{r} - \mathbf{r}') = 0$ at all points $\mathbf{r} \neq \mathbf{r}'$
2. For any scalar or vector function that is continuous at $\mathbf{r} = \mathbf{r}'$

$$\int_V \mathbf{F}(\mathbf{r}') \delta(\mathbf{r} - \mathbf{r}') dV' = \begin{cases} 0 & \mathbf{r} \text{ not in } V \\ \mathbf{F}(\mathbf{r}) & \mathbf{r} \text{ in } V \end{cases}$$

Present-day antenna theory and applications involve complex anisotropic media, in particular, gyrotropic media such as ferrites and plasmas, to a much greater extent than in the past. For this reason particular attention is paid to anisotropic media in the sections that follow.

1.2 Maxwell's Equations

In vacuum, or free space, Maxwell's equations are

$$\nabla \times \mathbf{E} = -\frac{\partial \mathbf{B}}{\partial t} \quad (1.1a)$$

$$\nabla \times \mathbf{H} = \frac{\partial \mathbf{D}}{\partial t} + \mathbf{J} \quad (1.1b)$$

$$\nabla \cdot \mathbf{B} = 0 \quad (1.1c)$$

$$\nabla \cdot \mathbf{D} = \rho \quad (1.1d)$$

where \mathbf{E} is the electric field in volts per meter, \mathbf{D} is the electric displacement in coulombs per meter², \mathbf{B} is the magnetic field in webers per meter², \mathbf{H} is the magnetic intensity in amperes per meter, \mathbf{J} is the conduction current density in

amperes per meter², and ρ is the charge density in coulombs per meter³. The divergence of (1.1b) together with (1.1d) yields the continuity equation

$$\nabla \cdot \mathcal{J} + \frac{\partial \rho}{\partial t} = 0 \quad (1.2)$$

In general the right-hand side of (1.1b) should also include a convection current term.

The force on a charge q moving with velocity \mathbf{v} is given by the Lorentz force law $q(\mathcal{E} + \mathbf{v} \times \mathcal{B})$, and hence \mathcal{E} and \mathcal{B} are usually regarded as the fundamental field quantities. \mathcal{H} and \mathcal{D} are then secondary field quantities and are related to \mathcal{B} and \mathcal{E} through the properties of the medium. In free space

$$\mathcal{D} = \epsilon_0 \mathcal{E} \quad \mathcal{H} = \frac{1}{\mu_0} \mathcal{B}$$

where ϵ_0 is the permittivity of vacuum and equal to 8.854×10^{-12} farad/m and μ_0 is the permeability of vacuum and equal to $4\pi \times 10^{-7}$ henry/m.

When solving certain types of electromagnetic field problems, it is often convenient to replace the actual sources by a set of equivalent sources located on the surface bounding the region of interest. It is then necessary to provide for a discontinuity in the tangential component of \mathcal{E} and the normal component of \mathcal{B} across the boundary surface. This requirement necessitates the introduction of a fictitious magnetic current density \mathcal{J}_m and associated magnetic charge ρ_m . Maxwell's equations (1.1) are now generalized to the following form (for a more detailed discussion see Stratton⁸ and Silver⁹):

$$\nabla \times \mathcal{E} = -\frac{\partial \mathcal{B}}{\partial t} - \mathcal{J}_m \quad (1.3a)$$

$$\nabla \times \mathcal{H} = \frac{\partial \mathcal{D}}{\partial t} + \mathcal{J} \quad (1.3b)$$

$$\nabla \cdot \mathcal{B} = \rho_m \quad (1.3c)$$

$$\nabla \cdot \mathcal{D} = \rho \quad (1.3d)$$

Taking the divergence of (1.3a) and utilizing (1.3c) gives the continuity equation

$$\nabla \cdot \mathcal{J}_m + \frac{\partial \rho_m}{\partial t} = 0 \quad (1.4)$$

For harmonic time variation, with an assumed time dependence of the form $e^{j\omega t}$, where ω is the angular frequency, the generalized set of Maxwell's equations (1.3) becomes

$$\nabla \times \mathbf{E} = -j\omega \mathbf{B} - \mathbf{J}_m \quad (1.5a)$$

$$\nabla \times \mathbf{H} = j\omega \mathbf{D} + \mathbf{J} \quad (1.5b)$$

$$\nabla \cdot \mathbf{B} = \rho_m \quad (1.5c)$$

$$\nabla \cdot \mathbf{D} = \rho \quad (1.5d)$$

where all quantities are now complex phasors and functions of the spatial coordinates and ω . The physical field is obtained by multiplying the phasor by $e^{j\omega t}$ and taking the real part, for example,

$$\mathfrak{B}(\mathbf{r}, t) = \text{Re } \mathbf{B}(\mathbf{r}, \omega) e^{j\omega t}$$

In material media the application of an electric field \mathfrak{E} produces a displacement of the charge bound to the atoms and molecules with the result that an average electric dipole polarization density \mathfrak{P} in coulombs per meter² is produced. The polarization density \mathfrak{P} acts as a secondary source and is accounted for by the auxiliary field vector \mathfrak{D} , which is defined, in general, by the relation

$$\mathfrak{D} = \epsilon_0 \mathfrak{E} + \mathfrak{P} \quad (1.6)$$

In a linear medium the classical theory relates \mathfrak{P} to \mathfrak{E} at each point in the medium by a differential equation which describes the dynamics of the polarization mechanism. For example, in a simple situation the equation describing the movement of the displaced charge would be

$$m \frac{d^2 \mathbf{r}}{dt^2} + m\nu \frac{d\mathbf{r}}{dt} + k\mathbf{r} = q\mathfrak{E} \quad (1.7)$$

where m is the effective mass of the charge q , ν is an effective damping coefficient or collision frequency, k is a constant giving the elastic restoring force, and \mathbf{r} is a vector giving the displacement of the charge from equilibrium. The induced dipole moment or polarization is $\mathfrak{P} = q\mathbf{r}$.

In the frequency domain (1.7) becomes

$$(k - m\omega^2 + jm\omega\nu)\mathbf{r} = q\mathbf{E} \quad (1.8)$$

from which it is seen that \mathbf{P} can be related to \mathbf{E} as follows:

$$\mathbf{P} = q\mathbf{r} = \frac{q^2 \mathbf{E}}{k - m\omega^2 + jm\omega\nu} = \epsilon_0 \chi_e(\omega) \mathbf{E} \quad (1.9)$$

where $\chi_e(\omega)$ is a suitable complex scalar function of ω and is called the electric susceptibility of the medium. The relation between \mathbf{D} and \mathbf{E} becomes

$$\mathbf{D} = \epsilon_0(1 + \chi_e)\mathbf{E} = \epsilon \mathbf{E} \quad (1.10)$$

where ϵ is called the permittivity of the medium. It should be noted that in the time domain it is not possible to relate \mathfrak{D} and \mathfrak{E} in as simple a form as in the frequency domain. Only if the frequency is sufficiently low that inertial and damping forces are negligible compared to the elastic restoring force can we write $\mathfrak{D} = \epsilon \mathfrak{E}$.†

The relation given by (1.10) is valid only in isotropic media in which \mathbf{P} has the same direction as \mathbf{E} . In anisotropic media \mathbf{P} and \mathbf{E} are not in the same

†For many materials this is true for frequencies up to and including the microwave band. In this frequency range the medium is said to be nondispersive, which implies that ϵ is not dependent on ω for these frequencies.

direction and χ_e and ϵ must then be replaced by tensors of rank 2 or dyadics. Thus in general we will have (for details see Landau and Lifshitz¹⁰)

$$\mathbf{P} = \epsilon_0 \chi_e \cdot \mathbf{E} \quad (1.11a)$$

$$\mathbf{D} = \epsilon_0 (\mathbf{I} + \chi_e) \cdot \mathbf{E} = \boldsymbol{\epsilon} \cdot \mathbf{E} \quad (1.11b)$$

where the dyadics χ_e and $\boldsymbol{\epsilon}$ (represented by boldface type) have components that are complex functions of ω . \mathbf{I} is the unit dyadic.

The dyadic $\boldsymbol{\epsilon}$ has nine components and written out in full is

$$\boldsymbol{\epsilon} = \begin{cases} \epsilon_{xx} \hat{\mathbf{x}}\hat{\mathbf{x}} + \epsilon_{xy} \hat{\mathbf{x}}\hat{\mathbf{y}} + \epsilon_{xz} \hat{\mathbf{x}}\hat{\mathbf{z}} \\ \epsilon_{yx} \hat{\mathbf{y}}\hat{\mathbf{x}} + \epsilon_{yy} \hat{\mathbf{y}}\hat{\mathbf{y}} + \epsilon_{yz} \hat{\mathbf{y}}\hat{\mathbf{z}} \\ \epsilon_{zx} \hat{\mathbf{z}}\hat{\mathbf{x}} + \epsilon_{zy} \hat{\mathbf{z}}\hat{\mathbf{y}} + \epsilon_{zz} \hat{\mathbf{z}}\hat{\mathbf{z}} \end{cases}$$

The scalar product $\boldsymbol{\epsilon} \cdot \mathbf{E}$ is formed by taking the scalar product between the unit vectors on adjacent sides of the dot, and it yields a vector. Alternatively, $\boldsymbol{\epsilon}$ may be represented by a 3×3 matrix with components ϵ_{ij} , $i, j = x, y, z$, and \mathbf{E} by a column vector. The scalar product $\boldsymbol{\epsilon} \cdot \mathbf{E}$ is then a conventional matrix product. In general the algebra of dyadics and vectors has a one-to-one correspondence with matrix algebra. For example, $\boldsymbol{\epsilon} \cdot \mathbf{E} = \mathbf{E} \cdot \boldsymbol{\epsilon}_t$, where $\boldsymbol{\epsilon}_t$ is the transposed dyadic corresponding to the transposed matrix. Corresponding to the inverse of the matrix there is an inverse dyadic $\boldsymbol{\epsilon}^{-1}$ such that $\boldsymbol{\epsilon}^{-1} \cdot \boldsymbol{\epsilon} = \mathbf{I}$, the unit dyadic. The unit dyadic $\mathbf{I} = \hat{\mathbf{x}}\hat{\mathbf{x}} + \hat{\mathbf{y}}\hat{\mathbf{y}} + \hat{\mathbf{z}}\hat{\mathbf{z}}$, or idemfactor, has the property that $\mathbf{I} \cdot \boldsymbol{\epsilon} = \boldsymbol{\epsilon}$. The corresponding matrix is the unit matrix with all off-diagonal elements equal to zero and diagonal elements equal to unity. Using the inverse dyadic, we can formally solve (1.11b) for \mathbf{E} to obtain $\mathbf{E} = \boldsymbol{\epsilon}^{-1} \cdot \mathbf{D}$. The use of dyadics in this book may be viewed as a convenient shorthand notation for matrix operations.

In magnetizable media a similar situation prevails. By convention the induced magnetic dipole polarization density \mathbf{M} is related to the magnetic intensity \mathbf{H} by a magnetic susceptibility tensor χ_m as follows:

$$\mathbf{M} = \chi_m \cdot \mathbf{H} \quad (1.12a)$$

The defining equation for \mathbf{H} in terms of \mathbf{M} and \mathbf{B} is

$$\mu_0 \mathbf{H} = \mathbf{B} - \mu_0 \mathbf{M}$$

or alternatively

$$\mathbf{B} = \mu_0 (\mathbf{H} + \mathbf{M}) = \mu_0 (\mathbf{I} + \chi_m) \cdot \mathbf{H} = \boldsymbol{\mu} \cdot \mathbf{H} \quad (1.12b)$$

where $\boldsymbol{\mu}$ is the permeability tensor. Both χ_m and $\boldsymbol{\mu}$ have components that are complex functions of ω . In the time domain the relation between \mathfrak{M} and \mathfrak{H} is again a differential equation describing the dynamics of the polarization.

Equations (1.11) and (1.12) are called constitutive equations, and $\boldsymbol{\epsilon}$ and $\boldsymbol{\mu}$ are referred to as constitutive parameters. The macroscopic interaction of material bodies with the electromagnetic field is accounted for through the use of these constitutive parameters and equations. Certain general properties of $\boldsymbol{\epsilon}$

and \mathbf{u} can be deduced from energy considerations, and this will be done in a later section. When ϵ and \mathbf{u} are independent of position, the medium is homogeneous. In an inhomogeneous medium the constitutive parameters vary with position.

For most conducting media the conduction current \mathbf{J} is proportional to \mathbf{E} and may be expressed in the form

$$\mathbf{J} = \sigma \mathbf{E} \quad (1.13)$$

where σ is a constant called the conductivity and is expressed in units of mhos per meter. Since σ is a constant, the same relation holds in the frequency domain.

If the conductivity σ of a material body is at all appreciable, the free charge density ρ in the interior can be taken as zero, since any initial charge distribution present will decay with a time constant $\tau = \epsilon/\sigma$ — which is very small, as the reader may readily verify.

Exercise 1.1 From (1.1d), the continuity equation (1.2) and the constitutive equation (1.13) show that $\partial\rho/\partial t = -(\sigma/\epsilon)\rho$ and hence $\rho(r,t) = \rho_0(r)e^{-\sigma t/\epsilon}$. Evaluate $\tau = \epsilon/\sigma$ for seawater, where $\sigma = 5$ mhos/m and $\epsilon \approx 80\epsilon_0$. As long as $\omega t \ll 1$ for the frequencies of interest, ρ can be taken as zero.

From Maxwell's equation for the curl of \mathbf{H} we can write

$$\nabla \times \mathbf{H} = j\omega\mathbf{D} + \mathbf{J} = j\omega\left(\epsilon - \frac{j\sigma}{\omega}\right)\mathbf{E}$$

for an isotropic medium. It is thus apparent that σ can be incorporated into an effective permittivity $\epsilon - j\sigma/\omega$. We shall generally write ϵ for the permittivity and assume that the conductivity of the medium is included. The real and imaginary parts of ϵ will be denoted by ϵ' and $-\epsilon''$, for example, $\epsilon = \epsilon' - j\epsilon''$. Similarly, we will write $\mu = \mu' - j\mu''$. In passive media both ϵ'' and μ'' are real positive functions of ω and give rise to energy loss in the medium. The physical basis for the energy loss is finite conductivity and the work that must be done to maintain the polarization against the viscous damping forces that are present.

1.3 Energy and Power

In a general anisotropic medium we have

$$\nabla \times \mathbf{E} = -j\omega\mathbf{u} \cdot \mathbf{H} \quad (1.14a)$$

$$\nabla \times \mathbf{H} = j\omega\epsilon \cdot \mathbf{E} + \mathbf{J} \quad (1.14b)$$

Using the results of the following exercise and integrating over a volume V , we obtain

Exercise 1.2 Expand $\nabla \cdot \mathbf{E} \times \mathbf{H}^*$ and use (1.14) to show that

$$\nabla \cdot \mathbf{E} \times \mathbf{H}^* = -j\omega \mathbf{H}^* \cdot \mathbf{u} \cdot \mathbf{H} + j\omega \mathbf{E} \cdot \boldsymbol{\epsilon}^* \cdot \mathbf{E}^* - \mathbf{E} \cdot \mathbf{J}^*$$

where the asterisk denotes the complex conjugate.

$$\frac{1}{2} \int_S \mathbf{E} \times \mathbf{H}^* \cdot d\mathbf{S} = 2j\omega \int \frac{1}{4} (\mathbf{H}^* \cdot \mathbf{u} \cdot \mathbf{H} - \mathbf{E} \cdot \boldsymbol{\epsilon}^* \cdot \mathbf{E}^*) dV + \frac{1}{2} \int \mathbf{E} \cdot \mathbf{J}^* dV \quad (1.15)$$

where the volume integral of the divergence has been converted to a surface integral by using the divergence theorem and the element of surface area $d\mathbf{S}$ is taken directed into the volume V . The quantity $\mathbf{E} \times \mathbf{H}^*$ is called the complex Poynting vector, and the result given by (1.15) is the complex Poynting vector theorem and has the following interpretation: The real part of the left-hand side, that is, $\text{Re } \frac{1}{2} \int \mathbf{E} \times \mathbf{H}^* \cdot d\mathbf{S}$, gives the time-average rate of energy flow into the volume V . In the interior this energy input is dissipated as heat by the conduction current \mathbf{J} and the polarization damping forces. The time-average rates of energy dissipation by these two mechanisms are given by

$$\frac{1}{2} \int \mathbf{E} \cdot \mathbf{J}^* dV = \frac{1}{2} \int \frac{\mathbf{J} \cdot \mathbf{J}^*}{\sigma} dV \quad (1.16a)$$

$$\text{Im } \frac{\omega}{2} \int (\mathbf{E} \cdot \boldsymbol{\epsilon}^* \cdot \mathbf{E}^* - \mathbf{H}^* \cdot \mathbf{u} \cdot \mathbf{H}) dV \quad (1.16b)$$

When ϵ and μ are scalars, it is readily seen that ϵ'' and μ'' , as defined earlier, must be positive if energy dissipation and not generation is to take place.

The time average of the imaginary part of the flux of the complex Poynting vector through the surface S is equal to 2ω times the difference in the time-average magnetic and electric energy stored in the interior volume. When ϵ and \mathbf{u} are scalars or dyadics that are independent of ω , that is, nondispersive media, the time-average magnetic and electric energy stored in V is given by

$$W_m = \text{Re } \frac{1}{4} \int \mathbf{H}^* \cdot \mathbf{u} \cdot \mathbf{H} dV = \text{Re } \frac{1}{4} \int \mathbf{H} \cdot \mathbf{u}^* \cdot \mathbf{H}^* dV \quad (1.17a)$$

$$W_e = \text{Re } \frac{1}{4} \int \mathbf{E} \cdot \boldsymbol{\epsilon}^* \cdot \mathbf{E}^* dV \quad (1.17b)$$

In dispersive media where ϵ and \mathbf{u} depend on ω the volume integrals in (1.17) do not give the time-average energy stored in the magnetic and electric fields. The reason for this apparent anomaly is as follows: When a medium is polarized, the increase in stored energy is essentially of two different kinds: the potential energy associated with charge displacement against elastic-type restoring forces and kinetic energy associated with the motion of the charge. The integral of the complex Poynting vector over a closed surface yields the difference in the free-space magnetic and electric energy stored and the difference in

the kinetic and potential energy associated with the polarization. Thus the quantity

$$\operatorname{Re} \frac{1}{4} \int_V (\mathbf{E} \cdot \boldsymbol{\epsilon}^* \cdot \mathbf{E}^* - \epsilon_0 \mathbf{E} \cdot \mathbf{E}^*) dV$$

gives only the increase in stored energy above the free space value arising from the difference between the potential and kinetic energy associated with the polarization. In a nondispersive medium or at sufficiently low frequencies the kinetic energy is negligible compared with the potential energy, in which case the total stored energy associated with the electric field is obtained from the given volume integral. Similar remarks apply to the expression (1.17a) for magnetic energy.

When the losses in the medium are negligible, the correct expressions for the time-average stored energy are

$$W_m = \operatorname{Re} \frac{1}{4} \int_V \mathbf{H} \cdot \frac{\partial(\omega \mathbf{u}^*)}{\partial \omega} \cdot \mathbf{H}^* dV \quad (1.18a)$$

$$W_e = \operatorname{Re} \frac{1}{4} \int_V \mathbf{E} \cdot \frac{\partial(\omega \boldsymbol{\epsilon}^*)}{\partial \omega} \cdot \mathbf{E}^* dV \quad (1.18b)$$

To obtain these results it is necessary to consider a process whereby the field is slowly built up from an initial value of zero to its final value and the resultant energy expended is evaluated. (For a derivation see Landau and Lifshitz¹¹ or Tonning¹².) The above expressions for stored energy bear a close relationship to Foster's reactance theorem for lossless reactive networks (Montgomery, Dicke, and Purcell¹³). Foster's reactance theorem states that the frequency derivative of the input susceptance B is given by $V V^* \partial B / \partial \omega = 4(W_e + W_m)$, where V is the applied voltage and $W_e + W_m$ is the total stored energy. For a lossless reactance X the corresponding result is $I I^* \partial X / \partial \omega = 4(W_e + W_m)$, where I is the input current. The quantities $\omega \boldsymbol{\epsilon}$ and $\omega \mathbf{u}$ may be regarded as generalized admittance and reactance functions for an anisotropic medium, and hence it is seen that (1.18) is similar in form to Foster's reactance theorem for lossless networks.

In the complex Poynting vector theorem (1.15) the current \mathbf{J} can be an impressed current (as in an antenna radiation problem), in which case the volume integral of $\mathbf{E} \cdot \mathbf{J}^*$ corresponds to the rate at which energy is produced. The real part of the complex Poynting vector flux is now directed outward corresponding to radiation of electromagnetic energy.

1.4 Some Properties of the Constitutive Parameters

In a lossless medium both of the dyadics $\boldsymbol{\epsilon}$ and \mathbf{u} are hermitian, that is, $\boldsymbol{\epsilon}^* = \boldsymbol{\epsilon}_t$ where $\boldsymbol{\epsilon}_t$ is the transposed dyadic, and similarly for \mathbf{u} , as we show below. Let $\boldsymbol{\epsilon}$ be expressed in the form

$$\boldsymbol{\epsilon} = \boldsymbol{\epsilon}' - j\boldsymbol{\epsilon}''$$

where $\epsilon' = \frac{1}{2}(\epsilon + \epsilon_t^*)$ is the hermitian part and $-j\epsilon'' = \frac{1}{2}(\epsilon - \epsilon_t^*)$ is the antihermitian part. For the quantity $2j\omega \mathbf{E} \cdot \epsilon^* \cdot \mathbf{E}^*$ we can write $2j\omega \mathbf{E} \cdot \epsilon'^* \cdot \mathbf{E}^* + 2\omega \mathbf{E} \cdot \epsilon''^* \cdot \mathbf{E}^*$. A hermitian dyadic, by definition, has the property $\epsilon' = \epsilon_t'^*$, while for an antihermitian tensor $-j\epsilon'' = -(-j\epsilon_t'')^*$, so that $\epsilon'' = \epsilon_t''^*$. Using these relations and the identity $\mathbf{E} \cdot \epsilon^* \cdot \mathbf{E}^* = \mathbf{E}^* \cdot \epsilon_t^* \cdot \mathbf{E}$, we find that

$$2j\omega \mathbf{E} \cdot \epsilon^* \cdot \mathbf{E}^* = j\omega (\mathbf{E} \cdot \epsilon'^* \cdot \mathbf{E}^* + \mathbf{E}^* \cdot \epsilon' \cdot \mathbf{E}) + \omega (\mathbf{E} \cdot \epsilon''^* \cdot \mathbf{E}^* + \mathbf{E}^* \cdot \epsilon'' \cdot \mathbf{E})$$

Each term in parentheses is the sum of a complex quantity and its complex conjugate and is pure real. For a loss-free medium the quantity $2j\omega \mathbf{E} \cdot \epsilon^* \cdot \mathbf{E}^*$ occurring in the complex Poynting vector theorem must be pure imaginary, which requires that ϵ'' be zero. The latter restricts ϵ to be a hermitian dyadic in a lossless medium. Similarly, μ must be hermitian for zero magnetic polarization loss. When a tensor of rank 2 or a dyadic is hermitian, the matrix representing this dyadic has pure real diagonal terms and off-diagonal terms that satisfy the symmetry property $\epsilon_{ij} = \epsilon_{ji}^*$. If $\epsilon_{ij} = \epsilon'_{ij} - j\epsilon''_{ij}$, then $\epsilon'_{ij} = \epsilon'_{ji}$ and $\epsilon''_{ij} = -\epsilon''_{ji}$. In isotropic loss-free media ϵ and μ are real, which is a special case of the above general result.

It is not possible to have a dispersive medium that is loss-free, although there may be frequency bands throughout which the loss is very small. Each element of the constitutive parameters ϵ and μ is an analytic function for which the real part determines the imaginary part, and vice versa, by means of the well-known Hilbert transforms. To see how these properties come about consider the polarization $\mathbf{P}(\omega) = \epsilon_0 \chi_e(\omega) \cdot \mathbf{E}(\omega)$. Let

$$\mathbf{\epsilon}(t) = \frac{1}{2\pi} \int_{-\infty}^{\infty} \mathbf{E}(\omega) e^{j\omega t} d\omega \quad \mathbf{E}(\omega) = \int_{-\infty}^{\infty} \mathbf{\epsilon}(t) e^{-j\omega t} dt$$

which are the usual Fourier transform relations. If $\mathbf{\epsilon}(t) \equiv 0$ for $t < 0$, then $\mathbf{E}(\omega)$ is free of all singularities in the lower $\omega + j\sigma$ complex plane, since for $t < 0$ the integral for $\mathbf{\epsilon}(t)$ can be evaluated by closing the contour in the lower half plane and must give zero. For $\mathbf{\epsilon}(t)$ to be a real function, $\mathbf{E}(\omega) = \mathbf{E}^*(-\omega)$. When $\mathbf{\epsilon}(t)$ is zero for $t < 0$, causality requires the polarization $\mathbf{P}(t)$ also to be zero for $t < 0$. Hence $\epsilon_0 \chi_e(\omega) \cdot \mathbf{E}(\omega)$, which is the Fourier transform of $\mathbf{P}(t)$, is also analytic in the lower half plane. Thus, $\chi_e(\omega)$ is analytic in the lower half plane. For a physical medium each element χ_{ij} of χ_e will vanish to order ω^{-a} , $a > 0$, as ω tends to infinity. For later use we also note that $\chi_{ij}(\omega) = \chi_{ij}^*(-\omega)$, since $\mathbf{P}(t)$ must be real. The above analytic properties of χ_e are a direct result of the physical properties of $\mathbf{P}(t)$ as given by

$$\mathbf{P}(t) = \frac{\epsilon_0}{2\pi} \int_{-\infty}^{\infty} \chi_e(\omega) \cdot \mathbf{E}(\omega) e^{j\omega t} d\omega$$

For the element $\chi_{ij} = \chi'_{ij} - j\chi''_{ij}$ the contour integral

$$I = \frac{1}{2\pi j} \int \frac{\chi_{ij}(\omega)}{\omega - \omega_0} d\omega = 0$$

since χ_{ij} is analytic within C and the contour C shown in Fig. 1.1 excludes the point ω_0 .

The contribution to the integral over the semicircle is zero, and hence

$$I = \pi j \chi_{ij}(\omega_0) + P \int_{-\infty}^{\infty} \frac{\chi_{ij}(\omega)}{\omega - \omega_0} d\omega = 0 \quad (1.19)$$

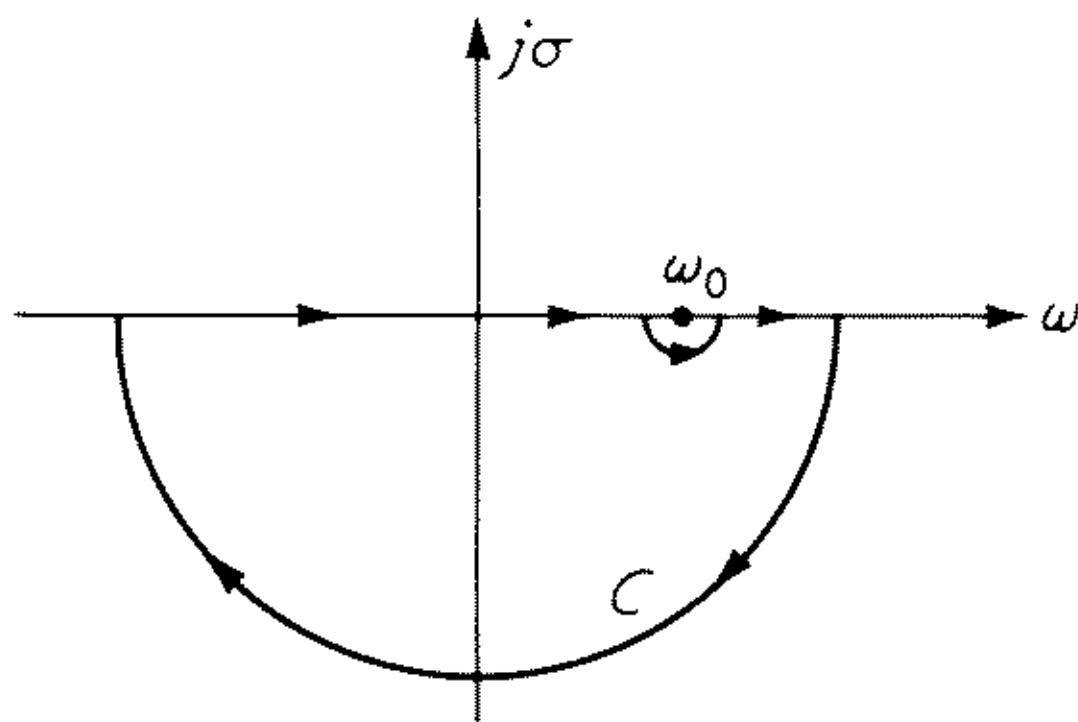


Fig. 1.1 Contour for the integral I leading to the Krönig-Kramers relations.

where P denotes the principal value. From this expression it is easy to show, as required in the exercise below, that

$$\chi'_{ij}(\omega_0) = \frac{2}{\pi} P \int_0^{\infty} \frac{\omega \chi''_{ij}(\omega)}{\omega^2 - \omega_0^2} d\omega \quad (1.20a)$$

$$\chi''_{ij}(\omega_0) = -\frac{2}{\pi} P \int_0^{\infty} \frac{\omega_0 \chi'_{ij}(\omega)}{\omega^2 - \omega_0^2} d\omega \quad (1.20b)$$

These relations, which are Hilbert transforms, are known in the literature as the Krönig-Kramers relations (for a discussion and reference to the original papers see Kerr¹⁴) and were extended to a ferrite medium by Gouray.¹⁵ If χ_{ij} has poles corresponding to loss-free resonances, these will lie on the real axis and the contour C must pass below these singular points and (1.20) must be modified accordingly.

In obtaining the above relations (1.20) we have followed the usual heuristic derivation without detailed consideration of the necessary conditions for their validity. For a careful and rigorous discussion the paper by Wu should be consulted.¹⁶

Exercise 1.3 Split (1.19) into its real and imaginary parts, use the property $\chi_{ij}(\omega) = \chi_{ij}^*(-\omega)$ to obtain $\chi'_{ij}(\omega) = \chi'_{ij}(-\omega)$ and $\chi''_{ij}(\omega) = -\chi''_{ij}(-\omega)$, and thus derive (1.20).

1.5 Wave Equation

The curl of (1.1a) together with (1.1b) gives

$$\nabla \times \nabla \times \mathbf{E} + \mu \epsilon \frac{\partial^2 \mathbf{E}}{\partial t^2} = -\mu \frac{\partial \mathbf{J}}{\partial t} \quad (1.21a)$$

Expanding the first term on the left into $\nabla\nabla\cdot\mathbf{E} - \nabla^2\mathbf{E}$ and using (1.1d) yields the wave equation

$$\nabla^2\mathbf{E} - \mu\epsilon\frac{\partial^2\mathbf{E}}{\partial t^2} = \mu\frac{\partial\mathbf{J}}{\partial t} + \frac{1}{\epsilon}\nabla\rho \quad (1.21b)$$

In deriving (1.21) we have assumed a nondispersive isotropic medium described by constitutive constants μ and ϵ . The magnetic field \mathbf{H} satisfies a similar equation that may be derived by taking the curl of (1.1b) and substituting the time derivative of (1.1a). Thus we find that

$$\nabla^2\mathbf{H} - \mu\epsilon\frac{\partial^2\mathbf{H}}{\partial t^2} = -\nabla\times\mathbf{J} \quad (1.22)$$

The above equations predict wave solutions having the characteristic velocity $(\mu\epsilon)^{-1/2}$

For monochromatic fields with a time dependence $e^{j\omega t}$ the wave equation becomes the vector Helmholtz equation, that is,

$$\nabla\times\nabla\times\mathbf{E} - k^2\mathbf{E} = -j\omega\mu\mathbf{J} \quad (1.23a)$$

$$\text{or equivalently} \quad \nabla^2\mathbf{E} + k^2\mathbf{E} = j\omega\mu\mathbf{J} + \frac{1}{\epsilon}\nabla\rho \quad (1.23b)$$

$$\text{and} \quad \nabla^2\mathbf{H} + k^2\mathbf{H} = -\nabla\times\mathbf{J} \quad (1.23c)$$

where $k = \omega(\mu\epsilon)^{1/2}$ is called the wave number or propagation constant. That is, k is the propagation constant for plane, spherical, or cylindrical transverse electromagnetic (TEM) waves in the medium.

In a source-free medium the plane wave solution to (1.23a) ($\mathbf{J} = \rho = 0$) is $\mathbf{E} = \mathbf{E}_0 e^{-j\mathbf{k}\cdot\mathbf{r}}$, where \mathbf{E}_0 is a constant vector and \mathbf{k} is the propagation vector. Substituting the assumed solution for \mathbf{E} into Maxwell's equations (1.5) with all source terms equated to zero gives

$$\mathbf{k}\times\mathbf{E}_0 e^{-j\mathbf{k}\cdot\mathbf{r}} = \omega\mu\mathbf{H} \quad (1.24a)$$

$$\mathbf{k}\times\mathbf{H} = -\omega\epsilon\mathbf{E}_0 e^{-j\mathbf{k}\cdot\mathbf{r}} \quad (1.24b)$$

$$\mathbf{k}\cdot\mathbf{H} = 0 \quad (1.24c)$$

$$\mathbf{k}\cdot\mathbf{E}_0 = 0 \quad (1.24d)$$

These equations show that \mathbf{H} is of the form $\mathbf{H}_0 e^{-j\mathbf{k}\cdot\mathbf{r}}$. The cross product of the first equation with \mathbf{k} yields

$$\mathbf{k}\times(\mathbf{k}\times\mathbf{E}_0) = (\mathbf{k}\cdot\mathbf{E}_0)\mathbf{k} - k^2\mathbf{E}_0 = \omega\mu\mathbf{k}\times\mathbf{H}_0$$

Use of the second and fourth equation gives $(\omega^2\mu\epsilon - k^2)\mathbf{E}_0 = 0$, which shows that a solution exists only if $k^2 = \omega^2\mu\epsilon$. Thus we were justified in calling $\omega(\mu\epsilon)^{1/2}$ the propagation constant earlier. We also readily find that

$$\mathbf{H}_0 = \frac{\mathbf{k}\times\mathbf{E}_0}{\omega\mu} = \left(\frac{\epsilon}{\mu}\right)^{1/2}\hat{\mathbf{k}}\times\mathbf{E}_0 \quad (1.25)$$

The parameter $(\mu/\epsilon)^{1/2}$ has the dimensions of an impedance and is called the intrinsic impedance of the medium. It will be represented by the symbol ζ ; thus

$$\zeta = \left(\frac{\mu}{\epsilon}\right)^{1/2} \quad (1.26)$$

In free space the propagation constant and intrinsic impedance are given by

$$k_0 = \omega(\mu_0\epsilon_0)^{1/2} \quad (1.27a)$$

$$\zeta_0 = (\mu_0/\epsilon_0)^{1/2} \quad (1.27b)$$

For the plane wave solution given above it may be noted that \mathbf{E} , \mathbf{H} , and \mathbf{k} are mutually perpendicular and that the Poynting vector $\mathbf{E} \times \mathbf{H}^*$ has the same direction as \mathbf{k} .

In anisotropic nonhomogeneous media simple wave solutions are a good deal more difficult, if not impossible, to construct. For a homogeneous anisotropic medium plane wave solutions of the form $\mathbf{E} = \mathbf{E}_0 e^{-j\mathbf{k} \cdot \mathbf{r}}$ and $\mathbf{H} = \mathbf{H}_0 e^{-j\mathbf{k} \cdot \mathbf{r}}$ do still exist, but the propagation vector \mathbf{k} is no longer a simple function of the constitutive parameters. A formal solution is outlined below in order to exhibit certain properties of the solution for later use.

If we substitute the assumed solutions into Maxwell's equations (1.14) with $\mathbf{J} = 0$, we obtain

$$\mathbf{k} \times \mathbf{E}_0 = \omega \mathbf{u} \cdot \mathbf{H}_0 \quad (1.28a)$$

$$\mathbf{k} \times \mathbf{H}_0 = -\omega \mathbf{\epsilon} \cdot \mathbf{E}_0 \quad (1.28b)$$

From (1.28a) we find $\mathbf{H}_0 = (1/\omega) \mathbf{u}^{-1} \cdot \mathbf{k} \times \mathbf{E}_0$, where \mathbf{u}^{-1} is the dyadic corresponding to the inverse of the matrix representing \mathbf{u} . Substitution into (1.28b) now gives

$$[\mathbf{k} \times (\mathbf{u}^{-1} \cdot \mathbf{k} \times \mathbf{I}) + \omega^2 \mathbf{\epsilon}] \cdot \mathbf{E}_0 = 0 \quad (1.29)$$

where we have replaced \mathbf{E}_0 by $\mathbf{I} \cdot \mathbf{E}_0$ in the expression for \mathbf{H}_0 . Equation (1.29) represents three homogeneous equations for the components of \mathbf{E}_0 . A solution will exist only if the determinant of the matrix that represents the dyadic operator in brackets in (1.29) vanishes. Equating the determinant to zero gives an equation for the propagation constant \mathbf{k} , that is,

$$D(k_x, k_y, k_z, \omega) = 0 \quad (1.30)$$

which in general is a function of ω and the direction in space along which the wave propagates. Thus we have represented the determinant D as a function of ω and the components k_x , k_y , k_z of \mathbf{k} , which are proportional to the direction cosines of \mathbf{k} . The equation obtained for \mathbf{k} is called the dispersion equation.

When the roots for \mathbf{k} have been determined, the components of \mathbf{E}_0 may be found in terms of the ratios of the cofactors of the determinant of the dyadic operator in (1.29). It should be noted that the components of \mathbf{E}_0 will be functions of ω and k_x , k_y , k_z in general. Similarly, \mathbf{H}_0 will be a function of these

parameters. Another feature of a general medium is that the Poynting vector will not usually be in the direction of the propagation vector \mathbf{k} , as may be seen by forming the expression $\mathbf{E} \times \mathbf{H}^*$.

1.6 Group and Energy Flow Velocities

The group velocity and energy flow velocity for electromagnetic waves in frequency-dispersive media have been discussed by many authors (see, for example, Brillouin,¹⁷ Hines,¹⁸ Rytov,¹⁹ Ginzburg,^{20,21} Budden,²² and Bunkin²³). A brief treatment is given below because of the importance of the results in formulating the proper radiation boundary condition at infinity in a medium such as a plasma.

The group velocity is usually defined as the velocity with which a signal composed of a narrow band or group of frequency components propagates, the definition being based on the time delay the packet undergoes in propagating a distance r . Consider a source located at the origin. The field radiated can be described by a superposition of plane waves. Let a component plane wave at the origin be

$$\boldsymbol{\varepsilon}(t,0) = \mathbf{C}f(t) \cos \omega_0 t$$

where \mathbf{C} is a constant vector and the modulating function $f(t)$ has a narrow-band frequency spectrum $g(\omega)$ which is zero outside the range $|\omega| > |\omega_1|$ and where $\omega_1 \ll \omega_0$. The spectrum of $\boldsymbol{\varepsilon}(t,0)$ is

$$\begin{aligned} \mathbf{E}_0(\omega,0) &= \mathbf{C} \int_{-\infty}^{\infty} \frac{1}{2} f(t) (e^{-j(\omega-\omega_0)t} + e^{-j(\omega+\omega_0)t}) dt \\ &= \frac{1}{2} \mathbf{C} [g(\omega - \omega_0) + g(\omega + \omega_0)] \end{aligned} \quad (1.31a)$$

The inverse transform relation is

$$\begin{aligned} \boldsymbol{\varepsilon}(t,0) &= \frac{1}{2\pi} \int_{-\infty}^{\infty} \mathbf{E}_0(\omega,0) e^{j\omega t} d\omega \\ &= \text{Re } \mathbf{C} \frac{1}{2\pi} \int_0^{\infty} g(\omega - \omega_0) e^{j\omega t} d\omega \end{aligned} \quad (1.31b)$$

since $g(-\omega) = g^*(\omega)$ for a real signal $f(t)$.

At a point \mathbf{r} the plane wave field is given by

$$\boldsymbol{\varepsilon}(t,\mathbf{r}) = \text{Re } \mathbf{C} \frac{1}{2\pi} \int_0^{\infty} g(\omega - \omega_0) e^{-j\mathbf{k}(\omega) \cdot \mathbf{r} + j\omega t} d\omega$$

For a narrow-band signal we can approximate $\mathbf{k}(\omega)$ by the first two terms of a Taylor series expansion, thus

$$\mathbf{k}(\omega) \approx \mathbf{k}(\omega_0) + \mathbf{k}'(\omega_0)(\omega - \omega_0) \quad \mathbf{k}' = \frac{\partial \mathbf{k}}{\partial \omega}$$

We now obtain

$$\begin{aligned}
 \mathbf{E}(t, \mathbf{r}) &= \operatorname{Re} \mathbf{C} \frac{1}{2\pi} e^{-j\mathbf{k}(\omega_0) \cdot \mathbf{r} + j\omega_0 t} \int_0^\infty g(\omega - \omega_0) e^{j(\omega - \omega_0)(t - \mathbf{k}' \cdot \mathbf{r})} d\omega \\
 &= \operatorname{Re} \mathbf{C} e^{-j\mathbf{k} \cdot \mathbf{r} + j\omega_0 t} f(t - \mathbf{k}' \cdot \mathbf{r}) \\
 &= \mathbf{C} f(t - \mathbf{k}' \cdot \mathbf{r}) \cos(\omega_0 t - \mathbf{k} \cdot \mathbf{r})
 \end{aligned} \tag{1.32}$$

The signal or modulating function is reproduced at \mathbf{r} without distortion but with a time delay $\tau = \mathbf{k}'(\omega_0) \cdot \mathbf{r}$. The signal or group speed is thus given by

$$v_g = \frac{r}{\tau} = \frac{r}{\partial \mathbf{k} / \partial \omega \cdot \mathbf{r}} \tag{1.33}$$

The plane wave propagates in the direction of \mathbf{k} , and if we place $\mathbf{r} = x\hat{\mathbf{x}}$, we obtain the component of the group velocity in the x direction, that is,

$$v_{gx} = \frac{x}{x \partial k_x / \partial \omega} = \frac{\partial \omega}{\partial k_x}$$

Similarly, we find that

$$v_{gy} = \frac{\partial \omega}{\partial k_y} \quad v_{gz} = \frac{\partial \omega}{\partial k_z}$$

and hence in vector form the group velocity is given by

$$\mathbf{v}_g = \nabla_{\mathbf{k}} \omega \tag{1.34}$$

where $\nabla_{\mathbf{k}}$ designates the gradient in \mathbf{k} space. The gradient of ω in \mathbf{k} space is evaluated from the dispersion equation given earlier.

The conditions under which \mathbf{k} may be approximated by a linear function of ω , for which only a time delay but no distortion occurs, depend on how rapidly \mathbf{k} varies with ω , the width of the signal frequency band, and the magnitude of \mathbf{r} . If \mathbf{r} is sufficiently large, additional terms in the expansion will always be required, leading to signal distortion. In this case the concepts of group and signal velocities are not applicable, because the signal is dispersed in the time domain. If the signal were originally a localized wave packet in both time and space, it would eventually be dispersed both in time and space if \mathbf{k} were a nonlinear function of ω .

We shall show that the velocity of energy propagation is equal to the group velocity. For this purpose it is convenient to utilize the following variation theorem, which is established in Exercise 1.4 for a lossless medium:

$$\nabla \cdot \left(\mathbf{E} \times \frac{\partial \mathbf{H}^*}{\partial \omega} + \frac{\partial \mathbf{E}^*}{\partial \omega} \times \mathbf{H} \right) = j \left(\mathbf{H} \cdot \frac{\partial \omega \mathbf{u}^*}{\partial \omega} \cdot \mathbf{H}^* + \mathbf{E} \cdot \frac{\partial \omega \mathbf{e}^*}{\partial \omega} \cdot \mathbf{E}^* \right) \tag{1.35}$$

The terms inside the brackets add up to give four times the electric plus magnetic energy density in the field, so that (1.35) can be written as

$$\nabla \cdot \left(\mathbf{E} \times \frac{\partial \mathbf{H}^*}{\partial \omega} + \frac{\partial \mathbf{E}^*}{\partial \omega} \times \mathbf{H} \right) = 4j(U_e + U_m) \tag{1.36}$$

Exercise 1.4 Expand the divergence, i.e., left-hand side of (1.35), and use Maxwell's source-free equations to show that the following result is obtained:

$$-j\omega \left(\frac{\partial \mathbf{H}^*}{\partial \omega} \cdot \mathbf{u} \cdot \mathbf{H} - \frac{\partial \mathbf{H}^*}{\partial \omega} \cdot \mathbf{u}_t^* \cdot \mathbf{H} + \mathbf{E} \cdot \boldsymbol{\epsilon}_t \cdot \frac{\partial \mathbf{E}^*}{\partial \omega} - \mathbf{E} \cdot \boldsymbol{\epsilon}^* \cdot \frac{\partial \mathbf{E}^*}{\partial \omega} \right) + j \left(\mathbf{H} \cdot \frac{\partial \omega \mathbf{u}^*}{\partial \omega} \cdot \mathbf{H}^* + \mathbf{E} \cdot \frac{\partial \omega \boldsymbol{\epsilon}^*}{\partial \omega} \cdot \mathbf{E}^* \right)$$

For a lossless medium $\mathbf{u} = \mu_t^*, \boldsymbol{\epsilon}^* = \boldsymbol{\epsilon}_t$, and the first term in parentheses vanishes, thus verifying (1.35). Next show that all the terms inside the parentheses on the right-hand side of (1.35) are real by comparing them with their complex conjugates. Using (1.18), the result given by (1.36) is then obtained.

If (1.36) is applied to the plane wave

$$\mathbf{E}_0(\omega)e^{-j\mathbf{k}(\omega) \cdot \mathbf{r}}, \mathbf{H}_0(\omega)e^{-j\mathbf{k}(\omega) \cdot \mathbf{r}}$$

in a loss-free (\mathbf{k} is then real) dispersive medium, we obtain

$$\begin{aligned} \nabla \cdot \left[\mathbf{E}_0 \times \frac{\partial \mathbf{H}_0^*}{\partial \omega} + j\mathbf{r} \cdot \frac{\partial \mathbf{k}}{\partial \omega} (\mathbf{E}_0 \times \mathbf{H}_0^* + \mathbf{E}_0^* \times \mathbf{H}_0) \right. \\ \left. + \frac{\partial \mathbf{E}_0^*}{\partial \omega} \times \mathbf{H}_0 \right] = j\nabla \cdot \left[\mathbf{r} \cdot \frac{\partial \mathbf{k}}{\partial \omega} (\mathbf{E}_0 \times \mathbf{H}_0^* \right. \\ \left. + \mathbf{E}_0^* \times \mathbf{H}_0) \right] = 4j(U_e + U_m) \quad (1.37) \end{aligned}$$

since the terms not involving \mathbf{r} are constants and have zero divergence. We may rewrite (1.37) in the form

$$\frac{1}{2} \text{Re} \mathbf{E}_0 \times \mathbf{H}_0^* \cdot \nabla \left(\mathbf{r} \cdot \frac{\partial \mathbf{k}}{\partial \omega} \right) = \frac{1}{2} \text{Re} \mathbf{E}_0 \times \mathbf{H}_0^* \cdot \frac{\partial \mathbf{k}}{\partial \omega} = U_e + U_m$$

since
$$\nabla \left(\mathbf{r} \cdot \frac{\partial \mathbf{k}}{\partial \omega} \right) = \nabla \left(x \frac{\partial k_x}{\partial \omega} + y \frac{\partial k_y}{\partial \omega} + z \frac{\partial k_z}{\partial \omega} \right) = \frac{\partial \mathbf{k}}{\partial \omega}$$

The time-average energy flow $\frac{1}{2} \text{Re} \mathbf{E}_0 \times \mathbf{H}_0^*$ is equal to the energy density $U_e + U_m$ multiplied by the energy flow velocity, which we shall designate by \mathbf{v}_g . Thus we have

$$(U_e + U_m)\mathbf{v}_g \cdot \frac{\partial \mathbf{k}}{\partial \omega} = U_e + U_m$$

and hence
$$\mathbf{v}_g \cdot \frac{\partial \mathbf{k}}{\partial \omega} = 1 \quad (1.38)$$

The dispersion equation (1.30) gives a functional relationship between k_x, k_y, k_z , and ω , but k_x, k_y, k_z are not explicit functions of ω . A change $\delta\omega$ does not uniquely specify the change $\delta\mathbf{k}$ in \mathbf{k} , since the dispersion equation requires only that

$$\delta D = \frac{\partial D}{\partial k_x} \delta k_x + \frac{\partial D}{\partial k_y} \delta k_y + \frac{\partial D}{\partial k_z} \delta k_z + \frac{\partial D}{\partial \omega} \delta \omega = 0 \quad (1.39)$$

We may, therefore, take $\delta k_y = \delta k_z = 0$, in which case $\delta k_x / \delta \omega$ is equal to $\partial k_x / \partial \omega$. From (1.38) and (1.39) we now see that

$$v_{gx} \frac{\partial k_x}{\partial \omega} = v_{gx} \frac{\delta k_x}{\delta \omega} = -v_{gx} \frac{\partial D / \partial \omega}{\partial D / \partial k_x} = 1$$

or
$$v_{gx} = \frac{\partial \omega}{\partial k_x} = -\frac{\partial D / \partial k_x}{\partial D / \partial \omega}$$

where $\partial \omega / \partial k_x$ is evaluated for k_y and k_z held constant. The other components of the energy flow velocity are determined in a similar manner. In vector form the final result is

$$\mathbf{v}_g = \nabla_{\mathbf{k}} \omega = -\frac{\nabla_{\mathbf{k}} D}{\partial D / \partial \omega} \quad (1.40)$$

which shows that the energy flow velocity is equal to the group velocity. It is also apparent that this relation establishes the direction of the real part of the complex Poynting vector as that of the gradient of ω in \mathbf{k} space.

The dispersion equation (1.30) determines a surface in \mathbf{k} space for each value of ω . This surface is called the index surface, since the index of refraction is given by k/k_0 . A given value of \mathbf{k} and ω determines a point on this surface. The energy flow corresponding to this value of \mathbf{k} has the direction of the normal to the index surface at the given point as illustrated in Fig. 1.2 for a two-dimensional case.

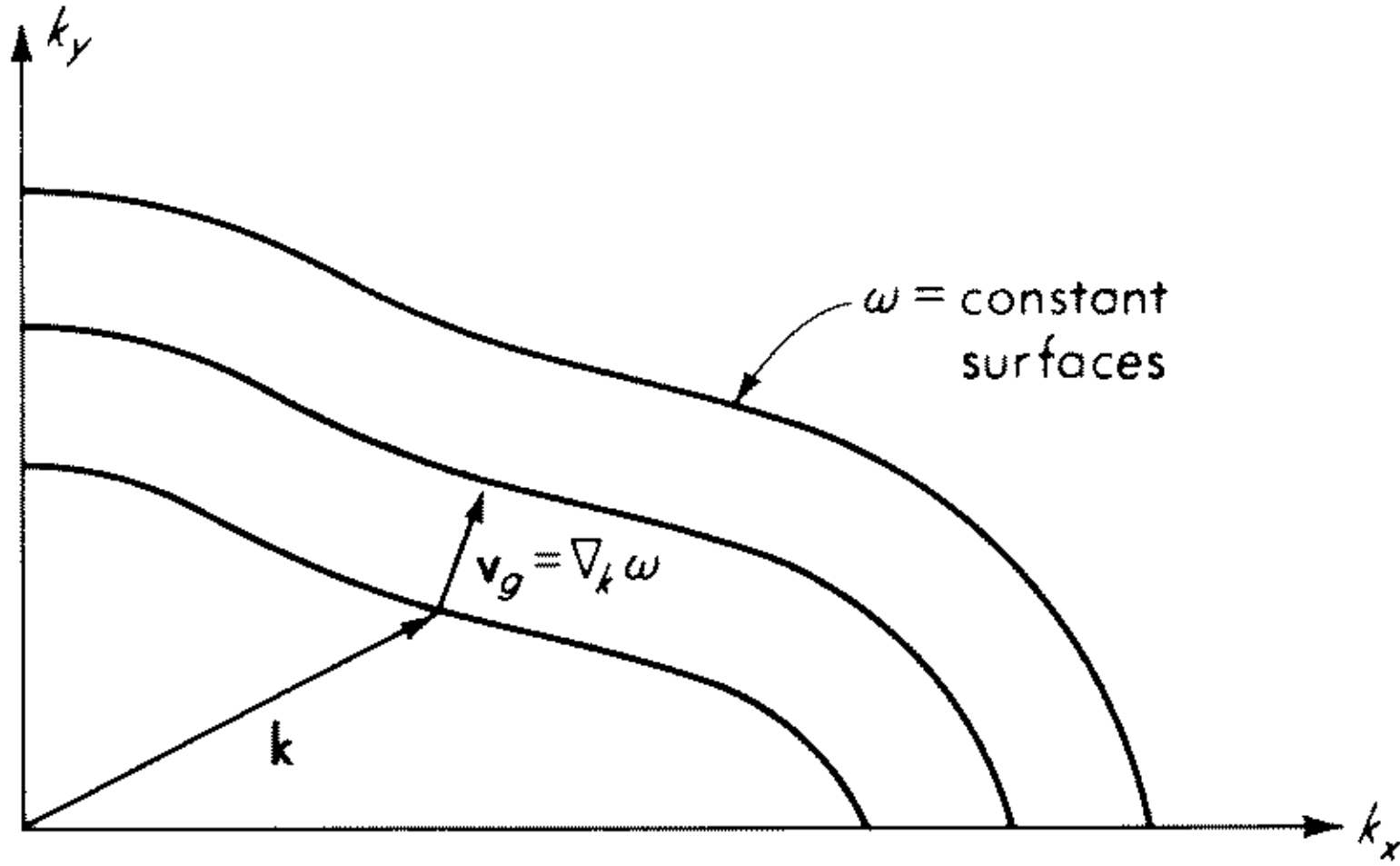


Fig. 1.2 Index surface showing directions of \mathbf{k} and \mathbf{v}_g .

1.7 Boundary Conditions

Boundary between Two Different Media

Figure 1.3 illustrates a boundary between two different media characterized by constitutive parameters ϵ_1, μ_1 and ϵ_2, μ_2 . The normal $\hat{\mathbf{n}}$ points into medium

1. At a separation boundary of this type the relationship between the field vectors on adjacent sides of the boundary are (see any standard text dealing with electromagnetic fields¹⁻⁸).

$$\hat{\mathbf{n}} \cdot \mathbf{D}_1 = \hat{\mathbf{n}} \cdot \mathbf{D}_2 \quad (1.41a)$$

$$\hat{\mathbf{n}} \cdot \mathbf{B}_1 = \hat{\mathbf{n}} \cdot \mathbf{B}_2 \quad (1.41b)$$

$$\hat{\mathbf{n}} \times \mathbf{E}_1 = \hat{\mathbf{n}} \times \mathbf{E}_2 \quad (1.41c)$$

$$\hat{\mathbf{n}} \times \mathbf{H}_1 = \hat{\mathbf{n}} \times \mathbf{H}_2 \quad (1.41d)$$

If an electric surface current of density \mathbf{J}_s per meter exists on the boundary separating regions 1 and 2, the tangential component of \mathbf{H} and normal component of \mathbf{D} will have a discontinuous change across the boundary according to the relations

$$\hat{\mathbf{n}} \times (\mathbf{H}_1 - \mathbf{H}_2) = \mathbf{J}_s \quad (1.42a)$$

$$\hat{\mathbf{n}} \cdot (\mathbf{D}_1 - \mathbf{D}_2) = \rho_s \quad (1.42b)$$

where ρ_s is the surface charge density and is related to \mathbf{J}_s by the surface continuity equation

$$\nabla_s \cdot \mathbf{J}_s = -j\omega\rho_s \quad (1.43)$$

with $\nabla_s = \nabla - \hat{\mathbf{n}}\hat{\mathbf{n}} \cdot \nabla$. Similarly, if a magnetic surface current of density \mathbf{J}_{ms} and associated magnetic surface charge ρ_{ms} exists on the separation boundary, we have

$$\hat{\mathbf{n}} \times (\mathbf{E}_1 - \mathbf{E}_2) = -\mathbf{J}_{ms} \quad (1.44a)$$

$$\hat{\mathbf{n}} \cdot (\mathbf{B}_1 - \mathbf{B}_2) = \rho_{ms} \quad (1.44b)$$

If medium 2 is a perfect conductor ($\sigma = \infty$), the fields in this region will vanish. A surface current of density \mathbf{J}_s and associated surface charge of density ρ_s will exist, and the boundary conditions are as follows:

$$\hat{\mathbf{n}} \times \mathbf{E}_1 = 0 \quad (1.45a)$$

$$\hat{\mathbf{n}} \times \mathbf{H}_1 = \mathbf{J}_s \quad (1.45b)$$

$$\hat{\mathbf{n}} \cdot \mathbf{D}_1 = \rho_s \quad (1.45c)$$

$$\hat{\mathbf{n}} \cdot \mathbf{B}_1 = 0 \quad (1.45d)$$

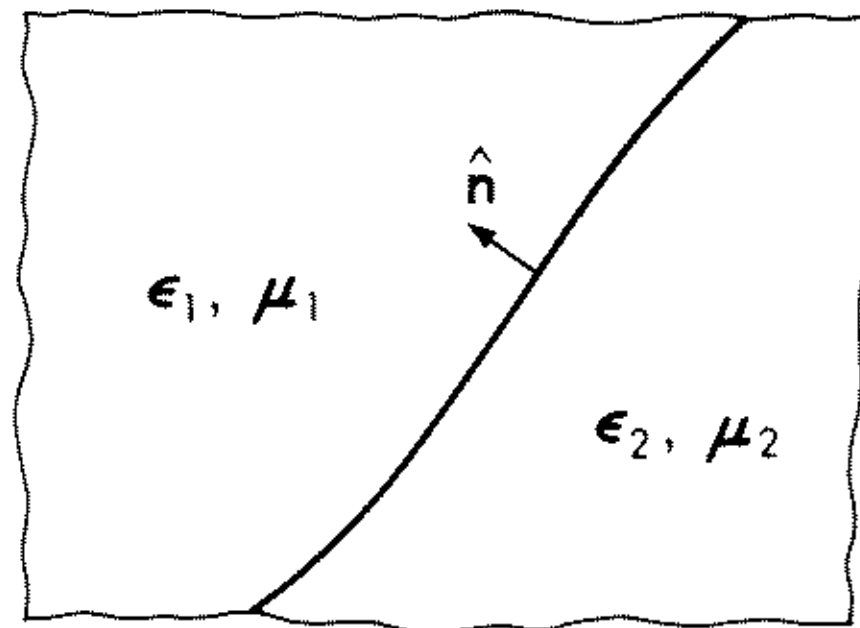


Fig. 1.3 Boundary between two different media.

If medium 2 is a good conductor (any metal falls in this category), the field will penetrate an effective distance equal to the skin depth d_s , which is given by

$$d_s = \left(\frac{2}{\omega \mu \sigma} \right)^{1/2} \quad (1.46)$$

At this depth the field amplitude has decayed by a factor e^{-1} compared to its value at the surface. When the radius of curvature is much larger than the skin depth, the boundary of the imperfect conductor may be described by an impedance boundary condition (occasionally called a Leontovich boundary condition in the literature^{24,25}). That is, a surface current of density \mathbf{J}_s given by

$$\mathbf{J}_s = \hat{\mathbf{n}} \times \mathbf{H}_1 \quad (1.47a)$$

produces a tangential electric field

$$\hat{\mathbf{n}} \times \mathbf{E}_1 = \zeta_s \hat{\mathbf{n}} \times \mathbf{J}_s \quad (1.47b)$$

where

$$\zeta_s = \frac{1 + j}{\sigma d_s} \quad (1.48)$$

is the surface impedance. The surface impedance is equal to the intrinsic impedance of the metal with the displacement current being neglected by comparison with the conduction current, that is,

$$\left(\frac{j\omega\mu}{j\omega\epsilon + \sigma} \right)^{1/2} \approx \left(\frac{j\omega\mu}{\sigma} \right)^{1/2} = \zeta_s$$

When (1.47a) and (1.47b) are combined, we obtain the impedance boundary condition

$$\hat{\mathbf{n}} \times \mathbf{E}_1 = \zeta_s \hat{\mathbf{n}} \times (\hat{\mathbf{n}} \times \mathbf{H}_1) = -\zeta_s (\mathbf{H}_1 - \hat{\mathbf{n}} \cdot \mathbf{H}_1 \hat{\mathbf{n}}) \quad (1.49)$$

Field Singularities at an Edge

The unique solution of electromagnetic boundary-value problems involving a sharp edge requires a statement of the nature of the singularity of the field

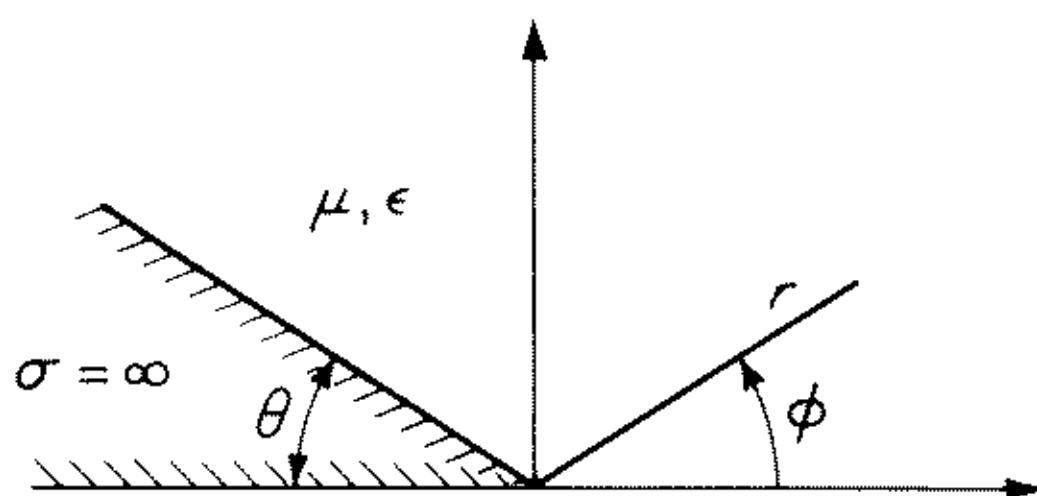


Fig. 1.4 A perfectly conducting wedge.

vectors at the edge. The edge conditions have been examined in detail by Bouwkamp,²⁶ Meixner,^{27,28} Jones,²⁹ Heins and Silver,³⁰ and others (for a discussion see Jones³¹). It is generally agreed that the maximum rate of growth of

the fields as the edge is approached must be limited by the condition that the energy stored in the field in a small volume about the edge should remain finite. Thus, for the two-dimensional perfectly conducting wedge illustrated in Fig. 1.4

$$\int_{-\pi}^{\pi-\theta} \int_0^r (\epsilon \mathbf{E} \cdot \mathbf{E}^* + \mu \mathbf{H} \cdot \mathbf{H}^*) r d\phi dr$$

must remain finite. It is apparent that $\mathbf{E} \cdot \mathbf{E}^*$ and $\mathbf{H} \cdot \mathbf{H}^*$ must then increase no faster than $r^{-(2-2\eta)}$, where η is an arbitrary small positive number. Thus the maximum permissible rate of growth of each field component is $r^{-(1-\eta)}$.

Meixner obtains exact results for the rate of growth of each field component in terms of the wedge angle θ by expanding the fields and Maxwell's equations in a power series in r . We may obtain the same results by using standard solutions for the fields with a radial dependence given in terms of Bessel functions.

For a two-dimensional wedge the fields separate into TE and TM fields with respect to the z axis. The r and ϕ components may be found in terms of E_z and H_z . Suitable solutions for E_z and H_z are

$$\begin{aligned} E_z &= J_\nu(\sqrt{k^2 - \beta^2} r) e^{\pm j\beta z} \sin \nu(\phi + \pi) \\ H_z &= J_\nu(\sqrt{k^2 - \beta^2} r) e^{\pm j\beta z} \cos \nu(\phi + \pi) \end{aligned}$$

where $k^2 = \omega^2 \mu \epsilon$ and $\nu = n\pi/(2\pi - \theta)$, $n = 0, 1, 2, \dots$, in order for the boundary conditions to hold at $\phi = -\pi, \pi - \theta$. For r very small, $J_\nu(\sqrt{k^2 - \beta^2} r)$ is given by $[(k^2 - \beta^2)^{\nu/2} r^\nu]/[2^\nu \Gamma(\nu + 1)]$, where Γ is the gamma function. The r and ϕ components of the fields increase by a factor r^{-1} faster, as Maxwell's equations show. Thus the field components normal to the edge will increase as $r^{-\alpha}$, where

$$\alpha = 1 - \nu = 1 - \frac{n\pi}{2\pi - \theta} \quad n = 0, 1, 2, \dots \quad (1.50)$$

The only values of ν allowed, i.e., integers n , are those that keep α less than $1 - \eta$. Hence, for a 90° wedge ($\theta = \pi/2$) we find that $\alpha = 1/3$, while for a flat, infinitely thin plate ($\theta = 0$) we obtain $\alpha = 1/2$. In both cases the smallest value of n allowed is $n = 1$. The field components tangential to the edge (E_z, H_z) always vanish at the edge. Likewise, the surface current directed normal to the edge vanishes, since this is related to H_z . The surface current parallel to the edge will increase as $r^{-\alpha}$ as the edge is approached. These results also apply to edges occurring in three-dimensional problems, since the singular behavior of the fields near the edge is determined only by the immediate currents and charges and hence a short segment of a curved edge behaves like the edge of a two-dimensional structure. The requirement that the stored energy be finite excludes the use of the second kind of Bessel function Y_ν as part of the solution. An equivalent statement is that the total real power across a surface surrounding the tip must be zero, i.e., the integral of $\text{Re } \mathbf{E} \times \mathbf{H}^*$ over the surface S in Fig. 1.4 must vanish, since no active sources are included. This condition also will exclude Y_ν as part of the solution.

Radiation Condition†

The unique solution of electromagnetic radiation problems requires a specification of boundary conditions to be imposed on the fields at infinity. To illustrate this point consider the scalar Helmholtz equation with a unit source at the origin, that is,

$$\nabla^2\psi(\mathbf{r}) + k^2\psi(\mathbf{r}) = -\delta(\mathbf{r}) \quad (1.51)$$

In the absence of all finite boundaries and assuming a homogeneous isotropic medium, the two solutions for ψ are

$$\psi_1 = \frac{e^{-jkr}}{4\pi r} \quad \psi_2 = \frac{e^{jkr}}{4\pi r}$$

Both solutions are mathematically valid, but only the first is physically possible, because it corresponds to a radially outward propagating wave and ψ_2 is a radially inward propagating wave. Only ψ_1 gives an energy flow directed radially outward at infinity. Thus in addition to boundary conditions imposed over finite boundaries it is necessary to specify a boundary condition or *radiation condition* at infinity. For a scalar wave Sommerfeld stated the radiation condition in the form (for a time dependence $e^{j\omega t}$)

$$|r\psi| < K \quad (1.52a)$$

$$\lim_{r \rightarrow \infty} r \left(\frac{\partial \psi}{\partial r} + jk\psi \right) = 0 \quad (1.52b)$$

where K is a finite constant. It is readily verified that ψ_1 satisfies (1.52), while ψ_2 does not satisfy (1.52b). The condition (1.52a) can be dropped, since it will be true whenever (1.52b) holds.

For the electromagnetic field let all sources, finite boundaries, inhomogeneities, etc., exist entirely within a sphere of radius r_m . Let the medium outside r_m be homogeneous and isotropic. Corresponding to (1.52), the mathematical statement of the radiation condition at infinity for the electromagnetic field is (see Jones³²):

$$|r\mathbf{E}| < K \quad (1.53a)$$

$$|r\mathbf{B}| < K \quad (1.53b)$$

$$\lim_{r \rightarrow \infty} r[\omega \hat{\mathbf{r}} \times \mathbf{B} + k\mathbf{E}] = 0 \quad (1.53c)$$

$$\lim_{r \rightarrow \infty} r[k \hat{\mathbf{r}} \times \mathbf{E} - \omega \mathbf{B}] = 0 \quad (1.53d)$$

These conditions essentially state that, as r tends toward infinity, the Poynting vector $\mathbf{E} \times \mathbf{H}^*$ must be directed radially outward and be decreasing as r^{-2}

†See also Sec. 8.2.

while the radial components \mathbf{E}_r , \mathbf{H}_r must be decreasing faster than r^{-1} . In other words, the field solution must represent an outward propagating wave and not an inward propagating wave at infinity. As a simple example consider the electric field arising from a solenoidal current distribution ($\nabla \cdot \mathbf{J} = 0$) located in a finite volume V in an isotropic homogeneous medium. The governing equation is (see 1.23b)

$$\nabla^2 \mathbf{E}(\mathbf{r}) + k^2 \mathbf{E}(\mathbf{r}) = j\omega\mu \mathbf{J}(\mathbf{r})$$

and the possible solutions are (these solutions are discussed in greater detail in Chap. 2)

$$\mathbf{E}(\mathbf{r}) = -j\omega\mu \int_V \frac{e^{\pm jk|\mathbf{r}-\mathbf{r}'|}}{4\pi|\mathbf{r}-\mathbf{r}'|} \mathbf{J}(\mathbf{r}') dV'$$

For $r \gg r'$ we can approximate $|\mathbf{r} - \mathbf{r}'|$ by $r - 2\hat{\mathbf{r}} \cdot \mathbf{r}'$ in the exponential term and by r in the denominator, thus as $r \rightarrow \infty$

$$\mathbf{E}(\mathbf{r}) \sim -j\omega\mu \frac{e^{\pm jkr}}{4\pi r} \int_V e^{\mp jk\hat{\mathbf{r}} \cdot \mathbf{r}'} \mathbf{J}(\mathbf{r}') dV'$$

When Maxwell's equations are used to determine \mathbf{H} , it is readily verified that only the use of the lower sign in the exponential term gives a solution that satisfies the radiation condition (1.53). The outward propagating wave is characterized by a radial dependence of the form $e^{-jkr}r^{-1}$ at infinity in the case of isotropic media.

In an isotropic homogeneous medium $\partial(\omega\epsilon)/\partial\omega$ and $\partial(\omega\mu)/\partial\omega$ are positive, since the average stored energy in the field must be positive (see 1.18). Since $k = \omega(\mu\epsilon)^{1/2}$, it follows that $\partial k/\partial\omega$ is also positive. Consequently, when \mathbf{k} is directed radially outward, the group velocity and energy flow have the same direction as \mathbf{k} .

For anisotropic media the proper radiation condition at infinity cannot be stated in as simple a form as (1.53), which holds for the isotropic case. From a physical point of view several equivalent statements regarding the behavior of the field at infinity can be made. These are (1) the energy flow at infinity must be radially outward, (2) the complex Poynting vector must be directed radially outward at infinity, and (3) the time delay must be positive and hence the group velocity must be in the outward radial direction. It is thus apparent that the direction of $\nabla_k \omega$ determines whether a propagation factor $e^{-j\mathbf{k} \cdot \mathbf{r}}$ or $e^{j\mathbf{k} \cdot \mathbf{r}}$ is appropriate rather than the direction of \mathbf{k} . To illustrate these features consider a two-dimensional problem for which the index surface is of the form shown in Fig. 1.5. Energy flow at infinity is in the direction of the normal to the index surface. Thus for a given value of k_y the waves with propagation vectors \mathbf{k}_1 and \mathbf{k}_3 in Fig. 1.5 contribute to energy flow in the positive x and y directions and the waves with propagation vectors \mathbf{k}_2 and \mathbf{k}_4 contribute to energy flow in the negative x direction. The wave with propagation vector \mathbf{k}_3

has a component of \mathbf{k}_3 in the negative x direction and hence has a positive phase velocity in the negative x direction. In the positive x direction the phase velocity is negative but the group velocity is positive. It is the requirement of positive group velocity that dictates the choice of \mathbf{k}_1 and \mathbf{k}_3 as suitable propagation vectors for waves in the region where x and y are positive.

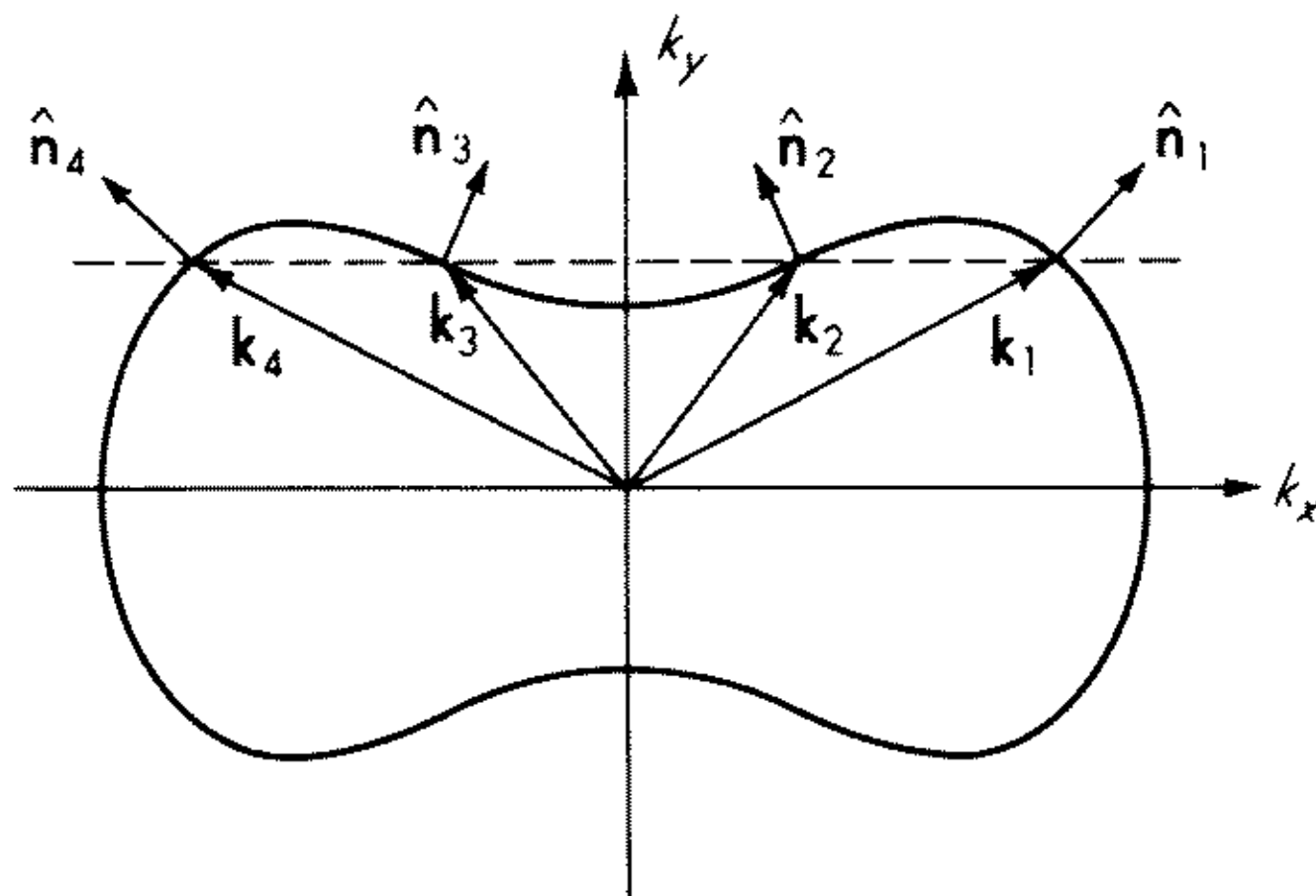


Fig. 1.5 Index surface for a two-dimensional case. Energy flow is in the direction of the outward normal to the surface.

1.8 Potential Theory

It usually proves to be more expedient to determine the electromagnetic field radiated by a given distribution of sources by first finding suitable vector and scalar potential functions. For this purpose we give a short review of potential theory in this section (see also Sec. 8.1). An isotropic homogeneous medium is assumed.

The divergence of \mathbf{B} is identically zero, and such a solenoidal field can always be expressed in terms of the curl of a suitable vector potential \mathbf{A} ; thus

$$\mathbf{B} = \nabla \times \mathbf{A} \quad (1.54)$$

We are tacitly assuming that fictitious magnetic charges and currents have not been introduced. Suitable potential functions for evaluating the partial field arising from equivalent magnetic sources are introduced later. From (1.5a) we obtain

$$\nabla \times \mathbf{E} = -j\omega \nabla \times \mathbf{A}$$

upon using (1.54). This latter equation may be integrated to give

$$\mathbf{E} = -j\omega \mathbf{A} - \nabla \Phi \quad (1.55)$$

where $\nabla \Phi$ is, as yet, the gradient of an arbitrary scalar potential function. In order that the remaining two Maxwell equations (1.5b) and (1.5d) will hold, we require that

$$\nabla \times \nabla \times \mathbf{A} = j\omega \mu \epsilon \mathbf{E} + \mu \mathbf{J} = k^2 \mathbf{A} - j\omega \mu \epsilon \nabla \Phi + \mu \mathbf{J} \quad (1.56a)$$

$$\nabla \cdot \epsilon \mathbf{E} = -j\omega \nabla \cdot \mathbf{A} - \epsilon \nabla^2 \Phi = \rho \quad (1.56b)$$

Upon expanding $\nabla \times \nabla \times \mathbf{A}$, we find that

$$\nabla^2 \mathbf{A} + k^2 \mathbf{A} = \nabla \nabla \cdot \mathbf{A} + j\omega\mu\epsilon \nabla \Phi - \mu \mathbf{J}$$

The equation for \mathbf{A} will simplify considerably if we choose $\nabla \cdot \mathbf{A}$ and Φ , which up to this point are unspecified, such that

$$\nabla \cdot \mathbf{A} = -j\omega\mu\epsilon \Phi \quad (1.57)$$

This particular relationship is called the Lorentz condition. The equation for \mathbf{A} is now an inhomogeneous Helmholtz equation, that is,

$$\nabla^2 \mathbf{A} + k^2 \mathbf{A} = -\mu \mathbf{J} \quad (1.58)$$

Use of the Lorentz condition in (1.56b) shows that the scalar potential Φ also satisfies an inhomogeneous Helmholtz equation; namely,

$$\nabla^2 \Phi + k^2 \Phi = -\frac{\rho}{\epsilon} \quad (1.59)$$

The use of the Lorentz condition enables the field to be expressed in terms of the vector potential \mathbf{A} alone, thus

$$\mathbf{B} = \nabla \times \mathbf{A} \quad (1.60a)$$

$$\mathbf{E} = -j\omega \mathbf{A} + \frac{\nabla \nabla \cdot \mathbf{A}}{j\omega\mu\epsilon} \quad (1.60b)$$

Since \mathbf{A} is completely determined by the current \mathbf{J} , it is seen that knowledge of the charge distribution ρ is not required. The latter is determined by $\nabla \cdot \mathbf{J}$ from the continuity equation and is not an independent source; for this reason, it could be eliminated from the equations specifying the time-dependent electromagnetic field.

If both electric and magnetic currents are present, the field determined by the vector potential \mathbf{A} is only a partial field. To this field must be added the partial field arising from magnetic sources. The magnetic currents and charges give rise to a field that may be evaluated in terms of a magnetic vector potential \mathbf{A}_m and a magnetic scalar potential Φ_m .

When all electric sources are zero, \mathbf{D} is a solenoidal field, so we may put

$$\mathbf{D} = -\nabla \times \mathbf{A}_m \quad (1.61a)$$

By following a development parallel to that employed to derive (1.58) to (1.60), we find that

$$\mathbf{H} = -j\omega \mathbf{A}_m - \nabla \Phi_m = -j\omega \mathbf{A}_m + \frac{\nabla \nabla \cdot \mathbf{A}_m}{j\omega\mu\epsilon} \quad (1.61b)$$

where

$$\nabla^2 \mathbf{A}_m + k^2 \mathbf{A}_m = -\epsilon \mathbf{J}_m \quad (1.62a)$$

$$\nabla^2 \Phi_m + k^2 \Phi_m = -\frac{\rho_m}{\mu} \quad (1.62b)$$

and a Lorentz condition

$$\nabla \cdot \mathbf{A}_m = -j\omega\mu\epsilon\Phi_m \quad (1.63)$$

has been invoked. The details of the derivation are called for in the following:

Exercise 1.5 Show that (1.61b) follows from (1.5b) when (1.61a) is used. Next show that (1.62a) results from substituting into (1.5a) and using the Lorentz condition (1.63). Finally, show that (1.62b) is obtained from (1.5c).

In addition to the electric- and magnetic-type vector potential functions introduced above, a similar set of hertzian vector potentials is often used in practice (see Stratton⁸). The relevant details are called for in problems given at the end of this chapter.

1.9 Reciprocity

The electromagnetic field satisfies certain reciprocity relations that are useful in deriving a number of different properties of electromagnetic devices. Of particular importance to antenna theory is the derivation of the relationship between the receiving and transmitting properties of an antenna. In this section we present the reciprocity theorems and postpone the application to antennas for a later section.

Consider a volume V bounded by a surface S and containing two possible sets of sources $\mathbf{J}_1, \mathbf{J}_{m1}$, and $\mathbf{J}_2, \mathbf{J}_{m2}$. The medium in V is assumed characterized by general unsymmetrical permeability and permittivity tensors \mathbf{y} and $\mathbf{\epsilon}$.

Let the sources $\mathbf{J}_1, \mathbf{J}_{m1}$ produce a field $\mathbf{E}_1, \mathbf{H}_1$ in V and on S . This field satisfies the equations

$$\nabla \times \mathbf{E}_1 = -j\omega\mathbf{y} \cdot \mathbf{H}_1 - \mathbf{J}_{m1} \quad (1.64a)$$

$$\nabla \times \mathbf{H}_1 = j\omega\mathbf{\epsilon} \cdot \mathbf{E}_1 + \mathbf{J}_1 \quad (1.64b)$$

Let $\mathbf{E}_2, \mathbf{H}_2$ be the field produced in V and on S by $\mathbf{J}_2, \mathbf{J}_{m2}$ when the medium in V is replaced by a medium characterized by permeability and permittivity tensors which are the transpose of those considered under the first situation. The field $\mathbf{E}_2, \mathbf{H}_2$ is a solution of

$$\nabla \times \mathbf{E}_2 = -j\omega\mathbf{y}_t \cdot \mathbf{H}_2 - \mathbf{J}_{m2} \quad (1.65a)$$

$$\nabla \times \mathbf{H}_2 = j\omega\mathbf{\epsilon}_t \cdot \mathbf{E}_2 + \mathbf{J}_2 \quad (1.65b)$$

where the subscript t denotes the transposed tensor, that is, μ_{xy} replaced by μ_{yx} , etc.

The expansion of $\nabla \cdot (\mathbf{E}_1 \times \mathbf{H}_2 - \mathbf{E}_2 \times \mathbf{H}_1)$ gives

$$\nabla \cdot (\mathbf{E}_1 \times \mathbf{H}_2 - \mathbf{E}_2 \times \mathbf{H}_1) = (\mathbf{E}_2 \cdot \mathbf{J}_1 - \mathbf{E}_1 \cdot \mathbf{J}_2) - (\mathbf{H}_2 \cdot \mathbf{J}_{m1} - \mathbf{H}_1 \cdot \mathbf{J}_{m2}) \quad (1.66)$$

since $\mathbf{H}_2 \cdot \mathbf{y} \cdot \mathbf{H}_1 = \mathbf{H}_1 \cdot \mathbf{y}_t \cdot \mathbf{H}_2$ and $\mathbf{E}_2 \cdot \mathbf{\epsilon} \cdot \mathbf{E}_1 = \mathbf{E}_1 \cdot \mathbf{\epsilon}_t \cdot \mathbf{E}_2$

The integral of (1.66) throughout the volume V gives

$$\oint_S (\mathbf{E}_1 \times \mathbf{H}_2 - \mathbf{E}_2 \times \mathbf{H}_1) \cdot d\mathbf{S} = \int_V (\mathbf{E}_2 \cdot \mathbf{J}_1 - \mathbf{E}_1 \cdot \mathbf{J}_2 - \mathbf{H}_2 \cdot \mathbf{J}_{m1} + \mathbf{H}_1 \cdot \mathbf{J}_{m2}) dV \quad (1.67)$$

after converting the volume integral of the divergence term to a surface integral by means of the divergence theorem. Equation (1.67) is the general form of the reciprocity theorem for the electromagnetic field (Harrington and Villeneuve³³).

If the surface S encloses all of the sources, the surface integral on the left-hand side in (1.67) vanishes. To show this, consider the application of (1.67) to the volume bounded by S and the surface S_∞ of a sphere of infinite radius. Let the medium have small but finite losses. In this case the fields will decrease in amplitude faster than $1/r$, and hence on S_∞ the surface integral vanishes. Since there are no sources in the volume bounded by S and S_∞ , the surface integral over S must also be zero. Now it seems reasonable to assume that the fields are analytic functions of the loss parameters. Hence the surface integral

$$\oint_S (\mathbf{E}_1 \times \mathbf{H}_2 - \mathbf{E}_2 \times \mathbf{H}_1) \cdot d\mathbf{S}$$

will be an analytic function of the loss parameters. Since the integral vanishes for infinitely small but finite loss parameters, it must still vanish as the loss parameters are reduced to zero in view of the analytic properties of the integral.

In the case of isotropic media the field on S_∞ satisfies the relation $\mathbf{E} = -\zeta \hat{\mathbf{r}} \times \mathbf{H}$ and the integrand $(\mathbf{E}_1 \times \mathbf{H}_2 - \mathbf{E}_2 \times \mathbf{H}_1) \cdot \hat{\mathbf{r}}$ vanishes identically at infinity independently of any loss that may be present.

If there are no sources in V , we obtain from (1.67) the generalization of the Lorentz form of the reciprocity theorem:

$$\oint_S \mathbf{E}_1 \times \mathbf{H}_2 \cdot d\mathbf{S} = \oint_S \mathbf{E}_2 \times \mathbf{H}_1 \cdot d\mathbf{S} \quad (1.68)$$

If the volume V contains all of the sources, the generalized Rayleigh-Carson form of the reciprocity theorem is obtained (Rayleigh,³⁴ Carson^{35,36}):

$$\int_V (\mathbf{E}_1 \cdot \mathbf{J}_2 - \mathbf{H}_1 \cdot \mathbf{J}_{m2}) dV = \int_V (\mathbf{E}_2 \cdot \mathbf{J}_1 - \mathbf{H}_2 \cdot \mathbf{J}_{m1}) dV \quad (1.69)$$

These relations are also valid in isotropic media, in which case the fields \mathbf{E}_2 , \mathbf{H}_2 are the fields produced by \mathbf{J}_2 , \mathbf{J}_{m2} in the actual medium.

It is also possible to obtain a reciprocity theorem relating two different electromagnetic fields with arbitrary time dependence (Welch³⁷). The derivation is straightforward and similar to that used to obtain (1.69). Since no application is made of the results in the present book, the details are not included.

PROBLEMS

1.1 A uniaxial dielectric medium is characterized by permittivities ϵ_1 , ϵ_2 , ϵ_2 along the principal axes which coincide with the x , y , z axes, respectively; i.e., the permittivity dyadic is diagonal. Show that for plane waves the dispersion relations are given by

$$k^2 = \omega^2 \epsilon_2 \mu_0 \quad \text{ordinary wave}$$

$$k_x^2 k_1^2 + (k_y^2 + k_z^2) k_2^2 - k_1^2 k_2^2 = 0 \quad \text{extraordinary wave}$$

where

$$k_i^2 = \omega^2 \epsilon_i \mu_0 \quad i = 1, 2$$

If

$$\epsilon_1 = \frac{\omega_1^2 - \omega^2}{\omega_2^2 - \omega^2} \epsilon_0 \quad \epsilon_2 = \frac{\omega_3^2 - \omega^2}{\omega_4^2 - \omega^2} \epsilon_0$$

where ω_i , $i = 1, 2, 3, 4$, are constants, obtain an expression for the energy flow velocity for the extraordinary wave.

1.2 From Maxwell's equations show that the normal components of \mathbf{D} and \mathbf{B} are continuous across the interface between two different media when the tangential components of \mathbf{E} and \mathbf{H} are continuous across the boundary. (Assume that there are no surface currents on the boundary.)

1.3 Figure P-1.3 illustrates a two-dimensional conducting wedge with a line charge source at x' . Find the electrostatic potential Φ and show that the surface charge density ρ_s induced on the wedge varies with distance r from the edge according to r^{-s} , where

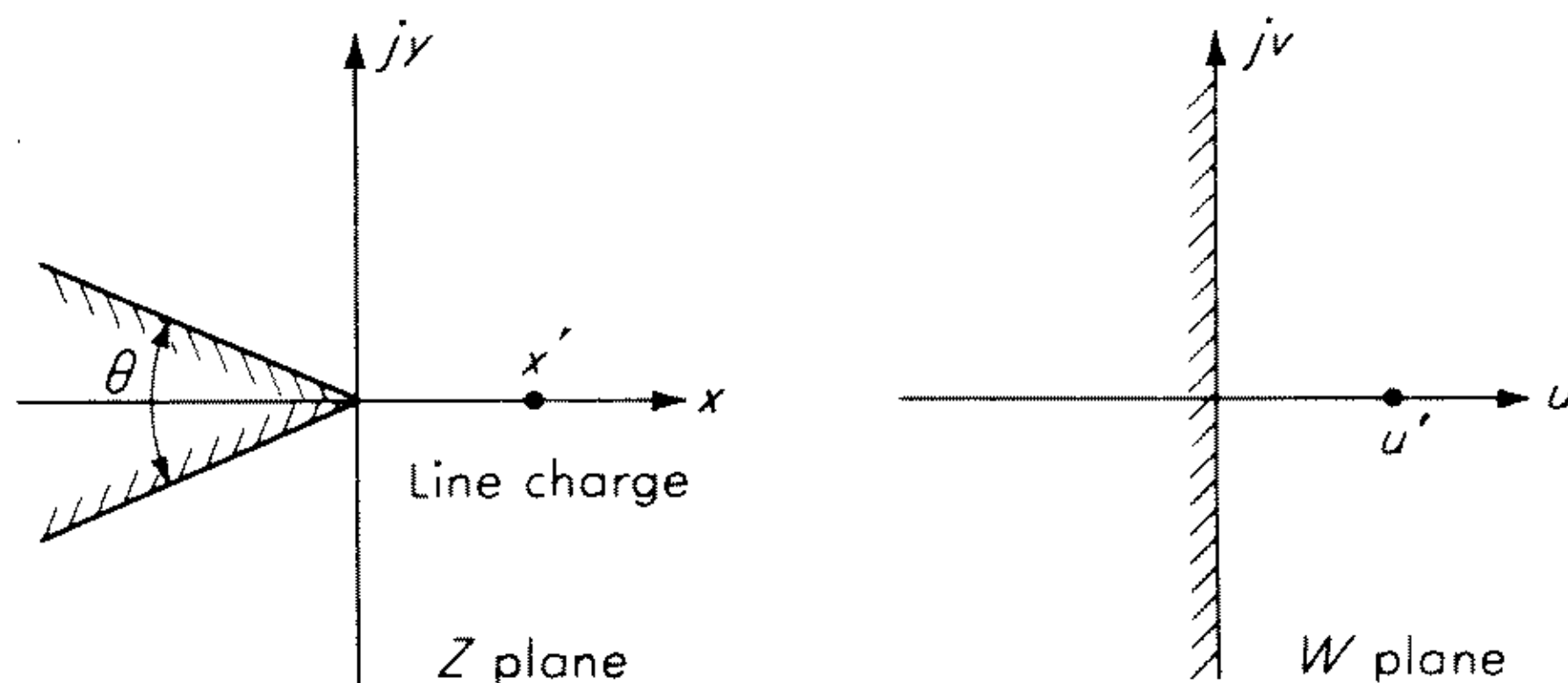


Fig. P-1.3

$s = (\pi - \theta)/(2\pi - \theta)$. Compare with the relation (1.50). Hint: Use conformal mapping ($W = Z^{1-s}$), $Z = x + jy$.

1.4 In a homogeneous isotropic medium where the only source present is an electric current, \mathbf{H} may be expressed in the form $\mathbf{H} = j\omega\epsilon\nabla \times \mathbf{\Pi}_e$, where $\mathbf{\Pi}_e$ is the electric hertzian potential. Show that $\mathbf{\Pi}_e$ is a solution of $(\nabla^2 + k^2)\mathbf{\Pi}_e = -\mathbf{J}/j\omega\epsilon$ and \mathbf{E} is given by $\mathbf{E} = (k^2 + \nabla\nabla\cdot)\mathbf{\Pi}_e$. Use a Lorentz condition and note that $k^2 = \omega^2\mu\epsilon$.

1.5 In a homogeneous isotropic medium where the only source term is a magnetic current density \mathbf{J}_m , the electric field may be derived from a magnetic-type hertzian potential; thus $\mathbf{E} = -j\omega\mu\nabla \times \mathbf{\Pi}_m$. Show that $\mathbf{\Pi}_m$ is a solution of

$$(\nabla^2 + k^2)\mathbf{\Pi}_m = -\frac{\mathbf{J}_m}{j\omega\mu}$$

and that \mathbf{H} is given by $\mathbf{H} = (k^2 + \nabla\nabla\cdot)\mathbf{\Pi}_m$.

1.6 In a source-free isotropic and homogeneous medium show that the hertzian potentials satisfy the relations

$$(\nabla^2 + k_0^2)\mathbf{\Pi}_e = -\frac{\mathbf{P}}{\epsilon_0} \quad (\nabla^2 + k_0^2)\mathbf{\Pi}_m = -\mathbf{M}$$

where \mathbf{P} and \mathbf{M} are the polarization densities in the material and $k_0^2 = \omega^2\mu_0\epsilon_0$. Hint: Express \mathbf{D} and \mathbf{B} in the form $\mathbf{D} = \epsilon_0\mathbf{E} + \mathbf{P}$, $\mathbf{B} = \mu_0(\mathbf{H} + \mathbf{M})$.

1.7 Establish the uniqueness theorem for a time-harmonic electromagnetic field. Let $\mathbf{E}_1, \mathbf{H}_1$ be a solution in a region V bounded by a closed surface S . Let $\mathbf{E}_2, \mathbf{H}_2$ be a second solution that has the same sources and is such that $\hat{\mathbf{n}} \times \mathbf{E}_2 = \hat{\mathbf{n}} \times \mathbf{E}_1$ on S or for which $\hat{\mathbf{n}} \times \mathbf{H}_2 = \hat{\mathbf{n}} \times \mathbf{H}_1$ on S . From the complex Poynting vector theorem show that the difference field $\mathbf{E} = \mathbf{E}_1 - \mathbf{E}_2$, $\mathbf{H} = \mathbf{H}_1 - \mathbf{H}_2$ must satisfy the condition

$$\int_V (\epsilon^* \mathbf{E} \cdot \mathbf{E}^* - \mu \mathbf{H} \cdot \mathbf{H}^*) dV = 0$$

If ϵ is complex, verify that the difference field must be identically zero in V . What happens to the proof if ϵ and μ are real? The uniqueness theorem shows that there is only one unique solution to Maxwell's equations.

REFERENCES

1. Jordan, E. C.: "Electromagnetic Waves and Radiating Systems," Prentice-Hall, Inc., Englewood Cliffs, N.J., 1950.
2. Kraus, J. D.: "Electromagnetics," McGraw-Hill Book Company, New York, 1953.
3. King, R. W. P.: "Fundamental Electromagnetic Theory," Dover Publications, Inc., New York, 1963.
4. Plonsey, R., and R. E. Collin: "Principles and Applications of Electromagnetic Fields," McGraw-Hill Book Company, New York, 1961.
5. Ramo, S., J. R. Whinnery, and T. Van Duzer: "Fields and Waves in Communication Electronics," John Wiley & Sons, Inc., New York, 1965.
6. Schelkunoff, S. A.: "Electromagnetic Waves," D. Van Nostrand Company, Inc., Princeton, N.J., 1943.
7. Toraldo di Francia, G.: "Electromagnetic Waves," Interscience Publishers, Inc., New York, 1956.
8. Stratton, J. A.: "Electromagnetic Theory," sec 8.14, McGraw-Hill Book Company, New York, 1941.
9. Silver, S.: "Microwave Antenna Theory and Design," M.I.T. Radiation Laboratory Series, vol. 12, Chap. 3, McGraw-Hill Book Company, New York, 1949.
10. Landau, L. D., and E. M. Lifshitz: "Electrodynamics of Continuous Media," chaps. IX and XI, Addison-Wesley Publishing Company, Inc., Reading, Mass., 1960.
11. Landau, L. D., and E. M. Lifshitz: Ref. 10, chap. IX.
12. Tonning, A.: Energy Density in Continuous Electromagnetic Media, *IRE Trans. Antennas Propagation*, vol. AP-8, pp. 428-434, July, 1960.
13. Montgomery, C. G., R. H. Dicke, and E. M. Purcell (eds.): "Principles of Microwave Circuits," M.I.T. Radiation Laboratory Series, vol. 8, secs. 5.20 and 5.21, McGraw-Hill Book Company, New York, 1948.
14. Kerr, D. E.: "Propagation of Short Radio Waves," chap. 8, McGraw-Hill Book Company, New York, 1951.
15. Gouray, B. S.: Dispersion Relations for Tensor Media and Their Applications to Ferrites, *J. Appl. Phys.*, vol. 28, pp. 283-288, 1957.
16. Wu, T. T.: Some Properties of Impedance as a Causal Operator, *J. Math. Phys.*, vol. 3, pp. 262-271, March-April, 1962.

17. Brillouin, L.: "Wave Propagation and Group Velocity," Academic Press Inc., New York, 1960.
18. Hines, C. O.: Wave Packets, the Poynting Vector, and Energy Flow, *J. Geophys. Res.*, vol. 56, pp. 63-72 and 191-220, 1951.
19. Rytov, S. M.: Some Theorems Concerning the Group Velocity of Electromagnetic Waves, *Zh. Eksperim. i Teor. Fiz.*, vol. 17, pp. 930-936, 1947.
20. Ginzburg, V. L.: On the Electrodynamics of Anisotropic Media, *J. Exptl. Theoret. Phys.*, vol. 10, pp. 601-607, 1940.
21. Ginzburg, V. L.: "Propagation of Electromagnetic Waves in Plasmas," secs. 22 and 24, Gordon and Breach, Science Publishers, Inc., New York, 1961. (Translated from 1960 Russian edition.)
22. Budden, K. G.: "Radio Waves in the Ionosphere," sec. 13.18, Cambridge University Press, London, 1961.
23. Bunkin, F. V.: On Radiation in Anisotropic Media, *J. Exptl. Theoret. Phys.*, vol. 32, pp. 338-346, 1957.
24. Leontovich, M. A.: "Investigations of Propagation of Radio Waves," Part II, Moscow, 1948.
25. Senior, T. B. A.: Impedance Boundary Conditions for Imperfectly Conducting Surfaces, *Appl. Sci. Res., Sec. B*, vol. 8, pp. 418-436, 1960-1961.
26. Bouwkamp, C. J.: A Note on Singularities at Sharp Edges in Electromagnetic Theory, *Physica*, vol. 12, pp. 467-474, October, 1946.
27. Meixner, J.: The Edge Conditions in the Theory of Electromagnetic Waves at Perfectly Conducting Plane Screens, *Ann. Physik*, vol. 6, pp. 2-9, September, 1949.
28. Meixner, J.: The Behavior of Electromagnetic Fields at Edges, *N.Y.U. Inst. Math. Sci. Res. Rept. EM-72*, December, 1954.
29. Jones, D. S.: Note on Diffraction by an Edge, *Quart. J. Mech. Appl. Math.*, vol. 3, pp. 420-434, December, 1950.
30. Heins, A. E., and S. Silver: The Edge Conditions and Field Representation Theorems in the Theory of Electromagnetic Diffraction, *Proc. Cambridge Phil. Soc.*, vol. 51, pp. 149-161, 1955.
31. Jones, D. S.: "The Theory of Electromagnetism," sec. 9.1, The Macmillan Company, New York, 1964.
32. Jones, D. S.: Ref. 31, sec. 1.27.
33. Harrington, R. F., and A. T. Villeneuve: Reciprocal Relations for Gyrotropic Media, *IRE Trans. Microwave Theory Tech.*, vol. MTT-6, pp. 308-310, July, 1958.
34. Lord Rayleigh: "The Theory of Sound," vol. I, pp. 98 and 150-157, and vol. II, p. 145, The Macmillan Company, New York, 1877 and 1937, 1878 and 1929.
35. Carson, J. R.: A Generalization of the Reciprocal Theorem, *Bell System Tech. J.*, vol. 3, pp. 393-399, July, 1924.
36. Carson, J. R.: Reciprocal Theorems in Radio Communication, *Proc. IRE*, vol. 17, pp. 952-956, June, 1929.
37. Welch, W. J.: Reciprocity Theorems for Electromagnetic Fields Whose Time Dependence Is Arbitrary, *IRE Trans. Antennas Propagation*, vol. AP-8, pp. 68-73, 1960.

CHAPTER 2

RADIATION FROM SIMPLE SOURCES

R. E. Collin

2.1 Introduction

This chapter deals with the problems of radiation from simple sources such as infinitesimal linear current elements, current loops (magnetic dipole radiation), and thin linear wire antennas. We also derive general expressions for the far-zone, or radiation, field from arbitrary current distributions. In addition, this chapter has another purpose, which is to introduce a number of parameters such as radiation pattern, gain, directivity, radiation resistance, etc., that are universally used to describe the characteristics of an antenna. The subject matter is well developed and discussed in all books on antennas, and hence an exhaustive treatment is not given here. (For further details see, for example, the books by Aharoni,¹ Kraus,² Jordan,³ Moullin,⁴ Schelkunoff and Friis,⁵ Silver,⁶ and Williams.⁷) A very extensive treatment of the linear antenna is given by King.⁸ We shall concentrate on the basic principles involved, with little or no reference to specific antenna structures. Applications of many of the results are made in later chapters.

2.2 Radiation from a Current Element

The simplest radiating source is an infinitesimal linear current element. A unit source of this type may be expressed as $\hat{\mathbf{a}}\delta(\mathbf{r} - \mathbf{r}')$, where \mathbf{r}' gives the location of the source and $\hat{\mathbf{a}}$ is a unit vector in the direction of the current. To begin with we shall consider the unit current source to be located at the origin and directed along the z axis as in Fig. 2.1. We shall also assume that the source radiates into free space and that the time dependence is given by $e^{j\omega t}$.

The current has only a z component, and consequently the vector potential \mathbf{A} also has only a z component A_z . The vector potential is a solution of the inhomogeneous Helmholtz equation (1.58), which in the present case simplifies to

$$(\nabla^2 + k_0^2)A_z\hat{\mathbf{z}} = -\mu_0\hat{\mathbf{z}}\delta(\mathbf{r})$$

or equivalently $(\nabla^2 + k_0^2)A_z = -\mu_0\delta(\mathbf{r})$ (2.1)

In view of the spherical symmetry involved, A_z will be a function of r only.

Expressing the laplacian operator in spherical coordinates and retaining only the part dependent on r , we obtain

$$\left(\frac{1}{r^2} \frac{\partial}{\partial r} r^2 \frac{\partial}{\partial r} + k_0^2\right) A_z = -\mu_0 \delta(\mathbf{r}) \quad (2.2)$$

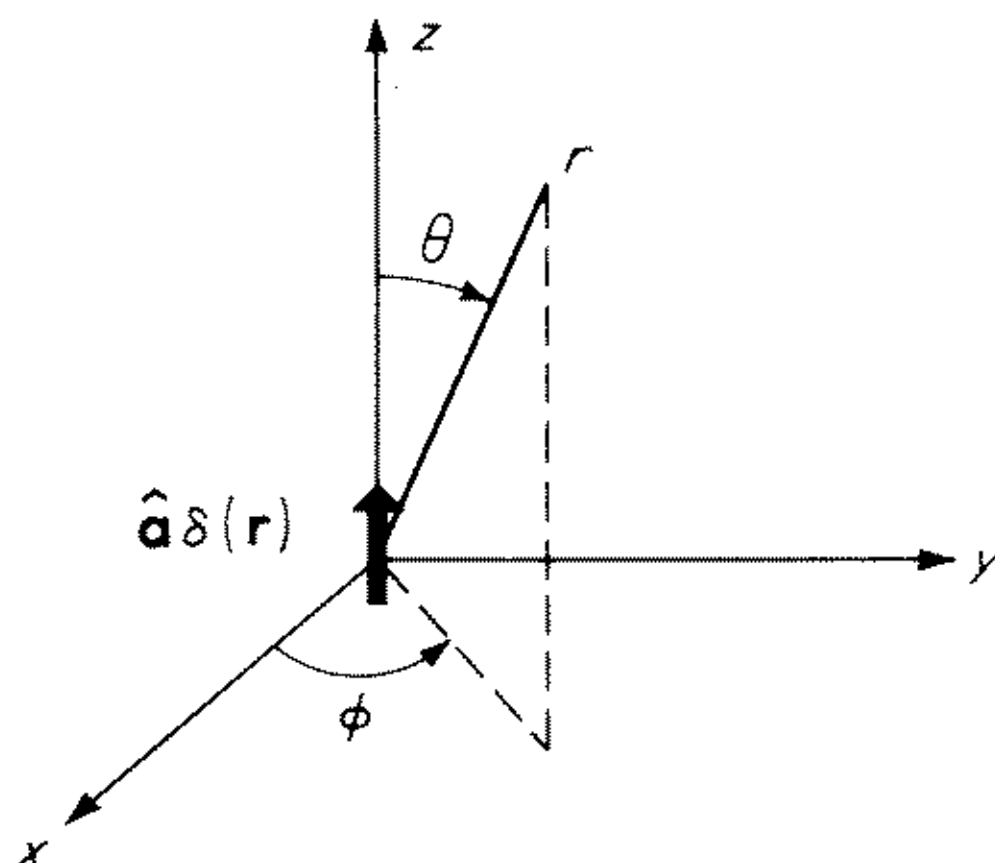


Fig. 2.1 The unit current source.

The homogeneous equation corresponding to (2.2) is the differential equation which defines the spherical Bessel functions of zero order (see, for example, Stratton⁹). The zero-order spherical Bessel functions of the first and second kind are given by

$$j_0(k_0 r) = \frac{\cos(k_0 r - \pi/2)}{k_0 r} = \frac{\sin k_0 r}{k_0 r}$$

$$n_0(k_0 r) = \frac{\sin(k_0 r - \pi/2)}{k_0 r} = \frac{\cos k_0 r}{k_0 r}$$

In order to satisfy the radiation condition at infinity a linear combination of the spherical Bessel functions must be used. The two following linear combinations are called the spherical Hankel functions of the first and second kind.

$$h_0^1(k_0 r) = j_0(k_0 r) + j n_0(k_0 r) = -j \frac{e^{jk_0 r}}{k_0 r}$$

$$h_0^2(k_0 r) = j_0(k_0 r) - j n_0(k_0 r) = j \frac{e^{-jk_0 r}}{k_0 r}$$

Only the second kind of spherical Hankel function corresponds to an outward propagating wave, and hence the solution for A_z must be of the form $A_z = C h_0^2(k_0 r)$, where C is a constant to be determined so as to give the right singularity at the origin.

To determine the constant C we integrate the equation for A_z over a small sphere of radius r to obtain

$$\int_V (\nabla \cdot \nabla A_z + k_0^2 A_z) dV = -\mu_0 \int_V \delta(\mathbf{r}) dV = -\mu_0$$

because of the property of the three-dimensional delta function. When we let the volume of the sphere tend to zero, the integral of $k_0^2 A_z$ will vanish, since V

is proportional to r^3 and A_z increases only as r^{-1} . Using the divergence theorem now gives

$$\lim_{V \rightarrow 0} \oint_S \nabla A_z \cdot d\mathbf{S} = -\mu_0$$

where $d\mathbf{S} = \hat{\mathbf{r}} r^2 d\Omega$ and $d\Omega$ is an element of solid angle. When we substitute for A_z , we obtain

$$\lim_{V \rightarrow 0} \int_0^{4\pi} C \left(r e^{-jk_0 r} - \frac{j}{k_0} e^{-jk_0 r} \right) d\Omega = -\frac{jC4\pi}{k_0} = -\mu_0$$

and hence $C = \mu_0 k_0 / j4\pi$. Thus the solution for A_z is

$$A_z = \frac{\mu_0 k_0}{4\pi j} h_0^2(k_0 r) = \frac{\mu_0 e^{-jk_0 r}}{4\pi r} \quad (2.3)$$

This solution may be immediately generalized to give the vector potential from a unit current element $\hat{\mathbf{a}}\delta(\mathbf{r} - \mathbf{r}')$ located at \mathbf{r}' and having the direction of $\hat{\mathbf{a}}$. For the general case we have

$$\mathbf{A}(\mathbf{r}) = \frac{\mu_0 \hat{\mathbf{a}}}{4\pi |\mathbf{r} - \mathbf{r}'|} e^{-jk_0 |\mathbf{r} - \mathbf{r}'|} \quad (2.4)$$

which is obtained by a simple change in the origin of the coordinate system and by noting that \mathbf{A} has the same direction as the unit vector $\hat{\mathbf{a}}$.

The electromagnetic field may be found from A_z by using (1.60). It is convenient to express the results in spherical coordinates, for which purpose \mathbf{A} is expressed as

$$\mathbf{A} = \hat{\mathbf{z}} A_z = (\hat{\mathbf{r}} \cos \theta - \hat{\boldsymbol{\theta}} \sin \theta) A_z(r)$$

We readily find that (see Exercise 2.1)

$$\mathbf{E} = -\frac{j\zeta_0}{2\pi k_0} \left(\frac{jk_0}{r^2} + \frac{1}{r^3} \right) e^{-jk_0 r} \cos \theta \hat{\mathbf{r}} + \frac{j\zeta_0}{4\pi k_0} \left(\frac{k_0^2}{r} - \frac{jk_0}{r^2} - \frac{1}{r^3} \right) e^{-jk_0 r} \sin \theta \hat{\boldsymbol{\theta}} \quad (2.5a)$$

$$\mathbf{H} = \frac{1}{4\pi} \left(\frac{jk_0}{r} + \frac{1}{r^2} \right) e^{-jk_0 r} \sin \theta \hat{\boldsymbol{\phi}} \quad (2.5b)$$

Exercise 2.1 Fill in the details in the derivation of (2.5). Note that $\nabla \times \hat{\mathbf{z}} A_z$ can be written as $-\hat{\mathbf{z}} \times \nabla A_z = (\hat{\mathbf{r}} \times \hat{\mathbf{z}}) \partial A_z / \partial r = -\hat{\boldsymbol{\phi}} \sin \theta \partial A_z / \partial r$.

If the expression for the electric field is examined, it will be seen that very close to the unit current source the field has the same structure, apart from the factor $e^{-jk_0 r}$, as the electrostatic field produced by an electric dipole. For this reason the radiation from a short linear current element is often referred to as electric dipole radiation. The terms involving r^{-2} and r^{-3} in the expressions for \mathbf{E} and \mathbf{H} constitute the near-zone, or induction, fields and do not contribute to the radiated power. The portion of the field that decreases as r^{-1} at infinity is called the far-zone, or radiation, field, since only this part of the field con-

tributes to the radiated power at infinity. For the unit current source the radiation field is given by

$$\mathbf{E} = \frac{j\zeta_0 k_0}{4\pi r} e^{-jk_0 r} \sin \theta \hat{\boldsymbol{\theta}} \quad (2.6a)$$

$$\mathbf{H} = \frac{jk_0}{4\pi r} e^{-jk_0 r} \sin \theta \hat{\boldsymbol{\phi}} \quad (2.6b)$$

and satisfies the relation

$$\zeta_0 \mathbf{H} = \hat{\mathbf{r}} \times \mathbf{E} \quad (2.6c)$$

which is characteristic of an outward propagating spherical TEM wave.

The time-average radiated power per unit area is given by

$$\frac{1}{2} \text{Re } \mathbf{E} \times \mathbf{H}^* = \frac{1}{2} \frac{\zeta_0 k_0^2 \sin^2 \theta}{(4\pi r)^2} \hat{\mathbf{r}} \quad (2.6d)$$

The power density decreases as r^{-2} ; but since the surface area of a sphere surrounding the source increases as r^2 , a finite amount of power given by

$$P = \frac{1}{2} \text{Re} \oint_S \mathbf{E} \times \mathbf{H}^* \cdot d\mathbf{S} = \frac{\zeta_0 k_0^2}{32\pi^2} \int_0^\pi \int_0^{2\pi} \sin^3 \theta d\theta d\phi = \frac{k_0^2 \zeta_0}{12\pi} \quad (2.6e)$$

is radiated.

2.3 Basic Antenna Parameters

We shall use the solution for the radiation from a unit current source to introduce a number of basic parameters used to describe antennas.

Radiation Pattern

Antennas do not radiate uniformly in all directions in space. Consequently, it is of interest to plot the relative strength of the radiation field as a function of the angles θ and ϕ for a constant value of r . The resultant surface describes the *radiation pattern* of the antenna. If the magnitude of the field is plotted, we obtain the field strength pattern, while if the power density is plotted, we obtain the power radiation pattern. Usually two-dimensional plots are used to show the relative or normalized field strength and radiated power in selected planes. For the unit current source the electric field is given by

$$E_\theta = \frac{j\zeta_0 k_0}{4\pi r} e^{-jk_0 r} \sin \theta$$

in the far-zone field. The maximum field strength occurs for $\theta = \pi/2$, and hence the normalized field strength is given by

$$\frac{|E_\theta(\theta, \phi)|}{|E_\theta(\pi/2, \phi)|} = |\sin \theta| \quad (2.7)$$

The radiated power is proportional to $|E_\theta|^2$, and so the normalized power radiation pattern is given by a plot of $\sin^2 \theta$. The radiation patterns for the unit current source are sketched in Fig. 2.2 for $\phi = 0$. Actually, the patterns are

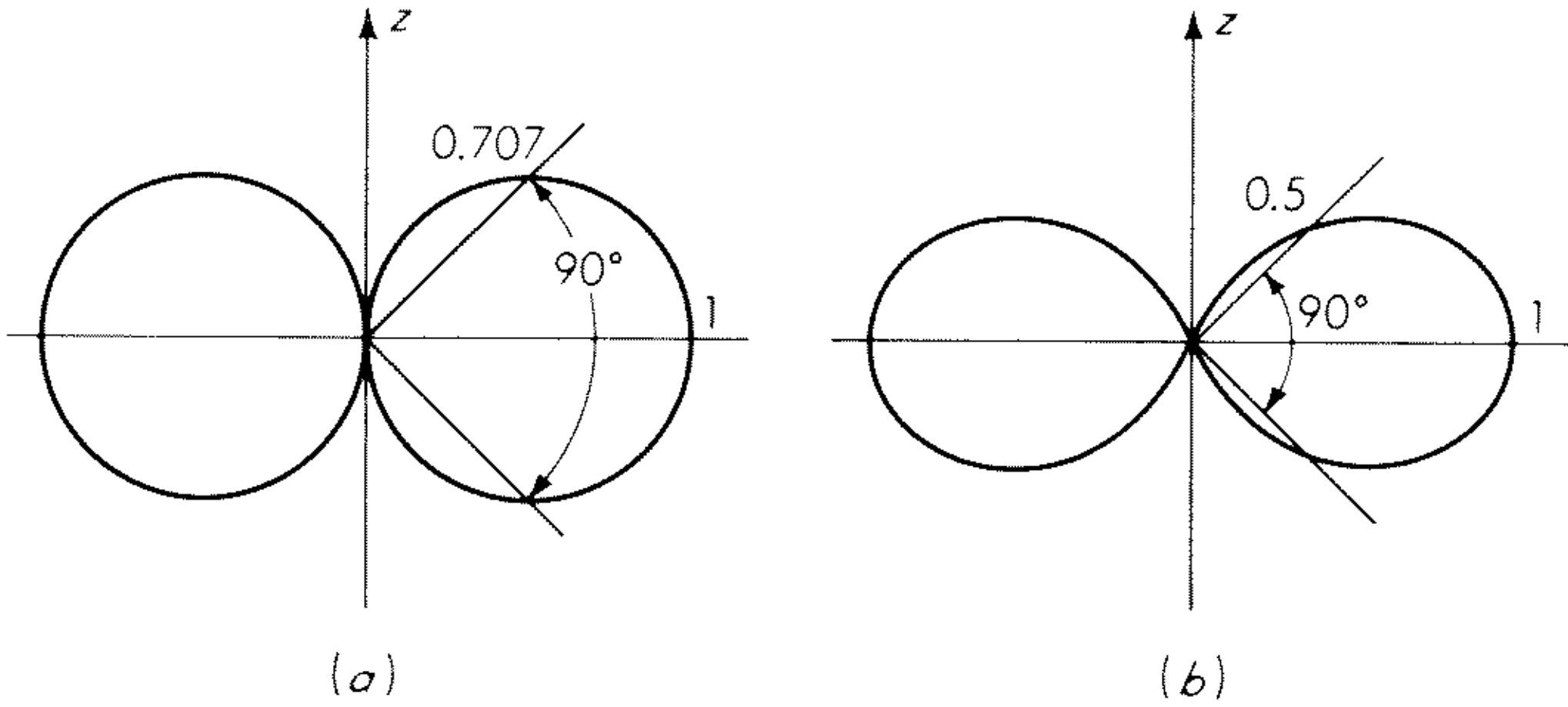


Fig. 2.2 Radiation patterns from a unit source. (a) Field strength pattern; (b) power radiation pattern.

independent of ϕ in the present case and may be visualized as the surfaces formed by revolving the given plots about the axis of the unit current source (z axis).

The radiation patterns of most antennas exhibit a main lobe and several minor lobes of smaller amplitude. The main lobe is described by giving its angular width in the two principal planes (we are assuming a linearly polarized field) that contain the electric field vector and magnetic field vector, respectively. Usually the beam width specified is that between the half-power points, although sometimes the full angular width of the main lobe between adjacent nulls is given. For the unit current source the half-power beam width in the E plane is 90° (see Fig. 2.2), while in the H plane the patterns are rotationally uniform.

Directivity

The directivity of an antenna is a measure of the directional properties or relative concentration of radiated power in different directions. Usually the directivity is specified with reference to an isotropic radiator. If an antenna radiated a total power P , the power density per unit solid angle would be $P/4\pi$ if the antenna radiated isotropically. In general, the antenna does not radiate isotropically. Its directivity in a given direction θ, ϕ is given by $D(\theta, \phi)$, where

$$D(\theta, \phi) = 4\pi \frac{\text{power radiated per unit solid angle in direction } \theta, \phi}{\text{total radiated power}} \quad (2.8)$$

and gives the power density in that direction relative to that which an isotropic radiator would produce.

The maximum directivity of an antenna (for brevity often called simply the

directivity) occurs in the direction of the main-lobe maximum and is a measure of the ability of an antenna to concentrate the radiated power in a given direction. A rough estimate of the maximum directivity of an antenna producing a single main lobe with narrow beam widths can be obtained by dividing 4π by the solid angle subtended by the main lobe between half-power points. It is apparent that a highly directive antenna will have a very sharp (narrow beam widths) main lobe.

For the unit current source the directivity is given by

$$D(\theta, \phi) = 4\pi \frac{(\xi_0 k_0^2 \sin^2 \theta)/32\pi^2}{\xi_0 k_0^2/12\pi} = 1.5 \sin^2 \theta \quad (2.9)$$

upon using (2.6), (2.7), and (2.8). The maximum directivity is 1.5.

Gain

The gain $G(\theta, \phi)$ of an antenna differs from the directivity by a factor which takes into account the efficiency of the antenna. Since all antennas have some dissipative loss, not all of the input power is radiated. The gain of an antenna is defined by

$$G(\theta, \phi) = 4\pi \frac{\text{power density per unit solid angle in the direction } \theta, \phi}{\text{total input power to antenna}} \quad (2.10)$$

and is less than the directivity by a factor equal to the efficiency. The antenna gain function $G(\theta, \phi)$ is obviously a more useful parameter than the directivity in describing the overall performance of a practical antenna. Both gain and directivity may be referred to any standard antenna such as a half-wave dipole antenna instead of the isotropic radiator used above.

Polarization

The unit current source produces a linearly polarized field; i.e., the electric field vector is always in the $\hat{\theta}$ direction. A more complicated antenna may radiate a field with components of electric field in both the $\hat{\theta}$ and $\hat{\phi}$ directions. If E_θ and E_ϕ are in phase everywhere, the electric field is linearly polarized, although the direction of polarization (direction of total \mathbf{E}) may vary with the direction in space as specified by the angles θ and ϕ . If E_θ and E_ϕ differ in phase, the direction of the resultant electric field at a given point in space will change periodically at an average angular rate ω . The tip of the vector representing the total electric field will trace out an ellipse in general, and the field is therefore said to be elliptically polarized. The polarization will generally also be different in different directions in space.

To illustrate how an elliptically polarized field arises, let

$$E_\theta = E_1 \cos \omega t \quad E_\phi = E_2 \cos (\omega t + \psi)$$

at a given point in space and where E_1 and E_2 are real constants. The curve traced out by the resultant electric field vector may be determined by eliminating the time t . We have

$$\frac{E_\phi}{E_2} - \cos \omega t \cos \psi = -\sin \omega t \sin \psi = \frac{E_\phi}{E_2} - \frac{E_\theta}{E_1} \cos \psi$$

and hence
$$\left(\frac{E_\phi}{E_2} - \frac{E_\theta}{E_1} \cos \psi \right)^2 = \sin^2 \omega t \sin^2 \psi = \left[1 - \left(\frac{E_\theta}{E_1} \right)^2 \right] \sin^2 \psi$$

After simplification we obtain

$$\left(\frac{E_\theta}{E_1} \right)^2 + \left(\frac{E_\phi}{E_2} \right)^2 - 2 \frac{E_\theta E_\phi}{E_1 E_2} \cos \psi = \sin^2 \psi \quad (2.11)$$

which is the equation of an ellipse. In the special case when $E_1 = E_2$ and $\psi = \pm\pi/2$ the field becomes circularly polarized. If $\psi = \pm\pi$, the ellipse degenerates to a straight line, which shows that the field is then linearly polarized. Further aspects of the polarization property of antennas will be dealt with later, so additional details will not be given in this section.

Antenna Impedance

An antenna must be coupled to a transmitter by means of a transmission line or waveguide in order to be excited and produce radiation. The antenna input impedance presented to the feed line is consequently an important parameter to know in order to design efficient coupling networks that will give maximum power transfer. The antenna input impedance will generally have both a resistive and a reactive part. The reactive part arises from the near-zone induction fields, because these fields give rise to a reactive energy storage in the region surrounding the antenna. The resistive part of the input impedance has contributions from all physical mechanisms that give rise to a loss of energy from the antenna. The radiated power is the desired loss mechanism, but other losses are also unavoidably present. In particular, there will always be ohmic losses present because of the finite conductivity of the antenna structure. When an antenna is operated near a lossy ground, additional losses arise from the currents that are induced in the ground. It is very desirable to have the resistance arising from radiated power (radiation resistance) be much greater than that arising from all other loss mechanisms. The radiation resistance of an antenna is defined as the equivalent resistance that would dissipate an amount of power equal to the total radiated power when the current through the resistance is equal to the current at the antenna input terminals. We shall illustrate the evaluation of radiation resistance by considering a short linear current radiator.

An antenna that approximates the unit current source as a radiator may be constructed by capacitive top loading of a short dipole antenna as illustrated

in Fig. 2.3. The ends of the dipole illustrated are loaded by capacitive disks in order to obtain essentially a uniform current along the antenna. If the maximum dimensions of the antenna are small compared to the wavelength, the

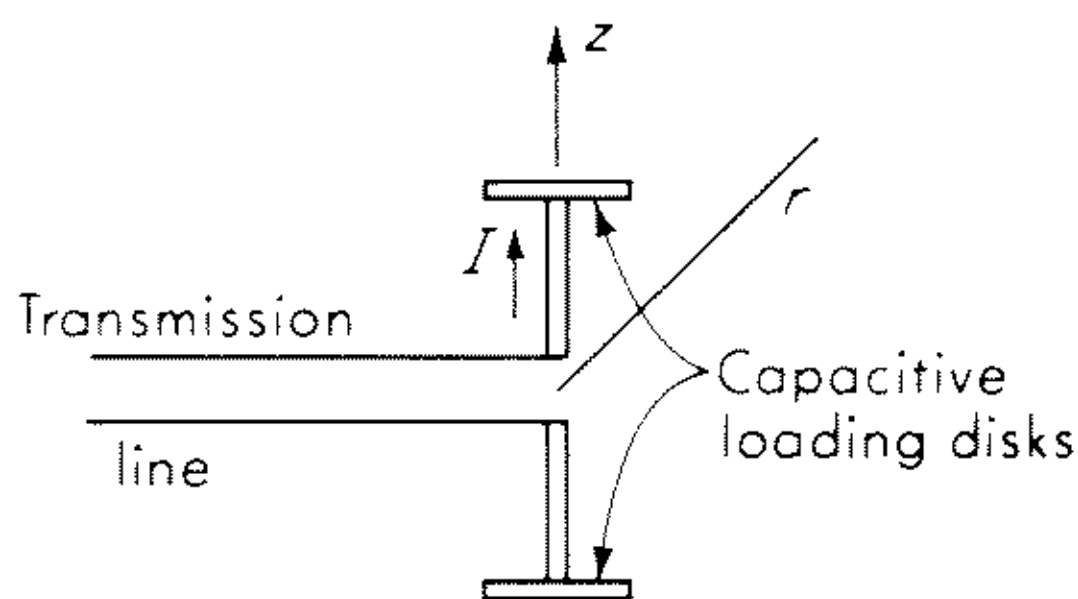


Fig. 2.3 A short dipole with capacitive loading.

antenna will radiate as a unit current source. For an antenna length l and a total current I the radiated field will be a factor Il greater than that produced by the unit current source. The total radiated power is thus given by $P = k_0^2 \zeta_0 |I|^2 l^2 / 12\pi$. The radiation resistance R_0 is

$$R_0 = \frac{P}{\frac{1}{2} |I|^2} = \frac{k_0^2 \zeta_0 l^2}{6\pi} = 80\pi^2 \left(\frac{l}{\lambda_0} \right)^2 \quad (2.12)$$

upon replacing ζ_0 by 120π ohms. As a typical example, if $l = 0.01\lambda_0$, the radiation resistance is found to be 0.08 ohms. This particular example shows that a short dipole antenna would be a very inefficient radiator because of the low value of radiation resistance. Ohmic losses and ground losses would normally contribute a much greater resistive component to the input impedance. A short dipole antenna also has a large capacitive reactance, which further compounds the difficulty of efficiently feeding power to the antenna.

The above discussion should have made it apparent that the evaluation of antenna input impedance is an important problem. It will be dealt with briefly in a later section and in considerable detail in later chapters.

2.4 Magnetic Dipole Radiation

Figure 2.4 illustrates a small circular current loop with a diameter much smaller than a wavelength. A current source of this kind may be regarded as a localized magnetic dipole of moment $\mathbf{M} = SI\hat{\mathbf{z}}$, where S is the area of the loop and I is the current. The radiated field is readily found by using the magnetic hertzian potential Π_m (see Probs. 1.5 and 1.6). The equations to be solved are

$$\nabla^2 \Pi_m + k_0^2 \Pi_m = -\mathbf{M} = -SI\hat{\mathbf{z}}\delta(\mathbf{r}) \quad (2.13)$$

$$\mathbf{E} = -j\omega\mu_0 \nabla \times \Pi_m \quad (2.14a)$$

$$\mathbf{H} = (k_0^2 + \nabla \nabla \cdot) \Pi_m \quad (2.14b)$$

Comparing these equations with the corresponding equations for electric dipole radiation shows that the two problems are duals. For magnetic dipole radiation the roles of the electric and magnetic fields are interchanged. The solution for Π_m is

$$\Pi_m = SI\hat{\mathbf{z}} \frac{e^{-jk_0 r}}{4\pi r} \quad (2.15)$$

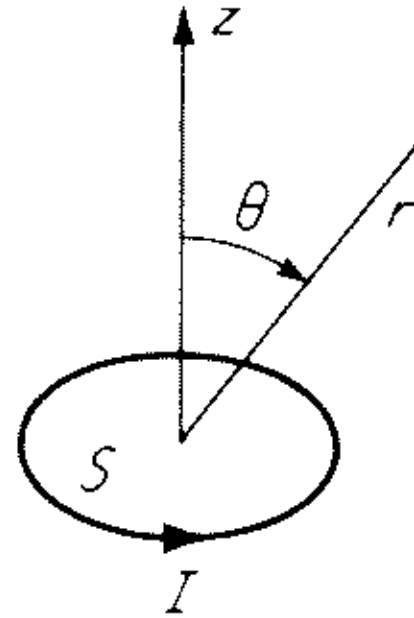


Fig. 2.4 The small current loop, or magnetic dipole.

as comparison with (2.1) and (2.3) shows. A straightforward analysis shows that the radiated field is given by

$$\mathbf{E} = \frac{-jk_0\zeta_0 SI}{4\pi} \left(\frac{jk_0}{r} + \frac{1}{r^2} \right) e^{-jk_0 r} \sin \theta \hat{\boldsymbol{\theta}} \quad (2.16a)$$

$$\mathbf{H} = \frac{SI}{2\pi} \left(\frac{jk_0}{r^2} + \frac{1}{r^3} \right) e^{-jk_0 r} \cos \theta \hat{\mathbf{r}} - \frac{SI}{4} \left(\frac{k_0^2}{r} - \frac{jk_0}{r^2} - \frac{1}{r^3} \right) e^{-jk_0 r} \sin \theta \hat{\boldsymbol{\theta}} \quad (2.16b)$$

In view of the dual nature of the solution it is apparent that the radiation patterns for electric and magnetic dipoles are identical. The total power radiated by the magnetic dipole is readily evaluated and is given by

$$P = \frac{k_0^4 \zeta_0 (S|I|)^2}{12\pi} \quad (2.17)$$

From this expression the radiation resistance of the small loop antenna is found to be

$$R_0 = \frac{2P}{|I|^2} = 320\pi^4 \frac{S^2}{\lambda_0^4} \quad (2.18)$$

Exercise 2.2 Carry out the detailed analysis leading to (2.16) and (2.17).

2.5 Radiation from Arbitrary Current Distributions

The electromagnetic field radiated by an arbitrary current distribution may be found by means of the superposition principle. An arbitrary current distribution can be regarded as a suitable weighted distribution of unit current

sources, and the vector potential that results is the linear sum of all the contributions from each current element. For a volume distribution of current as illustrated in Fig. 2.5 the vector potential is given by

$$\mathbf{A}(\mathbf{r}) = \frac{\mu_0}{4\pi} \int_V \mathbf{J}(\mathbf{r}') \frac{e^{-jk_0 R}}{4\pi R} dV' \quad (2.19)$$

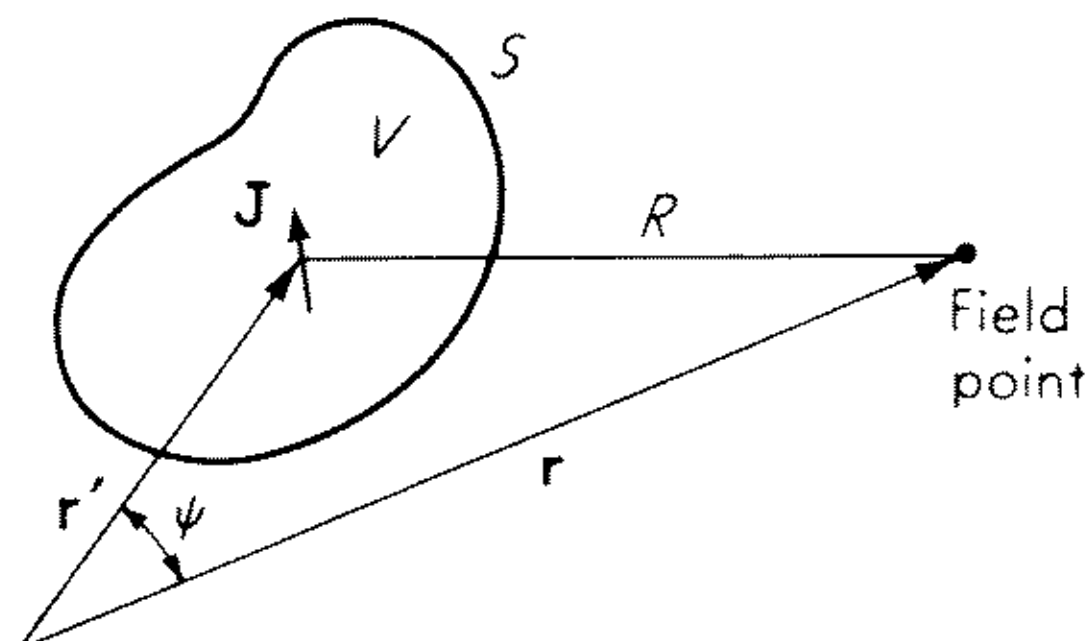


Fig. 2.5 An arbitrary current source.

where $R = |\mathbf{r} - \mathbf{r}'|$. This result is obtained by using (2.4) for the vector potential for a unit current element and integrating over the total current distribution.

From the vector potential we can obtain the magnetic and electric fields by using (1.60). Thus we find that the magnetic field is given by

$$\mathbf{H}(\mathbf{r}) = -\int_V \mathbf{J}(\mathbf{r}') \times \nabla \frac{e^{-jk_0 R}}{4\pi R} dV' \quad (2.20)$$

where the curl operator has been brought inside the integral sign. The electric field is given by

$$\begin{aligned} \mathbf{E}(\mathbf{r}) &= \frac{1}{j\omega\epsilon_0\mu_0} \nabla \times \nabla \times \mathbf{A} = \frac{1}{j\omega\epsilon_0} \nabla \times \mathbf{H} \\ &= -\frac{1}{j\omega\epsilon_0} \int_V \nabla \times \left[\mathbf{J} \times \nabla \frac{e^{-jk_0 R}}{4\pi R} \right] dV' \end{aligned}$$

If we use the vector expansion $\nabla \times (\mathbf{A} \times \mathbf{B}) = \mathbf{A}\nabla \cdot \mathbf{B} - \mathbf{B}\nabla \cdot \mathbf{A} + (\mathbf{B} \cdot \nabla)\mathbf{A} - (\mathbf{A} \cdot \nabla)\mathbf{B}$ and note that $\mathbf{J}(\mathbf{r}')$ is not a function of \mathbf{r} , we find that

$$\mathbf{E}(\mathbf{r}) = \frac{1}{j\omega\epsilon_0} \int_V \left[\mathbf{J}(\mathbf{r}') k_0^2 \frac{e^{-jk_0 R}}{4\pi R} + \mathbf{J}(\mathbf{r}') \cdot \nabla \nabla \frac{e^{-jk_0 R}}{4\pi R} \right] dV' \quad (2.21)$$

where the term $\nabla^2(e^{-jk_0 R}/4\pi R)$ has been replaced by $-k_0^2(e^{-jk_0 R}/4\pi R)$, since this latter function is a solution of the homogeneous scalar Helmholtz equation for $R \neq 0$. The solution (2.21) holds only in the region external to the volume containing the current source \mathbf{J} , since R is restricted to be nonzero.

In the general case the evaluation of the integrals in (2.20) and (2.21) is difficult to carry out. In radiation problems three regions of physical space are usually distinguished. The first region is the near-zone field region for which no general approximations may be made in the evaluation of (2.20) and (2.21)

for the fields. The second region, called the Fresnel region, is the region of physical space between the near-zone region and the far-zone or Fraunhofer region. The Fresnel and Fraunhofer regions are characterized by the type of approximations that may be made in the integrands in (2.20) and (2.21). Since the far-zone region is the least stringent, we shall consider it in detail first.

The far-zone region corresponds to the region in which the radiation field predominates and hence is the region of most interest in connection with antennas. The far-zone region is characterized by the conditions that r is much greater than the maximum value of r' and also much greater than the free-space wavelength λ_0 , that is, $k_0 r \gg 1$. Using the binomial expansion, we have

$$R = |\mathbf{r} - \mathbf{r}'| = (r^2 + r'^2 - 2\mathbf{r} \cdot \mathbf{r}')^{1/2} \approx r - \frac{\mathbf{r} \cdot \mathbf{r}'}{r} = r - \hat{\mathbf{r}} \cdot \mathbf{r}' = r - r' \cos \psi$$

where ψ is the angle between \mathbf{r} and \mathbf{r}' as in Fig. 2.5. We now approximate

$$\frac{1}{R} e^{-jk_0 R} \quad \text{by} \quad \frac{1}{r} \exp[-jk_0(r - \hat{\mathbf{r}} \cdot \mathbf{r}')]]$$

and then find that by including terms of order $1/r$ only

$$\begin{aligned} \nabla \frac{\exp[-jk_0(r - \hat{\mathbf{r}} \cdot \mathbf{r}')] }{r} \\ = \left[\hat{\mathbf{r}} \left\{ \frac{-jk_0}{r} - \frac{1}{r^2} \right\} - \frac{jk_0 r'}{r^2} \sin \psi \hat{\psi} \right] \exp[-jk_0(r - \hat{\mathbf{r}} \cdot \mathbf{r}')] \\ \approx \frac{-jk_0}{r} \exp(-jk_0 r) \exp(jk_0 \hat{\mathbf{r}} \cdot \mathbf{r}') \quad (2.22) \end{aligned}$$

where $\hat{\psi}$ is a unit vector in the direction of ψ increasing. When we use this result in (2.20), we obtain

$$\mathbf{H} = \frac{jk_0}{4\pi r} e^{-jk_0 r} \int_V \mathbf{J}(\mathbf{r}') \times \hat{\mathbf{r}} \exp(jk_0 \hat{\mathbf{r}} \cdot \mathbf{r}') dV' \quad (2.23a)$$

for the far-zone magnetic field. To the same order of approximation it may be verified that for the far-zone field (2.21) gives

$$\begin{aligned} \mathbf{E} = -\zeta_0 \hat{\mathbf{r}} \times \mathbf{H} &= \frac{jk_0 \zeta_0 e^{-jk_0 r}}{4\pi r} \int_V [(\hat{\mathbf{r}} \cdot \mathbf{J}) \hat{\mathbf{r}} - \mathbf{J}] \exp(jk_0 \hat{\mathbf{r}} \cdot \mathbf{r}') dV' \\ &= -\frac{jk_0 \zeta_0 e^{-jk_0 r}}{4\pi r} \int_V (J_\theta \hat{\theta} + J_\phi \hat{\phi}) \exp(jk_0 \hat{\mathbf{r}} \cdot \mathbf{r}') dV' \quad (2.23b) \end{aligned}$$

Thus it is seen that in the far-zone field the relation between \mathbf{E} and \mathbf{H} is that which is characteristic of spherical TEM waves. In the evaluation of (2.23a,b) it is useful to be able to transform the components in a spherical coordinate

frame to a rectangular coordinate frame, and vice versa. For this purpose the following relations are useful:

$$\begin{aligned}
 \hat{\mathbf{x}} &= \hat{\mathbf{r}} \sin \theta \cos \phi + \hat{\boldsymbol{\theta}} \cos \theta \cos \phi - \hat{\boldsymbol{\phi}} \sin \phi \\
 \hat{\mathbf{y}} &= \hat{\mathbf{r}} \sin \theta \sin \phi + \hat{\boldsymbol{\theta}} \cos \theta \sin \phi + \hat{\boldsymbol{\phi}} \cos \phi \\
 \hat{\mathbf{z}} &= \hat{\mathbf{r}} \cos \theta - \hat{\boldsymbol{\theta}} \sin \theta \\
 \hat{\mathbf{r}} &= \hat{\mathbf{x}} \sin \theta \cos \phi + \hat{\mathbf{y}} \sin \theta \sin \phi + \hat{\mathbf{z}} \cos \theta \\
 \hat{\boldsymbol{\theta}} &= \hat{\mathbf{x}} \cos \theta \cos \phi + \hat{\mathbf{y}} \cos \theta \sin \phi - \hat{\mathbf{z}} \sin \theta \\
 \hat{\boldsymbol{\phi}} &= -\hat{\mathbf{x}} \sin \phi + \hat{\mathbf{y}} \cos \phi
 \end{aligned} \tag{2.24}$$

We now return to a consideration of the Fresnel region. The usual approximations that are considered in defining the Fresnel region are $r \gg r'$, $k_0 r \gg 1$, but with r , r' , and λ_0 such that terms in r'^2 must be retained in the phase term in the exponential. We have

$$R = r - \hat{\mathbf{r}} \cdot \mathbf{r}' + \frac{1}{2r} [r'^2 - (\hat{\mathbf{r}} \cdot \mathbf{r}')^2]$$

to terms of order $(r'/r)^2$. Thus in the Fresnel region the vector potential is given by

$$\mathbf{A}(\mathbf{r}) = \frac{\mu_0 e^{-jk_0 r}}{4\pi r} \int_V \mathbf{J}(\mathbf{r}') \exp \left\{ jk_0 \left[\hat{\mathbf{r}} \cdot \mathbf{r}' + \frac{(\hat{\mathbf{r}} \cdot \mathbf{r}')^2}{2r} - \frac{r'^2}{2r} \right] \right\} dV' \tag{2.25}$$

In the evaluation of the field from \mathbf{A} , terms with amplitudes decreasing faster than $1/r$ are neglected. Thus the essential difference between the approximations involved in the Fraunhofer and Fresnel regions is only in the phase term in the exponential. There is no clearly marked boundary between the three regions, i.e., the near-zone, Fresnel, and far-zone regions, since the range of r in which the approximations outlined above may be made is dependent on the current distribution $\mathbf{J}(\mathbf{r}')$. In the case of radiation from a plane aperture with a maximum linear dimension L the far-zone or Fraunhofer region is commonly considered to begin for r somewhere between L^2/λ_0 and $2L^2/\lambda_0$ (see Silver¹⁰). The significance of this criterion may be seen by referring to the exponent $k_0[\hat{\mathbf{r}} \cdot \mathbf{r}' + (\hat{\mathbf{r}} \cdot \mathbf{r}')^2/2r - r'^2/2r]$ in (2.25). If the maximum value of r' is L , and r is equal to $2L^2/\lambda_0$, the two last terms in the exponent will correspond to a phase angle not exceeding $kr'^2/2r = k_0 L^2 \lambda_0 / 4L^2 = \pi/2$. Thus the phase angle of the various contributions to the field from the current distribution will be given by the term $k_0 \hat{\mathbf{r}} \cdot \mathbf{r}'$ alone with a maximum error not exceeding $\pi/2$. The additional terms will not introduce a phase angle large enough to cause the various contributions to add up to give a significantly different field intensity as long as r is greater than the specified minimum value. In order to have a significant Fresnel region, the term $k_0 r'^2/r$ should assume values as large as several π radians. Thus the condition $1 \ll (r/r') \ll (r'/\lambda_0)$ holds in the Fresnel zone. For a current distribution that is small compared with the wavelength it is possible to distinguish only two zones, the near- and far-field zones.

When measurements to determine the radiation pattern of an antenna are made, it is important that these measurements be taken in the far-zone, or Fraunhofer, region in order that they will be truly representative of the radiation pattern. In the Fresnel region the field amplitude will vary with direction and distance from the source in a manner quite different from the behavior in the far-zone region.

2.6 Free Space Dyadic Green's Functions

The evaluation of the fields produced by a given source distribution may be systematized by the use of dyadic Green's functions. An introduction to this topic is presented below. (For a more detailed discussion see Morse and Feshbach¹¹.)

To illustrate certain basic properties of a dyadic Green's function consider the solution (2.19) for the vector potential. If we note that the scalar product of the unit dyadic $\mathbf{I} = \hat{\mathbf{x}}\hat{\mathbf{x}} + \hat{\mathbf{y}}\hat{\mathbf{y}} + \hat{\mathbf{z}}\hat{\mathbf{z}}$ with a vector source \mathbf{J} gives $\mathbf{I} \cdot \mathbf{J} = \mathbf{J}$, we see that the solution for the vector potential can be written in the form

$$\mathbf{A}(\mathbf{r}) = \mu_0 \int_V \frac{e^{-jk_0|\mathbf{r}-\mathbf{r}'|}}{4\pi|\mathbf{r}-\mathbf{r}'|} \mathbf{I} \cdot \mathbf{J}(\mathbf{r}') dV' \quad (2.26)$$

The quantity

$$\mathbf{G}(\mathbf{r}|\mathbf{r}') = \frac{e^{-jk_0|\mathbf{r}-\mathbf{r}'|}}{4\pi|\mathbf{r}-\mathbf{r}'|} \mathbf{I} \quad (2.27)$$

is the free space dyadic Green's function for the vector potential. If the solution for \mathbf{A} is substituted into the inhomogeneous Helmholtz equation and the order of integration and differentiation interchanged, we obtain

$$\int_V (\nabla^2 + k_0^2) \mathbf{G}(\mathbf{r}|\mathbf{r}') \cdot \mathbf{J}(\mathbf{r}') dV' = -\mathbf{J}(\mathbf{r}) \quad (2.28)$$

If this equation is to be valid, it is necessary that \mathbf{G} be a solution of

$$(\nabla^2 + k_0^2) \mathbf{G}(\mathbf{r}|\mathbf{r}') = -\mathbf{I} \delta(\mathbf{r} - \mathbf{r}') \quad (2.29)$$

since then we obtain

$$\int_V \delta(\mathbf{r} - \mathbf{r}') \mathbf{I} \cdot \mathbf{J}(\mathbf{r}') dV' = \mathbf{J}(\mathbf{r})$$

The following two properties of the dyadic Green's function are thus apparent:

1. It is a linear dyadic operator that, when scalar-multiplied by a vector current source element, gives the required vector field from that source element.
2. It satisfies an equation of the same form as that for the field to be determined but with a source term $\mathbf{I} \delta(\mathbf{r} - \mathbf{r}')$. When the dyadic Green's function is known, the field from an arbitrary source distribution may be found by means of a superposition integral.

With the above introductory remarks we shall now consider the free space dyadic Green's function for the electric field. The electric field is a solution of the equation

$$(\nabla \times \nabla \times - k_0^2) \mathbf{E}(\mathbf{r}) = -j\omega\mu_0 \mathbf{J}(\mathbf{r}) \quad (2.30a)$$

The dyadic Green's function $\mathbf{G}(\mathbf{r}|\mathbf{r}')$ is a solution of

$$(\nabla \times \nabla \times - k_0^2) \mathbf{G}(\mathbf{r}|\mathbf{r}') = \mathbf{I} \delta(\mathbf{r} - \mathbf{r}') \quad (2.30b)$$

and is so chosen as to satisfy the radiation condition at infinity. To find the solution for the free space dyadic Green's function we shall use the method introduced by Levine and Schwinger.¹² The divergence of (2.30b) gives

$$-k_0^2 \nabla \cdot \mathbf{G}(\mathbf{r}|\mathbf{r}') = \nabla \cdot \mathbf{I} \delta(\mathbf{r} - \mathbf{r}') = \nabla \delta(\mathbf{r} - \mathbf{r}')$$

since the divergence of the curl of any vector is zero. If we also take the gradient of this last result, we obtain

$$\nabla \nabla \cdot \mathbf{G}(\mathbf{r}|\mathbf{r}') = -\frac{1}{k_0^2} \nabla \nabla \delta(\mathbf{r} - \mathbf{r}') \quad (2.31)$$

which we shall make use of later. We may rewrite (2.30b) in the form

$$(\nabla^2 + k_0^2) \mathbf{G}(\mathbf{r}|\mathbf{r}') - \nabla \nabla \cdot \mathbf{G}(\mathbf{r}|\mathbf{r}') = -\mathbf{I} \delta(\mathbf{r} - \mathbf{r}')$$

by using the identity $\nabla \times \nabla \times \mathbf{F} = \nabla \nabla \cdot \mathbf{F} - \nabla^2 \mathbf{F}$. If we now employ (2.31), we see that

$$(\nabla^2 + k_0^2) \mathbf{G}(\mathbf{r}|\mathbf{r}') = -\left(\mathbf{I} + \frac{\nabla \nabla}{k_0^2}\right) \delta(\mathbf{r} - \mathbf{r}') \quad (2.32)$$

which shows that \mathbf{G} can be obtained from a scalar Green's function $G_0(\mathbf{r}|\mathbf{r}')$ that satisfies the equation

$$(\nabla^2 + k_0^2) G_0(\mathbf{r}|\mathbf{r}') = -\delta(\mathbf{r} - \mathbf{r}') \quad (2.33)$$

by operating on G_0 by the dyadic operator $\mathbf{I} + \nabla \nabla / k_0^2$, since this operator and the $\nabla^2 + k_0^2$ operator commute, that is,

$$\left(\mathbf{I} + \frac{\nabla \nabla}{k_0^2}\right) (\nabla^2 + k_0^2) G_0 = (\nabla^2 + k_0^2) \left(\mathbf{I} + \frac{\nabla \nabla}{k_0^2}\right) G_0 = -\left(\mathbf{I} + \frac{\nabla \nabla}{k_0^2}\right) \delta(\mathbf{r} - \mathbf{r}')$$

The solution for the scalar Green's function is

$$G_0(\mathbf{r}|\mathbf{r}') = \frac{e^{-jk_0|\mathbf{r}-\mathbf{r}'|}}{4\pi|\mathbf{r}-\mathbf{r}'|} \quad (2.34)$$

Hence the required dyadic Green's function for the electric field is given by

$$\mathbf{G}(\mathbf{r}|\mathbf{r}') = \left(\mathbf{I} + \frac{\nabla \nabla}{k_0^2}\right) \frac{e^{-jk_0|\mathbf{r}-\mathbf{r}'|}}{4\pi|\mathbf{r}-\mathbf{r}'|} \quad (2.35)$$

In terms of this Green's function the electric field produced by an arbitrary current distribution is given by†

$$\mathbf{E}(\mathbf{r}) = -j\omega\mu_0 \int_V \mathbf{J}(\mathbf{r}') \cdot \mathbf{G}(\mathbf{r}'|\mathbf{r}) dV' \quad \mathbf{r} \text{ not in } V \quad (2.36)$$

The free space dyadic Green's function satisfies the reciprocity relationship

$$\mathbf{G}(\mathbf{r}|\mathbf{r}') = \mathbf{G}_t(\mathbf{r}'|\mathbf{r}) \quad (2.37a)$$

and the symmetry property

$$\mathbf{G}(\mathbf{r}|\mathbf{r}') = \mathbf{G}_t(\mathbf{r}|\mathbf{r}') \quad (2.37b)$$

as may be seen by examining the specific form of \mathbf{G} as given by (2.35). The modified dyadic Green's function that would be used in the presence of finite boundaries will satisfy the reciprocity relationship (2.37a) in a reciprocal medium, but, in general, it does not satisfy the symmetry property (2.37b) (see for example Collin¹³).

For a two-dimensional source (an infinite line source) the scalar Green's function is a solution of

$$(\nabla^2 + k_0^2)G_0(\mathbf{r}|\mathbf{r}') = -\delta(x - x')\delta(y - y') \quad (2.38)$$

The solution for G_0 is given by

$$G_0(x, y|x', y') = -\frac{j}{4} H_0^2[k_0 \sqrt{(x - x')^2 + (y - y')^2}] \quad (2.39)$$

where H_0^2 is the cylindrical Hankel function of the second kind and order zero. The corresponding two-dimensional dyadic Green's function is a solution of

$$(\nabla \times \nabla \times - k_0^2)\mathbf{G} = \mathbf{I}_t \delta(x - x')\delta(y - y') \quad (2.40)$$

and is given explicitly by

$$\mathbf{G}(x, y|x', y') = \left(\mathbf{I}_t + \frac{\nabla \nabla}{k_0^2} \right) G_0(x, y|x', y') \quad (2.41)$$

where \mathbf{I}_t is the two-dimensional unit dyadic $\hat{\mathbf{x}}\hat{\mathbf{x}} + \hat{\mathbf{y}}\hat{\mathbf{y}}$.

2.7 Radiation from Thin Wire Antennas

Since an antenna must be of the order of a wavelength in size before it will radiate efficiently, practical antennas at the longer wavelengths (50 m or more) are necessarily of simple form for structural reasons. Long straight wires of small cross section are commonly used. It has been verified both theoretically

†To obtain the correct field inside the source region a term $-(1/3k_0^2)\delta(\mathbf{r} - \mathbf{r}')$ must be added to the Green's dyadic and the principal value of (2.36) taken, or alternatively $\nabla \nabla$ should be replaced by $-\nabla \nabla'$.³²

and experimentally that the current distribution on long thin wire antennas may be approximated by a simple sinusoidal standing wave. Much of the early literature on antennas deals with the thin wire antenna. Some of the relevant early papers are those by Abraham,¹⁴ Pocklington,¹⁵ and Bechmann.¹⁶ For a comprehensive analysis the book by King should be consulted.⁸ We shall only be concerned with the evaluation of the far-zone or radiation field from long thin wire antennas for the purpose of illustrating the application of the superposition principle in calculating radiation fields from known current distributions

Figure 2.6 illustrates a thin long wire antenna fed at the center by a transmission line. The antenna cross-sectional dimensions are assumed to be very small compared with the wavelength, so that we may assume the current to be

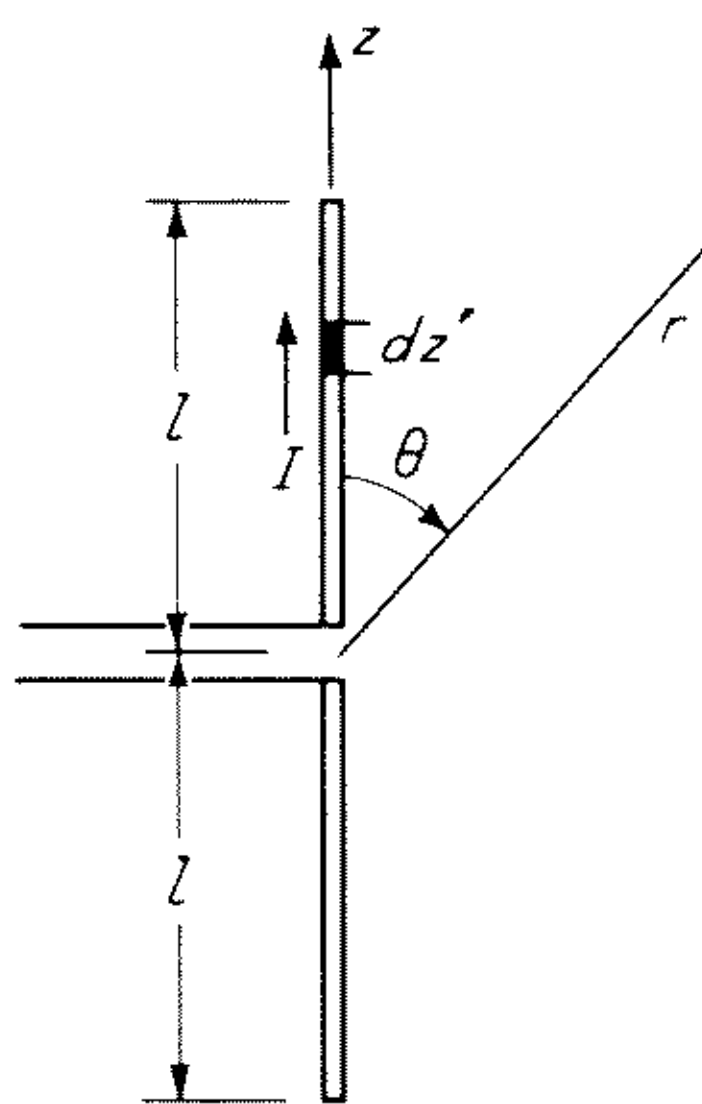


Fig. 2.6 A long thin wire antenna.

concentrated at the center. We shall evaluate the radiation field and radiation resistance under the assumption that the current distribution is sinusoidal and of the form $I(z) = I_0 \sin k_0(l - |z|)$, where $2l$ is the total antenna length. The far-zone field may be found by summing up the contribution from each element of current $I_0 \sin k_0(l - |z|) dz$ according to expression (2.23b). Thus we have

$$\begin{aligned} \mathbf{E} &= \frac{jk_0\zeta_0}{4\pi r} e^{-jk_0r} \int_{-l}^l I_0 \sin k_0(l - |z'|) (\hat{\mathbf{r}} \cdot \hat{\mathbf{z}} \hat{\mathbf{r}} - \hat{\mathbf{z}}) \exp(jk_0\hat{\mathbf{r}} \cdot \mathbf{r}') dz' \\ &= \frac{jk_0\zeta_0}{4\pi r} e^{-jk_0r} \int_{-l}^l I_0 \sin k_0(l - |z'|) \exp(jk_0z' \cos \theta) \hat{\theta} \sin \theta dz' \\ &= \frac{j\zeta_0 I_0}{2\pi r} e^{-jk_0r} \left[\frac{\cos(k_0l \cos \theta) - \cos k_0l}{\sin \theta} \right] \hat{\theta} \quad (2.42) \end{aligned}$$

The magnetic intensity H_ϕ is given by E_θ/ζ_0 .

The radiation pattern is independent of the angle ϕ because of the rotational symmetry of the antenna. As a function of θ the pattern exhibits a single

major lobe for $2l = \lambda_0/2$ and $2l = \lambda_0$. For greater lengths several lobes of unequal amplitude occur depending on the antenna length. As the antenna length is increased the lobes become sharper (narrower beam width). Typical patterns that are obtained for several different values of $2l/\lambda_0$ are illustrated in Fig. 2.7.

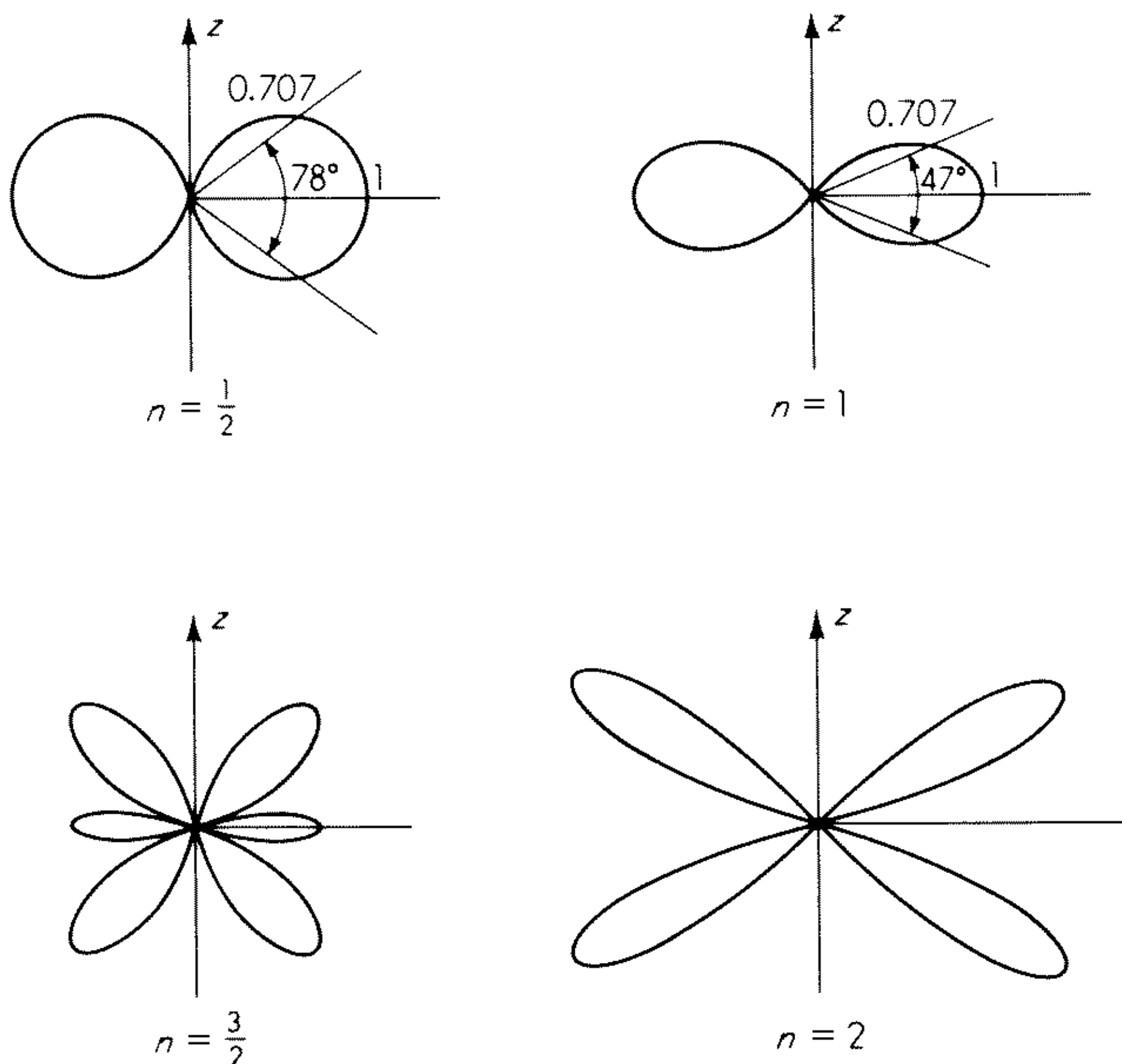


Fig. 2.7 Radiation patterns for thin center-fed long wire antennas for several values of $n = 2l/\lambda_0$.

An interesting feature of the expression (2.42) for the far-zone electric field from a line source is that it may be regarded as a Fourier transform of a finite-length current distribution. If we have a current distribution

$$I(z) = \begin{cases} F(z) & |z| \leq l \\ 0 & |z| > l \end{cases}$$

the corresponding far-zone electric field is given by

$$E_\theta = \frac{j\zeta_0 k_0 \sin \theta}{4\pi r} e^{-jk_0 r} f(k_0 \cos \theta) \quad (2.43)$$

where

$$f(k_0 \cos \theta) = \int_{-l}^l F(z') e^{jz' k_0 \cos \theta} dz' \quad (2.44)$$

The inverse Fourier transform relation gives

$$F(z') = \frac{1}{2\pi} \int_{-\infty}^{\infty} f(k_z) e^{-jk_z z'} dk_z \quad (2.45)$$

where we have put $k_0 \cos \theta = k_z$. The usefulness of this Fourier transform relationship stems from the possibility of applying well-known results about Fourier transform pairs to the problem of designing or synthesizing a line source distribution $F(z')$ to yield a desired radiation-pattern function $f(k_0 \cos \theta)$. We shall have a good deal more to say about Fourier transform relationships of the above type in the next chapter and shall, therefore, postpone the detailed discussion until later.

Radiation Resistance

The radiation resistance of a long wire antenna may be found by evaluating the total radiated power passing through a large spherical surface surrounding the antenna. For a sinusoidal standing-wave current distribution for which the electric field is given by (2.42) the total radiated power is

$$\begin{aligned} P &= \frac{1}{2\zeta_0} \int_0^{2\pi} \int_0^\pi |E_\theta|^2 r^2 \sin \theta d\theta d\phi \\ &= \frac{\zeta_0 I_0^2}{4\pi} \int_0^\pi \frac{[\cos(k_0 l \cos \theta) - \cos k_0 l]^2}{\sin \theta} d\theta \end{aligned} \quad (2.46)$$

The details for evaluating the integral are given in Exercise 2.3. It is found that

$$\begin{aligned} P &= \frac{\zeta_0 I_0^2}{4\pi} \left\{ \sin 2k_0 l [\text{Si}(2k_0 l) - \frac{1}{2} \text{Si}(4k_0 l)] \right. \\ &\quad + (1 + \cos 2k_0 l) [\ln 2k_0 l \gamma - \text{Ci}(2k_0 l)] \\ &\quad \left. - \frac{\cos 2k_0 l}{2} [\ln 4k_0 l \gamma - \text{Ci}(4k_0 l)] \right\} \end{aligned} \quad (2.47)$$

where

$$\text{Si}(x) = \int_0^x \frac{\sin x}{x} dx = \text{sine integral}$$

$$\text{Ci}(x) = -\int_x^\infty \frac{\cos x}{x} dx = \text{cosine integral}$$

$$\int_0^x \frac{1 - \cos x}{x} dx = \ln \gamma x - \text{Ci}(x) \quad \ln \gamma = 0.5772$$

Exercise 2.3 To evaluate the integral in (2.46) let $\cos \theta = u$ to obtain

$$I = \int_{-1}^1 \frac{(\cos k_0 l u - \cos k_0 l)^2}{1 - u^2} du$$

Next note that

$$\frac{1}{1 - u^2} = \frac{1}{2} \left(\frac{1}{1 - u} + \frac{1}{1 + u} \right)$$

and that the integrals involving $1 - u$ and $1 + u$ are equal so that

$$I = \int_{-1}^1 \frac{1 + \cos 2k_0 l u}{2(1 - u)} du + \cos k_0 l \int_{-1}^1 \frac{\cos k_0 l - 2 \cos k_0 l u}{1 - u} du$$

Now replace u by $1 - v$, expand the trigonometric functions, and regroup the terms to obtain

$$I = \sin 2k_0 l \int_0^2 \left(\frac{\sin 2k_0 l v}{2v} - \frac{\sin k_0 l v}{v} \right) dv \\ + (1 + \cos 2k_0 l) \int_0^2 \frac{1 - \cos k_0 l v}{v} dv - \cos 2k_0 l \int_0^2 \frac{1 - \cos 2k_0 l v}{v} dv$$

The result given by (2.47) now follows.

The radiation resistance referred to the antenna input terminals is obtained by dividing the total radiated power by one-half of the square of the input current, i.e., by $\frac{1}{2} I_0^2 \sin^2 k_0 l$. Thus, for example, for the half-wave dipole antenna we obtain ($2l = \lambda_0/2$)

$$R_0 = \frac{\zeta_0}{4\pi} [\ln 2\pi\gamma - \text{Ci}(2\pi)] = 73 \text{ ohms} \quad (2.48)$$

The integrals involved in (2.47) are tabulated in Jahnke and Emde.¹⁷

When the antenna length is a multiple of a wavelength λ_0 , our results predict an infinite radiation resistance referred to the feed point because the input current is now zero; i.e., a null in the standing-wave current distribution occurs at the feed point. An infinite radiation resistance is not observed in practice, although values of 1,000 ohms or more may occur. The theory breaks down because the assumed current distribution is not sufficiently accurate, at least in the vicinity of the feed point. More accurate theories are presented in Chaps. 8 to 10.

2.8 Radiation from a Traveling-wave Source

On certain practical long wire antennas the current distribution may be approximated as a traveling wave. One antenna in this class that is frequently used is the rhombic antenna. Its properties are discussed in detail by Laport in the "Antenna Engineering Handbook."¹⁸ To illustrate the features of radiation from a traveling-wave source we shall consider the simple case of a linear antenna of total length $2l$, as illustrated in Fig. 2.6, on which a current distribution $I = I_0 e^{-jk_0 z}$ has been excited.

The electric field from a traveling-wave line source may be found by using the Fourier transform relations (2.43) and (2.44). Thus we have

$$E_\theta = \frac{j\zeta_0 k_0 \sin \theta}{4\pi r} e^{-jk_0 r} \int_{-l}^l I_0 e^{-jk_0 z (1 - \cos \theta)} dz' \\ = \frac{j\zeta_0 k_0 \sin \theta}{2\pi r} e^{-jk_0 r} \frac{\sin k_0 l (1 - \cos \theta)}{1 - \cos \theta} \quad (2.49)$$

for the far-zone electric field. The radiation pattern, illustrated in Fig. 2.8, consists of a single major conical lobe tilted in the direction of propagation of the current wave, together with one or more minor lobes depending on antenna length. The most distinguishing difference between the radiation pattern of a

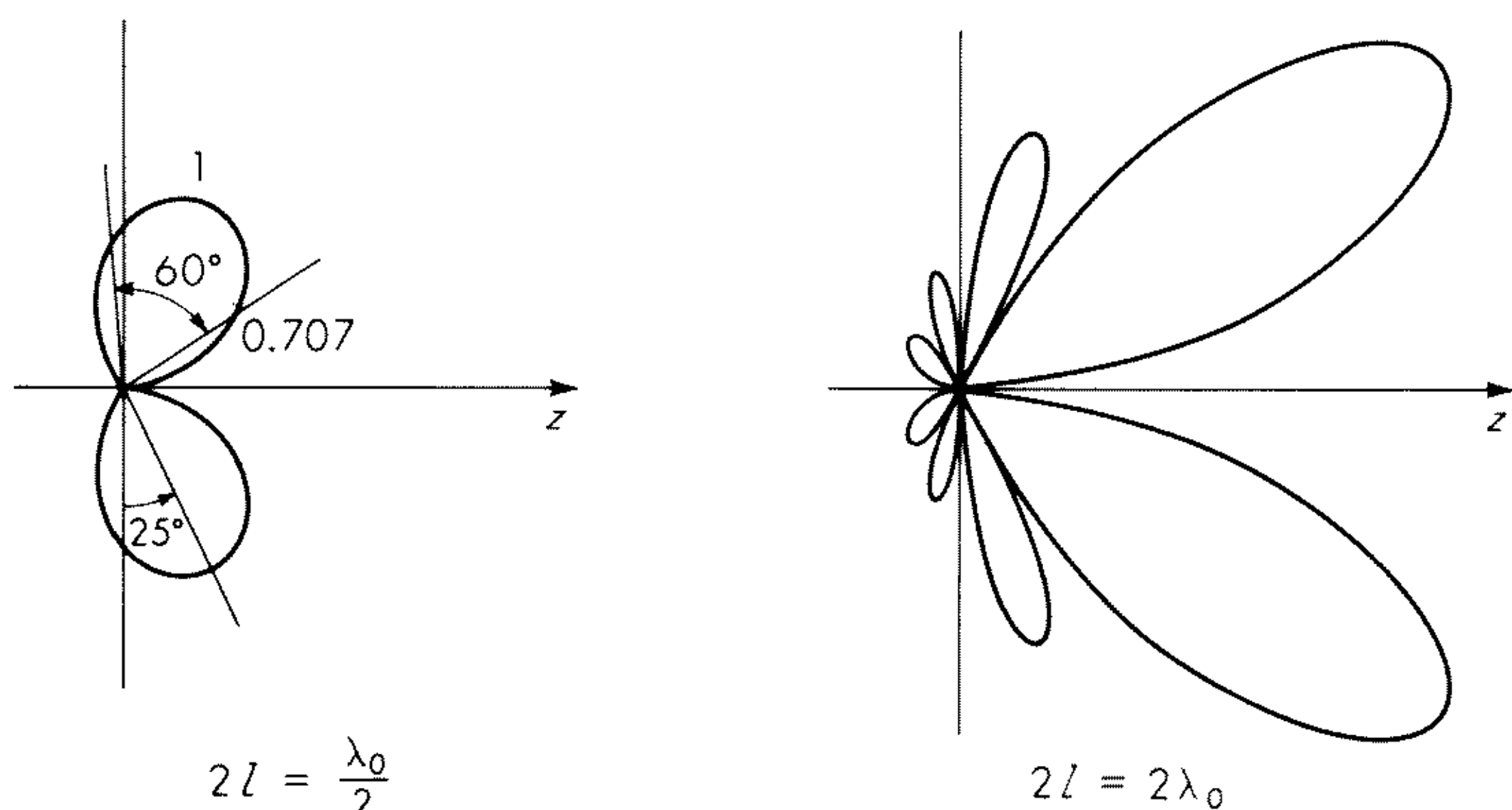


Fig. 2.8 Radiation patterns from a traveling-wave source.

standing-wave current source and a traveling-wave source is the forward tilt of the pattern in the latter case. The amount of tilt increases with the length of the antenna, and at the same time the major lobe becomes sharper. The tilt in the pattern can also be increased by loading the antenna wire, e.g., coating it with a dielectric sleeve, so as to reduce the phase velocity of the current wave. A detailed discussion of these aspects of traveling-wave sources is given in the text by Walter.¹⁹

2.9 Antenna Input Impedance

In this section we shall present two approximate methods for evaluating the antenna input impedance. More exact theories are given in Chaps. 8 to 10. The classical method of impedance evaluation for cylindrical antennas is the induced electromotive force or, briefly, the emf method. A somewhat more satisfactory method is the variational method. These two methods, as applied to the cylindrical antenna, are discussed below.

EMF Method for Antenna Impedance

The integral of the inward component of the complex Poynting vector over a closed surface S gives

$$\frac{1}{2} \oint_S \mathbf{E} \times \mathbf{H}^* \cdot d\mathbf{S} = 2j\omega(W_m - W_e) + P \quad (2.50)$$

where $W_m - W_e$ is the time-average net reactive energy stored within the volume bounded by S and P is the total power flow through S . When the

left-hand side of this equation can be expressed as the product of an equivalent voltage V and the complex conjugate of an equivalent current I , the theorem gives a means of defining the input impedance seen looking into the enclosed volume. The application of (2.50) to the evaluation of the antenna input impedance constitutes the classical emf method for evaluating the antenna input impedance.²⁰⁻²⁴

The antenna model which we shall consider is the thin cylindrical antenna of total length $2l$ illustrated in Fig. 2.6. The current on the antenna is assumed to be given by $I = I_0 \sin k_0(l - |z|)$ and to be uniformly distributed about the center with density $J_z = I/2\pi a$, where a is the antenna radius. To apply the emf method, the near-zone electric field component E_z is required. The vector potential is given by

$$A_z = \frac{\mu_0 I_0}{4\pi} \int_{-l}^l \sin k_0(|z'| - l) \frac{e^{-jk_0 R}}{R} dz'$$

where $R = [\rho^2 + (z - z')^2]^{1/2}$ and $\rho^2 = x^2 + y^2$ and the current has been assumed concentrated at $\rho = 0$ for the purpose of evaluating the vector potential. The field E_z is given by the expression

$$E_z = \frac{1}{j\omega\mu_0\epsilon_0} \left(k_0^2 A_z + \frac{\partial^2 A_z}{\partial z^2} \right)$$

and may be evaluated to give²⁵

$$E_z = -j \frac{\zeta_0 I_0}{4\pi} \left(2 \frac{e^{-jk_0 r}}{r} \cos k_0 l - \frac{e^{-jk_0 R_1}}{R_1} - \frac{e^{-jk_0 R_2}}{R_2} \right) \quad (2.51)$$

where

$$r = (\rho^2 + z^2)^{1/2} \quad R_1 = [\rho^2 + (z - l)^2]^{1/2} \quad R_2 = [\rho^2 + (z + l)^2]^{1/2}$$

The near-zone electric field given by (2.51) does not vanish on the perfectly conducting surface of the antenna. This results from the arbitrary assumption of a sinusoidal standing-wave current distribution on the antenna without any reference to the method of exciting the antenna. A possible way of making the resultant near-zone field and current distribution an exact solution is to assume that the antenna is driven by a magnetic current sheet $-\mathbf{n} \times \mathbf{E}$ placed on the surface of the antenna. The extent to which a practical method of exciting the antenna is equivalent to this magnetic current sheet as far as impedance calculations are concerned cannot be answered within the framework of the classical approach. Recourse to more exact theories or experimental results is necessary to judge the validity of the computed values of impedance.

If (2.50) is applied to the immediate surface surrounding the antenna and H_ϕ^* is replaced by J_z^* and end effects are neglected, we obtain

$$\begin{aligned} \frac{1}{2} \oint_S \mathbf{E} \times \mathbf{H}^* \cdot d\mathbf{S} &= -\frac{1}{2} \int_0^{2\pi} \int_{-l}^l E_z(a, z) J_z^* a d\phi dz \\ &= -\frac{1}{2} \int_{-l}^l E_z(a, z) I_z^* dz = 2j\omega(W_m - W_e) + P_r \end{aligned} \quad (2.52)$$

where P_r is the total radiated power. Referred to the current at the antenna input, the input impedance is given by

$$\frac{1}{2} I_0 I_0^* Z_{in} \sin^2 k_0 l = 2j\omega(W_m - W_e) + P_r$$

or from (2.52)

$$Z_{in} = -\frac{1}{I_0 I_0^* \sin^2 k_0 l} \int_{-l}^l E_z I_0^* \sin k_0(|z| - l) dz \quad (2.53)$$

Substituting for E_z from (2.51) and separating (2.53) into real and imaginary parts gives

$$R_{0m} = R_0 \sin^2 k_0 l = \frac{\zeta_0}{4\pi} \int_{-l}^l \left[2 \cos k_0 l \frac{\sin k_0 r}{r} - \frac{\sin k_0 R_1}{R_1} - \frac{\sin k_0 R_2}{R_2} \right] \sin k_0 (|z| - l) dz \quad (2.54a)$$

$$X_{0m} = X_0 \sin^2 k_0 l = \frac{\zeta_0}{4\pi} \int_{-l}^l \left[2 \cos k_0 l \frac{\cos k_0 r}{r} - \frac{\cos k_0 R_1}{R_1} - \frac{\cos k_0 R_2}{R_2} \right] \sin k_0 (|z| - l) dz \quad (2.54b)$$

where $Z_{in} = R_0 + jX_0$ and R_{0m} , X_{0m} are the resistance and reactance referred to the current antinode value I_0 .

In the integral for R_{0m} the antenna radius a may be placed equal to zero with negligible error when $a \ll l$ and $a \ll \lambda_0$. This is readily seen to be the case by noting that a affects the value of r , R_1 , and R_2 significantly only when these radii approach zero. But in this region $k_0 R_i$ is very small and $(\sin k_0 R_i)/k_0 R_i$ is approximately equal to unity. However, in the integral for X_{0m} the functions $(\cos k_0 R_i)/R_i$ become very large when R_i becomes small, so the effect of antenna radius must be retained in the evaluation of the reactance.

Upon placing a equal to zero, (2.54a) becomes

$$R_{0m} = \frac{\zeta_0}{4\pi} \int_{-l}^l \left[2 \cos k_0 l \frac{\sin k_0 z}{z} - \frac{\sin k_0(l - z)}{l - z} - \frac{\sin k_0(l + z)}{l + z} \right] \sin k_0(|z| - l) dz \quad (2.55)$$

The evaluation of this integral yields the result given by (2.47) if the latter is divided by $\frac{1}{2} I_0^2$. In the integral for X_{0m} the antenna radius a cannot be placed equal to zero. The two terms involving R_1 and R_2 contribute equal amounts, so we have

$$X_{0m} = \frac{\zeta_0}{2\pi} \int_{-l}^l \left(\cos k_0 l \frac{\cos k_0 r}{r} - \frac{\cos k_0 R_1}{R_1} \right) \sin k_0(|z| - l) dz \quad (2.56)$$

The evaluation of this integral is straightforward but tedious. The details may be found in Ref. 25. We shall give only the final results, which are

$$X_{0m} = \frac{\zeta_0}{4\pi} \left\{ 2 \text{Si}(2k_0 l) + [2 \text{Si}(2k_0 l) - \text{Si}(4k_0 l)] \cos 2k_0 l - \left[\ln \frac{\lambda_0 l}{a^2} - 2.414 - \text{Ci}(4k_0 l) + 2 \text{Ci}(2k_0 l) \right] \sin 2k_0 l \right\} \quad (2.57)$$

By a suitable choice of antenna length l the reactance X_{0m} can be made zero. Equating (2.57) for X_{0m} to zero determines the antenna resonant length for a given value of l/a^2 . Note that, as l/a^2 increases, $\sin 2k_0l$ must approach zero in order to make X_{0m} vanish. Thus the resonant length of an infinitely thin antenna occurs when $2k_0l = n\pi$, that is, $2l = n\lambda_0/2$.

The input resistances R_0 and R_{0m} are plotted in Fig. 2.9. Experimental

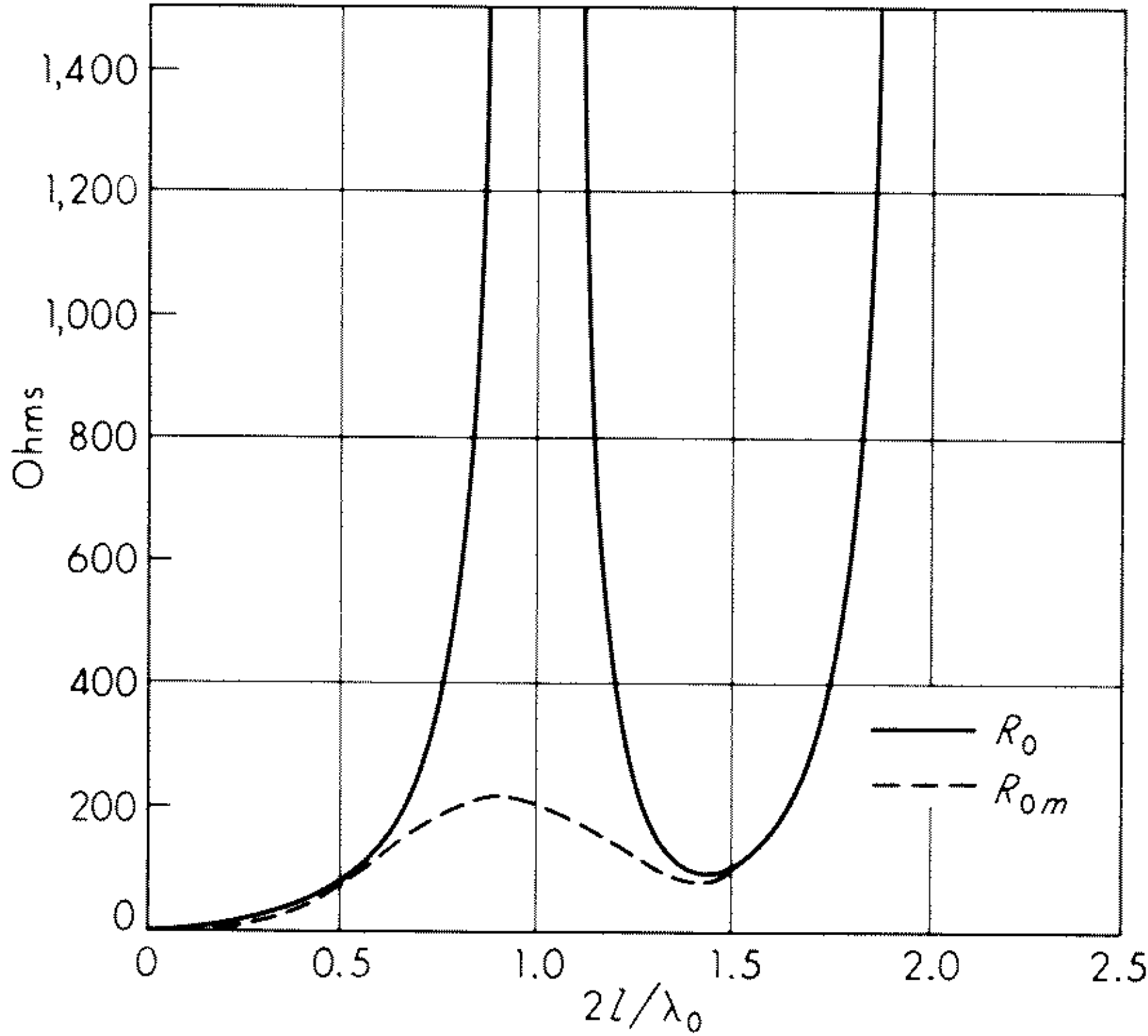


Fig. 2.9 Input resistance of a thin center-fed antenna as obtained by the emf method.

measurements show that for a thin antenna an input resistance of very nearly 73 ohms is obtained for $2l = \lambda_0/2$ and that the values of input resistance may exceed a few thousand ohms for $2l = \lambda_0$. The classical theory predicts an infinite value for R_0 when $2l = \lambda_0$, but this is not achieved in practice. A plot of X_0 is given in Fig. 2.11.

Variational Method for Antenna Impedance

Storer has demonstrated that a stationary or variational expression for the cylindrical antenna input impedance can be formulated.²⁶ The technique is similar to the variational methods introduced for waveguide discontinuity problems by Schwinger. The method was also developed and applied by Tai to both the cylindrical and biconical antennas.^{27,28}

The derivation of the variational principle for the thin cylindrical antenna will be presented here. An application of the method to the biconical antenna is discussed in Chap. 12. The antenna model to be considered consists of a

thin cylindrical conductor of length $2l$ and radius a and driven by a magnetic ring source at the center. The electric field satisfies the boundary condition

$$E_z = \begin{cases} 0 & \frac{d}{2} < |z| < l \\ -E_a & -\frac{d}{2} \leq z \leq \frac{d}{2} \end{cases} \quad (2.58)$$

where d is the width of the magnetic ring source and E_a is a cylindrically uniform but not necessarily constant applied electric field, that is, $E_a(z) = J_m(z)$, where J_m is the magnetic surface current density of the magnetic ring source. If $J_z(z)$ is the current flowing on the antenna and end effects are neglected (valid for $a \ll l$), the electric field in the z direction is given by

$$\begin{aligned} E_z(\rho, z) &= \int_0^{2\pi} \int_{-l}^l G(a, z' | \rho, z) J_z(z') a d\phi' dz' \\ &= \oint_S G(a, z' | \rho, z) J_z(z') dS' \end{aligned} \quad (2.59)$$

where the integration is over the surface of the antenna and the Green's function G is given by

$$G = \left(\frac{k_0^2 e^{-jk_0 R}}{4\pi R} + \frac{\partial^2}{\partial z^2} \frac{e^{-jk_0 R}}{4\pi R} \right) (j\omega\epsilon_0)^{-1}$$

where $R = [a^2 + \rho^2 - 2a\rho \cos(\phi - \phi') + (z - z')^2]^{\frac{1}{2}}$ and $\rho = (x^2 + y^2)^{\frac{1}{2}}$. Applying the boundary condition (2.58) leads to the following integral equation for the antenna current J_z ,

$$E_z = -E_a = \begin{cases} \oint_S G(a, z' | a, z) J_z(z') dS' & -\frac{d}{2} \leq z \leq \frac{d}{2} \\ 0 & \frac{d}{2} < |z| < l \end{cases} \quad (2.60)$$

When $d \ll l$, the current J_z may be considered constant over the source region. The total antenna current at $z = 0$ is $I_a = 2\pi a J_z(0)$. The applied voltage is

$$-\int_{-d/2}^{d/2} E_z dz = \int_{-d/2}^{d/2} E_a dz = V_a$$

and hence the input impedance is given by

$$Z_{in} = \frac{V_a}{I_a} = -\frac{1}{I_a} \int_{-d/2}^{d/2} E_z dz = \frac{1}{2\pi a I_a} \oint_S E_a dS \quad (2.61a)$$

where the integration may be extended over the whole antenna surface S , since

$E_z = E_a$ vanishes for $d/2 < |z| < l$. Since the current density is assumed constant over the region $|z| \leq d/2$, we can also write

$$Z_{\text{in}} = \frac{1}{I_a^2} \oint_S E_a J_z dS = \left| \frac{\int_{-d/2}^{d/2} E_a dz}{\oint_S E_a J_z dS} \right|^2 \oint_S E_a J_z dS \quad (2.61b)$$

Using (2.59) for E_a gives

$$Z_{\text{in}} = - \frac{\oint_S \oint_S G(z'|z) J_z(z') J_z(z) dS' dS}{\left(\oint_S E_a J_z dS \mid \int_{-d/2}^{d/2} E_a dz \right)^2} \quad (2.61c)$$

which is the required variational expression for Z_{in} . Equation (2.61c) may be derived also by multiplying both sides of the integral equation (2.60) by $J_z(z)$ and integrating over the antenna surface and then using the relation (2.61b).

To show that (2.61c) is a stationary expression for Z_{in} let the functional form of $J_z(z)$ be varied by a small amount δJ_z from its true value. Thus Z_{in} will vary by a small amount δZ_{in} . Carrying out the variation of (2.61c) gives

$$\begin{aligned} & \left(\frac{\oint_S E_a J_z dS}{\oint_S E_a dS} \right)^2 \delta Z_{\text{in}} + 2Z_{\text{in}} \frac{\oint_S E_a J_z dS}{\left(\oint_S E_a dS \right)^2} \oint_S E_a \delta J_z dS \\ &= - \oint_S \oint_S G(z'|z) [J_z(z') \delta J_z(z) + J_z(z) \delta J_z(z')] dS dS' \\ &= -2 \oint_S \oint_S G(z'|z) J_z(z') \delta J_z(z) dS dS' \end{aligned}$$

since G is symmetric in z and z' , that is, $G(z'|z) = G(z|z')$. Since Z_{in} has been so defined that

$$Z_{\text{in}} \oint_S E_a J_z dS = \left(\int_{-d/2}^{d/2} E_a dz \right)^2$$

we find that

$$\begin{aligned} & \left(\frac{\oint_S E_a J_z dS}{\oint_S E_a dS} \right)^2 \delta Z_{\text{in}} \\ &= -2 \oint_S \delta J_z(z) \left[\oint_S G(z'|z) J_z(z') dS' + E_a \right] dS = 0 \quad (2.62) \end{aligned}$$

by virtue of the boundary condition (2.60). We now see that a small variation in the current J_z from its correct value gives only a second-order change in Z_{in} when Z_{in} is computed from the variational expression (2.61c).

If a reasonably accurate expression for J_z can be found and is substituted into (2.61c), the resultant value of Z_{in} should be an excellent approximation to the correct value of Z_{in} .

The above variational formulation for Z_{in} can be criticized on several accounts. First of all it requires the assumption that the current J_z is constant over the source region $|z| \leq d/2$ so that the integral $\oint_S E_z J_z dS$ can, in some sense, be interpreted to give $-I_a^2 Z_{\text{in}} = -V_a I_a$. Thus, for the cylindrical antenna the variational expression does not account for the effect of the gap width d or the details of a practical method of exciting the antenna. In addition, since Z_{in} is a complex quantity, the stationary value of Z_{in} does not correspond to an absolute minimum or maximum for $|Z_{\text{in}}|$. Hence if two different trial functions for J_z are employed, there is no direct way to determine which of the two resultant expressions for Z_{in} is the most accurate.

The usual way of employing (2.61c) is to assume an expression for J_z that contains a number of variational parameters α_i , $i = 1, 2, \dots, N$, by which the functional form of J_z can be varied. The input impedance may then be computed and will be a function of the α_i . The stationary property of Z_{in} is now invoked and the α_i determined so that Z_{in} is stationary. The equations to be solved for the α_i are

$$\frac{\partial Z_{\text{in}}}{\partial \alpha_i} = 0 \quad i = 1, 2, \dots, N \quad (2.63)$$

together with (2.61c), which involves I_a , which is a function of the α_i also. The value of Z_{in} for these values of α_i is now considered to be the best value of input impedance that can be obtained with the assumed trial function. If the true current distribution is a member of the family of functions used to represent J_z , then the above procedure leads to the correct value of Z_{in} . If, however, the true current is not a member of the family of functions $J_z(z, \alpha_1, \alpha_2, \dots, \alpha_N)$, then there is no real reason why the stationary value of Z_{in} should be the most accurate one. A further difficulty arises here in that there is no unique way of measuring the accuracy of Z_{in} . A number of different criteria could be used. For example, if Z is the correct value and Z_{in} an approximate value, one measure of the accuracy of Z_{in} would be $|Z - Z_{\text{in}}|^2 = (R - R_{\text{in}})^2 + (X - X_{\text{in}})^2$. An equally valid measure might be the geometric mean of the errors in R_{in} and X_{in} , that is, $[(R - R_{\text{in}})^2(X - X_{\text{in}})^2]^{\frac{1}{2}} = |R - R_{\text{in}}| |X - X_{\text{in}}|$.

The main conclusion to be drawn from the above discussion is that the stationary value of Z_{in} , found from (2.61c) when a current J_z containing several variational parameters is used as a trial function, can be expected to be a good estimate or approximation to the true value of input impedance. However, no direct estimate of the accuracy of the result is available.

The use of the variational formulation (2.61c) is greatly facilitated if the kernel or Green's function G can be approximated by replacing R by $[\rho^2 + (z - z')^2]^{\frac{1}{2}}$. Tai has shown that for trial functions such as

$$J_z(z) = \sin k_0(|z| - l) + A[1 - \cos k_0(|z| - l)]$$

or
$$J_z(z) = \sin k_0(|z| - l) + A(|z| - l) \cos k_0(|z| - l)$$

the use of the approximate expression for R yields the same result as the exact kernel or Green's function yields when $a \ll l$.²⁹

Storer used $I_z = I_0 \{ \sin k_0(|z| - l) + A[1 - \cos k_0(|z| - l)] \}$ as a trial function and used the condition $\partial Z_{\text{in}}/\partial A = 0$ to determine the constant A . When $k_0 l = n\pi$, $n = 1, 2, \dots$, the current vanishes at $z = 0$ and the variational expression for Z_{in} becomes infinite. Tai overcame this difficulty by using $I_z = I_0 \{ \sin k_0(l - |z|) + A(l - |z|) \cos k_0(l - |z|) \}$ for a trial function together with the condition $\partial Z_{\text{in}}/\partial A = 0$ to determine A . The results of Tai's evaluation are

$$Z_{\text{in}} = \frac{Z_0}{4\pi} \frac{\nu_{11} + 2\nu_{12}A + \nu_{22}A^2}{(\sin k_0 l + A k_0 l \cos k_0 l)^2} \quad (2.64)$$

where

$$\begin{aligned} \nu_{11} &= 2 \text{Ein}(2k_0 l) + e^{2jk_0 l} \left[\ln 2 - \frac{\Omega}{2} - \text{Ein}(4k_0 l) \right. \\ &\quad \left. + 2 \text{Ein}(2k_0 l) \right] + e^{-2jk_0 l} \left(-\ln 2 + \frac{\Omega}{2} \right) \\ \nu_{12} &= jk_0 l [2 - \Omega + \text{Ein}(2k_0 l)] + e^{2jk_0 l} \left\{ \frac{1}{2} + jk_0 l \left[2 \ln 2 - \frac{\Omega}{2} \right. \right. \\ &\quad \left. \left. - 2 \text{Ein}(4k_0 l) + 3 \text{Ein}(2k_0 l) \right] \right\} + e^{-2jk_0 l} \left[-\frac{1}{2} + jk_0 l \left(2 \ln 2 - \frac{\Omega}{2} \right) \right] \\ \nu_{22} &= \text{Ein}(2k_0 l) + jk_0 l \left[-\frac{1}{2} - \Omega + \text{Ein}(2k_0 l) \right] + k_0^2 l^2 \left[-\frac{1}{2} + \text{Ein}(2k_0 l) \right] \\ &\quad + e^{2jk_0 l} \left\{ \frac{1}{4} \left[\frac{1}{2} + 2 \ln 2 - \Omega - 2 \text{Ein}(4k_0 l) + 4 \text{Ein}(2k_0 l) \right] \right. \\ &\quad + jk_0 l [1 + \ln 2 - \text{Ein}(4k_0 l) + \text{Ein}(2k_0 l)] \\ &\quad + k_0^2 l^2 \left[-2 \ln 2 + \frac{\Omega}{2} + 2 \text{Ein}(4k_0 l) - 3 \text{Ein}(2k_0 l) \right] \left. \right\} \\ &\quad + e^{-2jk_0 l} \left[\frac{1}{4} \left(-\frac{1}{2} - 2 \ln 2 + \Omega \right) + jk_0 l (1 + \ln 2) \right. \\ &\quad \left. + k_0^2 l^2 \left(\frac{1}{2} + 2 \ln 2 - \frac{\Omega}{2} \right) \right] \end{aligned}$$

and $\Omega = 2 \ln 2l/a$ and $\text{Ein}(x)$ is the exponential integral

$$\text{Ein}(x) = \text{Ci } x + j \text{Si } x = \int_0^x \frac{1 - e^{-ju}}{u} du$$

The solution obtained for A is

$$A = \frac{\nu_{11} k_0 l \sin k_0 l - \nu_{12} \sin k_0 l}{\nu_{22} \sin k_0 l - \nu_{12} k_0 l \cos k_0 l} \quad (2.65)$$

and hence

$$Z_{\text{in}} = \frac{Z_0}{4\pi} \frac{\nu_{11}\nu_{22} - \nu_{12}^2}{\nu_{11}k_0^2 l^2 \cos^2 k_0 l - k_0 l \nu_{12} \sin 2k_0 l + \nu_{22} \sin^2 k_0 l} \quad (2.66)$$

Chaney has obtained similar results by means of a generalized network approach.³⁰

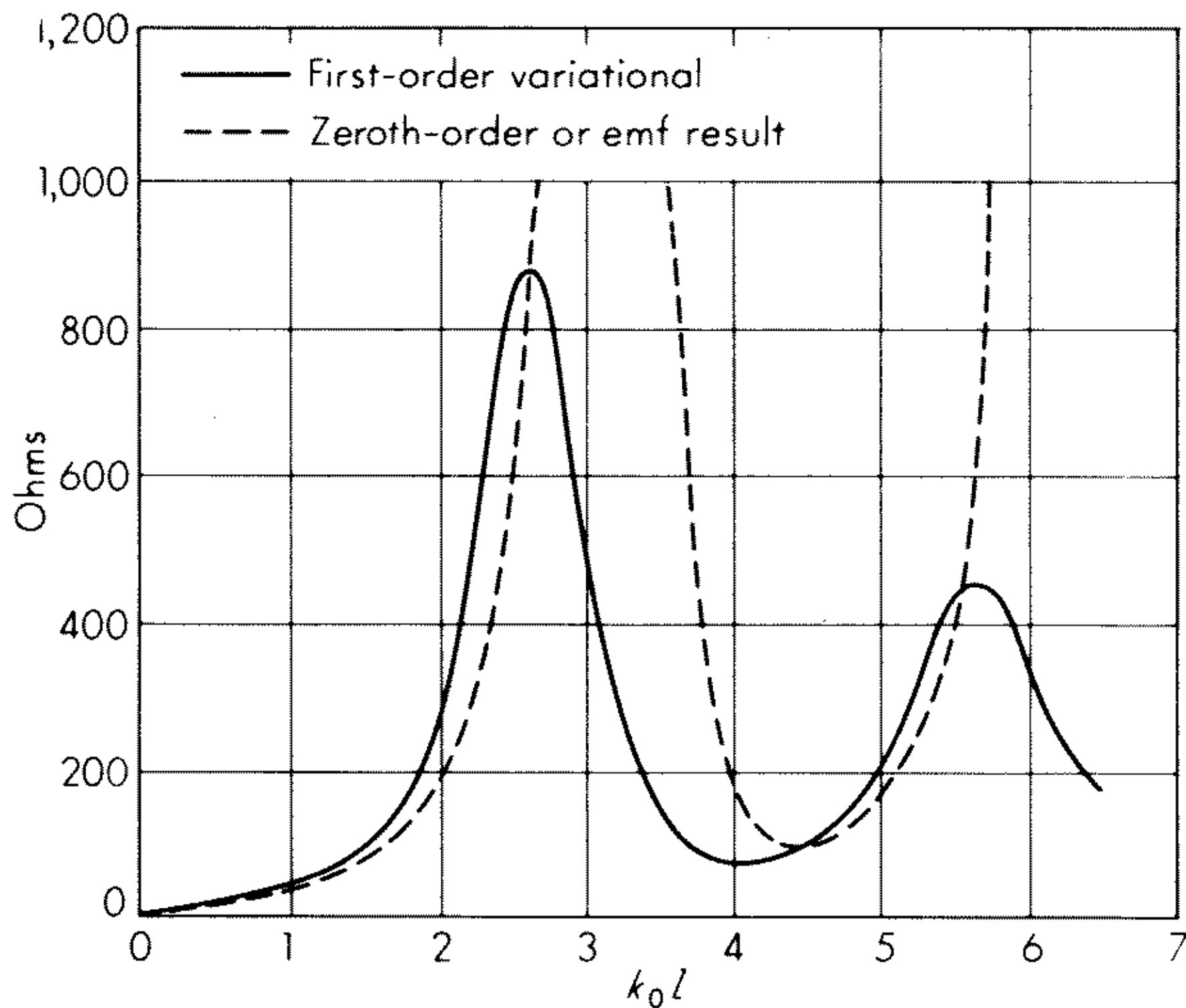


Fig. 2.10 Input resistance for a cylindrical antenna, $\Omega = 10$.

If A is chosen equal to zero, the variational formulation gives the same result for Z_{in} as the classical emf method does. The emf or zeroth-order solution is compared with the first-order solution given by (2.66) in Figs. 2.10 and 2.11. The first-order solution agrees quite well with the more exact King-

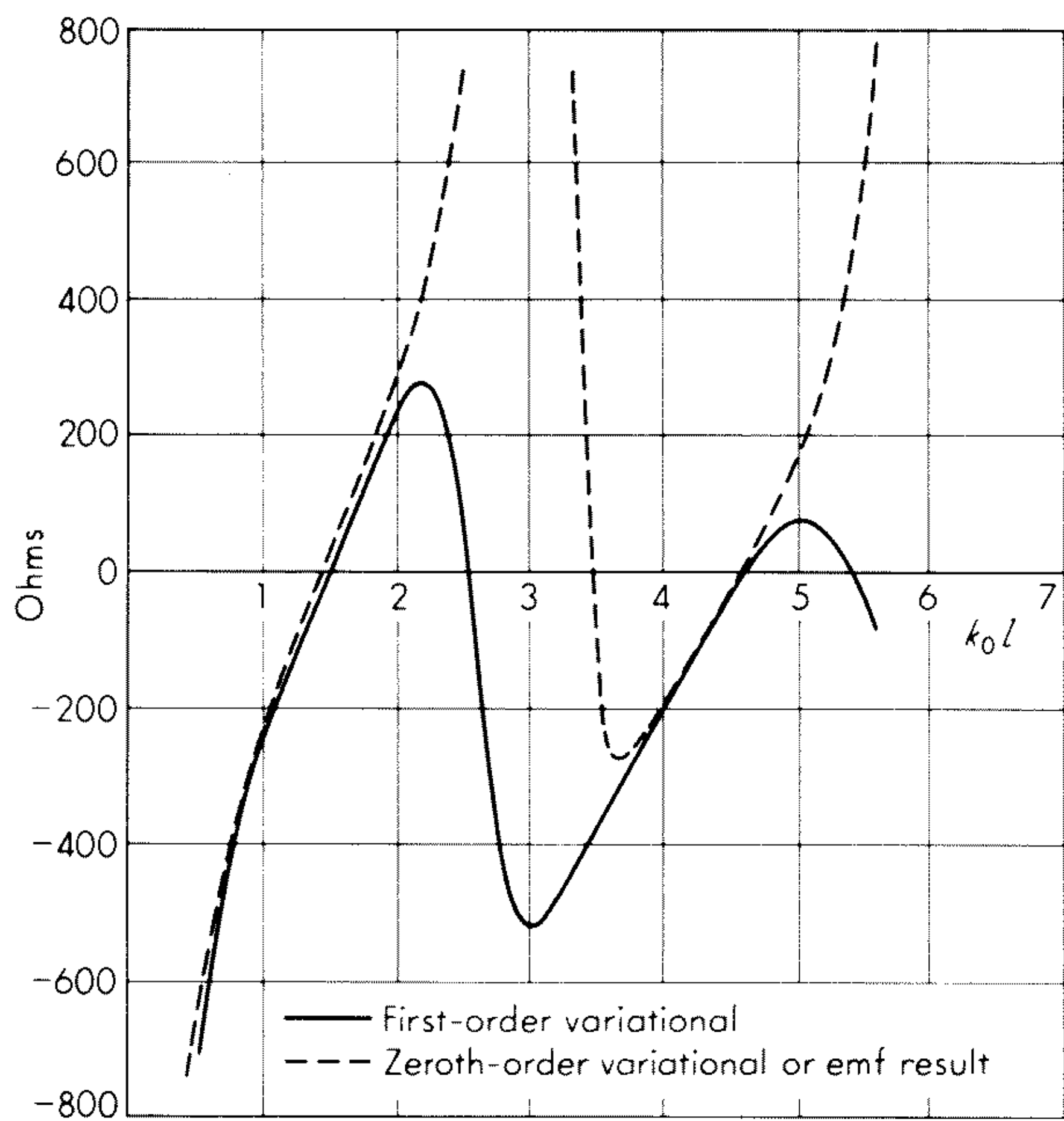


Fig. 2.11 Input reactance for a cylindrical antenna, $\Omega = 10$.

Middleton second-order theory, as we show in Fig. 2.12. The King-Middleton theory is covered in Ref. 31. In Chap. 9 a more refined theory is developed. The curves in Figs. 2.10 to 2.12 are based on calculations made by Tai.²⁷

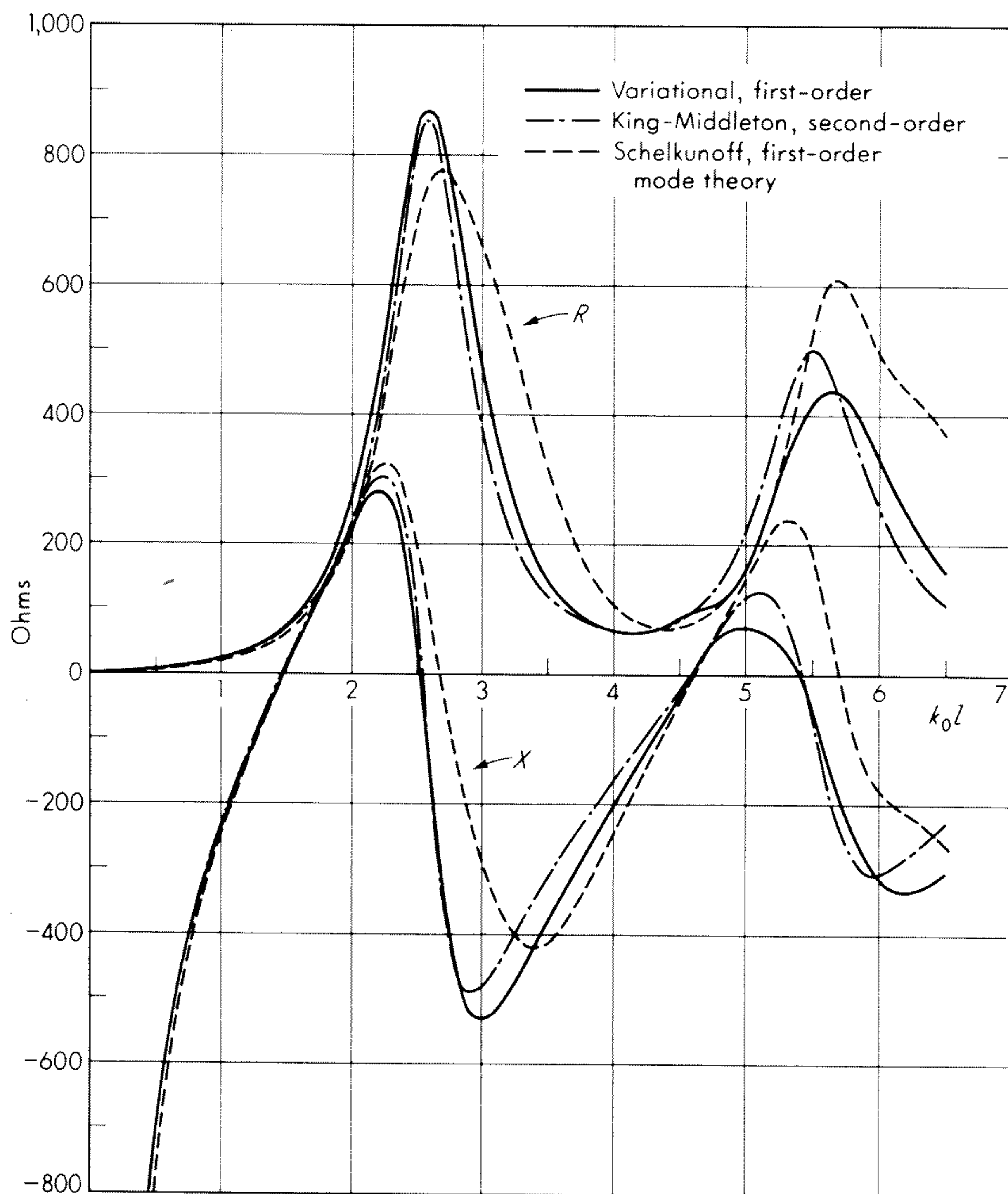


Fig. 2.12 Input impedance of a cylindrical antenna according to different theories, $\Omega = 10$, $2l/a = 150$.

PROBLEMS

2.1 Consider a short dipole antenna as illustrated in Fig. P-2.1. The length of the antenna is $l \ll \lambda_0$, and the antenna current is uniform with an amplitude I . Find the radiated fields by using the vector and scalar potentials. Hint: The scalar potential will arise from charges $\pm Q$ at the ends of the dipole $z = \pm l/2$. The rate at which charge accumulates at the ends is $j\omega Q$ and must equal the current at the end (from continuity equation).

Answer:

$$\Phi = \frac{Q}{4\pi\epsilon_0}\left(\frac{e^{-ik_0R_1}}{R_1} - \frac{e^{-ik_0R_2}}{R_2}\right) \approx \frac{Ql}{4\pi\epsilon_0}\left(\frac{\cos\theta}{r^2} + \frac{jk_0\cos\theta}{r}\right)e^{-ik_0r}$$
$$A_z = \frac{\mu_0Il}{4\pi r}e^{-ik_0r}$$

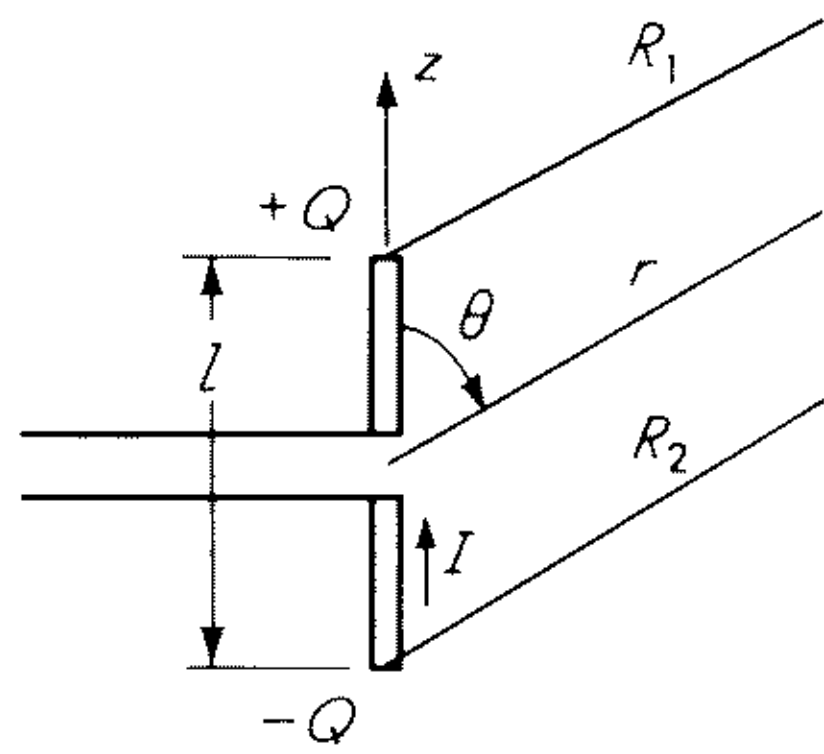


Fig. P-2.1

2.2 Consider the capacitive-loaded dipole antenna in Fig. 2.3. The antenna length is $0.02\lambda_0$. The circular disks have a diameter d equal to $0.02\lambda_0$. Evaluate the antenna input capacitive reactance by approximating the capacitance of the antenna as that between the two disks and neglecting fringing fields. Compare with the radiation resistance.

Answer: $1/\omega C = (2l\lambda_0\zeta_0)/(\pi d)^2$.

2.3 For the single-turn loop antenna described below evaluate the radiation resistance, ohmic resistance, and inductive reactance and compare. Loop diameter $d_1 = 0.04\lambda_0$; wire diameter $d_2 = 0.001\lambda_0$; σ = conductivity of wire = 5.8×10^7 mhos/m (copper). Hint: Use the low-frequency formula

$$L = \mu_0 2d_1 \left(\ln \frac{8d_1}{d_2} - 2 \right)$$

for the inductance of the loop. To calculate the ohmic resistance the current should be assumed to flow in a thin cylindrical shell of thickness equal to the skin depth d_s . Answer: Ohmic resistance = $d_1/(\sigma d_2 d_s)$.

2.4 Find the far-zone fields radiated by a current element

$$\mathbf{J} = I(\hat{\mathbf{x}} + \hat{\mathbf{y}}) \delta(x - 1) \delta(y - 1) \delta(z)$$

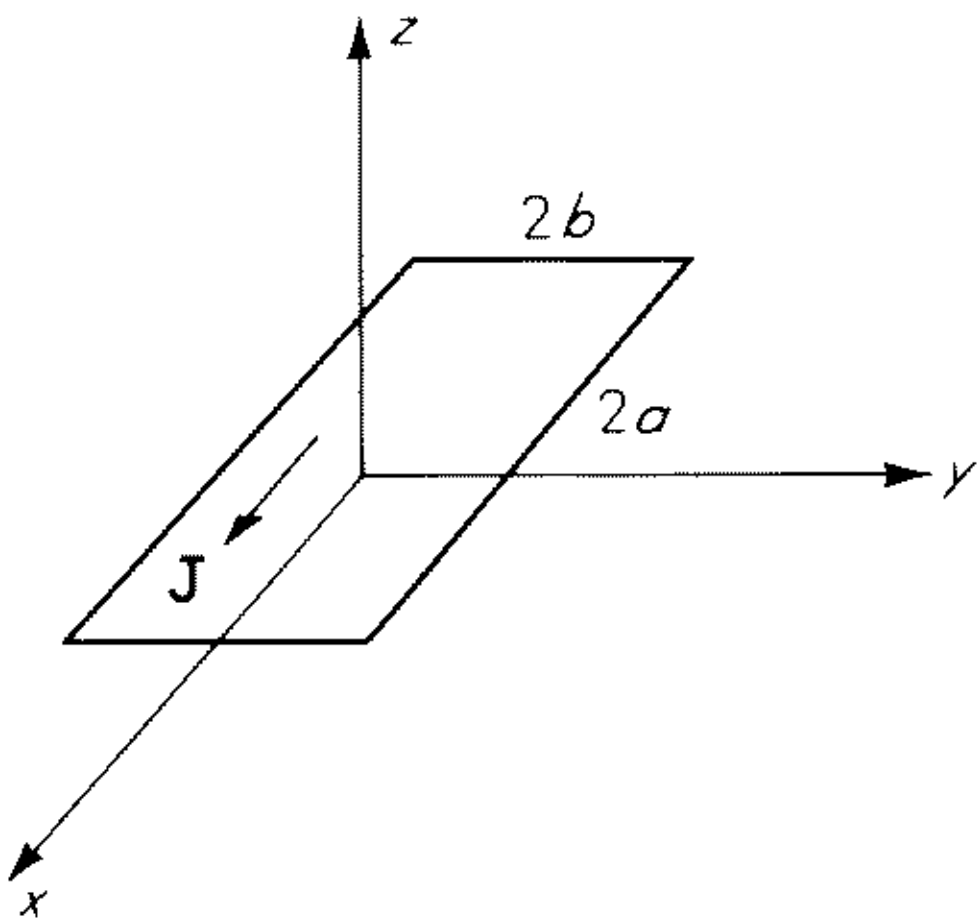


Fig. P-2.5

2.5 A rectangular current sheet of dimensions $2a$ by $2b$ in the xy plane has a uniform current distribution $J\mathbf{x}$. Find the far-zone fields, the directions in which maximum radiation occurs, and the half-power E - and H -plane beam widths. Assume a and b large compared with λ_0 . How do the beam widths vary with a and b ? The center of the current sheet is at the origin.

2.6 Show that if the sources of an electromagnetic field include both electric and magnetic currents, the expressions (2.43a,b) for the far-zone fields require the additional terms $-(\hat{\theta}J_{m\theta} + \hat{\phi}J_{m\phi})\zeta_0^{-1}$ and $\zeta_0\mathbf{J}_m \times \hat{\mathbf{r}}$, respectively, under the integral sign.

2.7 Show that in the Fresnel region the \mathbf{H} field is given by

$$\mathbf{H} = \frac{jk_0}{4\pi r} e^{-jk_0 r} \int_V \mathbf{J} \times \hat{\mathbf{r}} \exp \left\{ jk_0 \left[\hat{\mathbf{r}} \cdot \mathbf{r}' + \frac{(\hat{\mathbf{r}} \cdot \mathbf{r}')^2 - r'^2}{2r} \right] \right\} dV'$$

by neglecting terms of order r'/r . For the current sheet in Prob. 2.5 show that along the z axis \mathbf{H} is given by

$$\mathbf{H} = -\frac{jk_0 J}{\pi z} e^{-jk_0 z} (\hat{\theta} \sin \phi + \hat{\phi} \cos \theta \cos \phi) \int_0^{a/2} \int_0^{b/2} e^{-jk_0[(x'^2+y'^2)/z]} dx' dy'$$

2.8 By using the equation $\nabla \times \mathbf{H} = j\omega\epsilon_0\mathbf{E}$ and the expression given for \mathbf{H} in Prob. 2.7, obtain an expression for \mathbf{E} in the Fresnel region that is valid for $r \gg r'$; that is, neglect terms of order r'/r and higher.

2.9 Show that the radiation resistance of the traveling-wave antenna discussed in Sec. 2.8 is given by

$$R_0 = 60 \left(1.415 + \ln \frac{4l}{\lambda_0} + \frac{\sin 8\pi l/\lambda_0}{8\pi l/\lambda_0} - \text{Ci} \frac{8\pi l}{\lambda_0} \right)$$

REFERENCES

1. Aharoni, J.: "Antennae: An Introduction to Their Theory," Clarendon Press, Oxford, 1946.
2. Kraus, J. D.: "Antennas," McGraw-Hill Book Company, New York, 1950.
3. Jordan, E. C.: "Electromagnetic Waves and Radiating Systems," Prentice-Hall, Inc. Englewood Cliffs, N.J., 1950.
4. Moullin, E. B., "Radio Aerials," Oxford University Press, London, 1949.
5. Schelkunoff, S. A., and H. T. Friis: "Antennas: Theory and Practice," John Wiley & Sons, Inc., New York, 1952.
6. Silver, S.: "Microwave Antenna Theory and Design," McGraw-Hill Book Company, New York, 1949.
7. Williams, H. P.: "Antenna Theory and Design," 2 vols., Sir Isaac Pitman & Sons, Ltd., London, 1950.
8. King, R. W. P.: "The Theory of Linear Antennas," Harvard University Press, Cambridge, Mass., 1956.
9. Stratton, J. A.: "Electromagnetic Theory," sec. 7.4, McGraw-Hill Book Company, New York, 1941.
10. Silver, S.: "Microwave Antenna Theory and Design," sec. 6.9, McGraw-Hill Book Company, New York, 1949.
11. Morse, P. M., and H. Feshbach: "Methods of Theoretical Physics," part I, chap. 7, and part II, chap. 13, McGraw-Hill Book Company, New York, 1953.
12. Levine, H., and J. Schwinger: On the Theory of Diffraction by an Aperture in an Infinite Plane Screen, *Phys. Rev.*, vol. 75, pp. 1423-1432, 1949.

13. Collin, R. E.: "Field Theory of Guided Waves," chap. 2, McGraw-Hill Book Company, New York, 1960.
14. Abraham, M.: Die Electriscen Schwingungen um Einen Stabformigen Leiter, Behandelt Nach der Maxwell' schen Theorie, *Ann. Physik*, vol. 66, pp. 435-472, October, 1898.
15. Pocklington, H. C.: Electrical Oscillations on Wires, *Proc. Cambridge Phil. Soc.*, vol. 9, pp. 324-332, October, 1897.
16. Bechmann, R.: Calculations of Electric and Magnetic Field Strengths of Any Oscillating Straight Conductors, *Proc. IRE*, vol. 19, pp. 461-466, March, 1931.
17. Jahnke, E., and F. Emde: "Tables of Functions," 4th ed., Dover Publications, Inc., New York, 1945.
18. Jasik, H. (ed.): "Antenna Engineering Handbook," chap. 4, McGraw-Hill Book Company, New York, 1961.
19. Walter, C. H.: "Traveling Wave Antennas," McGraw-Hill Book Company, New York, 1965.
20. Brillouin, L.: Sur l'Origine de la Résistance de Rayonnement, *Radioélectricité*, vol. 3, p. 147, 1922.
21. Carter, P. S.: Circuit Relations in Radiating Systems and Applications to Antenna Problems, *Proc. IRE*, vol. 20, pp. 1004-1041, June, 1932.
22. Pistolcors, A. A.: The Radiation Resistance of Beam Antennas, *Proc. IRE*, vol. 17, pp. 562-579, March, 1929.
23. Bechmann, R.: On the Calculation of Radiation Resistance of Antennas and Antenna Combinations, *Proc. IRE*, vol. 19, pp. 1471-1480, August, 1931.
24. Tai, C. T.: A Study of the EMF Method, *J. Appl. Phys.*, vol. 20, pp. 717-723, July, 1949.
25. Schelkunoff, S. A.: "Electromagnetic Waves," pp. 369-374, D. Van Nostrand Company, Inc., Princeton, N.J., 1943.
26. Storer, J. E.: Variational Solution to the Problem of the Symmetrical Antenna, *Cruft Lab. Tech. Rept.* 101, Harvard University, 1950.
27. Tai, C. T.: A Variational Solution to the Problem of Cylindrical Antennas, *Stanford Res. Inst. Tech. Rept.* 12, Stanford, Calif., 1950.
28. Tai, C. T.: Application of a Variational Principle to Biconical Antennas, *J. Appl. Phys.*, vol. 20, pp. 1076-1084, November, 1949.
29. Tai, C. T.: A New Interpretation of the Integral Equation Formulation of Cylindrical Antennas, *IRE Trans. Antennas Propagation*, vol. AP-3, pp. 125-127, July, 1955.
30. Chaney, J. G.: A Simple Solution to the Problem of the Cylindrical Antenna, *IRE Trans. Antennas Propagation*, vol. AP-5, pp. 217-221, April, 1957.
31. King, R. W. P., and D. Middleton: The Cylindrical Antenna, Current and Impedance, *Quart. Appl. Math.*, vol. 3, pp. 302-335, January, 1946. For corrections see vol. 4, pp. 199-200, July, 1946, and vol. 6, p. 192, July, 1948.
32. Van Bladel, J.: Some Remarks on Green's Dyadic for Infinite Space, *IRE Trans. Antennas Propagation*, vol. AP-9, pp. 563-566, November, 1961.

RADIATION FROM APERTURES

R. E. Collin

3.1 Aperture-type Antennas

There are several types of antennas for which the radiated electromagnetic field may be viewed as emanating from a physical aperture or opening. Typical examples of antennas in this class, illustrated in Fig. 3.1, include the horn, lens, reflector, and some surface-wave antennas. The region of space may be divided into two regions by an infinite plane surface (called the aperture plane) con-

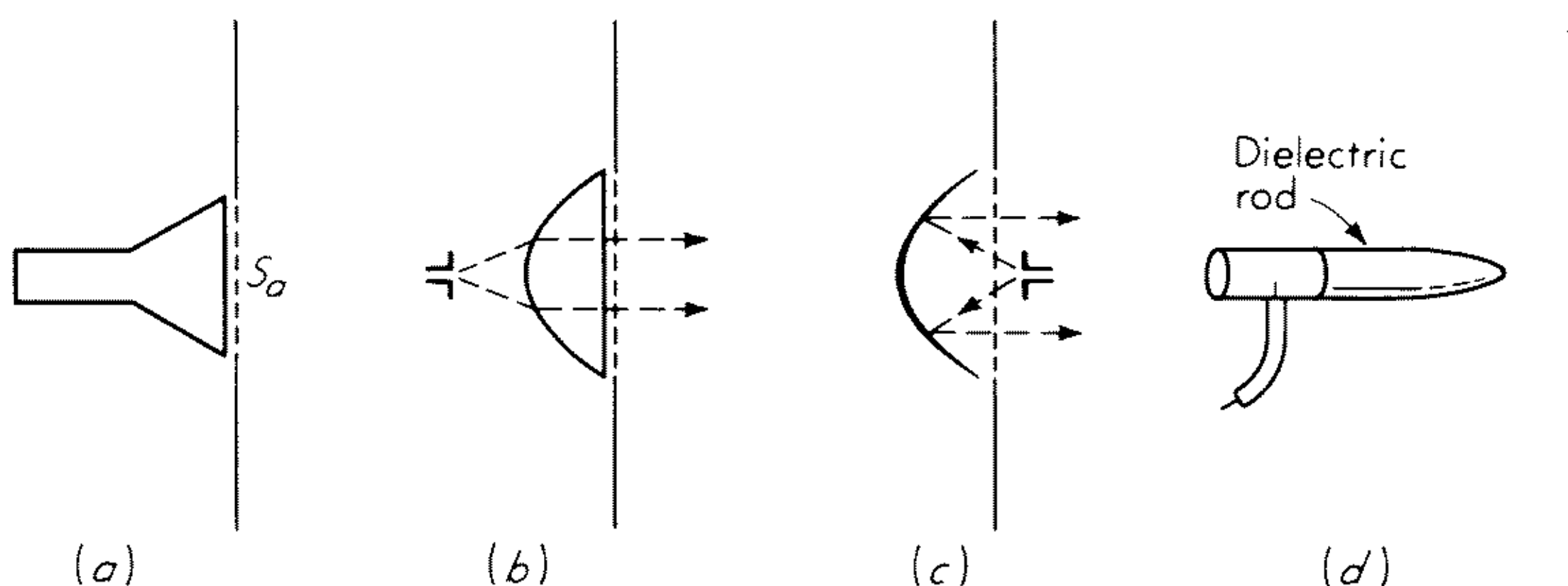


Fig. 3.1 Aperture-type antennas, S_a = aperture surface. (a) Horn; (b) lens; (c) reflector; (d) surface-wave antenna.

taining the antenna aperture. For physical apertures that are large compared with a wavelength the electromagnetic field amplitude will be small everywhere on the aperture plane except on the aperture surface. As a first approximation the far-zone radiation field may be found from the field on the aperture surface alone. The aperture field is usually determined by suitable approximate methods based on geometrical optics concepts (see Chaps. 16 to 18).

If the exact field were known everywhere on the aperture surface, the radiation field could be calculated exactly. However, for most antenna structures of practical interest exact solutions are very difficult to obtain, so approximate methods must be used. The main purpose of this chapter is to develop the theory leading to suitable formulas for calculating the radiation field in terms of the field distribution on the aperture plane and to examine the radiation patterns resulting from different types of aperture field distributions. Results similar to those included in this chapter have also been given by Silver,¹ and Fradin,² as well as many others.

3.2 Aperture in an Infinite Conducting Plane

For an aperture in an infinite perfectly conducting plane a number of exact results for the field radiated into space on one side of the screen can be readily obtained. These results will illustrate many of the features associated with the radiation from apertures and are dealt with for this reason in this section.

Figure 3.2 illustrates a rectangular aperture of dimensions $2a$ by $2b$ in an

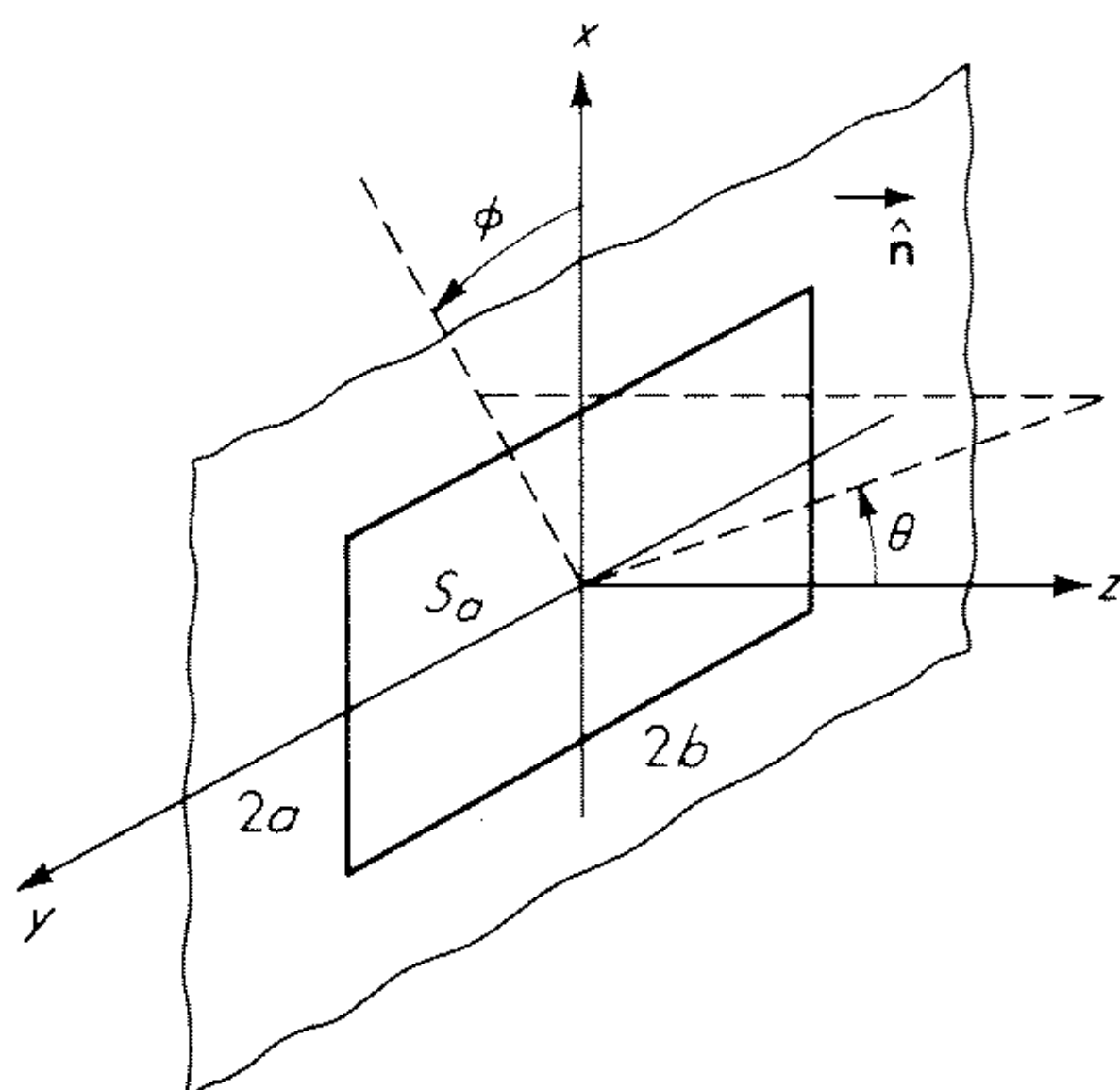


Fig. 3.2 Rectangular aperture in an infinite conducting plane.

infinite conducting plane coinciding with the $z = 0$ plane in a rectangular coordinate system. The electric and magnetic fields in the aperture are assumed known and have tangential components that will be denoted by \mathbf{E}_a and \mathbf{H}_a . According to the uniqueness theorem for the electromagnetic field the field in the half space $z > 0$ is uniquely determined by a knowledge of either the tangential electric field or tangential magnetic field on the plane $z = 0$ together with the radiation condition. Since $\hat{\mathbf{n}} \times \mathbf{E} = 0$ on the infinitely conducting plane outside the aperture opening whereas $\hat{\mathbf{n}} \times \mathbf{H}$ does not, it is more convenient to determine the radiated field in terms of the tangential electric field \mathbf{E}_a in the aperture surface S_a corresponding to $|x| \leq a$ and $|y| \leq b$.

In the source-free region $z > 0$ the electric field is a solution of $(\nabla^2 + k_0^2)\mathbf{E}(x, y, z) = 0$ and is solenoidal, that is, $\nabla \cdot \mathbf{E} = 0$. If we Fourier transform \mathbf{E} with respect to x and y and let

$$\mathbf{E}(k_x, k_y, z) = \iint_{-\infty}^{\infty} \mathbf{E}(x, y, z) e^{jk_x x + jk_y y} dx dy \quad (3.1)$$

we obtain

$$\left[\frac{\partial^2}{\partial z^2} + k_0^2 - (k_x^2 + k_y^2) \right] \mathbf{E}(k_x, k_y, z) = 0 \quad (3.2)$$

for the double Fourier transform of the equation satisfied by $\mathbf{E}(x, y, z)$. We may solve (3.2) to obtain

$$\mathbf{E}(k_x, k_y, z) = \mathbf{f}(k_x, k_y) e^{-jk_z z} \quad (3.3)$$

where \mathbf{f} is a vector function of k_x and k_y and $k_z = (k_0^2 - k_x^2 - k_y^2)^{1/2}$. The positive real root is chosen when k_z is real, and the root with a negative imaginary part is chosen when k_z is imaginary so as to satisfy the radiation condition. We now see that the electric field in the half space $z > 0$ can be represented in the form

$$\mathbf{E}(x, y, z) = \frac{1}{4\pi^2} \iint_{-\infty}^{\infty} \mathbf{f}(k_x, k_y) e^{-j\mathbf{k} \cdot \mathbf{r}} dk_x dk_y \quad (3.4)$$

where $\mathbf{k} = k_x \hat{\mathbf{x}} + k_y \hat{\mathbf{y}} + k_z \hat{\mathbf{z}}$ and $|\mathbf{k}| = k_0$. This expression simply states that the field may be regarded as made up of a superposition of plane waves of the form $\mathbf{f} e^{-j\mathbf{k} \cdot \mathbf{r}}$. Those waves for which k_z is real are propagating waves and will contribute to the energy flow at infinity, while those waves for which $k_x^2 + k_y^2 > k_0^2$ have a pure imaginary k_z and are evanescent. It is apparent that the far-zone radiation field must, therefore, arise only from that part of the k_x, k_y spectrum for which $k_x^2 + k_y^2 < k_0^2$. The components k_x and k_y of the propagation vector \mathbf{k} are sometimes called spatial frequencies, since they are the variables conjugate to the spatial variables x and y .†

†The following comments on terminology were supplied by F. J. Zucker:

In network theory one uses the Fourier transform relation

$$v(t) = \int_{-\infty}^{\infty} V(\omega) e^{j\omega t} d\omega \quad (1)$$

The conjugate variables are t , the time variable, and ω , which is called the angular or radian frequency.

In modal analysis one uses

$$F(x) = \int_{-\infty}^{\infty} f(k_x) e^{-jk_x x} dk_x \quad (2)$$

The conjugate variables are x and k_x , with x being called the distance in the source plane while k_x is called (a) wave number along x , (b) spatial frequency or periodicity along x , or (c) angular frequency along x . Booker and Clemmow introduced the terminology (c) in connection with aperture analysis, where the emphasis is on angle θ in $k_x = k_0 \sin \theta$. In modal analysis the emphasis is on k_x as the spectral variable and (c) is never used.

In pattern analysis and synthesis the relation

$$f(u) = \int_{-\infty}^{\infty} F(x') e^{jx' u} dx' \quad (3)$$

is used, where $u = \sin \theta$ is called the angle variable and $x' = k_0 x$ is called the normalized or reduced aperture distance. Now x' is the spectral variable with respect to u and could be called angular, radian, or spatial frequency (or periodicity) by analogy with (1) if u is considered analogous to time t .

Since a common terminology does not exist in the literature and it appears that no one single terminology could be made universally acceptable, we have not made any attempt to standardize on this point in this book. In context the reader should find it relatively easy to follow the terminology being used by the different authors.

Since $\mathbf{E}(x, y, z)$ is solenoidal, the divergence of (3.4) shows that, since $\nabla \cdot \mathbf{f} e^{-j\mathbf{k} \cdot \mathbf{r}} = \mathbf{f} \cdot \nabla e^{-j\mathbf{k} \cdot \mathbf{r}} = -j\mathbf{f} \cdot \mathbf{k} e^{-j\mathbf{k} \cdot \mathbf{r}}$, we must have

$$\mathbf{k} \cdot \mathbf{f} = 0 \quad (3.5)$$

and hence only two components of \mathbf{f} are independent. This result is consistent with the requirement that $\mathbf{E}(x, y, z)$ can be uniquely determined in terms of the tangential electric field on the aperture plane. When $z = 0$, we have

$$\mathbf{E}_t(x, y, 0) = \mathbf{E}_a(x, y) = \frac{1}{4\pi^2} \iint_{-\infty}^{\infty} \mathbf{f}_t(k_x, k_y) e^{-j(k_x x + k_y y)} dk_x dk_y \quad (3.6a)$$

where t denotes the x and y components. We may invert (3.6a) to obtain

$$\mathbf{f}_t = \iint_{S_a} \mathbf{E}_a(x, y) e^{j(k_x x + k_y y)} dx dy \quad (3.6b)$$

where the integration is over the aperture only, since \mathbf{E}_a is zero on the conducting screen. The z component of \mathbf{f} may be found from (3.5) in terms of \mathbf{f}_t given by (3.6b), that is,

$$f_z = -\frac{\mathbf{k}_t \cdot \mathbf{f}}{k_z} \quad (3.7)$$

The magnetic field \mathbf{H} may be found from the electric field by using Maxwell's equation $\nabla \times \mathbf{E} = -j\omega\mu_0\mathbf{H}$. Employing the expression (3.4) for \mathbf{E} , we readily find that

$$\mathbf{H}(x, y, z) = \frac{1}{4\pi^2 k_0 \zeta_0} \iint_{-\infty}^{\infty} \mathbf{k} \times \mathbf{f} e^{-j\mathbf{k} \cdot \mathbf{r}} dk_x dk_y \quad (3.8)$$

since $\nabla \times \mathbf{f} e^{-j\mathbf{k} \cdot \mathbf{r}} = -\mathbf{f} \times \nabla e^{-j\mathbf{k} \cdot \mathbf{r}} = j\mathbf{f} \times \mathbf{k} e^{-j\mathbf{k} \cdot \mathbf{r}}$

We are now in a position to evaluate a number of quantities of physical interest such as radiated power, average stored reactive energy, and the far-zone radiation field. The complex radiated power may be found by integrating the complex Poynting vector over the aperture plane. Thus

$$\begin{aligned} P + 2j\omega(W_m - W_e) &= \frac{1}{2} \iint_{S_a} \mathbf{E} \times \mathbf{H}^* \cdot \hat{\mathbf{z}} dx dy \\ &= \frac{1}{8\pi^2 \zeta_0 k_0} \iint_{-\infty}^{\infty} [(k_0^2 - k_t^2) \mathbf{f}_t \cdot \mathbf{f}_t^* + |\mathbf{k}_t \cdot \mathbf{f}_t|^2] \frac{dk_x dk_y}{k_z^*} \end{aligned} \quad (3.9)$$

The latter expression is obtained by using (3.4) and (3.8) for the fields as indicated in Exercise 3.1. For $k_t^2 \leq k_0^2$ the integrand is real, since in this region of k_x, k_y space k_z is real. For $k_t^2 > k_0^2$ the factor k_z is pure imaginary. Consequently, the real radiated power comes only from that portion of the plane wave spectrum for which k_x and k_y are located inside the circle $k_t^2 \leq k_0^2$. This

portion of the k_x, k_y space is, therefore, called the visible region. The average reactive energy $W_m - W_e$ stored in the evanescent waves arises from values of k_x and k_y corresponding to the invisible portion $k_t > k_0$ of the k_x, k_y space.

Exercise 3.1 Replace \mathbf{E} by (3.4) and \mathbf{H} by (3.8) in the complex Poynting vector and derive (3.9). Use \mathbf{k}'_t for the transform variable in the expression for \mathbf{E} , and use \mathbf{k}_t in the expression for \mathbf{H} . Also make use of the orthogonality property

$$\int_{-\infty}^{\infty} e^{-ik'_x x + ik_x x} dx = 2\pi \delta(k_x - k'_x)$$

to reduce the sixfold integral that is obtained for the complex power. Note that the integration over S_a may be extended over the whole xy plane, since $\hat{\mathbf{z}} \times \mathbf{E} = 0$ outside the aperture. The above orthogonality property shows that the plane waves do not interact, so that the complex power is the integral of that contributed by each separate plane wave.

The representation of an arbitrary electromagnetic field as a superposition of propagating and evanescent plane waves and its application to the problem of an aperture in an infinite conducting plane were first given by Booker and Clemmow.⁴ The theory has also been extended to give expressions for the energy stored in the electric and magnetic fields of the evanescent waves and the aperture Q (see Collin and Rothschild,⁵ also Probs. 3.1 and 3.2). This plane wave representation has also been discussed by Rhodes⁶ and Borgiotti.⁷

An expression for the far-zone radiation field may be obtained by evaluating the Fourier transform (3.4) asymptotically by the method of stationary phase (for a discussion of the method see Jeffreys and Jeffreys⁸). The method of stationary phase is based on the observation that, when r is very large, a function such as $e^{-j\mathbf{k} \cdot \mathbf{r}} = \cos \mathbf{k} \cdot \mathbf{r} - j \sin \mathbf{k} \cdot \mathbf{r}$ oscillates very rapidly between equal positive and negative values except for certain values of k_x and k_y for which $\mathbf{k} \cdot \mathbf{r}$ remains stationary, i.e., does not change for first-order changes in k_x and k_y . When a slowly varying function of k_x and k_y is multiplied by $e^{-j\mathbf{k} \cdot \mathbf{r}}$ and integrated over k_x and k_y , the contribution to the integral arises predominantly only from those values of k_x and k_y for which the phase remains stationary. For those values of k_x and k_y that make the phase $\mathbf{k} \cdot \mathbf{r}$ vary rapidly the integrand oscillates rapidly between plus and minus values and the contribution to the value of the integral is small. In the limit as r tends to infinity the leading term in the asymptotic expansion of the integral is given exactly by the contributions arising from the stationary phase points only.

The integral (3.4) to be evaluated is repeated here for reference:

$$\mathbf{E}(\mathbf{r}) = \frac{1}{4\pi^2} \int_{-\infty}^{\infty} \int \mathbf{f}(k_x, k_y) e^{-j\mathbf{k} \cdot \mathbf{r}} dk_x dk_y$$

We may express $\mathbf{k} \cdot \mathbf{r}$ as

$$k_x x + k_y y + k_z z = r [k_x \sin \theta \cos \phi + k_y \sin \theta \sin \phi + (k_0^2 - k_x^2 - k_y^2)^{1/2} \cos \theta]$$

where θ and ϕ are the usual angle variables in spherical coordinates (Fig. 3.2). The stationary phase points are determined by a solution of

$$\frac{\partial \mathbf{k} \cdot \mathbf{r}}{\partial k_x} = 0 \quad \frac{\partial \mathbf{k} \cdot \mathbf{r}}{\partial k_y} = 0$$

which are readily found to give

$$k_x = k_z \frac{\sin \theta \cos \phi}{\cos \theta} \quad k_y = k_z \frac{\sin \theta \sin \phi}{\cos \theta}$$

Since $k_x^2 + k_y^2 = k_0^2 - k_z^2$, we see that we must have $k_z = k_0 \cos \theta$, so that the stationary values of k_x and k_y are given by

$$k_x = k_1 = k_0 \cos \phi \sin \theta = k_0 u \quad (3.10a)$$

$$k_y = k_2 = k_0 \sin \phi \sin \theta = k_0 v \quad (3.10b)$$

The new angle variables $u = \sin \theta \cos \phi$ and $v = \sin \theta \sin \phi$ introduced here will be used in later chapters as an abbreviated notation. In the vicinity of the stationary phase point $\mathbf{k} \cdot \mathbf{r}$ can be approximated by the first few terms in a Taylor series expansion, i.e., by

$$\begin{aligned} \mathbf{k} \cdot \mathbf{r} &= \mathbf{k} \cdot \mathbf{r} \Big|_{k_1, k_2} + \frac{1}{2} \frac{\partial^2 \mathbf{k} \cdot \mathbf{r}}{\partial k_x^2} \Big|_{k_1, k_2} (k_x - k_1)^2 + \frac{1}{2} \frac{\partial^2 \mathbf{k} \cdot \mathbf{r}}{\partial k_y^2} \Big|_{k_1, k_2} (k_y - k_2)^2 + \\ &\quad \frac{\partial^2 \mathbf{k} \cdot \mathbf{r}}{\partial k_x \partial k_y} \Big|_{k_1, k_2} (k_x - k_1)(k_y - k_2) \\ &= k_0 r - (Au^2 + Bv^2 + Cuv) \end{aligned} \quad (3.11)$$

where A , B , and C are suitable constants and $u = k_x - k_1$, $v = k_y - k_1$ are new variables introduced for later convenience. (They should not be confused with the angle variables given by (3.10) which are not used in this chapter.)

In the vicinity of the stationary phase point $\mathbf{f}(k_x, k_y)$ is slowly varying, so it may be replaced by $\mathbf{f}(k_1, k_2)$. Hence the asymptotic value of the integral for $\mathbf{E}(\mathbf{r})$ is given by

$$\mathbf{E}(\mathbf{r}) \sim f(k_0 \cos \phi \sin \theta, k_0 \sin \phi \sin \theta) e^{-jk_0 r} \frac{1}{4\pi^2} \iint_{S_0} e^{j(Au^2 + Bv^2 + Cuv)} du dv \quad (3.12)$$

where S_0 is a small circle centered on the stationary phase point from which the major contribution to the integral comes. However, since the phase factor becomes large for large r as soon as u and v differ slightly from zero, the integration may be extended over the whole uv plane with little error because of the rapid oscillation of the integrand for nonzero values of u and v . When this is done according to Exercise 3.2, it is found that

$$\mathbf{E}(\mathbf{r}) \sim j \frac{e^{-jk_0 r}}{2\pi r} k_0 \cos \theta \mathbf{f}(k_0 \cos \phi \sin \theta, k_0 \sin \phi \sin \theta) \quad (3.13)$$

This result shows that the far-zone radiation field is related in a rather direct way to the Fourier transform of the aperture field. If we express (3.13) in terms of \mathbf{f}_t , we obtain

$$\begin{aligned}\mathbf{E}(\mathbf{r}) &\sim j \frac{e^{-jk_0 r}}{2\pi r} k_0 \cos \theta \left[\mathbf{f}_t(k_0 \cos \phi \sin \theta, k_0 \sin \phi \sin \theta) \right. \\ &\quad \left. - \frac{\sin \theta}{\cos \theta} (f_x \cos \phi + f_y \sin \phi) \hat{\mathbf{z}} \right] \\ &= j k_0 \frac{e^{-jk_0 r}}{2\pi r} [\hat{\Phi}(f_y \cos \phi - f_x \sin \phi) \cos \theta + \hat{\Theta}(f_x \cos \phi + f_y \sin \phi)]\end{aligned}\quad (3.14)$$

Exercise 3.2 In (3.12) introduce new variables $x = \sqrt{A}u$, $y = \sqrt{B}v$ to obtain

$$\frac{1}{\sqrt{AB}} \iint_{-\infty}^{\infty} \exp \left[j \left(x^2 + y^2 + \frac{Cxy}{\sqrt{AB}} \right) \right] dx dy$$

Complete the square for the x variable to obtain

$$\frac{1}{\sqrt{AB}} \iint_{-\infty}^{\infty} \exp \left\{ j \left[\left(x + \frac{Cy}{2\sqrt{AB}} \right)^2 + y^2 \left(1 - \frac{C^2}{4AB} \right) \right] \right\} dx dy$$

Integrate over x first and then over y , using the result

$$\int_{-\infty}^{\infty} e^{j\alpha(x-x_0)^2} dx = \sqrt{\frac{\pi}{\alpha}} e^{j\pi/4}$$

to obtain $2\pi j / \sqrt{4AB - C^2}$. If the coefficients A , B , C , are evaluated from (3.11), the result given by (3.12) will now be obtained.

The functions $\cos \theta$, $\cos \phi$, and $\sin \phi$ are slowly varying, so that the radiation pattern is seen to depend essentially only on f_x and f_y , which are the Fourier transforms of the x and y components of the electric field in the aperture. The results obtained here are very similar to those obtained in Sec. 2.7 for the radiation from an electric current line source. The Fourier transform relationship between the aperture field and the far-zone radiation field is a useful one, since it makes available all of the operational properties of Fourier transform pairs for the analysis of the radiation from given aperture fields. A detailed discussion of the use of Fourier transforms in antenna theory has been given by Ramsay⁹ and also by Spencer (see Silver¹⁰). The Fourier transform relationship may also be used as a basis for a synthesis technique to synthesize the aperture field required to give a desired specified radiation pattern. The synthesis problem is dealt with in Chap. 7 and for that reason will not be discussed here.

For a slit-type aperture of infinite width along y and an aperture field

independent of y the relations corresponding to (3.4), (3.6), (3.8), (3.9), and (3.13) are

$$\mathbf{E}(x, z) = \frac{1}{2\pi} \int_{-\infty}^{\infty} \mathbf{f}(k_x) e^{-j(k_x x + k_z z)} dk_x \quad (3.15a)$$

$$\mathbf{E}_a(x) = \frac{1}{2\pi} \int_{-\infty}^{\infty} \mathbf{f}_t(k_x) e^{-jk_x x} dk_x \quad (3.15b)$$

$$\mathbf{f}_t(k_x) = \int_{-a}^a \mathbf{E}_a(x) e^{jk_x x} dx \quad (3.15c)$$

$$\mathbf{H}(x, z) = \frac{1}{2\pi k_0 \zeta_0} \int_{-\infty}^{\infty} \mathbf{k} \times \mathbf{f} e^{-j(k_x x + k_z z)} dk_x \quad (3.15d)$$

$$P + 2j\omega(W_m - W_e) = \frac{1}{4\pi k_0 \zeta_0} \int_{-\infty}^{\infty} [(k_0^2 - k_x^2) \mathbf{f}_t \cdot \mathbf{f}_t^* + |\mathbf{k}_x \cdot \mathbf{f}_x|^2] \frac{dk_x}{k_z^*} \quad (3.15e)$$

$$\mathbf{E}(x, z) \sim \sqrt{\frac{j}{2\pi k_0 r}} k_0 \cos \theta \mathbf{f}(k_0 \sin \theta) e^{-jk_0 r} \quad (3.15f)$$

where $\mathbf{k} = k_x \hat{\mathbf{x}} + k_z \hat{\mathbf{z}}$ now and $|\mathbf{k}| = k_0$ as before. Note that (3.15e) gives the complex power per unit width of the slit aperture.

As an interesting alternative derivation of the far-zone radiation field from an aperture in an infinite conducting screen we note that if the aperture is closed by a perfectly conducting wall and a magnetic current $\mathbf{J}_{ms} = -\hat{\mathbf{z}} \times \mathbf{E}_a$ is placed on this closed aperture surface, the tangential electric field will be zero on the whole $z = 0$ plane but must change discontinuously to a value \mathbf{E}_a as the magnetic current sheet is crossed. Thus the radiated field can be found from this equivalent magnetic current sheet placed an infinitesimal distance in front of the closed aperture. But since the whole $z = 0$ plane is now a perfectly conducting plane, image theory tells us that the radiation from the magnetic current sheet in front of the conducting plane is the same as that from a current sheet of twice the amplitude and radiating in free space. We may determine the radiated field in terms of a magnetic vector potential \mathbf{A}_m (see Sec. 1.8). If we follow the same type of analysis as used in Sec. 2.5 to find the far-zone field radiated by an arbitrary electric current distribution, we obtain

$$\begin{aligned} \mathbf{E}(\mathbf{r}) &= -\frac{1}{4\pi} \nabla \times \iint_{S_a} 2\mathbf{J}_{ms}(\mathbf{r}') \frac{e^{-jk_0 R}}{R} dx' dy' \\ &\sim -\frac{jk_0}{4\pi r} e^{-jk_0 r} \iint_{S_a} 2\mathbf{J}_{ms}(\mathbf{r}') \times \hat{\mathbf{r}} \exp(jk_0 \hat{\mathbf{r}} \cdot \mathbf{r}') dx' dy' \end{aligned}$$

for the far-zone electric field. Replacing

$$\mathbf{J}_{ms} \times \hat{\mathbf{r}} \quad \text{by} \quad \hat{\mathbf{r}} \times (\hat{\mathbf{z}} \times \mathbf{E}_a) = (\hat{\mathbf{r}} \cdot \mathbf{E}_a) \hat{\mathbf{z}} - (\hat{\mathbf{r}} \cdot \hat{\mathbf{z}}) \mathbf{E}_a$$

and using the Fourier transform relation (3.6) to evaluate the integral, we find that

$$\begin{aligned}\mathbf{E}(\mathbf{r}) &\sim -jk_0 \frac{e^{-jk_0 r}}{2\pi r} [\hat{\mathbf{r}} \cdot \mathbf{f}_t (k_0 \sin \theta \cos \phi, k_0 \sin \theta \sin \phi) \hat{\mathbf{z}} - \cos \theta \mathbf{f}_t] \\ &= jk_0 \cos \theta \frac{e^{-jk_0 r}}{2\pi r} \left[\mathbf{f}_t - \frac{\sin \theta}{\cos \theta} (f_x \cos \phi + f_y \sin \phi) \hat{\mathbf{z}} \right]\end{aligned}$$

which is the same result as given by (3.14).

The above example has demonstrated for a particular case that the aperture field can be replaced by an equivalent current source and the field determined from the latter. The theory of equivalent sources, usually called field equivalence principles, is developed in a more general way in the next section.

3.3 Field Equivalence Principles

A field equivalence principle refers to the replacement of the actual sources of an electromagnetic field by a set of equivalent sources. Field equivalence principles are very useful in formulating scattering and diffraction problems even though they generally do not make the exact solution of the problem any easier to obtain. On the other hand, field equivalence principles often suggest approximate methods of obtaining solutions and for this reason are of importance in antenna theory.

In order to establish the basic concepts involved, consider a set of current sources \mathbf{J}_1 and \mathbf{J}_{m1} located in a region of space V_1 as shown in Fig. 3.3. Let S be

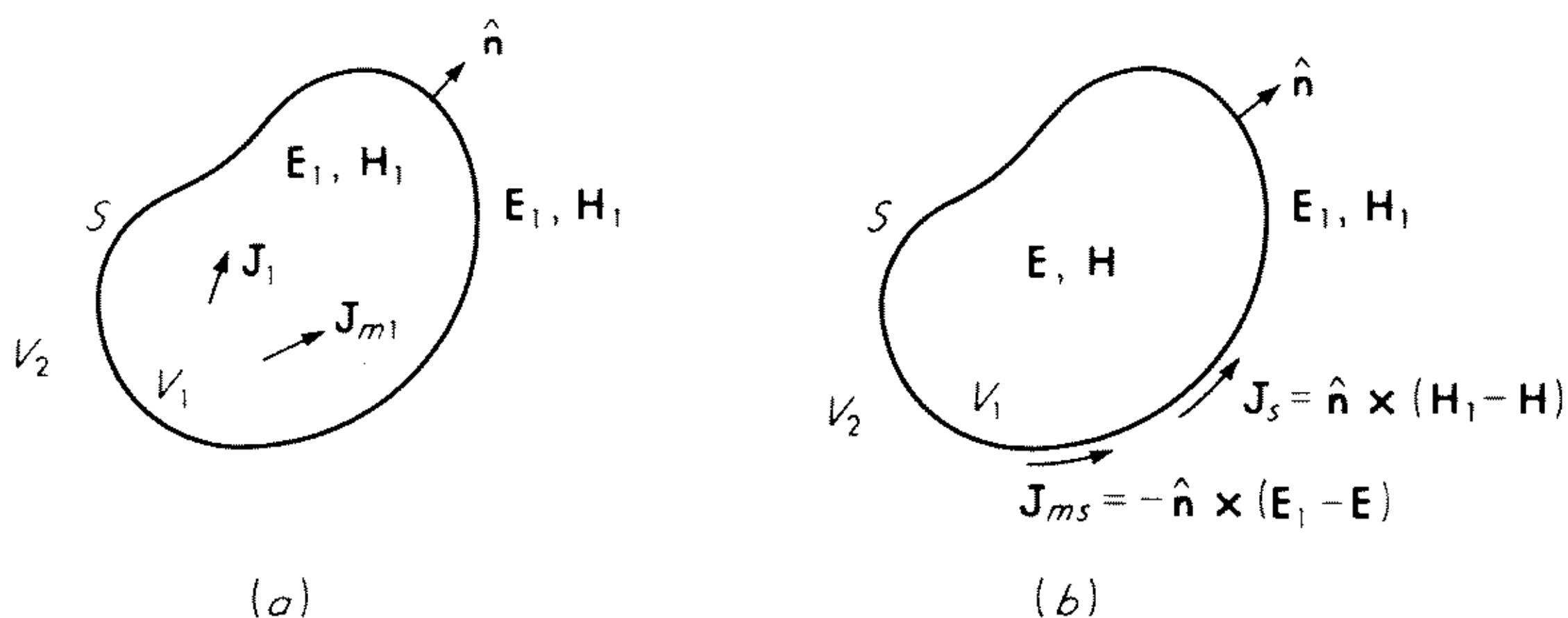


Fig. 3.3 Illustration of a field equivalence principle. (a) Original problem; (b) equivalent problem for region V_2 .

a closed surface enclosing all of the sources. The given sources will radiate a field $\mathbf{E}_1, \mathbf{H}_1$. In the region V_2 outside S the field $\mathbf{E}_1, \mathbf{H}_1$ is source-free. Let us now remove the sources in V_1 and postulate the existence of an arbitrary source-free field \mathbf{E}, \mathbf{H} inside V_1 and keep the original field $\mathbf{E}_1, \mathbf{H}_1$ outside S , that is, in V_2 . In order that the total field throughout V_1 and V_2 be a valid solution of Maxwell's equations it is necessary to postulate also the existence of equivalent sources on the surface S which separates V_1 and V_2 in order to

properly join the two solutions together. The equivalent sources on S must be so chosen as to provide for the discontinuous change in the tangential components of the electric and magnetic fields across S . Thus we require surface sources

$$\mathbf{J}_s = \hat{\mathbf{n}} \times (\mathbf{H}_1 - \mathbf{H}) \quad (3.16a)$$

$$\mathbf{J}_{ms} = -\hat{\mathbf{n}} \times (\mathbf{E}_1 - \mathbf{E}) \quad (3.16b)$$

The sources given by (3.16) may be viewed as those sources which will radiate a field $\mathbf{E}_1, \mathbf{H}_1$ in the region V_2 and a field \mathbf{E}, \mathbf{H} in V_1 . Since these fields are solutions of Maxwell's equations and satisfy proper boundary conditions at the surface S and the radiation condition at infinity, the uniqueness theorem shows that they represent the unique solution to the problem.

It is clear that the above procedure has led to the identification of a set of equivalent sources that, placed on the closed surface S , will produce the same field $\mathbf{E}_1, \mathbf{H}_1$ external to S that the original sources \mathbf{J}_1 and \mathbf{J}_{m1} in V_1 produced. However, internal to S the new sources produce a field \mathbf{E}, \mathbf{H} which is different from the original field, and consequently the equivalent sources are equivalent only for some given region that is external to the region in which the original sources had been located.

Several variations of the above basic field equivalence principle may be constructed. For example, we could postulate a null field inside S , in which case the required sources to be placed on S in order to maintain the original field $\mathbf{E}_1, \mathbf{H}_1$ outside S would be

$$\mathbf{J}_s = \hat{\mathbf{n}} \times \mathbf{H}_1 \quad (3.17a)$$

$$\mathbf{J}_{ms} = -\hat{\mathbf{n}} \times \mathbf{E}_1 \quad (3.17b)$$

In this form the field equivalence principle is known as Love's equivalence principle.¹¹

Two modifications of Love's equivalence principle of importance for the aperture antenna problem are given below. Since the field inside S is chosen as a null field, we can place a perfectly conducting surface just inside S . In this case the electric surface current $\mathbf{J}_s = \hat{\mathbf{n}} \times \mathbf{H}_1$ is short-circuited and does not radiate. Thus the field $\mathbf{E}_1, \mathbf{H}_1$ can be found from the magnetic current $\mathbf{J}_{ms} = -\hat{\mathbf{n}} \times \mathbf{E}_1$ alone placed on a perfectly conducting surface S . This is the field equivalence principle that was employed in the last part of Sec. 3.2 for the aperture in a conducting screen.

The dual of the above problem is obtained by replacing S by a perfect magnetic conductor, i.e., a fictitious surface on which the tangential magnetic field must vanish. In this case the magnetic current is short-circuited and the field may be found from the electric current $\mathbf{J}_s = \hat{\mathbf{n}} \times \mathbf{H}_1$ alone on S . In both of these two variations of Love's equivalence principle it is important to note that the equivalent sources radiate in the presence of the perfect electric or magnetic conducting surface S , respectively.

Schelkunoff has developed a number of other field equivalence principles also. For a discussion of these we refer the reader to the papers by Schelkunoff^{12,13} and the book by Harrington.¹⁴

3.4 Radiation from Aperture Fields

In this section we shall use the field equivalence principles discussed in the preceding section to obtain solutions for the far-zone radiation field arising from assumed known aperture fields. The problem of determining the aperture field is taken up in considerable detail in Chaps. 16 to 18.

Typical aperture antenna problems are illustrated in Fig. 3.4. We place in front of the antenna an aperture plane coinciding with the $z = 0$ plane. The aperture plane divides all of space into two regions, that for $z < 0$ containing

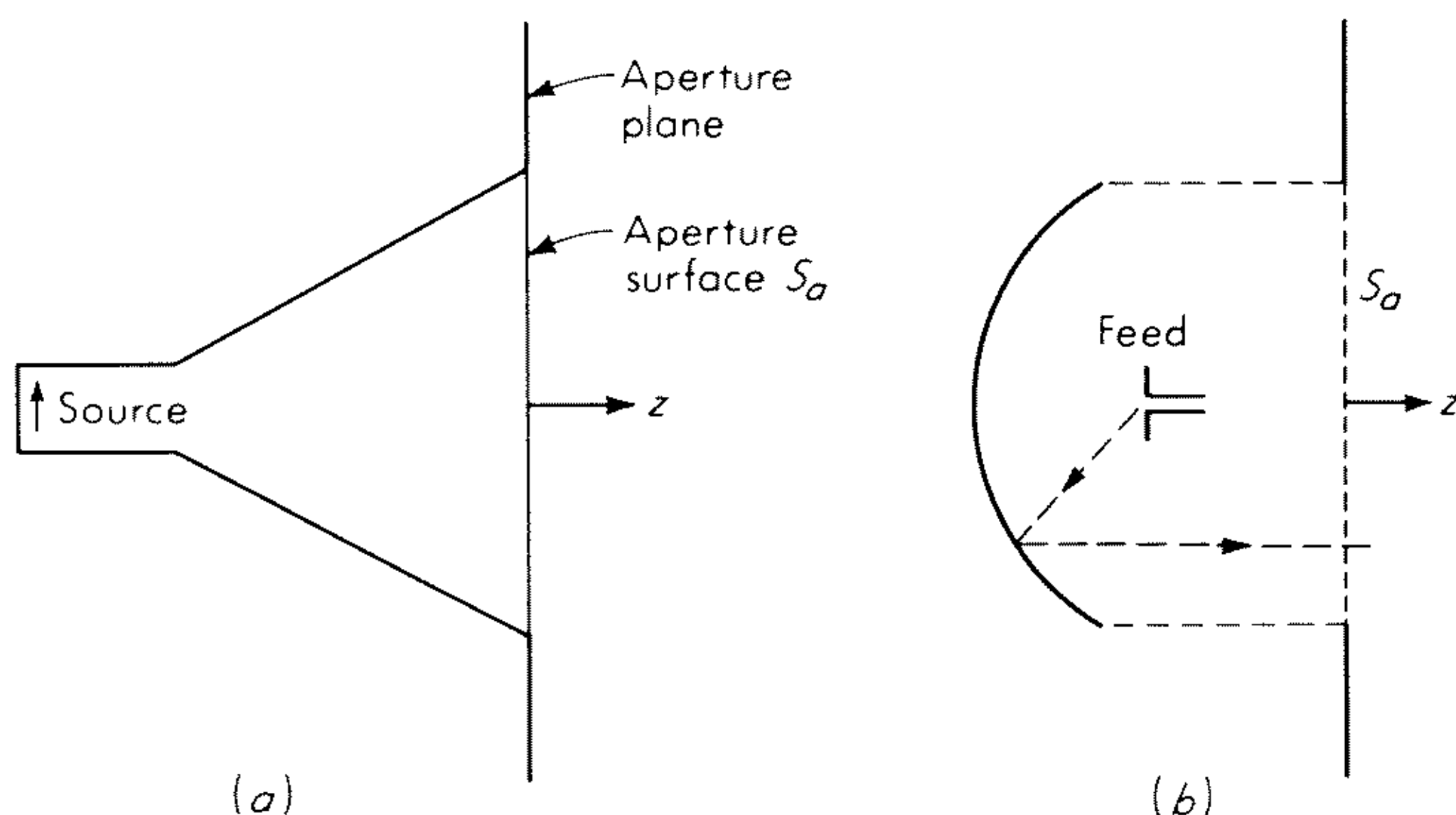


Fig. 3.4 Aperture antenna problems. (a) Horn; (b) reflector.

the antenna and impressed sources and that for $z > 0$ being source-free. For a typical aperture-type antenna such as a horn or parabolic reflector the field on the aperture plane will usually be small outside the surface S_a corresponding to the physical aperture. However, for the purpose of this section we shall assume that the tangential electric field \mathbf{E}_a and tangential magnetic field \mathbf{H}_a are known on the whole aperture plane $z = 0$.

According to the field equivalence principles discussed earlier, it is apparent that we can determine the field in the half space $z > 0$ in terms of electric and magnetic currents $\mathbf{J}_s = \hat{\mathbf{z}} \times \mathbf{H}_a$, $\mathbf{J}_{ms} = -\hat{\mathbf{z}} \times \mathbf{E}_a$ located on the aperture plane, or in terms of electric currents \mathbf{J}_s placed on a perfect magnetic conducting surface coinciding with the aperture plane, or in terms of magnetic currents \mathbf{J}_{ms} with the aperture plane replaced by a perfect electric conductor. In the latter two cases we may use image theory to remove the conducting plane and calculate the same field for $z > 0$ by doubling the current strengths and treating them as radiating into a free space environment.

In all three formulations the fields may be conveniently evaluated by first finding the vector potentials \mathbf{A} and \mathbf{A}_m . We are primarily interested in the far-zone radiation field, for which the solutions for the potentials for the three different formulations are as follows:

$$\mathbf{A}(\mathbf{r}) = \frac{\mu_0}{4\pi r} e^{-jk_0 r} \iint_S \mathbf{J}_s(\mathbf{r}') \exp(jk_0 \hat{\mathbf{r}} \cdot \mathbf{r}') dx' dy' \quad (3.18a)$$

$$\mathbf{A}_m(\mathbf{r}) = \frac{\epsilon_0}{4\pi r} e^{-jk_0 r} \iint_S \mathbf{J}_{ms}(\mathbf{r}') \exp(jk_0 \hat{\mathbf{r}} \cdot \mathbf{r}') dx' dy' \quad (3.18b)$$

$$\mathbf{A}(\mathbf{r}) = \frac{\mu_0}{4\pi r} e^{-jk_0 r} \iint_S 2\mathbf{J}_s(\mathbf{r}') \exp(jk_0 \hat{\mathbf{r}} \cdot \mathbf{r}') dx' dy' \quad (3.19)$$

$$\mathbf{A}_m(\mathbf{r}) = \frac{\epsilon_0}{4\pi r} e^{-jk_0 r} \iint_S 2\mathbf{J}_{ms}(\mathbf{r}') \exp(jk_0 \hat{\mathbf{r}} \cdot \mathbf{r}') dx' dy' \quad (3.20)$$

where $\mathbf{r}' = \hat{\mathbf{x}}x' + \hat{\mathbf{y}}y'$, S is the aperture plane surface, and

$$\mathbf{J}_s = \hat{\mathbf{z}} \times \mathbf{H}_a \quad (3.21a)$$

$$\mathbf{J}_{ms} = -\hat{\mathbf{z}} \times \mathbf{E}_a \quad (3.21b)$$

These solutions are obtained by approximating

$$\frac{e^{-jk_0 R}}{R} \quad \text{by} \quad \frac{e^{-jk_0 r}}{r} \exp(jk_0 \hat{\mathbf{r}} \cdot \mathbf{r}')$$

in the exact integrals for the potentials.

In the far-zone field, \mathbf{E} and \mathbf{H} are related as in a spherical TEM wave, i.e., by

$$\mathbf{E} = -\zeta_0 \hat{\mathbf{r}} \times \mathbf{H} \quad (3.22)$$

The far-zone fields are given in terms of the potentials by the expressions

$$E_\theta = -j\omega A_\theta - j\omega\zeta_0 A_{m\phi} \quad (3.23a)$$

$$E_\phi = -j\omega A_\phi + j\zeta_0 A_{m\theta} \quad (3.23b)$$

If electric currents alone or magnetic currents alone are used, then \mathbf{E} is determined by \mathbf{A} or \mathbf{A}_m alone, respectively. Equations (3.23) still apply, with the appropriate potential equated to zero. The solution (3.23) is obtained by using the formulas giving the field from the potentials and retaining only those terms that decrease as r^{-1} .

It is convenient to have the far-zone electric field expressed directly in terms of the aperture fields. For this purpose let us introduce the following Fourier transforms of the aperture fields:

$$\begin{aligned} \mathbf{f}_t(k_0 \sin \theta \cos \phi, k_0 \sin \theta \sin \phi) \\ = \iint_S \mathbf{E}_a(x, y) e^{jk_0(x \sin \theta \cos \phi + y \sin \theta \sin \phi)} dx dy \end{aligned} \quad (3.24a)$$

$$\begin{aligned} \mathbf{g}_t(k_0 \sin \theta \cos \phi, k_0 \sin \theta \sin \phi) \\ = \iint_S \mathbf{H}_a(x, y) e^{jk_0(x \sin \theta \cos \phi + y \sin \theta \sin \phi)} dx dy \end{aligned} \quad (3.24b)$$

where we have used the result

$$\hat{\mathbf{r}} = \hat{\mathbf{x}} \sin \theta \cos \phi + \hat{\mathbf{y}} \sin \theta \sin \phi + \hat{\mathbf{z}} \cos \theta$$

and dropped the prime on the aperture coordinates x, y . By making use of these Fourier transform relations in (3.18) to (3.20) and (3.23), a straightforward evaluation shows that the far-zone electric field is given by the following expressions for the three formulations being considered (the equivalent two-dimensional form is given in Prob. 3.9):

1. \mathbf{J}_s and \mathbf{J}_{ms} :

$$E_\theta = \frac{jk_0 e^{-jk_0 r}}{4\pi r} [f_x \cos \phi + f_y \sin \phi + \zeta_0 \cos \theta (g_y \cos \phi - g_x \sin \phi)] \quad (3.25a)$$

$$E_\phi = \frac{jk_0 e^{-jk_0 r}}{4\pi r} [\cos \theta (f_y \cos \phi - f_x \sin \phi) - \zeta_0 (g_y \sin \phi + g_x \cos \phi)] \quad (3.25b)$$

2. $2\mathbf{J}_s$:

$$E_\theta = \frac{jk_0 \zeta_0 \cos \theta e^{-jk_0 r}}{2\pi r} (g_y \cos \phi - g_x \sin \phi) \quad (3.26a)$$

$$E_\phi = \frac{-jk_0 \zeta_0 e^{-jk_0 r}}{2\pi r} (g_y \sin \phi + g_x \cos \phi) \quad (3.26b)$$

3. $2\mathbf{J}_{ms}$:

$$E_\theta = \frac{jk_0 e^{-jk_0 r}}{2\pi r} (f_x \cos \phi + f_y \sin \phi) \quad (3.27a)$$

$$E_\phi = \frac{jk_0 \cos \theta e^{-jk_0 r}}{2\pi r} (f_y \cos \phi - f_x \sin \phi) \quad (3.27b)$$

For a typical aperture antenna the aperture dimensions are large in terms of wavelength, and hence the Fourier transforms of the aperture field are highly peaked in the spatial frequency domain, i.e., in k_x, k_y space. Consequently, the radiation patterns are essentially determined by \mathbf{f}_t and \mathbf{g}_t , since the trigonometric functions $\cos \theta$, $\sin \phi$, and $\cos \phi$ are slowly varying functions of the angles. A number of examples that illustrate these remarks are discussed in the next section.

The equations (3.25) to (3.27) are exact and will yield identical results provided the exact aperture fields over the whole aperture plane are used to compute the Fourier transforms.† The results given by (3.25a,b) are the average of (3.26) and (3.27) and suffer from the disadvantage that they require a knowledge of both the tangential electric and magnetic field on the aperture plane. In practice the far-zone electric field is calculated by using one of the three formulations given together with only an approximate knowledge

†When the correct aperture fields are used in (3.25), the separate parts involving the functions \mathbf{f} and \mathbf{g} are equal, as comparison with (3.26) and (3.27) shows. Thus for $z < 0$, where $\pi/2 \leq \theta \leq \pi$ and $\cos \theta$ is negative, the fields given by (3.25) vanish, which is in accord with the field equivalence principle.

of the fields on the aperture plane. In this case the three formulations yield only approximate results which in general do not agree with each other. It is difficult to say a priori which formulation would yield the most accurate results, since this depends on the degree of approximation involved in specifying the aperture fields. It is usually more convenient to use either (3.26) or (3.27), since these require a knowledge of only the tangential magnetic field or tangential electric field, respectively, on the aperture plane.

If the formulation based on the use of an equivalent magnetic current sheet alone is used, all of the results derived in Sec. 3.2 for an aperture in a conducting screen are applicable. In particular, note that (3.14) and (3.27) are identical.

3.5 Radiation Patterns from Typical Aperture Fields

In this section we shall illustrate the theory developed in the preceding sections by evaluating the radiation patterns from a number of typical aperture field distributions. All of the significant features occur for an aperture electric field that is linearly polarized along a single coordinate axis. Therefore, for simplicity we shall assume that the aperture tangential electric field has only an x component.

Uniform Aperture Field

As a first example consider an aperture electric field $\mathbf{E}_a = E_0 \hat{\mathbf{x}}$ that is equal to a constant $E_0 \hat{\mathbf{x}}$ over a rectangular aperture surface $|x| \leq a$, $|y| \leq b$ and equal to zero outside this region. The Fourier transform of this aperture field gives the function \mathbf{f}_t as

$$\mathbf{f}_t = \hat{\mathbf{x}} 4ab E_0 \frac{\sin(k_0 a \sin \theta \cos \phi) \sin(k_0 b \sin \theta \sin \phi)}{(k_0 a \sin \theta \cos \phi)(k_0 b \sin \theta \sin \phi)} \quad (3.28)$$

The electric field in the two principal planes $\phi = 0$ and $\phi = \pi/2$ is given by (3.27) and is

$$\begin{aligned} E_\theta &= \frac{jk_0 ab E_0}{2\pi r} e^{-jk_0 r} f_x(\theta, \phi = 0) \\ &= \frac{j2k_0 ab E_0}{\pi r} e^{-jk_0 r} \frac{\sin(k_0 a \sin \theta)}{k_0 a \sin \theta} \end{aligned} \quad (3.29a)$$

$$\begin{aligned} E_\phi &= -\frac{jk_0 ab E_0 \cos \theta}{2\pi r} e^{-jk_0 r} f_x\left(\theta, \phi = \frac{\pi}{2}\right) \\ &= -\frac{j2k_0 ab E_0 \cos \theta}{\pi r} e^{-jk_0 r} \frac{\sin(k_0 b \sin \theta)}{k_0 b \sin \theta} \end{aligned} \quad (3.29b)$$

When $k_0 a$ and $k_0 b$ are large, a sharp main lobe is produced. The first null occurs when $k_0 a \sin \theta = \pi$ and $k_0 b \sin \theta = \pi$. For $k_0 a$ and $k_0 b$ large the corresponding values of θ are given to good accuracy by $\pi/k_0 a = \lambda_0/2a$ and $\lambda_0/2b$, respectively. To the same order of approximation the half-power beam widths in the princi-

pal planes are given by $0.88 \lambda_0/2a$ and $0.88 \lambda_0/2b$. It is thus apparent that the main-lobe angular width is inversely proportional to the aperture dimensions measured in wavelengths. For this reason the directivity is proportional to the aperture area measured in wavelengths squared. The pattern function

$$\frac{\sin(k_0 a \sin \theta)}{k_0 a \sin \theta}$$

is illustrated in Fig. 3.5. The side lobes decrease in amplitude as the point of observation moves away from the direction of the main lobe. The first side lobe has an amplitude which is a factor of 4.6 (or 13.3 db) below the main-lobe

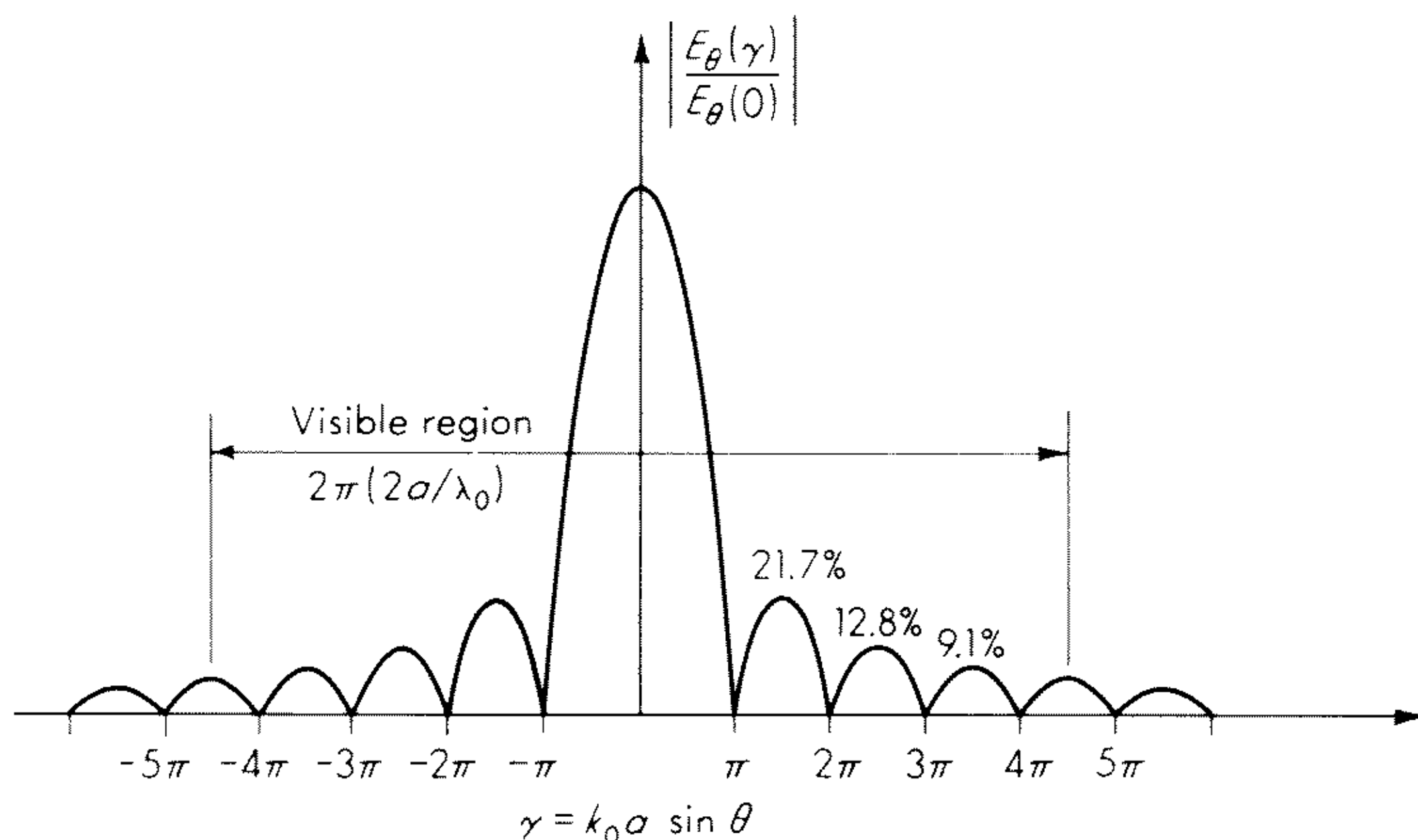


Fig. 3.5 Radiation pattern for a uniform aperture distribution ($\phi = 0$).

peak. The portion of the pattern shown in Fig. 3.5 that corresponds to physical space $-\pi/2 \leq \theta \leq \pi/2$ occurs for values of $\gamma = k_0 a \sin \theta$ between $-k_0 a$ and $k_0 a$ and represents the visible portion of the pattern.

In order to determine the directivity it is necessary to evaluate the total radiated power. An expression for the radiated power may be obtained from the expressions for the far-zone electric field. However, there is no simple way to evaluate the integral of $(1/2\zeta_0)(|E_\theta|^2 + |E_\phi|^2)$ over the surface of a sphere $0 \leq \theta \leq \pi$. As an alternative, a uniform aperture field such as $\mathbf{E}_a = E_0 \hat{\mathbf{x}}$, $\mathbf{H}_a = \zeta_0^{-1} E_0 \hat{\mathbf{y}}$ over a finite aperture $|x| \leq a$, $|y| \leq b$ and zero outside could be assumed. In this case the radiated power may be obtained by a simple integration of the complex Poynting vector over the aperture and gives $P = 4abE_0^2/2\zeta_0$. The far-zone electric field can be obtained from (3.25), where $\zeta_0 g_y$ would be equal to f_x in the present case. It can readily be verified that the maximum power density per unit solid angle is $2(k_0 ab)^2 E_0^2 / (\pi^2 \zeta_0)$ in the direction $\theta = 0$. Thus the maximum directivity is

$$D(\theta = 0, \phi) = 4\pi \frac{4ab}{\lambda_0^2}$$

or 4π times the aperture area measured in wavelengths squared. An alternative estimate of the directivity may be obtained by assuming that all of the radiated energy flows into an angular region bounded by the half-power beam widths. On this basis the directivity comes out to be

$$D = \frac{4\pi ab}{(0.44)^2 \lambda_0^2} = 4\pi \frac{5.2ab}{\lambda_0^2}$$

which is only 1.15 db larger. These expressions for directivity should be regarded as only indicating the dependence of the directivity on the aperture area, since a uniform aperture field of the kind that was assumed is not physically realizable.

Tapered Aperture Fields

It can be anticipated that tapering the amplitude of the aperture field down to a smaller value at the edges of the aperture is equivalent to an effective reduction in the aperture area and will result in a broader main lobe and a lower directivity. Both theory and experimental measurements verify these conclusions. However, tapering the aperture field distribution has the great advantage of giving a large reduction in the side-lobe amplitude, as the examples below will illustrate.

If the aperture field $E_{ax}(x, y)$ is separable, it can be expressed as a product $E_1(x)E_2(y)$, and the corresponding Fourier transform is then the product of the transforms of $E_1(x)$ and $E_2(y)$. We can, therefore, examine the effect of aperture field tapering by considering the one-dimensional problem only. That is, $E_1(x)$ determines the pattern in the principal plane $\phi = 0$, while $E_2(y)$ determines the pattern in the plane $\phi = \pi/2$.

As a first example consider a cosine distribution $E_1(x) = E_0 \cos(\pi x/2a)$. The Fourier transform of $E_1(x)$ is readily evaluated, and we find that in the $\phi = 0$ plane the pattern will be proportional to

$$\int_{-a}^a E_0 \cos \frac{\pi x}{2a} e^{jk_0 x \sin \theta} dx = \frac{E_0 \pi a \cos(k_0 a \sin \theta)}{(\pi/2)^2 - (k_0 a \sin \theta)^2} \quad (3.30)$$

The normalized pattern is illustrated in Fig. 3.6a. The angular width of the main lobe is $3\lambda_0/2a$ and the half-power beam width is $1.2\lambda_0/2a$. The first side lobe has an amplitude 23 db below the main-lobe maximum. This is approximately 10 db smaller than for the case of the uniform aperture field, but it is obtained at the expense of increased beam width and a smaller directivity.

As a second example consider a triangular distribution $E_0(1 - |x|/a)$. The Fourier transform of this aperture field is

$$\int_{-a}^a E_0 \left(1 - \frac{|x|}{a}\right) e^{jk_0 x \sin \theta} dx = a E_0 \left[\frac{\sin(1/2 k_0 a \sin \theta)}{(1/2 k_0 a \sin \theta)} \right]^2 \quad (3.31)$$

The triangular distribution gives a pattern with double zeros at each null, as

illustrated in Fig. 3.6b. The first nulls occur when $\theta = 2\lambda_0/2a$, the half-power beam width is $1.28\lambda_0/2a$, and the first side lobe is 26.4 db below the main-lobe peak.

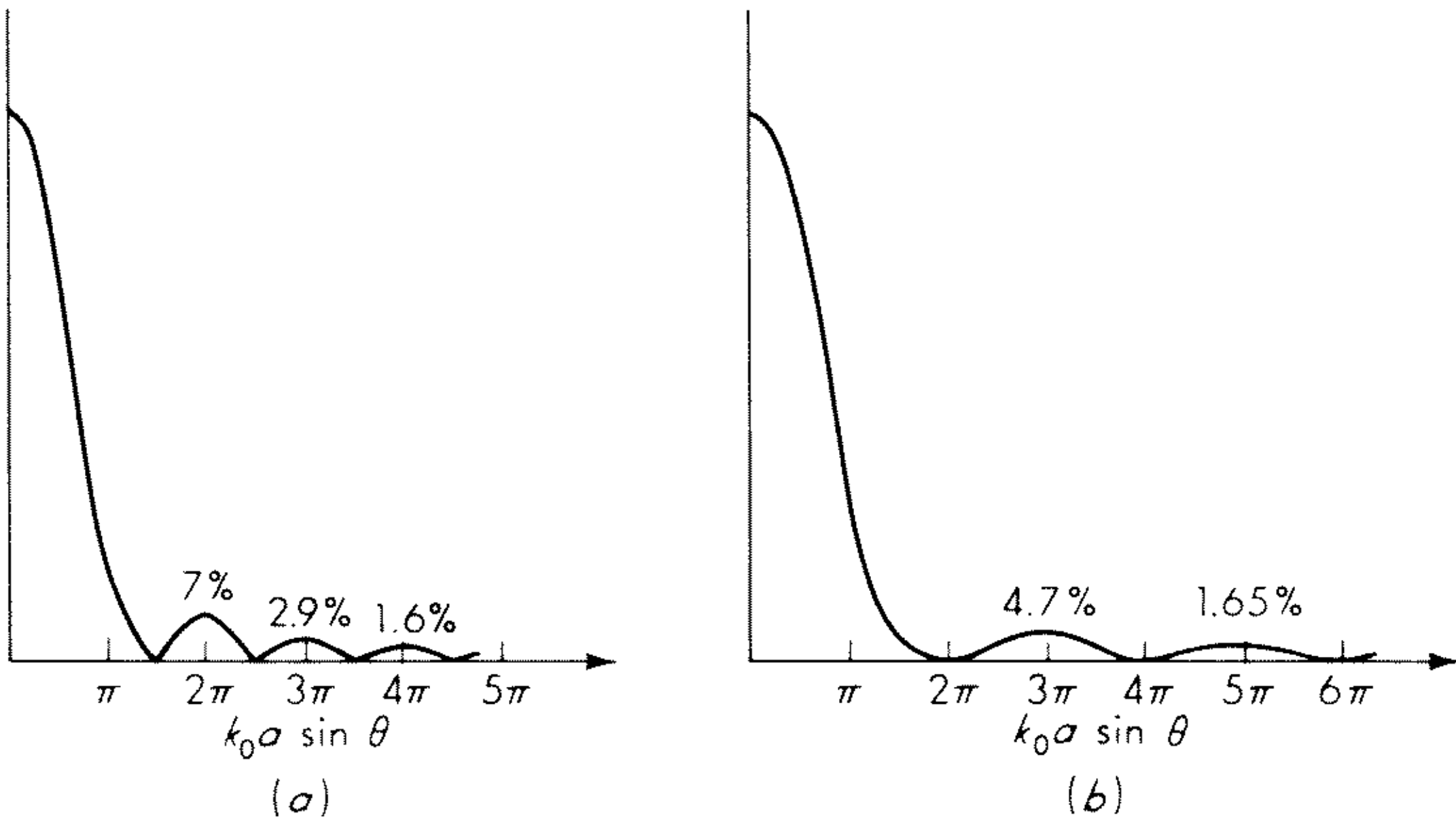


Fig. 3.6 Radiation patterns from tapered aperture distributions. (a) Cosine distribution; (b) triangular distribution.

Aperture Field with Linear Phase Variation

The preceding examples dealt with aperture fields having a constant uniform phase for which maximum radiation occurred in a direction normal to the aperture. If the aperture field has a linear phase variation, the main lobe will be swung away from the aperture normal. For specific results let us consider an aperture field of the form

$$E_{ax}(x) = E_1(x)e^{-jk_0x \sin \theta_0} \quad (3.32)$$

The Fourier transform of this field is

$$\int_{-a}^a E_1(x)e^{jk_0x (\sin \theta - \sin \theta_0)} dx = f_x[k_0(\sin \theta - \sin \theta_0)] \quad (3.33)$$

where f_x is the Fourier transform of $E_1(x)$. The effect of the linear phase variation is simply to replace $\sin \theta$ by $\sin \theta - \sin \theta_0$ in the Fourier transform of the constant-phase aperture field. For the uniform aperture field with a linear phase variation the pattern is therefore proportional to

$$\frac{\sin [k_0a(\sin \theta - \sin \theta_0)]}{k_0a(\sin \theta - \sin \theta_0)}$$

The main-lobe peak now occurs when $\theta = \theta_0$ for this pattern. Another effect of a linear phase variation is to increase the width of the main lobe, since the projected width of the aperture in the direction θ_0 is a factor $\cos \theta_0$ smaller than the physical width. We can demonstrate this effect analytically. The half-

power beam width occurs for $k_0 a (\sin \theta - \sin \theta_0) = 0.44\pi$. If we expand the quantity $k_0 a (\sin \theta - \sin \theta_0)$ in a Taylor series about θ_0 , we obtain

$$k_0 a (\sin \theta - \sin \theta_0) \approx k_0 a \cos \theta_0 (\theta - \theta_0)$$

for small values of $\theta - \theta_0$. When we solve for the value of $\theta - \theta_0$ at the half-power point, we find that $\theta - \theta_0 = 0.44 \lambda_0 / (2a \cos \theta_0)$, which gives a half-power beam width of $0.88 \lambda_0 / (2a \cos \theta_0)$. Thus the beam width is increased by a factor $(\cos \theta_0)^{-1}$, which may be viewed as the result of having reduced the projected width of the aperture in the direction θ_0 by the factor $\cos \theta_0$.

Directivity

In order to find the maximum directivity of an aperture antenna it is necessary to evaluate the total radiated power. The latter may be found by integrating the flux of the real part of the complex Poynting vector through the spherical surface $\theta \leq \pi$ at infinity. The complex Poynting vector may be found in terms of the far-zone electric field given by (3.25), (3.26), or (3.27). Alternatively, the radiated power may be found in terms of the Fourier transform of the electric field on the aperture plane by using the general formula (3.9) or (3.15e) for a slit aperture. As a general rule the integrals involved cannot be evaluated except by numerical methods.

An approximate method of obtaining the directivity can be obtained for the case when the tangential electric and magnetic fields in the aperture can be assumed to be related as in a plane TEM wave. This assumption is approximately correct when the aperture fields are slowly varying over distances comparable with a wavelength and are nearly of uniform phase over the aperture, i.e., maximum radiation in a direction along the normal to the aperture. In this case $\zeta_0 \mathbf{g}_t = \hat{\mathbf{z}} \times \mathbf{f}_t$ and (3.25) for the far-zone electric field becomes

$$E_\theta = \frac{jk_0 e^{-jk_0 r}}{4\pi r} (1 + \cos \theta) (f_x \cos \phi + f_y \sin \phi) \quad (3.34a)$$

$$E_\phi = \frac{jk_0 e^{-jk_0 r}}{4\pi r} (1 + \cos \theta) (f_y \cos \phi - f_x \sin \phi) \quad (3.34b)$$

The power per unit solid angle is given by

$$\frac{r^2}{2\zeta_0} (|E_\theta|^2 + |E_\phi|^2) = \frac{k_0^2}{32\pi^2 \zeta_0} (1 + \cos \theta)^2 (|f_x|^2 + |f_y|^2) \quad (3.35)$$

This expression is usually of form such that, after multiplication by $\sin \theta d\theta d\phi$, the integration cannot be performed. Instead of using the above formulation, the radiated power is obtained by integrating $|\mathbf{E}_a|^2 / 2\zeta_0$ over the aperture; thus

$$P = \frac{1}{2\zeta_0} \iint_{s_a} |\mathbf{E}_a|^2 dx dy \quad (3.36)$$

This expression can often be evaluated but must be regarded as only an approximate result, since it does not agree in general with the results obtained by using (3.35). The inconsistency between the two stems from the fact that the assumptions made about the field on the aperture plane are not in accord with Maxwell's equations. For example, the far-zone field E_ϕ will generally not vanish on the aperture plane, which contradicts the assumption made earlier that the tangential electric field on the aperture plane was zero outside the aperture surface. The field is uniquely determined by either the tangential electric or magnetic field on the aperture plane, so we are not at liberty to arbitrarily specify both. In spite of these objections, the formula (3.36) is commonly used and does give a useful estimate of the directivity from the expression

$$D = \frac{4\pi}{\lambda_0^2} \frac{|f_t(\theta = 0)|^2}{\iint_{S_a} |\mathbf{E}_a|^2 dx dy} = \frac{4\pi}{\lambda_0^2} \frac{\left| \iint_{S_a} \mathbf{E}_a dx dy \right|^2}{\iint_{S_a} |\mathbf{E}_a|^2 dx dy} \quad (3.37)$$

In formulating (3.37) we have used (3.35) with $\theta = 0$ for the maximum power per unit solid angle and replaced \mathbf{f}_t by its Fourier transform representation in terms of the aperture electric field.

3.6 General Formulas for Scattering and Diffraction

The theory developed in the preceding sections has shown that the far-zone radiation field can be evaluated in a straightforward manner provided either the tangential electric or magnetic field (or both) is known everywhere on the infinite aperture plane. However, in general it is not possible to evaluate exactly the tangential fields produced on an aperture plane by a given antenna system. Consequently, approximate techniques must be employed in order to readily obtain reasonably accurate estimates of the field on the aperture plane. Suitable methods based on geometrical optics concepts are discussed in later chapters. In this section we shall present some general formulas for the field radiated by a current source, in the presence of one or more obstacles such as a reflector, that can be used as a basis for finding approximate values of the fields on the aperture plane or for determining the radiation field directly. When the far-zone radiation field is found from an aperture field, with the latter determined by a separate analysis, the procedure is sometimes called the *aperture field method*. The other basic procedure for treating reflector-type antennas is based on an approximate determination of the induced currents on the reflector and the evaluation of the radiation field directly in terms of these currents. The latter procedure, called the *induced-current method*, has its basis in the general formulas developed below.

The literature on electromagnetic scattering and diffraction is very extensive and cannot be reviewed in detail here. Many of the results that have been obtained are of interest in connection with antennas even though they are

most often not directly applicable. The interested reader is referred to a very extensive review that has been given by Bouwkamp.¹⁵

Consider current sources $\mathbf{J}(\mathbf{r}')$, $\mathbf{J}_m(\mathbf{r}')$ radiating in the presence of one or more scattering obstacles as illustrated in Fig. 3.7. Let each obstacle be sur-

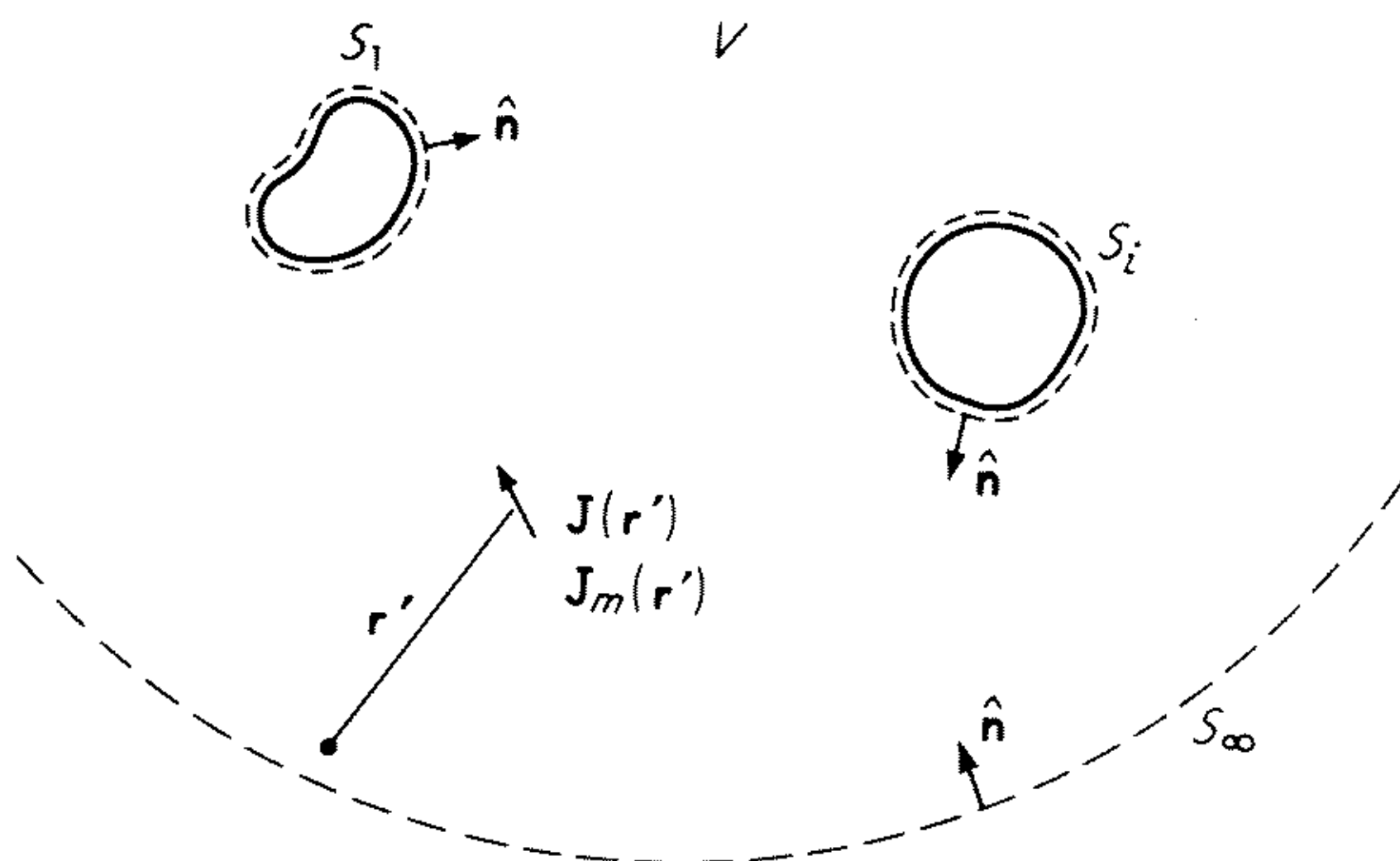


Fig. 3.7 A current source in the presence of scattering obstacles.

rounded by a closed surface S_i for the i th obstacle and let S_∞ denote the surface of a sphere of infinite radius. In the volume V bounded by the surface $S = S_1 + S_2 + \cdots + S_i + \cdots + S_\infty$ the electric and magnetic fields $\mathbf{E}(\mathbf{r})$ and $\mathbf{H}(\mathbf{r})$ are solutions of [see (1.5) and (1.23) with magnetic sources added]

$$(\nabla^2 + k_0^2)\mathbf{E} = j\omega\mu_0\mathbf{J} + \nabla \frac{\rho}{\epsilon_0} + \nabla \times \mathbf{J}_m \quad (3.38a)$$

$$(\nabla^2 + k_0^2)\mathbf{H} = -\nabla \times \mathbf{J} + j\omega\epsilon_0\mathbf{J}_m + \nabla \frac{\rho_m}{\mu_0} \quad (3.38b)$$

The field must also satisfy the boundary conditions on the surfaces of all scattering obstacles and the radiation condition on S_∞ .

We may regard the field as made up from a linear sum of the primary or incident field radiated directly by the sources into unbounded free space plus the field scattered by the various obstacles that are present. The primary field is obtained by multiplying the source terms in (3.38) by the negative of the free space scalar Green's function

$$G_0 = \frac{e^{-jk_0|\mathbf{r}-\mathbf{r}'|}}{4\pi|\mathbf{r}-\mathbf{r}'|} \quad (3.39)$$

and integrating over the source coordinates. Thus we have

$$\mathbf{E}_i(\mathbf{r}) = -\int_V \left[j\omega\mu_0\mathbf{J}(\mathbf{r}') + \frac{1}{\epsilon_0} \nabla' \rho(\mathbf{r}') + \nabla' \times \mathbf{J}_m(\mathbf{r}') \right] G_0(\mathbf{r}|\mathbf{r}') dV' \quad (3.40a)$$

$$\mathbf{H}_i(\mathbf{r}) = -\int_V \left[-\nabla' \times \mathbf{J}(\mathbf{r}') + j\omega\epsilon_0\mathbf{J}_m(\mathbf{r}') + \frac{1}{\mu_0} \nabla' \rho_m(\mathbf{r}') \right] G_0(\mathbf{r}|\mathbf{r}') dV' \quad (3.40b)$$

for the incident field.

The scattered field may be viewed as arising from the induced conduction and polarization currents that flow in and on the various scattering obstacles which are present. These secondary sources are external to the volume V bounded by the surfaces S_i in Fig. 3.7. Consequently, by Love's field equivalence principle the scattered field $\mathbf{E}_s, \mathbf{H}_s$ in V can be determined from equivalent current sources $\mathbf{J}_s = \hat{\mathbf{n}} \times \mathbf{H}_s, \mathbf{J}_{ms} = -\hat{\mathbf{n}} \times \mathbf{E}_s$ placed on the surfaces S_i surrounding the scattering obstacles. If we note that Love's field equivalence principle also states that equivalent sources $-\hat{\mathbf{n}} \times \mathbf{H}_i$ and $\hat{\mathbf{n}} \times \mathbf{E}_i$ placed on the surfaces S_i reproduce the incident field inside S_i but radiate a null field outside S_i , then it is clear that reversing the sign of these latter equivalent sources will still result in a null field radiated into the region V . Thus we can equally well use equivalent sources

$$\mathbf{J}_s = \hat{\mathbf{n}} \times (\mathbf{H}_s + \mathbf{H}_i) = \hat{\mathbf{n}} \times \mathbf{H} \quad (3.41a)$$

$$\mathbf{J}_{ms} = -\hat{\mathbf{n}} \times (\mathbf{E}_s + \mathbf{E}_i) = -\hat{\mathbf{n}} \times \mathbf{E} \quad (3.41b)$$

where \mathbf{E} and \mathbf{H} are the total fields in V , to reproduce the scattered field in V . These equivalent sources will now produce a field $-\mathbf{E}_i, -\mathbf{H}_i$ inside the surfaces S_i instead of a null field. However, this does not affect the field in the region of interest V .

Before proceeding further with the derivation of expressions for the total field in V it will be convenient to manipulate (3.40) into an alternative form. If we use the results

$$\nabla'(\rho G_0) = G_0 \nabla' \rho + \rho \nabla' G_0 \quad \nabla' \times (\mathbf{J}_m G_0) = G_0 \nabla' \times \mathbf{J}_m - \mathbf{J}_m \times \nabla' G_0$$

and the integral transformations

$$\begin{aligned} \int_V \nabla'(\rho G_0) dV' &= \oint_S \rho G_0 d\mathbf{S}' = 0 \\ \int_V \nabla' \times (\mathbf{J}_m G_0) dV' &= -\oint_S G_0 \mathbf{J}_m \times d\mathbf{S}' = 0 \end{aligned}$$

because ρ and \mathbf{J}_m are zero on S , we can express the incident fields in the form

$$\mathbf{E}_i(\mathbf{r}) = \int_V \left[-j\omega\mu_0 \mathbf{J}(\mathbf{r}') G_0 + \frac{\rho(\mathbf{r}')}{\epsilon_0} \nabla' G_0 - \mathbf{J}_m(\mathbf{r}') \times \nabla' G_0 \right] dV' \quad (3.42a)$$

$$\mathbf{H}_i(\mathbf{r}) = \int_V \left[\mathbf{J}(\mathbf{r}') \times \nabla' G_0 - j\omega\epsilon_0 \mathbf{J}_m(\mathbf{r}') G_0 + \frac{\rho_m(\mathbf{r}')}{\mu_0} \nabla' G_0 \right] dV' \quad (3.42b)$$

We can evaluate the scattered field in V from the equivalent surface currents given by (3.41) if we introduce vector potential functions \mathbf{A} and \mathbf{A}_m and invoke a Lorentz condition. If we use both the vector and scalar potentials, we require a knowledge of both the currents and the associated charge distributions. The formulas (3.42) are equivalent to the results which would have been obtained by introducing the vector and scalar potentials first. If we wish to use

these expressions to evaluate the scattered field by introducing the equivalent surface sources in place of the volume sources, we must determine the equivalent surface charge distributions. This latter source is readily found in terms of the discontinuity in the normal components of the fields across the surface S_i . Since the equivalent currents given by (3.41) produce the field $\mathbf{E}_s, \mathbf{H}_s$ outside the S_i and $-\mathbf{E}_i, -\mathbf{H}_i$ inside the S_i , it is clear that the equivalent surface charge distributions are given by

$$\rho_s = \epsilon_0[\hat{\mathbf{n}} \cdot \mathbf{E}_s - \hat{\mathbf{n}} \cdot (-\mathbf{E}_i)] = \epsilon_0 \hat{\mathbf{n}} \cdot \mathbf{E} \quad (3.43a)$$

$$\rho_{ms} = \mu_0[\hat{\mathbf{n}} \cdot \mathbf{H}_s - \hat{\mathbf{n}} \cdot (-\mathbf{H}_i)] = \mu_0 \hat{\mathbf{n}} \cdot \mathbf{H} \quad (3.43b)$$

When we make use of the equivalent sources given by (3.41) and (3.43) together with an adaptation of (3.42) to surface sources, we readily find that the scattered field is given by

$$\mathbf{E}_s(\mathbf{r}) = \oint_S [-j\omega\mu_0 \hat{\mathbf{n}} \times \mathbf{H}G_0 + \hat{\mathbf{n}} \cdot \mathbf{E} \nabla' G_0 + (\hat{\mathbf{n}} \times \mathbf{E}) \times \nabla' G_0] dS' \quad (3.44a)$$

$$\mathbf{H}_s(\mathbf{r}) = \oint_S [(\hat{\mathbf{n}} \times \mathbf{H}) \times \nabla' G_0 + j\omega\epsilon_0 \hat{\mathbf{n}} \times \mathbf{E}G_0 + \hat{\mathbf{n}} \cdot \mathbf{H} \nabla' G_0] dS' \quad (3.44b)$$

In these expressions for the scattered field the integration is taken over the surfaces S_i surrounding each obstacle. The surface S_∞ at infinity does not contribute, because the equivalent sources on this surface would reproduce the total field outside this surface but contribute only a null field to the region V (Love's principle again).

The results given by (3.42) and (3.44) were first developed by Larmor and Tedone (see Baker and Copson¹⁶ for details) and rederived by Stratton and Chu^{17,18} by using a vector form of Green's theorem. The derivation based on Green's theorem is outlined in Exercise 3.3.

In practice it is often desirable to find an approximate expression for the scattered field in terms of approximate equivalent sources located on an open surface with a boundary C . Formulas (3.44) are not directly applicable, since they hold only for the case of sources distributed over a closed surface. When we have an open surface and postulate equivalent current distributions that have a nonvanishing normal component at the boundary C , the continuity equation requires that line charges of density given by (in an exact solution these line charges would be zero because the edge condition requires the normal component of current to vanish at the edge; see Sec. 1.7)

$$j\omega\rho_l = \hat{\boldsymbol{\tau}} \cdot \mathbf{J}_s \quad (3.45a)$$

$$j\omega\rho_{ml} = \hat{\boldsymbol{\tau}} \cdot \mathbf{J}_{ms} \quad (3.45b)$$

be placed on the contour C . In (3.45a,b) $\hat{\boldsymbol{\tau}}$ is a unit vector perpendicular to C and directed outward from the boundary but in the tangent plane to the open surface S at the edge C . Equations (3.45) simply state that the rate at which charge accumulates on the boundary C is equal to the component of the surface

current directed toward the edge. If the line charges are added, then (3.44a,b) taken over an open surface together with the line integrals

$$\oint_C \frac{\hat{\mathbf{t}} \cdot \mathbf{J}_s}{j\omega\epsilon_0} \nabla' G_0 dl, \oint_C \frac{\hat{\mathbf{t}} \cdot \mathbf{J}_{ms}}{j\omega\mu_0} \nabla' G_0 dl \quad (3.46)$$

will be exact expressions for the fields radiated from specified sources located on an open surface. If instead the vector potential functions \mathbf{A} and \mathbf{A}_m are evaluated first, we can dispense with the line integrals, since these potentials are determined by the currents alone. A Lorentz condition must then, of course, be used to eliminate the scalar potentials so the fields can be found in terms of \mathbf{A} and \mathbf{A}_m alone. The choice of method to be used is one of individual preference. The necessary line charges and contour integrals were first introduced by Kottler (see Baker and Copson¹⁶). The need for these line sources is also discussed in an illuminating way in a recent paper by Sancer.³⁰

Exercise 3.3 Let $\mathbf{G}(\mathbf{r}|\mathbf{r}')$ be the dyadic Green's function for Helmholtz's equation as given by (2.27) in Sec. 2.6. By direct expansion verify that

$$-\nabla' \cdot [\mathbf{E} \times (\nabla' \times \mathbf{G}) + (\nabla' \times \mathbf{E}) \times \mathbf{G} + \mathbf{E} \nabla' \cdot \mathbf{G} - \mathbf{G} \nabla' \cdot \mathbf{E}] = (\nabla'^2 \mathbf{E}) \cdot \mathbf{G} - \mathbf{E} \cdot \nabla'^2 \mathbf{G}$$

By substituting for the right-hand side from the equations satisfied by \mathbf{G} and \mathbf{E} , show that

$$\begin{aligned} \mathbf{E}(\mathbf{r}) = & \int_V \left[-j\omega\mu_0 \mathbf{J} - \nabla' \frac{\rho}{\epsilon_0} - \nabla' \times \mathbf{J}_m \right] \cdot \mathbf{G} dV' \\ & + \oint_S [\mathbf{E} \times (\nabla' \times \mathbf{G}) + (\nabla' \times \mathbf{E}) \times \mathbf{G} + \mathbf{E} \nabla' \cdot \mathbf{G} - \mathbf{G} \nabla' \cdot \mathbf{E}] \cdot \hat{\mathbf{n}} dS' \end{aligned}$$

by using the divergence theorem. Next show that $\nabla'(\rho/\epsilon_0) \cdot \mathbf{G} = \nabla' \cdot (\mathbf{G} \rho/\epsilon_0) - (\rho/\epsilon_0) \nabla' \cdot \mathbf{G}$, $\nabla' \cdot \mathbf{G} = \nabla' G_0$, $\nabla' \times \mathbf{G} = \nabla' G_0 \times \mathbf{I} = \mathbf{I} \times \nabla' G_0$ and that $\hat{\mathbf{n}} \cdot \mathbf{E} \cdot (\nabla' \times \mathbf{G}) = \hat{\mathbf{n}} \times \mathbf{E} \cdot (\mathbf{I} \times \nabla' G_0) = (\hat{\mathbf{n}} \times \mathbf{E}) \times \nabla' G_0$. Note also that $\nabla' \times \mathbf{E}$ can be replaced by $-j\omega\mu_0 \mathbf{H}$ on S . When these results are used in the expression for $\mathbf{E}(\mathbf{r})$ and the volume integral of $\nabla' \cdot (\mathbf{G} \rho/\epsilon_0)$ is converted to a surface integral to cancel the contribution from the term $\mathbf{G} \nabla' \cdot \mathbf{E}$, the result given by the sum of (3.42a) and (3.44a) is obtained. A similar method may be used to derive the expression for $\mathbf{H}(\mathbf{r})$.

If the surface S consists of an open conducting surface, then on S we have $\hat{\mathbf{n}} \times \mathbf{E} = 0$ and $\hat{\mathbf{n}} \cdot \mathbf{E} = \rho_s/\epsilon_0$. The term $\hat{\mathbf{n}} \cdot \mathbf{E} \nabla' G_0$ in (3.44a) can now be written as

$$\frac{\nabla'_s \cdot \mathbf{J}_s}{-j\omega\epsilon_0} \nabla' G_0$$

where ∇'_s is the surface del operator. We can also write

$$\frac{\nabla'_s \cdot \mathbf{J}_s}{-j\omega\epsilon_0} \nabla' G_0 = \nabla'_s \cdot \left(\frac{\mathbf{J}_s \nabla' G_0}{-j\omega\epsilon_0} \right) + \frac{\mathbf{J}_s \cdot \nabla'_s \nabla' G_0}{j\omega\epsilon_0}$$

The surface integral of the divergence may be converted to a line integral around the boundary of the open surface by using the divergence theorem.

The line integral is easily seen to be the negative of that given by (3.46); and since the latter must be added to (3.44a) for an open surface, we finally get, after replacing $\hat{\mathbf{n}} \times \mathbf{H}$ by \mathbf{J}_s ,

$$\mathbf{E}_s(\mathbf{r}) = \int_S \left(-j\omega\mu_0 \mathbf{J}_s G_0 + \frac{\mathbf{J}_s \cdot \nabla' \nabla' G_0}{j\omega\epsilon_0} \right) dS'$$

since $\mathbf{J}_s \cdot \nabla'_s = \mathbf{J}_s \cdot \nabla'$. This expression is readily evaluated for the far-zone radiation field, i.e., to order $1/r$, by noting that in the far zone $\nabla' G_0 = -jk_0 \hat{\mathbf{R}} G_0 = -jk_0 \hat{\mathbf{r}} G_0$ to terms of order $1/r$. Note that $\hat{\mathbf{R}}$ and $\hat{\mathbf{r}}$ are essentially parallel unit vectors whenever $r \gg r'$. We thus find that the radiation field is given by

$$\mathbf{E}_s(\mathbf{r}) = -\frac{j\omega\mu_0 e^{-jk_0 r}}{4\pi r} \int_S (\mathbf{J}_s - \hat{\mathbf{r}} \cdot \mathbf{J}_s \hat{\mathbf{r}}) e^{jk_0 \hat{\mathbf{r}} \cdot \mathbf{r}'} dS' \quad (3.47)$$

This result is similar to that obtained in Chap. 2 for the far-zone field radiated by a volume distribution of current [see Eq. (2.23b)].

To illustrate how (3.44a) is used in practice consider a reflector illuminated by a dipole source as in Fig. 3.8. If we assume that the primary field \mathbf{E}_i , \mathbf{H}_i from the dipole is known, we can obtain an approximate expression for the

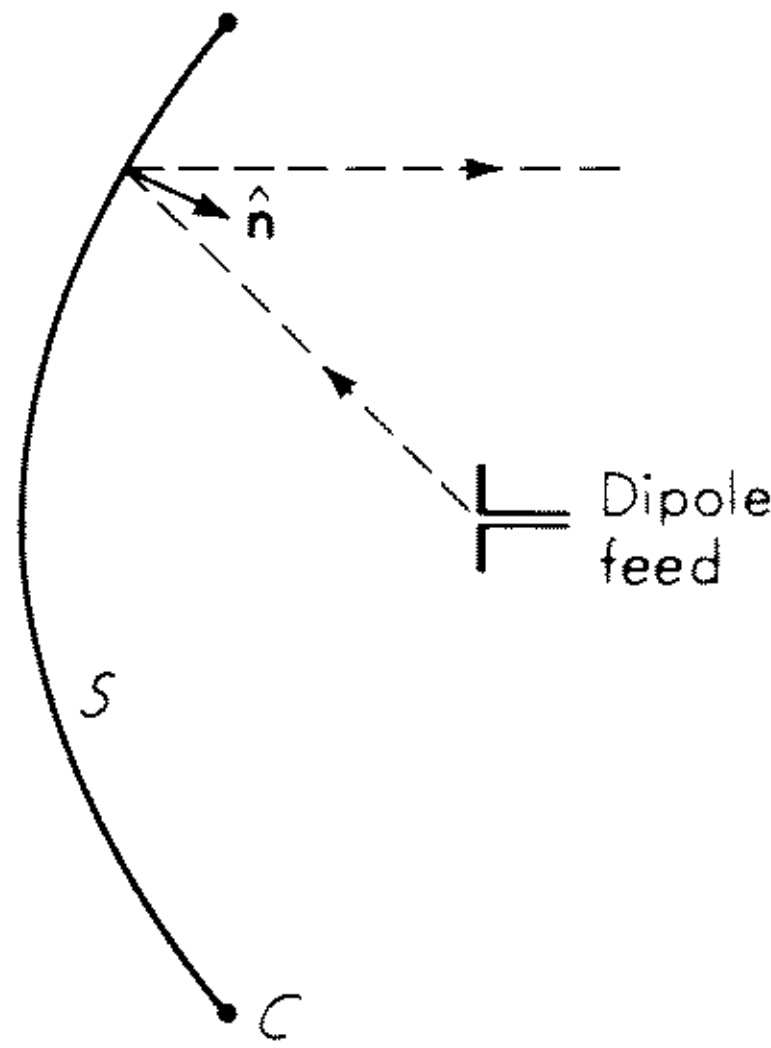


Fig. 3.8 A reflector-type antenna.

induced currents on the reflector as follows. On the shadow side of the reflector we may assume that the primary field is zero. (Because of diffraction this is only approximately true.) On the illuminated side $\hat{\mathbf{n}} \times \mathbf{E}$ is zero and $\hat{\mathbf{n}} \times \mathbf{H}$ can be approximated by $2\hat{\mathbf{n}} \times \mathbf{H}_i$ by considering that each point of the reflector behaves locally as though it were part of an infinite conducting plane. The radiation field may now be found from this induced current alone by using the vector potential \mathbf{A} . If (3.44a) is to be used, we must add the line charge contribution given by the contour integral involving $\mathbf{J}_s = 2\hat{\mathbf{n}} \times \mathbf{H}_i$ in (3.46), since the reflector surface is an open surface. The surface charge density ρ_s may be approximated by $2\epsilon_0 \hat{\mathbf{n}} \cdot \mathbf{E}_i$, the exact result for reflection from an infinite plane,

and replaces the term $\hat{\mathbf{n}} \cdot \mathbf{E}$ in (3.44a). Alternatively, (3.47) involving only the current \mathbf{J}_s may be used. Thus, the scattered field is approximated in terms of integrals involving only the known incident field. The total radiated field is the sum of the scattered field \mathbf{E}_s and the direct radiated field \mathbf{E}_i . It should be noted that, because the assumed current is not exact, the fields calculated from (3.44a) and (3.47) do not, in general, agree exactly.

Kirchhoff's Formula

In optical diffraction a scalar formulation based on Kirchhoff's formula is commonly used. Since the same method is also frequently used for large aperture-type antennas, a brief discussion of this formulation is given here.

Consider a region V bounded by a closed surface S in which the electric field is source-free. Thus in V , \mathbf{E} is a solution of

$$(\nabla^2 + k_0^2)\mathbf{E} = 0$$

The scalar Green's function

$$G_0 = \frac{e^{-jk_0|\mathbf{r}-\mathbf{r}'|}}{4\pi|\mathbf{r}-\mathbf{r}'|}$$

is a solution of $(\nabla^2 + k_0^2)G_0 = -\delta(\mathbf{r} - \mathbf{r}')$ in V . If we form the quantity

$$E_i \nabla^2 G_0 - G_0 \nabla^2 E_i = \nabla \cdot (E_i \nabla G_0 - G_0 \nabla E_i)$$

where E_i is one of the components of \mathbf{E} in a rectangular coordinate system, we find that

$$\nabla' \cdot [E_i(\mathbf{r}') \nabla' G_0 - G_0 \nabla' E_i(\mathbf{r}')] = -E_i(\mathbf{r}') \delta(\mathbf{r} - \mathbf{r}')$$

by interchanging the primed and unprimed variables. Let us now integrate over the volume V to obtain

$$E_i(\mathbf{r}) = \oint_S \left(E_i \frac{\partial G_0}{\partial n} - G_0 \frac{\partial E_i}{\partial n} \right) dS' \quad (3.48a)$$

where the normal derivative is taken with respect to the primed variables and the normal n is directed into the region V . By combining the results for each component of \mathbf{E} , we can write

$$\mathbf{E}(\mathbf{r}) = \oint_S \left(\mathbf{E} \frac{\partial G_0}{\partial n} - G_0 \frac{\partial \mathbf{E}}{\partial n} \right) dS' \quad (3.48b)$$

The equation given above is Kirchhoff's formula. If both \mathbf{E} and $\partial \mathbf{E} / \partial n$ are known everywhere on the closed surface S , then the field inside V is determined exactly. In practice the formula is often applied with only an approximate knowledge of the tangential electric field on an aperture plane. The term involving $\partial \mathbf{E} / \partial n$ and the normal component of \mathbf{E} would then be neglected. These approximations are quite drastic in nature, and it is difficult to estimate the magnitude of the error that results. In general, the use of (3.48) when the

surface S is taken as an open surface does not yield a solution for \mathbf{E} that satisfies Maxwell's equations in the region V . The vector formulas (3.44) together with the contour integrals (3.46) do not suffer from this deficiency.

In spite of the objections made above as regards the manner in which Kirchhoff's formula (3.48) is used in practice, it is still possible to formulate a satisfactory scalar or geometric optics theory on the basis of (3.48) for electromagnetic diffraction by large apertures.

3.7 The Focused Aperture

An aperture-type antenna with an aperture distribution having a constant or linearly varying phase is an aperture focused at infinity. In this section we shall consider radiation from an aperture which has a field with a phase variation corresponding to that of a converging spherical wave. This type of phase variation results in the radiated field being focused at a finite distance in front of the aperture. The characteristics of a focused aperture are of considerable interest in connection with the receiving properties of parabolic reflectors and lenses, since both are used to focus the incoming plane wave to a point at the location of the primary feed or receiving antenna located at the focus. Sometimes it is also desirable to focus an antenna at a finite distance for the purpose of measuring the radiation pattern at a much closer range to the antenna than is possible for an antenna focused at infinity. This is particularly true for large antennas, where the far-zone field could easily begin a distance of several miles from the antenna. This latter application has been discussed by Bickmore,¹⁹ Cheng,²⁰ and also Jull.²¹

As may be surmised, the properties of focused apertures have been of interest in optics for many years, and a large number of relevant papers are available. A notable early contribution was made by Lommel, who studied the properties of a focused circular aperture.²² Much more recent work, along with many references, has been published by Bachynski and Bekefi,²³ Matthews and

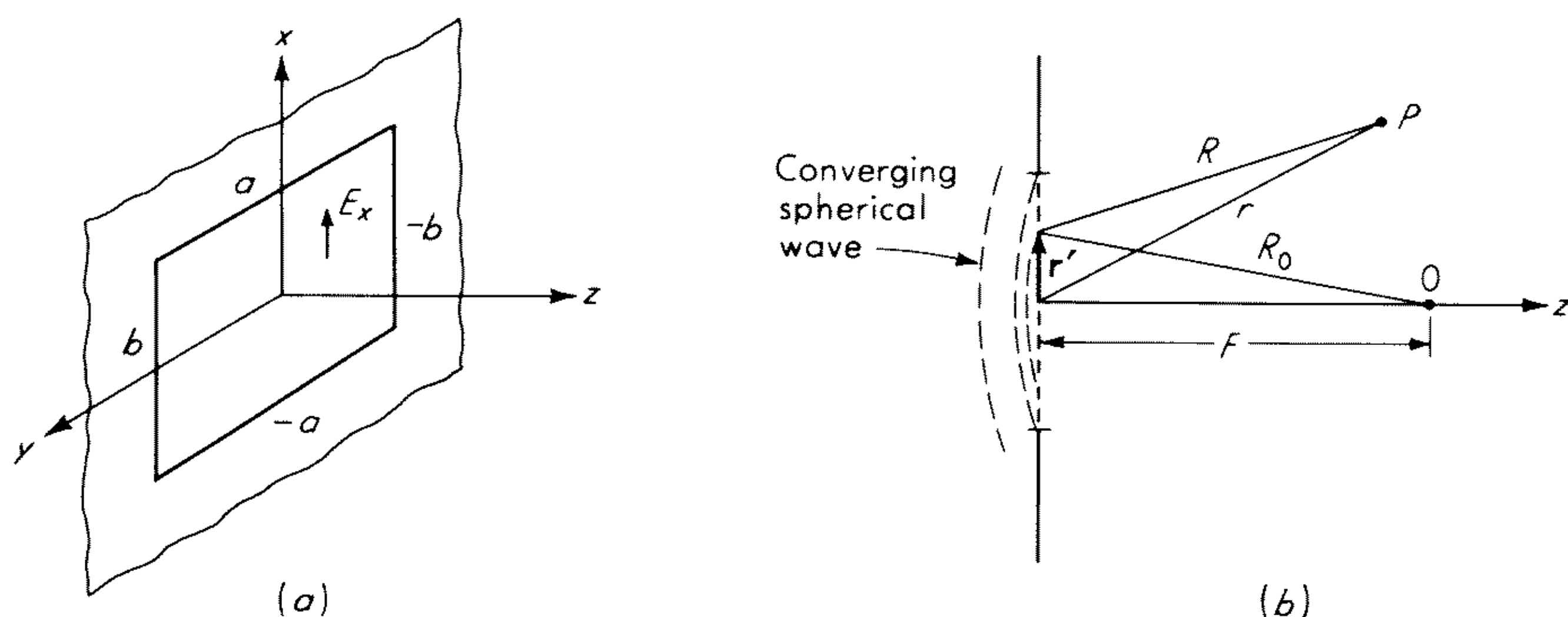


Fig. 3.9 The focused aperture.

Cullen,²⁴ and Boivin and Wolf.²⁵ The above authors present several plots of the field amplitude and phase in the region around the focus. Bachynski and Bekefi, and also Matthews and Cullen, give in addition measured results obtained at microwave frequencies. Focused apertures have also been studied by Bickmore²⁶ and Sherman.²⁷ (See too the discussion given by Hansen.²⁸)

As an illustration of a typical analysis we shall consider a rectangular aperture of size $2a$ by $2b$ in an infinite perfectly conducting screen as shown in Fig. 3.9. The aperture field is taken as linearly polarized in the x direction and having a phase variation corresponding to that of a spherical wave converging on the focus at O at a distance F from the aperture plane (see Fig. 3.9). We shall call F the focal length. The aperture field can be expressed as

$$\mathbf{E} = \hat{\mathbf{x}}A(x,y)e^{jk_0R_0} \quad (3.49)$$

where A is real. According to the discussion in Sec. 2.5, we approximate R , the distance from a source point to a field point, by

$$R = r - \hat{\mathbf{r}} \cdot \mathbf{r}' + \frac{1}{2r} [r'^2 - (\hat{\mathbf{r}} \cdot \mathbf{r}')^2] \quad (3.50)$$

since we are interested in the field in the Fresnel zone. For the amplitude variation of the field we replace R by r . The radiated field is given by (3.27) along with (3.24a), except that now we must use the more accurate expression (3.50) for R , thus

$$\mathbf{E}(P) = \frac{jk_0e^{-jk_0r}}{2\pi r} (\hat{\boldsymbol{\theta}} \cos \phi - \hat{\boldsymbol{\phi}} \sin \phi) \int_{-b}^b \int_{-a}^a A(x',y') e^{jk_0R_0} \exp(jk_0\hat{\mathbf{r}} \cdot \mathbf{r}') \exp \left\{ -jk_0 \left[r'^2 - \frac{(\hat{\mathbf{r}} \cdot \mathbf{r}')^2}{2r} \right] \right\} dx' dy' \quad (3.51)$$

To facilitate an evaluation of the integral we shall assume that F is large compared with both a and b , so that we may approximate $R_0 = [F^2 + r'^2]^{1/2}$ by $R_0 = F + r'^2/2F$. Hence the integral to be evaluated is

$$I = \int_{-b}^b \int_{-a}^a A(x',y') \exp \left(jk_0 \left\{ \hat{\mathbf{r}} \cdot \mathbf{r}' + \frac{r'^2}{2} \left[\frac{1}{F} - \frac{1}{r} + \frac{(\hat{\mathbf{r}} \cdot \mathbf{r}')^2}{r} \right] \right\} \right) dx' dy' \quad (3.52)$$

If we are interested in the field near the focus where $r \approx F$ and $x^2 + y^2 < a^2 + b^2$, then the term involving the factor $\hat{\mathbf{r}} \cdot \mathbf{r}'$ in the exponential is of order r'^4/F^3 . But terms of this order were dropped in approximating R_0 , and hence this term in (3.52) should be dropped for consistency. For $r = F$ and x and y small relative to F we see from (3.52) that in the focal plane $z = F$ the radiation field has a pattern which is essentially the same as the far-zone pattern, since the factor multiplying r'^2 is zero to the order of approximation being made here. As a typical example illustrating the order of approximation involved, let $a = b = 50$ cm, $\lambda_0 = 3$ cm, and $F = 200$ cm. Then the maximum value of r' is 70.7 cm and for $r = F$, $x = x' = y = y' = a$ the maximum value of $k_0(\hat{\mathbf{r}} \cdot \mathbf{r}')^2/2r$ is $\pi r'^4/(3r^3) = 1.04\pi$. If we keep x and y to less than $a/2$, the

surface S is taken as an open surface does not yield a solution for \mathbf{E} that satisfies Maxwell's equations in the region V . The vector formulas (3.44) together with the contour integrals (3.46) do not suffer from this deficiency.

In spite of the objections made above as regards the manner in which Kirchhoff's formula (3.48) is used in practice, it is still possible to formulate a satisfactory scalar or geometric optics theory on the basis of (3.48) for electromagnetic diffraction by large apertures.

3.7 The Focused Aperture

An aperture-type antenna with an aperture distribution having a constant or linearly varying phase is an aperture focused at infinity. In this section we shall consider radiation from an aperture which has a field with a phase variation corresponding to that of a converging spherical wave. This type of phase variation results in the radiated field being focused at a finite distance in front of the aperture. The characteristics of a focused aperture are of considerable interest in connection with the receiving properties of parabolic reflectors and lenses, since both are used to focus the incoming plane wave to a point at the location of the primary feed or receiving antenna located at the focus. Sometimes it is also desirable to focus an antenna at a finite distance for the purpose of measuring the radiation pattern at a much closer range to the antenna than is possible for an antenna focused at infinity. This is particularly true for large antennas, where the far-zone field could easily begin a distance of several miles from the antenna. This latter application has been discussed by Bickmore,¹⁹ Cheng,²⁰ and also Jull.²¹

As may be surmised, the properties of focused apertures have been of interest in optics for many years, and a large number of relevant papers are available. A notable early contribution was made by Lommel, who studied the properties of a focused circular aperture.²² Much more recent work, along with many references, has been published by Bachynski and Bekefi,²³ Matthews and

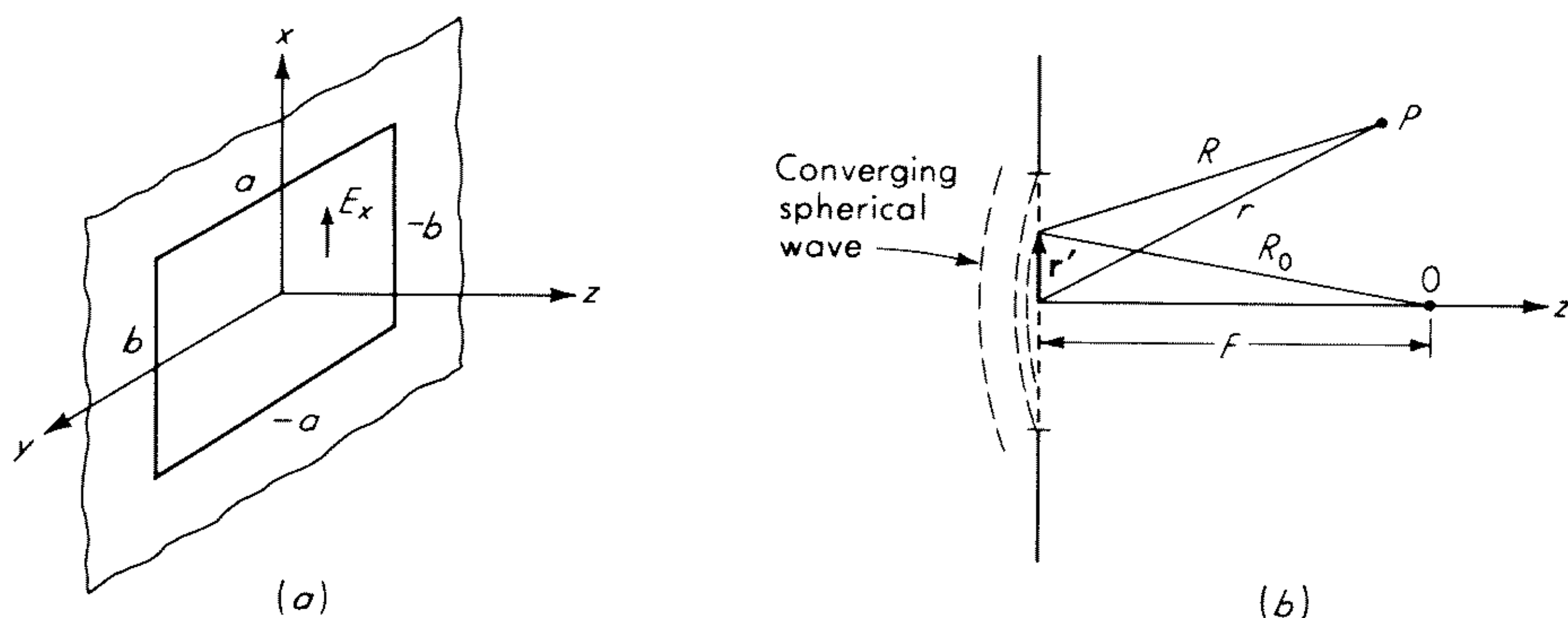


Fig. 3.9 The focused aperture.

Cullen,²⁴ and Boivin and Wolf.²⁵ The above authors present several plots of the field amplitude and phase in the region around the focus. Bachynski and Bekefi, and also Matthews and Cullen, give in addition measured results obtained at microwave frequencies. Focused apertures have also been studied by Bickmore²⁶ and Sherman.²⁷ (See too the discussion given by Hansen.²⁸)

As an illustration of a typical analysis we shall consider a rectangular aperture of size $2a$ by $2b$ in an infinite perfectly conducting screen as shown in Fig. 3.9. The aperture field is taken as linearly polarized in the x direction and having a phase variation corresponding to that of a spherical wave converging on the focus at O at a distance F from the aperture plane (see Fig. 3.9). We shall call F the focal length. The aperture field can be expressed as

$$\mathbf{E} = \hat{\mathbf{x}}A(x,y)e^{jk_0R_0} \quad (3.49)$$

where A is real. According to the discussion in Sec. 2.5, we approximate R , the distance from a source point to a field point, by

$$R = r - \hat{\mathbf{r}} \cdot \mathbf{r}' + \frac{1}{2r} [r'^2 - (\hat{\mathbf{r}} \cdot \mathbf{r}')^2] \quad (3.50)$$

since we are interested in the field in the Fresnel zone. For the amplitude variation of the field we replace R by r . The radiated field is given by (3.27) along with (3.24a), except that now we must use the more accurate expression (3.50) for R , thus

$$\mathbf{E}(P) = \frac{jk_0e^{-jk_0r}}{2\pi r} (\hat{\boldsymbol{\theta}} \cos \phi - \hat{\boldsymbol{\phi}} \sin \phi) \int_{-b}^b \int_{-a}^a A(x',y') e^{jk_0R_0} \exp(jk_0\hat{\mathbf{r}} \cdot \mathbf{r}') \exp \left\{ -jk_0 \left[r'^2 - \frac{(\hat{\mathbf{r}} \cdot \mathbf{r}')^2}{2r} \right] \right\} dx' dy' \quad (3.51)$$

To facilitate an evaluation of the integral we shall assume that F is large compared with both a and b , so that we may approximate $R_0 = [F^2 + r'^2]^{1/2}$ by $R_0 = F + r'^2/2F$. Hence the integral to be evaluated is

$$I = \int_{-b}^b \int_{-a}^a A(x',y') \exp \left(jk_0 \left\{ \hat{\mathbf{r}} \cdot \mathbf{r}' + \frac{r'^2}{2} \left[\frac{1}{F} - \frac{1}{r} + \frac{(\hat{\mathbf{r}} \cdot \mathbf{r}')^2}{r} \right] \right\} \right) dx' dy' \quad (3.52)$$

If we are interested in the field near the focus where $r \approx F$ and $x^2 + y^2 < a^2 + b^2$, then the term involving the factor $\hat{\mathbf{r}} \cdot \mathbf{r}'$ in the exponential is of order r'^4/F^3 . But terms of this order were dropped in approximating R_0 , and hence this term in (3.52) should be dropped for consistency. For $r = F$ and x and y small relative to F we see from (3.52) that in the focal plane $z = F$ the radiation field has a pattern which is essentially the same as the far-zone pattern, since the factor multiplying r'^2 is zero to the order of approximation being made here. As a typical example illustrating the order of approximation involved, let $a = b = 50$ cm, $\lambda_0 = 3$ cm, and $F = 200$ cm. Then the maximum value of r' is 70.7 cm and for $r = F$, $x = x' = y = y' = a$ the maximum value of $k_0(\hat{\mathbf{r}} \cdot \mathbf{r}')^2/2r$ is $\pi r'^4/(3r^3) = 1.04\pi$. If we keep x and y to less than $a/2$, the

maximum value of this term will be $\pi/4$, for which the value of the integral I is not significantly changed if the above term is dropped.

For large values of x and y the term $(\hat{\mathbf{r}} \cdot \mathbf{r}')^2/2r$ may not be negligible. Since this term involves a cross-product term in $x'y'$ because $(\hat{\mathbf{r}} \cdot \mathbf{r}')^2 = (xx' + yy')^2/r^2$, the integral I becomes difficult to evaluate. However, if we consider only the field variations in the principal planes $x = 0$ and $y = 0$, the cross-product term vanishes. For a separable aperture field amplitude of the form

$$A(x, y) = \sum_{n=0}^N \sum_{m=0}^M C_{nm} \cos \frac{n\pi x}{a} \cos \frac{m\pi y}{b}$$

the integral I can be evaluated in terms of Fresnel integrals. For simplicity we shall evaluate only the constant term in the aperture field expansion. A similar integral occurs in the theory of horn antennas, and the integral involving an aperture field with cosinusoidal variation is evaluated in Chap. 14 in connection with the analysis of the H -plane sectoral horn.

For the case when x and y are small we have

$$I = \int_{-b}^b \int_{-a}^a C_{00} \exp \left\{ j \frac{k_0}{r} \left[xx' + yy' + (x'^2 + y'^2) \left(\frac{r - F}{2F} \right) \right] \right\} dx' dy'$$

By completing the square in the exponential, it is readily found that

$$I = \frac{\pi r F}{k_0(r - F)} [C(u_2) \pm jS(u_2) - C(u_1) \mp jS(u_1)][C(v_2) \pm jS(v_2) - C(v_1) \mp jS(v_1)] \exp \left[-j \frac{k_0}{r} \frac{(x^2 + y^2)F}{2(r - F)} \right] \quad x^2 + y^2 \ll a^2 + b^2 \quad (3.53)$$

where the Fresnel integrals are given by

$$C(u) = \int_0^u \cos \frac{\pi u^2}{2} du$$

$$S(u) = \int_0^u \sin \frac{\pi u^2}{2} du$$

and

$$u_i = (-1)^i a \sqrt{\frac{k_0 |r - F|}{\pi r F}} \pm \sqrt{\frac{k_0 r F}{\pi |r - F|}} \frac{x}{r}$$

$$v_i = (-1)^i b \sqrt{\frac{k_0 |r - F|}{\pi r F}} \pm \sqrt{\frac{k_0 r F}{\pi |r - F|}} \frac{y}{r}$$

with $i = 1, 2$. The upper signs are used for $r > F$ and the lower signs for $r < F$. Tables of the Fresnel integrals may be found in Jahnke and Emde.²⁹ For $r - F$ very small we can use the results of Prob. 3.7 to obtain an alternative solution.

The labor involved in calculating the amplitude of the electric field is reduced if it is noted that (1) the field strength is proportional to $|I|/r$, (2) the function $|r - F|/rF$ has the same value at two points given by $r = F/(1 \pm \gamma)$, where γ is a variable constant, (3) the functions u_i, v_i are equal at the two values of r

specified in (2) provided the field is plotted as functions of x/r and y/r , (4) the functions $C(u)$ and $S(u)$ are odd functions of u , and hence $|I|$ has the same value at the two values of r given in (2) when plotted as a function of x/r and y/r , that is, when plotted as a function of $\sin \theta \cos \phi$ and $\sin \theta \sin \phi$.

In Fig. 3.10 we give the pattern in the $y = 0$ plane as a function of x/λ_0 for a

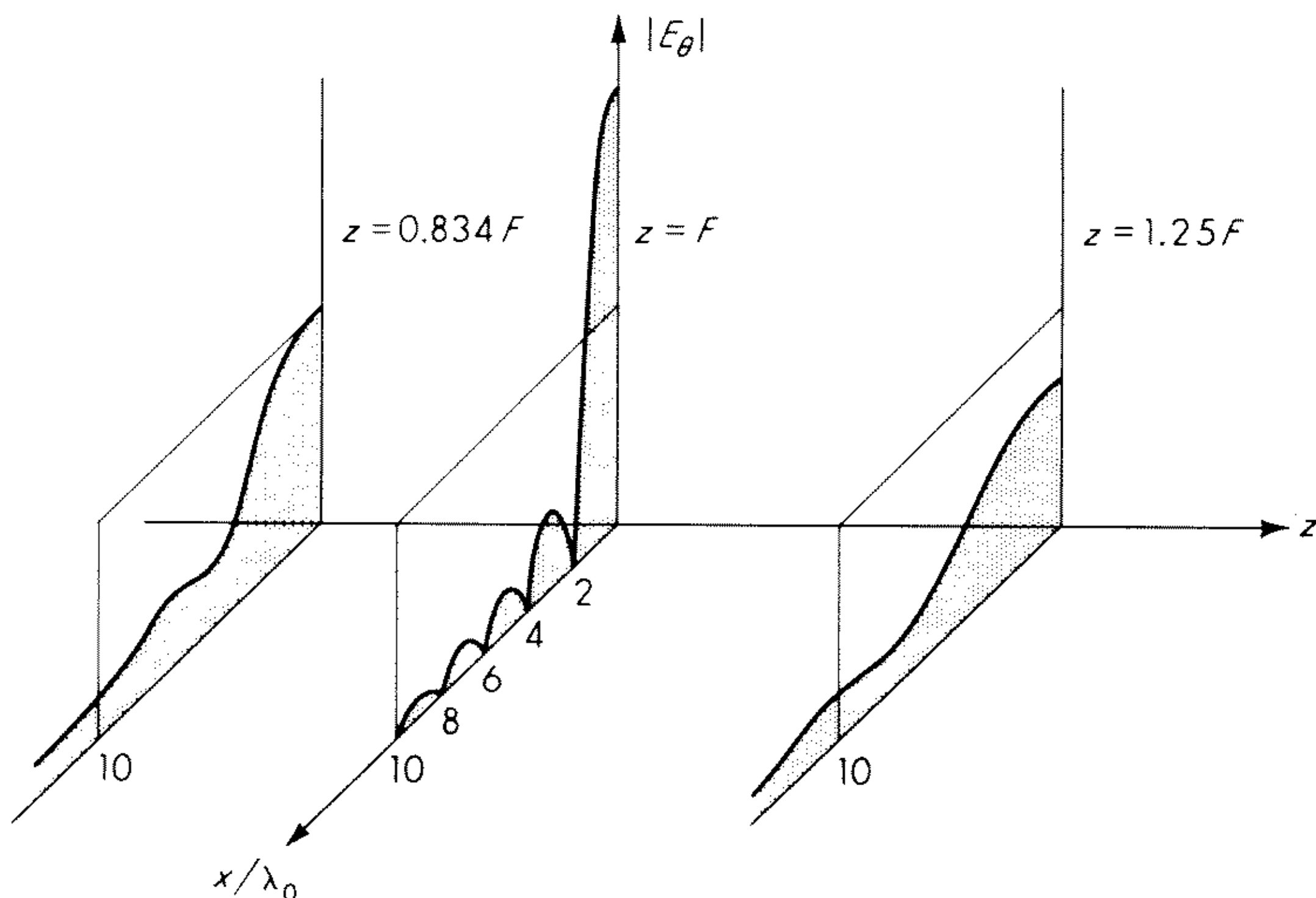


Fig. 3.10 Normalized electric field from a focused aperture in the $y = 0$ plane ($a = b = 50$ cm, $F = 200$ cm, $\lambda_0 = 3$ cm).

square aperture with $a = b = 50$ cm, $F = 200$ cm, $\lambda_0 = 3$ cm. The patterns given correspond to $z = 0.834F$, F , and $1.25F$ and are normalized relative to the field strength at the focus. For the small values of x involved r has been replaced by z . Note that the main lobe decreases rapidly in height and gets much broader with increasing distance away from the focal plane. Sherman gives similar plots of the pattern for a focused aperture.²⁷

The above analysis is also applicable for determining the Fresnel zone field from an aperture focused at infinity, i.e., as F tends to infinity.

PROBLEMS

3.1 Show that the time-average energies stored in the evanescent electric and magnetic fields arising from an aperture in a conducting screen are given by

$$W_m = \frac{\epsilon_0}{32\pi^2 k_0^2} \iint_{k_t > k_0} \left[(2k_t^2 - k_0^2) \mathbf{f}_t \cdot \mathbf{f}_t^* + \frac{k_0^2 |\mathbf{k}_t \cdot \mathbf{f}_t|^2}{k_t^2 - k_0^2} - 2|\mathbf{f}_t \cdot \mathbf{k}_t|^2 \right] \frac{dk_x dk_y}{(k_t^2 - k_0^2)^{1/2}}$$

$$W_e = \frac{\epsilon_0}{32\pi^2 k_0^2} \iint_{k_t > k_0} k_0^2 \left[\mathbf{f}_t \cdot \mathbf{f}_t^* + \frac{|\mathbf{k}_t \cdot \mathbf{f}_t|^2}{k_t^2 - k_0^2} \right] \frac{dk_x dk_y}{(k_t^2 - k_0^2)^{1/2}}$$

The following relations will be useful:

$$\mathbf{k} \cdot \mathbf{k}^* = 2k_t^2 - k_0^2 \quad \mathbf{k} \cdot \mathbf{f} = 0 \quad \mathbf{f} \cdot \mathbf{k}^* = 2\mathbf{k}_t \cdot \mathbf{f}_t \quad \text{for } k_t > k_0$$

3.2 In the visible region of $k_x - k_y$ space where \mathbf{k} is pure real show that the integrands for W_m and W_e in Prob. 3.1 are equal. This expresses the well-known property that the electric and magnetic energy density in a propagating plane wave are equal.

3.3 Derive the relations (3.15b) to (3.15f).

3.4 Use the Schwartz inequality

$$\left| \iint fg \, dx \, dy \right|^2 \leq \iint f^2 \, dx \, dy \iint g^2 \, dx \, dy$$

to show that of all constant-phase aperture fields the uniform field gives maximum directivity. Use (3.37) for the directivity and put $g = 1$ and f equal to the aperture field (assume a linearly polarized field).

3.5 Show that the radiation pattern of a circular aperture of radius a with a uniform linearly polarized aperture field is proportional to $J_1(k_0 a \sin \theta)/(k_0 a \sin \theta)$, where J_1 is the Bessel function of order 1. Show that the half-power beam width is equal to $1.02\lambda_0/2a$ and that the first side lobe is 17.5 db below the main-lobe peak.

3.6 For an aperture distribution given by $\cos^2(\pi x/2a)$ show that the half-power beam width is given by $1.45\lambda_0/2a$, that the side-lobe level is 32 db below the main-lobe peak, and that the directivity is smaller by a factor of 0.667 relative to that for a uniform aperture distribution.

3.7 Investigate the effect of a small quadratic phase error in the aperture field distribution. Assume an aperture field distribution $e^{-j\alpha x^2} \cos(\pi x/2a)$, where α is a small parameter.

Hint: Expand $e^{-j\alpha x^2}$ and note that integrals of the type

$$\int_{-a}^a x^{2n} e^{jk_0 x \sin \theta} \cos \frac{\pi x}{2a} \, dx$$

are equal to

$$\frac{d^{2n}}{d(jk_0 \sin \theta)^n} \int_{-a}^a e^{jk_0 x \sin \theta} \cos \frac{\pi x}{2a} \, dx$$

By using a two-term approximation for $e^{-j\alpha x^2}$, obtain an expression for the power radiation pattern. Estimate the increase in the half-power beam width and the decrease in directivity when $\alpha a^2 = \pi/2$.

3.8 Derive an expression for \mathbf{H} by using Green's second identity and a procedure similar to that outlined in Exercise 3.3 and thus verify (3.44b).

3.9 Let the tangential aperture fields be \mathbf{H}_a , \mathbf{E}_a on the aperture plane $z = 0$ over the region $|x| \leq a$, $-\infty \leq y \leq \infty$, and zero outside this region. Show that the two-dimensional form of (3.25) is

$$\mathbf{E} \sim \sqrt{\frac{j}{8\pi k_0 r}} e^{-jk_0 r} k_0 \cos \theta \left[\mathbf{f}(k_0 \sin \theta) - \frac{\zeta_0}{k_0} \mathbf{k} \times \mathbf{g}(k_0 \sin \theta) \right]$$

$$\mathbf{H} \sim \frac{1}{k_0 \zeta_0} \mathbf{k} \times \mathbf{E}$$

where $\mathbf{k} \cdot \mathbf{f} = \mathbf{k} \cdot \mathbf{g} = 0$, $\mathbf{k} = k_0(\hat{\mathbf{x}} \sin \theta + \hat{\mathbf{z}} \cos \theta)$

and

$$\mathbf{f}_t = \int_{-a}^a \mathbf{E}_a(x) e^{jk_x x} \, dx$$

$$\mathbf{g}_t = \int_{-a}^a \mathbf{H}_a(x) e^{jk_x x} \, dx$$

Hint: Use (3.15) and a similar procedure to find the magnetic field contributed by \mathbf{H}_a . Note that, because the equivalent currents $\mathbf{J}_s = \hat{\mathbf{z}} \times \mathbf{H}_a$ and $\mathbf{J}_{ms} = -\hat{\mathbf{z}} \times \mathbf{E}_a$ radiate into free space, (3.15) must be multiplied by $1/2$.

3.10 Use (2.39), the relation $E_y = -j\omega A_y = -(\omega\mu_0/4)H_0^2(k_0R)$ for the electric field from a unit line current along y , and the asymptotic form of the Hankel function to show that an aperture magnetic field $H_a(x)\hat{\mathbf{x}}$ over $-a \leq x \leq a$, $-\infty \leq y \leq \infty$, produces a far-zone electric field given by

$$E_y = -k_0\zeta_0\sqrt{\frac{j}{8\pi k_0r}}e^{-ik_0r}\int_{-a}^ae^{jk_0x'\sin\theta}H_a(x')dx'$$

where $R = [(x - x')^2 + z^2]^{1/2}$. Thus verify the result obtained in Prob. 3.9 by a different method for this special case.

REFERENCES

1. Silver, S.: "Microwave Antenna Theory and Design," McGraw-Hill Book Company, New York, 1949.
2. Fradin, A. Z.: "Microwave Antennas," Pergamon Press, New York, 1961.
3. Stratton, J. A.: "Electromagnetic Theory," sec. 9.2, McGraw-Hill Book Company, New York, 1941.
4. Booker, H. G., and P. C. Clemmow: The Concept of an Angular Spectrum of Plane Waves and Its Relation to That of Polar Diagram and Aperture Distribution, *Proc. IEEE*, vol. 97, part III, pp. 11-17, January, 1950.
5. Collin, R. E., and S. Rothschild: Reactive Energy in Aperture Fields and Aperture Q, *Can. J. Phys.*, vol. 41, pp. 1967-1979, December, 1963. See also Antennas and Propagation, *IEEE Trans.*, vol. AP-15, pp. 565-569, July, 1967.
6. Rhodes, D. R.: On a Fundamental Principle in the Theory of Planar Antennas, *Proc. IEEE*, vol. 52, pp. 1013-1021, September, 1964.
7. Borgiotti, G.: Fourier Transforms Method of Aperture Antennas Problem, *Alta. Freq.*, vol. 32, pp. 196-204, November, 1963.
8. Jeffreys, H., and B. S. Jeffreys: "Methods of Mathematical Physics," 2d ed., chap. 17, Cambridge University Press, London, 1950.
9. Ramsay, J. F.: Fourier Transforms in Aerial Theory, *Marconi Rev.*, parts I to VI, issue nos. 83-89, 1946.
10. Silver, S.: "Microwave Antenna Theory and Design," McGraw-Hill Book Company, New York, 1949. See chap. 6 for a discussion of Spencer's work.
11. Love, A. E. H.: The Integration of the Equations of Propagation of Electric Waves, *Phil. Trans. Roy. Soc. London, Ser. A*, vol. 197, pp. 1-45, 1901.
12. Schelkunoff, S. A.: Some Equivalence Theorems of Electromagnetics and Their Application to Radiation Problems, *Bell System Tech. J.*, vol. 15, pp. 92-112, 1936.
13. Schelkunoff, S. A.: Kirchhoff's Formula, Its Vector Analogue and Other Field Equivalence Theorems, *Commun. Pure Appl. Math.*, vol. 4, pp. 43-59, June, 1951. See also *Phys. Rev.*, vol. 56, pp. 308-316, 1939.
14. Harrington, R. F.: "Time-harmonic Electromagnetic Fields," chap. 3, McGraw-Hill Book Company, New York, 1961.
15. Bouwkamp, C. J.: Diffraction Theory, *Rept. Prog. Phys.*, vol. XVII, pp. 35-100, 1954.
16. Baker, B. B., and E. T. Copson: "The Mathematical Theory of Huygen's Principle," chap. III, Oxford University Press, London, 1939.
17. Stratton, J. A., and L. J. Chu: Diffraction Theory of Electromagnetic Waves, *Phys. Rev.*, vol. 56, pp. 99-107, 1939.

18. Stratton, J. A.: "Electromagnetic Theory," sec. 8.14, McGraw-Hill Book Company, New York, 1941.
19. Bickmore, R. W.: Fraunhofer Pattern Measurements in the Fresnel Zone, *Can. J. Phys.*, vol. 35, pp. 1299–1308, 1957.
20. Cheng, D. K.: On the Simulation of Fraunhofer Radiation Patterns in the Fresnel Zone, *IRE Trans. Antennas Propagation*, vol. AP-5, pp. 399–402, 1957.
21. Jull, E. V.: The Estimation of Aerial Radiation Patterns from Limited Near-zone Field Measurements, *Proc. Inst. Elec. Engrs. (London)*, vol. 110, pp. 501–506, 1963.
22. Lommel, E.: Theoretical and Experimental Investigations of Diffraction Phenomena at a Circular Aperture and Obstacle, *Bayer. Akad. Wiss. Jahrb.*, vol. 15, p. 233, 1884. See also the following papers by Lommel: Die Beugungserscheinungen Einer Öffnung und Eines Kreisrunden Schirmchens, *Königlich Bayer. Akad. der. Wiss., Abhandl. Math.-Physik.*, vol. 15, p. 229, 1886. Die Beugungserscheinungen Geradlinig Begrenzter Schirme, *ibid.*, p. 529.
23. Bachynski, M. P., and G. Bekefi: Study of Optical Diffraction Images at Microwave Frequencies, *J. Opt. Soc. Am.*, vol. 47, pp. 428–438, 1957.
24. Matthews, P. A., and A. L. Cullen: A Study of the Field Distribution at an Axial Focus of a Square Microwave Lens, *Proc. Inst. Elec. Engrs. (London)*, vol. 103, part C, pp. 449–456, 1956.
25. Boivin, A., and E. Wolf: Electromagnetic Field in the Neighborhood of the Focus of a Coherent Beam, *Phys. Rev.*, vol. 138, pp. B1561–B1565, 1965.
26. Bickmore, R. W.: On Focusing Electromagnetic Radiators, *Can. J. Phys.*, vol. 35, pp. 1292–1298, 1957.
27. Sherman, J. W.: Properties of Focused Apertures in the Fresnel Region, *IRE Trans. Antennas Propagation*, vol. AP-10, pp. 399–408, 1962.
28. Hansen, R. C.: "Microwave Scanning Antennas," vol. I, Academic Press Inc., New York, 1964.
29. Jahnke, E., and F. Emde: "Tables of Functions," 4th ed., Dover Publications, Inc., New York, 1945.
30. Sancer, M. I.: An Analysis of the Vector Kirchhoff Equations and the Associated Boundary Line Charge, *Radio Sci.*, vol. 3, pp. 141–144, 1968.

CHAPTER 4

THE RECEIVING ANTENNA

R. E. Collin

4.1 Introduction

In this chapter we shall examine the general properties of an antenna from the point of view that the antenna is used for the reception of electromagnetic radiation. We shall show that, when the antenna is located in a reciprocal medium, the directivity and pattern of an antenna used for the reception of electromagnetic radiation are the same as when the antenna is used to radiate energy. We shall also show that the antenna effective receiving cross section is related to the gain G by a universal constant $\lambda_0^2/4\pi$. In addition, the equivalent circuit of a receiving and transmitting antenna system, together with formulas for calculating the received power and the effects of noise, will be developed. The effects of varying polarization of the electromagnetic field on the performance of an antenna will also be dealt with.

The most general source of radiation that an antenna could be called upon to receive would have the following features:

1. Polychromatic, i.e., consist of a spectrum of frequencies
2. Spatial extent
3. Spatial and temporal variation of amplitude, phase, and polarization with varying degrees of spatial and temporal correlation between these quantities

The special case of monochromatic and nonrandomly polarized waves emanating from a point source has received the most extensive treatment in the literature and will be given major emphasis in this chapter. We shall, however, also discuss to some extent the reception of radiation with more general features.

When an antenna is used for radiating electromagnetic energy, the power output from the transmitter is fed to the antenna input terminals through a coaxial line, waveguide, or other suitable waveguiding structure. If the antenna input impedance is not equal to the characteristic impedance of the feed line, a portion of the incident power is reflected. This is an undesirable feature, since the maximum transmitter power output is not radiated and the resultant standing wave in the feed line yields a higher electric field strength than for a matched system, and hence a reduction of the power-handling capability before dielectric breakdown occurs. To overcome these undesirable

features a matching network is usually inserted between the antenna and the feed line in order to transform the antenna input impedance into an impedance equal to the characteristic impedance of the feed line. The transmitter must also be matched to the feed line in order to obtain maximum power transfer.

When an antenna is used to receive electromagnetic radiation, it is likewise desirable to have the antenna matched to the feed line and to have the load at the other end also matched to the feed line in order to maximize the received power. The matching networks should have as low a loss as possible in order to obtain a high efficiency, i.e., useful signal power output.

From an equivalent circuit point of view it makes no difference whether the feed line is a conventional TEM wave transmission line or a waveguide. If a transmission line is used, the TEM mode of propagation is uniquely described in terms of the voltage and current waves on the line and the characteristic impedance of the transmission line. If energy is coupled to and from the antenna by a waveguide, we can introduce equivalent transmission line voltage and current amplitudes proportional respectively to the transverse electric and magnetic fields in the waveguide. These equivalent voltage and current amplitudes may always be so chosen that the energy flow along the waveguide is given by $\frac{1}{2} \text{Re } VI^* = \frac{1}{2} \text{Re } II^* Z_c$, where Z_c is an equivalent characteristic impedance which can be arbitrarily chosen provided V and I are so defined that $V = IZ_c$ for a mode propagating in a single direction. In view of this equivalence between a waveguide and a transmission line we shall always assume a coaxial transmission line for the feed line whenever the analysis requires the use of a specific feed line. The theory will nevertheless be general, since the voltage, current, and characteristic impedance may always be interpreted as the equivalent parameters for a waveguide. For a detailed treatment of waveguide equivalent circuit theory, the reader is referred to the texts by Montgomery, Dicke, and Purcell¹ and Collin.²

4.2 Reciprocity for Antennas

Consider two arbitrary antennas fed from shielded sources by means of coaxial lines as in Fig. 4.1. The generators are denoted by g_a and g_b for antennas a and b , respectively. It is assumed that the antennas are located in an isotropic lossless medium and are separated by a distance sufficiently large that each antenna is located in the far-zone region of the other antenna. Let the impedance at reference plane S_1 looking toward g_a be Z_{i1} , the impedance at reference plane S_1 looking toward the antenna be $Z_{in,1}$, the impedance at reference plane S_2 looking toward the antenna be $Z_{in,2}$, and the impedance at reference plane S_2 looking toward g_b be Z_{i2} . With g_a on and g_b off the field produced by g_a is $\mathbf{E}_a, \mathbf{H}_a$ with components

$$E_r = \frac{V_{1a}}{r \ln(b/a)_1} \quad H_\phi = \frac{I_{1a}}{2\pi r} \quad \text{at } S_1 \quad \frac{V_{1a}}{I_{1a}} = Z_{in,1} \quad (4.1a)$$

$$E_r = \frac{V_{2a}}{r \ln(b/a)_2} \quad H_\phi = \frac{-I_{2a}}{2\pi r} \quad \text{at } S_2 \quad \frac{V_{2a}}{I_{2a}} = Z_{i2} \quad (4.1b)$$

With g_a off and g_b on the field produced by g_b is \mathbf{E}_b , \mathbf{H}_b with components

$$E_r = \frac{V_{1b}}{r \ln(b/a)_1} \quad H_\phi = \frac{-I_{1b}}{2\pi r} \quad \text{at } S_1 \quad \frac{V_{1b}}{I_{1b}} = Z_{11} \quad (4.1c)$$

$$E_r = \frac{V_{2b}}{r \ln(b/a)_2} \quad H_\phi = \frac{I_{2b}}{2\pi r} \quad \text{at } S_2 \quad \frac{V_{2b}}{I_{2b}} = Z_{in,2} \quad (4.1d)$$

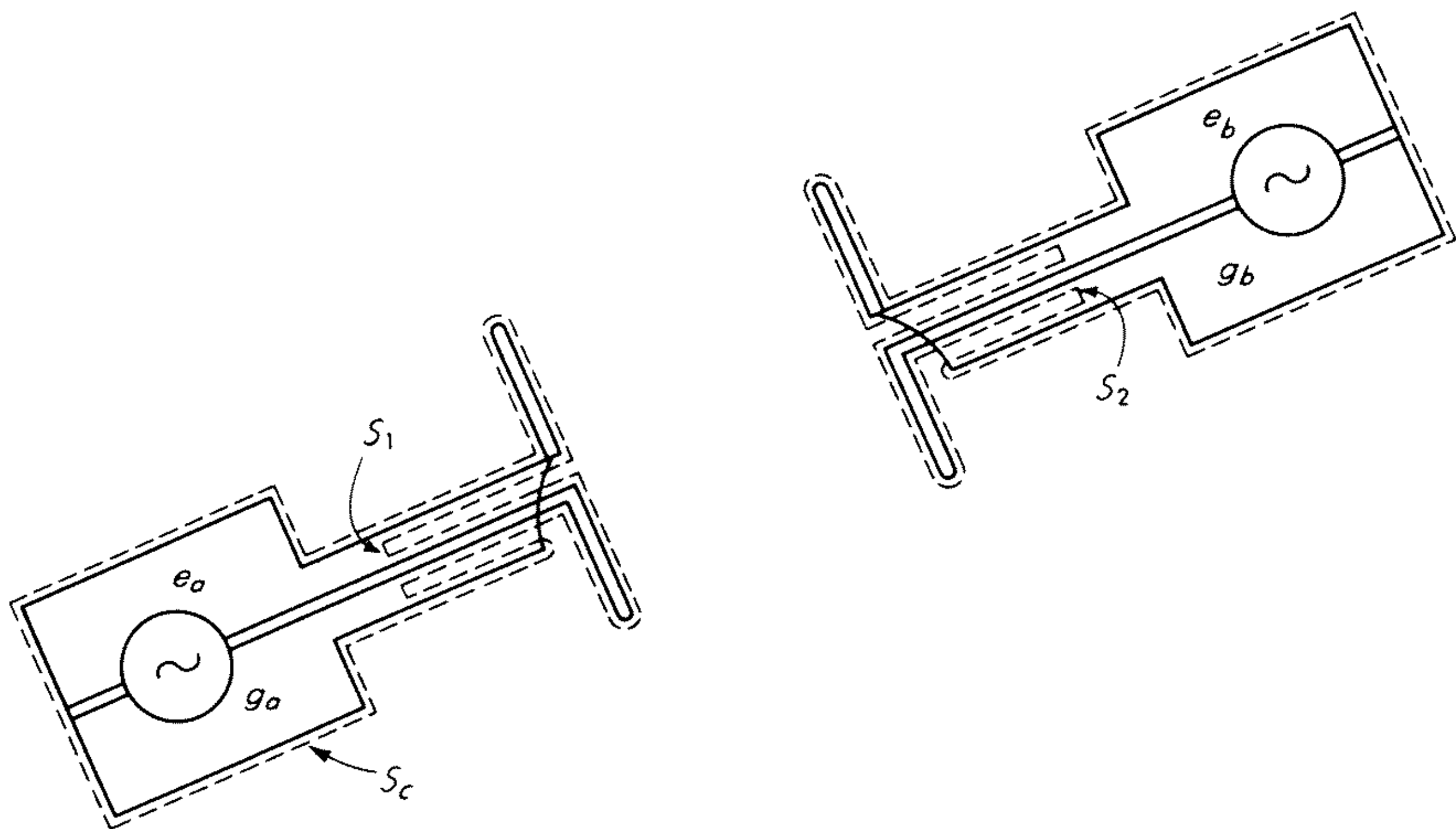


Fig. 4.1 A two-antenna system.

Note that the subscripts 1 and 2 refer to terminal planes S_1 and S_2 and subscripts a and b refer to which antenna is transmitting. The positive directions for I_{1a} and I_{2b} are toward the antennas, while the positive directions of I_{1b} and I_{2a} are away from the antennas.

If we use the fields \mathbf{E}_a , \mathbf{H}_a and \mathbf{E}_b , \mathbf{H}_b in the Lorentz reciprocity theorem given by (1.68) in Sec. 1.9, we obtain

$$\oint_S (\mathbf{E}_a \times \mathbf{H}_b - \mathbf{E}_b \times \mathbf{H}_a) \cdot d\mathbf{S} = 0 \quad (4.2)$$

where S consists of the surface S_c around the conductors making up each antenna system, the terminal planes S_1 and S_2 , and the surface of a sphere at infinity as shown in Fig. 4.1. Now at infinity $\zeta_0 \mathbf{H}_{a,b} = \hat{\mathbf{r}} \times \mathbf{E}_{a,b}$, while on the conducting surface S_c we have $\zeta_m \mathbf{H}_{(a,b)t} = \hat{\mathbf{n}} \times \mathbf{E}_{a,b}$, where $\mathbf{H}_{(a,b)t}$ denotes the tangential component. These relations show immediately that on the surface at infinity and on the imperfectly conducting surface S_c characterized by a surface impedance ζ_m the integrand is identically zero in (4.2). Thus we have

$$\int_{S_1} (\mathbf{E}_a \times \mathbf{H}_b - \mathbf{E}_b \times \mathbf{H}_a) \cdot d\mathbf{S} = \int_{S_2} (\mathbf{E}_b \times \mathbf{H}_a - \mathbf{E}_a \times \mathbf{H}_b) \cdot d\mathbf{S} \quad (4.3)$$

When we substitute from (4.1) for the fields and carry out the integration, we find that

$$V_{1a}I_{1b} + V_{1b}I_{1a} = V_{2b}I_{2a} + V_{2a}I_{2b} \quad (4.4)$$

From this expression we can obtain a relation giving the received signal voltage V_{2a} at the terminal plane S_2 , when g_b is short-circuited but g_a is on, in terms of the voltage V_{1b} that g_b would produce at S_1 when g_a is short-circuited. Replacing I_{1b} by V_{1b}/Z_{i1} and I_{2a} by V_{2a}/Z_{i2} in (4.4) gives

$$V_{2a} = \frac{Z_{i2}}{Z_{i1}} \frac{V_{1a} + I_{1a}Z_{i1}}{V_{2b} + I_{2b}Z_{i2}} V_{1b} \quad (4.5)$$

If we replace V_{1a} and V_{2b} in terms of the generator open-circuit voltages by using the relations given in Fig. 4.2, we obtain

$$V_{2a} = V_{1b} \frac{e_a/Z_{i1}}{e_b/Z_{i2}} \quad (4.6)$$

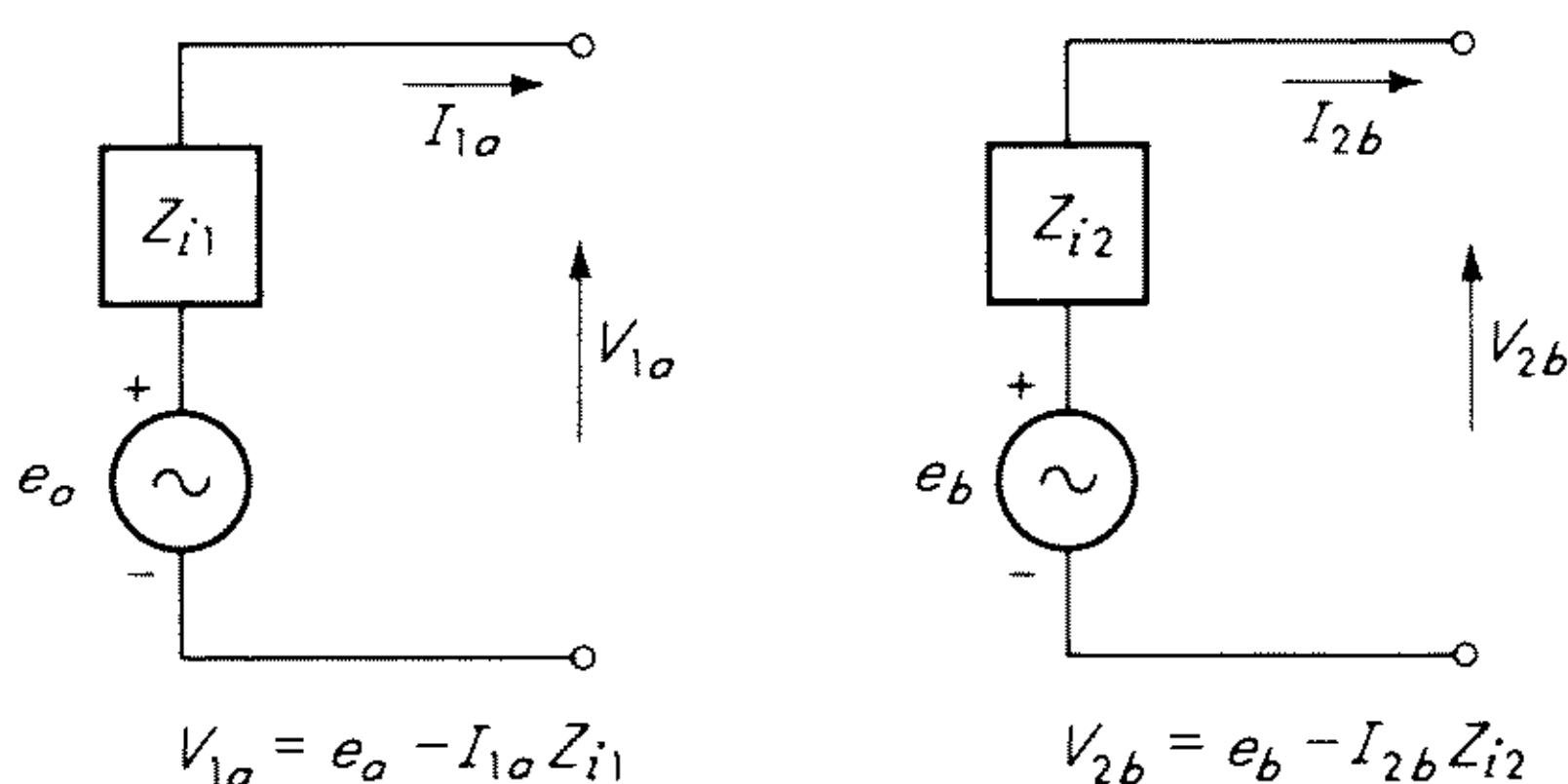


Fig. 4.2

a result which relates the received voltages at terminals S_1 and S_2 to each other in terms of the generator voltages and the internal impedances of the generators as seen from the terminal planes. Note that no assumptions about matched antennas or generators have been made.

If we replace V_{2a} by $Z_{i2} I_{2a}$ and V_{1b} by $Z_{i1} I_{1b}$, we obtain

$$e_b I_{2a} = e_a I_{1b} \quad (4.7)$$

This is a commonly quoted result for antennas and states that the generator voltage e_b times the current flowing at S_2 due only to e_a equals the generator voltage e_a times the current at S_1 as produced by e_b .

In deriving (4.6) and (4.7) it has been assumed that the terminal planes S_1 and S_2 are located just in front of the generators, so that the circuit between the generator terminals and the reference planes can be considered to be a simple series impedance. If this is not done, then an equivalent T network must be used to represent the structure between the generator terminals and the reference terminal plane. In this case V_{1a} is given by (see Fig. 4.3)

$$V_{1a} = \frac{Z_{2a}}{Z_{1a} + Z_{2a}} e_a - I_{1a}Z_{i1}$$

where $Z_{i1} = Z_{3a} + \frac{Z_{1a}Z_{2a}}{Z_{1a} + Z_{2a}}$. In place of (4.6) we have

$$V_{2a} = V_{1b} \frac{(e_a/Z_{i1})[Z_{2a}/(Z_{1a} + Z_{2a})]}{(e_b/Z_{i2})[Z_{2b}/(Z_{1b} + Z_{2b})]} = V_{1b} \frac{e'_a/Z_{i1}}{e'_b/Z_{i2}} \quad (4.8)$$

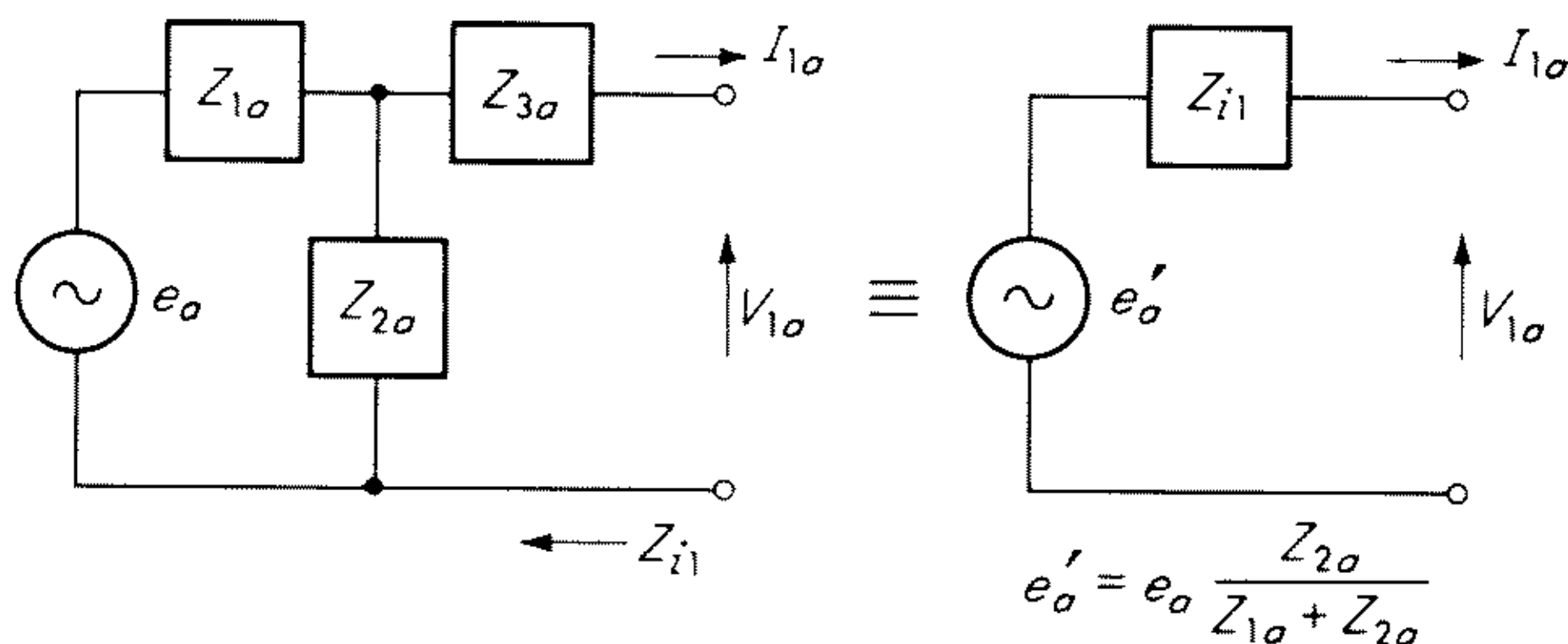


Fig. 4.3

where the subscript a refers to antenna a and b refers to antenna b . The quantities $e'_a = e_a Z_{2a}/(Z_{1a} + Z_{2a})$ and e'_b are the Thévenin equivalent voltages as seen from the terminal planes S_1 and S_2 , respectively.

We may specify an equivalent circuit to represent conditions between the terminals S_1 and S_2 also. The field at S_1 will be linearly proportional to e_a and e_b , and hence the total voltage at S_1 , and also at S_2 , will be linearly proportional to any linear combination of I_{1a} , I_{2a} and I_{1b} , I_{2b} . Thus we can write

$$V_1 = V_{1a} + V_{1b} = (I_{1a} - I_{1b})Z_{11} + (-I_{2a} + I_{2b})Z_{12} \quad (4.9a)$$

$$V_2 = V_{2a} + V_{2b} = (I_{1a} - I_{1b})Z_{21} + (-I_{2a} + I_{2b})Z_{22} \quad (4.9b)$$

The relation (4.4) will enable us to show that $Z_{12} = Z_{21}$. When $e_a = 0$, $e_b \neq 0$, we have

$$V_{1b} = -I_{1b}Z_{11} + I_{2b}Z_{12} \quad V_{2b} = -I_{1b}Z_{21} + I_{2b}Z_{22}$$

while if $e_a \neq 0$, $e_b = 0$, we have

$$V_{1a} = I_{1a}Z_{11} - I_{2a}Z_{12} \quad V_{2a} = I_{1a}Z_{21} - I_{2a}Z_{22}$$

Eliminating all voltages in (4.4) by means of these relations reduces (4.4) to $(I_{1b}I_{2a} - I_{1a}I_{2b})(Z_{12} - Z_{21}) = 0$. Since conditions a and b , that is, e_a and e_b ,

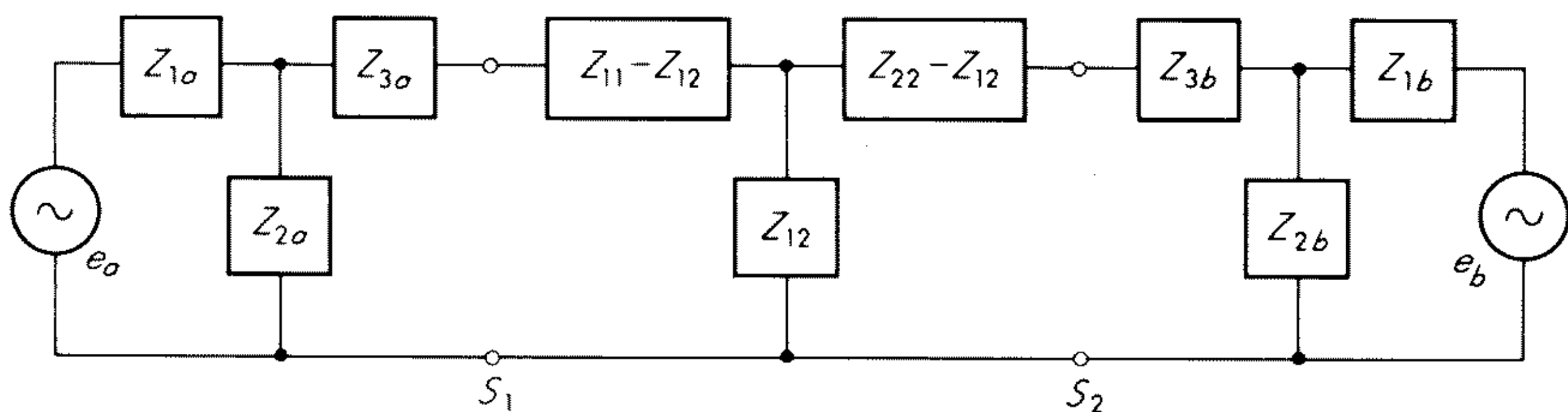


Fig. 4.4 Equivalent circuit for a two-antenna system.

are independent, this can hold in general only if $Z_{12} = Z_{21}$, that is, reciprocity holds. The overall general circuit of a two-antenna system is thus as illustrated in Fig. 4.4. The mutual impedance Z_{12} represents the coupling between the two antennas and will be a function of the distance separating the two antennas, the relative antenna orientation, and their polarization properties (see Probs. 4.3 and 4.4).

Exercise 4.1 Derive the result $(I_{1b}I_{2a} - I_{1a}I_{2b})(Z_{12} - Z_{21}) = 0$.

4.3 Directional Properties of a Receiving Antenna

We shall show in this section that the receiving and transmitting directional characteristics of an antenna are identical. Consider two antennas a and b that are matched to their respective feed lines, and with matched generators (or loads). Let the input resistance (reactance assumed zero) be R_a , R_b , respectively. Let antenna a be fixed in space and let antenna b be moved on the surface of a sphere with antenna a at the center as in Fig. 4.5. Let the orienta-

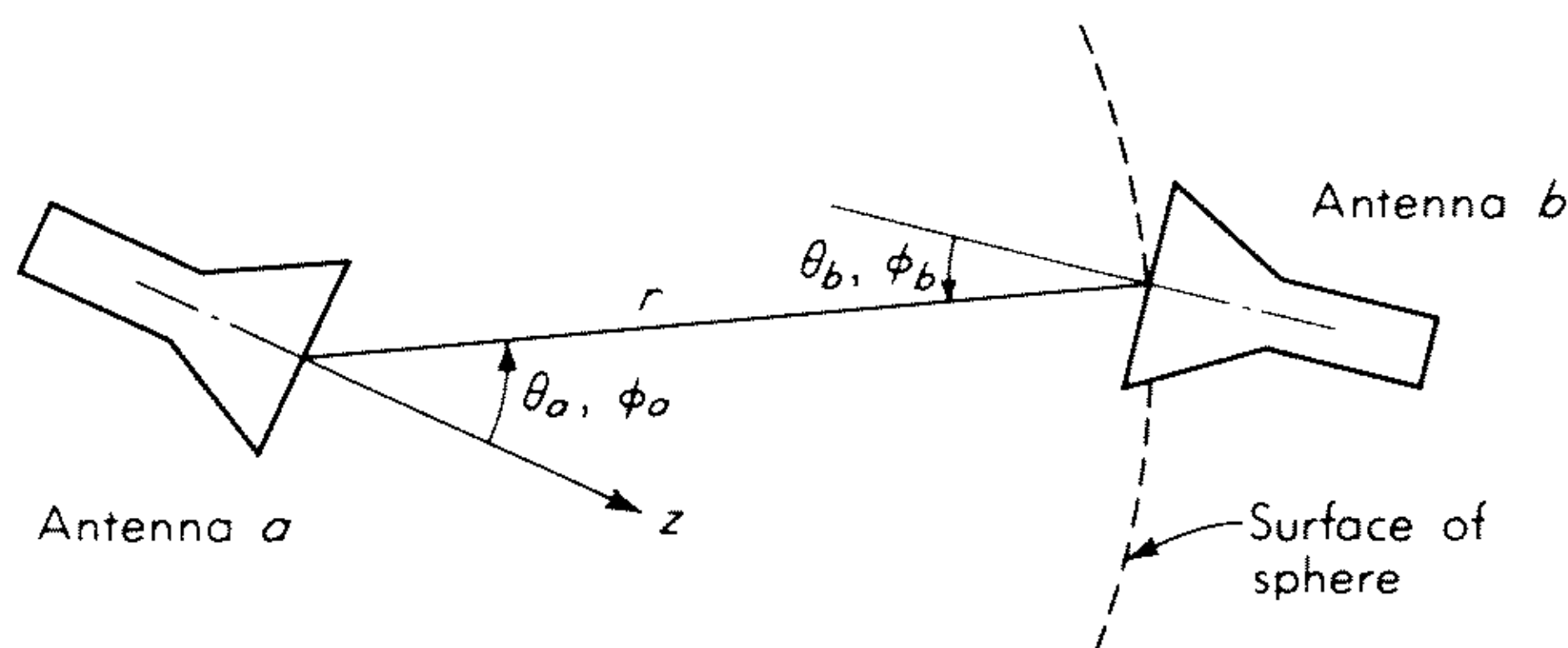


Fig. 4.5 Arrangement to measure the directional properties of a receiving antenna.

tion of the axis of antenna b be specified by the angles θ_b, ϕ_b with the radius vector from antenna a to antenna b as the polar axis. As antenna b moves on the sphere let θ_b, ϕ_b be kept constant. Let θ_a, ϕ_a specify the orientation of the axis of antenna b relative to antenna a . Let antenna a transmit and antenna b receive. As antenna b moves on the sphere around antenna a its received power is a measure of the directional properties of antenna a , provided the antennas are far enough apart that Z_{12} is so small that it does not change the power transmitted by antenna a to any appreciable extent. If this were not the case, the variation in Z_{12} with the angles θ_a, ϕ_a would result in an inaccurate relative measure of the gain $G_a(\theta_a, \phi_a)$. The coupling parameter Z_{12} is also a function of the polarization properties of the two antennas, a detailed discussion of which is given in a later section. For simplicity it is assumed here that both antennas transmit linearly polarized radiation and are always rotated

about their respective axis for maximum received power. (Rotation about the axis does not change the orientation angles θ and ϕ .)

Under the assumed conditions the power received by antenna b is readily computed from the equivalent circuit in Fig. 4.4, which is shown in Fig. 4.6 for

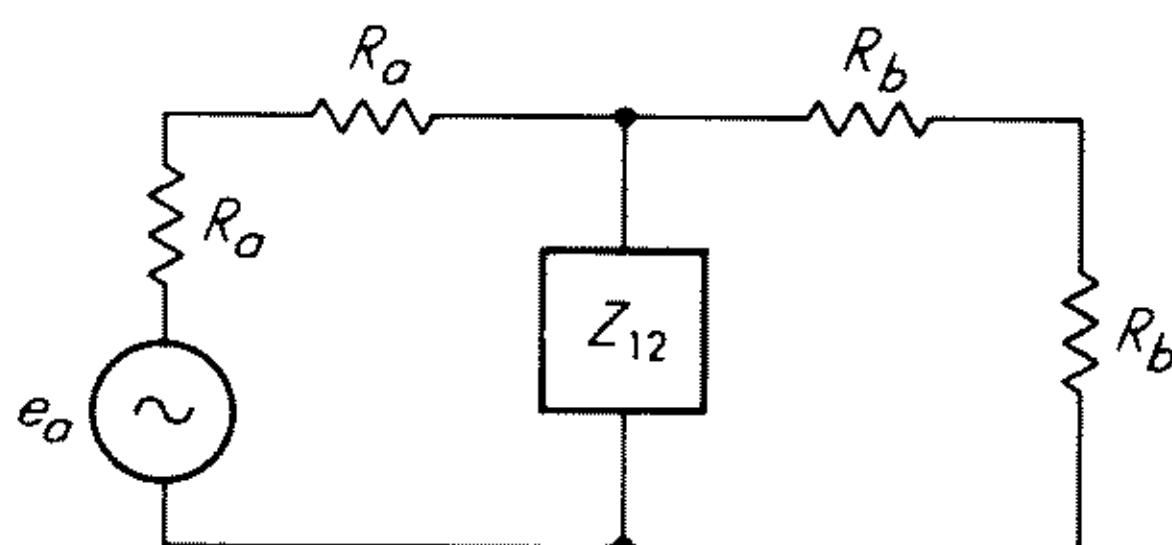


Fig. 4.6 Receiving circuit for antenna b .

the special conditions presently imposed. We find that the received power P_b is given by

$$\begin{aligned} P_b &= \frac{1}{2} \left| \frac{e_a}{2R_a} \right|^2 |Z_{12}(\theta_a, \phi_a)|^2 \frac{R_b}{(2R_b)^2} \\ &= \frac{|e_a|^2}{32R_a^2 R_b} |Z_{12}(\theta_a, \phi_a)|^2 \end{aligned} \quad (4.10)$$

Note that we have approximated $Z_{11} - Z_{12}$ and $Z_{22} - Z_{12}$ by $Z_{11} = R_a$ and $Z_{22} = R_a$, since Z_{12} is very small when the antennas are far apart. Since the power received by antenna b will be proportional to the power density incident on this antenna, and the latter is proportional to the gain $G_a(\theta_a, \phi_a)$ of antenna a in the direction of antenna b , $|Z_{12}(\theta_a, \phi_a)|^2$ is proportional to $G_a(\theta_a, \phi_a)$.

If antenna b is transmitting and antenna a is used for reception, similar considerations show that the power received by antenna a will be given by

$$P_a = \frac{|e_b|^2}{32R_b^2 R_a} |Z_{21}(\theta_a, \phi_a)|^2 \quad (4.11)$$

However, since $Z_{12} = Z_{21}$, the directional properties of antenna a under receiving conditions are the same as for transmitting conditions and in both cases are proportional to the gain $G_a(\theta_a, \phi_a)$. Since antenna a is arbitrary, this property is true for all antennas. Note that this result depends on reciprocity and would not be true for antennas located in a nonreciprocal medium such as a plasma with a static magnetic field present, e.g., the ionosphere in the presence of the earth's magnetic field, or if nonreciprocal devices were incorporated in the antenna structure or feed line. The former is strictly an environmental effect and not an intrinsic characteristic of the antenna itself (see discussion by Tai³).

Results similar to the above are obtained even if the antennas are not matched to their respective feed lines as long as the antenna separation is great enough that $|Z_{12}|$ is much smaller than $|Z_{11}|$ or $|Z_{22}|$ (see Prob. 4.1). For

closely spaced antennas such that $|Z_{12}|$ is comparable to $|Z_{11}|$ and $|Z_{22}|$, the input impedance at the antenna terminals is modified by the presence of a second antenna with a resultant change in radiated power (or received power).

4.4 Antenna Receiving Cross Section

A receiving antenna located in the far-zone region of a transmitting antenna has incident upon it a spherical TEM wave. This incident wave reacts with the receiving antenna to produce the received power in the terminating load. Clearly, the received power will be dependent only on the nature of the incident radiation and not on the specific properties of the transmitting antenna except insofar as they affect the amplitude, phase, and polarization of the incident radiation. Thus it is possible to express the received power in terms of a product of the incident power density per unit area and an effective receiving cross section or area A_r , which is a characteristic of the receiving antenna alone. In this section we shall show that the effective area A_r for any antenna is related to its gain $G(\theta, \phi)$ by a universal constant $\lambda_0^2/4\pi$, that is,

$$A_r(\theta, \phi) = \frac{\lambda_0^2}{4\pi} G(\theta, \phi) \quad (4.12)$$

Note that A_r is a function of the angles θ and ϕ which specify the direction of incidence relative to the antenna axis. In addition, (4.12) assumes that the polarization of the incoming radiation is that which gives maximum received power and that the antenna is matched to the terminating load. The effect of unmatched polarization is treated in detail in a later section.

With reference to Fig. 4.7 let antenna a be fed from a shielded source and let

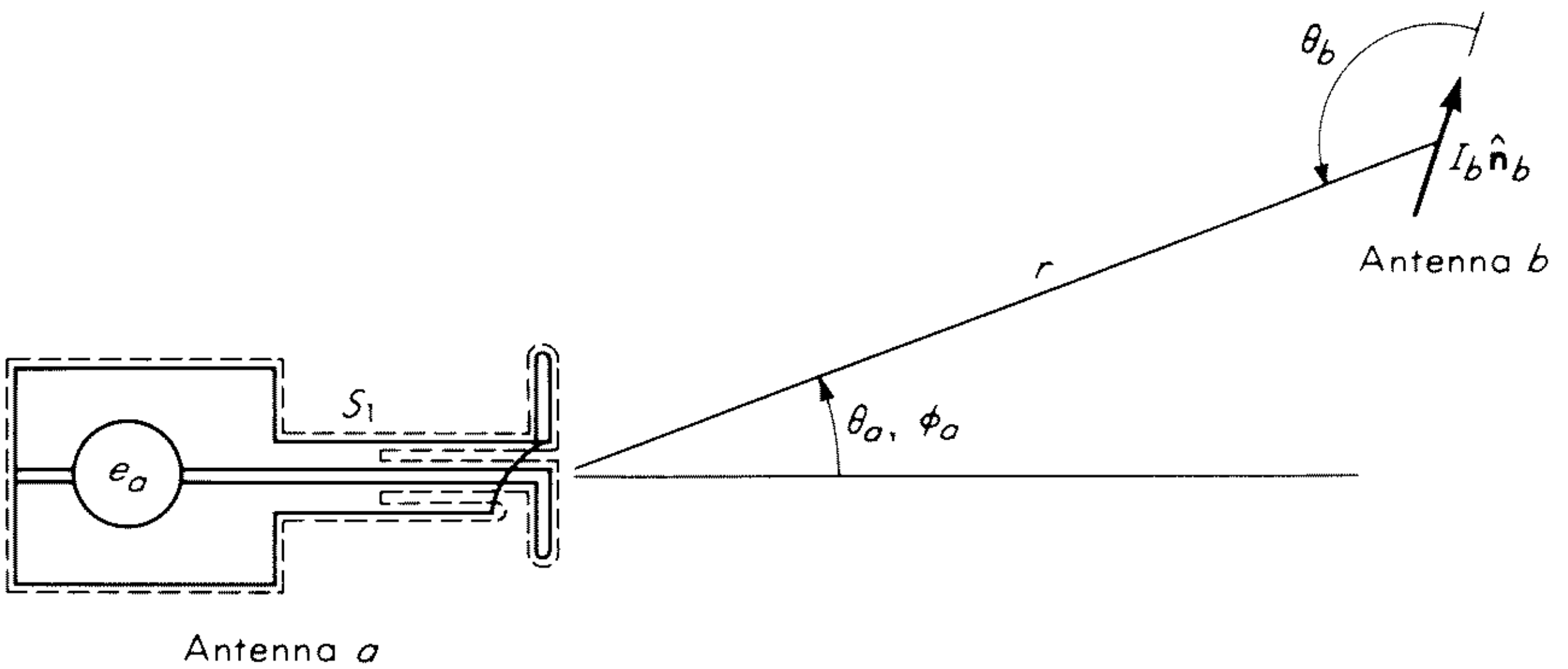


Fig. 4.7 An antenna excited by a current element.

antenna b be a short linear current element. When antenna a is transmitting, let $\mathbf{E}_a, \mathbf{H}_a$ be the fields produced. Similarly, let $\mathbf{E}_b, \mathbf{H}_b$ be the fields radiated by

the current element. An application of the Lorentz reciprocity theorem (1.67) as in Sec. 4.2 gives

$$\begin{aligned} \int_{S_1} (\mathbf{E}_a \times \mathbf{H}_b - \mathbf{E}_b \times \mathbf{H}_a) \cdot d\mathbf{S} &= - \int_V \mathbf{E}_a \cdot \mathbf{J}_b dV \\ &= V_{1a}I_{1b} + V_{1b}I_{1a} = -\mathbf{E}_a \cdot \hat{\mathbf{n}}_b I_b \Delta l \end{aligned} \quad (4.13)$$

where the current element (antenna b) has been included in the volume of integration. The current element is of length Δl , with total current I_b , and $\hat{\mathbf{n}}_b$ is a unit vector along the current element.

Exercise 4.2 Derive (4.13).

We may express the power received by antenna a in two alternative ways. Under receiving conditions the voltage at the terminal plane S_1 is V_{1b} and the received power is

$$P_a = \frac{1}{2} \operatorname{Re} V_{1b} I_{1b}^* = \frac{|V_{1b}|^2}{2} \operatorname{Re} (Z_{i1}^*)^{-1} = \frac{|V_{1b}|^2}{2|Z_{i1}|^2} \operatorname{Re} Z_{i1} \quad (4.14a)$$

where Z_{i1} is the impedance seen looking toward the generator from the terminal plane. Note that under receiving conditions the generator internal impedance is replaced by an equivalent load impedance. We can also express the received power in terms of the receiving cross section A_r ; thus

$$P_a = \frac{1}{2} \zeta_0^{-1} |\mathbf{E}_b|^2 A_r = \frac{A_r \zeta_0 k_0^2 (I_b \Delta l)^2 \sin^2 \theta_b}{32\pi^2 r^2} \quad (4.14b)$$

where we have used (2.6a) for the field from a current element. The angle θ_b measures the angle between the radius vector from antenna a and the axis of the current element, while r is the distance between the antenna and the current element.

In order to obtain an expression for A_r we equate (4.14a) and (4.14b) and eliminate V_{1b} by means of (4.13). First note that, according to the definitions given in Sec. 4.2, we can express (4.13) as follows:

$$\frac{V_{1a}V_{1b}}{Z_{i1}} + \frac{V_{1a}V_{1b}}{Z_{in,1}} = V_{1a}V_{1b} \frac{Z_{in,1} + Z_{i1}}{Z_{in,1}Z_{i1}} = -E_a I_b \Delta l \cos \psi$$

where $\cos \psi$ is the direction cosine between the current element and the electric field \mathbf{E}_a radiated by antenna a (assumed to be linearly polarized). The squared magnitude of this expression is

$$|V_{1a}V_{1b}|^2 \left| \frac{Z_{in,1} + Z_{i1}}{Z_{in,1}Z_{i1}} \right|^2 = |E_a|^2 (I_b \Delta l)^2 \cos^2 \psi \quad (4.15)$$

where we have assumed I_b to be real. To eliminate the voltage V_{1a} note that the power input to antenna a may be expressed as

$$\begin{aligned} \frac{1}{2} \operatorname{Re} V_{1a} I_{1a}^* &= \frac{1}{2} |V_{1a}|^2 \operatorname{Re} (Z_{in,1}^*)^{-1} \\ &= \frac{1}{2} \frac{|V_{1a}|^2}{|Z_{in,1}|^2} \operatorname{Re} Z_{in,1} \end{aligned}$$

and hence the quantity $|E_a|^2$ is given by

$$|E_a|^2 = 2\zeta_0 \frac{G_a(\theta_a, \phi_a)}{4\pi r^2} \frac{1}{2} \frac{|V_{1a}|^2}{|Z_{in,1}|^2} \operatorname{Re} Z_{in,1} \quad (4.16)$$

We can substitute (4.16) into (4.15) and thus eliminate V_{1a} and obtain an expression for V_{1b} . This expression is then used in (4.14a), which is subsequently equated to (4.14b) and solved for A_r . The details are omitted, but the reader can easily verify that the result is

$$A_r = G_a \frac{\lambda_0^2 \cos^2 \psi}{4\pi \sin^2 \theta_b} \frac{4 \operatorname{Re} Z_{in,1} \operatorname{Re} Z_{il}}{|Z_{in,1} + Z_{il}|^2} \quad (4.17)$$

Let us now assume that the current element is rotated for maximum received power ($\cos \psi = \sin \theta_b = 1$) and that we are dealing with a matched antenna system. Under matched conditions $Z_{il} = Z_{in,1}^*$, and if we let $\operatorname{Re} Z_{in,1} = R_a$, we find that

$$A_r(\theta_a, \phi_a) = \frac{\lambda_0^2}{4\pi} G_a(\theta_a, \phi_a) \quad (4.18)$$

which is the desired result relating the maximum receiving cross section to the antenna gain under matched conditions. Since antenna a is arbitrary, this result is true for any matched antenna. (It is also implied here that the polarization of the antenna matches that of the incoming radiation.)

Exercise 4.3 Fill in the details in the derivation of (4.17) and (4.18).

The general expression (4.17) can also be used to examine the effect of antenna mismatch on the receiving cross section. Let the transmission line be terminated in a pure resistive load impedance R_L equal to the characteristic impedance Z_c ; then $Z_{il} = Z_c = R_L$. In addition, let $Z_{in,1} = R_a + jX_a$ be the input impedance to the antenna. For a given antenna $Z_{in,1}$ is fixed, so that a matched condition must be obtained by means of a separate network which transforms $Z_{in,1}$ at the terminal plane S_1 into an impedance Z_c at the generator terminals. This network will transform the impedance Z_c into $Z_{in,1}^*$ at the terminal plane S_1 when looking toward the generator or load (see Prob. 4.2). Under matched conditions the receiving cross section is given by (4.18), but for the unmatched case as described above we obtain

$$A_r = \frac{\lambda_0^2}{4\pi} G_a \frac{4R_a R_L}{|R_a + jX_a + R_L|^2} \quad (4.19)$$

by using (4.17) with $\cos \psi = \sin \theta_b = 1$. The reflection coefficient Γ at the generator terminals is given by

$$\Gamma = \frac{Z_{in,1} - Z_c}{Z_{in,1} + Z_c}$$

and thus the fraction of the available power supplied to the antenna is

$$1 - |\Gamma|^2 = \frac{4R_a R_L}{(R_a + R_L)^2 + X_a^2}$$

Consequently, for a mismatched receiving antenna the receiving cross section can be expressed as

$$A_r(\theta_a, \phi_a) = (1 - |\Gamma|^2) \frac{\lambda_0^2}{4\pi} G_a(\theta_a, \phi_a) \quad (4.20)$$

For a mismatched antenna the loss in received power is the same as the loss in transmitted power. If G is taken to be the gain of the mismatched antenna, then we can still write $A_r = (\lambda_0^2/4\pi)G$. This requires that we define the gain as

$$\begin{aligned} G(\theta, \phi) &= 4\pi \frac{\text{power radiated per steradian in direction } \theta, \phi}{\text{maximum available power from generator}} \\ &= (1 - |\Gamma|^2) \frac{\text{power radiated per steradian in direction } \theta, \phi}{\text{power input to antenna}} \end{aligned} \quad (4.21)$$

In (4.21) the maximum available power from the generator is the power input to the antenna when a lossless matching network is used to transform the antenna impedance into the conjugate of the generator impedance.

4.5 Reception of Completely Polarized Waves

An electromagnetic wave may be elliptically, circularly, or linearly polarized, and as long as the state of polarization does not change with time it is said to be completely polarized. At the opposite extreme is the randomly polarized wave whose polarization varies continuously in a random fashion with a zero time-average value of polarization in any one state. In between these two extremes comes the partially polarized radiation which consists of two parts, namely, a randomly polarized component and a completely polarized component which can be elliptically, circularly, or linearly polarized. Randomly and partially polarized radiation is of particular interest to the radio astronomer. In this section we shall discuss the reception of completely polarized radiation, and in the following section partially polarized radiation will be dealt with.

The power received by an antenna depends on its polarization properties and also on the polarization of the incident radiation. In order to illustrate this effect in a simple situation, consider (4.13), which gives the received voltage V_{1b} . If we assume that the antenna is not terminated in a load, i.e., is open-circuited at the terminals, then $I_{1b} = 0$ and

$$V_{oc} = (V_{1b})_{oc} = -\frac{\mathbf{E}_a \cdot \hat{\mathbf{n}}_b}{I_{1a}} I_b \Delta l \quad (4.22)$$

is the open-circuit received voltage.

Let the current element be oriented in a plane perpendicular to the radius vector from the receiving antenna so that $\sin \theta_b = 1$. When the antenna is transmitting, it will in general radiate an elliptical polarized wave for which (see Sec. 2.3)

$$\mathbf{E}_a = E_\theta \hat{\boldsymbol{\theta}} + E_\phi \hat{\boldsymbol{\phi}} \quad (4.23)$$

where E_θ and E_ϕ are the complex phasor components at the position of the current element. The received voltage is thus

$$V_{oc} = C(E_\theta n_\theta + E_\phi n_\phi)$$

where C is a suitable proportionality constant and n_θ, n_ϕ are the components of $\hat{\mathbf{n}}_b$. The received power P_r will be proportional to $|V_{oc}|^2$, and hence

$$P_r \propto |E_\theta n_\theta + E_\phi n_\phi|^2$$

For simplicity let E_θ be real and positive and let $E_\phi = \tau e^{j\beta} E_\theta$, where τ and β are positive real constants. We can now write

$$\begin{aligned} P_r &\propto E_\theta^2 [(n_\theta + \tau n_\phi \cos \beta)^2 + (\tau n_\phi \sin \beta)^2] \\ &= E_\theta^2 (n_\theta^2 + \tau^2 n_\phi^2 + 2\tau n_\theta n_\phi \cos \beta) \end{aligned} \quad (4.24)$$

Exercise 4.4 Show that the received power is given by

$$\frac{|V_{oc}|^2 \operatorname{Re} Z_{i1}}{2|Z_{in,1} + Z_{i1}|^2}$$

Hint: By Thévenin's theorem the antenna is equivalent to a generator with voltage V_{oc} and internal impedance $Z_{in,1}$.

The polarization property of the antenna is completely specified by the polarization of the field that it radiates, i.e., by \mathbf{E}_a . The polarization of the incident radiation, which in this case is that from a linear current element, is determined by the unit vector $\hat{\mathbf{n}}_b$ and corresponds to linear polarization in the plane of $\hat{\mathbf{n}}_b$ and the unit radius vector $\hat{\mathbf{r}}$. It is readily shown from (4.24) that for maximum received power it is required that

$$\beta = 0 \quad \frac{E_\theta}{E_\phi} = \frac{n_\theta}{n_\phi} = \frac{1}{\tau} \quad (4.25)$$

that is, the antenna polarization should be linear and in the same direction as that of the unit vector $\hat{\mathbf{n}}_b$. In this case the received power is proportional to $E_\theta^2(1 + \tau^2)$.

As another simple example let the antenna radiate a circular polarized field with $E_\phi = jE_\theta$, which corresponds to $\beta = \pi/2$ and $|E_\theta| = |E_\phi|$. From (4.24)

Exercise 4.5 Verify that (4.25) maximizes P_r . Hint: Let $|E_\theta| = E_\theta(1 + \tau^2)^{1/2} \cos \delta$, $|E_\phi| = E_\theta(1 + \tau^2)^{1/2} \sin \delta$ and set $\partial P_r / \partial \beta = \partial P_r / \partial \delta = 0$ to obtain $\tan 2\delta = (2 \tan \delta) / (1 - \tan^2 \delta) = 2(n_\phi / n_\theta) / [1 - (n_\phi / n_\theta)^2]$.

we obtain

$$P_r \propto (E_\theta n_\theta)^2 + (E_\theta n_\phi)^2 = E_\theta^2$$

This result shows that, when a circularly polarized antenna is used to receive linearly polarized radiation, the received power is only one-half of the maxi-

mum [proportional to $(1 + \tau^2)E_\theta^2 = 2E_\theta^2$] that could be received if the antenna polarization were matched to that of the incident radiation.

The above results are very restricted, since they account only for linearly polarized incident radiation. However, we may easily generalize (4.22) by regarding $\hat{\mathbf{n}}_b$ as a complex vector which characterizes a more general state of polarization for the incident wave. The receiving properties of an antenna under these more general conditions are discussed by Sichak and Milazzo,⁴ Yeh,⁵ Roubine,⁶ Hatkin,⁷ Sinclair,⁸ and Morgan and Evans⁹ and also in a series of coordinated papers by Rumsey,¹⁰ Deschamps,¹¹ Kales,¹² and Bohnert.¹³

Sinclair introduces a complex effective vector length \mathbf{h} to characterize the receiving antenna.⁸ Under transmitting conditions the radiated field is expressed in the form

$$\mathbf{E}_a = \frac{j\zeta_0 I_{1a} \mathbf{h}}{2\lambda_0 r} e^{-jk_0 r} \quad (4.26)$$

where \mathbf{h} is a complex vector with complex phasor components h_θ and h_ϕ . For a current element $h_\phi = 0$, $h_\theta = \Delta l \sin \theta$, as reference to (2.6a) shows, and hence \mathbf{h} gives the radiated field relative to that from a current element of unit length. The incident field is expressed by its complex components $E_{0\theta}$ and $E_{0\phi}$. The open-circuit received voltage is then given by

$$V_{oc} = h_\theta E_{0\theta} + h_\phi E_{0\phi} = \mathbf{h} \cdot \mathbf{E}_0 \quad (4.27)$$

This equation is a generalization of (4.22), which we may show as follows: The incident field \mathbf{E}_0 may be regarded as originating from two perpendicular current elements $I_\theta \Delta l \hat{\boldsymbol{\theta}}$ and $I_\phi \Delta l \hat{\boldsymbol{\phi}}$ with suitable complex amplitudes I_θ and I_ϕ and with a location specified by the angles θ and ϕ relative to the axis (polar axis) of the receiving antenna (see Fig. 4.8). These current elements will produce an incident field given by (2.6a) as

$$\mathbf{E}_0 = -\frac{j\zeta_0 \Delta l}{2\lambda_0 r} e^{-jk_0 r} (I_\theta \hat{\boldsymbol{\theta}} + I_\phi \hat{\boldsymbol{\phi}}) \quad (4.28)$$

from which we obtain

$$I_\theta = -\frac{2\lambda_0 r e^{+jk_0 r}}{j\zeta_0 \Delta l} E_{0\theta} \quad (4.29a)$$

$$I_\phi = -\frac{2\lambda_0 r e^{+jk_0 r}}{j\zeta_0 \Delta l} E_{0\phi} \quad (4.29b)$$

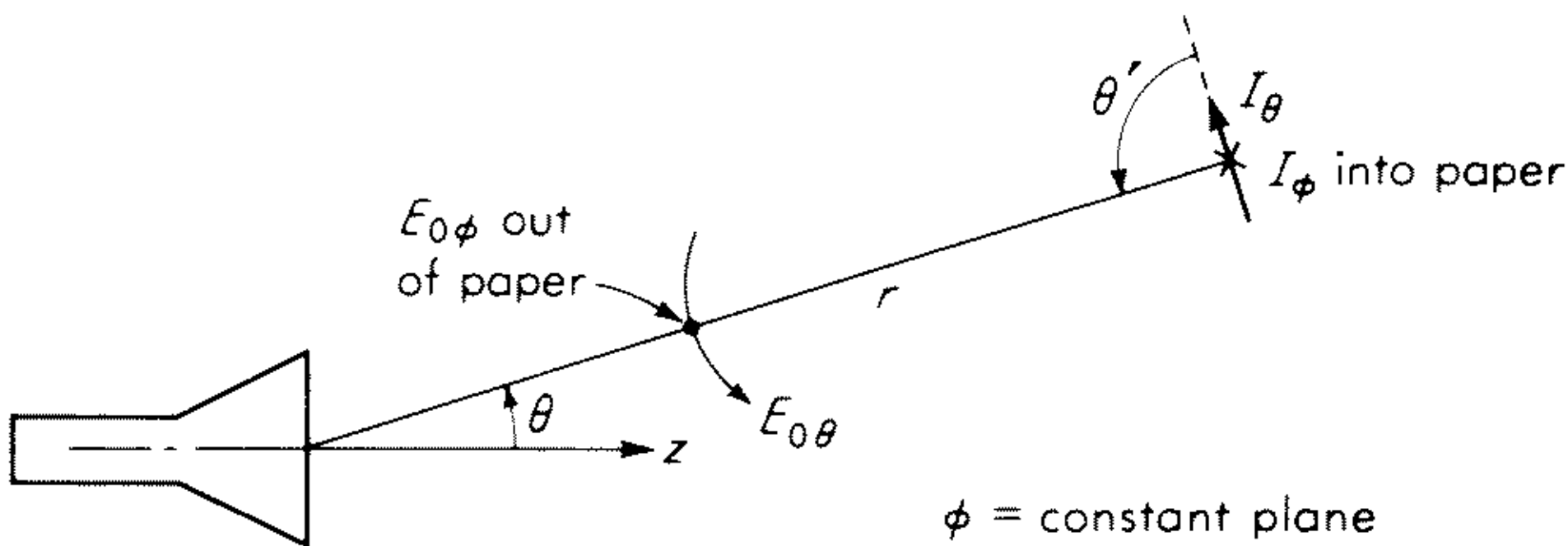


Fig. 4.8 Current elements producing a specified incident field.

Note that an additional minus sign occurs in (4.28) because the current elements are located at r, θ, ϕ and not the origin (this is clear from Fig. 4.8). At the position of the current elements the antenna produces a field given by (4.26). When we substitute (4.26) and (4.29) into the basic formula (4.22) for the received open-circuit voltage, we obtain Sinclair's result (4.27).

When the antenna polarization does not match that of the incident radiation, the effective receiving cross section is reduced. Since the received power will be proportional to $|V_{oc}|^2$ the reduction factor is clearly given by

$$p = \frac{|\mathbf{h} \cdot \mathbf{E}_0|^2}{|\mathbf{h}|^2 |\mathbf{E}_0|^2} \quad (4.30)$$

where the denominator is the maximum possible value of $|\mathbf{h} \cdot \mathbf{E}_0|^2$. This maximum occurs when \mathbf{h} is equal to a real constant times the complex conjugate of \mathbf{E}_0 (this is readily proved by an extension of Exercise 4.5). The receiving cross section is also reduced by a factor $1 - |\Gamma|^2$ when the antenna is not matched to the load. Thus in the general case of both mismatched polarizations and impedances we have

$$A_r(\theta, \phi) = (1 - |\Gamma|^2) p \frac{\lambda_0^2}{4\pi} G(\theta, \phi) \quad (4.31)$$

which is essentially the definition of effective receiving cross section proposed by Tai.¹⁴

A convenient way of visualizing the state of polarization of an antenna and the incident radiation has been described by Deschamps^{11,15} and will be outlined below. The antenna polarization is specified by the complex vector \mathbf{h} . Without loss in generality we can assume h_θ to be real and let $h_\phi = \tau e^{j\beta} h_\theta$, where τ and β are real positive constants. The physical field corresponding to \mathbf{h} is

$$E_\theta = \text{Re } h_\theta e^{j\omega t} = h_\theta \cos \omega t \quad E_\phi = \text{Re } h_\phi e^{j\omega t} = h_\theta \tau \cos(\omega t + \beta)$$

If we eliminate the time, we find that

$$(E_\theta)^2 + \left(\frac{E_\phi}{\tau}\right)^2 - \frac{2E_\theta E_\phi}{\tau} \cos \beta = h_\theta^2 \sin^2 \beta \quad (4.32)$$

This is the equation of an ellipse and shows that the field vector described by \mathbf{h} traces out an ellipse. When $0 \leq \beta \leq \pi/2$, the direction of rotation is from the ϕ axis into the θ axis. Viewed in the outward direction of propagation, the rotation is counterclockwise, so the polarization is said to be left elliptical polarization. When $\pi/2 \leq \beta \leq \pi$, the polarization is right elliptical polarization. The special case of $\beta = 0$ or π gives

$$\left(E_\theta \pm \frac{E_\phi}{\tau}\right)^2 = 0$$

which is a linearly polarized wave. Circular polarization is obtained when $\beta = \pi/2$ and $\tau = 1$, in which case (4.32) becomes $E_\theta^2 + E_\phi^2 = h_\theta^2$. An elliptically polarized wave can be decomposed into the sum of two linearly polarized waves or the sum of two left and right circularly polarized waves.⁷

The state of polarization represented by \mathbf{h} will vary with position as given by the angles θ and ϕ . However, for a specified value of θ and ϕ the polarization state can be uniquely described by giving the major and minor axis and the orientation of the major axis of the polarization ellipse. Each state of polarization can be represented by a point on a sphere called the Poincaré sphere.¹⁶ This representation is obtained by introducing the Stokes parameters, which are defined by the following relations:¹⁷

$$s_0 = h_\theta^2(1 + \tau^2) \quad (4.33a)$$

$$s_1 = h_\theta^2(1 - \tau^2) \quad (4.33b)$$

$$s_2 = 2\tau h_\theta^2 \cos \beta \quad (4.33c)$$

$$s_3 = 2\tau h_\theta^2 \sin \beta \quad (4.33d)$$

where $s_0^2 = s_1^2 + s_2^2 + s_3^2$. In terms of two auxiliary angles ψ and χ given by

$$\tan 2\psi = \frac{2\tau}{1 - \tau^2} \cos \beta \quad (4.34a)$$

$$\sin 2\chi = \frac{2\tau}{1 + \tau^2} \sin \beta \quad (4.34b)$$

we can also write

$$s_1 = s_0 \cos 2\chi \cos 2\psi \quad (4.35a)$$

$$s_2 = s_0 \cos 2\chi \sin 2\psi \quad (4.35b)$$

$$s_3 = s_0 \sin 2\chi \quad (4.35c)$$

The angle ψ is the orientation angle of the major axis relative to the θ axis, and χ is the ellipticity angle defined such that $\tan \chi$ equals the axial ratio.¹⁷ These latter equations show that s_1 , s_2 , s_3 may be regarded as the rectangular coordinates of a point on a sphere (the Poincaré sphere) of radius s_0 as shown in Fig. 4.9. Points on the equator correspond to $\chi = 0$, that is, $\beta = 0$, or linear

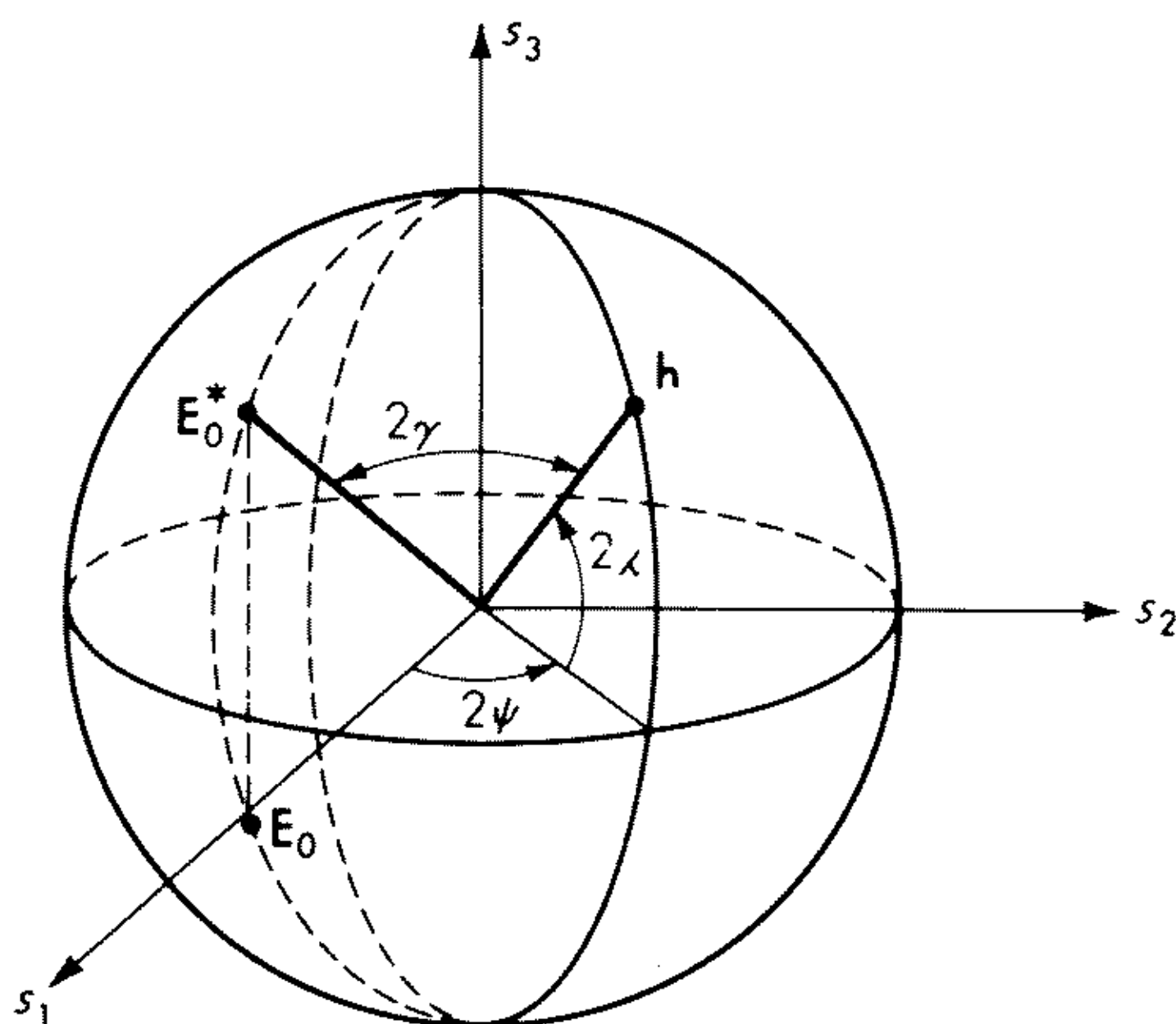


Fig. 4.9 The Poincaré sphere representation of the state of polarization.

polarization. The point at the pole $2\chi = \pi/2$ corresponds to $\beta = \pi/2$, $\tau = 1$, or left circular polarization, while the pole $2\chi = -\pi/2$ corresponds to right circular polarization. All other points on the upper or lower half of the sphere correspond to left or right elliptical polarization, respectively.

If we choose a proper phase reference, we can take $E_{0\theta}$ to be real and let $E_{0\phi} = E_{0\theta} \sigma e^{j\alpha}$, where σ and α are positive and real. It is then readily found that (4.30) can be expressed by

$$p = \frac{1 + \sigma^2 \tau^2 + 2\sigma\tau \cos(\alpha + \beta)}{(1 + \sigma^2)(1 + \tau^2)} \quad (4.36)$$

This result has an interesting interpretation in terms of the Poincaré sphere. The quantity $\mathbf{h}/|\mathbf{h}|$ is represented by a unit vector with components given by the normalized Stokes' parameters s_1/s_0 , s_2/s_0 , s_3/s_0 [see (4.33)]. Likewise, we can represent $\mathbf{E}_0^*/|\mathbf{E}_0|$ by a unit vector with components

$$\begin{aligned} \frac{s_1'}{s_0'} &= \frac{1 - \sigma^2}{1 + \sigma^2} \\ \frac{s_2'}{s_0'} &= \frac{2\sigma}{1 + \sigma^2} \cos \alpha \\ \frac{s_3'}{s_0'} &= -\frac{2\sigma}{1 + \sigma^2} \sin \alpha \end{aligned}$$

The scalar product between these two unit vectors gives

$$\cos 2\gamma = \left[1 + \sigma^2 \tau^2 - \sigma^2 - \tau^2 + \frac{4\sigma\tau \cos(\alpha + \beta)}{(1 + \tau^2)(1 + \sigma^2)} \right]$$

where 2γ is the angular distance between the two points on the unit Poincaré sphere representing the state of polarization defined by \mathbf{h} and \mathbf{E}_0^* . (The point corresponding to \mathbf{E}_0^* is the mirror image in the equatorial plane of the point representing \mathbf{E}_0 as shown in Fig. 4.9.) If we replace $\cos 2\gamma$ by $2 \cos^2 \gamma - 1$, we readily find that

$$p = \cos^2 \gamma \quad (4.37)$$

It is now clear that the maximum value of p corresponds to $\gamma = 0$ or π , which means that the angular distance between the points representing \mathbf{h} and \mathbf{E}_0^* is zero. Thus for maximum reception $\sigma = \tau$ and $\alpha = -\beta$, that is,

$$\frac{h_\theta}{h_\phi} = \left(\frac{E_\theta}{E_\phi} \right)^* \quad (4.38)$$

The received power will be zero whenever $2\gamma = \pi$ or the points representing \mathbf{h} and \mathbf{E}_0^* are diametrically opposite. For good polarization matching, these two points must be close together on the Poincaré sphere.

The polarization loss factor p can also be expressed as one-half of the scalar product between the two normalized four-component Stokes vectors with

components $(1, s_1/s_0, s_2/s_0, s_3/s_0)$ and $(1, s'_1/s'_0, s'_2/s'_0, s'_3/s'_0)$, as direct expansion and comparison with (4.34) shows; that is,

$$p = \frac{s_0 s'_0 + s_1 s'_1 + s_2 s'_2 + s_3 s'_3}{2s_0 s'_0} \quad (4.39)$$

4.6 Reception of Partially Polarized Waves

A strictly monochromatic wave is always completely polarized, since the phasors associated with such a wave are independent of time. A polychromatic wave can, however, be completely, partially, or randomly polarized. It is difficult to treat analytically the reception of a general polychromatic wave consisting of a broad frequency spectrum, since this would require a knowledge of the antenna characteristics over the corresponding frequency band. In practice, the receivers used are narrow-band devices so that, as a first approximation, the antenna characteristics can be assumed to remain constant over the frequency range of interest.[†] A narrow-band polychromatic wave is called a quasi-monochromatic wave and can be represented by

$$\mathbf{E}_0(\mathbf{r}, t) = \text{Re } \mathbf{E}_0(\mathbf{r}, t) e^{j\omega t} \quad (4.40)$$

where $\mathbf{E}_0(\mathbf{r}, t)$ is a slowly varying function of time, i.e., it has frequency components occupying a narrow range $\Delta\omega$ centered on $\omega = 0$.

The reception of a polychromatic wave of the form given by (4.40) can be treated by means of a modified set of Stokes' parameters or by introducing the polarization coherence matrix. We shall give a short discussion of the main features of the theory and refer the reader to papers by Ko¹⁸⁻²¹ and the texts by Born and Wolf¹⁷ and Papas²² for a more detailed treatment.

At any instant of time a narrow-band polychromatic wave has a definite state of polarization. Waves arriving at different angles θ and ϕ may, of course, have different states of polarization at the same instant of time. Since the wave is only quasi-monochromatic, the state of polarization will vary slowly with time. Therefore, the quantities of interest are time averages of the instantaneous signal. Consequently, we need to examine the time average of the product of two narrow-band signals before proceeding further. Actually, in practice, interest in partially polarized waves arises in problems in which little knowledge about the signal is available except in a statistical sense. However, for statistically stationary processes ensemble averages may be replaced by time averages.²³ We shall assume stationarity throughout in the discussion to follow.

Consider two narrow-band signals

$$e_1(t) = \text{Re } a_1(t) e^{j\omega t + j\phi_1(t)} = a_1 \cos(\omega t + \phi_1) \quad (4.41a)$$

$$e_2(t) = \text{Re } a_2(t) e^{j\omega t + j\phi_2(t)} = a_2 \cos(\omega t + \phi_2) \quad (4.41b)$$

[†]The general theory for the reception of wide-band stochastic fields has been given by Childers.⁴⁴

where a_1 , a_2 , ϕ_1 , ϕ_2 are all slowly varying real functions of time. The time average of the product is given by

$$\begin{aligned}\langle e_1(t)e_2(t) \rangle &= \lim_{T \rightarrow \infty} \frac{1}{2T} \int_{-T}^T e_1(t)e_2(t) dt \\ &= \lim_{T \rightarrow \infty} \frac{1}{2T} \int_{-T}^T \frac{a_1 a_2}{2} [\cos(\phi_1 - \phi_2) \\ &\quad + \cos(\phi_1 + \phi_2) \cos 2\omega t - \sin(\phi_1 + \phi_2) \sin 2\omega t] dt\end{aligned}$$

The last two terms average to essentially zero, so we obtain

$$\begin{aligned}\langle e_1 e_2 \rangle &= \frac{1}{2} \langle a_1 a_2 \cos(\phi_1 - \phi_2) \rangle \\ &= \frac{1}{2} \operatorname{Re} \langle a_1 e^{j\phi_1} a_2 e^{-j\phi_2} \rangle\end{aligned}\tag{4.42}$$

The analytic signals associated with e_1 and e_2 are (the analytic signal was introduced by Gabor and a good discussion is given in Born and Wolf¹⁷):

$$E_1(t) = a_1(t)e^{j\phi_1(t)+j\omega t}\tag{4.43a}$$

$$E_2(t) = a_2(t)e^{j\phi_2(t)+j\omega t}\tag{4.43b}$$

in terms of which we can express the time average as

$$\langle e_1 e_2 \rangle = \frac{1}{2} \operatorname{Re} \langle E_1 E_2^* \rangle\tag{4.44}$$

where E_2^* is the complex conjugate of E_2 . Note that when a_1 , a_2 , ϕ_1 , and ϕ_2 are slowly varying, they will have frequency components only in a narrow band $\Delta\omega$ which is very small compared to the mean radian frequency ω . The functions a_1 and a_2 may be conveniently viewed as the envelopes of the signals e_1 and e_2 .

In addition to the above result we shall also need the Fourier transform relation developed below. (For stochastic signals we implicitly assume that the time functions are truncated at $|t| = T$ so their Fourier transforms will exist. The limit $T \rightarrow \infty$ is taken when computing the time average, which is finite.²³) Let

$$A(\lambda) = \int_{-\infty}^{\infty} e(t)e^{-j\lambda t} dt\tag{4.45a}$$

$$\text{then} \quad e(t) = \frac{1}{2\pi} \int_{-\infty}^{\infty} A(\lambda)e^{j\lambda t} d\lambda\tag{4.45b}$$

Since $e(t)$ is real, $A(-\lambda) = A^*(\lambda)$. We can express $e(t)$ in the form

$$\begin{aligned}e(t) &= \frac{1}{2\pi} \int_0^{\infty} A(\lambda)e^{j\lambda t} d\lambda + \frac{1}{2\pi} \int_{-\infty}^0 A(\lambda)e^{j\lambda t} d\lambda \\ &= \frac{1}{2\pi} \int_0^{\infty} [A(\lambda)e^{j\lambda t} + A(-\lambda)e^{-j\lambda t}] d\lambda\end{aligned}$$

by replacing λ by $-\lambda$ in the last integral. But the above result may also be written

$$\begin{aligned} e(t) &= \frac{1}{2\pi} \int_0^\infty [A(\lambda)e^{j\lambda t} + A^*(\lambda)e^{-j\lambda t}] d\lambda \\ &= \operatorname{Re} \frac{1}{\pi} \int_0^\infty A(\lambda)e^{j\lambda t} d\lambda \end{aligned} \quad (4.46)$$

The analytic signal $E(t) = a(t)e^{j\omega t + j\phi(t)}$, with a real part $e(t)$, is now seen to be given by

$$E(t) = \frac{1}{\pi} \int_0^\infty A(\lambda)e^{j\lambda t} d\lambda \quad (4.47)$$

which is the required relation.

We now return to the problem of the reception of quasi-monochromatic waves. The basic relation (4.22) or its extension (4.27) holds for each Fourier component of the signal. Thus $\mathbf{h}(\theta, \phi, \omega)$ is the antenna transfer function in the frequency domain. When receiving a narrow-band signal, we can, as a first approximation, treat \mathbf{h} as a complex constant having a value corresponding to the mean value of frequency, which we still denote by ω .

Let $E_{\theta\theta^r}(t)$ and $E_{\phi\phi^r}(t)$ be the θ and ϕ components of the incident wave at the antenna in the time domain. These signals are the real parts of the associated analytic signals, which we denote by $E_{\theta\theta}(t)$ and $E_{\phi\phi}(t)$. The contribution of $E_{\theta\theta^r}(t)$ to the received open-circuit voltage will be

$$v_{oc,\theta} = \frac{1}{2\pi} \int_{-\infty}^\infty \int_{-\infty}^\infty h_\theta(\lambda) E_{\theta\theta^r}(t') e^{-j\lambda(t'-t)} dt' d\lambda$$

as obtained by expressing $E_{\theta\theta^r}$ in terms of its Fourier transform, multiplying by the transfer function $h_\theta(\lambda)$, and converting the result into the time domain. Now $E_{\theta\theta^r}(t)$ has frequency components in a small interval $\Delta\omega$ centered on ω only, and we may approximate $h_\theta(\lambda)$ by $h_\theta(\omega)$ in this interval and then, by steps analogous to the step used to obtain (4.46), find that

$$\begin{aligned} v_{oc,\theta} &= \operatorname{Re} \frac{1}{\pi} \int_{-\infty}^\infty \int_{\omega-\Delta\omega/2}^{\omega+\Delta\omega/2} h_\theta(\omega) E_{\theta\theta^r}(t') e^{-j\lambda(t'-t)} d\lambda dt' \\ &= \operatorname{Re} h_\theta(\omega) E_{\theta\theta}(t) \end{aligned} \quad (4.48)$$

by using the relation (4.47).

By an entirely similar procedure we find that

$$v_{oc,\phi} = \operatorname{Re} h_\phi(\omega) E_{\phi\phi}(t) \quad (4.49)$$

gives the contribution to the received open-circuit voltage from the ϕ com-

ponent of the incident wave. The time-average received power will be proportional to the time average of v_{oc}^2 ; thus by using (4.44), we obtain

$$\begin{aligned} P_r &\propto \frac{1}{2} \text{Re} \langle [h_\theta(\omega)E_{0\theta}(t) + h_\phi(\omega)E_{0\phi}(t)][h_\theta^*(\omega)E_{0\theta}^*(t) + h_\phi^*(\omega)E_{0\phi}^*(t)] \rangle \\ &= \frac{1}{2} [h_\theta h_\theta^* \langle E_{0\theta}(t)E_{0\theta}^*(t) \rangle + h_\phi h_\phi^* \langle E_{0\phi}(t)E_{0\phi}^*(t) \rangle \\ &\quad + 2 \text{Re} h_\theta h_\phi^* \langle E_{0\theta}(t)E_{0\phi}^*(t) \rangle] \end{aligned} \quad (4.50)$$

We shall now indicate how the above result can be expressed in terms of a suitable set of Stokes' parameters. For this purpose again assume that h_θ is real and $h_\phi = \tau e^{j\beta} h_\theta$. Also let

$$E_{0\theta} = \sigma_1(t) e^{j\alpha_1(t) + j\omega t} \quad E_{0\phi} = \sigma_2(t) e^{j\alpha_2(t) + j\omega t}$$

where σ_1 , σ_2 , α_1 , and α_2 are real functions of time. The Stokes parameters for the antenna are given by (4.33). The Stokes parameters for the incident wave are defined in terms of time averages as follows:

$$s'_0 = \langle \mathbf{E}_0 \cdot \mathbf{E}_0^* \rangle = \langle \sigma_1^2 \rangle + \langle \sigma_2^2 \rangle \quad (4.51a)$$

$$s'_1 = \langle E_{0\theta} E_{0\theta}^* \rangle - \langle E_{0\phi} E_{0\phi}^* \rangle = \langle \sigma_1^2 \rangle - \langle \sigma_2^2 \rangle \quad (4.51b)$$

$$s'_2 = \text{Re} 2 \langle E_{0\theta}^* E_{0\phi} \rangle = 2 \langle \sigma_1 \sigma_2 \cos(\alpha_1 - \alpha_2) \rangle \quad (4.51c)$$

$$s'_3 = \text{Im} 2 \langle E_{0\theta}^* E_{0\phi} \rangle = 2 \langle \sigma_1 \sigma_2 \sin(\alpha_2 - \alpha_1) \rangle \quad (4.51d)$$

Equation (4.50) can now be expressed in the form

$$P_r \propto \frac{1}{4} \mathbf{s} \cdot \mathbf{s}' \quad (4.52)$$

where \mathbf{s} and \mathbf{s}' are four-component vectors with components given by (4.33) and (4.51) that characterize the polarization properties of the antenna and the time-average polarization of the incident wave.

The effective receiving cross section for partially polarized waves is seen to be given by

$$A_r = (1 - |\Gamma|^2) \frac{\lambda_0^2}{4\pi} G \frac{1}{2} \frac{\mathbf{s} \cdot \mathbf{s}'}{s_0 s'_0} \quad (4.53)$$

as comparison with (4.31) and (4.39) shows. This definition includes the polarization mismatch factor p — which is not always desirable, since this factor is not purely a parameter of the antenna alone. An alternative definition would involve deleting the factor \mathbf{s}'/s'_0 , in which case the effective area would be a vector quantity.

The properties of partially polarized waves are more clearly illustrated by the polarization coherence matrix. The elements of the coherence matrix \mathbf{J}' are defined by¹⁷

$$J'_{\theta\theta} = \langle E_{0\theta}(t) E_{0\theta}^*(t) \rangle = \langle \sigma_1^2 \rangle \quad (4.54a)$$

$$J'_{\phi\phi} = \langle E_{0\phi}(t) E_{0\phi}^*(t) \rangle = \langle \sigma_2^2 \rangle \quad (4.54b)$$

$$\begin{aligned} J'_{\theta\phi} &= (J'_{\phi\theta})^* = \langle E_{0\theta}(t) E_{0\phi}^*(t) \rangle \\ &= \langle \sigma_1(t) \sigma_2(t) e^{j\alpha_1(t) - j\alpha_2(t)} \rangle \end{aligned} \quad (4.54c)$$

In general, we should take $J'_{\theta\theta}(\tau) = \langle E_{0\theta}(t)E_{0\theta}^*(t - \tau) \rangle$ etc., but for power calculations we only require the values for $\tau = 0$. The term *coherence* instead of the usual term *correlation* is used to emphasize the fact that the correlations involved in (4.54) are between analytic signals and are complex quantities (see remarks by Zucker²⁴). The coherence matrix is hermitian and is a function of the angles of incidence θ and ϕ .

In a similar way we can define a coherence matrix \mathbf{J} for the antenna; thus

$$\mathbf{J} = \begin{vmatrix} h_{\theta}h_{\theta}^* & h_{\theta}h_{\phi}^* \\ h_{\theta}^*h_{\phi} & h_{\phi}h_{\phi}^* \end{vmatrix} \quad (4.55)$$

The reader can now readily verify that the received power is given by

$$\begin{aligned} P_r &= A_r \frac{1}{2\zeta_0} \langle \mathbf{E}_0 \cdot \mathbf{E}_0^* \rangle \\ &= (1 - |\Gamma|^2) \frac{\langle \mathbf{E}_0 \cdot \mathbf{E}_0^* \rangle}{2\zeta_0} \frac{\lambda_0^2}{4\pi} G \frac{\text{tr } \mathbf{J} \cdot \mathbf{J}'_t}{|\mathbf{h}|^2 \langle \mathbf{E}_0 \cdot \mathbf{E}_0^* \rangle} \\ &= (1 - |\Gamma|^2) \frac{\lambda_0^2}{8\pi\zeta_0} G \frac{\text{tr } \mathbf{J} \cdot \mathbf{J}'_t}{|\mathbf{h}|^2} \end{aligned} \quad (4.56)$$

upon expanding the matrix product and forming the trace (sum of diagonal terms in the resultant matrix). Note that $(1/2\zeta_0)\langle \mathbf{E}_0 \cdot \mathbf{E}_0^* \rangle$ is the average incident power density per unit area and \mathbf{J}'_t denotes the transposed matrix.

The above expression suggests that the effective receiving cross section of the antenna should be defined by the matrix

$$\mathbf{A}_r = (1 - |\Gamma|^2) \frac{\lambda_0^2}{4\pi} G \frac{\mathbf{J}}{|\mathbf{h}|^2} = A_r \frac{\mathbf{J}}{|\mathbf{h}|^2} \quad (4.57)$$

since this expression involves only the antenna parameters. This is the working definition that Ko uses.^{19,21} Note that \mathbf{A}_r denotes a matrix and A_r is used for the factors $(1 - |\Gamma|^2)\lambda_0^2 G/4\pi$.

A number of useful results pertaining to the coherence matrix and its relation to the Stokes parameters can be established.^{17,22} For a completely unpolarized wave, i.e., a randomly polarized wave, the components $E_{0\theta}$ and $E_{0\phi}$ are statistically independent and have the same root-mean-square value, thus $J'_{\theta\theta} = J'_{\phi\phi} = \langle \sigma_1^2 \rangle$, $J'_{\theta\phi} = J'_{\phi\theta} = 0$, and the coherence matrix reduces to

$$\mathbf{J}' = \langle \sigma_1^2 \rangle \begin{bmatrix} 1 & 0 \\ 0 & 1 \end{bmatrix} \quad (4.58)$$

Note that $\zeta_0^{-1}\langle \sigma_1^2 \rangle = (1/2\zeta_0)\langle \mathbf{E}_0 \cdot \mathbf{E}_0^* \rangle$, which is the intensity of the incident wave.

The degree of polarization m is the ratio of the intensity of the polarized part to the total intensity of the wave. Hence for a partially polarized wave we can separate the polarized and unpolarized parts by subtracting

$$\frac{1 - m}{2} (\langle \sigma_1^2 \rangle + \langle \sigma_2^2 \rangle)$$

from the diagonal elements of the coherence matrix; thus

$$\mathbf{J}' = \mathbf{J}_1 + \mathbf{J}_2 \quad (4.59a)$$

where the unpolarized part is given by

$$\mathbf{J}_1 = \frac{1-m}{2} (\langle \sigma_1^2 \rangle + \langle \sigma_2^2 \rangle) \begin{bmatrix} 1 & 0 \\ 0 & 1 \end{bmatrix} \quad (4.59b)$$

and the polarized part is given by

$$\mathbf{J}_2 = \frac{1}{2} \begin{bmatrix} \langle \sigma_1^2 \rangle - \langle \sigma_2^2 \rangle + m(\langle \sigma_1^2 \rangle + \langle \sigma_2^2 \rangle) & 2\langle \sigma_1 \sigma_2 e^{j(\alpha_1 - \alpha_2)} \rangle \\ 2\langle \sigma_1 \sigma_2 e^{-j(\alpha_1 - \alpha_2)} \rangle & \langle \sigma_2^2 \rangle - \langle \sigma_1^2 \rangle + m(\langle \sigma_1^2 \rangle + \langle \sigma_2^2 \rangle) \end{bmatrix} \quad (4.59c)$$

For a completely polarized wave the reader may readily show that the determinant of the coherence matrix is zero. By equating the determinant of \mathbf{J}_2 to zero, we find that the degree of polarization m is given by

$$m = \left[1 - \frac{4 \det \mathbf{J}'}{(\text{tr } \mathbf{J}')^2} \right]^{\frac{1}{2}} \quad (4.60)$$

Exercise 4.6 Show that the determinant of the coherence matrix \mathbf{J} which characterizes the antenna is zero. Also, derive (4.60).

The contribution to the received power from the unpolarized component is independent of the antenna polarization. Hence for maximum power the antenna polarization should be matched to that of the completely polarized component of the incident radiation.

The connections between the elements of the coherence matrix and the Stokes parameters are given by^{17,22}

$$s'_0 = J'_{\theta\theta} + J'_{\phi\phi} \quad (4.61a)$$

$$s'_1 = J'_{\theta\theta} - J'_{\phi\phi} \quad (4.61b)$$

$$s'_2 = J'_{\theta\phi} + J'_{\phi\theta} \quad (4.61c)$$

$$s'_3 = j(J'_{\theta\phi} - J'_{\phi\theta}) \quad (4.61d)$$

$$\text{and} \quad 2J'_{\theta\theta} = s'_0 + s'_1 \quad (4.61e)$$

$$2J'_{\phi\phi} = s'_0 - s'_1 \quad (4.61f)$$

$$2J'_{\theta\phi} = 2(J'_{\phi\theta})^* = s'_2 - js'_3 \quad (4.61g)$$

In terms of the Stokes parameters the degree of polarization is given by

$$m = \frac{[(s'_1)^2 + (s'_2)^2 + (s'_3)^2]^{\frac{1}{2}}}{s'_0} \quad (4.62)$$

4.7 Radiation from Distributed Sources

In this section we shall give a brief introduction to the reception of radiation from source distributions with spatial extent. Distributed sources are of

interest in the field of radio astronomy, radio and radar mapping, multiple-target tracking, and so forth.

A source with spatial extent could be simulated by a suitable distribution of current elements $I_\theta(\theta, \phi, t)$ and $I_\phi(\theta, \phi, t)$ placed on the surface of a sphere of radius r . For generality we shall initially assume that there may be a degree of correlation between the sources at θ, ϕ and θ', ϕ' . With a proper choice of amplitudes such a source would reproduce the incident radiation (see Sec. 4.5).

Since we are now concerned with distributed sources, we shall let $\mathbf{E}_i(\theta, \phi) d\Omega$ be the incident analytic field from sources which subtend a solid angle $d\Omega$ at the antenna in the direction defined by θ and ϕ . The units of \mathbf{E}_i are volts per meter per steradian. For brevity we shall also represent the direction given by θ and ϕ by the single symbol Ω ; thus $\mathbf{E}_i(\Omega, t) d\Omega$ is the incident field from the direction Ω . The total received open-circuit voltage is the sum of the contributions from all directions seen by the antenna. If we let the antenna axis be pointed in the direction Ω_0 , we then have for the analytic signal representation of the open-circuit received voltage

$$V_{oc} = \int \mathbf{h}(\Omega - \Omega_0) \cdot \mathbf{E}_i(\Omega) d\Omega \quad (4.63)$$

by using (4.27). The integral is a double integral over all values of θ and ϕ from which radiation is incident. The received power will be given by

$$\begin{aligned} P_r &= \frac{1}{2} K_r \operatorname{Re} \langle V_{oc} V_{oc}^* \rangle \\ &= \frac{1}{2} K_r \iint \langle \mathbf{h}(\Omega - \Omega_0) \cdot \mathbf{E}_i(\Omega, t) \mathbf{h}^*(\Omega' - \Omega_0) \cdot \mathbf{E}_i^*(\Omega', t) \rangle d\Omega d\Omega' \end{aligned} \quad (4.64)$$

where K_r is a suitable constant given in Exercise 4.4. Note that we have changed the order of time averaging and integration over Ω and Ω' . A typical term in the integrand in (4.64) is

$$\langle E_{i\theta}(\Omega, t) E_{i\phi}^*(\Omega', t) \rangle$$

Since Ω and Ω' are not equal, this is not an element of the coherence matrix. If the radiation from the direction Ω' is independent of the radiation from the direction Ω , then there is zero correlation and the above quantity is zero except when $\Omega = \Omega'$. In general, we shall call quantities of the above type mutual coherence (see discussion in Born and Wolf¹⁷).

By analogy with the polarization coherence matrix, we shall introduce a mutual coherence matrix $\mathbf{\Gamma}'$ with elements (we take $\tau = 0$ as in 4.54)

$$\Gamma'_{\theta\theta}(\Omega, \Omega') = \langle E_{i\theta}(\Omega, t) E_{i\theta}^*(\Omega', t) \rangle \quad (4.65a)$$

$$\Gamma'_{\theta\phi}(\Omega, \Omega') = \langle E_{i\theta}(\Omega, t) E_{i\phi}^*(\Omega', t) \rangle \quad (4.65b)$$

$$\Gamma'_{\phi\theta}(\Omega, \Omega') = \langle E_{i\phi}(\Omega, t) E_{i\theta}^*(\Omega', t) \rangle = \Gamma_{\theta\phi}^*(\Omega', \Omega) \quad (4.65c)$$

$$\Gamma'_{\phi\phi}(\Omega, \Omega') = \langle E_{i\phi}(\Omega, t) E_{i\phi}^*(\Omega', t) \rangle \quad (4.65d)$$

In a similar manner we define the mutual coherence matrix $\mathbf{\Gamma}$ for the antenna with elements

$$\Gamma_{ij}(\Omega - \Omega_0, \Omega' - \Omega_0) = h_i(\Omega - \Omega_0)h_j^*(\Omega' - \Omega_0) \quad i, j = \theta, \phi \quad (4.66)$$

We now readily find that (4.64) can be expressed as

$$P_r = \frac{1}{2} K_r \iint \text{tr } \mathbf{\Gamma}(\Omega - \Omega_0, \Omega' - \Omega_0) \cdot \mathbf{\Gamma}'_t(\Omega, \Omega') d\Omega d\Omega' \quad (4.67)$$

It appears that in most cases of practical interest there is zero correlation between the radiation coming from the two directions Ω and Ω' except when $\Omega' = \Omega$. The mutual coherence matrix can then be replaced by the coherence matrix; that is

$$\mathbf{\Gamma}'_{ij}(\Omega, \Omega') = J'_{ij}(\Omega) \delta(\Omega - \Omega') \quad (4.68)$$

which corresponds to letting $\langle \mathbf{E}_i(\Omega, t) \mathbf{E}_i^*(\Omega', t) \rangle = \langle \mathbf{E}_i(\Omega, t) \mathbf{E}_i^*(\Omega, t) \rangle \delta(\Omega - \Omega')$. For this special case the integration over Ω' is eliminated and (4.67) reduces to

$$P_r = \frac{1}{2} K_r \int \text{tr } \mathbf{J}(\Omega - \Omega_0) \cdot \mathbf{J}'_t(\Omega) d\Omega \quad (4.69)$$

Actually, the coherence matrix \mathbf{J}' used here is slightly different from that used in Sec. 4.6 in that its elements are defined with units of (volts/meter)² per steradian. The expression (4.69) is the one of primary interest in radio astronomy, and it will therefore be appropriate to cast it in terms of more familiar quantities.

First of all, we shall introduce normalized coherence matrices $\mathbf{\rho}$ and $\mathbf{\rho}'$ with elements

$$\rho_{ij} = \frac{J_{ij}}{|\mathbf{h}|^2} \quad (4.70a)$$

$$\rho'_{ij} = \frac{J'_{ij}}{\langle \mathbf{E}_i \cdot \mathbf{E}_i^* \rangle} \quad (4.70b)$$

The effective antenna receiving cross section is now written as a matrix given by (4.57), that is,

$$\mathbf{A}_r = (1 - |\Gamma|^2) \frac{\lambda_0^2}{4\pi} G(\Omega - \Omega_0) \mathbf{\rho}(\Omega - \Omega_0) \quad (4.71)$$

The incident power per unit area and per unit solid angle from the element of solid angle $d\Omega$ is given by $\langle \mathbf{E}_i \cdot \mathbf{E}_i^* \rangle / 2\zeta_0$ in watts per meter² per steradian. This incident power has a spectral width Δf corresponding to the receiver band width. The incident power per unit area and per unit solid angle in a unit frequency interval is called the brightness $B(\theta, \phi)$ of the source; thus

$$B(\theta, \phi) \Delta f = \frac{\langle \mathbf{E}_i \cdot \mathbf{E}_i^* \rangle}{2\zeta_0} \quad (4.72)$$

In terms of the above quantities we can write

$$\frac{P_r}{\Delta f} = (1 - |\Gamma|^2) \frac{\lambda_0^2}{4\pi} \int G(\Omega - \Omega_0) B(\Omega) \operatorname{tr} \mathbf{e}(\Omega - \Omega_0) \cdot \mathbf{e}'_t(\Omega) d\Omega \quad (4.73)$$

for the received power per unit frequency interval.

If the incident radiation came from a blackbody, then Planck's law

$$B = \frac{2hc}{\lambda_0^3} (e^{hc/K\lambda_0 T} - 1)^{-1} \quad (4.74a)$$

which reduces to the Rayleigh-Jeans law

$$B = \frac{2Kf^2}{c^2} T \quad (4.74b)$$

at radio frequencies, may be used to relate the brightness to the temperature.²⁰⁻²² In the above, h is Planck's constant, K is Boltzmann's constant, and T is the temperature in degrees Kelvin. Even for nonthermal radiation the effective temperature of the source is defined in terms of the brightness by the above relations.

When the incident radiation is partially polarized, the total brightness B may be considered to be the sum of that associated with two mutually orthogonal but completely polarized beams.^{20,21} Consequently, for each position in the sky there are associated two values of brightness and two temperatures. Ko has shown that these two values of B are given by²¹

$$B' = \frac{1}{2}(1 + m)B \quad (4.75a)$$

$$B'' = \frac{1}{2}(1 - m)B \quad (4.75b)$$

where m is the degree of polarization given earlier by (4.60). The temperature associated with each polarization component is twice that given by (4.74b), that is,

$$T' = \frac{c^2}{Kf^2} B' \quad (4.76a)$$

$$T'' = \frac{c^2}{Kf^2} B'' \quad (4.76b)$$

since Planck's law applies to a randomly polarized wave which can be viewed as composed of two orthogonal polarized components.

The expression (4.67) gives the output power that would be measured by a receiver incorporating a square-law detector and a time-averaging (filtering) circuit. However, it is not necessary to use a single receiver. If two spaced antennas are used and the received voltages are cross-correlated, it is possible to measure the mutual coherence function, that is, $\langle \mathbf{E}_i(\Omega, t) \mathbf{E}_i^*(\Omega', t) \rangle$. For details on how this may be accomplished the reader is referred to the paper by MacPhie.²⁵

The special case of incoherent source distributions is of special interest to the radio astronomer. The function of the antenna and associated circuitry is to provide a map of the brightness or equivalent temperature distribution of the portion of sky or celestial body under study. The extent to which a measure of the true distribution can be obtained depends on the properties of the antenna. In order to illustrate the basic factors involved we shall consider a randomly polarized source. The received power is then given by

$$\begin{aligned} P_r(\Omega_0) &= \frac{\lambda_0^2 \Delta f}{8\pi} \int G(\Omega - \Omega_0) B(\Omega) d\Omega \\ &= \frac{\Delta f}{2} \int A_r(\Omega - \Omega_0) B(\Omega) d\Omega \end{aligned} \quad (4.77)$$

where we have assumed a conjugate matched load so that the reflection coefficient $\Gamma = 0$. If the antenna is slowly scanned across the sky, that is, Ω_0 is a slowly varying function of time such that the change in Ω_0 over an interval equal to the integration or averaging time is negligible, the power output as a function of Ω_0 is obtained. However, since the antenna beam width is finite, $P_r(\Omega_0)$ is not a direct measure of the true brightness distribution $B(\Omega_0)$. Only if $G(\Omega - \Omega_0) = \delta(\Omega - \Omega_0)$, that is, an antenna with infinite resolution, would $P_r(\Omega_0)$ be equal to a constant times $B(\Omega_0)$. In general, the antenna acts as a filter that smooths out the spatial variations in the brightness distribution. Nevertheless, it is possible to obtain a good deal of information about the brightness distribution by using suitable restoration techniques to recover $B(\Omega_0)$ from the measured $P_r(\Omega_0)$. The analysis employed has a great deal of similarity to analogous filtering problems that occur in communications. Since a whole chapter (Chap. 26) is devoted to the spatial filtering properties of an antenna, we shall not pursue the subject beyond the above introductory remarks in this section.

Exercise 4.7 Let $\mathbf{E}_i^r(t, \Omega) = \text{Re } \mathbf{E}_i(t, \Omega)$ be the incident stochastic (random) field. Truncate these stochastic signals at $|t| = T$ and define the Fourier transforms $\mathbf{E}_i^r(\omega, \Omega)$ and $\mathbf{E}_i(\omega, \Omega)$ by

$$\begin{aligned} \mathbf{E}_i^r(\omega, \Omega) &= \int_{-T}^T \mathbf{E}_i^r(t, \Omega) e^{-i\omega t} dt \\ \mathbf{E}_i(\omega, \Omega) &= \int_{-T}^T \mathbf{E}_i(t, \Omega) e^{-i\omega t} dt \end{aligned}$$

Show that

$$\mathbf{E}_i(\omega, \Omega) = \begin{cases} 2\mathbf{E}_i^r(\omega, \Omega) & \omega > 0 \\ 0 & \omega < 0 \end{cases}$$

The mutual coherence dyadic (matrix) is given by

$$\mathbf{\Gamma}'(\tau, \Omega, \Omega') = \langle \mathbf{E}_i(t, \Omega) \mathbf{E}_i^*(t - \tau, \Omega') \rangle$$

Show that

$$\mathbf{\Gamma}'(\tau, \Omega, \Omega') = \frac{1}{2\pi} \int_0^\infty \gamma(\omega, \Omega, \Omega') e^{j\omega\tau} d\omega$$

where

$$\gamma(\omega, \Omega, \Omega') = \lim_{T \rightarrow \infty} \frac{\mathbf{E}_i(\omega, \Omega) \mathbf{E}_i^*(\omega, \Omega')}{2T}$$

by evaluating the time average using the Fourier representation for the analytic signals $\mathbf{E}_i(t, \Omega)$ and $\mathbf{E}_i^*(t - \tau, \Omega')$.

The open-circuit voltage is given by

$$\begin{aligned} v_{oc}(t) &= \frac{1}{2\pi} \int_{-\infty}^{\infty} \int_{-\infty}^{\infty} \mathbf{h}(\omega, \Omega - \Omega_0) \cdot \mathbf{E}_i^r(\omega, \Omega) e^{j\omega t} d\omega d\Omega \\ &= \text{Re} \frac{1}{\pi} \int_0^\infty \int_{-\infty}^{\infty} \mathbf{h}(\omega, \Omega - \Omega_0) \cdot \mathbf{E}_i^r(\omega, \Omega) e^{j\omega t} d\omega d\Omega \\ &= \text{Re } V_{oc}(t) \end{aligned}$$

The latter complex integral gives the analytic signal $V_{oc}(t)$ and its Fourier ω spectrum is

$$\int_{-\infty}^{\infty} \mathbf{h}(\omega, \Omega - \Omega_0) \cdot \mathbf{E}_i(\omega, \Omega) d\Omega$$

In terms of the analytic signal representation of the load voltage and current, show that the average received power $\frac{1}{2} \text{Re}\langle V_L(t) I_L^*(t) \rangle$ is given by

$$\begin{aligned} P_r &= \text{Re} \frac{1}{4\pi} \int_0^\infty \lim_{T \rightarrow \infty} \frac{V_L(\omega) I_L^*(\omega)}{2T} d\omega \\ &= \frac{1}{4\pi} \int_0^\infty \lim_{T \rightarrow \infty} \frac{|V_{oc}(\omega)|^2}{2T} K_r(\omega) d\omega \\ &= \frac{1}{4\pi} \int_0^\infty K_r(\omega) \iint_{\Omega, \Omega'} \text{tr } \mathbf{\Gamma}(\omega, \Omega - \Omega_0, \Omega' - \Omega_0) \cdot \gamma_t(\omega, \Omega, \Omega') d\Omega d\Omega' d\omega \end{aligned}$$

For a narrow-band process this result can be approximated by

$$\frac{1}{4\pi} K_r(\omega) \iint_{\Omega, \Omega'} \text{tr } \mathbf{\Gamma}(\omega, \Omega - \Omega_0, \Omega' - \Omega_0) \cdot \int_0^\infty \gamma_t(\lambda, \Omega, \Omega') d\lambda d\Omega d\Omega'$$

The integration over λ replaces γ_t by $2\pi\mathbf{\Gamma}'$ with $\tau = 0$ so the result is seen to agree with (4.67).

In a similar way, generalize (4.56) and (4.69) so that they apply to wide-band stochastic signals.

4.8 Noise in Antenna Systems

The minimum signal power that can be detected is limited by the inherent noise always present in receiving systems. Part of the limitation is due to noise voltages generated within the mixers and amplifiers connected to the antenna terminals and will not be discussed in this book. The other source of noise which limits the minimum detectable signal is radiation of a noiselike character which is picked up along with the desired signal by the antenna. It is this latter aspect that we shall examine in this section.

Noiselike radiation received by an antenna has essentially two origins, namely, man-made disturbances such as ignition noise and commutator sparking from motors, etc., and thermal radiation from bodies surrounding the antenna. In the last category we also include radiation from galactic sources, the sun, the atmosphere, etc. Man-made noise will not be included in the discussion, because it has widely varying characteristics and can in principle be eliminated.

The elementary theory of noise in antenna systems is based on two basic laws, which are Nyquist's formula for the available noise power from an ideal resistor at temperature T and the second law of thermodynamics. The literature on noise is very extensive and will not be reviewed in detail here. The reader will find that the following papers will provide an excellent introduction and review of the subject: Pierce,²⁶ Bennett,²⁷ Siegman,²⁸ and Oliver.²⁹ We shall restrict the discussion to the minimum essentials needed to develop suitable working formulas for noise calculations involving antennas.

Nyquist's formula for the maximum available noise power from an ideal resistor at temperature T may be derived from Planck's radiation law and the second law of thermodynamics. Consider an ideal loss-free antenna connected to a load resistance R_L at its terminals by means of a loss-free transmission line. Let the antenna together with a small blackbody radiator be located in an otherwise empty universe, as indicated in Fig. 4.10. The blackbody has a

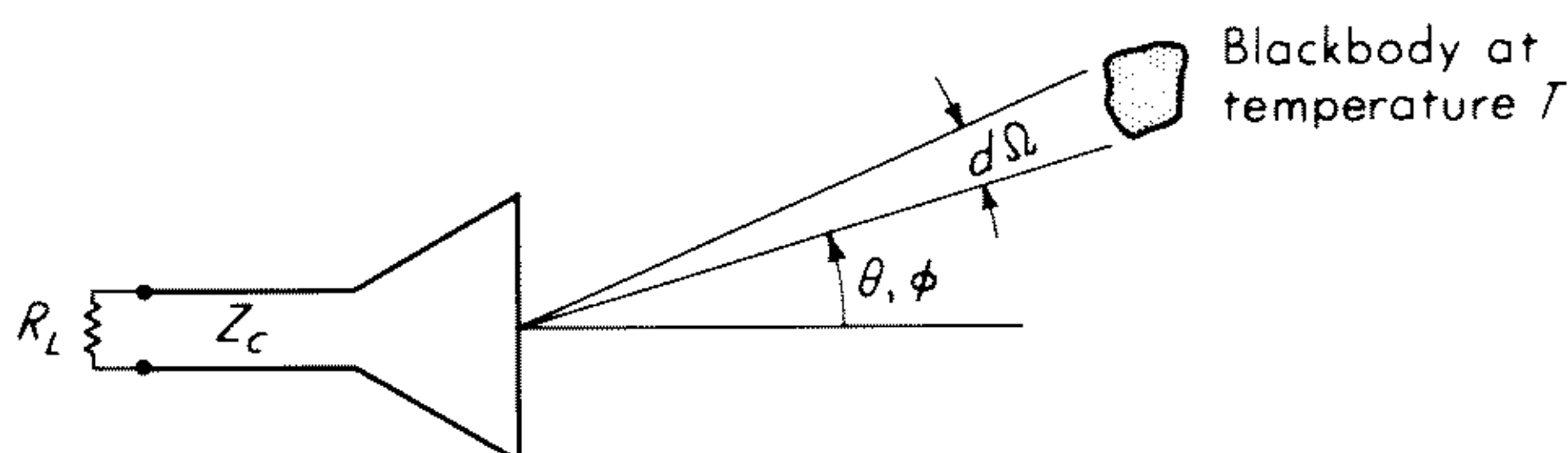


Fig. 4.10 An antenna and a blackbody radiator.

temperature T , is located at a position defined by the angles θ and ϕ relative to the antenna axis, and subtends a differential element of solid angle $d\Omega$ at the antenna. According to Planck's law (4.74a) or its approximate form the Rayleigh-Jeans law (4.74b), which is valid at radio frequencies, the power emitted by the blackbody in the direction of the antenna is $B = 2Kf^2T/c^2$ watts/m² — per steradian and per cycle. The received noise power is given by (4.77) and is

$$P_r = (1 - |\Gamma|^2) \frac{\Delta f}{2} \frac{\lambda_0^2}{4\pi} D(\theta, \phi) B d\Omega = (1 - |\Gamma|^2) K T \Delta f \frac{D d\Omega}{4\pi} \quad (4.78)$$

where $K = 1.380 \times 10^{-23}$ joules/degree is Boltzmann's constant, T is the absolute temperature in degrees Kelvin, and $D(\theta, \phi)$ is the antenna directivity ($D = G$ for a loss-free antenna). When thermodynamic equilibrium has been achieved, the temperature of the load resistor R_L must equal that of the black-

body radiator in order to maximize the entropy of the system. For equilibrium to be maintained the resistor R_L must radiate an amount of thermal power that will equal the received power into the element of solid angle $d\Omega$ and will be completely absorbed by the blackbody (a blackbody is a perfect absorber). If we let V_n be the root-mean-square noise voltage produced in R_L , then the available noise power from R_L will be $V_n^2/4R_L$. For an unmatched antenna the total radiated power will be $(1 - |\Gamma|^2)V_n^2/4R_L$. The total power radiated into the element of solid angle $d\Omega$ will be given by

$$(1 - |\Gamma|^2) \frac{V_n^2}{4R_L} D(\theta, \phi) \frac{d\Omega}{4\pi}$$

When we equate the radiated power to the received power given by (4.78), we obtain

$$V_n^2 = 4R_L K T \Delta f \quad (4.79a)$$

and hence the available noise power P_n from a resistor R_L is given by

$$P_n = \frac{V_n^2}{4R_L} = K T \Delta f \quad (4.79b)$$

which is Nyquist's formula. Although we used a specific example to derive (4.79), these formulas are perfectly general; in particular, the available noise power that a resistor can radiate is given by (4.79b) quite independently of whether any blackbody radiator is present or not.

As a first generalization of the above results we now consider an imperfect blackbody radiator, i.e., one that is not a perfect absorber. Let α_1 be the fraction of the power radiated by R_L that is absorbed by the imperfect blackbody. To maintain thermodynamic equilibrium the power delivered to R_L by the imperfect blackbody must then also be reduced by this same factor α_1 . Hence the received noise power in R_L will be

$$P_{r1} = \alpha_1 (1 - |\Gamma|^2) K T_1 \Delta f D \frac{d\Omega}{4\pi} \quad (4.80)$$

where T_1 is the temperature of the imperfect blackbody.

The above result may be extended to a collection of thermal radiators by the principle of superposition of power, since the thermal noise sources we are considering are incoherent and randomly polarized. Thus, consider a distribution of noise sources with a temperature $T(\theta, \phi)$ which is a function of direction. When the available input power at the antenna terminals is unity, let $\alpha(\theta, \phi)$ be the fraction of the radiated power which is absorbed by bodies located in the direction θ, ϕ . Also, let the fraction of the available input power that is absorbed in the feed line and antenna, which are at a temperature T_0 (usually ambient), be $(1 - |\Gamma|^2)\alpha_0$. Then the received noise power is given by

$$P_r = (1 - |\Gamma|^2) \frac{K \Delta f}{4\pi} \int_0^\pi \int_0^{2\pi} \alpha(\theta, \phi) G(\theta, \phi) T(\theta, \phi) \sin \theta d\theta d\phi + (1 - |\Gamma|^2) \alpha_0 K T_0 \Delta f \quad (4.81)$$

Each contribution to the received noise power as given by this expression is weighted by the factor α , which gives the fraction of the power transmitted by the antenna that the corresponding body would absorb. For example, the available power from R_L , if its temperature is T_0 , is $KT_0 \Delta f$. The power radiated and dissipated in the feed line and antenna losses is $(1 - |\Gamma|^2)\alpha_0 KT_0 \Delta f$. The lossy feed line and antenna act as thermal radiators and will return an equal amount of power to R_L in order to maintain equilibrium. Hence, $(1 - |\Gamma|^2)\alpha_0 KT_0 \Delta f$ is the contribution to the total received noise power from antenna and feed line losses.

It is convenient to introduce a single equivalent temperature T_a , called the antenna noise temperature, in terms of which the total received noise power can be expressed by means of Nyquist's formula. Thus, we let

$$P_r = (1 - |\Gamma|^2)KT_a \Delta f \quad (4.82)$$

from which we obtain

$$T_a = \alpha_0 T_0 + \frac{1}{4\pi} \int_0^\pi \int_0^{2\pi} \alpha(\theta, \phi) G(\theta, \phi) T(\theta, \phi) \sin \theta d\theta d\phi \quad (4.83)$$

for the equivalent antenna temperature by substituting into (4.81). The equivalent antenna temperature is a weighted average of the temperature of all surrounding bodies. As a special case, if $\alpha(\theta, \phi) = 1$ and $T = T_0$, we obtain $T_a = T_0$, since $G(\theta, \phi) = (1 - \alpha_0)D(\theta, \phi)$ and

$$\int_0^\pi \int_0^{2\pi} D(\theta, \phi) \sin \theta d\theta d\phi = 4\pi$$

from the definition of directivity. In terms of the antenna equivalent temperature, the received noise power may be viewed as coming from the radiation resistance of the antenna, the latter having a temperature T_a .

The above formula for the equivalent antenna noise temperature points out the great importance of keeping the feed line and antenna losses as small as possible and minimizing the level of the side lobes in the direction of the earth if a low noise temperature is to be obtained. The antenna proper and the earth would normally be at ambient temperature, while portions of the sky in certain frequency ranges may have a temperature of only a few degrees Kelvin, and hence the former could give the dominant contribution to the received noise power.

The actual observed temperature of the sky is dependent on many factors such as frequency and direction and exhibits daily as well as seasonal variations. Hogg and Mumford have given a summary of a number of measurements carried out by various people.³⁰ They point out that the effective temperature of the sun can be roughly approximated by the expression

$$\frac{T_{\text{sun}}}{290} = \frac{675}{f}$$

where f is the frequency in gigahertz in the frequency range 250 MHz to 35 GHz. At the lower frequencies the effective temperature is around a million degrees. The average noise temperature T_c due to cosmic sources is found to lie within the range

$$\frac{\lambda_0^2}{5} \leq \frac{T_c}{290} \leq 5\lambda_0^2$$

where λ_0 is the wavelength in meters. At 16 m a typical value of T_c is 140,000°K. In the microwave band of 10 to 100 GHz cosmic noise is relatively small but atmospheric attenuation is high owing to absorption by water vapor and oxygen. In this frequency range the antenna temperature can be approximated by the ambient temperature (290°K).

4.9 Scattering Properties of an Antenna

We shall conclude this chapter with a brief discussion of the scattering properties of an antenna. The scattering or reradiation characteristics are related to the receiving properties of the antenna, since the scattered radiation depends on the load impedance connected at the antenna terminals.

A detailed analysis of the scattering problem would involve the solution of a boundary-value problem in which a plane TEM wave (or other incident field) was incident on the antenna (see Chap. 9 for the cylindrical antenna case). This analysis would have to be repeated for every different kind of antenna of interest and does not lend itself to an easy determination of the general scattering properties of an antenna. The inherent difficulties of the boundary-value problem may be partially overcome by introducing a scattering matrix to represent the antenna, an approach which is completely analogous to the scattering matrix treatment of multiport waveguide junctions. The scattering matrix method was first introduced into antenna theory by Dicke.¹

We shall follow Dicke and assume that the antenna is fed from a single transmission line or waveguide supporting only one propagating mode. In general, the antenna could be excited by an N -port nonreciprocal network as discussed by Kahn and Kurss.³¹ All of space in the region outside a spherical surface which completely encloses the antenna can be represented by a denumerably infinite number of ports by expanding the field in spherical modes. The problem is thus analogous to a single-mode waveguide coupled through a junction to a multimode waveguide. In the antenna problem an infinite number of modes is required to represent the field in space exactly. However, for any practical antenna only a finite number of spherical modes would be required to give an acceptable accuracy.

With reference to Fig. 4.11 let S_1 be the terminal plane in the transmission line or waveguide feed line and let the spherical surface S_2 with $r = r_0$ be the reference plane for the region of space outside the antenna. The incident and

reflected waves in the feed line have amplitudes a^+ and a^- . The modal field is assumed to be normalized, so that $\frac{1}{2}(a^+)(a^+)^*$ gives the incident power.

The field outside the sphere $r = r_0$ may be expanded into inward and out-

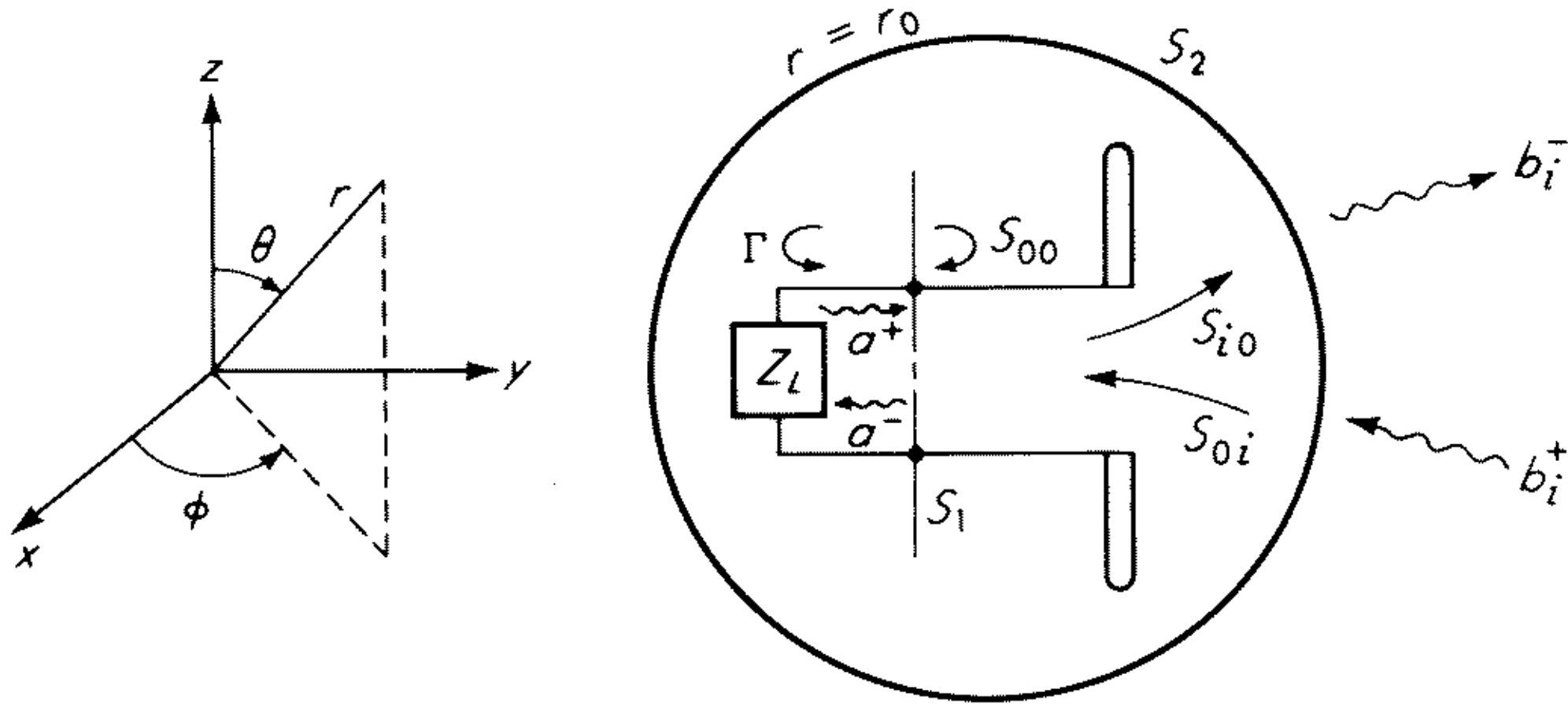


Fig. 4.11 Scattering matrix representation of an antenna.

ward propagating spherical modes. For this purpose the vector wave functions discussed by Stratton are appropriate.³² For solenoidal fields the required mode functions are given by

$$\mathbf{M}_{mn}^{e,0} = \mp \frac{m}{\sin \theta} z_n(k_0 r) P_n^m(\cos \theta) \begin{bmatrix} \sin m\phi \\ \cos m\phi \end{bmatrix} \hat{\mathbf{a}}_\theta - z_n(k_0 r) \frac{\partial P_n^m(\cos \theta)}{\partial \theta} \begin{bmatrix} \cos m\phi \\ \sin m\phi \end{bmatrix} \hat{\mathbf{a}}_\phi \quad (4.84a)$$

$$\mathbf{N}_{mn}^{e,0} = \frac{n(n+1)}{k_0 r} z_n(k_0 r) P_n^m(\cos \theta) \begin{bmatrix} \cos m\phi \\ \sin m\phi \end{bmatrix} \hat{\mathbf{a}}_r + \frac{1}{k_0 r} \frac{\partial}{\partial r} [r z_n(k_0 r)] \frac{\partial P_n^m(\cos \theta)}{\partial \theta} \begin{bmatrix} \cos m\phi \\ \sin m\phi \end{bmatrix} \hat{\mathbf{a}}_\theta \mp \frac{m}{k_0 r \sin \theta} \frac{\partial}{\partial r} [r z_n(k_0 r)] P_n^m(\cos \theta) \begin{bmatrix} \sin m\phi \\ \cos m\phi \end{bmatrix} \hat{\mathbf{a}}_\phi \quad (4.84b)$$

where $z_n(k_0 r)$ is a spherical Bessel function and P_n^m is the Legendre polynomial. These vector-mode functions are all mutually orthogonal. The normalization integrals are

$$\int_0^{2\pi} \int_0^\pi \mathbf{M}_{mn}^{e,0} \cdot \mathbf{M}_{mn}^{e,0} \sin \theta d\theta d\phi = \frac{4\pi n(n+1)}{\epsilon_m(2n+1)} \frac{(n+m)!}{(n-m)!} [z_n(k_0 r)]^2 \quad (4.85a)$$

$$\int_0^{2\pi} \int_0^\pi \mathbf{N}_{mn}^{e,0} \cdot \mathbf{N}_{mn}^{e,0} \sin \theta d\theta d\phi = \frac{4\pi n(n+1)}{\epsilon_m(2n+1)^2} \frac{(n+m)!}{(n-m)!} \left\{ (n+1)[z_{n-1}(k_0 r)]^2 + n[z_{n+1}(k_0 r)]^2 \right\} \quad (4.85b)$$

where $\epsilon_m = 1$ for $m = 0$ and 2 for $m > 0$. An arbitrary solenoidal electric field may be expanded in terms of these modes. As an example, we give the expansion for a plane wave,³²

$$E_0 \hat{\mathbf{a}}_x e^{-jk_0 z} = E_0 \sum_{n=1}^{\infty} j^{-n} \frac{2n+1}{n(n+1)} (\mathbf{M}_{1n}^0 + j\mathbf{N}_{1n}^e) \quad (4.86)$$

where $z_n(k_0r) = j_n(k_0r) = \frac{1}{2}[h_n^2(k_0r) + h_n^1(k_0r)]$ in the present case. The spherical Hankel functions have the following asymptotic behavior for large k_0r :

$$h_n^1(k_0r) \sim j^{-n-1} \frac{e^{jk_0r}}{k_0r} \quad (4.87a)$$

$$h_n^2(k_0r) \sim j^{n+1} \frac{e^{-jk_0r}}{k_0r} \quad (4.87b)$$

and thus (4.86) gives a representation of the plane wave in terms of inward and outward propagating spherical modes. If we replace $z_n(k_0r)$ in (4.84) by $h_n^2(k_0r)$, we see that the modal functions \mathbf{N}_{01} , \mathbf{N}_{11}^e , and \mathbf{N}_{11}^0 represent the electric field radiated by electric dipoles oriented along the z , x , and y axis, respectively. Similarly, \mathbf{M}_{01} , \mathbf{M}_{11}^e , and \mathbf{M}_{11}^0 represent the electric field radiated by magnetic dipoles (current loops).

It is now apparent that the field outside the reference sphere $r = r_0$ can be expressed as an infinite sum of inward and outward propagating spherical modes. It will be convenient to use a single index i to number the modes and let b_i^+ and b_i^- be the amplitudes of the i th incident and reflected modes. Also, we shall assume that the modal functions have been normalized, so that $\frac{1}{2}(b_i^+)(b_i^+)^*$, etc. gives the power flow across a spherical surface at infinity for this mode. It should be noted that this type of normalization cannot be made at a finite value of r , since the radial wave impedances for spherical modes are complex except at infinity, where the asymptotic forms for the Hankel functions can be used. In this respect there is a difficulty associated with the plane wave expansion (4.86), since the sum involves infinite values of n and the asymptotic formulas for the Hankel functions are valid only for $k_0r \gg n$. In actual fact, the plane wave has infinite power because of its infinite extent.

By following the usual waveguide theory, we can now write

$$\begin{bmatrix} a^- \\ b_1^- \\ b_2^- \\ \vdots \\ \vdots \\ b_i^- \\ \vdots \\ \vdots \\ \vdots \end{bmatrix} = \begin{bmatrix} S_{00} & S_{01} & S_{02} & \cdots \\ S_{10} & S_{11} & S_{12} & \cdots \\ S_{20} & \cdots & \cdots & \cdots \\ \vdots & \vdots & \vdots & \vdots \\ \vdots & \vdots & \vdots & \vdots \\ \vdots & \vdots & \vdots & \vdots \\ \vdots & \vdots & \vdots & \vdots \\ \vdots & \vdots & \vdots & \vdots \end{bmatrix} \begin{bmatrix} a^+ \\ b_1^+ \\ b_2^+ \\ \vdots \\ \vdots \\ b_i^+ \\ \vdots \\ \vdots \\ \vdots \end{bmatrix} \quad (4.88)$$

for the scattering matrix relationship between the incident and reflected wave amplitudes. When the antenna is used to radiate, all of the b_i^+ will be zero. In this case $a^- = S_{00}a^+$, so S_{00} is the reflection coefficient in the feed line looking toward the antenna. The i th radiated mode has an amplitude $b_i^- = S_{i0}a^+$, so a knowledge of the S_{i0} serves to determine the radiation pattern and radiated

power. For later convenience we shall partition the scattering matrix with the representations shown

$$\mathbf{S}_{00} = \left[\begin{array}{c|c} S_{00} & 0 \\ \hline 0 & 0 \end{array} \right] \tag{4.89a}$$

$$\mathbf{S}_{0i} = \left[\begin{array}{c|ccc} 0 & S_{10} & S_{20} & \cdots \\ \hline 0 & 0 & 0 & \cdots \end{array} \right] \tag{4.89b}$$

$$\mathbf{S}_{i0} = \left[\begin{array}{c|c} 0 & 0 \\ \hline S_{10} & \\ S_{20} & 0 \\ \vdots & \end{array} \right] \tag{4.89c}$$

$$\mathbf{S}_{ij} = \left[\begin{array}{c|cc} 0 & 0 \\ \hline 0 & S_{11} & S_{12} \\ \vdots & S_{21} & \cdots \\ \vdots & \end{array} \right] \tag{4.89d}$$

We shall also write

$$\mathbf{a} = \left[\begin{array}{c} a \\ \hline 0 \end{array} \right] \quad \text{and} \quad \mathbf{b} = \left[\begin{array}{c} 0 \\ \hline b_1 \\ b_2 \\ \vdots \\ \vdots \end{array} \right]$$

The antenna scattering matrix has a number of properties which may be derived in exactly the same way as in conventional waveguide theory. Thus when reciprocity holds, \mathbf{S} is symmetrical, that is, $S_{ij} = S_{ji}$. If the antenna is lossless, conservation of power requires that \mathbf{S} be a unitary matrix,^{1,2} that is,

$$\mathbf{S}_t^* \cdot \mathbf{S} = \mathbf{U} \tag{4.90}$$

where \mathbf{U} is the unit matrix and the subscript t denotes the transposed matrix. If there is no antenna present within the sphere $r = r_0$, then the incident

and reflected fields must remain finite at the origin, so $b_i^- = b_i^+$ (compare with the plane wave expansion). The scattering matrix then reduces to

$$\mathbf{S}_0 = \begin{bmatrix} 0 & 0 & \cdots & \cdots \\ 0 & 1 & 0 & \cdots \\ 0 & 0 & 1 & \cdots \\ \vdots & & & \ddots \end{bmatrix} \quad (4.91)$$

The difference between the outgoing waves when the antenna is present and those when the antenna is absent gives the field scattered by the antenna. If we denote the amplitudes of this field by the column vector \mathbf{b}_s with elements $b_{s,i}$, we have

$$\mathbf{b}_s = \mathbf{S}_{i0} \cdot \mathbf{a}^+ + (\mathbf{S}_{ij} - \mathbf{S}_0) \cdot \mathbf{b}_i^+ \quad (4.92)$$

The matrix b_s can be interpreted as the representation for the difference between the total field and the incident field. It should be noted that the contribution to the total outward propagating field from the wave a^+ reflected from the load is called the radiated field, since it has the same structure as the field radiated when the antenna is driven by a source. Some authors call the remaining term in (4.92) the scattered field. We are including both contributions for the scattered field, since these components are not orthogonal as regards power flow.

If the antenna is terminated in a load impedance Z_L with reflection coefficient Γ , we have $a^+ = \Gamma a^-$. The first equation in the set (4.88) gives

$$a^-(1 - S_{00}\Gamma) = S_{01}b_1^+ + S_{02}b_2^+ + \cdots$$

and hence the field scattered by the antenna is

$$\mathbf{b}_s = \left(\sum_{i=1}^{\infty} \frac{S_{0i}\Gamma}{1 - S_{00}\Gamma} b_i^+ \right) \mathbf{S}_{i0} + (\mathbf{S}_{ij} - \mathbf{S}_0) \cdot \mathbf{b}^+ \quad (4.93)$$

where the term $\mathbf{S}_{i0} \cdot \mathbf{a}^+ = a^+ \mathbf{S}_{i0}$. This equation may be used to examine the effect of the load termination on the scattered field. The scattered power is defined as that associated with the scattered field by

$$P_s = \frac{1}{2}(\mathbf{b}_s^*)_t \cdot \mathbf{b}_s = \frac{1}{2} \sum_i b_{s,i}^* b_{s,i} \quad (4.94)$$

where $(\mathbf{b}_s^*)_t$ is the transposed complex conjugate of \mathbf{b}_s .

As a simple example we shall consider scattering by a small electric dipole oriented along the x axis at the origin. We shall assume that the dipole is so small that it interacts only with the \mathbf{N}_{11}^e dipole mode. The interaction is proportional to the scalar product of the dipole current with the various modal functions in the expansion of the incident wave. If the incident wave is the

plane wave given by (4.86), only the \mathbf{N}_{11}^e mode interacts strongly, since all of the other modes have x components that vanish at the origin. At infinity the electric field of the \mathbf{N}_{11}^e mode with $z_1(k_0 r) = h_0^2(k_0 r)$ is

$$\mathbf{E} = \mathbf{N}_{11}^e = \frac{e^{-jk_0 r}}{k_0 r} (\hat{\mathbf{a}}_\theta \cos \theta \cos \phi - \hat{\mathbf{a}}_\phi \sin \phi)$$

The total outward power is readily evaluated to give

$$\int_0^\pi \int_0^{2\pi} \frac{|\mathbf{E}|^2}{2\zeta_0} r^2 \sin \theta d\theta d\phi = \frac{\lambda_0^2}{3\pi\zeta_0}$$

Hence the normalization factor for this mode is $(3\zeta_0\pi/2)\lambda_0^{-1}$. The outward propagating field will be

$$b_1^- \left(\frac{3\pi\zeta_0}{2\lambda_0^2} \right)^{1/2} \mathbf{N}_{11}^e$$

where $h_1^2(k_0 r)$ is used for $z_1(k_0 r)$. For the present problem the scattering matrix relation (4.88) becomes

$$\begin{bmatrix} a^- \\ b_1^- \\ b_2^- \\ \cdot \\ \cdot \\ \cdot \\ \cdot \end{bmatrix} = \begin{bmatrix} S_{00} & S_{01} & 0 & 0 & \cdots \\ S_{01} & S_{11} & 0 & 0 & \cdots \\ 0 & 0 & 1 & 0 & \cdots \\ 0 & 0 & 0 & 1 & \cdots \\ \cdot & \cdot & \cdot & \cdot & \cdot \\ \cdot & \cdot & \cdot & \cdot & \cdot \\ \cdot & \cdot & \cdot & \cdot & \cdot \end{bmatrix} \begin{bmatrix} a^+ \\ b_1^+ \\ b_2^+ \\ \cdot \\ \cdot \\ \cdot \\ \cdot \end{bmatrix} \quad (4.95)$$

since all modes except the $i = 1$ or \mathbf{N}_{11}^e mode are assumed to not interact with the dipole. The scattered field is given by (4.93) which reduces to

$$\begin{aligned} b_{s,1} &= \frac{S_{01}^2 \Gamma}{1 - S_{00} \Gamma} b_1^+ + (S_{11} - 1) b_1^+ \\ &= \frac{S_{01}^2 \Gamma + S_{11} - S_{11} S_{00} \Gamma + S_{00} \Gamma - 1}{1 - S_{00} \Gamma} b_1^+ \end{aligned} \quad (4.96)$$

From the properties of the scattering matrix for a lossless two port we have²

$$|S_{11}| = |S_{00}| \quad |S_{01}| = (1 - |S_{00}|^2)^{1/2}$$

and if

$$S_{00} = \rho e^{j\alpha_1} \quad S_{11} = \rho e^{j\alpha_2}$$

then

$$S_{01} = j(1 - \rho^2)^{1/2} e^{j(\alpha_1 + \alpha_2)/2}$$

It will be convenient to choose the reference planes S_1 and S_2 so that $\alpha_1 = \alpha_2 = 0$. We then obtain

$$b_{s,1} = \frac{(1 + \Gamma)(\rho - 1)}{1 - \rho\Gamma} b_1^+$$

We now replace the reflection coefficients ρ and Γ by

$$\rho = \frac{R_A - 1}{R_A + 1} \quad \Gamma = \frac{Z_L - 1}{Z_L + 1}$$

where R_A and Z_L are the normalized antenna and load impedances seen from the preferred reference plane. Our final result becomes

$$b_{s,1} = \frac{-2Z_L}{R_A + Z_L} b_1^+ \quad (4.97)$$

The scattered power is given by

$$P_s = 2 \left| \frac{Z_L}{R_A + Z_L} \right|^2 |b_1^+|^2$$

The incident field is given by (4.86), for which the incoming electric dipole component is

$$E_0^{3/4} \mathbf{N}_{11}^e \quad \text{with} \quad z_1(k_0 r) = h_0^1(k_0 r)$$

When we introduce the normalization factor, we have

$$\frac{E_0}{4} \left(\frac{6\lambda_0^2}{\pi\zeta_0} \right)^{1/2} \left[\left(\frac{3\pi\zeta_0}{2\lambda_0^2} \right)^{1/2} \mathbf{N}_{11}^e \right]$$

for the incident dipole component so

$$b_1^+ = \sqrt{\frac{6}{\pi\zeta_0}} \frac{E_0\lambda_0}{4}$$

Consequently, the power scattered by the dipole is

$$P_s = \frac{3E_0^2\lambda_0^2}{4\pi\zeta_0} \left| \frac{Z_L}{R_A + Z_L} \right|^2 \quad (4.98)$$

This equation shows that, by placing a short circuit ($Z_L = 0$) at the point on the transmission line where the impedance looking toward the antenna is pure resistive, the scattered power will vanish. If the load is matched to the antenna, $Z_L = R_A$ and the scattered power becomes

$$P_s = \frac{3E_0^2\lambda_0^2}{16\pi\zeta_0} \quad (4.99)$$

For a matched dipole the absorbed power is

$$P_A = \frac{E_0^2}{2\zeta_0} \frac{\lambda_0^2}{4\pi} G = P_s \quad (4.100)$$

since the gain $G = 1.5$. Thus a matched dipole scatters as much power as is absorbed. The reception mechanism may be viewed as one of destructive interference where the antenna scatters a field that cancels certain components (such as the dipole component above) of the incident field. Note that for the matched case $b_{s,1} = -b_1^+$.

We shall now return to the general equation (4.93) and cast it into a more useful form. Consider first the scattered field when $Z_L = 0$, in which case $\Gamma = -1$ and

$$\mathbf{b}_s^0 = - \left(\sum_i \frac{S_{0i}}{1 + S_{00}} b_i^+ \right) \mathbf{S}_{i0} + (\mathbf{S}_{ij} - \mathbf{S}_0) \cdot \mathbf{b}^+ \quad (4.101)$$

where $b_{s,i}^0$ are the amplitudes of the scattered modes for $Z_L = 0$. Next consider the case when the antenna radiates and is excited by a unit current. The total voltage at the terminals is $a^+ + a^- = a^+(1 + S_{00})$ and equals the normalized antenna input impedance Z_A for unit input current. Thus $a^+ = Z_A/(1 + S_{00})$ and the radiated field is

$$\mathbf{b}_r = \mathbf{S}_{i0} \cdot \mathbf{a}^+ = \left(\frac{Z_A}{1 + S_{00}} \right) \mathbf{S}_{i0} \quad (4.102)$$

where $b_{r,i}$ are the elements of \mathbf{b}_r and denote the amplitudes of the radiated modes. We now use (4.102) to eliminate \mathbf{S}_{i0} in (4.101) and (4.93). We also substitute for $(\mathbf{S}_{ij} - \mathbf{S}_0) \cdot \mathbf{b}^+$ from (4.101) into the general equation (4.93). In this reduction use is made of the fact that $\mathbf{S}_{i0} \cdot \mathbf{a}^+$ is a column matrix with elements $S_{i0}a^+$. It is readily found that

$$\mathbf{b}_s = \mathbf{b}_s^0 + \left[\sum_i \frac{S_{0i}}{Z_A} \left(1 + \Gamma \frac{1 + S_{00}}{1 - S_{00}\Gamma} \right) b_i^+ \right] \mathbf{b}_r$$

In order to eliminate the last explicit dependence on the scattering matrix parameters note that the antenna current $I(Z_L = 0)$ for zero load impedance is $a^+ - a^- = -2a^-$; and since $a^- = S_{00}a^+ + \sum_i S_{0i}b_i^+$, we get

$$I(Z_L = 0) = -\frac{2}{1 + S_{00}} \sum_i S_{0i}b_i^+$$

The factor multiplying \mathbf{b}_r above becomes

$$-\frac{I(Z_L = 0)(1 + S_{00})}{2Z_A} \frac{1 + \Gamma}{1 - \Gamma S_{00}} = \frac{-Z_L I(Z_L = 0)}{Z_A + Z_L}$$

Our desired result is now obtained and is

$$\mathbf{b}_s = \mathbf{b}_s^0 - \frac{I(Z_L = 0)Z_L}{Z_A + Z_L} \mathbf{b}_r \quad (4.103)$$

and expresses the scattered field as the sum of the field \mathbf{b}_s^0 scattered by the antenna with a short circuit at the terminals plus a field with amplitude which depends on the load impedance but otherwise is identical with the field that the antenna radiates when driven by a source. We can, of course, go from the scattering matrix representation directly to the field expressions, so (4.103) can be rewritten as

$$\mathbf{E}_s = \mathbf{E}_s(Z_L = 0) - \frac{I(Z_L = 0)Z_L}{Z_A + Z_L} \mathbf{E}_r \quad (4.104)$$

where \mathbf{E}_s is the scattered field in general, $\mathbf{E}_s(Z_L = 0)$ is the scattered field when $Z_L = 0$, and \mathbf{E}_r is the field radiated with unit current at the input terminals. The result (4.104) or its equivalent (4.103) is regarded as the fundamental equation in antenna scattering. In the form (4.104) it has been derived by a number of people (see for example King and Harrison,³³ Stevenson,³⁴ Hu,³⁵ and Aharoni³⁶).

Detailed studies of the scattering by small dipoles and loops have been carried out by Harrington.^{37,38} Scattering by loaded cylindrical antennas from a boundary-value point of view is described by King,³⁹ Chen and Liepa,⁴⁰ and Chen.⁴¹ The reader will also find a detailed discussion with additional references in the article by Garbacz.⁴²

Minimum Scattering Antennas

It is of interest to consider the relative amounts of power that an antenna absorbs and scatters under the condition that the antenna is matched to the transmission line. For this condition $S_{00} = 0$ and the scattering matrix relation (4.88) becomes

$$\begin{bmatrix} a^- \\ b_1^- \\ b_2^- \\ \vdots \\ \vdots \\ \vdots \end{bmatrix} = \begin{bmatrix} 0 & S_{01} & S_{02} & \cdots \\ S_{10} & S_{11} & S_{12} & \cdots \\ S_{20} & \cdots & \cdots & \cdots \\ \vdots & & & \\ \vdots & & & \\ \vdots & & & \end{bmatrix} \begin{bmatrix} a^+ \\ b_1^+ \\ b_2^+ \\ \vdots \\ \vdots \\ \vdots \end{bmatrix} \quad (4.105)$$

The absorbed and scattered powers are given by

$$P'_A = \frac{1}{2}(a^-)(a^-)^* = \frac{1}{2}[(\mathbf{b}^+)_t^* \cdot (\mathbf{S}_{0t})_t^*] \cdot (\mathbf{S}_{0t} \cdot \mathbf{b}^+) \quad (4.106)$$

$$\begin{aligned} P'_s &= \frac{1}{2}(\mathbf{b}^- - \mathbf{b}^+)_t^* \cdot (\mathbf{b}^- - \mathbf{b}^+) \\ &= \frac{1}{2}(\mathbf{b}^+)_t^* \cdot [(\mathbf{S}_{ij})_t^* - \mathbf{U}] \cdot (\mathbf{S}_{ij} - \mathbf{U}) \cdot \mathbf{b}^+ \end{aligned} \quad (4.107)$$

where we have followed Dicke¹ and Kahn and Kurss³¹ in defining the absorbed power P'_A and the scattered power P'_s . That is, the radiated field due to reflection from the load has not been included in the scattered field, in contrast with what was done in the definition (4.93) and (4.94). The true absorbed power is less than that given by (4.106), since power of amount $\frac{1}{2}(a^+)(a^+)^*$ is reflected from the load. Only when the load Z_L is matched to the antenna will P'_A and P'_s become equal to the true absorbed and scattered powers.

For $S_{00} = 0$ the unitary properties of the scattering matrix yield the following relations:

$$(\mathbf{S}_{i0})_t^* \cdot \mathbf{S}_{i0} = \mathbf{U} \quad (4.108a)$$

$$(\mathbf{S}_{i0})_t^* \cdot \mathbf{S}_{ij} = 0 \quad (4.108b)$$

$$(\mathbf{S}_{0i})_t^* \cdot \mathbf{S}_{0i} + (\mathbf{S}_{ij})_t^* \cdot \mathbf{S}_{ij} = \mathbf{U} \quad (4.108c)$$

We shall need these in the discussion to follow.

The concept of a minimum scattering antenna was introduced by Dicke, who showed that, for an incident field which was an eigenvector of the scattering matrix, i.e., a field for which

$$\mathbf{S} \cdot (\mathbf{a}^+ + \mathbf{b}^+) = \lambda(\mathbf{a}^+ + \mathbf{b}^+)$$

where λ is the eigenvalue, the scattered power P'_s was always greater than or equal to the absorbed power P'_A . An antenna for which $P'_s = P'_A$ was called a minimum-scattering antenna.¹ The results obtained by Dicke have been extended and generalized by Kahn and Kurss.³¹ According to the latter authors a minimum-scattering antenna may be defined as follows: A canonical minimum-scattering antenna is a lossless antenna, fed from an N -port matched and uncoupled waveguide system which may incorporate nonreciprocal elements, that is rendered invisible when all of the N waveguide ports are open-circuited. It has the property that $P'_s = P'_A$.

An antenna will in general scatter a field which is different from the field that it radiates. However, if the antenna is to be made invisible, it must scatter a field of structure identical with that which it radiates so that the reflected field and radiated field will cancel. Hence a minimum-scattering antenna scatters in exactly the same way that it radiates. We shall discuss the theory of minimum-scattering antennas only for reciprocal antennas fed from a single transmission line. For the more general case the paper by Kahn and Kurss should be consulted.

When the transmission line is open-circuited, $a^+ = a^-$ and we obtain

$$\begin{aligned} \mathbf{a}^- &= \mathbf{S}_{0i} \cdot \mathbf{b}^+ = \mathbf{a}^+ \\ \mathbf{b}^- &= \mathbf{S}_{i0} \cdot \mathbf{a}^+ + \mathbf{S}_{ij} \cdot \mathbf{b}^+ = (\mathbf{S}_{i0} \cdot \mathbf{S}_{0i} + \mathbf{S}_{ij}) \cdot \mathbf{b}^+ \end{aligned}$$

from (4.105). The antenna will be invisible only if $\mathbf{b}^- = \mathbf{b}^+$, which is the relation between the reflected and incident field when no antenna is present. Thus we must have

$$\mathbf{S}_{ij} = \mathbf{U} - \mathbf{S}_{i0} \cdot \mathbf{S}_{0i} \quad (4.109)$$

If we substitute for \mathbf{S}_{ij} from (4.109) into (4.107), we get

$$\begin{aligned} P'_s &= \frac{1}{2}(\mathbf{b}^+_i)^* \cdot [(\mathbf{S}_{0i})^* \cdot (\mathbf{S}_{i0})^* \cdot \mathbf{S}_{i0} \cdot \mathbf{S}_{0i}] \cdot \mathbf{b}^+ \\ &= \frac{1}{2}(\mathbf{b}^+)^* \cdot (\mathbf{S}_{0i})^* \cdot \mathbf{S}_{0i} \cdot \mathbf{b}^+ \end{aligned} \quad (4.110)$$

by using (4.108a) to simplify the product of the two innermost matrices. A comparison of this expression with (4.106) shows that

$$P'_s = P'_A \quad (4.111)$$

Hence the minimum-scattering antenna as defined has the property that, when terminated in a matched load, the true scattered power equals the true absorbed power, since $P'_s = P_s$ and $P'_A = P_A$ for a matched load. The dipole antenna discussed in the earlier part of this section is an example of a minimum-scattering antenna.

The pattern of the scattered field is the same as that when the antenna radiates, since from (4.109) the scattered field is given by

$$\mathbf{b}_s = -\mathbf{S}_{i0} \cdot \mathbf{S}_{0i} \cdot \mathbf{b}^+ \quad (4.112)$$

where

$$\mathbf{S}_{0i} \cdot \mathbf{b}^+ = \begin{bmatrix} S_{01}b_1^+ + S_{02}b_2^+ + \cdots \\ 0 \\ 0 \\ \vdots \\ \vdots \end{bmatrix}$$

and thus \mathbf{b}_s is a constant multiplying the column matrix with elements S_{i0} . The latter determines the radiation pattern of the antenna, because $\mathbf{b}^- = \mathbf{S}_{i0} \cdot \mathbf{a}^+$ when there is no incident field from space. When the antenna is reciprocal, each element $S_{i0} = S_{0i}$ and must be pure real, since from (4.109) we have

$$\begin{aligned} (\mathbf{S}_{i0})_t^* \cdot \mathbf{S}_{ij} &= 0 = (\mathbf{S}_{i0})_t^* - (\mathbf{S}_{i0})_t^* \cdot \mathbf{S}_{i0} \cdot \mathbf{S}_{0i} \\ &= (\mathbf{S}_{i0})_t^* - \mathbf{S}_{0i} \end{aligned}$$

or

$$(\mathbf{S}_{i0})_t^* = \mathbf{S}_{0i} \quad (4.113)$$

upon premultiplying by $(\mathbf{S}_{i0})_t^*$ and using (4.108a) and (4.108b). This property of the scattering matrix makes the radiation pattern symmetrical about any plane through the origin.

The question whether or not any antenna can absorb more power than it scatters naturally arises. Certainly for an antenna not matched to its load this is possible and may be shown in a simple manner in connection with the dipole antenna (see Prob. 4.10). Kahn and Kurss show that any antenna for which

$$|\mathbf{S}_{0i} \cdot \mathbf{b}^+| = |(\mathbf{S}_{i0})_t^* \cdot \mathbf{b}^+| \quad (4.114)$$

and which is connected to a matched receiver will scatter more power than it absorbs.³¹ However, (4.114) is a sufficient condition only for $P_s \geq P_A$. In actual fact Green has devised an antenna consisting of a dipole and a loop in combination which absorbs more power than it scatters.⁴³ The antenna is matched to its load, but its receiving properties do not optimize the received power when the dipole and loop are so phased as to make $P_s < P_A$. When phased for maximum received power, $P_s = P_A$. Green's antenna would not be invisible for a load replaced by an open circuit unless the dipole and loop were so phased that $P_s = P_A$, in which case the antenna would be a minimum-scattering antenna.

PROBLEMS

4.1 Show that the power received by antenna b when antenna a is transmitting (Fig. 4.5) is proportional to $|Z_{12}|^2$ when the equivalent circuit of Fig. 4.4 is valid. As-

sume that $|Z_{12}|$ is small compared with $|Z_{11}|$ and $|Z_{22}|$ and that a load resistance R_L is inserted in place of the generator e_b .

4.2 Consider a lossless matching network that transforms the antenna input impedance Z_a at terminals T_2 into the characteristic impedance Z_c at the terminals T_1 . Show that, when the transmission line is terminated in its characteristic impedance Z_c

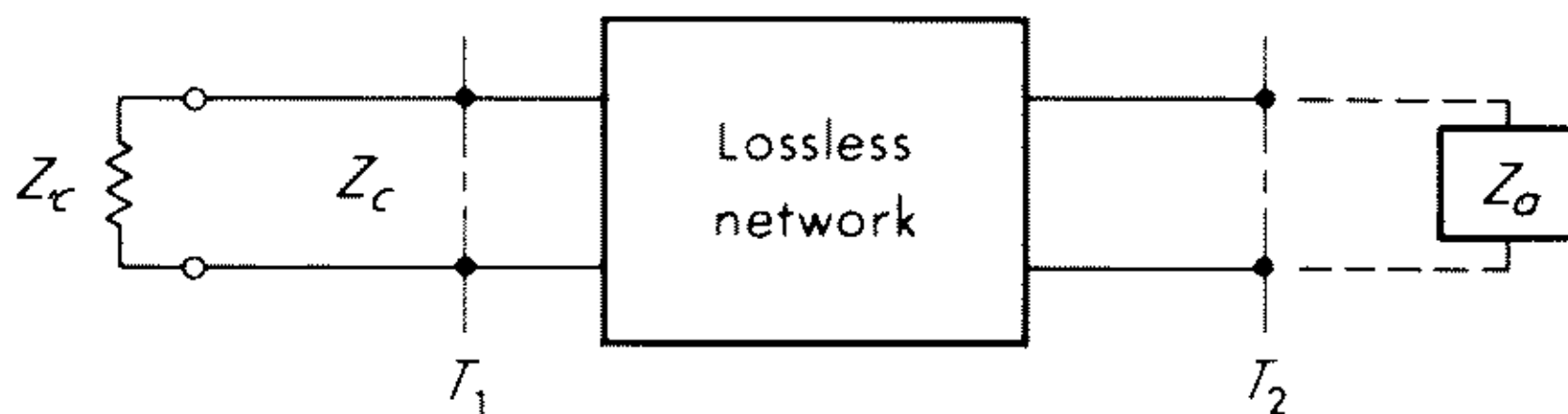


Fig. P-4.2

at T_1 , the impedance at T_2 looking into the matching network is Z_a^* , that is, a maximum power transfer match.

4.3 Show that, for a two-antenna system (matched),

$$|Z_{12}| = \left[4R_a R_b \left(\frac{\lambda_0}{4\pi r} \right)^2 G_a(\theta_a, \phi_a) G_b(\theta_b, \phi_b) \right]^{1/2}$$

Evaluate $|Z_{12}|$ for $R_a = R_b = 72$ ohms, $\lambda_0 = 10$ m, $r = 10^4$ m, $G_a = G_b = 10$. The quantity $|Z_{12}|/\sqrt{R_a R_b}$ is a measure of the relative magnitude of antenna coupling.

4.4 Consider the three-antenna system illustrated. Each antenna is matched to a transmission line with characteristic impedance Z_c . Antenna 1 is terminated in a resistive load $R_1 \neq Z_c$, and antenna 2 is terminated in a load $R_2 \neq Z_c$. Antenna 3 is

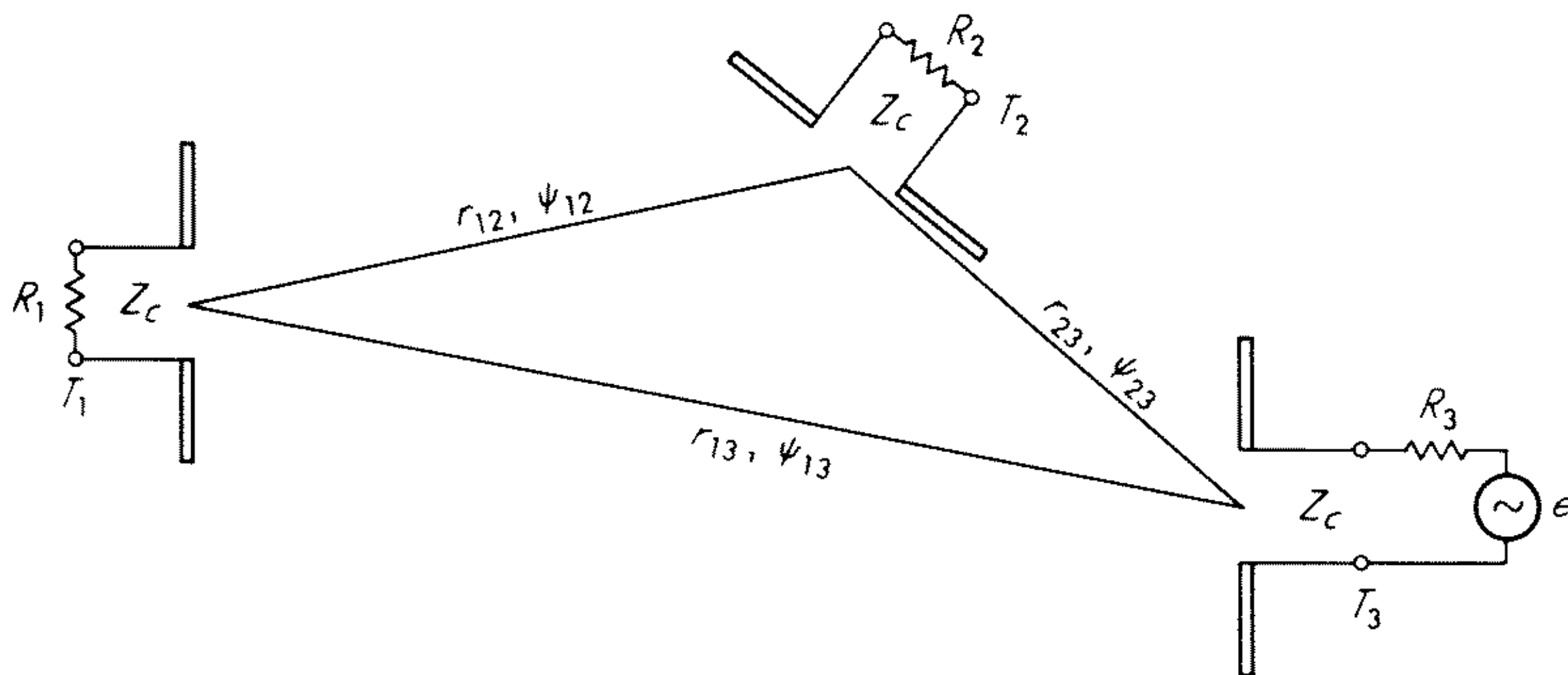


Fig. P-4.4

connected to a generator with internal resistance R_3 and open-circuit voltage e . Let the distance between antenna i and j be denoted r_{ij} , and let the phase of the received voltage at the reference plane of antenna j relative to the input terminal current of antenna i be ψ_{ij} ; that is, a factor $e^{-j\psi_{ij}}$ is used to account for propagation phase delay. Show that the mutual impedances are given by

$$Z_{ij} = \frac{\lambda_0}{2\pi} Z_c \frac{\sqrt{G_i(j)G_j(i)}}{r_{ij}} e^{-j\psi_{ij}}$$

where $G_i(j)$ is the gain of antenna i in the direction of antenna j . Derive expressions for the power received by antennas 1 and 2. How is the power received by antenna 1 affected by the presence of antenna 2? Assume all mutual impedances to be very small.

4.5 An elliptically polarized antenna radiates a field which is subsequently reflected from a large perfectly conducting plane perpendicular to the radius vector. Show that the loss in received power from the reflected wave due to polarization mismatching is given by

$$p = \frac{1 + \tau^4 + 2\tau^2 \cos 2\beta}{(1 + \tau^2)^2}$$

where $h_\theta, h_\phi = \tau e^{j\beta} h_\theta$ defines the state of polarization of the antenna. For a circularly polarized antenna show that the received power is zero.

4.6 Consider a receiving and transmitting antenna system with separation r . Show that the received power P_r when the incident power to the transmitting antenna terminals is P_t is given by

$$P_r = \frac{P_t \lambda_0^2}{16\pi^2 r^2} (1 - |\Gamma_t|^2)(1 - |\Gamma_r|^2) G_t(\theta_t, \phi_t) G_r(\theta_r, \phi_r) \frac{|\mathbf{h}_r \cdot \mathbf{h}_t|^2}{|\mathbf{h}_r|^2 |\mathbf{h}_t|^2}$$

The subscripts r and t refer to the receiving and transmitting antennas, respectively. This is a generalization of the well-known Friis formula (*Proc. IRE*, vol. 34, pp. 254–256, May, 1945).

4.7 A receiving antenna is elliptically polarized with polarization specified by the parameters $\tau = 2, \beta = \pi/3$. Evaluate the Stokes parameters and plot the representative point on the Poincaré sphere. Use the Poincaré sphere representation to find the parameters σ and α which characterize the polarization of an incident wave such that the received power will be zero. Compare the ellipticity and orientation of the two polarization ellipses.

4.8 Show that the coherence matrix for a circularly polarized wave is of the form

$$\langle \sigma^2 \rangle \begin{bmatrix} 1 & \pm j \\ \mp j & 1 \end{bmatrix}$$

4.9 Show that a linearly polarized antenna receives only one-half of the maximum possible power from a randomly polarized incident wave.

4.10 Show that, for the dipole antenna discussed in Sec. 4.8, the absorbed power P_A will exceed the scattered power P_s if the antenna is mismatched to the load, i.e., when $Z_L = R_L < R_A$.

Answer: $P_A/P_s = R_A/R_L$.

4.11 Determine the scattering matrix \mathbf{S}_{ij} for an antenna that becomes invisible when it is terminated in a pure reactive load. Show that this will also be a minimum-scattering antenna.

Hint: Let $a^+ = e^{j\alpha} a^-$.

REFERENCES

1. Montgomery, C. G., R. H. Dicke, E. M. Purcell: "Principles of Microwave Circuits," chaps. 2 and 3, McGraw-Hill Book Company, New York, 1948.
2. Collin, R. E.: "Foundations for Microwave Engineering," chaps. 3–5, McGraw-Hill Book Company, New York, 1966.
3. Tai, C. T.: On the Transposed Radiating Systems in an Anisotropic Medium, *IRE Trans. Antennas Propagation*, vol. AP-9, p. 502, September, 1961.

4. Sichak, W., and S. Milazzo: Antennas for Circular Polarization, *Proc. IRE*, vol. 36, pp. 997–1001, August, 1948.
5. Yeh, Y. C.: The Received Power of a Receiving Antenna and the Criteria for Its Design, *Proc. IRE*, vol. 37, pp. 155–158, February, 1949.
6. Roubine, E.: Les Propriétés des Antennas des Reception, *L'Onde Elec.*, vol. 30, pp. 259–266, June, 1950.
7. Hatkin, L.: Elliptically Polarized Waves, *Proc. IRE*, vol. 38, p. 1455, December, 1950.
8. Sinclair, G.: The Transmission and Reception of Elliptically Polarized Waves, *Proc. IRE*, vol. 38, pp. 148–151, February, 1950.
9. Morgan, M. G., and W. R. Evans: Synthesis and Analysis of Elliptic Polarization Loci in Terms of Space-quadrature Sinusoidal Components, *Proc. IRE*, vol. 39, pp. 552–556, May, 1961.
10. Rumsey, V. H.: Transmission between Elliptically Polarized Antennas, *Proc. IRE*, vol. 39, pp. 535–540, May, 1961.
11. Deschamps, G. A.: Geometrical Representation of the Plane Electromagnetic Wave, *Proc. IRE*, vol. 39, pp. 540–544, May, 1961.
12. Kales, M. L.: Elliptically Polarized Waves and Antennas, *Proc. IRE*, vol. 39, pp. 544–549, May, 1961.
13. Bohnert, J. I.: Measurements on Elliptically Polarized Antennas, *Proc. IRE*, vol. 39, pp. 549–552, May, 1951.
14. Tai, C. T.: On the Definition of the Effective Aperture of Antennas, *IRE Trans. Antennas Propagation*, vol. AP-9, pp. 224–225, March, 1961.
15. Deschamps, G. A.: A New Chart for the Solution of Transmission Line and Polarization Problems, *Elec. Commun.*, vol. 30, pp. 247–254, September, 1953.
16. Poincaré, H.: “Théorie Mathématique de la Lumière,” vol. 2, chap. 12, Paris, 1892.
17. Born, M., and E. Wolf: “Principles of Optics,” 2d ed., The Macmillan Company, New York, 1964.
18. Ko, H. C.: Theoretical Techniques for Handling Partially Polarized Radio Waves with Special Reference to Antennas, *Proc. IRE*, vol. 49, pp. 1446–1447, September, 1961.
19. Ko, H. C.: The Use of the Statistical Matrix and the Stokes Vector in Formulating the Effective Aperture of Antennas, *IRE Trans. Antennas Propagation*, vol. AP-9, pp. 581–582, November, 1961.
20. Ko, H. C.: On the Reception of Quasi-monochromatic, Partially Polarized Radio Waves, *Proc. IRE*, vol. 50, pp. 1950–1957, September, 1962.
21. Ko, H. C.: Radio-telescope Antenna Parameters, *IEEE Trans. Antennas Propagation*, vol. AP-12, pp. 891–898, December, 1964.
22. Papas, C. H.: “Theory of Electromagnetic Wave Propagation,” McGraw-Hill Book Company, New York, 1965.
23. Davenport, W. B., Jr., and W. L. Root: “Introduction to Random Signals and Noise,” McGraw-Hill Book Company, New York, 1958.
24. Zucker, F. J.: Introduction to Partially Coherent Electromagnetic Waves, in E. C. Jordan (ed.), “Electromagnetic Waves,” vol. 2, Pergamon Press, New York, 1963.
25. MacPhie, R. H.: On the Mapping by a Cross-correlation Antenna System of Partially Coherent Radio Sources, *IEEE Trans. Antennas Propagation*, vol. AP-12, pp. 118–124, January, 1964.
26. Pierce, J. R.: Physical Sources of Noise, *Proc. IRE*, vol. 44, pp. 601–608, May, 1956.
27. Bennett, W. R.: Methods of Solving Noise Problems, *Proc. IRE*, vol. 44, pp. 609–638, May, 1956.
28. Siegman, A. E.: Thermal Noise in Microwave Systems, *Microwave J.*, vol. 4, part I, pp. 81–90, March, 1961, part II, pp. 66–73, April, 1961, part III, pp. 93–104, May, 1961.

29. Oliver, B. M.: Thermal and Quantum Noise, *Proc. IEEE*, vol. 53, pp. 436–454, May, 1965.
30. Hogg, D. C., and W. W. Mumford: The Effective Noise Temperature of the Sky, *Microwave J.*, vol. 3, pp. 80–84, March, 1960.
31. Kahn, W. K., and H. Kurss: Minimum Scattering Antennas, *IEEE Trans. Antennas Propagation*, vol. AP-13, pp. 671–675, September, 1965.
32. Stratton, J. A.: "Electromagnetic Theory," chap. VII, McGraw-Hill Book Company, New York, 1941.
33. King, R. W. P., and C. W. Harrison, Jr.: The Receiving Antenna, *Proc. IRE.*, vol. 32, pp. 18–34, January, 1944. See also pp. 35–49 for a related paper by the same authors.
34. Stevenson, A. F.: Relations between the Transmitting and Receiving Properties of Antennas, *Quart. Appl. Math.*, vol. 5, pp. 140–148, January, 1948.
35. Hu, Y. Y.: Back-scattering Cross-section of a Center-loaded Antenna, *IRE Trans. Antennas Propagation*, vol. AP-6, pp. 140–148, January, 1958.
36. Aharoni, J.: "Antennas," pp. 164–176, Clarendon Press, Oxford, 1946.
37. Harrington, R. F.: Small Resonant Scatterers and Their Use for Field Measurements, *IRE Trans. Microwave Theory Tech.*, vol. MTT-10, pp. 165–174, May, 1962.
38. Harrington, R. F.: Theory of Loaded Scatterers, *Proc. IEEE*, vol. 111, pp. 617–623, April, 1964.
39. King, R. W. P.: "The Theory of Linear Antennas," chap. IV, pp. 456–521, Harvard University Press, Cambridge, Mass., 1956.
40. Chen, K. M., and V. Liepa: The Minimization of the Back Scattering of a Cylinder by Central Loading, *IEEE Trans. Antennas Propagation*, vol. AP-12, pp. 576–582, September, 1964.
41. Chen, K. M.: Minimization of Backscattering of a Cylinder by Double Loading, *IEEE Trans. Antennas Propagation*, vol. AP-13, pp. 262–270, March, 1965.
42. Garbacz, R. J.: Antennas as Scatterers, part of short-course notes on antenna and scattering theory, Electrical Engineering Dept., Ohio State University, 1965.
43. Green, R. B.: Scattering from Conjugate Matched Antennas, *IEEE Trans. Antennas Propagation*, vol. AP-14, pp. 17–21, January, 1966.
44. Childers, D. G.: Antenna Reception of Nonisotropic Stochastic Fields, *J. Frank. Inst.*, vol. 282, pp. 216–231, October, 1966.

CHAPTER 5

UNIFORMLY SPACED ARRAYS

H. Bach and J. E. Hansen

5.1 Introduction

For many applications in modern techniques it is not possible, with a single simple antenna, to obtain the values of directivity or beam width required. One convenient method of overcoming this difficulty is to form antenna systems composed of several similar antennas or elements. Such antenna systems are called arrays. By a suitable choice of the excitation in amplitude and phase of the individual radiators and of their spatial distribution, properties of the entire system which are essentially better than those of the separate elements may be obtained. This fact depends upon the displacement in time and space of the fields originating from the single antennas. In some directions, the null directions, these fields may interfere destructively, while in other directions they may be in phase and thus produce a maximum of radiation.

In this chapter we consider mainly antenna systems composed of identical antennas placed equidistantly along a curve. First the problem of analysis, i.e., the problem of determining the properties of an array from a given excitation and position of the elements, is treated. Later the reverse problem, the problem of synthesis, is discussed.

In Sec. 5.2 we show that the far field from an array of identical elements can be written as the product of two quantities. One of these, the element factor, is essentially equal to the field from one single element. For commonly employed elements such as dipoles and slots the element factor is a slowly varying function of the direction of radiation. Array theory may therefore concern itself only with the second (dimensionless, scalar, and element-independent) factor, the array factor, which controls the characteristic features of array radiation.

Not only the field but also other array quantities such as directivity and gain may be written as the product of an element-dependent part and a dimensionless "array-dependent" part. The basic parameters discussed in Sec. 5.3 are treated in this manner.

In Secs. 5.4 and 5.5 we consider classical methods for obtaining the array factor and the directivity for arrays with the elements arranged on a straight line and having particularly simple excitations. In Sec. 5.6 the circular array is treated in a similar manner.

Since, as mentioned, array theory is independent of the type of element

utilized, one may feel tempted to examine arrays in which the elements themselves are arrays. This leads to the principle of pattern multiplication which is discussed in Sec. 5.7.

In Sec. 5.8 an antenna array is treated as a network with n ports, where n is the number of elements. Some problems pertaining to transmitting and receiving properties of arrays are discussed there. Also, a brief derivation in terms of terminal quantities, such as impedances and currents, of the basic array parameters from Sec. 5.3 is given.

The last three sections are devoted to selected synthesis procedures for arrays. Section 5.9 covers methods yielding the excitation currents when the array factor is prescribed, while Sec. 5.10 concentrates upon the well-known Dolph-Chebyshev techniques for obtaining radiation patterns with narrow beam width and low side lobes. The chapter concludes with a section describing methods for optimizing directivity and other array parameters. In contrast with the schemes devised in Secs. 5.9 and 5.10, which apply to linear, uniformly spaced arrays, the methods of Sec. 5.11 are applicable to arbitrary arrays.

Throughout the chapter it is assumed that the arrays described are formed by infinitely thin identical oriented elements with similar current distributions. An exception is Sec. 5.8, where a brief mention is given with regard to the validity of idealized array theory for arrays of physical elements. In all sections the classical element-by-element approach to array theory is followed. Other approaches are in use; one notable example is the treatment of a uniformly spaced array as a periodic structure. The selection of topics for this chapter is by no means complete. For instance, the important aspect of array theory known as beam scanning is not mentioned. For a coverage of this subject the reader is referred to the specialized literature.¹

ANALYSIS OF ARRAYS

5.2 Radiation from an Array. Factorization

In this section we will calculate the far field generated by an array of antennas with specified current distributions. Of course, it is, in general, possible to set up exact formulas for the entire field, but they are complicated and usually difficult to apply. We therefore utilize the fact that in most applications the distance between the transmitter and the receiver is very large; this results in great simplification and leads to useful formulas.

First we consider a single antenna and derive expressions for its far field, i.e., the field at a distance from the antenna that is large compared to both the wavelength and the dimensions of the antenna. We introduce a spherical coordinate system (r, θ, ϕ) , the origin of which is located at a point 0 in the vicinity of the antenna, and let the current distribution on the antenna be given by $\mathbf{J}(\mathbf{r}')$. The vector potential \mathbf{A} at a field point \mathbf{r} is then expressed through

$$\mathbf{A} = \frac{\mu_0}{4\pi} \int_V \mathbf{J}(\mathbf{r}') \frac{e^{-jk_0 R}}{R} dV' \quad (5.1)$$

where $R = |\mathbf{r} - \mathbf{r}'|$ and V is the part of space in which $\mathbf{J}(\mathbf{r}') \neq 0$. We wish to calculate the far field only and introduce in the rapidly varying exponential term the approximation

$$k_0 R \approx k_0 r - k_0 \mathbf{r}' \cdot \hat{\mathbf{r}} \quad (5.2)$$

where $r = |\mathbf{r}|$, while in the denominator we use

$$k_0 R \approx k_0 r \quad (5.3)$$

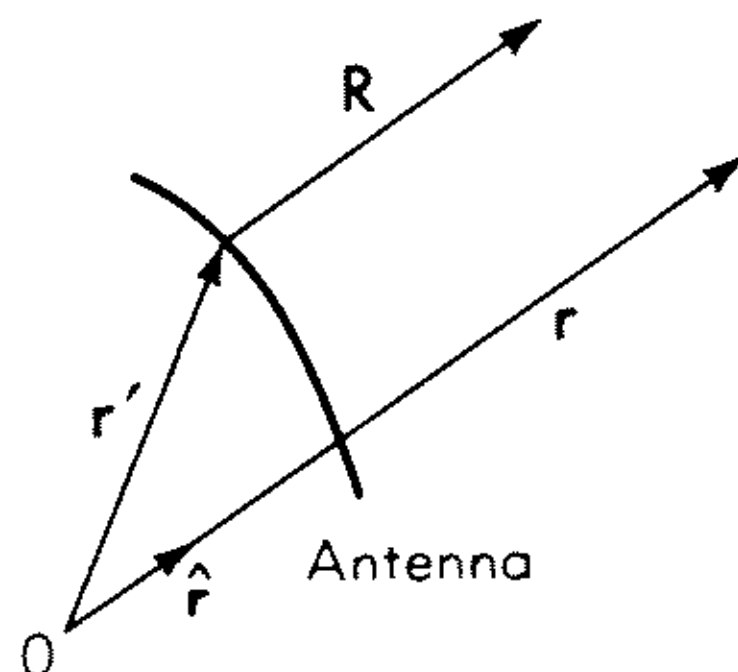


Fig. 5.1 For the computation of the far field from a single antenna.

Both of these approximations will hold at distances from the antenna which are large compared to its dimensions, as well as to the wavelength. We thus find the expression

$$\mathbf{A} = \frac{\mu_0}{4\pi} \frac{e^{-jk_0 r}}{r} \int_V \mathbf{J}(\mathbf{r}') \exp(jk_0 \mathbf{r}' \cdot \hat{\mathbf{r}}) dV' \quad (5.4)$$

for the vector potential corresponding to the far field.

We next consider an array of antennas. Let us introduce the convention that the current distributions on identical antennas are similar, differing from each other only by (possibly complex) constant multipliers. An array of antennas is then defined as a system of identical and identically oriented antennas with similar current distributions.

We shall now show that the field radiated from an array may be written as a product of two factors. One of these, the element factor, is the field radiated from a single (reference) element. The other, the array factor, is dependent on the quantities which precisely characterize the array as such, i.e., the relative positions and excitations of the elements. The process of separating the field expression into these two parts is termed factorization.

We denote the number of elements by n , and in order to obtain a simple specification of the array, we introduce a fictitious reference antenna; this is of the same type as the elements of the array, is oriented in the same manner, and possesses a current distribution similar to that of the elements. A reference point for the current distribution on the reference antenna is taken as the origin for a spherical coordinate system (r, θ, ϕ) . The position of, and current distribution on, the m th element of the array may now be specified simply by the translation \mathbf{r}_m , which must be applied to the reference antenna to bring it into

coincidence with the m th element, and the (possibly complex) constant a_m , the excitation coefficient, by which the current distribution of the reference antenna must be multiplied in order to become identical with that of the m th element. Let \mathbf{r}' be the position vector of a point on the reference antenna and \mathbf{r}'_m that of the congruent point on the m th element. We then have, as shown in Fig. 5.2,

$$\mathbf{r}'_m = \mathbf{r}' + \mathbf{r}_m \quad (5.5)$$

and the equation

$$\mathbf{J}_m(\mathbf{r}'_m) = a_m \mathbf{J}^{\text{ref}}(\mathbf{r}') \quad (5.6)$$

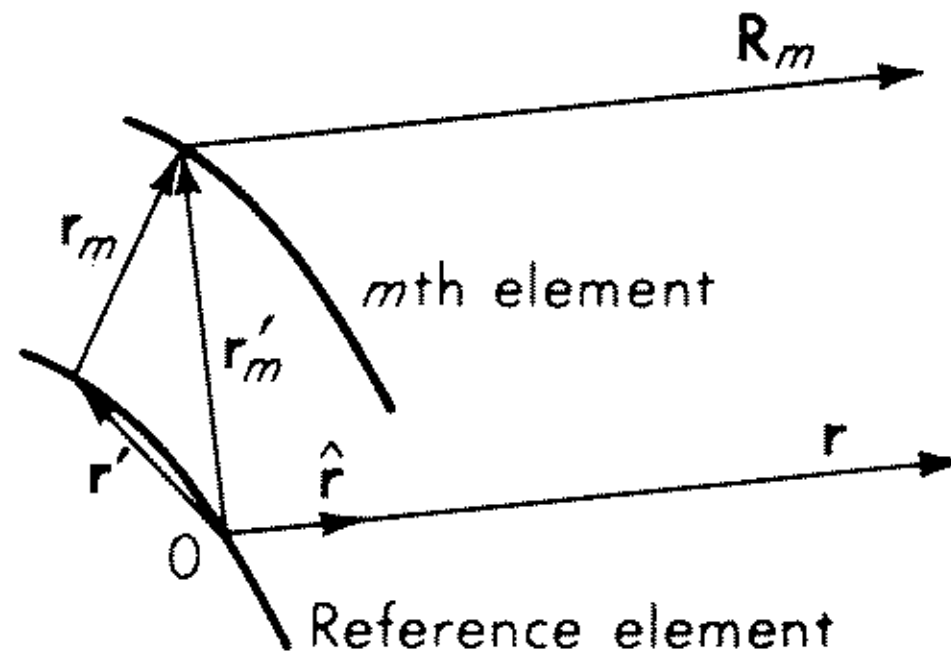


Fig. 5.2 For the computation of the far field from an array.

relating the current distributions on the m th element and the reference antenna.

Now, according to (5.4), the vector potential \mathbf{A}_m corresponding to the m th antenna may be expressed through

$$\mathbf{A}_m = \frac{\mu_0}{4\pi} \frac{e^{-jk_0 r}}{r} \int_{V_m} \mathbf{J}_m(\mathbf{r}'_m) \exp(jk_0 \mathbf{r}'_m \cdot \hat{\mathbf{r}}) dV'$$

Introducing into this equation formulas (5.5) and (5.6) and adding the contributions from the n elements to the total vector potential \mathbf{A} of the array, we arrive at

$$\mathbf{A} = \mathbf{A}^{\text{ref}}(r) f(\theta, \phi) \quad (5.7)$$

where

$$\mathbf{A}^{\text{ref}}(\mathbf{r}) = \frac{\mu_0}{4\pi} \frac{e^{-jk_0 r}}{r} \int_V \mathbf{J}^{\text{ref}}(\mathbf{r}') \exp(jk_0 \mathbf{r}' \cdot \hat{\mathbf{r}}) dV'$$

is the vector potential originating from the reference antenna and

$$f(\theta, \phi) = \sum_{m=1}^n a_m \exp(jk_0 \mathbf{r}_m \cdot \hat{\mathbf{r}}) \quad (5.8)$$

is the array factor, a dimensionless quantity.

Exercise 5.1 Fill in the details in the derivation of (5.8).

Hereby the factorization is accomplished. It is important to observe that the array factor is a quantity characteristic of the array; it depends only on the excitation coefficients a_m and the relative position of the elements, but it is

independent of the type of elements used. The array factor $f(\theta, \phi)$ is generally a complex function of (θ, ϕ) , but in the remainder of this chapter special attention will be paid to its absolute value $|f(\theta, \phi)|$, which we shall refer to as the array pattern.

By means of the formulas (1.60a,b)

$$\mathbf{E} = -j\omega \left(\frac{1}{k_0^2} \nabla \nabla \cdot \mathbf{A} + \mathbf{A} \right) \quad \mathbf{H} = \frac{1}{\mu_0} \nabla \times \mathbf{A}$$

it can be shown that the factorization also can be obtained for the electric and magnetic far field, which therefore may be expressed through

$$\mathbf{E} = \mathbf{E}^{\text{ref}} f(\theta, \phi) \quad \mathbf{H} = \mathbf{H}^{\text{ref}} f(\theta, \phi) \quad (5.9)$$

where \mathbf{E}^{ref} and \mathbf{H}^{ref} are the electric and magnetic field from the reference antenna and $f(\theta, \phi)$ is still determined by (5.8).

It is often convenient to introduce the rectangular components of the vectors

$$\mathbf{r}_m = x_m \hat{\mathbf{x}} + y_m \hat{\mathbf{y}} + z_m \hat{\mathbf{z}}$$

and

$$\hat{\mathbf{r}} = \hat{\mathbf{x}} \sin \theta \cos \phi + \hat{\mathbf{y}} \sin \theta \sin \phi + \hat{\mathbf{z}} \cos \theta$$

By inserting these expressions into (5.8), we find

$$f(\theta, \phi) = \sum_{m=1}^n a_m e^{jk_0(x_m \sin \theta \cos \phi + y_m \sin \theta \sin \phi + z_m \cos \theta)} \quad (5.10)$$

or

$$f(\theta, \phi) = \sum_{m=1}^n a_m e^{ju_m(\theta, \phi)} \quad (5.11)$$

where

$$u_m(\theta, \phi) = k_0 \mathbf{r}_m \cdot \hat{\mathbf{r}} \quad (5.12)$$

These formulas show that even if just a few elements are used, a relatively large number of parameters still occur. It is thus obvious that, even with the restriction imposed by the definition of an array, there exist many possibilities for constructing different arrays. For the sake of convenience, arrays are therefore classified in accordance with their geometrical structure into linear arrays in which the elements are placed along a straight line, circular or ring arrays in which they are placed along the circumference of a circle, etc. In this chapter, however, we shall confine ourselves to more specialized arrays, namely, arrays of equispaced elements. These can be defined as arrays for which the distance between two neighboring elements is a constant characteristic of the array. As the first example of such arrays we consider the linear array of equispaced elements. However, we shall first discuss some basic array parameters pertaining to arbitrary arrays.

5.3 Basic Array Parameters

In this chapter we represent the electrical field strength \mathbf{E} in the far field of an antenna which radiates the power P_{rad} in the form $\mathbf{E} = E \hat{\mathbf{p}}$, where

$$E = \sqrt{\frac{P_{\text{rad}}}{2\pi \zeta_0^{-1}}} \frac{e^{-jk_0 r}}{r} g(\theta, \phi) \quad (5.13)$$

and where $\hat{\mathbf{p}}$ is a (complex) polarization unit vector. In (5.13), ζ_0^{-1} is the intrinsic admittance of free space and $g(\theta, \phi)$ is the complex radiation pattern. The absolute value $|g(\theta, \phi)|$ is referred to as the radiation pattern of the antenna.

Exercise 5.2 Show, by integration of Poynting's vector over a sphere with its center at the antenna, that (5.13) implies the following normalization of the complex radiation pattern $g(\theta, \phi)$ of an antenna

$$\int_{4\pi} |g(\theta, \phi)|^2 d\Omega = 4\pi$$

where $d\Omega$ is an element of solid angle.

With this normalization of the radiation pattern we find that $\Phi(\theta, \phi)$, the power density per unit solid angle in the direction (θ, ϕ) , is given by

$$\Phi(\theta, \phi) = \frac{1}{4\pi} P_{\text{rad}} |g(\theta, \phi)|^2 \quad (5.14)$$

Accordingly, for the directivity $D(\theta, \phi)$ in this direction, we find

$$D(\theta, \phi) \equiv \frac{\Phi(\theta, \phi)}{(1/4\pi)P_{\text{rad}}} = |g(\theta, \phi)|^2 \quad (5.15)$$

Thus by the normalization of the complex radiation pattern implied by (5.13) the power pattern $|g(\theta, \phi)|^2$ and the directivity $D(\theta, \phi)$ are equal.

In the following we shall also consider lossy antennas. We introduce the dissipated power P_{loss} by the relation

$$P_{\text{tot}} = P_{\text{rad}} + P_{\text{loss}} \quad (5.16)$$

where P_{tot} is the total power supplied to the antenna. The efficiency η of the antenna is defined by

$$\eta = \frac{P_{\text{rad}}}{P_{\text{tot}}} \quad (5.17)$$

and we then find for the gain $G(\theta, \phi)$ in the direction (θ, ϕ)

$$G(\theta, \phi) \equiv \frac{\Phi(\theta, \phi)}{(1/4\pi)P_{\text{tot}}} = \eta |g(\theta, \phi)|^2 \quad (5.18)$$

or
$$G(\theta, \phi) = \eta D(\theta, \phi) \quad (5.19)$$

Now, since an array as a whole can be regarded as a composite antenna, the above concepts can be applied also to arrays. From (5.13) we have for the reference antenna, which is assumed to be lossless,

$$E^{\text{ref}} = \sqrt{\frac{P^{\text{ref}}}{2\pi\zeta_0^{-1}}} \frac{e^{-jk_0 r}}{r} g(\theta, \phi) \quad (5.20)$$

where P^{ref} denotes both input and radiated power. Insertion into (5.9) then yields the electric field from the array

$$E = \sqrt{\frac{P^{\text{ref}}}{2\pi\zeta_0^{-1}}} \frac{e^{-jk_0 r}}{r} g(\theta, \phi) f(\theta, \phi) \quad (5.21)$$

According to the normalization of complex radiation patterns implied by (5.13), (5.21) may be written

$$E = \sqrt{\frac{P_{\text{rad}}}{2\pi\zeta_0^{-1}}} \frac{e^{-jk_0 r}}{r} \frac{g(\theta, \phi)f(\theta, \phi)}{\sqrt{(1/4\pi) \int_{4\pi} |g(\theta, \phi)f(\theta, \phi)|^2 d\Omega}} \quad (5.22)$$

whereby the field from the array is expressed through its radiated power P_{rad} and the complex radiation pattern

$$\frac{g(\theta, \phi)f(\theta, \phi)}{\sqrt{(1/4\pi) \int_{4\pi} |g(\theta, \phi)f(\theta, \phi)|^2 d\Omega}} \quad (5.23)$$

which satisfies the equation in Exercise 5.2.

In this chapter we shall find it useful to express the properties of an array relative to the properties of the reference antenna. The relative directivity, for example, is defined by $D_{\text{rel}} = D/D^{\text{ref}}$, where the symbol without index refers to the entire array. In what follows all relative quantities are denoted by the subscript rel. Exceptions are the relative powers

$$p_{\text{rad}} = \frac{P_{\text{rad}}}{P^{\text{ref}}} \quad p_{\text{tot}} = \frac{P_{\text{tot}}}{P^{\text{ref}}} \quad p_{\text{loss}} = \frac{P_{\text{loss}}}{P^{\text{ref}}}$$

obtained by dividing the unnormalized power quantities by the power P^{ref} radiated by the reference antenna.

By comparing (5.21) and (5.22), we see that the ratio between P_{rad} and P^{ref} is given by

$$p_{\text{rad}} = \frac{1}{4\pi} \int_{4\pi} |g(\theta, \phi)f(\theta, \phi)|^2 d\Omega \quad (5.24)$$

We further have from (5.14)

$$\Phi^{\text{ref}}(\theta, \phi) = \frac{1}{4\pi} P^{\text{ref}} |g(\theta, \phi)|^2$$

The corresponding equation for the array is, by virtue of (5.23),

$$\Phi(\theta, \phi) = \frac{1}{4\pi} P_{\text{rad}} \frac{|g(\theta, \phi)f(\theta, \phi)|^2}{(1/4\pi) \int_{4\pi} |g(\theta, \phi)f(\theta, \phi)|^2 d\Omega}$$

We then have

$$\begin{aligned} \Phi_{\text{rel}}(\theta, \phi) &= \frac{\Phi(\theta, \phi)}{\Phi^{\text{ref}}(\theta, \phi)} = p_{\text{rad}} \frac{|f(\theta, \phi)|^2}{(1/4\pi) \int_{4\pi} |g(\theta, \phi)f(\theta, \phi)|^2 d\Omega} \\ &= |f(\theta, \phi)|^2 \end{aligned} \quad (5.25)$$

This result also follows immediately from (5.9). Finally, we have from (5.15) for the reference antenna

$$D^{\text{ref}}(\theta, \phi) = \frac{\Phi^{\text{ref}}(\theta, \phi)}{(1/4\pi)P^{\text{ref}}}$$

and for the array

$$D(\theta, \phi) = \frac{\Phi(\theta, \phi)}{(1/4\pi)P_{\text{rad}}}$$

This gives

$$\begin{aligned} D_{\text{rel}}(\theta, \phi) &= \frac{D(\theta, \phi)}{D^{\text{ref}}(\theta, \phi)} = \frac{\Phi_{\text{rel}}(\theta, \phi)}{p_{\text{rad}}} \\ &= \frac{|f(\theta, \phi)|^2}{(1/4\pi) \int_{4\pi} |g(\theta, \phi)f(\theta, \phi)|^2 d\Omega} \end{aligned} \quad (5.26)$$

In a similar manner we have

$$G_{\text{rel}}(\theta, \phi) = \frac{G(\theta, \phi)}{G^{\text{ref}}(\theta, \phi)} = \frac{\Phi_{\text{rel}}(\theta, \phi)}{p_{\text{rad}} + p_{\text{loss}}} \quad (5.27)$$

The concepts introduced above will be discussed further in later sections. In Sec. 5.8 D_{rel} and G_{rel} will be expressed in terms of the excitation coefficients. The formulas obtained in this way will form the basis of the optimization procedures described in Sec. 5.11.

5.4 Linear Arrays with Uniform Current Distribution

We consider a linear array consisting of n elements spaced equidistantly along the z axis of a rectangular coordinate system with distance d between consecutive elements and with the first element at the origin. We assume that the reference antenna and the first element coincide. From (5.10) we then have

$$f(\theta) = \sum_{m=1}^n a_m e^{jk_0 d(m-1) \cos \theta} \quad (5.28)$$

for the array factor of an equispaced linear array. We have not, apart from the requirements of similarity, made any assumptions above about the currents in the individual elements, but we assume now that the excitation coefficients a_m all have the same absolute value and that the difference in phase δ between one excitation coefficient and the next is a constant. If the currents in the first element ($m = 1$) and the reference antenna are in phase, and if the magnitude of the current in the reference antenna is equal to the sum of the magnitudes of the currents in the individual elements, the excitation coefficients may be written

$$a_m = \frac{1}{n} e^{j(m-1)\delta} \quad m = 1, 2, 3, \dots, n \quad (5.29)$$

The array factor for an equispaced array with uniform current distribution and a linear phase progression, or briefly, a uniform array, is then given by

$$f(\theta) = \frac{1}{n} \sum_{m=1}^n e^{j(m-1)(\delta + k_0 d \cos \theta)} \tag{5.30}$$

The array factor (5.30) may be written as a function of the variable

$$\gamma = \delta + k_0 d \cos \theta \tag{5.31}$$

By doing this we get

$$f(\gamma) = \frac{1}{n} \sum_{m=1}^n e^{j(m-1)\gamma}$$

where the symbol f for the array factor has been retained. The above finite series may be summed by the formula for a geometrical progression yielding the expression

$$f(\gamma) = \frac{1}{n} \frac{e^{jn\gamma} - 1}{e^{j\gamma} - 1}$$

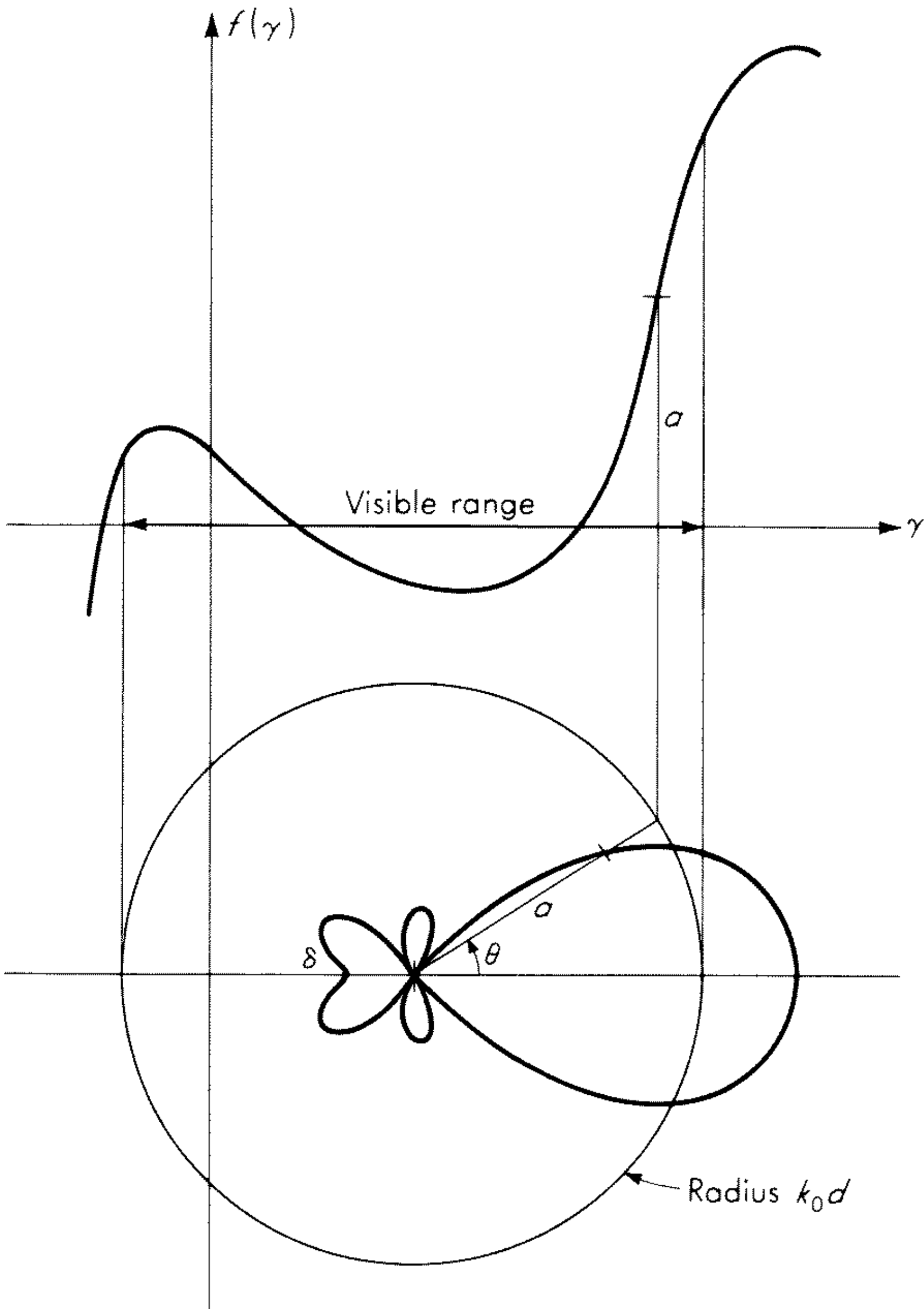


Fig. 5.3 Geometrical construction of polar diagram.

By using Euler's formulas, we finally find

$$f(\gamma) = e^{j(n-1)\gamma/2} \frac{\sin (n\gamma/2)}{n \sin (\gamma/2)} \quad (5.32)$$

for the complex array factor of a uniform array.

Array patterns

In the theory of antenna arrays, functions of the variable $\gamma = \delta + k_0 d \cos \theta$ often occur. A polar diagram of such functions can easily be obtained by means of the geometrical construction shown in Fig. 5.3. The function $f(\gamma)$ is plotted as a function of γ . The circle of radius $k_0 d$ is then drawn with its center at a distance δ from the line $\gamma = 0$. With the aid of this circle γ may be found for a given value of θ , and the corresponding value of $|f(\gamma)|$ can be determined from the curve. This length is then laid out from the center of the circle in the direction θ to give a point on the desired diagram. Now $0 \leq \theta \leq \pi$ and, accordingly, the interval for γ is of length $2k_0 d$ and is situated symmetrically with respect to $\gamma = \delta$. This interval corresponds to real values of the angle θ and is called the visible range. The part of the curve $f(\gamma)$ within the visible range is called the visible part of the curve. It is important to note that the *length* of the visible range is determined by the spacing d and the *position* of the visible range is determined by the phase constant δ . This construction is used extensively in the following, sometimes in a slightly modified form.

Now from (5.32) we find the array pattern

$$|f(\gamma)| = \left| \frac{\sin (n\gamma/2)}{n \sin (\gamma/2)} \right| \quad (5.33)$$

for a uniform array. We begin the investigation of this function with the special case $n = 2$ and find

$$|f| = |\cos \frac{1}{2}(\delta + k_0 d \cos \theta)| \quad (5.34)$$

for a two-element uniform array. We assume first that the two elements are driven in phase. Then $\delta = 0$ and we have

$$|f| = |\cos (\frac{1}{2}k_0 d \cos \theta)| \quad (5.35)$$

which shows that a maximum, independent of the spacing d , occurs in the direction $\theta = \pi/2$, i.e., perpendicular to the array axis. In this case the array is called a broadside array. If, furthermore, a null is to occur in the direction of the array axis ($\theta = 0$), we have $\cos (\frac{1}{2}k_0 d) = 0$ or $d = (2p + 1)(\lambda_0/2)$.

In the end-fire case, it is required that a maximum occur at $\theta = 0$ (or π). This yields $|\cos [\frac{1}{2}(\delta + k_0 d)]| = 1$ or $\delta + k_0 d = p2\pi$, $p = 0, \pm 1, \pm 2, \dots$. For $p = 0$ we have $\delta = -k_0 d$, which is known as the condition for ordinary end-fire radiation. If the two elements are fed in opposite phases, $\delta = -\pi$, we must have $d = (2p + 1)(\lambda_0/2)$. Hence the distance between the elements should be an odd multiple of half a wavelength.

Exercise 5.3 Give a physical explanation of the above results for a two-element array. Consider the phase difference between the fields from the elements in directions along and perpendicular to the array axis.

In Fig. 5.4 are shown polar diagrams for the array factor of a two-element array for some values of d and δ . The diagrams are obtained by means of the above geometrical construction. The function $f(\gamma) = \cos \gamma/2$ is shown, and the visible range is indicated by a heavy line. For $d = \delta = 0$ the two antennas coincide and the plot of the array pattern is a circle. When, for $d = 0$, δ de-

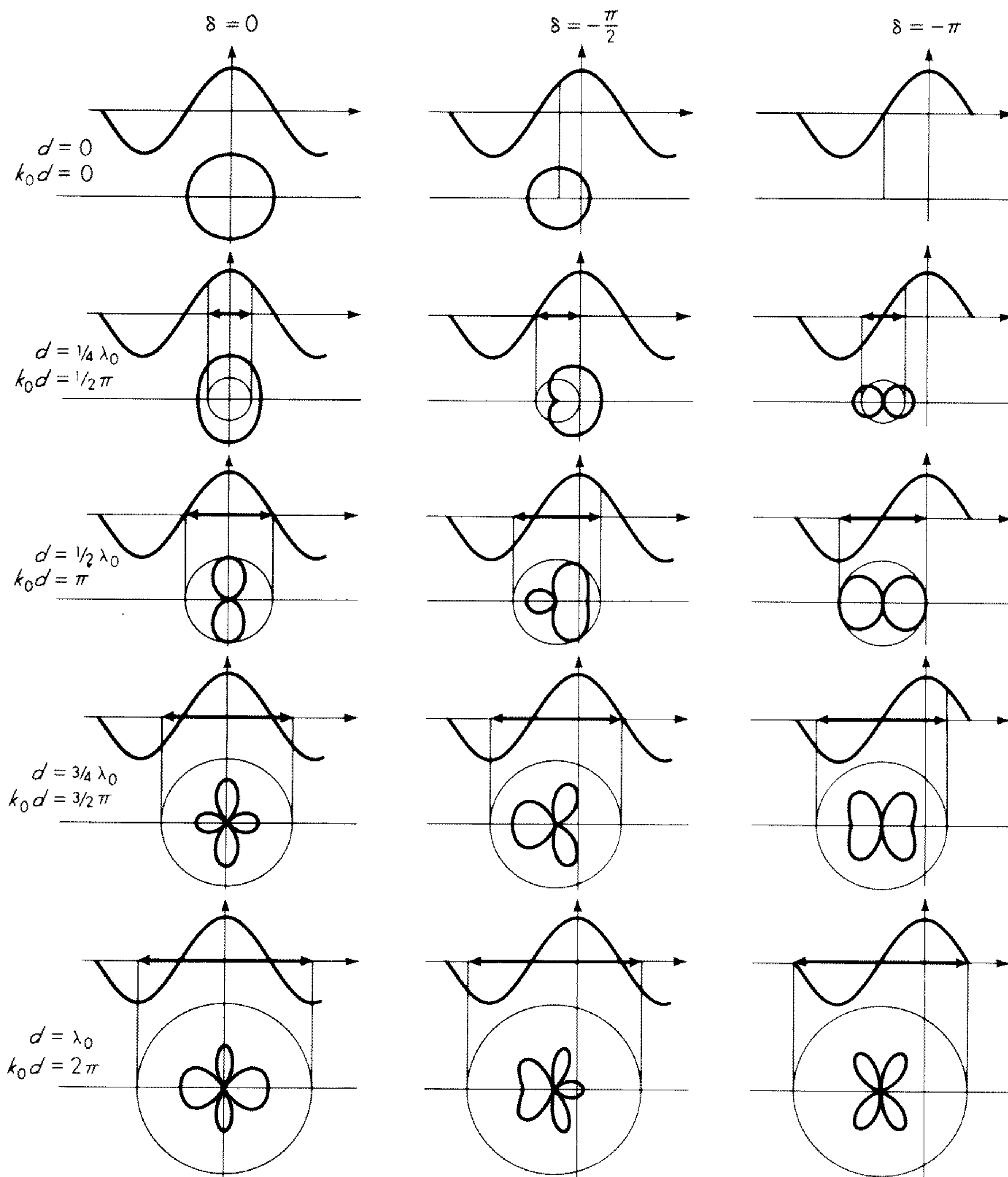


Fig. 5.4 Array patterns for a two-element array.

creases, the difference in phase of the currents in the two elements increases. The radius of the circular pattern therefore decreases and is finally equal to zero for $\delta = -\pi$, and the fields from the two antennas cancel. For a fixed value of δ , it is seen that the pattern, when d is increased, splits up into several lobes, the number of which increases with the distance d . For $\delta = 0$, $d = \frac{1}{4}\lambda_0$, the fields in the direction of the array axis are in phase quadrature and the value of the array pattern in these directions accordingly is $1/\sqrt{2}$ times the value in the transverse directions where the fields are in phase. For $\delta = 0$, $d = \frac{1}{2}\lambda_0$, the fields in the axial directions are in opposite phase, which results in a null in this direction, while the relative value $1/\sqrt{2}$ again is obtained for $d = \frac{3}{4}\lambda_0$. When $\delta = 0$, $d = \lambda_0$, the maximum value is obtained in both axial and transverse directions. In general, for $\delta = 0$, a maximum always occurs in the transverse direction, although other maxima also may appear. In contrast to this, for $\delta = -\pi$ a null always occurs in the transverse directions.

We now again consider the general expression

$$|f(\gamma)| = \left| \frac{\sin(n\gamma/2)}{n \sin(\gamma/2)} \right| \quad \gamma = \delta + k_0 d \cos \theta \quad (5.36)$$

for an array with n elements. This function has a period 2π and is symmetrical about $\gamma = 0$. We confine ourselves to the interval $-\pi \leq \gamma \leq \pi$ and find that the function is equal to zero for

$$\gamma = \frac{2\pi}{n} p \quad p = \pm 1, \pm 2, \dots, \pm p_0 \quad p_0 = \begin{cases} \frac{1}{2}(n-1) & n \text{ odd} \\ \frac{1}{2}n & n \text{ even} \end{cases} \quad (5.37)$$

Between these nulls the function attains secondary maxima which decrease from the principal maximum $|f| = 1$ at $\gamma = 0$ toward the ends of the interval under consideration. In Fig. 5.5 is shown a graph of the function for some

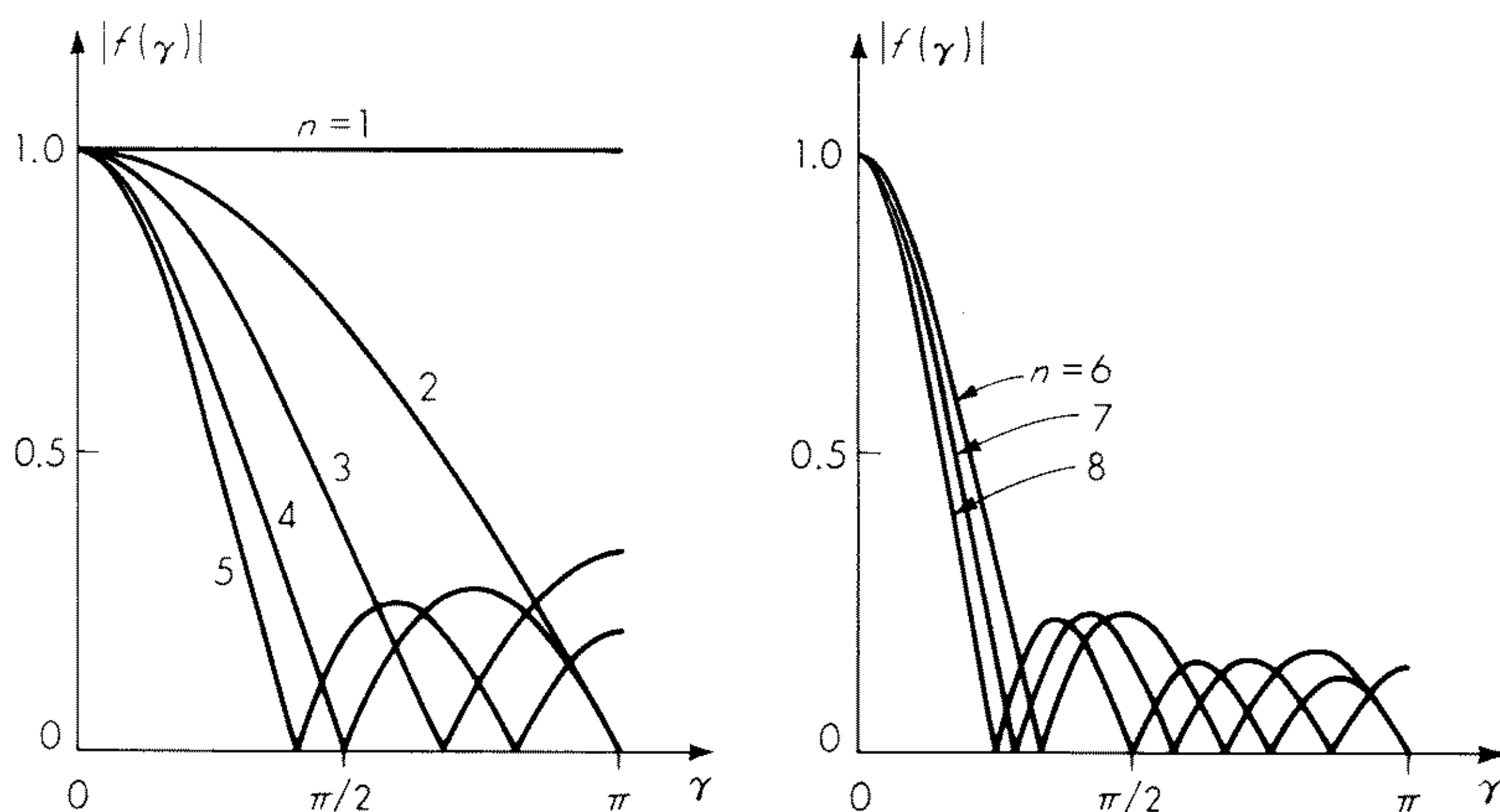


Fig. 5.5 The function $|f(\gamma)| = \left| \frac{\sin(n\gamma/2)}{n \sin(\gamma/2)} \right|$ for $n = 1-8$.

values of n . It is noted that the distance $4\pi/n$ between the two nulls surrounding the maximum value $\gamma = 0$ decreases with increase in the number of elements.

Now the function (5.36) is of the type $f(\delta + k_0d \cos \theta)$, and we therefore are able to obtain polar diagrams of the array patterns by the construction mentioned above. In Fig. 5.6 this has been carried out for two 6-element arrays, namely a broadside and an end-fire array. It is worthwhile to note that the broadside array has more side lobes than the end-fire array but, in compensation, a more narrow main lobe.

With knowledge of the curves, shown in Fig. 5.5, and the method for construction of array patterns at our disposal it is easy to form an estimate of the

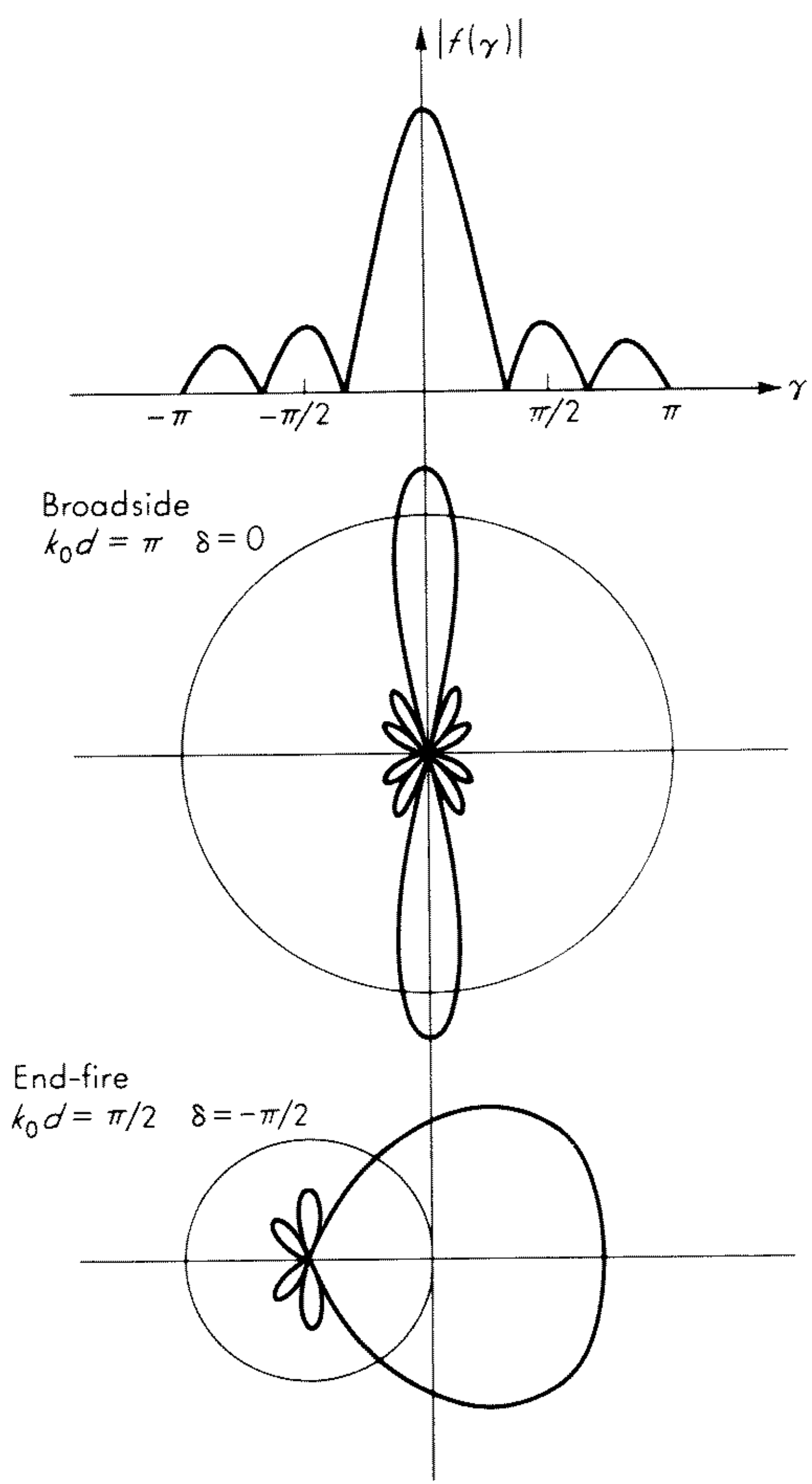


Fig. 5.6 Array pattern for uniform six-element broadside and end-fire arrays.

array pattern of an arbitrary uniform array. The curve corresponding to the number of elements in question can be taken from Fig. 5.5, and the size and location of the visible range are then determined from the values of d and δ . For $d = \frac{1}{2}\lambda_0$ the visible range is equal to 2π and a principal maximum will always occur in the visible range regardless of the value of δ . For sufficiently large values of d , more than one principal maximum will be within the visible range. These, usually unwanted, extra main lobes are often called grating lobes. It is furthermore seen that the number of side lobes is increased, both when the distance d is increased (for a fixed number of elements), as well as when the number of elements is increased (for fixed distance d). The length of the array is equal to $(n - 1)d$, and we accordingly have the rule that in general the number of side lobes increases with the array length.

Directive properties

We begin the discussion of the directive properties of uniform arrays with a computation of the beam width 2α and the side-lobe level r for the array pattern. We assume that α is a small angle, so that it is a good approximation to set

$$\theta_1 = \theta_0 - \alpha \quad \theta_2 = \theta_0 + \alpha$$

where θ_0 is the direction of the main lobe and θ_1 and θ_2 are the directions in which the nulls surrounding the main lobe occur as in Fig. 5.7. We then have the relations $\delta + k_0 d \cos \theta_2 = -2\pi/n$ and $\delta + k_0 d \cos \theta_0 = 0$. By subtraction we get

$$\cos \theta_2 - \cos \theta_0 = -\frac{2\pi}{nk_0 d}$$

If now we introduce the Taylor expansion

$$\cos \theta_2 = \cos (\theta_0 + \alpha) \approx \cos \theta_0 - \alpha \sin \theta_0 - \frac{\alpha^2}{2} \cos \theta_0$$

we find the equation

$$\alpha^2 \cos \theta_0 + 2\alpha \sin \theta_0 - \frac{2\lambda_0}{nd} = 0$$

for the determination of α . For a broadside ($\theta_0 = \pi/2$) and an end-fire array ($\theta_0 = 0$), respectively, we find

$$\alpha = \begin{cases} \frac{\lambda_0}{nd} & \text{broadside array} \\ \sqrt{\frac{2\lambda_0}{nd}} & \text{end-fire array} \end{cases} \quad (5.38)$$

It is thus seen to be a general rule that for the same array length a broadside array has a more narrow main lobe than an end-fire array. If the side lobes are large, a considerable part of the radiated energy is distributed in unwanted

directions. Usually the specification of the beam width of an array is therefore supplemented by the side-lobe level r defined as the ratio between the maximum values of the largest side lobe and the main lobe.

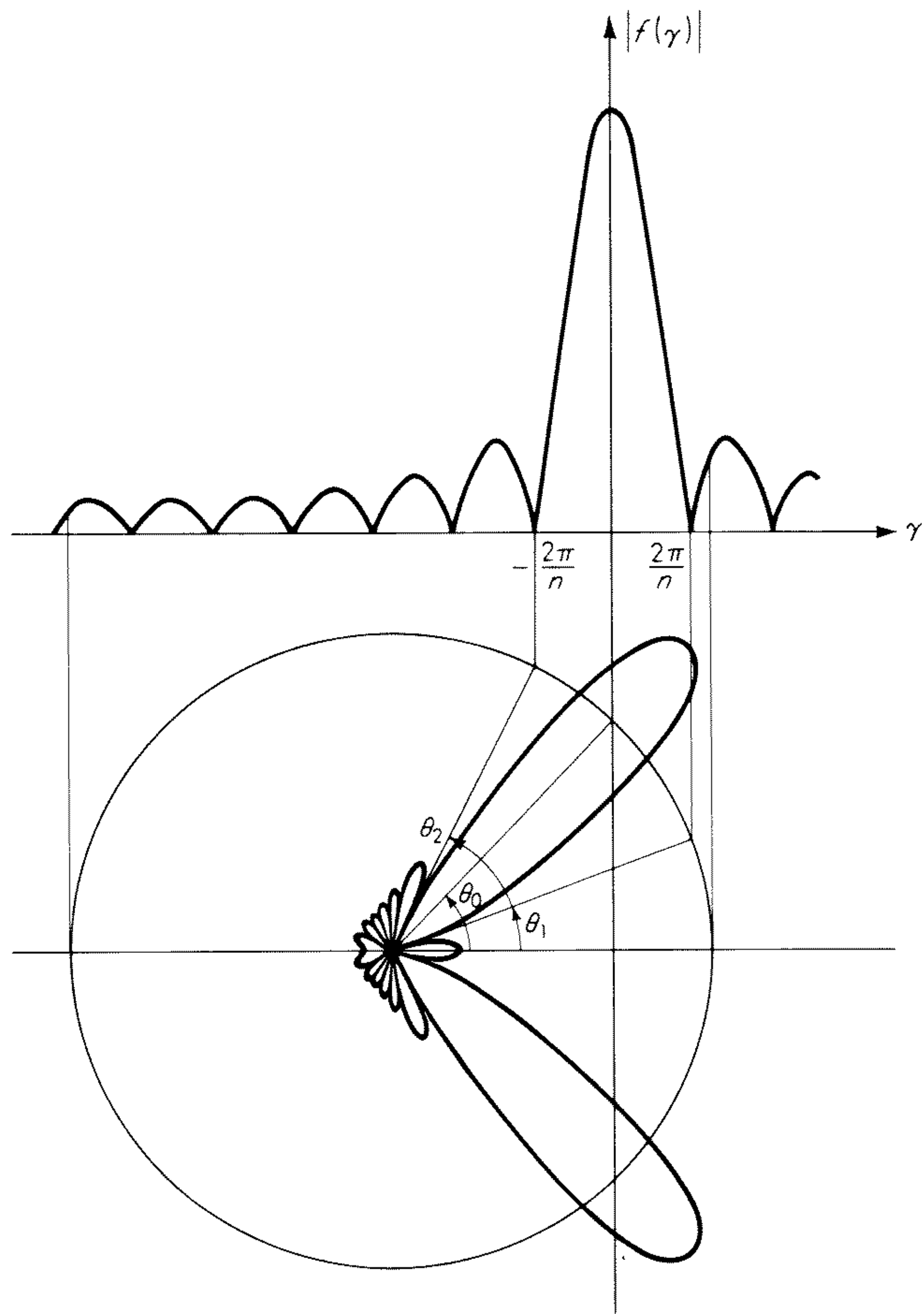


Fig. 5.7 For the computation of beam width and side-lobe level of uniform arrays.

For a uniform array, the side lobe next to the main lobe is usually the largest. The first secondary maximum of the function (5.36) is found for $\gamma = 3\pi/n$ approximately, and the side-lobe level accordingly is determined by

$$\left| \frac{\sin (3\pi/2)}{n \sin (3\pi/2n)} \right| = \frac{1}{|n \sin (3\pi/2n)|} \approx \frac{2}{3\pi} \quad \text{for large } n \quad (5.39)$$

For a linear uniform antenna array the lowest possible side-lobe level is -13.5 db, and it is seen that for arrays of many elements the side-lobe level is independent of the number of elements.

Next we consider the directivity D of the array. From Sec. 5.3 we get

$$D(\theta, \phi) = \frac{|f(\theta, \phi)|^2 |g(\theta, \phi)|^2}{(1/4\pi) \int_{4\pi} |f(\theta, \phi) g(\theta, \phi)|^2 d\Omega} \quad (5.40)$$

If the elements of the array are isotropic radiators, $|g(\theta, \phi)| \equiv 1$ and the above expression reduces to

$$D_f(\theta, \phi) = \frac{|f|^2}{(1/4\pi) \int_{4\pi} |f|^2 d\Omega} \quad (5.41)$$

which we shall call the geometrical directivity because it depends only on the “geometrical” quantities defining the array, i.e., the position vectors of the elements and the excitation coefficients. There is no simple relation between D , D_{rel} , and D_f , but nevertheless D_f is a useful concept because it is a quantity characteristic of the array, which does not depend on the type of elements used. As seen from the formulas, this is not the case for D and D_{rel} .

In general, D , D_{rel} , and D_f are all functions of the direction from the array to the field point. Of course, the maximum values obtained by variation of θ and ϕ are of particular interest. In the literature the term *directivity* often refers to these maximum values.

We shall now determine the geometrical directivity of a uniform array.² According to the definition (5.41) and the expression (5.36) we must then compute the integral

$$I = \frac{1}{4\pi} \int_{4\pi} \left| \frac{\sin(n\gamma/2)}{n \sin(\gamma/2)} \right|^2 d\Omega \quad \gamma = \delta + k_0 d \cos \theta$$

We utilize the formula³ [in Sec. 5.9 a method of deriving (5.42) is suggested]

$$\left| \frac{\sin(n\gamma/2)}{\sin(\gamma/2)} \right|^2 = n + 2 \sum_{m=1}^{n-1} (n-m) \cos m\gamma \quad (5.42)$$

and express the element of solid angle $d\Omega$ through

$$d\Omega = 2\pi \sin \theta d\theta$$

We then find

$$I = \frac{1}{n^2} \int_0^\pi \left[\frac{n}{2} + \sum_{m=1}^{n-1} (n-m) \cos m(\delta + k_0 d \cos \theta) \right] \sin \theta d\theta$$

or, by interchanging summation and integration,

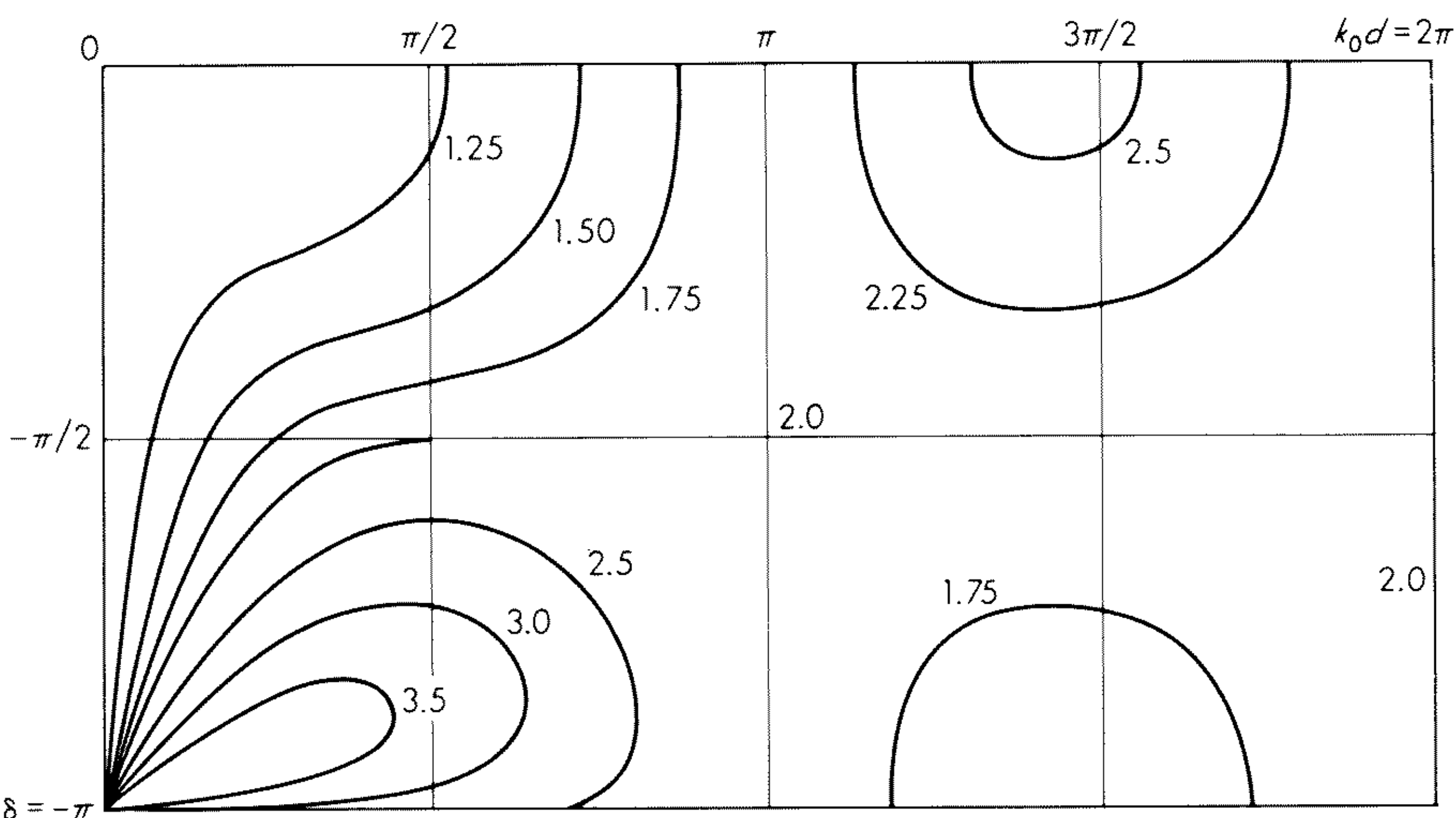
$$I = \frac{1}{n} + \frac{2}{n^2} \sum_{m=1}^{n-1} \frac{n-m}{mk_0 d} \sin mk_0 d \cos m\delta$$

Exercise 5.4 Fill in the details in the derivation of the above formula.

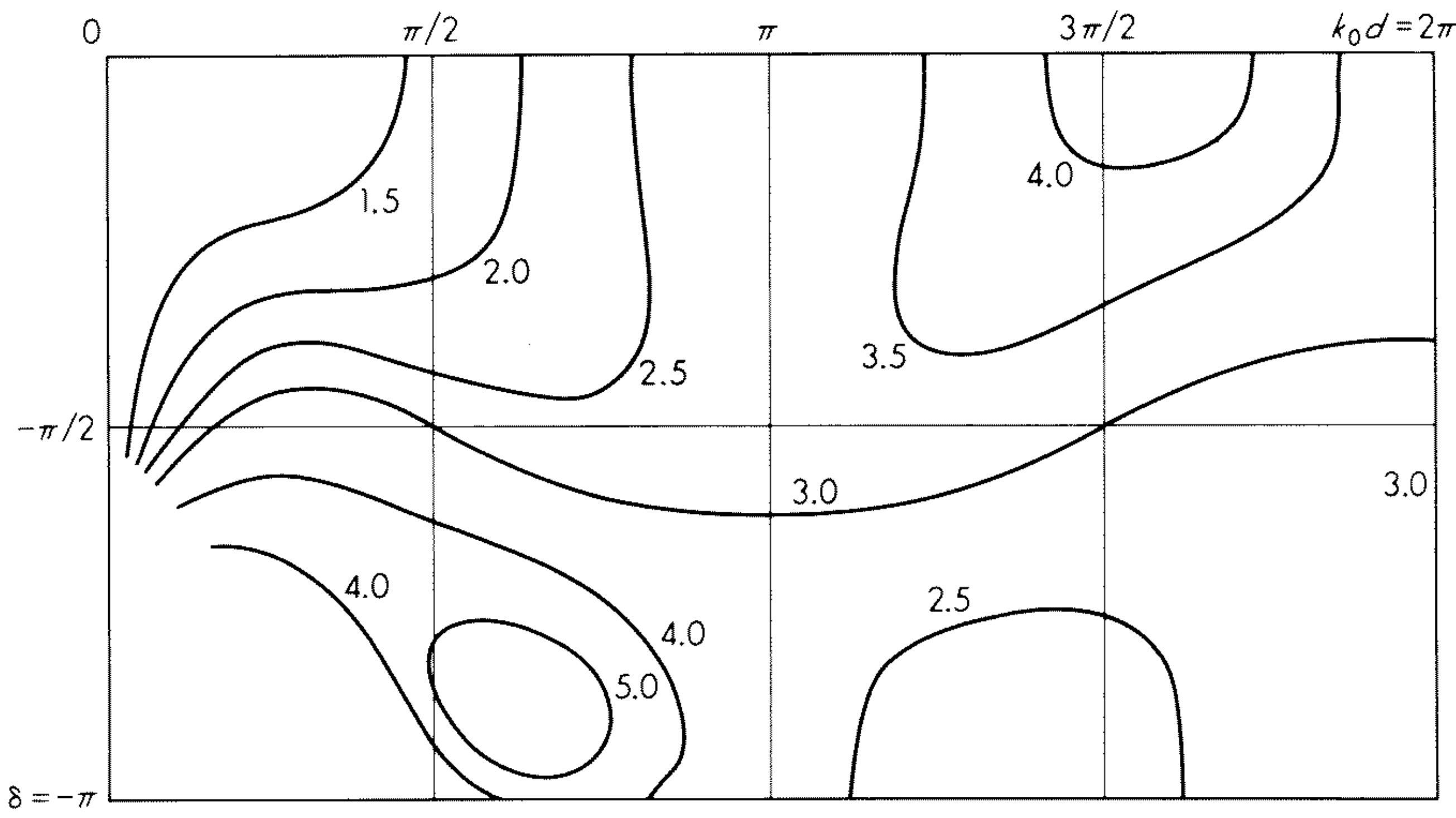
For the geometrical directivity of a uniform array we thus end up with the expression

$$D_f(\theta) = \frac{|f(\theta)|^2}{\frac{1}{n} + \frac{2}{n^2} \sum_{m=1}^{n-1} \frac{n-m}{mk_0 d} \sin mk_0 d \cos m\delta} \quad (5.43)$$

where $|f(\theta)|$ is given by (5.36).



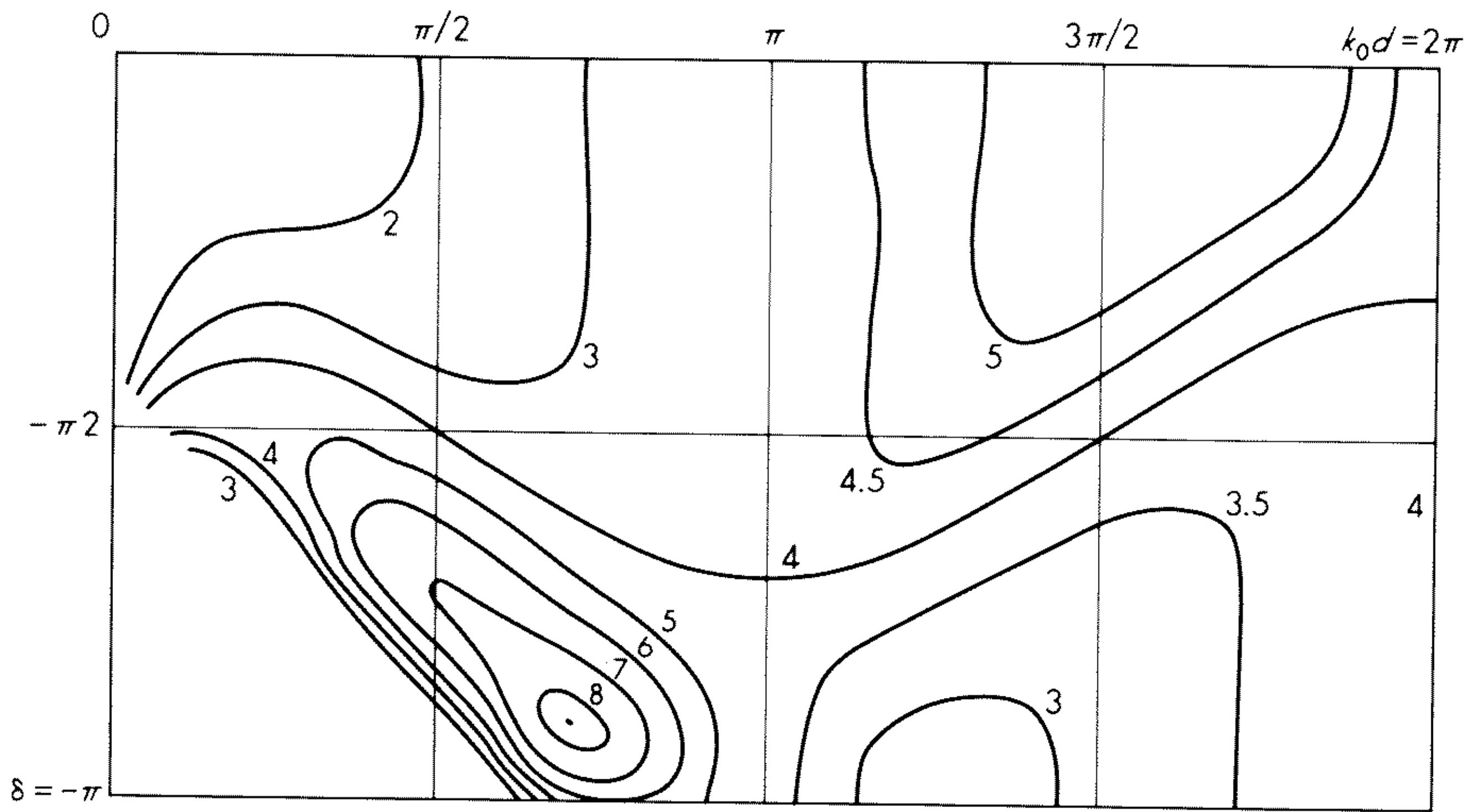
(a)



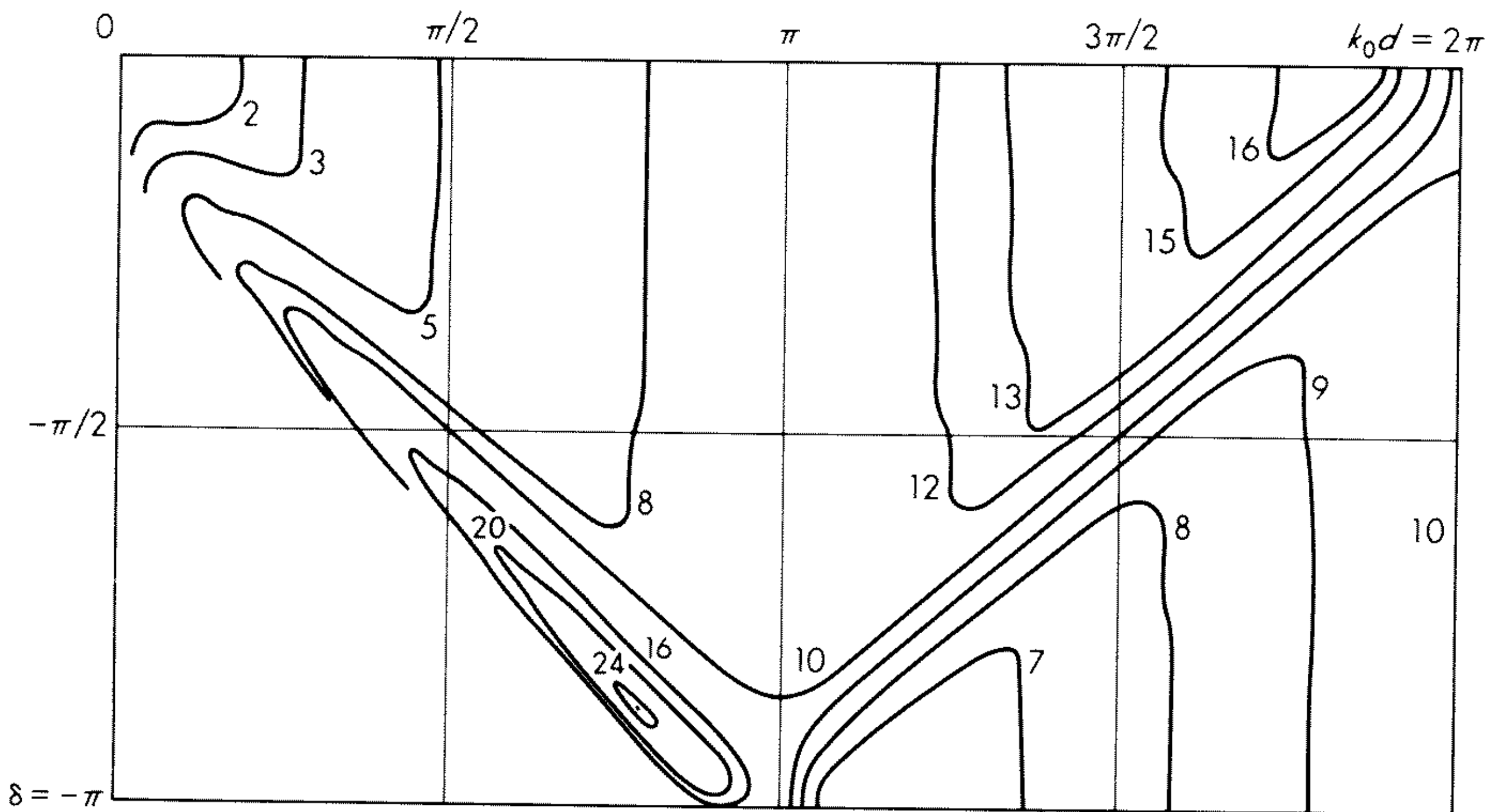
(b)

Fig. 5.8 Maximum geometrical directivity D_f of uniform arrays with (a) two elements, (b) three elements, (c) four elements, and (d) ten elements as a function of $k_0 d$ and δ [Eq. (5.43)].

It is observed from the above formula that, when the spacing $k_0 d$ is a multiple of half a wavelength ($k_0 d = p\pi$, $p = 1, 2, 3, \dots$), the denominator, independently of δ , is equal to $1/n$. Now, in this case the visible range is $2k_0 d = 2p\pi$; therefore, at least one direction θ_0 exists in which the numerator of (5.43) attains the maximum value 1. In this direction we thus find $D_f = n$, that is, the geometrical directivity is equal to the number of elements in the array.



(c)



(d)

Fig. 5.8 (Continued.)

The value of δ does not change the maximum geometrical directivity but does determine the direction θ_0 in which it occurs.

In the broadside case ($\delta = 0$) the formula reduces to

$$D_f\left(\frac{\pi}{2}\right) = \frac{1}{\frac{1}{n} + \frac{2}{n^2} \sum_{m=1}^{n-1} \frac{n-m}{mk_0d} \sin mk_0d}$$

From this it is seen that, for a broadside array, the directivity n again occurs when the spacing is half a wavelength. In the ordinary end-fire case ($\delta = -k_0d$)

$$D_f(0) = \frac{1}{\frac{1}{n} + \frac{1}{n^2} \sum_{m=1}^{n-1} \frac{n-m}{mk_0d} \sin 2mk_0d}$$

The directivity n thus is obtained when $-\delta = k_0d = \pi/2$. In Fig. 5.8a to d are shown curves for D_f for uniform arrays with two, three, four, and ten elements as a function of δ and k_0d with D_f as a parameter. The lines $\delta = 0$ and $\delta = -k_0d$ correspond to broadside and ordinary end-fire arrays, respectively, while the domain in between these lines corresponds to arrays with other maximum directions. In the area in between the lines $\delta = -k_0d$ and $\delta = -\pi$ the array is still end fire. However, for $n \geq 3$ the magnitude of the main lobe may become less than the largest side lobe, and the maximum directivity is then obtained in other directions. The part of each diagram corresponding to such values of δ and k_0d is left empty.

We shall illustrate these matters by means of a four-element array. In Fig. 5.9a the array factor is shown for an ordinary end-fire array determined by $\delta = -k_0d = -\pi$. The geometrical directivity of this array $D_f = 4$, and from Fig. 5.9e it is seen that the visible range is so placed that precisely two main lobes occur. In Fig. 5.9b is shown the array factor for δ increased to $-3\pi/4$. The length of the visible range is unchanged, but it is displaced by an amount $\pi/4$ to the right. Therefore two principal maxima still occur and D_f is still equal to 4. On the other hand, the directions of the principal maxima have been altered with respect to those of Fig. 5.9a. The very broad main lobe of Fig. 5.9b is due to the large visible range. If k_0d is reduced so that $k_0d = -\delta = -3\pi/4$, corresponding to Fig. 5.9c, only one principal maximum occurs (for $\theta = 0$) and the radiation is zero in the opposite direction. By insertion of these values into (5.43), it is found that $D_f = 5.58$ in contrast to 4.00 for an ordinary end-fire array. Now, from Fig. 5.8c it appears that, for $k_0d \approx 0.71\pi$ and $\delta \approx -0.89\pi$, the maximum directivity $D_f = 8.28$ is obtained. The corresponding array factor is shown in Fig. 5.9d. The side-lobe level is slightly increased with respect to Fig. 5.9c, but the main lobe simultaneously has become more narrow. This improvement has been obtained at the expense of the amplitude of the main lobe, which has been reduced by 20 percent approximately. As is seen from Fig. 5.9e, this is due to the fact that the principal maximum is now outside the visible range.

The problem of maximizing the directivity of an array will be treated later in more detail. However, at the present stage we shall mention the so-called Hansen-Woodyard condition⁴ for increased directivity, because it is often cited in the literature. By graphical methods these authors found that an increased directivity could be obtained if, for an ordinary end-fire array with the condition $\delta = -k_0d$, the phase constant was changed to

$$\delta = -k_0d - \frac{\pi}{n} \quad (5.44)$$

where n is the number of elements. This is the Hansen-Woodyard condition, and it is observed that the formula is not an equation which allows the determination of the optimum value of δ but is a condition which, when applied to

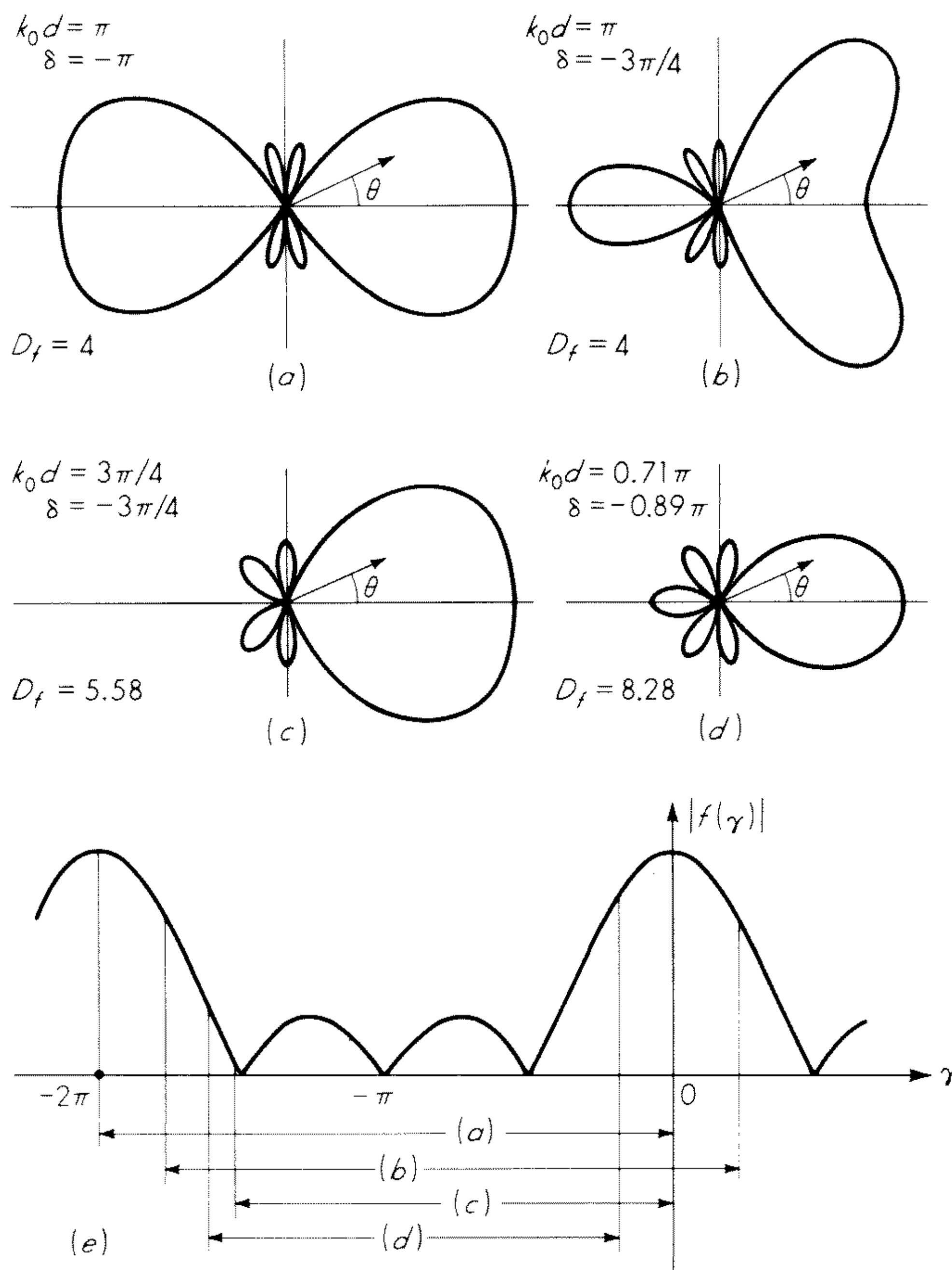


Fig. 5.9 Dependence of radiation pattern on visible range for a four-element uniform array.

an array with given spacing, yields a δ giving a larger directivity than obtained by $\delta = -k_0 d$. The condition is derived in principle for very long antenna arrays with many elements, and it therefore gives the best result in such cases. In the diagrams in Fig. 5.8 the condition (5.44) may be pictured as a straight line. It is seen that it generally yields larger directivity than the corresponding ordinary end-fire condition, but also that even higher directivities may be obtained by a uniform end-fire array. However, we shall later return to the problem of optimizing the directivity of a linear array. We shall find that the optimum directivity is obtained with an excitation which in the general case is not uniform.

5.5 Linear Arrays with Tapered Current Distribution.

The excitation coefficients a_m for a linear array can be thought of as complex numbers ascribed to the corresponding element positions $z = z_m$. We may visualize them by plotting the absolute values and the phases of a_1, a_2, \dots, a_n as points in a coordinate system with one axis coinciding with the array axis. By drawing a continuous curve through each set of points, a current (magnitude) distribution function and a phase distribution function can be constructed. Infinitely many complex distribution functions corresponding to the same set of excitation coefficients are, of course, possible. One of them may seem to be the most "natural." Often the situation is such that the excitation coefficients are defined in the first place as sampled values of some continuous function. A technique of analyzing arrays with excitation coefficients obtained in this manner is described later in this section.

In a linear array with tapered current distribution the phase of the excitation coefficients is usually taken as linearly progressing as for the uniform array. The absolute value of a_m , however, now depends on m . Accordingly, a larger variety of array patterns than for the uniform array can be produced. In particular, by this added degree of freedom, it is possible to gain control of the magnitude of the side lobes in the array pattern. This is obtained by tapering the current distribution function toward the ends of the array.

Schelkunoff's Polynomial Method

A convenient method for the analysis of linear arrays with tapered current distribution has been described by S. A. Schelkunoff.⁵ From (5.28) with $i = m - 1$ the array factor for an equispaced linear array with the z axis as array axis is given by

$$f(\theta) = \sum_{i=0}^{n-1} a_i e^{j i k_0 d \cos \theta} \quad (5.45)$$

By writing $a_i = |a_i| e^{j(\delta_i + i\delta)}$ we can separate the phase of a_i into a linear progressive part $i\delta$ and an individual part δ_i . This process is unique if we prescribe $\delta_i = 0$ for $i = n - 1$. With $\gamma = \delta + k_0 d \cos \theta$ as usual, we have

$$f = \sum_{i=0}^{n-1} |a_i| e^{j\delta_i} e^{j i \gamma} \quad (5.46)$$

By further introducing the new variable $\zeta = e^{j\gamma}$, the array factor can be written as a complex polynomial in ζ

$$f = \sum_{i=0}^{n-1} |a_i| e^{j\delta_i} \zeta^i \quad (5.47)$$

The polynomial is called Schelkunoff's polynomial or the array polynomial.

The importance of Schelkunoff's method lies in the recognition of the array factor as a complex polynomial. Hereby the whole theory of complex poly-

nomials, including the fundamental lemma of algebra, is at the disposal of array analysts.

We shall here restrict ourselves to arrays with linearly progressive phase i.e., current distributions with $\delta_i = 0, i = 0, 1, \dots, n - 1$. Then Schelkunoff's polynomial takes the simple form

$$f = \sum_{i=0}^{n-1} |a_i| \zeta^i \quad (5.48)$$

As θ varies through its range $0 \leq \theta \leq \pi$, ζ remains on the unit circle in the complex plane; the part of this circle which will be described depends on δ and d . Corresponding to $\theta = \pi/2$ is $\zeta = e^{j\delta}$; this point is the midpoint of the range on the unit circle traversed by ζ . The element spacing d determines the length of the range. For $d = \lambda_0/2$ the range is 2π . For $d < \lambda_0/2$ the range is less than one full circuit. The part of the circle which is covered is called the visible range of ζ . In the example illustrated in Fig. 5.10 the visible range of ζ is less than 2π .

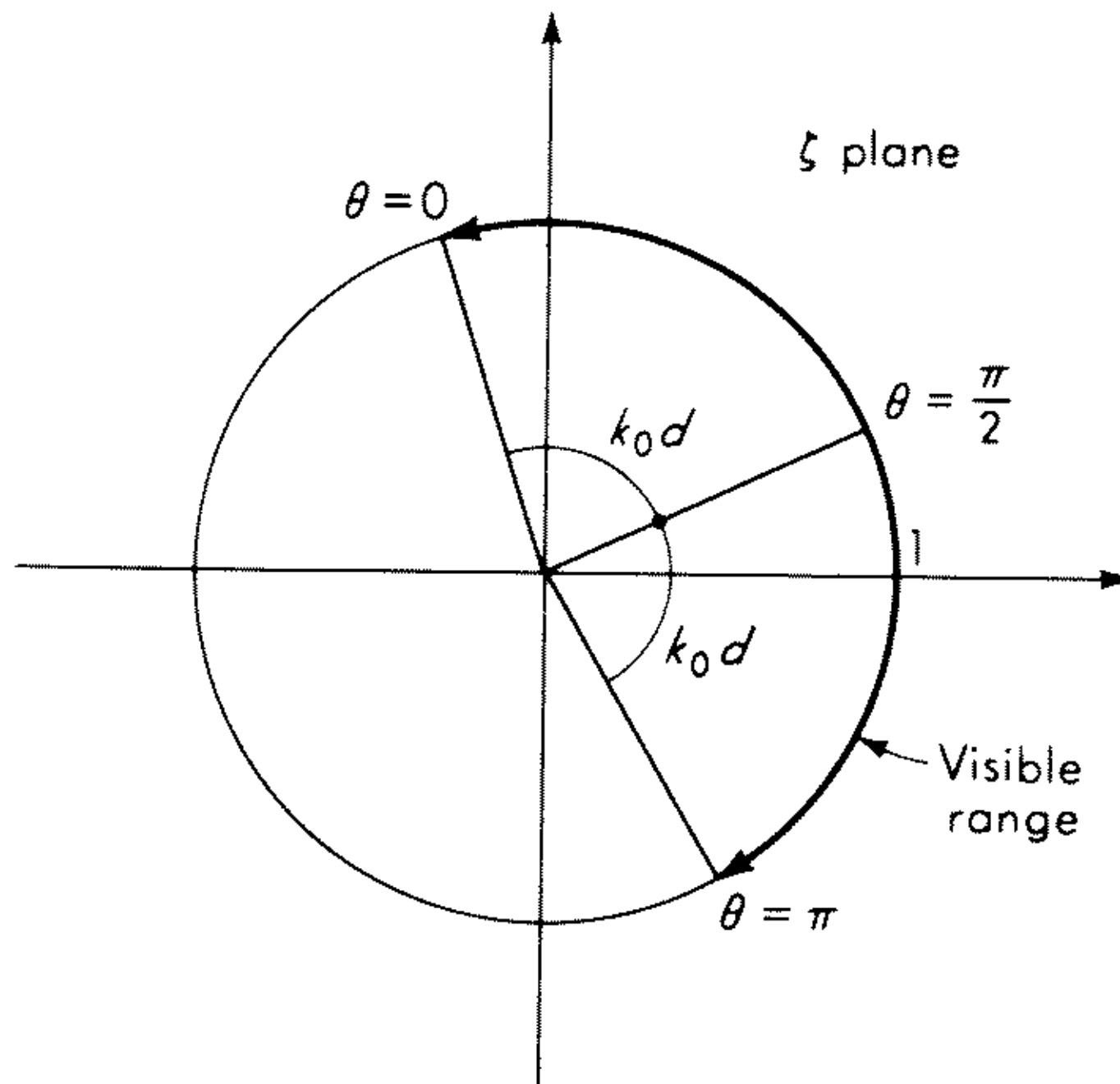


Fig. 5.10 Unit circle in ζ plane and visible range of ζ .

A clear insight into the connection between the algebraic form (5.48) of the array factor and the shape of the array pattern is obtained by using the fundamental lemma of algebra. According to this, we have

$$f = |a_{n-1}|(\zeta - \zeta_1)(\zeta - \zeta_2) \cdots (\zeta - \zeta_{n-1}) \quad (5.49)$$

where $\zeta_1, \zeta_2, \dots, \zeta_{n-1}$ are the zeros of the polynomial in (5.48). The absolute value and phase angle of f now have simple geometrical interpretations. For each value taken by θ , $|f|$ is proportional to the product of the lengths of the distances d_1, d_2, \dots, d_{n-1} between the zeros $\zeta_1, \zeta_2, \dots, \zeta_{n-1}$ and the point P on the unit circle corresponding to the value of θ in question. This is illustrated

for a simple case in Fig. 5.11. Likewise, apart from a constant, the phase angle of f is equal to the sum of the phase angles of each of the parentheses in (5.49). The zeros $\zeta_1, \zeta_2, \dots, \zeta_{n-1}$ will correspond to nulls of the array pattern only when they are located in the visible range of ζ . To each root configuration corresponds one particular set of excitation coefficients (apart from a constant

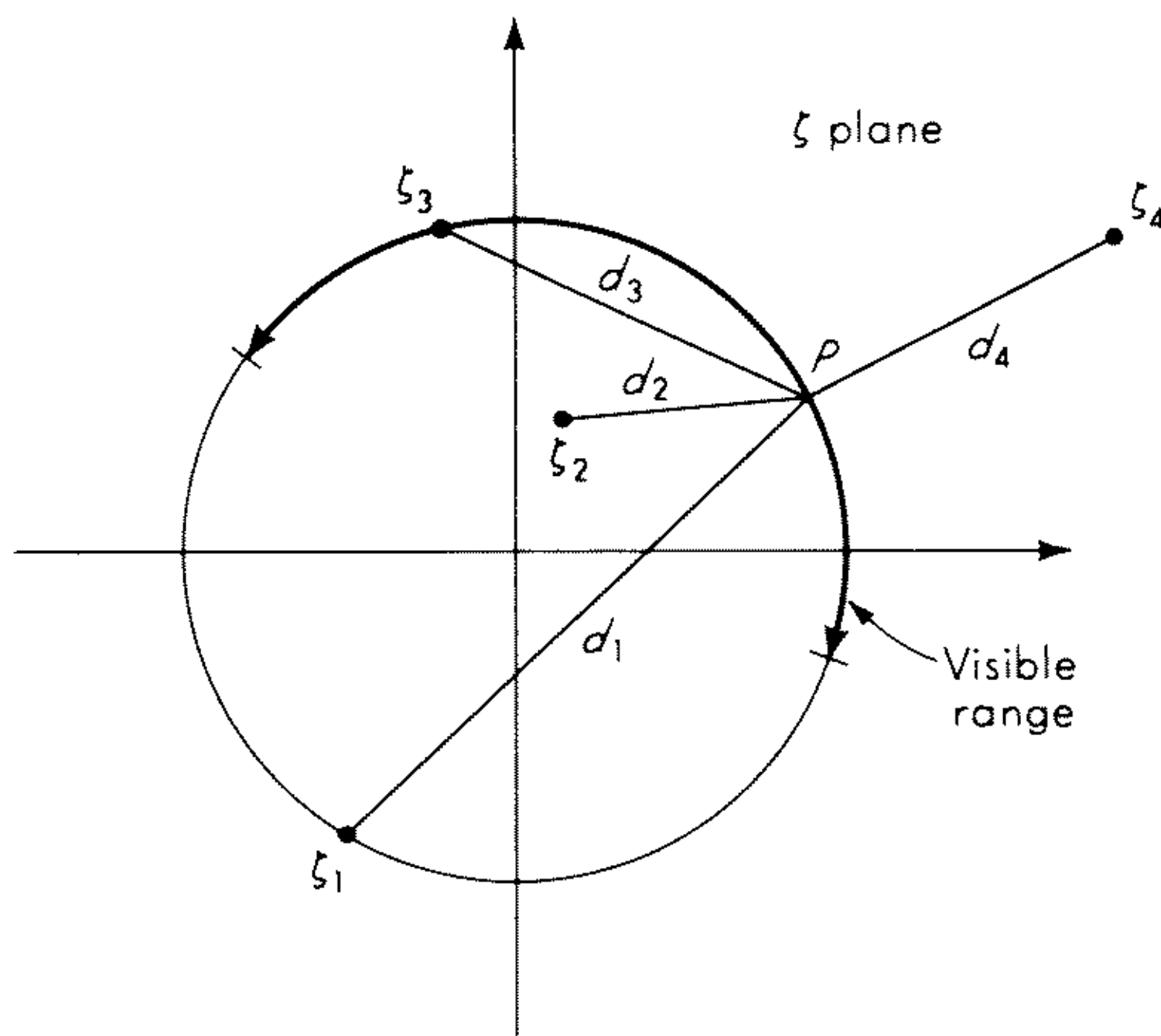


Fig. 5.11 Root configuration in complex ζ plane.

multiplier). In general, the converse is not true. However, if all roots are on the unit circle, there is a one-to-one correspondence between the relative variation of $|f|$ and the root configuration. The proof of this theorem as well as the proof of many other theorems regarding Schelkunoff's polynomial can be found in a paper by T. T. Taylor and J. R. Whinnery⁶ or in the original paper by Schelkunoff.

Exercise 5.5 Consider a four-element array with $d = \lambda_0/2$, $\delta = 0$ and excitation coefficients of magnitude 1, 3, 3, 1, respectively. Plot the zeros of ζ , and indicate the visible range. Sketch the array pattern. This current distribution is an example of the *binomial distribution*.

Z-transform Method

As shown by D. K. Cheng and M. T. Ma,⁷ the array factor for a large class of linear equispaced arrays with tapered current distribution can be expressed in "closed form." By this we mean that the summation (5.45) can be performed analytically. Formula (5.32) is a simple example of an array factor written in a closed form. It should be clear that the existence of an expression without summation sign for the array factor of an array will facilitate its analysis. The tool proposed by Cheng and Ma to achieve this is the theory of Z transforms originally developed for sampled data systems.⁸

The Z transform $\mathcal{Z} \{f(x)\}$ of a continuous function $f(x)$ of a real variable x is defined as the sum of the infinite series

$$\begin{aligned}\mathcal{Z} \{f(x)\} &= \sum_{i=0}^{\infty} f(id) \mathcal{Z}^{-i} \\ &= F(\mathcal{Z})\end{aligned}\tag{5.50}$$

where \mathcal{Z} is the transform variable and d the “sampling interval.” The Z transform has a simple relationship to the Laplace transform, but this will not be discussed here.† As examples of Z -transform pairs we refer to Table 5.1.

TABLE 5.1 Z -TRANSFORM PAIRS

<i>Function</i>	<i>Definition</i>	<i>Z transform</i>
Unit step	$u(x) = \begin{cases} 0 & x < 0 \\ 1 & x \geq 0 \end{cases}$	$\frac{1}{1 - \mathcal{Z}^{-1}}$
Unit gate with n sampling points	$g_n(x) = \begin{cases} 0 & x < 0 \\ 1 & 0 \leq x \leq (n - 1)d \\ 0 & x > (n - 1)d \end{cases}$	$\frac{1 - \mathcal{Z}^{-n}}{1 - \mathcal{Z}^{-1}}$

The theorems of Laplace transform theory have their Z -transform equivalents. We shall mention without proof the following:

$$\mathcal{Z} \{cf(x)\} = cF(\mathcal{Z})$$

and
$$\mathcal{Z} \{f_1(x) + f_2(x)\} = F_1(\mathcal{Z}) + F_2(\mathcal{Z})$$

which express the rules for multiplication by a constant and the sum of two transforms, respectively. Further, we have the theorem of complex translation

$$\mathcal{Z} \{e^{-bx}f(x)\} = F\{e^{bd}\mathcal{Z}\}$$

where b is a (complex) constant, and the theorem regarding differentiation with respect to a parameter

$$\mathcal{Z} \left\{ \frac{\partial}{\partial b} f(x,b) \right\} = \frac{\partial}{\partial b} \mathcal{Z} \{f(x,b)\}$$

Exercise 5.6 From the definition (5.50) derive the above theorem of complex translation.

The application of Z -transform theory to the treatment of linear antenna arrays is based on the fact that the array factor for an n -element array can be

†It is not difficult to show that $F(\mathcal{Z})$ is the Laplace transform of the function $f^*(x) = f(x) \sum_{i=0}^{\infty} \delta(x - id)$, where δ denotes the delta function.

written as a Z transform. To show this we let $\delta_i = 0$ in (5.45) and introduce the transform variable

$$\mathfrak{z} = e^{-j\gamma}$$

where $\gamma = \delta + k_0 d \cos \theta$ as usual. The array factor then becomes a function of \mathfrak{z}

$$\begin{aligned} f(\mathfrak{z}) &= \sum_{i=0}^{n-1} |a_i| \mathfrak{z}^{-i} \\ &= \mathcal{Z}\{a(z)g_n(z)\} \end{aligned} \quad (5.51)$$

Here $g_n(z)$ is the unit gate function defined previously and $a(z)$ any real continuous function (current distribution function) of argument z which takes the values of the magnitude of the excitation coefficients $|a_m|$ at the positions z_m of the array elements.

An example of the function $a(z)$ is illustrated in Fig. 5.12. In practice it is often possible to choose for $a(z)$ a simple algebraic or transcendental function of the z coordinate. In (5.51) the array factor for an n -element array with

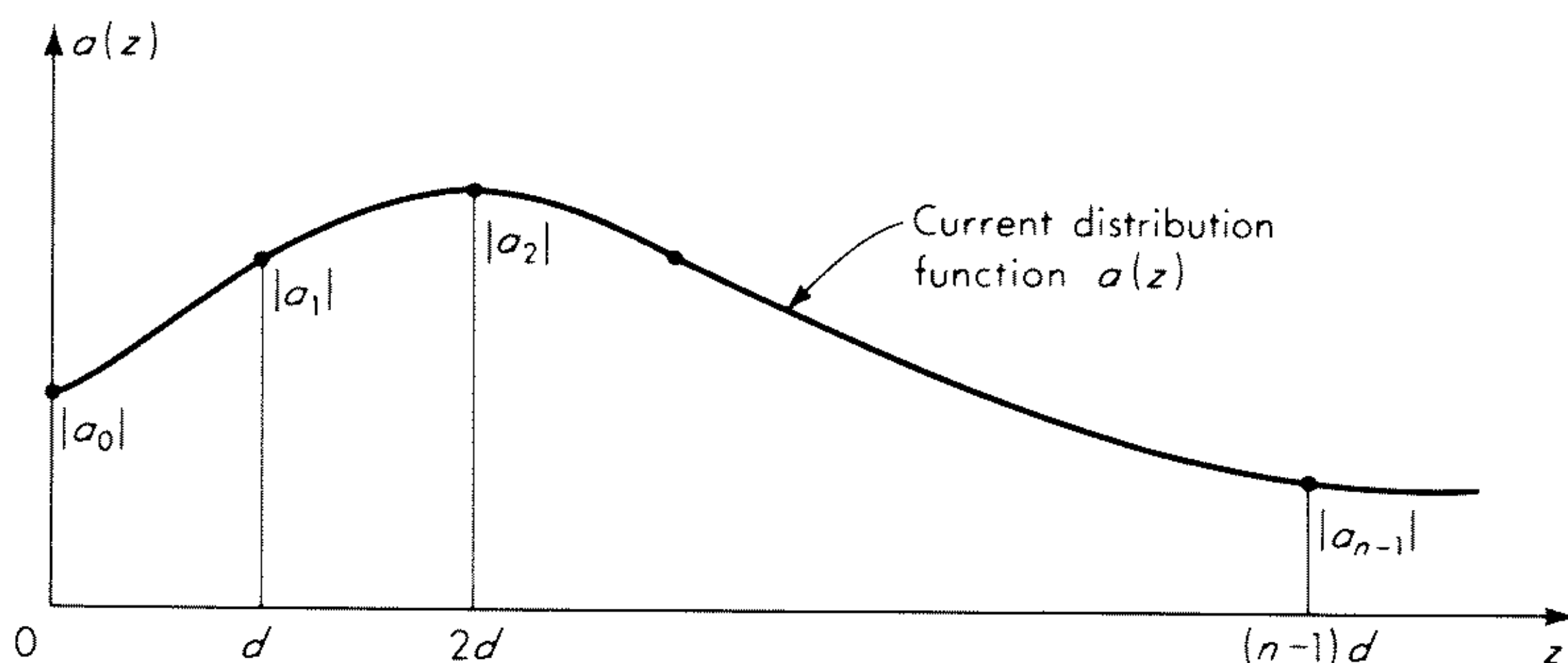


Fig. 5.12 Current distribution function for linear array.

tapered current distribution is expressed as the Z transform of the current distribution function $a(z)$ times the unit gate function $g_n(z)$.†

Let us now apply the rule of complex translation to the unit gate function. We thereby obtain

$$\begin{aligned} \mathcal{Z}\{e^{-bz}g_n(z)\} &= F(e^{bd}\mathfrak{z}) \\ &= \frac{1 - e^{-nbd}\mathfrak{z}^{-n}}{1 - e^{-bd}\mathfrak{z}^{-1}} \end{aligned} \quad (5.52)$$

By using the rules of multiplication by a constant [we choose the constant $(-h)^p$, where p is an integer] and differentiation with respect to a parameter

†Note that this result may be extended to cover the case of excitations with nonlinear phase distribution functions. We only need to allow $a(z)$ to attain complex values. The array factor then may be written as a Z transform plus the imaginary unit times another Z transform.

(we differentiate p times with respect to the constant b) we arrive at the following transform:⁹

$$\mathcal{Z}\{(hz)^p e^{-bz} g_n(z)\} = (-h)^p \frac{\partial^p}{\partial b^p} \frac{1 - e^{-nbd} \mathcal{Z}^{-n}}{1 - e^{-bd} \mathcal{Z}^{-1}} \quad (5.53)$$

With suitable choice of h , p , and b in (5.53) and with application of the previously given rules we are able to obtain in closed form the array factor for linear arrays with n equispaced elements when the current distribution function is linear, parabolic, exponential, sinusoidal, etc. The transform (5.53) is a generalization, particularly well adapted for array theory, of the well-known summation formula for a finite geometrical series.

Exercise 5.7 Carry out the detailed derivation of (5.53).

Exercise 5.8 Let us compute the array factor for an array with current distribution function $a(z) = \sin(hz)$. From (5.52) we have

$$\mathcal{Z}\{e^{\pm i h z} g_n(z)\} = \frac{1 - e^{\pm i h n d} \mathcal{Z}^{-n}}{1 - e^{\pm i h d} \mathcal{Z}^{-1}}$$

Application of Euler's formula then gives

$$\begin{aligned} \mathcal{Z}\{\sin(hz) g_n(z)\} &= \frac{\mathcal{Z} \sin(hd) - \mathcal{Z}^{-n+2} \sin(nhd) + \mathcal{Z}^{-n+1} \sin[(n-1)hd]}{\mathcal{Z}^2 - 2z \cos(hd) + 1} \\ &= f(\mathcal{Z}) \end{aligned} \quad (5.54)$$

where $\mathcal{Z} = e^{-j(\delta + k_0 d \cos \theta)}$. If we choose h so that $\sin(hd) = 0$ for $z = (n-1)d$, the array is excited symmetrically. In this case the expression for the array factor takes a particularly simple form. Derive the array factor for this special case.

5.6 Circular Arrays

Array Factor

A circular array, or ring array, is an array in which the elements are placed along the circumference of a circle.¹⁰⁻¹² We consider only the case when the elements are equidistantly spaced. If the reference antenna is placed at the center of the circle (of radius a), we find for the m th position vector

$$\mathbf{r}_m = \hat{\mathbf{x}}a \cos v_m + \hat{\mathbf{y}}a \sin v_m$$

where

$$v_m = \frac{2\pi}{n} m$$

and n is the number of elements. By insertion into the general expression (5.10) for the array factor we find

$$f(\theta, \phi) = \sum_{m=1}^n a_m e^{jk_0 a (\cos v_m \sin \theta \cos \phi + \sin v_m \sin \theta \sin \phi)} \quad (5.55)$$

For an equispaced circular array with excitation coefficients

$$a_m = |a_m|e^{j\delta_m}$$

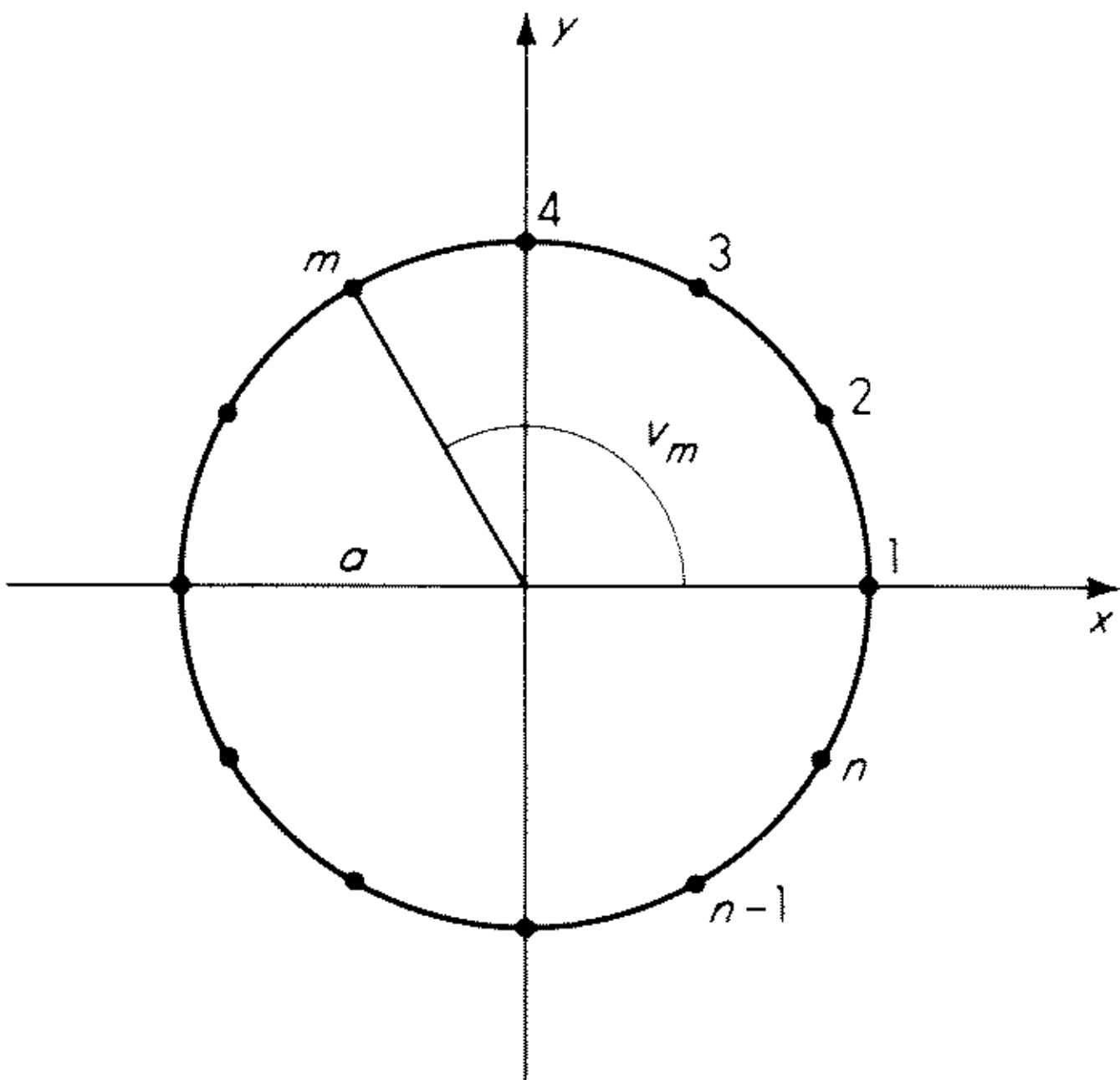


Fig. 5.13 Ring array.

the array factor becomes

$$f(\theta,\phi) = \sum_{m=1}^n |a_m|e^{j[\delta_m + \zeta \cos (\phi - \varphi_m)]} \tag{5.56}$$

with $\zeta = k_0a \sin \theta$. The main difference between this expression and that for an equispaced linear array is that the array factor is now a function of both θ and ϕ . This corresponds to the fact that a circular array does not have an axis of complete rotational symmetry.

In analogy with the definition of a uniform linear array, we define a uniform circular array as an equispaced circular array for which the phases of the excitation coefficients decrease uniformly along the circle so that the total decrease after one circuit is an integral multiple ν of 2π . If it is assumed that the current in the reference antenna is equal to the sum of the absolute values of the currents in the individual elements, the excitation coefficients may be expressed through

$$a_m = \frac{1}{n} e^{-j(2\pi \nu / n)m} \tag{5.57}$$

When this is inserted into (5.56), we obtain the expression

$$f(\theta,\phi) = \frac{1}{n} \sum_{m=1}^n e^{-j[\nu \varphi_m - \zeta \cos (\phi - \varphi_m)]} \tag{5.58}$$

for the array factor of a uniform circular array.

As an example of a nonuniform circular array we consider a directive array, i.e., a circular array which concentrates most of the radiated field within a small solid angle about some given direction (θ_0, ϕ_0) , called the main direction. In this case the excitation coefficients must be chosen in such a manner that the fields from the individual elements are all in phase in this direction. From (5.56) it is seen that if we let

$$\delta_m = -k_0 a \sin \theta_0 \cos (\phi_0 - v_m)$$

the fields from the individual elements will all have the relative phases zero in the main direction. If, further, $|a_m| = 1/n$, we obtain

$$f(\theta, \phi) = \frac{1}{n} \sum_{m=1}^n e^{-jk_0 a [\sin \theta_0 \cos (\phi_0 - v_m) - \sin \theta \cos (\phi - v_m)]} \quad (5.59)$$

For convenience we introduce the two quantities ξ and ρ by

$$\cos \xi = \frac{\sin \theta \cos \phi - \sin \theta_0 \cos \phi_0}{\sqrt{(\sin \theta \cos \phi - \sin \theta_0 \cos \phi_0)^2 + (\sin \theta \sin \phi - \sin \theta_0 \sin \phi_0)^2}}$$

$$\text{and } \rho = a \sqrt{(\sin \theta \cos \phi - \sin \theta_0 \cos \phi_0)^2 + (\sin \theta \sin \phi - \sin \theta_0 \sin \phi_0)^2}$$

After some elementary manipulations, we find the expression

$$f(\theta, \phi) = \frac{1}{n} \sum_{m=1}^n e^{jk_0 \rho \cos (\xi - v_m)} \quad (5.60)$$

for the array factor of a directive circular array with the main direction (θ_0, ϕ_0) .

In the theory of linear arrays it is convenient first to consider arrays with discrete elements and then proceed to continuous arrays. However, for the description of circular arrays the opposite procedure is preferable. This is due to the fact that the array factor of a discrete circular array is expressed most conveniently by the array factor for a corresponding continuous circular array plus some correction terms. These terms are then a measure of the deviation of the array factor for the discrete array from that of the corresponding continuous array. As will be seen from the following, the array factor for a continuous array can be expressed in a rather simple manner.

Continuous Circular Arrays

In order to determine the array factor for a continuous uniform circular array, we let the number of elements n tend to infinity; the angle between the radii to two adjacent elements, $\Delta v_m = 2\pi/n$, then goes to zero. From Eq. (5.58) we now find

$$f(\theta, \phi) = \lim_{n \rightarrow \infty} \frac{1}{2\pi} \sum_{m=1}^n e^{-j[v v_m - \xi \cos (\phi - v_m)]} \Delta v_m$$

When passing to the limit, v_m tends to v , which is then a continuous variable in the interval $(0, 2\pi)$. Simultaneously, the summation is replaced by an integration. Accordingly, we find

$$f(\theta, \phi) = \frac{1}{2\pi} \int_0^{2\pi} e^{-j[\nu v - \zeta \cos(\phi - v)]} dv$$

which may be written

$$f(\theta, \phi) = \frac{1}{2\pi} e^{-j\nu\phi} \int_0^{2\pi} e^{j[\nu(\phi - v) + \zeta \cos(\phi - v)]} dv$$

From the integral formula for the Bessel functions

$$j^\nu J_\nu(\zeta) = \frac{1}{2\pi} \int_0^{2\pi} e^{j(\nu v + \zeta \cos v)} dv \quad (5.61)$$

it is then seen that the array factor can be expressed through

$$f(\theta, \phi) = e^{-j\nu(\phi - \pi/2)} J_\nu(\zeta) \quad (5.62)$$

Thus the absolute value of the array factor is simply given by the Bessel function of ν th order

$$|f| = |J_\nu(\zeta)| = |J_\nu(k_0 a \sin \theta)| \quad (5.63)$$

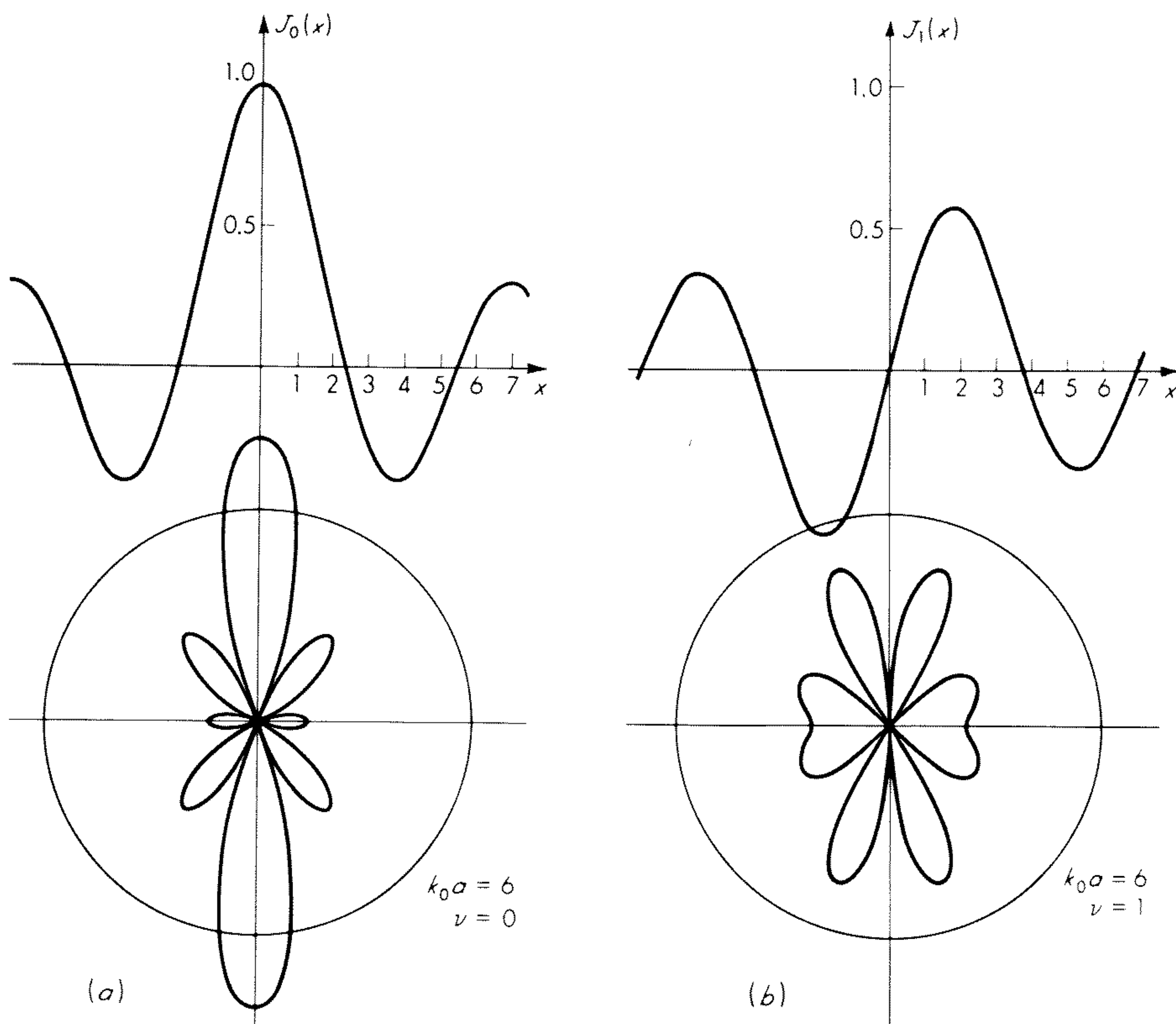


Fig. 5.14 Continuous uniform circular array with $k_0 a = 6$ and (a) $\nu = 0$, (b) $\nu = 1$.

In this case $|f|$ does not depend on ϕ ; accordingly, the continuous circular array is perfectly omnidirectional. The horizontal array pattern is therefore a circle, and the vertical pattern can be obtained in a simple manner by a slight modification of the previously mentioned method for constructing array patterns. Now $J_\nu(0) = \delta_{0\nu}$, and accordingly the array with $\nu = 0$ is the only circular array which radiates in the directions normal to the plane of the array. In Fig. 5.14 are shown the array patterns of two ring arrays with $k_0a = 6$ and $\nu = 0$ and 1, respectively. From graphs of the Bessel functions, it is immediately seen that the radiation in directions near $\theta = 0$ and π is reduced when ν is increased and that more minor lobes occur when the radius a is increased.

Exercise 5.9 By placing a center element in a circular array with $\nu = 0$ it is possible, by a suitable choice of the excitation coefficient a_0 for the center element, to reduce the radiation in the directions $\theta = \theta_0$. Under the condition that the original array can be considered as a uniform array, find the excitation coefficient a_0 for which the array factor of the entire system is zero for $\theta = \theta_0$.

In order to obtain the array factor for a continuous directive array, we let $n \rightarrow \infty$ in (5.60) and find

$$\begin{aligned} f(\theta, \phi) &= \lim_{n \rightarrow \infty} \frac{1}{2\pi} \sum_{m=1}^n e^{jk_0\rho \cos(\xi - v_m)} \Delta v_m \\ &= \frac{1}{2\pi} \int_0^{2\pi} e^{jk_0\rho \cos(\xi - v)} dv \end{aligned}$$

By means of formula (5.61), we obtain

$$f(\theta, \phi) = J_0(k_0\rho)$$

for the array factor of a continuous, directive circular array.

We first consider the special case in which the main direction is vertical ($\theta_0 = 0$). We then find $\rho = a \sin \theta$, which yields the expression

$$f(\theta, \phi) = J_0(k_0a \sin \theta)$$

Accordingly, this array is identical with the omnidirectional array with $\nu = 0$ as shown by the formula (5.63).

As another example, we consider an array with a horizontal main direction $(\theta_0, \phi_0) = (\pi/2, \phi_0)$ and find

$$\rho = a\sqrt{(1 - \sin \theta)^2 + 4 \sin \theta \sin^2 \frac{1}{2}(\phi - \phi_0)}$$

$$\text{and } |f(\theta, \phi)| = |J_0[k_0a\sqrt{(1 - \sin \theta)^2 + 4 \sin \theta \sin^2 \frac{1}{2}(\phi - \phi_0)}]|$$

The vertical pattern in a plane through the main direction is determined from

$$|f(\theta, \phi_0)| = |J_0[k_0a(1 - \sin \theta)]|$$

while the horizontal pattern is given by

$$\left| f\left(\frac{\pi}{2}, \phi\right) \right| = |J_0[2k_0 a \sin \frac{1}{2}(\phi - \phi_0)]|$$

From this formula it is seen that the horizontal pattern depends only on the angle $\nu = \phi - \phi_0$. Therefore, if the main direction is shifted through an angle $\Delta\phi_0$ by changing the phases of the excitation coefficients, the whole pattern will be shifted through the same angle $\Delta\phi_0$ without change of shape. In Fig. 5.15

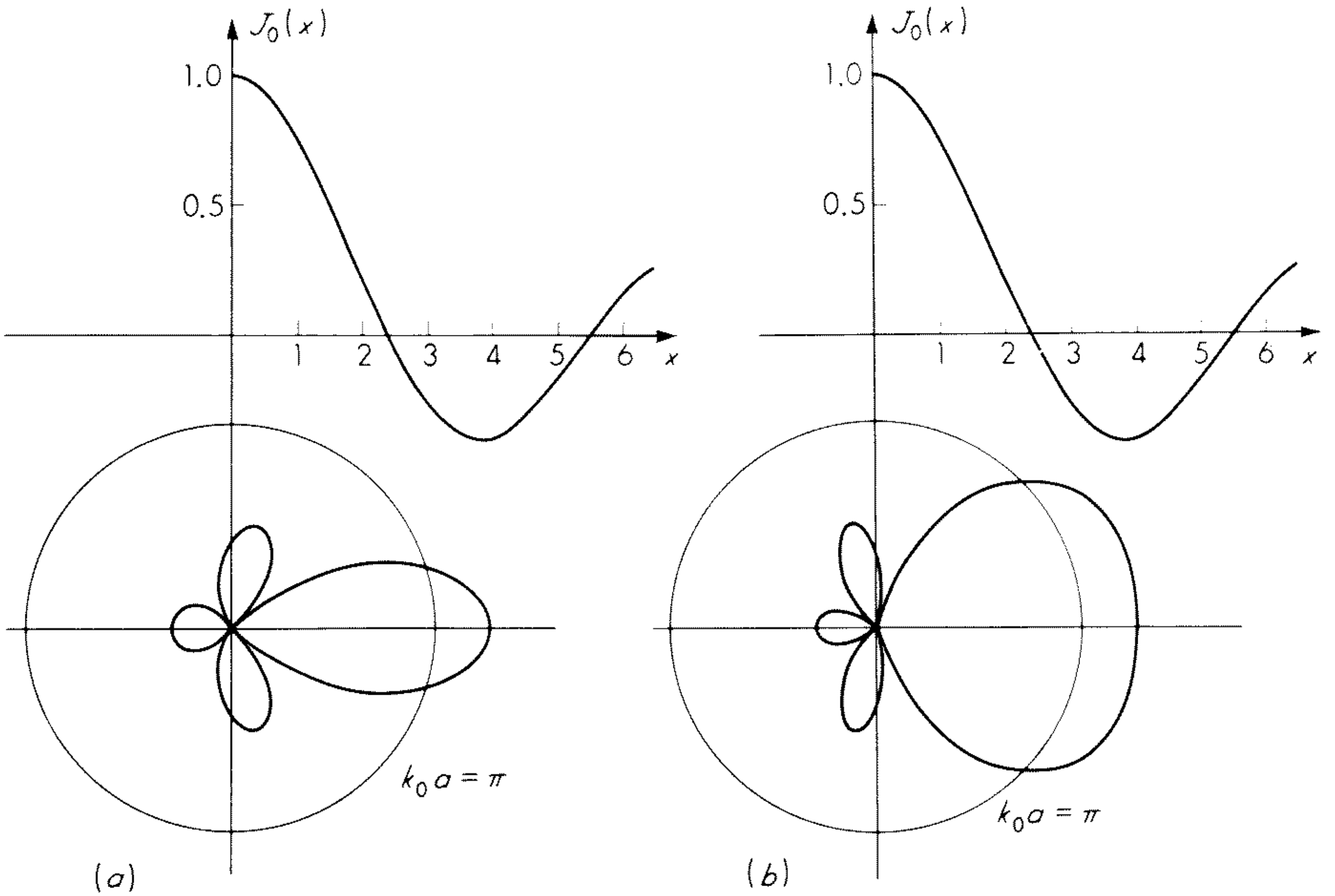


Fig. 5.15 Array pattern of continuous directive circular array. (a) Horizontal pattern; (b) vertical pattern.

the vertical and horizontal patterns are shown for $k_0 a = \pi$. Again it is obvious that, when the radius a is increased, in general the number of minor lobes increases and the beam width of the main lobe decreases.

Omnidirectional Circular Array

We now turn to the more complicated case of an omnidirectional circular array with discrete elements. We return to the formula (5.58) and introduce the relation¹³

$$e^{j\zeta \cos \alpha} = \sum_{k=0}^{\infty} \epsilon_k j^k \cos(k\alpha) J_k(\zeta) \quad (5.64)$$

where ϵ_k is Neumann's number defined by

$$\epsilon_k = \begin{cases} 1 & k = 0 \\ 2 & k \neq 0 \end{cases} \quad (5.65)$$

We then find

$$f(\theta, \phi) = \frac{1}{n} \sum_{m=1}^n \left[e^{-j\nu v_m} \sum_{k=0}^{\infty} \epsilon_k j^k \cos k(\phi - v_m) J_k(\zeta) \right]$$

By interchanging the order of summation and utilizing Euler's formulas, the expression can be rewritten in the following manner

$$\begin{aligned} f(\theta, \phi) &= \sum_{k=0}^{\infty} \left[\epsilon_k j^k J_k(\zeta) \frac{1}{n} \sum_{m=1}^n e^{-j\nu v_m} \cos k(\phi - v_m) \right] \\ &= \sum_{k=0}^{\infty} \left[\epsilon_k j^k J_k(\zeta) \frac{1}{2n} \left(e^{jk\phi} \sum_{m=1}^n e^{-j(\nu+k)v_m} + e^{-jk\phi} \sum_{m=1}^n e^{-j(\nu-k)v_m} \right) \right] \quad (5.66) \end{aligned}$$

Now, for k and n integers we have the formula

$$\frac{1}{n} \sum_{m=1}^n e^{-j2\pi(k/n)m} = \begin{cases} 1 & \frac{k}{n} \text{ integer} \\ 0 & \frac{k}{n} \text{ otherwise} \end{cases}$$

which shows that the finite series

$$\frac{1}{n} \sum_{m=1}^n e^{-j(\nu \pm k)v_m} = \frac{1}{n} \sum_{m=1}^n e^{-j2\pi(\nu \pm k)m/n}$$

contributes only when $(\nu \pm k)/n$ is an integer. Therefore, in the first sum with respect to m in (5.66), we let $q = (\nu + k)/n$; now $k \geq 0$ and therefore

$$k = nq - \nu \geq 0 \quad q \geq \frac{\nu}{n}$$

In the second we let $-q = (\nu - k)/n$, which yields

$$k = nq + \nu \geq 0 \quad q \geq -\frac{\nu}{n}$$

For the two series we then find

$$e^{\pm jk\phi} \sum_{m=1}^n e^{-j2\pi[(\nu \pm k)/n]m} = e^{j(nq \mp \nu)\phi}$$

When this result is inserted into the expression for $f(\theta, \phi)$ and q is introduced as a new index of summation, we get

$$\begin{aligned} f(\theta, \phi) &= \frac{1}{2} \sum_{q \geq \nu/n}^{\infty} \epsilon_{nq - \nu} J_{nq - \nu}(\zeta) e^{j(nq - \nu)(\phi + \pi/2)} \\ &\quad + \frac{1}{2} \sum_{q \geq -\nu/n}^{\infty} \epsilon_{nq + \nu} J_{nq + \nu}(\zeta) e^{j(nq + \nu)(\phi - \pi/2)} \end{aligned}$$

where the factor j^k has been included in the exponential. The notation $q \geq \nu/n$ and $q \geq -\nu/n$ means that the summation should begin with the first integer $\geq \nu/n$ or $\geq -\nu/n$ and that q assumes only the integral values of $(\nu \pm m)/n$ for $m = 0, 1, 2, \dots$.

We now assume that $n > |\nu|$, which is always the case in practical applications. We then have $|\nu|/n < 1$, which means that the summation always starts at $q = 0$ or at $q = 1$. When the above formula is written for convenience in the form

$$f(\theta, \phi) = \frac{1}{2} \sum F_1(nq - \nu) + \frac{1}{2} \sum F_2(nq + \nu)$$

we find, because ν is an integer, the following cases

$$f(\theta, \phi) = \begin{cases} \frac{1}{2} \sum_{q=0}^{\infty} F_1(nq - \nu) + \frac{1}{2} \sum_{q=1}^{\infty} F_2(nq + \nu) & \nu \leq -1 \\ \frac{1}{2} \sum_{q=0}^{\infty} F_1(nq - \nu) + \frac{1}{2} \sum_{q=0}^{\infty} F_2(nq + \nu) & \nu = 0 \\ \frac{1}{2} \sum_{q=1}^{\infty} F_1(nq - \nu) + \frac{1}{2} \sum_{q=0}^{\infty} F_2(nq + \nu) & \nu \geq 1 \end{cases}$$

These expressions may now be written in a simpler fashion. It is seen that the terms corresponding to $q \geq 1$ always appear; we therefore consider the terms corresponding to $q = 0$ in the three cases. When the formula

$$J_{-\nu}(\xi)e^{-j\nu(\phi + \pi/2)} = (-1)^\nu J_\nu(\xi)e^{-j\nu(\phi + \pi/2)} = J_\nu(\xi)e^{-j\nu(\phi - \pi/2)}$$

is introduced, the expressions for the zeroth term may be written

$$\begin{aligned} J_{-\nu}(\xi)e^{-j\nu(\phi + \pi/2)} &= \frac{1}{2}[J_{-\nu}(\xi)e^{-j\nu(\phi + \pi/2)} + J_\nu(\xi)e^{-j\nu(\phi - \pi/2)}] & \nu \leq -1 \\ \frac{1}{2}J_0(\xi) + \frac{1}{2}J_0(\xi) &= \frac{1}{2}[J_0(\xi) + J_0(\xi)] & \nu = 0 \\ J_\nu(\xi)e^{-j\nu(\phi - \pi/2)} &= \frac{1}{2}[J_{-\nu}(\xi)e^{-j\nu(\phi + \pi/2)} + J_\nu(\xi)e^{-j\nu(\phi - \pi/2)}] & \nu \geq 1 \end{aligned}$$

and accordingly we find the general formula

$$f(\theta, \phi) = \frac{1}{2} \sum_{q=0}^{\infty} \epsilon_q [J_{nq - \nu}(\xi)e^{j(nq - \nu)(\phi + \pi/2)} + J_{nq + \nu}(\xi)e^{-j(nq + \nu)(\phi - \pi/2)}] \quad (5.67)$$

for the array factor of a uniform circular array.

It is now easy to compare this result with the array factor for the corresponding continuous circular array. If we separate out the zeroth term, we find

$$\begin{aligned} f(\theta, \phi) &= J_\nu(\xi)e^{-j\nu(\phi - \pi/2)} \\ &+ \sum_{q=1}^{\infty} [J_{nq - \nu}(\xi)e^{j(nq - \nu)(\phi + \pi/2)} + J_{nq + \nu}(\xi)e^{-j(nq + \nu)(\phi - \pi/2)}] \quad (5.68) \end{aligned}$$

which, as seen from (5.62), expresses the array factor for a discrete circular array as the array factor for the corresponding continuous array plus an infinite series. The sum of this series thus is a measure of the difference between the array factors for the discrete array and the corresponding continuous array.

As seen from the above formula, the continuous array is a good approximation only when the sum of terms for $q = 1, 2, \dots$ is much smaller than the

term for $q = 0$. If $n > 2|\nu|$, which is usually the case in applications, the order of the Bessel function in the zeroth term will be lower than that of every Bessel function in the remainder. Now the value of a Bessel function, for a constant argument, tends to zero when the order increases and, accordingly, the terms in the series are decreasing. This not only shows that, when n is increased, the continuous array becomes a still better approximation but also indicates that only a few terms are usually necessary to obtain a good estimate of the sum of the series. In fact, for practical purposes, the first term alone often gives sufficient accuracy.

While the horizontal pattern for a continuous array is a circle, it is a nearly circular wave-line curve for a discrete array¹⁴ in accordance with the fact that this array is not perfectly omnidirectional. For $|\nu| \geq 1$ the amplitudes of the oscillations decrease when n is increased, as would be expected, but for $\nu = 0$ it turns out that $2n - 1$ antennas give a less wavy pattern than $2n$ antennas.¹⁵ This rather surprising fact is of importance in practical cases.

Directive Circular Array

To derive the array factor for a directive circular array with a finite number of elements we return to the expression (5.60)

$$f(\theta, \phi) = \frac{1}{n} \sum_{m=1}^n e^{jk_0 \rho \cos(\xi - v_m)}$$

We insert the expression

$$e^{jk_0 \rho \cos(\xi - v_m)} = \sum_{k=0}^{\infty} \epsilon_k j^k J_k(k_0 \rho) \cos k(\xi - v_m)$$

analogous to (5.64) and find by a procedure similar to that used in the preceding section

$$f(\theta, \phi) = \sum_{k=0}^{\infty} \left[\epsilon_k j^k J_k(k_0 \rho) \frac{1}{n} \sum_{m=1}^n \cos k(\xi - v_m) \right]$$

and

$$f(\theta, \phi) = \sum_{k=0}^{\infty} \left[\epsilon_k j^k J_k(k_0 \rho) \frac{1}{2n} \left(e^{jk\xi} \sum_{m=1}^n e^{-jk(2\pi/n)m} + e^{-jk\xi} \sum_{m=1}^n e^{jk(2\pi/n)m} \right) \right]$$

Again the sums of the finite series are different from zero only when $q \equiv k/n$ is an integer. Therefore, when q is introduced as a summation index, the expression may be written

$$\begin{aligned} f(\theta, \phi) &= \sum_{q=0}^{\infty} [\epsilon_q j^{nq} J_{nq}(k_0 \rho) \frac{1}{2} (e^{jnq\xi} + e^{-jnq\xi})] \\ &= \sum_{q=0}^{\infty} \epsilon_q j^{nq} J_{nq}(k_0 \rho) \cos(nq\xi) \end{aligned}$$

and, by isolating the zeroth term, the array factor for a discrete directive array may be expressed through

$$f(\theta, \phi) = J_0(k_0 \rho) + 2 \sum_{q=1}^{\infty} j^{nq} J_{nq}(k_0 \rho) \cos(nq\xi) \quad (5.69)$$

i.e., as the array factor for the corresponding continuous array plus an infinite series of correction terms. In this case, again because a Bessel function of constant argument goes rapidly to zero when the order is increased, the series is rapidly convergent when $n > k_0 a$, so that in practice only a few terms will suffice. Thus the array pattern again resembles that for the continuous array apart from some oscillations. While for the continuous array a shift of a horizontal main direction through $\Delta\phi_0$ makes the whole pattern turn by the same angle, this is not the case for a discrete array. In this case, a shift of the main direction will be accompanied by some deformation of the pattern.

Other Arrays

We conclude the section on circular arrays by briefly mentioning some other types of arrays which may be derived from the circular arrays. Among them the fading-reducing antenna consisting of a ring array plus a center element has attracted attention.¹⁶ In Ref. 17 is discussed the application of several concentric ring arrays in order to obtain reduced side-lobe level. A circular arc array consisting of a part of a ring array is described in Ref. 18. Recently a theory displaying a connection between elliptical and circular arrays has been presented.¹⁹ Antenna systems which possess some, but not all, of the properties of an array are called quasi-arrays. As an example of quasi-arrays we mention the tangential and radial dipole ring quasi-array. These antennas consist of dipoles arranged equidistantly along a circle and oriented tangentially or radially with respect to the circle.¹² The theory of quasi-arrays is more complicated because a factorization of the field, as discussed in Sec. 5.2, cannot be accomplished in general.

5.7 Array of Arrays

In this section we discuss an important method for the determination of the array factor for arrays which can be considered as a combination of simpler arrays. By f_1 we denote the array factor for an array with n elements, of which the p th element is employed as a reference element. We now look for the array factor of an array of mn antennas, which is formed by m identical arrays of the first-mentioned type. As previously shown, it is not necessary, when deriving the array factor for an array of antennas, to make any assumptions with regard to the type of elements used in the array. Therefore, we can consider each of the above-mentioned m arrays, the subarrays, as elements in an array with m elements, the superarray. We use the q th subarray as a reference element and

denote the corresponding array factor for the superarray by f_2 . It is then immediately seen that the array factor for the entire system may be expressed through

$$f = f_1 f_2$$

with the p th element in the q th subarray as a reference element.

This procedure, of course, can be repeated to form superarrays of still higher order, so that we find

$$f = \prod_{m=1}^p f_m$$

for the array factor for an array of p th order with an element in the array of lowest order as a reference element.

The most obvious application of this method, often referred to as the method of pattern multiplication, is the determination of array factors for two- and three-dimensional arrays. As an example we consider a simple curtain antenna consisting of two uniform arrays each with four elements located as shown in Fig. 5.16. We assume that the subarray is broadside ($\delta = 0$) with element spacing $\lambda_0/2$ and find the subarray factor shown in Fig. 5.16a. By the use of two arrays of this type we wish to suppress the lobe in the direction of the

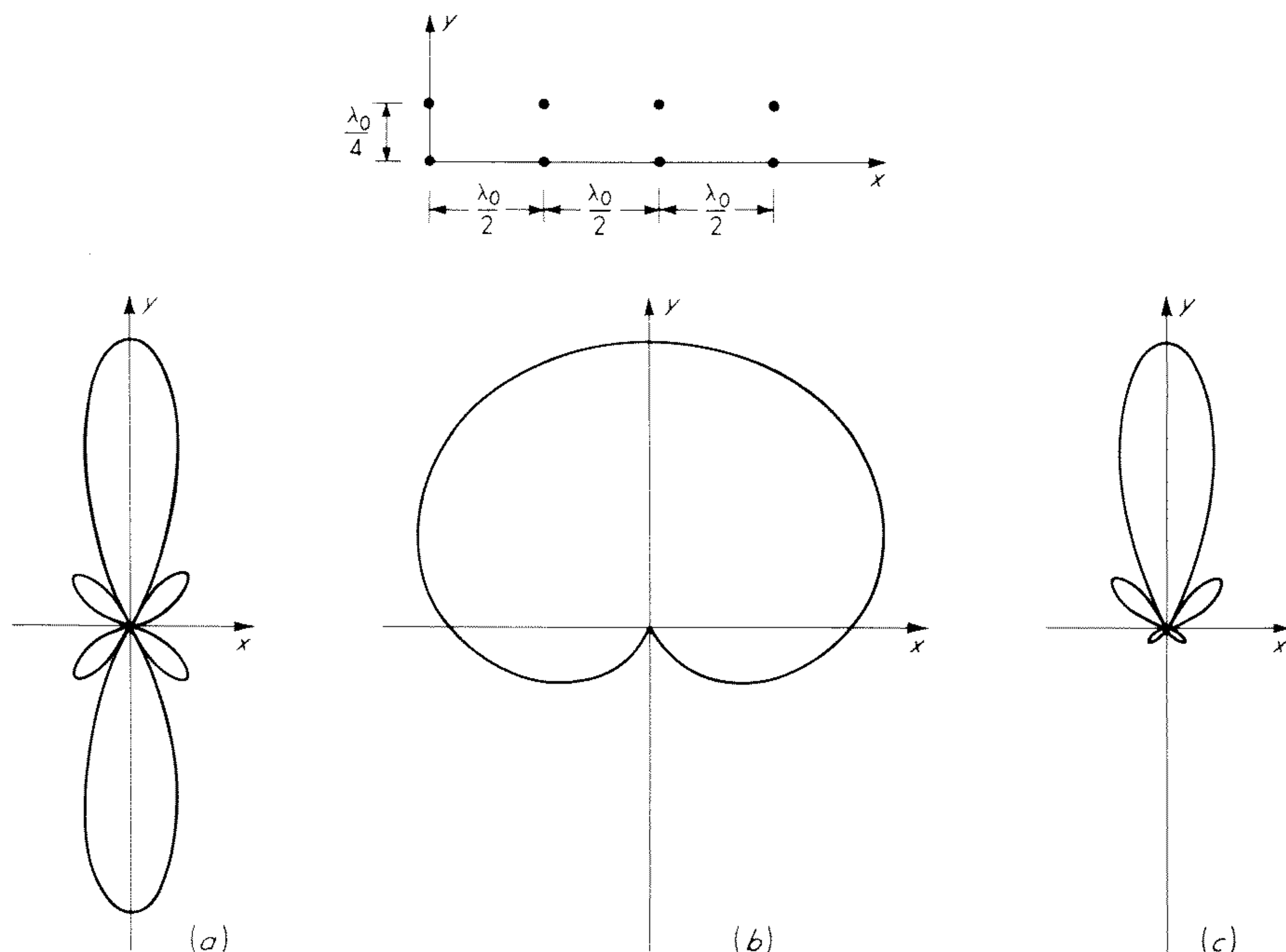


Fig. 5.16 Principle of pattern multiplication. The pattern (c) is obtained by multiplying the patterns (a) and (b).

negative y axis without appreciably disturbing the radiation in the opposite direction. From Fig. 5.4 it is seen that if, for the two subarrays, we choose the spacing $d = \lambda_0/4$ and the phase difference $\delta = \pi/2$, we obtain the superarray factor shown in Fig. 5.16*b*. By multiplication, the pattern for the whole array, shown in Fig. 5.16*c*, results. This simple example illustrates that it is possible, with knowledge of the array patterns of simple arrays, to estimate the patterns of more complicated arrays.

The application sketched above does not exhaust the possibilities of the method of pattern multiplication. Thus we shall show that it is easy to derive the array factors for some tapered arrays by this method. As an example we take the linear array with a triangular current distribution. We consider as the subarray a uniform linear array of n elements with spacing d and phase difference δ between adjacent elements and excited by currents of magnitude 1. From n of these subarrays we construct a superarray, which we imagine to be formed when the subarray is translated $n - 1$ times an amount d in the direction of the array axis. Simultaneously, at each translation, the phase of the excitation coefficient in each element is increased by δ . As shown by the summation in Fig. 5.17, we hereby obtain an antenna system which can be regarded

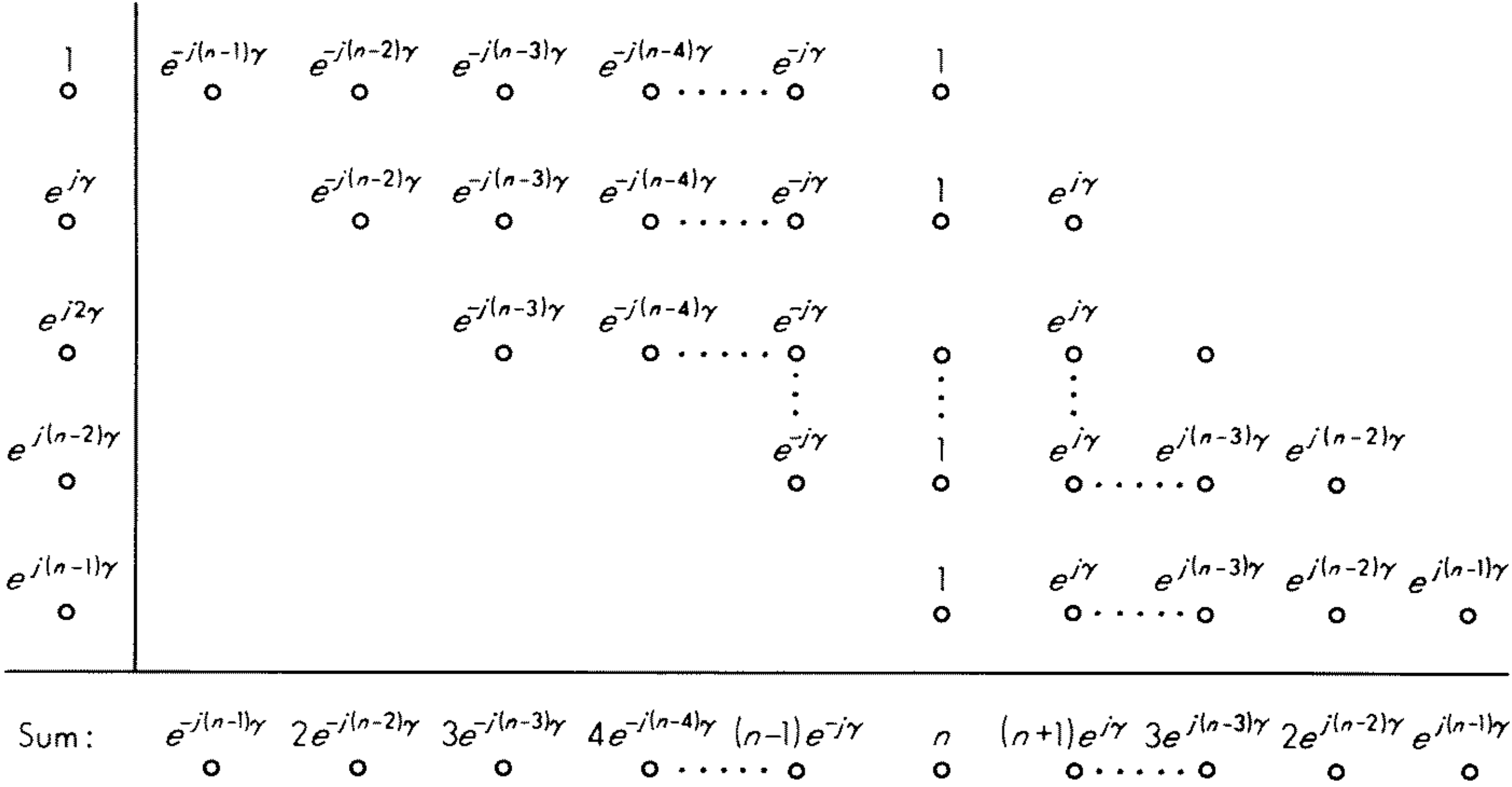


Fig. 5.17 Array factor for a linear array with triangular current distribution obtained by the principle of pattern multiplication. At right the subarrays are shown separately. At left the excitation coefficients of these, when considered as elements of the superarray, are shown. Below is the resulting array.

as a linear array of $2n - 1$ elements with a triangular current distribution and linear phase progression and with the center element as a reference element. The pattern of this array is immediately found because the subarray factor is expressed through

$$f_1 = e^{-j(n-1)(\gamma/2)} \frac{\sin (n\gamma/2)}{\sin (\gamma/2)}$$

while the superarray factor is given by

$$f_2 = e^{j(n-1)(\gamma/2)} \frac{\sin (n\gamma/2)}{\sin (\gamma/2)}$$

when the first subarray is used as a reference element. The array factor for the entire system is thus given by

$$f = f_1 f_2 = \left[\frac{\sin (n\gamma/2)}{\sin (\gamma/2)} \right]^2$$

with the center element as a reference element. The array factor for the triangular array may, of course, also be computed directly from (5.11). By doing this and equating the result with the above expression, we obtain a simple derivation of the summation formula (5.42).

Exercise 5.10 Find the array factor for a linear array of an even number of elements with triangular current distribution and linear phase progression when the reference antenna is placed in the center of the array. Then derive the formula

$$2 \sum_{m=0}^{n-1} (n-m) \cos (m + 1/2)\gamma = \frac{\sin (n\gamma/2)}{\sin (\gamma/2)} \frac{\sin (n+1)\gamma/2}{\sin (\gamma/2)}$$

As another example we shall derive the array factor for the binomial array. We consider a uniform array with two elements separated by the distance d and with the phase difference δ as shown in Fig. 5.18a. We now construct a

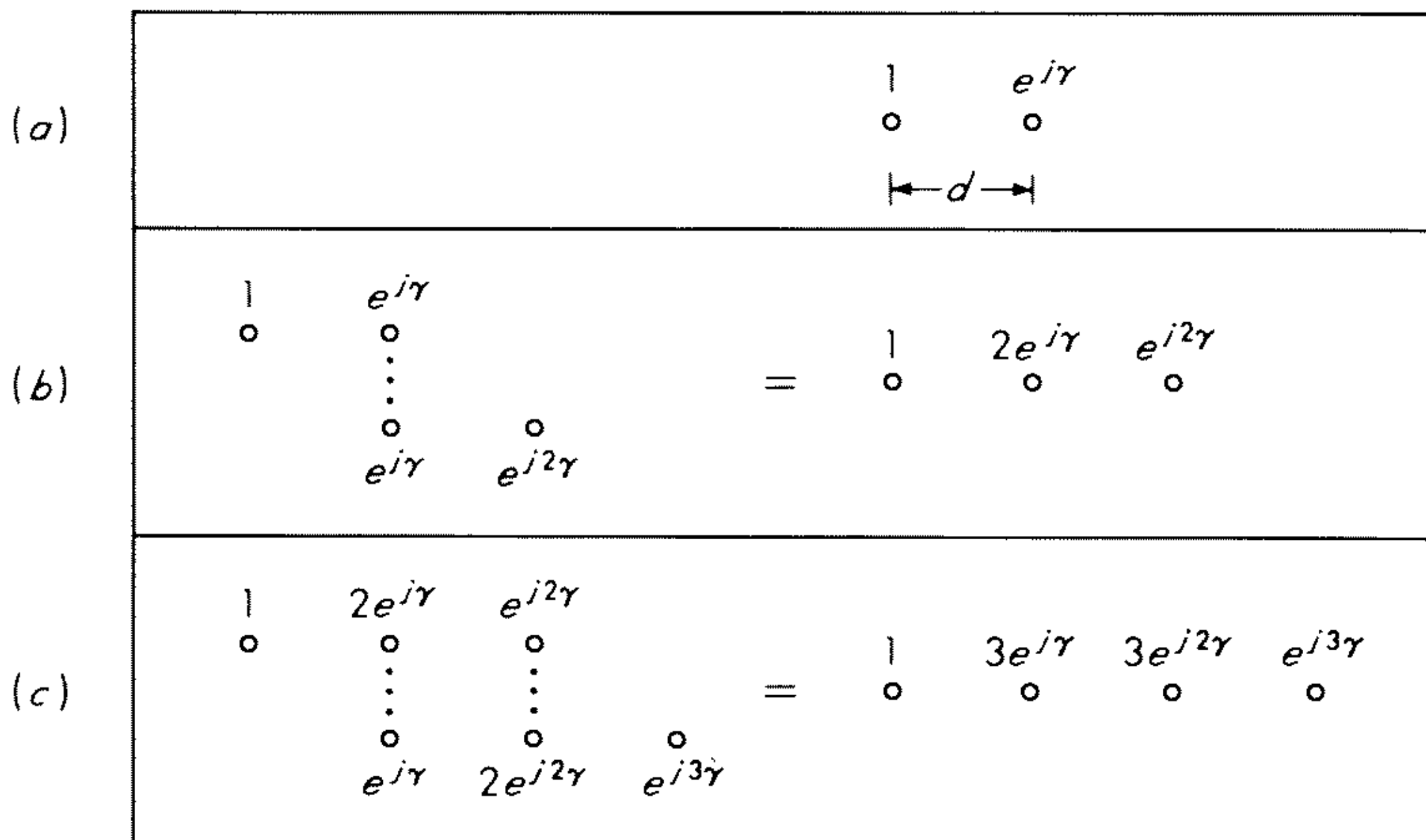


Fig. 5.18 Array factor for binomial arrays obtained by the principle of pattern multiplication. (a) two elements; (b) three elements; (c) four elements.

superarray by adding to this array an array formed by a translation d in the direction of the array axis and a simultaneous increase of the phase by an amount δ . We then have the configuration shown in Fig. 5.18b. In an

analogous manner we form from this array a new superarray (of third order) as shown in Fig. 5.18c. It is now seen that the repetition of this procedure leads to the following excitation coefficients for the superarray of p th order

$$\begin{aligned} a_1 &= \binom{p}{0} = 1 \\ a_2 &= \binom{p}{1} e^{j\gamma} \\ a_3 &= \binom{p}{2} e^{j2\gamma} & \binom{p}{q} &= \frac{p!}{q!(p-q)!} \\ &\dots\dots\dots \\ a_p &= \binom{p}{p-1} e^{j(p-1)\gamma} \\ a_{p+1} &= \binom{p}{p} e^{jp\gamma} \end{aligned}$$

Thus the excitation coefficients are given by the binomial coefficients and, accordingly, the array is called the binomial array. It is immediately seen that the array factor is given by

$$f = (1 + e^{j\gamma})^p$$

where $\gamma = \delta + k_0 d \cos \theta$ which shows that the array pattern for the binomial array has the same nulls as the two-element array from which it is derived.

In Fig. 5.19 the array patterns for broadside arrays with seven elements, $d = \lambda_0/2$, and uniform, triangular, and binomial current distributions are shown. As mentioned earlier, it is seen that a certain tapering of the current magnitudes reduces the number and the level of the side lobes, but simultaneously gives rise to a broader main lobe. Accordingly, the binomial array is in a certain sense optimal because the side lobes for this array have completely disappeared.

5.8 Excitation of an Array

The Array as an n -Pair Terminal Network

Until now we have completely avoided the problem of realizing a given system of element currents on an array. In order to obtain control over the current distribution we now consider the currents and voltages at the terminals of the array. As in any linear system with n pairs of terminals, the following set of linear equations connecting the terminal currents I_m and voltages V_m , $m = 1, 2, \dots, n$, is valid:

$$\begin{aligned} V_1 &= Z_{11}I_1 + Z_{12}I_2 + \dots + Z_{1n}I_n \\ V_2 &= Z_{21}I_1 + Z_{22}I_2 + \dots + Z_{2n}I_n \\ &\dots\dots\dots \\ V_n &= Z_{n1}I_1 + Z_{n2}I_2 + \dots + Z_{nn}I_n \end{aligned} \tag{5.70}$$

where the quantities Z_{ml} are called self-impedances when $l = m$ and mutual impedances for $l \neq m$. Because of reciprocity the impedance matrix is symmetric, that is, $Z_{ml} = Z_{lm}$.

The self- and mutual impedance Z_{ml} in (5.70) may be separated into real and imaginary parts. The real part has the form $R_{ml} + \delta_{ml}R_{\text{loss}}$ in general. Here R_{ml} is the mutual radiation resistance, whereas R_{loss} is the equivalent loss resistance; δ_{ml} is the Kronecker delta. We have here made the assumption that all elements have the same equivalent loss resistance R_{loss} . For lossless arrays $Z_{ml} = R_{ml} + jX_{ml}$.

In the following we shall use normalized impedances mainly. These are obtained by dividing Z_{ml} by the radiation resistance for a reference antenna.

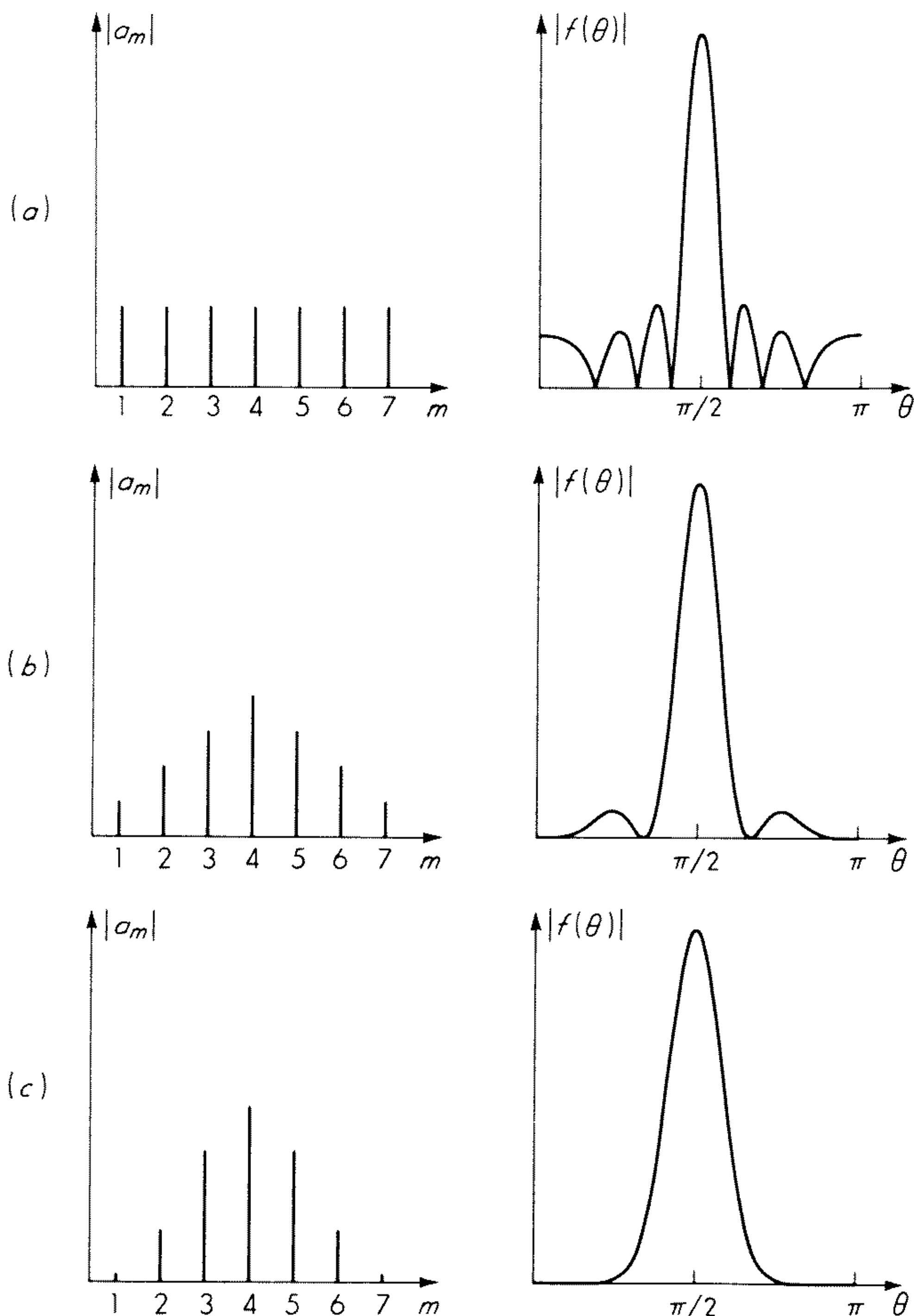


Fig. 5.19 Excitation coefficients and array patterns for a seven-element linear broadside array with $d = \lambda_0/2$ and (a) uniform, (b) triangular, and (c) binomial current distribution.

Element No. 1 may conveniently serve as a reference antenna. We shall denote normalized impedances by small letters. In this way we have, for instance, $z_{ml} = Z_{ml}/R^{\text{ref}}$, where $R^{\text{ref}} = R_{11}$.

In general, the impedances depend in a complicated manner on the specific type of element employed and on the position of all elements. Numerical values are therefore usually difficult to compute. Often one makes the simplifying assumption that every array element experiences the same surroundings as all other elements in the array. This implies that the mutual interaction between any two elements is independent of the location of the rest of the elements and that all self-impedances are equal. The first discussion of impedance relations for arrays, given by Carter,²⁰ was based on this assumption. If the elements are far from each other in comparison with their size and the wavelength, the mentioned approximation may be rather good, but frequently a more refined theory is necessary.^{21,22} In any case, however, for a physical array, the impedances involved are well-defined quantities, which can be determined by measurement.

A related question is how the current distribution on the individual radiators is influenced by the other elements in the array. We must remember that, although it can be generalized to different elements,²³ the whole pattern theory as we have derived it depends on the assumption that the current distributions on the antennas that together form the array are similar. However, the spatial distribution of the radiated field from an element is usually relatively independent of the actual form of the current distribution on it. This means that in general the array concept and the factorization of the field are meaningful for physical arrays.

Corresponding to the impedance matrix for the array, an equivalent n -pair terminal network can be constructed. This network will be passive for a transmitting array but active (provided an incident field is present) for receiving or diffracting arrays. For the two last cases the following extension²⁴ of Thévenin's theorem applies:

Every active n -terminal linear network (such as an antenna array) can be simulated — so far as the action on another network is concerned — by the corresponding inactive network, provided we place in series with (across) the terminals voltage (current) sources such that, on open circuit (closed circuit), the original network and the simulating network are indistinguishable. The corresponding inactive network is derived from the active network by replacing voltage generators by short circuits and current generators by open circuits.

In the applications the n ports of the array are usually either connected through some $(n + 1)$ -port network to a single generator or load or merely interconnected through an n -port network. The modes of operation mentioned correspond to the transmitting, receiving, and diffracting cases, respectively. They are illustrated symbolically in Fig. 5.20.

It is well known that the transmitting and receiving patterns for any antenna (or antenna plus connecting network) are similar. This is a consequence of the reciprocity theorem and is derived in Chap. 4. The reradiation pattern,

however, is usually different from the pattern characterizing receiving and transmitting. This follows from the fact that the current distribution on an array is different in the receiving and transmitting cases.

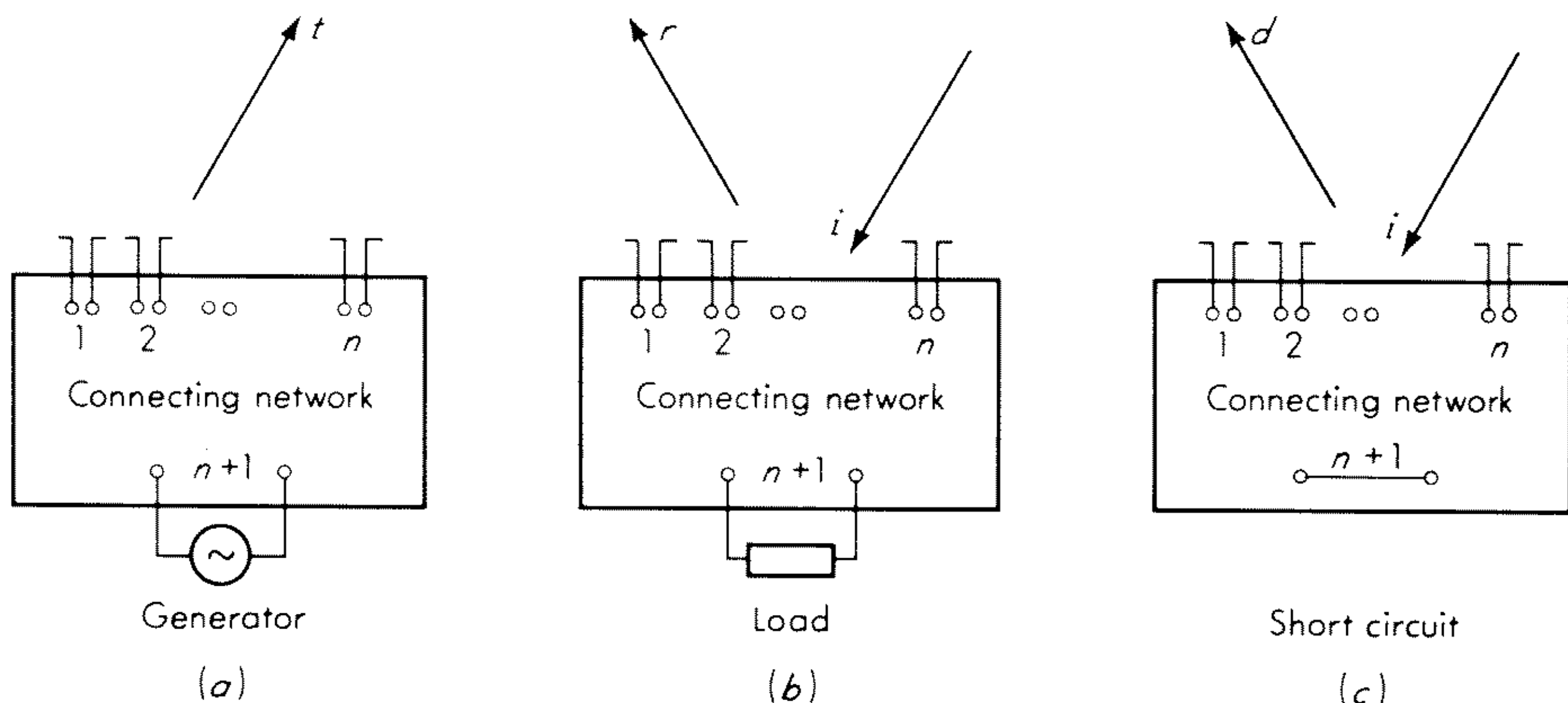


Fig. 5.20 (a) Transmitting array; (b) receiving array; (c) diffracting array.

To see this we place in series with the load in Fig. 5.20 a voltage source E_1 of such magnitude that it just balances the open-circuit voltage from the network. In this case, the current through the load will be zero. The element currents, however, will clearly not be zero in general. They will, rather, adopt a current distribution, the *idling current distribution*, of a shape dependent on the incident field, the array, and the connecting network. The array can now be brought back to its normal state if we add another voltage source E_2 in series with E_1 to cancel it. But E_2 will produce on the array a pure transmitting current distribution. Thus, the receiving current distribution on the array is formed by the superposition of the idling current distribution and the transmitting current distribution. Only when these two current distributions have the same shape, which cannot be expected in general, will the reradiation take place with the same polar diagram as transmitting and receiving.

In order to illustrate the use of the above we shall consider the primitive case of a two-element array in a qualitative manner. In Fig. 5.21 an equivalent

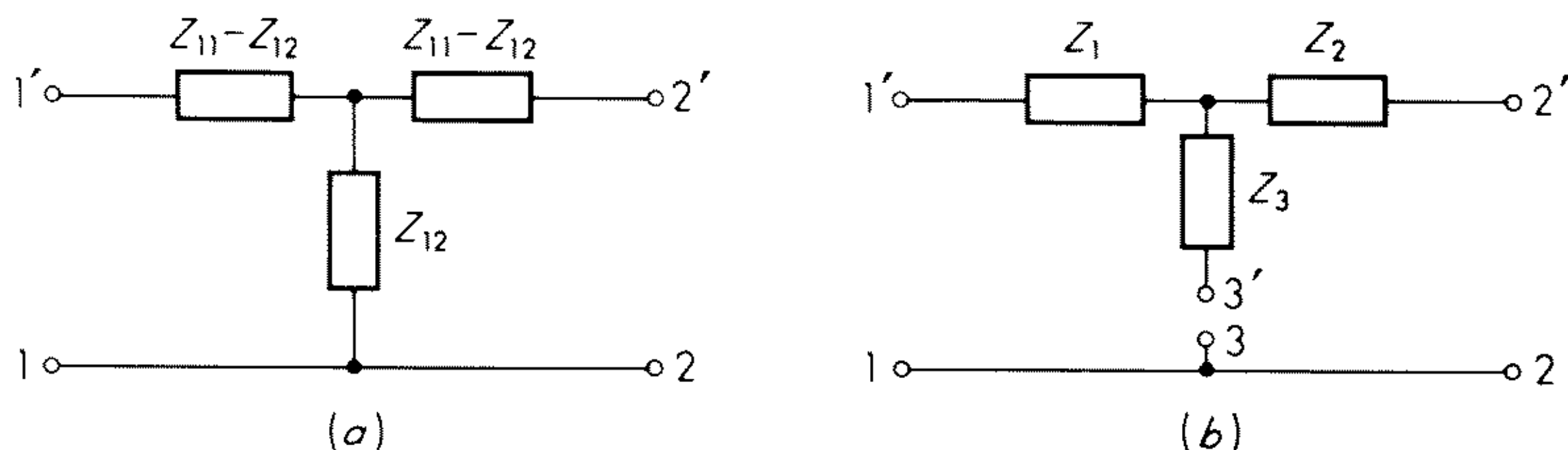


Fig. 5.21 (a) Equivalent circuit and (b) connecting network for a two-element array.

circuit of two coupled antennas with terminals 1-1' and 2-2' is shown together with a simple connecting network to be placed in parallel with it. In the transmitting case a generator is connected to the terminals 3-3'. With all impedances known the resulting element currents I_1 and I_2 are then easily found. In the receiving case a load must replace the generator. Further, in accordance with the theorem, the now active equivalent circuit of the two antennas can be thought of as being the circuit in Fig. 5.21a with voltage sources inserted in series with the terminals 1' and 2'. These sources are to be the open-circuit voltages across the array terminals when receiving. Hence they are merely equal to $\mathbf{h} \cdot \mathbf{E}$, where \mathbf{h} is the effective height of one element and \mathbf{E} is the electric field of the primary (plane) wave at the terminals. With the open-circuit voltages known, the current through the load and the element currents — which give rise to the scattered field — are determined. This type of array is a simple example of the so-called Van Atta array.^{25,26}

Exercise 5.11 Consider a two-element diffracting array as shown in Fig. 5.22. The array consists of two dipoles of self-impedance Z_1 and mutual impedance Z_2 separated by a distance d . The elements are interconnected by a transmission line of length l and

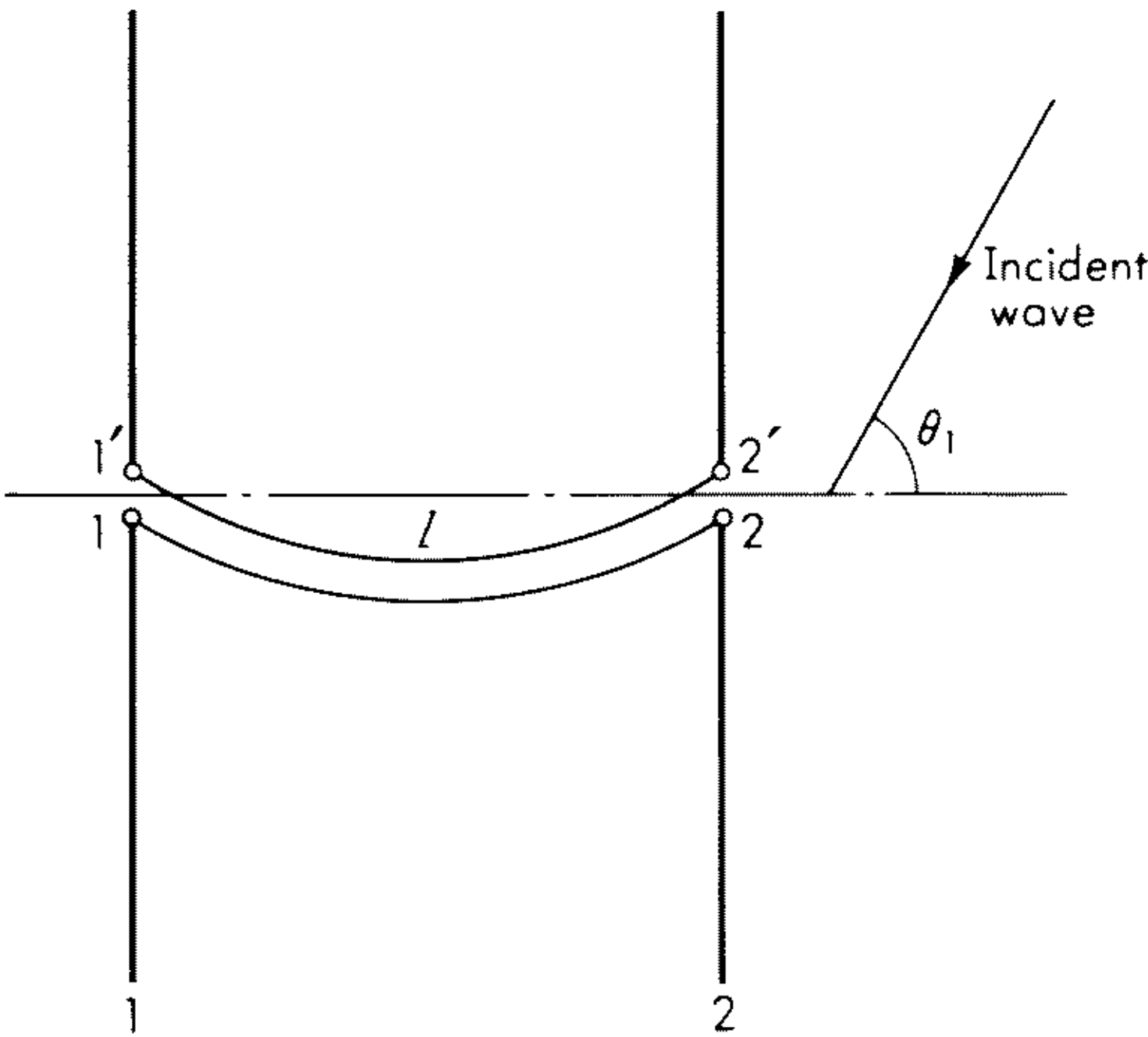


Fig. 5.22 Two-element diffracting array with the elements interconnected by a transmission line of length l .

characteristic impedance Z_3 . The array is exposed to a plane wave of field strength \mathbf{E} with the direction of propagation forming an angle θ_1 with the array axis. By assuming an equivalent T network for the transmission line, compute the array factor $f(\theta_1, \theta)$, with respect to one of the elements as a reference antenna, for the reradiated field.

The above discussion of an array (of idealized elements) viewed as an n -pair terminal network in parallel with an $(n + 1)$ -pair connecting network is based on a paper by Bloch.²⁴ A rigorous formulation, in terms of network parameters, of the receiving and transmitting problems for antenna arrays consisting of

physical elements has been given by Harrington.²⁷ (See also Chap. 4 for a discussion of the receiving antenna.) The impedance behavior of single elements and arrays has been discussed by Oliner and Malech.¹

Array Parameters Expressed by Terminal Quantities

We shall now express some of the array parameters discussed in Sec. 5.3 by the excitation coefficients and the mutual and self-impedances for the elements. We consider an arbitrary array of n elements. The relationships between terminal voltages and currents are then given by (5.70). For convenience, we take the first element (with losses neglected) as the reference antenna. The input resistance of the reference antenna (with all other antennas open-circuited) is then $R^{\text{ref}} = R_{11}$. The input power P^{ref} to the reference antenna becomes

$$P^{\text{ref}} = \frac{1}{2} I_1 I_1^* R^{\text{ref}} \quad (5.71)$$

where the factor $\frac{1}{2}$ arises because I_1 denotes the maximum value of the current. The array input power is expressed by

$$P_{\text{tot}} = \frac{1}{2} \sum_{m=1}^n \sum_{l=1}^n I_m I_l^* (R_{ml} + \delta_{ml} R_{\text{loss}}) \quad (5.72)$$

Only a part of the input power

$$P_{\text{rad}} = \frac{1}{2} \sum_{m=1}^n \sum_{l=1}^n I_m I_l^* R_{ml} \quad (5.73)$$

is radiated. The rest

$$\begin{aligned} P_{\text{loss}} &= \frac{1}{2} \sum_{m=1}^n \sum_{l=1}^n I_m I_l^* \delta_{ml} R_{\text{loss}} \\ &= \frac{1}{2} \sum_{m=1}^n |I_m|^2 R_{\text{loss}} \end{aligned} \quad (5.74)$$

is lost as heat. As mentioned in the preceding subsection, we use the approximation that all elements have the same equivalent loss resistance R_{loss} .

Exercise 5.12 Derive the result given by (5.72).

As in Sec. 5.3, it is convenient to introduce dimensionless quantities. The relative input power to the array is

$$p_{\text{tot}} = \frac{P_{\text{tot}}}{P^{\text{ref}}} = \sum_{m=1}^n \sum_{l=1}^n a_m a_l^* (r_{ml} + \delta_{ml} r_{\text{loss}}) \quad (5.75)$$

where, according to (5.8), $a_m = I_m/I_1$ is the excitation coefficient for the m th antenna and where $r_{ml} = R_{ml}/R^{\text{ref}}$ is the normalized mutual radiation resistance between element m and l . The relative radiated power is obtained in a similar manner

$$p_{\text{rad}} = \frac{P_{\text{rad}}}{P^{\text{ref}}} = \sum_{m=1}^n \sum_{l=1}^n a_m a_l^* r_{ml} \quad (5.76)$$

Finally, from (5.71) and (5.74) we find

$$\begin{aligned} p_{\text{loss}} &= \frac{P_{\text{loss}}}{P_{\text{ref}}} = \sum_{m=1}^n \sum_{l=1}^n a_m a_l^* \delta_{ml} r_{\text{loss}} \\ &= r_{\text{loss}} \sum_{m=1}^n |a_m|^2 \end{aligned} \quad (5.77)$$

From (5.11) we have for the array factor

$$\begin{aligned} f(\theta, \phi) &= \sum_{m=1}^n a_m e^{ju_m(\theta, \phi)} \\ |f|^2 &= \sum_{m=1}^n \sum_{l=1}^n a_m a_l^* e^{ju_m} e^{-ju_l} \end{aligned} \quad (5.78)$$

where $u_m(\theta, \phi) = k_0(x_m \sin \theta \cos \phi + y_m \sin \theta \sin \phi + z_m \cos \theta)$ as before. We are now in a position to write down formulas for the relative directivity and gain. From (5.76) and (5.78)

$$\begin{aligned} D_{\text{rel}} &= \frac{|f|^2}{p_{\text{rad}}} \\ &= \frac{\sum_{m=1}^n \sum_{l=1}^n a_m a_l^* e^{ju_m} e^{-ju_l}}{\sum_{m=1}^n \sum_{l=1}^n a_m a_l^* r_{ml}} \end{aligned} \quad (5.79)$$

The relative gain becomes

$$\begin{aligned} G_{\text{rel}} &= \frac{|f|^2}{p_{\text{tot}}} \\ &= \frac{\sum_{m=1}^n \sum_{l=1}^n a_m a_l^* e^{ju_m} e^{-ju_l}}{\sum_{m=1}^n \sum_{l=1}^n a_m a_l^* (r_{ml} + \delta_{ml} r_{\text{loss}})} \end{aligned} \quad (5.80)$$

It is seen that the relative gain is less than or equal to the relative directivity. We have

$$\frac{1}{G_{\text{rel}}} = \frac{1}{D_{\text{rel}}} + \frac{r_{\text{loss}}}{F} \quad (5.81)$$

The deviation of G_{rel} from D_{rel} depends on the ratio r_{loss}/F , where

$$F = \frac{\sum_{m=1}^n \sum_{l=1}^n a_m a_l^* e^{ju_m} e^{-ju_l}}{\sum_{m=1}^n |a_m|^2} \quad (5.82)$$

is called the efficiency index. We shall see later that the highest value that can be taken by F is obtained when the so-called ordinary or normal excitation is

used; in this case F is equal to the number of elements. Other excitations, in particular those which yield high values of the relative directivity, will lead to lower values of F . For such excitations the relative gain may deviate considerably from the relative directivity.

In a later section we shall use the above-derived expressions for the relative directivity, gain, and efficiency index. We conclude this section by giving — without derivation — some numerical values of the normalized mutual radiation resistance between two-array elements in the idealized cases for which the elements are (1) isotropic radiators, (2) infinitesimal (hertzian) parallel dipoles (perpendicular to the array axis), and (3) infinitely thin, half-wave dipoles with sinusoidal transmitting current distribution and the same orientation as in (2).

TABLE 5.2 NORMALIZED MUTUAL RADIATION
RESISTANCE r_{12} BETWEEN TWO ANTENNAS

<i>Distance in wave lengths between antennas d/λ_0</i>	<i>Isotropic radiators</i>	<i>Hertzian dipoles</i>	<i>Half-wave dipoles</i>
0.00	1.00000	1.00000	1.00000
0.10	0.93549	0.92270	0.92074
0.20	0.75683	0.70987	0.70282
0.30	0.50455	0.41336	0.40006
0.40	0.23387	0.10315	0.08501
0.50	0.00000	-0.15198	-0.17137
0.60	-0.15592	-0.30280	-0.31879
0.70	-0.21624	-0.33155	-0.33998
0.80	-0.18921	-0.25423	-0.25287
0.90	-0.10394	-0.11309	-0.10242
1.00	0.00000	0.03800	0.05486
1.10	0.08504	0.15030	0.16852
1.20	0.12614	0.19403	0.20856
1.30	0.11644	0.16509	0.17220
1.40	0.06682	0.08325	0.08165
1.50	0.00000	-0.01689	-0.02581
1.60	-0.05847	-0.09884	-0.11155

More values of r_{12} may be computed by the principle outlined in Prob. 5.8. For isotropic radiators we have simply $r_{12} = \sin(k_0 d)/k_0 d$. For hertzian dipoles we have^{2,28}

$$r_{12} = \frac{\sin k_0 d}{k_0 d} + \frac{\cos k_0 d}{(k_0 d)^2} - \frac{\sin k_0 d}{(k_0 d)^3} \quad (5.83)$$

A table of mutual radiation resistance for thin half-wave dipoles with assumed

sinusoidal current distribution has been published by Stearns.²⁹ For values pertaining to physical antennas the reader is referred, for example, to the papers by King and Sandler^{21,22} and to later chapters.

SYNTHESIS OF ARRAYS

5.9 Synthesis of Array Patterns

The theory of synthesis of antenna arrays usually deals with the problem of evaluating the system of excitation coefficients on an antenna array that will produce a prescribed array factor to within specified error limits. For practical purposes, the complex array factor f , defined for all directions in space, seldom forms the basis of a synthesis process. Often the array pattern $|f|$ is the only specified function. This gives the designer the extra problem of choosing a convenient phase function.

Historically, the first treatments of the array synthesis problem were given by Berndt,³⁰ Wolff,³¹ and Schelkunoff.⁵ Basically these papers deal with the development of the prescribed array factor into a Fourier series which is then truncated to a finite number of terms. The trigonometric polynomial obtained in this way may then in turn be realized exactly by an array with the proper number of elements. Examples of the method are shown in the book by Jordan.³² When only the magnitude of the array factor is specified, the synthesis problem becomes more involved and the solution is not, in general, unique. This case has been considered by Eaton, Eyges, and Macfarlane³³ and by Taylor and Whinnery.⁶

If the prescribed array factor contains discontinuities, which is often the case, the Fourier series method leads to difficulties. This is because a truncated Fourier series can approximate a given function in the vicinity of a discontinuity only within a tolerance >9 percent. This results in a relatively high side-lobe level when synthesis of patterns with a steep slope is attempted. Methods for improving this situation may be based on, for example, Féjér's summation technique. Such methods have been devised by Jaeckle.³⁴

A more general approach has been described by Simon,³⁵ who viewed the synthesis problem for linear arrays as being a question of approximating a periodic function (the prescribed array pattern) by a sum of trigonometric functions. Instead of the total-mean-square-error criterion, which leads to the Fourier series, Simon suggested the use of the maximum-error criterion. Several theorems from the mathematical theory of approximations are concerned with this problem.³⁶ Further development of the synthesis of array patterns based on approximation theory or interpolation theory has been described by Ma³⁷ and by Jagermann.³⁸ Synthesis of arrays by a direct numerical method has been described by Michelson and Schomer.³⁹ Recently, array synthesis procedures based on eigenfunction expansions have been suggested.^{40,41}

simple example of an array factor for a ten-element array with $d = \lambda_0/4$ obtained by the application of the method sketched above is illustrated in Fig. 5.23.

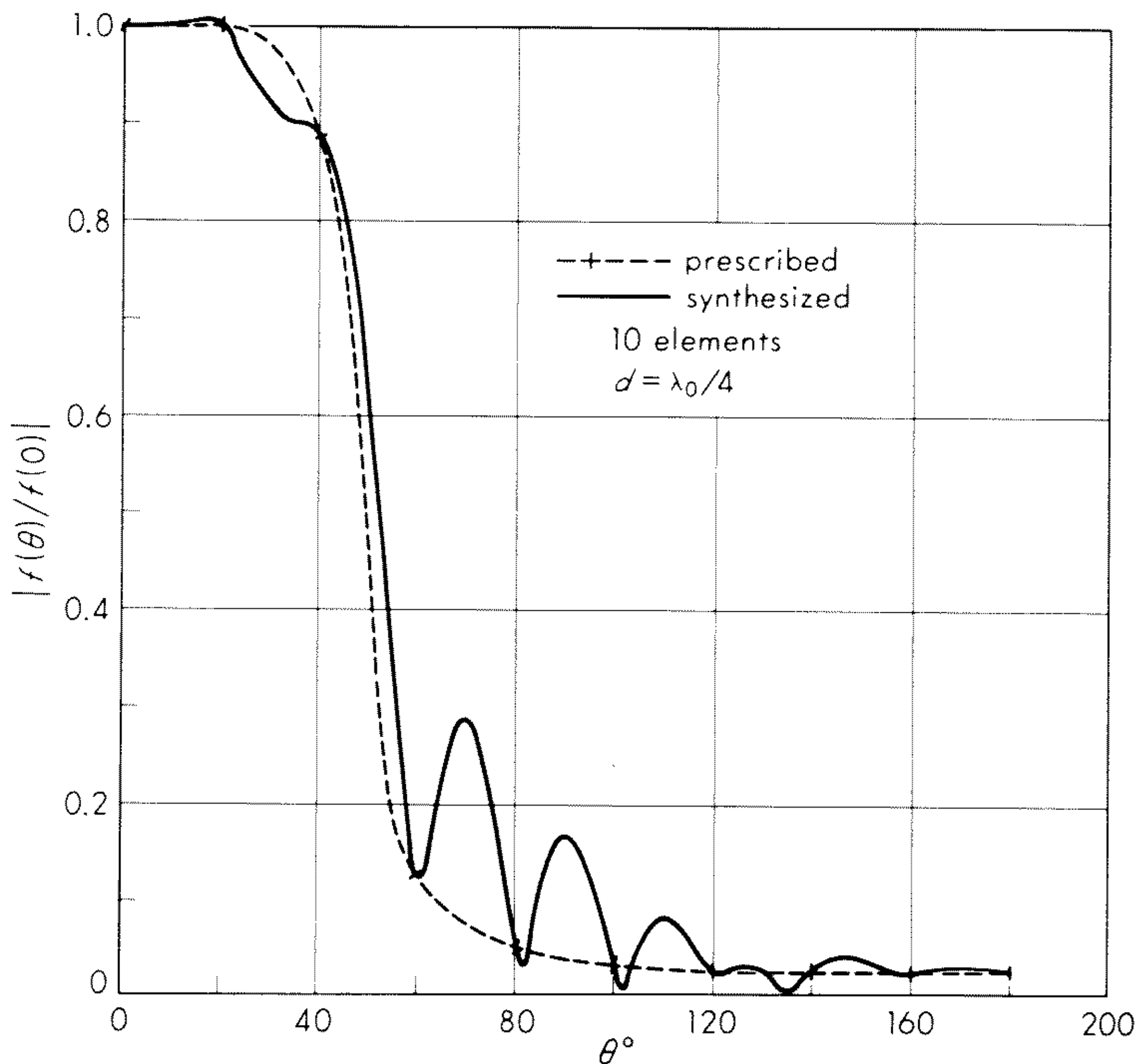


Fig. 5.23 Synthesis of array pattern of a 10-element end-fire array with $d = \lambda_0/4$.

5.10 Optimization of Array Patterns (Dolph-Chebyshev Arrays)

By comparison of the array patterns produced by the uniform, the triangular, and the binomial current distributions (Sec. 5.7) it appears that a high degree of tapering of the current distribution on a broadside array leads to a low level of side lobes. This is obtained, however, at the expense of a broad main beam. We may therefore expect that the design of an array from which the main radiation takes place within a sharp beam and which has vanishing radiation in other directions is bound to involve a compromise between beam width and side-lobe level.

In this section we consider a one-parameter family of current distributions with linearly progressive phase which selects the best compromise in the sense that for a prescribed beam width the side-lobe level is as low as possible. If, on the other hand, the side-lobe level is prescribed, the beam width between the first nulls is minimized. Not surprisingly, it turns out that this optimum

property is obtained when for a given number of elements the array pattern contains as many side lobes as possible and these all have the same level.⁴⁴

The current distribution mentioned was proposed by Dolph⁴⁵ for the case of broadside arrays. The derivation is based on the optimum properties of Chebyshev polynomials. We shall give a brief account of these polynomials first.

The Chebyshev Polynomials

The Chebyshev polynomials may be defined by

$$T_n(x) = \begin{cases} (-1)^n \cosh (n \cosh^{-1} |x|) & x < -1 \\ \cos (n \cos^{-1} x) & |x| \leq 1 \\ \cosh (n \cosh^{-1} x) & x > 1 \end{cases} \quad (5.86)$$

The first few polynomials are

$$T_0(x) = 1$$

$$T_1(x) = x$$

$$T_2(x) = 2x^2 - 1$$

$$T_3(x) = 4x^3 - 3x$$

$$T_4(x) = 8x^4 - 8x^2 + 1$$

Polynomials of higher degree can be obtained from the recurrence relationship $T_{n+1}(x) = 2xT_n(x) - T_{n-1}(x)$ or from the functional equation $T_{mn}(x) = T_m[T_n(x)] = T_n[T_m(x)]$.

Some of the Chebyshev polynomials are plotted in Fig. 5.24. They have the following properties: The polynomial $T_n(x)$ is of n th degree. For n even (odd) it contains x in the even (odd) powers only. The polynomials pass through the points $(1,1)$ and $(-1,(-1)^n)$ and oscillate between the bounds ± 1 in the interval $|x| \leq 1$. For $n > 1$ the extrema are all in the interval $|x| < 1$ and occur at $x = \cos [(\pi/n)p]$, $p = 1, 2, \dots, n-1$. For $n > 0$ the zeros are all in the interval $|x| < 1$ and occur at $x = \cos [(\pi/2n)(2p+1)]$, $p = 0, 1, \dots, n-1$. For any n th degree polynomial $P_n(x)$ through (x_0, R) , $R > 1$, which crosses the x axis at a point x_2 in the interval $x_1 \leq x_2 < x_0$, where x_1 is the largest zero of $T_n(x)$, we must have $|P_n(x)| > 1$ for at least a part of the interval $|x| \leq 1$. This follows from the fundamental lemma of algebra, since $P_n(x)$ and $T_n(x)$ must have at least $n+1$ points in common. In other words, among all polynomials of degree n which pass through two given points (x_0, R) and $(x_2, 0)$, $T_n(x)$ minimizes the largest absolute value in the interval $|x| \leq 1$. The opposite is also true: Among all polynomials $P_n(x)$ of degree n which pass through a given point (x_0, R) and which remain within the bounds ± 1 in the interval $|x| \leq 1$, the Chebyshev polynomial $T_n(x)$ minimizes the distance $x_0 - x_2$, where x_2 is the largest zero of $P_n(x)$.

We shall make use of the above-mentioned optimum properties of Chebyshev polynomials in the design of optimum arrays. For information about other aspects of the theory of Chebyshev polynomials, the reader is referred to the literature.⁴⁶

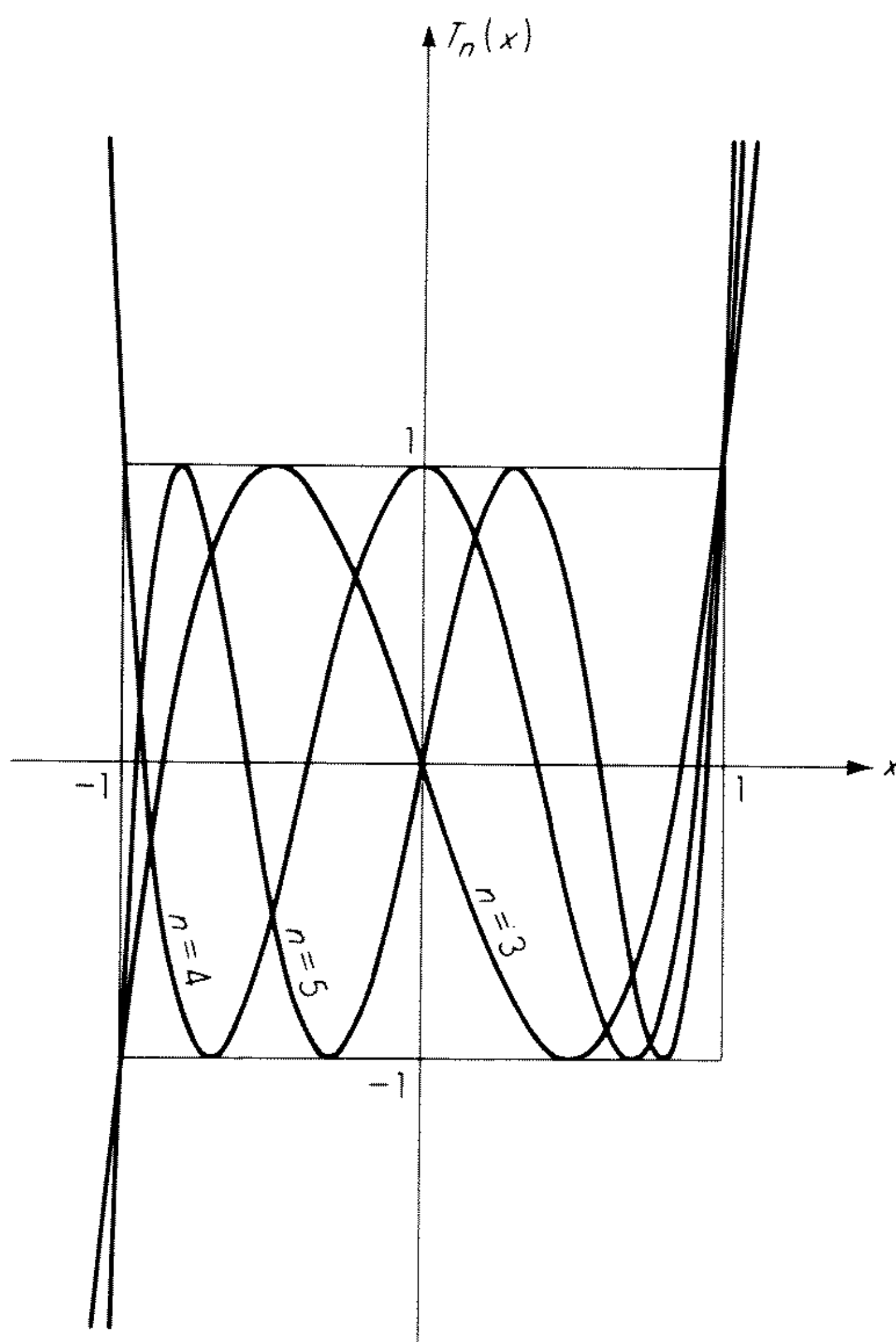


Fig. 5.24 The Chebyshev polynomials $T_n(x)$ for $n = 3, 4, 5$.

Application to Arrays

As the starting point for the derivation of the Dolph-Chebyshev current distribution we consider symmetric excitations, i.e., excitations with $|a_m| = |a_{n-m+1}|$. It is then advantageous to let the midpoint of the array coincide with $z = 0$. With the numbering of the elements being slightly modified from the numbering used for the tapered array with linearly progressive phase in Sec. 5.5, the array factor may now be expressed in the following way

$$f(\gamma) = \begin{cases} 2 \sum_{m=1}^{n/2} |a_m| \cos \frac{(2m-1)\gamma}{2} & n \text{ even} \\ a_0 + 2 \sum_{m=1}^{(n-1)/2} |a_m| \cos m\gamma & n \text{ odd} \end{cases} \quad (5.87)$$

where a_m are the excitation coefficients and $\gamma = \delta + k_0 d \cos \theta$ as usual. The function $\cos px$, where p is an integer, can be expressed as a polynomial of degree p in $\cos x$. Consequently, the array factor can be written as a polynomial in $\cos \gamma$ when n is odd and as a polynomial in $\cos (\gamma/2)$ in both cases. Choosing the latter possibility, we write

$$f(\gamma) = \begin{cases} \sum_{m=1}^{n/2} a_m \left(\cos \frac{\gamma}{2} \right)^{2m-1} & n \text{ even} \\ a'_0 + \sum_{m=1}^{(n-1)/2} a'_m \left(\cos \frac{\gamma}{2} \right)^{2m} & n \text{ odd} \end{cases} \quad (5.88)$$

where a'_m are new (real) coefficients. The degree of both polynomials is $n - 1$. When n is even (odd), the corresponding polynomial contains only odd (even) powers of $\cos (\gamma/2)$.

The idea of Dolph is to optimize the polynomials (5.88) by identifying them with Chebyshev polynomials. The Chebyshev polynomial chosen obviously must be $T_{n-1}(x)$. The identification can be accomplished in many ways depending upon the transformation of variables used. We introduce the following family of transformations

$$x = b \cos \frac{\gamma}{2} \quad (5.89)$$

where $b > 1$ is a parameter. Expressed in terms of the Chebyshev polynomial, the array factor thus obtained is

$$f(\gamma) = T_{n-1} \left(b \cos \frac{\gamma}{2} \right) \quad (5.90)$$

Exercise 5.13 When the number of elements is known, the excitation coefficients yielding an array factor of the form (5.90) may be obtained in the following two steps. To obtain the coefficients a'_m equate the explicit form of the right-hand side of (5.90) with the explicit form of the appropriate right-hand side of (5.88). To obtain $|a_m|$ equate (5.88) with (5.87).

Show that for a five-element optimum array $a_0 = 3b^4 - 4b^2 + 1$, $|a_1| = 2b^4 - 2b^2$, $|a_2| = \frac{1}{2}b^4$.

In order to illustrate how the transformation (5.89) works we shall refer to a geometrical construction which is a simple extension of the geometrical construction described earlier for the uniform array. The construction is shown in Fig. 5.25 for a broadside array and in Fig. 5.26 for an end-fire array. For Fig. 5.25 the element spacing is $\lambda_0/2$. The quantity δ and the radius $k_0 d$ of the circle determine the part of the curve $x = b \cos (\gamma/2)$ that applies. As θ increases from 0 through $\pi/2$ to π , x goes from $b \cos [(k_0 d + \delta)/2]$ through $b \cos (\delta/2)$ to $b \cos [(-k_0 d + \delta)/2]$. In the (γ, x) and (x, f) coordinate systems the corresponding points on the curves $x = b \cos (\gamma/2)$ and $f = T_{n-1}(x)$ move from A through B to C and A' through B' to C' , respectively. The array factor $f(\gamma)$ obtained in this manner will have an absolute maximum R corresponding

to a main lobe and extrema ± 1 corresponding to side lobes. The side-lobe level is $1/R$.

Let us examine the broadside array (Fig. 5.25). For a broadside array maxi-

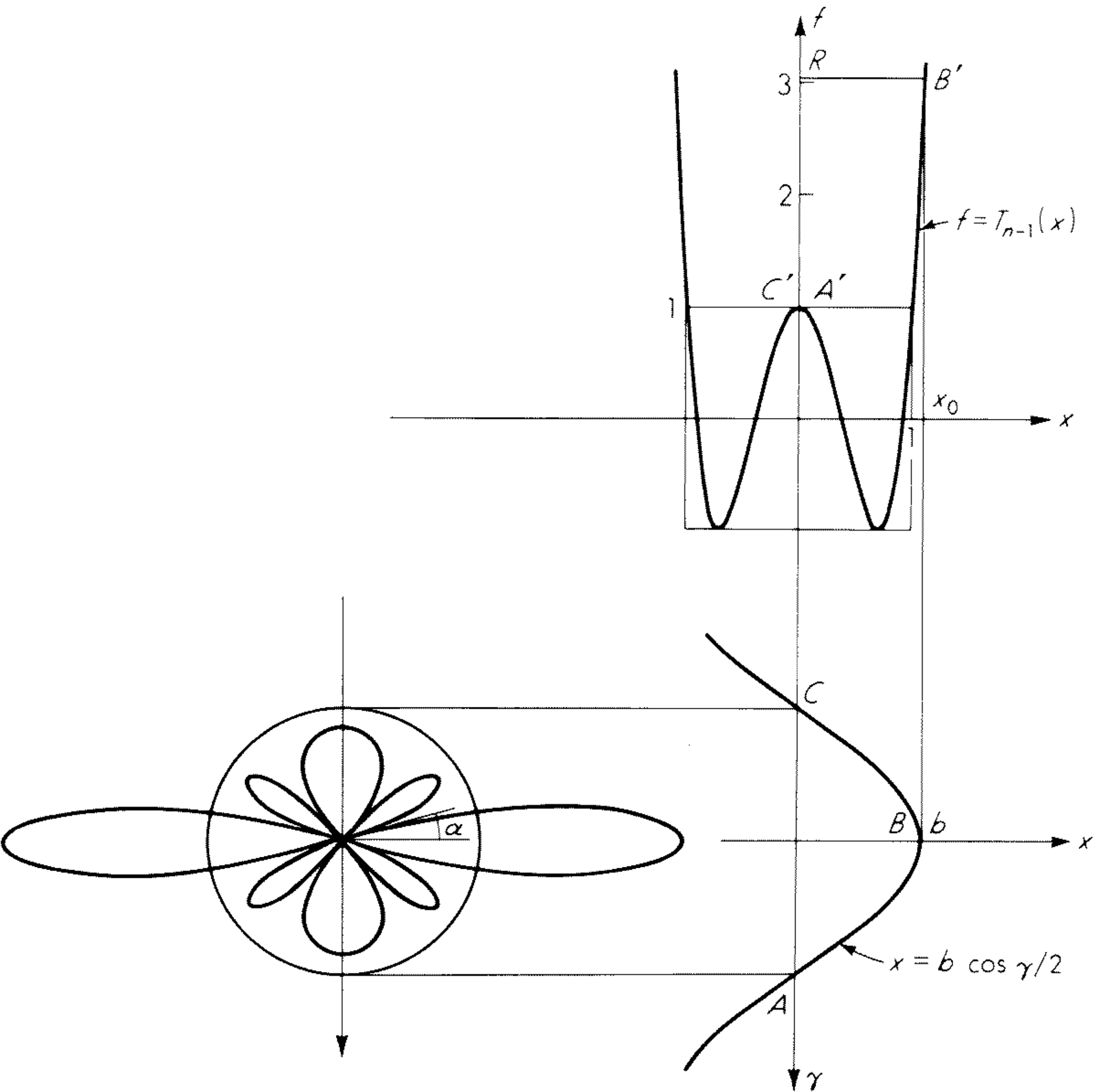


Fig. 5.25 Geometrical construction of array pattern for broadside Dolph-Chebyshev array with $d = \lambda_0/2$.

imum radiation takes place in the direction $\theta = \pi/2$. Therefore, we have $\delta = 0$. Assuming the number of elements n and the spacing k_0d to be fixed quantities, we first consider the case when the beam width 2α between the first nulls of the pattern is specified.

The first null of the pattern corresponds to the largest zero $x_1 = \cos[\pi/(2n - 2)]$ of the Chebyshev polynomial $T_{n-1}(x)$. This determines the parameter b in the transformation (5.89)

$$\begin{aligned} \cos \frac{\pi}{2n - 2} &= b \cos \frac{k_0d \cos (\pi/2 - \alpha)}{2} \\ b &= \frac{\cos [\pi/(2n - 2)]}{\cos [(k_0d \sin \alpha)/2]} \end{aligned} \tag{5.91}$$

With b known, the side-lobe level follows from $R = T_{n-1}(b)$, or, since $b > 1$,

$$R = \cosh [(n - 1) \cosh^{-1} b] \quad (5.92)$$

Equations (5.91) and (5.92) express the relation between the prescribed beam width 2α and the corresponding side-lobe level $1/R$, which, according to the optimum property of the Chebyshev polynomial, is as small as possible.

If, instead of the beam width, the side-lobe level $1/R$ is the required quantity, we must have

$$T_{n-1}(b) = R \quad R > 1$$

The solution to this algebraic equation follows directly from (5.86)

$$b = \cosh \left(\frac{1}{n-1} \cosh^{-1} R \right) \quad (5.93)$$

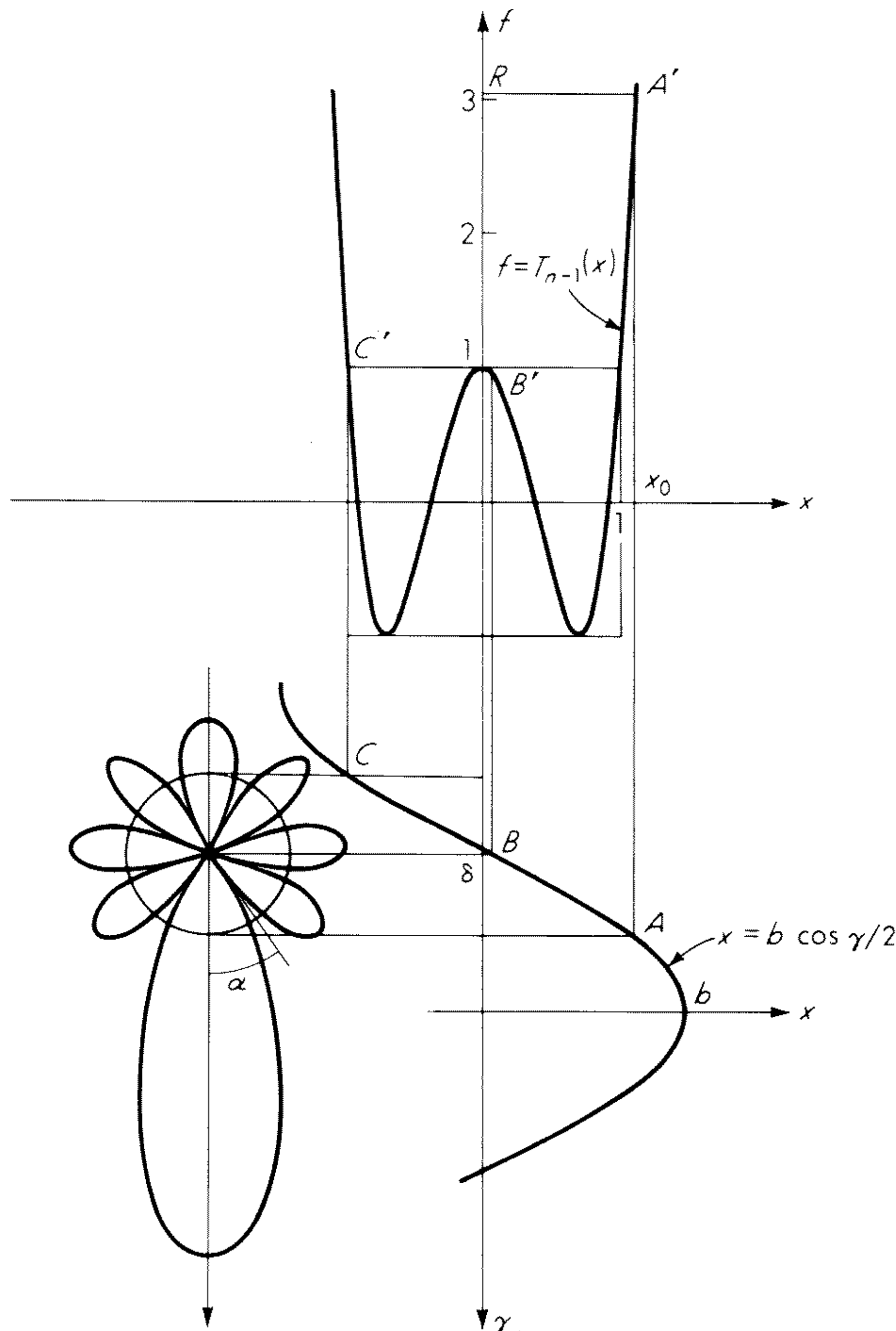


Fig. 5.26 Geometrical construction of array pattern for end-fire Dolph-Chebyshev array with $d = \lambda_0/4$.

The optimum beam width, which goes together with the specified side-lobe level, can be obtained by solving (5.91) for α .

Since $\delta = 0$, the points A' and C' in Fig. 5.25 coincide. Note that if the radius k_0d of the circle is so small that the abscissa x_3 of A' and C' is positive, the transformation (5.89) does not make full use of the Chebyshev polynomial. In this case it might well be that there exists a polynomial $P_{n-1}(x)$ of degree $n - 1$ and correct parity which passes through the point (x_0, R) , $R > 1$, and which yields a "better" array factor than the array factor produced by the Chebyshev polynomial. The reason for this is that $P_{n-1}(x)$ is restricted to stay within the bounds ± 1 only in the range $x_3 < |x| \leq 1$, where $x_3 > 0$, and may therefore cross the x axis at a point x_2 in the interval $x_1 < x_2 < x_0$, where x_1 is the largest zero of $T_{n-1}(x)$. Hence, for $d < \lambda_0/2$ the Chebyshev polynomial does not yield an optimum array factor for a broadside array. Note also that if the radius k_0d of the circle is taken so large that $x_0 \cos(k_0d/2) < -1$, additional main lobes will start to appear.

Exercise 5.14 Compare the beam width of the five-element broadside arrays with $d = \lambda_0/3$ and $R > 3.3$ generated by the polynomials $T_4(x) = 8x^4 - 8x^2 + 1$ and $P_4(x) = 14.2x^4 - 19.3x^2 + 5.56$.

We now turn to the end-fire array. Here the maximum radiation is in the direction $\theta = 0$. The geometrical construction is shown in Fig. 5.26. We must now have $x = x_0$ at $\theta = 0$ and $x = -1$ at $\theta = \pi$, respectively. The last condition ensures that the full number of complete side lobes is included in the array pattern. If the side-lobe level is specified, we have

$$x_0 = \cosh \left(\frac{1}{n-1} \cosh^{-1} R \right)$$

The transformation (5.89) yields

$$\begin{aligned} x_0 &= b \cos \frac{k_0d + \delta}{2} \\ -1 &= b \cos \frac{-k_0d + \delta}{2} \end{aligned}$$

with the solutions

$$b = \frac{[(1 + x_0^2) + 2x_0 \cos k_0d]^{1/2}}{\sin k_0d} \quad (5.94)$$

$$\delta = -2 \tan^{-1} \frac{(x_0 + 1) \cot(k_0d/2)}{x_0 - 1} \quad (5.95)$$

If instead the beam width is specified, we must solve the equations

$$\begin{aligned} \cos \frac{\pi}{2n-2} &= b \cos \frac{k_0d \cos \alpha + \delta}{2} \\ -1 &= b \cos \frac{-k_0d + \delta}{2} \end{aligned}$$

for b and δ .

Hereby the derivation is complete. The array factor is given by (5.90), and the excitation coefficients may be found in the same way as indicated in Exercise 5.13.

We conclude this section by remarking that the method described yields optimum array patterns for broadside arrays with interelement spacing not less than one-half wavelength. For end-fire arrays there is no lower limit for the interelement spacing. A discussion of the range of validity of the Dolph-Chebyshev approach to the design of optimum antenna arrays has been given by Pritchard.⁴⁷

Review of Dolph-Chebyshev Theory

As mentioned earlier, the idea of using the Chebyshev polynomials for the purpose of constructing linear arrays with the narrowest beam width for a prescribed side-lobe level, or with the lowest side-lobe level for a prescribed beam width, originated in the now classical paper by Dolph.⁴⁵ Dolph applied the transformation (5.89) in identifying the array factor for an n -element broadside array with the Chebyshev polynomial of order $n - 1$. However, as pointed out by Riblet,⁴⁸ the method of Dolph will lead to a nonoptimum design (as we have seen is the case for $d < \lambda_0/2$), if fewer than the maximum possible number of complete side lobes are included in the visible range. The task of obtaining the excitation coefficients by the process of identification of the array factor with a Chebyshev polynomial becomes rather involved as more elements are used. Dolph's expressions for the currents were simplified by Barbieri,⁴⁹ who used the orthogonality properties of the cosine functions to obtain them. Barbieri's formulas, however, required the subtraction of two (large) numbers of almost the same magnitude. Methods better adapted to computation, especially for arrays with a large number of elements, were given by Stegen,⁵⁰ Van der Maas,⁵¹ and Van der Maas and Gruenberg.⁵² In the last-mentioned paper the limiting cases for small side-lobe levels and for a large number of elements received special attention. The question of the directivity obtained was considered by Stegen.⁵³ Tables of excitation coefficients, directivities, and beam widths for broadside arrays have been published by Brown and Sharp.⁵⁴ Dolph's method was also used by Rhodes⁵⁵ to produce an end-fire pattern with a single main beam, but only for one specific element spacing. However, it was demonstrated by Pritchard⁴⁷ that the method of Dolph could be used for end-fire arrays also — even without any restrictions on the interelement spacing. The Dolph-Pritchard approach has been described in the preceding section. The directivity of optimum end-fire arrays was considered by Ma⁵⁶ and by Ma and Hyovalti.⁵⁷

The above-mentioned restriction for the broadside array was removed by Riblet,⁴⁸ who used the transformation $x = b \cos \gamma + c$ in connection with the Chebyshev polynomial $T_n(x)$ for a $(2n + 1)$ -element array. This approach, which is restricted to arrays with an odd number of elements, was extended by

DuHamel⁵⁸ to cover the end-fire case also. DuHamel's expressions for the excitation coefficients were rather complicated, and much effort has been devoted since then to their simplification. DuHamel showed that the problem of obtaining the excitation coefficients could be reduced to the determination of b_m in the expansion $T_n(bx + c) = \sum_{m=1}^n b_m T_m(x)$. An elegant matrix method of solving this problem was proposed by Herscovici.⁵⁹ Other methods were given by Salzer⁶⁰ and by Brown,^{61,62} who applied the orthogonality properties of the Chebyshev polynomials. Drane⁶³ derived a recurrence relation for the b_m coefficients, thereby simplifying the current expressions given previously by Salzer and Brown. A general approach to the design of arrays in which the ratio between beam width and side-lobe level is optimized and where all cases of end-fire, off-axis, and broadside radiation for arrays with an even as well as an odd number of elements are covered has been given by Pokrovskii.^{64,65} Numerical data, however, are not yet available.

Two-dimensional optimum arrays have been considered by Baklanov.⁶⁶

5.11 Optimization of Performance Indices

We conclude this chapter on uniformly spaced arrays by considering procedures for optimizing such array performance indices as the relative directivity and the efficiency index. These quantities were defined in Sec. 5.8.

One of the main purposes of dealing with arrays is to obtain large values of directivity, or gain. As we shall see, a theoretical maximum exists for the relative directivity of an array with a given element configuration. This upper limit is a function of the element type and spacing. For closely spaced arrays it may be considerably higher than the relative directivity obtained with the ordinary end-fire excitation or the Hansen-Woodyard excitation referred to earlier. Unfortunately, however, the current distributions which lead to these large relative directivities for closely spaced arrays simultaneously yield low values of the efficiency index. Arrays with such excitations are called *super-gain arrays*.

In this section we consider criteria for optimizing the efficiency index F and the relative directivity D_{rel} . Since these quantities cannot in general be maximized by the same set of excitation coefficients, the design of an array usually involves a compromise between them. Here, however, we consider the two optimizing criteria separately.

We shall need some of the basic array quantities expressed in the language of algebra.⁶⁷ As shown in Sec. 5.2, the array factor for an arbitrary array may be written

$$f(\theta, \phi) = \sum_{m=1}^n a_m e^{ju_m(\theta, \phi)}$$

where $u_m(\theta, \phi) = k_0(x_m \sin \theta \cos \phi + y_m \sin \theta \sin \phi + z_m \cos \theta)$ in the usual notation. By introducing the following complex vectors of n dimensions

$$\mathbf{a} = (a_1, a_2, \dots, a_n) \quad (5.96)$$

$$\mathbf{e} = [\exp(-ju_1), \exp(-ju_2), \dots, \exp(-ju_n)] \quad (5.97)$$

which we shall call respectively excitation vector and radiation vector, the array factor can be expressed as the complex scalar product

$$f = (\mathbf{a}, \mathbf{e}) = \mathbf{a} \cdot \mathbf{e}^* \quad (5.98)$$

The square of the modulus of the array factor can be written simply

$$|f|^2 = |(\mathbf{a}, \mathbf{e})|^2 \quad (5.99)$$

or, alternatively, as the hermitian quadratic form

$$|f|^2 = (\mathbf{a}, \mathbf{C} \cdot \mathbf{a}) \quad (5.100)$$

where \mathbf{C} is an $n \times n$ hermitian matrix with the elements $C_{ml} = C_{lm}^* = \exp(-ju_m) \exp(ju_l)$. The dot signifies the matrix product of \mathbf{C} with \mathbf{a} .

Exercise 5.15 By using the definition of the complex scalar product adopted here, that is, $(\mathbf{a}, \mathbf{b}) = \sum_{m=1}^{n-1} a_m b_m^*$, where b_m^* denotes the complex conjugate of b_m , show that (5.99) and (5.100) are equivalent.

The relative radiated power (5.76)

$$p_{\text{rad}} = \sum_{m=1}^n \sum_{l=1}^n a_m a_l^* r_{ml}$$

may be written as the positive definite hermitian form $(\mathbf{a}, \mathbf{R} \cdot \mathbf{a})$, where the elements of the matrix \mathbf{R} are the normalized mutual radiation resistances r_{ml} . Further,

$$\sum_{m=1}^n |a_m|^2 = (\mathbf{a}, \mathbf{a})$$

We now have from (5.79), (5.80), and (5.82), respectively,

$$D_{\text{rel}} = \frac{(\mathbf{a}, \mathbf{C} \cdot \mathbf{a})}{(\mathbf{a}, \mathbf{R} \cdot \mathbf{a})} \quad (5.101)$$

$$G_{\text{rel}} = \frac{(\mathbf{a}, \mathbf{C} \cdot \mathbf{a})}{(\mathbf{a}, \mathbf{R} \cdot \mathbf{a}) + r_{\text{loss}}(\mathbf{a}, \mathbf{a})} \quad (5.102)$$

$$F = \frac{(\mathbf{a}, \mathbf{C} \cdot \mathbf{a})}{(\mathbf{a}, \mathbf{a})} \quad (5.103)$$

whereby the relative directivity, relative gain, and the efficiency index have been written as ratios of hermitian forms in which the denominators are positive definite. On the basis of the expressions derived for D_{rel} and F , we shall now consider their optimization.

The Traveling-wave Theorems

The efficiency index F has been introduced in Sec. 5.8 in connection with considerations of the decrease in relative gain due to the presence of power losses in the elements. We found

$$\frac{1}{G_{\text{rel}}} = \frac{1}{D_{\text{rel}}} + \frac{r_{\text{loss}}}{F} \quad (5.104)$$

As seen from this formula, high values of F will diminish the influence of the (normalized) loss resistance.

Another interpretation can be given to F . Let us assume that we have synthesized an array which has a prescribed radiation pattern. In any physical realization we cannot expect to be able to establish precisely the designed values of element positions and excitation coefficients. They will contain small (random) errors. The effect of these on the relative directivity must be disclosed by a statistical analysis.

The numerator in the expression for D_{rel} is equal to the array factor absolute squared, or relative power pattern, of the array. Based on simple assumptions with regard to the nature of the errors, it has been shown⁶⁸ that the mean expected value $\langle (\mathbf{a}, \mathbf{C} \cdot \mathbf{a}) \rangle$ of the numerator is proportional to $(\mathbf{a}, \mathbf{C} \cdot \mathbf{a}) + \Delta^2(\mathbf{a}, \mathbf{a})$, where Δ^2 is a small number (an aggregate variance) describing the effect of both position and excitation errors. The effect of the errors is thus to add (small) positive numbers to the diagonal terms in the \mathbf{C} matrix. In other words, in the average (of a large number of sample arrays) an omnidirectional "background" pattern $\Delta^2(\mathbf{a}, \mathbf{a})$ is superimposed on the prescribed pattern $(\mathbf{a}, \mathbf{C} \cdot \mathbf{a})$. The extent to which the desired pattern dominates over the background pattern depends on Δ^2 and on $(\mathbf{a}, \mathbf{C} \cdot \mathbf{a})/(\mathbf{a}, \mathbf{a}) = F$.

Likewise, the effect on the denominator, which is equal to the relative radiated power, is to add positive numbers Δ^2 to the diagonal terms of the \mathbf{R} matrix. We then have

$$\langle D_{\text{rel}} \rangle = \frac{(\mathbf{a}, \mathbf{C} \cdot \mathbf{a}) + \Delta^2(\mathbf{a}, \mathbf{a})}{(\mathbf{a}, \mathbf{R} \cdot \mathbf{a}) + \Delta^2(\mathbf{a}, \mathbf{a})} \quad (5.105)$$

Obviously, for $D_{\text{rel}} \gg 1$, we may disregard the second term in the numerator in (5.105). We then have

$$\frac{1}{\langle D_{\text{rel}} \rangle} = \frac{1}{D_{\text{rel}}} + \frac{\Delta^2}{F} \quad (5.106)$$

which is of the same form as (5.104). An analogous expression for $1/\langle G_{\text{rel}} \rangle$ may be obtained by adding the term r_{loss}/F to the right-hand side of (5.106).

From the above remarks it is seen that the efficiency index is a measure of the reluctance† of the array radiation against element losses and random errors in element position and excitation coefficients. $F = F(\theta, \phi)$ has the same dependence on the direction in space as $|f(\theta, \phi)|^2$; its maximum value occurs in the direction (θ_0, ϕ_0) of the main beam. The magnitude of F in this direction depends on the particular set of excitation coefficients.

We now have motivation for considering the following optimization problem: For a given element configuration and main beam direction (θ_0, ϕ_0) , determine the set of excitation coefficients which will maximize $F(\theta_0, \phi_0)$ absolutely. The solution to this problem follows immediately from Schwartz's inequality $|(\mathbf{a}, \mathbf{e})| \leq |\mathbf{a}| |\mathbf{e}|$, where the equality sign is valid only when $\mathbf{a} = c\mathbf{e}$, where c is a constant. Hence

$$F \leq \frac{|\mathbf{a}|^2 |\mathbf{e}|^2}{|\mathbf{a}|^2} = |\mathbf{e}|^2 = n \quad (5.107)$$

where n is the number of elements. The excitation vector which yields the maximum value n is determined by $\mathbf{a} = c\mathbf{e}$, where c is an arbitrary constant.

This result can be formulated in the following *traveling-wave theorem I*: For any array the maximum efficiency index $F(\theta_0, \phi_0)$ is less than or equal to the number of elements. The particular excitation coefficients which yield the absolute maximum value n are proportional to the values at each element position of the field strength of a plane electromagnetic wave traveling across the array in the given main-beam direction (θ_0, ϕ_0) . The excitation indicated in this theorem is the so-called normal or ordinary excitation referred to earlier. In the sense described above this excitation is an optimum excitation.

We next consider the problem of maximizing the relative directivity D_{rel} of an arbitrary array in some specified direction (θ_0, ϕ_0) . The solution to this problem can also be found in a theorem from linear algebra: The maximum value that can be taken by a ratio of hermitian quadratic forms $D_{\text{rel}} = (\mathbf{a}, \mathbf{C} \cdot \mathbf{a}) / (\mathbf{a}, \mathbf{R} \cdot \mathbf{a})$, where the denominator is positive definite, is equal to the largest eigenvalue $\lambda = \lambda_0$ of the (extended) eigenvalue problem $\mathbf{C} \cdot \mathbf{a} = \lambda \mathbf{R} \cdot \mathbf{a}$. Hence, the maximum possible relative directivity that can be obtained in a given direction from an array with prescribed element positions is the largest solution $\lambda = \lambda_0$ to the determinantal equation $\det(\mathbf{C} - \lambda \mathbf{R}) = 0$. It can be shown (see Exercise 5.17) that of the n roots of the determinantal equation only one, λ_0 , differs from zero.

An excitation vector \mathbf{a} with which the maximum value of D_{rel} is actually obtained satisfies the characteristic equation $\mathbf{C} \cdot \mathbf{a} = \lambda_0 \mathbf{R} \cdot \mathbf{a}$. Since the elements of the matrix \mathbf{C} are of a form which is separated with respect to the indices, the corresponding eigenvector \mathbf{a} can be found almost by inspection and without

†Instead of the efficiency index F the reciprocal quantity $K = 1/F$ is often used. K is called the sensitivity factor.

any prior knowledge of λ_0 . Explicitly written, the characteristic equation is as follows

$$\sum_{l=1}^n e^{-ju_m(\theta_0, \phi_0)} e^{ju_l(\theta_0, \phi_0)} a_l = \lambda_0 \sum_{l=1}^n r_{ml} a_l \quad m = 1, 2, \dots, n$$

The last two factors under the summation sign on the left-hand side are independent of the index m . We therefore conclude that the unknown excitation coefficient a_l must satisfy the set of inhomogeneous linear equations

$$\sum_{l=1}^n r_{ml} a_l = ce^{-ju_m(\theta_0, \phi_0)} \quad m = 1, 2, \dots, n \quad (5.108)$$

$$\text{or} \quad \mathbf{R} \cdot \mathbf{a} = c\mathbf{e} \quad (5.109)$$

$$\mathbf{a} = c\mathbf{R}^{-1} \cdot \mathbf{e} \quad (5.110)$$

where c is an arbitrary constant. The quantity on the left-hand side of (5.108) is called the resistance voltage of the m th element and is equal to the voltage that would exist across the terminals of this element provided all mutual and self-reactances were canceled.

This result may be formulated in the following *traveling-wave theorem II*: For any array with n elements the relative directivity $D_{\text{rel}} \leq \lambda_0$, λ_0 being the

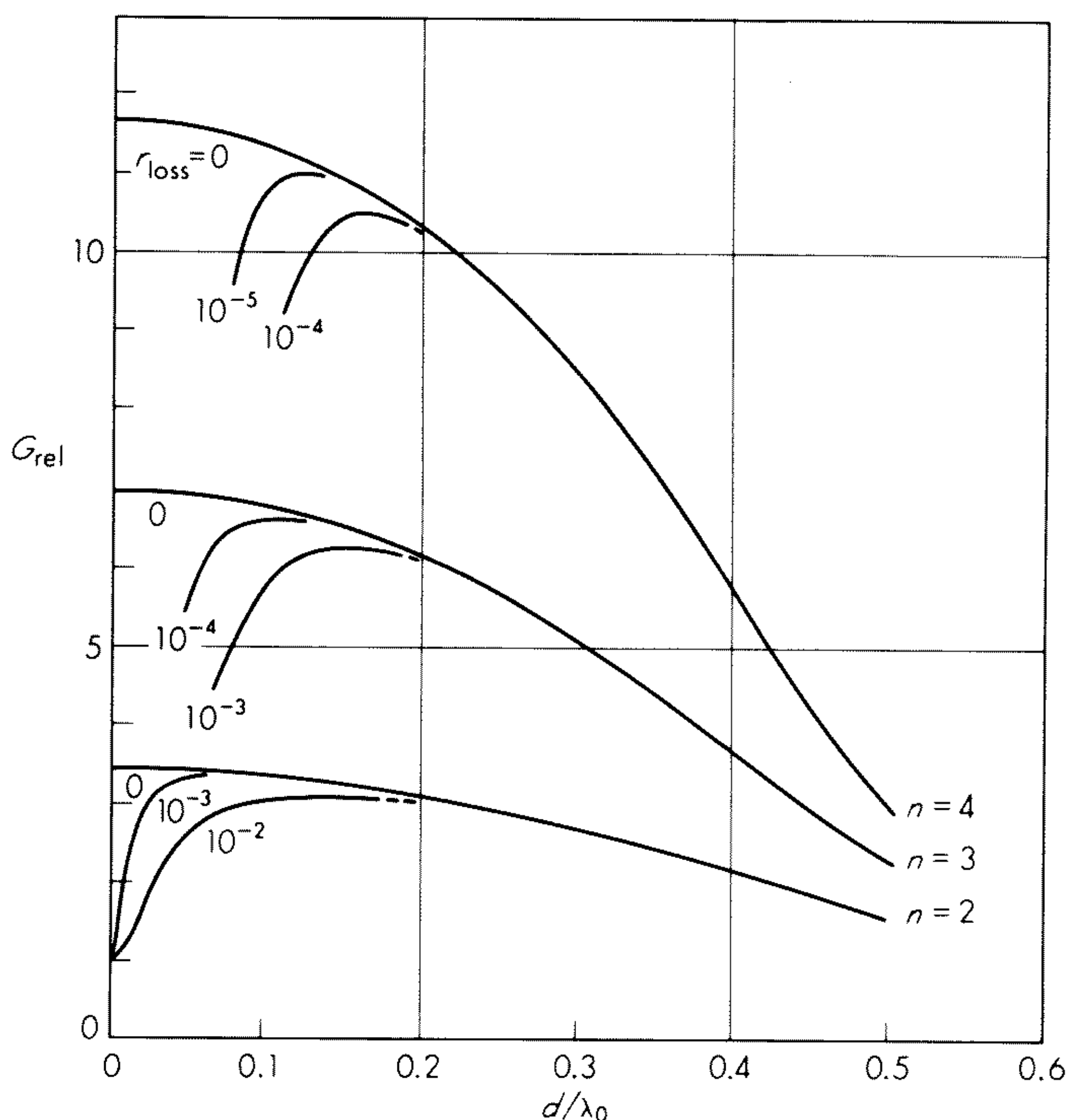


Fig. 5.27 Curves of maximum relative gain G_{rel} of two-, three-, and four-element equally spaced end-fire arrays of thin parallel half-wave dipoles with r_{loss} as a parameter.

largest eigenvalue of the eigenvalue problem $\mathbf{C} \cdot \mathbf{a} = \lambda \mathbf{R} \cdot \mathbf{a}$. The particular excitation coefficients which yield the maximum value λ_0 are determined by the condition that the resistance voltages across the terminals of the elements be proportional to the field strength of a plane electromagnetic wave traveling across the array in the given main beam direction (θ_0, ϕ_0) .

The excitation required for maximum gain may also be found from the theorem. To do this we need only add r_{loss} to the diagonal elements of \mathbf{R} in (5.109). Curves of optimum directivity and gain for end-fire arrays of two, three, and four thin parallel half-wave dipoles, obtained by the above method, are shown in Fig. 5.27.

Exercise 5.16 In order to illustrate the optimizing criteria considered above we now examine the simplest array possible, i.e., the two-element array. We assume the elements to be situated at $z = 0$ and $z = d$ on the z axis of a rectangular coordinate system. With the reference antenna at the origin we have $\mathbf{a} = [a_1, a_2]$ and $\mathbf{e} = [1, \exp(-ju_2)]$, where $u_2 = k_0 d \cos \theta$. Further

$$\mathbf{C} = \begin{bmatrix} 1 & \exp(ju_2) \\ \exp(-ju_2) & 1 \end{bmatrix} \quad \text{and} \quad \mathbf{R} = \begin{bmatrix} 1 & r \\ r & 1 \end{bmatrix}$$

where r denotes the normalized mutual radiation resistance between the antennas.

Show that the excitation corresponding to traveling-wave theorem I yields $F = 2$ and $D_{\text{rel}} = 1/(1 + r \cos u_2)$. Further, show that the excitation corresponding to traveling-wave theorem II yields $D_{\text{rel}} = 2(1 - r \cos u_2)/(1 - r^2)$, $F = (1 - r \cos u_2)/(1 + r^2)$ and $\mathbf{a} = [(1 - r \exp(-ju_2))/(1 - r^2), (\exp(-ju_2) - r)/(1 - r^2)]$.

Exercise 5.17 By performing row operations (or otherwise), show that $\lambda = 0$ is an $(n - 1)$ -double root of the determinantal equation $\det(\mathbf{C} - \lambda \mathbf{R}) = 0$.

Exercise 5.18 Show that the maximum relative directivity of an array is given by $D_{\text{rel}} = \lambda_0 = (\mathbf{e}, \mathbf{R}^{-1} \cdot \mathbf{e})$.

Review of Optimization Theory

The first solution to an optimization problem for antenna arrays was given by Uzkov,⁶⁹ who observed that if there is no mutual power exchange between the antennas in an array, i.e., if $r_{ml} = 0$ for $m \neq l$, the maximum directivity is equal to the sum of the directivities of the individual radiators (see Fig. 5.28). In arrays of isotropic elements, for example, we have $r_{ml} = \delta_{ml}$ when the distances between the elements are multiples of $\lambda_0/2$. In this case $D_{\text{rel}} = F$; hence from traveling-wave theorem I, the maximum value is n . (Note that here the uniform and the optimum excitation coincide.) For other spacings the maximum value of D_{rel} may be obtained by an orthogonalization process. For $d \rightarrow 0$ a maximum end-fire relative directivity of n^2 is obtained. This represents the absolute maximum of the relative directivity that can be obtained with arrays. Bloch, Medhurst, and Pool⁷⁰ solved the same problem by a variational principle and obtained explicit expressions for the maximum relative directivity of

arrays of arbitrary spacings. The formulation of the condition that the currents must satisfy in order to yield the maximum D_{rel} was given by these authors as the traveling-wave theorem II discussed in the preceding subsection. Numerical calculations for end-fire arrays of half-wave dipoles based upon the

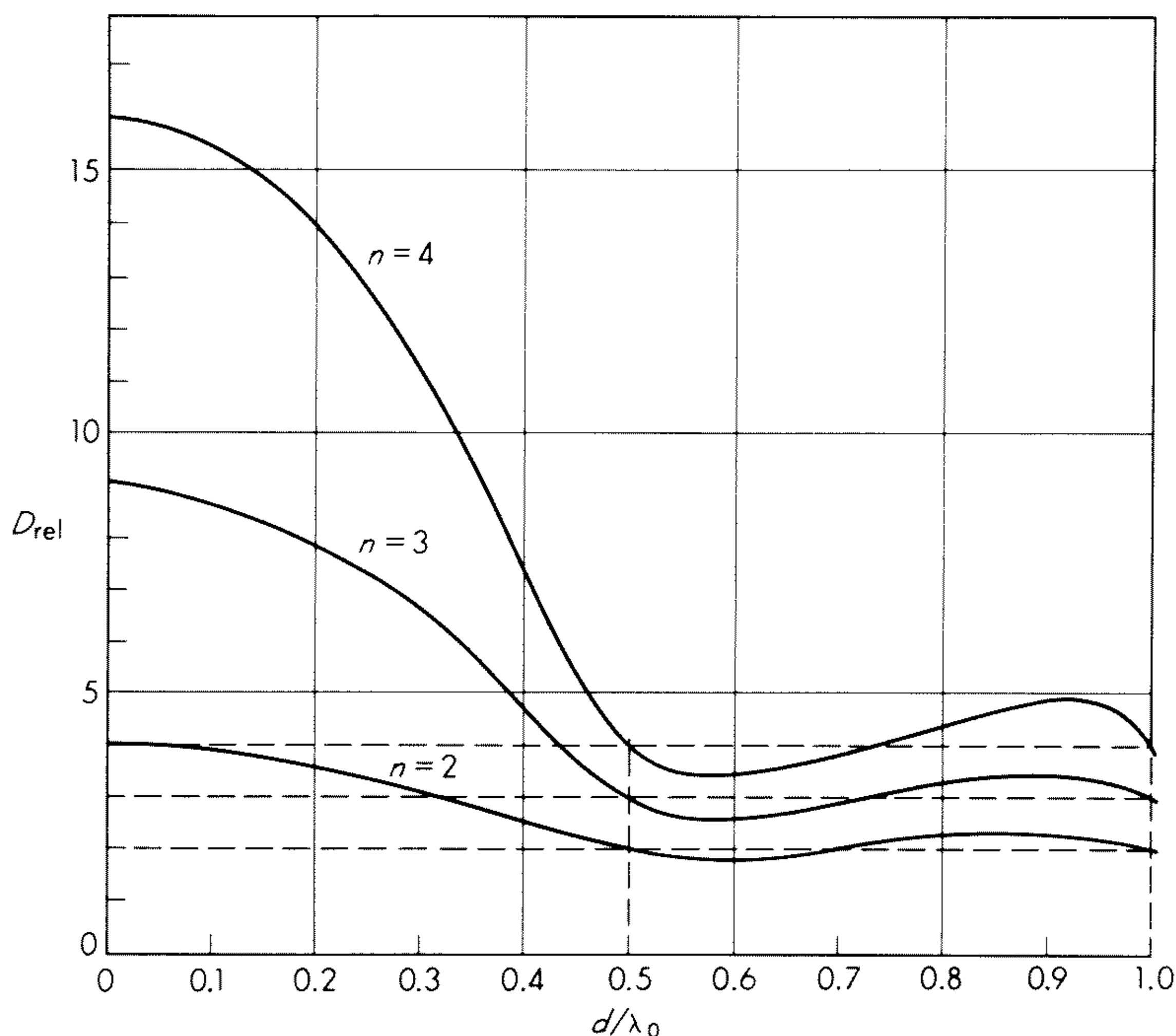


Fig. 5.28 Maximum end-fire directivity of equally spaced isotropic elements. (After Uzkov.⁶⁹)

mentioned paper were reported by Stearns.⁷¹ The traveling-wave theorem I as well as the solution to the problem of optimizing the relative directivity subject to the constraint that the efficiency index, or, alternatively, the Q factor, defined by $Q = (\mathbf{a}, \mathbf{a}) / (\mathbf{a}, \mathbf{R} \cdot \mathbf{a}) = D_{\text{rel}} / F$, take a prescribed value was given by Gilbert and Morgan⁶⁸ and, independently, by Uzsoky and Solymár.⁷² The problem considered by the above writers is of importance because it estimates construction requirements in a quantitative manner.⁷³ The statistical analysis of the influence of random errors on array parameters on which the above papers (and the preceding subsection of this chapter) are based has recently been generalized considerably.⁷⁴

In an interesting paper, Bloch²⁴ gave an independent proof of the traveling-wave theorem II by applying to the equivalent network of the array (considered as a receiving antenna) a generalization to n -pair terminal networks of the well-known condition $Z_L = Z^*$ for the maximum power transfer from a two-terminal active network with internal impedance Z to a load Z_L .

The uniqueness of the solution of Bloch, Medhurst, and Pool to the optimum-directivity problem follows, as shown by Krupitskii,⁷⁵ directly from the fact that all eigenvalues of $\mathbf{C} - \lambda \mathbf{R}$ are zero except $\lambda_0 = \max (D_{\text{rel}})$ (see Exercise 5.17).

The above-cited papers on optimization of the performance of arbitrary antenna arrays have been followed by many papers dealing with these problems. A bibliography of superdirective antennas covering the period until 1960 has been given by Bloch et al.⁷⁶ Later work includes investigations of optimum broadside arrays of collinear and parallel short dipoles,²⁸ optimum arrays of nonidealized physical elements,²⁷ and optimum circular and elliptical arrays.⁷⁷

Another aspect of (receiving) array performance that can be treated by the optimization techniques described in this section is the signal-to-noise problem also considered by Gilbert and Morgan and, in more detail, by Kritikos.⁷⁸ The signal-to-noise ratio can be expressed as the quotient of hermitian quadratic forms $(\mathbf{a}, \mathbf{C} \cdot \mathbf{a}) / (\mathbf{a}, \mathbf{A} \cdot \mathbf{a})$, where the denominator represents relative noise power. The elements a_{ml} of \mathbf{A} are determined from

$$a_{ml} = \frac{1}{4\pi} \int_{4\pi} e^{-j\mathbf{u}_m \cdot \mathbf{u}_l} t(\theta, \phi) d\Omega$$

where the weight function $t(\theta, \phi)$ is the normalized noise temperature distribution and the other symbols have their usual meaning. This optimization problem can also be solved with the constraint that the Q factor is prescribed. This was done in a paper by Lo, Lee, and Lee,⁷⁹ who also gave explicit solutions to several other optimization problems for arrays.

Optimization of arrays for broadband signals or signals with other frequency spectra can be carried out by the use of principles similar to those used above. This problem has been considered by Sharpe and Crane.⁸⁰

We conclude this section by stressing that the formulation and solution of array-optimization problems in the above manner provide no guarantee in regard to the details of the radiation pattern. The optimization criteria are all of an integrated type. Optimization problems with what we might call differential criteria are far more difficult. A simple example of the latter type of optimization problem would be to maximize the directivity of an array in some given direction subject to the condition that the radiation in all other directions outside the main lobe is below a prescribed level. This problem has not yet been treated in the literature.

PROBLEMS

5.1 Determine the horizontal and the vertical radiation patterns for:

- a. A four-element broadside array of collinear half-wave dipoles
- b. A four-element end-fire array of parallel half-wave dipoles

In both cases $d = \frac{1}{2}\lambda_0$.

5.2 The antennas 1 to 4 are similar and similarly orientated and located at the points

$(d,0)$, $(0,d)$, $(-d,0)$ and $(0,-d)$ in the xy plane. Neighboring antennas are excited in opposite phases with currents of the same magnitude. For $d = \frac{3}{8}\lambda_0$ find and plot the absolute value of the array factor:

- a. By means of the general formula (5.10)
- b. By means of the method of pattern multiplication
- c. By considering the array as two crossed two-element arrays
- d. By considering the array as a ring array

5.3 An antenna system is constructed from four short dipoles tangential to the circle $x^2 + y^2 = 1$ and located at the intersections of the circle and the x and y axes. The dipoles are oriented in accordance with the positive sense of the circle. They are fed by currents of the same magnitude while the phase increases by 90° from dipole to dipole in the positive sense of the circle. Find in a spherical coordinate system the far-field components of the electrical field from this antenna system.

5.4 Find the directivity D of an n -element array of:

- a. Collinear short dipoles
- b. Parallel short dipoles

with spacing d and phase progression constant δ .

Answer:

$$D = \frac{|f(\theta)g(\theta,\phi)|^2}{a_0 + \frac{2}{n^2} \sum_{m=1}^{n-1} \frac{n-m}{mk_0d} |a_1 \sin mk_0d + a_2 \cos mk_0d| \cos m\delta}$$

where

Elements	$g^2(\theta,\phi)$	a_0	a_1	a_2
Isotropic	1	$\frac{1}{n}$	1	0
Collinear dipoles . . .	$\sin^2 \theta$	$\frac{2}{3n}$	$\frac{2}{(mk_0d)_2}$	$-\frac{2}{mk_0d}$
Parallel dipoles	$1 - \sin^2 \theta \cos^2 \phi$	$\frac{2}{3n}$	$1 - \frac{1}{(mk_0d)^2}$	$\frac{1}{mk_0d}$

The case of an isotropic element has been included for comparison.

5.5 As shown in the text, the maximum geometrical directivity of a two-element array is $D_f^0 = n^2 = 4$. This maximum is achieved with a uniform excitation for $\delta \rightarrow -\pi$ and simultaneously $k_0d \rightarrow 0$. From a study of the behavior along a small circle in the $k_0d - \delta$ plane with its center at $(k_0d,\delta) = (0,-\pi)$ determine the constraint between δ and k_0d which for $k_0d \rightarrow 0$ yields the desired result.

Answer: $\delta = \frac{1}{3}k_0d - \pi$.

5.6 For an n -element binomial array of isotropic sources $d = \frac{1}{4}\lambda_0$

- a. Show that the maximum geometrical directivity is independent of δ and given by

$$D_f^0 = \frac{2n-1}{4} \frac{\Gamma(n)\Gamma(1/2)}{\Gamma(n+1/2)}$$

where $\Gamma(x+1) = x\Gamma(x) = x!$ and $\Gamma(1/2) = \sqrt{\pi}$

- b. Find D_f^0 for $n = 6$.

5.7 By the Z -transform method compute the array factor for a linear equispaced array with the current distribution function

a. $a(z) = \cos hz$

b. $a(z) = hz$

where h is a real constant.

5.8 The elements of a two-element array are located at the points $(d/2, 0, 0)$ and $(-d/2, 0, 0)$ in a rectangular coordinate system xyz . The elements are assumed to be parallel to the z axis, so that their radiation pattern $g(\theta)$ is a function of the polar angle only. By equating the input power, as computed from terminal quantities, to the radiated power, as computed from far-field quantities, derive the following formula for the mutual radiation resistance between the elements

$$r_{12} = \frac{1}{2} \int_0^\pi |g(\theta)|^2 J_0(k_0 d \sin \theta) \sin \theta d\theta$$

Hint: Use the formula $J_0(\alpha) = \frac{1}{2\pi} \int_0^{2\pi} \cos(\alpha \cos v) dv$.

5.9 In a uniformly spaced linear array a uniform current distribution with the phase constant $\delta = -k_0 d - \delta_0$ is assumed. Show that, for this current distribution, which for $\delta_0 = 0$ and $\delta_0 = \pi/n$ yields the normal excitation and the Hansen-Woodyard excitation, respectively, the efficiency index is given by

$$F = \frac{1}{n} \left[\frac{\sin(n\delta_0/2)}{\sin(\delta_0/2)} \right]^2$$

for all values of the element spacing.

5.10 Show that, for an arbitrary array, the maximum relative directivities obtainable in the direction (θ_0, ϕ_0) and in the opposite direction $(\pi - \theta_0, \phi_0 + \pi)$ are equal.

5.11 By using the expressions derived in Exercise 5.16 for the optimum relative directivity and the efficiency index of a two-element end-fire array, compute the limiting values of D_{rel} and F for $d \rightarrow 0$. Assume isotropic elements with $r_{12} = \sin(k_0 d)/k_0 d$. Answer: $D_{\text{rel}} = 4$, $F = 0$.

REFERENCES

1. Hansen, R. C. (ed.): "Microwave Scanning Antennas," vol. II, "Array Theory and Practice," Academic Press Inc., New York, 1966.
2. Sterba, E. J.: Theoretical and Practical Aspects of Directional Transmitting Systems, *Proc. IRE*, vol. 19, pp. 1184-1215, July, 1931.
3. Whittaker, E. T., and G. N. Watson: "A Course of Modern Analysis," p. 170, Cambridge University Press, London, 1958.
4. Hansen, W. W., and J. R. Woodyard: A New Principle in Directional Antenna Design, *Proc. IRE*, vol. 26, pp. 333-45, March, 1938.
5. Schelkunoff, S. A.: A Mathematical Theory of Linear Arrays, *Bell System Tech. J.*, vol. 22, pp. 80-107, 1943.
6. Taylor, T. T., and J. R. Whinnery: Applications of Potential Theory to the Design of Linear Arrays, *J. Appl. Phys.*, vol. 22, pp. 19-29, January, 1951.
7. Cheng, D. K., and M. T. Ma: A New Mathematical Approach for Linear Array Analysis, *IRE Trans. Antennas Propagation*, vol. AP-8, pp. 255-259, May, 1960.
8. Jury, E. I.: "Theory and Application of the Z -transform Method," John Wiley & Sons, Inc., New York, 1964.

9. Christiansen, P. L.: On the Closed Form of the Array Factor for Linear Arrays, *IEEE Trans. Antennas Propagation*, vol. AP-11, p. 198, March, 1963.
10. Page, H.: Ring Aerial Systems, *Wireless Engr.*, pp. 308–315, October, 1948.
11. Knudsen, H. L.: Bidrag til Teorien for Antennesystemer med Hel eller Delvis Rotationssymmetri (Contribution to the Theory of Antennas with Complete or in Part Rotational Symmetry), I Kommission hos Teknisk Forlag, Copenhagen, Denmark, 1953.
12. Knudsen, H. L.: Radiation from Ring Quasi Arrays, *IRE Trans. Antennas Propagation*, vol. AP-4, pp. 452–72, July, 1956.
13. Watson, G. N.: "A Treatise on the Theory of Bessel Functions," Cambridge University Press, London, 1962.
14. Chu, Ta-Shing: On the Use of Uniform Circular Arrays to Obtain Omnidirectional Patterns, *IRE Trans. Antennas Propagation*, vol. AP-7, pp. 436–438, October, 1959.
15. Knudsen, H. L.: The Necessary Number of Elements in a Directional Ring Aerial, *J. Appl. Phys.*, vol. 22, pp. 1299–1306, November, 1951.
16. Simpson, T. L., and J. D. Tillmann: Parasitic Excitation of Circular Antenna Arrays, *IRE Trans. Antennas Propagation*, vol. AP-9, pp. 263–267, May, 1961.
17. Stearns, C. O., and A. C. Stewart: An Investigation of Concentric Ring Antennas with Low Sidelobes, *IEEE Trans. Antennas Propagation*, vol. AP-13, pp. 856–863, November, 1965.
18. Lee, S. W., and Y. T. Lo: On the Pattern Function of Circular Arc Arrays, *IEEE Trans. Antennas Propagation*, vol. AP-13, pp. 649–650, July, 1965.
19. Lo, T. Y., and H. C. Hsuan: An Equivalence Theory between Elliptical and Circular Arrays, *IEEE Trans. Antennas Propagation*, vol. AP-13, pp. 247–256, March, 1965.
20. Carter, P. S.: Circuit Relations in Radiating Systems and Applications to Antenna Problems, *Proc. IRE*, vol. 20, pp. 1004–1041, June, 1932.
21. King, R. W. P., and S. S. Sandler: The Theory of Broadside Arrays, *IEEE Trans. Antennas Propagation*, vol. AP-12, pp. 269–75, May, 1964.
22. King, R. W. P., and S. S. Sandler: The Theory of Endfire Arrays, *IEEE Trans. Antennas Propagation*, vol. AP-12, pp. 276–280, May, 1964.
23. Hines, J. N., V. H. Rumsey, and T. E. Tice: On the Design of Arrays, *Proc. IRE*, vol. 42, pp. 1262–1267, August, 1954.
24. Bloch, A.: *N*-terminal Networks, *Wireless Engr.*, vol. 33, pp. 295–300, December, 1956.
25. Larsen, T.: Reflector Arrays, *IEEE Trans. Antennas Propagation*, vol. AP-14, pp. 689–693, November, 1966.
26. Appel-Hansen, J.: A Van Atta Reflector Consisting of Half-wave Dipoles, *IEEE Trans. Antennas Propagation*, vol. AP-14, pp. 694–700, November, 1966.
27. Harrington, R. F.: Antenna Excitation for Maximum Gain, *IEEE Trans. Antennas Propagation*, vol. AP-13, pp. 896–903, November, 1965.
28. Tai, C. T.: The Optimum Directivity of Uniformly Spaced Broadside Arrays of Dipoles, *IEEE Trans. Antennas Propagation*, vol. AP-12, pp. 447–454, July, 1964.
29. Stearns, C. O.: Mutual Impedances between Parallel, Side-by-Side, Infinitesimally Thin, Half-wave Dipoles, *Natl. Bur. Std. (U.S.) Rept.* 6798, September, 1961.
30. Berndt, W.: Amplituden, Abstands und Phasenbedingungen bei Antennenkombinationen, *Hochfrequenz Elektroakustik*, vol. 44, no. 1, pp. 23–28, July, 1934.
31. Wolff, I.: Determination of the Radiating System Which Will Produce a Specified Directional Characteristic, *Proc. IRE*, vol. 25, pp. 630–643, May, 1937.
32. Jordan, E. C.: "Electromagnetic Waves and Radiating System," Prentice-Hall, Inc., Englewood Cliffs, N.J., 1950.
33. Silver, S. (ed.): "Microwave Antenna Theory and Design," M.I.T. Radiation Laboratory Series, vol. 12, chap. 9, McGraw-Hill Book Company, New York, 1949.
34. Jaekle, W. G.: Antenna Synthesis by Weighted Fourier Coefficients, *IEEE Trans. Antennas Propagation*, vol. AP-12, pp. 369–370, May, 1964.

35. Simon, J. C.: Application of Periodic Functions Approximation to Antenna Pattern Synthesis and Circuit Theory, *IRE Trans. Antennas Propagation*, vol. AP-4, pp. 429-440, July, 1956.
36. Fröberg, C. E.: "Introduction to Numerical Analysis," Addison-Wesley Publishing Company, Inc., Reading, Mass., 1966.
37. Ma, M. T.: Applications of Bernstein Polynomials and Interpolation Theory to Linear Array Synthesis, *IEEE Trans. Antennas Propagation*, vol. AP-12, pp. 668-677, November, 1964.
38. Jagermann, D.: Cosine Sum Approximation and Synthesis of Array Antennas, *Bell System Tech. J.*, vol. 44, pp. 1761-1777, October, 1965.
39. Michelson, R. A., and J. W. Schomer: A Three Parameter Antenna Pattern Synthesis Technique, *Microwave J.*, vol. 8, pp. 88-94, September, 1965.
40. Garbacz, R. J.: Modal Expansions for Resonance Scattering Phenomena, *Proc. IRE*, vol. 53, pp. 856-865, August, 1965.
41. Butler, J. K., and H. Unz: Optimization of Beam Efficiency and Synthesis of Non-uniformly Spaced Arrays, *Proc. IEEE*, vol. 54, pp. 2007-2008, December, 1966.
42. Fel'd, Ya. N., and L. D. Bakhrakh: Present State of Antenna Synthesis Theory, *Radio Eng. Electron. Phys.*, vol. 8, pp. 163-179, February, 1963.
43. Hoffman, M.: The Utility of the Array Pattern Matrix for Linear Array Computations, *IRE Trans. Antennas Propagation*, vol. AP-9, pp. 97-100, January, 1961.
44. Pokrovskii, V. L.: A General Method of Determining the Optimum Distribution for Linear Antennas, *Soviet Phys.*, vol. 6, pp. 435-436, November, 1961.
45. Dolph, C. L.: A Current Distribution for Broadside Arrays Which Optimizes the Relationship between Beam Width and Side-lobe Level, *Proc. IRE*, vol. 34, pp. 335-348, June, 1946.
46. Tables of Chebyshev polynomials, *Natl. Bur. of Std. (U.S.) Appl. Math. Ser. 9*, 1952.
47. Pritchard, R. L.: Discussion on Optimum Patterns for Endfire Arrays, *IRE Trans. Antennas Propagation*, vol. AP-3, pp. 40-43, January, 1955.
48. Riblet, H. J.: Discussion on "A Current Distribution for Broadside Arrays Which Optimizes the Relationship between Beam Width and Side Lobe Level," *Proc. IRE*, vol. 35, pp. 489-492, May, 1947.
49. Barbieri, D.: A Method for Calculating the Current Distribution of Tschebyscheff Arrays, *Proc. IRE*, vol. 40, pp. 78-82, January, 1952.
50. Stegen, R. J.: Excitation Coefficients and Beamwidth of Tchebycheff Arrays, *Proc. IRE*, vol. 41, pp. 1671-1674, November, 1953.
51. Van der Maas, G. J.: A Simplified Calculation for Dolph-Tchebycheff Arrays, *J. Appl. Phys.*, vol. 25, pp. 121-124, January, 1954.
52. Van der Maas, G. J., and H. Gruenberg: Note on a Simplified Calculation for Dolph-Tchebycheff Arrays, *J. Appl. Phys.*, vol. 27, pp. 962-963, August, 1956.
53. Stegen, R. J.: Gain of Tchebyscheff Arrays, *IRE Trans. Antennas Propagation*, vol. AP-8, pp. 629-631, November, 1960.
54. Brown, L. B., and G. A. Sharp: "Tschebyscheff Antenna Distribution, Beamwidth, and Gain Tables," Naval Ordnance Laboratory, Corona, 1958.
55. Rhodes, D. R.: The Optimum Linear Array for a Single Main Beam, *Proc. IRE*, vol. 41, pp. 793-794, June, 1953.
56. Ma, M. T.: Directivity of Uniformly Spaced Optimum Endfire Arrays with Equal Sidelobes, *Radio Sci. J. Res. Natl. Bur. Std. (U.S.)*, vol. 69D, no. 9, pp. 1249-1255, September, 1965.
57. Ma, M. T., and D. C. Hyovalti: A Table of Radiation Characteristics for Uniformly Spaced Optimum Endfire Arrays with Equal Sidelobes, *Natl. Bur. Std. (U.S.), Monograph 95*, December, 1965.

58. DuHamel, R. H.: Optimum Patterns for Endfire Arrays, *Proc. IRE*, vol. 41, pp. 652–659, May, 1953.
59. Herscovici, S.: Calcul des Réseaux Linéaires Produisant le Diagramme de Rayonnement le Plus Avantageux, *Ann. Radioélec.*, pp. 352–359, October, 1954.
60. Salzer, H. E.: Note on the Fourier Coefficients for Chebyshev Patterns, *Proc. Inst. Elec. Engrs. (London)*, vol. 103C, pp. 286–288, February, 1956.
61. Brown, J. L., Jr.: A Simplified Derivation of the Fourier Coefficients for Chebyshev Patterns, *Proc. Inst. Elec. Engrs. (London)*, vol. 105C, pp. 167–168, March, 1958.
62. Brown, J. L., Jr.: On the Determination of Excitation Coefficients for a Tchebycheff Pattern, *IRE Trans. Antennas Propagation*, vol. AP-10, pp. 215–216, March, 1962.
63. Drane, C. J.: Derivation of Excitation Coefficients for Chebyshev Arrays, *Proc. Inst. Elec. Engrs. (London)*, vol. 110, pp. 1755–1758, October, 1963.
64. Pokrovskii, V. L.: The Design of Optimum Aerials Radiating Along the Axis, *Radio Eng. Electron.*, vol. 2, pp. 28–35, 1957.
65. Pokrovskii, V. L.: Optimum Linear Aerials Radiating at a Given Angle to the Axis, *Radio Eng. Electron.*, vol. 2, pp. 61–69, 1957.
66. Baklanov, Y. V.: On the Theory of Optimal Linear Antennas, *Radio Eng. Electron. Phys.*, vol. 7, pp. 857–859, May, 1962.
67. Gel'fand, I. M.: "Lectures on Linear Algebra," Interscience Publishers, Inc., New York, 1961.
68. Gilbert, E. N., and S. P. Morgan: Optimum Design of Directive Antenna Arrays Subject to Random Variations, *Bell System Tech. J.*, vol. 34, pp. 637–663, May, 1955.
69. Uzkov, A. I.: An Approach to the Problem of Optimum Directive Antenna Design, *Compt. Rend. (Doklady) Acad. Sci. U.S.S.R.*, vol. 53, pp. 35–38, 1946.
70. Bloch, A., R. G. Medhurst, and S. D. Pool: A New Approach to the Design of Super-directive Aerial Arrays, *Proc. Inst. Elec. Engrs. (London)*, part 3, vol. 100, pp. 303–314, September, 1953.
71. Stearns, C. O.: Computed Performance of Moderate Size Super-gain Antennas, *IEEE Trans. Antennas Propagation*, vol. AP-14, pp. 241–242, March, 1966.
72. Uzsoky, M., and L. Solymár: Theory of Super-directive Linear Arrays, *Acta Phys. (Budapest)*, vol. 6, pp. 185–204, 1956.
73. Smaryshev, M. D.: Maximizing the Directive Gain of an Antenna Array, *Radio Eng. Electron. Phys.*, vol. 9, pp. 1399–1400, September, 1964.
74. Howard, J. E.: Statistical Patterns of a General Array, *IEEE Trans. Antennas Propagation*, vol. AP-15, pp. 60–65, January, 1967.
75. Krupitskii, É. I.: On the Maximum Directivity of Antennas Consisting of Discrete Radiators, *Soviet Phys. "Doklady" (English Transl.)*, vol. 7, no. 3, pp. 257–259, September, 1962.
76. Bloch, A., R. G. Medhurst, S. D. Pool, and W. E. Kock: Superdirectivity, *Proc. IRE*, vol. 48, p. 1164, June, 1960.
77. Cheng, D. K., and F. I. Tseng: Maximization of Directive Gain for Circular and Elliptical Arrays, *Proc. IEE*, vol. 114, pp. 589–594, May, 1967.
78. Kritikos, H. N.: Optimal Signal-to-Noise Ratio for Linear Arrays by the Schwartz Inequality, *J. Franklin Inst.*, vol. 276, pp. 295–304, October, 1963.
79. Lo, Y. T., S. W. Lee, and Q. H. Lee: Optimization of Directivity and Signal-to-Noise Ratio of an Arbitrary Antenna Array, *Proc. IEEE*, vol. 54, pp. 1033–1045, August, 1966.
80. Sharpe, C. B., and R. B. Crane: Optimization of Linear Arrays for Broad Band Signals, *IEEE Trans. Antennas Propagation*, vol. AP-14, pp. 422–427, July, 1966.

CHAPTER 6

NONUNIFORM ARRAYS

Merrill I. Skolnik

6.1 Introduction

Most array antennas employ equal spacings between adjacent elements. The theory is well understood, and convenient analytical procedures are available for antenna design and radiation pattern synthesis. It is possible, however, to operate array antennas with nonuniform, or unequal, spacings between adjacent elements. The element spacings provide another parameter, in addition to the amplitude and phase of the element current, with which to control the radiation pattern. This chapter is concerned with arrays of this type.

Following this introductory section the various methods available for synthesizing radiation patterns with unequally spaced elements are briefly described (Sec. 6.2). The specific technique known as *density tapering* is selected for detailed discussion. In this method, the density of unequally spaced, equal-amplitude elements at any point within the aperture is made proportional to the amplitude that a conventional array of equally spaced elements would have at the same point if designed with an amplitude illumination taper (Sec. 5.5). A deterministic method of density-taper design is discussed in Sec. 6.3, and a statistical method in Sec. 6.4. The analysis of an array with randomly missing elements (such as might occur because of catastrophic failure) is similar to that of the unequally spaced array and is therefore included in this chapter in Sec. 6.5. The chapter closes with a discussion of the effects of phase and amplitude errors in conventional arrays, Sec. 6.6. This section is included because the analysis is similar to that of the statistical density taper and because an array with random errors is one which can be called nonuniform.

The pattern of a linear array of M identical isotropic radiating elements with arbitrary spacing between elements and with equal current at each element may be written.

$$|f(u)| = \left[\left(\sum_{n=1}^M \cos 2\pi\xi_n u \right)^2 + \left(\sum_{n=1}^M \sin 2\pi\xi_n u \right)^2 \right]^{1/2} \quad (6.1)$$

where $u = \sin \theta$, θ is the angle measured with respect to the normal to the array, and ξ_n is the distance of the n th element, measured in wavelengths, with

respect to some reference.[†] The array is assumed located along the x axis, and since the pattern has rotational symmetry about the array axis, the angle variable is chosen for convenience as $u = \sin \theta$ instead of $u = \sin \theta \cos \phi$. This is equivalent to looking at the pattern in the xz or $\phi = 0$ plane, which is sufficient in view of the rotational symmetry. In general, this expression, called the *array factor* or *space factor*, is difficult to handle analytically. For convenience it is usually assumed that the elements are arranged symmetrically in pairs

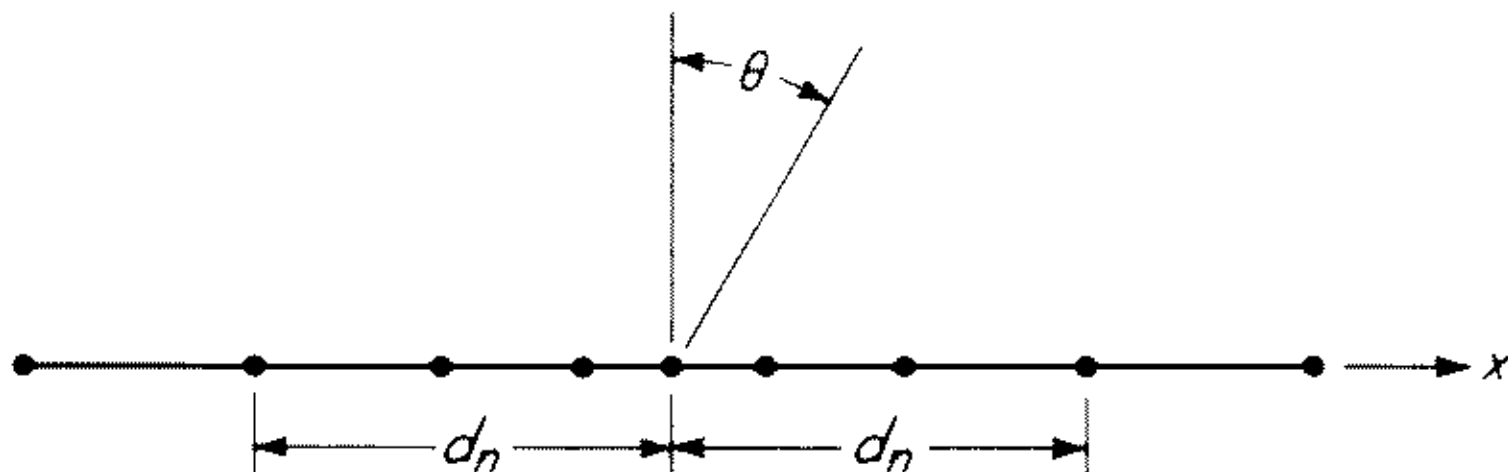


Fig. 6.1 Unequally spaced elements symmetrically arranged in pairs about the center element.

about the center element and that the center element is the reference from which the phase is measured (Fig. 6.1). With these assumptions the array pattern of (6.1) becomes

$$f(u) = 1 + 2 \sum_{n=1}^N \cos 2\pi d_n u \quad (6.2)$$

where d_n is the element distance, measured in wavelengths, from the center element. The total number of elements is $2N + 1$. The problem in unequally spaced array design is to select the N values of the element-pair spacings d_n to achieve some desired radiation pattern.

The array of unequally spaced elements whose pattern is given by (6.2) has N degrees of freedom with which to specify the pattern. In principle it should be possible to approximate a desired radiation pattern with the expression of (6.1) just as with a conventional, equally spaced array of $2N + 1$ elements occupying the same aperture. The pattern of the equally spaced array is

$$f_{eq}(u) = 1 + 2 \sum_{n=1}^N i_n \cos 2\pi n d u \quad (6.3)$$

where d is the spacing between adjacent elements. In the equally spaced array, it is the N values of the currents i_n at the N element pairs that are to be determined. With the unequally spaced array, it is the N values of d_n .

There is an important limitation, however, which does not permit the practical unequally spaced array to achieve a pattern equivalent to that of the equally spaced array. This limitation is the minimum spacing between adjacent elements. For (6.2) and (6.3) to yield equivalent patterns there should be

[†]The notation in this chapter differs from that used in Chap. 5, since for the problems treated here it is convenient to normalize the element spacing relative to the wavelength.

no restriction on the element spacings d_n . In practice, however, array elements cannot be located much closer than a half wavelength. Closer spacing results in increased mutual coupling which changes the aperture illumination. Furthermore, the sizes of practical antenna elements are of the order of a half-wavelength dimension, and it would be difficult to make elements much smaller without loss of efficiency.

An aperture that contains M elements equally spaced at half-wavelength intervals contains more elements than if the spacings are made unequal and if the minimum spacing is a half-wavelength. Since the unequally spaced array contains fewer elements than the conventional array occupying the same aperture, it is said to be "thinned." The conventional array with half-wavelength spacing is called a "filled" array. The degree of thinning is expressed by the percentage of elements removed from the filled array. For example, a 90 percent thinned unequally spaced array of 1,000 elements means that the filled array would contain 10,000 elements. The pattern of the thinned array cannot be controlled as well as that of a filled array, and its average side lobes, relative to the peak gain, will not be as low. If the thinning is not too severe (of the order of half the elements removed) the peak side lobe can be kept to a reasonable value and can be made competitive with that of a conventional design. The side lobes of an array severely thinned (perhaps 90 percent of the elements removed) will not be at all similar in amplitude to the side lobes of the filled array.

Unequally spaced arrays may be used to obtain radiation patterns with low peak side lobes without the need for an amplitude taper. This might be of importance in applications where it is not convenient to individually adjust the amplitude of the current at the elements. Since the beam width of an array is determined primarily by the extent of the aperture and is relatively insensitive to the arrangement of elements within the aperture (compare, for example, the pattern of the circular planar aperture with that of a ring), the unequally spaced array can approximate the beam width of a conventional filled array. Although the beam width of the unequally spaced array may be as narrow as that of the filled array, the theoretical resolution capabilities are not as good, since resolution depends on both the beam width and the received signal-to-noise ratio. The latter depends on the number of elements.

It is difficult to operate a conventional equally spaced array over a wide frequency range without the formation of undesirable grating lobes. (Grating lobes, as explained in Sec. 5.4, are equal in magnitude to the main lobe and are formed in equally spaced arrays when the electrical spacing between elements is wide enough to cause phase differences between adjacent elements of more than 2π radians.) The unequally spaced array permits the antenna to operate over a wide frequency range without the appearance of grating lobes. Similarly, the unequally spaced array can be scanned over a wide angle without the formation of the grating lobes that could appear with the equally spaced array.

The availability of the spacing as an additional parameter provides, in

principle, more flexibility in array-pattern synthesis. But, as mentioned previously, this property is restricted in utility by practical requirements on the permitted spacings.

The gain of a thinned array of isotropic elements each radiating equal power is approximately equal to the number of elements within the aperture. The beam width is of the order of λ_0/D , where λ_0 is the wavelength and D is the aperture dimension. Removing elements in the thinned array results in reduced gain compared with a filled array with the same beam width. In a receiving array there is a decrease in signal-to-noise ratio. The average side-lobe level of a highly thinned array relative to that of the main beam approaches a value equal to the reciprocal of the number of elements remaining in the array. The fraction of the total energy within the side lobes is approximately equal to the fraction of elements removed. For comparison, the energy in the side lobes of a uniformly illuminated circular aperture is about 15 percent of the total.

6.2 Synthesis with Unequally Spaced Arrays

A number of methods exist for synthesizing radiation patterns of conventional-array antennas with equally spaced elements, as discussed in Chaps. 5 and 7. The theoretical basis for the synthesis of equally spaced array radiation patterns is well developed; practical procedures have been devised for its implementation; and the limitations to be expected in design are understood. The same is roughly true for unequally spaced arrays, but not to the same extent. The theory developed for equally spaced arrays is in general not directly applicable to arrays with unequally spaced elements. The theoretical analyses that have been applied to unequally spaced arrays are of limited utility in practice and are difficult to employ with arrays of a large number of elements. One of the few theoretical approaches that has been applied to unequally spaced arrays is the finite Fourier series approximation,¹² but, because of the need to invert a matrix equal to the number of elements contained in the array, this method is difficult to use in practice.

In situations where theory is difficult to formulate in simple terms it is not surprising to find that much of the initial exploration is performed by trial-and-error experimentation in order to obtain some appreciation of the problem. This was true with unequally spaced arrays. Likely element configurations were postulated and the resulting radiation patterns examined. Obviously poor techniques can be eliminated and guides can be provided for the designer. The empirical trial-and-error approach is generally inefficient for discovering optimum procedures, if indeed the optimum can be found at all by such methods. Digital computers may be employed to remove some of the drudgery of the trial-and-error approach and to speed the examination of the many possible configurations of element locations. Three approaches to the trial-and-error method of unequally spaced array design with the aid of digital computers have been considered in the past. These may be classified as (1) total enumeration, (2) perturbation, and (3) dynamic programming.

Total enumeration as applied to unequally spaced arrays consists in examining all possible configurations of element locations and selecting that which is best. It is often an impractical method because of the large number of cases that must be examined. For example, if the array consists of ten element pairs which can be placed in any of 50 possible locations, approximately 1 billion combinations must be examined in order to ensure obtaining the best pattern.

In the perturbation method of design a likely configuration of elements is chosen and the computer is programmed to vary, or perturb, the location of each element one at a time and to select that position which produces the best pattern. After the locations of all the elements are perturbed, the process is repeated until perturbing the element locations offers no significant improvement of the radiation pattern. The success of this method depends on the choice of the initial element locations and how much freedom the computer is allowed in the examination of the possible alternate locations for each element. The perturbation method is an approximation to the total enumeration method. It eliminates many of the possible combinations to be examined by the proper selection of the initial configuration and the choice of element locations. The limit to this method is computer capacity and speed.

Another application of computers to unequally spaced array pattern synthesis is the technique of *dynamic programming*.¹ This is a method for determining an optimum solution to a multistage problem by optimizing each stage of the problem on the basis of the input to that stage. As applied to arrays, the various "stages" of the dynamic programming problem are the selection of the spacings of each element pair. Unlike the perturbation method, an initial set of element locations need not be postulated. Although a computer is not a fundamental part of the technique, it is difficult to solve practical problems without it.

The advantage of dynamic programming as compared with total enumeration is that it drastically reduces the number of combinations that must be examined. This is accomplished by converting a single N -dimensional optimization problem into a sequence of N one-dimensional optimization problems. A considerable reduction in the computations that must be performed in dynamic programming is had by using the fact that many of the computations in total enumeration need not be performed more than once. Dynamic programming will give the same answer as total enumeration if the so-called *principle of optimality* applies. Unfortunately, it has not been proved that the principle of optimality applies to the problem of unequally spaced array design. Nevertheless, dynamic programming has been employed for unequally spaced arrays with interesting and useful results. A similar situation occurs in the application of scalar Kirchhoff theory to the analysis of the radiation pattern from an aperture (Sec. 3.6), in which useful results, consistent with experiment, are obtained in spite of theoretical objections.

In both the perturbation and the dynamic programming methods (as well as with total enumeration) the criterion for selecting the optimum radiation pattern must be carefully formulated and programmed into the computer. One

criterion that has been used with dynamic programming is that of minimizing the maximum side-lobe level over a specified region of angle.

Dynamic programming, applied to the design of linear arrays of unequally spaced elements, has achieved results equal or superior to results with arrays designed by other methods. It is capable of application to planar arrays except that it becomes economically prohibitive in terms of computer time to design large planar arrays with many elements.² Other techniques, such as density tapering, are easier to apply to planar apertures and give satisfactory results. Planar arrays with circular symmetry which can be reduced to a one-angular coordinate problem present no more difficulty than linear arrays.

It has been said previously that there is little theoretical guide for the synthesis of unequally spaced arrays. Conventional antenna theory, however, describes the type of aperture illumination that is needed to obtain a desired radiation characteristic (Sec. 3.5). This is based on the fact that the far-field pattern and the distribution of current density across the aperture are Fourier transform pairs. The theory of pattern synthesis and design developed for continuous apertures can be applied to unequally spaced arrays by arranging the elements so that the *density* of elements across the aperture is of the same form as the *amplitude* of the current density distribution of classical antenna theory. This is called *density* or *space* taper and is discussed in more detail in the following two sections.

Although it is not generally considered as an unequally spaced array technique, the design of arrays with regular spacings other than the rectangular grid can be used to obtain a thinned array. Elements can be arranged on triangular and hexagonal grids or located at the intersections of rings and radials.

This brief review does not include all of the many methods that have been considered for unequally spaced arrays. The technique of density tapering is one of the more practical methods, especially for large planar apertures, and it will be used to illustrate further the nature of this class of array antenna.

6.3 Density Taper — Deterministic

When the element spacings are of the order of one-half wavelength, the radiation pattern of the equally spaced array is a close approximation to that from a continuous aperture of the same size and illumination function (Sec. 7.4). With this as a guide it is of interest to consider the design of an unequally spaced array by attempting to approximate the continuous-aperture current density with equal-amplitude samples spaced nonuniformly. In so doing, the density of the equally excited, unequally spaced radiating elements as a function of location within the aperture will be of the same form as the continuous current density function of the conventional antenna used as the model. This design procedure is called *density tapering* to distinguish it from the more usual *amplitude tapering*. It has also been known as *space tapering*. The continuous aperture illumination from which the density taper is derived is called the *model illumination function* and will be denoted by $i_0(x)$.

The quality of the approximation to a continuous aperture current density function by an array depends on the number of elements. The thinner the array the poorer the approximation. It is found that the main lobe of the density-tapered array and the main lobe of the continuous aperture used as the amplitude-tapered model are close approximations of one another. Also, the near-in side lobes are generally similar. However, the far-out side lobes can deviate considerably and generally rise to relatively large values. This will be illustrated later in the discussion pertaining to Fig. 6.4.

One method of selecting the element locations of the density-tapered array is trial and error. Although this can often produce satisfactory engineering results, it can be a tedious procedure, especially when the number of elements is large. This section describes a systematic procedure for finding the element locations by a method other than trial and error. It is based on the equal-area approximation to the aperture illumination function and uses the cumulative current distribution (integral of the current density) rather than the current density itself. It is called a *deterministic method* to distinguish it from the *statistical method* discussed in the next section.

To employ density tapering, an amplitude-tapered illumination function is first selected as a model. One criterion for its selection is that, when used with a continuous aperture, its radiation pattern should be similar to that desired of the density-tapered array. The illumination function of the amplitude-tapered model might be as shown in Fig. 6.2a. To locate the positions of the M elements the area under the curve is divided into M equal parts and an element is placed at the center of each of the intervals defined by the equal areas, as illustrated in Fig. 6.2b. The density of the equally excited, unequally spaced discrete currents depicted in (b) is seen to approximate the continuous current density function of (a).

The element locations in a linear array may be determined with the equal-area approximation applied to the cumulative distribution $I_0(x)$ of the model aperture illumination, rather than the current density $i_0(x)$. The relationship between the two is given by

$$I_0(x) = \int_{-a/2}^x i_0(x) dx \quad (6.4)$$

which is the integral of the amplitude-tapered current density $i_0(x)$ taken over the limits $(-a/2, x)$, or $(-\infty, x)$, since $i_0(x) = 0$ for $x < -a/2$. The cumulative distribution is plotted in Fig. 6.2c. The equal areas may be found by dividing the ordinate into M equal increments and projecting these points onto the x axis, as shown. The elements are then located within the center of each interval. The procedure is similar to the trapezoidal rule for approximating an integral.

The justification for considering the density-taper method of unequally spaced array design is that the discrete, equally excited currents of the array elements approximate the continuous-aperture amplitude-taper illumination function used as the model. There is no guarantee, however, that the radiation

pattern of the density-tapered array will be a suitable approximation to the radiation pattern of the amplitude-tapered model. It is of interest to inquire, therefore, what relation the pattern of the density-tapered array has to the

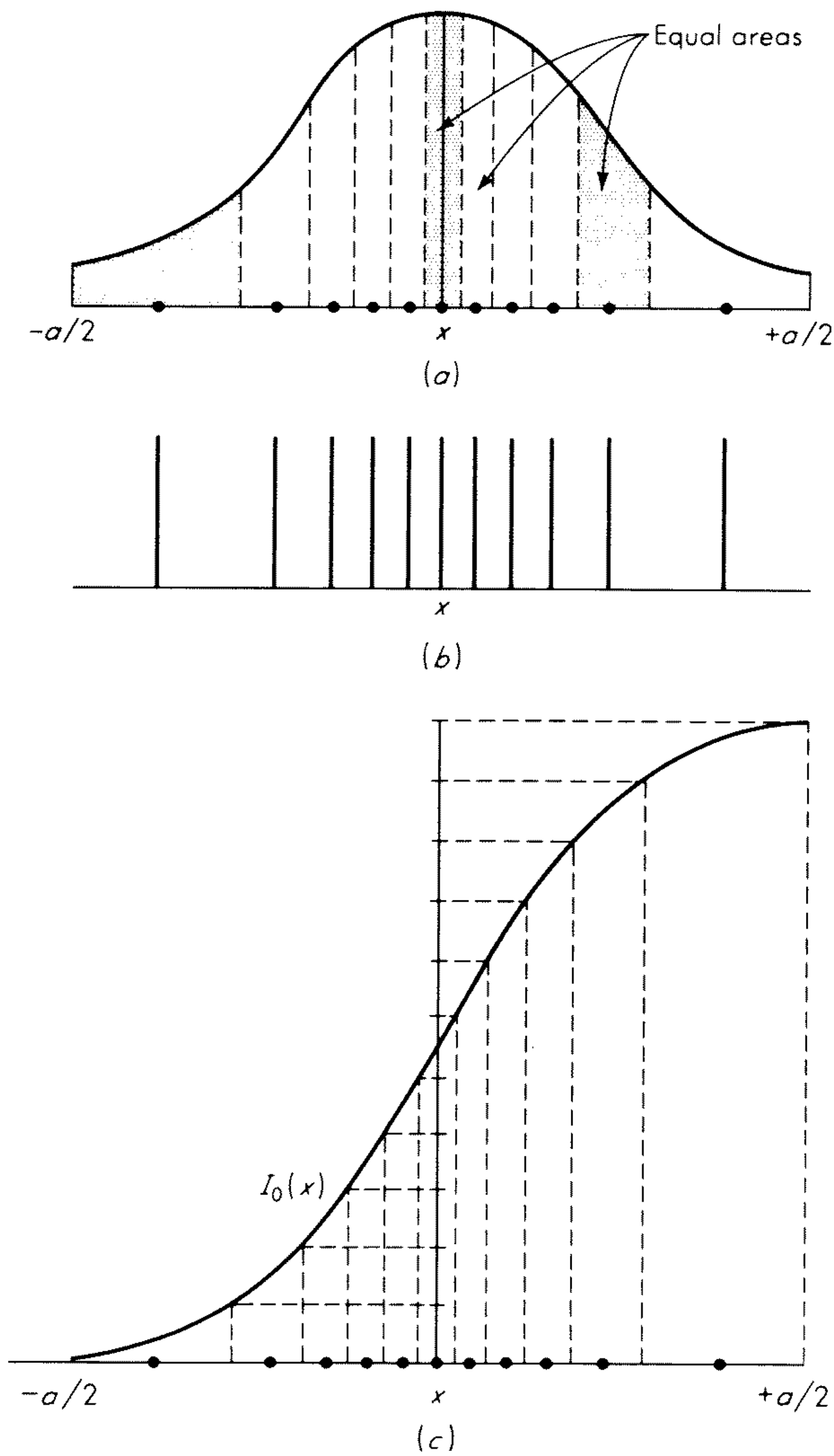


Fig. 6.2 Deterministic density taper. (a) Model current density illumination function (amplitude taper) divided into 11 equal subarrays; (b) location of density-tapered elements; (c) cumulative current distribution.

pattern of the model. This problem was examined by Doyle,³ who has shown that the density-tapered pattern is equivalent to the least-mean-square approximation to the model amplitude-tapered pattern with weighting propor-

tional to the inverse square of the normalized pattern argument. This is shown below as an analysis adapted from that of Doyle.

The antenna pattern produced by an aperture extending from $-a/2$ to $+a/2$ with amplitude taper $i_0(x)$ is

$$f_0(u) = \int_{-a/2}^{a/2} i_0(x) \cos 2\pi x u \, dx \quad (6.5)$$

The cosine is employed in the integral rather than the exponential because the aperture illumination function is assumed symmetrical about the origin and therefore will be real. The function $i_0(x)$ is used as the model for the density taper. The unequally spaced array is also symmetrical and, following (6.2), is

$$f_a(u) = 1 + 2 \sum_{n=1}^N \cos 2\pi d_n u \quad (6.6)$$

The array illumination function can be expressed as a summation of delta functions, or

$$i_a(x) = \delta(x) + \sum_{n=1}^N \delta(x \pm d_n) \quad (6.7)$$

The array pattern may be written similar to the model pattern of (6.5)

$$f_a(u) = \int_{-a/2}^{a/2} i_a(x) \cos 2\pi x u \, dx \quad (6.8)$$

The difference between the model pattern (6.5) and the array pattern (6.8) may be expressed in a number of ways. In this analysis the least-mean-square difference between the two is selected as the criterion for expressing how well the density-tapered pattern matches that of the model. The difference between the two, or the error, may be written

$$\epsilon = \int_{-\infty}^{\infty} [f_0(u) - f_a(u)]^2 W(u) \, du \quad (6.9)$$

where $W(u) \geq 0$ is a weighting function which expresses the relative importance of agreement as a function of the angular variable u . The weighting function is taken to be $1/u^2$, so that the difference between the two patterns becomes progressively greater with increasing distance from the main beam. The error to be minimized is then

$$\epsilon = \int_{-\infty}^{\infty} [f_0(u) - f_a(u)]^2 \frac{du}{u^2} \quad (6.10)$$

The behavior of $1/u^2$ near the origin is of no concern in the integral, since $[f_0(u) - f_a(u)]^2/u^2 = O(u^2)$. (Show as an exercise.)

The difference in the radiation patterns is related to the difference in the aperture current densities by a Fourier transform

$$f_0(u) - f_a(u) = \int_{-a/2}^{a/2} [i_0(x) - i_a(x)] \cos 2\pi x u \, dx \quad (6.11)$$

By integrating by parts, introducing the definition of the cumulative distribution function of (6.4), and assuming that the cumulative distributions of the model aperture illumination and the array illumination are equal at the end points [that is, $I_0(-a/2) = I_a(-a/2) = 0$, and $I_0(a/2) = I_a(a/2)$], it can be shown (do as an exercise) that

$$\frac{f_0(u) - f_a(u)}{2\pi u} = \int_{-a/2}^{a/2} [I_0(x) - I_a(x)] \sin 2\pi x u \, dx \quad (6.12)$$

This establishes a Fourier sine transform relationship between the pattern difference and the distribution difference. Applying Parseval's theorem gives

$$\int_{-\infty}^{\infty} \frac{[f_0(u) - f_a(u)]^2}{u^2} \, du = 4\pi^2 \int_{-a/2}^{a/2} [I_0(x) - I_a(x)]^2 \, dx \quad (6.13)$$

Minimizing the mean-square difference of the patterns with $1/u^2$ weighting [left side of (6.13)] is thus equivalent to minimizing the mean-square difference between the current distributions [right side of (6.13)] if the total integrated currents across the apertures in the two cases are equal; that is, $I_0(a/2) = I_a(a/2)$. (This condition was not always satisfied in many previous density-taper designs.)

The function $I_a(x)$ has the form of a sum of steps of equal height. To minimize (6.13), $I_0(x)$ should pass through each step of $I_a(x)$. If the k th equal interval of $I_a(x)$ lying between $(k-1)/N$ and k/N defines a region on the x axis, $\alpha < x < \beta$ (Fig. 6.3), the problem is to determine x_k within the interval

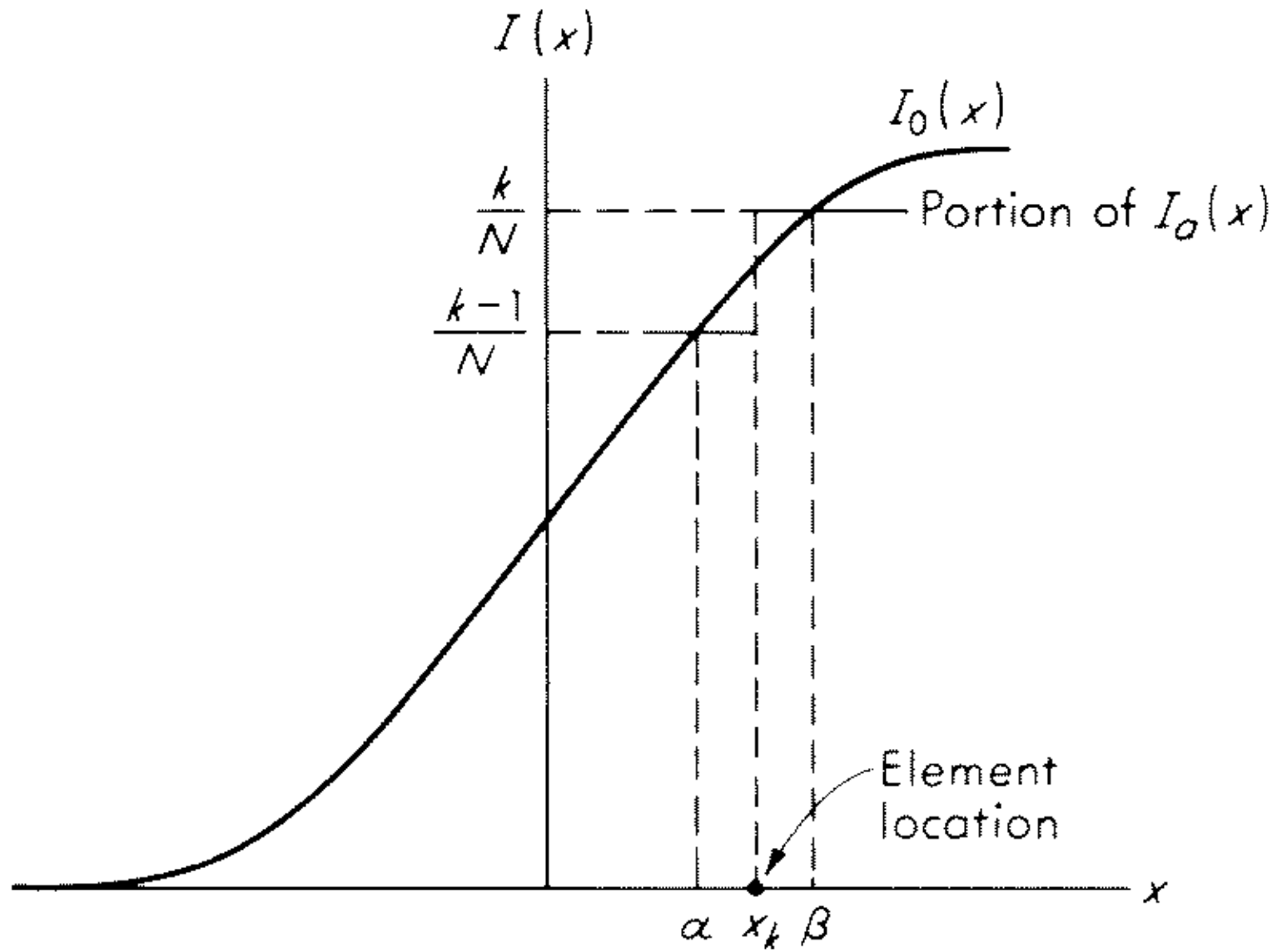


Fig. 6.3 Fitting of $I_a(x)$ to $I_0(x)$ so as to minimize mean-square difference [Eq. (6.12)].

(α, β) so that the mean-square difference between the model distribution and the array distribution is a minimum. Thus it is required to minimize

$$\int_{\alpha}^{\beta} [I_0(x) - I_a(x)]^2 \, dx = \int_{\alpha}^{x_k} \left[I_0(x) - \frac{k-1}{N} \right]^2 \, dx + \int_{x_k}^{\beta} \left[\frac{k}{N} - I_0(x) \right]^2 \, dx \quad (6.14)$$

Differentiating with respect to x_k and solving gives

$$I_0(x_k) = \frac{2k - 1}{2N} \quad (6.15)$$

which states that each step of $I_a(x)$ should be so chosen that $I_0(x)$ crosses the middle of the step.

Figure 6.4 shows the radiation patterns (array factors) of a density tapered array with 12, 18, and 24 isotropic elements. These examples are taken from Doyle.³ The abscissa is a generalized parameter that includes the aperture size measured in wavelengths, the angle, and the number of elements. The visible region for a 20-wavelength array aperture is shown. Also shown is the model pattern, which is designed with 20-db equal side lobes according to Taylor's "ideal space factor" (Sec. 7.8). As more elements are added the fit between the two patterns becomes progressively better. In Fig. 6.4c, with 24 elements, the degree of thinning is 60 percent if a 20-wavelength aperture is assumed. The closest spacing between adjacent elements, 0.52 wavelength, occurs between the outer two elements of the array. If considerably more elements were to be employed in the 20-wavelength, unequally spaced aperture, the fit between the theoretical density-tapered array and the model array would be even better, but it is likely that element spacings less than one-half wavelength would be necessary. This would make the design an impractical one. When practical elements are employed in the array, the element factor will suppress the far-out high side lobes in an array with a radiation pattern like that of Fig. 6.4c and good side lobes would be expected throughout the visible region.

The patterns of Fig. 6.4, as well as other density-tapered array patterns, indicate that the density-tapered pattern is in close agreement with the model pattern for a number of side lobes, measured from the main beam, approximately equal to the number of independent element locations to be chosen. For example, in an 18-element design there are eight locations to be determined in a symmetrical array in which the end elements are fixed beforehand. It can be seen that the first eight side lobes in Fig. 6.4b follow the model pattern reasonably well. Beyond the eighth side lobe, however, the differences are quite marked.

The selection of the model amplitude-tapered illumination function is an important part of the density-taper design. There does not seem to be a unique criterion for selecting the best model. One can be guided, however, by the pattern that the model illumination would produce if radiated by a continuous aperture and by the fact that the density-tapered pattern is a good approximation to the model pattern in the vicinity of the main beam and the near-in side lobes. One model illumination function that is not satisfactory is the uniform current density. (Explain why!)

The density-taper method described for the linear array can be extended to the planar array.⁴ The density of elements in the unequally spaced planar array is made to approximate the double integral representing the current on a

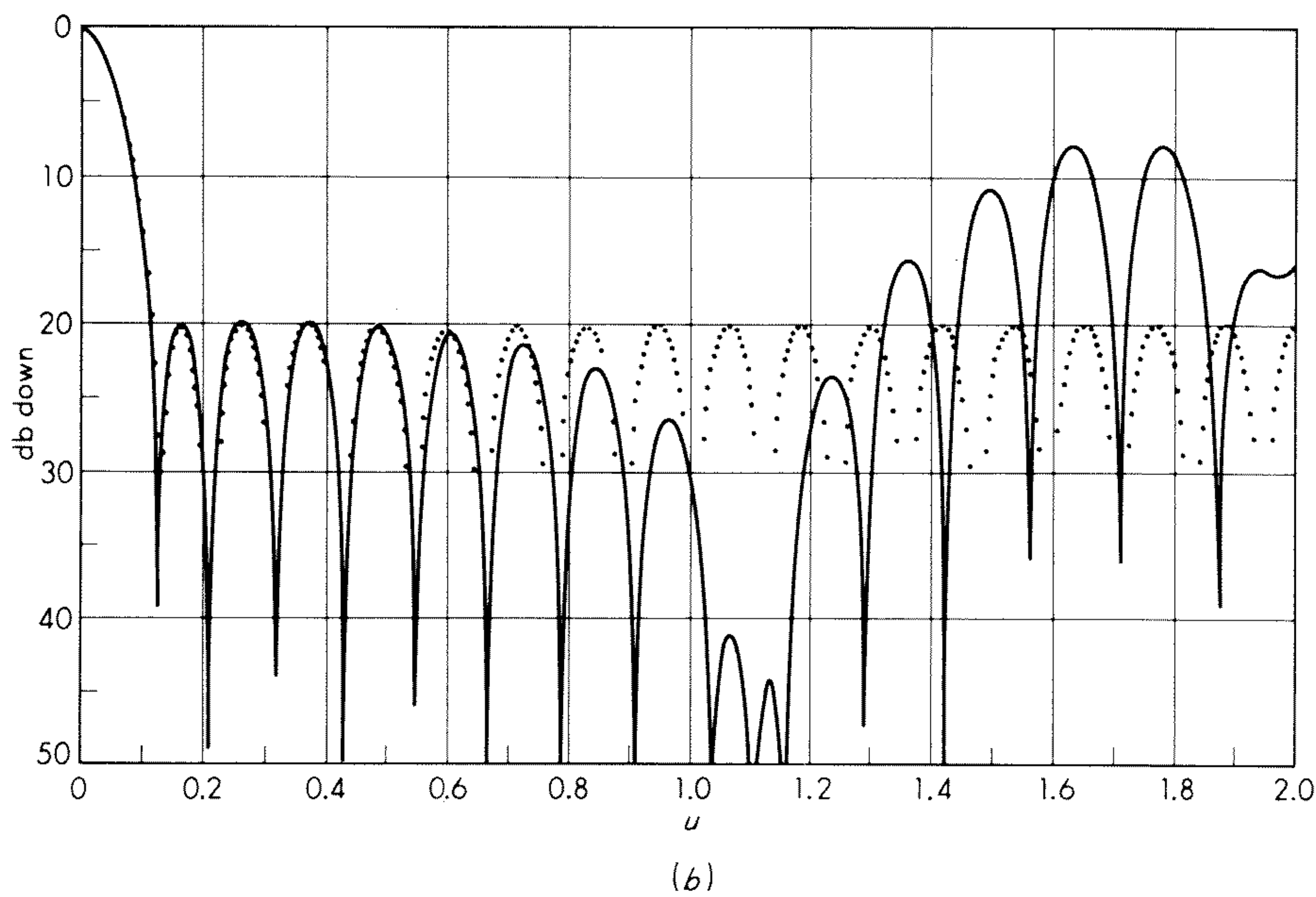
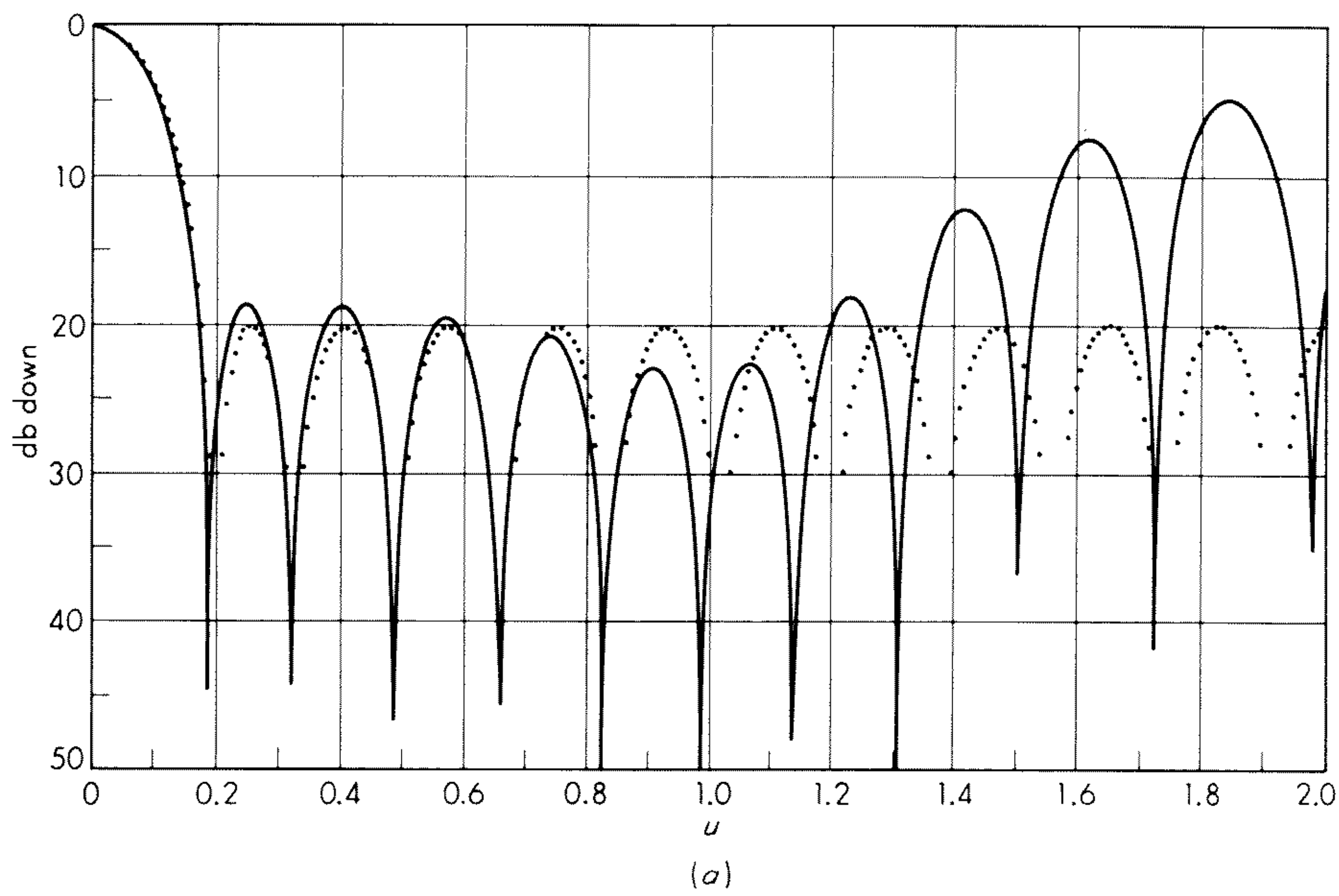


Fig. 6.4 Comparison of density-tapered array pattern (solid curve) and the model amplitude-tapered array pattern (dotted curve). (a) 12 elements; (b) 18 elements; (c) 24 elements. (From Doyle.³)

planar aperture rather than the single integral of the linear array. The volume under the surface defining the planar aperture current-density illumination

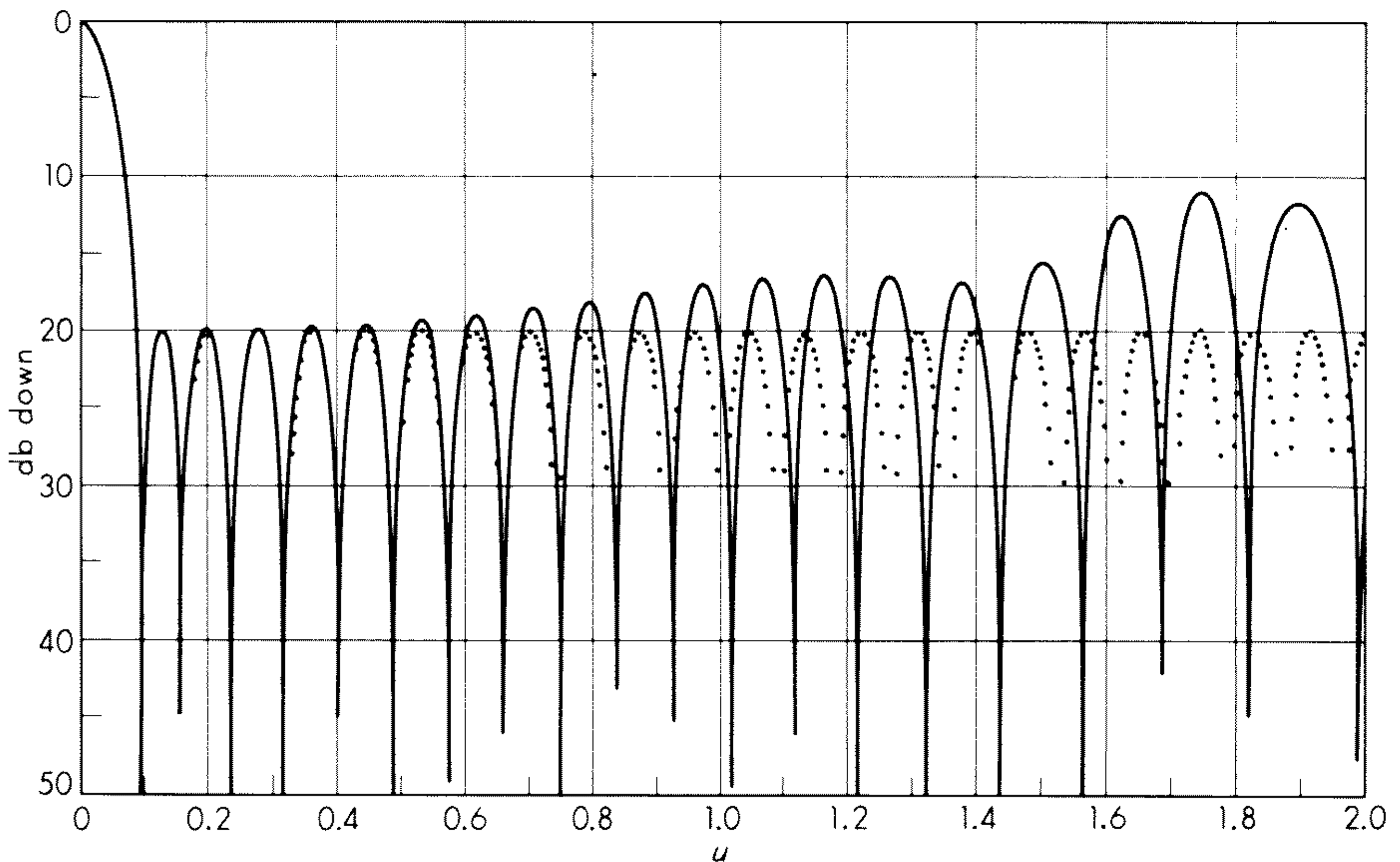


Fig. 6.4 (Continued.)

(c)

function is divided into M equal parts, where M is the number of elements. One element is placed within each subvolume at the center of the area projected onto the aperture plane. In general it is not as convenient to implement the design of a density-tapered planar array as of a linear array.

The use of the density-taper technique as described above is basically a graphical method with a bit of trial and error involved. Another method for locating the elements in a large planar array is the probabilistic or statistical method of the next section. This method offers a definite, yet simple, procedure for determining the element locations so as to approximate a density taper.

6.4 Density Taper — Statistical

In this approach to the design of the density-tapered array, the model amplitude-taper illumination function is employed to determine, on a probabilistic basis, whether or not an element should be located at a particular point within the aperture.⁵ The model illumination function serves a role analogous to that of the probability density function of probability theory, although it does not necessarily conform to the strict definition of a probability density function. The elements are located randomly (actually pseudorandomly) rather than in some definite manner as in the deterministic density taper of the preceding section. However, the elements are not uniformly random across the aperture, but their average density, computed statistically, follows the form of the model amplitude-taper illumination function. This method is called a

statistical density taper, since the radiation pattern of a particular class of design can be specified beforehand only in statistical terms.

The procedure for designing a statistical, density-tapered array may be illustrated with the aid of Fig. 6.5. The curve represents the amplitude taper

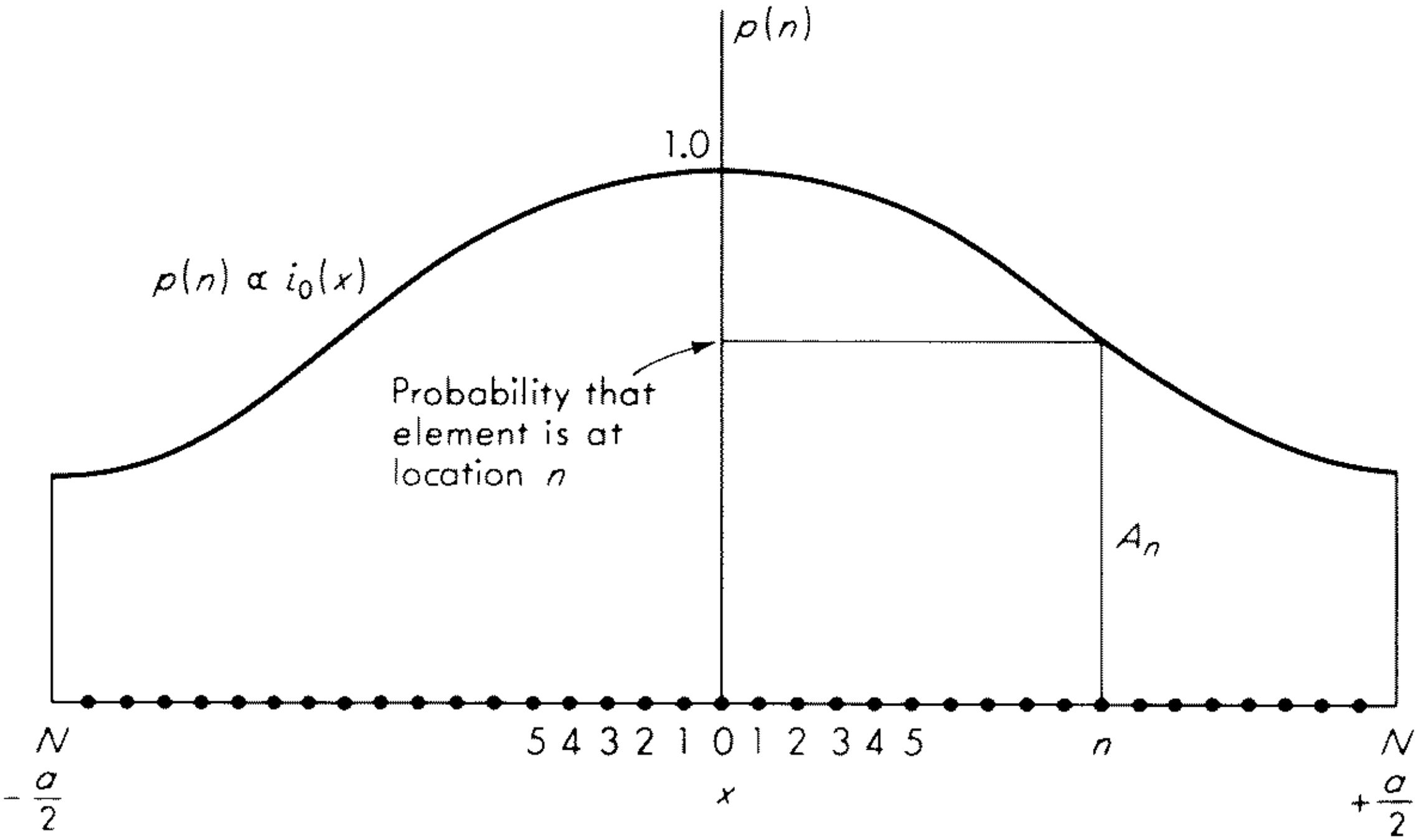


Fig. 6.5 Model aperture illumination used to determine placement of elements in statistical density-taper method of designing unequally spaced arrays.

$i_0(x)$ of the model aperture illumination. The scale of the ordinate is so adjusted that the maximum of the model amplitude taper is equal to k , where $0 \leq k \leq 1$. In the present discussion and in Fig. 6.5, $k = 1$. Along the abscissa are N possible element-pair locations. (The array consists of pairs of elements, since symmetry is assumed throughout this chapter when considering linear arrays.) The possible element locations are equally spaced (generally one-half wavelength). The model amplitude taper specifies the probability that an element pair will be located at the n th equally spaced position of the aperture.

The design of the statistical density taper begins by selecting a continuous amplitude taper $i_0(x)$ whose pattern is to be approximated by the density-tapered array. From the continuous distribution $i_0(x)$, a discrete approximation is obtained. This is denoted A_n and is the aperture illumination of an amplitude-tapered filled array used as the model for the density taper, where $0 \leq A_n \leq 1$. Each possible element location is examined in turn to determine whether or not an element is to be located there. An element is placed at a particular point if the value of the amplitude taper A_n at that location is less than a number, chosen at random, between the values of 0 and 1. Let us say that the amplitude taper A_n at some element location n has a value of 0.7. A random-number generator or table is consulted, and a number between zero and one is selected. If it is less than A_n (in this case 0.7), the element remains. If the random number is greater, it is removed. If this is repeated in many

designs, the element will remain at that particular location a fraction of times equal to the value of the model amplitude taper at that point. Thus an element will be allowed to remain seven times out of ten on the average in this example. With enough elements, the pattern of the statistically designed density-tapered array will approximate that of the amplitude-tapered filled array used as the model. This is a relatively simple design procedure and can be readily implemented with a digital computer.

The degree of thinning achieved will depend upon the value of k and the shape of the amplitude taper. With typical amplitude tapers, the degree of thinning with $k = 1$ is about 40 to 60 percent for circular planar apertures. When $k = 1$, the design is said to be *naturally thinned*. Greater thinning is obtained with values of k less than unity.

The above discussion of the statistical density-tapered array assumed a linear aperture for convenience of discussion. The extension to a planar aperture is straightforward.

If elements are removed from an N -element "filled" array, the field intensity (array factor) in the far field may be written

$$f(\theta, \phi) = \sum_{n=1}^N F_n \exp(j\psi_n) \quad (6.16)$$

where θ, ϕ are the angular coordinates describing the field, ψ_n is the phase of the signal at the n th element, and F_n is a factor which is either zero or unity according to whether the n th element is removed or left in place. The elements are assumed isotropic. This expression for the field intensity does not require the geometry of the aperture to be specified, since it is "hidden" in the phase factor ψ_n . Hence, it is applicable to planar as well as linear apertures. Unlike most of the other expressions for the field intensity given in this chapter, (6.16) uses complex notation. This is done for convenience, although, it should be cautioned, it is the magnitude of the complex expression which is generally of concern in practice. In the statistically designed density-tapered array, F_n is selected randomly and independently from element to element so that its ensemble average is $\overline{F_n} = kA_n$, where the bar denotes average value and $0 \leq k \leq 1$ is the factor introduced to account for greater thinning than would be obtained from natural thinning ($k = 1$). In what follows k is taken to be unity. A_n is the amplitude of the current excitation that would be applied to the n th element of the model amplitude-tapered filled array whose field intensity is

$$f_0(\theta, \phi) = \sum_{n=1}^N A_n \exp(j\psi_n) \quad (6.17)$$

The field-intensity pattern of the density-tapered array (6.16) is statistical, since F_n is statistical. By the central limit theorem of statistics, the distribution of the quantity $f(\theta, \phi)$ for a given θ and ϕ will be approximately gaussian if the number of elements N is large. The mean value of the statistical pattern of

(6.16) is found by using the fact that the mean of the sum is the sum of the means:

$$\overline{f(\theta, \phi)} = \sum_{n=1}^N \overline{F_n} \exp(j\psi_n) = \sum_{n=1}^N A_n \exp(j\psi_n) = f_0(\theta, \phi) \quad (6.18)$$

Thus the average field-intensity pattern of a density-tapered array is identical with the field-intensity pattern of the amplitude-tapered array used as the model. The square of the field-intensity pattern is the power pattern, or radiation pattern, and is

$$\begin{aligned} |f(\theta, \phi)|^2 &= f(\theta, \phi) f^*(\theta, \phi) \\ &= \sum_n \sum_m F_n F_m \exp j(\psi_n - \psi_m) \end{aligned} \quad (6.19)$$

where $f^*(\theta, \phi)$ denotes the complex conjugate. There is a theorem in statistics which states that the mean of a product of statistically independent random variables is equal to the product of the means of those random variables. The variables F_n and F_m in (6.19) are independent if and only if $n \neq m$. If $n = m$, they are, of course, identical and not independent. Therefore, the double summation is separated into terms with $n = m$ and terms with $n \neq m$, and the average is taken as follows:

$$\overline{|f(\theta, \phi)|^2} = \sum_n \overline{F_n^2} + \sum_n \sum_{\substack{m \\ n \neq m}} \overline{F_n F_m \exp j(\psi_n - \psi_m)} \quad (6.20)$$

Since the values of F_n are either 0 or 1, $F_n^2 = F_n$ and the first summation of (6.20) becomes

$$\sum_n \overline{F_n^2} = \sum_n \overline{F_n} = \sum_n A_n \quad (6.21)$$

Using the theorem mentioned above, the second summation of (6.20) involving terms with $n \neq m$ becomes

$$\sum_n \sum_{\substack{m \\ n \neq m}} A_n A_m \exp j(\psi_n - \psi_m) \quad (6.22)$$

This is simply the power pattern corresponding to the model array of (6.17) except that the terms with $n = m$ are missing. When these terms are restored and subtracted from the result, the following average power pattern for the density-tapered array is obtained:

$$\overline{|f(\theta, \phi)|^2} = |f_0(\theta, \phi)|^2 + \sum_n A_n (1 - A_n) \quad (6.23)$$

where $|f_0(\theta, \phi)|^2$ is the power pattern of the model array with the amplitude taper A_n applied.

The first term of the average radiation (power) pattern of (6.23) is the same as the radiation pattern of the model amplitude-tapered array which depends on the aperture illumination A_n . The second term is independent of angle and

depends only on the model aperture illumination and the number of elements. Thus the average radiation pattern can be predicted from a knowledge of the model amplitude taper A_n . The second term of (6.23) defines the average level of the statistical side lobes. This term dominates the pattern outside the vicinity of the main beam and the near-in side lobes.

An example of a radiation pattern of a statistical density-tapered array is shown in Fig. 6.6. The solid curve is the computed radiation pattern in one principal plane of a 50-wavelength-diameter circular aperture array containing

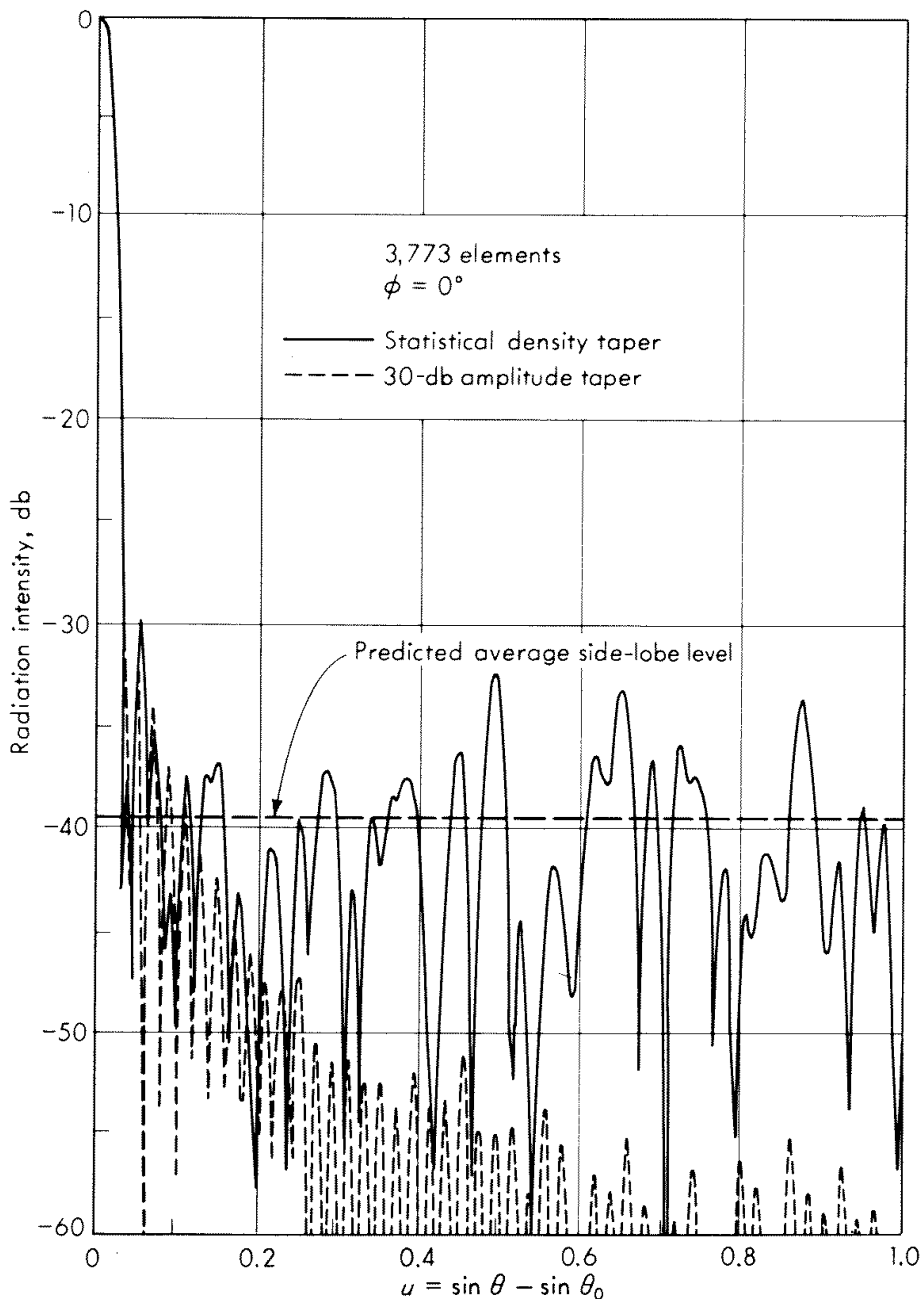


Fig. 6.6 Statistical density-taper radiation pattern designed with a 30-db Taylor distribution as the model.

3,773 elements. The model aperture illumination is a Taylor circular distribution designed to give 30-db near-in side lobes ($\bar{n} = 3$). The array was naturally thinned ($k = 1$) and, if filled, would have contained about 7,800 elements. Consequently, the degree of thinning is about 50 percent. The dashed pattern is that of the model aperture illumination. The predicted average statistical side-lobe level [second term of (6.23)] is also shown. Close to the main beam the pattern is determined by the model pattern, but in the angular region removed from the main beam the statistical average pattern dominates. The side lobes of the density-tapered array are seen to be higher than those of the model pattern. Thus the gain of the density-tapered array will be less, in general, than that of the amplitude-tapered array that is used as the model. With natural thinning this difference might not be too large when it is considered that the differences in the two side-lobe patterns are not large when measured on an absolute scale (rather than a decibel scale), even though the differences may appear impressive with the logarithmic ordinate on which the pattern is plotted. Furthermore, the low side lobes predicted for the amplitude-tapered array might not always be achieved in practice because of the ever-present imprecision which enters into the construction of practical antennas (Sec. 6.6). Figure 6.7 gives the location of elements for the particular array whose pattern is shown in Fig. 6.6.

As with any statistical process, there must be enough "samples" to ensure statistical regularity. Thus the statistical density-taper design requires that the array contain a sufficient number of elements. Empirically, it has been found that arrays of more than 100 elements are probably adequate for applying this technique, but arrays with as few as 25 elements are likely to result in poorer patterns with the statistical design than with other methods. For this reason statistical density taper is more applicable to the design of large planar arrays than of linear arrays with only a moderate number of elements. In practice it is found that, for linear arrays, the deterministic density taper is slightly better than the statistical density taper. However, other methods (for example, dynamic programming) usually produce better designs for linear arrays than either type of density taper. Although both density-taper techniques are of academic interest, the statistical density taper has had application in large array implementations; notably the Bendix Corporation ESAR array, which contains 760 unequally spaced elements arranged within a 50-wavelength-diameter circular aperture capable of 8,000 elements if fully filled.

It is of interest to note the basic difference between the radiation patterns obtained by the two density-taper methods. Equation (6.23) predicts that the average pattern of the statistical density taper is the superposition of the model pattern and a statistical side-lobe pattern whose average value is independent of angle. Thus for angles beyond those corresponding to the near-in side lobes the side-lobe level should be, on the average, uniform. (However, in any particular design, statistical variation about the average is to be expected.) With the deterministic density-taper method the pattern in the vicinity of the

main beam is essentially that of the model pattern, just as with the statistical design. But as the angle increases from the main beam the side lobes rise and become progressively worse because the model pattern and the density-taper pattern are least-mean-square fits with a weighting inversely proportional to the square of the angle.

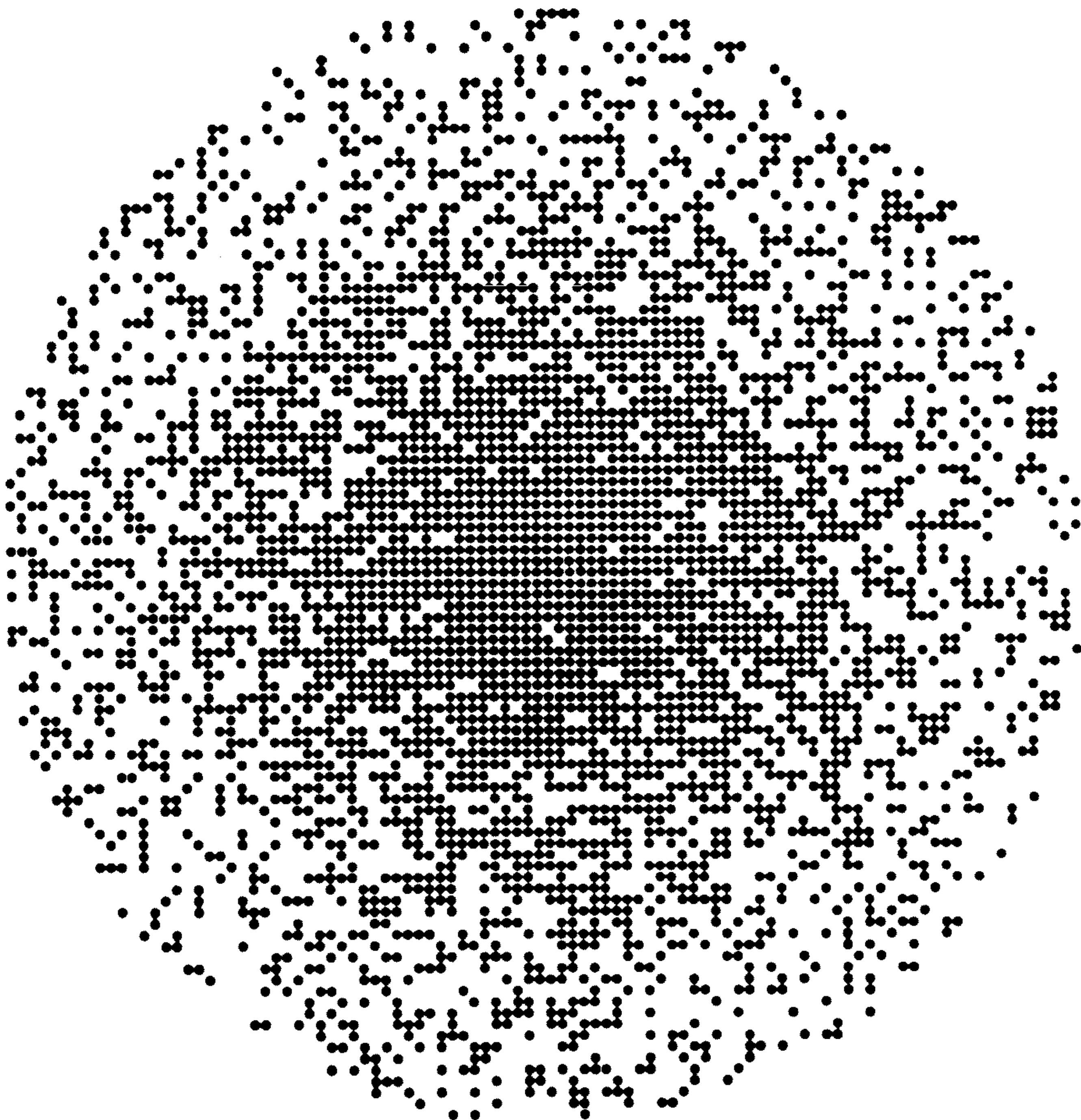


Fig. 6.7 Actual locations of elements determined statistically for the naturally thinned 30-dB density-taper array whose pattern is shown in Fig. 6.6.

6.5 Missing Elements in Equally Spaced Arrays

It was seen in the preceding section that the unequally spaced array designed with a statistical density taper can be considered as a filled array of equally excited, equally spaced elements in which elements are removed at random (or not included in the first place) according to some specified probabil-

ity criterion. The results of the preceding section may also be applied to predict the effect of random element failures in large arrays with equally excited elements. Although many arrays are designed with an amplitude taper rather than equally excited elements, the analysis of the antenna with equally excited elements is included here because it is a straightforward extension of the work already developed. It is a convenient means for obtaining an insight into this problem without resorting to the more complete analysis required to account for random element failure in arrays with amplitude taper. (This is reserved for the next section.) The results for equally excited elements are qualitatively not too unlike those for amplitude-tapered arrays.

In any practical phased array, failures can be expected in the individual elements. This is especially true if the elements contain some active device such as a transmitter or a receiver. The phase shifter can also be a source of failure. Although the failure of a few elements in a large array is not likely to affect the radiation pattern sufficiently to be noticed, eventually the failure of enough elements will result in a degradation that must be corrected. (Unfortunately, the fact that an array can tolerate a certain amount of element failures can lead to the implementation of a marginal array. It is sometimes argued that if 10 percent failure of elements can be tolerated, then these elements may be left out of the array in the first place. Failure of 10 percent of the elements from this "starved" array might then be of concern.)

The accidental failure of elements in an equally excited array results in a thinned array and can be considered as a statistical density taper where the model aperture illumination is uniform and of a value which accounts for the probability of an element failure. The model aperture distribution is $A_n = 1$, and the factor $k < 1$ of the preceding section is the probability that a particular element location will contain a working element. The fraction of elements that fail is $1 - k$.

The average radiation (power) pattern of the statistical density-taper array with the factor k included is

$$\overline{|f(\theta, \phi)|^2} = k^2 |f_0(\theta, \phi)|^2 + \sum_{n=1}^N k A_n (1 - k A_n) \quad (6.24)$$

where $|f_0(\theta, \phi)|^2$ is the radiation pattern of the filled array with aperture illumination A_n . With equally excited elements $A_n = 1$ and the radiation pattern is

$$\overline{|f(\theta, \phi)|^2} = k^2 |f_0(\theta, \phi)|^2 + (k - k^2)N \quad (6.25)$$

Thus the effect of random failures is to cause a reduction of k^2 in the peak of the no-error pattern (because less energy is radiated) and to produce a statistically uniform, average side-lobe level (independent of angle) superimposed on the side lobes of the original pattern. Assuming the side lobes of the original pattern decrease with increasing angle (as they do for an equally excited array with half-wave spacing between elements), the statistical side lobes will eventually dominate the side lobes of the original pattern at angles far enough

removed from the main beam. Consider the case when 10 percent of the elements of an equally excited planar array randomly fail. The fraction of the elements remaining is thus $k = 0.9$. Assuming the original no-error array consisted of 10,000 isotropic elements, the peak intensity would be reduced by a factor of 0.81, from a value of 10^8 to 8.1×10^7 , in the units appropriate to (6.25). The average statistical side lobes on this scale would be 900 according to the second term of (6.25). There will, of course, be statistical variations about this value. The average statistical side lobes, however, are almost 50 db down from the main beam. The gain of the array is reduced in proportion to the number of elements removed, so that the 10,000-element array with 40 db gain is reduced to 39 db when 10 percent of the elements are removed. If 30 percent of the elements fail, the peak intensity will be 4.9×10^7 in units appropriate to (6.25) and the average side lobe level will be 2,100, with the result that the average side-lobe intensity will be -43.6 db relative to the peak intensity.

Only the average level of the statistical side lobes has been considered. It is sometimes important to know the variation to be expected about the average. This is described by the *variance* which may be obtained from a knowledge of the probability density function describing the behavior of the statistical side lobes.

6.6 Random Errors in Arrays

One of the fundamental principles of antenna theory is that the radiation pattern is determined by the amplitude and phase of the alternating currents along the aperture (Chap. 3). The antenna designer can, in principle, specify the form of the current across the aperture and expect the resulting radiation pattern to be as predicted. In practice, however, there will be unavoidable errors in the currents excited on the aperture and the actual radiation pattern will differ from the theoretical. The agreement between the two depends on how well the desired distribution of current across the aperture can be achieved.

Errors in the aperture currents can be divided into two types depending on whether they are predictable or random. An example of a predictable error is the finite quantization of the phase produced by a digital phase shifter. Another example is the step approximation to the linear phase shift introduced by an array consisting of subarrays. The effects of such errors are predictable, and the resulting radiation pattern can be computed by classical methods from a knowledge of the array design.

Random errors are caused by the accidental deviations of the antenna parameters from their design value. Although they may be small, they are ever-present and can limit the minimum side-lobe level that can be achieved just as random noise limits the sensitivity of a radio receiver. Random errors cause a rise in the side-lobe level, a reduction in the gain, and an error in the direction of the main beam. Only the first two will be considered here.

If errors in an existing antenna can be measured, the pattern can be calculated in the classical manner. It is not possible, however, to know the exact nature of the random errors that might be encountered in some particular antenna from a knowledge of its design. The actual existence of the antenna is necessary. It is possible, however, to predict in statistical terms the pattern behavior of a collection, or ensemble, of antennas. The average, or expected, value of the pattern and the standard deviation about the average are used to describe the antenna performance. More generally, the statistical character of the array pattern due to random errors can be described by the *probability density function*. The statistical description of random errors cannot be applied to any *particular* antenna but applies to the *collection* of similar antennas whose errors are described by the same statistical parameters.

The calculation of the effect of random errors in array antennas requires the application of probability theory, in particular the concept of the probability density function and the calculation of the average value. It is realized that probability theory is not generally one of the more familiar working tools of the antenna engineer. However, the mathematics needed for the understanding of errors in arrays is often introduced to the electrical engineering student in courses in information theory or the statistical theory of communications and is similar to the mathematics used in the discussion of the statistical density taper in Sec. 6.4. Therefore, rather than review the required probability theory, the necessary concepts will be stated as needed in the discussion.

An array antenna radiation pattern might differ from the desired pattern because of (1) errors in the amplitude of the currents at each element, (2) errors in the phase of the current, (3) missing elements (due to catastrophic failure), (4) rotation of the radiating elements, (5) translational errors in the element location, and (6) errors in the radiation pattern of each element. Although all of these have been treated in the literature,⁶⁻¹⁰ only the first three will be discussed here. A special case of an array with missing elements was the subject of Sec. 6.5. The analysis presented in this section is based, in large part, on the basic work of Ruze⁶ and the extensions made by Allen.⁷ In the following the average radiation (power) pattern will be derived by taking account of phase and amplitude errors as well as missing elements. Those wishing to avoid the derivation may skip over to (6.40), the expression for the average radiation pattern.

The array factor of a planar array of M by N isotropic elements, arranged on a rectangular grid in the xy plane with equal spacing d between the elements, can be written

$$f(\theta, \phi) = \sum_{m=1}^M \sum_{n=1}^N i'_{mn} \exp [jk_0 d \sin \theta (m \cos \phi + n \sin \phi)] \quad (6.26)$$

where i'_{mn} is the current at the m nth element, $k_0 = 2\pi/\lambda_0$, $\lambda_0 =$ wavelength, and θ, ϕ define the usual angular coordinate system (see, for example, the coordinate system of Fig. 2.1). The field intensity is proportional to $f(\theta, \phi)$. The

radiation, or power, pattern (which is proportional to the radiation intensity) is obtained by multiplying (6.26) by its complex conjugate

$$|f(\theta, \phi)|^2 = f(\theta, \phi) f^*(\theta, \phi) \\ = \sum_{m=1}^M \sum_{n=1}^N \sum_{p=1}^M \sum_{q=1}^N i'_{mn} i'^*_{pq} \exp \{jk_0 d \sin \theta [(m - p) \cos \phi + (n - q) \sin \theta]\} \quad (6.27)$$

The currents i'_{mn} (and i'_{pq}) are the actual currents at the elements and are related to the desired (no-error) currents i_{mn} in the following manner

$$i'_{mn} = i_{mn} r_{mn} (1 + \Delta_{mn}) \exp(j\delta_{mn}) \quad (6.28)$$

where Δ_{mn} is the fractional error in the amplitude of the current at the mn th element and δ_{mn} is the error in the phase (measured in radians) at each element. The average value of the phase error δ and amplitude error Δ is assumed to be zero. The phase and amplitude errors at any element are taken to be independent of the errors in any other element. The factor r_{mn} accounts for missing elements such as might be caused by catastrophic failure. It has the value of unity with probability P_e and the value zero with probability $1 - P_e$. Thus the probability of the element mn being operative is designated P_e and is assumed to be independent of the location of the element within the array. The probability P_e is also equal to the average fractional number of elements that remain operating and is similar to the parameter k introduced in Sec. 6.5.

Inserting the current as given by (6.28) into the power pattern expression of (6.27) yields

$$|f(\theta, \phi)|^2 = \sum_{m=1}^M \sum_{n=1}^N \sum_{p=1}^M \sum_{q=1}^N i_{mn} i^*_{pq} r_{mn} r_{pq} (1 + \Delta_{mn})(1 + \Delta_{pq}) \exp[j(\delta_{mn} - \delta_{pq})] \\ \exp \{jk_0 d \sin \theta [(m - p) \cos \phi + (n - q) \sin \phi]\} \quad (6.29)$$

The power pattern of (6.29) is statistical, since r , Δ , and δ are statistical. The average power pattern may be considered as the average of a large number of similar arrays whose errors are governed by the same statistical laws and parameters. In obtaining the average of (6.29) it is convenient to separate the summation into two parts by separating those terms in which $m = p, n = q$ from the remaining terms in which $m \neq p, n \neq q$. This is done so that use can be made of the theorem in probability theory which states that the mean of a product of statistically independent random variables is equal to the product of the means of these random variables. The variables Δ_{mn} and Δ_{pq} are independent if and only if $m \neq p, n \neq q$.

Considering only those terms in the power pattern $|f(\theta, \phi)|^2$ which are statistically independent and applying the theorem mentioned above gives an average contribution

$$\overline{|f(\theta, \phi)|^2}_{m \neq p, n \neq q} = P_e^2 \sum_m \sum_n \sum_p \sum_q i_{mn} i^*_{pq} \overline{\exp[j(\delta_{mn} - \delta_{pq})]} \\ \exp \{jk_0 d \sin \theta [(m - p) \cos \phi + (n - q) \sin \phi]\} \quad (6.30)$$

In obtaining the above, use was made of the assumption that $\overline{\Delta_{mn}} = 0$ and $\overline{\Delta_{pq}} = 0$ and that $\overline{r_{mn}} = \overline{r_{pq}} = P_e$. It remains to evaluate the average of the exponential factor involving the difference of the phase errors. Most of the analysis is involved in this task. To evaluate the average a description must be given of the statistical behavior of the random phase error δ_{mn} (or δ_{pq}). It is assumed that the phase error δ (the subscripts are dropped for simplicity) is described by the gaussian probability density function with zero mean

$$p_1(\delta) = \frac{1}{(2\pi\overline{\delta^2})^{1/2}} \exp\left(-\frac{\delta^2}{2\overline{\delta^2}}\right) \quad (6.31)$$

where $\overline{\delta^2}$ is the variance (generally denoted σ^2) or mean-square value of the deviation about the average (the average in this case is zero). The probability density function $p_1(\delta)$, when multiplied by the infinitesimal $d\delta$, gives the probability of finding the variable δ between the values of δ and $\delta + d\delta$. The gaussian probability density function is chosen not only for mathematical convenience but also because it is a good description of many types of errors that occur in practice. The gaussian assumption will be asymptotically true if the phase error δ is due to a number of causes and such errors are small so that a linear relation exists between the cause of the phase error and the error itself.

Let $y = \delta_{mn} - \delta_{pq}$ so that the problem becomes that of finding the average value of $\exp(jy)$. From the definition of the average value we get

$$\overline{\exp(jy)} = \int_{-\infty}^{\infty} \exp(jy)p(y) dy \quad (6.32)$$

where $p(y)$ is the probability density function for the variable y . The probability density function for δ is given by (6.31) and is needed in determining $p(y)$. The variable y is a function of two independent variables δ_{mn} and δ_{pq} (by definition they are independent so long as $m \neq p$, $n \neq q$). The joint probability density function for the two independent variables is the product

$$p(\delta_{mn}, \delta_{pq}) = p_1(\delta_{mn})p_1(\delta_{pq}) = p_1(y + \delta_{pq})p_1(\delta_{pq}) \quad (6.33)$$

The density function $p(y)$ can be found by integrating the above over the variable $\delta_{pq} = \delta$.

$$p(y) = \int_{-\infty}^{\infty} p_1(y + \delta)p_1(\delta) d\delta \quad (6.34)$$

By substituting $p_1(\delta)$ as given by (6.31) into the integral for $p(y)$, the reader can verify that the desired probability density function is

$$p(y) = \frac{1}{(4\pi\overline{\delta^2})^{1/2}} \exp\left(-\frac{y^2}{4\overline{\delta^2}}\right) \quad (6.35)$$

The integral of (6.32) for the average value of the exponent may be written as

$$\overline{\exp(jy)} = \int_{-\infty}^{\infty} \cos y p(y) dy + j \int_{-\infty}^{\infty} \sin y p(y) dy \quad (6.36)$$

The second term is equal to zero. (Why?) Substituting the probability density function of (6.35) into the first term and performing the integration by using (863.3) of Dwight¹¹ gives

$$\overline{\exp(jy)} = \overline{\cos y} = \exp(-\delta^2) \quad (6.37)$$

By substituting this result back into the expression of (6.30), the average value of the power pattern for those terms in which $m \neq p, n \neq q$ is found. We hold this result in abeyance and next consider the remaining terms of the power pattern expression not included in (6.30).

When $m = p, n = q$ in the power pattern of (6.29), the average value of these terms becomes

$$\begin{aligned} \overline{|f(\theta, \phi)|^2}_{m=p, n=q} &= \sum_{m=1}^M \sum_{n=1}^N \overline{i_{mn}^2 r_{mn}^2} \overline{(1 + \Delta_{mn})^2} \\ &= P_e (1 + \overline{\Delta_{mn}^2}) \sum_m \sum_n \overline{i_{mn}^2} \end{aligned} \quad (6.38)$$

where use has been made of the statistical independence between the amplitude errors and the probability of a missing element. Since r_{mn} takes on only the values 0 or 1, $\overline{r_{mn}^2} = \overline{r_{mn}} = P_e$, the probability that any particular element will be present.

The average power pattern is given by the sum of (6.38) and (6.30) (with 6.37 included in 6.30). Combining the two equations gives

$$\begin{aligned} \overline{|f(\theta, \phi)|^2} &= P_e^2 \exp(-\delta^2) \sum_m \sum_n \sum_p \sum_q \overline{i_{mn} i_{pq}} \\ &\quad \exp\{jk_0 d \sin \theta [(m - p) \cos \phi + (n - q) \sin \phi]\} \\ &\quad + P_e (1 + \overline{\Delta^2}) \sum_m \sum_n \overline{i_{mn}^2} \end{aligned} \quad (6.39)$$

The first summation is similar to the no-error power pattern [(6.27) with i_{mn} and i_{pq} substituted instead of i'_{mn}] and i'_{pq} except that the terms with $m = p$ and $n = q$ are missing. Adding these terms to the first summation to obtain the no-error power pattern $|f_0(\theta, \phi)|^2$ and subtracting them as a separate term so as not to include them twice, the average power pattern becomes

$$\begin{aligned} \overline{|f(\theta, \phi)|^2} &= P_e^2 \exp(-\delta^2) |f_0(\theta, \phi)|^2 \\ &\quad + [(1 + \overline{\Delta^2}) P_e - P_e^2 \exp(-\delta^2)] \sum_m \sum_n \overline{i_{mn}^2} \end{aligned} \quad (6.40)$$

This is the sought-for result. Thus the effect of random errors is to produce an average power pattern that is the superposition of two terms. One term is the no-error power pattern multiplied by the square of the fraction of elements remaining and by a factor proportional to the phase error. The other term depends on both the amplitude and the phase errors as well as on the fraction of elements remaining. It also depends on the aperture illumination, but it is independent of the angular coordinates θ, ϕ . This second term can be thought of

as a "statistically omnidirectional" pattern. It causes the far-out side lobes to differ in the presence of error as compared with the no-error pattern. The shapes of the main lobe and the near-in side lobes, however, are relatively unaffected by errors. Note that when the phase and amplitude errors are zero, and if the aperture illumination is uniform ($i_{mn} = 1$), the expression for the average power pattern reduces to that of (6.25) (with $P_e = k$) derived in Sec. 6.5 in a different manner.

For $P_e = 1$ and small errors the normalized pattern is

$$\overline{|f(\theta, \phi)|^2} = |f_0(\theta, \phi)|^2 + (\overline{\Delta^2} + \overline{\delta^2}) \frac{\sum_m \sum_n i_{mn}^2}{\left(\sum_m \sum_n i_{mn}\right)^2} \quad (6.41)$$

This is the expression originally derived by Ruze.⁶ For a given error, the second term of (6.41) indicates that the larger the number of elements the smaller will be the statistical side-lobe level.

The average power pattern is, of course, never realized in practice. It represents the average pattern of many similar arrays. The pattern of any particular array will exhibit variation about the mean. Although it will not be proved here, the statistics of the field-intensity pattern can be described by the modified Rayleigh probability density function

$$p(v) = \frac{2v}{\sigma^2} \exp \left[-\frac{(a^2 + v^2)}{\sigma^2} \right] I_0 \left(\frac{2av}{\sigma^2} \right) \quad (6.42)$$

where $p(v) dv$ is the probability of the field intensity (at some particular angle) lying within the value of v and $v + dv$, $a^2 =$ first term of (6.41), $\sigma^2 =$ second term of (6.41), and $I_0(\cdot)$ is the modified Bessel function of the first kind. [Note that (6.42) is the same distribution that describes the statistics of the output envelope of a narrow-band filter when the input is noise of mean-square value $\sigma^2/2$ and a sine wave of amplitude a .]

When the errors are small ($a^2 \gg \sigma^2$), (6.42) approaches the gaussian probability. This applies in the vicinity of the main beam where the no-error pattern is large compared with the statistical side-lobe pattern. For large errors ($a^2 \ll \sigma^2$) the original minor-lobe radiation may be neglected and (6.42) approaches the modified Rayleigh density function

$$p(v) = \frac{2v}{\sigma^2} \exp \left(-\frac{v^2}{\sigma^2} \right) \quad (6.43)$$

From a knowledge of the probability density function the probability that the field intensity at angle (θ, ϕ) will exceed a specified value v_0 may be computed as follows:

$$\text{Probability } (v > v_0) = \int_{v_0}^{\infty} p(v) dv \quad (6.44)$$

In that portion of the radiation pattern where the side lobes are determined by the statistical pattern rather than by the no-error pattern ($a^2 \ll \sigma^2$) the proba-

bility that a particular side-lobe level v_0 is exceeded is found by substituting the Rayleigh probability density function of (6.43) into (6.44).

$$\text{Probability } (v > v_0) = \exp\left(\frac{-v_0^2}{\sigma^2}\right) \quad (6.45)$$

The probability that the field intensity exceeds twice the average statistical field intensity (exceeds the average by 6 db) is 1.8 percent. The probability of it exceeding a value 8 db above the average is 0.18 percent, while the probability of it exceeding the average is 36.8 percent.

Errors in arrays can also cause a reduction in the gain (directivity) of an antenna. By substituting the radiation intensity of (6.40) into the definition of directivity [Eq. (2.8)], the reader can show as an exercise that

$$\frac{D}{D_0} = \frac{P_e}{(1 + \overline{\Delta^2}) \exp(-\overline{\delta^2})} \approx \frac{P_e}{1 + \overline{\Delta^2} + \overline{\delta^2}} \quad (6.46)$$

where D is the directivity of the array with errors, D_0 is the no-error directivity, P_e , as before, is the probability that any particular element will be present, $\overline{\Delta^2}$ is the mean-square amplitude error, and $\overline{\delta^2}$ is the mean-square phase error. In the derivation of (6.46) it was assumed that the statistical side-lobe level could be neglected compared with the peak intensity in the numerator of the expression for directivity. Note that the relative reduction in directivity is independent of the number of elements and depends only on the mean-square value of the errors and the fraction of elements that remain.

The effect of errors on the direction in which the beam points can also be derived but will not be derived here.^{7,9} The assumption that the elements are isotropic radiators can be removed and the element factor properly taken into account.⁷ These and other more detailed analyses of the effect of errors on array antennas may be found in the literature.

PROBLEMS

6.1 Determine the spacings of an 11-element linear array designed with a model amplitude taper $i_0(x) = 1.0 + 0.4 \cos(2\pi x/a)$, where x is the distance from the array center and a is the aperture size, both measured in wavelengths. Assume $a = 20$ wavelengths.

6.2 Derive the average power pattern of a statistical density-taper array when $k \neq 1$. [Answer: Eq. (6.24)]

6.3 If a 1-db reduction in directivity is allowed with a 100-element uniform amplitude illumination array, what rms value may be specified for the phase error, assuming no amplitude error and no missing elements? What amplitude error, if $\overline{\delta^2} = 0$, $P_e = 0$? What P_e , if $\overline{\Delta^2} = 0$, $\overline{\delta^2} = 0$? Repeat for a 10,000-element array.

6.4 Show that the average directivity of a statistical density-taper array of isotropic elements is approximately equal to the average number $\overline{N_e}$ of elements remaining. [Assume the directivity of the model amplitude-tapered filled array is $(\sum A_n)^2 / \sum A_n^2$

and use the fact that $\overline{N_e} = \sum_{n=1}^N A_n$, where the symbols are as defined in Sec. 6.4.]

REFERENCES

1. Skolnik, M. I., G. Nemhauser, and J. W. Sherman III: Dynamic Programming Applied to Unequally Spaced Arrays, *IEEE Trans. Antennas Propagation*, vol. AP-12, pp. 35–43, January, 1964.
2. Skolnik, M. I., and J. W. Sherman III: Planar Arrays with Unequally Spaced Elements, *Radio Electron. Engr.*, vol. 28, pp. 173–184, September, 1964.
3. Doyle, W.: On Approximating Linear Array Factors, *RAND Corp. Mem. RM-3530-PR*, February, 1963.
4. Willey, R. E.: Space Tapering of Linear and Planar Arrays, *IRE Trans. Antennas Propagation*, vol. AP-10, pp. 369–377, July, 1962.
5. Skolnik, M. I., J. W. Sherman III, and F. C. Ogg, Jr.: Statistically Designed Density-tapered Arrays, *IEEE Trans. Antennas Propagation*, vol. AP-12, pp. 408–417, 1964.
6. Ruze, J.: The Effect of Aperture Errors on the Antenna Radiation Pattern, *Nuovo Cimento Suppl.*, vol. 9, no. 3, pp. 364–380, 1952.
7. Allen, J. L.: Some Extensions of the Theory of Random Error Effects on Array Patterns, chap. III, part 3 of Phased Array Radar Studies, July 1, 1960 to July 1, 1961, *M.I.T. Lincoln Lab. Tech. Rept. 236*, Nov. 13, 1961.
8. Elliott, R. S.: Mechanical and Electrical Tolerances for Two-dimensional Scanning Antenna Arrays, *IRE Trans. Antennas Propagation*, vol. AP-6, pp. 114–120, January, 1958.
9. Rondinelli, L. A.: Effects of Random Errors on the Performance of Antenna Arrays of Many Elements, *IRE Natl. Conv. Record*, vol. 7, part 1, pp. 174–187, 1959.
10. Bracewell, R. N.: Tolerance Theory of Large Antennas, *IRE Trans. Antennas Propagation*, vol. AP-9, pp. 49–58, January, 1961.
11. Dwight, H. B.: "Tables of Integrals and Other Mathematical Data," 3d ed., The Macmillan Company, New York, 1957.
12. Unz, H.: Linear Arrays with Arbitrarily Distributed Elements, *IRE Trans. Antennas Propagation*, vol. AP-8, pp. 222–223, March, 1960.

CHAPTER 7

ANTENNA PATTERN SYNTHESIS

A. C. Schell and A. Ishimaru

7.1 Introduction

Most of this book is concerned with the determination of the radiation characteristics of a given current distribution on an antenna. The assessment of these characteristics can be termed the analysis of antennas. A complementary problem is the one of determining the antenna that produces a given radiation characteristic. Because this problem involves procedures that are inverse to those of analysis, we shall describe it as the synthesis problem, or simply as antenna pattern synthesis.

The synthesis of antenna patterns has analogies in the fields of circuit theory and waveform construction. In these fields we may analyze the outputs of a number of networks and choose the most desirable among them, or we may attempt the inverse (and often more difficult) problem of finding the network that produces the desired output as nearly as possible. Frequently the output of a network is assumed to extend over an infinite range of time; however, in antenna synthesis, the radiation pattern extends over a finite range of angle. This distinction has caused a great deal of controversy regarding the applicability of network theory techniques to antennas and has pointed out the need for the ratio of reactive to radiative power to be determined, at least approximately, for a given antenna pattern synthesis result.

There are many methods of antenna pattern synthesis. At first glance, it might appear that many of these methods are duplicates and that there is little or no distinction between them. This is not the case. Each method of synthesis is developed in response to a given class of problems. It should be clear that one has no a priori assurance that the technique for determining the best linear array will yield the optimum aperture distribution on a curved surface. It is necessary to judge synthesis techniques in the light of the intended use of the antenna; otherwise, the word optimum has little or no meaning. To distinguish among techniques, we shall divide the synthesis problems into two parts.

The first part is the approximation problem. Each antenna is intended to meet the requirements for a given set of system applications. These requirements are stated in terms of the impedance characteristics, the size and shape of the overall structure, and the radiation pattern. The desired pattern statement is invariably given such that it cannot be exactly satisfied by a realistic antenna. For example, the desired pattern may be one with sharp corners or no

side lobes or an arbitrarily narrow beam. The desired pattern must be approximated by a functional representation that is consistent with the general type of antenna under consideration and that satisfies the error conditions that are relevant. Thus the first part of the synthesis procedure, the approximation, requires the use of pertinent criteria. Some representative criteria are:

1. *The gaussian, or minimum-mean-square-error match.*¹ This basic criterion is the error measure for the finite Fourier series approximation of any piecewise continuous function. Because the use of a truncated Fourier series provides the best fit in the mean-square sense, the application of this criterion to a desired field pattern results in the best use of the available aperture power to match the desired pattern. Thus, the Fourier series approximation provides the maximum-gain answer to the approximation of a point source function. (There are exceptions to this rule that are relevant when Fourier transforms do not accurately describe the relation between far-field and antenna current distribution, but they are not germane here.)

The gaussian error criterion is an average-error measure: it does not specify the excursion of the approximation function from the desired function at any arbitrary point. In the vicinity of a discontinuity or impulsive behavior of the desired pattern, there occur ripples or lobes that are the result of the slow rate of decrease of the coefficients of the higher terms of the approximating series. These oscillations near discontinuities, commonly referred to as the Gibbs phenomenon, are an inevitable result of mean-square-error matching, and it is often necessary to modify either the desired pattern or the approximating function to reduce them.

2. *The Chebyshev, or minimum-deviation match.* This criterion limits the maximum excursion of the approximating function from the desired pattern, often by the use of Chebyshev polynomials as the basis of expansion. In this way the overshoot and ripple that are attendant on pattern discontinuities can be limited to a specified value. Relating the Chebyshev polynomials to the antenna characteristics usually involves a tedious and lengthy computation, and as a result the Chebyshev criterion tends to be used only for approximating an impulse function. It does not necessarily follow that the expansion of a desired pattern in terms of a truncated series of Chebyshev polynomials will result in approximation error consisting of equal ripple lobes. A special computation procedure, often referred to as "minimax" matching, is needed to find a truly equal deviation pattern fit. Generally the Chebyshev polynomials will provide an equal ripple approximation if the error can be expanded in terms of a single Chebyshev polynomial.

The second part of the synthesis problem is the realization of the antenna. Once a suitable approximation to the desired pattern that satisfies the error criterion has been found, the next step is to translate the functional representation into the currents on the antenna structure. This part of the procedure re-

quires the statement of the constraints that are pertinent in a given realization. The constraint specification restricts the choice of realizations to the one that is relevant to the intended application. Some representative constraints are:

1. *The physical size and shape of the antenna.* This is an obvious constraint, and it has a direct bearing on the choice of the functional representation of the pattern. Related constraints are the applicability of a ground plane and whether the antenna currents are located on a curved surface.
2. *The antenna Q .* For most antennas it is very difficult to compute the bandwidth of the antenna, and a commonly used measure is the *aperture Q* , which is the ratio of the reactive power to the radiative power at the aperture. Although this quantity is not in general equal to the Q as seen from the input terminals, it provides a reliable indication of high- Q systems, and the discrepancy between aperture Q and the actual Q is relatively unimportant if both quantities are large.
3. *The phase of the far field.* There are many applications for which only the magnitude of the radiation pattern is specified; the phase of the far field has no effect on system performance. An example of this is a conventional radar, which measures the power returned from a given direction. Since most synthesis methods deal with field quantities, it is necessary to specify the far-field phase to carry out the procedure. This imposes a set of constraints that may unnecessarily restrict the solution. A common choice of phase constraints is to specify that the desired far-field phase be a constant.

Synthesis procedures cannot in general be dissected into the two distinct parts of approximation, involving the criteria, and realization, involving the constraints. Most methods fuse the two parts by considering a functional representation that is intended to apply to a specific set of constraints and truncating a series expansion of the functions to provide the approximation.

There is a broad class of synthesis techniques for which the pattern specification is a single beam with side lobes below a given level. This sort of loose description of the desired pattern has resulted in the evolution of several widely differing approaches to the approximation with controlled Gibbs phenomenon of an impulse by the pattern of an array or continuous current distribution. Some of these methods use the element locations as well as the amplitude and phase of the element currents to control the pattern behavior. However, most of these techniques are not true synthesis procedures: they cannot be used to synthesize an arbitrary pattern, and there is not a well-defined error measure. In fact, many of these quasi-synthesis procedures are the results of the analysis of a large number of antenna distributions of a given type by which heightened intuition is gained in order to select a distribution that will satisfy a loose pattern specification.

The antenna pattern synthesis problem is basically the same whether the final antenna structure is an array or an aperture-type antenna. Therefore,

we shall include both types of antennas in the discussion. Some specific antenna array synthesis techniques are discussed in Chaps. 5 and 6, specifically in Secs. 5.9 to 5.11 and 6.3 and 6.4. With the exception of Sec. 5.11, which treats the problem of optimizing the relative directivity and efficiency index for an array, the emphasis was on array design to yield patterns which were optimum in a rather loosely defined way, e.g., narrow beam width and low side-lobe level. The aim of this chapter is to examine the synthesis problem from a much broader and general point of view.

7.2 Gaussian Error — Rectangular Array

The synthesis methods that have as their error criterion the gaussian, or minimum-mean-square-error, match are the most basic and general approaches, and they were the first to be developed.

Consider an error criterion of the form

$$\varepsilon = \int_{u^2+v^2<1} |f_D - f|^2 du dv \quad \begin{array}{l} u = \sin \theta \cos \phi \\ v = \sin \theta \sin \phi \end{array} \quad (7.1)$$

where the square of the difference between the desired radiation pattern function f_D and the approximation function f is averaged over the visible region. The coordinate system is given in Fig. 3.2, and the k_x and k_y of Chap. 3 correspond to $k_0 u$ and $k_0 v$, respectively. If f_D is piecewise continuous, it can be expanded in a double Fourier series with a periodicity equal to 2 in both u and v as

$$f_D(u, v) = \sum_{n=-\infty}^{\infty} \sum_{m=-\infty}^{\infty} A_{Dnm} e^{jn\pi u + jm\pi v}$$

where

$$A_{Dnm} = \frac{1}{4} \int_{-1}^1 \int_{-1}^1 f_D(u, v) e^{-jn\pi u - jm\pi v} du dv$$

With a similar expansion for f , the error criterion (7.1) can be written

$$\varepsilon = \int_{-1}^1 \int_{-1}^1 \left| \sum_{n,m} (A_{Dnm} - A_{nm}) e^{jn\pi u + jm\pi v} \right|^2 du dv = 4 \sum_{n,m} |A_{Dnm} - A_{nm}|^2$$

where the integration has been extended to include the corners of the pattern range outside the visible region, for which $u, v \approx 1$. Let us assume that we are capable of realizing an antenna that permits adjusting the coefficients of the first $(2N + 1)(2M + 1)$ terms of the summation, corresponding to $-N \leq n \leq N$, $-M \leq m \leq M$. All other coefficients of the approximation series are zero. It is obvious that the minimum-error condition occurs when each coefficient of the desired function is equated to the corresponding coefficient of the approximation function:

$$A_{Dnm} = A_{nm}$$

leaving an error

$$\varepsilon_{\min} = 4 \sum_{\substack{|n| > N \\ \text{or } |m| > M}} |A_{Dnm}|^2$$

The approximation function is therefore

$$f(u,v) = \sum_{n=-N}^N \sum_{m=-M}^M A_{Dnm} e^{jn\pi u + jm\pi v} \quad (7.2)$$

The next step is to find a physical realization for this function (7.2). This is particularly simple in this instance, because elementary array theory states that a rectangular array of point sources, each with an excitation current i_{nm} , has a far-field radiation pattern given by

$$f(u,v) = \sum_{n=-N}^N \sum_{m=-M}^M i_{nm} e^{jk_0 n d_x u + jk_0 m d_y v} \quad (7.3)$$

The function $f(u,v)$ is often referred to as the array factor in order to distinguish the properties of the array from the properties of the individual elements. In this chapter we are concerned only with patterns and we shall not deal with the structure or size of individual radiating elements. Hence, the arrays are assumed to consist of isotropic radiators. (See Chap. 2 or 5 for further discussion of element factors.)

The spacing between elements in any one of the $2N + 1$ rows is d_y ; the inter-element spacing in each of the $2M + 1$ columns is d_x ; and the frequency of operation is $f_0 = c/\lambda_0 = k_0 c/2\pi$. Therefore, if the desired pattern f_D is a far-field pattern and we choose $k_0 d_x = k_0 d_y = \pi$, Eqs. (7.2) and (7.3) are identical if the element currents are equated to the coefficients of the Fourier series expansion of the desired pattern.

The match of the array pattern to the desired pattern over the entire visible region results in interelement spacings

$$d_x = d_y = \frac{\pi}{k_0} = \frac{\lambda_0}{2}$$

The half-wavelength spacing is the “natural” choice for visible-range pattern fit. If a match over a different angular extent is desired, the interelement spacing should be adjusted accordingly.

The simple relation between array pattern and truncated Fourier expansion was pointed out by Wolff² in 1937 and was later treated in detail by Schelkunoff.³ As an example, consider the desired pattern of Fig. 7.1, which is

$$f_D(u,v) = \begin{cases} 3(v^2 u + v^3 u^2) & 0 \leq u, v \leq 0.5 \\ 0 & \text{elsewhere} \end{cases}$$

The coefficients of the Fourier series are

$$A_{nm} = \frac{3}{4} \int_0^{0.5} \int_0^{0.5} (v^2 u + v^3 u^2) e^{-jn\pi u - jm\pi v} du dv$$

Note that the desired pattern function is not symmetric or separable and that the array coefficients are complex. The radiation pattern for the gaussian

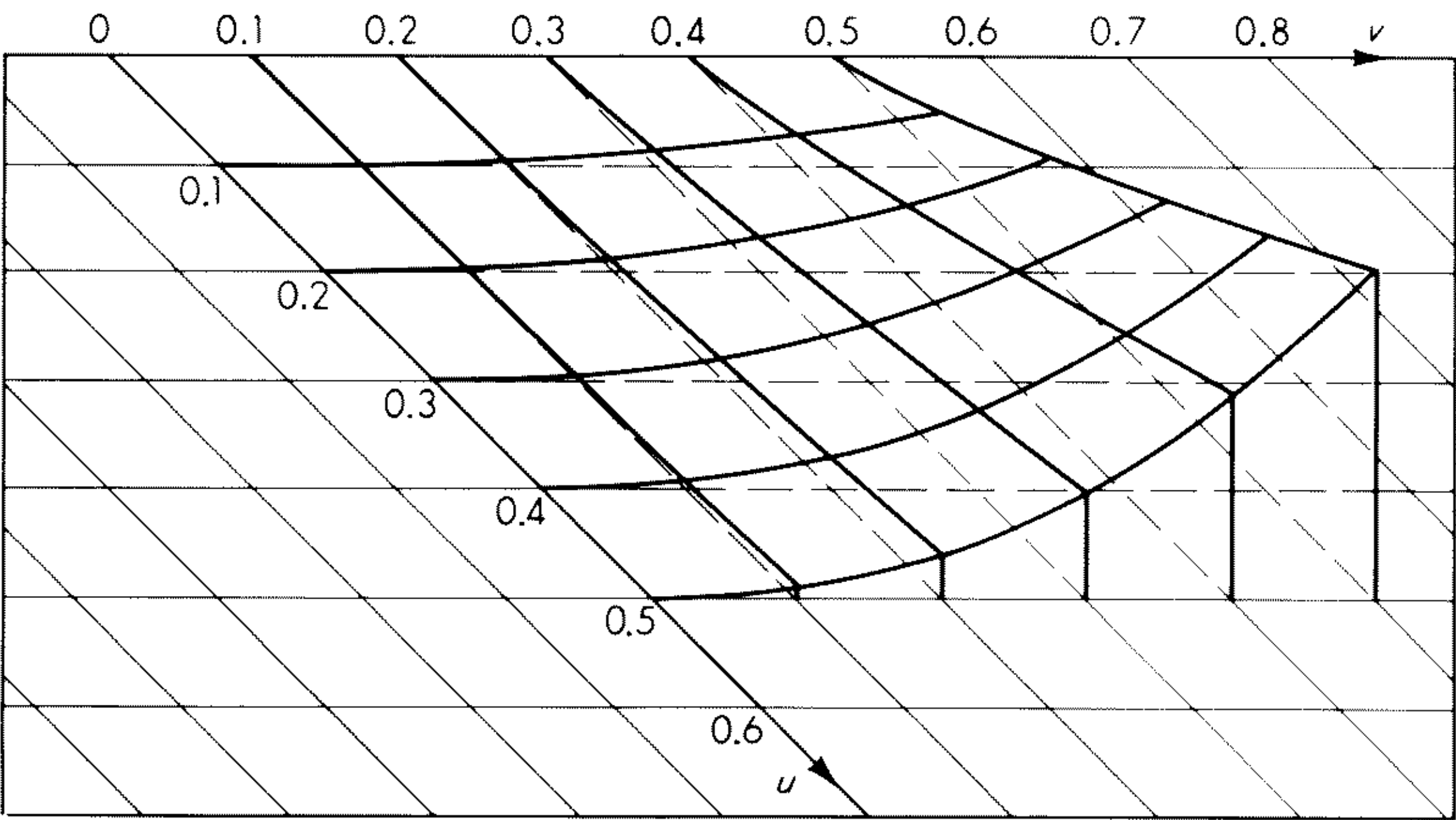


Fig. 7.1 A specified “ideal” pattern.

error synthesis using a 35×35 array of point sources is shown in Fig. 7.2. Notice that the ripple of the approximation pattern in the v coordinate for negative v is small, because the desired pattern and its first derivative in v are zero at $v = 0$. The approximation pattern exhibits large ripples near the other boundaries of the desired pattern, where the finite discontinuities in f_D produce the Gibbs phenomenon.

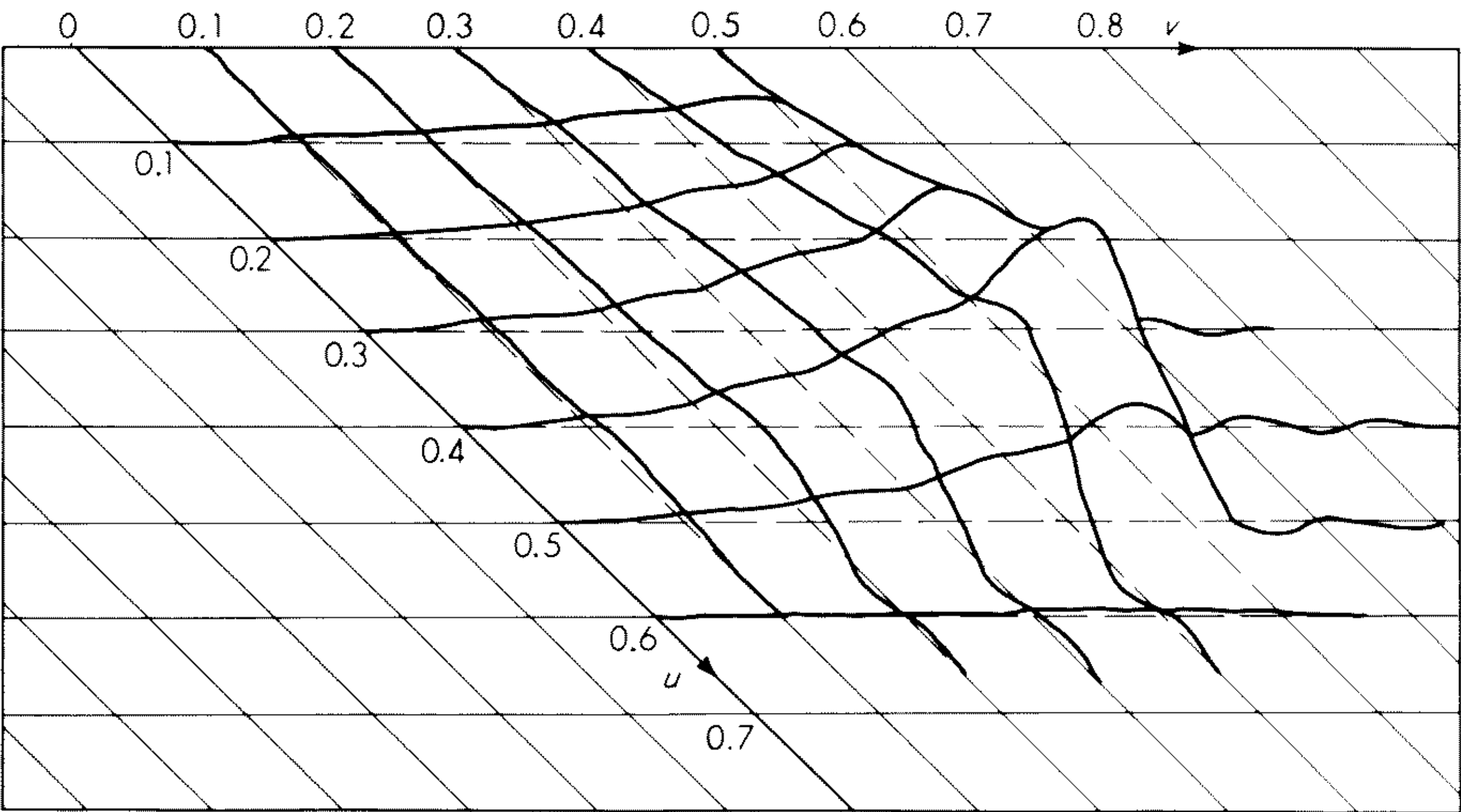


Fig. 7.2 A minimum-mean-square-error approximation to the pattern of Fig. 7.1 by a 35×35 array.

Exercise 7.1 Will matching the Fourier coefficients as was done to minimize (7.1) also provide the minimum error for higher-order averaged errors? Consider the mean-fourth-error criterion

$$\epsilon' = \int_{-1}^1 |f_D - f|^4 du$$

Is the error of a finite series approximation of $2N + 1$ terms minimized by $A_{Dn} = A_n$ for $(|n| \leq N)$? Try a three-term series ($N = 1$), matching $A_{D0} = 1$, $A_{D1} = A_{D(-1)} = 1$, $A_{D2} = A_{D(-2)} = 1/2$, $A_{D3} = A_{D(-3)} = 1/2$.

Gaussian Error, Rectangular Array; Even Number of Elements

The synthesis method described in the preceding section used a series expansion of the desired pattern that consisted of an odd number of terms. Since there is a one-to-one correspondence between expansion coefficient and array current with this method, the realized array has an odd number of elements. This is not a fundamental restriction to the method. Implicit in the choice of an odd number of half-wavelength spaced elements is that the desired pattern repeats in the angular intervals adjacent to the visible region as

$$f_D(u + 2, v) = f_D(u, v)$$

$$f_D(u, v + 2) = f_D(u, v)$$

Instead, we may consider the desired pattern to be antisymmetrically periodic in u and v ; that is,

$$f_D(u + 2, v) = -f_D(u, v) \quad (7.4a)$$

$$\text{and} \quad f_D(u, v + 2) = -f_D(u, v) \quad (7.4b)$$

The coefficients of the Fourier decomposition of this pattern are, considering the four angular regions of u and v ,

$$\begin{aligned} A_{nm} &= \frac{1}{4} \int_{-1}^1 \int_{-1}^1 f_D(u, v) e^{-jnk_0 d_x u - jmk_0 d_y v} du dv \\ &\quad - \frac{1}{4} \int_{-1}^1 \int_{-1}^1 f_D(u, v) e^{-jnk_0 d_x (u+2) - jmk_0 d_y v} du dv \\ &\quad - \frac{1}{4} \int_{-1}^1 \int_{-1}^1 f_D(u, v) e^{-jnk_0 d_x u - jmk_0 d_y (v+2)} du dv \\ &\quad + \frac{1}{4} \int_{-1}^1 \int_{-1}^1 f_D(u, v) e^{-jnk_0 d_x (u+2) - jmk_0 d_y (v+2)} du dv \\ &= \frac{1}{4} \int_{-1}^1 \int_{-1}^1 f_D(u, v) e^{-jnk_0 d_x u - jmk_0 d_y v} du dv (1 - e^{-j2nk_0 d_x} - e^{-j2mk_0 d_y} \\ &\quad + e^{-j2nk_0 d_x - j2mk_0 d_y}) \quad (7.5) \end{aligned}$$

Let us choose the spacings $d_x = d_y = \lambda_0/4$. Then

$$\begin{aligned} A_{nm} &= \frac{1}{4} \int_{-1}^1 \int_{-1}^1 f_D(u, v) e^{-jn(\pi/2)u - jm(\pi/2)v} du dv \\ &\quad (1 - e^{jn\pi} - e^{jm\pi} + e^{-jn\pi - jm\pi}) \\ &= \frac{1}{4} \int_{-1}^1 \int_{-1}^1 f_D(u, v) e^{-jn(\pi/2)u - jm(\pi/2)v} du dv (1 - e^{-jn\pi})(1 - e^{-jm\pi}) \quad (7.6) \end{aligned}$$

All coefficients of (7.6) for n or m even are zero. The nonzero coefficients form a set that can be identified with an array of an even number of elements spaced $\lambda_0/2$ apart having a far-field pattern of the form

$$f(u, v) = \sum_{\substack{n=-N \\ (m, n \text{ odd})}}^N \sum_{m=-M}^M A_{nm} e^{jn(\pi/2)u + jm(\pi/2)v}$$

This procedure can, of course, be carried out for only one variable, resulting in an array of an even number of columns and an odd number of rows or vice versa.

Gaussian Error — Rectangular Array; Spacings Smaller than $\lambda_0/2$

The choice of half-wavelength interelement spacings results in a coincidence of the period of the desired pattern expansion along the u or v axis and the period of the array pattern. If the element spacing of the array is chosen to be greater than $\lambda_0/2$, the radiation pattern will begin to repeat in the visible region $u^2 + v^2 \leq 1$, which is usually undesirable for most antenna applications. The use of interelement spacings smaller than $\lambda_0/2$ implies a pattern periodicity greater than the visible region; the additional interval in which the desired pattern is not specified can be used for very large values of the approximation function, which will have an effect on the part that appears in the visible region. Thus, while the mean-square error between pattern and approximation will not be minimized over the interval corresponding to the reciprocal of the element spacing, a closer fit in the visible region can be achieved.

Let us consider the error criterion

$$\varepsilon = \int_{-\lambda_0/2d}^{\lambda_0/2d} (f_D - f)^2 H^2(u) du \quad (7.7)$$

which is a mean-square match weighted by $H^2(u)$ over the interval corresponding to an interelement spacing d for a single angular variable. If $H(u) = 1$ for all u , this criterion would lead to a Fourier expansion as was obtained previously.

Expanding f_D as a Fourier series over the integration interval,

$$f_D(u) = \sum_{n=-\infty}^{\infty} A_{Dn} e^{jk_0 n d u}$$

The pattern of an array of $2N + 1$ elements that minimizes (7.7) for $H = 1$ everywhere is

$$f(u) = \sum_{n=-N}^N A_{Dn} e^{jk_0 n d u}$$

If we choose $H(u) = 1$ for $-1 < u < 1$, and $H = 0$ elsewhere, we free the approximation pattern function f outside the visible region to improve the match to the desired function f_D in the visible region. For an error criterion that measures pattern fit only in the visible region, we can determine the array coefficients by using $G_D = Hf_D$ and $G = Hf$ such that we minimize

$$\varepsilon = \int_{-1}^1 (f_D - f)^2 du = \int_{-\lambda_0/2d}^{\lambda_0/2d} (f_D - f)^2 H^2 du = \int_{-\lambda_0/2d}^{\lambda_0/2d} (G_D - G)^2 du$$

Expanding G_D and G in Fourier series,

$$G_D = \sum B_{Dn} e^{jk_0 n d u} \quad \text{and} \quad G = \sum B_n e^{jk_0 n d u}$$

we can satisfy the error criterion by equating

$$B_{Dn} = B_n$$

for the first $2N + 1$ terms. To relate B_n to the array element currents we use the fact that the product of f and H is equivalent to a convolution of their Fourier transforms. Hence for $H = 1$ within $|u| \leq 1$, $H = 0$ elsewhere,

$$B_n = \frac{2d}{\lambda_0} \sum_{m=-N}^N A_m \frac{\sin(m-n)\pi(2d/\lambda_0)}{(m-n)\pi(2d/\lambda_0)} \quad (7.8)$$

As an example, consider the desired pattern f_D to be an impulse at $u = 0$. Then

$$B_{Dn} = A_{Dn} = \frac{d}{\lambda_0} = B_n$$

Let us find the coefficients for an array of five elements with $\lambda_0/8$ interelement spacings. The symmetry of f_D about $u = 0$ results in three independent equations from (7.8), since $A_{-2} = A_2$, $A_{-1} = A_1$. These are

$$\begin{aligned} \frac{1}{2} &= A_2 + A_1 \frac{8\sqrt{2}}{3\pi} + \frac{2}{\pi} A_0 \\ \frac{1}{2} &= \frac{8\sqrt{2}}{3\pi} A_2 + \left(\frac{2}{\pi} + 1\right) A_1 + \frac{2\sqrt{2}}{\pi} A_0 \\ \frac{1}{2} &= \frac{4}{\pi} A_2 + \frac{4\sqrt{2}}{\pi} A_1 + A_0 \end{aligned} \quad (7.9)$$

The above equations can be solved to yield the coefficients $A_0 = 103.38$, $A_1 = -72.44$, $A_2 = 21.65$. The far-field pattern of the five-element array with these feeding currents is shown in Fig. 7.3. Also plotted is the far-field pattern of an array of five elements with $\lambda_0/2$ spacings and equal currents.

Exercise 7.2 Derive (7.8) by carrying out the integration of the error

$$\varepsilon' = \int_{-1}^1 |f_D - f|^2 du$$

for f_D expanded as

$$f_D(u) = \sum_{n=-\infty}^{\infty} A_{Dn} e^{jnk_0 d u}$$

and a similar expression for $f(u)$. Differentiate the error to find its minimum, and match like terms.

The large coefficients that result from the solution of (7.9) are to be expected from attempting to synthesize a pattern by using functions of limited variation. The result can be regarded as using interference to produce the main beam as well as the side lobes or as using the visible tails of pattern components in the

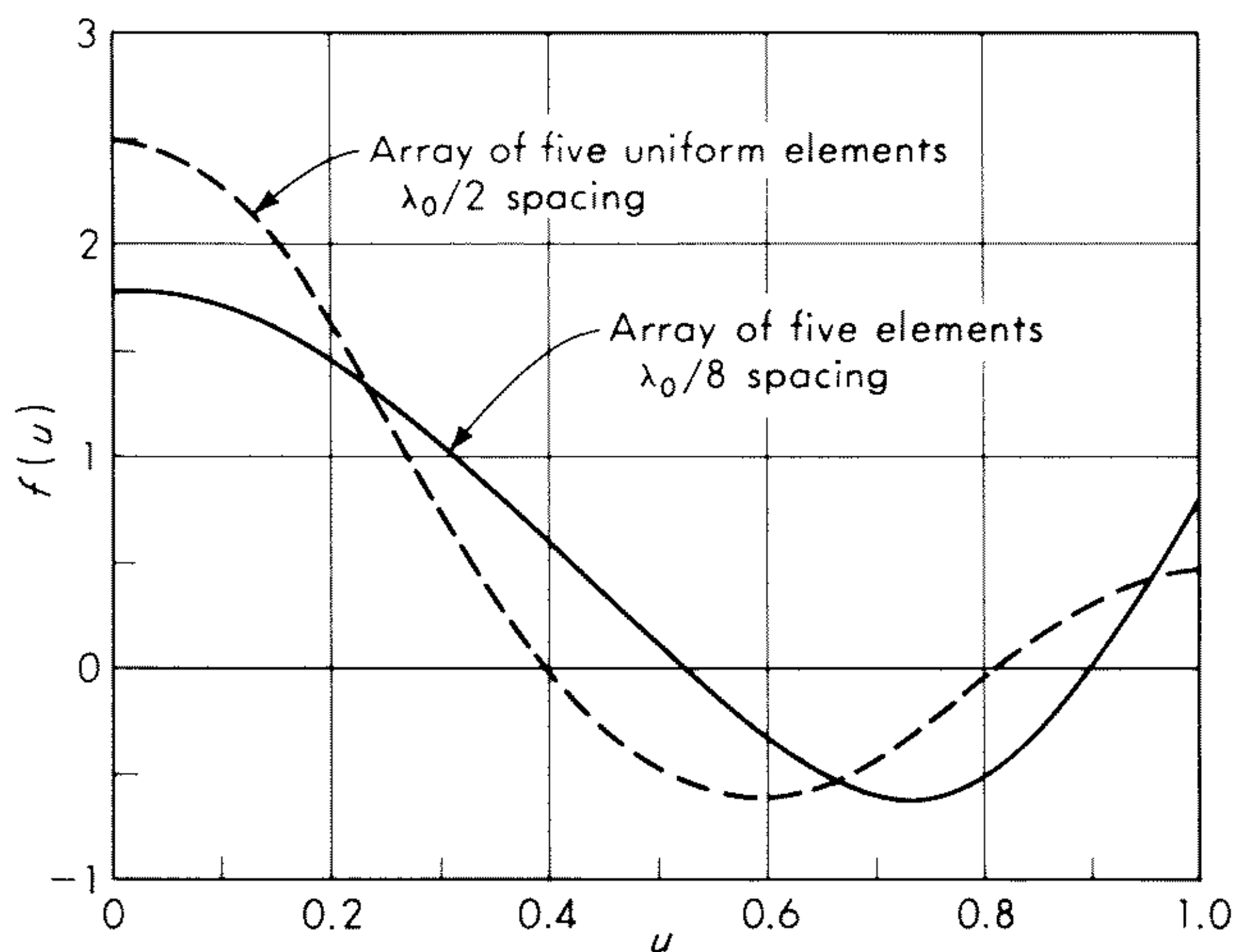


Fig. 7.3 The pattern approximations to an impulse by five-element arrays with $\lambda_0/8$ and $\lambda_0/2$ spacings.

invisible region to shape the pattern. Perhaps a better way to regard this effect, which is often referred to as *supergain*, or more properly *superdirectivity*, is as a poor design of the feeding structure of the antenna. If, instead of dealing only with patterns, the electromagnetic properties of the radiation from a supergain array are analyzed, it will be found that a field distribution corresponding to that produced by a larger conventional array occupies the space in front of the supergain elements and that the high currents in these elements are producing this virtual aperture. Thus the supergain array is in effect a poor feed for the creation of a much larger virtual aperture. Nevertheless, the patterns shown in Fig. 7.3 represent the minimum-mean-square-error match to the desired pattern over the visible range for the given interelement spacing.

The topic of superdirectivity has received considerable attention in the literature, and we shall return to the considerations involving pattern synthesis in Sec. 7.7.

7.3 Gaussian Error — Rectangular Aperture

The error criterion (7.1) has been used in the preceding sections with the constraint that an array of a finite number of point sources is realized. In this section we shall use the realization constraint of a rectangular aperture with a continuous current distribution. The approximation to the desired pattern will

be governed by the finite number of terms of the Fourier series expansion of the current distribution.

A transverse current wave

$$K(x, y) = K_{nm} e^{-jk_x x - jk_y y}$$

across a rectangular aperture that extends from $-a$ to $+a$ in the x direction and from $-b$ to $+b$ in y produces a far-field pattern

$$f(u, v) = 4ab K_{nm} \frac{\sin k_0 a (u - k_x/k)_0}{k_0 a (u - k_x/k_0)} \frac{\sin k_0 b (v - k_y/k_0)}{k_0 b (v - k_y/k_0)}$$

If the aperture distribution consists of a sum of current waves, the far field is a superposition of cardinal functions, each shifted by an amount proportional to the transverse phase velocity.⁴ If the values for k_x and k_y are chosen to be

$$k_x = \frac{n\pi}{a} \quad k_y = \frac{m\pi}{b}$$

then the cardinal functions form an orthogonal set:

$$\begin{aligned} \frac{k_0 a}{\pi} \int_{-\infty}^{\infty} \frac{\sin (k_0 a u - n\pi)}{k_0 a u - n\pi} \frac{\sin (k_0 a u - p\pi)}{k_0 a u - p\pi} du &= \delta_{np} \\ \frac{k_0 b}{\pi} \int_{-\infty}^{\infty} \frac{\sin (k_0 b v - m\pi)}{k_0 b v - m\pi} \frac{\sin (k_0 b v - q\pi)}{k_0 b v - q\pi} dv &= \delta_{mq} \end{aligned}$$

The properties of the cardinal functions can be used to develop a synthesis method based on the Fourier harmonic expansion of the current or field across a plane rectangular aperture. Consider a field pattern $f_D(u, v)$, for which it is desired to synthesize a best fit in the mean-square sense by using a rectangular aperture of size $2a$ in the x direction and $2b$ in the y direction. Equate a set of sample values of the desired pattern to the current harmonics by

$$f_D\left(u_n = \frac{n\pi}{k_0 a}, v_m = \frac{m\pi}{k_0 b}\right) = 4ab K_{nm}$$

Then the aperture distribution

$$K(x, y) = \sum_{n, m} K_{nm} e^{-j(n\pi x/a) - j(m\pi y/b)}$$

produces a far-field pattern

$$f(u, v) = \sum_{n, m} f_D(u_n, v_m) \frac{\sin (k_0 a u - n\pi)}{k_0 a u - n\pi} \frac{\sin (k_0 b v - m\pi)}{k_0 b v - m\pi}$$

that equals the desired pattern at each of the sample points. Between the sample points the pattern deviates from the desired function, and the maximum error can usually be controlled by shifting the entire set of sample points or by altering the specified values near or at singularities in the desired pattern.

Since the desired pattern is usually specified only over the visible region, all samples can be chosen to be zero when

$$u^2 + v^2 = \frac{n^2 \pi^2}{k_0^2 a^2} + \frac{m^2 \pi^2}{k_0^2 b^2} > 1$$

Thus the maximum value of n is $N = 2a/\lambda_0$ and the maximum value of m is $M = 2b/\lambda_0$. The total number of samples in the visible region is approximately the area of the visible region, divided by the area of a sample cell, bounded by the bisectors of the lines between a sample and its neighbors. This is

$$\text{Total number of samples} \approx \frac{\pi}{(\pi/k_0a)(\pi/k_0b)} = \frac{k_0^2}{\pi} ab = \frac{\pi}{\lambda_0^2} (4ab) = \pi NM$$

for large N and M .

The restriction that all nonzero samples lie within the visible region constrains the aperture current or field to have no nonzero wave components with transverse velocities greater than the velocity of light in free space. The result is that there are no supergain synthesis solutions.

To obtain a superdirective result, namely, one that contains large evanescent wave components, a set of sample values of the desired pattern is chosen closer together than the "natural" spacings $\Delta u = \lambda_0/2a$, $\Delta v = \lambda_0/2b$. The set of cardinal functions is then equated to the desired pattern values, and the current components are found. The result is analogous to that shown previously for an array with interelement spacings less than $\lambda_0/2$.

The interval over which the cardinal functions are orthogonal and complete is the infinite range of u (or v). Since any function that is piecewise continuous can be approximated by these functions to an error that decreases to zero as the number of terms goes to infinity, there is an aperture distribution (albeit a supergain one) that will exactly reproduce the desired pattern. This aperture distribution $K_D(u,v)$ is a Fourier series expansion: choosing the first $(2M+1)(2N+1)$ terms results in the best approximation, in the mean-square sense, to that aperture distribution. By Parseval's theorem

$$\lambda_0^2 \int |K_D - K|^2 dx dy = \int_{-\infty}^{\infty} |f_D - f|^2 du dv$$

Hence the truncated Fourier expansion of an aperture distribution corresponding to equally spaced samples of the desired pattern produces the minimum-mean-square pattern match for the given number of terms and aperture size.⁵

7.4 An Equivalence between Arrays and Apertures

The synthesis of patterns for arrays and apertures can be treated separately, or the results can be interrelated. In practice an aperture distribution is often used as an envelope of array current coefficients, and vice versa. There is, however, an equivalence relation that permits the determination of a unique array of M equally spaced elements from an aperture distribution of N harmonic terms. The patterns produced by an aperture distribution and its equivalent array are not identical, but for most practical cases they are very nearly so. The difference occurs because the patterns of arrays are periodic in the variable u , while those of continuous distributions are not. It is therefore necessary to specify the interval over which the equivalence exists.

An aperture distribution of the form

$$F(x) = \frac{1}{2a_N} \sum_{\text{terms}} f_n e^{-jn\pi x/a}$$

produces a far-field pattern that is specified by the N sample values f_n spaced $\Delta u = \lambda_0/2a$ apart, as discussed in Sec. 7.3. The radiation pattern is a series of shifted cardinal functions

$$f(u) = \sum_{N \text{ terms}} f_n \frac{\sin(k_0 a u - n\pi)}{k_0 a u - n\pi} \quad (7.10)$$

As one member of an equivalent set of functions, consider the far-field pattern of a uniform in-phase array of M elements

$$f_u(u) = e^{-j[(M-1)/2]k_0 d u} (1 + e^{jk_0 d u} + e^{2jk_0 d u} + \cdots + e^{jk_0(M-1)d u}) = \frac{\sin[Mk_0(d/2)u]}{\sin[k_0(d/2)u]}$$

This function can be used to construct a set of orthogonal functions with the relation

$$\frac{Md}{\lambda_0} \int_{-\lambda_0/2d}^{\lambda_0/2d} \frac{\sin[k_0 M(d/2)u - n\pi]}{M \sin[k_0(d/2)u - n\pi/M]} \frac{\sin[k_0 M(d/2)u - m\pi]}{M \sin[k_0(d/2)u - m\pi/M]} du = \delta_{mn} \quad (7.11)$$

where the interval λ_0/d is the pattern period. The pattern of any array of M elements with interelement spacings of d can be represented by a sum of terms as

$$f(u) = \sum_{M \text{ terms}} f_m \frac{\sin[M(k_0 d u/2) - m\pi]}{M \sin(k_0 d u/2 - m\pi/M)} \quad (7.12)$$

If the patterns (7.10) and (7.12) are to be equal at the sample points, $u_m = m\lambda_0/Md$, the corresponding coefficients of terms must be equal, and

$$Md = 2a$$

Exercise 7.3 Verify the orthogonality property expressed by (7.11).

To complete the equivalence it is necessary to state the interval over which the equivalence exists. Typically, this might be chosen to be the region that is bounded by the first zero-value samples of the pattern. The region of equivalence determines the number of elements in the array, since the pattern begins to repeat for values of $1/2 k_0 d u$ larger than $\pi/2$. Hence, the total number of samples included in the region of equivalence is M . Of these, N are nonzero, corresponding to the coefficients of the harmonics of the equivalent aperture.

The complex amplitude of the m th element of the equivalent array is

$$A_m = \frac{1}{M_N} \sum_{N \text{ terms}} f_n e^{-j2mn\pi/M}$$

In this manner an array can be found that provides a far-field pattern that is equal to the pattern of a continuous distribution at a set of sample points. The

total extent over which the pattern is to be equivalent defines d , the element spacing, and the frequency of the samples in angle defines M . Since the array pattern exactly equals the aperture pattern at the sample points, one can be obtained from the other, and they may be termed equivalent.

The difference between the patterns at points between the samples must be calculated for each case. As an example, consider the mean-square difference between a uniform array pattern and that of a constant aperture over the array-pattern period:

$$\epsilon = \int_{-\lambda_0/2d}^{\lambda_0/2d} \left[\frac{\sin k_0 a u}{k_0 a u} - \frac{\sin M k_0 (d/2) u}{M \sin k_0 (d/2) u} \right]^2 du$$

Using $Md = 2a$

$$\epsilon \approx \frac{2\lambda_0}{Md} \left(1 - \frac{1}{\pi^2 M} \right) - 2 \int_{-\lambda_0/2d}^{\lambda_0/2d} \frac{\sin^2 M k_0 (d/2) u}{M^2 k_0 (d/2) u \sin (k_0 d/2) u} du$$

or
$$\epsilon \approx \frac{0.3\lambda_0}{M^2 d} \quad M \gg 1$$

7.5 Gaussian Error — Circular Array

The synthesis of far-field patterns is not, of course, limited to the constraint of rectangular apertures or arrays. Similar techniques have been developed for circular antennas. The methods for circular or ring arrays usually apply to the control of the radiation pattern in the plane of the ring, whereas the methods involving circular apertures tend to be concerned principally with the pattern variation with the polar angle measured from the aperture normal.

Consider an array of N point sources equispaced around the circumference of a ring of radius a as shown in Fig. 7.4. The far-field radiation pattern is

$$f(\phi) = \sum_{n=0}^{N-1} i_n e^{j k_0 a \sin \theta \cos [\phi - (n/N)2\pi]} \quad (7.13)$$

The current at each element can be written as a series of terms

$$i_n = \frac{1}{N} \sum_{m=0}^M I_m e^{j m n 2\pi / N} \quad (7.14)$$

This is a representation of the element currents in a Fourier series of *sequence currents*, which are current components that have equal magnitude at each element and a progressive phase increase around the array. Substituting (7.14) into (7.13),

$$f(\phi) = \sum_m \sum_n I_m e^{j k_0 a \sin \theta \cos [\phi - (n/N)2\pi] + j m n 2\pi / N}$$

and using the identities

$$e^{j\beta \cos x} = \sum_n (2 - \delta_{0n}) j^n J_n(\beta) \cos nx \quad (7.15)$$

and

$$\sum_{n=0}^{N-1} e^{j2\pi mn/N} = \begin{cases} N & \text{for } m/N \text{ an integer} \\ 0 & \text{otherwise} \end{cases}$$

the pattern is (see Sec. 5.6)

$$f = \frac{1}{2} \sum_{m=0}^M I_m \sum_{n=0}^{\infty} (2 - \delta_{0n}) [J_{m+nN}(\beta) e^{j(m+nN)(\phi + \pi/2)} + J_{-m+nN}(\beta) e^{-j(-m+nN)(\phi - \pi/2)}] \quad (7.16)$$

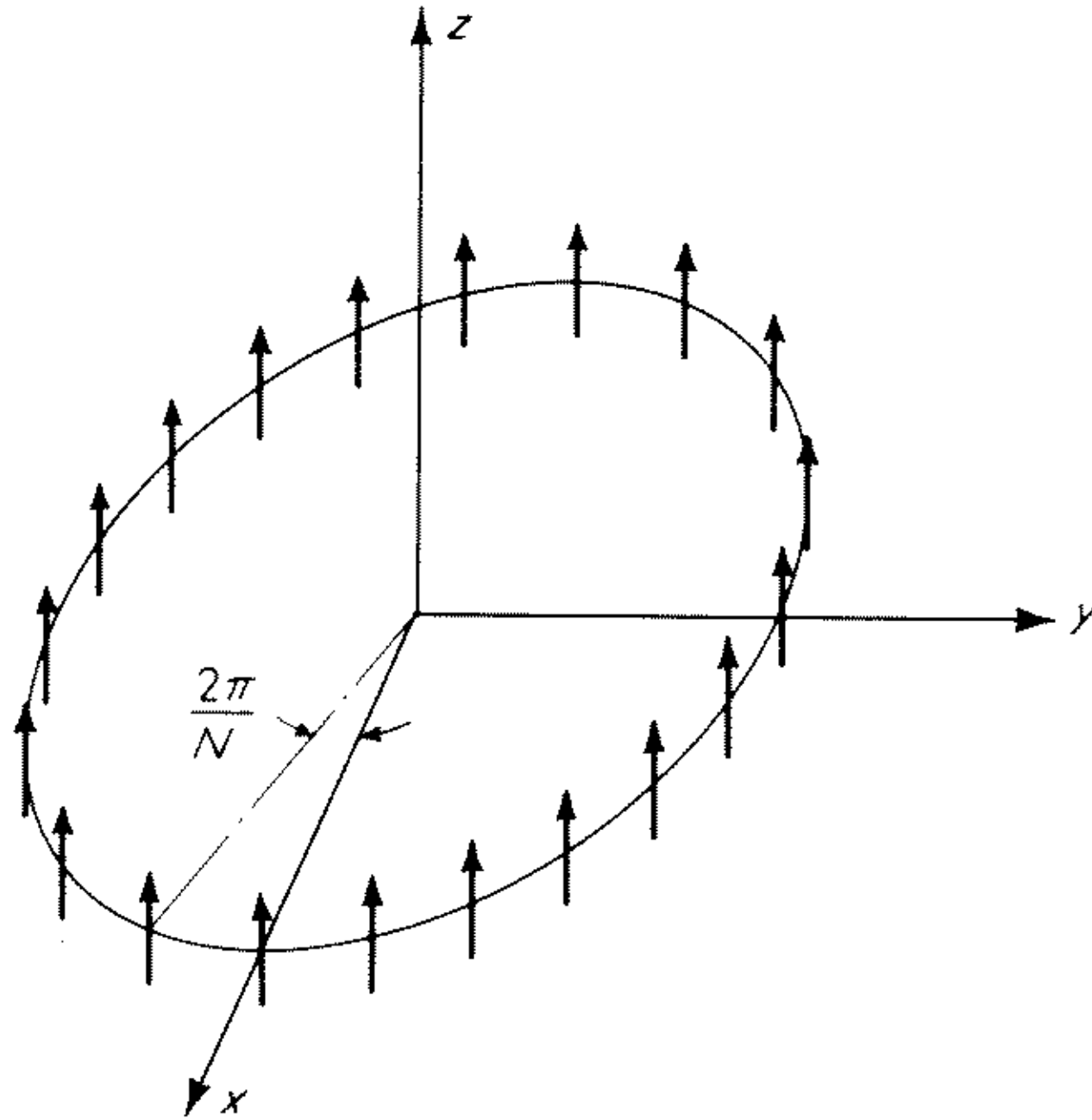


Fig. 7.4 The coordinate system for a circular array.

where $\beta = k_0 a \sin \theta$. The terms for $n = 0$ in (7.16) are called the principal terms; all of the remainder are called residuals. By choosing β to be approximately equal to N , the residuals are almost always small because the largest value that m attains is less than or equal to $N/2$, and the value of a Bessel function is small when the order exceeds the argument. Neglecting residuals, the pattern of the ring of elements is

$$f(\theta, \phi) = \sum_{m=0}^M I_m j^m J_m(k_0 a \sin \theta) e^{jm\phi} \quad (7.17)$$

Let the azimuthal ϕ variation of the desired pattern be specified for some fixed polar angle θ_0 . If $f_D(\theta_0, \phi)$ is piecewise continuous, it can be represented as a Fourier series

$$f_D(\theta_0, \phi) = \sum_{m=-\infty}^{\infty} A_m e^{jm\phi}$$

where

$$A_m = \frac{1}{2\pi} \int_{-\pi}^{\pi} f_D(\theta_0, \phi) e^{-jm\phi} d\phi$$

We can synthesize a pattern that achieves a mean-square match to the desired pattern to the extent that the residuals can be neglected by choosing

$$A_m = I_m j^m J_m(k_0 a \sin \theta_0) \quad (7.18)$$

The coefficients of the Fourier expansion of the desired pattern are related to the sequence currents I_m . Note that the pattern expansion is directly in terms of the angle ϕ and not of the sine of the angle, as was the case for the linear array. The sequence currents having been found from (7.18), the element currents are given by (7.14). Since there cannot be more independently specified coefficients than there are elements, the maximum number of sequence current terms is equal to N , and hence $M \leq N/2$.

The description of a synthesis method for circular arrays of discrete elements using Fourier analysis was presented by Taylor⁶ in 1952. A similar method, in which the elements were approximated by a continuous current sheet, was given by DuHamel.⁷ Further exposition of this topic is in articles by Knudsen⁸ and Patton and Tillman.⁹ The analysis of uniform omnidirectional and directional circular arrays is given in Sec. 5.6.

7.6 Gaussian Error — Circular Aperture

A method of synthesis has been developed that provides a minimum-mean-square-error fit to the desired pattern by the far field of a circular aperture or current disk.¹⁰ For circularly symmetric distributions this technique uses the Hankel-Bessel transform pair

$$\begin{aligned} f(u) &= \int_0^\infty F(r) J_0(k_0 u r) r dr \\ F(r) &= k_0^2 \int_0^\infty f(u) J_0(k_0 u r) u du \end{aligned} \tag{7.19}$$

and the orthogonality property of Bessel functions

$$\int_0^1 J_0(\beta_m r) J_0(\beta_n r) r dr = \frac{1}{2} J_0^2(\beta_n) \delta_{mn}$$

where β_m and β_n are roots of the first-order Bessel function

$$J_1(\beta_m) = 0$$

of which the first four are

$$\begin{aligned} \beta_0 &= 0 \\ \beta_1 &= 3.8317 \\ \beta_2 &= 7.0156 \\ \beta_3 &= 10.1735 \end{aligned}$$

Consider a circularly symmetric distribution of current or field over a circular aperture of radius a lying in the xy plane. The polar angle θ is measured

from the normal to the aperture. Expanding the aperture distribution in the form

$$F(r) = \frac{1}{a^2} \sum_n b_n J_0\left(\frac{\beta_n r}{a}\right) \quad (7.20)$$

the far-field pattern is

$$f(u) = \sum_n b_n J_0(\beta_n) \frac{(k_0 a u) J_1(k_0 a u)}{(k_0 a u)^2 - \beta_n^2} \quad (7.21)$$

where $u = \sin \theta$

Exercise 7.4 Derive (7.21) by using (7.20) and (7.19) and invoking the properties of the Bessel function roots.

The expression (7.21) can be used for a synthesis procedure that is analogous to the Woodward method⁴ of Sec. 7.3, because the field at an angle given by $k_0 a u_m = \beta_m$ is produced by the m th term in the series, all other contributions being zero at this angle. Therefore, we may match the desired pattern $f_D(u)$ at a set of angles

$$u_m = \frac{\beta_m}{k_0 a} \quad (7.22)$$

where

$$f_D(u_m) = \frac{1}{2} b_m J_0^2(\beta_m)$$

The aperture distribution that will produce the pattern that coincides with the desired pattern at the points given by (7.22) is

$$F(r) = 2 \sum \frac{f_D(\beta_m/k_0 a)}{a^2 J_0^2(\beta_m)} J_0\left(\beta_m \frac{r}{a}\right)$$

The directivity of the synthesized pattern in the direction $u = 0$ is

$$D(0) = \frac{4\pi}{\lambda_0^2} (\pi a^2) \frac{|f(0)|^2}{\sum_m \left| f\left(\frac{\beta_m}{k_0 a}\right) \right|^2 / J_0^2(\beta_m)}$$

As was the case for the Woodward method, we have expanded the aperture distribution in the form of orthogonal functions. A truncated series of these functions results in a least-mean-square-error match over the aperture and, by Parseval's theorem, a least-mean-square-error match to the desired pattern over the infinite interval of u . In order to avoid oscillations in the aperture distribution that occur in a shorter distance than a free-space wavelength, no nonzero samples should be chosen for $u_m > 1$.

The above synthesis technique can be extended to include patterns from circular apertures that are not symmetric. Consider an aperture distribution of the form

$$F(r, \phi') = \sum_m \sum_n C_{mn} e^{jn\phi'} J_n\left(\alpha_{mn} \frac{r}{a}\right) \quad (7.23)$$

where α_{mn} is the m th root of the n th order Bessel function and ϕ' is the angle of rotation in the $z = 0$ plane. The radiation pattern is given by substituting (7.23) into

$$f(u, \phi) = \frac{1}{2\pi a^2} \int_0^{2\pi} \int_0^a F(r, \phi') e^{jk_0 u r \cos(\phi - \phi')} r dr d\phi'$$

and using (7.15) to obtain

$$f(u, \phi) = \sum_n j^n e^{jn\phi} \sum_m C_{mn} \alpha_{mn} J_{n-1}(\alpha_{mn}) \frac{J_n(k_0 a u)}{(k_0 a u)^2 - \alpha_{mn}^2}$$

The first step of this synthesis procedure is to expand the desired pattern in its angular Fourier components, given by

$$f_{Dn}(u) = \frac{1}{2\pi} \int_0^{2\pi} f_D(u, \phi) e^{-jn\phi} d\phi$$

Then the n th Fourier component of the desired pattern is equated at the points $k_0 a u_{mn} = \alpha_{mn}$ to the pattern expansion by

$$f_{Dn}(u_{mn}) = j^n \frac{C_{mn}}{2} J_{n-1}^2(\alpha_{mn}) \quad (7.24)$$

The aperture coefficients are determined by (7.24) and substituted into (7.23) to yield the aperture distribution that matches each angular harmonic of f_D at a set of selected angles.

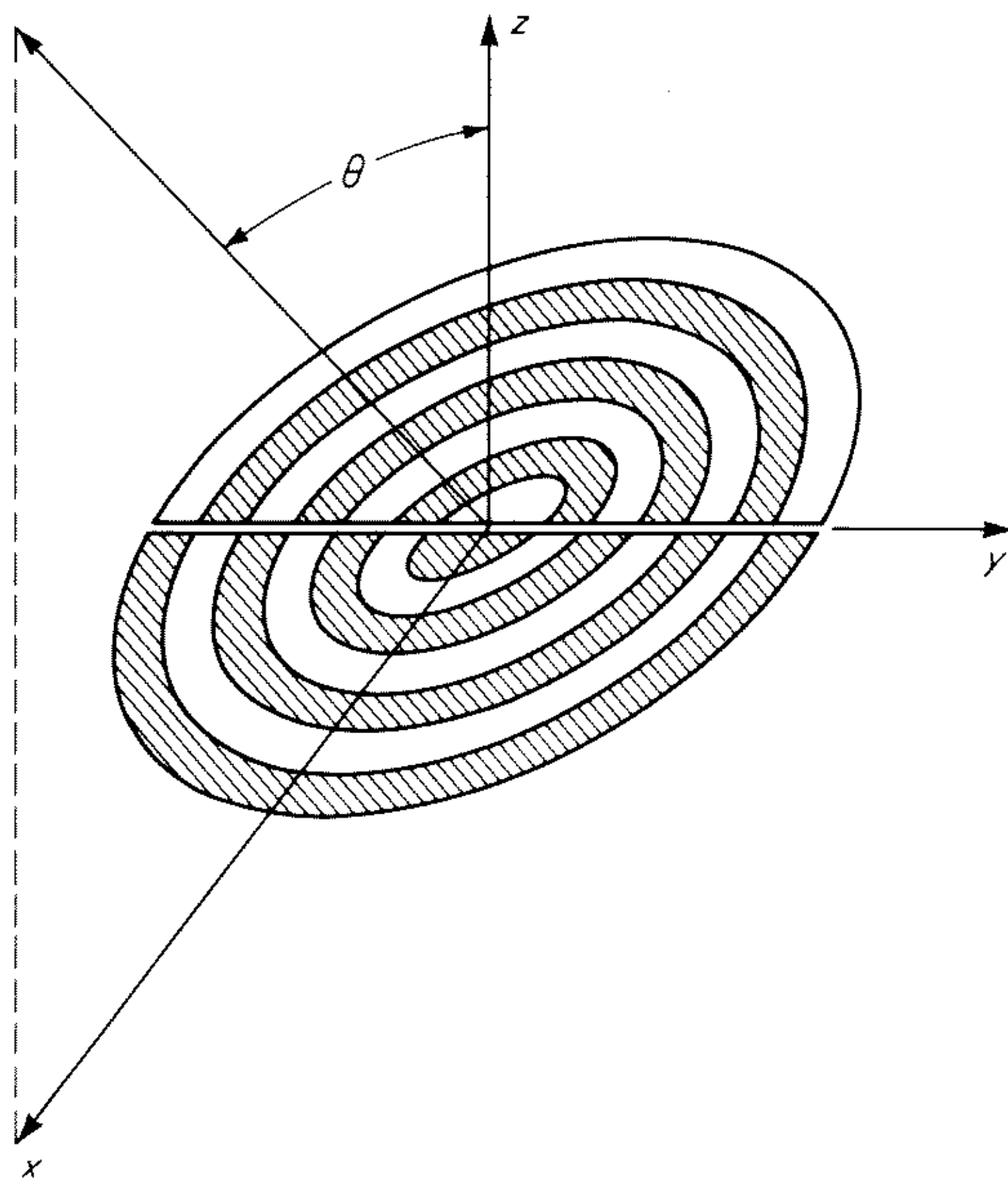


Fig. 7.5 The semicircular zones for the alternate method of Sec. 7.6.

Circular Aperture Synthesis — Alternate Method 1

An alternative method for pattern synthesis uses a circular aperture consisting of two semicircular sectors with a radial amplitude distribution $F(r)$ and a phase difference of 2α radians between the two halves. The aperture is divided into semicircular zones with a common diameter, as shown in Fig. 7.5. The amplitude and phase within each zone are constants.¹¹ This method is particularly applicable to shaping the pattern of a circular aperture in one plane.

Consider a circular aperture consisting of two semicircular sectors with a radial amplitude distribution $F(r)$ and a phase difference of 2α radians between the two halves. The far-field pattern of this aperture measured in the plane that is perpendicular to the diameter that divides the two halves of the aperture is

$$a^2 f(u) = \cos \alpha \int_0^a F(r) J_0(k_0 r) r dr + \sin \alpha \int_0^a F(r) \Omega_0(k_0 r) r dr$$

where $u = \sin \theta$, J_0 is the zeroth-order Bessel function, and Ω_0 is the zeroth order Lommel-Weber function.¹² If the radial variation of the aperture distribution $F(r)$ is a constant F_n in the zone between $r_{n-1} = (n-1)a/N$ and $r_n = na/N$ and if there are N such zones across each half of the aperture, the far-field pattern is

$$f(u) = \sum_{n=1}^N F_n \left\{ \cos \alpha_n \left[\frac{n}{N} \frac{J_1\left(\frac{n}{N} k_0 a u\right)}{k_0 a u} - \frac{(n-1)}{N} \frac{J_1\left(\frac{n-1}{N} k_0 a u\right)}{k_0 a u} \right] + \sin \alpha_n \left[\frac{n}{N} \frac{H_1\left(\frac{n}{N} k_0 a u\right)}{k_0 a u} - \frac{(n-1)}{N} \frac{H_1\left(\frac{n-1}{N} k_0 a u\right)}{k_0 a u} \right] \right\}$$

where $H_1(x)$ is the first-order Struve function.¹² Collecting terms, the above equation can be rewritten

$$f(u) = \sum_{n=1}^N \frac{n}{N k_0 a} \left[A_n J_1\left(\frac{n}{N} k_0 a u\right) + B_n H_1\left(\frac{n}{N} k_0 a u\right) \right] \quad (7.25)$$

with

$$A_n = F_n \cos \alpha_n - F_{n+1} \cos \alpha_{n+1}$$

$$B_n = F_n \sin \alpha_n - F_{n+1} \sin \alpha_{n+1}$$

$$F_{N+1} = 0$$

The series (7.25), when multiplied by u , is a generalized Schlömilch¹² series and can be used to represent functions in the range $|u| < N\pi/k_0 a$.

The first step of the synthesis procedure is to introduce an intermediate function that is well behaved in u and can be expanded in a series

$$f_I(u) = \sum_{n=1}^{\infty} \left[A_{In} J_0 \left(\frac{n}{N} k_0 a u \right) + B_{In} H_0 \left(\frac{n}{N} k_0 a u \right) \right] \quad (7.26)$$

where

$$A_{In} = \frac{k_0 a}{N \pi} \int_{-1}^1 \int_0^{\pi/2} \sec \phi \frac{d}{d\phi} [f_I(u \sin \phi)] \cos \left(\frac{k_0 a n u}{N} \right) d\phi du \quad (7.27)$$

and

$$B_{In} = \frac{k_0 a}{N \pi} \int_{-1}^1 \int_0^{\pi/2} \sec \phi \frac{d}{d\phi} [f_I(u \sin \phi)] \sin \left(\frac{k_0 a n u}{N} \right) d\phi du \quad (7.28)$$

Differentiating (7.26) term by term yields

$$f'_I(u) = \frac{k_0 a}{N} \left[\sum_{n=1}^{\infty} -n A_{In} J_1 \left(\frac{k_0 a n u}{N} \right) - n B_{In} H_1 \left(\frac{k_0 a n u}{N} \right) + B_{In} \frac{2}{\pi} \right] \quad (7.29)$$

Examination of (7.29) and (7.25) shows that the derivative of the intermediate function is of the same form as the radiation pattern of the zoned aperture. Hence, the function f_I provides a convenient means of expanding the desired pattern in a series that is relevant to the zoned aperture pattern. If the desired pattern is $f_D(u)$, we set

$$f'_I(u) = -(k_0 a)^2 u f_D(u)$$

and solve for $f_I(u)$. Then, using (7.27) and (7.28) we determine the constants A_{In} and B_{In} from $f_I(u)$. The far-field pattern of the zoned aperture is a truncated series of terms using the expansion coefficients of $f_I(u)$, that is, (7.25), where

$$A_n = A_{In} \quad B_n = B_{In}$$

The sum $\sum (2/\pi) B_{In}$ can be considered a constant (provided the series is convergent) that is included in the condition on f at $u = 0$,

$$f(0) = \sum_{n=1}^N \frac{n^2}{N^2} \frac{A_n}{2}$$

The limits of ± 1 on u imply that for real values of θ , N must be less than or equal to $2a/\lambda_0$, from which the minimum zone width is

$$\Delta r = r_{n+1} - r_n = \frac{a}{N} = \frac{\lambda_0}{2}$$

As an example, consider the synthesis of a flat-topped beam,

$$f_D(u) = 1 \quad -u_0 \leq u \leq u_0$$

$$f_D(u) = 0 \quad u_0 < |u| < 1$$

$$f'_I(u) = -(k_0 a)^2 u f_D(u)$$

$$\begin{aligned} A_n &= -\frac{2k_0 a}{N\pi} \int_0^{u_0} \int_0^{\pi/2} \sec \phi \frac{d}{d\phi} \left[\frac{(k_0 a u \sin \phi)^2}{2} \right] \cos \left(\frac{k_0 a n u}{N} \right) d\phi du \\ &= -\frac{2N^2}{\pi} \left[\frac{(k_0 a u_0)^2}{N^2 n} \sin \left(\frac{k_0 a n u_0}{N} \right) + \frac{2k_0 a u_0}{N n^2} \cos \left(\frac{k_0 a n u_0}{N} \right) \right. \\ &\quad \left. - \frac{2}{n^3} \sin \left(\frac{k_0 a n u_0}{N} \right) \right] \quad (7.30) \end{aligned}$$

For the correct value at the origin,

$$\sum \frac{1}{2} \frac{n^2}{N^2} A_n = 1$$

For this example, assume $N = 20$ and $k_0 a u_0 = 99\pi/25$. By substituting into (7.30) and using the resultant values of A_n in (7.25), the pattern shown in Fig. 7.6 is obtained.

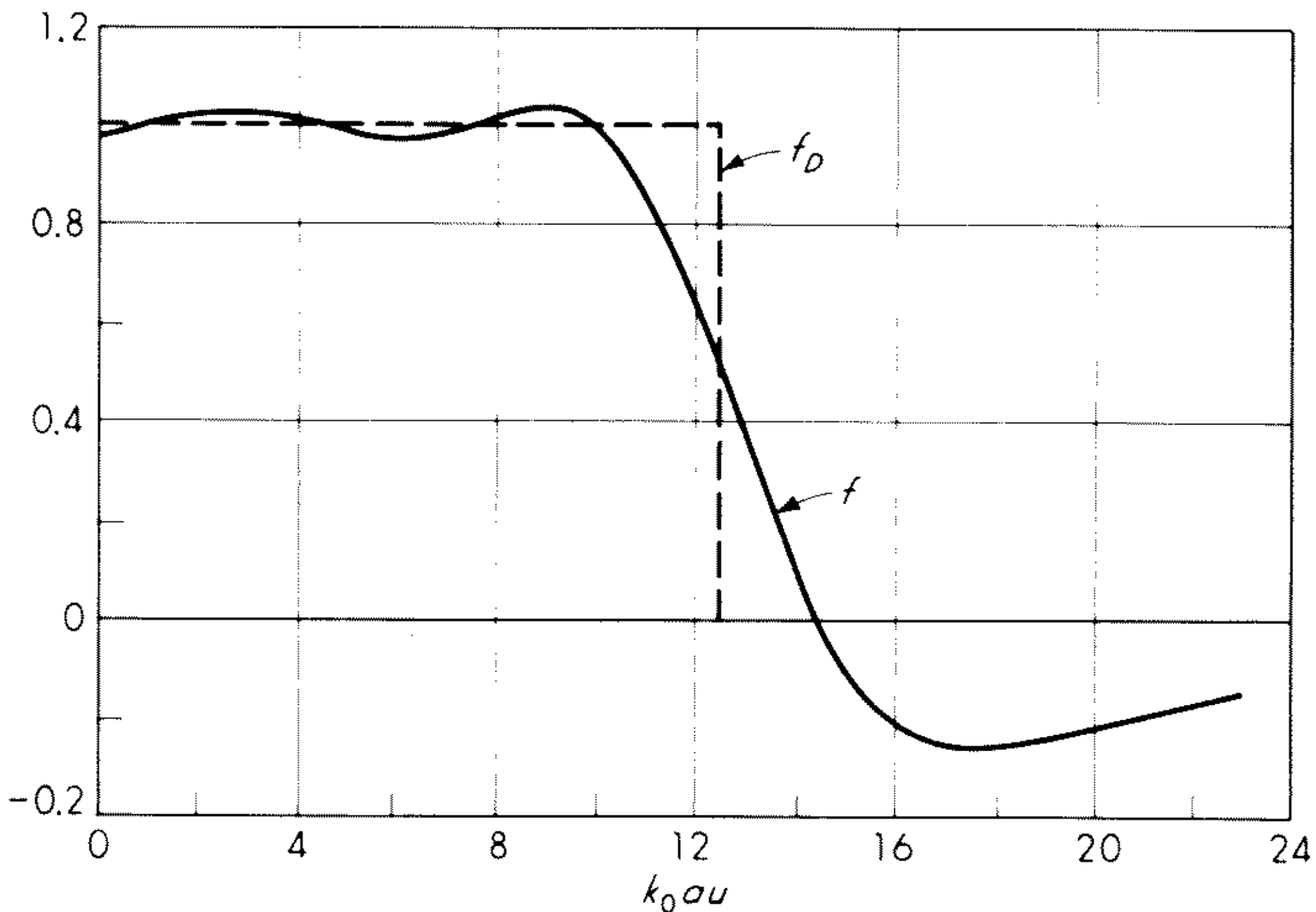


Fig. 7.6 The far-field pattern approximation to a square-top pattern using the semicircular zone synthesis method. (From Cornbleet.¹¹)

Circular Aperture Synthesis — Alternate Method 2

There is another method of synthesis of circularly symmetric patterns that has a particularly simple physical interpretation. Consider a circular aperture

of radius a , located in the $z = 0$ plane and containing a field or current distribution $F(r)$ that depends only upon r . The far-field pattern is

$$f(\sin \theta) = \int_0^{2\pi} \int_0^a F(r) e^{jk_0 r \sin \theta \cos(\phi - \phi')} r dr d\phi' \quad (7.31)$$

As the pattern (7.31) is independent of ϕ , we may choose $\phi = 0$ for convenience.

Writing (7.31) in terms of the variables x and y , and using $u = \sin \theta$

$$f(u) = \int_{-a}^a \int_{-\sqrt{a^2-x^2}}^{\sqrt{a^2-x^2}} F(\sqrt{x^2+y^2}) e^{jk_0 x u} dy dx \quad (7.32)$$

The expression (7.32) can be interpreted as the far-field pattern of an equivalent line source of length $2a$ lying along the x axis. The current on the equivalent line source is

$$F_e(x) = \int_{-\sqrt{a^2-x^2}}^{\sqrt{a^2-x^2}} F(\sqrt{x^2+y^2}) dy$$

or, by changing variables,

$$F_e(x) = 2 \int_x^a \frac{F(r)}{\sqrt{r^2-x^2}} r dr \quad (7.33)$$

To invert (7.33) so that $F(r)$ can be found from a given $F_e(x)$, consider the integral

$$\int_w^a \frac{x F_e(x)}{\sqrt{x^2-w^2}} dx$$

From (7.33)

$$\int_w^a \frac{x F_e(x)}{\sqrt{x^2-w^2}} dx = 2 \int_w^a \frac{x dx}{\sqrt{x^2-w^2}} \int_x^a \frac{r F(r)}{\sqrt{r^2-x^2}} dr \quad (7.34)$$

Interchanging the order of integration in (7.34) and regrouping terms, we obtain

$$\int_w^a \frac{x F_e(x)}{\sqrt{x^2-w^2}} dx = 2 \int_w^a F(r) r dr \int_w^r \frac{x dx}{\sqrt{x^2-w^2} \sqrt{r^2-x^2}} \quad (7.35)$$

Substituting $x^2 = (r^2 - w^2)t + w^2$, (7.35) becomes

$$\int_w^a \frac{x F_e(x)}{\sqrt{x^2-w^2}} dx = \int_w^a r F(r) dr \int_0^1 \frac{dt}{\sqrt{t(1-t)}} \quad (7.36)$$

The second integral on the right side of (7.36) can be evaluated as

$$\int_0^1 \frac{dt}{\sqrt{t(1-t)}} = \pi$$

yielding

$$\int_w^a \frac{x F_e(x)}{\sqrt{x^2-w^2}} dx = \pi \int_w^a F(r) r dr \quad (7.37)$$

Differentiating both sides of (7.37),

$$\frac{d}{dw} \int_w^a \frac{x F_e(x) dx}{\sqrt{x^2 - w^2}} = -\pi w F(w)$$

and since w is a dummy variable for r , we may rewrite the final form as

$$F(r) = -\frac{1}{\pi r} \frac{d}{dr} \int_r^a \frac{x F_e(x) dx}{\sqrt{x^2 - r^2}} \quad (7.38)$$

or as
$$F(r) = -\frac{1}{\pi r} \frac{d}{dr} \int_0^{\sqrt{a^2 - r^2}} F_e(\sqrt{r^2 + w^2}) dw \quad (7.39)$$

Exercise 7.5 Check (7.38) or (7.39) by finding the circular aperture distribution that produces the same field pattern variation as a uniform line source ($F_e = 1$).

This synthesis method for circular apertures rests upon the integral (7.38) or (7.39). The first step is to find F_e , the current distribution of the equivalent line source that meets the desired error criterion. Then, by using (7.38), the field or current distribution on a circular aperture that produces the same pattern variation can be determined. This method, which was developed by Minkovich and Davidchevskiy,¹³ provides an interesting equivalence between circular apertures and line sources and can also be applied to elliptical apertures. The derivation given here was developed independently by Chu and Glaser.¹⁴

7.7 The Reactive Power Constraint

The synthesis methods described in the preceding sections have not dealt directly with the problem of constraining the amount of reactive power resulting from the antenna current distribution. In fact, each of the methods can be used or extended to provide an arbitrarily close fit to a desired pattern, usually resulting in large, highly oscillatory terms in the current distribution, as illustrated in Sec. 7.2.

The reactive power in the vicinity of the antenna is linked to the radiation pattern in the invisible region of the angular variable (see Sec. 3.2). This connection was explored by Woodward and Lawson¹⁵ for the two-dimensional case and by Rhodes¹⁶ for a planar aperture and three dimensions.

A frequently used measure of the ratio of reactive to radiative power of an antenna is the superrain ratio¹⁷ given by

$$\gamma = \frac{\int_{-\infty}^{\infty} |f(u)|^2 du}{\int_{-1}^1 |f(u)|^2 du} \quad (7.40)$$

for a single angular variable.

The relation between the superratio and the antenna band width is not apparent, since (7.40) takes into account only the radiation field and not the antenna circuitry. However, it has been shown that a suitably modified form of aperture Q calculation can yield the correct input Q for a small planar dipole.¹⁸ It is a certainty that a large value of γ implies that the energy storage terms will dominate the input characteristics of the antenna. Although the input Q and the aperture Q may be numerically different, it is necessary to constrain the latter if the former is to be kept small.

A method of pattern synthesis has been developed that incorporates an explicit constraint on the superratio.^{19,20} It applies to the case of a continuous line source and a single angular variable. The key to the method is the use of a set of functions that are orthogonal over both a finite interval, corresponding to the visible region, and the infinite interval. The functions that exhibit this property of dual orthogonality are the spheroidal wave functions, and it is the prolate spheroidal functions of zero degree that are pertinent to the problem of energy-constrained synthesis by a line source. The properties of these functions are described by Slepian and Pollak²¹ and Flammer.²² Let us choose a set of prolate spheroidal functions ψ_n that are normalized so that

$$\int_{-1}^1 \psi_n(c,z) \psi_m(c,z) dz = \delta_{nm} \quad (7.41)$$

and
$$\int_{-\infty}^{\infty} \psi_n(c,z) \psi_m(c,z) dz = G_n(c) \delta_{nm} \quad (7.42)$$

Values of the normalization constant $G_n(c)$ versus c are given by Slepian and Pollak,²¹ where the reciprocal of G_n is called λ_n . A prolate spheroidal function is its own Fourier transform; these functions are the eigenfunctions of the finite-range Fourier transform equation

$$j^n \sqrt{\frac{2\pi}{cG_n}} \psi_n(c,u) = \int_{-1}^1 e^{jcuz} \psi_n(c,z) dz$$

Thus a current distribution along the z axis from $-a$ to $+a$ of the form $\psi_n(z/a)$ produces a far-field pattern $\psi_n(u)$, where $u = \cos \theta$ and θ is the polar angle, measured from the z axis. In the literature involving these functions it is customary to call the function over the finite range the angular wave function, whereas the same function considered over the infinite range is termed the radial prolate spheroidal wave function. This distinction arises because these functions are the bases of expansion along the prolate spheroidal coordinate axes. The parameter c is related to the line source length $2a$ and the wavelength by $c = k_0 a$.

The prolate spheroidal wave functions form a complete and orthogonal set over the finite interval corresponding to the visible region, $-1 \leq u \leq 1$; hence the desired radiation pattern can be expanded in a series of these functions

$$f_D(u) = \sum_{n=0}^{\infty} A_{Dn} \psi_n(c,u) \quad (7.43)$$

where the coefficients A_{Dn} are given by

$$A_{Dn} = \int_{-1}^1 f_D(u) \psi_n(c, u) du \quad (7.44)$$

The line source pattern can be expanded in a similar fashion:

$$f(u) = \sum_{n=0}^N A_n \psi_n(c, u) \quad (7.45)$$

where

$$A_n = \int_{-1}^1 f(u) \psi_n(c, u) du \quad (7.46)$$

A synthesis technique to determine the coefficients of the line source pattern for a fixed superratio can now be developed by using the Lagrange multiplier method. The error criterion is that of the minimum-mean-square-error match of f to f_D for a specified γ , given by

$$\epsilon = \int_{-1}^1 |f_D(u) - f(u)|^2 du + \mu \left[\int_{-\infty}^{\infty} |f(u)|^2 du - \gamma \int_{-1}^1 |f(u)|^2 du \right] \quad (7.47)$$

Substituting (7.43) and (7.45) into (7.47) and using (7.41) and (7.42) leads to

$$\epsilon = \sum_n [|A_{Dn} - A_n|^2 + \mu |A_n|^2 (G_n - \gamma)] \quad (7.48)$$

which is minimized by

$$A_n = \frac{A_{Dn}}{1 + \mu(G_n - \gamma)} \quad (7.49)$$

The Lagrange multiplier is a positive number satisfying the equation

$$0 = \sum_{n=0}^N |A_n|^2 (G_n - \gamma) = \sum_{n=0}^N \frac{|A_{Dn}|^2 (G_n - \gamma)}{[1 + \mu(G_n - \gamma)]^2} \quad (7.50)$$

From examination of tables of the normalization constants $G_n(c)$ it is found that the values of G_n increase very rapidly after $4a/\lambda_0 + 1$ terms, provided γ is not chosen to be excessively large. Hence the ratio A_n/A_{Dn} , given by (7.49), decreases rapidly for $n > N = 4a/\lambda_0$ for realistic γ . The resultant approximation pattern is determined for all practical purposes by the same number of terms as would be employed in a Woodward synthesis over the visible region. The basic difference between the two methods is that the use of the prolate spheroidal terms results in a straightforward means of synthesizing a pattern with a specified value of superratio.

Solving (7.50) for μ , given A_{Dn} and γ , permits the determination of A_n from (7.49), and thus the synthesized pattern. The line source current distribution that produces this pattern is

$$F(z) = \sum_{n=0}^N j^{-n} \sqrt{cG_n/2\pi} A_n \psi_n(c, z/a) \quad -a \leq z \leq a$$

This method of reactive-power-constrained synthesis requires extensive tables of the prolate spheroidal functions, which are not as yet available, particularly for large values of the parameter c . Also, the determination of the expansion coefficients A_{Dn} is a tedious job. There are many aspects of this problem remaining to be studied, such as the conversion of these results to sets of more convenient functions.

Although this synthesis method is limited in applicability by the use of the gaussian error criterion and the supergain ratio, it provides a formally straightforward method of energy-constraint synthesis. Extensions of this technique that are applicable to planar antennas and that relate the reactive and radiative power at the planar antenna surface to the angular spectrum of the wave components are the next steps in the development of synthesis with reactive power constraints.^{18,23}

7.8 Methods Suited to the Production of Narrow-beam, Low-side-lobe Patterns

The problem that occurs most frequently in antenna design is to determine a current distribution that will produce a radiation pattern with a specified main-beam width and side-lobe level. A number of synthesis techniques have been developed for this particular problem, rather than the synthesis of arbitrary patterns, as discussed in the other sections of this chapter.

The single-beam low-side-lobe problem can be characterized as one for which the desired pattern is an impulse. Error criteria other than gaussian can be used for this case because the mathematical manipulations are not overly involved, and the results can be conveniently tabulated. The Chebyshev methods, which in this instance provide a minimum deviation match, were developed for arrays by Dolph²⁴ and for continuous line sources by Taylor.¹⁷ The application to arrays is discussed in detail in Sec. 5.10, so only the principal results for the broadside array are briefly summarized here.

Chebyshev Error — Linear Array

The Dolph-Chebyshev technique consists in expressing the pattern function of a linear, uniformly spaced array as a Chebyshev polynomial. The order of the polynomial is related to the number of elements of the array. In the following the Chebyshev polynomial will be related to the field pattern; therefore, the order of the polynomial associated with an array of $N + 1$ elements is N .

Within the range $-1 \leq w \leq 1$ the polynomial

$$T_N(w) = \cos(N \cos^{-1} w)$$

is oscillatory, having a magnitude no greater than unity. For values of $|w|$ greater than 1 the Chebyshev polynomial increases rapidly with $|w|$. To

specify a pattern with a side-lobe level that is $1/R$ that of the main beam of $N + 1$ elements, set

$$R = \cosh (N \cosh^{-1} w_0) \quad (7.51)$$

where w_0 is the end point of w . Since w_0 is the point at which the largest value of T_N occurs, it is the main beam direction. Let us now relate the Chebyshev polynomial to the array factor $f(u)$ of a broadside array by

$$f(u) = T_N \left(w_0 \cos \frac{k_0 d}{2} u \right)$$

where d is the interelement spacing. If the pattern periodicity is to correspond to the visible region $-1 \leq u \leq 1$, the spacing $d = \lambda_0/2$. For patterns symmetric about $u = 0$, the array factor can be written [Eq. (5.87)]

$$f(u) = \sum_{m=0}^{(N-1)/2} A_m \cos (2m + 1) \frac{k_0 d}{2} u \quad \begin{array}{l} N \text{ odd (even number} \\ \text{of elements)} \end{array} \quad (7.52)$$

$$\text{or } f(u) = \sum_{m=0}^{N/2} A_m \cos m k_0 d u \quad \begin{array}{l} N \text{ even (odd number} \\ \text{of elements)} \end{array} \quad (7.53)$$

Having determined w_0 from the specified side-lobe level and number of elements by (7.51), the next step is to relate $T_N(w)$ to $f(u)$ by equating terms of the Chebyshev expansion to those given by (7.52) or (7.53). The array factors are expanded in Chebyshev polynomials of $w/w_0 = \cos [(k_0 d/2)u]$. As an example, for N odd the array factor is

$$\begin{aligned} f(u) &= A_0 T_1 \left(\frac{w}{w_0} \right) + A_1 T_3 \left(\frac{w}{w_0} \right) + A_2 T_5 \left(\frac{w}{w_0} \right) + \cdots \\ &= A_0 \left(\frac{w}{w_0} \right) + A_1 \left[4 \left(\frac{w}{w_0} \right)^3 - 3 \left(\frac{w}{w_0} \right) \right] \\ &\quad + A_2 \left[16 \left(\frac{w}{w_0} \right)^5 - 20 \left(\frac{w}{w_0} \right)^3 + 5 \left(\frac{w}{w_0} \right) \right] + \cdots \end{aligned}$$

while the Chebyshev polynomial that is to be matched to the array factor is $T_N(w)$. Equating the two and matching like powers of w determines the coefficients A_m , from which the element currents can be found.

In Sec. 5.10 it is shown that the Chebyshev polynomial method provides the lowest side-lobe level for a given number of elements and a fixed beam width, measured between first nulls. The Dolph-Chebyshev method is a simple yet elegant technique for a minimum-deviation fit to an impulse function. The feeding coefficients for the array elements have been tabulated for a large number of cases,²⁵ and there are highly accurate approximation methods for determining the coefficients of arrays of many elements that are much simpler than the term-matching procedure outlined above.^{26,27}

Chebyshev Error — Continuous Line Source

A side-lobe level control technique similar to that for arrays can be developed for continuous current distributions, but in this case the infinite angular range of the pattern function forces a modification of the basic method.

Consider a radiation pattern of the form

$$f(u) = \cos k_0 a (\sqrt{u^2 - c^2}) \quad (7.54)$$

For the angular range $c^2 \leq u^2 < \infty$ this function oscillates between $+1$ and -1 ; however, when $u = 0$,

$$f(u = 0) = \cosh k_0 a c$$

and the side-lobe level of a pattern with a main beam at $u = 0$ is given by

$$R = \cosh k_0 a c \quad (7.55)$$

Using (7.55), the value of c can be determined for a given side-lobe level, aperture size, and wavelength.

To determine the current distribution that produces the pattern of (7.54), let us use the Woodward technique of Sec. 7.3. Sampling the pattern function $f(u)$ at the intervals $u_n = n\pi/k_0 a$ yields the Fourier expansion of the current as

$$F(z) = \frac{1}{2a} \sum_{n=0}^{\infty} \cos k_0 a \sqrt{\left(\frac{n\pi}{k_0 a}\right)^2 - c^2} e^{-j(\pi/a)nz} \quad (7.56)$$

If the pattern (7.54) is allowed to continue for large values of u , the coefficients of the current expansion for large n will tend to $\cos n\pi$. These are the terms that provide impulsive behavior at the edges of the line source. Large values of current or aperture field at the edges of the antenna are difficult to produce and represent an unrealistic result from two standpoints. First, for many antennas it is desirable to have the edge current values low, not high; second, the reason that we are led to these peaks is to sustain the equal-lobe pattern for large values of u . In fact, this is rarely a feature. It would generally be preferred if the side lobes decreased in value for large u . Calculation of the pattern directivity shows that power expended in the far-out lobes is at the expense of main-beam gain.

A simple method of eliminating the higher terms of the current distribution that contribute to impulsive behavior is to terminate the series (7.56) after the N th term. In effect, this requires that the pattern function of the terminated series must have zeros occurring at the sample points $u_n = n\pi/k_0 a$, when $n > N$. The pattern is thus forced to revert to $(\sin k_0 a u)/k_0 a u$ behavior for $u > u_N$. The choice of N is dependent upon the desired side-lobe level, the amount of gain decrease from a uniform distribution that can be tolerated, and the desirability of uniform side lobes from system considerations.

A more sophisticated method for the adjustment of pattern zeros to terminate the series expansion of current terms was given by Taylor.¹⁷ He introduced a factor σ that stretches the zeros of the pattern function so that for

$u_N = N\pi/k_0a$ a zero coincides with the sample points for the Woodward synthesis. The Taylor pattern function for $u < u_N$ corresponding to (7.54) is

$$f_1(u) = \cos k_0a \sqrt{\left(\frac{u}{\sigma}\right)^2 - c^2}$$

which has zeros at

$$u_n = \sigma \sqrt{\frac{\pi^2(2n-1)^2}{4k_0^2a^2} + c^2}$$

In order that a zero of f_1 coincides with the N th sample point,

$$u_N = \frac{N\pi}{k_0a} = \sigma \sqrt{\frac{\pi^2(2N-1)^2}{4k_0^2a^2} + c^2}$$

or

$$\sigma = \frac{N}{\sqrt{(N-1/2)^2 + (2k_0ac/\pi)^2}}$$

The parameter σ provides a smooth transition between the two pattern regions, at the expense of slight beam broadening. The Taylor pattern is

$$f_1(u) = R \frac{\sin k_0au}{k_0au} \prod_{n=1}^{N-1} \frac{1 - (u/u_n)^2}{1 - (k_0au/n\pi)^2}$$

where

$$u_n = \pm \sigma \sqrt{c^2 + \left[\frac{\pi(n-1/2)}{k_0a}\right]^2} \quad 1 \leq n \leq N$$

$$u_n = \pm n \frac{\pi}{k_0a} \quad N \leq n \leq \infty$$

The result is that this method provides approximately a specified deviation match to an impulse, using a continuous current distribution, over an angular range that is so chosen that the directivity of the antenna is not seriously reduced.

The One-parameter Taylor Line Source

Another method of partial-pattern synthesis that is intended for side-lobe control was developed by Taylor.²⁸ This method, which is not based on an error criterion, uses a modified $(\sin k_0au)/k_0au$ pattern as its basis and benefits from the high efficiency that is achieved by using patterns resembling $(\sin k_0au)/k_0au$.

Consider a pattern function

$$f(u) = \frac{\sin k_0a \sqrt{u^2 - c^2}}{k_0a \sqrt{u^2 - c^2}}$$

For large values of u , this pattern behaves as $(\sin k_0au)/k_0au$. For $u = 0$, the pattern height is

$$f(0) = \frac{\sinh k_0ac}{k_0ac}$$

The first side lobe occurs when

$$k_0 a \sqrt{u^2 - c^2} = 4.603 \quad \text{or} \quad u \approx \sqrt{\frac{9}{16} \frac{\lambda_0^2}{a^2} + c^2}$$

and has a height relative to the main beam of

$$\frac{1}{R} = \frac{k_0 a c}{4.603 \sinh k_0 a c} \approx \frac{4 a c}{3 \lambda_0 \sinh k_0 a c}$$

If R , the height of the main beam over the first side lobe, is specified, the constant c can be determined, given the aperture size ($2a$) and the wavelength. The aperture distribution that produces this pattern is

$$F(z) = \frac{1}{2a} I_0 \left[k_0 a c \sqrt{1 - \left(\frac{z}{a} \right)^2} \right] \quad |z| \leq a$$

where I_0 is the modified Bessel function of zero order. The value of this method is that it is a simple way of obtaining an aperture distribution that produces a main beam with relatively high efficiency and side lobes that do not exceed a specified value.

Chebyshev Error — Circular Aperture

The Chebyshev side-lobe control technique for line sources can be restated for a circular aperture. The far-field radiation pattern of a current distribution $F(r)$ that varies only as a function of the radius r and extends to $r = a$ is

$$f(u) = \int_0^a F(r) J_0(k_0 r u) r dr$$

where the variable u is the sine of the polar angle θ measured from the normal to the circular aperture.

Let us choose a desired pattern of the form

$$f_D(u) = \cos k_0 a \sqrt{u^2 - c^2} \quad (7.57)$$

The height of the main beam above the side-lobe level is, as before,

$$R = \cosh k_0 a c$$

Using the Ruze method¹⁰ of circular aperture synthesis that is analogous to the Woodward method⁴ for line sources, we find that the aperture distribution that produces the pattern (7.57) is

$$F(r) = 2 \sum_{n=0}^{\infty} \frac{\cos k_0 a \sqrt{(\beta_n/k_0 a)^2 - c^2}}{a^2 J_0^2(\beta_n)} J_0 \left(\beta_n \frac{r}{a} \right)$$

where the Bessel roots β_n are defined by $J_1(\beta_n) = 0$. As was shown previously, the sampling of (7.57) for large n leads to impulsive behavior of $F(r)$ at $r \rightarrow a$. It is necessary to terminate the series at some value $n = N$, thereby shifting

the zeros of the pattern to coincide with the zeros of $J_1(k_0 au)$. This forces the pattern to decrease with large u , resulting in a controlled-side-lobe, high-directivity pattern.†

Tables of aperture distributions have been calculated by using the expressions derived by Taylor, for which there is a stretching factor σ that shifts the zeros up to $n = N$ so that the N th zero coincides with a zero of the uniform aperture distribution.³⁰

7.9 Non-uniformly Spaced Array Pattern Synthesis

The classical approaches to array-pattern analysis and synthesis have considered only the case of uniformly spaced elements. There is rarely, however, any clear requirement for uniform spacing, although under certain conditions it may be desirable to have all elements in identical environments. There have been a number of studies of the properties of arrays of unequally spaced elements in which attempts were made to use the additional freedoms of element placement to improve the radiation pattern. The electromagnetic interaction that occurs between closely spaced elements usually precludes the consideration of spacings of less than $\lambda_0/2$, and so most nonuniform spacing techniques apply to the reduction of the number of elements from that needed for a conventional uniformly spaced array.

There are two categories in which the nonuniform array method can be grouped. The first of these are the deterministic, or analytical techniques, some of which will be covered in this section. The second category includes the random or pseudorandom methods, in which the pattern of an array is intended to resemble the average pattern of an ensemble of arrays constructed by the same technique. These methods are not synthesis techniques, although they may have as their goal the production of a beam with a specified side-lobe level. Rather, they are analysis methods that provide heightened intuition by which a given choice of element placement can be selected to approximately fulfill the desired criterion. The random, or statistical, methods are given in Chap. 6.

The first significant work on nonuniformly spaced arrays was carried out by Unz and was reported in his University of California (Berkeley, 1956) doctoral dissertation. Since that time, a large number of contributions to this field have been made. We shall discuss only a selected few of the many different approaches that have been proposed and refer the reader to the literature for further details (see references listed for Sec. 7.9 at the end of this chapter).

The Source Position Function

To calculate the pattern of a nonuniformly spaced array, it is first necessary to choose a descriptor of the element positions, since they are no longer con-

†The method described by Taylor differs somewhat from the approach outlined here. The interested reader should consult Ref. 29.

sidered to be located at regular intervals. A source number function $v(z)$ is used to locate elements according to the rule that at the location of the n th element $z = z_n$, $v(z_n) = n$. Thus a continuous curve $v(z)$ defines the element locations or, conversely, provides the number of the element for a given position along the array axis z (Fig. 7.7).

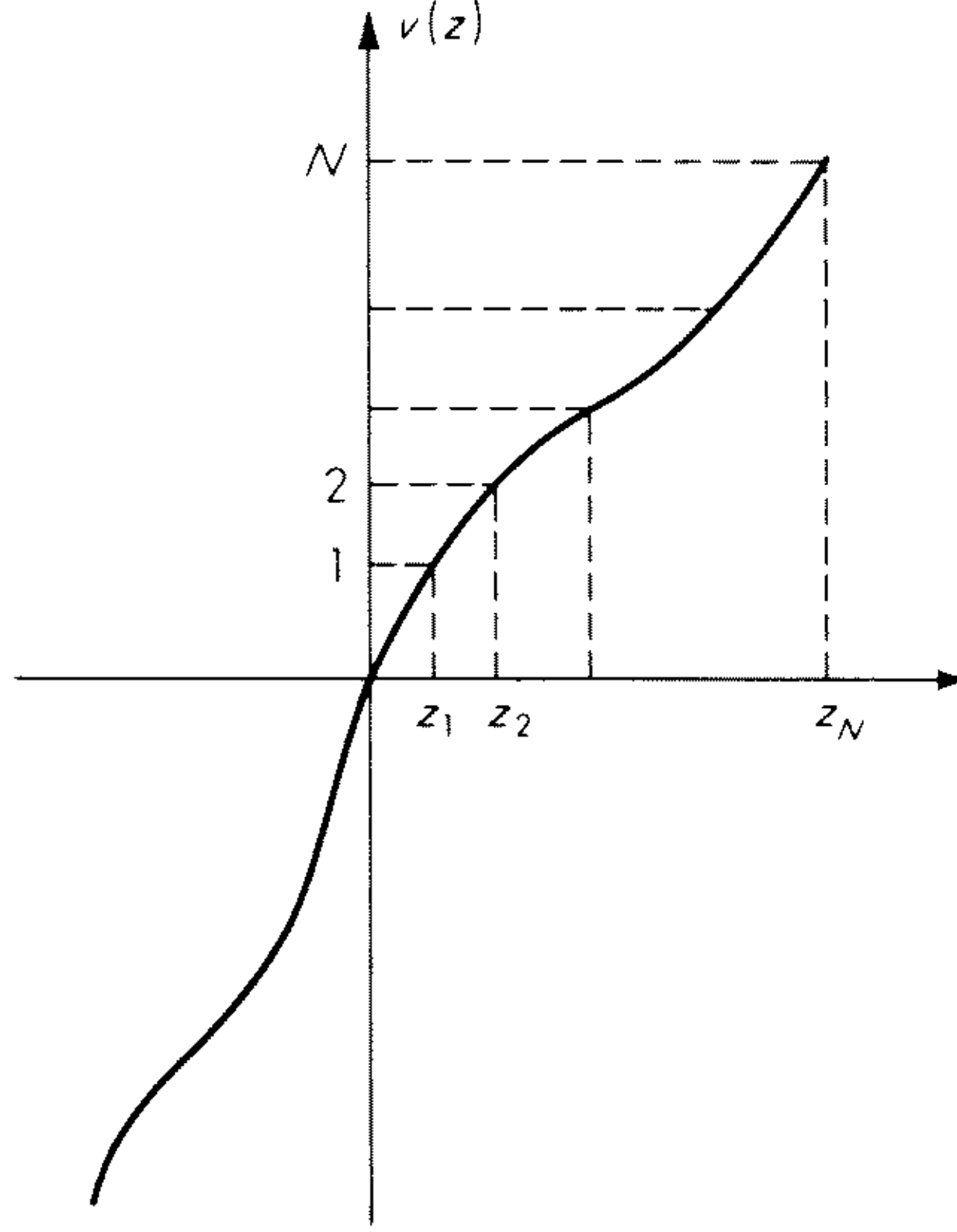


Fig. 7.7 The source number function.

The radiation pattern of an array of N elements on the z axis is given by

$$f(u) = \sum_{n=1}^N i_n e^{jk_0 z_n u} \quad (7.58)$$

where i_n is the current in the n th element, z_n is its location, and $u = \sin \theta$. This equation can be transformed by using the Poisson sum formula, which states

$$\sum_{n=-\infty}^{\infty} F(n) = \sum_{m=-\infty}^{\infty} \int_{-\infty}^{\infty} F(v) e^{j2m\pi v} dv$$

Thus (7.58) becomes

$$f(u) = \sum_{m=-\infty}^{\infty} \int_0^N i(v) e^{j2m\pi v + jk_0 z u} dv \quad (7.59)$$

where the limits of integration are from 0 to N because there are no elements outside the range. Changing the variable in (7.59) from v to z , we obtain

$$f(u) = \sum_{m=-\infty}^{\infty} \int_{z_0}^{z_N} i(z) \frac{dv}{dz} e^{j2\pi m v(z) + jk_0 z u} dz$$

and writing

$$f(u) = \sum_{m=-\infty}^{\infty} f_m(u) \quad (7.60)$$

we may consider a single term of the expansion

$$f_m(u) = \int_{z_0}^{z_N} i(z) \frac{dv}{dz} e^{j2\pi m v(z) + jk_0 z u} dz \quad (7.61)$$

Thus we have transformed the array sum (7.58) into a sum of integrals of continuous functions. The functions $i(z)$ and $v(z)$ are understood to be the envelope of the current distribution and the source positions; that is, at the location of the n th element, $z = z_n$, $i(z_n) = i_n$, and $v(z_n) = n$.

The physical interpretation of (7.61), however, is the radiation pattern of a continuous line source with a current distribution

$$i(z) \frac{dv}{dz} e^{j2\pi m v(z)}$$

The series (7.60) tends to be a rapidly convergent one for most problems. The main contribution to $f(u)$ for small u comes from the $m = 0$ term.³¹

The synthesis techniques that have been developed for continuous current distributions can now be applied to the case of nonuniformly spaced arrays. For example, suppose it is desired to find an array of elements with equal currents that produce a pattern approximating a Taylor distribution, as described in Sec. 7.8. First, set $i(z) = 1$; considering only the $m = 0$ term in (7.60), we have

$$f_0(u) = \int \frac{dv}{dz} e^{jk_0 z u} dz$$

The results in Sec. 7.8 that would specify the current distribution apply here to the derivative of the source position function, dv/dz .

*The Anger Function Method*³³

Consider the case of an array of uniformly illuminated elements ($i_n = 1/N$). The source position function is chosen to be

$$v(z) = \left(\frac{z}{2a} + \frac{2A_1}{\pi} \sin \frac{\pi z}{2a} \right) N^2 \quad (7.62)$$

where $2a$ is the total length of the array and $|A_1| < 1/2$, so that $v(z)$ is a single-valued function. Substitution of (7.62) into (7.61) yields

$$f_m(u) = J_{2au/\lambda_0 - mN}(2mNA_1) + A_1[J_{2au/\lambda_0 - mN+1}(2mNA_1) + J_{2au/\lambda_0 - mN-1}(2mNA_1)] \quad (7.63)$$

where $J_p(z)$ is the Anger function defined by³²

$$J_p(z) = \frac{1}{\pi} \int_0^\pi \cos(px - z \sin x) dx$$

Using the recursion formulas for the Anger function, the pattern $f(u)$ can be written

$$f(u) = f_0(u) + \sum_{m=1}^{\infty} (-1)^{m(N-1)} [f_m(u) + f_{-m}(u)]$$

where
$$f_0(u) = \frac{\sin k_0 a u}{k_0 a u} \frac{1 - u^2/u_1^2}{1 - (2au/\lambda_0)^2} \quad u_1^2 = \frac{(2a/\lambda_0)^{-2}}{1 - 2A_1}$$

$$f_m(u) + f_{-m}(u) = \frac{2au}{mN\lambda_0} [J_{2au/\lambda_0 - mN}(2mNA_1) - J_{-2au/\lambda_0 - mN}(2mNA_1)]$$

Considering the pattern range $u > 0$, we can approximate $f(u)$ by

$$f(u) \approx f_0(u) + \sum_{m=1}^{\infty} (-1)^{m(N-1)} G_{-m}(u) \quad (7.64)$$

where
$$G_{-m}(u) = \frac{2au}{mN\lambda_0} J_{2au/\lambda_0 - mN}(2mNA_1)$$

Choosing $|A_1| = 1/6$ so that there is no overlap of the G_{-m} terms, the magnitude of the maximum side lobe of the pattern (7.64) can be shown to be

$$|f(u)|_{\max} = |G_{-1}|_{\max} \approx \frac{1 + 2|A_1|}{\sqrt{N\pi|A_1|}}$$

The radiation pattern from this unequal spacing arrangement consists of a main beam and a distributed series of side lobes that are given by the $G_{-m}(u)$.³³ In Fig. 7.8 a typical pattern is shown.

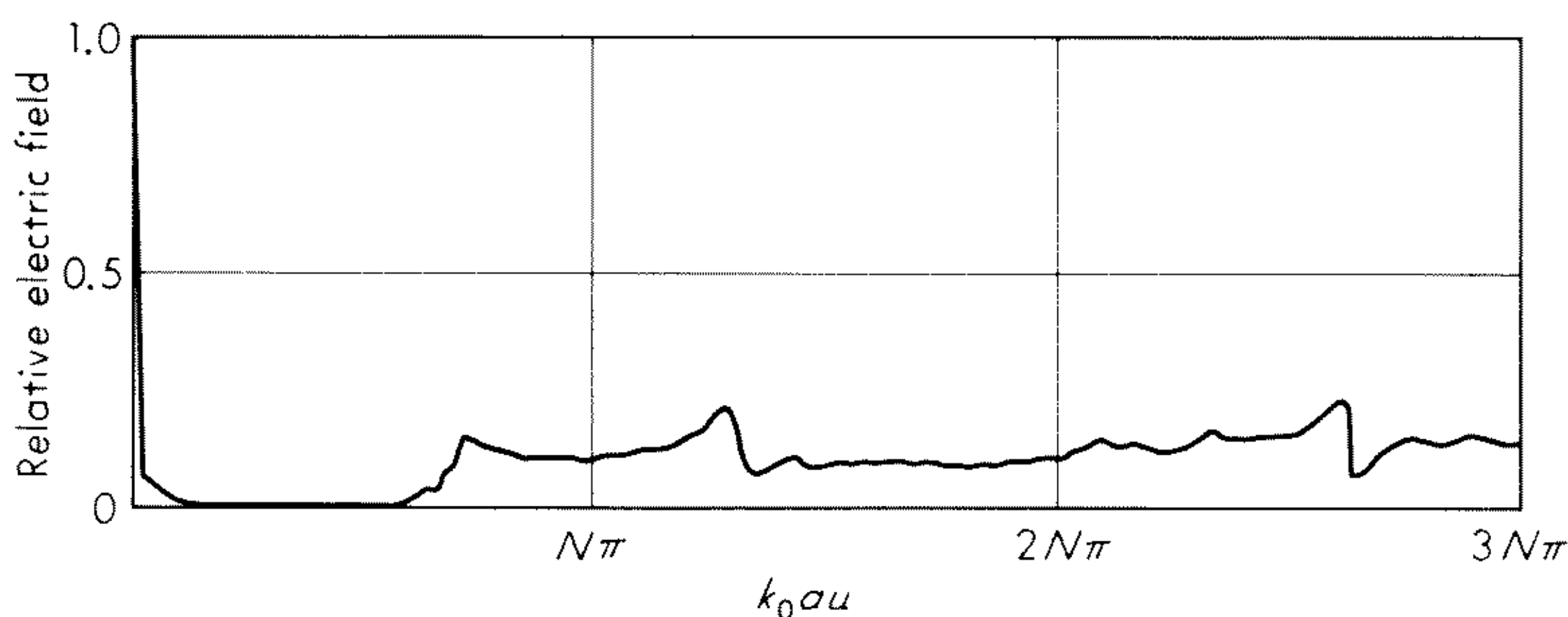


Fig. 7.8 A typical far-field pattern obtained by application of the Anger function method. The array consists of 151 elements with uniform current distribution. (From Ishimaru and Chen.³³)

The Grating Plateau Method³⁴

The Poisson sum formulation can be used to develop a technique for the production of approximately flat plateaus of side lobes by an array of non-uniformly spaced, equal-current elements. Let us consider the pattern of a non-uniformly spaced array in the form given by (7.59). The element currents

are assumed to be equal, and z is written as a function of v to imply that, when $v = n$, $z = z_n$. A single term of (7.59) is

$$f_{-m}(u) = \int_0^N e^{-j2m\pi v + jk_0 u z(v)} dv \quad (7.65)$$

The main contribution to (7.65) comes from the vicinity of the point of stationary phase, $v = n_0$, for which

$$k_0 u \left. \frac{dz}{dv} \right|_{v=n_0} - 2m\pi = 0 \quad (7.66)$$

Evaluating (7.65) by the stationary phase method we obtain, for an n_0 that is not near the ends of the array,

$$f_{-m}(u) = \left[\frac{2\pi}{k_0 u z''(n_0)} \right]^{1/2} e^{jk_0 u z(n_0) - j2m\pi n_0 + j\pi/4}$$

Let us now require that the magnitude of the function f_{-m} be approximately constant in the vicinity of the stationary phase point. Then

$$k_0 u \left. \frac{d^2 z(v)}{dv^2} \right|_{v=n_0} = \text{constant} \quad (7.67)$$

Using (7.66) and (7.67), we find that

$$\left. \frac{d^2 z(v)}{dv^2} \right|_{v=n_0} - \ln(1 + \delta) \left. \frac{dz(v)}{dv} \right|_{v=n_0} = 0$$

where δ is a constant chosen for convenience of notation. Dropping the subscript on n , the form of the source position function for constant grating plateaus is

$$v(n) = \frac{s_1}{(1 + \delta) \ln(1 + \delta)} [(1 + \delta)^n - 1]$$

where s_1 is the minimum spacing and δ is the exponential increment between any two adjacent element spacings; that is,

$$z_{n+1} - z_n = (1 + \delta)(z_n - z_{n-1})$$

The maximum spacing occurs at the ends of the array and is

$$z_N - z_{N-1} = (1 + \delta)^{N-1} s_1 \quad (7.68)$$

The level of the plateaus is found from (7.67) and (7.68) to be, for large N , given by

$$f_{-m}(u) \approx \frac{e^{jk_0 u z(n_0) - j2m\pi n_0 + j\pi/4}}{\sqrt{m \ln(1 + \delta)}}$$

The main beam can be found by direct integration of (7.59). A pattern with an approximately constant side-lobe level can be generated by this technique.³⁴

The ratio of side-lobe level to main beam, in conjunction with the number of elements, determines the exponential spacing increment δ . A typical pattern of a symmetric array of elements with the exponential spacing distribution is shown in Fig. 7.9.

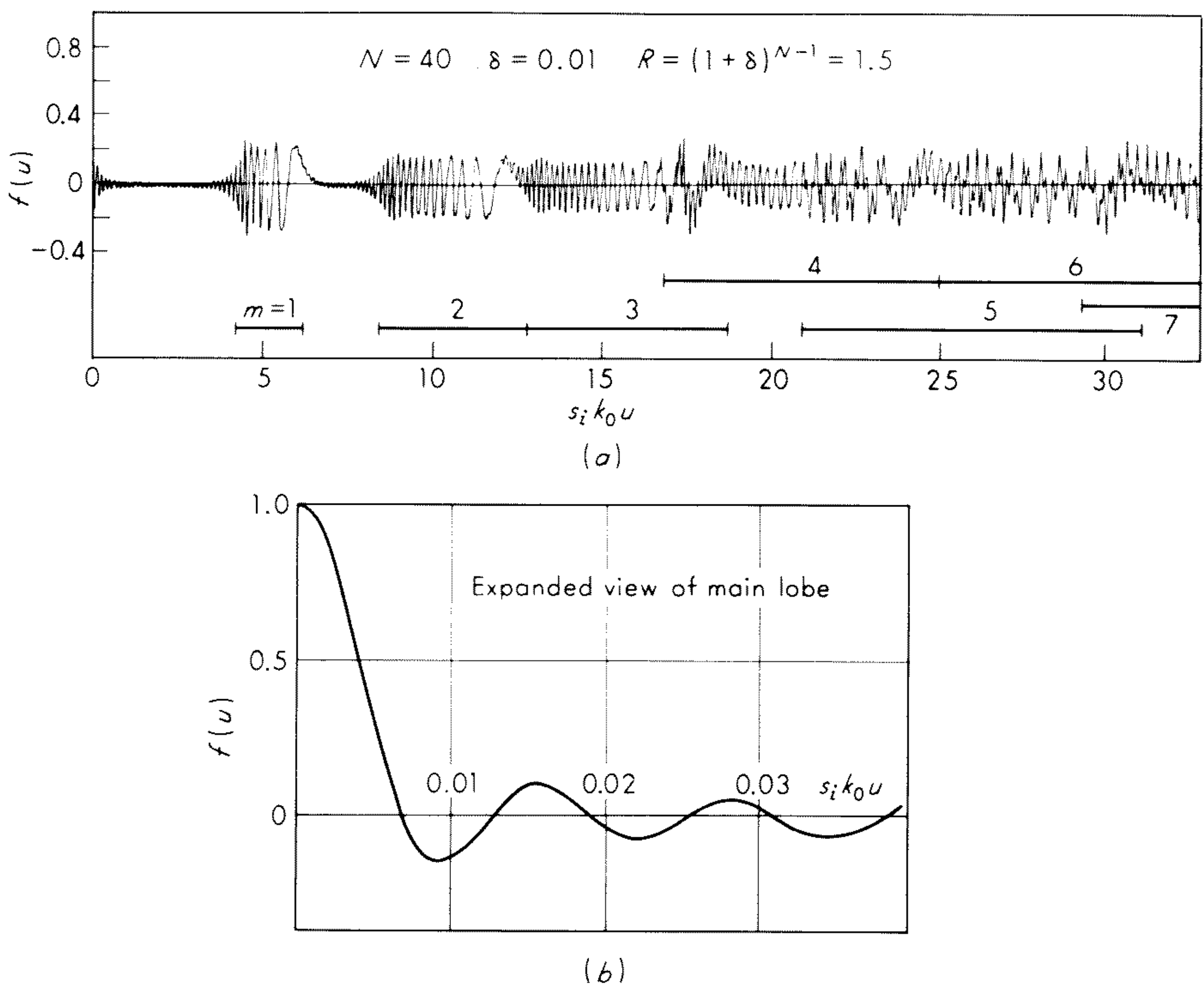


Fig. 7.9 A typical pattern resulting from the grating plateau method. (From Chow.³⁴)

7.10 The Phase Constraint: Power-pattern Synthesis

Most synthesis techniques require a statement of the phase of the far-field pattern. The applicable mathematical methods describe field quantities and depend upon the Fourier transform relation between the current distribution and the radiation field.

However, it is frequently the case that the antenna designer is interested only in the power pattern, and the far-field phase has no effect on system performance. An example of this is a radar with a shaped-beam radiation pattern. The radar output displays the reflected power from the illuminated targets, and the phases of the returns are discarded at the detector.

The specification of the phase of the far field imposes a set of constraints on the radiation pattern that may be unnecessary for the desired result. These constraints restrict the pattern behavior in ways that are not obvious to one

accustomed to dealing with the conventional Fourier techniques. For example, it is commonly accepted that the rate of ripple of the approximation pattern is given by the reciprocal of the antenna size in wavelengths. This is the usual result for constant-phase patterns; however, if the constraints used to produce spherical waves are released for further amplitude control, a ripple rate of twice that of the field methods frequently occurs.

There are difficulties inherent in the synthesis of power patterns. The first is that the convenient linearity of the Fourier transform relations is lost. Power is an inherently nonlinear quantity, so the methods of analysis result in nonlinear equations. Another troublesome aspect to power-pattern synthesis is that a unique array is rarely found. Rather, a unique set of arrays or apertures is determined. All members of the set produce the same power pattern that satisfies the error criterion. The number of antennas that produce the same pattern is finite, but in many cases it is very large.³⁵

An appreciation of the intractability of the equations of power-pattern synthesis can be gained by examination of the problem of the minimum-mean-square match of the power pattern of an array to a desired pattern.³⁶

Consider the far-field pattern of an array of $N + 1$ equispaced elements, given by

$$f(u) = \sum_{n=0}^N A_n e^{jk_0 n d u}$$

Using $Z = e^{jk_0 d u}$, we obtain the associated polynomial

$$\begin{aligned} f(Z) &= A_0 + A_1 Z + A_2 Z^2 + \cdots + A_N Z^N \\ &= A_N (Z - Z_1)(Z - Z_2) \cdots (Z - Z_N) \end{aligned}$$

The N zeros of this polynomial can be plotted in the complex Z plane, and the field pattern can be found by multiplying the vectors from the zeros to points on the unit circle corresponding to values of u (see Sec. 5.5).

The power pattern of the array is

$$\begin{aligned} P(Z) &= ff^* = |A_0 + A_1 Z + \cdots + A_N Z^N|^2 \\ &= |A_N|^2 |Z - Z_1|^2 |Z - Z_2|^2 \cdots |Z - Z_N|^2 \end{aligned} \quad (7.69)$$

While it is relatively simple to determine the power pattern (7.69) if the coefficients A_n are given, the inverse process is another matter altogether. The reason is that in writing the polynomial representing the power pattern (7.69), we have formed products

$$|Z - Z_n|^2 \quad (7.70)$$

that cannot be distinguished from those of the conjugate image point $1/Z_n^*$, that is,

$$|Z_n|^2 \left| Z - \frac{1}{Z_n^*} \right|^2 \quad (7.71)$$

for a Z that traverses the unit circle. This can be seen by expanding (7.70) and (7.71), using $Z = e^{j\psi}$ and $Z_n = \rho_n e^{j\psi_n}$, as

$$\begin{aligned} |Z - Z_n|^2 &= (e^{j\psi} - \rho_n e^{j\psi_n})(e^{-j\psi} - \rho_n e^{-j\psi_n}) \\ &= 1 - \rho_n(e^{j(\psi_n - \psi)} + e^{-j(\psi_n - \psi)}) + \rho_n^2 \\ &= 1 + \rho_n^2 - 2\rho_n \cos(\psi_n - \psi) \end{aligned}$$

and

$$\begin{aligned} |Z_n|^2 \left| Z - \frac{1}{Z_n^*} \right|^2 &= \rho_n^2 \left(e^{j\psi} - \frac{1}{\rho_n} e^{-j\psi_n} \right) \left(e^{-j\psi} - \frac{1}{\rho_n} e^{j\psi_n} \right) \\ &= \rho_n^2 + 1 - 2\rho_n \cos(\psi_n - \psi) \end{aligned}$$

In reconstructing an array from the power pattern $P(Z)$ we must choose between each root and its conjugate image, unless the root lies on the unit circle, for which $1/Z_n^* = Z_n$. If there are Q single roots of the field pattern lying off the unit circle, there are 2^Q combinations of these roots or their conjugate images that will produce the same power pattern.

The power pattern of an array is also a polynomial in Z and, if written in terms of the variable u , it is

$$P(u) = \sum_{n=-N}^N B_n e^{jnk_0 u} \quad (7.72)$$

Let us suppose that the desired power pattern is expanded as a Fourier series,

$$P_D(u) = \sum_{n=-\infty}^{\infty} B_{Dn} e^{jnk_0 u} \quad (7.73)$$

If (7.72) and (7.73) were field-pattern expansions, the coefficients of like terms could be equated. However, this is almost never possible for power patterns, for the reason that a truncated series expansion of $P_D(u)$ is rarely positive for all angles in the visible region. The coefficients B_n are values of the autocorrelation of the array currents. Since

$$P(u) = f(u)f^*(u) = \sum_{m=0}^N A_m e^{jk_0 m u} \sum_{p=0}^N A_p^* e^{-jk_0 p u} = \sum_m \sum_p A_m A_p^* e^{jk_0(m-p)u}$$

if $m - p = n$

$$P(u) = \sum_{n=0}^N \left\{ \sum_{m=n}^N A_m A_{m-n}^* \right\} e^{jk_0 n u} + \sum_{n=-1}^{-N} \left\{ \sum_{m=0}^{N+n} A_m A_{m-n}^* \right\} e^{jk_0 n u}$$

and the coefficients B_n of the expansion (7.72) are

$$B_n = \sum_{m=n}^N A_m A_{m-n}^* \quad n \geq 0$$

and

$$B_n = \sum_{m=0}^{N+n} A_m A_{m-n}^* \quad n < 0$$

Exercise 7.6 Show $B_{-n} = B_n^*$.

A solution for the coefficients A_m cannot be obtained for $B_n = B_{Dn}$ unless

$$\sum_{n=-N}^N B_{Dn} e^{jk_0 n d u} \geq 0 \quad \text{for} \quad -\frac{\lambda_0}{2d} \leq u \leq \frac{\lambda_0}{2d} \quad (7.74)$$

If (7.74) does not hold, an error criterion must be used, such as minimizing

$$\varepsilon = \sum_{n=-N}^N |B_{Dn} - B_n|^2 \quad (7.75)$$

Note that this is a second approximation; the first was a truncation of the series of terms of P_D . No matter what coefficients are chosen for the array of $N + 1$ elements, it cannot reproduce any terms of (7.73) for $|n| > N$. In addition, the requirement that the resultant power pattern must be everywhere positive further restricts the B_n so that they cannot equal B_{Dn} for $|n| < N$. Minimizing (7.75) leads to

$$\frac{\partial}{\partial \operatorname{Re} A_n} \left| \sum_{n=0}^N \left(B_{Dn} - \sum_{m=n}^N A_m A_{m-n}^* \right) + \sum_{n=-1}^{-N} \left(B_{Dn} - \sum_{m=0}^{N+n} A_m A_{m-n}^* \right) \right|^2 = 0 \quad (7.76)$$

and a similar expression for the imaginary part of A_n . As might be suspected from a cursory examination of (7.76), this set of simultaneous equations is very difficult to solve, and straightforward manipulation often leads to errors unless the results are tested to assure that (7.75) is minimized.

The Pattern Logarithm Method

There is a method of power-pattern synthesis that is relatively simple to carry out but does not apply to all cases.³⁵ The key to this technique is that the logarithm of a complex function separates the phase and amplitude of the function.

Consider a desired power pattern that is expressed in terms of the magnitude of the field pattern as

$$P_D(u) = |f_D(u)|^2$$

Let us assume that we can take the logarithm of the magnitude of f_D , and, further, that the function

$$\log |f_D(Z)| \quad Z = e^{jk_0 d u}$$

has no singularities inside the unit circle. Those singularities that are on the unit circle we shall exclude by taking an appropriately indented contour.

The logarithm of a complex function f can be written

$$\log f = \log |f| + j \arg f$$

thus effectively separating the magnitude and phase of f . If $\log f$ is an analytic function in a region, its real and imaginary parts are laplacian and one can be determined from the other by the Cauchy-Riemann equation relating harmonic functions.

As we have seen before, there is no difference between the array power pattern that is constructed by using the zeros of the associated polynomial and the one from the conjugate image points. Hence, the determination of the array pattern that has an analytic logarithm inside the unit circle is equivalent to finding the particular array polynomial that has all zeros outside or on the unit circle. Restricting our consideration to an analytic $\log f$ within the unit circle, the array pattern can be expanded in a power series about the origin as

$$\log f = \sum_{n=0}^{\infty} C_n Z^n$$

and the coefficients C_n can be found by a Fourier decomposition of the real part of $\log f$ around the unit circle

$$C_n = \frac{1}{\pi} \int_{-\pi}^{\pi} \log |f| e^{-jn\psi} d\psi \quad n \neq 0 \quad (7.77)$$

where $\psi = k_0 du$. The coefficient C_0 is unimportant, since it is a constant multiplying the array polynomial. By replacing $\log |f|$ by $\log |f_D|$ in (7.77), we are in effect using the Fourier decomposition of the logarithm of the desired pattern to determine the expansion coefficients of the log of the array pattern.

To find the associated polynomial of the array,

$$f(Z) = \sum_{m=0}^N A_m Z^m$$

a series expansion of the function $e^{\log f}$ is used, for which

$$A_m = \frac{1}{m!} \left[\frac{d^m}{dZ^m} \exp \left(\sum_{n=0}^{\infty} C_n Z^n \right) \right]_{z=0} \quad (7.78)$$

The terms are

$$A_0 = e^{C_0}$$

$$A_1 = A_0 C_1$$

$$A_2 = \frac{1}{2}(2A_0 C_2 + A_1 C_1)$$

$$A_3 = \frac{1}{3}(3A_0 C_3 + 2A_1 C_2 + A_2 C_1)$$

etc.

The expression (7.78) yields the excitation coefficients of the linear array of $N + 1$ elements that provide a match to the first $N + 1$ harmonic terms of the logarithm of the desired field pattern magnitude. The synthesis procedure consists of the Fourier decomposition of $\log |f_D|$, given by (7.77), and the series expansion for the array coefficients using the C_n 's as given by (7.78).

As an example, consider the desired power pattern

$$P_D(u) = e^{-2bu^2} \quad (7.79)$$

for which

$$\log |f_D(u)| = -bu^2$$

The coefficients of the series expansion about $Z = 0$ are

$$\begin{aligned} C_n &= \frac{1}{\pi} \int_{-\pi}^{\pi} \log |f_D(\psi)| e^{-jn\psi} d\psi \quad \psi = k_0 du \\ &= \frac{1}{\pi} \int_{-\pi}^{\pi} \left(-\frac{b\psi^2}{k_0^2 d^2} \right) e^{-jn\psi} d\psi \\ &= (-1)^{n-1} \frac{4b}{k_0^2 d^2 n^2} \end{aligned}$$

The constant C_0 is arbitrarily set equal to zero. Then, from (7.78)

$$A_0 = 1$$

$$A_1 = 4 \left(\frac{b}{k_0^2 d^2} \right)$$

$$A_2 = - \left(\frac{b}{k_0^2 d^2} \right) + 8 \left(\frac{b}{k_0^2 d^2} \right)^2$$

$$A_3 = \frac{32}{3} \left(\frac{b}{k_0^2 d^2} \right)^3 - 4 \left(\frac{b}{k_0^2 d^2} \right)^2 + \frac{4}{9} \left(\frac{b}{k_0^2 d^2} \right)$$

$$A_4 = \frac{32}{3} \left(\frac{b}{k_0^2 d^2} \right)^4 - 8 \left(\frac{b}{k_0^2 d^2} \right)^3 + \frac{41}{18} \left(\frac{b}{k_0^2 d^2} \right)^2 - \frac{1}{4} \left(\frac{b}{k_0^2 d^2} \right)$$

A graph of $P_D(u)$ and $P(u)$ for an array of five elements with $\lambda_0/2$ interelement spacings is shown in Fig. 7.10 for the case $b = 6$.

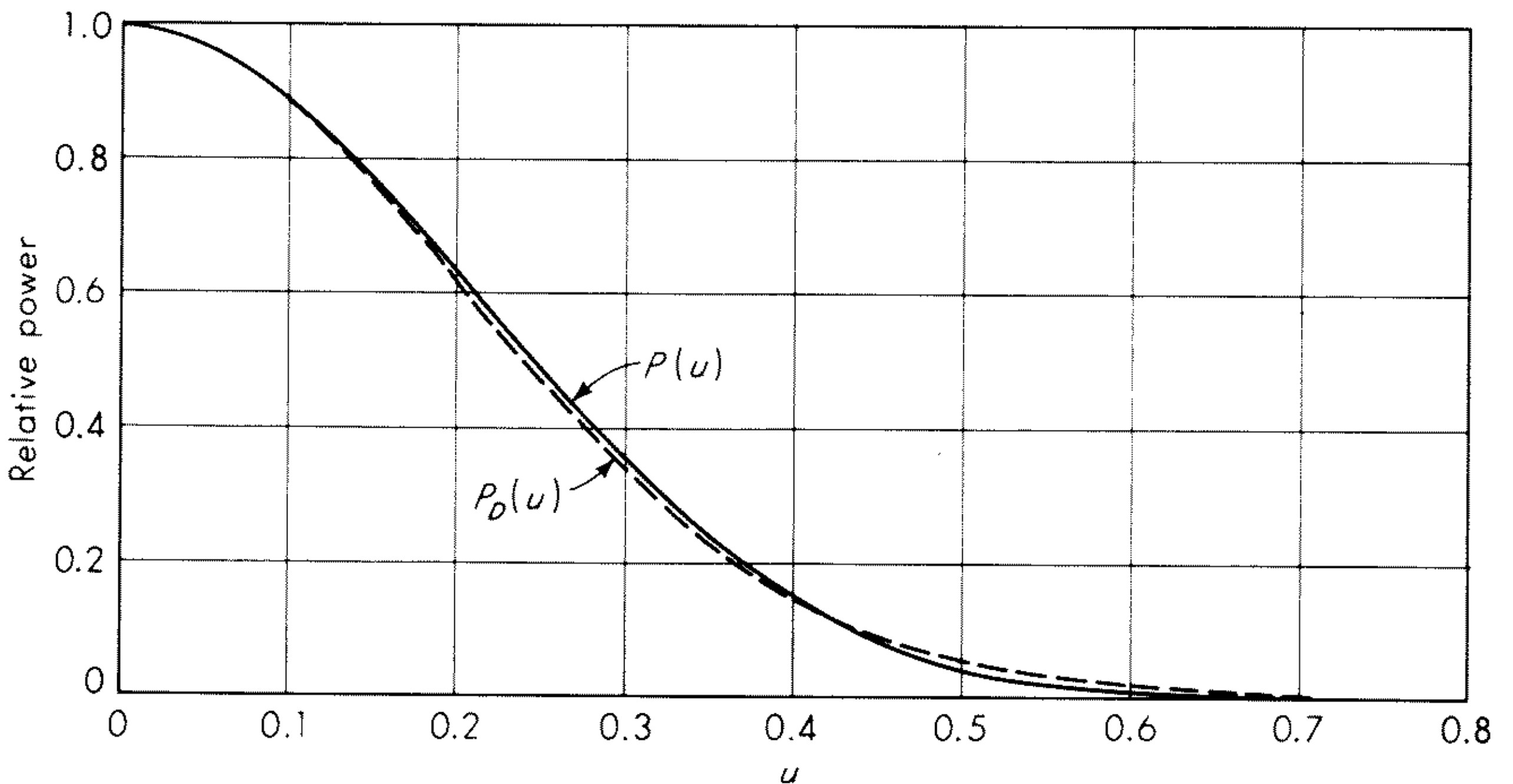


Fig. 7.10 The approximation to a gaussian pattern obtained by the potential-theory method.

The step on which this method depends, the use of the logarithm of the desired pattern, is also its chief limitation. Zeros of the desired pattern produce singularities in the logarithm, and small changes near the pattern nulls result in large changes in the logarithm and in the coefficients of the approximation. There is no guarantee that the use of the first N coefficients will provide a good pattern fit, particularly if the desired pattern and the approximation pattern differ substantially. If, for example, the coefficient b in (7.79) had been chosen to be $b = (2k_0d)^2$, the array excitation coefficients increase with m until $m = 12$. To apply this method of synthesis effectively, it is necessary to choose the total number of array elements, $N + 1$, to be sufficiently large that the magnitudes of the coefficients for $m > N + 1$ are small relative to the average in the array. Otherwise, it is necessary to examine groups of coefficients corresponding to different arrays, $A_l, A_{l+1}, \dots, A_{l+N}$, in order to find which provides the most satisfactory pattern approximation.

A Variational Method of Power-pattern Synthesis

The synthesis of radiation patterns without the a priori specification of far-field phase can be accomplished by the use of a variational calculus.³⁷ This method can be applied to problems other than pattern synthesis, but we shall consider as an error criterion the minimum of the squared difference between the desired power pattern $P_D(u)$ and the power pattern of an array of $N + 1$ elements, averaged over a single angular variable:

$$\epsilon = \int_{-1}^1 [P_D(u) - P(u)]^2 du \quad (7.80)$$

Previously, the error criterion (7.80) was shown to be equivalent to (7.75):

$$\epsilon = \sum_{n=-N}^N |B_{Dn} - B_n|^2 \quad (7.75)$$

If we introduce a variation in each of the array-feeding coefficients, so that

$$A_m \rightarrow A_m + \delta A_m$$

there will be a variation in the array autocorrelations,

$$B_n \rightarrow B_n + \delta B_n$$

that will change ϵ . There are sets of array-feeding coefficients for which any small variation δA_m causes an increase in ϵ . These coefficients yield the power pattern that minimizes (7.80). We shall determine the equation that defines the minimum ϵ coefficients and devise a method of testing a set of coefficients so that we are sure that a solution has been obtained.

First, it is necessary to prevent a simple scale change from affecting the answer. We are concerned with pattern shape, and not the absolute value of

the field intensity. By constraining the total power in the array to be a constant, we obtain

$$B_0 = \sum_{m=0}^N A_m A_m^* = \sum_{m=0}^N (A_m + \delta A_m)(A_m^* + \delta A_m^*) \quad (7.81)$$

This is equivalent to stating that the antenna gain, averaged over all angles, is a constant independent of the current distribution. From (7.81)

$$\sum_{m=0}^N (A_m \delta A_m^* + A_m^* \delta A_m) = - \sum_{m=0}^N \delta A_m \delta A_m^* \quad (7.82)$$

The desired pattern is also normalized so that

$$B_0 = B_{D0} = 1 \quad (7.83)$$

Let us consider a set of real array coefficients in order to simplify the analysis. Note that this will not, in general, result in a real far field. Rather, it makes the real and imaginary parts of the far field into Hilbert transforms. The case of real A_m represents a particular set of answers that do not necessarily yield the lowest error; however, it illustrates the method and permits a convenient introduction to the complex case.

A real variation δA_m of each array coefficient changes B_n according to

$$\begin{aligned} B_n + \delta B_n &= \sum_{m=n}^N A_m A_{m-n} + \sum_{m=n}^N \delta A_m A_{m-n} + \sum_{m=n}^N A_m \delta A_{m-n} \\ &\quad + \sum_{m=n}^N \delta A_m \delta A_{m-n} \quad n \geq 0 \\ &= \sum_{m=0}^{N+n} A_m A_{m-n} + \sum_{m=0}^{N+n} \delta A_m A_{m-n} + \sum_{m=0}^{N+n} A_m \delta A_{m-n} \\ &\quad + \sum_{m=0}^{N+n} \delta A_m \delta A_{m-n} \quad n < 0 \end{aligned}$$

$$\begin{aligned} \text{Thus } \delta B_n &= \sum_{m=n}^N \delta A_m A_{m-n} + \sum_{k=0}^{N-n} \delta A_k A_{k+n} \\ &\quad + \sum_{m=n}^N \delta A_m \delta A_{m-n} \quad n \geq 0 \end{aligned} \quad (7.84)$$

$$\begin{aligned} \text{or } \delta B_n &= \sum_{m=0}^{N+n} \delta A_m A_{m-n} + \sum_{k=-n}^N \delta A_k A_{k+n} \\ &\quad + \sum_{m=0}^{N+n} \delta A_m \delta A_{m-n} \quad n < 0 \end{aligned} \quad (7.85)$$

The variation in the error ε is given by

$$\varepsilon + \delta\varepsilon = \sum_{n=-N}^N [B_{Dn} - (B_n + \delta B_n)]^2$$

$$\text{or } \delta\varepsilon = -2 \sum_{n=-N}^N (B_{Dn} - B_n) \delta B_n + \sum_{n=-N}^N (\delta B_n)^2 \quad (7.86)$$

Substituting (7.84) and (7.85) into (7.86), and writing $B_{Dn} - B_n = \Delta_n$, yields

$$\begin{aligned} \delta\epsilon = & -2 \sum_{n \geq 0} \Delta_n \left(\sum_{m=n}^N \delta A_m A_{m-n} + \sum_{m=0}^{N-n} \delta A_m A_{m+n} \right) \\ & - 2 \sum_{n < 0} \Delta_n \left(\sum_{m=0}^{N+n} \delta A_m A_{m-n} + \sum_{m=-n}^N \delta A_m A_{m+n} \right) \\ & - 2 \sum_{n \geq 0} \sum_{m=n}^N \Delta_n \delta A_m \delta A_{m-n} - 2 \sum_{n < 0} \sum_{m=0}^{N+n} \Delta_n \delta A_m \delta A_{m-n} \\ & + 2 \sum_{n=-N}^N (\delta B_n)^2 \quad (7.87) \end{aligned}$$

Interchanging the m and n summations in the first two expressions in (7.87), and using the property that $\Delta_n = \Delta_{-n}$, we obtain the result

$$\begin{aligned} \delta\epsilon = & -4 \sum_{m=0}^N \delta A_m \sum_{n=-(N-1-m)}^m \Delta_n A_{m-n} - 2 \sum_{n \geq 0} \sum_{m=n}^N \Delta_n \delta A_m \delta A_{m-n} \\ & - 2 \sum_{n < 0} \sum_{m=0}^{N+n} \Delta_n \delta A_m \delta A_{m-n} + 2 \sum_{n=-N}^N (\delta B_n)^2 \quad (7.88) \end{aligned}$$

Exercise 7.7 Verify (7.88) by checking that the limits of the sums of (7.88) follow from interchanging the order of summation of (7.87).

In order to find the set of A_m 's that produce the minimum ϵ , consider a variation in δA_m of the form

$$\delta A_m = e a_m$$

A necessary condition for an extremum of (7.88) is that

$$\left. \frac{d(\delta\epsilon)}{de} \right|_{e=0} = 0 \quad (7.89)$$

Each part of (7.88) except the first contains terms in e^2 , thus the application of (7.89) leads to the requirement that

$$\sum_{m=0}^N a_m \sum_{n=-(N-m)}^m \Delta_n A_{m-n} = 0 \quad (7.90)$$

for any arbitrarily chosen set of a_m , and $e = 0$. A first guess at the solution of (7.90) might be to make the summation on n identically equal to zero for any m . However, a glance at (7.88) would evoke the suspicion that if the first double sum of (7.88) is zero, the variation in the error is negative, and hence the choice

$$\sum_{n=-(N-m)}^m \Delta_n A_{m-n} = 0$$

leads to a maximization of the error, rather than a minimization. This does, indeed, turn out to be the case in most instances.

To minimize (7.88), let us reexamine the constraint equation (7.82) written in terms of real coefficients:

$$\sum_{m=0}^N \delta A_m A_m = -1/2 \sum_{m=0}^N (\delta A_m)^2$$

This equation states that if each variation $\delta A_m = e a_m$ is weighted by the minimum-error amplitudes A_m , the sum is a function of e^2 . Therefore we have an alternate choice in satisfying (7.89). By requiring that

$$\sum_{n=-(N-m)}^m \Delta_n A_{m-n} = C A_m \quad (7.91)$$

all terms in (7.88) vary as e^2 , and the requirement (7.89) is met.

The result (7.91) is the defining equation for the minimization of the error criterion (7.75) for real coefficients A_m and B_{Dm} . If the preceding manipulations are carried out for complex coefficients, the defining equation is the same.

To determine the normalization constant C , multiply both sides of (7.91) by A_m^* and sum:

$$\sum_{m=0}^N \sum_{n=-(N-m)}^m \Delta_n A_{m-n} A_m^* = C \sum_{m=0}^N A_m A_m^* = B_0 C = C$$

or, by interchanging the order of summation on the left,

$$\sum_{n=-N}^N \Delta_n B_n^* = C \quad (7.92)$$

Equation (7.91) and the normalization (7.92) can be combined in a single equation that defines any one of the sets of coefficients of an array of $N + 1$ elements that yields a pattern with the least-mean-square fit to a desired power pattern:

$$\sum_{n=-(N-m)}^m (B_{Dn} - B_n) A_{m-n} = \left[\sum_{n=-N}^N (B_{Dn} - B_n) B_n^* \right] A_m \quad (7.93)$$

As is readily apparent, (7.93) is nonlinear in A_m , since B_n contains products of the coefficients. However, this equation is amenable to iteration techniques, and by using a high-speed computer, the coefficients of arrays of large numbers of elements can be determined. Alternatively, techniques similar to those employed for the Wiener-Hopf equation can be used for analytic solutions of (7.93). The disadvantage of these techniques is that approximations are necessary to make the equations amenable to analysis. As a consequence, it is usually simpler to iterate (7.93) directly than to attempt analytic solutions that require an excessive number of terms in order to reduce approximation errors.

As an example of power-pattern synthesis, consider the square-top pattern shown in Fig. 7.11. The desired power pattern P_D is a constant from $u = -0.5$ to $u = 0.5$. The application of the Schelkunoff synthesis method (see Sec. 7.2) for a 21-element linear array with $\lambda_0/2$ interelement spacings, considering the phase of f_D to be a constant, results in the set of excitation coefficients given in the first column of Table 7.1. The second column of Table 7.1 is a set of co-

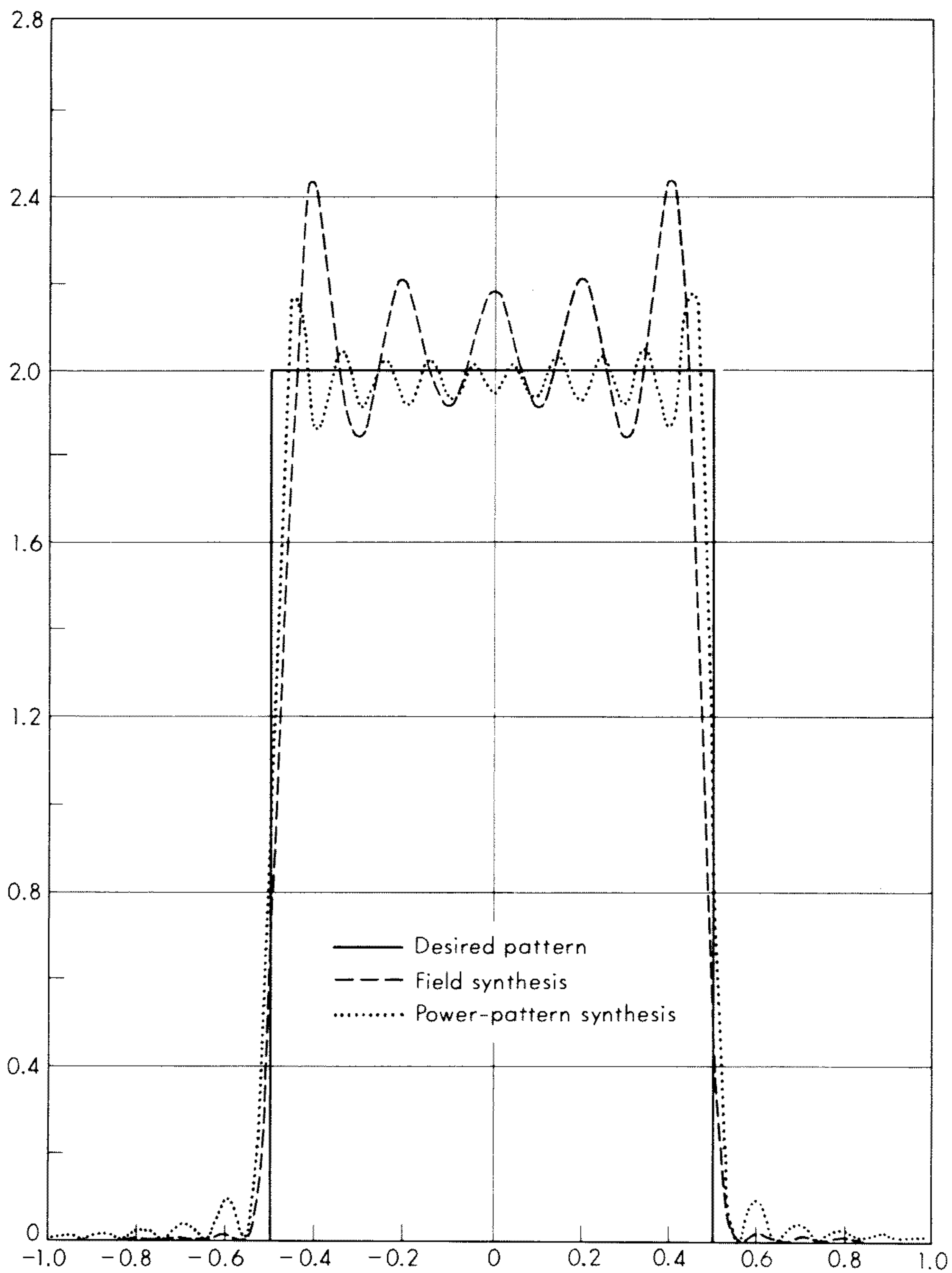


Fig. 7.11 The approximations to a square-top pattern that are obtained by field and power-pattern synthesis methods.

efficients for a 21-element array that is the result of the solution of (7.93) by iteration for this case. The third column is a list of B_{Dn} , and the fourth and fifth columns are the B_n determined from the A_n of columns 1 and 2, respec-

TABLE 7.1

Array coefficients			Pattern coefficients			
<i>Fourier series method</i>		<i>Power-pattern method</i>	<i>Desired pattern Fourier coefficient</i>	<i>Pattern coefficient from Fourier series method</i>	<i>Pattern coefficient from PPS method</i>	
N	A_n	A_n	N	B_{Dn}	B_n	B_n
-10	0	$0.0819 + j0.1108$	-21	0	0	0
-9	0.0505	$0.0116 + j0.1228$	-20	0	0	-0.0163
-8	0	$-0.1825 - j0.0125$	-19	-0.0335	0	-0.0256
-7	-0.0650	$-0.1533 - j0.0564$	-18	0	0.0025	0.0074
-6	0	$0.0919 + j0.0652$	-17	0.0374	0	0.0308
-5	0.0910	$0.1646 + j0.1932$	-16	0	0.0066	-0.0050
-4	0	$-0.1317 + j0.1715$	-15	-0.0424	0	-0.0359
-3	-0.1516	$-0.4548 + j0.0660$	-14	0	0.0134	0.0034
-2	0	$-0.4039 + j0.0106$	-13	0.0490	0	0.0423
-1	0.4548	$-0.1017 - j0.0217$	-12	0	-0.0271	-0.0021
0	0.7144	$0.0244 - j0.1177$	-11	-0.0579	0	-0.0510
1	0.4548	$-0.1183 - j0.1966$	-10	0	0.0739	0.0009
2	0	$-0.2280 - j0.0963$	-9	0.0707	0.0722	0.0635
3	-0.1516	$-0.1263 + j0.1437$	-8	0	-0.0407	0.0005
4	0	$0.0283 + j0.2929$	-7	-0.0909	-0.0928	-0.0833
5	0.0910	$0.0785 + j0.2375$	-6	0	0.0313	-0.0021
6	0	$0.0928 + j0.1003$	-5	0.1273	0.1300	0.1191
7	-0.0650	$0.1420 + j0.0173$	-4	0	-0.0263	0.0044
8	0	$0.1273 - j0.0324$	-3	-0.2122	-0.2166	-0.2031
9	0.0505	$-0.0122 - j0.1087$	-2	0	0.0230	-0.0084
10	0	$-0.0705 - j0.0954$	-1	0.6366	0.6497	0.6257
			0	1.0000	1.0000	1.0000
				$B_{Dn} = B_{D-n}^*$	$B_n = B_{-n}^*$	

tively. The patterns of the arrays with the coefficients of Table 7.1 are shown in Fig. 7.11. The power-pattern synthesis result has a ripple rate that is approximately twice that of the field synthesis result, because of the interaction of the real and imaginary parts of the radiation pattern.

If a set of array coefficients is found from (7.93) by iteration, it may not be obvious that the set is the minimum-error solution. There is a sensitive test that can be applied to prove that (7.75) has been minimized. The test involves only the B_n , as does the error criterion.

Let us assume that we have found a set of coefficients A_m that satisfy (7.93). Substituting (7.93) into (7.88) yields (for real A_m and B_{Dn})

$$\begin{aligned} \delta\epsilon = 2 \sum_{m=0}^N (\delta A_m)^2 \sum_{n=-N}^N \Delta_n B_n - 2 \sum_{n>0}^N \sum_{m=n}^N \Delta_n \delta A_m \delta A_{m-n} \\ - 2 \sum_{n<0}^{-N} \sum_{m=0}^{N+n} \Delta_n \delta A_m \delta A_{m-n} + 2 \sum_{n=-N}^N (\delta B_n)^2 \end{aligned}$$

and using the notation

$$\sum_{n=-N}^N \Delta_n B_n^* = D \quad \delta A_m = e\eta_m \quad (7.94)$$

$$\begin{aligned} \delta\epsilon = 2e^2 \left(D \sum_{m=0}^N \eta_m^2 - \sum_{n>0} \Delta_n \sum_{m=n}^N \eta_m \eta_{m-n} - \sum_{n<0} \Delta_n \sum_{m=0}^{N+n} \eta_m \eta_{m-n} \right) \\ + \text{terms in } e^4 \text{ and terms independent of } \Delta_n \quad (7.95) \end{aligned}$$

Examining (7.95), we see that we can write the part of (7.95) between the brackets in matrix form as

$$\mathbf{n}_t \cdot \mathbf{D} \cdot \mathbf{n} \quad (7.96)$$

where \mathbf{n} is a column vector with elements η_m and \mathbf{n}_t is the corresponding row vector (transposed vector).

The theory of quadratic forms states that this matrix product will always be positive for any \mathbf{n} if the matrix \mathbf{D} is positive definite, that is, if the determinant of each submatrix consisting of the first p rows and columns of \mathbf{D} , where $1 < p < N$, is greater than or equal to zero. The matrix \mathbf{D} is

$$\begin{bmatrix} D & -\Delta_1 & -\Delta_2 & -\Delta_3 & \cdots & \cdots & \cdots \\ -\Delta_{-1} & D & -\Delta_1 & -\Delta_2 & \cdots & \cdots & \cdots \\ -\Delta_{-2} & -\Delta_{-1} & D & -\Delta_1 & -\Delta_2 & \cdots & \cdots \\ -\Delta_{-3} & -\Delta_{-2} & -\Delta_{-1} & D & -\Delta_1 & -\Delta_2 & \cdots \\ \cdots & -\Delta_{-3} & -\Delta_{-2} & -\Delta_{-1} & D & -\Delta_1 & -\Delta_2 \\ \cdots & \cdots & -\Delta_{-3} & -\Delta_{-2} & -\Delta_{-1} & D & -\Delta_1 \\ \cdots & \cdots & \cdots & \cdots & \cdots & -\Delta_{-1} & D \end{bmatrix} \quad (7.97)$$

Note that, from (7.83), $\Delta_0 = 0$, and, from (7.97),

$$D \geq 0$$

$$D^2 - \Delta_1 \Delta_{-1} \geq 0$$

etc.

The development given above can be restated for complex coefficients, using the definition for D given by (7.94), by introducing conjugate values at the appropriate places. The matrix that must be tested for positive definiteness is the same as (7.97) for complex Δ_n .

Exercise 7.8 Show that D is always real.

The Reduction of Gibbs' Phenomenon

There usually occur relatively large ripples in the synthesized pattern near the angles at which there are discontinuities in the desired pattern. These ripples are the result of the mean-square-error criterion, which weights a mismatch of any Fourier coefficient equally with that of any other. This equality of weighting of Fourier coefficients, and the subsequent abrupt termination of the matching of Fourier coefficients of the desired pattern that is imposed by the finite number of freedoms present in the antenna, results in lobes that may be undesirable for the antenna application. There are methods by which the Gibbs phenomenon can be reduced. One method that has been discussed by Simon³⁸ is the weighting of the coefficients of the Fourier expansion so that the terms of the series decrease in magnitude to zero as the end of the series is approached. This can be stated as an error criterion similar to (7.75) as

$$\varepsilon = \sum_{n=-N}^N H_n |B_{Dn} - B_n|^2 \quad (7.98)$$

where

$$H_n = \left[1 - \left(\frac{n}{N} \right)^2 \right]$$

Carrying out an analysis similar to that of (7.80) to (7.93), using (7.98) in place of (7.75), yields a defining equation for the array coefficients of

$$\sum_{n=-(N-m)}^m H_n (B_{Dn} - B_n) A_{m-n} = \left[\sum_{n=-N}^N H_n (B_{Dn} - B_n) B_n^* \right] A_m \quad (7.99)$$

Exercise 7.9 Derive (7.99) by using the steps (7.75) to (7.93).

As an example of this weighting method, consider the synthesis of a $\csc^2 \theta$ sector pattern by a 21-element array. The desired pattern is shown in Fig. 7.12 along with the power-pattern synthesis result determined by iterating (7.93) with the appropriate B_{Dn} . Note the poor match and the large ripple near $\theta = 45^\circ$ due to the mean-square power criterion. Using the error criterion (7.98), and iterating (7.99) yields the pattern shown in Fig. 7.12. This synthesis result for a 21-element array is a much smoother pattern at the expense of the high gain values near $\theta = 10^\circ$.

A second technique, used by Haywood,³⁹ for the reduction of Gibbs phenomenon is to avoid discontinuities in the desired pattern. Since the antenna cannot produce a pattern with extremely steep slopes unless an inordinately large number of elements is used, the choice of a desired pattern such as that shown in Fig. 7.12 represents a poor choice in terms of realistic antenna patterns. A desired pattern having discontinuities can be modified by adding "tails" that reduce the maximum pattern slope to values that can be achieved

by an antenna of the size under consideration. As an example, Fig. 7.13 shows the desired pattern of Fig. 7.12 modified by the addition of sinusoidal segments. Using this modified pattern as P_D , a power-pattern synthesis result for a 21-element array was found, and it is shown in Fig. 7.13. The reduction in ripple over the result in Fig. 7.12 is apparent. These techniques for reducing unwanted lobes near discontinuities can be applied to cases other than power-pattern synthesis

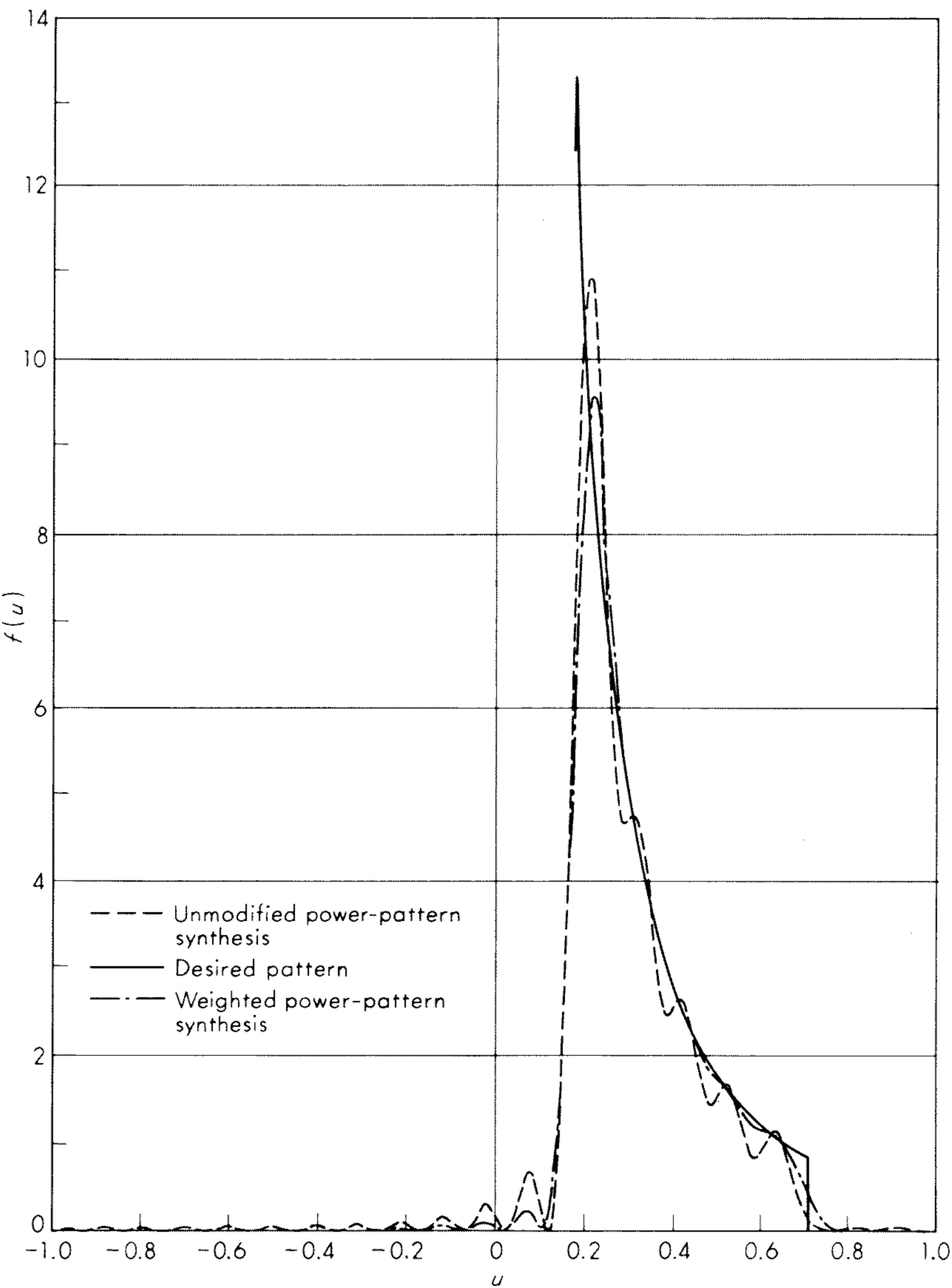


Fig. 7.12 The unmodified and weighted power-pattern synthesis matches to a $\csc^2 \theta$ pattern.

The Bernstein Polynomial Method

One of the principal difficulties inherent in the application of Fourier series to the synthesis of power patterns is the determination of an approximation that is everywhere greater than or equal to zero and that can be identified as a

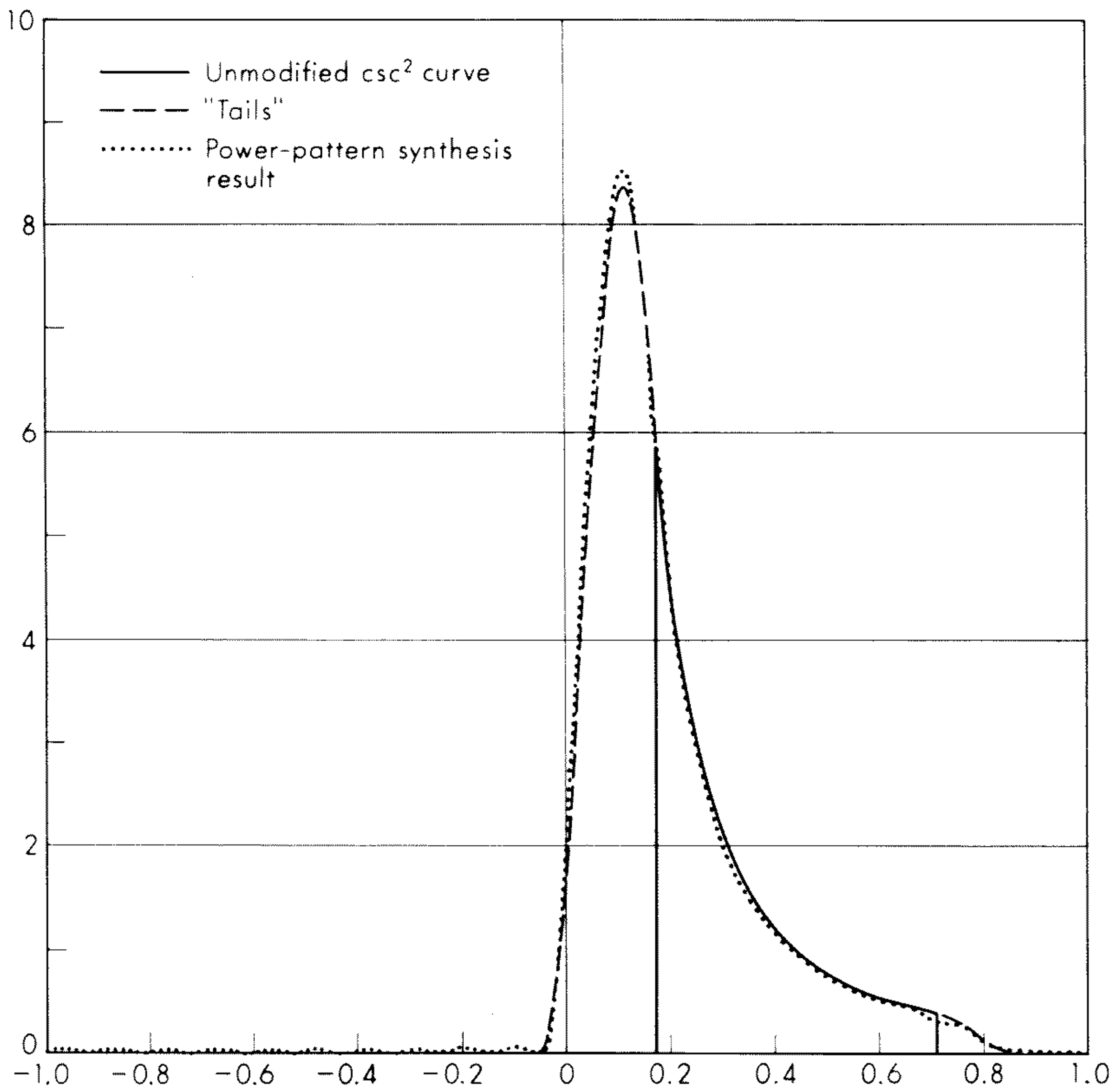


Fig. 7.13 The power-pattern synthesis match to a modified $\csc^2 \theta$ pattern.

power pattern. A synthesis method that avoids this difficulty can be developed by approximating the power pattern by a Bernstein polynomial.⁴⁰

Consider a desired power pattern $P_D(u)$ that is symmetric about $u = 0$. An approximation to $P_D(u)$ is sought by using a linear array of $N + 1$ equispaced elements. The polynomial $P(Z)$ associated with the array power pattern is given by (7.69). Because the patterns are symmetric, the coefficients B_n are real. We shall restrict our consideration to a set of $N + 1$ real feeding coefficients, A_n , and write the array polynomial in terms of the real variable

$$y = \frac{1}{2}(Z + Z^{-1}) \quad (7.100)$$

which is equivalent to an expansion of the pattern in cosines, as $Z = e^{ik_0 d u}$. The

approximation of a function $P_D(x)$ over the interval $0 \leq x \leq 1$ by the Bernstein polynomial of order N is given by

$$P_B(x) = \sum_{m=0}^N C_m^N P_D(x = m/N) x^m (1-x)^{N-m} \quad (7.101)$$

where

$$C_m^N = \frac{N!}{m!(N-m)!}$$

The interval $0 \leq x \leq 1$ coincides with half the visible region for a symmetric pattern if

$$y = 1 - 2x \quad (7.102)$$

The first step is to use Eqs. (7.100) and (7.102) to find the points $x = m/N$ at which P_D must be specified. Substitution of the values of P_D into (7.101) determines the approximation to the desired pattern. It can be shown that the Bernstein polynomial approximation to $P_D(x)$ will uniformly approach $P_D(x)$ as the order N increases and that $P_B(x)$ will have the same upper and lower bounds as $P_D(x)$, although the minima and maxima need not occur at the same points as those of $P_D(x)$. Therefore if

$$P_D(x) \geq 0 \quad \text{for } 0 \leq x \leq 1$$

then

$$P_B(x) \geq 0 \quad \text{for } 0 \leq x \leq 1$$

Bounds on the approximation error can be set in terms of the modulus of continuity, defined as

$$\omega(\delta) = \max |P_D(x_1) - P_D(x_2)|$$

and the modulus of continuity of the first derivative,

$$\omega'(\delta) = \max |P_D'(x_1) - P_D'(x_2)|$$

where

$$|x_1 - x_2| \leq \delta \quad \text{for } 0 \leq x_1, x_2 \leq 1$$

The bounds on the deviation of P_B from P_D are

$$|P_D(x) - P_B(x)| \leq \frac{5}{4} \omega(N^{-1/2})$$

and

$$|P_D(x) - P_B(x)| \leq \frac{3}{4} N^{-1/2} \omega'(N^{-1/2})$$

Note that these bounds are not very restrictive if P_D has a discontinuity in value or slope. For example, suppose there is a step in $P_D'(y)$ of unity height occurring at $y = y_0$. Then if

$$y_1 = y_0 - \frac{\epsilon}{2} \quad y_2 = y_0 + \frac{\epsilon}{2} \quad \omega'(\delta) = 1$$

for any δ , since ϵ can always be chosen less than δ . Hence the bound on the maximum excursion for this case is

$$|P_D(y) - P_B(y)| \leq \frac{3}{4} N^{-1/2}$$

For functions with smoothly changing slopes, however, these bounds are usually conservative.

The Bernstein polynomial of order N given by (7.101) can be written as an array polynomial in the form of (7.69) by substituting (7.100). The roots can then be factored and an array determined. An alternative approach is to factor $P_B(y)$ directly into its roots. Since $P_B(y)$ is a nonnegative polynomial with real coefficients and defined for the region $-1 \leq y \leq 1$, it must contain a combination of the following factors:

1. $y + c_k$ c_k real, $c_k \geq 1$
2. $-(y - c_k)$ c_k real, $c_k \geq 1$
3. $(y + c_k)^2$ c_k real, $|c_k| \leq 1$
4. $y^2 + 2c_{k1}y + c_{k1}^2 + c_{k2}^2$ c_{k1} real, c_{k2} real

The elementary array polynomials corresponding to these factors are:

1. $\frac{1}{\sqrt{a_k}} (1 + a_k Z)$ $a_k = c_k \pm \sqrt{c_k^2 - 1}$
2. $\frac{1}{\sqrt{a_k}} (a_k Z - 1)$ $a_k = c_k \pm \sqrt{c_k^2 - 1}$
3. $1 + 2c_k Z + Z^2$
4. $\frac{1}{\sqrt{a_{k1}a_{k2}}} [1 + (a_{k1} + a_{k2})Z + a_{k1}a_{k2}Z^2]$ $a_{k1} = c_{k1} + jc_{k2}$
 $a_{k2} = a_{k1}^*$
 $+ \sqrt{(c_{k1} + jc_{k2})^2 - 1}$

To determine the array coefficients, it is necessary to factor $P_B(y)$ into its linear or quadratic factors, determine the corresponding elementary array polynomials, and multiply them together to obtain the polynomial in Z that describes the array. Since the elementary array polynomials are not uniquely determined, different combinations will yield the different arrays that produce the given power pattern.

As an example, consider the application of the Bernstein polynomial to the synthesis of the square-top pattern of Fig. 7.11. Considering an array of six elements with $\lambda_0/2$ interelement spacings, (7.101) is

$$P_B(x) = \sum_{m=0}^5 C_m^5 x^m (1-x)^{5-m} P_D\left(x = \frac{m}{5}\right)$$

or
$$P_B(y) = \sum_{m=0}^5 C_m^5 P_D\left(x = \frac{m}{5}\right) \left(\frac{1-y}{2}\right)^m \left(\frac{1+y}{2}\right)^{5-m}$$

where $y = \cos \pi u$. For the desired pattern of Fig. 7.11

$$\begin{aligned} P_B(y) &= \sum_{m=0}^2 C_m \left(\frac{1-y}{2}\right)^m \left(\frac{1+y}{2}\right)^{5-m} \\ &= \frac{1}{32} [(1+y)^5 + 5(1-y)(1+y)^4 + 10(1-y)^2(1+y)^3] \\ &= \frac{3}{16} (1+y)^3 \left(y^2 - 3y + \frac{8}{3}\right) \\ &= \frac{3}{16} (1+y)^3 \left(y - \frac{23}{12} + \frac{\sqrt{145}}{12}\right) \left(y - \frac{23}{12} - \frac{\sqrt{145}}{12}\right) \end{aligned} \tag{7.103}$$

The elementary array polynomials corresponding to the factors of (7.103) are

$$(1 + Z)^3 \quad \text{and} \quad 1 - 0.57450Z + 0.10589Z^2$$

and an array polynomial constructed from the elementary array polynomials is

$$f(Z) = 1 + 2.4255Z + 1.3824Z^2 - 0.4058Z^3 - 0.2568Z^4 + 0.1059Z^5$$

The power pattern of the array representing the Bernstein polynomial approximation is shown in Fig. 7.14.

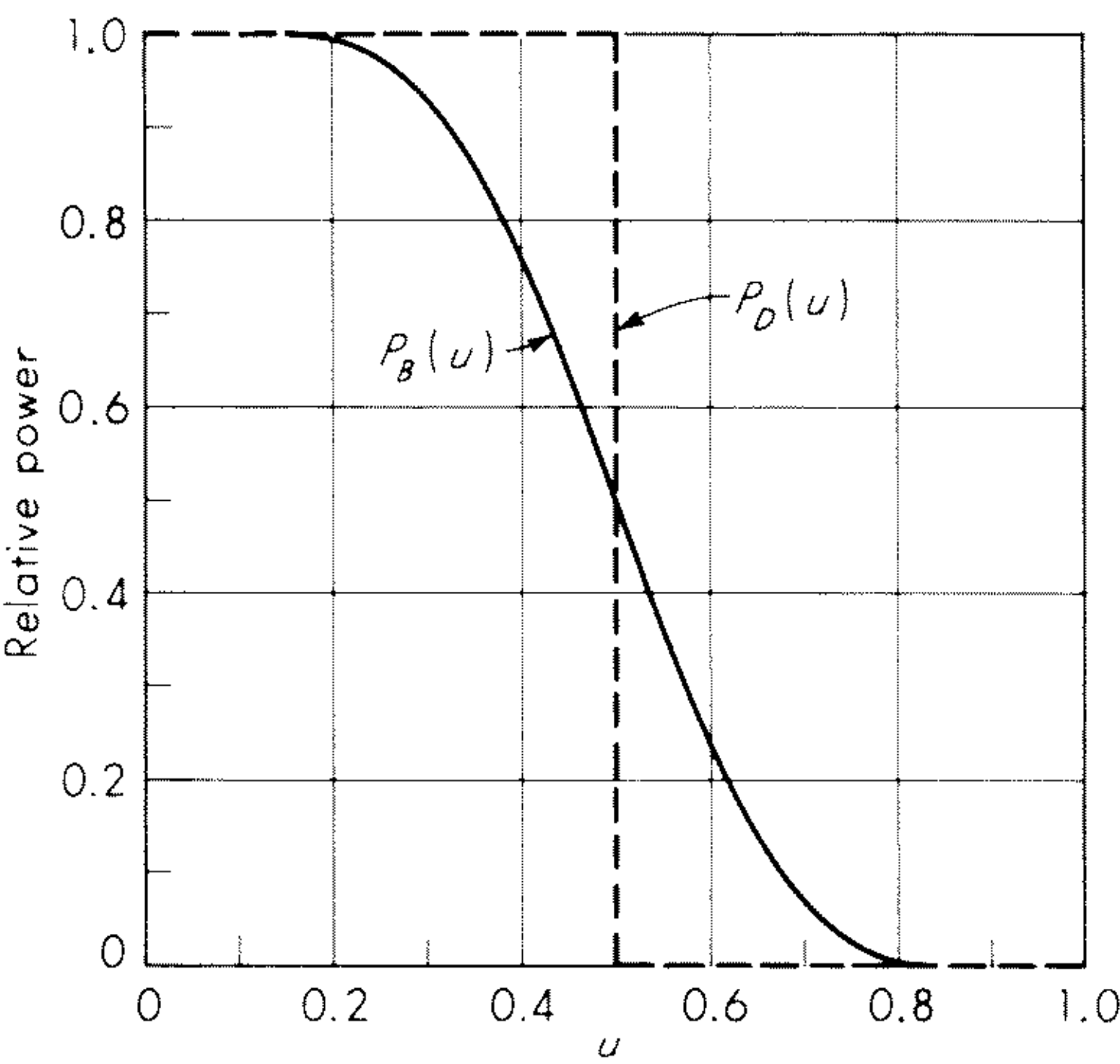


Fig. 7.14 The Bernstein polynomial method approximation to a square-top pattern.

This technique has been applied to patterns that are not symmetric in u and that involve complex B_n . However, the realization of an array polynomial from (7.101) in this case is more involved.⁴⁰

7.11 Other Synthesis Techniques

There are many other synthesis methods that have been developed to meet special problems or to achieve a result different from the results described in

the preceding sections. A list of papers following the references contains many synthesis methods that are not described in the chapter. Some of these methods are modifications of the described techniques, others are incomplete; however, most deserve examination by anyone wishing to cover the topic of synthesis in depth.

In this section a number of specialized synthesis techniques are presented. The first two methods deal with error criteria that are not mean-square or maximum deviation. The next method is one which contains the constraint that the phases of the antenna currents are fixed. The fourth is a true maximum-deviation method, and at the end is an introduction to the quadrature methods, which represent an adaptation of a well-known and important aspect of interpolation theory.

Antenna Pattern Synthesis by Derivative Control

The error criteria for most synthesis techniques involve functions of the difference between the desired and approximating patterns. As a result, the available constraints are used to make the approximating pattern oscillate about the desired pattern. For some applications, however, it is important that the pattern in a specified sector be more rigidly controlled. For example, a linear pattern variation over a given angular range may be necessary. The matching of the derivatives of the antenna pattern to those of the desired pattern can reduce or, in some instances, eliminate the oscillations of the pattern over a given range. By properly spacing the points at which the pattern and its first derivative are matched to the desired value near a discontinuity, the overshoot associated with the Gibbs phenomenon can be substantially reduced.⁴¹

Maximally Flat Antenna Pattern Synthesis

In certain applications it is desirable to have an antenna that provides a constant illumination over a sector with very little power radiated outside the sector. An equivalent transfer function in network theory is the maximally flat, or Butterworth function, given by

$$f(\omega) = \frac{1}{1 + \omega^{2n}}$$

in the frequency domain. The first $2n - 1$ derivatives of the function vanish at the origin, producing a flat top for $\omega < 1$. At $\omega = \infty$, $f(\omega)$ has a zero of order $2n$ which produces high attenuation for $\omega > 1$. A breakpoint other than $\omega = 1$ can be obtained by simple scaling of the frequency variable.

Let us consider the problem of synthesizing a radiation pattern similar to the Butterworth function, using a linear array of $2N + 1$ elements. The range of the pattern variable is $-1 \leq u \leq 1$, and since the sector beam is symmetric

in u , we shall use the range $0 \leq u \leq 1$. The far-field radiation pattern of the array with $\lambda_0/2$ interelement spacings is

$$f(u) = \sum_{n=-N}^N A_n e^{jn\pi u}$$

and if

$$f(u) = f(-u)$$

the pattern can be written as

$$f(u) = A_0 + 2 \sum_1^N A_n \cos n\pi u \quad (7.104)$$

or as

$$f(x) = \sum_0^N B_n x^n \quad (7.105)$$

where

$$x = \cos \pi u \quad (7.106)$$

A symmetric field pattern from an array of $2N + 1$ elements has N parameters, and its derivative is controlled by $N - 1$ zeros. To produce a pattern analogous to the Butterworth pattern, we shall divide the zeros of the pattern derivative between the sector center ($x = 1$) and the pattern edge ($x = -1$). If the zeros are divided equally, the pattern breakpoint is $x = 1/2$. For this case

$$f'(x) = (x + 1)^{(N-1)/2} (x - 1)^{(N-1)/2} = (x^2 - 1)^{(N-1)/2} \quad (7.107)$$

To find the array coefficients, integrate (7.107) to obtain

$$f(x) = \int_0^x (x^2 - 1)^{(N-1)/2} dx + A_0 \quad (7.108)$$

where A_0 is so chosen that

$$f(-1) = 0$$

Substituting (7.106) into (7.105) and expanding the powers of $\cos \pi u$ then yields the pattern in the form of (7.104) and the array coefficients.

For pattern breakpoints other than $x = 1/2$ the zeros of $f'(x)$ are so divided that

$$f'(x) = (x + 1)^n (x - 1)^{\alpha n}$$

where the integer α satisfies the equation

$$n + \alpha n = N - 1$$

The breakpoint is given by

$$f''(x) = 0 = \frac{d}{dx} [(x + 1)^n (x - 1)^{\alpha n}]$$

which has the solution

$$x_\beta = \frac{\alpha - 1}{\alpha + 1}$$

By choosing values of α the breakpoint can be adjusted throughout the range of x . Note that the case

$$f'(x) = (1 + x)^{N-1}$$

corresponds to the binomial pattern, where all pattern parameters are used to produce zeros at the end of the visible region.

As an example, let us find the array of 15 elements that generates a maximally flat beam with a breakpoint at $x = 0$ ($u = 1/2$). Using (7.108)

$$f(x) = \int_0^x (x^2 - 1)^3 dx + A_0 = x - x^3 + \frac{3}{5}x^5 - \frac{x^7}{7} + A_0$$

Applying the condition $f(-1) = 0$ and substituting (7.106) yields

$$f(u) = -0.143 \cos^7 \pi u + 0.600 \cos^5 \pi u - 1.000 \cos^3 \pi u + 1.000 \cos \pi u + 0.457$$

which can be expanded as

$$f(u) = 0.457 + 0.547 \cos \pi u - 0.109 \cos 3\pi u + 0.0215 \cos 5\pi u - 0.002 \cos 7\pi u \quad (7.109)$$

The pattern (7.109) is plotted in Fig. 7.15 along with the desired pattern and the minimum-mean-square match by the same number of elements. The omission of the last two terms of (7.109) would introduce no more than 2 per cent of oscillation

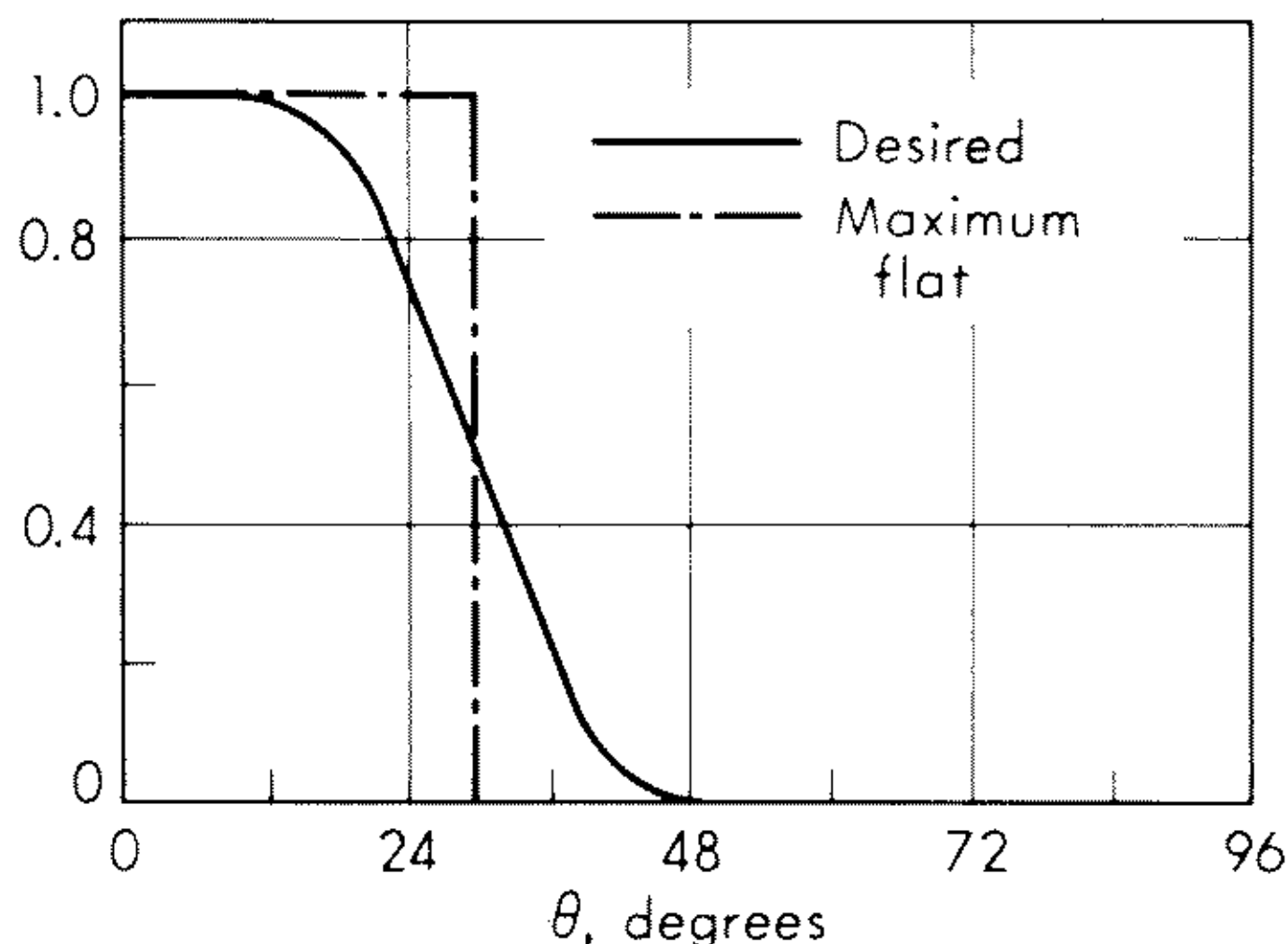


Fig. 7.15 A maximally flat approximation to a square-top pattern. (From Ksienski.⁴²)

Derived Sector Beams

The use of pattern derivatives in the formulation of the approximation suggests a simple method of synthesis of sector beams that draws on the available data for pencil beams.⁴² Consider a desired sector beam pattern as shown in Fig. 7.16a. The derivative of this pattern with respect to u is a pair of impulses, as shown in Fig. 7.16b. By using one of the techniques of Sec. 7.8, a narrow-beam, low-side-lobe pattern can be generated for each of these impulses. Integrating the resultant pattern yields the approximation to the desired pattern. The result will not be optimum in any conventional sense, but

satisfactory patterns can usually be found with few calculations. For example, let the pattern of Fig. 7.16a be approximated by an array of $2N + 1$ elements, which could produce a broadside Chebyshev error pencil-beam pattern,

$$T_N(u) = \sum_{n=0}^N A_n \cos n\pi u$$

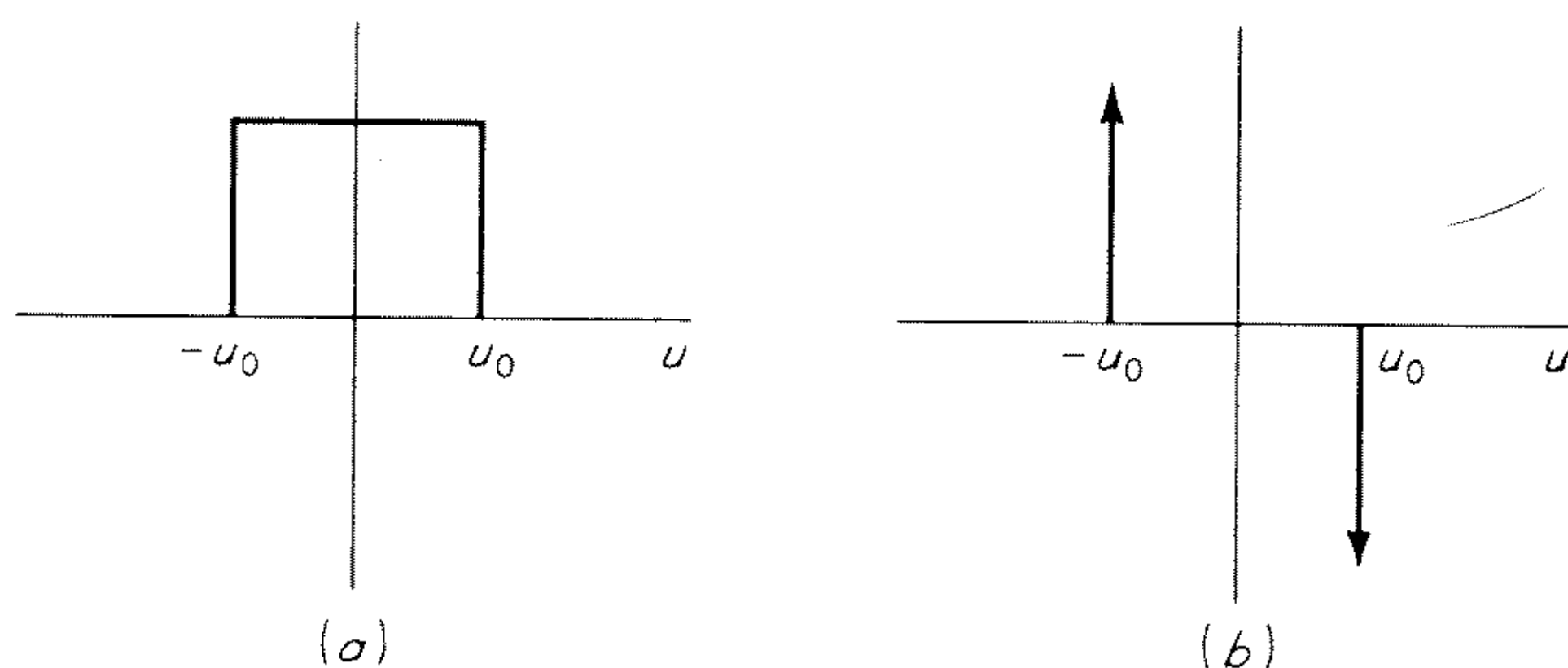


Fig. 7.16 (a) The desired pattern; (b) its derivative.

The approximation to the pattern of Fig. 7.16b is

$$\begin{aligned} f'(u) &= \sum A_n \cos n\pi(u - u_0) - \sum A_n \cos n\pi(u + u_0) \\ &= \sum A_n \sin n\pi u_0 \sin n\pi u \end{aligned}$$

from which the approximation to the pattern of Fig. 7.16a is given by

$$f(u) = \sum \left(\frac{A_n}{n} \sin n\pi u_0 \right) \cos n\pi u$$

where the A_n are the original excitation coefficients of the Chebyshev pattern. The coefficient A_0 is chosen to set the pattern level, usually such that $f(1) = 0$. The choice of the number of elements and the side-lobe level of the pencil-beam pattern will determine the ripple size and the rate of dropoff of the sector beam. If the side-lobe level of the Chebyshev pattern is $1/R$ that of the main beam, the side-lobe level of the derived sector beam pattern is given by

$$\frac{\text{Main beam}}{\text{Side-lobe level}} \geq \left(\frac{\pi}{2} \cosh^{-1} R \right) \Omega_1(j \cosh^{-1} R)$$

where $\Omega_1(x)$ is the first-order Lommel-Weber function.

In a related method of pattern approximation, the desired sector pattern is convolved with a Chebyshev pattern directly to yield the approximation pattern. The array coefficients for this approximation are the product of the Fourier harmonics of the sector pattern and the Chebyshev array coefficients.⁴³

Gaussian Error — Rectangular Array; Fixed Element Phase

The synthesis method of Sec. 7.2 produced a least-mean-square-error fit of the desired pattern to the pattern of rectangular array of elements. If the pattern is not symmetric in u or v , the currents are complex.

A synthesis technique in which the phases of the currents are constrained has been developed. Pattern variation is achieved by control of the amplitudes of the currents. The resultant array can be considered as two interleaved sub-arrays that separately provide the real and imaginary currents necessary for a nonsymmetric far-field pattern.

A desired real far-field pattern can be decomposed into a series of terms

$$f_D(u) = A_0 + 2 \sum_{n=1}^{\infty} A_n \cos n\pi u + 2 \sum_{n=1}^{\infty} B_n \sin n\pi u = f_{De}(u) + f_{Do}(u)$$

where $A_n = \frac{1}{2} \int_{-1}^1 f_D(u) \cos n\pi u du$ and $B_n = \frac{1}{2} \int_{-1}^1 f_D(u) \sin n\pi u du$

The first $N + 1$ terms of $f_{De}(u)$ can be produced by an array of $2N + 1$ elements, where elements occupying positions symmetric about the center have the same currents. To approximate the odd-pattern variation, an array of $2N$ elements with excitations $B_{-n} = -B_n$ will reproduce the first N terms of f_{Do} . The interelement spacings in either array are $\lambda_0/2$; interleaving the even- and odd-pattern arrays results in spacings of $\lambda_0/4$ between adjacent elements. The odd-pattern elements must be fed in phase quadrature to the even-pattern elements. As an example, consider the synthesis of an impulse at $u = u_0$. For this case

$$A_0 = \frac{1}{2} \quad A_n = \frac{1}{2} \cos n\pi u_0 \quad B_n = \frac{1}{2} \sin n\pi u_0$$

The beam position can be shifted by changing the amplitudes of the element coefficients. This is commonly referred to as amplitude scanning.⁴⁴

Minimax Error Pattern Synthesis

It has been pointed out earlier in this chapter and repeatedly in the literature that the least-mean-square-error criterion often is not desirable because of Gibbs phenomenon effects. In Sec. 7.8 the use of Chebyshev polynomials to obtain a minimized maximum deviation fit to an impulse was presented. The approximation of a function by a truncated set of Chebyshev polynomials is no guarantee of an equal-ripple fit such as occurs when the approximation error is proportional to a single Chebyshev polynomial.

In fact, the expansion of a function in a series of Chebyshev polynomials is equivalent to a power series of Fourier harmonic terms. To illustrate the relation between Chebyshev and Fourier expansions, consider a truncated Fourier series of an even function in the variable u :

$$f(u) = \sum_{n=0}^N A_n \cos n\pi u \tag{7.110}$$

The Chebyshev polynomial of order n is

$$T_n(x) = \cos (n \cos^{-1} x) \tag{7.111}$$

If we choose $x = \cos \pi u$, $T_n(x) = \cos n\pi u$, and the series (7.110), written in the variable x , is

$$f(x) = \sum_{n=0}^N A_n T_n(x) \quad (7.112)$$

The choice of the variable determines whether f is a Fourier series or Chebyshev series. The relation between a representation of f as a power series or Chebyshev series is provided by a table of the polynomials,

$$\begin{aligned} T_0 &= 1 \\ T_1 &= x \\ T_2 &= 2x^2 - 1 \\ T_3 &= 4x^3 - 3x \\ T_4 &= 8x^4 - 8x^2 + 1 \end{aligned} \quad (7.113)$$

or the inverted set

$$\begin{aligned} 1 &= T_0 \\ x &= T_1 \\ x^2 &= \frac{1}{2}T_2 + \frac{1}{2}T_0 \\ x^3 &= \frac{1}{4}T_3 + \frac{3}{4}T_1 \\ x^4 &= \frac{1}{8}T_4 + \frac{1}{2}T_2 + \frac{3}{8}T_0 \end{aligned} \quad (7.114)$$

and the recurrence relation

$$T_{n+1}(x) = 2xT_n - T_{n-1}$$

A method of pattern synthesis by which the error of approximation to the desired pattern consists of lobes of equal height is known as the minimax procedure.⁴⁵ There are restrictions on the types of desired functions for which this procedure will yield satisfactory results. If the desired pattern has a step discontinuity in value at some point in the visible range, any approximation function consisting of a finite number of harmonic terms will have an error of at least one-half the height of the discontinuity at that point.

Let us restrict our consideration to desired functions that are real, even, continuous and have continuous finite derivatives. We wish to find the coefficients of a linear array of $2N + 1$ elements that provide the minimax fit. The array pattern can be expressed as

$$f_M(u) = A_0 + 2 \sum_{n=1}^N A_n \cos n\pi u$$

or as

$$f_M(x) = \sum_{n=0}^N a_n x^n$$

where

$$x = \cos \pi u$$

The error criterion is to minimize $|\epsilon_{\max}| = E$, where

$$\epsilon(x) = f_M(x) - f_D(x)$$

over the visible region, which is $-1 \leq x \leq 1$. A necessary condition for the solution is that the approximation error $\epsilon(x)$ at its maximum values can be written as

$$(-1)^k \epsilon(x_k) = E = (-1)^k [f_M(x_k) - f_D(x_k)] \quad (7.115)$$

implying an oscillating error consisting of equal-amplitude lobes. There are $N + 2$ points x_k at which the error is a maximum. At these points the derivative of $\epsilon(x)$ is zero, yielding a set of N equations

$$\left. \frac{df_M}{dx} \right|_{x=x_k} = \sum_{n=1}^N n a_n x_k^{n-1} = \left. \frac{df_D(x)}{dx} \right|_{x=x_k} \quad (7.116)$$

The simultaneous solution of the $2N + 2$ equations given by (7.115) and (7.116) yields the unknowns a_n , x_k , and E . The end points of the interval usually correspond to error maxima; hence $x_0 = -1$, $x_{N+1} = 1$ in most cases. For large N and an f_D that is transcendental, the solution of (7.115) and (7.116) can become quite involved. However, with a high-speed computer an iterative result can usually be obtained without inordinate difficulty.

As an example of the minimax method, consider the desired function

$$f_D(u) = e^{\cos \pi u} \quad -1 \leq u \leq 1 \quad (7.117)$$

which we shall approximate by using a linear array of five elements with $\lambda_0/2$ spacings. The Fourier series coefficients are found by using the expansion

$$e^{\cos \pi u} = I_0(1) + 2 \sum_{m=1}^{\infty} I_m(1) \cos m\pi u$$

where $I_m(x)$ is the modified Bessel function of m th order. The least-mean-square approximation of (7.117) is therefore

$$f(u) = 1.266 + 1.130 \cos \pi u + 0.272 \cos 2\pi u \quad (7.118)$$

corresponding to array coefficients $A_2 = A_{-2} = 0.136$, $A_1 = A_{-1} = 0.565$, $A_0 = 1.266$. The pattern (7.118) is shown in Fig. 7.17 with the desired pattern (7.117). If we had represented (7.117) as a function of x , the Fourier series (7.118) would be the truncated Chebyshev series

$$f(x) = 1.266 + 1.130 T_1(x) + 0.272 T_2(x)$$

We can examine a truncated power series fit to the desired pattern to observe the improvement in error distribution by the Chebyshev series. Expanding $f_D(x)$ yields the three-term approximation

$$f(x) = 1 + x + \frac{x^2}{2}$$

or, using (7.114),

$$f(u) = 1.25 + \cos \pi u + 0.250 \cos 2\pi u \quad (7.119)$$

The power series fit (7.119) is also shown in Fig. 7.17.

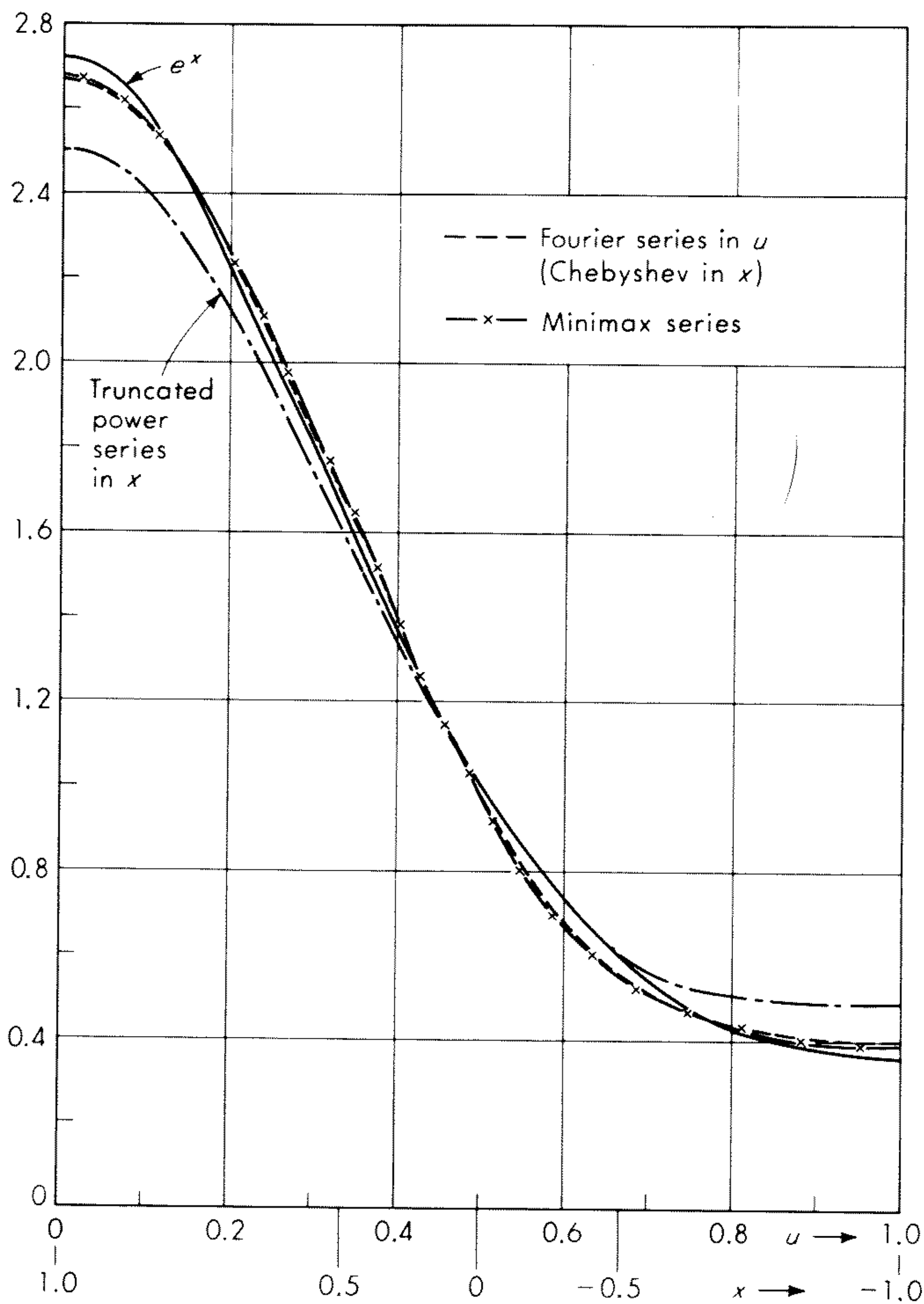


Fig. 7.17 The approximation of a desired pattern by three methods: Taylor series, Fourier series, and minimax.

Applying the minimax method by substituting into (7.115) and (7.116) yields the equations

$$\begin{aligned} E &= a_0 - a_1 + a_2 - e^{-1} \\ -E &= a_0 + a_1x_1 + a_2x_1^2 - e^{x_1} \\ E &= a_0 + a_1x_2 + a_2x_2^2 - e^{x_2} \\ -E &= a_0 + a_1 + a_2 - e^1 \\ a_1 + 2a_2x_1 - e^{x_1} &= 0 \\ a_1 + 2a_2x_2 - e^{x_2} &= 0 \end{aligned} \tag{7.120}$$

where the end points -1 and $+1$ have been used as the maximum error points x_0 and x_3 , respectively.

The solution to the set of equations (7.120) is

$$f(x) = 0.990 + 1.13x + 0.553x^2$$

or
$$f(u) = 1.267 + 1.13 \cos \pi u + 0.277 \cos 2\pi u \quad (7.121)$$

corresponding to array coefficients $A_2 = A_{-2} = 0.138$, $A_1 = A_{-1} = 0.565$, $A_0 = 1.267$. Note the small difference between (7.121), which is plotted on Fig. 7.17, and (7.118). However, there is a difference in the error of approxima-

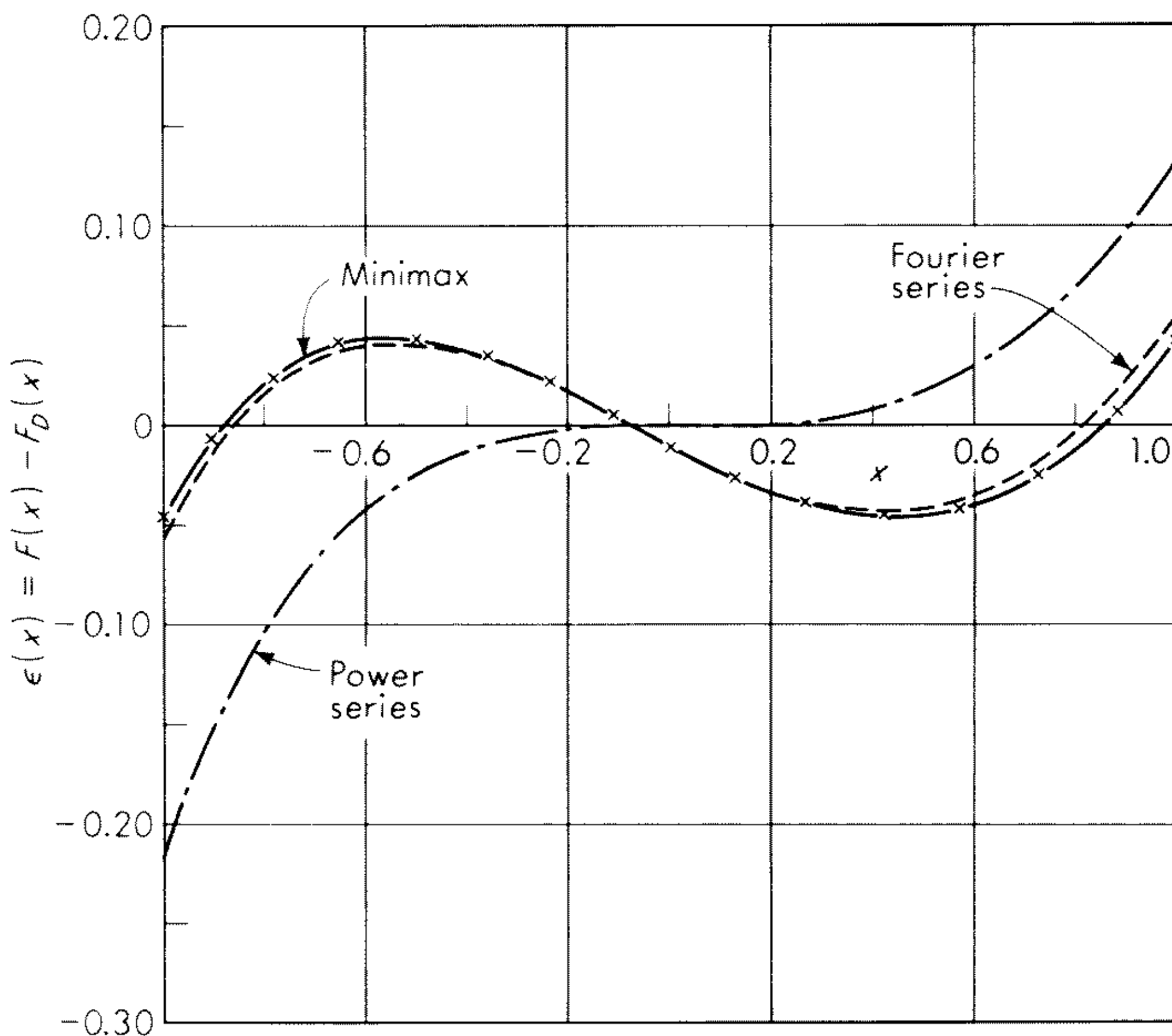


Fig. 7.18 The error of approximation by Taylor series, Fourier series, and minimax.

tion. The errors, $f_D - f$, for the three approximations (7.118), (7.119), and (7.121) are shown in Fig. 7.18, and it can be seen that it is the minimax approximation that has lobes of equal deviation about the desired pattern value.

The Quadrature Methods

Most of the array-pattern synthesis techniques described in this chapter contain the constraint of equal interelement spacings. In Sec. 7.4 a number of quasi-synthesis techniques involving non-uniformly spaced arrays were discussed in the light of the production of narrow-beam, low side-lobe patterns. There is, however, an important branch of numerical analysis that can be

Synthesis method			Constraints			Criteria		
Section	Reference	Array or aperture	Dimensions	Shape	Reactive power or Q	Full or partial pattern specification	Synthesized quantity	Error measured
7.2	3	Array	1 or 2	Linear or rect.	None	Full	Field	Min. mean square (gaussian)
7.3	4	Aperture	1 or 2	Linear or rect.	None	Full	Field	Min. mean square (gaussian)
7.5	6	Array	2	Circular	None	Arbitrary†	Field	Approx. gaussian
7.6	10	Aperture	2	Circular	None	Arbitrary†	Field	Gaussian
7.6	11	Aperture	2	Circular zones	None	Arbitrary†	Field	—
7.6	13	Aperture	2 (1.var.)	Circular	None	Arbitrary†	Field	—
7.7	20	Continuous			Aperture			
		line source	1	Linear	Q spec.	Full†	Field	Gaussian
7.8	24	Array	1	Linear	None	BW-SLL‡	Field	Chebyshev
7.8	17	Continuous						
		line source	1	Linear	None	BW-SLL	Field	Approx. Chebyshev
7.8	28	Continuous						
		line source	1	Linear	None	BW-SLL	Field	—
7.8	29	Aperture	2 (1 var.)	Circular	None	BW-SLL	Field	Approx. Chebyshev
7.9	31-34	Array	1	Linear non-uniform spacing	None	BW-SLL	Field	—
7.10	35	Array	1	Linear	None	Full§	Power	Gaussian error for pattern logarithm
7.10	37	Array	1 or 2	Linear	None	Full	Power	Gaussian
7.10	40	Array	1	Linear	None	Full	Power	Mod. of continuity limit
7.11	41	Array	1	Linear	None	Sector	Field	Pattern value and derivative match
7.11	44	Array	1 or 2	Linear	None	Full	Field	Gaussian
7.11	—	Array	1	Linear	None	Full	Field	True Chebyshev

†Pattern in one variable.

‡BW-SLL = Beam-width or side-lobe level specification.

§With restriction

applied to antenna pattern synthesis to reduce the approximation error in certain instances. This is the topic of interpolation by quadratures.⁴⁶

The approximation of a desired function by a specially selected set of samples has been investigated for many spacings of samples corresponding to different weightings of the match between the desired and approximating functions. For example, the sampling points for the Gaussian-Chebyshev quadrature method coincide with the zeros of a selected Chebyshev polynomial. Most interpolation formulas, however, are intended to approximate the desired function over a specified range, and the use of nonuniform sample points to synthesize a pattern for the entire visible region may result in array spacings that are less than $\lambda_0/2$. Nevertheless, the quadrature methods may provide a systematic approach to the synthesis of arbitrary patterns by non-uniformly spaced arrays.

PROBLEMS

7.1 Find the excitation coefficients of a linear array of $2N + 1$ uniformly spaced isotropic elements lying along the x axis with $d_x = 3\lambda_0/4$ for a minimum-mean-square-error match in the visible range to an impulse located at $u = 1/2$. Plot the array factor.

7.2 Repeat the last part of Exercise 7.1 with $A_{D3} = A_{D(-3)} = 0$ and all other A_{Dn} the same. What general characteristic changes this problem from Exercise 7.1? Try to generalize your results for higher-order averaged errors.

7.3 Find the gaussian match, over the visible range, to an impulse at $u = 0$ by an array of three elements by using (7.8). Plot the ratio of array input power ($\sum A_m^2$) to main beam height $f^2(0)$ versus d for $0 < d \leq \lambda_0/2$. For small d , use a two-term approximation for the sine function in (7.8).

7.4 Apply the cardinal function synthesis technique of Sec. 7.3 to a desired pattern of one angular variable, given by

$$\begin{aligned} f_D(u) &= (u^{-1} - 1) & 0 < u \leq 1 \\ f_D(u) &= 0 & \infty < u \leq 0, u > 1 \end{aligned}$$

for $a = 2\lambda_0$. Calculate the far-field pattern for the following cases:

- The first sample, u_0 , is at $u = 0$.
- The set of samples is so shifted that the first sample is at $u_0 = 1/8$.
- The samples are at $u_n = n\pi/k_0a$, but the sample value at $u = 0$ is set equal to 1.

This last case was studied by Woodward, who used the sample values at the edges of the desired pattern for side-lobe control.⁴

7.5 The taper of the illumination pattern of a conventional aperture is a slowly varying function, although the aperture may be many wavelengths in extent. A typical distribution (in one dimension) is

$$F(x) = \frac{1 + \Delta}{2} + \frac{1 - \Delta}{2} \cos \frac{\pi x}{a} \quad -a \leq x \leq a$$

Expand $F(x)$ in the form

$$F(x) = \sum_m f_m e^{jm(\pi/a)x}$$

and calculate the radiation pattern in the form of (7.10). Sketch the pattern. Find the equivalent array, given by (7.12). Calculate the array coefficients for the case

- a. The region of equivalence ends at the nonzero samples.
- b. The region of equivalence includes the first zero-value samples adjacent to the region of equivalence of case a.

Compare the array coefficients with the values of $F(x)$ at the element locations. Note that the number of elements of the equivalent array is very small in this example, although the aperture could be many wavelengths across. Plot the array patterns for cases a and b by using $\Delta = 1/4$. Compare with the aperture pattern.

7.6 Find the circular array of six isotropic elements that provides a gaussian match to an impulse at $\phi = \phi_0$. Select the ring radius by trying a few values and determining the contributions of the strongest residuals. Plot the patterns and determine the beam widths and side-lobe levels. How do the feeding coefficients change if the beam is rotated ($\phi_0 = \omega_0 t$)?

7.7 Find the line source distribution that provides a minimum-mean-square match to an impulse at $u = 0$, with the constraint that the supergain ratio $\gamma = 2$, and $c = 4$. The normalization constants of the prolate spheroidal functions are as follows:

n	$G_n(4)$
0	1.00413
1	1.09636
2	1.92660
3	9.07359
4	113.2772
5	2,622.676

7.8 What is the lowest supergain ratio possible for a distribution on a line source of length $2a = 4\lambda_0/\pi$? Use the table of Prob. 7.7.

7.9 Program an iterative solution of (7.93) for an 11-element linear array with $\lambda_0/2$ interelement spacings. After each iteration compute the error ϵ . Consider the desired power pattern to be an impulse at $u = 0$. Use as an initial set of A_m a set of real coefficients. Do the iterated coefficients remain real? Try a set of complex coefficients. Is the resultant error ϵ after several iterations nearly the same as that for the real coefficients? Why?

7.10 Compute the periods of the sinusoidal "tails," such as those shown on the curve of Fig. 7.13, that vary at the fastest rate possible for a linear array of $N + 1$ elements with interelement spacings of d . Would you expect a synthesis result to approximate closely tails that vary at the maximum rate?

7.11 Carry out the Bernstein polynomial synthesis for a desired pattern

$$P_D = 1 \quad -0.25 < u < 0.25$$

$$P_D = 0 \quad \text{elsewhere}$$

and a six-element array. Plot the result. State whether the results would differ if the desired pattern were the following:

$$P_D = 1 \quad -0.35 < u < 0.35$$

$$P_D = 0 \quad \text{elsewhere}$$

REFERENCES

1. Lanczos, C.: "Applied Analysis," Prentice-Hall, Inc., Englewood Cliffs, N.J., 1956.
2. Wolff, I.: Determination of the Radiating System Which Will Produce a Specified Directional Characteristic, *Proc. IRE*, vol. 25, p. 630, 1937.

3. Schelkunoff, S. A.: A Mathematical Theory of Linear Arrays, *Bell System Tech. J.*, vol. 22, pp. 80–107, January, 1943.
4. Woodward, P. M.: A Method of Calculating the Field over a Plane Aperture Required to Produce a Given Polar Diagram, *Proc. Inst. Elec. Engrs. (London)*, vol. 93, part IIIA, pp. 1554–1558, 1947.
5. Yen, J. L.: On the Synthesis of Line-sources and Infinite Strip-sources, *IRE Trans. Antennas Propagation*, vol. AP-5, pp. 40–46, January, 1957.
6. Taylor, T. T.: A Synthesis Method for Circular and Cylindrical Antennas Composed of Discrete Elements, *IRE Trans. Antennas Propagation*, vol. PGAP-3, pp. 251–261, August, 1952.
7. DuHamel, R. H.: Pattern Synthesis for Antenna Arrays on Circular, Elliptical, and Spherical Surfaces, *Univ. Illinois, Elec. Eng. Res. Lab., Tech. Rept.*, no. 16, Urbana, Ill., May, 1952.
8. Knudsen, H. L.: Radiation from Ring Quasi-arrays, *IRE Trans. Antennas Propagation*, vol. AP-4, pp. 452–472, July, 1956.
9. Patton, W. T., and J. D. Tillman: An Analysis of the Terminal Properties of a Circular Antenna Array with a Synthesis Technique for Obtaining a Prescribed Radiation Pattern, *Univ. Tennessee Eng. Expt. Stat. Sci. Rept. 2*, Contract AF 19(604)-1557, Knoxville, Tenn., June, 1958. Astia No. AD 152379, or C. E. Hickman, H. P. Neff, and J. D. Tillman, The Theory of a Single Ring Antenna Array, *Trans. AIEE*, vol. 80, part 1, May, 1961.
10. Ruze, J.: Circular Aperture Synthesis, *IEEE Trans. Antennas Propagation*, vol. AP-12, pp. 691–694, November, 1964.
11. Cornbleet, S.: Pattern Synthesis from Zoned Circular Apertures, *IEEE Trans. Antennas Propagation*, vol. AP-14, pp. 646–648, September, 1966.
12. Watson, G. N.: "Theory of Bessel Functions," Cambridge University Press, London, 1962.
13. Minkovich, B. M., and Yu. I. Davidchevskiy: Synthesis of Circular Aperture Antennas, *Radiotekhn. Elektron.*, vol. 6, pp. 1395–1396, 1961.
14. Chu, L. J.: private communication, Oct. 11, 1966.
15. Woodward, P. M., and J. D. Lawson, The Theoretical Precision with Which an Arbitrary Radiation Pattern May Be Obtained from a Source of Finite Size, *Proc. Inst. Elec. Engrs. (London)*, vol. 95, part IIIA, pp. 363–369, 1948.
16. Rhodes, D. R.: On a Fundamental Principle in the Theory of Planar Antennas, *Proc. IEEE*, vol. 52, pp. 1013–1021, September, 1964.
17. Taylor, T. T.: Design of Line Source Antennas for Narrow Beamwidth and Low Side-lobes, *IRE Trans. Antennas Propagation*, vol. AP-3, pp. 16–28, January, 1955.
18. Rhodes, D. R.: On the Stored Energy and Reactive Power of Planar Apertures, *IEEE Trans. Antennas Propagation*, vol. AP-14, pp. 676–683, November, 1966.
19. Leonard, D. J.: Synthesis of the Aperture Field from an Arbitrary Radiation Pattern, *McGill Symp. Microwave Optics*, part II, AFCRC-TR-59-118(II), Astia No. AD211500, pp. 337–343, April, 1959.
20. Rhodes, D. R.: The Optimum Line Source for the Best Mean-Square Approximation to a Given Radiation Pattern, *IEEE Trans. Antennas Propagation*, vol. AP-11, pp. 440–446, July, 1963.
21. Slepian, D., and H. O. Pollak: Prolate Spheroidal Wave Functions, Fourier Analysis, and Uncertainty, pt. 1, *Bell System Tech. J.*, vol. 40, pp. 43–64, January, 1961.
22. Flammer, C.: "Spheroidal Wave Functions," Stanford University Press, Stanford, Calif., 1957.
23. Collin, R. E., and S. Rothschild: Reactive Energy in Aperture Fields and Aperture Q , *Can. J. Phys.*, vol. 41, pp. 1967–1979, December, 1963.
24. Dolph, C. L.: A Current Distribution for Broadside Arrays Which Optimizes the Relationship between Beam Width and Side-lobe Level, *Proc. IRE*, vol. 34, pp. 335–348, June, 1946.

25. Brown, L. B., and G. A. Scharp: Tchebycheff Antenna Distribution, Beamwidth and Gain Tables, *Naval Ordnance Lab., Corona, Calif., NAVORD Rept.* 4629, 1958.
26. Drane, C. J.: Derivation of Excitation Coefficients for Chebyshev Arrays, *PROC. Inst. Elec. Engrs. (London)*, vol. 110, pp. 1755–1758, October, 1963.
27. Drane, C. J.: Dolph-Chebyshev Excitation Coefficient Approximation, *IEEE Trans. Antennas Propagation*, vol. AP-12, pp. 781–782, November, 1964.
28. Taylor, T. T.: One Parameter Family of Line Sources Producing Modified $(\sin \pi u)/\pi u$ Patterns, *Hughes Aircraft Tech. Mem.* 324, September, 1953.
29. Taylor, T. T.: Design of Circular Apertures for Narrow Beamwidth and Low Sidelobes, *IRE Trans. Antennas Propagation*, vol. AP-8, pp. 17–22, January, 1960.
30. Hansen, R. C.: Tables of Taylor Distributions for Circular Aperture Antennas, *IRE Trans. Antennas Propagation*, vol. AP-8, pp. 23–26, January, 1960.
31. Ishimaru, A.: Theory of Unequally Spaced Arrays, *IRE Trans. Antennas Propagation*, vol. AP-10, pp. 691–702, November, 1962.
32. Jahnke, E., F. Emde, and F. Losch: "Tables of Higher Functions," 6th ed., McGraw-Hill Book Company, New York, 1960.
33. Ishimaru, A., and Y. S. Chen: Thinning and Broadbanding Antenna Arrays by Unequal Spacings, *IEEE Trans. Antennas Propagation*, vol. AP-13, pp. 34–42, January, 1965.
34. Chow, Y. L.: On Grating Plateaux of Nonuniformly Spaced Arrays, *IEEE Trans. Antennas Propagation*, vol. AP-13, pp. 208–215, March, 1965.
35. Taylor, T. T., and J. R. Whinnery: Applications of Potential Theory to the Design of Linear Arrays, *J. Appl. Phys.*, vol. 22, pp. 19–29, January, 1951.
36. Wolff, E. A.: Linear Antenna Array Synthesis, doctoral dissertation, University of Maryland, 1961.
37. Morison, J. E., and A. C. Schell: A Technique for Power Pattern Synthesis, *PTGAP Intl. Symp. Digest*, pp. 160–163, July, 1963.
38. Simon, J. C.: Application of Periodic Functions Approximation to Antenna Pattern Synthesis and Circuit Theory, *IRE Trans. Antennas Propagation*, vol. AP-4, pp. 429–440, July, 1956.
39. Haywood, A. L.: An Analog Computer for Linear Array Antenna Analysis, *WADD Tech. Rept.* 60-666, November, 1960.
40. Ma, M. T.: Application of Bernstein Polynomial and Interpolation Theory to Linear Array Synthesis, *IEEE Trans. Antennas Propagation*, vol. AP-12, pp. 668–677, November, 1964.
41. Ksienski, A.: Derivative Control in Shaping Antenna Patterns, *Hughes Aircraft Sci. Rept.* 3508-6, Contract AF19(604)-3508, Culver City, Calif., September, 1959.
42. Ksienski, A.: Maximally Flat and Quasi-smooth Sector Beams, *IRE Trans. Antennas Propagation*, vol. AP-8, pp. 476–484, September, 1960.
43. Ruze, J.: Physical Limitations on Antennas, *M.I.T. Radiation Lab. Eng. Tech. Rept.* 248, pp. 64–72, October, 1952.
44. Sletten, C. J., P. Blacksmith, and G. Forbes: New Method of Antenna Array Synthesis Applied to Generation of Double-step Patterns, *IRE Trans. Antennas Propagation*, vol. AP-5, pp. 369–373, October, 1957.
45. Todd, J. (ed.): "Survey of Numerical Analysis," McGraw-Hill Book Company, New York, 1962.
46. Bruce, J. D., and H. Unz: Mechanical Quadratures to Synthesize Nonuniformly Spaced Antenna Arrays, *Proc. IRE*, vol. 50, p. 2128, October, 1962.

ADDITIONAL REFERENCES

General

- Fel'd, Ya. N., and L. D. Bakrakh: The Present State of the Antenna Synthesis Theory, *Radiotekhn. Elektron.*, vol. 8, pp. 187–205, 1963.

Zelkin, Ye. G.: Design of Radiating Systems on the Basis of a Given Radiation Pattern, *Gosenergoizdat*, 1963.

Geometrical Optics Synthesis

Chu, L. J.: Microwave Beam Shaping Antennas, *M.I.T. Res. Lab. Electron. Tech. Rept.* 40, June, 1947.

Dunbar, A. S.: On the Theory of Antenna Beam Shaping, *J. Appl. Phys.*, vol. 23, p. 847, August, 1952.

Keller, J. B.: The Inverse Scattering Problem in Geometrical Optics and the Design of Reflectors, *IRE Trans. Antennas Propagation*, vol. AP-7, pp. 146–149, April, 1959.

Shanks, H. E.: A Geometrical Optics Method of Pattern Synthesis for Linear Arrays, *IRE Trans. Antennas Propagation*, vol. AP-8, p. 485, September, 1960.

Also see Chap. 16.

Papers Relevant to Sec. 7.2

Cheng, D. K., and M. T. Ma: A New Mathematical Approach for Linear Array Analysis, *IRE Trans. Antennas Propagation*, vol. AP-8, pp. 255–259, May, 1960.

Ksienski, A.: Synthesis of Nonseparable Two-dimensional Patterns by Means of Planar Arrays, *IRE Trans. Antennas Propagation*, vol. AP-8, pp. 224–225, March, 1960.

Ma, M. T.: An Application of the Inverse Z-transform Theory to the Synthesis of Linear Antenna Arrays, *IEEE Trans. Antennas Propagation*, vol. AP-12, p. 798, November, 1964.

Papers Relevant to Sec. 7.3

Collin, R. E.: Pattern Synthesis with Nonseparable Aperture Fields, *IEEE Trans. Antennas Propagation*, vol. AP-12, p. 502, July, 1964.

Ksienski, A.: Equivalence between Continuous and Discrete Radiating Arrays, *Can. J. Phys.*, vol. 39, pp. 335–349, February, 1961.

Minkovich, B. M.: Use of the Double Fourier Transform for the Synthesis of Antennas with Planar Aperture, *Radiotekhn. Elektron.*, vol. 7, no. 1, pp. 171–173, 1962.

Pistolkors, A. A.: Use of Mathieu Functions for Computing Field Distribution in an Antenna to Obtain a Directional Diagram, *Doklady Akad. Nauk SSSR*, vol. 89, pp. 849–852, 1953.

Tartakovsky, L. B.: Synthesis for a Linear Radiator and Its Analogy in the Problem of Broadband Matching, *Radiotekhn. Elektron.*, vol. 3, p. 1463, 1958.

Zelkin, Ye. G.: Synthesis of Planar-aperture Antennas, *Radiotekhn. Elektron.*, pp. 1843–1848, December, 1963.

Papers Relevant to Sec. 7.7

Chu, L. J.: Physical Limitations of Omnidirectional Antennas, *J. Appl. Phys.*, vol. 19, pp. 1163–1175, December, 1948.

Collin, R. E., and S. Rothschild: Evaluation of Antenna Q , *IEEE Trans. Antennas Propagation*, vol. AP-12, pp. 23–27, January, 1964.

Minkovich, B. M.: The Selection of Antenna Length, *Radiotekhn. Elektron.*, vol. 10, pp. 1311–1314, 1965.

Parad, L.: The Real and Reactive Power of a Planar Array, *IEEE Trans. Antennas Propagation*, vol. AP-13, pp. 990–992, November, 1965.

Slepian, D.: Some Asymptotic Expansions for Prolate Spheroidal Wave Functions, *J. Math. Phys.*, vol. 44, pp. 99–140, 1965.

Yakovlev, V. P.: Synthesis of a Linear Antenna Whose Current Distribution Is Represented by a Fourier Series with a Finite Number of Harmonics, *Radiotekhn. Elektron.*, vol. 9, pp. 12–23, 1964.

Yaru, N.: A Note on Supergain Antenna Arrays, *Proc. IRE*, vol. 39, pp. 1081–1085, 1951.

Papers Relevant to Sec. 7.9

Bruce, J. D., and H. Unz: Broadband Nonuniformly Spaced Arrays, *Proc. IRE*, vol. 50, pp. 228–229, February, 1962.

Butler, J. K., and H. Unz: Fourier Transform Methods for Analyzing Nonuniform Arrays, *Proc. IEEE*, vol. 53, no. 2, pp. 191–192, February, 1965.

——— and ———: Optimization of Beam Efficiency and Synthesis of Nonuniformly Spaced Arrays, *Proc. IEEE*, vol. 54, no. 12, pp. 2007–2008, December, 1966.

——— and ———: Beam Efficiency and Gain Optimization of Antenna Arrays with Nonuniform Spacings, *Radio Sci.*, vol. 2 (new series), no. 7, pp. 711–720, July, 1967.

Chow, Y. L., and J. L. Yen: On Grating Plateaux of the Conformal Array, *IEEE Trans. Antennas Propagation*, vol. AP-14, pp. 590–600, September, 1966.

Galejs, J.: Minimization of Side Lobes in Space Tapered Linear Arrays, *IEEE Trans. Antennas Propagation*, vol. AP-12, p. 497, July, 1964.

Harrington, R. F.: Side Lobe Reduction by Nonuniform Element Spacing, *IRE Trans. Antennas Propagation*, vol. AP-9, p. 187, March, 1961.

King, D. D., R. F. Packard, and R. K. Thomas: Unequally Spaced, Broadband Antenna Arrays, *IRE Trans. Antennas Propagation*, vol. AP-8, pp. 380–385, July, 1960.

Lo, Y. T.: A Spacing Weighted Antenna Array, *IRE Conv. Record*, 1962.

———: A Mathematical Theory of Antenna Arrays with Randomly Spaced Elements, *IEEE Trans. Antennas Propagation*, vol. AP-12, p. 257, May, 1964.

——— and S. W. Lee: Side Lobe Level of Nonuniformly Spaced Antenna Arrays, *IEEE Trans. Antennas Propagation*, vol. AP-13, p. 817, September, 1965.

Ma, M. T.: Another Method of Synthesizing Nonuniformly Spaced Arrays, *IEEE Trans. Antennas Propagation*, vol. AP-13, p. 833, September, 1965.

Maffett, A. L.: Array Factors with Nonuniform Spacing Parameter, *IRE Trans. Antennas Propagation*, vol. AP-10, pp. 131–136, March, 1962.

Maher, T. M., and D. K. Cheng: Random Removal of Radiators from Large Linear Arrays, *IEEE Trans. Antennas Propagation*, vol. AP-11, pp. 106–111, March, 1963.

Pokrovskiy, V. L.: A General Method for Determining the Optimum Distribution for Linear Antennas, *Doklady Akad. Nauk SSSR*, vol. 138, pp. 584–586, 1961.

Sandler, S. S.: Some Equivalences between Equally and Unequally Spaced Arrays, *IRE Trans. Antennas Propagation*, vol. AP-8, p. 496, September, 1960.

Shubert, H. A., J. K. Butler, and H. Unz: Comments on Optimization of Beam Efficiency and Synthesis of Nonuniformly Spaced Arrays, *Proc. IEEE*, vol. 55, no. 7, pp. 1205–1206, July, 1967.

Skolnik, M. I., G. Neinhauser, and J. W. Sherman: Dynamic Programming Applied to Unequally Spaced Arrays, *IEEE Trans. Antennas Propagation*, vol. AP-12, pp. 35–43, January, 1964.

———, J. W. Sherman, and F. C. Ogg: Statistically Designed Density-tapered Arrays, *IEEE Trans. Antennas Propagation*, vol. AP-12, p. 408, July, 1964.

Strait, B. J.: Synthesis of Unequally Spaced Arrays with Uniform or Stepped Amplitude Distribution, *Proc. Natl. Electron. Conf.*, vol. XXII, pp. 50–55, 1966.

Tang, C. H.: An Approximate Method of Designing Nonuniformly Spaced Arrays, *IEEE Trans. Antennas Propagation*, vol. AP-13, p. 177, January, 1965.

- Unz, H.: Antenna Arrays with Arbitrarily Distributed Elements, doctoral dissertation, Electrical Engineering Department, University of California, Berkeley, Calif., November, 1956.
- : Linear Arrays with Arbitrarily Distributed Elements, *Electron. Res. Lab.*, University of California, Berkeley, Calif. ser. 60, issue 168, pp. 1–58, Nov. 2, 1956.
- : Multi-dimensional Lattice Arrays with Arbitrarily Distributed Elements, *Univ. California Electron. Res. Lab.*, ser. 60, issue 172, pp. 1–43, Berkeley, Calif., Dec. 19, 1956.
- : Linear Arrays with Arbitrarily Distributed Elements, *IRE Trans. Antennas Propagation*, vol. AP-8, pp. 222–223, March, 1960.
- : Matrix Relations for a Linear Array with Dipole Elements in the Fresnel Zone, *IRE Trans. Antennas Propagation*, vol. AP-9, no. 2, p. 220, March, 1961.
- : Nonuniform Arrays with Spacings Larger Than One Wavelength, *IRE Trans. Antennas Propagation*, vol. AP-10, no. 5, pp. 647–648, September, 1962.
- : New Methods for Synthesis of Nonuniformly Spaced Antenna Arrays, *Ohio State Univ. Antenna Lab. Rept.* 1423-1, pp. 1–31, Columbus, Ohio, Nov. 15, 1962.
- : Nonuniformly Spaced Arrays: The Orthogonal Method, *IEEE Proc.*, vol. 54, no. 1, pp. 53–54, January, 1966.
- : Nonuniformly Spaced Arrays: The Eigenvalues Method, *IEEE Proc.*, vol. 54, no. 4, pp. 676–678, April, 1966.

Papers Relevant to Sec. 7.10

- Hyneman, R. F., and R. M. Johnson: A Technique for the Synthesis of Shaped-beam Radiation Patterns with Approximately Equal-percentage Ripple, *Hughes Aircraft FR66-14-241*, Fullerton, Calif., Oct. 3, 1966.
- Proctor, E., and C. Ablow: A Variational Method of Synthesizing Antenna Power Patterns, *Stanford Res. Inst. Sci. Rept.* 9, Contract AF19(604)-3502, March, 1961.
- Zelkin, Ye. G.: Phase Radiation Pattern and Problem of Antenna Synthesis, *Radiotekhn. Elektron.*, vol. 8, pp. 42–52, 1963.

Papers Relevant to Sec. 7.11

- Brecout, P. A.: Pattern Synthesis Using Weighted Functions, *IRE Trans. Antennas Propagation*, vol. AP-8, pp. 441–444, 1960.
- Fradin, A. L.: A Method for the Synthesis of the Radiator Best Approximating an Isotropic Radiator, *Radiotekhn. Elektron.*, vol. 8, pp. 759–764, 1963.
- Harris, J. H., and H. E. Shanks: A Method for Synthesis of Optimum Directional Patterns from Nonplanar Apertures, *IRE Trans. Antennas Propagation*, vol. AP-10, p. 228, May, 1962.
- Jaekle, W. G.: Antenna Synthesis by Weighted Fourier Coefficients, *IEEE Trans. Antennas Propagation*, vol. AP-12, pp. 369–370, May, 1964.
- Ksienski, A.: Interpolation Techniques Applied to Pattern Synthesis, *Hughes Aircraft Sci. Rept.* 8, Contract AF19(608)-3508, October, 1960.
- Minkovich, B. M.: On One Type of Partial Radiation Patterns, *Radiotekhn. Elektron.*, vol. 7, pp. 708–710, 1962.
- : Representation of the Radiation Pattern of an Antenna as the Sum of N Functions, *Radiotekhn. Elektron.*, vol. 9, pp. 1073–1076, 1964.
- : On Plane Aperture Antenna Design, *Radiotekhn. Elektron.*, vol. 9, pp. 1308–1310, 1964.
- Zelkin, Ye. G.: Synthesis of a Linear Radiator of Arbitrary Shape, *Radiotekhn. Elektron.*, vol. 9, pp. 24–32, 1964.

CHAPTER 8

INTRODUCTION TO LINEAR ANTENNAS

Tai Tsun Wu

8.1 Maxwell's Equations

In this chapter we consider some questions of principle encountered in the theory of linear antennas. We shall not be concerned here with any problems of actually obtaining numerical results. These are to be dealt with in later chapters.

For definiteness, we consider the antenna to be in vacuum, so that

$$\mathfrak{B} = \mu_0 \mathfrak{H} \quad \text{and} \quad \mathfrak{D} = \epsilon_0 \mathfrak{E} \quad (8.1)$$

The velocity of light and the characteristic impedance of free space are then given by

$$c = (\mu_0 \epsilon_0)^{-1/2} \quad \text{and} \quad \zeta_0 = \mu_0^{1/2} \epsilon_0^{-1/2} \quad (8.2)$$

To generalize the results to an arbitrary homogeneous isotropic medium characterized by the scalars μ and ϵ , it is sufficient to replace μ_0 by μ and ϵ_0 by ϵ . Of course, c and ζ_0 are also redefined by using μ and ϵ ; all four quantities may be complex.

We shall use \mathfrak{B} and \mathfrak{E} to write the Maxwell equations

$$\nabla \times \mathfrak{E} = -\frac{\partial \mathfrak{B}}{\partial t} \quad (8.3)$$

$$\mu_0^{-1} \nabla \times \mathfrak{B} = \epsilon_0 \frac{\partial \mathfrak{E}}{\partial t} + \mathfrak{J} \quad (8.4)$$

$$\nabla \cdot \mathfrak{B} = 0 \quad (8.5)$$

and
$$\epsilon_0 \nabla \cdot \mathfrak{E} = \rho \quad (8.6)$$

In (8.4) and (8.6), \mathfrak{J} and ρ are respectively the current and charge densities. The current and charge densities satisfy the *equation of continuity*

$$\nabla \cdot \mathfrak{J} + \frac{\partial \rho}{\partial t} = 0 \quad (8.7)$$

Equations (8.3) and (8.4) are the dynamic equations of motion for determining \mathfrak{B} and \mathfrak{E} for given \mathfrak{J} . It follows from (8.3), (8.4), and (8.7) that

$$\frac{\partial}{\partial t} (\nabla \cdot \mathfrak{B}) = 0 \quad (8.8)$$

$$\frac{\partial}{\partial t} (\epsilon_0 \nabla \cdot \mathfrak{E} - \rho) = 0 \quad (8.9)$$

(We have assumed that the order of differentiation can be changed. Such mathematical questions are not considered in this chapter.) Thus (8.5) and (8.6) are boundary conditions in the sense of initial conditions. If they hold at a particular time, they hold for all times.

We introduce the vector potential \mathfrak{A} by

$$\mathfrak{B} = \nabla \times \mathfrak{A} \quad (8.10)$$

Since, by (8.3), $\nabla \times \left(\mathfrak{E} + \frac{\partial \mathfrak{A}}{\partial t} \right) = 0$, we introduce the scalar potential φ by

$$\mathfrak{E} = -\frac{\partial \mathfrak{A}}{\partial t} - \nabla \varphi \quad (8.11)$$

Then the substitution of (8.10) and (8.11) into (8.4) and (8.6) gives

$$\nabla^2 \mathfrak{A} - c^{-2} \frac{\partial^2 \mathfrak{A}}{\partial t^2} = -\mu_0 \mathfrak{J} + \nabla \chi \quad (8.12)$$

$$\nabla^2 \varphi - c^{-2} \frac{\partial^2 \varphi}{\partial t^2} = -\epsilon_0^{-1} \rho - \frac{\partial \chi}{\partial t} \quad (8.13)$$

where
$$\chi = \nabla \cdot \mathfrak{A} + c^{-2} \frac{\partial \varphi}{\partial t} \quad (8.14)$$

In view of the form of the right-hand sides of (8.12) and (8.13), it is convenient for a number of purposes to choose

$$\chi = 0 \quad (8.15)$$

This is known as the Lorentz condition. With (8.15), (8.12) and (8.13) simplify to the familiar form

$$\nabla^2 \mathfrak{A} - c^{-2} \frac{\partial^2 \mathfrak{A}}{\partial t^2} = -\mu_0 \mathfrak{J} \quad (8.16)$$

and
$$\nabla^2 \varphi - c^{-2} \frac{\partial^2 \varphi}{\partial t^2} = -\epsilon_0^{-1} \rho \quad (8.17)$$

It is important to realize that (8.17) is a dynamic equation for the scalar potential, while (8.13) is a boundary condition. Although it seems that we have five equations (8.15) to (8.17) for the four quantities \mathfrak{A} and φ , one of them is really a boundary condition. In particular, for various reasons such as Lorentz invariance, it is convenient to use (8.16) and (8.17) as the dynamic equations, and it follows from these two equations that χ satisfies, by (8.7), the *homogeneous* equation

$$\nabla^2 \chi - c^{-2} \frac{\partial^2 \chi}{\partial t^2} = -\mu_0 \left(\nabla \cdot \mathfrak{J} + \frac{\partial \rho}{\partial t} \right) = 0 \quad (8.18)$$

Thus, (8.15) holds for all times if we have the boundary conditions

$$\chi = \frac{\partial \chi}{\partial t} = 0 \quad (8.19)$$

at any one time. That there are two boundary conditions here instead of the one (8.6) merely reflects the fact that (8.17) contains two time derivatives and (8.15) contains only one. For further discussion of (8.19) see, for example, Wentzel.¹

In view of the role played by the equation of continuity in (8.18), it is often desirable, even in approximate calculations of electromagnetic problems, to satisfy (8.7) *exactly*.

Although Maxwell's equations in free space are invariant under Lorentz transformations, this invariance is often of no importance in engineering applications. For example, if we want to study the behavior of an antenna system, such a system is usually at rest in a particular Lorentz frame. It is then natural and convenient to carry out all the analysis in this particular frame.

On the other hand, invariance under time translation often holds. In such cases, it is desirable in most instances to use Fourier transforms with respect to t , and thus we can replace the independent variable t by a parameter ω , the frequency. More precisely, let

$$\mathbf{E}(\mathbf{r}, t) = \frac{1}{2\pi} \int_{-\infty}^{\infty} \mathbf{E}(\mathbf{r}, \omega) e^{-i\omega t} d\omega \quad (8.20)$$

$$\varphi(\mathbf{r}, t) = \frac{1}{2\pi} \int_{-\infty}^{\infty} \Phi(\mathbf{r}, \omega) e^{-i\omega t} d\omega \quad (8.21)$$

and so on. Note that $\mathbf{E}(\mathbf{r}, t)$ is real, that is,

$$\mathbf{E}(\mathbf{r}, t) - \mathbf{E}^*(\mathbf{r}, t) = 0 \quad (8.22)$$

$$\text{or} \quad \int_{-\infty}^{\infty} [\mathbf{E}(\mathbf{r}, \omega) - \mathbf{E}^*(\mathbf{r}, -\omega)] e^{-i\omega t} d\omega = 0 \quad (8.23)$$

for all t . Since zero is the only function whose Fourier transform is zero, we get

$$\mathbf{E}(\mathbf{r}, \omega) = \mathbf{E}^*(\mathbf{r}, -\omega) \quad (8.24)$$

This symmetry holds also for \mathbf{B} , \mathbf{A} , Φ , \mathbf{J} , ρ , etc. It is thus often sufficient to consider only positive values of ω . Maxwell's equations imply that

$$\nabla \times \mathbf{E} = i\omega \mathbf{B} \quad (8.25)$$

$$\mu_0^{-1} \nabla \times \mathbf{B} = -i\omega \epsilon_0 \mathbf{E} + \mathbf{J} \quad (8.26)$$

$$\nabla \cdot \mathbf{B} = 0 \quad (8.27)$$

$$\text{and} \quad \epsilon_0 \nabla \cdot \mathbf{E} = \rho \quad (8.28)$$

The equation of continuity is

$$\nabla \cdot \mathbf{J} - i\omega \rho = 0 \quad (8.29)$$

The vector and scalar potentials are given by

$$\mathbf{B} = \nabla \times \mathbf{A} \quad (8.30)$$

$$\text{and} \quad \mathbf{E} = i\omega \mathbf{A} - \nabla \Phi \quad (8.31)$$

If the Lorentz condition is retained, that is,

$$c^2 \nabla \cdot \mathbf{A} - i\omega \Phi = 0 \quad (8.32)$$

then

$$(\nabla^2 + k^2) \mathbf{A} = -\mu_0 \mathbf{J} \quad (8.33)$$

and

$$(\nabla^2 + k^2) \Phi = -\epsilon_0^{-1} \rho \quad (8.34)$$

where

$$k = \frac{\omega}{c} \quad (8.35)$$

Note that, for convenience, we have dropped the subscript on k . Also $e^{-i\omega t}$ is used in this chapter in place of $e^{j\omega t}$.

8.2 Green's Functions and Radiation Conditions

The connection between the time-dependent quantities \mathcal{E} , \mathcal{B} , \mathcal{A} , φ , etc. on the one hand and the time-independent quantities \mathbf{E} , \mathbf{B} , \mathbf{A} , Φ , etc. on the other is not as straightforward as it may seem. The reason is briefly as follows. The partial differential equations for the time-dependent quantities, (8.16) and (8.17), for example, are hyperbolic and hence have unique solutions for given initial conditions, while the corresponding equations for the time-independent quantities, (8.33) and (8.34), for example, are elliptic partial differential equations and hence some boundary conditions are needed in order to get unique solutions. These additional boundary conditions are the radiation conditions of Sommerfeld.²

In order to avoid being confused by irrelevant details, we study the Green's functions in some detail. Because of (8.16) and (8.17), consider the Green's function \mathcal{G} defined by

$$\nabla^2 \mathcal{G} - c^{-2} \frac{\partial^2 \mathcal{G}}{\partial t^2} = -\delta(\mathbf{r})\delta(t) \quad (8.36)$$

together with the boundary condition that, for $t < 0$,

$$\mathcal{G} = 0 \quad (8.37)$$

This is known as the retarded Green's function. Although other Green's functions defined by different boundary conditions are more useful in quantum theory, this is by far the most useful Green's function in classical problems of wave propagation, and antenna theory in particular. By rotational invariance,

$$\mathcal{G} = \mathcal{G}(r, t) \quad (8.38)$$

Suppose that we want to represent this \mathcal{G} in the manner of (8.21),

$$\mathcal{G}(r, t) = \frac{1}{2\pi} \int_{-\infty}^{\infty} G(r, \omega) e^{-i\omega t} d\omega \quad (8.39)$$

then G satisfies

$$(\nabla^2 + k^2)G = -\delta(\mathbf{r}) \quad (8.40)$$

Equation (8.40) does not determine $G(r, \omega)$ uniquely; we still need to use the boundary condition (8.37). The general solution of (8.40) is

$$G(r, \omega) = (4\pi r)^{-1}(a_1 e^{ikr} + a_2 e^{-ikr}) \quad (8.41)$$

$$\text{where} \quad a_1 + a_2 = 1 \quad (8.42)$$

The substitution of (8.41) into (8.39) gives

$$\mathcal{G}(r, t) = (4\pi r)^{-1} \left[a_1 \delta\left(t - \frac{r}{c}\right) + a_2 \delta\left(t + \frac{r}{c}\right) \right] \quad (8.43)$$

The boundary condition (8.37) is satisfied if and only if

$$a_2 = 0 \quad (8.44)$$

and, hence, by (8.42),

$$a_1 = 1 \quad (8.45)$$

$$\text{Therefore} \quad G(r, \omega) = (4\pi r)^{-1} e^{ikr} \quad (8.46)$$

$$\text{and} \quad \mathcal{G}(r, t) = (4\pi r)^{-1} \delta\left(t - \frac{r}{c}\right) \quad (8.47)$$

It is interesting to note that (8.47) can be written alternatively as

$$\mathcal{G}(r, t) = (2\pi c)^{-1} \delta(c^2 t^2 - r^2) H(t) \quad (8.48)$$

$$\text{where} \quad H(t) = \begin{cases} 1 & t > 0 \\ 0 & t < 0 \end{cases} \quad (8.49)$$

Equation (8.48) exhibits explicitly the invariance of \mathcal{G} under orthochronous Lorentz transformations.

The result (8.47) can be obtained directly from (8.36) and (8.37) without using Fourier transforms. We proceed to discuss (8.46) in some further detail. Equation (8.46) differs from (8.41) only in the absence of the term proportional to e^{-ikr} . We therefore need to add to (8.40) some rule or condition to eliminate this term. This may be done in a number of different ways.

1. The simplest way is to add the following rule. All terms that are proportional to the sources \mathbf{J} and ρ and behave like e^{-ikr} as $r \rightarrow \infty$ must be deleted. This is adequate for most antenna problems.

2. A second way is to apply Sommerfeld's radiation condition²

$$\lim_{r \rightarrow \infty} r \left(\frac{\partial Q}{\partial r} - ikQ \right) = 0 \quad (8.50)$$

for any fixed direction. Here Q is any scalar physical quantity or any rectangular component of a vector physical quantity.

3. The third method makes use of the fact that Q must be analytic and bounded in the upper half of the ω plane. This comes from (8.37) and the inverse Fourier transform of (8.39), and it is illustrated in Sec. 8.4. This method of choosing the proper solution is particularly useful in cases involving anisotropic media.³

4. Another method is to choose a Q that remains bounded at infinity when c becomes complex with $\text{Im } c < 0$. (This means that the medium becomes lossy.) This condition is, however, difficult to apply in practice.

This list is not intended to be exhaustive, and we can easily think of other ways of eliminating the term e^{-ikr} . For example, we may demand that power flow, obtained from the Poynting vector, is outward at infinity. This is a useful criterion, but it must be used carefully since it fails to eliminate, for example, the solution with $a_1 = 2/3$ and $a_2 = 1/3$.

We conclude with the remark that, since

$$\frac{1}{4\pi} \int_{-\infty}^{\infty} \frac{e^{ik\sqrt{r^2+z^2}}}{\sqrt{r^2+z^2}} e^{i\zeta z} dz = \frac{1}{4} i H_0^{(1)}(r\sqrt{k^2 - \zeta^2}) \quad (8.51)$$

for $|\zeta| < k$, the right-hand side of (8.51) is the retarded Green's function in two dimensions. Terms proportional to $H_0^{(2)}$ are absent. In most antenna problems, it is only necessary to remember to use $H_0^{(1)}$ whenever there is an ambiguity. However, when one studies problems involving anisotropic media extending to infinity, one has to be much more careful; there are known cases when $H_0^{(2)}$ must be used.³

So far we have been discussing Maxwell's equations in general. The remainder of this chapter deals entirely with linear antennas.

8.3 Preliminary Formulation of the Problem of Linear Antennas

In this section, we obtain one form of Hallén's integral equation.⁴ This is the basis of many of the developments in later chapters, and more detailed derivations can be found in the monumental work of King⁵ on linear antennas. We shall then discuss some mathematical difficulty connected with this equation.

Consider two circular rods of radius a and length h placed end to end as shown in Fig. 8.1. Choose the cylindrical coordinate system (r, θ, z) such that

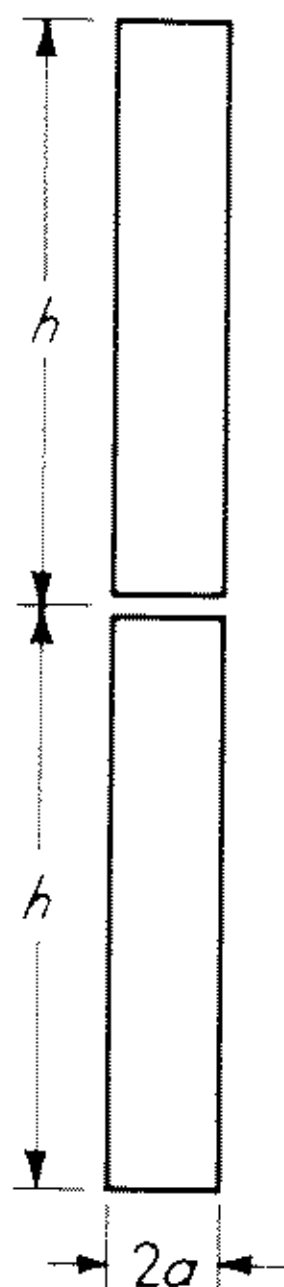


Fig. 8.1 The cylindrical dipole antenna.

the ends of one rod are at $-h$ and $0-$, with those of the other at $0+$ and h . We maintain a potential difference $\text{Re } Ve^{-i\omega t}$ between the ends at $0-$ and $0+$ and ask how the current on the rods, assumed to be perfectly conducting, can be found approximately when a/λ is very small (λ is the free space wavelength).

Since \mathbf{E} , \mathbf{J} , and \mathbf{A} are vectors, while \mathbf{B} is a pseudovector (or axial vector) it follows from rotational symmetry that

$$E_\theta = J_\theta = A_\theta = B_r = B_z = 0 \quad (8.52)$$

Since the rods are of uniform cross sections, J_r can be nonvanishing at most in the vicinities of $z = 0, \pm h$. Since a/λ is very small, we get approximately that

$$A_r = 0 \quad (8.53)$$

and hence by (8.32) and (8.35)

$$\Phi = -ik^{-1}c \frac{\partial A_z}{\partial z} \quad (8.54)$$

Accordingly, on the surface of the rods between $z = -h$ and $z = h$,

$$ik^{-1}c \left(\frac{\partial^2 A_z}{\partial z^2} + k^2 A_z \right) = E_z = -V \delta(z) \quad (8.55)$$

the solution of which is

$$A_z = \frac{iV}{2c} \sin k|z| + C \mu_0 \cos kz \quad (8.56)$$

since A_z is an even function of z . In (8.56), C is a constant to be determined.

Since a/λ is very small, all the current is located near $r = 0$. We therefore make the approximation that the current is located at $r = 0$; that is,

$$J_z(r, \theta, z) = (2\pi r)^{-1} \delta(r) I(z) \quad (8.57)$$

With (8.57), a comparison of (8.33), (8.46), and (8.56) gives, for $|z| \leq h$,

$$\int_{-h}^h I(z') K(z - z', a) dz' = \frac{1}{2} \zeta_0^{-1} iV \sin k|z| + C \cos kz \quad (8.58)$$

where

$$K(z, a) = (4\pi)^{-1} (z^2 + a^2)^{-1/2} \exp [ik(z^2 + a^2)^{1/2}] \quad (8.59)$$

Equation (8.58) is the desired integral equation for the current $I(z)$. It contains an as yet unknown constant C to be determined by the boundary condition

$$I(h) = 0 \quad (8.60)$$

Most of our knowledge about linear antennas comes from this integral equation, and some of the more recent developments will be given later in this book. However, we shall see presently that (8.58) can have no solution for $V \neq 0$, or more precisely, if $I(z)$ is integrable,

$$\int_{-h}^h |I(z)| dz \text{ exists} \quad (8.61)$$

then $I(z)$ does not satisfy (8.58). [The condition (8.61) can be considerably weakened, but again we shall not be concerned with such mathematical problems.] We are therefore faced with the difficult task of interpreting a vast amount of existing theoretical and numerical results. This task will be partially carried out in the next few sections.

The reason why (8.58) has no solution is roughly as follows. As defined by (8.59), $K(z, a)$ is an analytic function of z when z is real. Therefore, the left-hand side of (8.58) is analytic for real z , while the right-hand side has a discontinuous first derivative. For the sake of completeness, we give below a more detailed proof. For $z \geq h$, define

$$\alpha(z) = \int_{-h}^h I(z') K(z - z', a) dz' \quad (8.62)$$

We also define Fourier transforms as follows

$$\bar{I}(\zeta) = \int_{-h}^h I(z) e^{i\zeta z} dz \quad (8.63)$$

$$\bar{K}(\zeta, a) = \int_{-\infty}^{\infty} K(z, a) e^{i\zeta z} dz \quad (8.64)$$

$$\bar{V}(\zeta) = \int_{-h}^h (\frac{1}{2}\zeta_0^{-1}iV \sin k|z| + C \cos kz) e^{i\zeta z} dz \quad (8.65)$$

and
$$\bar{\alpha}(\zeta) = \int_h^{\infty} \alpha(z) e^{i\zeta z} dz \quad (8.66)$$

Then it follows from (8.58) and (8.62) that, for ζ real,

$$\bar{I}(\zeta) \bar{K}(\zeta, a) = \bar{V}(\zeta) + \bar{\alpha}(\zeta) + \bar{\alpha}(-\zeta) \quad (8.67)$$

It follows from (8.61) and (8.62) that

$$|\alpha(z)| \leq (4\pi)^{-1} [(z - h)^2 + a^2]^{-1/2} \int_{-h}^h |I(z)| dz \quad (8.68)$$

$$|\alpha'(z)| \leq (4\pi)^{-1} [1 + k^2(z - h)^2 + k^2a^2]^{1/2} [(z - h)^2 + a^2]^{-1} \int_{-h}^h |I(z)| dz \quad (8.69)$$

etc. Accordingly, by integrations by parts, we get

$$\bar{\alpha}(\zeta) = e^{ik\zeta} [i\alpha(h)\zeta^{-1} - \alpha'(h)\zeta^{-2} + O(\zeta^{-3})] \quad (8.70)$$

and
$$\bar{\alpha}(-\zeta) = -e^{-ik\zeta} [i\alpha(h)\zeta^{-1} + \alpha'(h)\zeta^{-2} + O(\zeta^{-3})] \quad (8.71)$$

as $\zeta \rightarrow \infty$. Furthermore, by explicit computation, we also know that

$$\begin{aligned} \bar{V}(\zeta) &= (i\zeta_0^{-1}V \sin kh + 2C \cos kh) \sin k\zeta \zeta^{-1} \\ &+ [k(i\zeta_0^{-1}V \cos kh - 2C \sin kh) \cos k\zeta - ik\zeta_0^{-1}V] \zeta^{-2} + O(\zeta^{-3}) \end{aligned} \quad (8.72)$$

Equations (8.70) to (8.72) give the asymptotic behavior of the right-hand side of (8.67). More explicitly, since by (8.62),

$$\alpha(h) = \frac{1}{2}i\zeta_0^{-1}V \sin kh + C \cos kh \quad (8.73)$$

and
$$\alpha'(h) = k(\frac{1}{2}i\zeta_0^{-1}V \cos kh - C \sin kh) \quad (8.74)$$

we get, for $\zeta \rightarrow \infty$

$$\bar{V}(\zeta) + \bar{\alpha}(\zeta) + \bar{\alpha}(-\zeta) = -ik\zeta_0^{-1}V\zeta^{-2}[1 + O(\zeta^{-1})] \quad (8.75)$$

On the other hand, $\bar{I}(\zeta)$ is bounded because of (8.61), and the asymptotic behavior of $\bar{K}(\zeta, a)$ can be easily found to be

$$\bar{K}(\zeta, a) = \frac{1}{2}(2\pi\zeta a)^{-\frac{1}{2}}e^{-\zeta a}[1 + O(\zeta^{-1})] \quad (8.76)$$

as $\zeta \rightarrow \infty$. Thus the left-hand side of (8.67) decreases exponentially as $\zeta \rightarrow \infty$, while the right-hand side approaches zero only as ζ^{-2} by (8.75). Therefore, (8.67) cannot be satisfied, and hence (8.58) has no solution that is integrable. (This detailed calculation also demonstrates the well-known connection between the behavior of a function at small distances and the behavior of its Fourier transform at infinity.)

8.4 The Circular Tubular Antenna

In view of the failure of (8.58) to have a solution, it is necessary for us to construct a more precisely defined model for the dipole antenna. In this section, we consider a model for the infinite dipole antenna. This model can be very easily modified to give the finite dipole antenna.

The model consists of an infinitely long circular tube of radius a and zero thickness. We take its axis to be the z axis, and we imagine the tube to have an infinitesimal gap at $z = 0$ so that a scalar potential difference $\text{Re}(Ve^{-i\omega t})$ can be maintained between the two halves across the gap. The tube is perfectly conducting so that the tangential component of the electric field is zero on this tube except at the gap. We also assume

$$ka \ll 1 \quad (8.77)$$

[For all the considerations in this section, (8.77) can be replaced by the less restrictive assumption that ka is less than the first zero of the Bessel function J_0 so that there is no propagating waveguide mode inside the tube.]

By (8.52), we can write Maxwell's equations in the following form

$$-ikE_r = -c \frac{\partial B_\theta}{\partial z} \quad (8.78)$$

$$-ikE_z = c \frac{1}{r} \frac{\partial}{\partial r}(rB_\theta) \quad (8.79)$$

and
$$ikcB_\theta = \frac{\partial E_z}{\partial z} - \frac{\partial E_r}{\partial r} \quad (8.80)$$

These three equations hold both for $r > a$ and for $r < a$. The boundary condition at $r = a$ is

$$E_z = -V \delta(z) \quad (8.81)$$

Define the Fourier transform in the usual way by

$$\bar{E}_z(r, \zeta) = \int_{-\infty}^{\infty} E_z(r, z) e^{i\zeta z} dz \quad (8.82a)$$

$$\bar{E}_r(r, \zeta) = \int_{-\infty}^{\infty} E_r(r, z) e^{i\zeta z} dz \quad (8.82b)$$

and
$$\bar{B}_\theta(r, \zeta) = \int_{-\infty}^{\infty} B_\theta(r, z) e^{i\zeta z} dz \quad (8.82c)$$

then (8.78) to (8.81) can be rewritten as

$$k\bar{E}_r(r, \zeta) = -\zeta c\bar{B}_\theta(r, \zeta) \quad (8.83)$$

$$k\bar{E}_z(r, \zeta) = \frac{ic}{r} \frac{\partial}{\partial r} [r\bar{B}_\theta(r, \zeta)] \quad (8.84)$$

and
$$kc\bar{B}_\theta(r, \zeta) = -\zeta\bar{E}_r(r, \zeta) + i \frac{\partial}{\partial r} \bar{E}_z(r, \zeta) \quad (8.85)$$

together with the boundary condition

$$\bar{E}_z(a, \zeta) = -V \quad (8.86)$$

Equations (8.83) to (8.85) imply that

$$\frac{1}{r} \frac{\partial}{\partial r} r \frac{\partial}{\partial r} \bar{E}_z(r, \zeta) + (k^2 - \zeta^2) \bar{E}_z(r, \zeta) = 0 \quad (8.87)$$

Together with the radiation condition, (8.50) for example, (8.86) and (8.87) determine \bar{E}_z completely:

If $r < a$,
$$\bar{E}_z(r, \zeta) = -V \frac{J_0(r\sqrt{k^2 - \zeta^2})}{J_0(a\sqrt{k^2 - \zeta^2})} \quad (8.88)$$

If $r > a$,
$$\bar{E}_z(r, \zeta) = \begin{cases} -V \frac{H_0^{(1)}(r\sqrt{k^2 - \zeta^2})}{H_0^{(1)}(a\sqrt{k^2 - \zeta^2})} & \text{for } |\zeta| < k \\ -V \frac{K_0(r\sqrt{\zeta^2 - k^2})}{K_0(a\sqrt{\zeta^2 - k^2})} & \text{for } |\zeta| > k \end{cases} \quad (8.89)$$

Before proceeding any further, we discuss (8.89) in some detail. So far, we have always taken $\omega = kc$ to be positive and also ζ to be real. Indeed, in (8.82), the integrals certainly fail to converge if ζ is not real. Accordingly, (8.89) can be used to define \bar{E}_z for $\omega > 0$ and real ζ . We proceed to enlarge this domain of definition.

1. Consider first the case of negative ω still with real ζ . The applied scalar potential difference is

$$\text{Re}(Ve^{-i\omega t}) = (\text{Re } V) \cos \omega t + (\text{Im } V) \sin \omega t \quad (8.90)$$

Since the real part of $Ve^{-i\omega t}$ is the only physical part, we can alternatively use its complex conjugate, that is,

$$\operatorname{Re}(Ve^{-i\omega t}) = \operatorname{Re}(V^*e^{i\omega t})^* \quad (8.91)$$

In other words, precisely the same physical situation can be described with $-\omega$ and V^* . Therefore, in the present problem, any field quantity Q at $-\omega$ must be obtained from the same field quantity at ω by [compare with (8.24)]

$$Q(-\omega) = [Q(\omega)|_{V \rightarrow V^*}]^* \quad (8.92)$$

By applying this prescription to (8.89), we get

$$\bar{E}_z(r, \zeta) = \begin{cases} -V \frac{H_0^{(1)}(r\sqrt{k^2 - \zeta^2})}{H_0^{(1)}(a\sqrt{k^2 - \zeta^2})} & \text{for } |\zeta| < k \\ -V \frac{K_0(r\sqrt{\zeta^2 - k^2})}{K_0(a\sqrt{\zeta^2 - k^2})} & \text{for } |\zeta| > |k| \\ -V \frac{H_0^{(2)}(r\sqrt{k^2 - \zeta^2})}{H_0^{(2)}(a\sqrt{k^2 - \zeta^2})} & \text{for } |\zeta| < -k \end{cases} \quad (8.93)$$

2. In (8.93), both k and ζ are still real. We now consider complex ζ , keeping k real. For the sake of definiteness, let k be positive for the time being, and hence (8.89) may be used. We analytically continue the functions

$$\frac{H_0^{(1)}(r\sqrt{k^2 - \zeta^2})}{H_0^{(1)}(a\sqrt{k^2 - \zeta^2})}$$

to values of ζ larger than k , and we get the result

$$\frac{K_0(r\sqrt{\zeta^2 - k^2}) + i\pi I_0(r\sqrt{\zeta^2 - k^2})}{K_0(a\sqrt{\zeta^2 - k^2}) + i\pi I_0(a\sqrt{\zeta^2 - k^2})}$$

if the analytic continuation is carried out via the upper half plane, or

$$\frac{K_0(r\sqrt{\zeta^2 - k^2})}{K_0(a\sqrt{\zeta^2 - k^2})}$$

if the lower half plane is used instead. The second result coincides with what we want, but the first result does not. We therefore reach the conclusion that there is a branch cut in the upper half of the ζ plane with the branch point at $\zeta = k$. Similarly, there is a branch cut in the lower half plane starting from the point $\zeta = -k$. These two statements hold for both positive and negative k . The precise position of the branch cuts are, of course, not defined and may be taken in any convenient way. One possible choice is shown in Fig. 8.2a.

3. We next let ζ be real but ω complex. Starting with (8.93), and employing precisely the same kind of argument as in the last paragraph, we reach the conclusion that there are two branch cuts with branch points at $\pm\zeta c$ and that both

of these branch cuts are in the lower half of the ω plane. Two possible choices are shown in Fig. 8.2*b* and Fig. 8.2*c*. Note that there is no branch cut in the upper half of the ω plane, as discussed in Sec. 8.2.

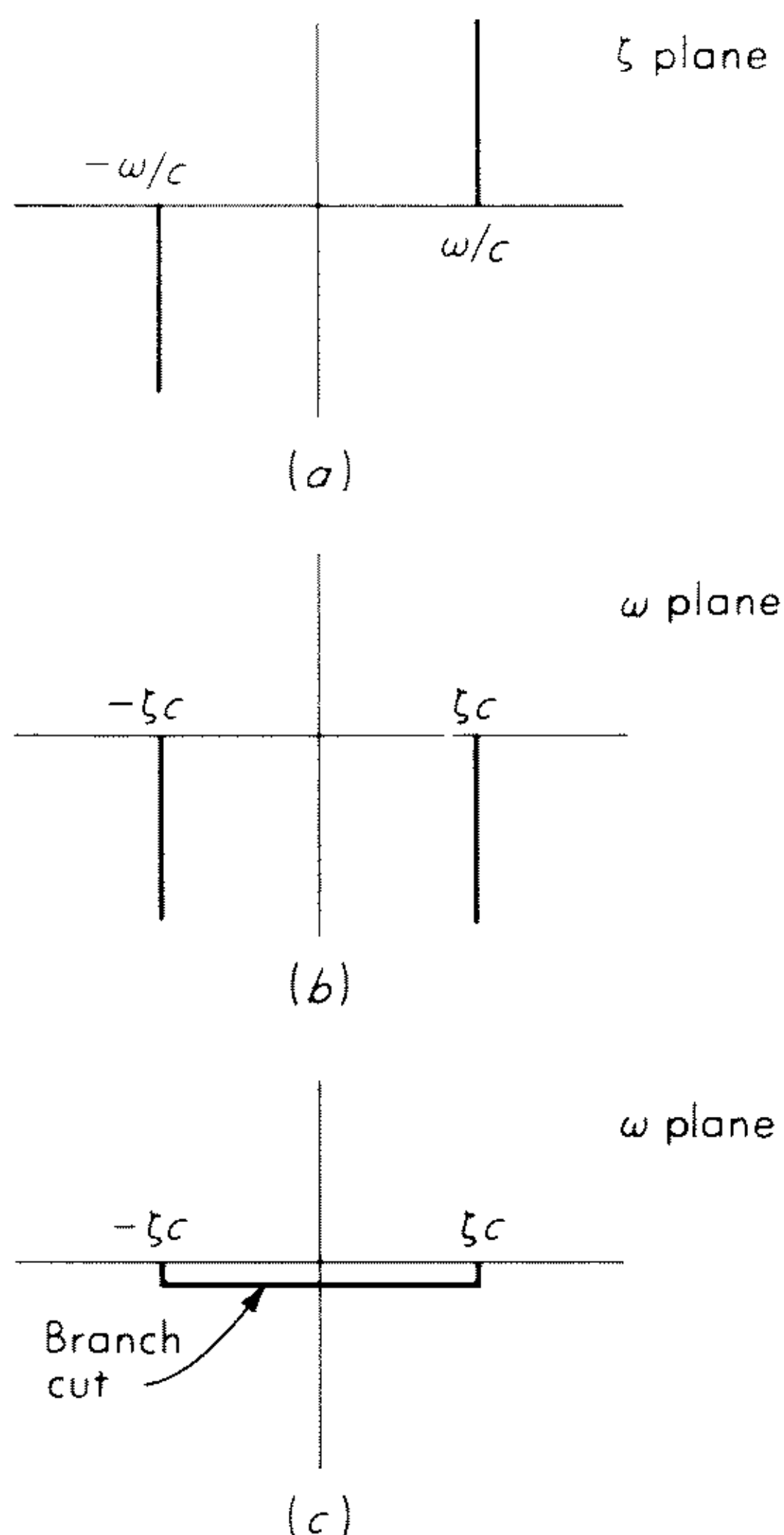


Fig. 8.2 Positions of the branch cut.

4. Finally, let both ζ and ω be complex. Suppose we choose the branch cuts in the two cases above as follows: If k is real, the two branch cuts are

$$\zeta - k \geq 0 \quad (8.94a)$$

and

$$\zeta + k \leq 0 \quad (8.94b)$$

[Equation (8.94*a*) means that $\zeta - k$ is real and nonnegative.] If ζ is real, the branch cuts are taken to be

$$k - \zeta \leq 0 \quad (8.95a)$$

$$k + \zeta \leq 0 \quad (8.95b)$$

The choice corresponds to those shown in Fig. 8.2*a* and Fig. 8.2*b*. We now note that (8.94) and (8.95) are formally the same equations. Thus we can extend the domain of definition for $\bar{E}_z(r, \zeta)$, with $r > a$, to the direct product of the complex ζ plane and the complex k plane with the exception of two cuts de-

finer by either (8.94) or (8.95). This is one of the simplest choices of cuts, but it is by no means the only one.

We can therefore write (8.89) or (8.93) more simply in the form, for $r > a$,

$$\bar{E}_z(r, \zeta) = -V \frac{H_0^{(1)}(r\sqrt{k^2 - \zeta^2})}{H_0^{(1)}(a\sqrt{k^2 - \zeta^2})} \quad (8.96)$$

with the understanding that analytical continuation can be carried out provided that the two branch cuts are not crossed. [Analytical continuation of (8.88) is trivial.]

After this long digression, we return to the computation of other field quantities. By (8.83), (8.85), (8.88), and (8.96), we get

$$c\bar{B}_\theta(r, \zeta) = \begin{cases} -ikV(k^2 - \zeta^2)^{-1/2} \frac{J'_0(r\sqrt{k^2 - \zeta^2})}{J_0(a\sqrt{k^2 - \zeta^2})} & \text{for } r < a \\ -ikV(k^2 - \zeta^2)^{-1/2} \frac{H_0^{(1)'}(r\sqrt{k^2 - \zeta^2})}{H_0^{(1)}(a\sqrt{k^2 - \zeta^2})} & \text{for } r > a \end{cases} \quad (8.97)$$

$$\bar{E}_r(r, \zeta) = \begin{cases} i\zeta V(k^2 - \zeta^2)^{-1/2} \frac{J'_0(r\sqrt{k^2 - \zeta^2})}{J_0(a\sqrt{k^2 - \zeta^2})} & \text{for } r < a \\ i\zeta V(k^2 - \zeta^2)^{-1/2} \frac{H_0^{(1)'}(r\sqrt{k^2 - \zeta^2})}{H_0^{(1)}(a\sqrt{k^2 - \zeta^2})} & \text{for } r > a \end{cases} \quad (8.98)$$

In particular, it follows from (8.97) that the surface current density on the outside of the tube is

$$J_+(z) = \frac{-ikV}{2\pi\zeta_0} \int_C e^{-i\zeta z} (k^2 - \zeta^2)^{-1/2} \frac{H_0^{(1)'}(a\sqrt{k^2 - \zeta^2})}{H_0^{(1)}(a\sqrt{k^2 - \zeta^2})} d\zeta \quad (8.99)$$

and the surface current density on the inside is

$$J_-(z) = \frac{ikV}{2\pi\zeta_0} \int_C e^{-i\zeta z} (k^2 - \zeta^2)^{-1/2} \frac{J'_0(a\sqrt{k^2 - \zeta^2})}{J_0(a\sqrt{k^2 - \zeta^2})} d\zeta \quad (8.100)$$

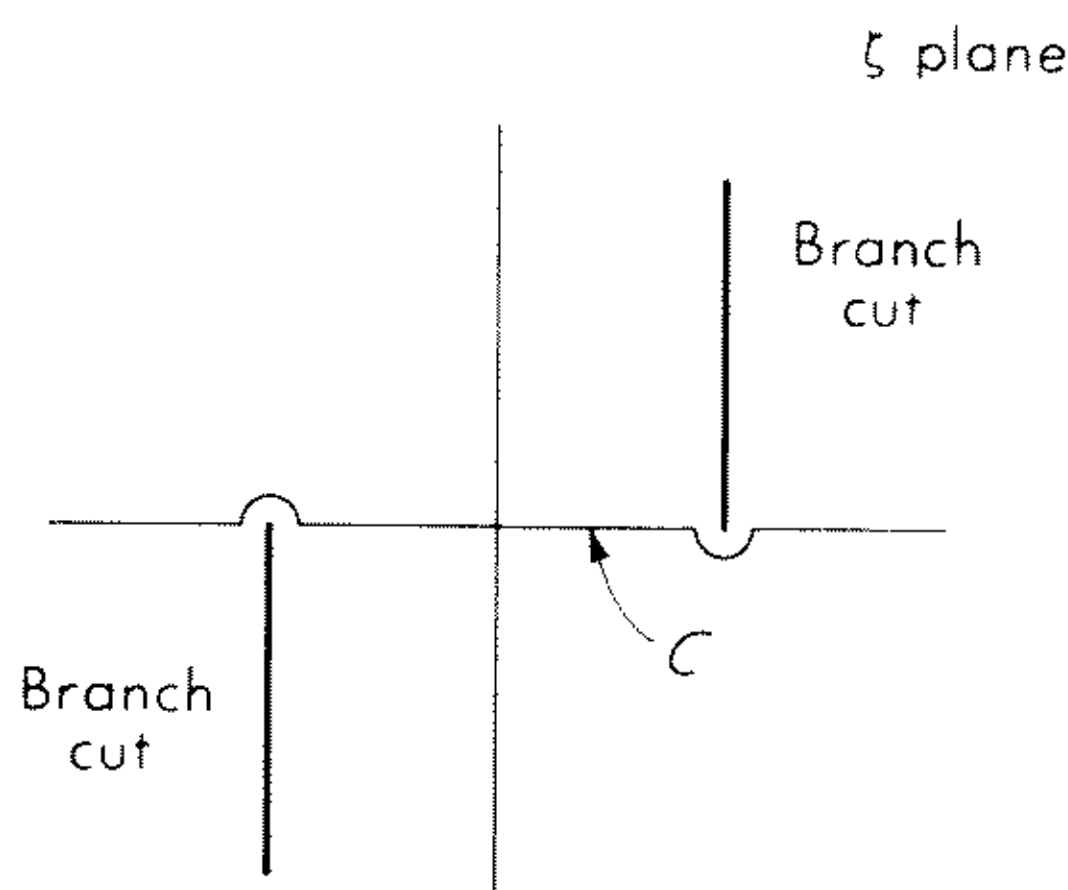


Fig. 8.3 The contour of integration C .

In both (8.99) and (8.100) the contour of integration C is that shown in Fig. 8.3. The total current $I_\infty(z)$ is defined to be

$$I_\infty(z) = 2\pi a[J_+(z) + J_-(z)] \quad (8.101)$$

or

$$I_\infty(z) = \frac{ikV}{2\pi\zeta_0} \int_C e^{-i\zeta z} \left[\frac{i}{4} (k^2 - \zeta^2) J_0(a\sqrt{k^2 - \zeta^2}) H_0^{(1)}(a\sqrt{k^2 - \zeta^2}) \right]^{-1} d\zeta \quad (8.102)$$

Equation (8.102) implies that the current on the infinite tubular antenna is well defined and finite for all $z \neq 0$. For $z = 0$, the integral on the right-hand side diverges logarithmically. Let us thus investigate the behavior of the current near $z = 0$. It follows from (8.99) and (8.100) that, for $|z| \ll a$,

$$J_+(z) \approx -\frac{ikV}{\pi\zeta_0} \ln \frac{1}{|z|} \quad (8.103)$$

and

$$J_-(z) \approx -\frac{ikV}{\pi\zeta_0} \ln \frac{1}{|z|} \quad (8.104)$$

Hence, again for $|z| \ll a$,

$$I_\infty(z) \approx -4ika\zeta_0^{-1}V \ln \frac{1}{|z|} \quad (8.105)$$

Equation (8.105) means that there is an infinite input capacitance. This is easy to understand physically as follows. The two edges of the halves of the tubular antenna, namely, the part with $z > 0$ and the part with $z < 0$, are kept at different potentials but separated only infinitesimally. Thus, there is an infinite capacitance between the two circular knife edges. This also explains why the right-hand side of (8.105) is proportional to the circumference of the tube and also why the two right-hand sides of (8.103) and (8.104) are equal to each other and independent of a .

On the other hand, by (8.103), the input conductance

$$\mathcal{G}_\infty = \lim_{z \rightarrow 0} \operatorname{Re} \frac{\mathcal{G}_\infty(z)}{V} \quad (8.106)$$

is given by the convergent integral

$$\mathcal{G}_\infty = 2\pi^{-1}\zeta_0^{-1}k \int_{-k}^k (k^2 - \zeta^2)^{-1} \{ [J_0(a\sqrt{k^2 - \zeta^2})]^2 + [Y_0(a\sqrt{k^2 - \zeta^2})]^2 \}^{-1} d\zeta \quad (8.107)$$

Therefore, we get finite answers from this model of the infinite tubular antenna, with the exception of the input susceptance. This infinite capacitance has a very simple physical interpretation, and it must be blamed on the overidealized driving condition of the delta-function generator [see (8.81)]. This problem is discussed further in Chap. 10.

8.5 Integral Equations for the Current Distributions

We proceed to study the finite tubular antenna, which consists of a circular tube of length $2h$, radius a , and zero thickness. We assume it to be perfectly conducting and center-driven, which means that there is an infinitesimal gap at the middle of the tube, of distance h to either end, and that a scalar potential difference $\text{Re}(Ve^{-i\omega t})$ is maintained across the gap. The geometry is shown in Fig. 8.4.

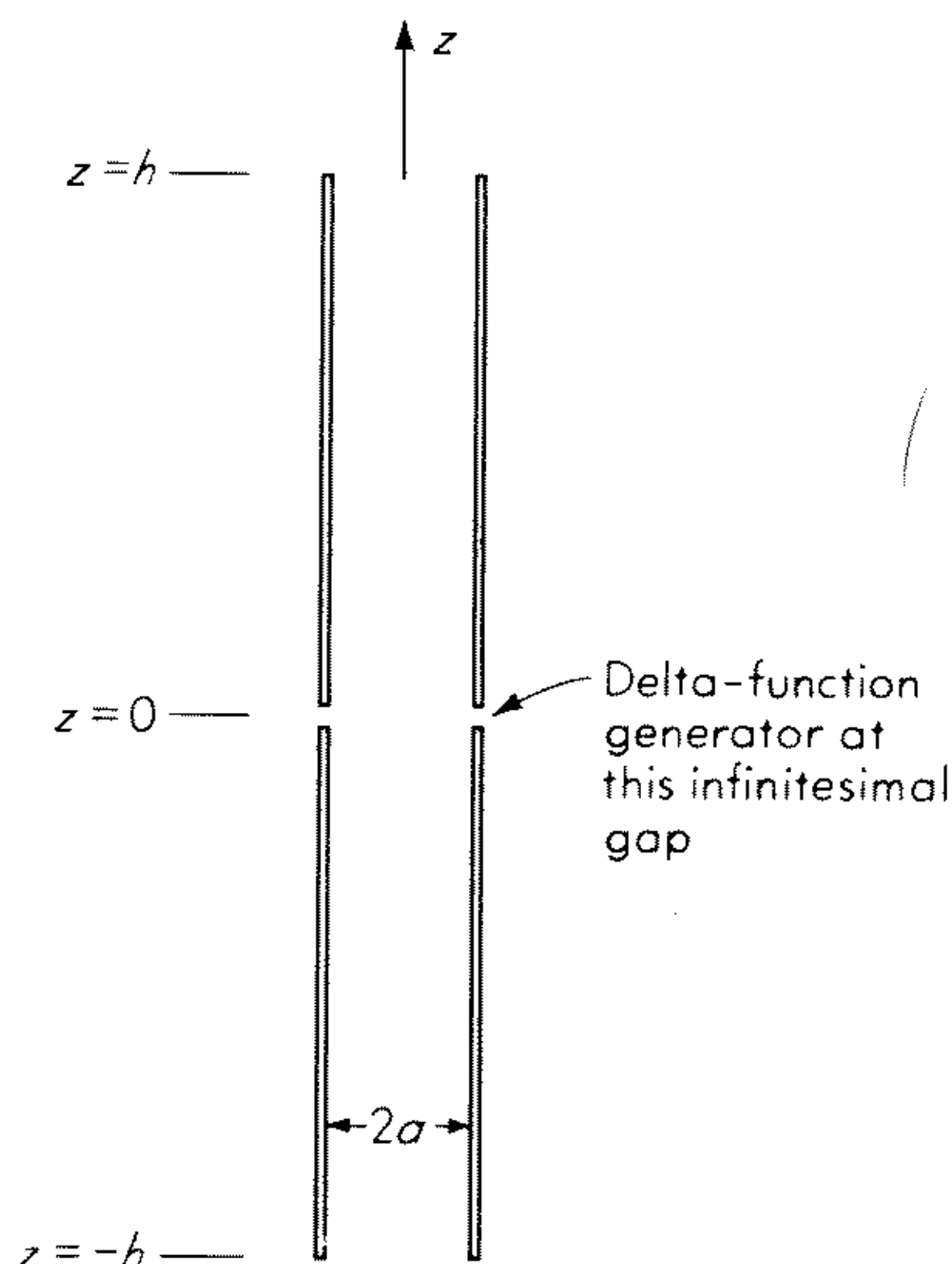


Fig. 8.4 The finite circular tubular antenna.

Maxwell's equations in the form (8.78) to (8.80) hold everywhere except on the circular tube, i.e., except when $r = a$ and $|z| \leq h$. The boundary condition on this finite tube is

$$E_z(a, z) = -V \delta(z) \quad (8.108)$$

for $|z| < h$. Unlike the case studied in detail in the preceding section, we cannot solve (8.78) to (8.80) and (8.108) explicitly for finite h . Instead we try to formulate the problem in terms of an integral equation.

As seen in the preceding section, there is a current on both the inner surface and the outer surface of the circular tube. Both current densities, to be designated as $J_-(z)$ and $J_+(z)$, respectively, are in the direction of the z axis and are given by, for $|z| \leq h$,

$$J_-(z) = -\lim_{r \rightarrow a-} \mu_0^{-1} B_\theta(r, z) \quad (8.109)$$

$$J_+(z) = \lim_{r \rightarrow a+} \mu_0^{-1} B_\theta(r, z) \quad (8.110)$$

These two current densities must satisfy, by the continuity of current,

$$J_+(h) = -J_-(h) \quad (8.111)$$

Similar to (8.101), the total current is, for $|z| \leq h$,

$$g(z) = 2\pi a[J_+(z) + J_-(z)] \quad (8.112)$$

which, by (8.111), satisfies the boundary condition

$$g(h) = 0 \quad (8.113)$$

The current density is actually

$$(2\pi a)^{-1}g(z) \delta(r - a)\hat{\mathbf{z}} \quad (8.114)$$

Because of the symmetry of the geometry, E_z , H_θ , $J_+(z)$, $J_-(z)$, and $g(z)$ are all even functions of z , while E_r and the charge distribution on the tube are odd functions of z .

We introduce the vector potential \mathbf{A} in the manner discussed in Sec. 8.1. Because of (8.30) and (8.114), \mathbf{A} has only a z component, which is given by

$$\begin{aligned} A_z(a, z) &= \mu_0 \int G(\mathbf{r} - \mathbf{r}') (2\pi a)^{-1} g(z') \delta(r' - a) d\mathbf{r}' \big|_{r=a} \\ &= \mu_0 \int_{-h}^h g(z') \mathcal{K}(z - z') dz' \end{aligned} \quad (8.115)$$

$$\text{where} \quad \mathcal{K}(z) = \frac{1}{2\pi} \int_{-\pi}^{\pi} K\left(z, 2a \left| \sin \frac{\theta}{2} \right| \right) d\theta \quad (8.116)$$

with K defined by (8.59). More explicitly, $\mathcal{K}(z)$ is

$$\mathcal{K}(z) = \frac{1}{8\pi^2} \int_{-\pi}^{\pi} \left(z^2 + 4a^2 \sin^2 \frac{\theta}{2} \right)^{-1/2} \exp \left[ik \left(z^2 + 4a^2 \sin^2 \frac{\theta}{2} \right)^{1/2} \right] d\theta$$

Note that $\mathcal{K}(z)$ has a logarithmic singularity at $z = 0$ and that the Fourier transform of $\mathcal{K}(z)$ has branch-cuts from the points $\pm k$, as shown in Fig. 8.2a. On the other hand, the derivation of (8.56) holds here, and, in fact, (8.56) is exact for the present model of a finite tubular antenna. A comparison of (8.115) with (8.56) then yields the integral equation for the current distribution

$$\int_{-h}^h g(z') \mathcal{K}(z - z') dz' = \frac{1}{2} i \zeta_0^{-1} V \sin k|z| + \mathcal{C} \cos kz \quad (8.117)$$

where \mathcal{C} is again to be determined by the boundary condition $g(h) = 0$.

Equation (8.117) differs from (8.58) only in the replacement of K by \mathcal{K} . While (8.58) does not have a solution, the same argument as given in Sec. 8.3 does not lead to the same conclusion about (8.117). The reason is that the crucial equation (8.76) does not hold for the Fourier transform of \mathcal{K} ; that is, $\mathcal{K}(z)$ is not an analytic function of z for real z , and hence its Fourier transform has a rather different asymptotic behavior from that of \bar{K} . Indeed, we can

show that (8.117) has a unique solution, which is qualitatively rather similar to the current distribution on the infinite tubular antenna, i.e., the solution $g(z)$ is finite everywhere except for a logarithmic singularity at $z = 0$ given by (8.105):

$$g(z) = -4ika \zeta_0^{-1} V \left[\ln \frac{1}{|z|} + O(1) \right] \quad (8.118)$$

for $z \rightarrow 0$. In other words, the infinite knife-edge capacitance is not changed by making the tubular antenna finite in length.

We also write down the integral equation for the current on an infinite antenna

$$\int_{-\infty}^{\infty} g_{\infty}(z') \mathcal{K}(z - z') dz' = \frac{1}{2} \zeta_0^{-1} V e^{ik|z|} \quad (8.119)$$

By Fourier transformation, it is straightforward to solve (8.119) and to verify that its solution is indeed (8.102).

Similarly, analogous to (8.58), we would also study the following integral equation for the infinite antenna

$$\int_{-\infty}^{\infty} I_{\infty}(z') K(z - z', a) dz' = \frac{1}{2} \zeta_0^{-1} V e^{ik|z|} \quad (8.120)$$

By the argument of Sec. 8.3, (8.120) does not have a solution that is integrable. However, we can still ask the question whether we can meaningfully interpret the component of the current I_{∞} in phase with V . More precisely, we are raising the question whether we can find a real function $I_{\infty 1}(z)$ such that the quantity

$$iI_{\infty 2}(z) = \zeta_0 V^{-1} I_{\infty}(z) - I_{\infty 1}(z) \quad (8.121)$$

is formally imaginary.

We answer this question in the following way. First, the Fourier transform of $K(z, a)$ as defined by (8.64) is explicitly

$$\bar{K}(\zeta, a) = \begin{cases} \frac{1}{4} i H_0^{(1)}(a \sqrt{k^2 - \zeta^2}) & \text{for } |\zeta| < k \\ (2\pi)^{-1} K_0(a \sqrt{\zeta^2 - k^2}) & \text{for } |\zeta| > k \end{cases} \quad (8.122)$$

Thus the structure of the branch cuts for $\bar{K}(\zeta, a)$ in the ζ plane is precisely that shown in Fig. 8.2a. In particular, (8.76) is an immediate consequence of (8.122). Consider the expression, for $k_1 > k$,

$$I_{\infty}(z; k_1) = \frac{ikV}{2\pi\zeta_0} \int_{C(k_1)} e^{-i\zeta z} [(k^2 - \zeta^2) \bar{K}(\zeta, a)]^{-1} d\zeta \quad (8.123)$$

where $C(k_1)$ is the portion of the contour C , shown in Fig. 8.3, that is between $-k_1$ and k_1 . [The motivation of considering this $I_{\infty}(z; k_1)$ is this: formally, analogous to (8.102), the solution of (8.120) is the right-hand side of (8.123)

with $C(k_1)$ replaced by C . But no meaning can be attached to this divergent integral because of (8.66), and thus we truncate the path of integration.] Let

$$\hat{I}_\infty(z; k_1) = I_\infty(z) - I_\infty(z; k_1), \quad (8.124)$$

and let us try to get an integral equation for $\hat{I}_\infty(z, k_1)$. By direct evaluation

$$\begin{aligned} \int_{-\infty}^{\infty} I_\infty(z'; k_1) K(z - z', a) dz' \\ = \frac{ikV}{2\pi\zeta_0} \int_{C(k_1)} [(k^2 - \zeta^2) \bar{K}(\zeta, a)]^{-1} d\zeta \int_{-\infty}^{\infty} e^{-i\zeta z'} K(z - z', a) dz' \\ = \frac{ikV}{2\pi\zeta_0} \int_{C(k_1)} e^{-i\zeta z} (k^2 - \zeta^2)^{-1} d\zeta \end{aligned} \quad (8.125)$$

Accordingly, by (8.120) and (8.124),

$$\int_{-\infty}^{\infty} \hat{I}_\infty(z'; k_1) K(z - z', a) dz' = \frac{ikV}{2\pi\zeta_0} \left(\int_{-\infty}^{-k_1} + \int_{k_1}^{\infty} \right) e^{-i\zeta z} (k^2 - \zeta^2)^{-1} d\zeta \quad (8.126)$$

Define a kernel $R(z)$ by requiring that its Fourier transform is

$$\bar{R}(\zeta) = \begin{cases} \frac{iJ_0(a\sqrt{k^2 - \zeta^2})}{Y_0(a\sqrt{k^2 - \zeta^2})} & \text{for } |\zeta| < k \\ 0 & \text{for } |\zeta| > k \end{cases} \quad (8.127)$$

that is, we define $R(z)$ by

$$R(z) = \frac{i}{2\pi} \int_{-k}^k e^{-i\zeta z} \frac{J_0(a\sqrt{k^2 - \zeta^2})}{Y_0(a\sqrt{k^2 - \zeta^2})} d\zeta \quad (8.128)$$

Using $R(z)$, we define the kernel K_R by

$$K_R(z, a) = K(z, a) + \int_{-\infty}^{\infty} R(z - z') K(z', a) dz' \quad (8.129)$$

We can explicitly compute \bar{K}_R as

$$\begin{aligned} \bar{K}_R(\zeta, a) &= \int_{-\infty}^{\infty} e^{i\zeta z} K_R(z, a) dz = \bar{K}(\zeta, a) [1 + R(\zeta)] \\ &= \begin{cases} \frac{-1/4 \{ [J_0(a\sqrt{k^2 - \zeta^2})]^2 + [Y_0(a\sqrt{k^2 - \zeta^2})]^2 \}}{Y_0(a\sqrt{k^2 - \zeta^2})} & \text{for } |\zeta| < k \\ (2\pi)^{-1} K_0(a\sqrt{\zeta^2 - k^2}) & \text{for } |\zeta| > k \end{cases} \end{aligned} \quad (8.130)$$

Note that this \bar{K}_R , and hence $K_R(z, a)$, is real. We next compute

$$\begin{aligned} \int_{-\infty}^{\infty} R(z - z') dz' \left(\int_{-\infty}^{-k_1} + \int_{k_1}^{\infty} \right) e^{-i\zeta z'} (k^2 - \zeta^2)^{-1} d\zeta \\ = \left(\int_{-\infty}^{-k_1} + \int_{k_1}^{\infty} \right) e^{-i\zeta z} (k^2 - \zeta^2)^{-1} \bar{R}(\zeta) d\zeta = 0 \end{aligned} \quad (8.131)$$

by (8.127). Therefore, (8.126) is *equivalent to* the integral equation

$$\int_{-\infty}^{\infty} \hat{I}_{\infty}(z'; k_1) K_R(z - z', a) dz' = \frac{ikV}{\pi\zeta_0} \int_{k_1}^{\infty} \frac{\cos \zeta z}{k^2 - \zeta^2} d\zeta \quad (8.132)$$

In this equation, the kernel is real as remarked above and the right-hand side is purely imaginary except for the factor V . Thus $\hat{I}_{\infty}(z; k_1)/V$ is formally purely imaginary. We have thus shown that, by (8.124), the current distribution $I_{\infty}(z)$ can be split into two parts; one part $I_{\infty}(z; k_1)$ is explicitly given by (8.123), and the other part is formally purely imaginary after multiplying by V^{-1} . We can therefore choose the required $I_{\infty 1}(z)$ as

$$\begin{aligned} I_{\infty 1}(z) &= \operatorname{Re} \frac{\zeta_0 I_{\infty}(z; k_1)}{V} \\ &= \frac{2k}{\pi} \int_{-k}^k \frac{e^{-i\zeta z}}{k^2 - \zeta^2} \frac{J_0(a\sqrt{k^2 - \zeta^2})}{[J_0(a\sqrt{k^2 - \zeta^2})]^2 + [Y_0(a\sqrt{k^2 - \zeta^2})]^2} d\zeta \\ &= \frac{4k}{\pi} \int_0^k \frac{\cos \zeta z}{k^2 - \zeta^2} \frac{J_0(a\sqrt{k^2 - \zeta^2})}{[J_0(a\sqrt{k^2 - \zeta^2})]^2 + [Y_0(a\sqrt{k^2 - \zeta^2})]^2} d\zeta \end{aligned} \quad (8.133)$$

which is convergent for all z and independent of the choice of k_1 . With this $I_{\infty 1}(z)$, the quantity $I_{\infty 2}(z)$ defined by (8.121) is formally real.

It is perhaps of some interest to compare the $I_{\infty 1}(z)$ of (8.133) with the corresponding quantity for the integral equation (8.119), namely, from (8.102),

$$\operatorname{Re} \frac{\zeta_0 I_{\infty}(z)}{V} = \frac{4k}{\pi} \int_0^k \frac{\cos \zeta z}{k^2 - \zeta^2} \frac{1}{[J_0(a\sqrt{k^2 - \zeta^2})]^2 + [Y_0(a\sqrt{k^2 - \zeta^2})]^2} d\zeta \quad (8.134)$$

The right-hand sides of (8.133) and (8.134) differ only in the factor $J_0(a\sqrt{k^2 - \zeta^2})$. Thus, for small a ,

$$I_{\infty 1}(z) - \operatorname{Re} \frac{\zeta_0 I_{\infty}(z)}{V} = O(k^2 a^2) \quad (8.135)$$

uniformly for all z . It is also interesting to study the case where k_1 is very, very large, but we shall not dwell further on this topic.

So far as the author is aware, the corresponding problem for the finite antenna has not been solved. We make the following conjecture: For the integral equation (8.58) with the boundary condition (8.60), the current distribution can be written in the form

$$V^{-1}\zeta_0 I(z) = I_1(z) + iI_2(z) \quad (8.136)$$

where $I_1(z)$ is finite and real for all z and $I_2(z)$ is formally real in the same sense as in the case of the infinite antenna discussed above.

8.6 Iterative Solutions for the Current Distributions

Neither (8.58) nor (8.117) can be solved exactly in terms of known functions. Many approximate procedures have been suggested over the years to get

valuable information about the center-driven dipole antenna, and the literature in this connection is extensive. Almost all of these procedures are equally applicable to (8.58) and to (8.117). However, since the kernel $K(z, a)$ is significantly simpler than that of (8.117), which involves an integration, most of the numerical computation has been carried out on the basis of (8.58). On the other hand, it is shown in Sec. 8.3 by a very simple argument that (8.58) has no integrable solution. Hence, the best we can hope is that these approximate solutions to (8.58) are actually *in some sense* approximate solutions to (8.117). (Of course, as stated at the end of Sec. 8.4, the model of the circular tubular antenna has a difficulty of its own, but here we are not concerned with that difficulty.) To find out whether this hope is actually realized or not, we can apply the same approximate procedure to (8.58) and (8.117) and then compare the two resulting approximate solutions. If they are close to each, then we may make use of the numerical results obtained on the basis of (8.58), even though (8.58) is devoid of a solution.

We shall carry out this comparison for the so-called iterative solutions. Since we are interested only in questions of principle here, the various iterative solutions are not very different. For definiteness, we shall treat the iterative procedure of King and Middleton.⁶ In order to avoid obscuring the essential points, we shall use operator notations. For example, operator K on I gives KI defined by

$$(KI)(z) = \int_{-h}^h K(z - z', a) I(z') dz' \quad (8.137)$$

Similarly, define the operator \mathcal{K} by

$$(\mathcal{K}g)(z) = \int_{-h}^h \mathcal{K}(z - z') g(z') dz' \quad (8.138)$$

$$\text{If} \quad f(z) = \frac{1}{2} i \zeta_0^{-1} V \sin k|z| \quad (8.139)$$

$$\text{and} \quad g(z) = \cos kz \quad (8.140)$$

then (8.58) and (8.117) can be written respectively as

$$KI = f + Cg \quad (8.141)$$

$$\text{and} \quad \mathcal{K}g = f + \mathcal{C}g \quad (8.142)$$

The King-Middleton procedure was originally designed for (8.141). It sought to approximate KI by ΨI , where Ψ is a number. For the present purpose, we need not go into the details of the choice of Ψ ; indeed, we are not even concerned about whether Ψ is real or complex. King and Middleton iterated the equation

$$\Psi I = f + Cg - (K - \Psi)I \quad (8.143)$$

n times to get the n th iterated solution

$$I^{(n)} = \Psi^{-1} \sum_{m=0}^n (1 - \Psi^{-1}K)^m (f + C^{(n)}g) \quad (8.144)$$

where 1 denotes the identity operator. An operator raised to the m th power merely means the operator applied repeatedly for m times. (The Ψ here actually differs from the expansion parameter of King and Middleton by a factor of 4π .) The constant $C^{(n)}$ for the n th iterated solution is determined by

$$I^{(n)}(h) = 0 \quad (8.145)$$

$$C^{(n)} = - \frac{\sum_{m=0}^n [(1 - \Psi^{-1}K)^m f](h)}{\sum_{m=0}^n [(1 - \Psi^{-1}K)^m g](h)} \quad (8.146)$$

For example, the first-order solution is

$$I^{(1)} = \Psi^{-1}[(2f - \Psi^{-1}Kf) + C^{(1)}(2g - \Psi^{-1}Kg)] \quad (8.147)$$

and

$$C^{(1)} = \frac{2f(h) - \Psi^{-1}(Kf)(h)}{2g(h) - \Psi^{-1}(Kg)(h)} \quad (8.148)$$

A rather large amount of numerical calculation has been carried out on the basis of (8.147) and (8.148).

The procedure is, of course, equally applicable to (8.142) with the result

$$g^{(n)} = \Psi^{-1} \sum_{m=0}^n (1 - \Psi^{-1}\mathcal{K})^m (f + \mathfrak{C}^{(n)}g) \quad (8.149)$$

with

$$\mathfrak{C}^{(n)} = - \frac{\sum_{m=0}^n [(1 - \Psi^{-1}\mathcal{K})^m f](h)}{\sum_{m=0}^n [(1 - \Psi^{-1}\mathcal{K})^m g](h)} \quad (8.150)$$

Note that we have used the same Ψ in both cases; this choice is certainly permissible, although not unavoidable.

So far as the author is aware, virtually nothing is known about the convergence of the iterative procedure in the form (8.149) and (8.150). It is conjectured that, for a finite antenna, these series indeed converge with a suitably chosen Ψ . This conjecture, however, is by no means obvious and indeed may be incorrect. In this connection, we shall study in some detail the case of the infinite tubular antenna of Sec. 8.4 and show that the series (8.149) has rather interesting structures.

We first write down this series in some detail. Instead of (8.138), we use

$$(\mathcal{K}g)(z) = \int_{-\infty}^{\infty} \mathcal{K}(z - z')g(z') dz' \quad (8.151)$$

In this notation, the integral equation (8.119) is

$$\mathcal{K}g_{\infty} = f_0 \quad (8.152)$$

where

$$f_0(z) = \frac{1}{2}\zeta_0^{-1}V e^{ik|z|} \quad (8.153)$$

No boundary condition is involved. The case is therefore particularly simple, and, instead of (8.149) and (8.150), we have

$$\mathcal{G}_\infty^{(n)} = \Psi^{-1} \sum_{m=0}^n (1 - \Psi^{-1}\mathcal{K})^m f_0 \quad (8.154)$$

This current $\mathcal{G}_\infty^{(n)}(z)$ can be written more explicitly by Fourier transforms. Similar to (8.63) to (8.66), we define

$$\bar{\mathcal{G}}_\infty^{(n)}(\zeta) = \int_{-\infty}^{\infty} \mathcal{G}_\infty^{(n)}(z) e^{i\zeta z} dz \quad (8.155a)$$

$$\bar{\mathcal{K}}(\zeta) = \int_{-\infty}^{\infty} \mathcal{K}(z) e^{i\zeta z} dz \quad (8.155b)$$

and
$$\bar{f}_0(\zeta) = \int_{-\infty}^{\infty} f_0(z) e^{i\zeta z} dz = ik\zeta_0^{-1} V (k^2 - \zeta^2)^{-1} \quad (8.155c)$$

By (8.116) and (8.122),

$$\bar{\mathcal{K}}(\zeta) = \frac{1}{4} i H_0^{(1)}(a\sqrt{k^2 - \zeta^2}) J_0(a\sqrt{k^2 - \zeta^2}) \quad (8.156)$$

with the branch cuts as shown in Fig. 8.2a. Equation (8.154) implies that

$$\bar{\mathcal{G}}_\infty^{(n)}(\zeta) = \Psi^{-1} \sum_{m=0}^n [1 - \Psi^{-1}\bar{\mathcal{K}}(\zeta)]^m \bar{f}_0(\zeta) \quad (8.157)$$

Note that the operator notation is used in (8.154), but not in (8.157). Therefore

$$\bar{\mathcal{G}}_\infty^{(n)}(\zeta) = \{1 - [1 - \Psi^{-1}\bar{\mathcal{K}}(\zeta)]^{n+1}\} \frac{\bar{f}_0(\zeta)}{\bar{\mathcal{K}}(\zeta)} \quad (8.158)$$

and a comparison with (8.102) shows that

$$\begin{aligned} \mathcal{G}_\infty(z) - \mathcal{G}_\infty^{(n)}(z) &= \frac{ikV}{2\pi\zeta_0} \int_C e^{-i\zeta z} [\frac{1}{4} i (k^2 - \zeta^2) J_0(a\sqrt{k^2 - \zeta^2}) H_0^{(1)}(a\sqrt{k^2 - \zeta^2})]^{-1} \\ &\quad \times [1 - \frac{1}{4} i \Psi^{-1} J_0(a\sqrt{k^2 - \zeta^2}) H_0^{(1)}(a\sqrt{k^2 - \zeta^2})]^{n+1} d\zeta \end{aligned} \quad (8.159)$$

How does this integral behave for large n ? We shall discuss this question from several points of view.

1. If n is fixed and $z \rightarrow 0$, (8.105) also holds in the sense that

$$\mathcal{G}_\infty(z) - \mathcal{G}_\infty^{(n)}(z) \approx -4ika \zeta_0^{-1} V \ln \frac{1}{|z|} \quad (8.160)$$

Hence the iterative solution does not reproduce the logarithmic singularity in the current distribution. This is certainly to be expected, since $\mathcal{K}^n f_0$ is bounded for all n .

2. We consider next the case where n is fixed and $z \rightarrow \infty$. In this case, we can shift the contour of integration C until it wraps around the left branch cut

of Fig. 8.1a, and the contribution comes mostly from the vicinity of the point $\zeta = -k$. Thus

$$g_{\infty}(z) - g_{\infty}^{(n)}(z) \approx \mathfrak{F}^{(n)}(z) \quad (8.161)$$

where

$$\mathfrak{F}^{(n)}(z) = \frac{ikV}{2\pi\zeta_0} \int_{C_-} e^{-i\zeta z} (k^2 - \zeta^2)^{-1} \left\{ \frac{1}{4}i \left[1 + \frac{2i}{\pi} \left(\gamma + \ln \frac{a}{2} \sqrt{k^2 - \zeta^2} \right) \right] \right\}^{-1} \\ \left\{ 1 - \frac{1}{4}i\Psi^{-1} \left[1 - \frac{2i}{\pi} \left(\gamma + \ln \frac{a}{2} \sqrt{k^2 - \zeta^2} \right) \right] \right\}^{n+1} d\zeta \quad (8.162)$$

The right-hand side of (8.162) is obtained from that of (8.159) by the approximations

$$J_0(a\sqrt{k^2 - \zeta^2}) \approx 1$$

and
$$H_0^{(1)}(a\sqrt{k^2 - \zeta^2}) \approx 1 + \frac{2i}{\pi} \left(\gamma + \ln \frac{a}{2} \sqrt{k^2 - \zeta^2} \right) \quad (8.163)$$

Moreover, the contour C_- is obtained from C by the rule that, wherever there is a pole on the real axis, C_- is considered to be in the lower half plane. The change from C to C_- is necessary because the right-hand side of (8.163) has zeros at

$$\zeta = \pm(4a^{-2}e^{-2\gamma} + k^2)^{1/2} \quad (8.164)$$

In (8.163) and (8.164), γ is Euler's constant, roughly 0.577217.

To find $\mathfrak{F}^{(n)}(z)$ approximately for large z and fixed n let

$$x = (k + \zeta)z \quad (8.165)$$

Thus we may find $\mathfrak{F}^{(n)}(z)$ by setting

$$k + \zeta = \frac{1}{z} \quad \text{and} \quad \zeta = -k$$

in the two braces. The resulting integral can be evaluated from the residue of the integral at $\zeta = -k$, and the answer is

$$\mathfrak{F}^{(n)}(z) \approx \pi\zeta_0^{-1}V e^{ikz} \left\{ -\ln a\sqrt{\frac{k}{z}} \right\}^{-1} \left\{ 1 - (2\pi\Psi)^{-1} \ln \left(a\sqrt{\frac{k}{z}} \right) \right\}^{n+1} \quad (8.166)$$

or, more simply, by (8.161),

$$g_{\infty}(z) - g_{\infty}^{(n)}(z) \approx \frac{1}{2}\zeta_0^{-1}V\Psi^{-1}(4\pi\Psi)^{-n}(\ln z)^n e^{ikz} \quad (8.167)$$

for $z \rightarrow \infty$. Thus the difference between $g_{\infty}(z)$ and $g_{\infty}^{(n)}(z)$ is unbounded for large z . The case $n = 1$ can be derived more simply by integrating (8.151) directly.

3. We finally let z be fixed and nonzero while $n \rightarrow \infty$. The behavior of $g_{\infty}(z) - g_{\infty}^{(n)}(z)$ in this case depends on the choice of Ψ . For a given Ψ , it may or may not be possible to deform the contour of integration C such that

$$|1 - \frac{1}{4}i\Psi^{-1}J_0(a\sqrt{k^2 - \zeta^2})H_0^{(1)}(a\sqrt{k^2 - \zeta^2})| < 1 \quad (8.168)$$

on the entire deformed contour. If this is possible, then

$$g_{\infty}(z) - g_{\infty}^{(n)}(z) \rightarrow 0 \quad (8.169)$$

for every fixed $z \neq 0$ and $n \rightarrow \infty$. If for every deformation of the contour,

$$|1 - \frac{1}{4}i\Psi^{-1}J_0(a\sqrt{k^2 - \zeta^2})H_0^{(1)}(a\sqrt{k^2 - \zeta^2})| > 1 \quad (8.170)$$

on some part of the contour, then

$$g_{\infty}(z) - g_{\infty}^{(n)}(z) \rightarrow \infty \quad (8.171)$$

for every fixed $z \neq 0$ and $n \rightarrow \infty$.

We conclude with a short discussion of the finite antenna. We have seen from the derivation of (8.167) that the unboundedness of $g_{\infty}^{(n)}(z)$ is due to the fact that the spectrum set of \mathcal{K} , as defined in (8.151), is unbounded. In this case, the spectrum set is just the set of values taken by $\bar{\mathcal{K}}(\zeta)$ for real ζ . Similarly, for the finite antenna, the convergence of the iterative solution depends on whether the spectrum set of \mathcal{K} , as defined in (8.138), lies in a circle with center at Ψ and radius $|\Psi|$. In this case, since \mathcal{K} is a Fredholm operator, its spectrum set is just the set of its eigenvalues. The answer to this question is not known by the author.

8.7 Comparison of the Iterative Solutions

In this section, we attempt to compare the two iterative solutions (8.144) and (8.149). The iterative solutions are useful only when a is sufficiently small and kh not large. Thus we shall assume that $ka \ll 1$, $a/h \ll 1$, and also, for the sake of definiteness, kh is of the order of unity. In other words, we shall study the limit $a \rightarrow 0$ for fixed λ and h .

It is easily seen from (8.144) and (8.149) that

$$I^{(0)}(z) = g^{(0)}(z) = \frac{f(z)g(h) - f(h)g(z)}{\Psi g(h)} \quad (8.172)$$

We compare in detail $I^{(1)}(z)$ and $g^{(1)}(z)$. To begin with, note that, by (8.122)

$$\int_{-\infty}^{\infty} K(z, a) dz = \bar{K}(0, a) = \frac{1}{4}iH_0^{(1)}(ka) \quad (8.173)$$

$$\text{and} \quad \int_{-\infty}^{\infty} \mathcal{K}(z) dz = \bar{\mathcal{K}}(0) = \frac{1}{4}iH_0^{(1)}(ka)J_0(ka) \quad (8.174)$$

Therefore, for $a \rightarrow 0$ with fixed λ and h

$$\lim_{a \rightarrow 0+} \frac{1}{4}iH_0^{(1)}(ka)g(z) = \frac{f(z)g(h) - f(h)g(z)}{g(h)} \quad (8.175)$$

provided that $z \neq 0$ and that $g(h) \neq 0$. A comparison of (8.172) and (8.175) shows that

$$\Psi = O(-\ln ka) \quad (8.176)$$

In order to compare $I^{(1)}$ and $g^{(1)}$, it is sufficient to compare Kf and Kg with $\mathcal{K}f$

and $\mathcal{K}g$, respectively. Let F be a smooth function independent of a ; F may be f or g in particular. The difference between KF and $\mathcal{K}F$ is, by (8.137) and (8.138),

$$\begin{aligned} (\mathcal{K}F)(z) - (KF)(z) &= \int_{-h}^h [\mathcal{K}(z - z') - K(z - z', a)]F(z') dz' \\ &= \Delta_1(z) + F(z)\Delta_2(z) + \Delta_3(z) \end{aligned} \quad (8.177)$$

where

$$\begin{aligned} \Delta_1(z) &= \int_{-h}^h \{[\mathcal{K}(z - z') - K(z - z', a)] \\ &\quad - [\mathcal{K}(z - z') - K(z - z', a)]|_{k=0}\} F(z') dz' \end{aligned} \quad (8.178)$$

$$\Delta_2(z) = \int_{-h}^h [\mathcal{K}(z - z') - K(z - z', a)]|_{k=0} dz' \quad (8.179)$$

$$\text{and } \Delta_3(z) = \int_{-h}^h [\mathcal{K}(z - z') - K(z - z', a)]|_{k=0} [F(z') - F(z)] dz' \quad (8.180)$$

Consider first $\Delta_1(z)$. Let F_0 be the maximum of $|F(z)|$; then by (8.176)

$$\begin{aligned} &\int_{-h}^h F(z') [\exp \{ik[(z - z')^2 + a^2]^{1/2}\} dz' \\ &\quad - (2\pi)^{-1} \int_{-\pi}^{\pi} \exp \left\{ ik \left[(z - z')^2 + 4a^2 \sin^2 \frac{\theta}{2} \right]^{1/2} \right\} d\theta] \\ &\leq \pi^{-1} F_0 \int_{-h}^h dz' \int_{-\pi}^{\pi} \left| \sin k \left\{ [(z - z')^2 + a^2]^{1/2} - \left[(z - z')^2 + 4a^2 \sin^2 \frac{\theta}{2} \right]^{1/2} \right\} \right| d\theta \\ &\leq 2\pi^{-1} F_0 \int_{-\pi}^{\pi} d\theta \int_0^{2h} \left| \sin \left\{ k \left[(z'^2 + a^2)^{1/2} - \left(z'^2 + 4a^2 \sin^2 \frac{\theta}{2} \right)^{1/2} \right] \right\} \right| dz' \\ &\leq 2\pi^{-1} F_0 \int_{-\pi}^{\pi} d\theta \int_0^{2h} \min(1, \frac{3}{2}ka^2/z') dz' \\ &= 6ka^2 F_0 \ln \frac{4eh}{3ka^2} = O(ka^2\Psi) \end{aligned} \quad (8.181)$$

Therefore, by (8.59),

$$|\Delta_1(z)| \leq 6F_0 \int_0^k ka^2 \ln \frac{4eh}{3ka^2} dk = 3F_0(ka)^2 \ln \frac{4e^{3/2}h}{3ka^2} = O(k^2a^2\Psi) \quad (8.182)$$

This difference is indeed small.

The function $\Delta_2(z)$ can be written in the form

$$\begin{aligned} \Delta_2(z) &= (8\pi^2)^{-1} \int_{-\pi}^{\pi} \left[\sinh^{-1} \frac{h - z}{2a|\sin(\theta/2)|} + \sinh^{-1} \frac{h + z}{2a|\sin(\theta/2)|} \right. \\ &\quad \left. - \sinh^{-1} \frac{h - z}{a} - \sinh^{-1} \frac{h + z}{a} \right] d\theta \\ &= (8\pi^2)^{-1} \int_{-\pi}^{\pi} \left[\ln \left(1 + \left\{ 1 + \left[2a(h - z)^{-1} \sin \frac{\theta}{2} \right]^2 \right\}^{1/2} \right) \right. \\ &\quad \left. + \ln \left(1 + \left\{ 1 + \left[2a(h + z)^{-1} \sin \frac{\theta}{2} \right]^2 \right\}^{1/2} \right) \right. \\ &\quad \left. - \ln(1 + \{1 + [a(h - z)^{-1}]^2\}^{1/2}) - \ln(1 + \{1 + [a(h + z)^{-1}]^2\}^{1/2}) \right] d\theta \end{aligned} \quad (8.183)$$

In (8.183) use has been made of the identity

$$\int_0^\pi \ln \left(2 \sin \frac{\theta}{2} \right) d\theta = 0 \quad (8.184)$$

It is seen from (8.183) that

$$\Delta_2(z) = k^{-4}(h^2 - z^2)^{-2}O(k^2a^2) \quad (8.185)$$

and

$$\Delta_2(\pm h) = O(k^2a^2) \quad (8.186)$$

Thus $\Delta_2(z)$ is small except when z is close to, but not equal to, h or $-h$.

Finally, $\Delta_3(z)$ is comparatively not so small. Since

$$\begin{aligned} & \int_0^h [\mathcal{K}(z) - K(z, a)]|_{k=0} z F(z) dz \\ &= (8\pi^2)^{-1} \int_{-\pi}^{\pi} d\theta \int_0^h \left[\left(z^2 + 4a^2 \sin^2 \frac{\theta}{2} \right)^{-\frac{1}{2}} - (z^2 + a^2)^{-\frac{1}{2}} \right] z F(z) dz \\ &= (8\pi^2)^{-1} \int_{-\pi}^{\pi} \left\{ \left[\left(z^2 + 4a^2 \sin^2 \frac{\theta}{2} \right)^{\frac{1}{2}} - (z^2 + a^2)^{\frac{1}{2}} \right] F(z) \Big|_0^h \right. \\ & \quad \left. - \int_0^h F'(z) \left[\left(z^2 + 4a^2 \sin^2 \frac{\theta}{2} \right)^{\frac{1}{2}} - (z^2 + a^2)^{\frac{1}{2}} \right] dz \right\} d\theta \\ &= (8\pi^2)^{-1} \int_{-\pi}^{\pi} \left(a - 2a \left| \sin \frac{\theta}{2} \right| \right) F(0) d\theta + O(ka^2 \Psi) \\ &= (4\pi)^{-1} \left(1 - \frac{4}{\pi} \right) a F(0) + O(ka^2 \Psi) \end{aligned} \quad (8.187)$$

we get the following orders of magnitudes for $\Delta_3(z)$:

$$\Delta_3(z)|_{F=f} = O(k^2a^2\Psi V) \quad (8.188)$$

for z not close to $\pm h$ or 0;

$$\Delta_3(z)|_{F=g} = O(k^2a^2\Psi) \quad (8.189)$$

for z not close to $\pm h$;

$$\Delta_3(0)|_{F=f} = (4\pi)^{-1} i \zeta_0^{-1} V k a \left(1 - \frac{4}{\pi} \right) [1 + O(ka\Psi)] \quad (8.190)$$

$$\Delta_3(\pm h)|_{F=f} = -(8\pi)^{-1} i \zeta_0^{-1} V k a \left(1 - \frac{4}{\pi} \right) \cos kh [1 + O(ka\Psi)] \quad (8.191)$$

$$\text{and } \Delta_3(\pm h)|_{F=g} = (4\pi)^{-1} k a \left(1 - \frac{4}{\pi} \right) \sin kh [1 + O(ka\Psi)] \quad (8.192)$$

Substitution of these results into (8.177) gives that

$$\begin{aligned} & (\mathcal{K}f)(z) - (Kf)(z) \\ &= \begin{cases} -(8\pi)^{-1} i \zeta_0^{-1} V k a \left(1 - \frac{4}{\pi} \right) \cos kh [1 + O(ka\Psi)] & \text{for } z = \pm h \\ (4\pi)^{-1} i \zeta_0^{-1} V k a \left(1 - \frac{4}{\pi} \right) [1 + O(ka\Psi)] & \text{for } z = 0 \\ O\left(\frac{k^2a^2\Psi V}{\zeta_0}\right) & \text{for } z \text{ not close to } \pm h \text{ or } 0 \end{cases} \end{aligned} \quad (8.193)$$

and $(\mathcal{K}g)(z) - (Kg)(z)$

$$= \begin{cases} (4\pi)^{-1}ka\left(1 - \frac{4}{\pi}\right)\sin kh[1 + O(ka\Psi)] & \text{for } z = \pm h \\ O(k^2a^2\Psi) & \text{for } z \text{ not close to } \pm h \end{cases} \quad (8.194)$$

Thus the difference is at most of the order of ka .

The conclusion is therefore reached that, by (8.185), (8.193), and (8.194),

$$I^{(1)}(z) - g^{(1)}(z) = O\left(\frac{kaV}{\xi_0}\right) \quad (8.195)$$

provided that both $k(h - z)$ and $k(h + z)$ are not much less than $(ka)^{1/2}$. The coefficient of kaV in (8.195) can be calculated easily if so desired.

This result (8.195) holds for any order of iteration, namely

$$I^{(n)}(z) - g^{(n)}(z) = O\left(\frac{kaV}{\xi_0}\right) \quad (8.196)$$

More precisely, (8.196) means that, for $a \rightarrow 0$ with fixed λ , fixed h , and fixed n , the difference $I^{(n)}(z) - g^{(n)}(z)$ is of the order of magnitude kaV/ξ_0 . As discussed in the preceding section, no such result holds if $n \rightarrow \infty$ also.

We shall not derive (8.196) in any detail. We shall merely say that for $n = 2$, the following identity is useful:

$$\begin{aligned} \int_{-\pi}^{\pi} d\theta_1 \int_{-\pi}^{\pi} d\theta_2 \int_0^{\delta} \left(z^2 + 4a^2 \sin^2 \frac{\theta_1}{2}\right)^{-1/2} \sinh^{-1} \left[\left(2a \sin \frac{\theta_2}{2}\right)^{-1} z \right] dz \\ = 1/2 \left\{ \int_{-\pi}^{\pi} \sinh^{-1} \left[\left(2a \left|\sin \frac{\theta}{2}\right|\right)^{-1} \delta \right] \right\}^2 d\theta \end{aligned} \quad (8.197)$$

This trick can also be generalized to the cases where $n > 2$.

Equation (8.196) gives the answer to the question raised at the beginning of Sec. 8.6: when ka is very small, the first few iterations of (8.58) are indeed good approximations to the corresponding iterations of (8.117). We do not have any good estimate of the permissible number of iterations for given ka and kh , but this number is expected to be less than

$$\frac{\ln(1/ka)}{\ln \ln(1/ka)} \quad (8.198)$$

for small ka .

8.8 The Circular Tubular Antenna (Continued)

The finite circular tubular antenna of Fig. 8.4 is an idealization of a number of physical situations, for example, a monopole driven from a coaxial line. In Fig. 8.5 we show two possible geometries intermediary between the physical situation and that of Fig. 8.4; that is, in Fig. 8.5 we have two idealizations where the coaxial lines are not eliminated. In order that the development given in the preceding sections be physically meaningful, the solutions of (8.117)

must be good approximations to the current distributions for the geometries of Fig. 8.5a and Fig. 8.5b.

In particular, let $h \rightarrow \infty$. Then the integral equation (8.117) becomes (8.119), the solution of which is already given in Sec. 8.4. On the other hand,

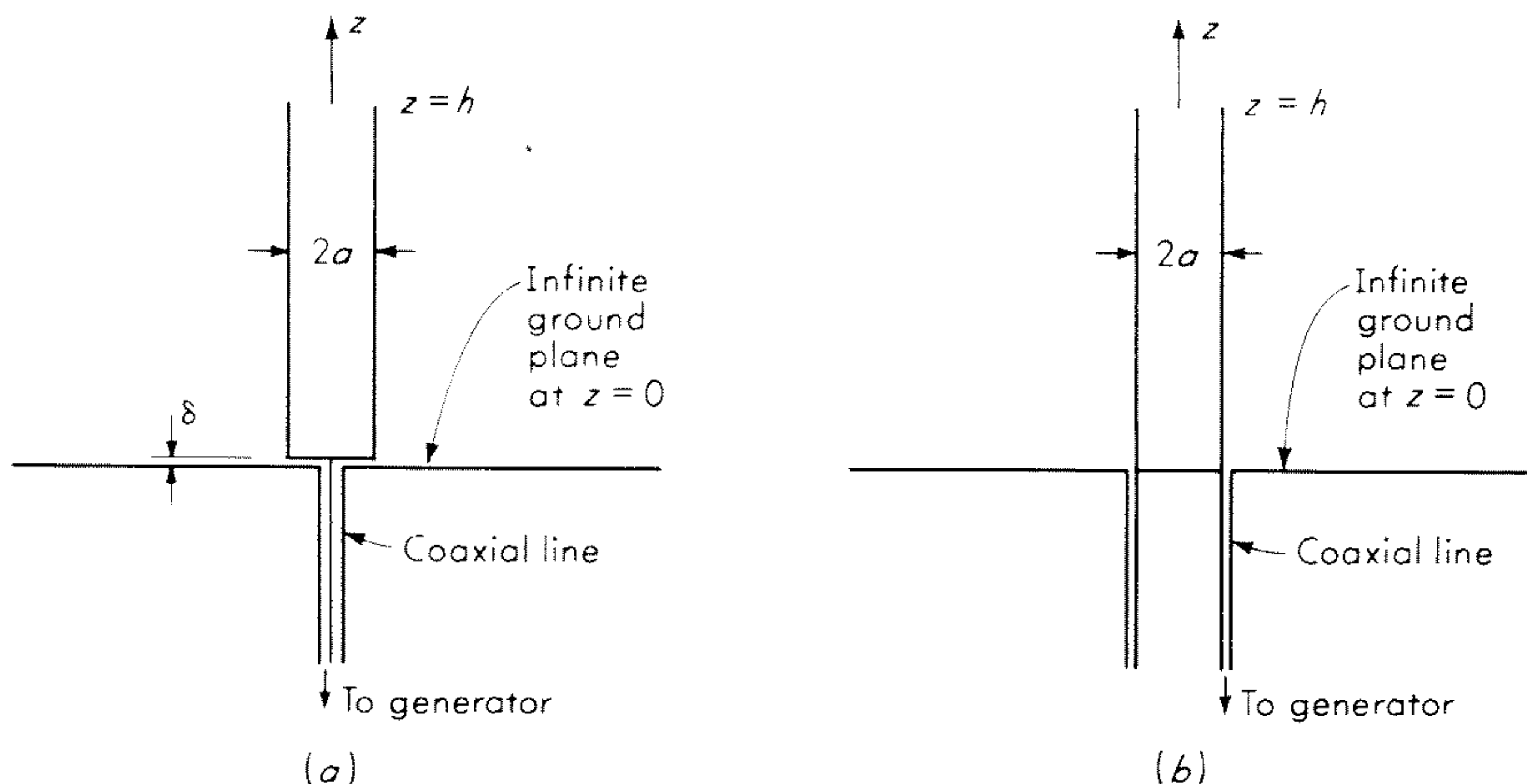


Fig. 8.5 Linear antennas driven from coaxial lines.

as $h \rightarrow \infty$ it is clear that the electromagnetic field is zero when $z > \delta$ and $r < a$ for the geometry of Fig. 8.5a and that it is also zero when $r < a$ for that of Fig. 8.5b. Therefore, the desired field for the infinite circular tubular antenna is *not* that obtained from (8.97) and (8.98); instead, the Fourier transforms of B_θ and E_r are given by

$$c\bar{B}_\theta(r, \xi) = \begin{cases} 0 & \text{for } r < a \\ -ikV(k^2 - \xi^2)^{-1/2} \frac{H_0^{(1)'}(r\sqrt{k^2 - \xi^2})}{H_0^{(1)}(a\sqrt{k^2 - \xi^2})} & \text{for } r > a \end{cases} \quad (8.199)$$

and

$$\bar{E}_r(r, \xi) = \begin{cases} 0 & \text{for } r < a \\ i\xi V(k^2 - \xi^2)^{-1/2} \frac{H_0^{(1)'}(r\sqrt{k^2 - \xi^2})}{H_0^{(1)}(a\sqrt{k^2 - \xi^2})} & \text{for } r > a \end{cases} \quad (8.200)$$

In particular, it follows from (8.81) that

$$E_z(a+, z) = \lim_{r \rightarrow a+} E_z(r, z) = -V\delta(z) \quad (8.201)$$

and

$$E_z(a-, z) = \lim_{r \rightarrow a-} E_z(r, z) = 0 \quad (8.202)$$

Thus the infinite circular tubular antenna is driven by a δ -function generator on the *outside* of the tube but not on the inside of the tube.

We study in this section the solution given by (8.199) and (8.200) and ask how (8.119) may be modified to yield this solution. In the next section, we apply these considerations to the finite tubular antenna.

The first step is to introduce the vector potential \mathbf{A} . In order for this vector potential to be useful, it must satisfy at least the following conditions: (1) $\mathbf{A} = \hat{\mathbf{z}}A_z$, that is, \mathbf{A} has only a z component, (2) $\mathbf{A} \rightarrow 0$ as $r \rightarrow \infty$, and (3) \mathbf{A} is continuous. Accordingly, by (8.30),

$$B_\theta = -\frac{\partial A_z}{\partial r} \quad (8.203)$$

and hence by the second condition

$$A_z(r, z) = \int_r^\infty B_\theta(r', z) dr' \quad (8.204)$$

By the third condition, (8.204) must hold both for $r > a$ and $r < a$. Therefore, by (8.199), for $r < a$

$$A_z(r, z) = A_z(a, z) \quad (8.205)$$

More explicitly, also by (8.199), for $r \geq a$,

$$\bar{A}_z(r, \zeta) = ikc^{-1}V(k^2 - \zeta^2)^{-1} \frac{H_0^{(1)}(r\sqrt{k^2 - \zeta^2})}{H_0^{(1)}(a\sqrt{k^2 - \zeta^2})} \quad (8.206)$$

The substitution of (8.206) into (8.205) yields immediately that, for $r \leq a$,

$$\bar{A}_z(r, \zeta) = ikc^{-1}V(k^2 - \zeta^2)^{-1} \quad (8.207)$$

$$A_z(r, z) = \frac{1}{2}c^{-1}Ve^{ik|z|} \quad (8.208)$$

The important point here is that $\partial A_z / \partial z$ is *discontinuous* for $z = 0$ and $r \leq a$.

The next step is to calculate $(\nabla^2 + k^2)A_z$. This is zero except on the tube $r = a$ and on the disk $z = 0$ and $r < a$. Instead of (8.101), the total current $\mathcal{G}_\infty^+(z)$ is more simply

$$\mathcal{G}_\infty^+(z) = 2\pi a J_+(z) = 2\pi a \mu_0^{-1} B_\theta(a+, z) \quad (8.209)$$

By (8.208) and (8.209), we get

$$(\nabla^2 + k^2)A_z(r, z) = -(2\pi a)^{-1} \mu_0 \mathcal{G}_\infty^+(z) \delta(r - a) + ikc^{-1}V\delta(z)H(a - r) \quad (8.210)$$

where H is defined by (8.49). By (8.116), we can compute the vector potential on the tube from (8.210)

$$A_z(a, z) = \mu_0 \int_{-\infty}^{\infty} \mathcal{G}_\infty^+(z) \mathcal{K}(z - z') dz' - ikc^{-1}VW(z, a) \quad (8.211)$$

where

$$W(z, a) = \frac{1}{4\pi} \int_0^a r dr \int_{-\pi}^{\pi} (z^2 + r^2 + a^2 - 2ra \cos \theta)^{-1/2} \exp[ik(z^2 + r^2 + a^2 - 2ra \cos \theta)^{1/2}] d\theta \quad (8.212)$$

Note that $W(z, a)$ is a completely known function.

A comparison of (8.211) with (8.208) then yields

$$\int_{-\infty}^{\infty} g_{\infty}^{+}(z') \mathcal{K}(z - z') dz' = \frac{1}{2} \zeta_0^{-1} V e^{ik|z|} + ik \zeta_0^{-1} V W(z, a) \quad (8.213)$$

This is the required integral equation for the current on an infinitely long circular tubular antenna driven by a δ -function generator on the outside of the tube. Equation (8.213) differs from (8.119) only in the presence of an extra term on the right-hand side.

We conclude this section with a brief discussion of the function W . First, it can easily be expressed as a single integral

$$W(z, a) = \frac{1}{2\pi} \int_0^{2a} \cos^{-1} \left(\frac{r}{2a} \right) (z^2 + r^2)^{-1/2} \exp [ik(z^2 + r^2)^{1/2}] r dr \quad (8.214)$$

Let $r = 2a \sin \theta$, then by integrating (8.214) by parts we get

$$ikW(z, a) = -\frac{1}{4} e^{ik|z|} + \frac{1}{2\pi} \int_0^{\pi/2} \exp [ik(z^2 + 4a^2 \sin^2 \theta)^{1/2}] d\theta \quad (8.215)$$

The limiting behaviors of W are as follows:

$$ikW(0, a) = -\frac{1}{4} + \frac{1}{4\pi} \int_0^{\pi} e^{2ika \sin \theta} d\theta$$

$$\text{or} \quad W(0, a) = \frac{i}{4k} [1 - J_0(2ka) + iE_0(2ka)] \quad (8.216)$$

where E_0 is the Anger-Weber function of order zero;⁷ and, as $|z| \rightarrow \infty$,

$$W(z, a) \approx \frac{a^2}{4|z|} e^{ik|z|} \quad (8.217)$$

Furthermore, as $k \rightarrow 0$, $W(z, a)$ reduces simply to

$$\begin{aligned} W(z, a)|_{k=0} &= -\frac{1}{4}|z| + \frac{1}{2\pi} \int_0^{\pi/2} (z^2 + 4a^2 \sin^2 \theta)^{1/2} d\theta \\ &= -\frac{1}{4}|z| + \frac{1}{2\pi} (z^2 + 4a^2)^{1/2} E(k_0) \end{aligned} \quad (8.218)$$

where E is the complete elliptic integral, and

$$k_0 = 2a(z^2 + 4a^2)^{-1/2} \quad (8.219)$$

As a check, it follows from either (8.216) or (8.219) that

$$W(0, a) \Big|_{k=0} = \frac{a}{\pi} \quad (8.220)$$

It is interesting to note that, by (8.215), the integral equation (8.213) may be written as

$$\begin{aligned} \int_{-\infty}^{\infty} g_{\infty}^{+}(z) \mathcal{K}(z - z') dz' &= \frac{1}{4} \zeta_0^{-1} V e^{ik|z|} \\ &+ \frac{V}{2\pi \zeta_0} \int_0^{\pi/2} \exp [ik(z^2 + 4a^2 \sin^2 \theta)^{1/2}] d\theta \end{aligned} \quad (8.221)$$

That the coefficient of $Ve^{ik|z|}$ is reduced by a factor of 2 is intimately related to the fact that

$$\lim_{z \rightarrow 0} \frac{g_{\infty}^{+}(z)}{g_{\infty}(z)} = 1/2 \quad (8.222)$$

which is a direct consequence of (8.209), (8.101), (8.103), and (8.104).

8.9 Integral Equations for the Current Distributions (Continued)

We have seen from (8.213) that a term $ik\zeta_0^{-1}VW(z,a)$ needs to be added to the right-hand side of (8.119) in the case of an infinite antenna. In this section we shall show that the same term should be added to the right-hand side of (8.117) for the finite antenna.

In view of (8.201) and (8.202), we may formulate the problem as follows. Solve (8.78) to (8.80), which hold except where $r = a$ and $|z| \leq h$, with the boundary conditions (8.201) and (8.202), which hold when $|z| < h$. Again, this means that the circular tubular antenna is driven by a δ -function generator on the outside of the tube but not on the inside. However, in the present case the field is, in general, not zero inside the tube.

The main point in this section is that we must be extremely careful in introducing the vector and scalar potentials. Since $\mathbf{B} = \hat{\mathbf{0}}B$, we try to define a vector potential which satisfies the three conditions enumerated in the preceding section. By (8.203), (8.204) must hold also for the finite circular tubular antenna, and it defines the vector potential unambiguously. It is seen from (8.208) that, for $r < a$,

$$\left. \frac{\partial}{\partial z} A_z(r,z) \right|_{z=0+} - \left. \frac{\partial}{\partial z} A_z(r,z) \right|_{z=0-} = \frac{ikV}{c} \quad (8.223)$$

for the infinite antenna. Equation (8.223) also holds for the finite antenna. To see this, we use (8.204) and (8.78) to get, for $r < a$,

$$\begin{aligned} \left. \frac{\partial}{\partial z} A_z(r,z) \right|_{z=0+} - \left. \frac{\partial}{\partial z} A_z(r,z) \right|_{z=0-} &= \int_r^{\infty} \left[\left. \frac{\partial}{\partial z} B_{\theta}(r',z) \right|_{z=0+} - \left. \frac{\partial}{\partial z} B_{\theta}(r',z) \right|_{z=0-} \right] dr' \\ &= ikc^{-1} \int_r^{\infty} [E_r(r',0+) - E_r(r',0-)] dr' \\ &= ikc^{-1} \int_{0+}^{0-} E_z(a+,z) dz = \frac{ikV}{c} \end{aligned} \quad (8.224)$$

We have used the fact that, locally near the δ -function generator, the field has approximately the form of the static field.

Attention is next turned to the scalar potential. It is easily verified that

$$\nabla \times (\mathbf{E} - i\omega\mathbf{A}) = 0 \quad (8.225)$$

and hence there exists a function Φ such that

$$\mathbf{E} = i\omega\mathbf{A} - \nabla\Phi \quad (8.226)$$

The important point is that, since the region exterior to the tubular antenna is

not simply connected, Φ is in general *not single-valued*. It is therefore convenient to introduce a cut at

$$z = l \quad \text{and} \quad r \leq a \quad (8.227)$$

where $|l| \leq h$, as shown in Fig. 8.6. We say that Φ is defined in the exterior of the tubular antenna and the cut taken together, and we attempt to compute

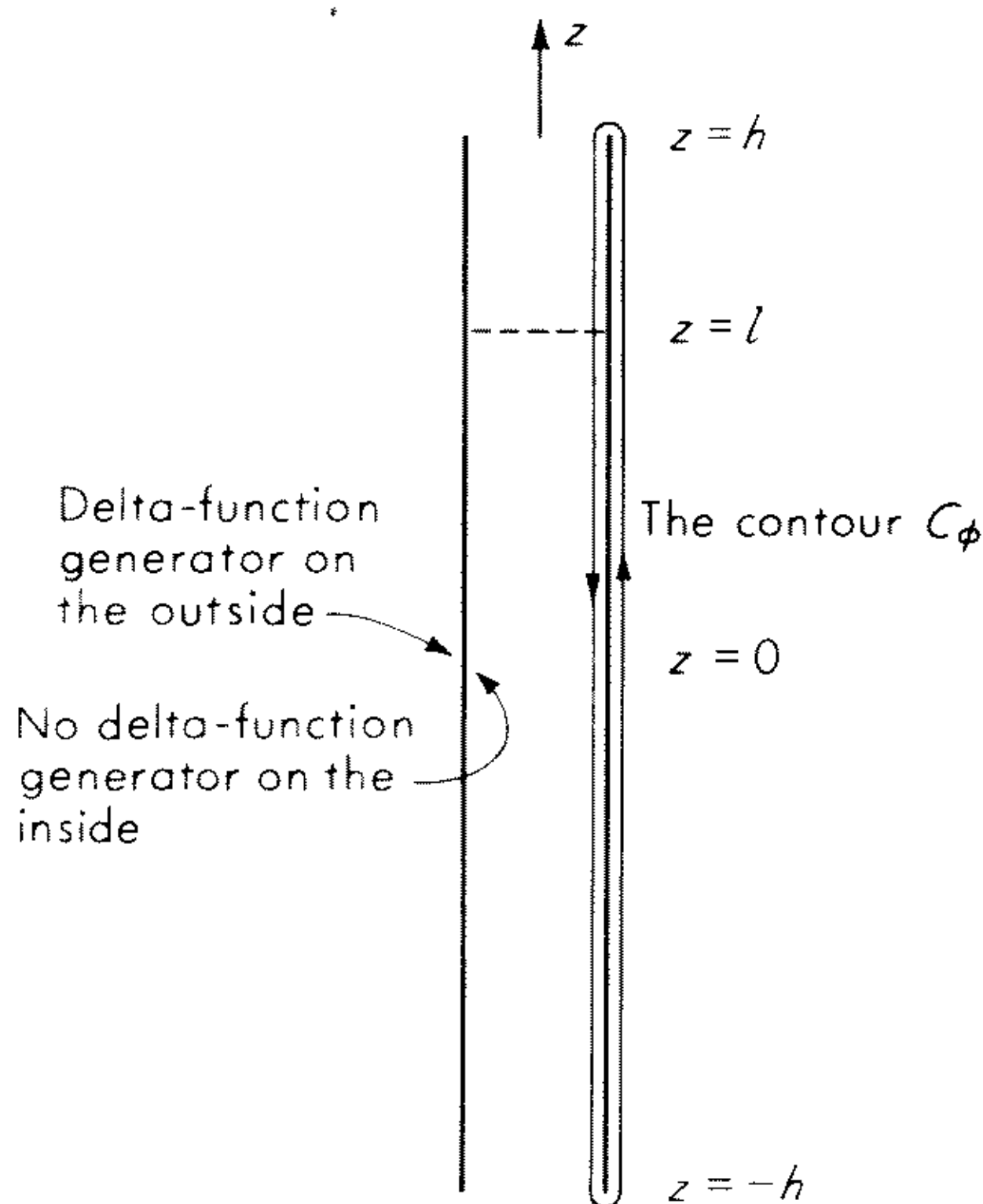


Fig. 8.6 Circular tubular antenna driven on the outside surface only.

the discontinuity of Φ across this cut. Let C_Φ be the contour shown in Fig. 8.6, and we integrate (8.226) along the contour. By (8.201) and (8.202),

$$\int_{C_\Phi} \mathbf{E} \cdot d\mathbf{s} = -V \quad (8.228)$$

By the continuity of the vector potential

$$\int_{C_\Phi} \mathbf{A} \cdot d\mathbf{s} = 0 \quad (8.229)$$

Therefore

$$\Phi(r, l+) - \Phi(r, l-) = V \quad (8.230)$$

for $r < a$. Note that, given the cut by (8.227), Φ is unambiguously defined by (8.226) together with the condition that Φ vanishes at infinity.

We have defined the vector and scalar potentials with no reference to the Lorentz condition (8.32). Let

$$\chi = \nabla \cdot \mathbf{A} - \frac{ik\Phi}{c} = \frac{\partial A_z}{\partial z} - \frac{ik\Phi}{c} \quad (8.231)$$

then, by (8.12),

$$\nabla^2 \mathbf{A} + k^2 \mathbf{A} = \nabla \chi \quad (8.232)$$

exterior to the tubular antenna. Since \mathbf{A} has only a z component, (8.232) implies that

$$\frac{\partial \chi}{\partial x} = \frac{\partial \chi}{\partial y} = 0 \quad (8.233)$$

Since $\chi = 0$ at infinity, (8.233) may be solved to yield that

$$\chi(r, z) = \begin{cases} \text{function of } z & \text{for } r < a \text{ and } |z| < h \\ 0 & \text{otherwise} \end{cases} \quad (8.234)$$

By (8.224) and (8.230), χ has the following discontinuities for $r < a$:

$$\chi(r, 0+) - \chi(r, 0-) = \frac{ikV}{c} \quad (8.235)$$

and
$$\chi(r, l+) - \chi(r, l-) = \frac{-ikV}{c} \quad (8.236)$$

Indeed, since χ is an analytic function of r and z , it follows from (8.234) to (8.236) that, if $l \geq 0$,

$$\chi(r, z) = \begin{cases} \frac{ikV}{c} & \text{for } r < a \text{ and } 0 < z < l \\ 0 & \text{otherwise} \end{cases} \quad (8.237)$$

and if $l \leq 0$,

$$\chi(r, z) = \begin{cases} \frac{-ikV}{c} & \text{for } r < a \text{ and } l < z < 0 \\ 0 & \text{otherwise} \end{cases} \quad (8.238)$$

Therefore, the Lorentz condition $\chi = 0$ is satisfied if and only if we choose

$$l = 0 \quad (8.239)$$

in connection with the scalar potential.

By (8.232), A_z satisfies the homogeneous Helmholtz equation except possibly on the tubular antenna and the disk $z = 0$ and $r < a$. Let $\mathcal{G}^+(z)$ be the total current on the circular tubular antenna driven on the outside surface only,

$$\mathcal{G}^+(z) = 2\pi a \mu_0^{-1} [B_\theta(a+, z) - B_\theta(a-, z)] \quad (8.240)$$

then, by (8.224),

$$(\nabla^2 + k^2)A_z(r, z) = -(2\pi a)^{-1} \mu_0 \mathcal{G}^+(z) \delta(r - a) + ikc^{-1} V \delta(z) H(a - r) \quad (8.241)$$

similar to (8.210). Hence, by (8.212),

$$A_z(a, z) = \mu_0 \int_{-h}^h \mathcal{G}^+(z') \mathcal{K}(z - z') dz' - ikc^{-1} V W(z, a) \quad (8.242)$$

By (8.234) and (8.56), (8.242) is an integral equation for the current $\mathcal{G}^+(z)$:

$$\int_{-h}^h \mathcal{G}^+(z') \mathcal{K}(z - z') dz' = \frac{1}{2} i \zeta_0^{-1} V [\sin k|z| + 2W(z, a)] + \mathcal{C}^+ \cos kz \quad (8.243)$$

where the constant \mathcal{C}^+ is to be determined by the boundary condition

$$g^+(h) = 0 \quad (8.244)$$

Equation (8.243) is the desired integral equation, and it differs from (8.117) only in the appearance of the additional term $ik\zeta_0^{-1}VW(z,a)$ on the right-hand side.

Some properties of $W(z,a)$ have already been given in the preceding section. By (8.217) to (8.220), when ka is small, $W(z,a)$ is of the order of magnitude of $a^2/(a + |z|)$. Thus for a thin antenna, the term $ikVW(z,a)$ gives only a small correction to the right-hand side of the integral equation. In particular, when $ka \ll 1$, this term does not appreciably alter the first few terms of the iterative solution discussed in Secs. 8.6 and 8.7; however, its effect on the behavior of the iterative solution after many iterations is not understood.

For numerous technical reasons, there is now a great deal of interest in the case when ka is not very much smaller than 1. In that case, the term $ik\zeta_0^{-1}VW(z,a)$ is, of course, very important, and calculations based on (8.117) without this term must be considered to be irrelevant to the problem of a monopole driven from a coaxial line. Investigations on this problem have been carried out by Chang.⁸

8.10 A More General Case

It is shown in the preceding section that, in the case of a tubular antenna driven only on the outside, the scalar potential is discontinuous. Moreover, this discontinuity occurs across a surface in free space. Under these circumstances, it may be considered desirable to avoid introducing a scalar potential. To understand this point better, we study in detail here a more general case, where a tubular antenna is driven on the outside by a δ -function generator that *depends* on the angular variable θ . In this case, it is very cumbersome to use vector and scalar potentials; instead we deal with the field quantities directly.

Consider the geometry of Fig. 8.6. Instead of (8.201) and (8.202), the boundary conditions are

$$E_z(a+, \theta, z) = \lim_{r \rightarrow a+} E_z(r, \theta, z) = -Ve^{in\theta}\delta(z) \quad E_\theta(a+, \theta, z) = 0 \quad (8.245)$$

and

$$E_z(a-, \theta, z) = \lim_{r \rightarrow a-} E_z(r, \theta, z) = 0 \quad E_\theta(a-, \theta, z) = 0 \quad (8.246)$$

for $|z| < h$. In writing down (8.245) and (8.246) we have made use of the rotational invariance and linearity of the Maxwell equations. When $n = 0$, (8.245) and (8.246) reduce to (8.201) and (8.202). Unlike the cases treated in

Secs. 8.3 to 8.9, no field component vanishes, and we need the entire set of Maxwell's equations in free space:

$$\frac{1}{r} \frac{\partial E_z}{\partial \theta} - \frac{\partial E_\theta}{\partial z} = i\omega B_r \quad (8.247)$$

$$\frac{\partial E_r}{\partial z} - \frac{\partial E_z}{\partial r} = i\omega B_\theta \quad (8.248)$$

$$\frac{1}{r} \left[\frac{\partial}{\partial r} (rE_\theta) - \frac{\partial E_r}{\partial \theta} \right] = i\omega B_z \quad (8.249)$$

$$\frac{1}{r} \frac{\partial B_z}{\partial \theta} - \frac{\partial B_\theta}{\partial z} = -i\omega\mu_0\epsilon_0 E_r \quad (8.250)$$

$$\frac{\partial B_r}{\partial z} - \frac{\partial B_z}{\partial r} = -i\omega\mu_0\epsilon_0 E_\theta \quad (8.251)$$

and
$$\frac{1}{r} \left[\frac{\partial}{\partial r} (rB_\theta) - \frac{\partial B_r}{\partial \theta} \right] = -i\omega\mu_0\epsilon_0 E_z \quad (8.252)$$

The problem is to solve (8.247) to (8.252), which hold except where $r = a$ and $|z| \leq h$, together with the boundary conditions (8.245) and (8.246).

The dependence of each field component on θ is given by $e^{in\theta}$. Accordingly, we define Fourier transforms by

$$\bar{E}_i(r, \zeta) = e^{-in\theta} \int_{-\infty}^{\infty} E_i(r, \theta, z) e^{i\zeta z} dz \quad (8.253)$$

and
$$\bar{B}_i(r, \zeta) = e^{-in\theta} \int_{-\infty}^{\infty} B_i(r, \theta, z) e^{i\zeta z} dz \quad (8.254)$$

where $i = r, \theta, z$. In terms of these Fourier transforms, it follows from (8.248) and (8.250) that

$$(k^2 - \zeta^2) \bar{E}_r(r, \zeta) = -i\zeta \frac{\partial}{\partial r} \bar{E}_z(r, \zeta) - \frac{\omega n}{r} \bar{B}_z(r, \zeta) \quad (8.255)$$

and
$$(k^2 - \zeta^2) \bar{B}_\theta(r, \zeta) = i\omega\mu_0\epsilon_0 \frac{\partial}{\partial r} \bar{E}_z(r, \zeta) + \frac{n\zeta}{r} \bar{B}_z(r, \zeta) \quad (8.256)$$

Similarly, it follows from (8.247) and (8.251) that

$$(k^2 - \zeta^2) \bar{E}_\theta(r, \zeta) = \frac{n\zeta}{r} \bar{E}_z(r, \zeta) - i\omega \frac{\partial}{\partial r} \bar{B}_z(r, \zeta) \quad (8.257)$$

and
$$(k^2 - \zeta^2) \bar{B}_r(r, \zeta) = \frac{n\omega\mu_0\epsilon_0}{r} \bar{E}_z(r, \zeta) - i\zeta \frac{\partial}{\partial r} \bar{B}_z(r, \zeta) \quad (8.258)$$

The substitution of (8.255) to (8.258) into (8.249) and (8.252) then yields the differential equations for \bar{E}_z and \bar{B}_z as follows:

$$\left(\frac{\partial^2}{\partial r^2} + \frac{1}{r} \frac{\partial}{\partial r} - \frac{n^2}{r^2} + k^2 - \zeta^2 \right) \bar{E}_z = \left(\frac{\partial^2}{\partial r^2} + \frac{1}{r} \frac{\partial}{\partial r} - \frac{n^2}{r^2} + k^2 - \zeta^2 \right) \bar{B}_z = 0 \quad (8.259)$$

It is important to note that we do not retain any term involving the currents. Any attempt to write down these terms leads to confusion. Equations (8.255) to (8.259) hold both for $r > a$ and $r < a$.

The current densities are given by the sum of those on the outside of the tubular antenna (denoted by $+$) and those on the inside (denoted by $-$):

$$J_\theta(\theta, z) = J_\theta^+(\theta, z) + J_\theta^-(\theta, z) \quad (8.260)$$

$$\text{and} \quad J_z(\theta, z) = J_z^+(\theta, z) + J_z^-(\theta, z) \quad (8.261)$$

where all the J 's are zero for $|z| > h$, while for $|z| \leq h$

$$J_\theta^\pm(\theta, z) = \mp \mu_0^{-1} B_z(a \pm, \theta, z) \quad (8.262)$$

$$\text{and} \quad J_z^\pm(\theta, z) = \pm \mu_0^{-1} B_\theta(a \pm, \theta, z) \quad (8.263)$$

Define Fourier transforms similar to (8.253) and (8.254); for example,

$$\bar{J}_i(\zeta) = e^{-in\theta} \int_{-h}^h J_i(\theta, z) e^{i\zeta z} dz \quad (8.264)$$

where $i = \theta, z$. Then, by (8.260) to (8.263),

$$\bar{B}_\theta(a+, \zeta) - \bar{B}_\theta(a-, \zeta) = \mu_0 \bar{J}_z(\zeta) \quad (8.265)$$

$$\text{and} \quad \bar{B}_z(a+, \zeta) - \bar{B}_z(a-, \zeta) = -\mu_0 \bar{J}_\theta(\zeta) \quad (8.266)$$

The corresponding boundary conditions for \bar{E} follow from (8.245) and (8.246):

$$\bar{E}_\theta(a+, \zeta) - \bar{E}_\theta(a-, \zeta) = 0 \quad (8.267)$$

$$\text{and} \quad \bar{E}_z(a+, \zeta) - \bar{E}_z(a-, \zeta) = -V \quad (8.268)$$

Equation (8.268) is responsible for the difficulties encountered in attempts to include the current terms in Maxwell's equations. It follows from (8.257), (8.267), and (8.268) that

$$\frac{\partial}{\partial r} \bar{B}_z(a+, \zeta) - \frac{\partial}{\partial r} \bar{B}_z(a-, \zeta) = \frac{in\zeta V}{\omega a} \quad (8.269)$$

Similarly, it follows from (8.256), (8.265), and (8.266) that

$$\frac{\partial}{\partial r} \bar{E}_z(a+, \zeta) - \frac{\partial}{\partial r} \bar{E}_z(a-, \zeta) = (i\omega\epsilon_0 a)^{-1} [a(k^2 - \zeta^2) \bar{J}_z(\zeta) + n\zeta \bar{J}_\theta(\zeta)] \quad (8.270)$$

Because of the boundary conditions (8.266) and (8.268) to (8.270), the differential equations (8.259) can be solved with the radiation condition to give the following results. For $r > a$:

$$\begin{aligned} \bar{E}_z(r, \zeta) = & \{ -\frac{1}{2}\pi(\omega\epsilon_0)^{-1} [a(k^2 - \zeta^2) \bar{J}_z(\zeta) + n\zeta \bar{J}_\theta(\zeta)] J_{|n|}(\sqrt{k^2 - \zeta^2}a) \\ & - \frac{1}{2}i\pi a V \sqrt{k^2 - \zeta^2} J'_{|n|}(\sqrt{k^2 - \zeta^2}a) \} H_{|n|}^{(1)}(\sqrt{k^2 - \zeta^2}r) \end{aligned} \quad (8.271)$$

and

$$\begin{aligned} \bar{B}_z(r, \zeta) = & \{ -\frac{1}{2}i\pi a \mu_0 \sqrt{k^2 - \zeta^2} \bar{J}_\theta(\zeta) J'_{|n|}(\sqrt{k^2 - \zeta^2}a) \\ & + \frac{1}{2}\pi n \zeta \omega^{-1} V J_{|n|}(\sqrt{k^2 - \zeta^2}a) \} H_{|n|}^{(1)}(\sqrt{k^2 - \zeta^2}r) \end{aligned} \quad (8.272)$$

For $r < a$:

$$\begin{aligned} \bar{E}_z(r, \zeta) = & \{ -\frac{1}{2}\pi(\omega\epsilon_0)^{-1}[a(k^2 - \zeta^2)\bar{J}_z(\zeta) + n\zeta\bar{J}_\theta(\zeta)]H_{|n|}^{(1)}(\sqrt{k^2 - \zeta^2}a) \\ & - \frac{1}{2}i\pi aV\sqrt{k^2 - \zeta^2}H_{|n|}^{(1)'}(\sqrt{k^2 - \zeta^2}a)\}J_{|n|}(\sqrt{k^2 - \zeta^2}r) \end{aligned} \quad (8.273)$$

$$\begin{aligned} \text{and } \bar{B}_z(r, \zeta) = & \{ -\frac{1}{2}i\pi a\mu_0\sqrt{k^2 - \zeta^2}\bar{J}_\theta(\zeta)H_{|n|}^{(1)'}(\sqrt{k^2 - \zeta^2}a) \\ & + \frac{1}{2}\pi n\zeta\omega^{-1}VH_{|n|}^{(1)}(\sqrt{k^2 - \zeta^2}a)\}J_{|n|}(\sqrt{k^2 - \zeta^2}r) \end{aligned} \quad (8.274)$$

where the branch cuts for $\sqrt{k^2 - \zeta^2}$ are in every case again taken to be those shown in Fig. 8.2a. In order to use the boundary conditions (8.245) or (8.246), it remains to write down the expressions for $\bar{E}_\theta(r, \zeta)$ from (8.257). For $r > a$:

$$\begin{aligned} \bar{E}_\theta(r, \zeta) = & -\frac{1}{2}\pi an\zeta(\omega\epsilon_0 r)^{-1}\bar{J}_z(\zeta)J_{|n|}(\sqrt{k^2 - \zeta^2}a)H_{|n|}^{(1)}(\sqrt{k^2 - \zeta^2}r) \\ & + \bar{J}_\theta(\zeta)[-\frac{1}{2}\pi(\omega\epsilon_0 r)^{-1}n^2\zeta^2(k^2 - \zeta^2)^{-1}J_{|n|}(\sqrt{k^2 - \zeta^2}a)H_{|n|}^{(1)}(\sqrt{k^2 - \zeta^2}r) \\ & - \frac{1}{2}\pi a\omega\mu_0J'_{|n|}(\sqrt{k^2 - \zeta^2}a)H_{|n|}^{(1)'}(\sqrt{k^2 - \zeta^2}r)] \\ & - \frac{1}{2}i\pi n\zeta V(k^2 - \zeta^2)^{-\frac{1}{2}}[ar^{-1}J'_{|n|}(\sqrt{k^2 - \zeta^2}a)H_{|n|}^{(1)}(\sqrt{k^2 - \zeta^2}r) \\ & + J_{|n|}(\sqrt{k^2 - \zeta^2}a)H_{|n|}^{(1)'}(\sqrt{k^2 - \zeta^2}r)] \end{aligned} \quad (8.275)$$

For $r < a$:

$$\begin{aligned} \bar{E}_\theta(r, \zeta) = & -\frac{1}{2}\pi an\zeta(\omega\epsilon_0 r)^{-1}\bar{J}_z(\zeta)H_{|n|}^{(1)}(\sqrt{k^2 - \zeta^2}a)J_{|n|}(\sqrt{k^2 - \zeta^2}r) \\ & + \bar{J}_\theta(\zeta)[-\frac{1}{2}\pi(\omega\epsilon_0 r)^{-1}n^2\zeta^2(k^2 - \zeta^2)^{-1}H_{|n|}^{(1)}(\sqrt{k^2 - \zeta^2}a)J_{|n|}(\sqrt{k^2 - \zeta^2}r) \\ & - \frac{1}{2}\pi a\omega\mu_0H_{|n|}^{(1)'}(\sqrt{k^2 - \zeta^2}a)J'_{|n|}(\sqrt{k^2 - \zeta^2}r)] \\ & - \frac{1}{2}i\pi n\zeta V(k^2 - \zeta^2)^{-\frac{1}{2}}[ar^{-1}H_{|n|}^{(1)'}(\sqrt{k^2 - \zeta^2}a)J_{|n|}(\sqrt{k^2 - \zeta^2}r) \\ & + H_{|n|}^{(1)}(\sqrt{k^2 - \zeta^2}a)J'_{|n|}(\sqrt{k^2 - \zeta^2}r)] \end{aligned} \quad (8.276)$$

Let $r \rightarrow a-$; then it follows from (8.273) and (8.276) that

$$\bar{E}_z(a-, \zeta) = (k^2 - \zeta^2)\bar{M}_{zz}(\zeta)\bar{J}_z(\zeta) + \bar{M}_{z\theta}(\zeta)\bar{J}_\theta(\zeta) + V\bar{g}_z(\zeta) \quad (8.277)$$

$$\text{and } \bar{E}_\theta(a-, \zeta) = \bar{M}_{\theta z}(\zeta)\bar{J}_z(\zeta) + \bar{M}_{\theta\theta}(\zeta)\bar{J}_\theta(\zeta) + V\bar{g}_\theta(\zeta) \quad (8.278)$$

$$\text{where } \bar{M}_{zz}(\zeta) = -\frac{1}{2}\pi a(\omega\epsilon_0)^{-1}J_{|n|}(\sqrt{k^2 - \zeta^2}a)H_{|n|}^{(1)}(\sqrt{k^2 - \zeta^2}a) \quad (8.279)$$

$$\bar{M}_{z\theta}(\zeta) = \bar{M}_{\theta z}(\zeta) = -\frac{1}{2}\pi n\zeta(\omega\epsilon_0)^{-1}J_{|n|}(\sqrt{k^2 - \zeta^2}a)H_{|n|}^{(1)}(\sqrt{k^2 - \zeta^2}a) \quad (8.280)$$

$$\begin{aligned} \bar{M}_{\theta\theta}(\zeta) = & -\frac{1}{2}\pi(\omega\epsilon_0 a)^{-1}[n^2\zeta^2(k^2 - \zeta^2)^{-1}J_{|n|}(\sqrt{k^2 - \zeta^2}a)H_{|n|}^{(1)}(\sqrt{k^2 - \zeta^2}a) \\ & + k^2 a^2 J'_{|n|}(\sqrt{k^2 - \zeta^2}a)H_{|n|}^{(1)'}(\sqrt{k^2 - \zeta^2}a)] \end{aligned} \quad (8.281)$$

$$\bar{g}_z(\zeta) = -\frac{1}{2}i\pi a\sqrt{k^2 - \zeta^2}J_{|n|}(\sqrt{k^2 - \zeta^2}a)H_{|n|}^{(1)'}(\sqrt{k^2 - \zeta^2}a) \quad (8.282)$$

and

$$\begin{aligned} \bar{g}_\theta(\zeta) = & -\frac{1}{2}i\pi n\zeta(k^2 - \zeta^2)^{-\frac{1}{2}}[J_{|n|}(\sqrt{k^2 - \zeta^2}a)H_{|n|}^{(1)'}(\sqrt{k^2 - \zeta^2}a) \\ & + J'_{|n|}(\sqrt{k^2 - \zeta^2}a)H_{|n|}^{(1)}(\sqrt{k^2 - \zeta^2}a)] \end{aligned} \quad (8.283)$$

Let $M_{zz}(z)$ etc. be the functions whose Fourier transforms are $\overline{M}_{zz}(\zeta)$ etc., that is,

$$M_{ij}(z) = (2\pi)^{-1} \int_C \overline{M}_{ij}(\zeta) e^{-i\zeta z} d\zeta \quad (8.284)$$

and

$$g_i(z) = (2\pi)^{-1} \int_C \bar{g}_i(\zeta) e^{-i\zeta z} d\zeta \quad (8.285)$$

where $i, j = z, \theta$ and the contour of integration C is that shown in Fig. 8.3. It then follows from (8.246) that, for $|z| < h$,

$$\left(\frac{d^2}{dz^2} + k^2 \right) \int_{-h}^h M_{zz}(z - z') J_z(z') dz' + \int_{-h}^h M_{z\theta}(z - z') J_\theta(z') dz' + V g_z(z) = 0 \quad (8.286)$$

and

$$\int_{-h}^h M_{\theta z}(z - z') J_z(z') dz' + \int_{-h}^h M_{\theta\theta}(z - z') J_\theta(z') dz' + V g_\theta(z) = 0 \quad (8.287)$$

The behavior of J_z and J_θ near $z = \pm h$ is, of course,

$$J_z(z) = O(\sqrt{h^2 - z^2}) \quad (8.288)$$

and

$$J_\theta(z) = O \frac{1}{\sqrt{h^2 - z^2}} \quad (8.289)$$

Equations (8.286) and (8.287) are the desired integral equations. The behavior of the various functions near $z = 0$ is as follows:

$$M_{zz}(z) = -i(2\pi\omega\epsilon_0)^{-1} \ln |z| + O(1) \quad (8.290)$$

$$M_{z\theta}(z) = M_{\theta z}(z) = -n(2\pi\omega\epsilon_0 a)^{-1} z^{-1} + O(1) \quad (8.291)$$

$$M_{\theta\theta}(z) = -i(2\pi\omega\epsilon_0)^{-1} \left(k^2 - \frac{n^2}{a^2} \right) \ln |z| + O(1) \quad (8.292)$$

$$g_z(z) = \frac{1}{2} \delta(z) + O(\ln |z|) \quad (8.293)$$

and

$$g_\theta(z) = O(1) \quad (8.294)$$

In particular, the integrals in (8.286) and (8.287) involving $M_{z\theta}$ or $M_{\theta z}$ should be interpreted in the sense of principal values.

So far, n can be any integer, positive, zero, or negative. We now consider briefly the case $n = 0$. It follows from (8.280) and (8.283) that in this case

$$\overline{M}_{z\theta}(\zeta) = \overline{M}_{\theta z}(\zeta) = \bar{g}_\theta(\zeta) = 0 \quad (8.295)$$

Or, by (8.284) and (8.285),

$$M_{z\theta}(z) = M_{\theta z}(z) = g_\theta(z) = 0 \quad (8.296)$$

Moreover, by (8.296) and the integral equation (8.287),

$$J_\theta(z) = 0 \quad (8.297)$$

which is already contained in (8.52). The substitution of (8.296) and (8.297) into (8.286) gives

$$\left(\frac{d^2}{dz^2} + k^2 \right) \int_{-h}^h M_{zz}(z - z') J_z(z') dz' + V g_z(z) = 0 \quad (8.298)$$

Since $n = 0$, a comparison of (8.156) and (8.279) shows that

$$M_{zz}(z) = 2\pi i a (\omega \epsilon_0)^{-1} \mathcal{K}(z) \quad (8.299)$$

Since the total current is $2\pi a$ times the current density, that is,

$$g^+(z) = 2\pi a J_z(z) \quad (8.300)$$

the substitution of (8.299) into (8.298) gives

$$\left(\frac{d^2}{dz^2} + k^2 \right) \int_{-h}^h \mathcal{K}(z - z') g^+(z') dz' = i\omega \epsilon_0 V g_z(z) \quad (8.301)$$

To find the relation between g_z and W , we note, from (8.212) and (8.51), that

$$\begin{aligned} \bar{W}(\zeta, a) &= \int_{-\infty}^{\infty} W(z, a) e^{i\zeta z} dz \\ &= \int_0^a r dr \int_{-\pi}^{\pi} \frac{1}{4} i H_0^{(1)}(\sqrt{k^2 - \zeta^2} \sqrt{r^2 + a^2 - 2ra \cos \theta}) d\theta \\ &= \frac{1}{2} \pi i \int_0^a H_0^{(1)}(\sqrt{k^2 - \zeta^2} a) J_0(\sqrt{k^2 - \zeta^2} r) r dr \\ &= -\frac{1}{2} i \pi a (k^2 - \zeta^2)^{-1/2} H_0^{(1)}(\sqrt{k^2 - \zeta^2} a) J_0'(\sqrt{k^2 - \zeta^2} a) \end{aligned} \quad (8.302)$$

Accordingly, by (8.282),

$$\bar{g}_z(\zeta) = 1 + (k^2 - \zeta^2) \bar{W}(\zeta, a) \quad (8.303)$$

The inverse Fourier transform of (8.303) is simply

$$g_z(z) = \delta(z) + \left(\frac{d^2}{dz^2} + k^2 \right) W(z, a) \quad (8.304)$$

which can be substituted into (8.298) to give

$$\left(\frac{d^2}{dz^2} + k^2 \right) \left[\int_{-h}^h \mathcal{K}(z - z') g^+(z') dz' - ik\zeta_0^{-1} V W(z, a) \right] = ik\zeta_0^{-1} V \delta(z) \quad (8.305)$$

Equation (8.305) is equivalent to (8.243). It is interesting to note that the Fourier transform of $W(z, a)$, as given by (8.302), is of a rather simple form.

We conclude this section with a discussion of the case when the δ -function generator is *inside* the tubular antenna. In this case, the boundary conditions are, instead of (8.245) and (8.246),

$$E_z^{\text{ins}}(a+, \theta, z) = 0, \quad E_{\theta}^{\text{ins}}(a+, \theta, z) = 0 \quad (8.306)$$

$$\text{and} \quad E_z^{\text{ins}}(a-, \theta, z) = -V e^{in\theta} \delta(z) \quad E_{\theta}^{\text{ins}}(a-, \theta, z) = 0 \quad (8.307)$$

for $|z| < h$. Moreover, (8.271) to (8.276) still hold provided that V is replaced by $-V$. Let $r \rightarrow a+$; it follows from (8.271) and (8.275) that

$$\bar{E}_z^{\text{ins}}(a+, \zeta) = (k^2 - \zeta^2) \bar{M}_{zz}(\zeta) \bar{J}_z^{\text{ins}}(\zeta) + \bar{M}_{z\theta}(\zeta) \bar{J}_\theta^{\text{ins}}(\zeta) + V \bar{g}_z^{\text{ins}}(\zeta) \quad (8.308)$$

$$\text{and } \bar{E}_\theta^{\text{ins}}(a+, \zeta) = \bar{M}_{\theta z}(\zeta) \bar{J}_z^{\text{ins}}(\zeta) + \bar{M}_{\theta\theta}(\zeta) \bar{J}_\theta^{\text{ins}}(\zeta) + V \bar{g}_\theta^{\text{ins}}(\zeta) \quad (8.309)$$

$$\text{where } \bar{g}_z^{\text{ins}}(\zeta) = \frac{1}{2} i \pi a \sqrt{k^2 - \zeta^2} J'_{|n|}(\sqrt{k^2 - \zeta^2} a) H_{|n|}^{(1)}(\sqrt{k^2 - \zeta^2} a) \quad (8.310)$$

$$\text{and } \bar{g}_\theta^{\text{ins}}(\zeta) = -\bar{g}_\theta(\zeta) \quad (8.311)$$

Therefore, the coupled integral equations are in this case

$$\begin{aligned} \left(\frac{d^2}{dz^2} + k^2 \right) \int_{-h}^h M_{zz}(z - z') J_z^{\text{ins}}(z') dz' \\ + \int_{-h}^h M_{z\theta}(z - z') J_\theta^{\text{ins}}(z') dz' + V g_z^{\text{ins}}(z) = 0 \end{aligned} \quad (8.312)$$

$$\begin{aligned} \text{and } \int_{-h}^h M_{\theta z}(z - z') J_z^{\text{ins}}(z') dz' \\ + \int_{-h}^h M_{\theta\theta}(z - z') J_\theta^{\text{ins}}(z') dz' + V g_\theta^{\text{ins}}(z) = 0 \end{aligned} \quad (8.313)$$

for $|z| < h$. Or, by (8.310) and (8.311),

$$\begin{aligned} \left(\frac{d^2}{dz^2} + k^2 \right) \int_{-h}^h M_{zz}(z - z') J_z^{\text{ins}}(z') dz' \\ + \int_{-h}^h M_{z\theta}(z - z') J_\theta^{\text{ins}}(z') dz' + V \delta(z) - V g_z(z) = 0 \end{aligned} \quad (8.314)$$

and

$$\begin{aligned} \int_{-h}^h M_{\theta z}(z - z') J_z^{\text{ins}}(z') dz' \\ + \int_{-h}^h M_{\theta\theta}(z - z') J_\theta^{\text{ins}}(z') dz' - V g_\theta(z) = 0 \end{aligned} \quad (8.315)$$

If (8.314) is added to (8.286), and (8.315) to (8.287), then

$$\begin{aligned} \left(\frac{d^2}{dz^2} + k^2 \right) \int_{-h}^h M_{zz}(z - z') [J_z(z') + J_z^{\text{ins}}(z')] dz' \\ + \int_{-h}^h M_{z\theta}(z - z') [J_\theta(z') + J_\theta^{\text{ins}}(z')] dz' + V \delta(z) = 0 \end{aligned} \quad (8.316)$$

and

$$\begin{aligned} \int_{-h}^h M_{\theta z}(z - z') [J_z(z') + J_z^{\text{ins}}(z')] dz' \\ + \int_{-h}^h M_{\theta\theta}(z - z') [J_\theta(z') + J_\theta^{\text{ins}}(z')] dz' = 0 \end{aligned} \quad (8.317)$$

for $|z| < h$. These are the integral equations for the case where a δ -function generator is present both inside and outside the tubular antenna.

8.11 Conclusions

In this chapter, we have developed the integral equation for the current in a transmitting dipole antenna. Much of the material is not new, but is well known to people working in the field. Rather, we attempt to present the argument in a reasonably systematic way, with emphasis on what we do or do not know. It is beyond the ability of the author to trace the history of the development; we shall merely summarize the content of this chapter and give a few references.

Most of the existing numerical calculation about properties of the transmitting dipole antenna is carried out on the basis of (8.58). It was realized a long time ago, for example, by Schelkunoff,⁹ that this rather naive equation has no integrable solution, as shown in Sec. 8.3. This does not mean, however, that numerical results obtained on the basis of (8.58) are meaningless. In searching for an integral equation without this defect, it is useful to study the model of an infinite circular tubular antenna. This model is solved in Sec. 8.4, part of which may be compared with the work of Hallén.¹⁰ It then becomes clear how (8.58) should be modified to give (8.117), which can be found, for example, in the book by Schelkunoff⁹ or in the work of Kapitza, Fok, and Vainshtein.¹¹ Inasmuch as the kernel of the integral equation (8.117) is very much more complicated than that of (8.58), relatively little numerical calculation has been carried out on the basis of (8.117). Fortunately, as shown in Secs. 8.6 and 8.7, the iterative solutions of (8.58) and (8.117) are virtually identical for thin antennas except near the driving point, at least when the number of iterations is small. Thus most of the existing numerical calculations on the basis of (8.58) are still useful in the sense that they are also applicable approximately to (8.117). On closer examination, as first noticed by King and the author,¹² (8.117) still needs to be modified by the inclusion of an additional term, because (8.117) actually corresponds to a problem with an extraneous generator inside the tubular antenna. In order to eliminate the extraneous generator, the scalar potential cannot be continuous. When this is properly taken into account, (8.117) is further modified to (8.243). For thin antennas, the solution of (8.117) and that of (8.243) are again close except near the driving point. For better understanding, a more general problem¹³ is studied in Sec. 8.10, where the driving voltage depends on the angle θ .

Both of the integral equations (8.117) and (8.243) still have the defect that the reactive component of the input current is not finite. This is intimately connected with the δ -function generator,¹⁴ and the removal of this infinity requires an examination of the transmission line.¹⁵ In the case of a coaxial line driving the antenna, this problem of the end correction is treated in Chap. 10. A similar problem exists in the more general case of Sec. 8.10. However, for $n \neq 0$, we have at present no understanding whatsoever of the problem of end corrections.

At the beginning of this chapter, in Sec. 8.1, the time-dependent problem is formulated. However, so far we have failed to discuss the transient problem

connected with linear antennas. Most of the existing work on antenna transients gives results in terms of the Fourier transforms of steady-state solutions. Although these results are very interesting and very useful, they are outside the scope of the chapter. In the next section, the last one of the chapter, we shall discuss an exactly solved problem of transients on linear antennas, the solution involves more than straightforward Fourier transformation.

8.12 Transient Response of a Dipole Antenna

Although many approximate methods have been devised to deal with the dipole antenna of finite length, rather few cases have been solved exactly. In this section we present such a case; more precisely, we consider the initial behavior of the transient response of the circular tubular antenna, as shown in Fig. 8.4. For $t \leq h/c$, the dipole behaves as though it were infinitely long, and, for this reason, an exact solution is possible. We restrict ourselves to this time interval $t \leq h/c$, and accordingly it is sufficient to study the infinite tubular antenna. The driving voltage is chosen to be a step function in time:¹⁶

$$\mathcal{E}_z(a, \theta, z, t) = \begin{cases} 0 & \text{for } t < 0 \\ -V\delta(z) & \text{for } t > 0 \end{cases} \quad (8.318)$$

The problem is rotationally symmetrical with respect to θ , provided that

$$\mathcal{E}_\theta(a, \theta, z, t) = 0 \quad (8.319)$$

This problem was solved in Ref. 16, and also later by Morgan.¹⁷ However, in both of these papers, an infinite number of terms is incorrectly omitted. We shall follow the procedure of Ref. 16.

It follows from (8.11) and (8.15) that

$$\frac{\partial \mathcal{E}_z}{\partial t} = -\frac{\partial^2 \mathcal{Q}_z}{\partial t^2} + c^2 \frac{\partial^2 \mathcal{Q}_z}{\partial z^2} \quad (8.320)$$

In (8.320) we have made use of the fact that \mathcal{Q} has only a z component. The substitution of (8.318) into (8.320) gives, for $r = a$,

$$\left(\frac{\partial^2}{\partial z^2} - c^{-2} \frac{\partial^2}{\partial t^2} \right) \mathcal{Q}_z = -c^{-2} V \delta(z) \delta(t) \quad (8.321)$$

On the other hand, let $\hat{\mathbf{z}}g(z, t)$ be the total current on the dipole antenna. Then, by (8.36) and (8.16), the vector potential may be expressed as

$$\mathcal{Q}_z(\mathbf{r}, t) = \mu_0 \int_{-\infty}^{\infty} dz' \int_{-\infty}^{\infty} g(z', t') dt' (2\pi)^{-1} \int_{-\pi}^{\pi} \mathcal{G}(\mathbf{r} - \mathbf{r}', t - t') d\theta' \quad (8.322)$$

Because of (8.322), it is convenient to define the kernel κ by

$$\kappa(z, t) = (2\pi)^{-1} \int_{-\pi}^{\pi} \mathcal{G}(\mathbf{r} - \mathbf{r}', t) d\theta' \quad (8.323)$$

where $\mathbf{r} = (a, 0, z)$ and $\mathbf{r}' = (a, \theta, 0)$. By (8.47), κ is more explicitly

$$\kappa(z, t) = (8\pi^2 ct)^{-1} \int_{-\pi}^{\pi} \delta \left[\sqrt{z^2 + \left(2a \sin \frac{\theta}{2} \right)^2} - ct \right] d\theta \tag{8.324}$$

In terms of this kernel, the integral equation resulting from the substitution of (8.322) into (8.321) is

$$\left(\frac{\partial^2}{\partial z^2} - c^{-2} \frac{\partial^2}{\partial t^2} \right) \int_{-\infty}^{\infty} dz' \int_{-\infty}^{\infty} g(z', t') \kappa(z - z', t - t') dt' = -c^{-1} \zeta_0^{-1} V \delta(z) \delta(t) \tag{8.325}$$

Equation (8.325) is invariant under the formal one-dimensional orthochronous Lorentz transformation

$$\begin{aligned} \mathcal{L}z &= z \cosh \phi + ct \sinh \phi \\ \mathcal{L}ct &= z \sinh \phi + ct \cosh \phi \end{aligned} \tag{8.326}$$

This is the underlying reason for the simplicity of the present problem. To make use of this invariance, introduce a formal “photon mass” $m > 0$ and consider (8.325) to be the limit as $m \rightarrow 0+$ of

$$\begin{aligned} \left(\frac{\partial^2}{\partial z^2} - c^{-2} \frac{\partial^2}{\partial t^2} - m^2 \right) \int_{-\infty}^{\infty} dz' \int_{-\infty}^{\infty} g(z', t) \kappa(z - z', t - t') dt' \\ = -c^{-1} \zeta_0^{-1} V \delta(z) \delta(t) \end{aligned} \tag{8.327}$$

The Green’s function g for the one-dimensional Klein-Gordon equation

$$\left(\frac{\partial^2}{\partial z^2} - c^{-2} \frac{\partial^2}{\partial t^2} - m^2 \right) g(z, t) = -\delta(z) \delta(t) \tag{8.328}$$

has the representation

$$g(z, t) = -(2\pi)^{-2} \int_{S_0} (c^{-2} \omega^2 - k^2 - m^2)^{-1} \exp [i(kz - \omega t)] dk d\omega \tag{8.329}$$

It is desired to choose the complex surface of integration S_0 so that the g of

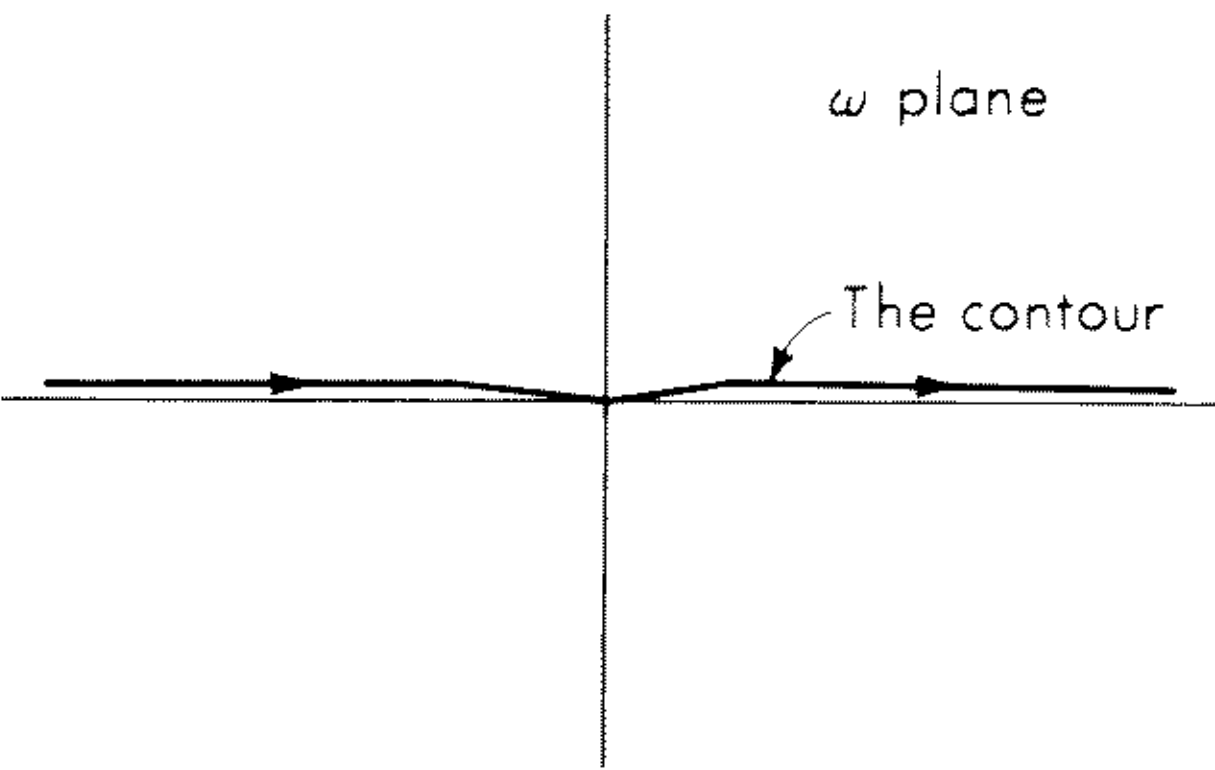


Fig. 8.7 Projection of C_0 on the ω plane.

(8.329) is the *retarded* Green's function and also that S_0 is invariant under the formal Lorentz transformation in the momentum space

$$\begin{aligned}\mathcal{L}k &= k \cosh \phi + c^{-1}\omega \sinh \phi \\ \mathcal{L}c^{-1}\omega &= k \sinh \phi + c^{-1}\omega \cosh \phi\end{aligned}\quad (8.330)$$

Let C_0 be a contour where $k = 0$ and ω ranges from $-\infty$ to ∞ slightly above the real axis except for a dip to pass through the origin, as shown in Fig. 8.7. (This contour is different from that of Ref. 16.) Then a possible choice for S_0 is

$$\begin{aligned}S_0: \quad k, \omega \text{ both real if } |ck| > |\omega| \\ S_0 = \mathcal{L}C_0 \quad \text{if } |\omega| > |ck|\end{aligned}\quad (8.331)$$

The kernel κ has the integral representation

$$\kappa(z, t) = (2\pi)^{-2} \int_{-\infty}^{\infty} dk \int_{-\infty}^{\infty} \bar{\kappa}(k, \omega) \exp [i(kz - \omega t)] d\omega \quad (8.332)$$

where

$$\bar{\kappa}(k, \omega) = \begin{cases} \frac{1}{4}iH_0^{(1)}(a\sqrt{\omega^2 - k^2c^2}/c)J_0(a\sqrt{\omega^2 - k^2c^2}/c) & \text{for } \omega > |ck| \\ -\frac{1}{4}iH_0^{(2)}(a\sqrt{\omega^2 - k^2c^2}/c)J_0(a\sqrt{\omega^2 - k^2c^2}/c) & \text{for } \omega < -|ck| \\ (2\pi)^{-1}K_0(a\sqrt{k^2c^2 - \omega^2}/c)I_0(a\sqrt{k^2c^2 - \omega^2}/c) & \text{for } |\omega| < |ck| \end{cases} \quad (8.333)$$

Thus the solution of (8.327) is

$$\mathcal{g}(z, t) = (2\pi)^{-2} \int_{S_0} \bar{\mathcal{g}}(k, \omega) \exp [i(kz - \omega t)] dk d\omega \quad (8.334)$$

$$\text{where} \quad \bar{\mathcal{g}}(k, \omega) = -c^{-1}\zeta_0^{-1}V(c^{-2}\omega^2 - k^2 - m^2)^{-1}[\bar{\kappa}(k, \omega)]^{-1} \quad (8.335)$$

In order to evaluate (8.334), divide the surface S_0 into four pieces: (1) $\text{Re } \omega > |ck|$; (2) $ck > |\omega|$; (3) $-\text{Re } \omega > |ck|$; and (4) $-ck > |\omega|$. Let \mathcal{g}_i , $i = 1, \dots, 4$, be the contributions to \mathcal{g} of (8.334) from these four regions, respectively. With the variable $\sqrt{\omega^2 - c^2k^2}/c$, it may be verified that

$$\mathcal{g}_i(z, t) = -(\pi\zeta_0)^{-1}V \int_{C_i} (\zeta^2 - m^2)^{-1}[\frac{1}{4}iH_0^{(1)}(a\zeta)J_0(a\zeta)]^{-1}\mathfrak{F}_i(z, t; \zeta)\zeta d\zeta \quad (8.336)$$

In (8.336), the four contours of integration are as follows: C_1 is from 0 to ∞ just above the positive real axis, C_2 and C_4 are both from $i\infty$ to 0 along the positive imaginary axis, and C_3 is from 0 to $-\infty$ just above the negative real axis. The functions \mathfrak{F}_i are explicitly given in Table 8.1. From Table 8.1, it is seen that

$$\mathcal{g}_1(z, t) + \mathcal{g}_4(z, t) = \mathcal{g}_2(z, t) + \mathcal{g}_3(z, t) = 0 \quad (8.337)$$

for $z > ct$, and

$$\mathcal{g}_1(z, t) + \mathcal{g}_2(z, t) = \mathcal{g}_3(z, t) + \mathcal{g}_4(z, t) = 0 \quad (8.338)$$

for $z < -ct$. Therefore

$$\mathcal{g}(z, t) = 0 \quad (8.339)$$

unless $|z| \leq ct$. For $|z| < ct$, it follows from Table 8.1 that

$$\mathcal{g}(z, t) = 2(\pi\zeta_0)^{-1}V \int (\zeta^2 - m^2)^{-1}J_0(\zeta\sqrt{c^2t^2 - z^2})[H_0^{(1)}(a\zeta)J_0(a\zeta)]^{-1}\zeta d\zeta \quad (8.340)$$

TABLE 8.1 VALUES OF \mathfrak{F}_i

[For example, in the region $z > c|t|$, $\mathfrak{F}_1 = (2\pi)^{-1}K_0(\zeta\sqrt{z^2 - c^2t^2})$]

Region	$ z < ct$	$z > c t $	$ z < -ct$	$z < -c t $
Argument	$\zeta\sqrt{c^2t^2 - z^2}$	$\zeta\sqrt{z^2 - c^2t^2}$	$\zeta\sqrt{c^2t^2 - z^2}$	$\zeta\sqrt{z^2 - c^2t^2}$
\mathfrak{F}_1	$-\frac{1}{4}iH_0^{(2)}$	$(2\pi)^{-1}K_0$	$\frac{1}{4}iH_0^{(1)}$	$(2\pi)^{-1}K_0$
\mathfrak{F}_2	$\frac{1}{4}iH_0^{(1)}$	$(2\pi)^{-1}K_0 + \frac{1}{2}iI_0$	$\frac{1}{4}iH_0^{(1)}$	$(2\pi)^{-1}K_0$
\mathfrak{F}_3	$\frac{1}{4}iH_0^{(1)} + \frac{1}{2}iJ_0$	$(2\pi)^{-1}K_0 + \frac{1}{2}iI_0$	$\frac{1}{4}iH_0^{(1)}$	$(2\pi)^{-1}K_0 + \frac{1}{2}iI_0$
\mathfrak{F}_4	$\frac{1}{4}iH_0^{(1)}$	$(2\pi)^{-1}K_0$	$\frac{1}{4}iH_0^{(1)}$	$(2\pi)^{-1}K_0 + \frac{1}{2}iI_0$

where the contour of integration is that shown in Fig. 8.7 and the limit $m \rightarrow 0+$ remains to be taken.

We note that the integrand on the right-hand side of (8.340) has poles at the zeros of $J_0(a\zeta)$. Let τ_j be the values where J_0 vanishes; thus, approximately, $\tau_1 = 2.4048$, $\tau_2 = 5.5201$, $\tau_3 = 8.6537$, etc. Consequently, with $m \rightarrow 0+$, the current is given by

$$g(z,t) = 4\zeta_0^{-1}V\left\{\frac{1}{\pi}\int_0^\infty \frac{J_0(\zeta\sqrt{c^2t^2 - z^2}/a)}{[J_0(\zeta)]^2 + [Y_0(\zeta)]^2} \frac{d\zeta}{\zeta} - \sum_{j=1}^\infty \frac{J_0(\tau_j\sqrt{c^2t^2 - z^2}/a)}{\tau_j J'_0(\tau_j) Y_0(\tau_j)}\right\} \tag{8.341}$$

for $|z| < ct$. The sum in (8.341) represents currents associated with the various circularly symmetric waveguide modes excited inside the tubular antenna. It is this sum that is incorrectly omitted in the papers.^{16,17} It is perhaps interesting to note that

$$J'_0(\tau_j)Y_0(\tau_j) < 0 \tag{8.342}$$

for all j . It is trivial to write down separately expressions for the currents inside and outside the tubular antenna. But we shall not go into this point here.

The desired answer (8.341) is already quite complicated. If the tubular antenna is finite, (8.341) holds only for $t \leq h/c$. It is in principle straightforward to use the Wiener-Hopf procedure to find exactly the current for $h/c < t \leq 3h/c$, $3h/c < t \leq 5h/c$, etc., but, so far as the author is aware, this has not been explicitly carried out. In any case, for $t > h/c$, there is no invariance under (8.326), and consequently the results are most probably too complicated to be instructive.

It is worth emphasizing that our knowledge about the transient response of antennas is very meager indeed. Any progress in this rather neglected field is certainly going to be of tremendous value.

Acknowledgments

I am greatly indebted to Professor Ronold W. P. King for his guidance on the subject of antennas since my student days. For helpful discussions, I am also grateful to Professors S. R. Seshadri and David Chang.

REFERENCES

1. Wentzel, G.: "The Quantum Theory of Fields," Interscience Publishers, Inc., New York, 1949.
2. Sommerfeld, A.: *Jahrb. Deut. Math. Ver.*, vol. 21, p. 326, 1912.
3. Seshadri, S. R., and T. T. Wu: to be published
4. King, L. V.: Radiation Field of a Perfectly Conducting Base Insulated Cylindrical Aerial over a Perfectly Conducting Plane Earth and the Calculation of Radiation Resistance and Reactance, *Phil. Trans. Roy. Soc. (London)*, vol. 236A, pp. 381-422, 1937. E. Hallén: Theoretical Investigations into the Transmitting and Receiving Qualities of Antennae, *Nova Acta Regiae Soc. Sci. Upsaliensis*, vol. 11, no. 4, 1938.
5. King, R. W. P.: "Linear Antennas," Harvard University Press, Cambridge, Mass., 1956.
6. King, R. W. P., and D. Middleton: The Cylindrical Antenna; Current and Impedance, *Quart. Appl. Math.*, vol. 3, pp. 302-335, 1946.
7. Bateman Project Staff, A. Erdelyi (ed.): "Higher Transcendental Functions," vol. II, McGraw-Hill Book Company, New York, 1953.
8. Chang, David: doctoral dissertation, Harvard University, 1967.
9. Schelkunoff, S. A.: "Advanced Antenna Theory," chap. 5, John Wiley & Sons, Inc., New York, 1952.
10. Hallén, E.: "Electromagnetic Theory," John Wiley & Sons, Inc., New York, 1962.
11. Kapitza, P. L., V. A. Fok, and L. A. Vainshtein: Symmetric Electric Oscillation of an Ideally Conducting Hollow Cylinder of Finite Length, *Soviet Phys.-Techn. Phys.*, vol. 4, pp. 1088-1105, 1960.
12. Wu, T. T., and R. W. P. King: The Thick Tubular Transmitting Antenna, *Radio Sci.*, vol. 2, pp. 1061-1065, 1967.
13. Seshadri, S. R., and T. T. Wu: An Integral Equation for the Current in an Asymmetrically Driven Cylindrical Antenna, *Proc. IEEE*, vol. 55, p. 1097, 1967.
14. Wu, T. T., and R. W. P. King: Driving Point and Input Admittance of Linear Antennas, *J. Appl. Phys.*, vol. 30, pp. 74-76, 1959.
15. Wu, T. T.: Input Admittance of Linear Antennas Driven from a Coaxial Line, *J. Res. Natl. Bur. Std. (U.S.)*, vol. 67D, pp. 83-89, 1963. See also T. T. Wu, Input Admittance of Infinitely Long Dipole Antennas Driven from Coaxial Lines, *J. Math. Phys.*, vol. 3, pp. 1298-1301, 1962.
16. Wu, T. T.: Transient Response of a Dipole Antenna, *J. Math. Phys.*, vol. 2, pp. 892-894, 1961.
17. Morgan, S. P.: Transient Response of a Dipole Antenna, *J. Math. Phys.*, vol. 3, pp. 564-565, 1962.

CHAPTER 9

CYLINDRICAL ANTENNAS AND ARRAYS

Ronold W. P. King

9.1 Introduction

The purpose of this chapter is to develop a practical theory of the thin cylindrical antenna and arrays of such antennas when used for transmission or reception. Beginning with the basic integral equations, solutions are to be sought for the circuit and field properties. These are the distribution of current along and the driving-point admittance of each element, the radiation field of transmitting antennas, and the effective length of receiving antennas. Related quantities of interest are the distributions of charges and the electromagnetic field near each antenna. Solutions are called practical if they combine reasonable quantitative accuracy with formal simplicity in a physically meaningful representation. Such solutions can be used, on the one hand, to solve engineering problems and, on the other hand, to illuminate the underlying physical principles in their relation to actual situations.

The first problem considered is the isolated center-driven cylindrical antenna of relatively small radius constructed of a metallic conductor that need not be perfect. It is imbedded in an infinite homogeneous and isotropic medium characterized by arbitrary dielectric constant and permeability. Initially the conductivity is also arbitrary, but eventually the conductivity of the medium is restricted to values that are not too high. Owing to algebraic complications the actual solution for currents and admittances is carried out for a nonconducting medium, but the application to a more general medium is pointed out. It is shown that highly conducting antennas may be treated as if perfectly conducting, and the complete electromagnetic field is determined for this case. Its evaluation in the more general situation of an imperfectly conducting antenna involves somewhat greater mathematical difficulties.

The second problem is the analysis of the center-loaded receiving antenna in a plane-wave incident field. The distributions of currents and charges, the effective length, the power in the load, and the electromagnetic field near the antenna when functioning as a scatterer are determined.

The final problem is that of an array of parallel nonstaggered antennas in circular or curtain arrays. The currents in the several elements, their driving-point admittances, and the distant electromagnetic field are studied.

9.2 The Internal Impedance and the Vector Potential of a Transmitting Antenna

Consider the antenna shown in Fig. 9.1. It consists of a thin metal cylinder of radius a and half length h center-driven by a δ -function generator with

emf V_0^e at an angular frequency ω . The internal impedance per unit length¹ of the conductor is z^i . For solid conductors for which $a\sqrt{\omega\mu_1\sigma_1} \geq 10$ or tubular conductors with walls that have a thickness d that is large compared to the skin

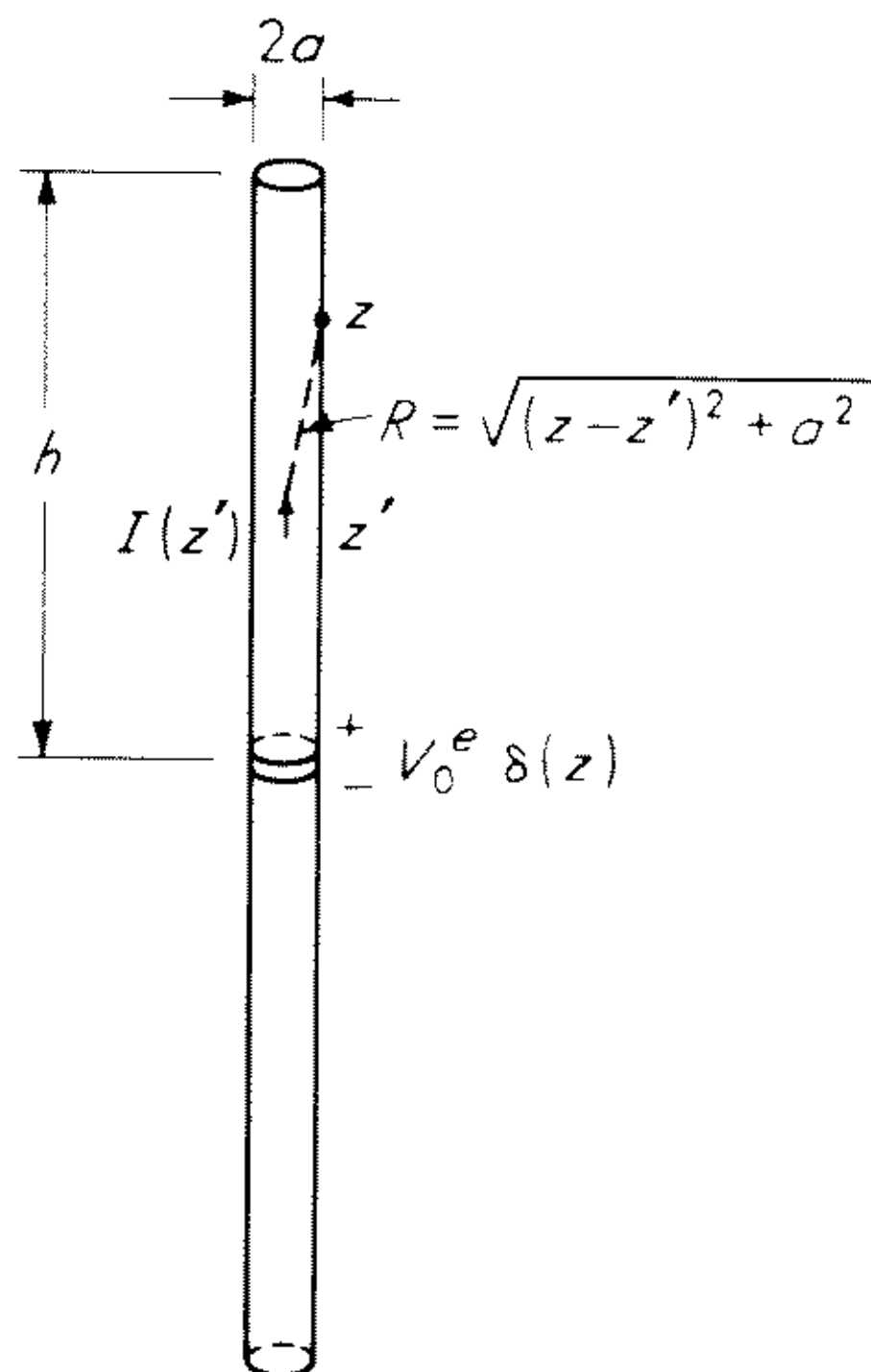


Fig. 9.1 Cylindrical antenna.

depth d_s ($d \gg d_s = \sqrt{2/\omega\mu_1\sigma_1}$), it is given by $z^i = (1+j)(2\pi a\sigma_1 d_s)^{-1} = \zeta_s/2\pi a$ (see Sec. 1.7). If the walls of the tube are thinner than the skin depth ($d < d_s$), the impedance per unit length is essentially the dc resistance, $z^i \doteq r_0 = (2\pi a\sigma_1 d)^{-1}$. The antenna is immersed in an infinite medium characterized by the constants σ , ϵ , and μ . It is assumed that the conductivity of the medium is small compared with that of the cylindrical conductor ($\sigma_1 \gg \sigma$).

From the definition of the internal impedance per unit length, the electric field at the surface $r = a$ of the antenna is given by $E_z(r = a) = I_z z^i$. In terms of the scalar and vector potentials Φ and \mathbf{A} at points outside the antenna, this same field is given by $E_z = -\partial\Phi/\partial z - j\omega A_z$. This is true except at $z = 0$, where the generator maintains the additional field $E_z = -V_0^e \delta(z)$. If use is made of the Lorentz condition $\nabla \cdot \mathbf{A} + j(k^2/\omega)\Phi = 0$ and the boundary condition $E_z(r = a)$ is continuous, the following equation is obtained at $r = a$, $-h \leq z \leq h$:

$$\left(\frac{\partial^2}{\partial z^2} + k^2\right)A_z(z) = j\frac{k^2}{\omega}[z^i I_z(z) - V_0^e \delta(z)] \quad (9.1)$$

where

$$k = \beta - j\alpha = \omega\sqrt{\mu\epsilon}\left(1 - \frac{j\sigma}{\omega\epsilon}\right) = \omega\sqrt{\mu\epsilon} \quad (9.2)$$

is the complex propagation constant of the infinite medium. The complex parameter

$$\epsilon = \epsilon - \frac{j\sigma}{\omega} = \epsilon' - j\epsilon'' - \frac{j(\sigma' - j\sigma'')}{\omega} = \left(\epsilon' - \frac{\sigma''}{\omega}\right) - j\left(\epsilon'' + \frac{\sigma'}{\omega}\right)$$

Exercise 9.1 Show that the real and imaginary parts of k in (9.2) may be separated by means of the tabulated functions², $f(p) = \cosh (1/2 \sinh^{-1} p)$, $g(p) = \sinh (1/2 \sinh^{-1} p)$ in $\sqrt{1 \pm jp} = f(p) \pm jg(p)$.

If the radius a and the real part of the propagation constant satisfy the inequality $\beta a \ll 1$, the vector potential on the surface of the antenna is given approximately by†

$$A_z(z) = \frac{\mu}{4\pi} \int_{-h}^h I_z(z') K(z, z') dz' \quad (9.3)$$

where
$$K(z, z') = \frac{e^{-jkR}}{R} \quad R = \sqrt{(z - z')^2 + a^2} \quad (9.4)$$

The kernel (9.4) may be separated into the following two parts:

$$K(z, z') = K_R(z, z') + jK_I(z, z') \quad (9.5)$$

where
$$K_R(z, z') = R^{-1} \cos kR \quad (9.6a)$$

$$K_I(z, z') = -R^{-1} \sin kR \quad (9.6b)$$

[Note that (9.5) does not separate real and imaginary parts of the kernel except when $\alpha = 0$.] This separation is made because the properties of the two parts of the kernel are very different when the variable point z' on the surface of the antenna approaches the fixed point z where the vector potential is evaluated. Consider specifically the associated parts (not the real and imaginary parts) of the vector potential $A_z(z) = A_R(z) + jA_I(z)$, where

$$A_R(z) = \frac{\mu}{4\pi} \int_{-h}^h I_z(z') K_R(z, z') dz' \quad (9.7a)$$

$$A_I(z) = \frac{\mu}{4\pi} \int_{-h}^h I_z(z') K_I(z, z') dz' \quad (9.7b)$$

When $z' \rightarrow z$, $R \rightarrow a$, so that, with $\alpha \leq \beta$ and $\beta a \ll 1$, $|ka| \ll 1$ and

$$\frac{K_R(z, z')}{k} \rightarrow \frac{\cos ka}{ka} \doteq \frac{1}{ka} \gg 1 \quad (9.8a)$$

$$\frac{K_I(z, z')}{k} \rightarrow \frac{-\sin ka}{ka} \doteq -1 \quad (9.8b)$$

†Extensive computations in R. W. P. King, E. A. Aronson, and C. W. Harrison, Jr., Determination of the Admittance and Effective Length of Cylindrical Antennas, *Radio Sci.*, vol. 1, July, 1966, show that the approximate kernel (9.4) yields essentially the same results as the exact kernel for a tubular antenna,

$$K(z, z') = \frac{1}{2\pi} \int_{-h}^h \frac{e^{-jkR(\theta)}}{R(\theta)} d\theta$$

with $R(\theta) = \sqrt{(z - z')^2 + [2a \sin (\theta/2)]^2}$ for antennas with $|ka| \leq 0.1$.

Clearly, $K_R(z, z')$ has a sharp peak near $z' = z$, so that whatever the distribution of current $I_z(z)$, provided only that it varies slowly over distances comparable with $10a$, the function $A_R(z)$ must vary with z much as does $I_z(z)$, since the kernel greatly magnifies the contributions to the integral from elements of current at and near $z' = z$. Since $I_z(h) = 0$, the vector potential difference $A_R(z) - A_R(h)$ should be approximately proportional to $I_z(z)$ at all points along the antenna. That is,

$$4\pi\mu^{-1}[A_R(z) - A_R(h)] = \Psi(z)I_z(z) \doteq \Psi I_z(z) \quad (9.9)$$

where Ψ is the approximately constant value of $\Psi(z)$ defined at a suitable reference value of z . In general, this is at the maximum of current.

The kernel $K_I(z, z')$ has no peak at $z' = z$, so that contributions to $A_I(z)$ must come almost equally from elements of current over a range of values of $|z' - z|$ which is quite wide when αh is small or zero. It follows that an approximate form of $K_I(z, z')/k$ is

$$\frac{K_I(z, z')}{k} = -\frac{2 \sin \frac{1}{2}kR \cos \frac{1}{2}kR}{kR} \doteq -\cos \frac{1}{2}kR \quad (9.10)$$

over a range $|kR| \leq 3.5$. Hence,

$$A_I(z) \doteq -\frac{k\mu}{4\pi} \int_0^h I(z') (\cos \frac{1}{2}kR_1 + \cos \frac{1}{2}kR_2) dz' \quad (9.11)$$

where $R_1 = \sqrt{(z' - z)^2 + a^2} \doteq |z' - z|$ and $R_2 = \sqrt{(z' + z)^2 + a^2} \doteq |z' + z|$.

Exercise 9.2 Compare the functions $(\sin kR)/kR$ and $\cos (kR/2)$ in the range $kR \leq 3.5$ when $\alpha = 0$ and so verify that (9.11) is a very good approximation of (9.7b).

The principal part of (9.11) is

$$A_I(z) \doteq A_I(0) \cos \frac{1}{2}kz \quad (9.12a)$$

$$\text{where} \quad A_I(0) = -\frac{k\mu}{4\pi} \int_{-h}^h I(z') \cos \frac{1}{2}kz' dz' \quad (9.12b)$$

is a constant. It is seen that in this approximation the z dependence of $A_I(z)$ is actually independent of the distribution of current $I_z(z')$. For values of βh that do not much exceed π , the representation (9.12a,b) is a satisfactory approximation.

If use is made of (9.9) to eliminate $I_z(z)$ from (9.1) and $k^2 A_z(h)$ is subtracted from both sides, it becomes

$$\begin{aligned} \left(\frac{\partial^2}{\partial z^2} + k^2 \right) [A_z(z) - A_z(h)] &= \frac{j4\pi z^i k}{\zeta \Psi} [A_R(z) - A_R(h)] \\ &\quad - k^2 A_z(h) - j \frac{k^2}{\omega} V_0^e \delta(z) \end{aligned} \quad (9.13)$$

where $\zeta = \omega\mu/k$. It is now convenient to define the complex constant k_c by

$$k_c^2 = k^2 \left(1 - \frac{j4\pi z^i}{k\zeta\Psi} \right) \quad (9.14)$$

and make use of (9.12a). With these, (9.13) becomes

$$\begin{aligned} \left(\frac{\partial^2}{\partial z^2} + k_c^2 \right) [A_z(z) - A_z(h)] &= j(k_c^2 - k^2)A_I(0) \cos \frac{1}{2}kz \\ &\quad - [k^2 A_R(h) + jk_c^2 A_I(h)] - j \frac{k^2}{\omega} V_0^e \delta(z) \end{aligned} \quad (9.15)$$

This is a differential equation for the vector potential difference. It has the solution

$$\begin{aligned} 4\pi\mu^{-1}[A_z(z) - A_z(h)] \\ = \frac{-j4\pi k}{\zeta k_c} [C_1 \cos k_c z + \frac{1}{2}V_0^e \sin k_c |z| + D \cos \frac{1}{2}kz + U_k] \end{aligned} \quad (9.16)$$

$$\text{where} \quad U_k = \frac{-j\omega k_c}{k^2} \left[\frac{k^2}{k_c^2} A_R(h) + jA_I(h) \right] \quad (9.17)$$

$$D = \frac{-\omega k_c}{k^2} \left(\frac{k_c^2 - k^2}{k_c^2 - k^2/4} \right) A_I(0) \quad (9.18)$$

The arbitrary constant C_1 can be expressed in terms of U_k , D , and V_0^e if z is set equal to h in (9.16). Thus,

$$C_1 = -(\frac{1}{2}V_0^e \sin k_c h + D \cos \frac{1}{2}kh + U_k) \sec k_c h \quad (9.19)$$

9.3 Integral Equation for the Current and Its Approximate Solution

If (9.19) is substituted in (9.16), the quantity $\cos \frac{1}{2}kh \cos k_c h$ is added and subtracted in the coefficient of D , and the integral (9.3) is used on the left, the following integral equation is obtained for the current $I_z(z)$ in the antenna:

$$\int_{-h}^h I_z(z') K_d(z, z') dz' = \frac{j4\pi k}{k_c \zeta \cos k_c h} (\frac{1}{2}V_0^e M_{kz} + U'_k F_{kz} - DH_{0z} \cos k_c h) \quad (9.20)$$

$$\text{where} \quad U'_k = U_k + D \cos \frac{1}{2}kh \quad (9.21)$$

$$\begin{aligned} M_{kz} &= \sin k_c(h - |z|) & F_{kz} &= \cos k_c z - \cos k_c h \\ H_{0z} &= \cos \frac{1}{2}kz - \cos \frac{1}{2}kh \end{aligned} \quad (9.22)$$

and the difference kernel is

$$K_d(z, z') = K(z, z') - K(h, z') = R^{-1}e^{-jkR} - R_h^{-1}e^{-jkR_h} \quad (9.23)$$

with $R_h = \sqrt{(h - z')^2 + a^2}$. R is defined in (9.4). Also let $K_{dR}(z, z') = K_R(z, z') - K_R(h, z')$, $K_{dI}(z, z') = K_I(z, z') - K_I(h, z')$.

A solution of the integral equation (9.20) for the current $I_z(z)$ along an imperfectly conducting antenna immersed in an infinite imperfect dielectric medium may be carried out with the help of the principles that are involved in

(9.9) and (9.12a). Specifically, the leading terms in the integral in (9.20) obey the following relations:

$$\int_{-h}^h I_z(z') K_{dR}(z, z') dz' \approx I_z(z) \quad (9.24a)$$

$$\int_{-h}^h I_z(z') K_{dI}(z, z') dz' \approx H_{0z} \quad (9.24b)$$

where H_{0z} is defined in (9.22). With these considerations and an examination of the right side of (9.20), it is clear that the principal part of the current in the antenna may be expressed quite accurately in the form

$$I_z(z) = I_V(z) + I_U(z) + I_D(z) \quad (9.25)$$

where $I_V(z) \doteq I_V M_{kz} \quad I_U(z) \doteq I_U F_{kz} \quad I_D(z) \doteq I_D H_{0z} \quad (9.26)$

If (9.25) is substituted in (9.20), the following integrals are obtained; they may be approximated as shown

$$\int_{-h}^h I_V(z') K_{dR}(z, z') dz' = I_V(z) \Psi_{dR} + \gamma_V(z) \quad (9.27a)$$

$$\int_{-h}^h I_U(z') K_{dR}(z, z') dz' = I_U(z) \Psi_{dUR} + \gamma_U(z) \quad (9.27b)$$

$$\int_{-h}^h I_D(z') K_d(z, z') dz' = I_D(z) \Psi_{dD} + \gamma_D(z) \quad (9.27c)$$

$$\int_{-h}^h I_V(z') K_{dI}(z, z') dz' = I_D(z) T_D^{-1} \Psi_{dI} + \gamma_I(z) \quad (9.27d)$$

$$\int_{-h}^h I_U(z') K_{dI}(z, z') dz' = I_D(z) T_U T_D^{-1} \Psi_{dUI} + \gamma_J(z) \quad (9.27e)$$

where the shorthands $T_D = I_D/I_V$, $T_U = I_U/I_V$ are used. The γ 's are small correction terms that are neglected in a zero-order solution. Explicit formulas for the several Ψ functions are given later. With these approximate formulas, (9.20) is reduced to an algebraic equation which is satisfied by

$$I_V(z) = I_V M_{kz} - \frac{\gamma_V(z)}{\Psi_{dR}} \quad I_V = \frac{j2\pi k V_0^e}{\zeta k_c \Psi_{dR} \cos k_c h} \quad (9.28a)$$

$$I_U(z) = I_U F_{kz} - \frac{\gamma_U(z)}{\Psi_{dUR}} \quad I_U = \frac{j4\pi k (U_k + D \cos \frac{1}{2}kh)}{\zeta k_c \Psi_{dUR} \cos k_c h} \quad (9.28b)$$

$$I_D(z) = I_D H_{0z} - \frac{\gamma_D(z)}{\Psi_{dD}} \quad I_D = \frac{-j}{\Psi_{dD}} \left(\frac{4\pi D k}{\zeta k_c} + I_V \Psi_{dI} + I_U \Psi_{dUI} \right) \quad (9.28c)$$

Exercise 9.3 Verify the solution (9.28). Hint: Solve for the current amplitudes I_V , I_U , and I_D first by neglecting the γ 's.

For a zero-order solution the small correction terms $\gamma(z)$ can be neglected. It follows that an approximate solution for the current $[I_z(z)]_0$ has been obtained in the form (9.25) with (9.26). It remains to evaluate the several parameters.

Since the zero-order currents are given by (9.25), (9.26), and (9.28a–c) with the γ 's equal to zero, it is possible to substitute (9.25) directly in the original differential equation (9.1) and evaluate I_V , I_U , and I_D directly with the aid of (9.27a–c). It is also necessary to determine Ψ in the expression (9.14) for k_c .

The subtraction of $k^2 A_z(h)$ from both sides of (9.1) and the multiplication by $4\pi\mu^{-1}$ gives

$$4\pi\mu^{-1}\left(\frac{d^2}{dz^2} + k^2\right)[A_z(z) - A_z(h)] = \frac{j4\pi k}{\zeta} [z^i I_z(z) - V_0^e \delta(z) + j\omega A_z(h)] \quad (9.29)$$

where, with (9.27a–c)

$$4\pi\mu^{-1}[A_z(z) - A_z(h)] = \bar{I}_V M_{kz} + \bar{I}_U F_{kz} + \bar{I}_D H_{0z} \quad (9.30a)$$

with

$$\bar{I}_V = I_V \Psi_{dR} \quad \bar{I}_U = I_U \Psi_{dUR} \quad \bar{I}_D = I_D(\Psi_{dD} + jT_D^{-1}\Psi_{dI} + jT_D^{-1}T_U \Psi_{dUI}) \quad (9.30b)$$

$T_D = I_D/I_V$, $T_U = I_U/I_V$ as defined following (9.27e). If the differential operator $(d^2/dz^2 + k^2)$ is applied to (9.30a), it follows that

$$\begin{aligned} [\text{Left side of (9.29)}] &= \bar{I}_V[(k^2 - k_c^2)M_{kz} - 2k_c \cos k_ch \delta(z)] \\ &+ \bar{I}_U[(k^2 - k_c^2)F_{kz} - k_c^2 \cos k_ch] - \bar{I}_D k^2(\cos \frac{1}{2}kh - \frac{3}{4} \cos \frac{1}{2}kz) \end{aligned} \quad (9.31a)$$

Similarly,

$$\begin{aligned} [\text{Right side of (9.29)}] &= \frac{j4\pi k}{\zeta} [z^i(I_V M_{kz} + I_U F_{kz} + I_D H_{0z}) - V_0^e \delta(z) + j\omega A_z(h)] \end{aligned} \quad (9.31b)$$

Exercise 9.4 Obtain (9.31a) from the left side of (9.29) and (9.30b).

If these two expressions are equated, the coefficients of $\delta(z)$ must be equal, and also the coefficients of M_{kz} . These give

$$I_V = \frac{\bar{I}_V}{\Psi_{dR}} = \frac{j2\pi k V_0^e}{\zeta k_c \Psi_{dR} \cos k_ch} \quad (9.32)$$

$$k_c^2 = k^2 \left(1 - \frac{j4\pi z^i}{k\zeta \Psi_{dR}}\right) \quad (9.33)$$

Note that k_c^2 as defined in (9.22) is the same in form as (9.14), but the more refined parameter Ψ_{dR} appears instead of the tentative rough constant Ψ .

With the principal amplitude I_V evaluated, it remains to determine I_U and I_D . With (9.32) and (9.33) the remaining equation obtained when (9.31a) is set equal to (9.31b) is

$$\begin{aligned} \bar{I}_U[(k^2 - k_c^2)F_{kz} - k_c^2 \cos k_ch] - \bar{I}_D k^2(\cos \frac{1}{2}kh - \frac{3}{4} \cos \frac{1}{2}kz) \\ = \Psi_{dR}(k^2 - k_c^2)(I_U F_{kz} + I_D H_{0z}) - 4\pi\mu^{-1}k^2 A_z(h) \end{aligned} \quad (9.34)$$

This relation reveals its approximate nature, since the independent equating of the coefficients of F_{kz} and H_{0z} is possible only when $k_c = k$ or $z^i = 0$. However, for antennas that are not too long, $|kh| \leq 3.5$, the distributions $F_{kz} = \cos k_c z - \cos k_c h$ and $H_{0z} = \cos \frac{1}{2}kz - \cos \frac{1}{2}kh$ both have maxima at $z = 0$, vanish at $z = h$, and vary smoothly between these values. If the coefficient of each is quite accurately evaluated at $z = 0$, so that the admittance of the antenna is well approximated, a moderate error in the distribution F_{kz} or H_{0z} is tolerable, since it affects only a part of the electromagnetic field very near the antenna. It follows that (9.34) may be satisfied exactly at $z = 0$ and $z = h$, and the fact that it is not satisfied for z between these extremes ignored. In this evaluation the vector potential at $z = h$ may be expressed in terms of the distribution (9.25). That is

$$4\pi\mu^{-1}A_z(h) = I_V\Psi_V(h) + I_U\Psi_U(h) + I_D\Psi_D(h) \quad (9.35)$$

$$\text{where} \quad \Psi_V(h) = \int_{-h}^h \sin k_c(h - |z'|) \frac{e^{-jkR_h}}{R_h} dz' \quad (9.36a)$$

$$\Psi_U(h) = \int_{-h}^h (\cos k_c z' - \cos k_c h) \frac{e^{-jkR_h}}{R_h} dz' \quad (9.36b)$$

$$\Psi_D(h) = \int_{-h}^h (\cos \frac{1}{2}kz' - \cos \frac{1}{2}kh) \frac{e^{-jkR_h}}{R_h} dz' \quad (9.36c)$$

where $R_h = \sqrt{(h - z')^2 + a^2}$. When (9.35) is substituted in (9.34), two equations are obtained, one with $z = 0$, the other with $z = h$. These may be solved simultaneously to obtain first I_U and I_D in terms of I_V and then the coefficients $T_U = I_U/I_V$, $T_D = I_D/I_V$. The results are

$$T_U = \frac{C_V E_D - C_D E_V}{C_U E_D - C_D E_U} \quad T_D = \frac{C_U E_V - C_V E_U}{C_U E_D - C_D E_U} \quad (9.37)$$

$$\text{where} \quad C_U = (1 - n^2)(\Psi_{dUR} - \Psi_{dR})(1 - c_c) - n^2\Psi_{dUR}c_c + j\Psi_{dUI}(\frac{3}{4} - c) + \Psi_U(h) \quad (9.38a)$$

$$C_D = \Psi_{dD}(\frac{3}{4} - c) - (1 - n^2)\Psi_{dR}(1 - c) + \Psi_D(h) \quad (9.38b)$$

$$C_V = -[j\Psi_{dI}(\frac{3}{4} - c) + \Psi_V(h)] \quad (9.38c)$$

$$E_U = -n^2\Psi_{dUR}c_c - j\frac{1}{4}\Psi_{dUI}c + \Psi_U(h) \quad (9.38d)$$

$$E_D = -\frac{1}{4}\Psi_{dD}c + \Psi_D(h) \quad (9.38e)$$

$$E_V = j\frac{1}{4}\Psi_{dI}c - \Psi_V(h) \quad (9.38f)$$

In these formulas the shorthands $n^2 = k_c^2/k^2$, $c_c = \cos k_c h$, and $c = \cos \frac{1}{2}kh$ have been used. The several Ψ functions are obtained from (9.27a-e) with z fixed at z_m with $m = M, F$, and H which specified the maximum values of M_{kz} , F_{kz} , and H_{0z} , respectively. It is readily verified that these maxima occur when $z_F = z_H = 0$ and when z_M satisfies the equation $\sin 2\beta_c(h - z_M) =$

$-(\alpha_c/\beta_c) \sinh 2\alpha_c(h - z_M)$. When $\alpha_c(h - z_M)$ is small, this reduces to $\beta_c z_M = \beta_c h - \pi/[2(1 - \alpha_c^2/\beta_c^2)]$. As α_c/β_c increases from small values toward 1, $\beta_c z_M$ moves from $\beta_c h - \pi/2$ toward zero while the largest amplitude $|\sin k_c(h - z_M)| = [\cosh^2 \alpha_c(h - z_M) - \cos^2 \beta_c(h - z_M)]^{1/2}$ increases from 1 to $\cosh \alpha_c h$. It follows that

$$\Psi_{dR} = \csc k_c(h - |z_M|) \int_{-h}^h \sin k_c(h - |z'|) \left(\frac{\cos kR_m}{R_m} - \frac{\cos kR_h}{R_h} \right) dz' \quad (9.39a)$$

$$\Psi_{dUR} = (1 - \cos k_ch)^{-1} \int_{-h}^h (\cos k_c z' - \cos k_ch) \left(\frac{\cos kR_0}{R_0} - \frac{\cos kR_h}{R_h} \right) dz' \quad (9.39b)$$

$$\Psi_{dD} = (1 - \cos \frac{1}{2}kh)^{-1} \int_{-h}^h (\cos \frac{1}{2}kz' - \cos \frac{1}{2}kh) \left(\frac{e^{-jkR_0}}{R_0} - \frac{e^{-jkR_h}}{R_h} \right) dz' \quad (9.39c)$$

$$\Psi_{dI} = -(1 - \cos \frac{1}{2}kh)^{-1} \int_{-h}^h \sin k_c(h - |z'|) \left(\frac{\sin kR_0}{R_0} - \frac{\sin kR_h}{R_h} \right) dz' \quad (9.39d)$$

$$\Psi_{dUI} = -(1 - \cos \frac{1}{2}kh)^{-1} \int_{-h}^h (\cos k_c z' - \cos k_ch) \left(\frac{\sin kR_0}{R_0} - \frac{\sin kR_h}{R_h} \right) dz' \quad (9.39e)$$

where $R_0 = \sqrt{z'^2 + a^2}$, $R_h = \sqrt{(h - z')^2 + a^2}$, $R_m = \sqrt{(z_m - z')^2 + a^2}$. Note that $\Psi_{dD} = \Psi_{dDR} + j\Psi_{dDI}$. When k and k_c are complex, the subscripts R and I do not refer to real and imaginary parts.

The parameter Ψ_{dR} is contained in the definition (9.33) of the propagation constant k_c . On the other hand, k_c appears explicitly in the integral (9.39a) which defines Ψ_{dR} . Since Ψ_{dR} is relatively insensitive to the value of k_c , a process of iteration may be used in which $(\Psi_{dR})_0$ is determined from (9.33) with k substituted for k_c . The value $(\Psi_{dR})_0$ is then used in (9.33) to determine $(\Psi_{dR})_1$. It is to be expected that, when z^i is small, $(\Psi_{dR})_0$ is a satisfactory approximation to determine k_c but that one or more iterations may be necessary for larger values of z^i .

9.4 Distributions of Current and Charge; Admittance

The zero-order solution for the current in an imperfectly conducting cylindrical antenna is

$$[I_z(z)]_0 = \frac{j2\pi k V_0^e}{\zeta k_c \Psi_{dR} \cos k_ch} [\sin k_c(h - |z|) + T_U(\cos k_c z - \cos k_ch) + T_D(\cos \frac{1}{2}kz - \cos \frac{1}{2}kh)] \quad (9.40)$$

The driving-point admittance is

$$Y_0 = \frac{I_z(0)}{V_0^e} = \frac{j2\pi k}{\zeta k_c \Psi_{dR} \cos k_ch} [\sin k_ch + T_U(1 - \cos k_ch) + T_D(1 - \cos \frac{1}{2}kh)] \quad (9.41)$$

The charge per unit length is obtained from the equation $dI_z(z)/dz + j\omega q(z) = 0$. For $z \geq 0$ it is

$$[q(z)]_0 = \frac{2\pi k V_0^e}{\omega \zeta \Psi_{dR} \cos k_c h} \left[\cos k_c(h - z) + T_U \sin k_c z + \frac{k T_D}{2k_c} \sin \frac{1}{2} k z \right] \quad (9.42)$$

For $z < 0$, $q(-z) = -q(z)$.

When the antenna is perfectly conducting ($z^i = 0$, $k_c = k_0 = \omega/c$) and immersed in air ($\sigma = 0$, $\epsilon = \epsilon_0$, $\mu = \mu_0$, $k = k_0 = \omega\sqrt{\mu_0\epsilon_0}$),

$$[I_z(z)]_0 = \frac{j2\pi V_0^e}{\zeta_0 \Psi_{dR} \cos k_0 h} [\sin k_0(h - |z|) + T_U(\cos k_0 z - \cos k_0 h) + T_D(\cos \frac{1}{2} k_0 z - \cos \frac{1}{2} k_0 h)] \quad (9.43)$$

where now T_U and T_D are simply

$$T_U = Q^{-1}[\Psi_{dD}\Psi_V(h) - j\Psi_{dI}\Psi_D(h)] \quad (9.44a)$$

$$T_D = -jQ^{-1}\{\Psi_{dI}[\Psi_{dUR} \cos k_0 h - \Psi_U(h)] + \Psi_{dUI}\Psi_V(h)\} \quad (9.44b)$$

$$\text{with} \quad Q = \Psi_{dD}[\Psi_{dUR} \cos k_0 h - \Psi_U(h)] + j\Psi_{dUI}\Psi_D(h) \quad (9.44c)$$

The Ψ functions are defined in (9.36a-c) and (9.39a-e), but with $k_c = k = k_0$.

Since $\cos k_c h$, which occurs in the denominator of (9.40), becomes quite small when $\beta_c h = \pi/2$ and $\alpha_c h$ is small—it vanishes when $\alpha_c = 0$, an alternative but equivalent form for $I_z(z)$ is convenient when $\beta_c h$ is at or near $\pi/2$ and $\alpha_c h$ is small. It is

$$[I_z(z)]_0 = \frac{-j2\pi k V_0^e}{\zeta k_c \Psi_{dR}} [(\sin k_c |z| - \sin k_c h) + T'_U(\cos k_c z - \cos k_c h) - T'_D(\cos \frac{1}{2} k z - \cos \frac{1}{2} k h)] \quad (9.45a)$$

$$\text{where} \quad T'_U = -\frac{T_U + \sin k_c h}{\cos k_c h} \quad T'_D = \frac{T_D}{\cos k_c h} \quad (9.45b)$$

Exercise 9.5 Show that, when $\alpha = 0$, T'_U and T'_D are both finite when $\cos k_c h = 0$

For $z \geq 0$:

$$[q(z)]_0 = \frac{2\pi k V_0^e}{\omega \zeta \Psi_{dR}} (\cos k_c z - T'_U \sin k_c z + \frac{1}{2} T'_D \sin \frac{1}{2} k z) \quad (9.46)$$

For $z \leq 0$, the symmetry relation $q(-z) = -q(z)$ obtains.

Typical numerical values of the parameters for a perfectly conducting antenna with $a/\lambda_0 = 7.022 \times 10^{-3}$ in air are as follows. For $k_0 h = \pi$ and $\Omega = 2 \ln(2h/a) = 9.92$: $\Psi_{dR} = 5.737$, $T_U = -0.117 + j0.114$, $T_D = -0.106 + j0.108$, $Y_0 = (0.976 + j0.988) \times 10^{-3}$ mhos. For $k_0 h = \pi/2$ and $\Omega = 8.58$: $\Psi_{dR} = 6.218$, $T'_U = 3.085 + j3.581$, $T'_D = 1.061 + j0.025$, $Y_0 = (9.578 - j4.756) \times 10^{-3}$ mhos.

It is instructive to compare the approximate theoretical currents and charges given by (9.40) and (9.42) with measured values. Data are available for monopoles in air base-driven from a coaxial line over a very large ground

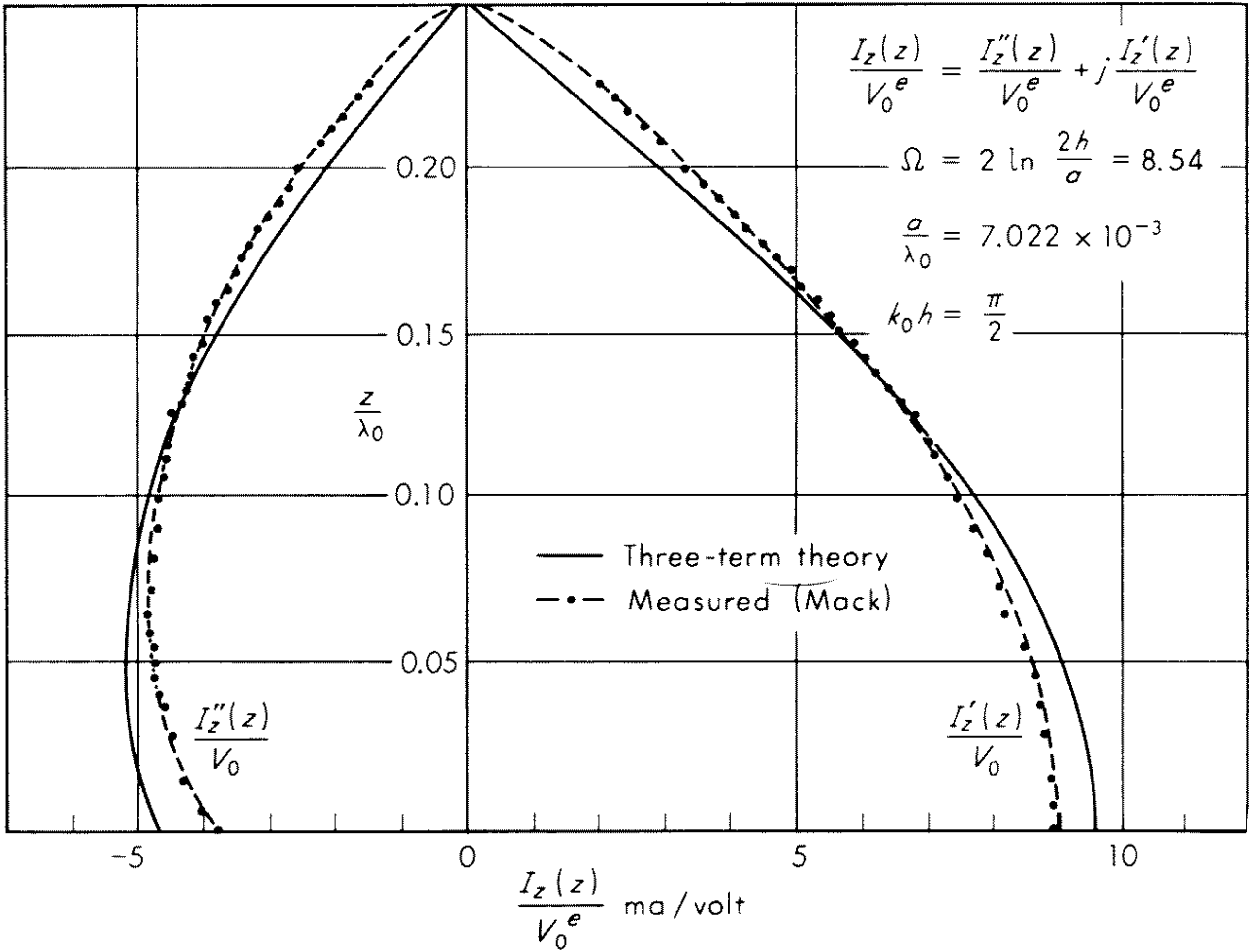


Fig. 9.2 Current in half-wave dipole.

screen.³ In this case, $\alpha_c = 0$, $\beta_c = \beta = k_0 = \omega/c$. For the antenna in question $k_0 a = 0.044$, which still satisfies the requirement $k_0 a \ll 1$. The measured and calculated normalized components of current for $k_0 h = \pi/2$ are shown in Fig. 9.2, and those for $k_0 h = \pi$ in Fig. 9.3. Note that $I_z''(0)/V_0^e = G_0$ is the conductance and $I_z'(0)/V_0^e = B_0$ is the susceptance. The associated normalized distributions of charge per unit length are shown in Figs. 9.4 and 9.5. In general, the agreement is quite good in view of the fact that only the leading trigonometric terms have been used. Results for imperfectly conducting antennas in air are in the literature.

For determining admittances and electromagnetic fields at some distance from the antenna a simpler and only slightly less accurate formula for the current may be satisfactory for highly conducting antennas in air for which $k_c = k = k_0$. When $k_0 h \leq \pi$, the two distribution functions $\cos k_0 z - \cos k_0 h$ and $\cos (k_0 z/2) - \cos (k_0 h/2)$ are quite similar. The latter is important primarily in the vicinity of the ends of the antenna, where it maintains a larger amplitude than the former. If $\cos (k_0 z/2) - \cos (k_0 h/2)$ is replaced everywhere by $\cos k_0 z - \cos k_0 h$, $\Psi_{aD} = \Psi_{aU}$, $\Psi_D(h) = \Psi_U(h)$, so that (9.43) is reduced to

$$[I_z(z)]_0 = \frac{j2\pi V_0^e}{\xi_0 \Psi_{aR} \cos k_0 h} [\sin k_0(h - |z|) + T(\cos k_0 z - \cos k_0 h)] \quad (9.47a)$$

with
$$T = \frac{\Psi_V(h) - j\Psi_{aI} \cos k_0 h}{\Psi_{aU} \cos k_0 h - \Psi_U(h)} \quad (9.47b)$$

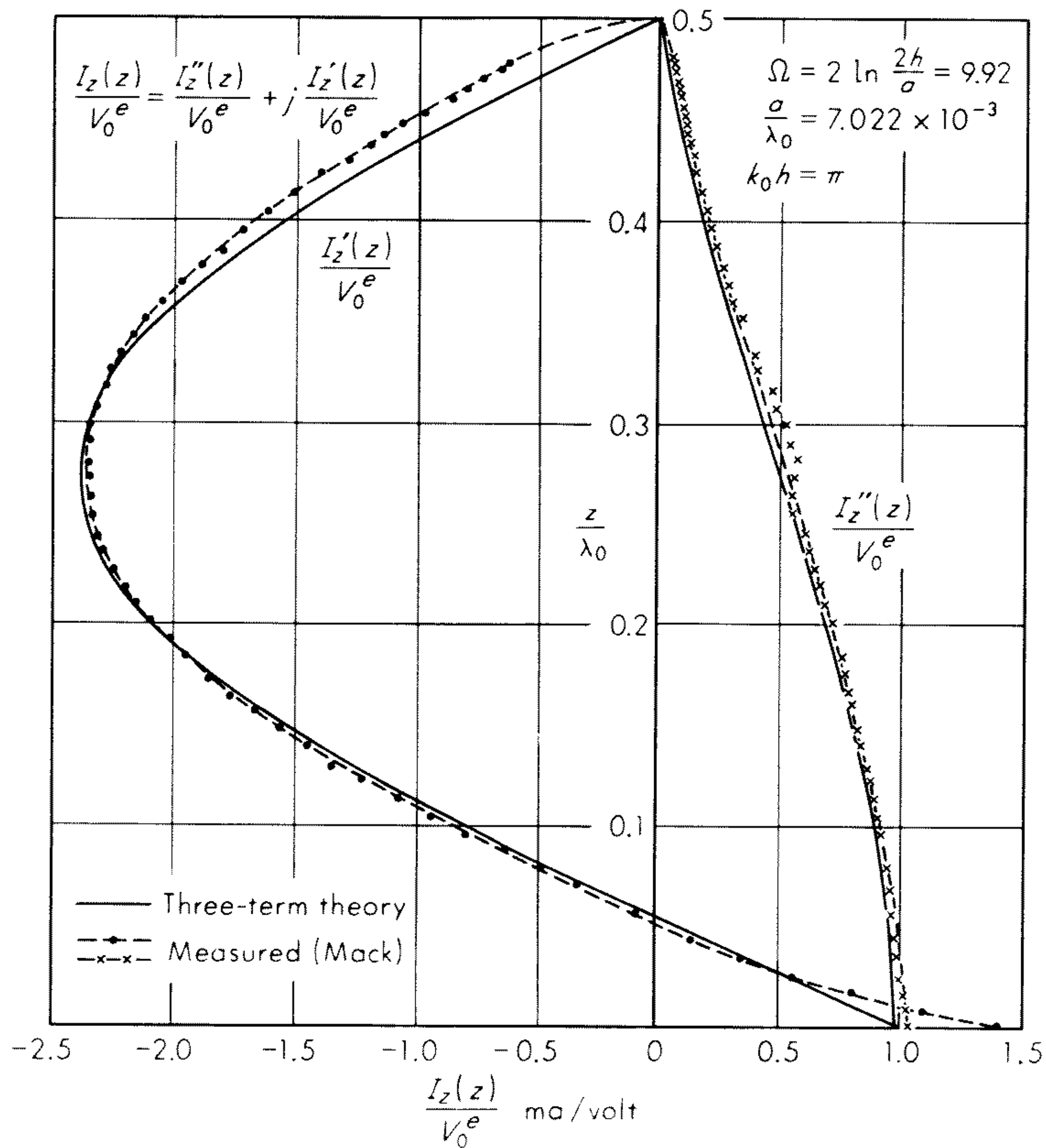


Fig. 9.3 Current in full-wave dipole.

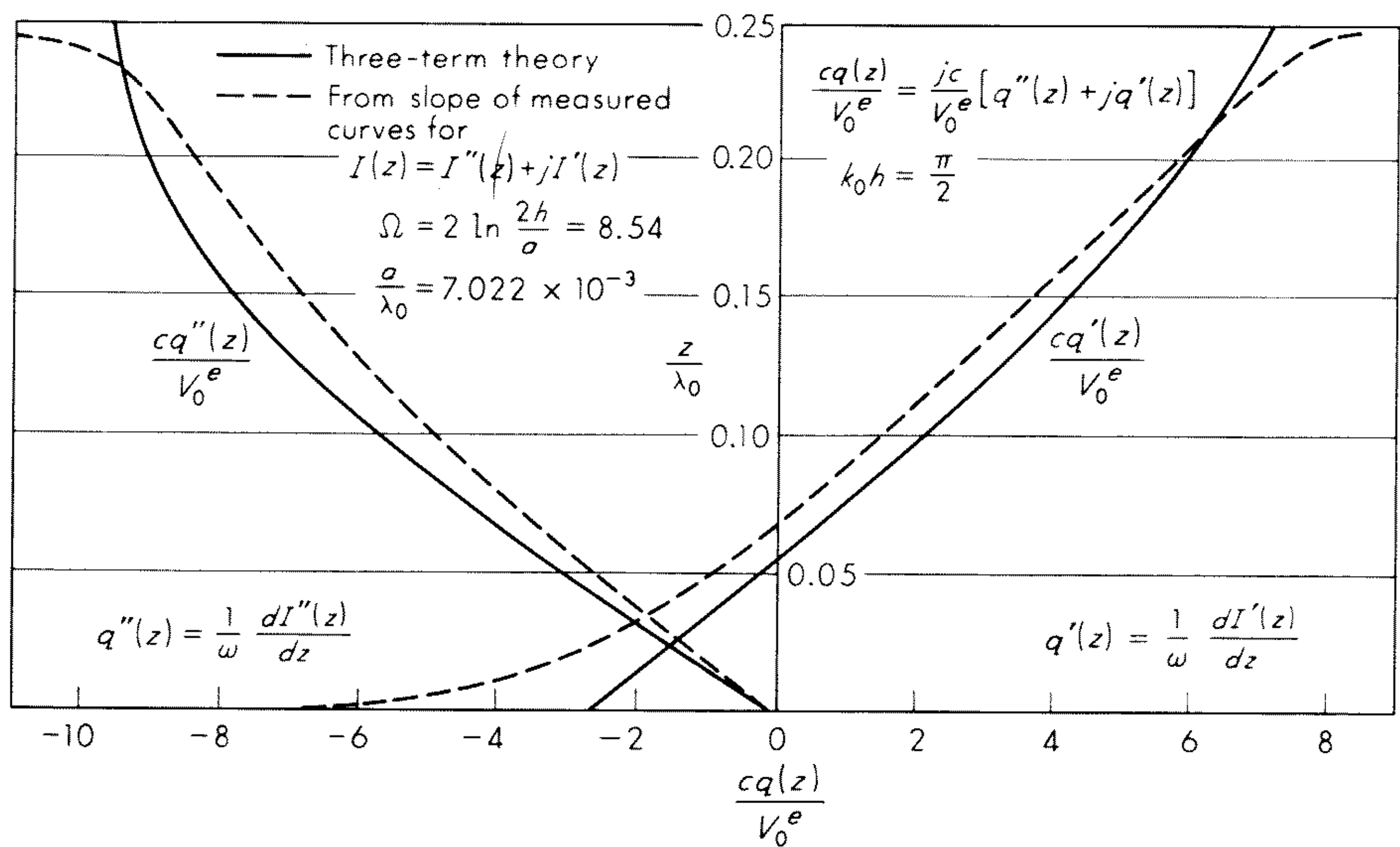


Fig. 9.4 Charge in half-wave dipole.

A similar simplification may be made in the alternative form (9.45a). Numerical values for $a/\lambda_0 = 7.022 \times 10^{-3}$ are, for $k_0h = \pi$, $T = -0.172 + j0.175$, $Y_0 = (1.021 + j1.000) \times 10^{-3}$ mhos. For $k_0h = \pi/2$, $T' = 2.65 + j3.79$,

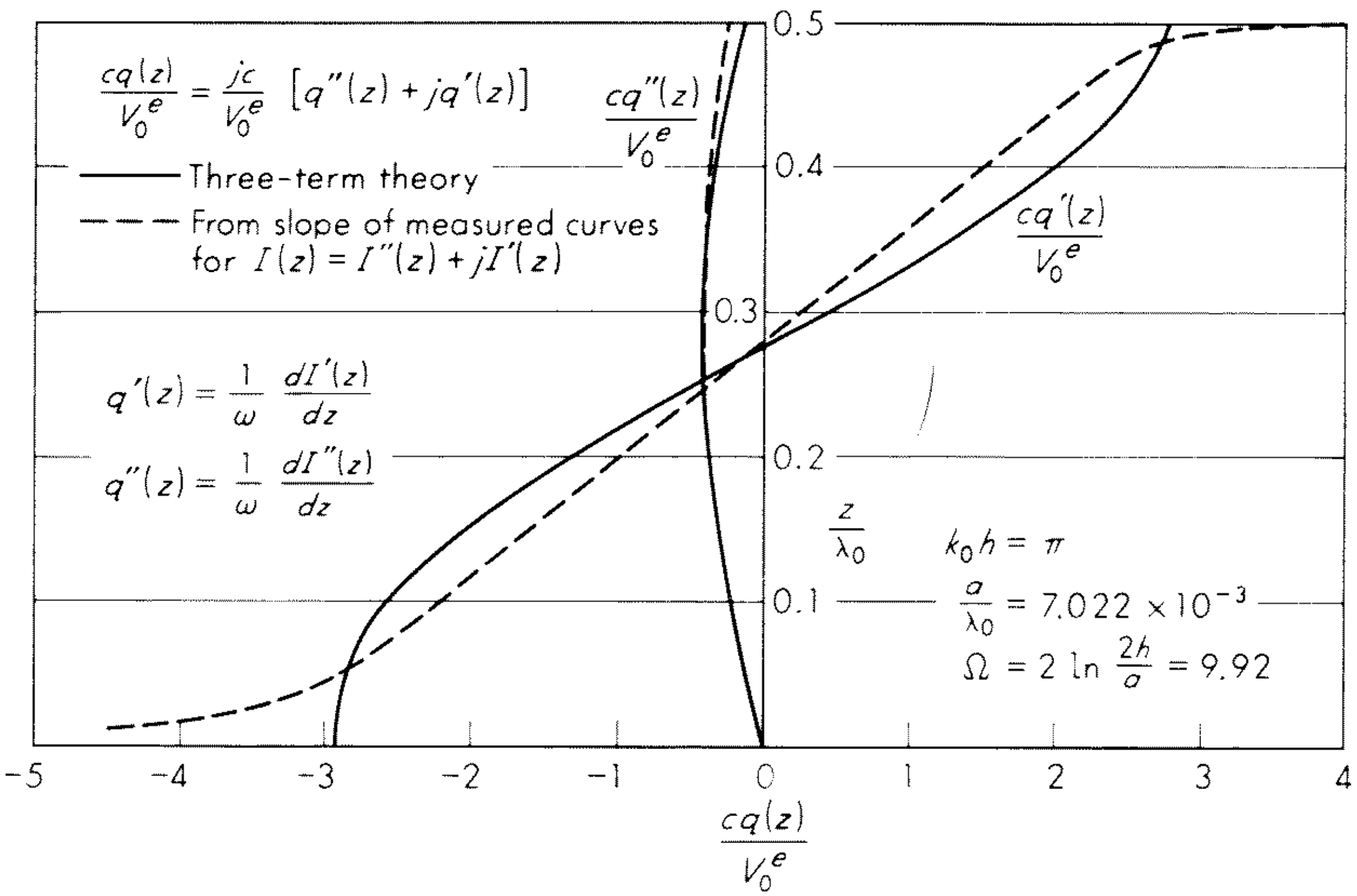


Fig. 9.5 Charge in full-wave dipole.

$Y_0 = (10.17 - j4.43) \times 10^{-3}$ mhos. The values of Y_0 differ only slightly from those obtained with the three-term formulas.

A comparison of the two-term admittance $Y_0 = [I_z(0)]_0/V_0^e$ as determined from (9.47a) and its alternative form near $k_0h = \pi/2$ with the King-Middleton second-order admittance is given in Fig. 9.6, together with the measured curves. The measured susceptance involves the difference between the local geometry near the driving point of the actual antenna and that of the idealized δ -function generator. An approximate correction has been made in the measured curve by including a lumped terminal-zone network.^{4,5} As seen especially in Fig. 9.3, the trigonometric functions are incapable of representing accurately the sharp peak in $I'_z(z)/V_0^e$ near $z = 0$. An empirical correction may be made for this error by adding a constant lumped susceptance to B_0 . The value required when $k_0h = \pi$ is 0.72. It is seen from Fig. 9.6 that this correction improves the agreement of B_0 with the King-Middleton second-order values (Table 9.1) and the measured values.

A more accurate distribution of current is required if the charges near $z = 0, \pm h$ and the electric field very near the antenna $r \leq 10a$ are to be determined with quantitative precision. A first-order current is readily obtained if

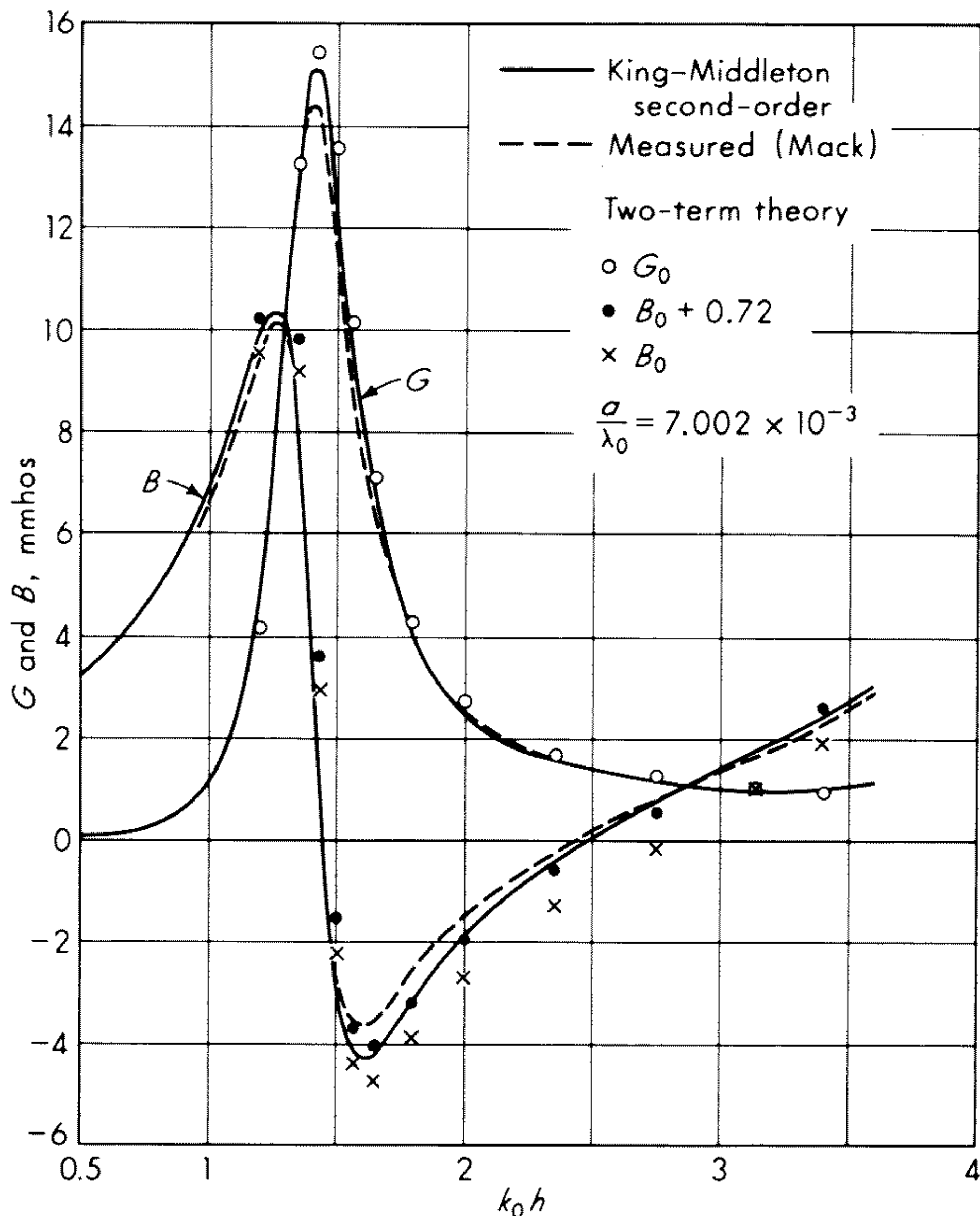


Fig. 9.6 King-Middleton second-order admittance $Y = G + jB$, two-term zero-order admittance $Y_0 = G_0 + jB_0$, and measured curves.

the correction terms $\gamma(z)$ are retained in (9.28a-c). It follows from (9.27a-c), that first-order values of these quantities are

$$[\gamma_V(z)]_1 = \int_{-h}^h M_{kz'} K_{dR}(z, z') dz' - M_{kz} \Psi_{dR} \quad (9.48a)$$

$$[\gamma_U(z)]_1 = \int_{-h}^h F_{kz'} K_{dR}(z, z') dz' - F_{kz} \Psi_{dUR} \quad (9.48b)$$

$$[\gamma_D(z)]_1 = \int_{-h}^h H_{0z'} K_{dR}(z, z') dz' - H_{0z} \Psi_{dD} \quad (9.48c)$$

where the zero-order currents have been substituted for $I(z)$. If (9.48a-c) are substituted in (9.28a-c) the following first-order currents are obtained:

$$[I_z(z)]_1 = 2[I_z(z)]_0 - I_{c1}(z) \quad (9.49a)$$

with

$$I_{c1}(z) = I_V \left[\Psi_{dR}^{-1} \int_{-h}^h M_{kz'} K_{dR}(z, z') dz' + T_U \Psi_{dUR}^{-1} \int_{-h}^h F_{kz'} K_{dR}(z, z') dz' + T_D \Psi_{dD}^{-1} \int_{-h}^h H_{0z'} K_{dR}(z, z') dz' \right] \quad (9.49b)$$

TABLE 9.1 SECOND-ORDER ADMITTANCE, IMPEDANCE, EFFECTIVE LENGTH, AND DIRECTIVITY OF CYLINDRICAL ANTENNA; $\Omega = 2 \ln 2h/a = 10$

k_0h	$Y, \text{ mmhos}$	$Z, \text{ ohms}$	βh_e	D
0.5	$0.00985 + j1.40329$	$4.9993 - j712.5738$	$0.24218 - j0.00053$	1.40783
0.6	$0.02298 + j1.76626$	$7.3644 - j566.0731$	$0.29524 - j0.00113$	1.42037
0.7	$0.04942 + j2.18972$	$10.3026 - j456.4468$	$0.35102 - j0.00218$	1.43521
0.8	$0.10165 + j2.70219$	$13.9011 - j369.5470$	$0.41015 - j0.00390$	1.45230
0.9	$0.20576 + j3.34929$	$18.2737 - j297.4484$	$0.47333 - j0.00658$	1.47152
1.0	$0.42137 + j4.20717$	$23.5695 - j235.3288$	$0.54140 - j0.01062$	1.49291
1.1	$0.89990 + j5.40415$	$29.9820 - j180.0505$	$0.61532 - j0.01657$	1.51648
1.2	$2.07678 + j7.11904$	$37.7639 - j129.4519$	$0.69620 - j0.02518$	1.54220
1.3	$5.27830 + j9.15773$	$47.2439 - j81.9671$	$0.78535 - j0.03746$	1.57018
1.4	$12.28788 + j7.60298$	$58.8508 - j36.4132$	$0.88430 - j0.05478$	1.60063
1.48	$14.27641 + j0.14974$	$70.0379 - j0.7346$	$0.97169 - j0.07354$	1.62699
1.5	$13.50489 - j1.50120$	$73.1434 + j8.1306$	$0.99481 - j0.07906$	1.63388
$\pi/2$	$9.65893 - j4.46911$	$85.2751 + j39.4561$	$1.08112 - j0.10186$	1.65938
1.6	$8.25871 - j4.76188$	$90.8731 + j52.3964$	$1.11895 - j0.11303$	1.67023
1.7	$5.08984 - j4.35364$	$113.4588 + j97.0480$	$1.26015 - j0.16218$	1.70735
1.8	$3.51213 - j3.50121$	$142.8070 + j142.3630$	$1.42159 - j0.23399$	1.74417
1.9	$2.65621 - j2.75171$	$181.5916 + j188.1206$	$1.60586 - j0.33972$	1.78039
2.0	$2.14531 - j2.14009$	$233.6347 + j233.0658$	$1.81334 - j0.49682$	1.81567
2.1	$1.81653 - j1.63501$	$304.1220 + j273.7312$	$2.03788 - j0.73163$	1.84988
2.2	$1.59258 - j1.20581$	$399.1128 + j302.1859$	$2.25702 - j1.08107$	1.88303
2.3	$1.43327 - j0.82995$	$522.5034 + j302.5626$	$2.41333 - j1.58608$	1.91535
2.4	$1.31604 - j0.49158$	$666.8191 + j249.0787$	$2.39191 - j2.25819$	1.94727
2.5	$1.22746 - j0.17953$	$797.6292 + j116.6627$	$2.03778 - j3.00063$	1.97931
2.6	$1.15923 + j0.11424$	$854.3421 - j84.1965$	$1.29575 - j3.55619$	2.01214
2.7	$1.10619 + j0.39569$	$801.4512 - j286.6857$	$0.37447 - j3.67786$	2.04632
2.8	$1.06527 + j0.66940$	$672.9909 - j422.8962$	$-0.40256 - j3.39356$	2.08234
2.9	$1.03491 + j0.93903$	$529.9562 - j480.8611$	$-0.89144 - j2.92740$	2.12040
3.0	$1.01475 + j1.20777$	$407.7867 - j485.3552$	$-1.13515 - j2.46030$	2.16044
3.1	$1.00537 + j1.47858$	$314.4768 - j462.4952$	$-1.22571 - j2.06609$	2.20217
π	$1.00494 + j1.59254$	$283.3940 - j449.0990$	$-1.23629 - j1.92723$	2.21993
3.2	$1.00811 + j1.75453$	$246.2016 - j428.4926$	$-1.23458 - j1.75564$	2.24521
3.3	$1.02500 + j2.03920$	$196.7771 - j391.4790$	$-1.20490 - j1.51726$	2.28921
3.4	$1.05889 + j2.33712$	$160.8428 - j355.0024$	$-1.16018 - j1.33492$	2.33373
3.5	$1.11390 + j2.65438$	$134.4233 - j320.3261$	$-1.11253 - j1.19408$	2.37776
3.6	$1.19644 + j2.99924$	$114.7455 - j287.6447$	$-1.06773 - j1.08295$	2.41874
3.7	$1.31719 + j3.38293$	$99.9443 - j256.6868$	$-1.02801 - j0.99241$	2.45138
3.8	$1.49467 + j3.82032$	$88.8155 - j227.0097$	$-0.99364 - j0.91558$	2.46661
3.9	$1.76194 + j4.32984$	$80.6308 - j198.1446$	$-0.96379 - j0.84744$	2.45124
4.0	$2.17958 + j4.93036$	$75.0053 - j169.6670$	$-0.93712 - j0.78451$	2.38967

The zero-order current $[I_z(z)]_0$ is given in (9.40) or (9.45a). The three integrals in (9.49b) can be expressed in terms of tabulated generalized sine and cosine integral functions, or they may be evaluated numerically by computer.

9.5 The Electromagnetic Field near a Cylindrical Antenna

The electromagnetic field at all points outside the cylindrical antenna of radius a may be expressed in terms of the scalar and vector potentials in the cylindrical coordinates r, ϕ, z . Specifically, with

$$A_z(r, z) = \frac{\mu}{4\pi} \int_{-h}^h I_z(z') K_r(z, z') dz' \quad (9.50a)$$

$$\Phi(r, z) = \frac{1}{4\pi\epsilon} \int_{-h}^h q_z(z') K_r(z, z') dz' \quad (9.50b)$$

where $K_r(z, z') = e^{-jkR}/R$ with $R = \sqrt{(z' - z)^2 + r^2}$, $I_z(z)$ is given in (9.40), and $q(z)$ in (9.42), the components of the electromagnetic field are

$$B_\phi(r, z) = \frac{-\partial A_z(r, z)}{\partial r} \quad (9.51a)$$

$$E_r(r, z) = \frac{-\partial \Phi(r, z)}{\partial r} = \frac{-j\omega}{k^2} \frac{\partial^2 A_z(r, z)}{\partial z \partial r} \quad (9.51b)$$

$$E_z(r, z) = \frac{-\partial \Phi(r, z)}{\partial z} - j\omega A_z(r, z) = \frac{-j\omega}{k^2} \left[\frac{\partial^2 A_z(r, z)}{\partial z^2} + k^2 A_z(r, z) \right] \quad (9.51c)$$

Note that at $r = a$, $-h \leq z \leq h$ the square bracket in (9.51c) vanishes, so that $E_z(a, z) = 0$ everywhere on the surface of the antenna. The evaluation of these components in closed form is not possible in general. Even when the antenna is a perfect conductor so that $k_c = k$, only the first term in the distribution of current can be integrated directly. Specifically, if the amplitude $I_m = (j2\pi V_0^e / \zeta \Psi_{dR} \cos kh)$ is introduced, the part of the field due to the current $I_V(z) = I_m \sin k(h - |z|)$ may be shown to be⁷

$$[B_\phi(r, z)]_{V0} = \frac{j\mu I_m}{4\pi r} (e^{-jkR_{1h}} + e^{-jkR_{2h}} - 2e^{-jkR_0} \cos kh) \quad (9.52a)$$

$$[E_r(r, z)]_{V0} = \frac{j\zeta I_m}{4\pi r} \left(\frac{z - h}{R_{1h}} e^{-jkR_{1h}} + \frac{z + h}{R_{2h}} e^{-jkR_{2h}} - \frac{2z}{R_0} e^{-jkR_0} \right) \quad (9.52b)$$

$$[E_z(r, z)]_{V0} = \left(\frac{-j\zeta I_m}{4\pi} \left(\frac{e^{-jkR_{1h}}}{R_{1h}} + \frac{e^{-jkR_{2h}}}{R_{2h}} - \frac{2}{R_0} e^{-jkR_0} \cos kh \right) \right) \quad (9.52c)$$

where $R_0 = \sqrt{z^2 + r^2}$, $R_{1h} = \sqrt{(z - h)^2 + r^2}$, $R_{2h} = \sqrt{(z + h)^2 + r^2}$. This part of the field is the complete field *only* if the distribution of current is given accurately by the first term in (9.40) instead of the sum of all three terms. For an antenna of finite radius this is possible only if it is maintained by a suitable continuous distribution of generators instead of by a single generator at $z = 0$. The contributions to the field obtained by substituting $I_U(z) = I_m T_U(\cos kz - \cos kh)$ and $I_D(z) = I_m T_D(\cos \frac{1}{2}kz - \cos \frac{1}{2}kh)$ have not been evaluated in general. However, the fields very close to the antenna and very far from it are readily obtained.

At points that are electrically near the antenna so that $r^2 \ll h^2$ and

$|kr| \ll 1$, and not too near the ends, $h^2 \gg z^2$, contributions to the vector and scalar potentials (9.48a,b) come principally from elements of current or charge at z' that are electrically near the point z where the potential is calculated. Over such distances the current and charge vary only slightly and retardation is negligible. Hence,

$$A_z(r,z) \doteq \frac{\mu I_z(z)}{4\pi} \int_{-h}^h \frac{dz'}{R} \doteq \frac{\mu I_z(z)}{2\pi} \ln \frac{2h}{r} \quad (9.53a)$$

$$\Phi(r,z) \doteq \frac{q(z)}{4\pi\epsilon} \int_{-h}^h \frac{dz'}{R} \doteq \frac{q(z)}{2\pi\epsilon} \ln \frac{2h}{r} \quad (9.53b)$$

It follows from (9.51a,b) that

$$B_\phi(r,z) \doteq \frac{\mu I_z(z)}{2\pi r} \quad E_r(r,z) \doteq \frac{q(z)}{2\pi\epsilon r} \quad (9.53c)$$

where $I_z(z)$ and $q(z)$ are given by (9.40) and (9.42). Within the approximations implied in (9.53), $E_z(r,z)$ can be calculated directly from Maxwell's equation in the form

$$\frac{\partial E_r(r,z)}{\partial z} - \frac{\partial E_z(r,z)}{\partial r} = -j\omega B_\phi(r,z) \quad (9.54a)$$

Thus,

$$\begin{aligned} E_z(r,z) &= \int_a^r \left[\frac{\partial E_r(r,z)}{\partial z} + j\omega B_\phi(r,z) \right] dr \\ &= \frac{1}{2\pi} \left[\frac{1}{\epsilon} \frac{\partial q(z)}{\partial z} + j\omega\mu I_z(z) \right] \ln \frac{r}{a} \\ &= \frac{j}{2\pi\omega\epsilon} \left[\frac{\partial^2 I_z(z)}{\partial z^2} + k^2 I_z(z) \right] \ln \frac{r}{a} \end{aligned} \quad (9.54b)$$

With (9.40) and (9.42) specialized to have $k_c = k$,

$$E_z(r,z)]_0 \doteq \frac{kV^e}{\Psi_{dR} \cos kh} [T_U \cos kh - T_D(\frac{3}{4} \cos \frac{1}{2}kz - \cos \frac{1}{2}kh)] \ln \frac{r}{a} \quad (9.55a)$$

Alternatively, when βh is near $\pi/2$, form (9.46) gives

$$E_z(r,z)]_0 = \frac{-kV^e}{\Psi_{dR}} [\sin kh + T'_U \cos kh + T'_D(\frac{3}{4} \cos \frac{1}{2}kz - \cos \frac{1}{2}kh)] \ln \frac{r}{a} \quad (9.55b)$$

Note that (9.54b) satisfies the boundary conditions $E_z(a,z) = 0$ on the surface $r = a$ of the perfectly conducting antenna. Clearly, the component (9.51c) alone does not.

It follows from Figs. 9.2 and 9.3 that $I_z(z)$ and, hence, $B_\phi(r,z)$ near the antenna are well represented, respectively, by (9.40) and (9.52c). Similarly, Figs. 9.4 and 9.5 indicate that $q(z)$ and with it $E_r(r,z)$ near the antenna are quite well approximated by (9.42) and (9.53c) except quite near $z = 0, \pm h$.

Since $E_z(r, z)$ depends on both $I_z(z)$ and $\partial q(z)/\partial z$, it is clear from Figs. 9.2 to 9.5 that (9.54a,b) is at best a rough approximation at some distance from $z = 0, \pm h$.

In order to obtain a better approximation of $q(z) \approx \partial I_z(z)/\partial z$ and $\partial q(z)/\partial z \approx \partial^2 I_z(z)/\partial z^2$, the first-order current (9.49a,b) may be used.

Since the more accurate current is needed primarily to calculate $E_z(r, z)$ close to the antenna, it is sufficient to obtain $(\partial^2/\partial z^2 + k_0^2)I_z(z) = 2(\partial^2/\partial z^2 + k_c^2)[I_z(z)]_0 - (\partial^2/\partial z^2 + k_c^2)I_{c1}(z)$ with (9.48a,b) and a repeated integration by parts. Thus,

$$\left(\frac{\partial^2}{\partial z^2} + k^2\right)I_{c1}(z) = J_V \Psi_{dR}^{-1} + J_U T_U \Psi_{dUR}^{-1} + J_D T_D \Psi_{dD}^{-1} \quad (9.56)$$

$$\begin{aligned} \text{where } J_V &= \int_{-h}^h I_V(z') \left(\frac{\partial^2}{\partial z^2} + k^2\right) K_{dR}(z, z') dz' \\ &= \int_{-h}^h I_V(z') \frac{\partial^2}{\partial z^2} K_R(z, z') dz' + k^2 \int_{-h}^h I_V(z') K_{dR}(z, z') dz' \end{aligned} \quad (9.57)$$

Use has been made of the relations $K_{dR}(z, z') = K_R(z, z') - K_R(h, z')$ and $\partial^2 K_R(z, z')/\partial z^2 = \partial^2 K_R(z, z')/\partial z'^2$. Corresponding expressions for J_U and J_D are obtained with changes in subscripts on $I(z')$ and the omission of the subscript R for J_D . Integration by parts twice and the condition $I_V(h) = 0$ yield

$$\begin{aligned} J_V &= \frac{-\partial I_V(z')}{\partial z'} K_R(z, z') \Big|_{z'=-h}^h \\ &+ \int_{-h}^h K_R(z, z') \left(\frac{\partial^2}{\partial z^2} + k^2\right) I_V(z') dz' - k^2 \int_{-h}^h K_R(h, z') I_V(z') dz' \end{aligned} \quad (9.58)$$

Analogous expressions apply to J_U and J_D . Since for use in (9.58), $I_V(z') = I_V \sin k(h - |z|) = I_V \{H(z) \cos k(h - z) - [1 - H(z)] \cos k(h - z)\}$, where $H(z) = 1$ for $z \geq 1$, $H(z) = 0$ for $z < 1$, $I_U(z) = I_V T_U (\cos kz - \cos kh)$, $I_D(z) = I_V T_D (\cos \frac{1}{2} k_c z - \cos \frac{1}{2} k_c h)$, it follows that $\partial I_V(z)/\partial z = -I_V k_c \{H(z) \cos k(h - z) - [1 - H(z)] \cos k_c(h + z)\}$, $\partial I_U(z)/\partial z = -I_V k_c T_U \sin kz$, and $\partial I_D(z)/\partial z = -\frac{1}{2} I_V T_D \sin \frac{1}{2} k_c z$, and $(\partial^2/\partial z^2 + k^2)I_V(z) = -2I_V k \cos kh \delta(z)$, $(\partial^2/\partial z^2 + k^2)I_U(z) = -I_V k^2 T_U \cos kh$, $(\partial^2/\partial z^2 + k^2)I_D(z) = I_V k^2 T_D (\frac{3}{4} \cos \frac{1}{2} k_c z - \cos \frac{1}{2} k_c h)$. With these values

$$J_V = I_V k^2 \operatorname{Re} \left[L_1(z, h) - 2 \cos kh \frac{K(z, 0)}{k} - L_2(h) \right] \quad (9.59a)$$

$$J_U = I_V k^2 T_U \operatorname{Re} \{ L_1(z, h) \sin kh - [E_a(h, z) - E_a(h, h)] \cos kh - C_a(h, h) \} \quad (9.59b)$$

$$\begin{aligned} J_D &= I_V k^2 T_D \{ \frac{1}{2} L_1(z, h) \sin \frac{1}{2} k_c h - [E_a(h, z) - E_a(h, h)] \cos \frac{1}{2} k_c h \\ &\quad + \frac{3}{4} \mathcal{G}_a(h, z) - \mathcal{G}_a(h, h) \} \end{aligned} \quad (9.59c)$$

The following new symbols have been introduced:

$$L_1(z, h) = \frac{K(z, h) + K(z, -h)}{k} \quad (9.60a)$$

$$L_2(h) = C_a(h, h) \sin kh - S_a(h, h) \cos kh \quad (9.60b)$$

$$S_a(h, z) = \int_0^h [K(z, z') + K(z, -z')] \sin kz' dz' \quad (9.60c)$$

$$C_a(h, z) = \int_0^h [K(z, z') + K(z, -z')] \cos kz' dz' \quad (9.60d)$$

$$E_a(h, z) = \int_0^h [K(z, z') + K(z, -z')] dz' \quad (9.60e)$$

$$\mathcal{G}_a(h, z) = \int_0^h [K(z, z') + K(z, -z')] \cos \frac{1}{2}kz' dz' \quad (9.60f)$$

$$\text{where } K(z, z') = K_R(z, z') + jK_I(z, z') = \frac{e^{-jkR}}{R} \quad (9.60g)$$

in which $R = \sqrt{(z - z')^2 + a^2}$.

The functions $S_a(h, z)$, $C_a(h, z)$, and $E_a(h, z)$ may be expressed in terms of the tabulated generalized sine and cosine integral functions.⁸ The functions $S_a(h, h)$, $C_a(h, h)$, and $E_a(h, h)$ have been tabulated.⁹ The function $\mathcal{G}_a(h, z)$ may also be expressed in terms of the generalized sine and cosine integrals.[†]

With (9.59a-c) and (9.56) used in (9.54b),

$$[E_z(r, z)]_1 = 2[E_z(r, z)]_0 - E_{c1}(r, z)$$

where

$$\begin{aligned} E_{c1}(r, z) &= \frac{j}{2\pi\omega\epsilon} (J_V \Psi_{dR}^{-1} + J_U T_U \Psi_{dU}^{-1} + J_D T_D \Psi_{dD}^{-1}) \ln \frac{r}{a} \\ &= \frac{-Vk}{\Psi_{dR} \cos kh} \left(\text{Re} \left[L_1(z, h) - 2 \cos kh \frac{K(z, 0)}{k} - L_2(h) \right] \Psi_{dR}^{-1} \right. \\ &\quad + \text{Re} \{ L_1(z, h) \sin kh - [E_a(h, z) - E_a(h, h)] \cos kh - C_a(h, h) \} T_U \Psi_{dU}^{-1} \\ &\quad + \{ \frac{1}{2} L_1(z, h) \sin \frac{1}{2}kh - [E_a(h, z) - E_a(h, h)] \cos \frac{1}{2}kh \\ &\quad \left. + \frac{3}{4} \mathcal{G}_a(h, z) - \mathcal{G}_a(h, h) \} T_D \Psi_{dD}^{-1} \right) \ln \frac{r}{a} \quad (9.61a) \end{aligned}$$

$$\begin{aligned} \dagger \mathcal{G}_a(h, z) &= \left(\sinh^{-1} \frac{U_2}{A} + \sinh^{-1} \frac{U_1}{A} \right) \cos \frac{1}{2}U_0 \\ &\quad - \frac{1}{2} e^{jU_0/2} \left[C\left(A', \frac{U_1}{2}\right) + C\left(A', \frac{3U_2}{2}\right) + jS\left(A', \frac{U_1}{2}\right) + jS\left(A', \frac{3U_2}{2}\right) \right] \\ &\quad - \frac{1}{2} e^{-jU_0/2} \left[C\left(A', \frac{U_2}{2}\right) + C\left(A', \frac{3U_1}{2}\right) + jS\left(A', \frac{U_2}{2}\right) + jS\left(A', \frac{3U_1}{2}\right) \right] \end{aligned}$$

where $U_0 = kz$, $U_1 = k(h - z)$, $U_2 = k(h + z)$, $A' = A\sqrt{3}/2$ with $A = ka$. Also,

$$C(A, U) = \int_0^U \frac{1 - \cos \sqrt{U^2 + A^2}}{\sqrt{U^2 + A^2}} dU \quad S(A, U) = \int_0^U \frac{\sin \sqrt{U^2 + A^2}}{\sqrt{U^2 + A^2}} dU$$

An alternative convenient form of $E_{c1}(r, z)$ when kh is at or near $\pi/2$ is obtained with the parameters T'_U and T'_D , which remain finite when $kh = \pi/2$. They are defined by $T_U = -[T'_U \cos kh + \sin kh]$, $T_D = T'_D \cos kh$. The desired expression for $E_{c1}(r, z)$ very near the antenna is

$$\begin{aligned}
 E_{c1}(r, z) = & \frac{-Vk}{\Psi_{dR}} \left(\text{Re} \left\{ \left(\frac{1}{\Psi_{dR}} - \frac{\sin^2 kh}{\Psi_{dUR}} \right) \frac{L_1(z, h)}{\cos kh} - \frac{2K(z, 0)}{k\Psi_{dR}} \right. \right. \\
 & - \left(\frac{1}{\Psi_{dR}} - \frac{1}{\Psi_{dUR}} \right) C_a(h, h) \tan kh \\
 & \left. - \frac{S_a(h, h)}{\Psi_{dR}} + \frac{[E_a(h, z) - E_a(h, h)] \sin kh}{\Psi_{dUR}} \right\} \\
 & - \frac{T'_U}{\Psi_{dUR}} \text{Re} \{ L_1(z, h) \sin kh - [E_a(h, z) - E_a(h, h)] \cos kh - C_a(h, h) \} \\
 & + \frac{T'_D}{\Psi_{dD}} \{ \frac{1}{2} L_1(z, h) \sin \frac{1}{2} kh - [E_a(h, z) - E_a(h, h)] \cos \frac{1}{2} kh \\
 & \left. + \frac{3}{4} g_a(h, z) - g_a(h, h) \} \right) \ln \frac{r}{a} \quad (9.61b)
 \end{aligned}$$

Numerical values for antennas in air with $a/\lambda_0 = 7.022 \times 10^{-3}$ or $k_0 a = 0.044$ are

$$\begin{aligned}
 k_0 h = \pi: \quad \Psi_{dR} &= 5.737 \quad \Psi_{dU} = 7.572 - j4.449 \quad \Psi_{dD} = 7.224 - j2.398 \\
 T_U &= -0.117 + j0.114 \quad T_D = -0.106 + j0.108 \\
 k_0 h = \pi/2: \quad \Psi_d &= \Psi_{dU} = 6.218 - j2.161 \quad \Psi_{dD} = 6.120 - j0.652 \\
 T'_U &= 3.085 + j3.581 \quad T'_D = 1.061 + j0.025
 \end{aligned}$$

The functions $C_a(h, h)$, $S_a(h, h)$, and $E_a(h, z)$ have been tabulated¹⁰ or may be evaluated from tables of the generalized sine and cosine integral functions.

Note that, when $kh = \pi/2$, $\Psi_{dUR} = \Psi_{dR}$. Since $K_R(0, 0)/k \approx 1/ka$ and $L_1(\pm h, h) \approx 1/ka$, it is clear that $E_z(r, z)$ as given in (9.61a,b) has large values at $z = 0, \pm h$ which are not given by (9.55a,b). On the other hand, at small distances from these points, the order of magnitude of $|E_z(r, z)|$ in (9.61a,b) is roughly approximated by (9.55a,b). Graphical representations of the component of the electric field $E_z(r, z)$ near a half-wave dipole and a full-wave dipole are shown in Figs. 9.7a and b, where the results computed from (9.55) and (9.61) are compared. A comparison with the field obtained from (9.50c) alone for an assumed sinusoidally distributed current is given in Fig. 9.8.

9.6 The Radiation Field of a Cylindrical Antenna

The radiation field E_θ^r of a cylindrical antenna in air is given by

$$E_\theta^r = j\omega A_z^r \sin \theta \quad A_z^r = \frac{\mu_0}{4\pi} \frac{e^{-jk_0 R_0}}{R_0} \int_{-h}^h I_z(z) e^{jk_0 z' \cos \theta} dz' \quad (9.62)$$

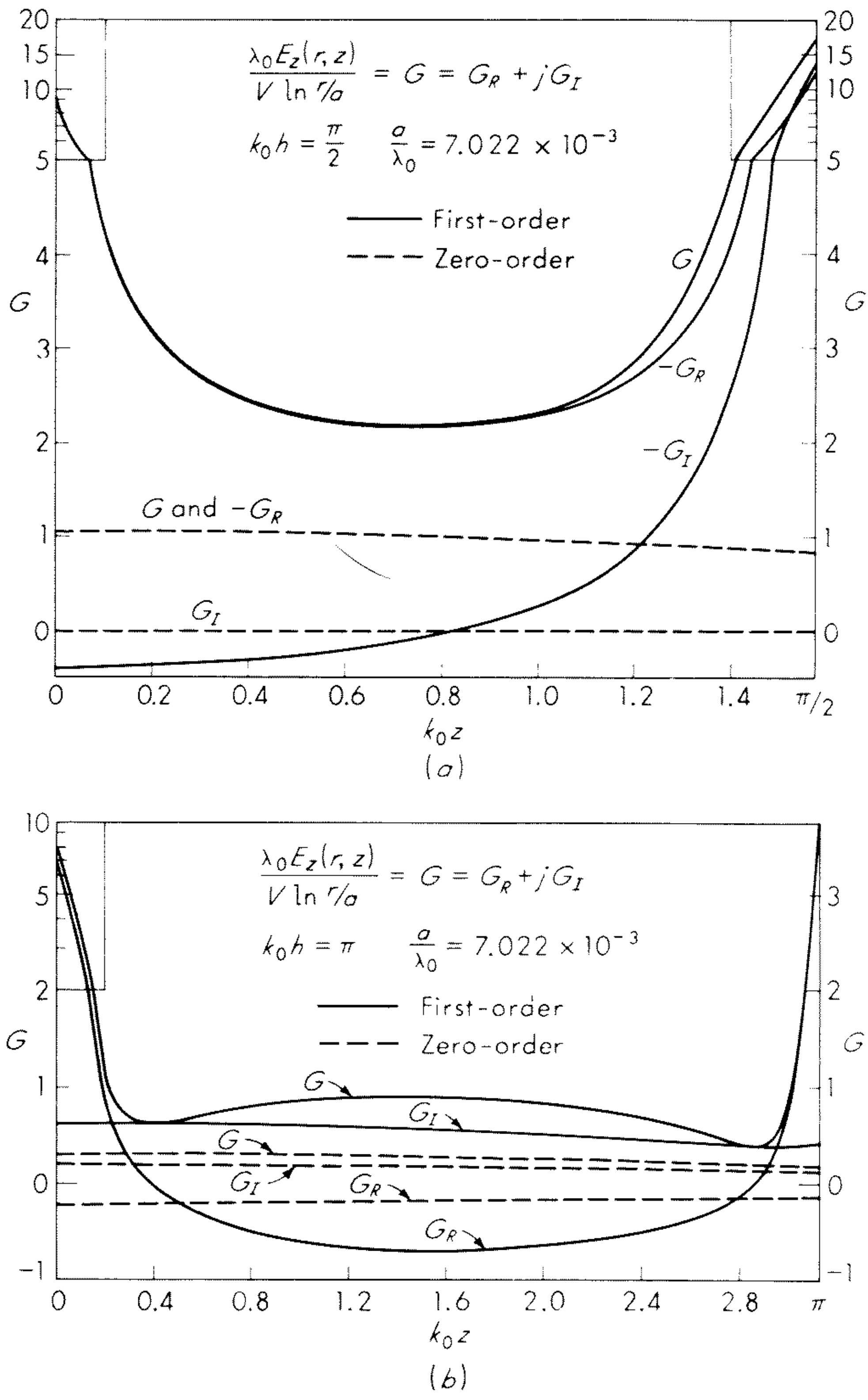


Fig. 9.7 (a) Normalized electric field near center-driven antenna; $k_0 h = \pi/2$, $a/\lambda_0 = 7.022 \times 10^{-3}$, $G(z) = \lambda_0 E_z(r, z)/V \ln r/a$; (b) normalized electric field $G(z) = \lambda_0 E_z(r, z)/V \ln r/a$ near center-driven antenna; $k_0 h = \pi$, $a/\lambda_0 = 7.022 \times 10^{-3}$.

where $I_z(z) \doteq [I_z(z)]_0$ is in (9.45a). It may be expressed as follows:

$$E_{\theta}^r = \frac{-V_0^e}{\Psi_{dR}} \frac{e^{-jk_0 R_0}}{R_0 \cos kh} [F_m(\theta, k_0 h) + T_U G_m(\theta, k_0 h) + T_D D_m(\theta, k_0 h)] \quad (9.63)$$

where

$$F_m(\theta, k_0 h) = \frac{k_0}{2} \int_{-h}^h \sin k_0(h - |z'|) e^{jk_0 z' \cos \theta} \sin \theta \, dz' \\ = \frac{\cos(k_0 h \cos \theta) - \cos k_0 h}{\sin \theta} \quad (9.64a)$$

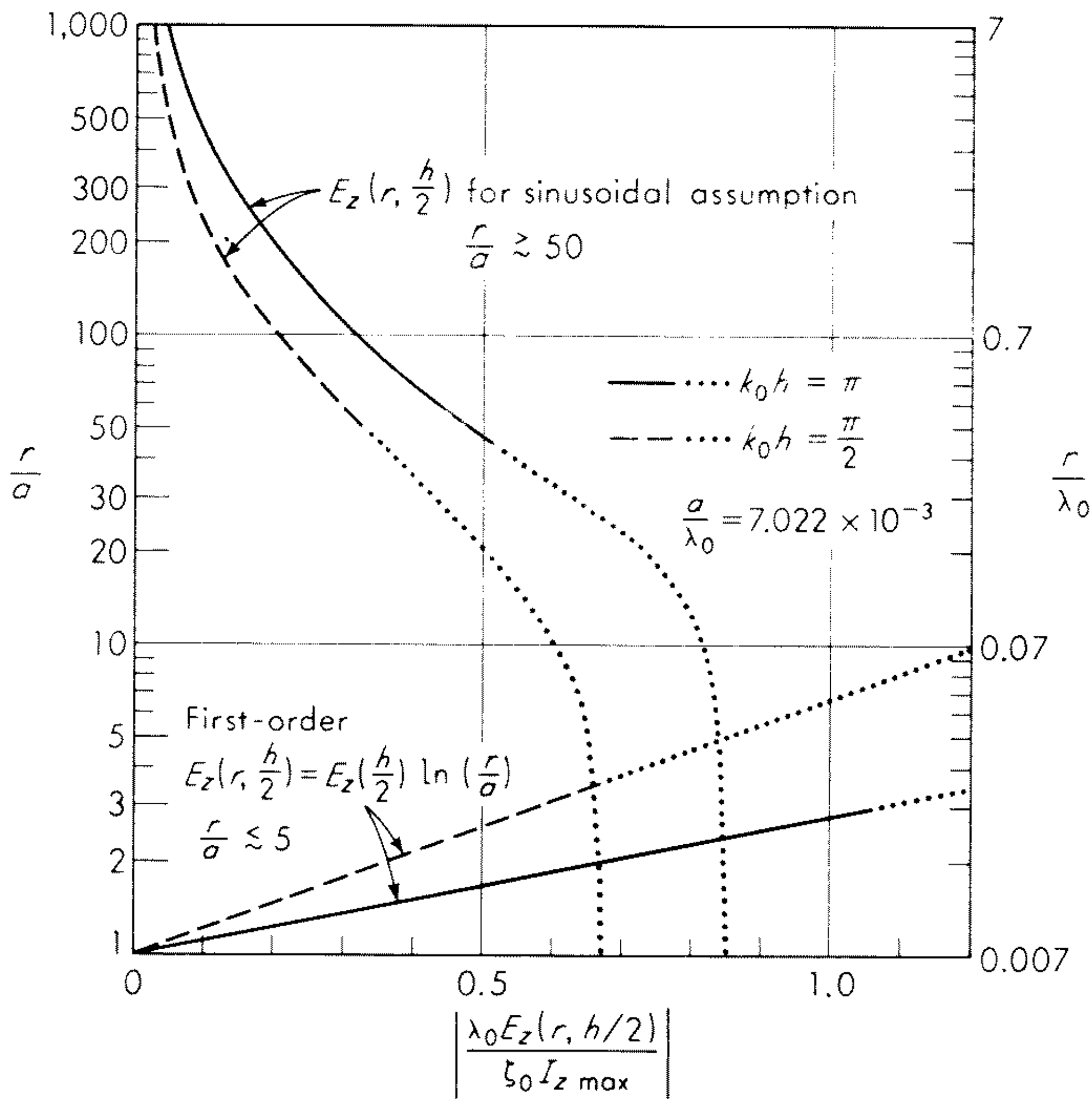


Fig. 9.8 $E_z(r, h/2)$ near half- and full-wave dipoles; $a/\lambda_0 = 7.022 \times 10^{-3}$.

$$G_m(\theta, k_0 h) = \frac{k_0}{2} \int_{-h}^h (\cos k_0 z' - \cos k_0 h) e^{jk_0 z' \cos \theta} \sin \theta dz'$$

$$= \frac{\sin k_0 h \cos (k_0 h \cos \theta) \cos \theta - \cos k_0 h \sin (k_0 h \cos \theta)}{\sin \theta \cos \theta} \quad (9.64b)$$

$$D_m(\theta, k_0 h) = \frac{k_0}{2} \int_{-h}^h (\cos \frac{1}{2} k_0 z' - \cos \frac{1}{2} k_0 h) e^{jk_0 z' \cos \theta} \sin \theta dz'$$

$$= \left[\frac{2 \cos (k_0 h \cos \theta) \sin \frac{1}{2} k_0 h - 4 \sin (k_0 h \cos \theta) \cos \frac{1}{2} k_0 h \cos \theta}{1 - 4 \cos^2 \theta} - \frac{\sin (k_0 h \cos \theta) \cos \frac{1}{2} k_0 h}{\cos \theta} \right] \sin \theta \quad (9.64c)$$

If the alternative form (9.46a) is used for the current,

$$E_{\theta^r} = \frac{V_0^e e^{-jk_0 R_0}}{\Psi_{dR} R_0} [H_m(\theta, k_0 h) + T'_U G_m(\theta, k_0 h) - T'_D D_m(\theta, k_0 h)] \quad (9.65a)$$

where

$$H_m(\theta, k_0 h) = \frac{k_0}{2} \int_{-h}^h (\sin k_0 |z'| - \sin k_0 h) e^{jk_0 z' \cos \theta} \sin \theta dz'$$

$$= \frac{\cos \theta [1 - \cos k_0 h \cos (k_0 h \cos \theta)] - \sin k_0 h \sin (k_0 h \cos \theta)}{\sin \theta \cos \theta} \quad (9.65b)$$

Note that, when $k_0h = \pi/2$,

$$H_m\left(\theta, \frac{\pi}{2}\right) = \frac{\cos \theta - \sin [(\pi/2) \cos \theta]}{\sin \theta \cos \theta} \quad (9.66a)$$

$$G_m\left(\theta, \frac{\pi}{2}\right) = \frac{\cos [(\pi/2) \cos \theta]}{\sin \theta} \quad (9.66b)$$

$$D_m\left(\theta, \frac{\pi}{2}\right) = \frac{\sqrt{2}}{2} \left\{ \frac{2 \cos [(\pi/2) \cos \theta] - 4 \sin [(\pi/2) \cos \theta] \cos \theta}{1 - 4 \cos^2 \theta} - \frac{\sin [(\pi/2) \cos \theta]}{\cos \theta} \right\} \sin \theta \quad (9.66c)$$

The associated magnetic field is $B_\phi^r = E_\theta^r/c$.

The field obtained with the conventionally assumed sinusoidal distribution of current is the same as (9.63) with $T_U = T_D = 0$. However, the usual reference for phase and amplitude is the current instead of the voltage. Since $I_z(0) = V_0^e/Z_0$, where Z_0 is the driving-point impedance, the substitution is easily made. For the sinusoidal assumption $Z_0 \doteq (j\zeta_0\Psi/2\pi) \cot k_0h$, so that the coefficient $V_0^e/\Psi_{dR} \cos k_0h$ becomes $jI_z(0)\zeta_0/2\pi \sin k_0h = jI_m\zeta_0/2\pi$, where $I_m = I_z(0)/\sin k_0h$ is the maximum of the sinusoidally distributed current.

The so-called far-field factor or far-field pattern $\mathfrak{F}_0(\theta, k_0h)$ is contained in

$$E_\theta^r = \frac{j\zeta_0 I_z(0)}{2\pi} \frac{e^{-jk_0 R_0}}{R_0} \mathfrak{F}_0(\theta, k_0h) \quad (9.67a)$$

Evidently (9.63) may be reduced to this form if V_0^e is eliminated by means of (9.44) with $z = 0$. It follows that

$$\mathfrak{F}_0(\theta, k_0h) = \frac{F_m(\theta, k_0h) + T_U G_m(\theta, k_0h) + T_D D_m(\theta, k_0h)}{\sin k_0h + T_U(1 - \cos k_0h) + T_D(1 - \cos \frac{1}{2}k_0h)} \quad (9.67b)$$

Note that if a sinusoidally distributed current were assumed, $T_U = T_D = 0$ and

$$\mathfrak{F}_0(\theta, k_0h) = F_0(\theta, k_0h) = \frac{F_m(\theta, k_0h)}{\sin k_0h} \quad (9.67c)$$

where $F_m(\theta, k_0h)$ is given by (9.64a). This is a conventional form.

9.7 Distributions of Current and Charge in a Center-loaded Receiving Antenna

The electromagnetic field maintained by the periodically varying currents in a transmitting antenna induces currents in more or less distant parasitic antennas that may be loaded with a receiver or simply reradiate as scatterers. The important quantities in a receiver are the current or voltage or power in the load. For the scatterer, the reradiated field is of interest, particularly the field very close to the antenna in certain problems involving radio-frequency hazards.

The current and power in the load of a cylindrical receiving antenna in an arbitrarily directed plane wave incident field are readily obtained by a simple generalization of the formulation for the transmitting antenna. The geometry and notation are shown in Fig. 9.9. The angle θ is measured between the axis of the antenna (z axis) and the ray of the plane wave that passes through the

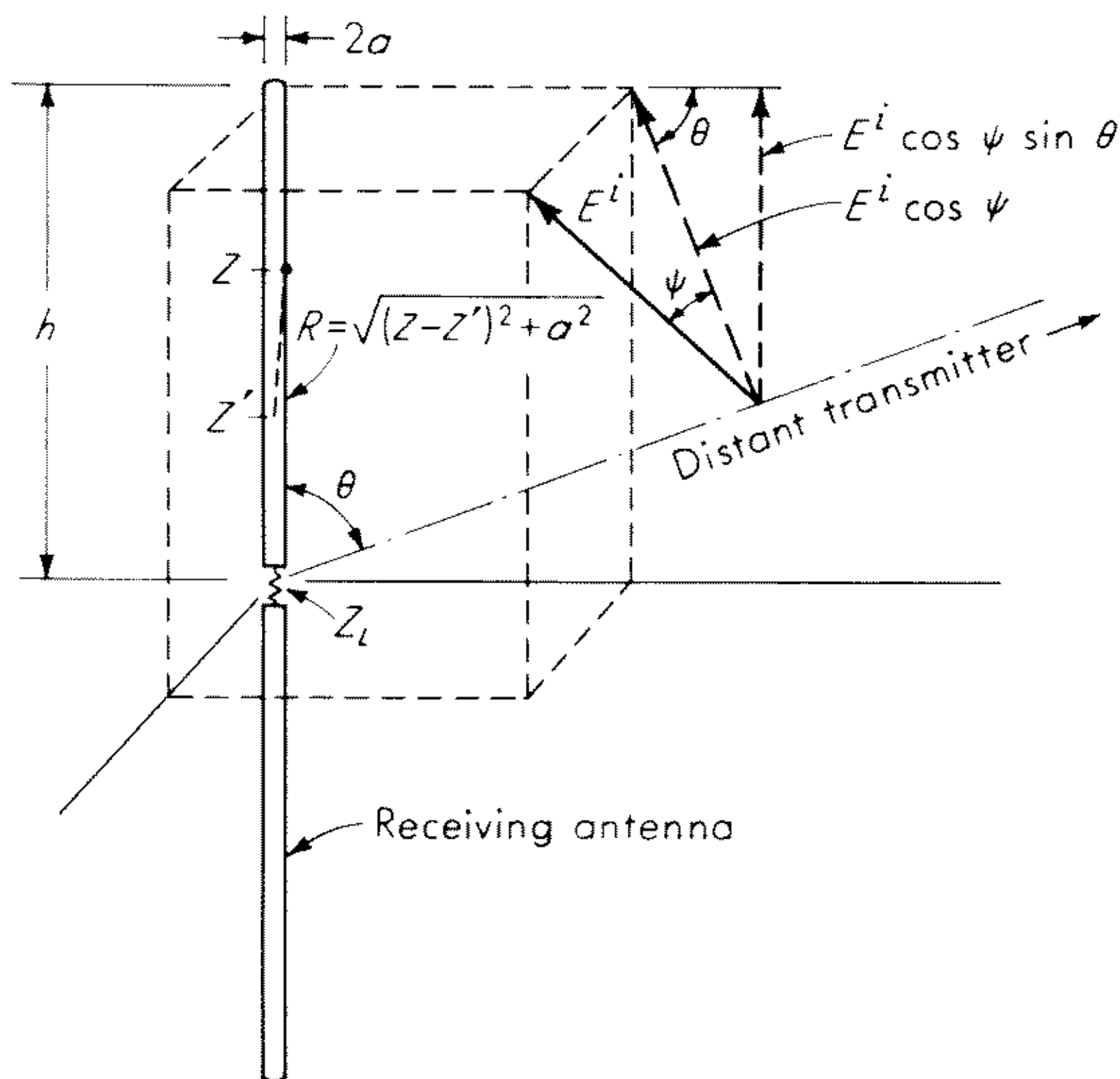


Fig. 9.9 Center-loaded receiving antenna in an incident plane wave field. The plane of the incident wave front is perpendicular to the dash-dot line.

center of the antenna at $z = 0$. The angle ψ is between the incident electric vector \mathbf{E}^i and the plane defined by the z axis and the ray through $z = 0$.

The differential equation for the vector potential $A_z(z)$ at the surface $r = a$ of an antenna in which a part of the current is induced by an incident field E^i and a part maintained by a δ -function generator with emf V_0^e at its center is like (9.1) with an added term. If, for simplicity, the antenna is assumed to be perfectly conducting so that $z^i = 0$ and immersed in air so that $k = k_0$, the equation is

$$\left(\frac{\partial^2}{\partial z^2} + k_0^2\right)A_z(z) = \frac{-jk_0^2}{\omega}\left(1 - \frac{q_0^2}{k_0^2}\right)U^i e^{jq_0 z} - \frac{jk_0^2}{\omega}V_0^e \delta(z) \quad (9.68)$$

with $q_0 = k_0 \cos \theta$ and $U^i = -(E^i \cos \psi)/k_0 \sin \theta$. It is anticipated that the emf V_0^e will be replaced by the negative of the voltage drop across a lumped load impedance Z_L at $z = 0$. That is, V_0^e will be set equal to $-I_z(0)Z_L$. As for the transmitting antenna, it is assumed that the radius a of the antenna satisfies the inequalities $k_0 a \ll 1$ and $a \ll h$, where h is the half-length of the antenna.

The general solution of (9.68) when $0 \leq z \leq h$ is

$$A_z(z) = \frac{-j}{c}(C_1 \cos k_0 z + C_2 \sin k_0 z + U^i e^{jk_0 z}) \quad (9.69)$$

The solution for $-h \leq z \leq 0$ is like (9.69) but with the different constants C_3 and C_4 substituted for C_1 and C_2 . These constants must be evaluated from the driving and boundary conditions at $z = 0$ and $z = h$.

The solution of (9.69) and its analog with z negative is more involved than the corresponding problem for the center-driven antenna owing to the absence of symmetry when the direction of incidence is arbitrary. It is convenient to separate the symmetric problem with even currents and vector potentials and odd charges and scalar potentials from the antisymmetric problem with odd currents and vector potentials and even charges and scalar potentials. With $A_z(z) = A_z^s(z) + A_z^a(z)$, $I_z(z) = I_z^s(z) + I_z^a(z)$, the symmetric part of (9.69) is defined by $A_z^s(z) = \frac{1}{2}[A_z(z) + A_z(-z)]$, $I_z^s(z) = \frac{1}{2}[I_z(z) + I_z(-z)]$ and the antisymmetric part by $A_z^a(z) = \frac{1}{2}[A_z(z) - A_z(-z)]$, $I_z^a(z) = \frac{1}{2}[I_z(z) - I_z(-z)]$. With these defining relations, the driving condition $V_0^e = \Phi^s(+0) + \Phi^a(-0)$, the boundary condition $I_z(h) = 0$, and rearrangements like those previously carried out for the transmitting antenna, the following two integral equations may be derived for the symmetric (even) and antisymmetric (odd) parts of the current in an antenna that is immersed in an incident plane wave electromagnetic field and simultaneously center driven by an emf V_0^e :

$$\begin{aligned} \int_{-h}^h I_z^s(z') K_d^s(z, z') dz' \\ = \frac{j4\pi}{\zeta_0 \cos k_0 h} [\frac{1}{2} V^e \sin k_0(h - |z|) + U^s(\cos q_0 z - \cos q_0 h) \\ + U^i(\cos k_0 z \cos q_0 h - \cos q_0 z \cos k_0 h)] \quad (9.70a) \end{aligned}$$

$$\begin{aligned} \int_{-h}^h I_z^a(z') K_d^a(z, z') dz' = \frac{j4\pi}{\zeta_0 \sin k_0 h} [U^a(\sin k_0 |z| - \sin k_0 h) \\ \pm jU^i(\sin q_0 z \sin k_0 h - \sin k_0 z \sin q_0 h)] \quad (9.70b) \end{aligned}$$

where the upper sign is for $z \geq 0$, the lower sign for $z \leq 0$. The following notation has been introduced:

$$K_d^s(z, z') = K(z, z') - K(h, z') \quad K_d^a(z, z') = K(z, z') - \frac{h}{z} K(h, z') \quad (9.71a)$$

$$U^s = \frac{-j\omega}{k_0} A_z^s(h) = \frac{-j\zeta_0}{4\pi} \int_{-h}^h I_z^s(z') K^s(h, z') dz' \quad (9.71b)$$

$$U^a = \frac{-j\omega}{k_0} \frac{z}{h} A_z^a(h) = \frac{-j\zeta_0 z}{4\pi h} \int_{-h}^h I_z^a(z') K^a(h, z') dz' \quad (9.71c)$$

The solution of the integral equations (9.70a,b) is complicated by the presence (in $q_0 = k_0 \cos \theta$) of the angle θ between the axis of the antenna and the propagation vector k_0 of the incident field. Since great simplification is achieved when the antenna lies in the plane wave front of the incident field ($\theta = \pi/2$) and since at this angle the maximum current with respect to θ is obtained for antennas with $k_0 h \leq \pi$, only this practically most important case is discussed in the following. The more general case has been treated elsewhere in a somewhat different form.¹¹

When $\theta = \pi/2$, no antisymmetric currents are induced, $I_z(z) = I_z^s(z)$,

$I_z^a(z) = 0$, and the integral equation (9.70b) is obviated. Furthermore, since $q_0 = 0$, the complicated angle-dependent coefficient of U^i in (9.70a) reduces simply to the shifted cosine. It follows that (9.70a) reduces to

$$\int_{-h}^h I_z(z) K_d(z, z') dz' = \frac{j4\pi}{\zeta_0 \cos k_0 h} [1/2 V_0^e \sin k_0(h - |z|) + U(\cos k_0 z - \cos k_0 h)] \quad (9.72)$$

where $U = U^i + U^s$ with $U^i = -(E^i \cos \psi)/k_0 \sin \theta$ and U^s given by (9.71b). This equation is formally like (9.20) for the transmitting antenna when written for perfectly conducting antennas in air, i.e., with $k_c = k = k_0$, $D = 0$. Indeed, if $E^i = 0$, it reduces identically to (9.20) so specialized. It follows that an approximate solution may be found by the same procedure. The resulting current is like (9.40) but with an added term due to the contribution by U^i . The final result is

$$I_z(z) = V_0^e v(z) + U^i u(z) \quad (9.73a)$$

$$v(z) = \frac{j2\pi}{\zeta_0 \Psi_{dR} \cos k_0 h} [\sin k_0(h - |z|) + T_U(\cos k_0 z - \cos k_0 h) + T_D(\cos 1/2 k_0 z - \cos 1/2 k_0 h)] \quad (9.73b)$$

$$u(z) = \frac{j4\pi}{\zeta_0 Q} [\Psi_{dD}(\cos k_0 z - \cos k_0 h) - j\Psi_{dUI}(\cos 1/2 k_0 z - \cos 1/2 k_0 h)] \quad (9.73c)$$

where the coefficients T_U , T_D , and Q are defined in (9.45a-c) and the Ψ functions in (9.36a-c) and (9.39a-c) with $k = k_c = k_0$.

The current in an antenna that is center-loaded with an arbitrary lumped impedance Z_L is obtained from (9.73a) with $V_0^e = -I_z(0)Z_L$ used to eliminate V_0^e . The result is

$$I_z(z) = U^i \left[u(z) - v(z)u(0) \frac{Z_L Z_0}{Z_L + Z_0} \right] \quad (9.74)$$

where Z_0 is the driving-point impedance of the antenna. This expression shows that the current in a center-loaded receiving antenna is composed of two parts: the one distributed as in an unloaded antenna and the other distributed as in a center-driven antenna. Depending on the relative magnitudes of the load Z_L and the impedance, the one or the other of these two distributions predominates. It is evident that, when $Z_L Z_0 / (Z_L + Z_0)$ is maximized by setting $Z_L = Z_0^*$, the distribution will resemble that on a transmitting antenna. On the other hand, when $|Z_L| \ll |Z_0|$, the distribution is more like that on an unloaded receiving antenna.

The distribution of charge per unit length is readily obtained with the equation of continuity, $q(z) = (j/\omega)(\partial I_z / \partial z)$. When $h \geq z \geq 0$, it is

$$q(z) = \frac{jU^i}{\omega} \left[u'(z) - v'(z)u(0) \frac{Z_0 Z_L}{Z_0 + Z_L} \right] \quad (9.75a)$$

$$\text{where } u'(z) = \frac{-j4\pi k_0}{\zeta_0 Q} \left[\Psi_{dD} \sin k_0 z - \frac{j}{2} \Psi_{dUI} \sin 1/2 k_0 z \right] \quad (9.75b)$$

$$v'(z) = \frac{-j2\pi k_0}{\zeta_0 \Psi_{dR} \cos k_0 h} [\cos k_0(h - z) + T_U \sin k_0 z + 1/2 T_D \sin 1/2 k_0 z] \quad (9.75c)$$

With normal incidence ($\theta = \pi/2$), $q(-z) = q(z)$.

When k_0h is near $\pi/2$, a convenient alternative expression for $v(z)$ with $z \geq 0$ is

$$v(z) = \frac{-j2\pi}{\xi_0\Psi_{dR}} [(\sin k_0z - \sin k_0h) + T'_U(\cos k_0z - \cos k_0h) - T'_D(\cos \frac{1}{2}k_0z - \cos \frac{1}{2}k_0h)] \quad (9.76)$$

where $T'_U = -(T_U + \sin k_0h)/\cos k_0h$ and $T'_D = T_D/\cos k_0h$ are finite when $k_0h \rightarrow \pi/2$.

9.8 Effective Length and Directivity of a Center-loaded Receiving Antenna

The current in the load Z_L of a receiving antenna with an impedance Z_0 is obtained from (9.74) with $z = 0$. It may be expressed as follows:

$$I_z(0) = \frac{U^i u(0) Z_0}{Z_0 + Z_L} = \frac{V}{Z_0 + Z_L} \quad (9.77)$$

This is the equation for the current in a simple series circuit consisting of the impedances Z_0 and Z_L and the emf $V = U^i u(0) Z_L$. This is readily found to be the voltage across the load in the limit as it becomes infinite. Thus

$$V = \lim_{Z_L \rightarrow \infty} I_z(0) Z_L = U^i u(0) Z_0 \lim_{Z_L \rightarrow \infty} \frac{Z_L}{Z_0 + Z_L} = U^i u(0) Z_0 \quad (9.78)$$

Since the incident electric field is a factor in U^i , it is convenient to express the open-circuit voltage V in the form

$$V = -E^i 2h_e \left(\frac{\pi}{2} \right) \cos \psi \quad (9.79)$$

where $2h_e(\pi/2)$ is known as the complex effective length of the antenna of length $2h$. In general, it is a function of θ . However, since (9.74) is specialized to $\theta = \pi/2$, h_e in (9.79) must also be. The electrical half length of the antenna in radians when $\theta = \pi/2$ is given by

$$k_0 h_e \left(\frac{\pi}{2} \right) = \frac{1}{2} u(0) Z_0 \quad (9.80)$$

In (9.78) and (9.80)

$$u(0) = \frac{j4\pi}{\xi_0 Q} [\Psi_{dD}(1 - \cos k_0h) - j\Psi_{dUI}(1 - \cos \frac{1}{2}k_0h)] \quad (9.81)$$

where Q is given in (9.45c) and the Ψ functions in (9.39c,e). When only the leading shifted-cosine term is used as an approximation of the current in the unloaded receiving antenna, $k_0 h_e(\pi/2) = \tan \frac{1}{2}k_0h$. The formula (9.80) is more accurate than this simple form — which is useful only when $k_0h < \pi$ — but less accurate than the more complicated iterated expression in the literature.¹²

In order to derive the complete expression for $h_e(\theta)$ it is possible to solve the θ -dependent integral equation (9.70a). Alternatively, and more simply, the Rayleigh-Carson reciprocal theorem¹³ may be applied, which reduces to

$$k_0 h_e(\theta) = \mathfrak{F}_0(\theta, k_0h) \quad (9.82)$$

where $\mathfrak{F}_0(\theta, k_0h)$ is the far-field function of the same antenna when center driven.

It is given in the three-term approximation by (9.67*b*). Note, however, that $k_0 h_e(\pi/2)$ as given by (9.82) does not reduce identically to (9.80) with (9.81) used for $u(0)$ and Z_0 obtained from (9.44). The reason is that both expressions are approximate, so that they agree only approximately. More accurate calculations of actual numerical values have been made from the general relation

$$k_0 h_e(\theta) = \frac{u(0)Z_0}{2 \sin \theta} \quad (9.83)$$

with King-Middleton second-order values of $u(0)$ and Z_0 . A short table taken from more extensive computations¹⁴ is in Table 9.1.

The power in the load is given by $P_L = \frac{1}{2} I_z(0) I_z^*(0) R_L$, where $I_z(0)$ is given by (9.77) with (9.79). It is readily verified that P_L is maximized when $Z_L = Z_0^*$. The maximum so obtained is conveniently expressed in the form

$$(P_L)_{\max} = \frac{\lambda_0 E^i \cos \psi}{8\pi \zeta_0} D\left(\frac{\pi}{2}, k_0 h\right) \quad (9.84a)$$

$$\text{where} \quad D\left(\frac{\pi}{2}, k_0 h\right) = \frac{\zeta_0}{\pi} \frac{k_0^2 h_e^2(\pi/2)}{R_0} \quad (9.84b)$$

is the dimensionless directivity. [Note that in general $D(\theta, k_0 h)$ is a function of θ as well as of $k_0 h$. However, when $k_0 h \leq 3\pi/2$, $(P_L)_{\max}$ occurs at $\theta = \pi/2$.] Values of $D(\pi/2, k_0 h)$ are given in Table 9.1 as computed from (9.80) by using second-order King-Middleton values of Z_0 and $u(0)$. The maximum directivity is seen to occur when $k_0 h \approx 4$.†

9.9 The Electromagnetic Field near a Thin Scattering Cylinder

For some purposes, notably in problems related to radio-frequency hazards, a knowledge of the electromagnetic field very near to a conducting cylinder is required. This field is composed of the incident field and the scattered field. For simplicity, let the conducting cylinder be oriented parallel to the incident electric field so that the induced current is a maximum. The incident magnetic field is then transverse. Since it has been assumed that the cross section of the cylinder is electrically small with $k_0 a \ll 1$, the scattered field will be approximately rotationally symmetrical. The average magnetic field and the radial electric field very close to the cylinder are well approximated by (9.53). Hence,

$$B_\phi(r, z) = \frac{\mu_0 I_z(z)}{2\pi r} = \frac{\mu_0 U^i u(z)}{2\pi r} \quad (9.85)$$

$$E_r(r, z) = \frac{q(z)}{2\pi \epsilon_0 r} = \frac{j U^i u'(z)}{2\pi \epsilon_0 \omega r} \quad (9.86)$$

†The corresponding results (table 10.1 and fig. 10.1 in chap. IV) in King, "Theory of Linear Antennas" were determined from second-order values of Z_0 and first-order values of $u(0)$ in (9.80) — the best data then available. The new results in Table 9.2 have been recomputed by Harrison and Aronson at the Sandia Corporation by using second-order values for both Z_0 and $u(0)$. While the general behavior as a function of $k_0 h$ is the same, the directivity of fat antennas now turns out to be less instead of greater than that of thin antennas.

where $u(z)$ is in (9.73c) and $u'(z)$ in (9.75b). The z component of the total electric field satisfies Maxwell's equations and may be obtained in the same manner as in (9.54a) to (9.55b). The result in zero order is

$$[E_z(r, z)]_0 = \frac{2U^i k_0}{Q} [\Psi_{aD} \cos k_0 h - j\Psi_{aUI} (\frac{3}{4} \cos \frac{1}{2} k_0 z - \cos \frac{1}{2} k_0 h)] \ln \frac{r}{a} \quad (9.87)$$

$$\text{where} \quad Q = \Psi_{aD} [\Psi_{aUR} \cos k_0 h - \Psi_U(h)] + j\Psi_{aUI} \Psi_D(h) \quad (9.88)$$

The several Ψ functions are the same as in (9.36a-c) and (9.39a-e). Since the formula (9.54b) for $E_z(r, z)$ near an antenna actually involves the very small difference between two fairly large quantities, both $\partial q(z)/\partial z$ and $I(z)$ must be known accurately. For this purpose an improved value of $E_z(r, z)$ may be obtained from a first-order current in the manner described in conjunction with the transmitting antenna. The first-order current is

$$[I_z(z)]_1 = 2[I_z(z)]_0 - I_{c1}(z) \quad (9.89a)$$

where

$$I_{c1} = \frac{j4\pi U^i}{\zeta_0 Q} \left[\frac{\Psi_{aD}}{\Psi_{aUR}} \int_{-h}^h (\cos k_0 z' - \cos k_0 h) K_{aR}(z, z') dz' - j \frac{\Psi_{aUI}}{\Psi_{aD}} \int_{-h}^h (\cos \frac{1}{2} k_0 z' - \cos \frac{1}{2} k_0 h) K_a(z, z') dz' \right] \quad (9.89b)$$

and the corresponding first-order expression for $E_z(r, z)$ is

$$[E_z(r, z)]_1 = 2[E_z(r, z)]_0 - E_{c1}(r, z) \quad (9.90a)$$

where

$$E_{c1} = \frac{-2U^i k_0}{Q} \ln \frac{r}{a} \left\{ \frac{\Psi_{aD}}{\Psi_{aUR}} \operatorname{Re} [L_1(z, h) \sin k_0 h - [E_a(z, h) - E_a(h, h)] \cos k_0 h - C_a(h, h)] - j \frac{\Psi_{aUI}}{\Psi_{aD}} [\frac{1}{2} L_1(z, h) \sin \frac{1}{2} k_0 h - [E_a(z, h) - E_a(h, h)] \cos \frac{1}{2} k_0 h + \frac{3}{4} g_a(h, z) - g_a(h, h)] \right\} \quad (9.90b)$$

The several functions in (9.90) are defined in Sec. 9.5.

It is convenient to set

$$\frac{E_z(r, z)}{E^i} = C(z) \ln \frac{r}{a} \cos \psi$$

where $C(z)$ is $2/Q$ times the brace in (9.90b). The magnitude of the coefficient $C(z)$ is shown graphically for both zero-order and first-order in Fig. 9.10 for a parasitic antenna with $k_0 h = \pi/2$ and $k_0 a = 0.044$ lying in the plane of the incident plane wave front. Corresponding results for $k_0 h = \pi$ are given in Fig. 9.11. It is seen that very close to the antenna the axial electric field is greatest near the charged ends.

A study of Figs. 9.10 and 9.11 shows that, when $k_0 h = \pi$, the simple zero-order approximation is very good indeed except very near the ends. The same

statement cannot be made for $k_0 h = \pi/2$. The reason for the difference lies in the fact that the zero-order charge distribution has a maximum at the ends of the antenna when $k_0 h = \pi/2$, whereas it vanishes there when $k_0 h = \pi$. The

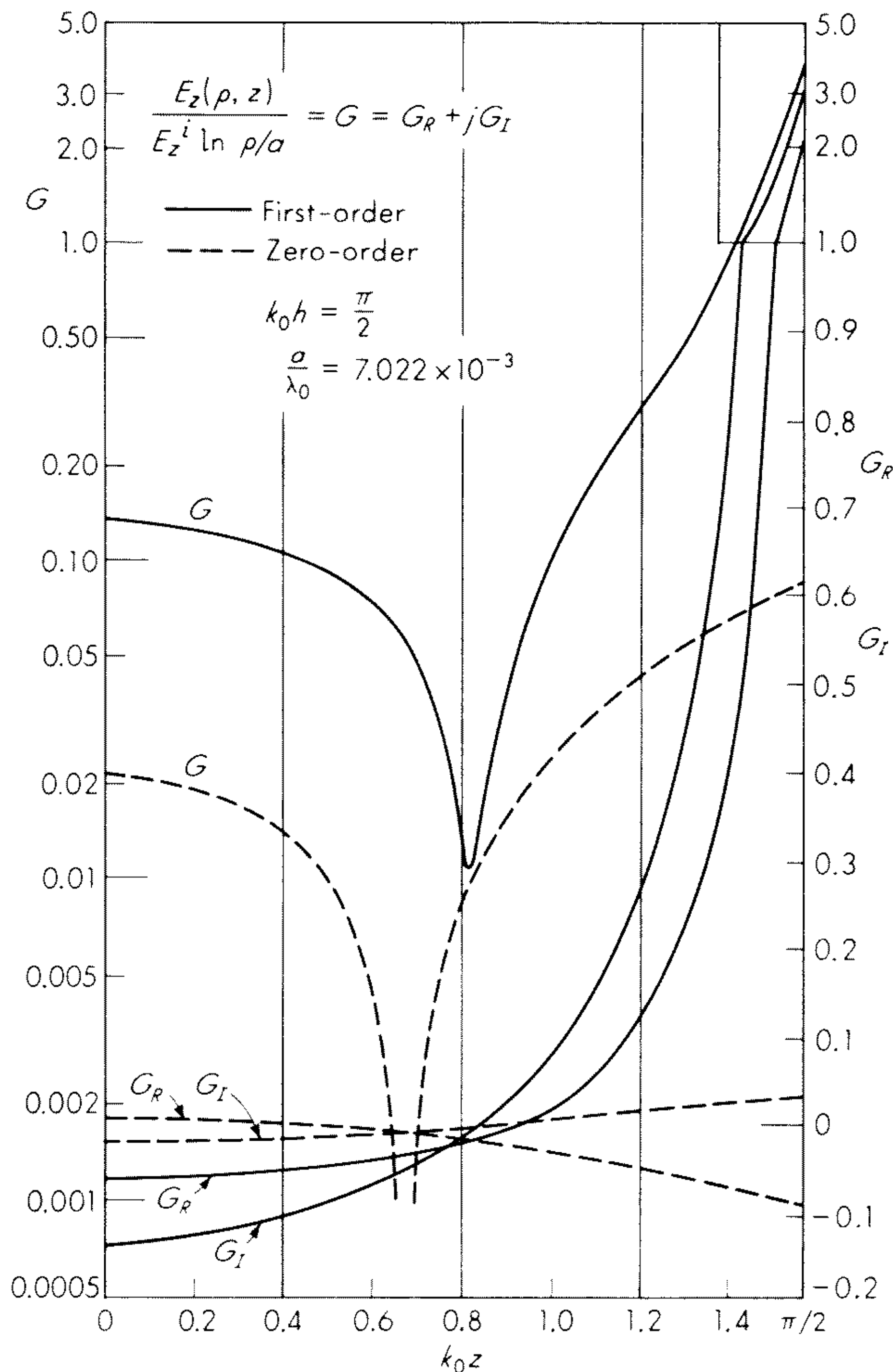


Fig. 9.10 Normalized electric field near parasitic antenna for an incident plane wave; $k_0 h = \pi/2$.

zero-order approximation of $q(z)$ near $z = \pm h$ is quite poor, and this is more significant in its effect on E_z when $q(h)$ is large than when it is very small.

9.10 The Simultaneous Integral Equations for the Parallel Array

The horizontal field pattern of an isolated vertical cylindrical antenna is a circle. In order to achieve directional patterns in the horizontal plane, two or more identical antennas may be arranged in a parallel, nonstaggered array

such as the curtain and the circle shown in Fig. 9.12. In order to determine the electromagnetic fields maintained by an array of N parallel elements, the current in each must be known. Conventional array theory assumes that the distributions of current along the several elements are the same in both ampli-

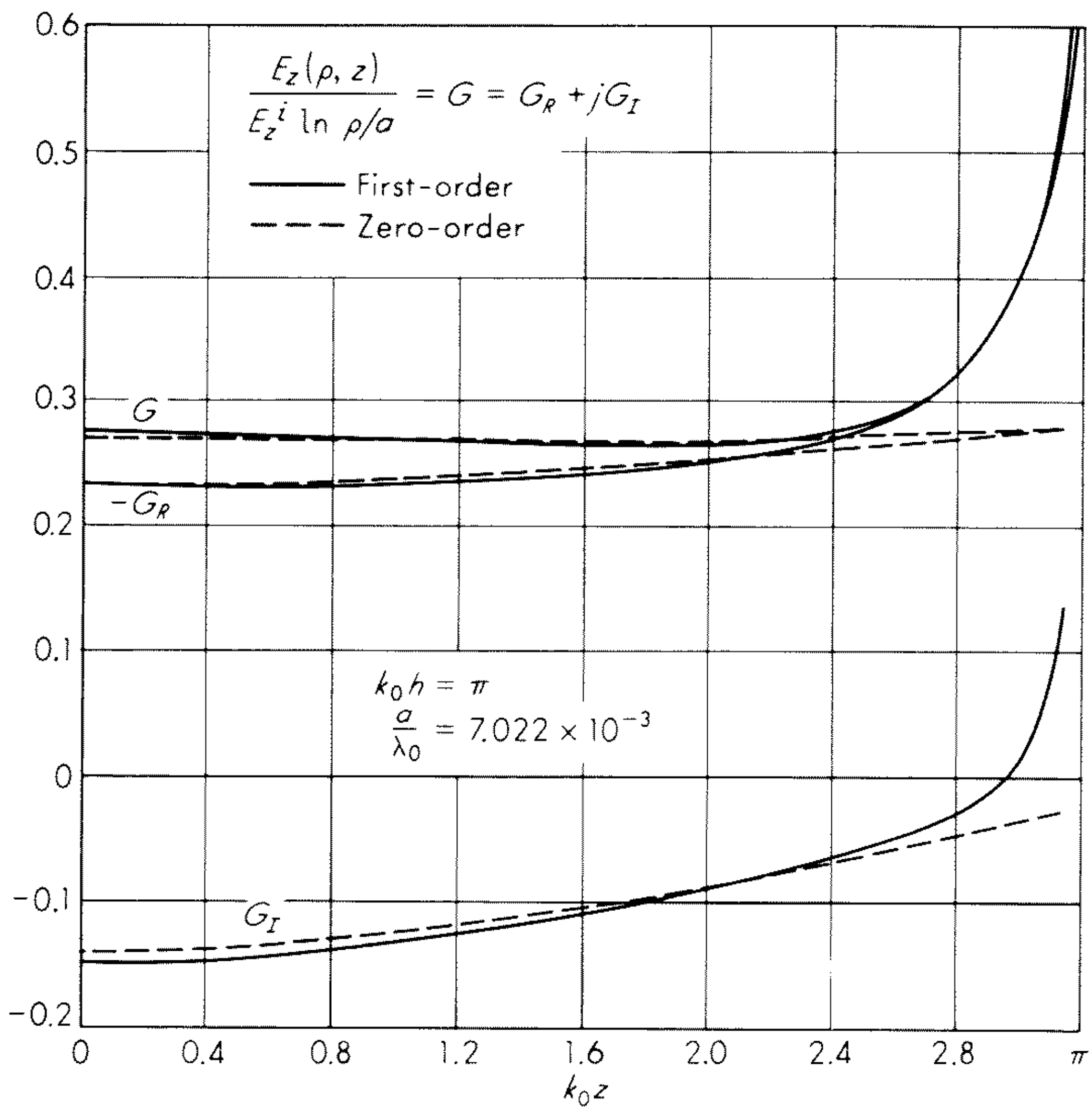


Fig. 9.11 Normalized electric field near parasitic antenna for an incident plane wave; $k_0 h = \pi$.

tude and phase. The usual assumption for the current in element i is $I_i(z) = k_i I_1(z)$, where k_i is a complex constant and the current in the reference element 1 is $I_1(z) = I_m \sin k_0(h - |z|)$. If suitable values are assigned to the k_i , a variety of theoretical far-field patterns may be obtained. Although conventional array theory is simple and useful in certain engineering applications that involve very narrow band operation of arrays of very thin half-wave elements, it does not, in fact, provide a solution of the general electromagnetic problem of coupled antennas and arrays in which the distributions of current as well as the values at the driving points are significantly affected by coupling and in which the sinusoidal approximation is not adequate.

The currents in the several elements of an array of parallel elements are governed by a set of simultaneous integral equations. These are individually like (9.20) for the isolated antenna except that the left side, which is proportional to the vector potential difference $A_z(z) - A_z(h)$ on the surface $r = a$ of

the antenna, must now include contributions from currents in all of the coupled elements and the function U_k on the right, which is proportional to $A_z(h)$, must contain similar contributions. Let it be assumed for simplicity that all an-

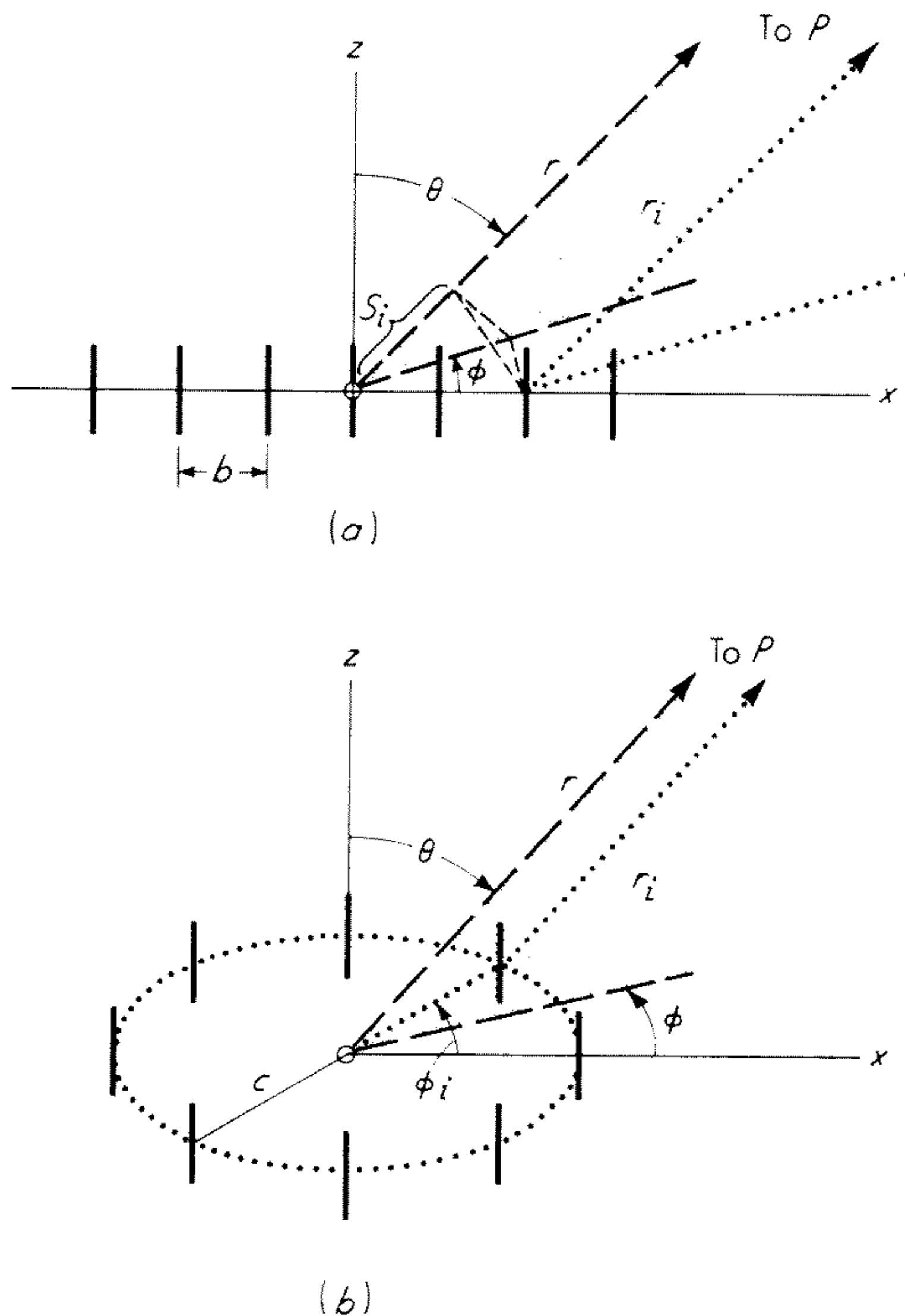


Fig. 9.12 (a) Broadside array, $N = 7$; (b) circular array, $N = 8$.

tennas are perfectly conducting, parallel, nonstaggered, and physically identical (half-length h , radius a); also let the medium in which they are immersed be air. It follows that $k = k_c = k_0$, so that the integral equation for the k th element is

$$\int_{-h}^h \sum_{i=1}^N I_z(z'_i) K_d(z_k, z'_i) dz'_i = \frac{j4\pi}{\zeta_0 \cos k_0 h} [1/2 V_k M_{0z_k} + U_k F_{0z_k}] \quad k = 1, 2, \dots, N \quad (9.91)$$

where $M_{0z_k} = \sin k_0(h - |z_k|)$, $F_{0z_k} = \cos k_0 z_k - \cos k_0 h$

$$\text{and} \quad K_d(z_k, z'_i) = K(z_k, z'_i) - K(h_k, z'_i) = \frac{e^{-jk_0 R_{ki}}}{R_{ki}} - \frac{e^{-jk_0 R_{kih}}}{R_{kih}} \quad (9.92a)$$

$$R_{ki} = \sqrt{(z_k - z'_i)^2 + b_{ki}^2} \quad R_{kih} = \sqrt{(h_k - z'_i)^2 + b_{ki}^2} \quad b_{kk} = a \quad (9.92b)$$

$$U_k = \sum_{i=1}^N U_{ki} = \frac{-j\zeta_0}{4\pi} \int_{-h}^h \sum_{i=1}^N I_z(z'_i) K(h_k, z'_i) dz'_i \quad (9.92c)$$

Note that b_{ki} is the distance between the center of antenna k and a point on the surface of antenna i at $z = 0$. The notation $b_{kk} = a$ is used, where a is the radius of antenna k . R_{ki} is the distance from the element of current $I_{zi}(z') dz'$ at z' on the axis of antenna i to the element dz on the surface of antenna k . It is assumed that $b_{ki}^2 \gg a^2$, $k \neq i$.

9.11 The Circular Array — Phase-sequence Currents

The solution of the N simultaneous integral equations (9.91) can be carried out readily when the N elements are symmetrically arranged around a circle so that geometrically there is no difference between their relative locations. Electrical differences resulting from unequal driving voltages may be treated by expressing each of the N currents $I_{z1}(z), \dots, I_{zN}(z)$ as the sum of N phase-sequence currents $I_z^{(0)}, \dots, I_z^{(N)}$ excited by N phase-sequence voltages at the driving points. A phase-sequence voltage has the same amplitude for each element, but its phase increases progressively by a constant angle from element to element around the array. It follows that in each phase sequence the currents in the N elements all have identical distributions and equal amplitudes but are shifted progressively in phase by a constant angle from element to element. There are N possible combinations with phase increments $\theta_m = 2\pi m/N$, where $m = 0, 1, 2, \dots, N-1$. The N driving voltages for phase sequence m are

$$V_i^{(m)} = V_1 p^{(i-1)m} \quad p = e^{j2\pi/N} \quad (9.93)$$

The reference antenna is arbitrary and has been selected to be number 1. Since in any one phase sequence all elements are geometrically and electrically equivalent, the integral equation for the current in the m th phase sequence among the N values $m = 0, 1, 2, \dots, N$ is simply

$$\int_{-h}^h I_z^{(m)}(z'_i) K_d^{(m)}(z, z'_i) dz'_i = \frac{j4\pi}{\xi_0 \cos k_0 h} (\frac{1}{2} V^{(m)} M_{0z} + U^{(m)} F_{0z}) \quad (9.94)$$

$$\text{where} \quad K_d^{(m)}(z, z'_i) = K^{(m)}(z, z'_i) - K^{(m)}(h, z'_i) = \sum_{i=1}^N p^{(i-1)m} K_d(z_1, z'_i) \quad (9.95a)$$

$$U^{(m)} = \frac{-j\xi_0}{4\pi} \int_{-h}^h I_z^{(m)}(z'_i) K^{(m)}(h, z'_i) dz'_i \quad (9.95b)$$

The currents on the N elements when driven in the m th phase sequence by the voltages (9.93) are given by $I_{zi}^{(m)}(z) = I_z^{(m)}(z) p^{(i-1)m}$, $i = 1, 2, \dots, N$, where $I_z^{(m)}(z)$ is the solution of (9.94). When m is assigned the N values, $m = 0, 1, \dots, N-1$, the N phase-sequence currents, $I_z^{(0)}(z), \dots, I_z^{(N)}(z)$, are determined. Evidently, the introduction of the method of symmetrical components has reduced the solution of N simultaneous integral equations with the N elements driven by the arbitrary voltages V_1, \dots, V_N to N independent integral equations with the N elements driven by the phase-sequence voltages $V^{(m)}$ given by (9.93).

The integral equation (9.94) is formally the same as (9.20) with $D = 0$. However, the kernel now consists of a sum of terms of the form $(R_{ki}^{-1}e^{-jk_0R_{ki}} - R_{kih}^{-1}e^{-jk_0R_{kih}})$ instead of the single term with $i = k$ and $b_{kk} = a$. This term will, of course, behave just as before. It may be expected that if one or more of the N coupled antennas are extremely close to antenna k so that for each of them $b_{ik} < 1$, they will behave similarly. It is convenient to express separately the part of the kernel that involves these very close elements numbered $k - n \leq i \leq k + n$. Thus, let

$$K_{dR1}^{(m)}(z_k, z'_i) = \sum_{k-n}^{k+n} p^{(i-k)m} \left(\frac{\cos k_0 R_{ki}}{R_{ki}} - \frac{\cos k_0 R_{kih}}{R_{kih}} \right) \quad (9.96a)$$

The remaining, more distant, elements for which $b_{ki} \geq 1$ involve the kernel

$$K_{dR2}^{(m)}(z_k, z'_i) = \left(\sum_1^{k-1} + \sum_{k+n}^N \right) p^{(i-k)m} \left(\frac{\cos k_0 R_{ki}}{R_{ki}} - \frac{\cos k_0 R_{kih}}{R_{kih}} \right) \quad (9.96b)$$

Note that $K_{dR}^{(m)}(z_k, z'_i) = K_{dR1}^{(m)}(z_k, z'_i) + K_{dR2}^{(m)}(z_k, z'_i)$ is the real part of (9.95a). A little thought reveals that the vector potential difference due to the current in any more distant element i for which $b_{ki} \geq 1$ is distributed along antenna k in a manner that is relatively insensitive to the axial distribution of current $I_z^{(m)}(z_i)$ that maintains it. Indeed, direct calculation in typical special cases shows the following to be good approximations:

$$\int_{-h}^h I_z^{(m)}(z'_i) K_{dR2}^{(m)}(z_k, z'_i) dz'_i \approx F_{0z_k} \quad (9.97a)$$

$$\int_{-h}^h I_z^{(m)}(z'_i) K_{dI}^{(m)}(z_k, z'_i) dz'_i \approx H_{0z_k} \quad (9.97b)$$

where $K_{dI}^{(m)}(z_k, z'_i)$ is the imaginary part of (9.95a) and $F_{0z_k} = \cos k_0 z_k - \cos k_0 h$, $H_{0z_k} = \cos \frac{1}{2} k_0 z_k - \cos \frac{1}{2} k_0 h$.

With this information regarding the behavior of the kernels and integrals, the procedure in Sec. 9.3 may be generalized. Clearly, the principal part of the m th phase-sequence current in antenna k has the form given in (9.25) and (9.26) for the isolated antenna, viz.,

$$I_z^{(m)}(z_k) = I_V^{(m)}(z) + I_U^{(m)}(z) + I_D^{(m)}(z) \quad (9.98)$$

where $I_V^{(m)}(z) \doteq I_V^{(m)} M_{0z}$, $I_U^{(m)}(z) = I_U^{(m)} F_{0z} = I_V^{(m)} T_U^{(m)} F_{0z}$, $I_D^{(m)}(z) = I_D^{(m)} H_{0z} = I_V^{(m)} T_D^{(m)} H_{0z}$ with $T_U^{(m)} = I_U^{(m)} / I_V^{(m)}$, $T_D^{(m)} = I_D^{(m)} / I_V^{(m)}$. If this current is substituted in (9.91a), the integral on the left may be treated as a sum of integrals in the following manner:

$$\int_{-h}^h I_V^{(m)}(z'_i) K_{dR1}^{(m)}(z_k, z'_i) dz'_i = I_V^{(m)}(z_k) \Psi_{dR1}^{(m)} \doteq I_V^{(m)} \Psi_{dR1} M_{0z} \quad (9.99a)$$

where all the elements in the range $k - n \leq i \leq k + n$ are so close to antenna

k that for them $b_{ki} < 1$. (Frequently $n = 0$, and $i = k$ is the only element that satisfies this condition.) The remaining integrals are conveniently chosen to be

$$\int_{-h}^h I_V^{(m)}(z'_i) K_{dR2}^{(m)}(z_k, z'_i) dz'_i = \frac{I_U^{(m)}(z_k) \Psi_{dR2}^{(m)}}{T_U^{(m)}} \doteq I_V^{(m)} \Psi_{dR2}^{(m)} F_{0z} \quad (9.99b)$$

$$\int_{-h}^h I_U^{(m)}(z'_i) K_{dR}^{(m)}(z_k, z'_i) dz'_i = I_U(z_k) \Psi_{dUR}^{(m)} \doteq I_V^{(m)} T_U^{(m)} \Psi_{dUR} F_{0z} \quad (9.99c)$$

$$\int_{-h}^h I_D^{(m)}(z'_i) K_d^{(m)}(z_k, z'_i) dz'_i \doteq I_D^{(m)}(z_k) \Psi_{dD}^{(m)} \doteq I_V^{(m)} T_D^{(m)} \Psi_{dD}^{(m)} H_{0z} \quad (9.99d)$$

$$\int_{-h}^h I_V^{(m)}(z'_i) K_{dI}^{(m)}(z_k, z'_i) dz'_i \doteq \frac{I_D^{(m)}(z_k) \Psi_{dI}^{(m)}}{T_D^{(m)}} = I_V^{(m)} \Psi_{dI}^{(m)} H_{0z} \quad (9.99e)$$

$$\int_{-h}^h I_U^{(m)}(z'_i) K_{dI}^{(m)}(z_k, z'_i) dz'_i \doteq \frac{I_D^{(m)}(z_k) \Psi_{dUI}^{(m)} T_U^{(m)}}{T_D^{(m)}} \doteq I_V^{(m)} T_U^{(m)} \Psi_{dUI}^{(m)} H_{0z} \quad (9.99f)$$

Explicit formulas for the Ψ functions are:

$$\Psi_{dR1}^{(m)} = \csc k_0(h - |z_M|) \int_{-h}^h M_{0z'} K_{dR1}^{(m)}(z_M, z'_i) dz'_i \quad (9.100a)$$

$$\Psi_{dR2}^{(m)} = (1 - \cos k_0 h)^{-1} \int_{-h}^h F_{0z'} K_{dR2}^{(m)}(0, z'_i) dz'_i \quad (9.100b)$$

$$\Psi_{dUR}^{(m)} = (1 - \cos k_0 h)^{-1} \int_{-h}^h F_{0z'} K_{dR}^{(m)}(0, z'_i) dz'_i \quad (9.100c)$$

$$\Psi_{dD}^{(m)} = (1 - \cos \frac{1}{2} k_0 h)^{-1} \int_{-h}^h H_{0z'} K_d^{(m)}(0, z'_i) dz'_i \quad (9.100d)$$

$$\Psi_{dI}^{(m)} = (1 - \cos \frac{1}{2} k_0 h)^{-1} \int_{-h}^h M_{0z'} K_{dI}^{(m)}(0, z'_i) dz'_i \quad (9.100e)$$

$$\Psi_{dUI}^{(m)} = (1 - \cos \frac{1}{2} k_0 h)^{-1} \int_{-h}^h F_{0z'} K_{dI}^{(m)}(0, z'_i) dz'_i \quad (9.100f)$$

Note that if $N = 1$, these formulas reduce directly to (9.39a-e) with $\Psi_{dR1}^{(m)} \rightarrow \Psi_{dR}$ and $\Psi_{dR2}^{(m)} = 0$, since $K_{dR2}^{(m)}(z_k, z'_i)$ vanishes. With (9.98) the function $U^{(m)}$ as defined in (9.95b) may be expressed as follows:

$$U^{(m)} = \frac{-j\check{\zeta}_0}{4\pi} [I_V^{(m)} \Psi_V^{(m)}(h) + I_U^{(m)} \Psi_U^{(m)}(h) + I_D^{(m)} \Psi_D^{(m)}(h)] \quad (9.101)$$

$$\text{where} \quad \Psi_V^{(m)}(h) = \int_{-h}^h M_{0z'} K^{(m)}(h, z'_i) dz'_i \quad (9.102a)$$

$$\Psi_U^{(m)}(h) = \int_{-h}^h F_{0z'} K^{(m)}(h, z'_i) dz'_i \quad (9.102b)$$

$$\Psi_D^{(m)}(h) = \int_{-h}^h H_{0z'} K^{(m)}(h, z'_i) dz'_i \quad (9.102c)$$

$$\text{where} \quad K^{(m)}(h, z'_i) = \sum_{i=1}^N p^{(i-k)m} K(h, z'_i) = \sum_{i=1}^N p^{(i-k)m} \frac{e^{-jk_0 R_{ikh}}}{R_{ikh}}$$

with $R_{ikh} = \sqrt{(h - z'_i)^2 + b_{ik}^2}$.

If (9.99a-f) and (9.102a-c) are substituted in the integral equation (9.94) and the coefficients of the three functions of z are separately equated to zero, the following values are obtained for $I_V^{(m)}$, $T_U^{(m)}$, and $T_D^{(m)}$:

$$I_V^{(m)} = \frac{j2\pi V^{(m)}}{\xi_0 \Psi_{dR1} \cos k_0 h} \quad (9.103a)$$

$$T_U^{(m)} = (Q^{(m)})^{-1} \{ \Psi_{dD}^{(m)} [\Psi_V^{(m)}(h) - \Psi_{dR2}^{(m)} \cos k_0 h] - j \Psi_{dI}^{(m)} \Psi_D^{(m)}(h) \} \quad (9.103b)$$

$$T_D^{(m)} = j(Q^{(m)})^{-1} \{ \Psi_{dI}^{(m)} [\Psi_U^{(m)}(h) - \Psi_{dUR}^{(m)} \cos k_0 h] - \Psi_{dUI}^{(m)} [\Psi_V^{(m)}(h) - \Psi_{dR2}^{(m)} \cos k_0 h] \} \quad (9.103c)$$

$$Q^{(m)} = -\Psi_{dD}^{(m)} [\Psi_U^{(m)}(h) - \Psi_{dUR}^{(m)} \cos k_0 h] + j \Psi_{dUI}^{(m)} \Psi_D^{(m)}(h) \quad (9.103d)$$

Comparison of (9.103b) to (9.103d) with (9.45b) to (9.45c) shows that the values for N coupled antennas reduce identically to the earlier values for the single antenna when $N = 1$ and $\Psi_{dR2} = 0$.

With all coefficients evaluated, the explicit form for the leading terms for the current in the element k of a circular array driven in the m th phase sequence as obtained from (9.98) is

$$I_z^{(m)}(z) = \frac{j2\pi V^{(m)}}{\xi_0 \Psi_{dR1}^{(m)} \cos k_0 h} [\sin k_0(h - |z|) + T_U^{(m)}(\cos k_0 z - \cos k_0 h) + T_D^{(m)}(\cos \frac{1}{2}k_0 z - \cos \frac{1}{2}k_0 h)] \quad (9.104)$$

The currents in the other $N - 1$ elements are given by $I_{zi}^{(m)}(z_i) = I_z^{(m)}(z)p^{(i-k)m}$, where $p = e^{j2\pi/N}$. Note that they differ only by a constant phase factor. Higher-order terms may be obtained by iteration, but for most purposes (9.104) is adequate. The m th phase-sequence admittance is

$$Y^{(m)} = \frac{I_z^{(m)}(0)}{V^{(m)}} \quad (9.105)$$

9.12 Arbitrarily Driven Circular Array

The N phase-sequence currents given by (9.104) with $m = 0, 1, 2, \dots, N - 1$, may be combined to give the currents in N arbitrarily driven elements by means of the following set of formulas, where $p = e^{j2\pi/N}$. The N individual driving voltages V_i and currents $I_{zi}(z)$ in an arbitrarily driven circular array are related to the phase-sequence voltages $V^{(m)}$ and currents $I_z^{(m)}(z)$ of the same circular array successively driven in the N phase sequences by the relations

$$V_i = \sum_{m=0}^{N-1} p^{(i-k)m} V_i^{(m)} \quad I_{zi}(z) = \sum_{m=0}^{N-1} p^{(i-k)m} I_z^{(m)}(z) \quad (9.106)$$

which are referred to antenna k . The inverse relations are

$$V^{(m)} = N^{-1} \sum_{i=1}^N p^{-(i-k)m} V_i \quad I_z^{(m)}(z) = N^{-1} \sum_{i=1}^N p^{-(i-k)m} I_{zi}(z) \quad (9.107)$$

For any given set of driving voltages V_i , it is possible to determine the necessary phase-sequence voltages $V^{(m)}$ by solving the set of equations in (9.106). For each of the $V^{(m)}$ the distribution of current $I_z^{(m)}(z)$ is obtained from (9.104). With all of the currents $I_z^{(m)}(z)$, $m = 0, 1, 2, \dots, N - 1$, known, the individual currents $I_{zi}(z)$, $i = 1, 2, \dots, N$, may be obtained directly from (9.106) in the form

$$I_{zi}(z) = \sum_{m=0}^{N-1} p^{(i-k)m} V^{(m)} Y^{(m)}(z) \quad (9.108)$$

where $Y^{(m)}(z) = I_z^{(m)}(z)/V^{(m)}$ and $Y^{(m)} = Y^{(m)}(0) = I_z^{(m)}(0)/V^{(m)}$ is the m th phase-sequence admittance.

The circuit properties of an array are conveniently expressed in terms of self- and mutual admittances. This is readily accomplished by the elimination of $V^{(m)}$ from (9.108) by means of (9.107). The result is a set of N algebraic equations

$$I_{zi}(z) = \sum_{j=1}^N V_j Y_{ij}(z) \quad i = 1, 2, \dots, N \quad (9.109a)$$

where

$$Y_{ij}(z) = N^{-1} \sum_{m=0}^{N-1} p^{(i-j)m} Y^{(m)}(z) \quad (9.109b)$$

In particular, the driving-point currents satisfy the equations

$$I_{zi}(0) = \sum_{j=1}^N V_j Y_{ij} \quad i = 1, 2, \dots, N \quad (9.110)$$

where $Y_{ij} = Y_{ij}(0)$, Y_{ii} is the self-admittance of antenna i and the Y_{ji} , $j \neq i$, are the mutual admittances of antenna i in the given circular array. Note that in general $Y_{ij} = Y_{ji}$. It is important to recognize that Y_{ii} and Y_{ij} in a given N -element array are *not the same* as Y_{ii} and Y_{ij} when any or all of the N elements except i and j are removed. The N equations (9.110) may be solved for the N voltages in the form

$$V_i = \sum_{j=1}^N I_{zj}(0) Z_{ij} \quad (9.111)$$

where the Z_{ij} are the self- ($j = i$) and mutual ($j \neq i$) impedances.

Exercise 9.6 Obtain formulas for the Z_{ij} in terms of the Y_{ij} .

It follows from (9.106) with (9.104) that the approximate current in element i is given by

$$I_{zi}(z) = \frac{j2\pi}{\zeta_0 \cos k_0 h} [s_i \sin k_0(h - |z|) + g_i(\cos k_0 z - \cos k_0 h) + h_i(\cos \frac{1}{2}k_0 z - \cos \frac{1}{2}k_0 h)] \quad (9.112)$$

$$\text{where} \quad s_i = \sum_{m=0}^{N-1} p^{(i-1)m} \frac{V^{(m)}}{\Psi_{dR1}^{(m)}} \quad (9.113a)$$

$$g_i = \sum_{m=0}^{N-1} p^{(i-1)m} \frac{T_U^{(m)} V^{(m)}}{\Psi_{dR1}^{(m)}} \quad (9.113b)$$

$$h_i = \sum_{m=0}^{N-1} p^{(i-1)m} \frac{T_D^{(m)} V^{(m)}}{\Psi_{dR1}^{(m)}} \quad (9.113c)$$

If the N driving voltages V_1, \dots, V_N are specified, the voltages $V^{(m)}$ may be obtained from (9.107) with $k = 1$ and used in (9.113a-c). On the other hand, if the N driving-point currents $I_{z1}(0), \dots, I_{zN}(0)$ are specified, the associated N phase-sequence currents $I_z^{(0)}(0), \dots, I_z^{(N-1)}(0)$ may be obtained from (9.107). Since the phase-sequence admittances $Y^{(m)}$ are known, the voltages $V^{(m)} = I_z^{(m)}(0)/Y^{(m)}$ are available for use in (9.113a-c).

The radiation field of an array of N parallel elements with their centers at $z = 0$ uniformly spaced around a circle of radius ρ is given by

$$E_\theta(R, \theta, \phi) = \frac{j\omega\mu_0}{4\pi} \frac{e^{-jk_0 R_0}}{R_0} \sin \theta \sum_{i=1}^N e^{jk_0 S_i} \int_{-h}^h I_{zi}(z') e^{jk_0 z' \cos \theta} dz' \quad (9.114)$$

where $I_{zi}(z)$ is the current in antenna i and $R_i = R_0 - S_i$ with $S_i = \rho \sin \theta \cos(\phi - \phi_i)$ and $\phi_i = 2\pi(i-1)/N$. The notation is illustrated in Fig. 9.12. With (9.112) substituted in (9.114), it follows that

$$E_\theta(R, \theta, \phi) = \frac{-e^{-jk_0 R_0}}{R_0 \cos k_0 h} \left[F_m(\theta, k_0 h) \sum_{i=1}^N s_i e^{jk_0 S_i} + G_m(\theta, k_0 h) \sum_{i=1}^N g_i e^{jk_0 S_i} + D_m(\theta, k_0 h) \sum_{i=1}^N h_i e^{jk_0 S_i} \right] \quad (9.115)$$

where s_i , g_i , and h_i are in (9.113a-c) and where $F_m(\theta, k_0 h)$, $G_m(\theta, k_0 h)$, and $D_m(\theta, k_0 h)$ are defined in (9.64a-c). When $k_0 h$ is near $\pi/2$, a more convenient formula in terms of the function $H_m(\theta, k_0 h)$ defined in (9.65b) and $G_m(\theta, k_0 h)$ and $D_m(\theta, k_0 h)$ is readily derived.

Computations for currents, admittances, and field patterns of circular arrays have not been made from (9.112) and (9.115). However, a somewhat simpler and slightly less accurate formulation has been studied in detail. This is based on the fact that the distributions $F_{0z} = \cos k_0 z - \cos k_0 h$ and $H_{0z} = \cos \frac{1}{2}k_0 z - \cos \frac{1}{2}k_0 h$ are not very different when $k_0 h \leq \pi$ except near the ends of the antenna, where the amplitude is relatively small. It follows that the substitution of F_{0z} for H_{0z} should make no great difference in the admittance and far field (this is not true of the near field). If this substitution is made, the phase sequence currents are

$$I_z^{(m)}(z) \doteq \frac{j2\pi V^{(m)}}{\zeta_0 \Psi_{dR1} \cos k_0 h} [\sin k_0(h - |z|) + T^{(m)}(\cos k_0 z - \cos k_0 h)] \quad (9.116a)$$

where, since now $\Psi_{dD} \rightarrow \Psi_{dU}$, $\Psi_D(h) \rightarrow \Psi_U(h)$

$$T^{(m)} = T_U^{(m)} + T_D^{(m)} = -\frac{\Psi_V(h) - (\Psi_{dR2} + j\Psi_{dI}) \cos k_0 h}{\Psi_U(h) - \Psi_{dU} \cos k_0 h} \quad (9.116b)$$

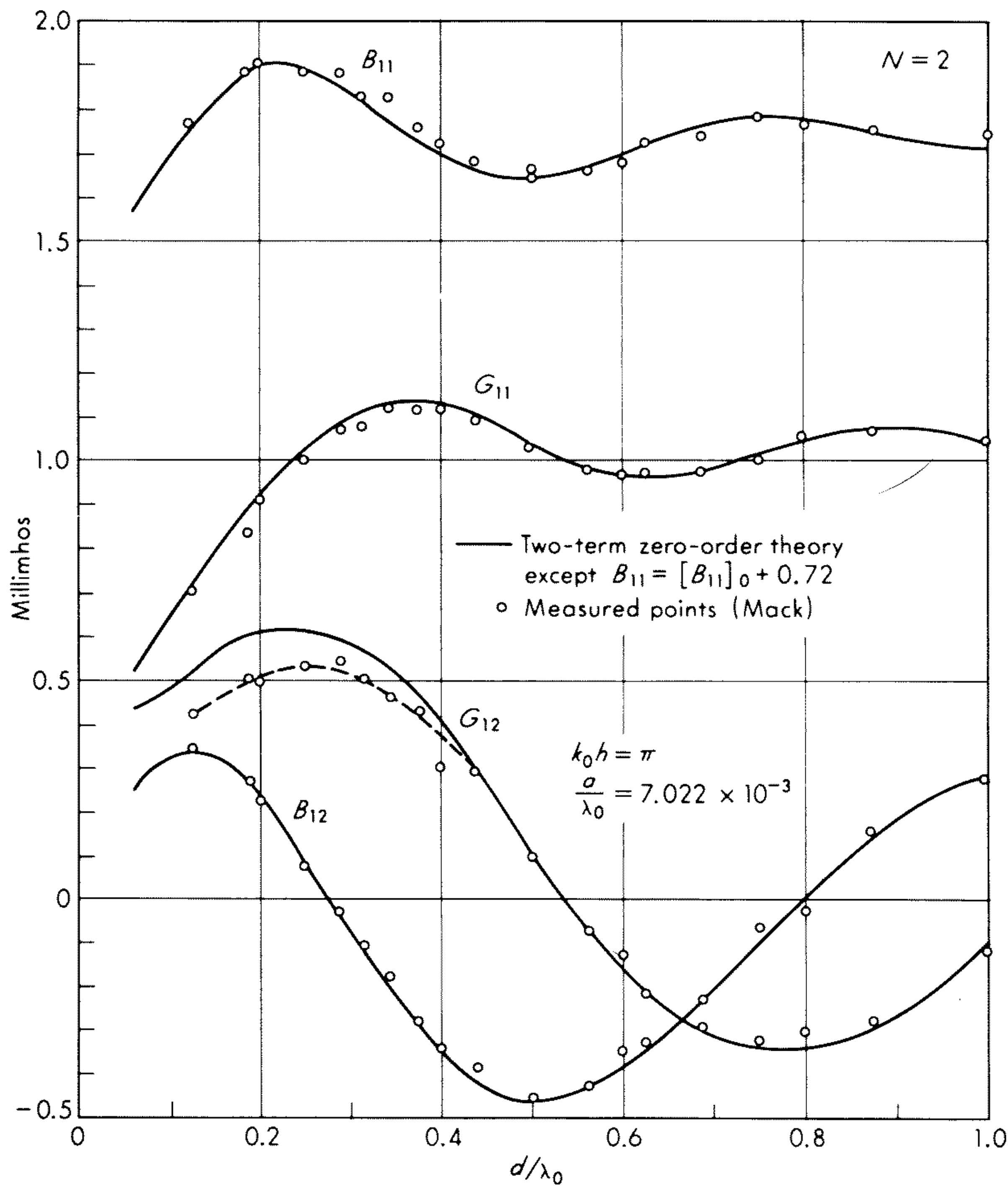


Fig. 9.13 Self- and mutual admittances of two-element array; d is the distance between elements.

If this current is used to obtain field patterns, the expression (9.115) is obtained but with the last term [with $D_m(\theta, k_0 h)$ as coefficient] absent and $T^{(m)}$ as given in (9.116b) substituted for $T_U^{(m)}$ in (9.113b).

In order to show the accuracy of the two-term theory in the complete analysis of arrays, values of self- and mutual conductances for a two-element and a five-element circular array are shown in Figs. 9.13 and 9.14 specifically for full-wave elements — which cannot be handled at all by conventional array theory. Zero-order values of G and B are shown together with measured values¹⁵ except that B_{11} is corrected by adding a lumped susceptance of 0.72 mmhos to correct for the error in $I(z)$ very near and at $z = 0$, which results from the inadequacy of trigonometric functions to account for the rapid change in the current near the driving point. The agreement is seen to be very good

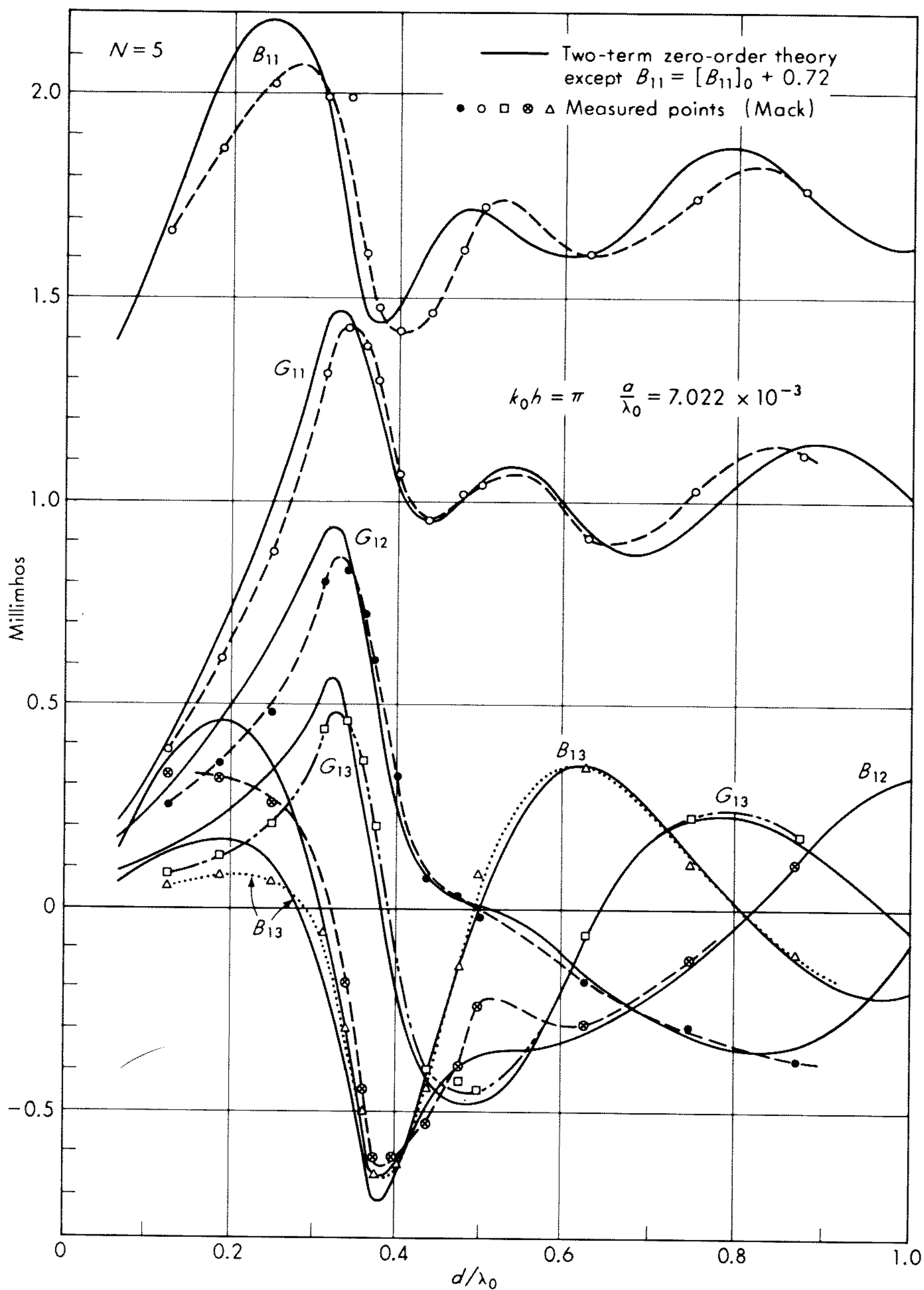


Fig. 9.14 Self- and mutual admittances of five-element circular array; d is the distance between adjacent elements.

throughout. The same can be said of the field patterns shown in Fig. 9.15 for which one element is driven, the others parasitic. Similar agreement has been obtained for antennas in the range $k_0 h \leq 5\pi/4$.

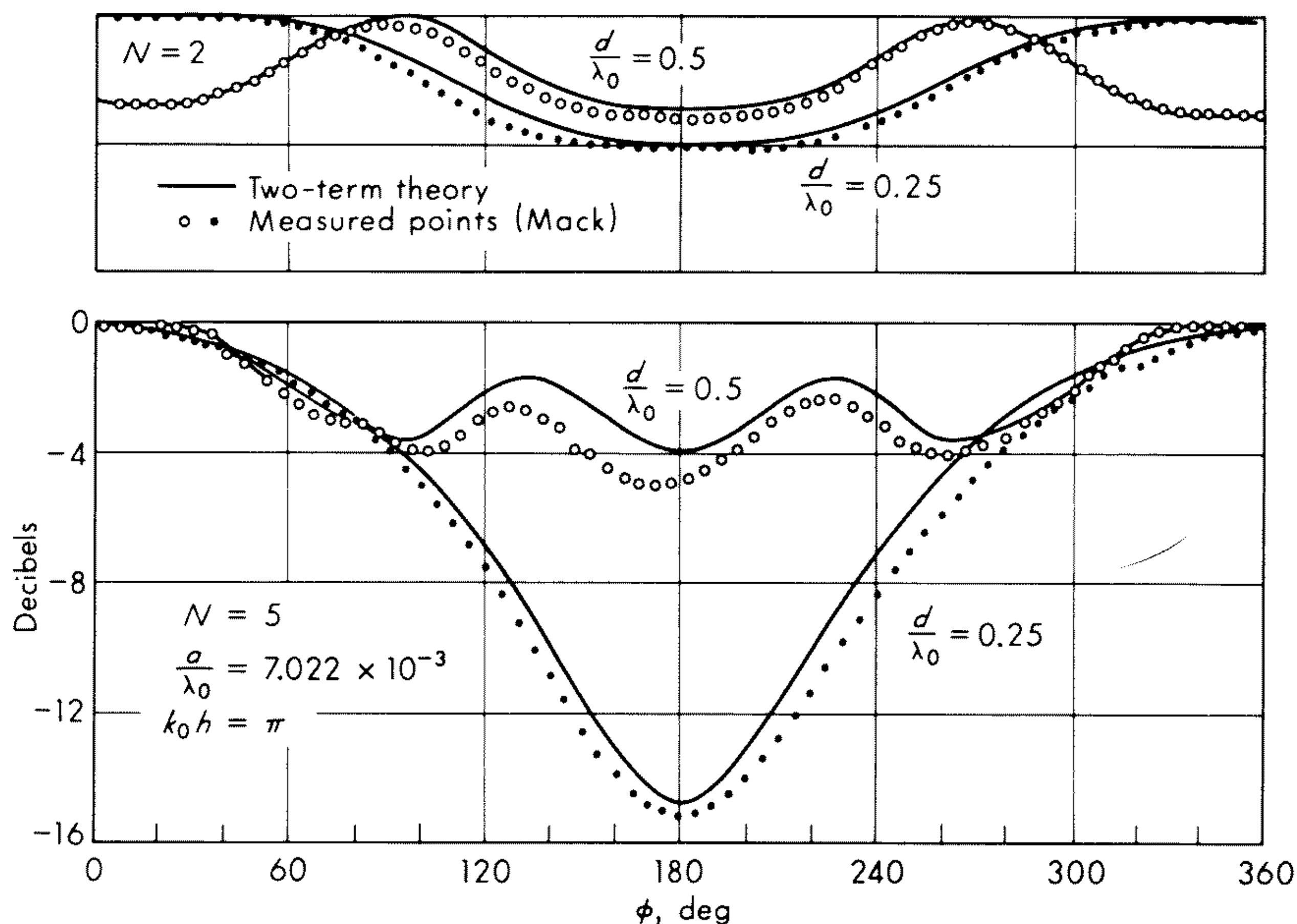


Fig. 9.15 Horizontal field pattern of parasitic arrays of N elements in a circle; d is the distance between adjacent elements.

It may be concluded that circular arrays may be treated with quantitative accuracy in determining currents, admittances, and far fields if use is made of the simple two-term formula for the current in each element supplemented with a small lumped susceptance in parallel with the antenna to correct for the inability of trigonometric functions to represent the current very near to and at the driving point accurately. Actually, this correction is needed only when $k_0 h > \pi/2$.

9.13 The Curtain Array

When the N geometrically identical elements of a parallel array are located with their centers equally spaced along a straight line instead of around a circle, the N simultaneous integral equations (9.91) for the N currents cannot be solved by replacing them with N independent integral equations. Since the relative positions of the elements are all different in pairs, there is no physical equivalence between them no matter how they are driven. However, since the distributions of current on all the elements of a circular array of any size can be well approximated by the three-term expression (9.112), it is logical to assume that the same distribution with suitably defined coefficients must be a good approximation for the elements of a curtain array. Specifically, let the current on element i be approximated by

$$I_{zi}(z) = I_{Vi}(z) + I_{Ci}(z) + I_{Di}(z) \doteq jA_i M_{0z} + C_i F_{0z} + D_i H_{0z} \quad (9.117)$$

where, as before, $M_{0z} = \sin k_0(h - |z|)$, $F_{0z} = \cos k_0z - \cos k_0h$, and $H_{0z} = \cos \frac{1}{2}k_0z - \cos \frac{1}{2}k_0h$. If this current is substituted in the sum of integrals on the left in (9.91) and in the expression (9.92c) for U_k and if the same properties are assumed to apply to the kernel as are introduced in (9.96a-f) for the circular array, a set of Ψ functions may be defined for each element just as is done in (9.100a-f) and (9.102a-c) for all elements in a phase sequence. With them the integral equations (9.91) reduce to the following set of N simultaneous algebraic equations for the coefficients of the zero-order currents:

$$A_k M_{0z} + C_k F_{0z} + D_k H_{0z} = \frac{j4\pi}{\zeta_0 \cos k_0h} (\frac{1}{2}V_k M_{0z} + U_k F_{0z}) \quad (9.118)$$

where $k = 0, 1, 2, \dots, N$ and

$$U_k = \frac{-j\zeta_0}{4\pi} \sum_{i=1}^N [I_{Vi}\Psi_{Vki}(h) + I_{Ui}\Psi_{Uki}(h) + I_{Di}\Psi_{Dki}(h)] \quad (9.119)$$

$$A_k = \sum_{i=k-m}^{k+m} I_{Vi}\Psi_{dRki} \quad (9.120a)$$

$$C_k = \left(\sum_{i=0}^{k-m} + \sum_{k+m}^N \right) I_{Vi}\Psi_{dRki} + \sum_{i=0}^N I_{Ui}\Psi_{dURki} \quad (9.120b)$$

$$D_k = \sum_{i=0}^N (jI_{Vi}\Psi_{dIki} + jI_{Ui}\Psi_{dUIki} + I_{Di}\Psi_{dDki}) \quad (9.120c)$$

In (9.120a) m is a number such that all elements in the range $k - m \leq i \leq k + m$ are sufficiently close to element k that $b_{ki} < 1$. The several Ψ functions in (9.119)–(9.120c) are defined as follows:

$$\Psi_{dRki} = \csc k_0(h - |z_M|) \int_{-h}^h M_{0z'} K_{dRki}(z_M, z'_i) dz'_i \quad (9.121a)$$

$$\Psi_{dURki} = (1 - \cos k_0h)^{-1} \int_{-h}^h F_{0z'} K_{dRki}(z_M, z'_i) dz'_i \quad (9.121b)$$

$$\Psi_{dDki} = (1 - \cos \frac{1}{2}k_0h)^{-1} \int_{-h}^h H_{0z'} K_{dki}(z, z'_i) dz'_i \quad (9.121c)$$

$$\Psi_{dIki} = (1 - \cos \frac{1}{2}k_0h)^{-1} \int_{-h}^h H_{0z'} K_{dki}(0, z'_i) dz'_i \quad (9.121d)$$

$$\Psi_{dUIki} = (1 - \cos \frac{1}{2}k_0h)^{-1} \int_{-h}^h F_{0z'} K_{dI}(0, z'_i) dz'_i \quad (9.121e)$$

$$\Psi_{Vki}(h) = \int_{-h}^h M_{0z'} K_{ki}(h, z'_i) dz'_i \quad (9.121f)$$

$$\Psi_{Uki}(h) = \int_{-h}^h F_{0z'} K_{ki}(h, z'_i) dz'_i \quad (9.121g)$$

$$\Psi_{Dki}(h) = \int_{-h}^h H_{0z'} K_{ki}(h, z'_i) dz'_i \quad (9.121h)$$

The subscript d denotes a difference kernel; R and I denote real and imaginary parts of the kernel; and k and i are indices. The kernels are

$$K_{dki}(z, z') = K_{ki}(z, z') - K_{ki}(h, z') = \frac{e^{-jk_0 R_{ki}}}{R_{ki}} - \frac{e^{-jk_0 R_{hki}}}{R_{hki}} \quad (9.122a)$$

$$\begin{aligned} K_{dki}(z, z'_i) &= K_{dRki}(z, z'_i) + jK_{dIki}(z, z'_i) \\ &= \frac{\cos k_0 R_{ki}}{R_{ki}} - \frac{\cos k_0 R_{hki}}{R_{hki}} - j \left(\frac{\sin k_0 R_{ki}}{R_{ki}} - \frac{\sin k_0 R_{hki}}{R_{hki}} \right) \end{aligned} \quad (9.122b)$$

$$\text{where } R_{ki} = [(z - z')^2 + b_{ki}^2]^{\frac{1}{2}} \quad R_{hki} = [(h - z')^2 + b_{ki}^2]^{\frac{1}{2}} \quad (9.122c)$$

A solution of the set of simultaneous equations (9.118) with $k = 0, 1, \dots, N$, may be obtained if the coefficients of each of the three distribution functions is separately equated to zero. This yields three sets of N simultaneous equations. In order to simplify the problem let it be assumed that all antennas are sufficiently far from their next adjacent neighbors that $b_{ki} \geq 1$ for all $k \neq i$. In this case

$$\Psi_{dRki} = \Psi_{dRkk} \equiv \Psi_{dR} \quad (9.123)$$

It follows that

$$A_k = \frac{j2\pi V_k}{\zeta_0 \cos k_0 h} \quad C_k = \frac{j4\pi U_k}{\zeta_0 \cos k_0 h} \quad D_k = 0 \quad (9.124)$$

With (9.119) to (9.120c) and $m = 0$, it follows that

$$I_{Vk} = \frac{j2\pi V_k}{\zeta_0 \Psi_{dR} \cos k_0 h} \quad k = 1, 2, \dots, N \quad (9.125)$$

$$\sum_{i=1}^N \left\{ I_{Vi} [\Psi_{Vki}(h) - \Psi_{dRki}(1 - \delta_{ki}) \cos k_0 h] + I_{Ui} [\Psi_{Uki}(h) - \Psi_{dRki} \cos k_0 h] \right. \\ \left. + I_{Di} [\Psi_{Dki}(h) - \Psi_{dDki} \cos k_0 h] \right\} = 0 \quad (9.126)$$

$$\sum_{i=1}^N (jI_{Vi} \Psi_{dIki} + jI_{Ui} \Psi_{dUIki} + I_{Di} \Psi_{dDki}) = 0 \quad (9.127)$$

The two sets of N equations (9.126) and (9.127) must be solved for the N quantities I_{Ui} , $i = 1, \dots, N$, and the N quantities I_{Di} , $i = 1, \dots, N$, in terms of the N quantities I_{Vk} , $k = 1, \dots, N$. If the N driving voltages V_k are given, all of the amplitudes I_{Vk} , I_{Uk} , and I_{Dk} are then determined and with them the currents in the N coupled antennas.

Since the solution of (9.126) and (9.127) is somewhat involved, a simplifying approximation is desirable. It has already been pointed out that for antennas with half lengths h in the range, $h < 3\pi/2$, the difference between the distributions of current $F_{0z} = \cos k_0 z - \cos k_0 h$ and $H_{0z} = \cos \frac{1}{2}k_0 z - \cos \frac{1}{2}k_0 h$ is not so great that the field at some distance from each antenna is greatly altered. (This is not true of the field very near each antenna.) Since it has been assumed that the nearest distance between any pair of elements satisfies the inequality $k_0 b_{ik} \geq 1$ for all i and k with $i \neq k$, the substitution of F_{0z} for H_{0z} should be an acceptable approximation. Note that the current at the driving points and,

hence, the driving-point admittance is not affected significantly, since the total current at $z = 0$ is maintained substantially the same with either choice of distribution.

If $H_{0z} \rightarrow F_{0z}$, it follows that $\Psi_{dDki} \rightarrow \Psi_{dUki}$, $\Psi_{Dki}(h) \rightarrow \Psi_{Uki}(h)$, and $I_{Ui} + I_{Di} \rightarrow I_{Ui}$. With these substitutions in (9.126) and (9.127), the latter may be multiplied by $\cos k_0 h$ and subtracted from (9.126) to give the following single set of equations:

$$\sum_{i=1}^N I_{Vi} \{ \Psi_{Vki}(h) - [\Psi_{dRki}(1 - \delta_{ki}) + j\Psi_{dIki}] \cos k_0 h \} = \sum I_{Ui} [\Psi_{dUki} \cos k_0 h - \Psi_{Uki}(h)] \quad (9.128)$$

This is now conveniently put in matrix form with

$$\Phi_{Vki} = \Psi_{Vki}(h) - [\Psi_{dRki}(1 - \delta_{ki}) + j\Psi_{dIki}] \cos k_0 h \quad (9.129a)$$

$$\Phi_{Uki} = \Psi_{dUki} \cos k_0 h - \Psi_{Uki}(h) \quad (9.129b)$$

It follows that

$$\Phi_U \cdot \mathbf{I}_U = \Phi_V \cdot \mathbf{I}_V \quad (9.130)$$

where \mathbf{I}_U and \mathbf{I}_V are column matrices and Φ_U and Φ_V square $N \times N$ matrices of the form

$$\mathbf{I}_U = \begin{Bmatrix} I_{U1} \\ I_{U2} \\ \vdots \\ I_{UN} \end{Bmatrix} \quad \Phi_U = \begin{bmatrix} \Phi_{U11} & \Phi_{U12} & \cdots & \Phi_{U1N} \\ \cdots & \cdots & \cdots & \cdots \\ \Phi_{UN1} & \Phi_{UN2} & \cdots & \Phi_{UNN} \end{bmatrix} \quad (9.131)$$

The solution of (9.130) may be carried out for two important physical situations: (1) the N voltages V_k are specified and the N currents $I_{zk}(z)$ are to be determined, and (2) the N driving-point currents $I_{zk}(0)$ are specified and the N voltages V_k are to be determined. In both cases the ratio $I_{zk}(0)/V_k = Y_k$ yields the driving-point admittance.

1. **Driving voltages specified.** If the N voltages V_k are given, the N amplitudes I_{Vk} are known from (9.125), $I_{Vk} = j2\pi V_k / \zeta_0 \Psi_{dR} \cos k_0 h$. The amplitudes I_U are then obtained from (9.130) in the form

$$\mathbf{I}_U = \Phi_U^{-1} \cdot \Phi_V \cdot \mathbf{I}_V = \frac{j2\pi}{\zeta_0 \Psi_{dR} \cos k_0 h} \Phi_U^{-1} \cdot \Phi_V \cdot \mathbf{V} \quad (9.132)$$

It follows that the complete solutions are given by

$$\begin{aligned} \mathbf{I}_z(z) &= \mathbf{I}_V M_{0z} + \mathbf{I}_U F_{0z} \\ &= \frac{j2\pi}{\zeta_0 \Psi_{dR} \cos k_0 h} [\mathbf{V} \sin k_0(h - |z|) + \Phi_U^{-1} \cdot \Phi_V \cdot \mathbf{V} (\cos k_0 z - \cos k_0 h)] \end{aligned} \quad (9.133)$$

2. Driving-point currents specified. If each of the complex currents $I_{zi}(0) = I''_{zi}(0) + jI'_{zi}(0)$ is specified in

$$I_{zi}(0) = j(I_{Vi}) \sin k_0 h + (I_{URi} + jI_{UIi})(1 - \cos k_0 h) \quad (9.134)$$

where $|I_{Vi}| = 2\pi V_i / \zeta_0 \Psi_{dR} \cos k_0 h$, it follows that

$$I_{URi} = \frac{I''_{zi}(0)}{1 - \cos k_0 h} \quad (9.135a)$$

$$I_{UIi} = \frac{I'_{zi}(0) - |I_{Vi}| \sin k_0 h}{1 - \cos k_0 h} \quad (9.135b)$$

Hence, with $I''_{zi}(0)$ and $I'_{zi}(0)$ given, the quantities I_{URi} and I_{UIi} can be determined directly, so that the I_{Ui} are known. Thus

$$I_{Ui} = \frac{I_{zi}(0) - I_{Vi} \sin k_0 h}{1 - \cos k_0 h} \quad (9.136a)$$

$$\frac{I_{zi}(0)}{1 - \cos k_0 h} = I_{Ui} + I_{Vi} \frac{\sin k_0 h}{1 - \cos k_0 h} \quad (9.136b)$$

It follows that

$$\frac{\mathbf{I}_z(0)}{1 - \cos k_0 h} = \left(\mathbf{I}_U + \mathbf{I}_V \frac{\sin k_0 h}{1 - \cos k_0 h} \right) = \mathbf{I}_U + \mathbf{I}_V \frac{\sin k_0 h}{1 - \cos k_0 h} \quad (9.137)$$

The premultiplication of (9.137) on both sides by Φ_U and the use of (9.130) with the distributive law leads to

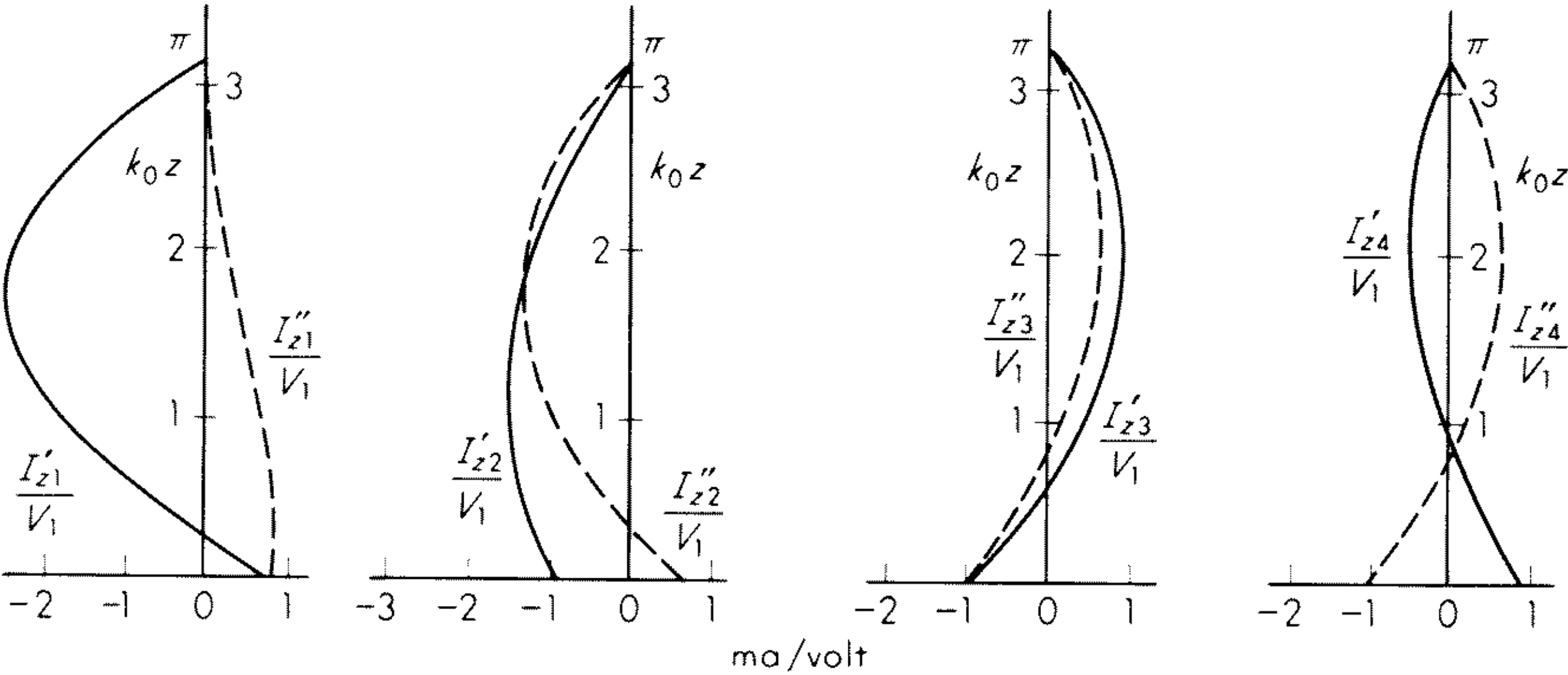
$$\mathbf{I}_V = \left(\Phi_V + \Phi_U \frac{\sin k_0 h}{1 - \cos k_0 h} \right)^{-1} \cdot \Phi_U \cdot \frac{\mathbf{I}_z(0)}{1 - \cos k_0 h} \quad (9.138a)$$

or
$$\mathbf{V} = \frac{-j\zeta_0 \Psi_{dR} \cos k_0 h}{2\pi(1 - \cos k_0 h)} \left(\Phi_V + \Phi_U \frac{\sin k_0 h}{1 - \cos k_0 h} \right)^{-1} \cdot \Phi_U \cdot \mathbf{I}_z(0) \quad (9.138b)$$

The N values of V_i that are required to maintain the N specified currents $I_{zi}(0)$ may be determined from this equation and used to obtain the associated amplitudes I_{Vi} . With $I_{zi}(0)$ given and I_{Vi} known, (9.136a) may be used to find $I_{Ui} = I_{URi} + jI_{UIi}$. The substitution of these values in $I_{zi}(z) = I_{Vi}M_{0z} + I_{Ui}F_{0z}$ expresses the current in each element in terms of the N driving voltages V_i . The ratio $I_{zi}(0)/V_i = Y_i$ is the driving-point admittance of element i .

The distribution of current on a four-element end-fire array in which the identical elements are spaced one-quarter wavelength apart ($b_{i,i+1} = \lambda_0/4$) and are a full wavelength long ($2h = \lambda_0$) is shown in Fig. 9.16 for two cases. In the upper row the driving-point currents are required to have equal amplitudes and to be shifted progressively in phase by one-quarter period. The currents higher up on the elements are seen to differ greatly, with much more current in element No. 1 than in No. 4. In the lower row the driving voltages are equal in magnitude and shifted progressively by one-quarter period in phase. Although

Driving-point currents specified; $I_{z4}(0) = jI_{z3}(0) = -I_{z2}(0) = -jI_{z1}(0)$



Driving voltages specified; $V_4 = jV_3 = -V_2 = -jV_1$

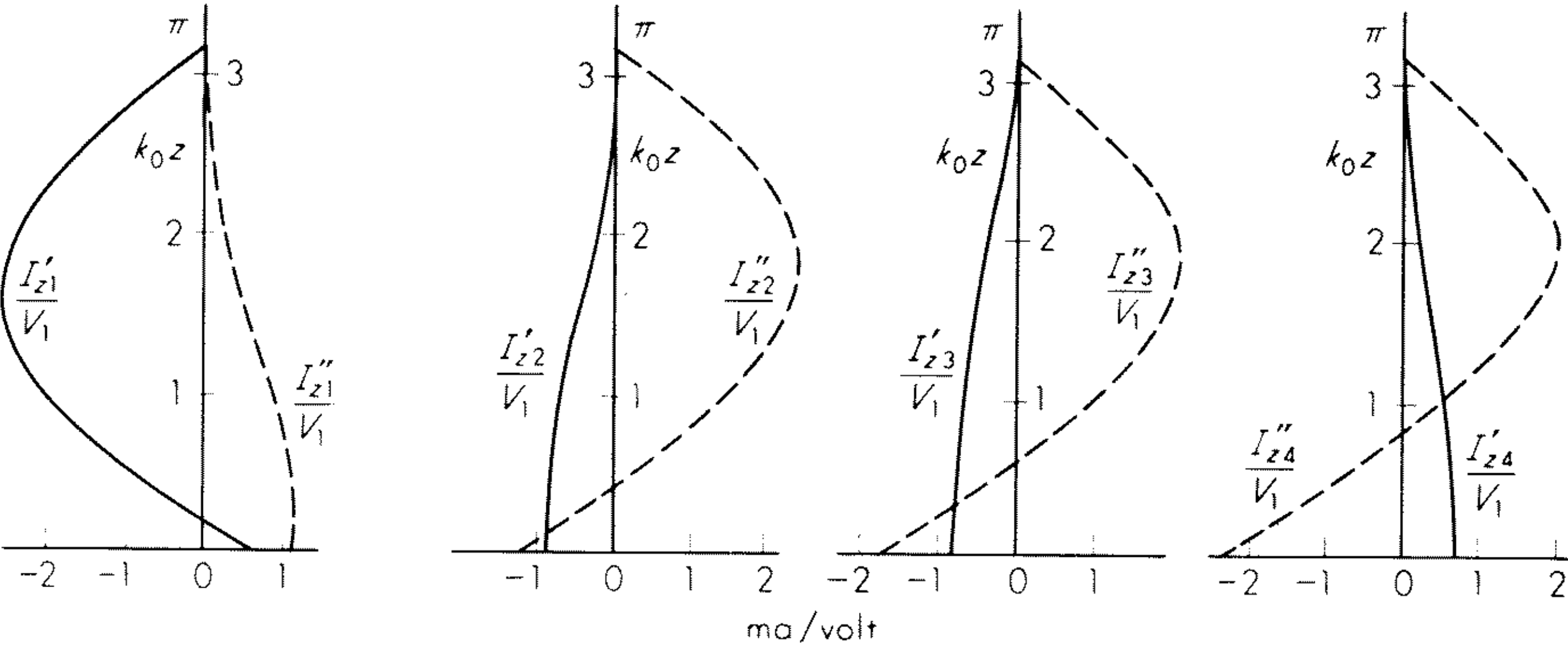


Fig. 9.16 Normalized currents in four-element end-fire array; $\Omega = 10, k_0h = \pi, k_0b = \pi/2$.

the distributions on the elements differ, the total currents are quite comparable. The associated driving-point admittances $Y_{0j} = G_{0j} + jB_{0j}$ in millimhos are:

Millimhos	Y_{01}	Y_{02}	Y_{03}	Y_{04}
Currents specified . .	$0.824 + j0.797$	$0.433 + j1.611$	$0.216 + j1.921$	$0.049 + j2.363$
Voltages specified . . .	$1.209 + j0.459$	$0.884 + j1.234$	$0.848 + j1.710$	$0.681 + j2.339$

The power supplied to each of the elements is $P_i = |I_{zi}(0)|^2R_{0i} = |V_i|^2G_{0i}$. Referred to element No. 4 the relative powers are:

	P_1	P_2	P_3	P_4
Currents specified . .	71.4	17.7	10.1	1
Voltages specified . . .	1.76	1.29	1.24	1

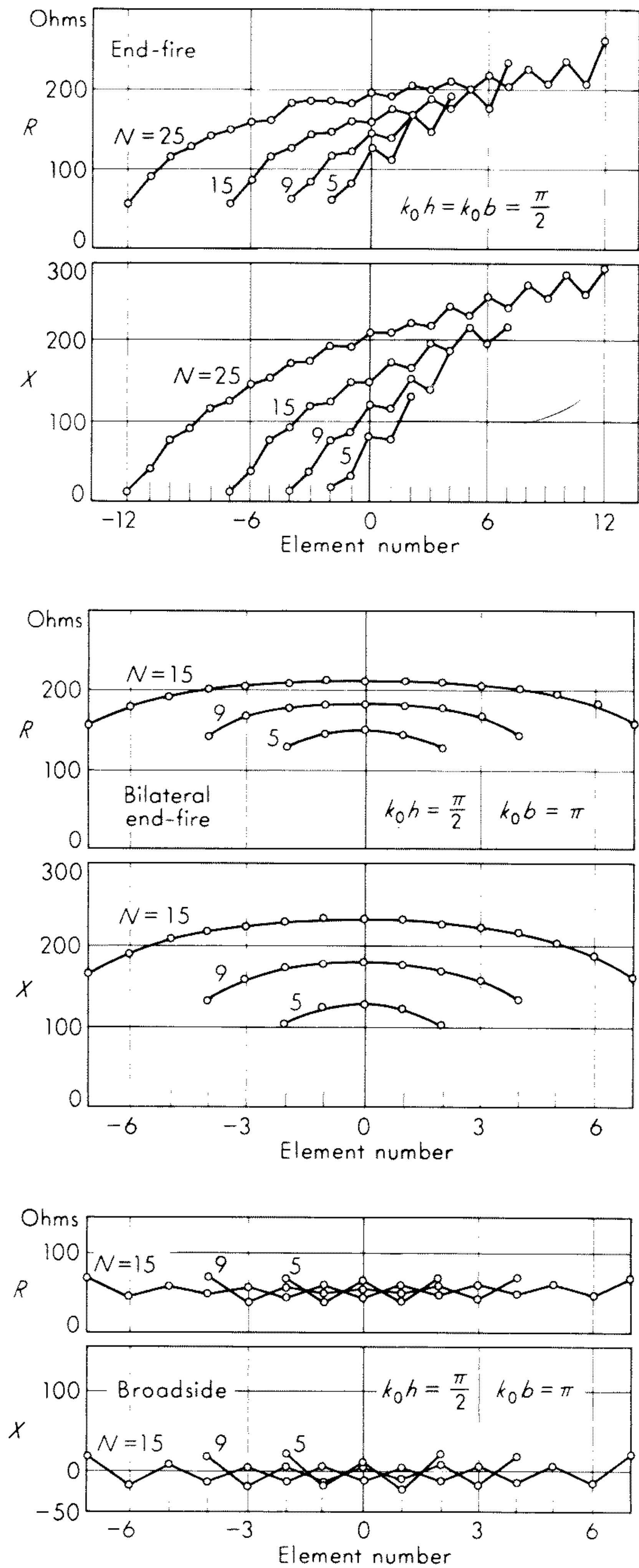


Fig. 9.17 Impedance of N -element curtain arrays; half-wave elements; $I(0)$ specified.

These results are consistent with the relative amplitudes of the currents on the four elements. When driving-point currents are kept equal in magnitude, antenna 1 carries much more current than the others and, therefore, radiates much more power. When the voltages are equal in magnitude, the amplitudes of the currents along the antennas (but not at the driving points) are quite comparable, so that they contribute fairly equally to the radiated power.

The driving-point impedances of typical broadside and end-fire arrays are shown in Fig. 9.17 for several values of N for half-wave elements and in Fig. 9.18 for full-wave elements.

The far fields of curtain arrays may be determined from a formula similar to (9.115) with $\phi_i = 0$ and ρ suitably defined. The horizontal field patterns of the

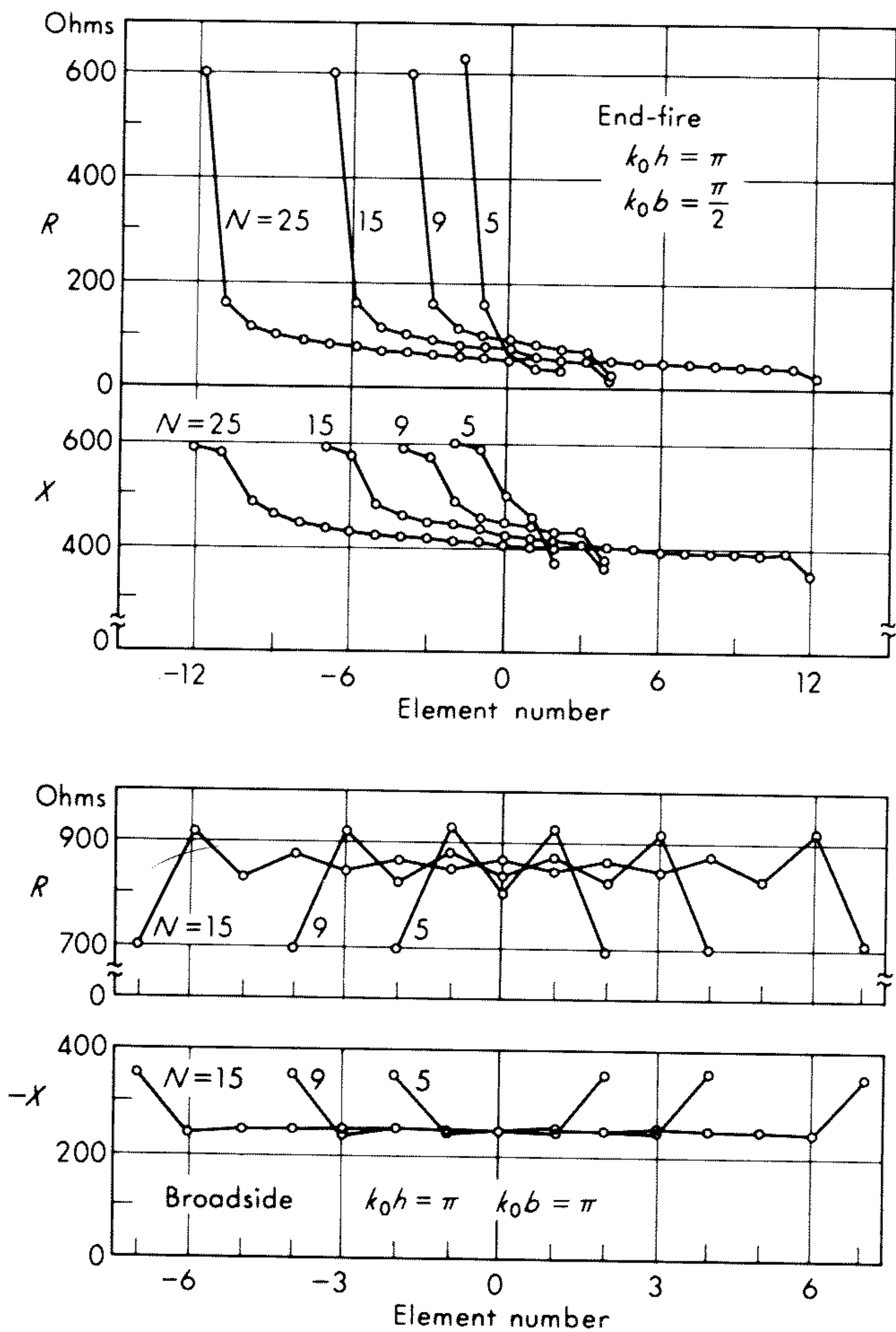
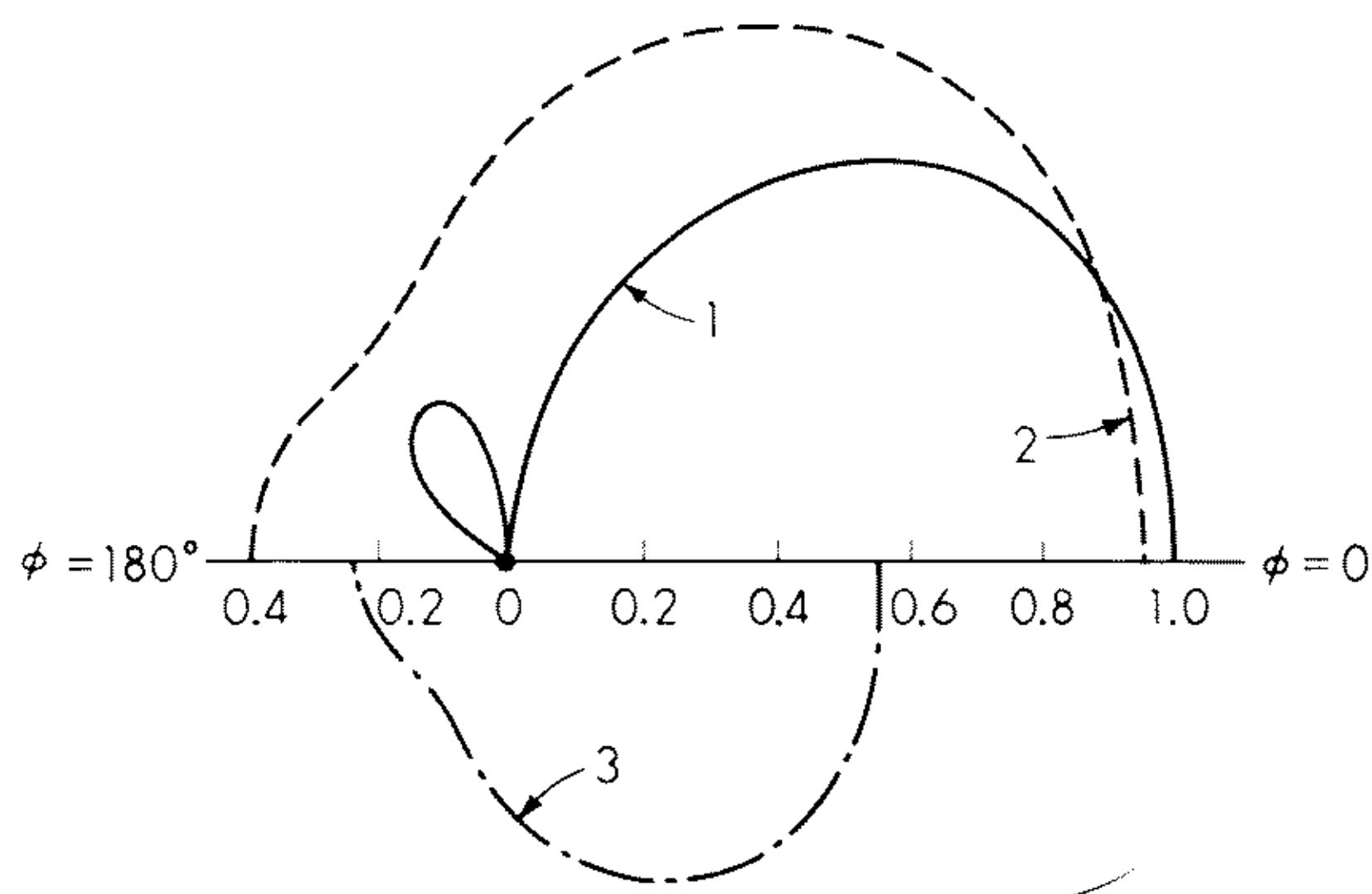


Fig. 9.18 Impedance of N -element curtain arrays; full-wave elements; $I(0)$ specified.



- 1. Ideal pattern, normalized at $\phi_{\max} = 0^\circ$
- 2. Actual theoretical pattern, normalized at $\phi_{\max} = 40^\circ$
- 3. Actual theoretical pattern, normalized for equal power with 1

Fig. 9.19 Radiation pattern of four-element end-fire array; driving-point currents specified so that $I_4 = jI_3 = -I_2 = -jI_1$, $k_0b = \pi/2$, $k_0h = \pi$, $\Omega = 2 \ln 2h/a = 10$.

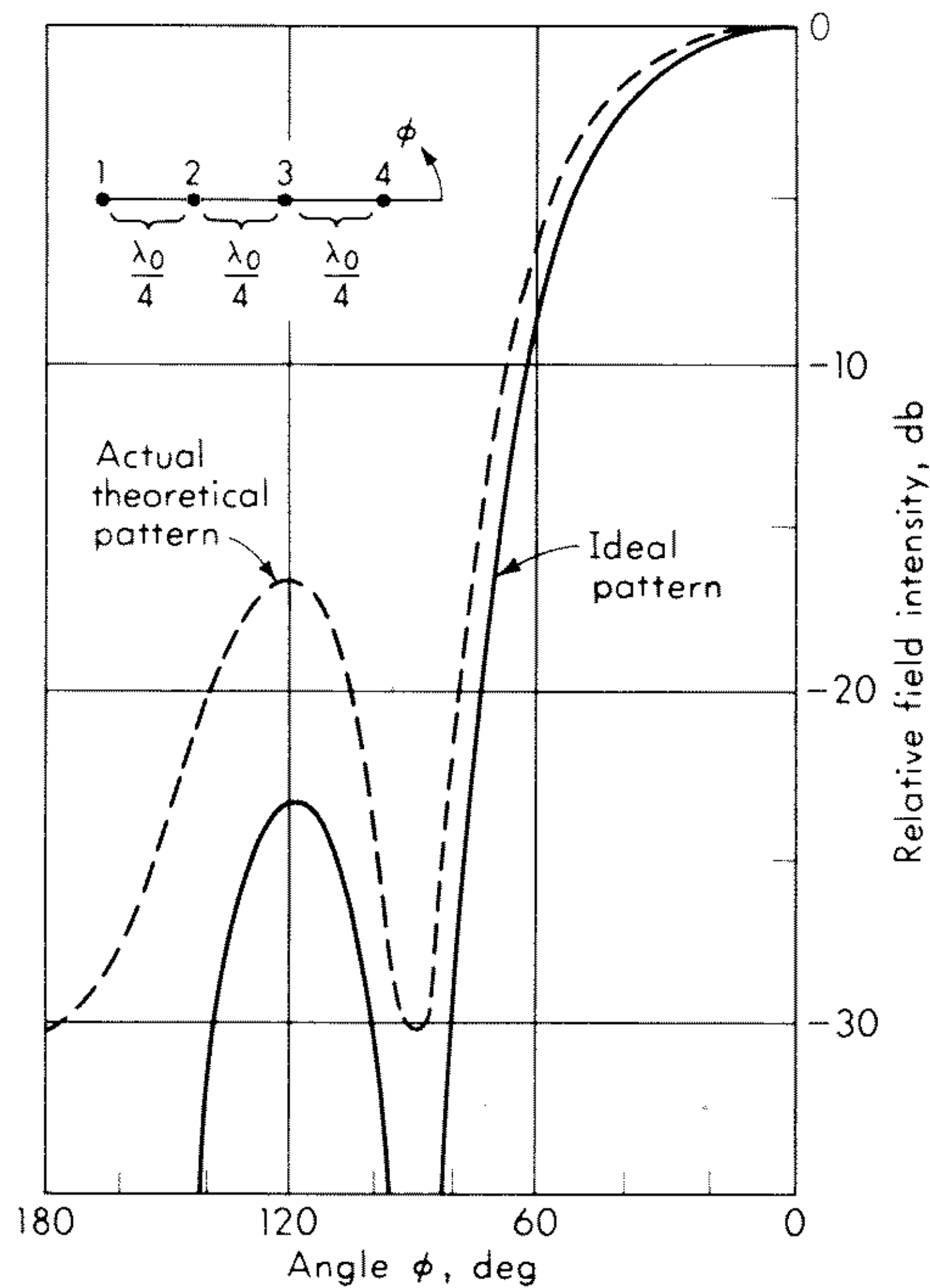


Fig. 9.20 Horizontal field patterns for four-element end-fire array; driving voltage specified so that $V_4 = jV_3 = -V_2 = -jV_1$; $k_0b = \pi/2$, $k_0h = \pi$, $\Omega = 2 \ln 2h/a = 10$.

four-element end-fire array of full-wave elements is shown in Fig. 9.19 when the currents are specified and in Fig. 9.20 when the voltages are specified. Note

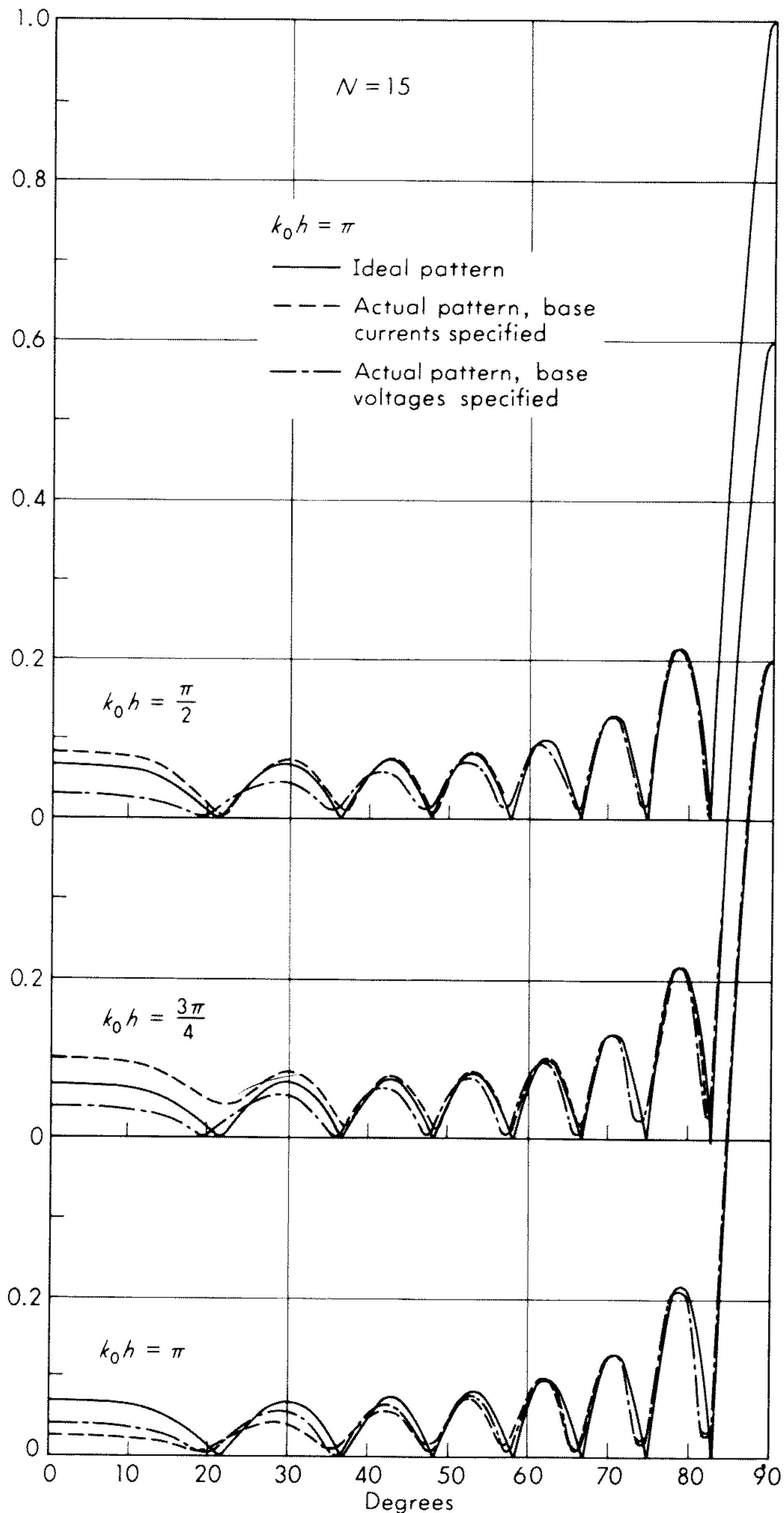


Fig. 9.21 Fields of 15-element broadside array.

how much more closely the latter agrees with the conventional pattern which assumes sinusoidally distributed currents with no phase shift along the element. The reason for this is that, when the voltages are specified in a full-wave array, this is equivalent to specifying the amplitudes and phases of the large sinusoidal component of the current which contributes a major part to the electromagnetic field. Typical field patterns for longer broadside arrays are shown in Fig. 9.21 and for end-fire arrays in Fig. 9.22.

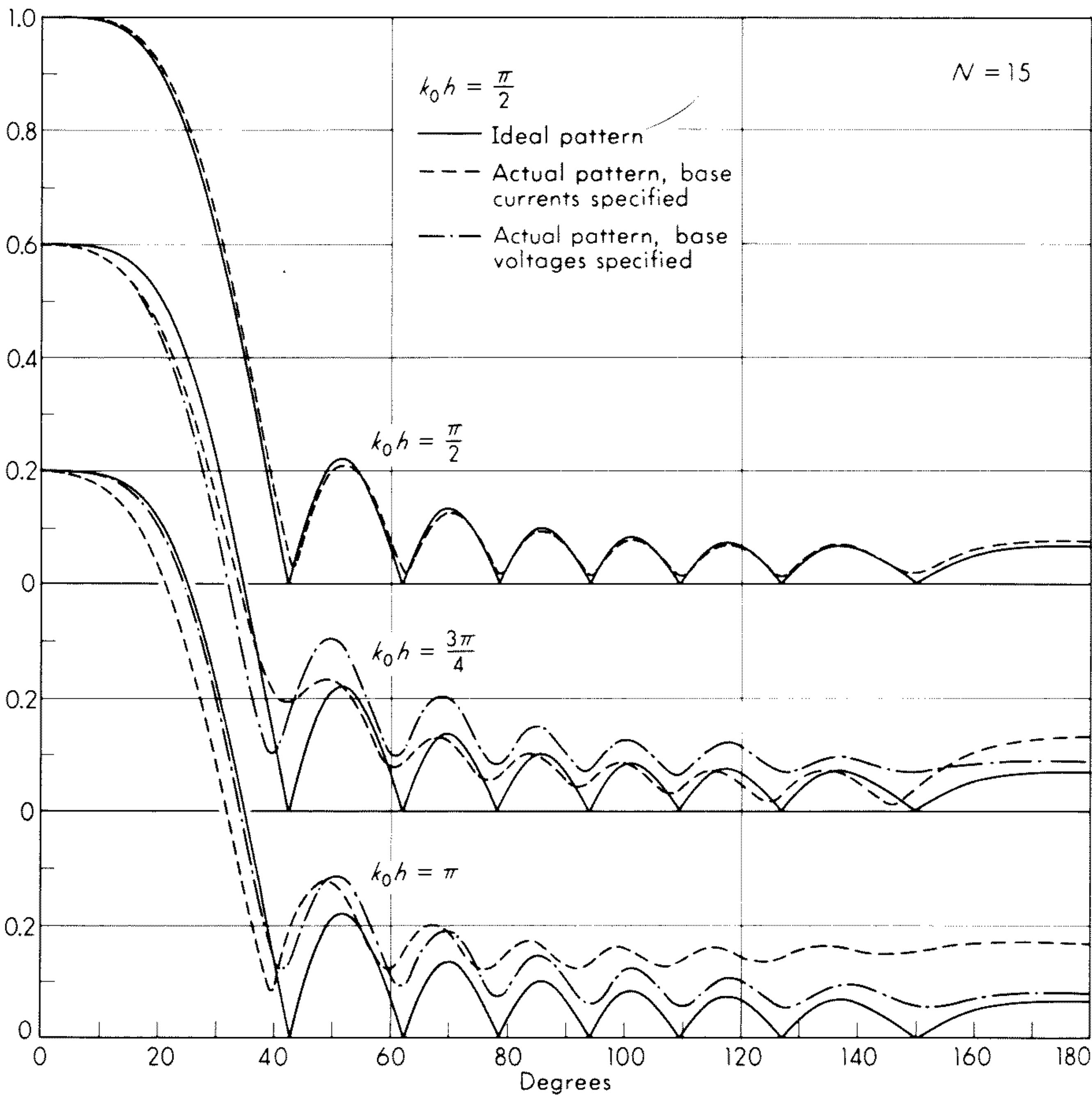


Fig. 9.22 Fields of 15-element end-fire array.

9.14 Parasitic Arrays

In the discussion in the preceding section reference is made specifically to certain arrays in which all of the elements are driven. The theory is, however, also applicable to an important class of directional arrays in which only one element is active and all others are parasitic. A simple array of this type is

shown in Fig. 9.23. It involves only the driving voltage V_{01} with $V_{0i} = 0$; $i = 2, \dots, N$. This implies that the distributions of current in the three-term form become

$$I_{z1}(z) = jA_1 \sin k_0(h - |z|) + B_1(\cos k_0z - \cos k_0h) + D_1\left(\cos \frac{k_0z}{2} - \cos \frac{k_0h}{2}\right) \quad (9.139a)$$

$$I_{zi}(z) = B_i(\cos k_0z - \cos k_0h) + D_i\left(\cos \frac{k_0z}{2} - \cos \frac{k_0h}{2}\right) \quad i = 2, 3, \dots, N \quad (9.139b)$$

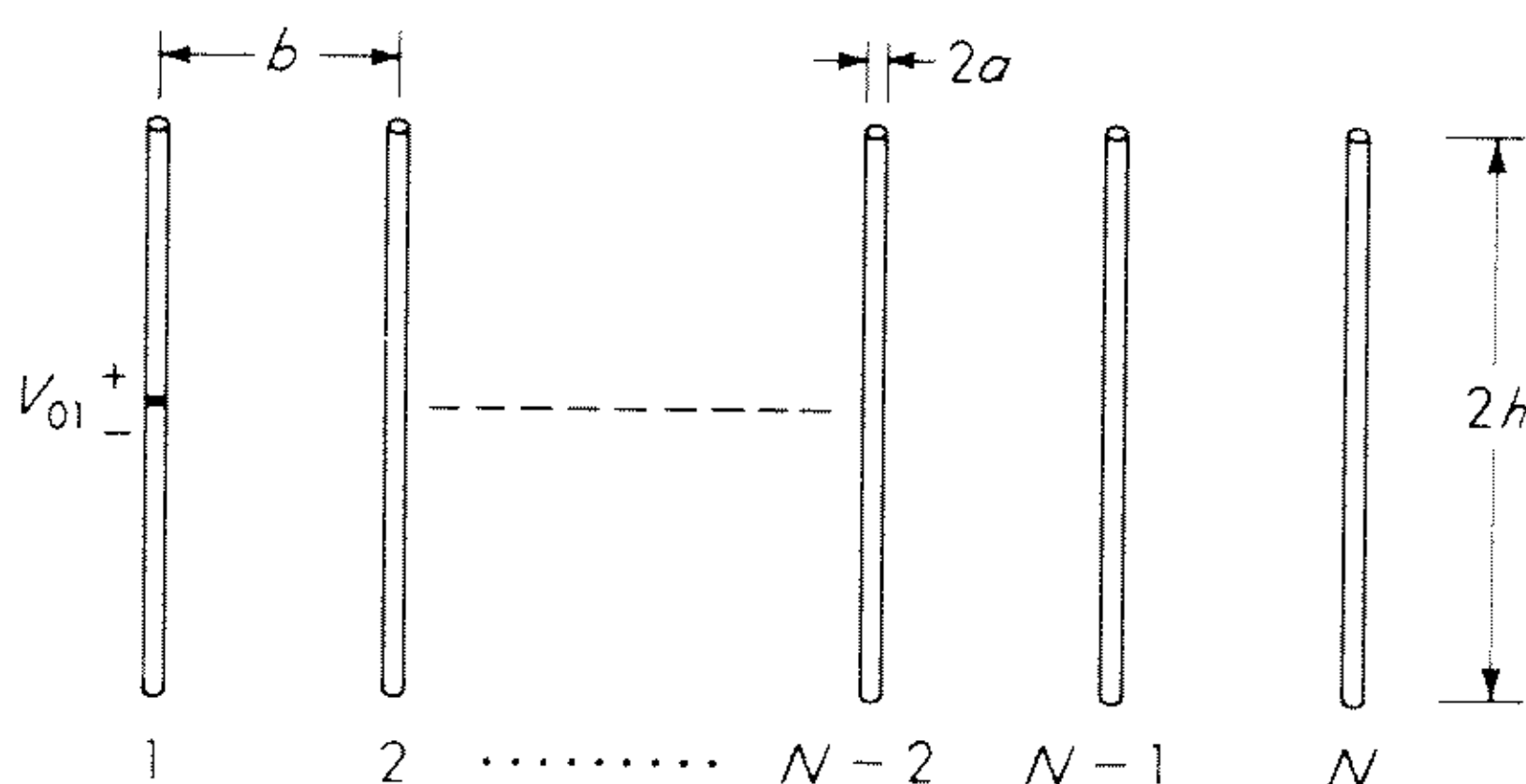


Fig. 9.23 Array of N identical equally spaced antennas of which only No. 1 is driven.

since A_i is proportional to V_{0i} . The simpler two-term form, which is a very satisfactory approximation for most driven curtain arrays, is obtained from (9.139 *a,b*) with $D_i = 0$, $i = 1, 2, \dots, N$. Note, however, that, when $D_i = 0$, the currents in all of the parasitic elements are represented by the simple term $B_i(\cos k_0z - \cos k_0h)$, where the complex coefficient B_i is, in general, different for the several elements. This approximation by a single term is more than a restriction on the distribution of the amplitude of the current along each parasitic element, since it actually eliminates the possibility of taking account of possible changes in phase. Specifically, it implies that the phase of the current in each parasitic antenna is the same at all points along its length as at its center. It is to be anticipated that such an assumption is likely to be satisfactory only for elements that are not much longer than a half wavelength. Since the most useful types of parasitic arrays make use of elements that satisfy this requirement, the simple representation obtained from (9.139 *a,b*) with $D_1 = D_i = 0$ should be adequate except possibly for very long end-fire arrays in which cumulative effects can occur.

A detailed study of a 20-element array like that shown in Fig. 9.23 was made by Mailloux.¹⁶ He used the two-term theory with distributions of current given by (9.139 *a,b*) with $D_1 = D_i = 0$. Measurements were made with monopoles erected over a large aluminum ground plane. Graphs of the theoretically determined and measured distributions of current on the driven element No. 1

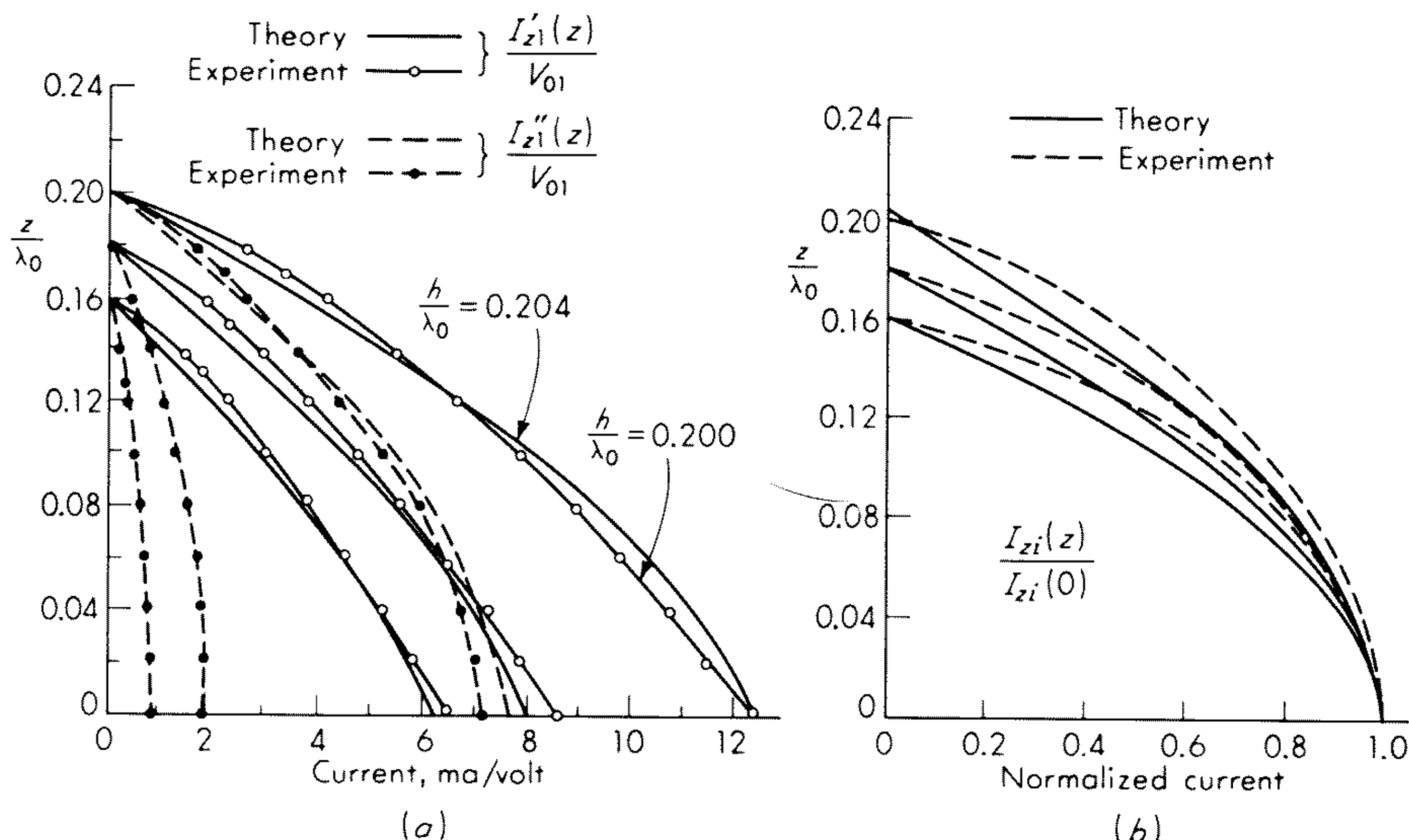


Fig. 9.24 Current distributions in array of one driven and 19 parasitic elements with $a/\lambda_0 = 0.00635$, $b/\lambda_0 = 0.2$, $h/\lambda_0 = 0.16$, 0.18 , and 0.20 . (a) Components of current in driven element No. 1: $I_{z1}(z) = I'_{z1}(z) + jI''_{z1}(z)$, where $I'_{z1}(z)$ is in phase with V_{01} ; (b) normalized currents in a typical parasitic element. (From Mailloux.¹⁶)

in the form $I_{z1}(z) = I'_{z1}(z) + jI''_{z1}(z)$ are shown in Fig. 9.24a. The normalized current along a typical parasitic element is shown in Fig. 9.24b. Three lengths, $h/\lambda_0 = 0.16$, 0.18 , and 0.20 , were investigated by Mailloux. The amplitudes and phases of all of the 20 currents at $z = 0$, that is, $I_{zi}(0)$ with $i = 1, 2, \dots, 20$, are represented in Fig. 9.25. Note that in this figure the continuous curves are meaningless except at the discrete points corresponding to a dipole number. The measured points are shown; the corresponding theoretical points used to construct the curves have been omitted. The driving-point admittances of element No. 1 are shown in Fig. 9.26, the horizontal field patterns in Fig. 9.27. The agreement between theory and measurement is seen to be very good throughout. Note that measurements for monopoles of axial length $h = 0.200\lambda_0$ are compared with theoretical results for $h = 0.204\lambda_0$. The difference, $0.004\lambda_0$, is less than the radius $a = 0.00635\lambda_0$ of the antenna. However, as resonance is approached, the currents in the parasitic elements become increasingly sensitive to the precise length of the elements. The agreement between theory and measurements is considerably improved if a small end correction in the form of an extra length $0.004\lambda_0$ is introduced. Actually, the quasi-one-dimensional theory may be expected to be in error by lengths corresponding to a fraction of the radius, since no account is taken of the nature of the ends at $z = \pm h$. Note in particular from Fig. 9.27 that the complete minor-lobe structure is correctly given by the approximate theory.

The operation of the array with 19 parasitic directors may be inferred from Fig. 9.25. When h/λ_0 is sufficiently small, for example, $h/\lambda_0 = 0.16$ or 0.18 , the

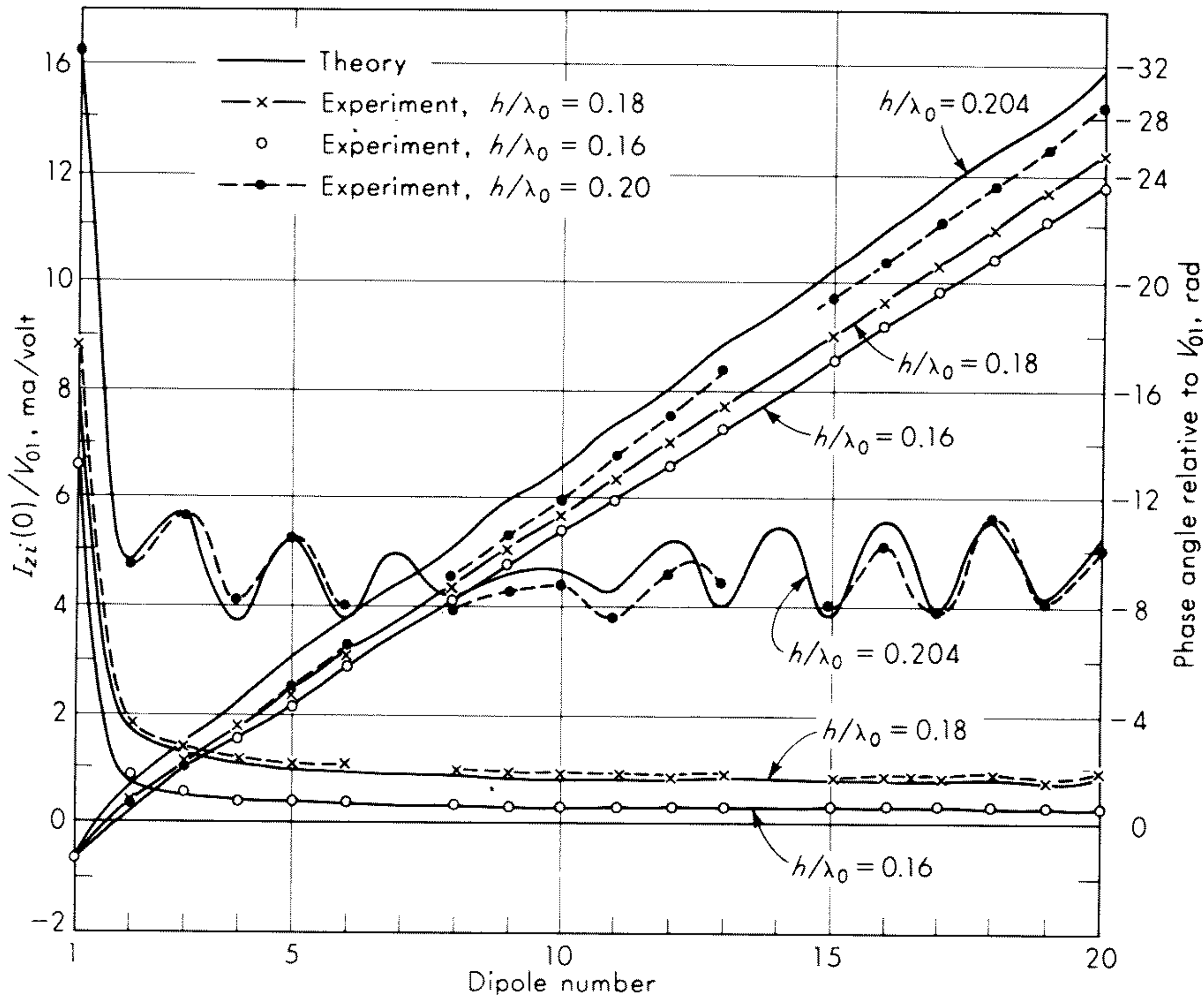


Fig. 9.25 Amplitudes and relative phases of currents $I_{zi}(0)$ in the 20 elements; $a/\lambda_0 = 0.00635$, $b/\lambda_0 = 0.2$. (From Mailloux.¹⁶) (The continuous curves are meaningful only at discrete points corresponding to the elements.)

amplitudes of the currents in the directors are quite constant and the phase change from element to element is proportional to the distance. The resulting field pattern is strongly end-fire with very small minor lobes. When h/λ_0 is increased to 0.2, the amplitudes of the currents increase greatly, but they are no

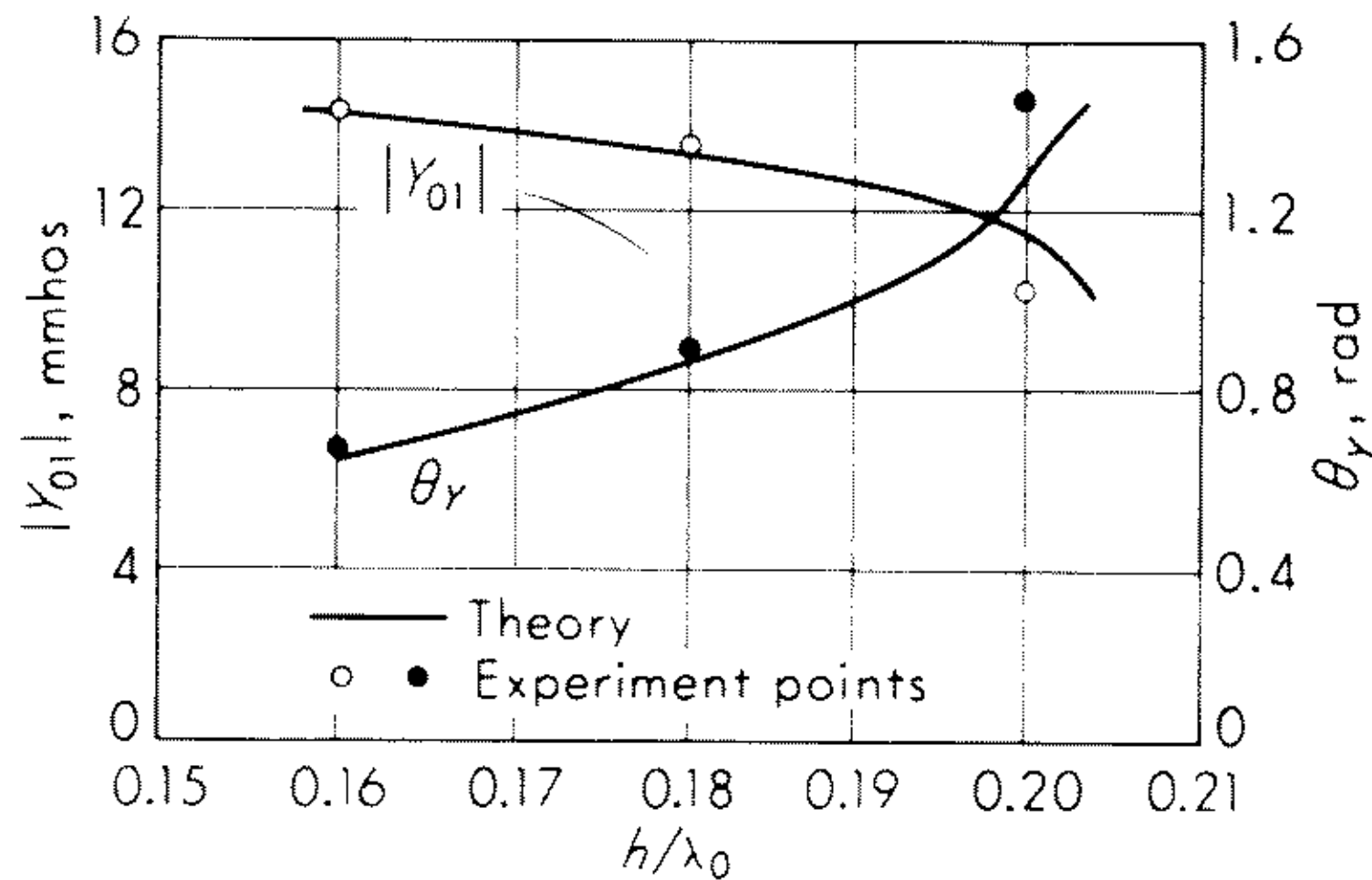


Fig. 9.26 Admittance $Y_{01} = |Y_{01}| e^{i\delta_Y}$ of driven element in 20-element array; $a/\lambda_0 = 0.00635$, $b/\lambda_0 = 0.2$. (From Mailloux.¹⁶)

longer constant from element to element. As a consequence, significant minor lobes begin to appear. The array is still strongly end-fire. However, with a further increase in h/λ_0 , the resonant value, where the director action of the parasitic elements stops and reflector action begins, is soon reached.

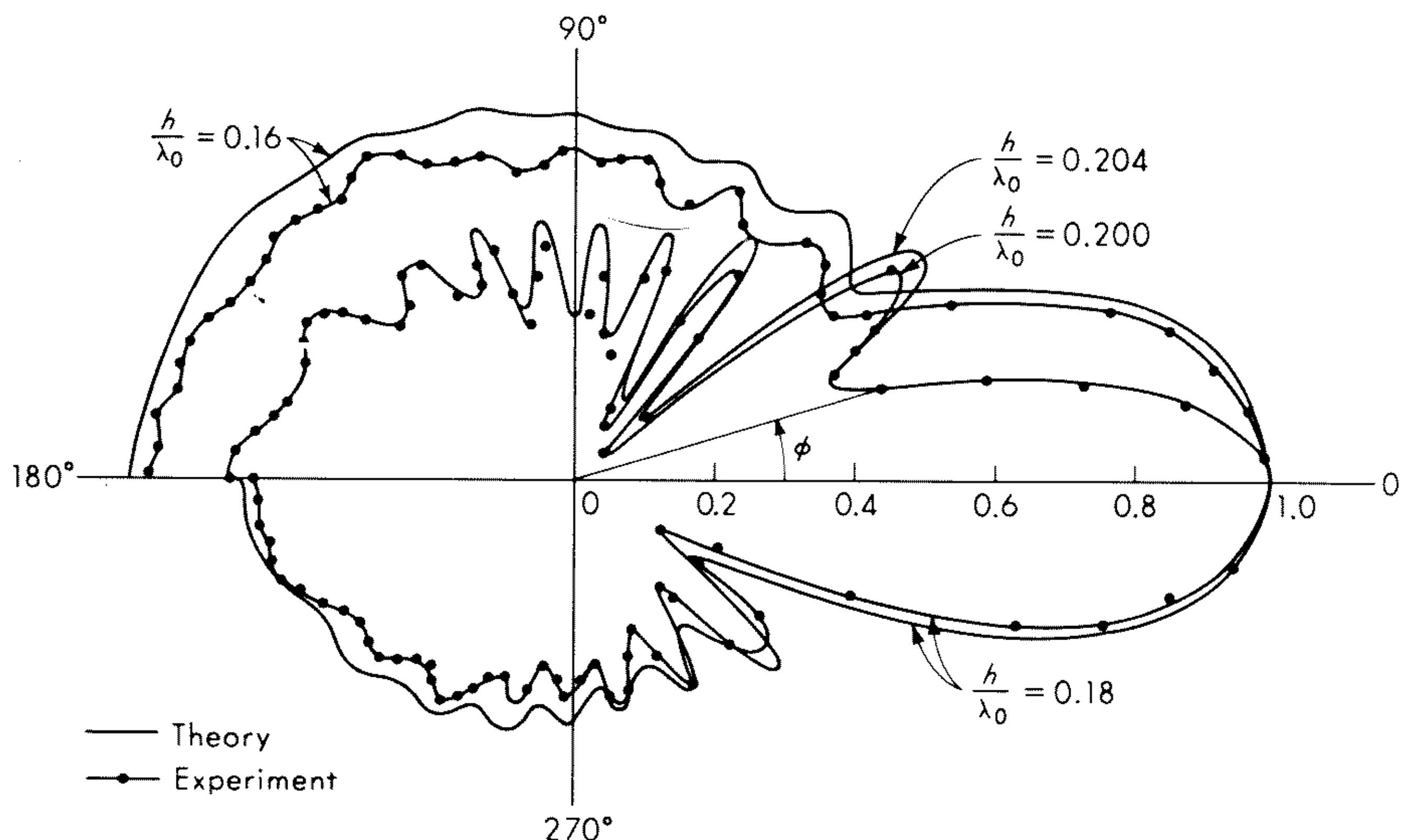


Fig. 9.27 Horizontal field patterns of 20-element array. (From Mailloux.¹⁶)

The familiar Yagi antenna resembles the array shown in Fig. 9.23. It usually consists of a single driven element (No. 2) with $h/\lambda_0 = 0.25$, a reflecting element (No. 1) with $h/\lambda_0 = 0.25$, and $N - 2$ directors with $h/\lambda_0 \leq 0.2$. A complete study of such an array has been made by Morris^{17,18} by using currents of the form $I_{z1}(z) = jA_1 \sin k_0(h - |z|) + B_1(\cos k_0 z - \cos k_0 h)$ for the driven element and $I_{zi} = B_i(\cos k_0 z - \cos k_0 h) + D_i(\cos \frac{1}{2}k_0 z - \cos \frac{1}{2}k_0 h)$ for the parasitic elements. Computer programs to determine optimum values of the forward gain and the front-to-back ratio have been developed; they provide the complete distributions of current in all elements, the impedance and admittance of the driven element, and the field pattern of the array. Morris' work leads to the conclusion that one important mode with near optimum forward gain is the one studied by Mailloux in which the amplitudes and phases of the currents in the parasitic directors all have equal amplitudes and a constant phase angle along the antenna. However, there are other modes with quite different currents that have comparable field patterns.

9.15 More General Curtain Arrays

The analytical formulation of the theory of arrays as developed in this chapter has been concerned with circular and curtain arrangements of parallel,

nonstaggered elements that have the same or nearly the same lengths. A careful theoretical and experimental study by Cheong^{19,20} has shown that, when elements that differ greatly in length are coupled, the currents can still be represented adequately by the three-term form (9.139a) provided $k_0 h \leq 5\pi/4$. This verification justified the application of the theory to the log-periodic dipole array which was originally treated by Carrel²¹ by using the emf method and an assumed sinusoidally distributed current in all elements. The log-periodic antenna consists of a curtain of dipoles which have a constant h/a ratio and increase in length and spacing from the driven end of the two-wire line to the loaded end as shown in Fig. 9.28. The conductors of the line are

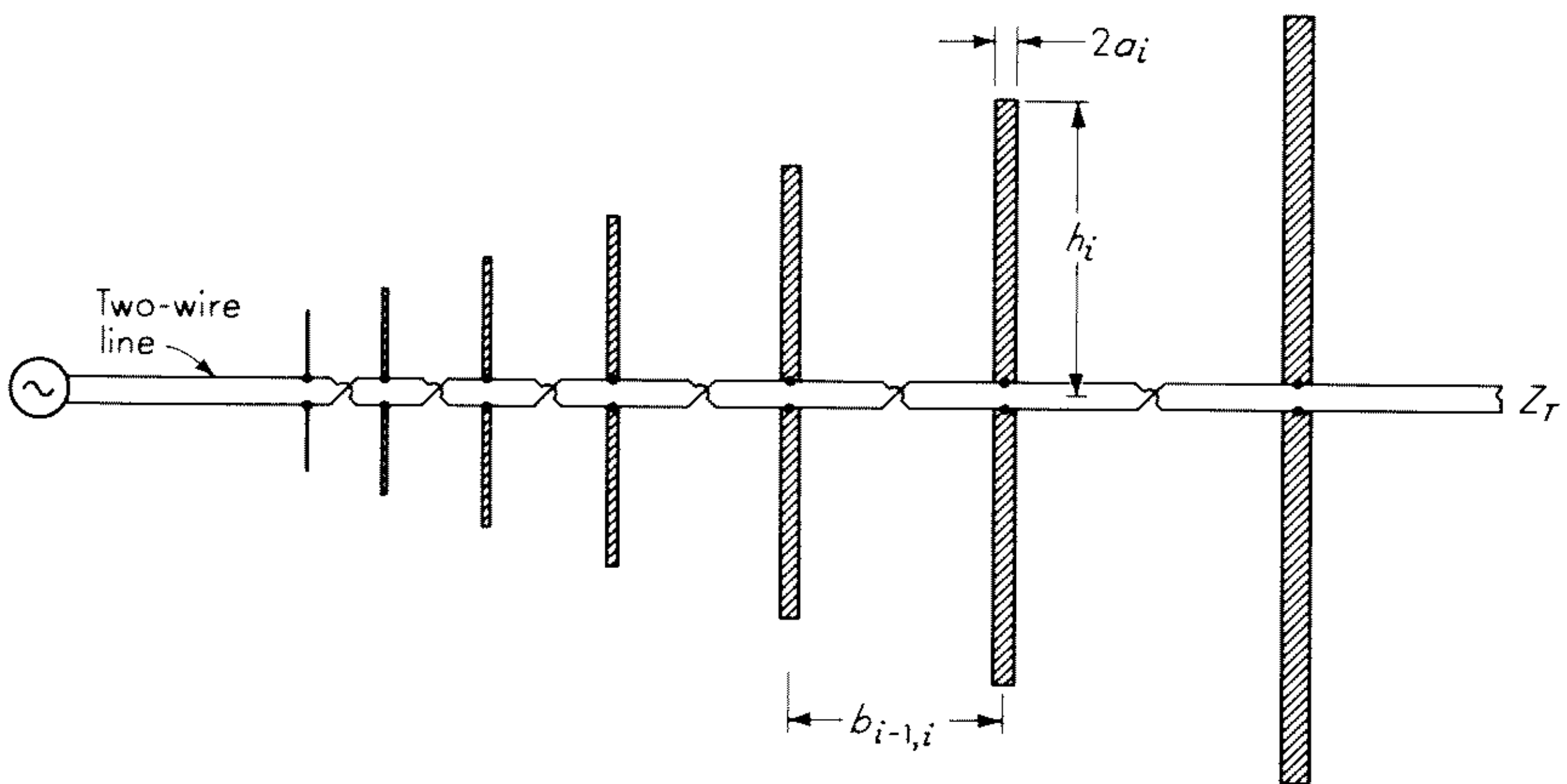


Fig. 9.28 Log-periodic dipole array.

crossed between each adjacent pair of elements in order to achieve a 180° phase shift that is independent of frequency. The variable parameters are $\Omega = 2 \ln (2h_i/a_i)$, $\tau = h_i/h_{i+1}$, $\sigma = h_{i+1}/b_{i,i+1}$, Z_T , and N , where h_i and a_i are respectively the half length and radius of element i , $b_{i,i+1}$ is the distance between elements i and $i + 1$, Z_T is the impedance terminating the line, and N is the total number of elements. Cheong has analyzed completely a log-periodic array with the following parameters independent of i : $\Omega = 11.4$, $\tau = 0.93$, $\sigma = 0.7$, $Z_T = R_c$, and $N = 12$ using the three-term representation of current (9.139a) for all elements. The numerical solution includes the distribution of current along and the driving-point admittance of each element, the power in each element and in the termination, the admittance of the array across its terminals at element No. 1, and the field pattern.

Important properties of the array may be understood from Fig. 9.29, where the admittances of the 12 elements are shown in the complex plane when a frequency for which element No. 7 is nearly resonant is used. The inner circle connects the admittances when the elements are all isolated, the outer curve connects the admittances of the same elements when they are active in the

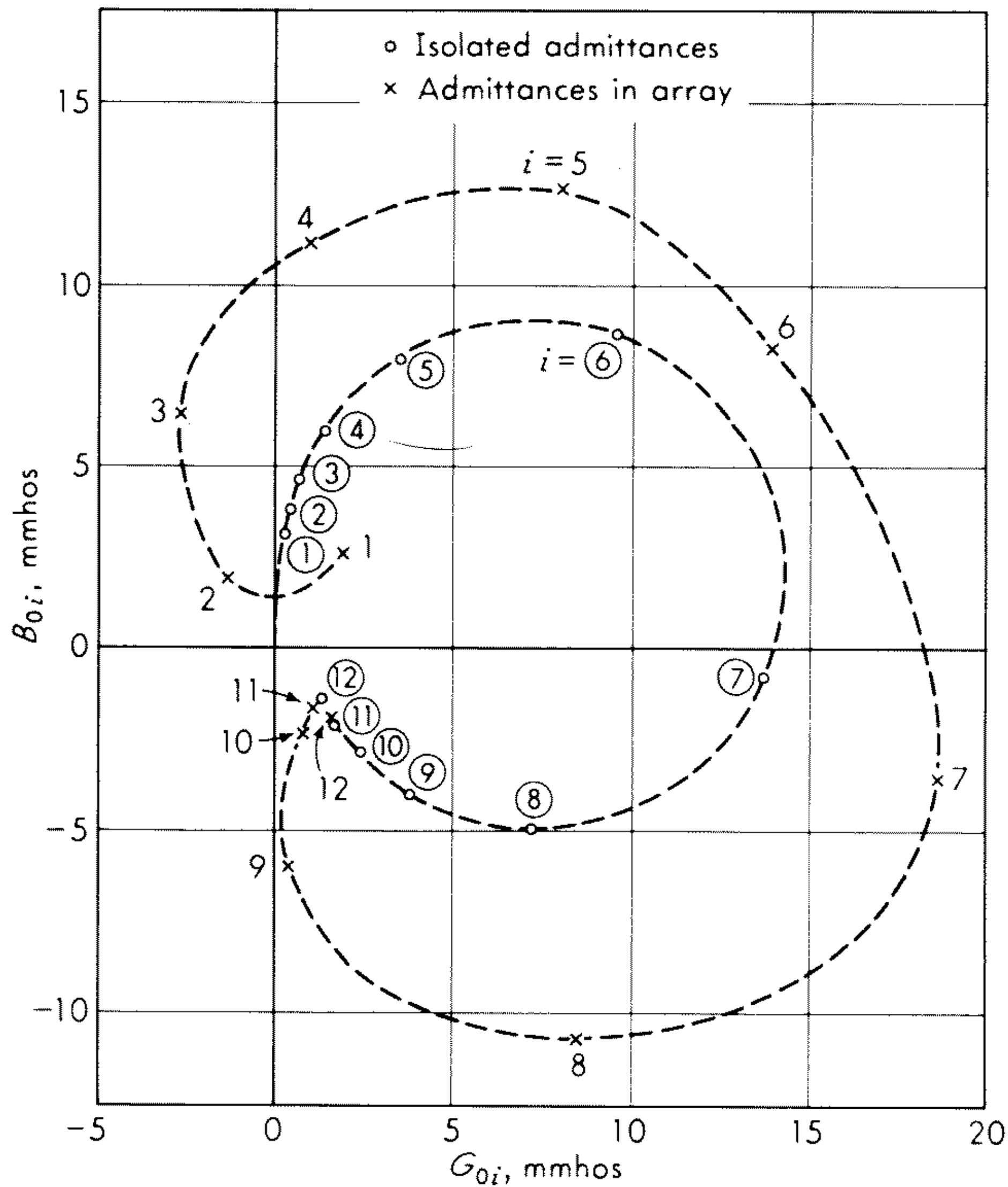


Fig. 9.29 Theoretical admittances of elements in log-periodic array when individually isolated and when in array with $\tau = 0.93$, $\sigma = 0.7$, $\Omega = 11.8$, $Z_T = Z_c$, $N = 12$, frequency f_7 .

array. It is seen that, for a few elements on each side of the one near resonance, the admittances of the elements when isolated differ greatly from those when the elements are part of the array, but that, beyond these few, the admittances cluster or spiral closely around the circle for the isolated elements. Since the impedance of an element in an array can be the same as the impedance of the same element when isolated only if the element carries an insignificant current so that it contributes negligibly to the far field, it must be concluded that only a relatively small group of elements near resonance is active in the array. This group includes three subgroups: (1) The element nearest resonance and the next two shorter elements. It is to these that most of the power is supplied from the line. (2) The element longer than the resonant one. This receives some power from the line but carries a large induced inductive current that makes this element act primarily like a parasitic reflector. (3) The three shorter elements beyond subgroup 1. These are also supplied with very little power from the line; indeed two of them have negative conductances and feed power back into the line. These elements have relatively large induced capacitive currents that make them behave like parasitic directors. The reflecting and

directing elements are very significant much as in a parasitic array in providing a typical end-fire beam with only small side lobes.

When the frequency is changed, the admittances and their connecting curves in Fig. 9.29 rotate to bring a longer or shorter element near resonance. This means that the cluster or spiral of points near one end of the admittance curve of the array unwinds and that at the other winds up. So long as neither end unwinds so far that it is removed from the vicinity of the admittance circle of the isolated elements, the array is essentially frequency independent in both its admittance properties and its field pattern. Over this frequency-independent range virtually all of the power is radiated and only a small portion is dissipated in the terminating impedance Z_T .

When the frequency is changed sufficiently that one end of the admittance curve of the array in Fig. 9.28 becomes widely separated from the admittance circle of the isolated elements, the frequency-independent behavior ceases: the driving-point admittance changes, a large fraction of the power is dissipated in the termination, and the minor lobes in the field pattern become large. A more detailed description of the operating characteristics of the log-periodic array is in the literature.¹⁹⁻²¹

9.16 Arrays with Collinear and Staggered Elements

When the restriction that all elements in an array be nonstaggered is removed, a much more complicated situation arises, since the currents and associated vector potentials can no longer be assumed to have even symmetry with respect to their respective centers. Even when all elements in a planar or three-dimensional array are individually center driven, their relative positions are such that induced currents cannot be the same in the halves of many of the elements. That is, the condition $I_{zi}(-z_i) = I_{zi}(z_i)$ is not satisfied with respect to the axial coordinate z_i which has its origin at the center of element i . It has been shown^{22,23} that the current in each arbitrarily located element can be separated into a part that is even and satisfies the condition $I_{zi}(-z_i) = I_{zi}(z_i)$ and a part that is odd and satisfies the condition $I_{zi}(-z_i) = -I_{zi}(z_i)$. The total current is the sum of the odd and the even parts.

As might be expected, the previously used three-term representation (9.139a) is a good approximation of the even part of the current in a typical, arbitrarily located element i . By an analysis similar to that carried out earlier in the chapter for even currents, it has been shown²² that the odd part is well represented by the sum of two terms. Thus, the total current is represented by the following five terms, of which the first three are the same as those previously used for even currents:

$$\begin{aligned}
 I_{zi}(z_i) = & A_i \sin k_0(h - |z_i|) + B_i(\cos k_0 z_i - \cos k_0 h) \\
 & + D_i \left(\cos \frac{k_0 z_i}{2} - \cos \frac{k_0 h}{2} \right) + Q_i \left(\sin k_0 z_i - \frac{z_i}{h} \sin k_0 h \right) \\
 & + R_i \left(\sin \frac{k_0 z_i}{2} - \frac{z_i}{h} \sin \frac{k_0 h}{2} \right) \quad (9.140)
 \end{aligned}$$

The use of this expression in the simultaneous integral equations for the currents in the N elements of an arbitrary array permits the reduction of these equations to algebraic form and the evaluation of the $5N$ coefficients A_i , B_i , D_i , Q_i , and R_i by high-speed computer. The resulting distributions of current, driving point admittances, and field patterns may also be read out.

In this manner detailed studies have been made²³ of the two-element array of collinear and staggered elements and of planar arrays and three-dimensional arrays for half- and full-wave dipoles with either driving-point currents or driving-point voltages assigned. In each case the distributions of current and admittances of all elements were computed together with the field patterns. Of particular interest is the fact that the distributions of current even along half-wave elements differ greatly from the conventionally assumed cosinusoid.

9.17 Dipole Coupled to an Open-wire Line

In most arrays the individual elements are either directly connected to a transmission line or are parasitic with currents induced by coupling to the other elements. A novel array originally suggested by Sletten²⁴ and analyzed by Chen and King²⁵ consists of dipoles that are coupled to an open-wire line in the simple manner indicated in Fig. 9.30. Each antenna is in a plane parallel to

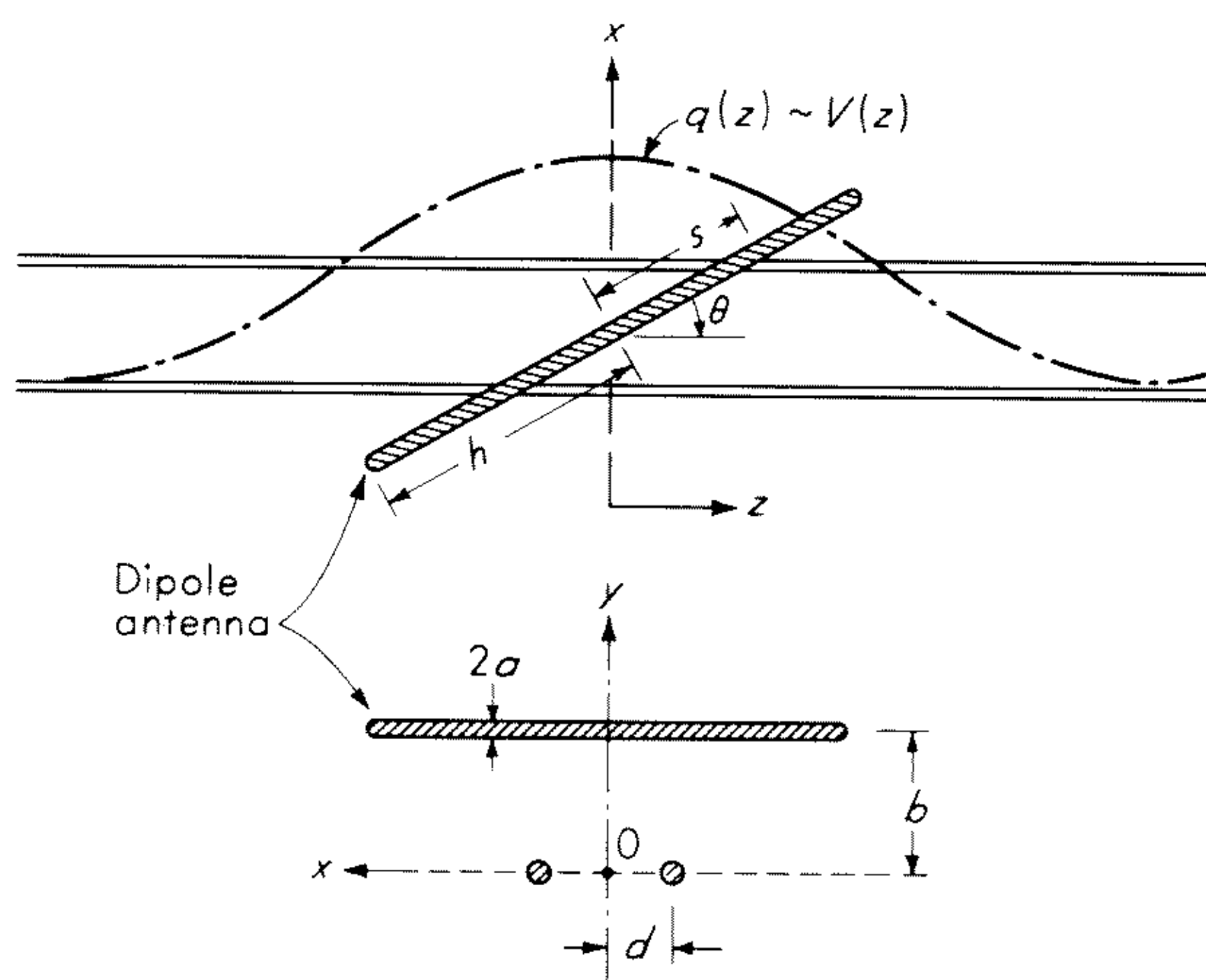


Fig. 9.30 Dipole coupled to two-wire line.

and at a distance b from the plane of the two-wire line, the conductors of which are separated by the distance $2d$. The coupled dipoles are located at half-wave intervals along the transmission line, as shown in Fig. 9.31, with centers at voltage maxima in the standing-wave pattern. Owing to the loading of the line by the dipoles, the standing-wave ratio can be quite low with a predominantly traveling-wave distribution.

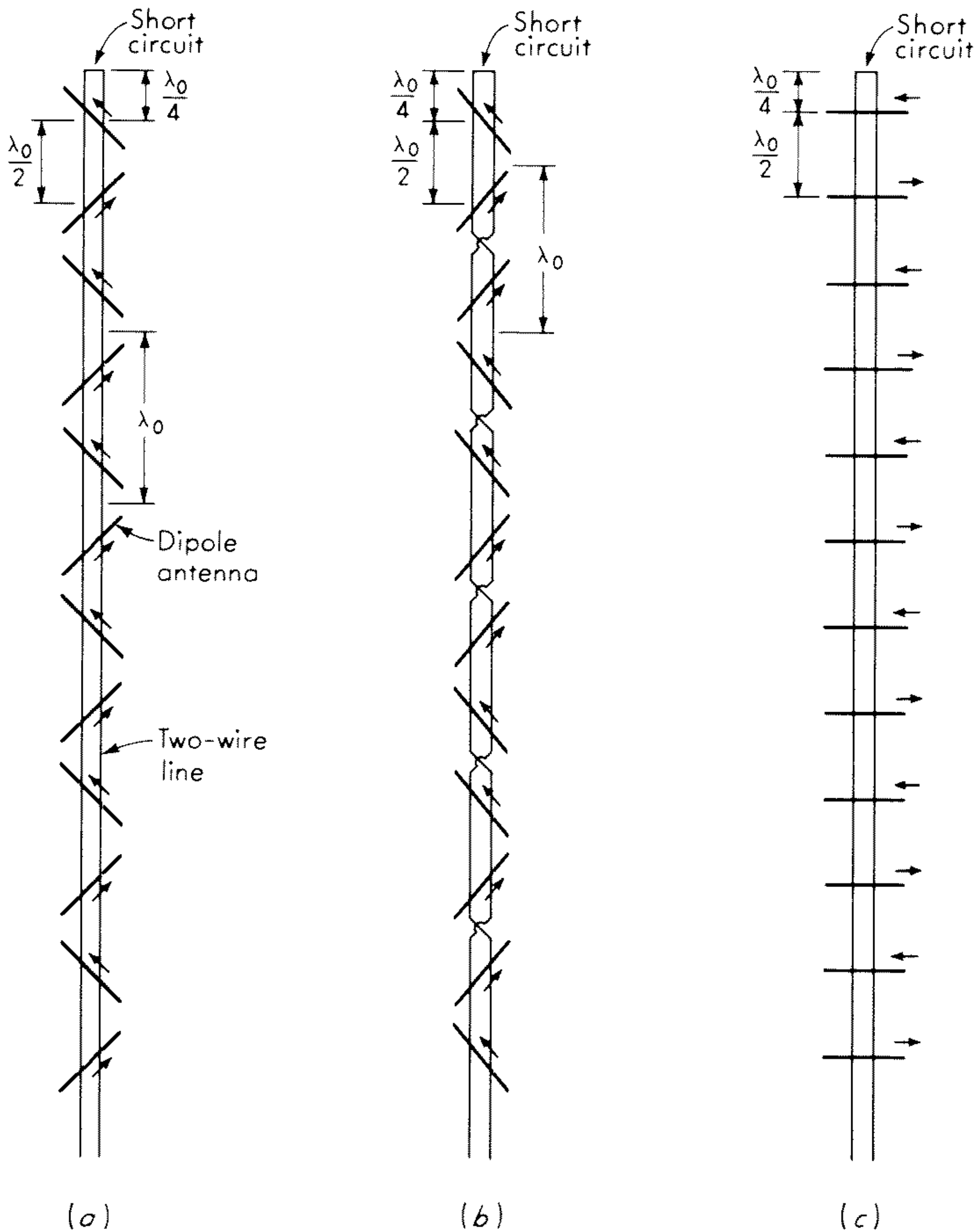


Fig. 9.31 Arrays of dipoles coupled to two-wire line. (a) Broadside and end-fire array; (b) broadside array; (c) end-fire array.

When the axis of the typical dipole in Fig. 9.30 is parallel to the conductor of the line so that $\theta = 0$, no currents are induced in the antenna, since it is in the neutral plane of the transmission line. However, when the antenna is rotated from that neutral plane through an angle θ , currents are excited in the antenna by the charges and currents in the line. The magnitude and distribution of the induced current vary with the angle of rotation θ of the antenna from the neutral position, the length $2h$ of the antenna, the distance b between the planes containing the antenna and the line, and the spacing $2d$ of the transmission line.

A first step in the study of arrays of the type shown in Fig. 9.31 is to determine the circuit and field properties of a radiating system that consists of a single dipole when coupled to a two-wire line in the manner shown in Fig. 9.30.

In general, the complex amplitude of the charge per unit length along the line (which is assumed to be lossless) is

$$q(z) = q_1 \cos k_0 z + j q_2 \sin k_0 z \quad (9.141)$$

where q_1 and q_2 are amplitude coefficients. The voltage distribution corresponding to (9.141) is $V(z) = q(z)/c$, where c is the capacitance per unit length. The associated current, as obtained from (9.141) with the equation of continuity, is

$$I(z) = -j v_0 q_1 \sin k_0 z + v_0 q_2 \cos k_0 z \quad (9.142a)$$

where v_0 is the velocity of light. These charges and currents maintain a transverse electric field in the plane perpendicular to the axis of the line. It can be calculated from $\mathbf{E} = -\nabla\Phi - j\omega\mathbf{A}$, where the scalar and vector potentials are²⁶

$$A_z(z) = \frac{I_z(z)U_0}{2\pi} \ln \left[\frac{(x+d)^2 + y^2}{(x-d)^2 + y^2} \right] \quad (9.142b)$$

$$\Phi(z) = \frac{q(z)}{2\pi\epsilon_0} \ln \left[\frac{(x+d)^2 + y^2}{(x-d)^2 + y^2} \right] \quad (9.142c)$$

The component of the field in the direction \hat{s} along the axis of the antenna has a symmetrical (even) and an antisymmetrical (odd) part with respect to the center ($s = 0$) of the dipole. These may be shown to be

$$E_t^s(s) = \frac{-dq_1}{\pi\epsilon_0} D(\theta, s) \cos(k_0 s \cos \theta) \sin \theta \quad (9.143a)$$

$$E_t^a(s) = \frac{j dq_2}{\pi\epsilon_0} D(\theta, s) \sin(k_0 s \cos \theta) \sin \theta \quad (9.143b)$$

where

$$D(\theta, s) = \frac{b^2 + d^2 - s^2 \sin^2 \theta}{[(s \sin \theta + d)^2 + b^2][(s \sin \theta - d)^2 + b^2]} \quad (9.144)$$

in which s is the distance from the center of the dipole to the point along its axis at which the electric field $E_t(s)$ is evaluated. The symmetrical part of the electric field maintained along the dipole by the currents and charges in the transmission line generates a symmetrical current $I_s^s(s) = \frac{1}{2}[I_s(s) + I_s(-s)]$ in the antenna. Similarly, the antisymmetrical part of the field generates an antisymmetrical current $I_s^a(s) = \frac{1}{2}[I_s(s) - I_s(-s)]$. The total current in the antenna is $I_s(s) = I_s^s(s) + I_s^a(s)$.

Exercise 9.7 Derive (9.143a,b) from (9.142a,b). Plot the electric field in the transverse plane of a two-wire line.

If the antenna is assumed to be perfectly conducting, the differential equations for the symmetrical and antisymmetrical part of the vector potential on the surface of the antenna are

$$\left(\frac{\partial^2}{\partial s^2} + k_0^2 \right) A_s^s(s) = -j \frac{k_0^2}{\omega} E_t^s(s) \quad (9.145a)$$

$$\left(\frac{\partial^2}{\partial s^2} + k_0^2 \right) A_s^a(s) = -j \frac{k_0^2}{\omega} E_t^a(s) \quad (9.145b)$$

These have the solutions

$$A_s^s(s) = \frac{-j}{v_0} [C_s \cos k_0 s - \Theta_s(s)] \quad (9.146a)$$

$$A_s^a(s) = \frac{-j}{v_0} [C_a \sin k_0 s - \Theta_a(s)] \quad (9.146b)$$

where $\Theta_s(s)$ and $\Theta_a(s)$ are the particular integrals

$$\Theta_s(s) = -\int_0^s E_t^s(w) \sin k_0(s-w) dw \quad (9.147a)$$

$$\Theta_a(s) = -\int_0^s E_t^a(w) \sin k_0(s-w) dw \quad (9.147b)$$

and C_s and C_a are constants to be determined from the conditions $I_s^s(\pm h) = I_s^a(\pm h) = 0$. The component of the vector potential along the surface of the dipole is given by (9.3) with z replaced by s . If its even and odd parts in s are used in (9.146a,b), the following integral equations are obtained for the symmetrical and antisymmetrical parts of the current:

$$\int_{-h}^h I_s^s(s') K(s, s') ds' = \frac{-j4\pi}{h_0} [C_s \cos k_0 s + \Theta_s(s)] \quad (9.148a)$$

$$\int_{-h}^h I_s^a(s') K(s, s') ds' = \frac{-j4\pi}{h_0} [C_a \sin k_0 s + \Theta_a(s)] \quad (9.148b)$$

where
$$K(s, s') = \frac{e^{-jk_0 R}}{R} \quad R = \sqrt{(s-s')^2 + a^2} \quad (9.149)$$

Satisfactory zero-order approximations of the even and odd currents in antennas that satisfy the requirement $\beta_0 h \leq 5\pi/4$ are

$$|I_s^s(s')|_0 = \frac{-j4\pi C_s}{\zeta_0 \Psi_s} (\cos k_0 s' - \cos k_0 h) \quad (9.150a)$$

$$|I_s^a(s')|_0 = \frac{-j4\pi C_a}{\zeta_0 \Psi_a} \left(\sin k_0 s' - \frac{s'}{h} \sin k_0 h \right) \quad (9.150b)$$

If these are substituted in (9.148a,b) with $s = h$, the following expressions are obtained for C_s and C_a :

$$C_s = \frac{\Psi_s \Theta_s(h)}{[\Psi_s + E_a(h, h)] \cos k_0 h - C_a(h, h)} \quad (9.151a)$$

$$C_a = \frac{\Psi_a \Theta_a(h)}{[\Psi_a + \varepsilon_a(h, h)] \sin k_0 h - S_a(h, h)} \quad (9.151b)$$

where
$$\Psi_s = \frac{C_a(h, 0) - \cos k_0 h E_a(h, 0)}{1 - \cos k_0 h} \quad (9.152a)$$

$$\Psi_a = \frac{S_a(h, 0) - \sin k_0 h \varepsilon_a(h, 0)}{\sin(k_0 h/2) - \frac{1}{2} \sin k_0 h} \quad (9.152b)$$

and $\Theta_s(h)$ and $\Theta_a(h)$ are obtained from (9.147a,b) with $s = h$. The following integrals occur:

$$C_a(h,s) = \int_{-h}^h \cos k_0 s' K(s,s') ds' \quad (9.153)$$

$$E_a(h,s) = \int_{-h}^h K(s,s') ds' \quad (9.154)$$

$$S_a(h,s) = \int_{-h}^h \sin k_0 s' K(s,s') ds' \quad (9.155)$$

$$\mathcal{E}_a(h,s) = \int_{-h}^h \frac{s'}{h} K(s,s') ds' \quad (9.156)$$

The total zero-order current is now given by

$$[I_s(s)]_0 = \frac{-j4\pi}{\zeta_0} \left[\frac{C_s}{\Psi_s} (\cos k_0 s - \cos k_0 h) + \frac{C_a}{\Psi_a} \left(\sin k_0 s - \frac{s}{h} \sin k_0 h \right) \right] \quad (9.157)$$

where all quantities are expressed in terms of the charge distribution (9.141) on the transmission line.

It is to be noted that a more accurate analysis of the dipole can be carried out if the full two-term representation of both the even and odd parts of the current is used, that is, if the term $\cos(k_0 s/2) - \cos(k_0 h/2)$ is added to (9.150a) and $\sin(k_0 s/2) - (s/h) \sin(k_0 h/2)$ to (9.150b), each with an arbitrary complex coefficient. Separate Ψ functions are then defined with the real and imaginary part of the kernel in the manner carried out earlier in this chapter. Actually, since the dipole is parasitic with no discontinuity at its center and since it is useful primarily when $k_0 h$ is near $\pi/2$, the simpler forms (9.150a,b) are adequate. Indeed, for elements of this length or shorter the odd part of the current, although in general not zero, is sufficiently small to be negligible for most engineering purposes.

The approximate current in the coupled dipole as given by (9.157) involves the two coefficients q_1 and q_2 in the charge distribution (9.141) which is assumed to exist along the line. The ratio $V(0)/V(\lambda_0/4) = q(0)/q(\lambda_0/4) = q_1/q_2$ is the voltage standing-wave ratio on the line; it varies with the nature of the load. When $q_2 = q_1$, a pure traveling wave exists and the line is perfectly matched; when $q_2 = 0$, a pure standing wave with voltage and charge maxima at $z = 0$ obtains and the line is unloaded. The degree in which a coupled dipole antenna loads the line depends on its length, the distance b , the angle θ , and the line spacing $2d$. Since the current in the dipole also depends on these quantities, it is clear that the ratio of the coefficients q_1/q_2 and the current $I_s(s)$ are, in general, interrelated in a complicated manner. However, since the coefficient q_1 occurs only in the symmetrical and the coefficient q_2 only in the antisymmetrical parts of $E_t(s)$ and $I_s(s)$, it follows that, whenever the antisymmetrical part is negligible, q_2 may be treated as if zero. The symmetrical part of the current is excited entirely by the part of the distribution of charge, viz., $q_1 \cos k_0 z$, that is characteristic of an ideal standing wave. The following

quantitative investigation applies to a dipole antenna with $k_0 h$ in a relatively small range near $\pi/2$ in which the antisymmetrical current can be neglected.

Measurements by Chen and King²⁵ of the distribution of current along a dipole of length $\lambda_0/4 = 10$ cm when located at a distance $b = 3$ cm above a two-wire line with spacing $2d = 2.2$ cm at the angles $\theta = 23.6^\circ, 53.1^\circ$, and 90° indicate that its cosinusoidal approximation is satisfactory. The relative amplitudes of the current at $s = 0$ as a function of the angle of rotation θ are shown in Fig. 9.32 for three values of b . Agreement between the zero-order

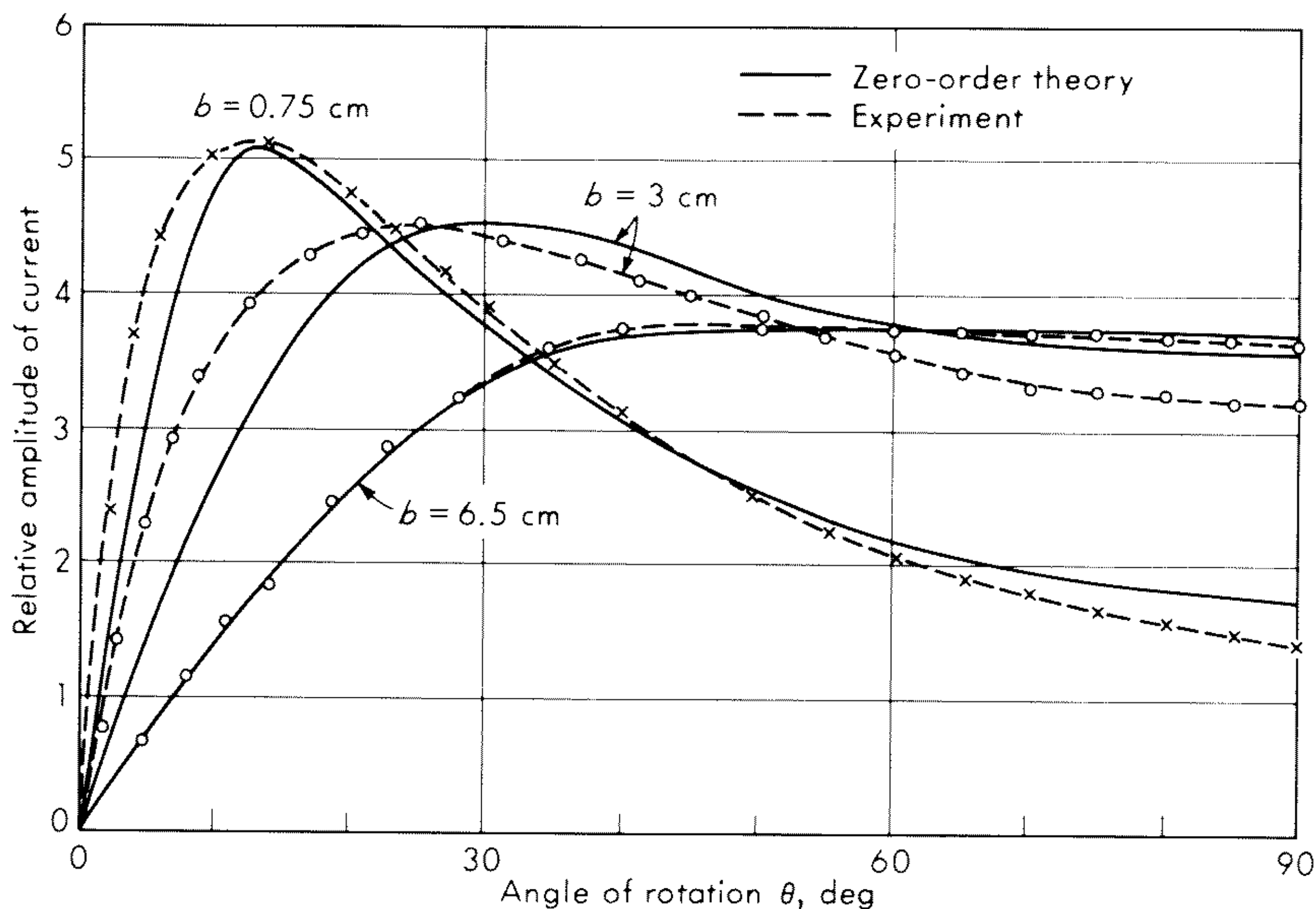


Fig. 9.32 Relative currents at $s = 0$ in dipole as function of angle of rotation; $\lambda_0 = 40$ cm, $h = 10$ cm, $2d = 2.2$ cm. (The scales for the three values of b are not comparable. See Fig. 9.33 for current vs. distance b .) (From Chen and King.²⁵)

theory and measured values is sufficiently good to make a higher-order theory unnecessary. It is seen that, as the antenna is coupled more closely to the line, the angle θ of maximum response becomes more critical and moves toward smaller values. Since the curves for the three different values of b have been drawn with different scale factors, they cannot be used to compare the relative magnitudes of $I_s(s)$ as a function of b . Such a comparison is in Fig. 9.33 for five values of θ . As is to be expected, the induced current increases with decreasing b for all angles θ . The increase is more rapid when θ is below about 45° . Measured and theoretical values agree quite well except with very close coupling and relatively small angles θ . Since no account is taken in the zero-order theory of the effects of close coupling, this disagreement is not surprising.

It is evident from Fig. 9.34 that the maximum induced current in its coupled dipole does not occur when $h/\lambda_0 = 0.25$ but more nearly when $h/\lambda_0 = 0.23$.

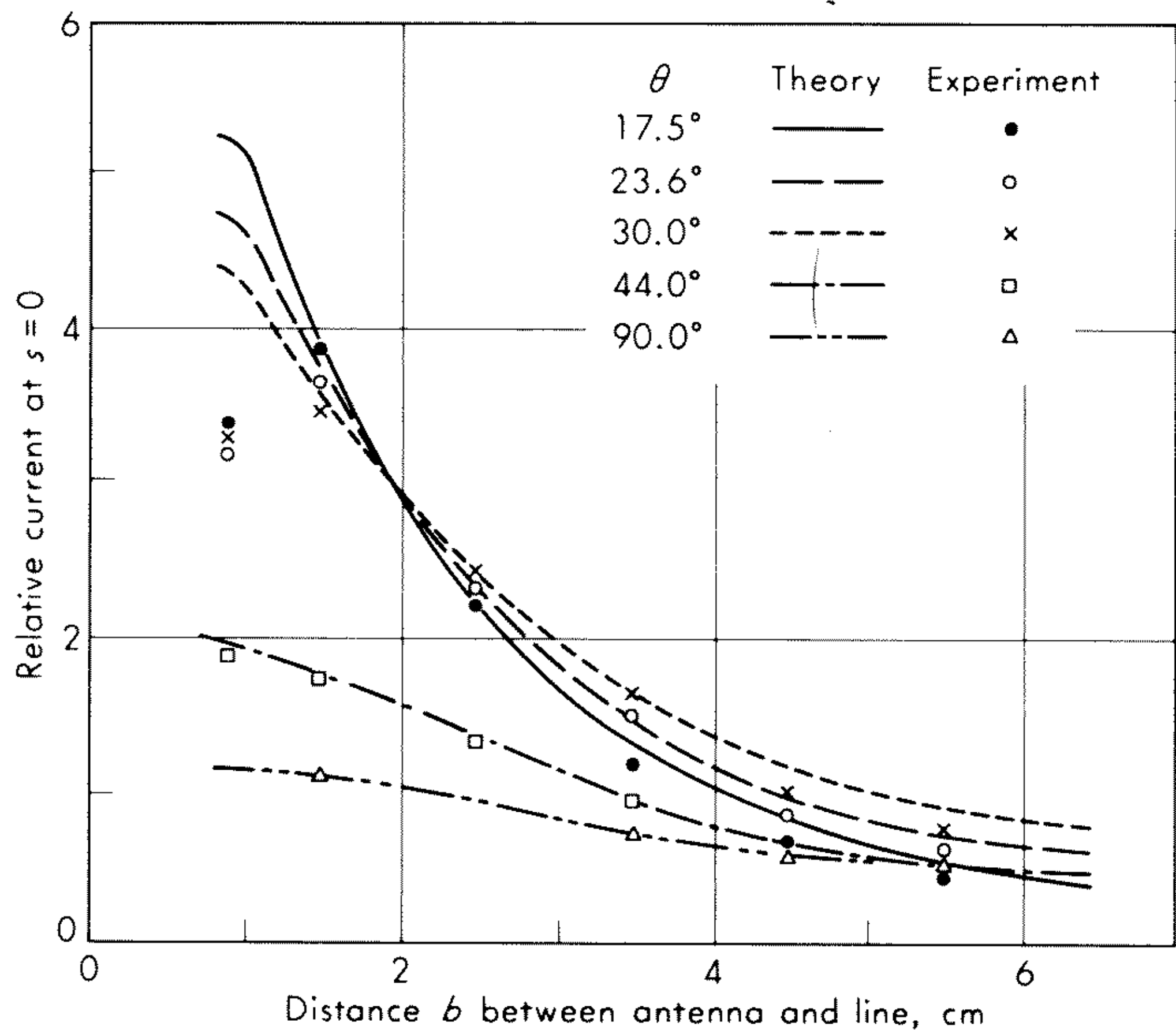


Fig. 9.33 Current at center of dipole as a function of its distance from the transmission line; $\lambda_0 = 40$ cm, $h = 10$ cm, $2d = 2.2$ cm. (From Chen and King.²⁵)

Measurements and theory agree that this length, the resonant length for the particular ratio of a/λ_0 , does not depend on the value of θ .

When a dipole antenna is coupled to a two-wire line, as in Fig. 9.32, with its center opposite a voltage maximum, the antenna constitutes a shunt

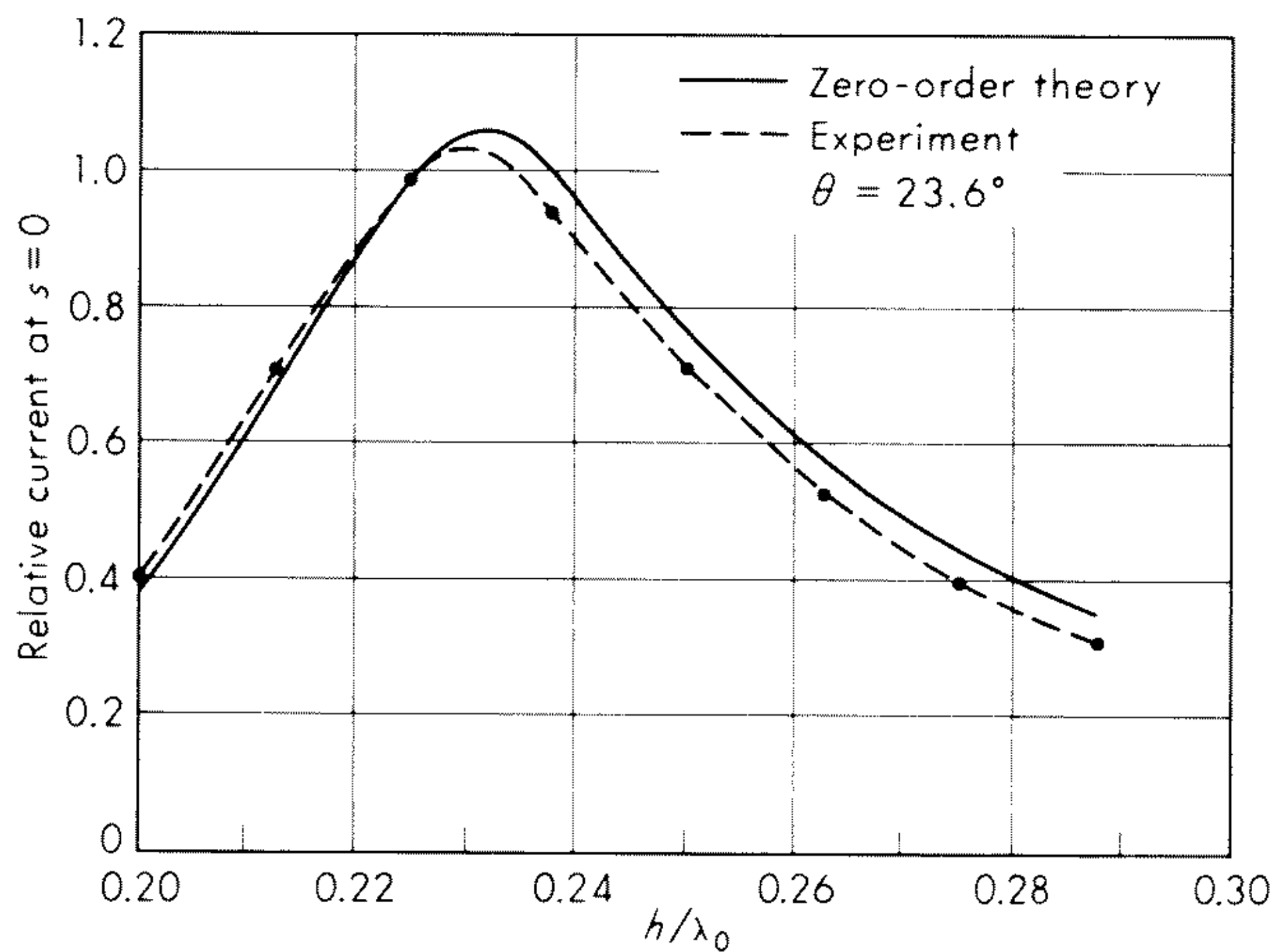


Fig. 9.34 Relative current at $s = 0$ in dipole as function of the half length h of the dipole; $\lambda_0 = 40$ cm, $b = 3$ cm, $2d = 2.2$ cm. (From Chen and King.²⁵)

admittance across the line at the voltage maximum. For a lossless line, the power in that equivalent admittance is $P = \text{Re} (VI^*/2) = |V|^2 G/2$, where V is the voltage across the equivalent admittance $Y = G + jB$. Note that $V = q_1/c = (q_1/\pi\epsilon_0) \ln (2d/a_1)$, where a_1 is the radius of the line wire. This power must equal the power radiated by the lossless antenna, $P = |I_s(0)|^2 R_0$, where R_0 is the input resistance of the antenna. When these two expressions for the power are equated and use is made of (9.157) with $s = 0$, the equivalent conductance of the dipole as a load across the line is

$$G = \left[\frac{K\pi}{\xi_0 \ln (2d/a_1)} \right]^2 R_0 \quad (9.158)$$

with
$$K = \frac{4(1 - \cos k_0 h) \Theta_s(h)}{[\Psi_s + E_a(h, h)] \cos k_0 h - C_a(h, h)} \quad (9.159)$$

and
$$\Theta_s(h) = d \sin \theta \int_0^h D(\theta, w) \cos (k_0 w \cos \theta) \sin k_0 (h - w) dw \quad (9.160)$$

The field pattern of the single coupled dipole has the well-known form for a half-wave dipole with a cosinusoidally distributed current.

9.18 Arrays of Dipoles Coupled to an Open-wire Line

The fundamental unit of the arrays shown in Fig. 9.31 is a pair of tilted dipoles as shown in Fig. 9.35. Let it be assumed that $k_0 h = \pi/2$ and that the current is well approximated by

$$[I_s(s)]_0 = I_0 \cos k_0 s \quad (9.161a)$$

where
$$I_0 = \frac{j4\pi}{\xi_0 C_a(\lambda_0/4, \lambda_0/4)} \Theta_s(\lambda_0/4) \quad (9.161b)$$

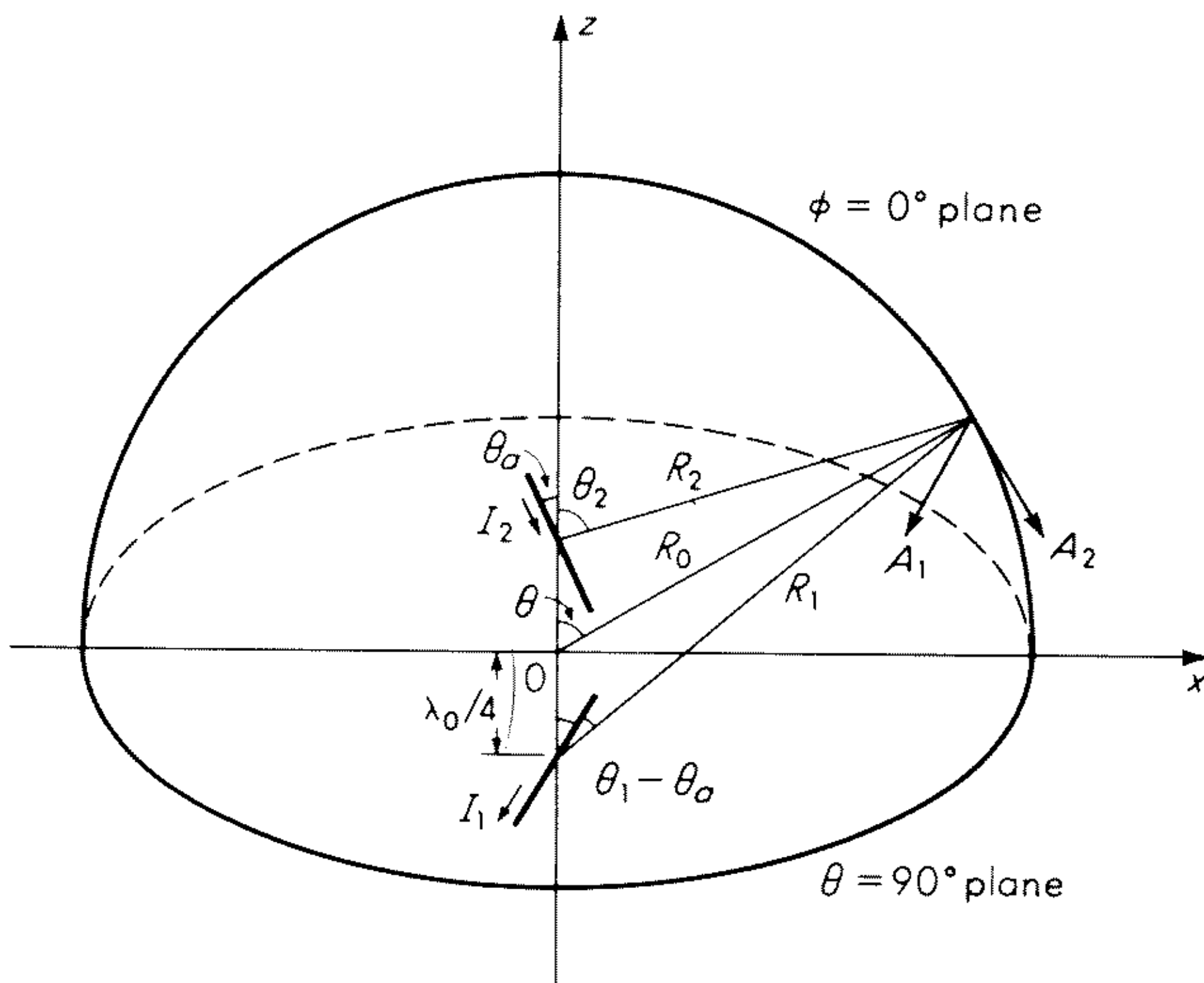


Fig. 9.35 Coordinate system for determination of radiation pattern.

with $\Theta_s(\lambda_0/4)$ given by (9.147a) with $s = h = \lambda_0/4$. The dipoles lie in the plane $\phi = 0$ at a tilt angle θ_a measured from the z axis. It is then readily verified that the radiation field in the E plane ($\phi = 0, \pi$ plane) is given by

$$E_{\theta^r}(\theta, \theta_a) = \frac{-j\zeta_0 I_0 e^{-jk_0 R}}{2\pi R} F_s(\theta, \theta_a) \quad (9.162a)$$

where

$$F_s(\theta, \theta_a) = \frac{\cos [(\pi/2) \cos (\theta - \theta_a)]}{\sin (\theta + \theta_a)} e^{-j(\pi/2) \cos \theta} + \frac{\cos [(\pi/2) \cos (\theta + \theta_a)]}{\sin (\theta + \theta_a)} e^{j(\pi/2) \cos \theta} \quad (9.162b)$$

This has four major lobes: two along the lines $\theta = 0, \pi$ (broadside effect) and two along the lines $\phi = 0, \pi$ (end-fire effect). Evidently this type of antenna functions as a combined broadside and end-fire array. The ratio of the maximum broadside to maximum end-fire field is

$$\frac{F_s(90^\circ, \theta_a)}{F_s(0^\circ, \theta_a)} = \tan \theta_a \left\{ \frac{\cos [(\pi/2) \sin \theta_a]}{\cos [(\pi/2) \cos \theta_a]} \right\} \quad (9.163)$$

When the tilt angle θ_a is small, this ratio is large and the two-element array is primarily a broadside array; when the tilt angle θ_a is large (near $\pi/2$), the ratio is small and the end-fire property is dominant. When $\theta_a = 45^\circ$, the end-fire and broadside lobes in the field pattern are equal in amplitude.

The field in the H plane ($\theta = 90^\circ$ plane) is

$$E_{\theta^r}(\phi, \theta_a) = \frac{-j\zeta_0 I_0 e^{-jk_0 R}}{\pi R} G(\phi, \theta_a) \quad (9.164a)$$

where

$$G(\phi, \theta_a) = \frac{\cos [(\pi/2) \sin \theta_a \cos \phi]}{1 - \sin^2 \theta_a \cos^2 \phi} \quad (9.164b)$$

When the tilt angle θ_a is small, $G(\phi, \theta_a)$ is nearly independent of ϕ . Hence, in practical application for which θ_a is nearly 20° , the pattern in the H plane is nearly omnidirectional.

A number of different arrays can be constructed of suitable combinations of the two-element array shown in Fig. 9.35. Three are shown in Fig. 9.31. An array with both broadside and end-fire characteristics is shown in Fig. 9.31a. Its radiation pattern in the E plane is

$$F(\theta, \theta_a) = F_s(\theta, \theta_a) \frac{\sin [(N\pi/2) \cos \theta]}{\sin (\pi \cos \theta)} \quad (9.165)$$

The array in Fig. 9.31b has broadside properties. The far-field pattern is given by

$$F(\theta, \theta_a) = f_z(\theta, \theta_a) \left\{ \frac{\sin [(N\pi/2) \cos \theta]}{\sin [(\pi/2) \cos \theta]} \right\} + 2f_x(\theta, \theta_a) \sin \left(\frac{\pi}{2} \cos \theta \right) \left\{ \frac{\sin [(N\pi/2) (\frac{1}{2} \cos \theta)]}{\cos (\pi \cos \theta)} \right\} \quad (9.166)$$

where
$$f_z(\theta, \theta_a) = \left\{ \frac{\cos [(\pi/2) \cos \theta_a \cos \theta]}{1 - \cos^2 \theta_a \cos^2 \theta} \right\} \cos \theta_a \sin \theta \quad (9.167a)$$

$$f_x(\theta, \theta_a) = \left\{ \frac{\cos [(\pi/2) \sin \theta_a \sin \theta]}{1 - \sin^2 \theta_a \sin^2 \theta} \right\} \sin \theta_a \cos \theta \quad (9.167b)$$

Finally, the simple transverse arrangement shown in Fig. 9.33c is an end-fire array with the pattern

$$F(\theta, \theta_a) = \left\{ \frac{\cos [(\pi/2) \cos \theta]}{\sin \theta} \right\} \left\{ \frac{\sin [(N\pi/2)(1 - \cos \theta)]}{\cos [(\pi/2) \cos \theta]} \right\} \quad (9.168)$$

Other possible arrangements are described in the literature.²⁵

PROBLEMS

- 9.1 Determine the impedance per unit length of solid and tubular copper and brass cylinders of different radii at broadcast and microwave frequencies. Repeat for dielectric tubes coated with layers of silver or carbon as thin as 10^{-4} to 10^{-7} m.
- 9.2 Verify that (9.16) is a solution of (9.15).
- 9.3 Begin with (9.56) and carry out the steps in the evaluation of (9.59a-c).
- 9.4 Compare the vertical field patterns for $E_\theta r$ when the three-term form (9.63) is used with the corresponding pattern for the sinusoidally distributed currents when $k_0 h = \pi/2$ and $k_0 h = \pi$ (refer to Sec. 9.7).
- 9.5 Carry out the derivation of Eq. (9.68) beginning with the boundary condition $E_z = 0$ at $r = a$.
- 9.6 Carry out the steps leading to (9.70a,b) beginning with (9.69) and its analog for $-h \leq z \leq 0$.
- 9.7 Derive (9.90a,b).
- 9.8 Obtain explicit formulas for the currents and the driving-point admittance of a four-element circular array when driven by four different voltages. (Refer to Sec. 9.12.)
- 9.9 Derive the integral formula for $E_\theta(R, \theta, \phi)$ for the far field of a curtain array. (Refer to end of Sec. 9.13.)

REFERENCES

1. King, R. W. P.: "Fundamental Electromagnetic Theory," pp. 356ff., Dover Publications, Inc., New York, 1963.
2. King, R. W. P.: "Fundamental Electromagnetic Theory," appendix I, Dover Publications, Inc., New York, 1963.
3. Mack, R. B.: A Study of Circular Arrays, pts. 2 and 3, *Cruft Lab. Tech. Repts.* 382 and 383, Harvard University, May, 1963; R. W. P. King and T. T. Wu: Currents, Charges, and Near Fields of Cylindrical Antennas, *Radio Sci.*, vol. 69D, pp. 429-446, March, 1965; vol. 1 (new series), pp. 353-359, March, 1966.
4. King, R. W. P., and T. T. Wu: The Imperfectly Conducting Cylindrical Antenna, *IEEE Trans. Antennas Propagation*, vol. AP-14, pp. 524-534, September, 1966; R. W. P. King, C. W. Harrison, Jr., and E. A. Aronson: The Imperfectly Conducting Cylindrical Antenna: Numerical Results, *IEEE Trans. Antennas Propagation*, vol. AP-14, pp. 535-542, September, 1966; L. C. Shen: An Experimental Study of Imperfectly Conducting Dipoles, *IEEE Trans. Antennas Propagation*, vol. AP-15, pp. 782-784, November, 1967.

5. King, R. W. P.: "Transmission Line Theory," pp. 405-411 and 430-437, Dover Publications, Inc., New York, 1965; "Theory of Linear Antennas," chap. II, sec. 10, Harvard University Press, Cambridge, Mass., 1956.
6. Iizuka, K., and R. W. P. King: Terminal-zone Corrections for a Dipole Driven by a Two-wire Line, *J. Res. Natl. Bur. Std. (U.S.)*, vol. 66D, pp. 775-782, November-December, 1962.
7. See, for example, R. W. P. King: "Theory of Linear Antennas," pp. 525 and 528, Harvard University Press, Cambridge, Mass., 1956.
8. King, R. W. P.: "Theory of Linear Antennas," sec. II.19, Harvard University Press, Cambridge, Mass., 1956.
9. Harrison, C. W., Jr., and R. W. P. King: Tables of the Integrals $C(h,0)$, $S(h,0)$, $E(h,0)$, $C(h,h)$, $S(h,h)$, and $E(h,h)$ for Complex Arguments, *Sandia Corp. Monograph SCR-667*.
10. Mack, R. B.: A Study of Circular Arrays, Part 5, Tables of $E(h,z)$, $C(h,z)$, $S(h,z)$, *Cruft Lab. Tech. Rept.* 385, Harvard University, May 1, 1963.
11. King, R. W. P.: "Theory of Linear Antennas," chap. IV, Harvard University Press, Cambridge, Mass., 1956.
12. King, R. W. P.: "Theory of Linear Antennas," p. 487, eq. (19), Harvard University Press, Cambridge, Mass., 1956.
13. King, R. W. P.: "Transmission Line Theory," p. 568, Dover Publications, Inc., New York, 1965.
14. Computed at Sandia Corporation under direction of C. W. Harrison, Jr. Programming by Aronson.
15. Mack, R. B.: A Study of Circular Arrays, Parts II and III, *Cruft Lab. Tech. Repts.* 382, 383, Harvard University, May, 1963.
16. Mailloux, R. J.: The Long Yagi-Uda Array, *IEEE Trans. Antennas Propagation*, vol. AP-14, pp. 128-137, 1966.
17. Morris, I. L.: Optimization of the Yagi Array, doctoral dissertation, Harvard University, 1965.
18. King, R. W. P., R. B. Mack, and S. S. Sandler: "Arrays of Cylindrical Dipoles," chap. 6, Cambridge University Press, New York, 1968.
19. Cheong, W. M.: Arrays of Unequal and Unequally Spaced Dipoles with Application to the Log-periodic Antenna, doctoral dissertation, Harvard University, 1967; *Radio Sci.*, vol. 2 (new series), pp. 1303-1325, November, 1967.
20. King, R. W. P., R. B. Mack, and S. S. Sandler: "Arrays of Cylindrical Dipoles," chap. 6, Cambridge University Press, New York, 1968.
21. Carrel, R. L.: Analysis and Design of the Log-periodic Dipole Antenna, *Univ. Illinois Elec. Eng. Res. Lab. Tech. Rept.* 52, October, 1961.
22. King, R. W. P., and T. T. Wu: The Cylindrical Antenna with Arbitrary Driving Point, *IEEE Trans. Antennas Propagation*, vol. AP-13, pp. 710-718, 1965.
23. King, R. W. P., R. B. Mack, and S. S. Sandler: "Arrays of Cylindrical Dipoles," chap. 7, Cambridge University Press, New York, 1968.
24. Sletten, C. J.: A New Antenna Radiator for VHF-UHF Communications, *AFCRC, Cambridge, Mass., Tech. Rept.*, 57-114, 1957.
25. Chen, K. M., and R. W. P. King: Dipole Antennas Coupled Electromagnetically to a Two-wire Transmission Line, *IEEE Trans. Antennas Propagation*, vol. AP-9, pp. 405-432, 1961.
26. King, R. W. P.: "Transmission Line Theory," p. 25, eq. (12), Dover Publications, Inc., New York, 1965.

CHAPTER 10

THEORY OF THE LONG DIPOLE ANTENNA

Chin-Lin Chen and Tai Tsun Wu

10.1 Introduction†

In order for a dipole antenna to radiate, power must be supplied through a transmission line, which is usually a two-wire line or a coaxial line. It should be emphasized that the transmission line and the antenna are inseparable parts of the same problem. For instance, to measure the input admittance of the antenna, the standing-wave ratio and the position of the current or voltage minimum on the transmission line are determined. Therefore, what we actually measure is the admittance of the antenna as it appears to the transmission line, or the apparent input admittance.¹ This problem, as it stands, is extremely difficult to analyze theoretically. Therefore, we consider an idealized model of a dipole antenna driven by a δ -function generator. This idealized problem has been studied in detail in Chap. 8. However, we have shown in Sec. 8.4 that the input susceptance so obtained is infinite. This suggests that this idealized problem is oversimplified. In order to have a better understanding, we shall consider in this chapter first the case of an infinite antenna driven by a coaxial line, as shown in Fig. 10.1. In this case, we find² that if $kb \ll 1$, it is possible to express the apparent input admittance approximately as the sum of two parts: one part is a function of ka only, while the other part, divided by ka , depends on a and b , but not k . It is perhaps natural to interpret the first part as the intrinsic admittance of the antenna, since it does not depend on the geometry of the coaxial transmission line. Similarly, the second part, being a property of the coaxial line, may be interpreted as a capacitive end correction. However, it should be noted that this separation is not unique and is possible only for thin antennas driven by a thin coaxial line. As discussed in Sec. 10.2, in order to apply this splitting of the apparent input admittance to a finite antenna, it is necessary to have a theory of the long dipole antenna.

In some applications the transient operation of a dipole antenna is of interest. Since a dipole antenna is a linear system, its transient responses may be obtained by the superposition of the responses to the individual frequency components of the Fourier representation of the applied signal.³ This is not only possible in principle but also practical, since high-speed computers are available. It has been shown⁴ that the initial transient response of a dipole antenna

†In this chapter we use the same notation as in Chap. 8, i.e., the subscript on k is dropped and $e^{-i\omega t}$ is used in place of $e^{i\omega t}$.

is closely related to the properties of the antenna at high frequencies. For this purpose, a solution of the long dipole antenna is again necessary.

As discussed in Sec. 10.3, this problem of a long dipole antenna is conveniently analyzed by the Wiener-Hopf technique. In Sec. 10.4, we describe

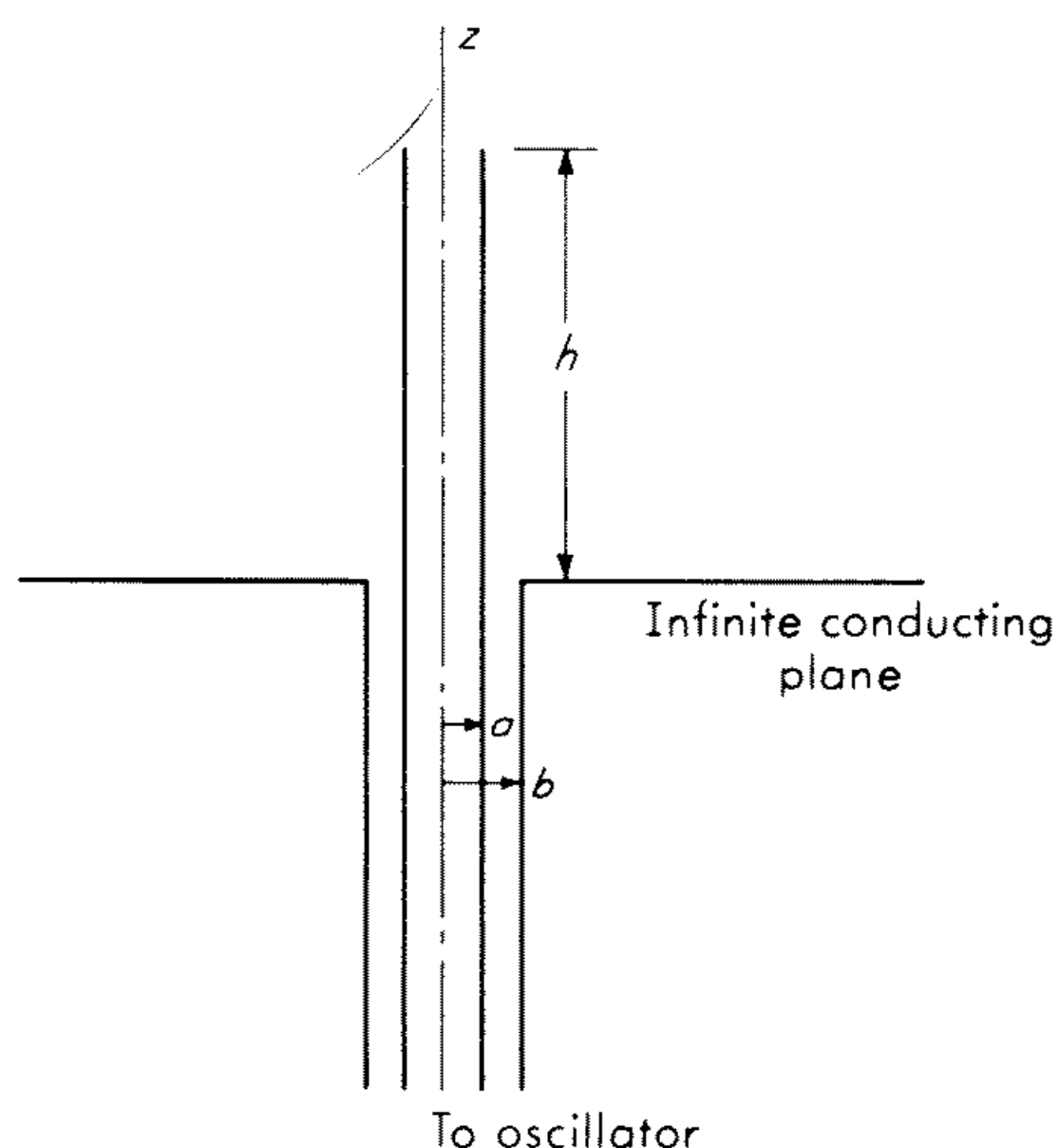


Fig. 10.1 A dipole antenna driven from a coaxial line.

in some detail how the Wiener-Hopf technique can be applied to this problem. The details of the calculation are presented in Secs. 10.5 and 10.6, and in Sec. 10.7 we collect all the results on the input admittances, the current and charge distributions, the field patterns, etc., and discuss their range of validity. It is hoped that those who are not interested in the mathematical details can omit Secs. 10.5 and 10.6 and can still follow the rest of the chapter without difficulty. The development and discussion in this chapter follow rather closely those of Refs. 2, 5, and 6, and the notation and conventions adopted here are those introduced in Chapter 8.

10.2 The Infinitely Long Dipole Antenna Driven from a Coaxial Line

In this section we shall study the problem of an infinite dipole antenna driven from a coaxial line, as depicted in Fig. 10.1. By solving this canonical problem, we shall provide the basis for separating the antenna from the antenna-transmission line system and thereby interpret the experimental data. We shall also compare the solution obtained in this section with the solutions given in Chap. 8, i.e., an infinite dipole antenna driven by a δ -function generator. Through these comparisons, we wish to find out what necessary steps and corrections should be taken to overcome the shortcomings of the idealized δ -function generators and provide guidance for further approximation. In

short, we hope to furnish the links between the theoretical results and the experimental data and between the problem of an antenna driven by a coaxial line and that of one driven by a δ -function generator.

a. Green's Functions

Let (r, ϕ, z) be the cylindrical coordinate system. The system under investigation is evidently independent of ϕ , and it is therefore suppressed. Let $\mathcal{G}_0(r, r'; z, z'; k)$ be the Green's function for the region above the ground plane. It is defined by the partial differential equation

$$\left(\frac{\partial^2}{\partial r'^2} + \frac{1}{r'} \frac{\partial}{\partial r'} - \frac{1}{r'^2} + \frac{\partial^2}{\partial z'^2} + k^2 \right) \mathcal{G}_0(r, r'; z, z'; k) = -\frac{1}{r} \delta(r - r') \delta(z - z') \quad r, r' \geq a \quad 0 \leq z, z' < \infty \quad (10.1)$$

the radiation condition at infinity, and the boundary conditions

$$\frac{\partial}{\partial r'} [r' \mathcal{G}_0(r, r'; z, z'; k)] = 0 \quad \text{at } r' = a \quad (10.2)$$

$$\frac{\partial}{\partial z'} [\mathcal{G}_0(r, r'; z, z'; k)] = 0 \quad \text{at } z' = 0 \quad (10.3)$$

Because of (10.3), \mathcal{G}_0 can be written as

$$\mathcal{G}_0(r, r'; z, z'; k) = G_0(r, r'; z, z'; k) + G_0(r, r'; z, -z'; k) \quad (10.4)$$

where G_0 is given by the same partial differential equation (10.1), the radiation condition and the boundary condition (10.2), with the domain of validity extended to $(-\infty, \infty)$ for z and z' . Let \bar{G}_0 be the Fourier transform of G_0 defined by

$$\bar{G}_0(r, r'; z, \zeta; k) = \int_{-\infty}^{\infty} G_0(r, r'; z, z'; k) e^{i\zeta z'} dz' \quad (10.5)$$

Then the standard methods can be used to solve for \bar{G}_0 ;

$$\bar{G}_0(r, r'; z, \zeta; k) = \frac{i\pi}{2} \frac{H_1^{(1)}(\xi r_>)}{H_0^{(1)}(\xi a)} [H_0^{(1)}(\xi a) J_1(\xi r_<) - J_0(\xi a) H_1^{(1)}(\xi r_<)] e^{i\zeta z} \quad (10.6)$$

where $r_>$ and $r_<$ are respectively the larger and the smaller of r and r' , and

$$\xi = (k^2 - \zeta^2)^{1/2} \quad (10.7)$$

is defined by $\xi = k$ for $\zeta = 0$ and by the branch cut shown in Fig. 10.2.

In the coaxial region, the Green's function $\mathcal{G}_c(r, r'; z, z'; k)$ is defined by the partial differential equation

$$\left(\frac{\partial^2}{\partial r'^2} + \frac{1}{r'} \frac{\partial}{\partial r'} - \frac{1}{r'^2} + \frac{\partial^2}{\partial z'^2} + k^2 \right) \mathcal{G}_c(r, r'; z, z'; k) = -\frac{1}{r} \delta(r - r') \delta(z - z') \quad a \leq r, r' \leq b \quad -\infty < z, z' \leq 0 \quad (10.8)$$

the radiation condition for $z' \rightarrow -\infty$, and the boundary conditions

$$\frac{\partial}{\partial r'} [r' \mathcal{G}_c(r, r'; z, z'; k)] = 0 \quad \text{at } r' = a \text{ and } r' = b \quad (10.9)$$

$$\frac{\partial}{\partial z'} \mathcal{G}_c(r, r'; z, z'; k) = 0 \quad \text{at } z' = 0 \quad (10.10)$$

For the same reason and in a similar fashion $G_c(r, r'; z, z'; k)$ and its Fourier transform \bar{G}_c are introduced.

$$\mathcal{G}_c(r, r'; z, z'; k) = G_c(r, r'; z, z'; k) + G_c(r, r'; z, -z'; k) \quad (10.11)$$

$$\begin{aligned} \bar{G}_c(r, r'; z, z'; k) &= \frac{i\pi}{2} \\ &\times \frac{[H_0^{(1)}(\xi b)J_1(\xi r_>) - J_0(\xi b)H_1^{(1)}(\xi r_>)][H_0^{(1)}(\xi a)J_1(\xi r_<) - J_0(\xi a)H_1^{(1)}(\xi r_<)]e^{i\zeta z}}{J_0(\xi a)H_0^{(1)}(\xi b) - J_0(\xi b)H_0^{(1)}(\xi a)} \end{aligned} \quad (10.12)$$

We note that \bar{G}_c has no branch cut; its only singularities are poles. For $kb \ll 1$, all these poles are complex except two located at $\zeta = \pm k$. These two real poles correspond to the TEM mode in the coaxial line. Thus as $z' \rightarrow -\infty$, with z fixed, the only dominant term is due to the residue at $\zeta = k$,

$$G_c(r, r'; z, z'; k) \approx \frac{i}{2k \ln(b/a)} \frac{e^{ik(z-z')}}{rr'}$$

Thus, as $z' \rightarrow -\infty$,

$$\mathcal{G}_c(r, r'; z, z'; k) \approx \frac{i}{k \ln(b/a)} \frac{\cos kz}{rr'} e^{-ikz'} \quad (10.13)$$

Furthermore, as $z \rightarrow -\infty$

$$G_c(r, r'; z, 0; k) \approx \frac{i}{2k \ln(b/a)} \frac{e^{-ikz}}{rr'} \quad (10.14)$$

b. Formulation of the Problem

Let the incident current on the inner conductor of the coaxial line be

$$I^{\text{inc}}(z) = e^{ikz} \quad (10.15)$$

Because of the rotational symmetry, $E_r(r, z)$, $E_z(r, z)$, and $H_\phi(r, z)$ are the only nonvanishing components of the electromagnetic field excited by (10.15). The components of the electric field can be expressed in terms of $H_\phi(r, z)$

$$E_r(r, z) = \frac{1}{i\omega\epsilon_0} \frac{\partial H_\phi(r, z)}{\partial z} \quad (10.16)$$

$$E_z(r, z) = -\frac{1}{i\omega\epsilon_0} \frac{1}{r} \frac{\partial}{\partial r} [rH_\phi(r, z)] \quad (10.17)$$

and $H_\phi(r, z)$ satisfies the wave equation

$$\left(\frac{\partial^2}{\partial r^2} + \frac{1}{r} \frac{\partial}{\partial r} - \frac{1}{r^2} + \frac{\partial^2}{\partial z^2} + k^2 \right) H_\phi(r, z) = 0 \quad (10.18)$$

subject to the radiation condition and the proper boundary conditions. We wish to find an integral expression for $H_\phi(r, z)$ for $z \leq 0$, $a \leq r \leq b$. For this purpose Green's theorem can be employed:

$$\begin{aligned} & \int [\mathcal{G}_c(r, r'; z, z'; k) \nabla'^2 H_\phi(r', z') - H_\phi(r', z') \nabla'^2 \mathcal{G}_c(r, r'; z, z'; k)] dV' \\ &= \int \hat{\mathbf{n}}' \cdot [\mathcal{G}_c(r, r'; z, z'; k) \nabla' H_\phi(r', z') - H_\phi(r', z') \nabla' \mathcal{G}_c(r, r'; z, z'; k)] dS' \end{aligned} \quad (10.19)$$

where the integrals are over the coaxial region. It follows from (10.8) and (10.18) that the volume integral yields $2\pi H_\phi(r, z)$. From (10.9) and the boundary conditions $E_z(a, z') = E_z(b, z') = 0$, it can be demonstrated that there is no contribution from the surface integral over the cylindrical surface $r' = a$ and $r' = b$. The surface integral over the surface $z' = 0$, $a \leq r' \leq b$ can be simplified by (10.10). The surface integral over the surface $a \leq r' \leq b$, $z' \rightarrow -\infty$ can be carried out explicitly by noting (10.13) and (10.15) and the radiation condition. Thus we have, in terms of $E_r(r, 0)$ and G_c , for $z \leq 0$, $a \leq r \leq b$

$$H_\phi(r, z) = \frac{\cos kz}{\pi r} + \frac{i2k}{\xi_0} \int_a^b G_c(r, r'; z, 0; k) E_r(r', 0) dr' \quad (10.20)$$

Similarly, for $z \geq 0$, $r \geq a$,

$$H_\phi(r, z) = -\frac{i2k}{\xi_0} \int_a^b G_0(r, r'; z, 0; k) E_r(r', 0) dr' \quad (10.21)$$

The continuity of $H_\phi(r, z)$ for $z = 0$, $a \leq r \leq b$ gives the desired integral equation for $E_r(r, z)$

$$\int_a^b E_r(r', 0) [G_0(r, r'; 0, 0; k) + G_c(r, r'; 0, 0; k)] r' dr' = \frac{i\xi_0}{2\pi k r} \quad (10.22)$$

c. Approximation for Small kb

When $|\xi b| \ll 1$, \bar{G}_c is approximated by

$$\bar{G}_c^{(0)}(r, r'; z, \xi; k) = -\frac{1}{\xi^2} \frac{e^{i\xi z}}{rr' \ln(b/a)} \quad (10.23)$$

Let $G_c^{(0)}(r, r'; z, z'; k)$ be the inverse Fourier transform of $\bar{G}_c^{(0)}(r, r'; z, \xi; k)$. Then

$$G_c^{(0)}(r, r'; z, 0; k) = \frac{i}{2k \ln(b/a)} \frac{e^{ik|z|}}{rr'} \quad (10.24)$$

Clearly, for $kb \ll 1$, $G_c^{(0)}(r, r'; z, 0; k)$ is a good approximation for $G_c(r, r'; z, 0; k)$ except when $|z|$ is small. When $z = 0$, the difference is given by

$$\begin{aligned} D_c(r, r'; k) = G_c(r, r'; 0, 0; k) - G_c^{(0)}(r, r'; 0, 0; k) &= \frac{1}{2\pi} \int_{-\infty}^{\infty} \\ &\left\{ i \frac{\pi}{2} \frac{[J_1(\xi r_<) H_0^{(1)}(\xi a) - H_1^{(1)}(\xi r_<) J_0(\xi a)][J_1(\xi r_>) H_0^{(1)}(\xi b) - H_1^{(1)}(\xi r_>) J_0(\xi b)]}{J_0(\xi a) H_0^{(1)}(\xi b) - J_0(\xi b) H_0^{(1)}(\xi a)} \right. \\ &\quad \left. + \frac{1}{rr' \ln(b/a)} \frac{1}{\xi^2} \right\} d\xi \end{aligned} \quad (10.25)$$

Under the assumption of a thin coaxial line, $kb \ll 1$, the right-hand side of (10.25) can be approximated by its static value at $k = 0$,

$$D_c(r, r'; k) \approx D_c(r, r'; 0) = \frac{1}{\pi} \int_0^\infty \left\{ \frac{[I_1(\xi r_<)K_0(\xi a) + K_1(\xi r_<)I_0(\xi a)][I_1(\xi r_>)K_0(\xi b) + K_1(\xi r_>)I_0(\xi b)]}{I_0(\xi b)K_0(\xi a) - I_0(\xi a)K_0(\xi b)} - \frac{1}{rr' \ln(b/a)} \frac{1}{\xi^2} \right\} d\xi \quad (10.26)$$

which is obviously frequency independent. Then,

$$G_c(r, r'; 0, 0; k) \approx \frac{i}{2k \ln(b/a)} \frac{1}{rr'} + D_c(r, r'; 0) \quad (10.27)$$

In a similar fashion, for $|\xi r_>| \ll 1$, \bar{G}_0 can be approximated by

$$\bar{G}_0(r, r'; z, \xi; k) = \frac{i2}{\pi} \frac{1}{rr'} \frac{e^{i\xi z}}{\xi^2 \{1 + (i2/\pi)[\gamma + \ln(\xi a/2)]\}} \quad (10.28)$$

where γ is Euler's constant. Analogous to (10.26) and (10.27) we have, for $kr_> \ll 1$,

$$D_0(r, r'; k) \approx D_0(r, r'; 0) = \frac{1}{\pi} \int_0^\infty \left\{ \frac{K_1(\xi r_>)}{K_0(\xi a)} [K_0(\xi a)I_1(\xi r_<) + I_0(\xi a)K_1(\xi r_<)] + \frac{1}{[rr' \ln(b/a)]\xi^2} \right\} d\xi \quad (10.29)$$

and

$$G_0(r, r'; 0, 0; k) \approx D_0(r, r'; 0) + \frac{1}{rr'} \frac{i}{\pi^2} \int_{C_0} \frac{d\xi}{\xi^2 \{1 + (i2/\pi)[\gamma + \ln(\xi a/2)]\}} \quad (10.30)$$

The contour C_0 is shown in Fig. 10.2.

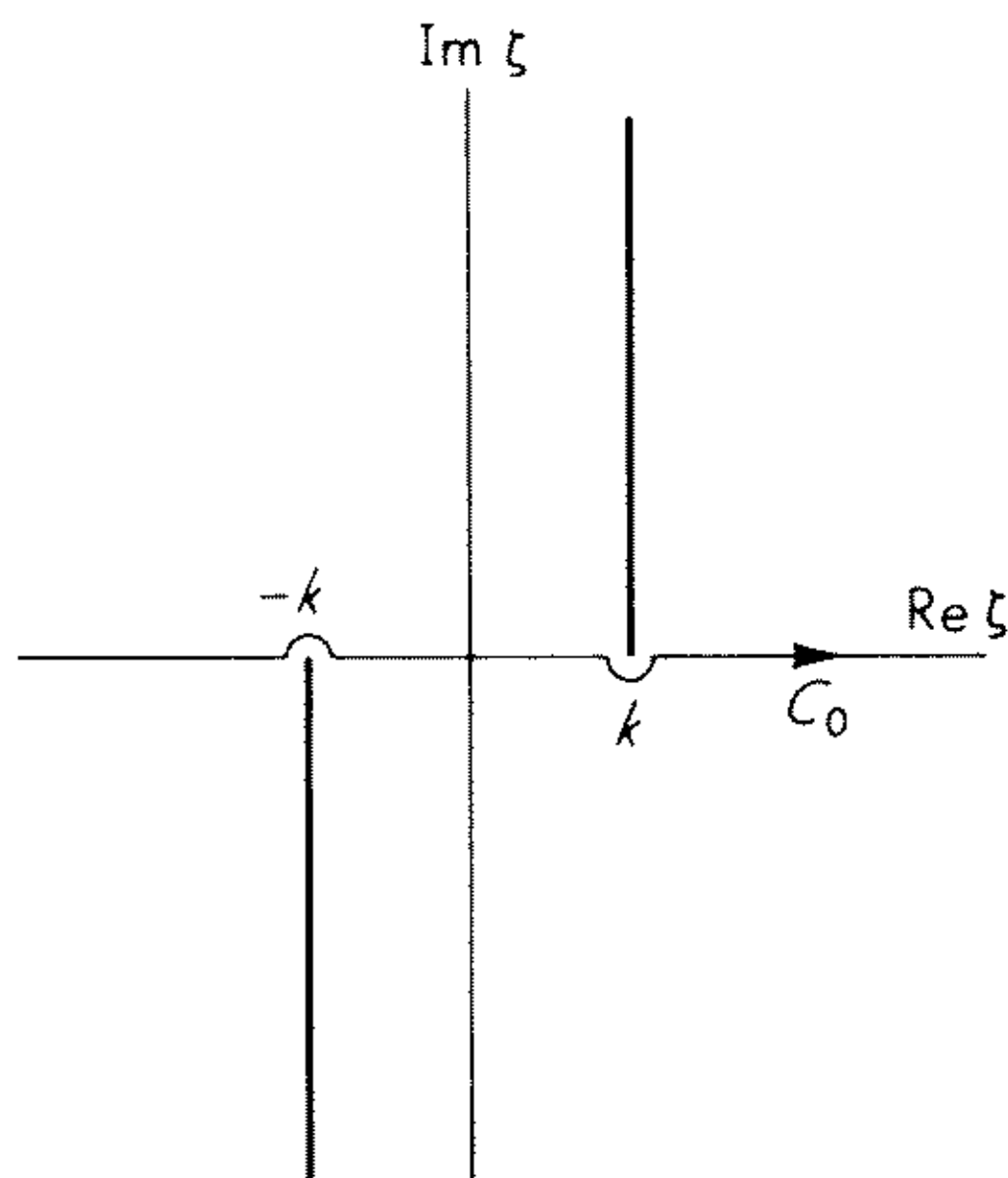


Fig. 10.2 The ξ plane and the contour C_0 ($\text{Im } k = 0$).

If (10.27) and (10.30) are substituted into (10.22) and

$$D(r, r'; 0) = D_0(r, r'; 0) + D_c(r, r'; 0) \quad (10.31)$$

$$\tau = \frac{i}{2k \ln(b/a)} + \frac{i}{\pi^2} \int_{c_0} \frac{d\xi}{\xi^2 \{1 + (i2/\pi)[\gamma + \ln(\xi a/2)]\}} \quad (10.32)$$

then (10.22) becomes

$$\int_a^b r' D(r, r'; 0) E_r(r', 0) dr' = \frac{1}{r} \left[\frac{i\xi_0}{2\pi k} - \tau \int_a^b E_r(r', 0) dr' \right] \quad (10.33)$$

Let $f(r)$ be the solution of the integral equation

$$\int_a^b r' f(r') D(r, r'; 0) dr' = \frac{1}{r} \quad (10.34)$$

and define

$$\alpha = a \int_a^b f(r) dr \quad (10.35)$$

$f(r)$ is a rather complicated function of r/a and r/b . However, we wish to extract as much information as possible, short of actually solving the integral equation. We note that $D(r, r'; 0)$ is real, and hence $f(r)$ and α are also real. Furthermore, α is independent of the wavelength. It can also be shown that α is a function of b/a only.

A comparison of (10.33) with (10.34) leads to the desired result:

$$E_r(r, 0) = \chi f(r) \quad (10.36)$$

where

$$\chi = \frac{i\xi_0}{2\pi k} \frac{1}{1 + \tau\alpha/a} \quad (10.37)$$

d. Application to the Thin Dipole Antenna Driven by a Thin Coaxial Line

These results can now be applied to the case $kb \ll 1$. As $z \rightarrow -\infty$ it follows from (10.14) and (10.21) and $H_\phi(r, z)$ can be put into a more descriptive form as follows:

$$H_\phi(r, z) = \frac{1}{2\pi r} \left\{ e^{ikz} + e^{-ikz} \left[1 - \frac{2\pi}{\xi_0 \ln(b/a)} \int_a^b E_r(r', 0) dr' \right] \right\} \quad (10.38)$$

The reflection coefficient is thus

$$\Gamma = 1 - \frac{2\pi}{\xi_0 \ln(b/a)} \int_a^b E_r(r', 0) dr' \quad (10.39)$$

By transmission line theory⁷ the apparent input admittance Y_a is related to the reflection coefficient by

$$Y_a = Y_c \frac{1 + \Gamma}{1 - \Gamma} \quad (10.40)$$

where the characteristic admittance of the coaxial line is

$$Y_c = \frac{2\pi}{\xi_0 \ln(b/a)} \quad (10.41)$$

The substitution of (10.39) and (10.41) into (10.40) gives the apparent input admittance of the infinite dipole antenna as seen from a coaxial line,

$$Y_{a\infty} = -\frac{2\pi}{\zeta_0 \ln(b/a)} + \frac{2}{\int_a^b E_r(r',0) dr'} \quad (10.42)$$

In terms of τ and α , we have

$$Y_{a\infty} = -\frac{2\pi}{\zeta_0 \ln(b/a)} - i \frac{4\pi}{\zeta_0} \left(k\tau + \frac{ka}{\alpha} \right) \quad (10.43)$$

Or, more explicitly,

$$Y_{a\infty} = 2Y_\infty - i \frac{4ka}{\zeta_0} \frac{1}{\alpha} \quad (10.44)$$

where

$$Y_\infty = \frac{2k}{\pi\zeta_0} \int_{c_0} \frac{d\zeta}{\xi^2 \{1 + (i2/\pi)[\gamma + \ln(\xi a/2)]\}} \quad (10.45)$$

In calculating the integral (10.32), we have ignored the poles at $\zeta = \pm(k^2 + 4e^{-2\gamma}a^{-2})^{1/2}$. However, these poles are of no consequence for our purpose, and they can be properly taken care of through more elaborate manipulation.²

The current along the antenna is given by

$$I(z) = 2\pi a H_\phi(a, z)$$

For kz not too small, $G_0^{(0)}$ can be used to approximate G_0 . Then $I(z)$ can be written as

$$I(z) = \frac{4k}{\pi\zeta_0} \frac{\chi\alpha}{a} \int_{c_0} \frac{e^{i\zeta z} d\zeta}{\xi^2 \{1 + (i2/\pi)[\gamma + \ln(\xi a/2)]\}} \quad (10.46)$$

Equation (10.21) can be used to compute the radiation field. For this purpose the asymptotic expression of $G_0(r, r'; z, 0; k)$ is needed, and it can be obtained by the usual saddle-point technique. The final result is, in terms of the spherical coordinate system (R, θ, ϕ) ,

$$H_\phi(r, z) \approx \frac{i2k}{\pi\zeta_0} \frac{\chi\alpha}{a} \frac{1}{\sin \theta} \frac{1}{1 + (i2/\pi)[\gamma + \ln(ka \sin \theta/2)]} \frac{e^{ikR}}{R} \quad (10.47)$$

e. Discussion of Results

This completes our investigation of the canonical problem. We have shown in (10.44) that, when $kb \ll 1$, the apparent input admittance $Y_{a\infty}$, as seen from the coaxial line, can be split into two parts. The first and dominant part $2Y_\infty$ depends on ka only and hence may be considered to be an intrinsic part of the antenna. The other part $-i(4ka/\zeta_0\alpha)$ is called the capacitive end correction. Note that this splitting is arbitrary up to a constant in the capacitance. Physically, this lumped capacitance is due to the geometrical discontinuity at $z = 0$ and is a local effect. Thus this same lumped capacitance is present not only in the case of the infinite antenna but also for finite antennas, provided

that the length is not too short. More precisely, consider a linear antenna of length h driven from a coaxial line. If $h \gg b$, and $kb \ll 1$, then the apparent input admittance Y_a can be approximately expressed as follows:

$$Y_a = 2Y - i \frac{4ka}{\zeta_0 \alpha} \quad (10.48)$$

Here again $2Y$ can be considered to be the intrinsic admittance of the antenna, while $-i(4ka/\zeta_0 \alpha)$ is the capacitive end correction. The important point is that Y depends only on ka and kh but not kb .

Many theories, such as the King-Middleton procedure,¹ yield a finite intrinsic admittance for dipole antennas. Because of the ambiguity in the splitting of the apparent input admittance, the results of these theories cannot be used in conjunction with (10.48) to get Y_a . In other words, the value of the capacitive end correction depends on the theory. In order to use (10.48) Y must satisfy

$$\lim_{h \rightarrow \infty} Y = Y_\infty \quad (10.49)$$

This condition removes the ambiguity in the splitting of Y_a . Note that for theories valid only for relatively short dipole antennas it is not meaningful to ask whether (10.49) is satisfied or not.

Since it is much easier to solve the problem of a dipole antenna driven by a δ -function generator than that of one driven by a coaxial line, only the δ -function generator will be used in the following sections. It is therefore essential to establish the connection between these two problems. For this purpose, we note that the current distribution along and the radiation field of an infinite dipole antenna driven by a δ -function generator are given by

$$I_\infty(z) = \frac{2kV}{\pi\zeta_0} \int_{c_0} \frac{e^{-i\zeta z}}{\xi^2 J_0(\xi a) H_0^{(1)}(\xi a)} d\zeta \quad (10.50)$$

$$H_\phi(r, z) \approx \frac{ik}{\pi\zeta_0} \frac{V}{\sin \theta H_0^{(1)}(ka \sin \theta)} \frac{e^{ikR}}{R} \quad (10.51)$$

In particular,

$$\frac{I_\infty(0)}{V} = \frac{2k}{\pi\zeta_0} \int_{c_0} \frac{1}{\xi^2 J_0(\xi a) H_0^{(1)}(\xi a)} d\zeta \quad (10.52)$$

In order to compare (10.50) and (10.51) with (10.46) and (10.47) we have to define an equivalent driving voltage. A natural choice of such a driving voltage is, from (10.35) and (10.36),

$$V' = \int_a^b E_r(r, 0) dr = \frac{\chi \alpha}{a} \quad (10.53)$$

The right-hand sides of (10.50) and (10.51) are approximately equal to those of (10.46) and (10.47) if V' is identified as $V/2$. Physically this is because (10.46) and (10.47) are the current and radiation field of an infinite dipole antenna

driven at its base against a ground plane, by an equivalent voltage source V' , while (10.50) and (10.51) are for the antenna driven at its center. This is also the reason for introducing the factor 2 in (10.44).

We also observe that if the leading terms of the power series expansion of the Bessel functions are used, then the right-hand side of (10.52) becomes formally identical with that of (10.46) even though $I_\infty(0)/V$ is infinite and Y_∞ is finite. Therefore, in order to use (10.48) for finite dipole antennas we must use only the leading terms for the Bessel functions that appear in the Fourier transform of the kernel. This replacement of the Bessel functions by their leading terms is not for convenience, but is mandatory. One may ask whether there is a way of including the higher-order terms in the series expression of the Bessel functions in the interest of obtaining better accuracy. The answer is that, if this better accuracy is desired, it is not possible to split the apparent input admittance additively into an intrinsic part and an end correction. That is, it would then be necessary to consider the coupled system of the dipole antenna together with the driving coaxial line. These remarks apply to both the infinite antenna with $kb \ll 1$ and the finite antenna with $h \gg b$ and $kb \ll 1$. [The consideration can be generalized to the case $h \gg b - a$ and $k(b - a) \ll 1$, but we shall not discuss this point any further.]

In the following sections, where we investigate the problem of the long, thin, dipole antenna driven by a δ -function generator, we prescribe that all Bessel functions in the Fourier transform of the kernel are replaced by their leading terms in their series expansions and that the extraneous poles caused by this replacement are ignored. The resulting input admittance is identified with the intrinsic admittance Y . It is then found that (10.49) is indeed satisfied.

10.3 Discussion of the Existing Solutions for Short Dipole Antennas

The integral equation for the current distribution along a thin, finite, circular, tubular antenna is

$$\int_{-h}^h g(z') \mathcal{K}(z - z') dz' = \frac{iV}{2\xi_0} (\sin k|z| + \mathcal{C} \cos kz) \quad |z| < h \quad (10.54)$$

where \mathcal{C} is to be determined by the boundary condition

$$g(\pm h) = 0 \quad (10.55)$$

This integral equation has previously been introduced in Sec. 8.5, except that a factor of $2\xi_0/iV$ has been absorbed in \mathcal{C} for convenience. The following assumptions have been made in its derivation:

1. The antenna is perfectly conducting.
2. The antenna is very thin, $ka \ll 1$, so that the complication discussed in Secs. 8.8 and 8.9 has negligible effect on the final solution.

3. The voltage source used as the excitation is angularly independent, or more explicitly,

$$E_z(a, \phi, z) = -V\delta(z) \quad (10.56)$$

These assumptions are made throughout this chapter. However, we shall comment on the first assumption at the end of this chapter.

There exist principally five different approaches to the problem so imposed. They are the variational method, Fourier series expansions, numerical technique, iterative method, and the Wiener-Hopf technique. The last procedure is adapted specifically for the long dipole antenna, while the first four procedures are valid only for relatively short antennas. We shall comment on these four methods briefly.

The variational technique^{8,9} is a very powerful tool for estimating the input admittance or impedance of the antenna *if* we know roughly what the current distribution is. For the case of a thin dipole antenna with $h \leq \lambda$, it does give results comparable with the King-Middleton solution.[†] If we were able to find such a reasonable guess of the first approximation for longer antennas, the variational method would certainly be applicable. The trouble is that it is difficult to make such an intelligent guess. Besides, it really does not solve the antenna problem, and even if the impedance computation yields a good result, very little could be said about the current distribution itself. A variational expression in terms of the electric field has been investigated by Hurd.¹⁰

The usefulness and accuracy of the Fourier series method¹¹⁻¹³ have been greatly improved since the introduction of digital computers. The success of Duncan and Hinchey¹³ must not be attributed to the Fourier series; rather, it is due to the inclusion of King's quasi-zero-order solution¹⁴ in addition to the Fourier series expansion. Since the quasi-zero-order solution itself is already rather accurate, it is not surprising that they are able to obtain a good result for antennas with $h \leq \lambda$. But the quasi-zero-order solution is not applicable for antennas with $h > \lambda$, and there is also the question of how to subtract out the logarithmic singularity or the knife-edge capacitance from the solution. Although these obstacles are not insurmountable,^{15,16} the rate of convergence and the accuracy of the solution deteriorate as the antenna becomes longer. Furthermore, the Fourier series method and the numerical techniques^{17,18} have one disadvantage in common. That is, very little can be said about the problem until the numerical computation has been carried out specifically for those parameters of interest.

Among the methods used to solve the antenna problem, the iterative procedure stands out as the most useful one. Our present-day knowledge of the linear antenna is primarily due to the successful application of the iterative procedure, or more specifically, the King-Middleton procedure.¹ However, it fails to yield accurate results for the case $h > \lambda$. Since the iterative procedure itself can hardly be questioned, an explanation of the discrepancy in the iterative solution may be sought in the adequacy of the initial approximation. One

[†]See Sec. 2.9.

of the major steps of the King-Middleton procedure is the introduction of the iterative parameter Ψ . Physically Ψ is the ratio of the vector potential to the current at the same point. In order to get the zero-order solution for the current, it is assumed that Ψ , real or complex, is sensibly constant over the whole antenna. This assumption is reasonable except on two occasions, i.e., (1) if the antenna is too long, say $h > \lambda$, or (2) near the end points of the antenna, $z \approx \pm h$, even if the antenna is short. Since the current vanishes at the ends $z = \pm h$, while the vector potential remains finite there, it should be obvious that Ψ would vary rapidly there. Unfortunately, the value of the constant \mathcal{C} is determined at $z = \pm h$, precisely where the approximation is poor.

To see why Ψ fails to remain constant for the case when $h > \lambda$, we shall give a rough estimate of the vector potential at $0 < z < h$. For this purpose, the kernel $K(z, a)$ instead of $\mathcal{K}(z)$ may be used conveniently.¹⁹

$$A_z(a, z) = \frac{\mu_0}{4\pi} \int_{-h}^h g(z') \frac{e^{ik\sqrt{(z-z')^2 + a^2}}}{\sqrt{(z-z')^2 + a^2}} dz' \quad (10.57)$$

As a rough approximation we could use $I_0 e^{ik|z|}$ as the current distribution function. Then the integral can be split into two parts

$$\begin{aligned} A_z(z, a) &\approx \frac{\mu_0}{4\pi} I_0 e^{ikz} \int_{z-d}^{z+d} \frac{dz'}{\sqrt{(z-z')^2 + a^2}} \\ &\quad + \frac{\mu_0}{4\pi} I_0 \left(\int_{-h}^{z-d} + \int_{z+d}^h \right) e^{ik|z'|} \frac{e^{ik|z-z'|}}{|z-z'|} dz' \\ &= \frac{\mu_0}{4\pi} I_0 e^{ikz} \ln \left(\frac{2d}{a} \right)^2 + \frac{\mu_0}{4\pi} I_0 e^{ikz} \ln \frac{z}{d} + O\left(\frac{1}{2kz} \right) \end{aligned} \quad (10.58)$$

where d is some constant satisfying the relation $a \ll d \ll \lambda$. The first term is the vector potential contributed by the current at a neighboring point $(z-d, z+d)$, and the second term is the contribution from the current at the other portion of the antenna. For thin antennas, the first term is the dominant part, since $a \ll \lambda$ under usual circumstances. This is the reason why Ψ is reasonably constant for $h \leq \lambda$. However, for longer antennas h , and hence z , could be much larger than a wavelength; the importance of the second term can no longer be ignored.

To overcome these two obstacles just mentioned, we shall employ the Wiener-Hopf technique.^{20,21}

10.4 Plan for the Wiener-Hopf Approach

The content of the integral equation (10.54) and its boundary condition (10.55) may be qualitatively described by saying that the current on the antenna is determined by the following conditions (Fig. 10.3a):

1. The vector potential is as prescribed on the antenna, $|z| \leq h$.
2. The current vanishes outside the antenna, $z > h$ and $z < -h$.

The constant \mathcal{C} has a direct bearing on the input admittance of the antenna,

and, roughly speaking, large values of \mathcal{C} indicate resonance while small values indicate antiresonance. Therefore, the determination of \mathcal{C} is a crucial step in finding the solution. Since the constant \mathcal{C} is determined by the condition that

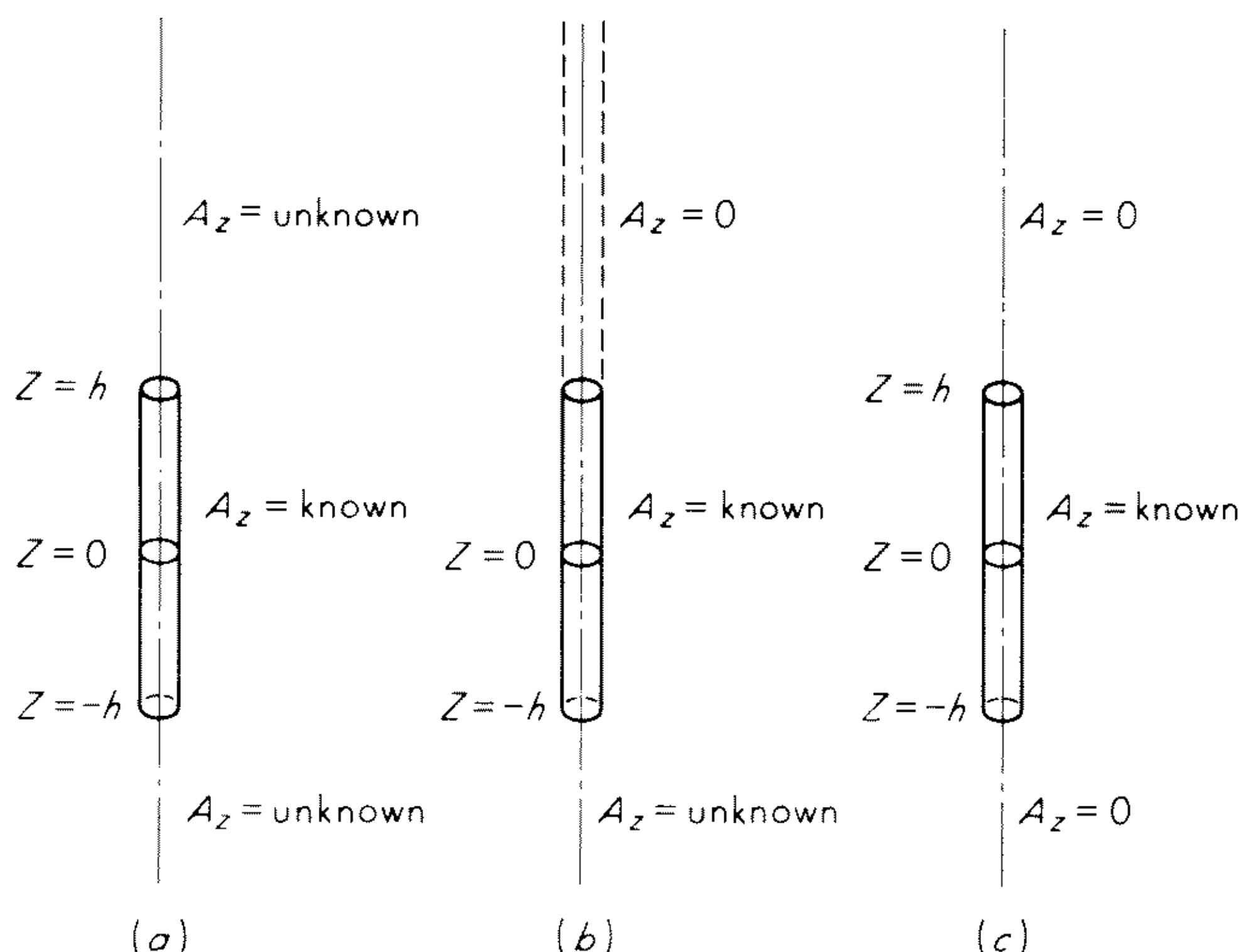


Fig. 10.3 Antenna models, δ -function generator located at $z = 0$. (a) Idealized model; (b) model of semi-infinite antenna for the determination of \mathcal{C} ; (c) simplified model.

the current vanish at the ends of the antenna, it is necessary to express the current at $z = \pm h$ in terms of \mathcal{C} . For thin antennas, the kernel of the integral equation is relatively large for small $k|z - z'|$ and relatively small and oscillatory for large $k|z - z'|$. Accordingly, the vector potential is comparatively small for $|z| > h$. For long or moderately long antennas, the value of the current at $z \approx -h$ is not sensitive to the condition at $z > h$. Consequently, the current at $z = -h$ may be found approximately by assuming instead the following conditions:

1'. The vector potential is as prescribed on the antenna, $-h \leq z \leq h$, and *vanishes for* $z > h$.

2'. The current vanishes for $z < -h$.

Then the antenna may be approximated by a semi-infinite one which extends from $z = -h$ to $+\infty$ and is driven by a vector potential distribution given by condition 1'. This semi-infinite antenna (Fig. 10.3b) is described by an integral equation of the Wiener-Hopf type:

$$\int_{-h}^{\infty} g(z') \mathcal{K}(z - z') dz' = \mathfrak{F}(z) \quad z \geq -h \quad (10.59)$$

$$\text{where } \mathfrak{F}(z) = \begin{cases} \frac{iV}{2\zeta_0} (\sin k|z| + \mathcal{C} \cos kz) & -h \leq z \leq h \\ 0 & z > h \end{cases} \quad (10.60)$$

As the solution of (10.59), $g(z)$ is in general unbounded near $z = -h$. If, however, $\mathfrak{F}(z)$ satisfies a certain integral condition, $g(z)$ becomes bounded near $z = -h$ and, furthermore, $\lim_{z \rightarrow -h^+} g(z) = 0$. The Wiener-Hopf technique is here employed to find such an integral condition. The result is given in (10.91).

This condition (10.91) for the vanishing of the current at the end of the semi-infinite antenna is exact. However, this rather complicated condition can be greatly simplified if the antenna is thin, that is, $ka \ll 1$, and if the characteristic distance for the variation of $\mathfrak{F}(z)$ is much larger than a . Under these circumstances the Fourier transform of the kernel $\mathcal{K}(z)$ may be replaced by its small-argument approximation as indicated in Sec. 10.2. When this is done, the constant \mathcal{C} can be determined explicitly.

Once \mathcal{C} is known, some of the properties of the antenna, such as the input admittance, the current and the charge distribution along the major portion of the antenna, and the radiation pattern, may be found by assuming the somewhat less accurate but considerably simpler conditions that

- 1''. The vector potential is as prescribed, with \mathcal{C} already determined on the antenna, $-h \leq z \leq h$, and *vanishes for both* $z > h$ *and* $z < -h$.
- 2''. There is no condition on the current.

This simplified model (Fig. 10.3c) may be solved by the Fourier transform method. However, as is well-known, the solution of the Wiener-Hopf equations and the result of the Fourier transform method are in general extremely complicated, being contour integrals with complicated integrands. Since a direct evaluation of these integrals seems extremely difficult, it is a necessary task to obtain simpler approximations to these rather involved expressions. For this purpose, the smallness of the radius of the antenna is used repeatedly. Although the procedure is very complicated and detailed, the final result is simple and quite accurate for long antennas. These results are summarized in Sec. 10.7, and the mathematical derivations are presented in Secs. 10.5 and 10.6.

10.5 Integral Condition

One of the major steps in Wiener-Hopf procedure is to write a function as the sum or product of two functions, one being analytic in the upper half plane and the other in the lower half plane. For any function f of ζ analytic in a strip, say $|\text{Im } \zeta| < \epsilon$, define

$$f_+(\zeta) = \frac{1}{2\pi i} \int_{-\infty - i\epsilon/2}^{\infty - i\epsilon/2} \frac{f(\zeta')}{\zeta' - \zeta} d\zeta' \quad (10.61)$$

and
$$f_-(\zeta) = \frac{-1}{2\pi i} \int_{-\infty + i\epsilon/2}^{\infty + i\epsilon/2} \frac{f(\zeta')}{\zeta' - \zeta} d\zeta' \quad (10.62)$$

where the Cauchy principal values are taken at infinity. If these integrals are absolutely convergent, then $f_-(\zeta)$ is analytic for $\text{Im } \zeta < \epsilon/2$ and $f_+(\zeta)$ is analytic for $\text{Im } \zeta > -\epsilon/2$. Furthermore, in the strip $|\text{Im } \zeta| < \epsilon/2$,

$$f(\zeta) = f_+(\zeta) + f_-(\zeta) \quad (10.63)$$

The corresponding formulas for multiplicative splitting can be found by noting

$$\ln f(\zeta) = [\ln f(\zeta)]_+ + [\ln f(\zeta)]_- \quad (10.64)$$

We shall not discuss any of the mathematical problems connected with the Wiener-Hopf procedure. For this, the reader is referred to Klein.²¹ Rather, we shall use the heuristic device of considering the medium to be slightly lossy, i.e.,

$$\text{Im } k = \epsilon > 0$$

Eventually ϵ is allowed to approach zero.

The integral equation for the semi-infinite antenna is given by (10.59) and (10.60). After a translation of coordinate systems, $z_1 = z + h$, $z'_1 = z' + h$, and with the following definitions:

$$g(z) = g(z_1 - h) \equiv I(z_1) \quad (10.65)$$

$$\begin{aligned} \mathfrak{F}(z) &= \mathfrak{F}(z_1 - h) \equiv F(z_1) \\ &= \begin{cases} \frac{iV}{2\zeta_0} [\sin k|z_1 - h| + \mathcal{C} \cos k(z_1 - h)] H(2h - z_1) & z_1 \geq 0 \\ 0 & z_1 < 0 \end{cases} \end{aligned} \quad (10.66)$$

where $H(x)$ is the Heaviside function

$$H(x) = \begin{cases} 1 & x > 0 \\ 0 & x < 0 \end{cases}$$

then, for $z_1 \geq 0$,

$$\int_0^\infty I(z'_1) \mathcal{K}(z_1 - z'_1) dz'_1 = F(z_1) \quad (10.67)$$

Define

$$G(z_1) = \begin{cases} 0 & z_1 \geq 0 \\ \int_0^\infty I(z'_1) \mathcal{K}(z_1 - z'_1) dz'_1 & z_1 < 0 \end{cases} \quad (10.68)$$

Then, for all real z_1 ,

$$\int_0^\infty I(z'_1) \mathcal{K}(z_1 - z'_1) dz'_1 = F(z_1) + G(z_1) \quad (10.69)$$

The relevant Fourier transforms are defined by

$$\bar{\mathcal{K}}(\zeta) = \int_{-\infty}^{\infty} \mathcal{K}(z_1) e^{i\zeta z_1} dz_1 = \frac{i}{4} J_0(\xi a) H_0^{(1)}(\xi a) \quad (10.70)$$

$$\bar{I}_+(\zeta) = \int_0^{\infty} I(z_1) e^{i\zeta z_1} dz_1 \quad (10.71)$$

$$\bar{F}_+(\zeta) = \int_0^{\infty} F(z_1) e^{i\zeta z_1} dz_1 \quad (10.72)$$

$$\bar{G}_-(\zeta) = \int_{-\infty}^0 G(z_1) e^{i\zeta z_1} dz_1 \quad (10.73)$$

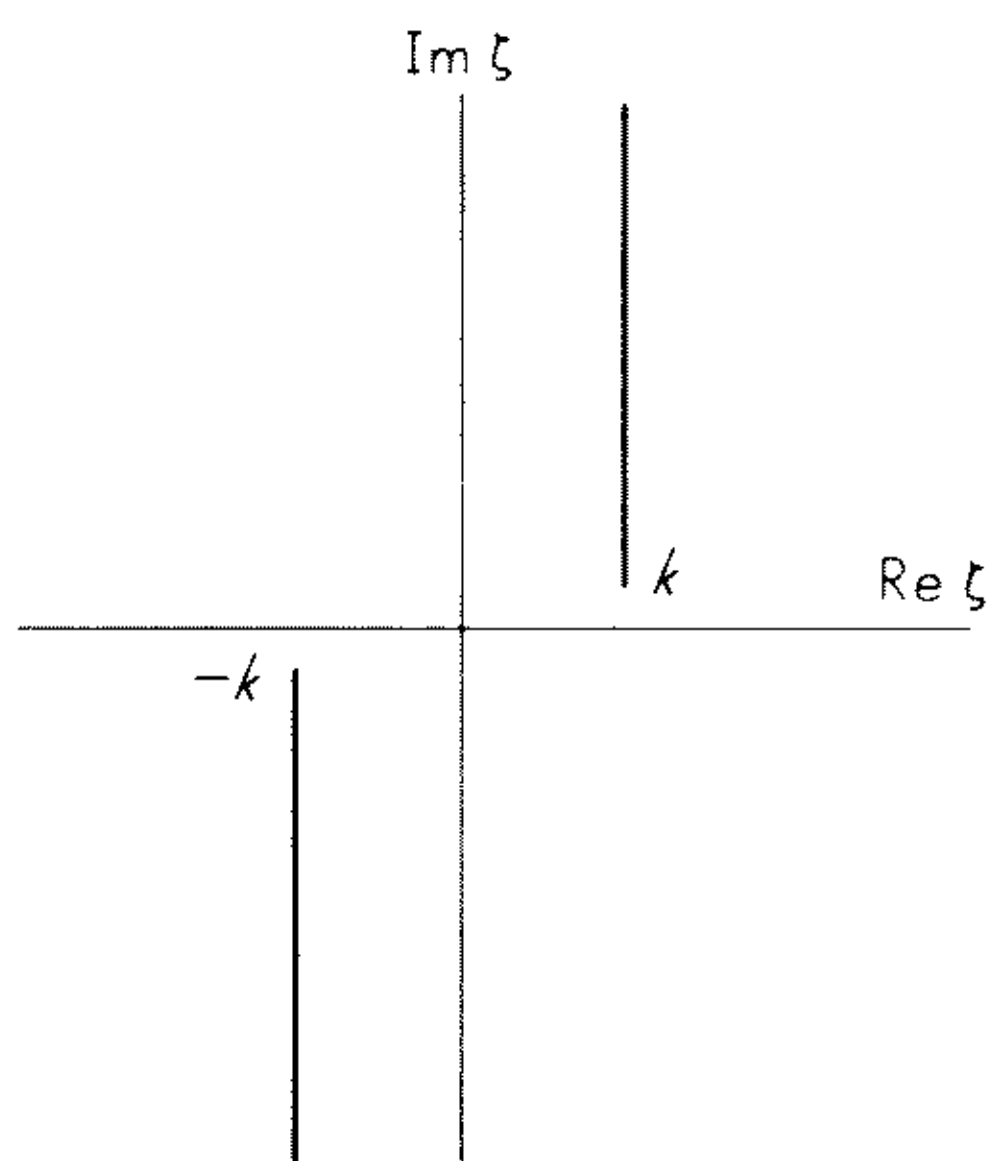


Fig. 10.4 The ζ -plane branch cut with $\text{Im } k = \epsilon > 0$.

where $\xi = \sqrt{k^2 - \zeta^2}$. For the sake of definiteness we take $\zeta = k$ when $\zeta = 0$ and draw the branch cuts in the first and the third quadrants as shown in Fig. 10.4. Clearly $\bar{\mathcal{K}}(\zeta)$ is analytic in the strip $|\text{Im } \zeta| < \epsilon$, and as $|\zeta| \rightarrow \infty$ in that strip

$$\bar{\mathcal{K}}(\zeta) \approx O(|\zeta|^{-1}) \quad (10.74)$$

From our previous study of the current on an infinite antenna¹⁹ we learned that, as $z_1 \rightarrow \infty$,

$$I(z_1) e^{-ikz_1} \rightarrow 0 \quad (10.75)$$

Thus $I_+(\zeta)$ is analytic for $\text{Im } \zeta > -\epsilon/2$. Since $I(z_1) \rightarrow 0$ as $z_1 \rightarrow 0+$, it follows from (8.97) that, as $|\zeta| \rightarrow \infty$ in the half plane $\text{Im } \zeta > -\epsilon/2$,

$$\bar{I}_+(\zeta) \approx O(|\zeta|^{-1}) \quad (10.76)$$

The Fourier transforms defined in (10.70) to (10.73) have a common strip of analyticity, which includes the real ζ axis. In this common strip we have, from (10.69)

$$\bar{I}_+(\zeta) \bar{\mathcal{K}}(\zeta) = \bar{F}_+(\zeta) + \bar{G}_-(\zeta) \quad (10.77)$$

Making use of (10.61) to (10.64), we define

$$\bar{L}_{\pm}(\zeta) = \exp [\pm \ln \bar{\mathcal{K}}(\zeta)]_{\pm} \quad (10.78)$$

Then, in the strip $|\operatorname{Im} \zeta| < \epsilon/2$, we have

$$\bar{\mathcal{K}}(\zeta) = \frac{\bar{L}_+(\zeta)}{\bar{L}_-(\zeta)} \quad (10.79)$$

Since $\bar{\mathcal{K}}(\zeta)$ is an even function of ζ , it follows from (10.61) and (10.62) that

$$\bar{L}_-(-\zeta) = \frac{1}{\bar{L}_+(\zeta)} \quad (10.80)$$

Furthermore, as $|\zeta| \rightarrow \infty$,

$$\bar{L}_+(\zeta) \approx O(|\zeta|^{-1/2}) \quad (10.81)$$

$$\bar{L}_-(\zeta) \approx O(|\zeta|^{1/2}) \quad (10.82)$$

From (10.77) and (10.79) it follows that

$$\bar{I}_+(\zeta)\bar{L}_+(\zeta) = \bar{L}_-(\zeta)\bar{F}_+(\zeta) + \bar{L}_-(\zeta)\bar{G}_-(\zeta)$$

One further additive splitting leads to

$$\bar{I}_+(\zeta)\bar{L}_+(\zeta) - [\bar{L}_-(\zeta)\bar{F}_+(\zeta)]_+ = [\bar{L}_-(\zeta)\bar{F}_+(\zeta)]_- + \bar{L}_-(\zeta)\bar{G}_-(\zeta) \quad (10.83)$$

The right-hand side of this equation is analytic in the lower half plane, whereas the left-hand side is analytic in the upper half plane, and they are equal in the common strip. Thus, (10.83) defines an entire function, which must be zero because of the behavior at infinity. Therefore,

$$\bar{I}_+(\zeta)\bar{L}_+(\zeta) = [\bar{L}_-(\zeta)\bar{F}_+(\zeta)]_+ \quad (10.84)$$

It then follows from (10.76) and (10.81) that, as $|\zeta| \rightarrow \infty$,

$$[\bar{F}_+(\zeta)\bar{L}_-(\zeta)]_+ = O(|\zeta|^{-1}) \quad (10.85)$$

This is the required condition on $F(z_1)$.

In order to simplify this integral condition, we observe that $\bar{\mathcal{K}}(\zeta)$ is analytic in the cut plane and both $\bar{L}_+(\zeta)$ and $\bar{L}_-(\zeta)$ are analytic in the entire plane except, respectively, the left and the right branch cuts of $\bar{\mathcal{K}}(\zeta)$, as shown in Fig. 10.4. Since the leading term of $\bar{F}_+(\zeta)$ as $|\zeta| \rightarrow \infty$ is causing difficulty, it is taken out, and we define

$$\bar{F}_+^0(\zeta) = \bar{F}_+(\zeta) + \frac{F(0^+)}{i(\zeta - k)} \quad (10.86)$$

Therefore

$$[\bar{F}_+(\zeta)\bar{L}_-(\zeta)]_+ = [\bar{F}_+^0(\zeta)\bar{L}_-(\zeta)]_+ + iF(0^+)\left[\frac{\bar{L}_-(\zeta)}{\zeta - k}\right]_+ \quad (10.87)$$

Clearly, the last term is identically zero, since $1/(\zeta - k)$ and $\bar{L}_-(\zeta)$ are both analytic functions in the lower half plane. Thus

$$[\bar{F}_+(\zeta)\bar{L}_-(\zeta)]_+ = \frac{1}{2\pi i} \int_{-\infty-i\epsilon/2}^{\infty-i\epsilon/2} \frac{\bar{F}_+^0(\zeta')\bar{L}_-(\zeta')}{\zeta' - \zeta} d\zeta' \quad (10.88)$$

A comparison of (10.88) with (10.85) shows that

$$\int_{-\infty-i\epsilon/2}^{\infty-i\epsilon/2} \bar{F}_+^0(\zeta')\bar{L}_-(\zeta') d\zeta' = 0 \quad (10.89)$$

Or, more simply,

$$\int_{-\infty}^{\infty} \bar{F}_+^0(\zeta)\bar{L}_-(\zeta) d\zeta = 0 \quad (10.90)$$

where the integration is along the real axis. Let $\epsilon \rightarrow 0^+$, then (10.90) becomes

$$\int_{C_0} \bar{F}_+^0(\zeta)\bar{L}_-(\zeta) d\zeta = 0 \quad (10.91)$$

where the contour of integration C_0 is shown in Fig. 10.2.

10.6 Finite Dipole Antennas

a. Approximation for Thin Dipole Antennas

The approximate condition (10.91) for the vanishing of the current at the end of the long dipole antenna can be simplified if the antenna is thin. As discussed near the end of Sec. 10.2, for $ka \ll 1$, the Bessel and Hankel functions in $\bar{\mathcal{K}}(\zeta)$ can be approximated by the leading terms of their series expansions:

$$\bar{\mathcal{K}}(\zeta) = \frac{1}{4\pi} \left(2\Omega_1 - \ln \frac{k^2 - \zeta^2}{k^2} \right) \quad (10.92)$$

$$\text{where} \quad \Omega_1 = \Omega_0 + i\frac{\pi}{2} \quad (10.93)$$

$$\text{and} \quad \Omega_0 = \ln \frac{2}{ka} - \gamma \quad (10.94)$$

In (10.94) γ is Euler's constant, numerically about 0.5772. We shall use the approximation (10.92) but ignore the real zeros at $\zeta = \pm(k^2 + 4e^{-2\gamma}a^{-2})^{1/2}$. [See the discussion after (10.45).] Then, and only then, is it possible to define the functions $M(z_1)$ and $L_-(z_1)$ by

$$\bar{M}(\zeta) = \frac{1}{\bar{\mathcal{K}}(\zeta)} = \int_{-\infty}^{\infty} M(z_1)e^{i\zeta z_1} dz_1 \quad (10.95)$$

$$\text{and} \quad \bar{L}_-(\zeta) = \int_{-\infty}^{\infty} L_-(z_1)e^{i\zeta z_1} dz_1 \quad (10.96)$$

Note that the exact $\bar{M}(\zeta)$ and $\bar{L}_-(\zeta)$, without (10.92), are not the Fourier transforms of integrable functions.

We wish to emphasize that the approximation (10.92) is not only mathematically necessary but also physically desirable. If (10.92) is used, a finite input admittance can be obtained. And if we let $h \rightarrow \infty$, as shown in Sec. 10.8, the final result so obtained is exactly the intrinsic admittance of an infinite antenna driven from a coaxial line, as discussed in Sec. 10.2. Thus it is this approximation for thin antennas which yields a plausible answer to the question "How do we obtain the intrinsic admittance of a finite dipole antenna driven by a coaxial line *without* really considering the coaxial line?" Furthermore, for large z_1 , $M(z_1)$ behaves like $e^{ikz_1}/kz_1(\ln kz_1)^2$. This rapid decrease of $M(z_1)$ implies that the behavior of A_z is relatively unimportant in the present calculation. The choice of the semi-infinite antenna model is therefore justified.

b. The Determination of \mathcal{C}

We are now in a position to determine the constant \mathcal{C} approximately. From (10.72) and (10.86) we note

$$\bar{F}_+^0(\xi) = \int_0^\infty [F(z_1) - F(0^+)e^{-ikz_1}]e^{i\xi z_1} dz_1$$

$$\text{or} \quad F^0(z_1) = \begin{cases} F(z_1) - F(0^+)e^{ikz_1} & z_1 \geq 0 \\ 0 & z_1 < 0 \end{cases} \quad (10.97)$$

Making use of (10.66) we have the explicit expression for $z_1 \geq 0$:

$$\begin{aligned} F^0(z_1) = & \frac{iV}{\xi_0} \sin kh [\cos kz_1 H(h - z_1) - e^{ikz_1}] - \frac{iV}{\xi_0} \cos kh [\sin kz_1 H(h - z_1)] \\ & - \frac{iV}{2\xi_0} (\sin kh - \mathcal{C} \cos kh) [\cos kz_1 H(2h - z_1) - e^{-ikz_1}] \\ & + \frac{iV}{2\xi_0} (\cos kh + \mathcal{C} \sin kh) [\sin kz_1 H(2h - z_1)] \end{aligned} \quad (10.98)$$

The terms of (10.98) are so arranged that, as $|\xi| \rightarrow \infty$, the Fourier transforms of each term in brackets decay faster than $1/|\xi|$. Thus each bracket can be treated separately when (10.98) is substituted into (10.61). Define

$$S_1(X) = \int_{c_0} \bar{L}_-(\xi) d\xi \int_0^\infty e^{i\xi z_1} \sin kz_1 H(X - z_1) dz_1 \quad (10.99)$$

$$T_1(X) = \int_{c_0} \bar{L}_-(\xi) d\xi \int_0^\infty e^{i\xi z_1} [\cos kz_1 H(X - z_1) - e^{ikz_1}] dz_1 \quad (10.100)$$

When (10.97) and (10.98) are substituted into (10.61), the result is, using (10.99) and (10.100),

$$\begin{aligned} \sin kh T_1(h) - \cos kh S_1(h) + \frac{1}{2}(\cos kh + \mathcal{C} \sin kh) S_1(2h) \\ - \frac{1}{2}(\sin kh - \mathcal{C} \cos kh) T_1(2h) = 0 \end{aligned}$$

$$\text{or} \quad \mathcal{C} = - \frac{\sin kh [2T_1(h) - T_1(2h)] - \cos kh [2S_1(h) - S_1(2h)]}{\sin kh S_1(2h) + \cos kh T_1(2h)} \quad (10.101)$$

It remains to evaluate the functions defined in (10.99) and (10.100). However, we know very little about $\bar{L}_-(\zeta)$ except its integral form. Since we are mainly interested in the case of long dipole antennas, where $kh > \pi$, we shall evaluate these integrals for large X approximately. In (10.99) and (10.100) the contour C_0 can be deformed so that it is wrapped around the right branch cut. The deformation of contour is possible because $\bar{L}_-(\zeta)$ is analytic over the entire complex ζ plane except the right branch cut; there is no contribution from the large arc, since as $|\zeta| \rightarrow \infty$, the z_1 integral of (10.99) and (10.100) decays faster than $1/|\zeta|$. The advantage of the particular arrangement of the terms made in (10.98) should now be appreciated. For large kX the contributions to these two integrals, insofar as the ζ integral is concerned, come mainly from the region $|\zeta - k|X \ll 1$. We shall therefore approximate $\bar{L}_-(\zeta)$ around the branch point $\zeta = k$. On the other hand, from (10.79), $\bar{L}_-(\zeta)$ is exactly the same as $\bar{M}(\zeta)\bar{L}_+(\zeta)$, where $\bar{L}_+(\zeta)$ is analytic in the vicinity of $\zeta = k$. Thus, in (10.99) and (10.100) $\bar{L}_-(\zeta)$ can be replaced by $\bar{L}_+(k)\bar{M}(\zeta)$. Therefore, approximately,

$$S_1(X) = \bar{L}_+(k)S(X) \quad (10.102)$$

$$T_1(X) = \bar{L}_+(k)T(X) \quad (10.103)$$

where
$$S(X) = \int_{C_0} \bar{M}(\zeta) d\zeta \int_0^\infty e^{i\zeta z_1} \sin kz_1 H(X - z_1) dz_1 \quad (10.104)$$

$$T(X) = \int_{C_0} \bar{M}(\zeta) d\zeta \int_0^\infty e^{i\zeta z_1} [\cos kz_1 H(X - z_1) - e^{ikz_1}] dz_1 \quad (10.105)$$

Since the expression of $\bar{M}(\zeta)$ is known, the advantage of (10.104) and (10.105) over (10.99) and (10.100) is obvious. If the approximations (10.102) and (10.103) are used in (10.101), the factor $\bar{L}_+(k)$ cancels out and we have an explicit expression for \mathcal{C} :

$$\mathcal{C} = -\frac{\sin kh [2T(h) - T(2h)] - \cos kh [2S(h) - S(2h)]}{\sin kh S(2h) + \cos kh T(2h)} \quad (10.106)$$

The derivation of the functions $S(X)$ and $T(X)$ is postponed until Sec. 10.6e.

c. The Current and Charge Distribution and the Input Admittance

Once the constant \mathcal{C} is obtained, we can use the approximate condition 1'' to find the current distribution along the antenna. The integral equation with this prescription is

$$\int_{-\infty}^{\infty} \mathcal{G}(z') \mathcal{K}(z - z') dz' = \mathcal{F}(z)[H(z + h) - H(z - h)] \quad |z| < \infty \quad (10.107)$$

In contrast with (10.71) the Fourier transforms are defined as follows:

$$\bar{\mathcal{G}}(\zeta) = \int_{-\infty}^{\infty} \mathcal{G}(z) e^{i\zeta z} dz \quad (10.108)$$

and

$$\bar{\mathcal{F}}(\zeta) = \int_{-h}^h \mathcal{F}(z) e^{i\zeta z} dz \quad (10.109)$$

From (10.107) to (10.109), (10.66), (10.92), and (10.95) it follows that

$$\bar{g}(\zeta) = \overline{M}(\zeta)\bar{\mathcal{F}}(\zeta) \quad (10.110)$$

or
$$g(z) = \frac{1}{2\pi} \int_{c_0} \overline{M}(\zeta)\bar{\mathcal{F}}(\zeta)e^{-i\zeta z} d\zeta \quad (10.111)$$

For convenience define $U(X)$, analogous to (10.104) and (10.105), as follows:

$$U(X) = \int_{c_0} \overline{M}(\zeta) d\zeta \int_{-X}^X \cos kz e^{i\zeta z} dz \quad (10.112)$$

In terms of $S(X)$ and $U(X)$, (10.111) becomes (10.132). The input admittance is given by $g(0)/V$ or (10.134). If the equation of continuity of charge is used in conjunction with (10.111), the charge distribution is then given by

$$q(z) = -\frac{1}{2\pi\omega} \int_{c_0} \zeta \overline{M}(\zeta)\bar{\mathcal{F}}(\zeta)e^{-i\zeta z} d\zeta \quad (10.113)$$

Again this equation can be expressed in terms $S(X)$, $U(X)$, and $M(X)$ as given in (10.133).

d. Radiation Field

Let a spherical coordinate system (R, θ, ϕ) be set up such that the ends of the antenna are located around $(h, 0, \phi)$ and (h, π, ϕ) . All the field quantities are independent of ϕ because of the rotational symmetry. Thus in the far field,²² that is, $kR \rightarrow \infty$,

$$E_\theta(R, \theta) \approx i\omega \sin \theta A_z(r, z) \quad (10.114)$$

The z component of the vector potential at (r, z) is given by

$$A_z(r, z) = \frac{\mu_0}{4\pi} \int_{-h}^h g(z') dz' \frac{1}{2\pi} \int_{-\pi}^{\pi} \frac{e^{ik\sqrt{(z-z')^2 + r^2 + a^2 - 2ra \cos \theta'}}}{\sqrt{(z-z')^2 + r^2 + a^2 - 2ra \cos \theta'}} d\theta'$$

When the terms proportional to $(ka)^2$ are neglected, and for large $kR = k\sqrt{r^2 + z^2}$, this simplifies to

$$A_z(r, z) \approx \frac{\mu_0}{4\pi} \frac{e^{ikR}}{R} \bar{g}(k \cos \theta) \quad (10.115)$$

Define the field pattern by

$$E(\theta) = -\lim_{R \rightarrow \infty} R e^{-ikR} E_\theta(R, \theta) \quad (10.116)$$

or
$$E(\theta) = -i \frac{\omega\mu_0}{4\pi} \sin \theta \bar{g}(k \cos \theta) \quad (10.117)$$

The explicit expression for the field pattern is obtained by substituting (10.110) into (10.117), and is given in (10.135).

e. *Derivation of $S(X)$*

This subsection is devoted to the detailed derivation of $S(X)$, which, as given in (10.104), can be simplified to read

$$S(X) = 2\pi \int_{c_0} \left[\frac{e^{i(\zeta-k)X}}{\zeta-k} - \frac{e^{i(\zeta+k)X}}{\zeta+k} + \frac{2k}{\zeta^2 - k^2} \right] \frac{d\zeta}{2\Omega_1 - \ln [(k^2 - \zeta^2)/k^2]} \quad (10.118)$$

A change of variable, $\zeta = k(1 + 2\eta)$, yields

$$S(X) = -2\pi \int_0^\infty \left[\frac{1}{2(\Omega_0 - \ln 2) - \ln \eta(1 + \eta)} - \frac{1}{2(\Omega_0 - \ln 2) + i2\pi - \ln \eta(1 + \eta)} \right] \left[\frac{e^{i2kX(1+\eta)}}{1 + \eta} - \frac{e^{i2kX\eta}}{\eta} + \frac{1}{\eta(1 + \eta)} \right] d\eta \quad (10.119)$$

Since the Cauchy principal values are taken at infinity, we introduce an arbitrarily large number \equiv , then,

$$\int_0^\equiv \left[\frac{1}{2(\Omega_0 - \ln 2) - \ln \eta(1 + \eta)} - \frac{1}{2(\Omega_0 - \ln 2) + i2\pi - \ln \eta(1 + \eta)} \right] \times \left(\frac{1}{\eta} + \frac{1}{1 + \eta} \right) d\eta = \ln \left(1 + \frac{\pi i}{\Omega_0 - \ln 2 - \ln \equiv} \right) \quad (10.120)$$

and

$$2 \int_0^\equiv \left[\frac{1}{2(\Omega_0 - \ln 2) - 2 \ln (1 + \eta)} - \frac{1}{2(\Omega_0 - \ln 2) + i2\pi - 2 \ln (1 + \eta)} \right] \times \frac{1}{1 + \eta} d\eta = \ln \left(1 + \frac{\pi i}{\Omega_0 - \ln 2 - \ln \equiv} \right) - \ln \left(1 + \frac{\pi i}{\Omega_0 - \ln 2} \right) \quad (10.121)$$

On the other hand, approximately

$$\begin{aligned} \int_0^\infty \left[\frac{1}{2(\Omega_0 - \ln 2) - \ln \eta(1 + \eta)} - \frac{1}{2(\Omega_0 - \ln 2) - 2 \ln (1 + \eta)} \right] \frac{1}{1 + \eta} d\eta \\ \approx - \int_0^\infty \frac{\ln [(1 + \eta)/\eta]}{[2(\Omega_0 - \ln 2) - 2 \ln (1 + \eta)]^2} \frac{1}{1 + \eta} d\eta \\ \approx - \int_0^\infty \frac{\ln [(1 + \eta)/\eta]}{[2(\Omega_0 - \ln 2) - 2 \ln 2]^2} \frac{d\eta}{1 + \eta} = - \frac{\pi^2}{6} \frac{1}{[2(\Omega_0 - 2 \ln 2)]^2} \end{aligned} \quad (10.122)$$

Similarly,

$$\begin{aligned} \int_0^\infty \left[\frac{1}{2(\Omega_0 - \ln 2) + 2\pi i - \ln \eta(1 + \eta)} - \frac{1}{2(\Omega_0 - \ln 2) + 2\pi i - 2 \ln (1 + \eta)} \right] \frac{1}{1 + \eta} d\eta \\ \approx - \frac{\pi^2}{6} \frac{1}{[2(\Omega_0 - 2 \ln 2) + i2\pi]^2} \end{aligned} \quad (10.123)$$

Letting $\equiv \rightarrow \infty$, (10.119) to (10.123) give

$$\begin{aligned} & \int_0^\infty \left[\frac{1}{2(\Omega_0 - \ln 2) - \ln \eta(1 + \eta)} \right. \\ & \quad \left. - \frac{1}{2(\Omega_0 - \ln 2) + i2\pi - \ln(1 + \eta)\eta} \right] \frac{1}{(1 + \eta)\eta} d\eta \\ &= \ln \left(1 + \frac{\pi i}{\Omega_0 - \ln 2} \right) + \frac{\pi^2}{3} \frac{1}{[2(\Omega_0 - 2 \ln 2)]^2} - \frac{\pi^2}{3} \frac{1}{[2(\Omega_0 - 2 \ln 2) + i2\pi]^2} \end{aligned} \quad (10.124)$$

It remains to study the other two terms of (10.118). For this purpose, it is convenient to introduce two functions

$$\Omega_2(X) = 2(\Omega_0 - \ln 2) + \ln(2kX) + \gamma - i\frac{\pi}{2} \quad (10.125)$$

$$\Omega_3(X) = 2(\Omega_0 - \ln 2) + \ln(2kX) + \gamma + i\frac{3\pi}{2} \quad (10.126)$$

and note that

$$\gamma = -\psi(1) \quad \gamma' = \psi'(1) \quad (10.127)$$

where, in terms of the gamma function $\Gamma(z)$,

$$\psi(z) = \frac{d}{dz} \ln \Gamma(z) \quad (10.128)$$

In terms of these functions we have

$$\begin{aligned} & \int_0^\infty \left[\frac{1}{2(\Omega_0 - \ln 2) - \ln \eta(1 + \eta)} \right. \\ & \quad \left. - \frac{1}{2(\Omega_0 - \ln 2) + i2\pi - \ln \eta(1 + \eta)} \right] \frac{e^{i2kX\eta}}{\eta} d\eta \\ & \approx \int_0^\infty \frac{e^{-\eta'}}{\eta'} \left[\frac{1}{\Omega_2(X) - (\gamma + \ln \eta')} - \frac{1}{\Omega_3(X) - (\gamma + \ln \eta')} \right] d\eta' \\ & = \int_0^\infty e^{-\eta'} \ln \left[\frac{\Omega_3(X) - (\gamma + \ln \eta')}{\Omega_2(X) - (\gamma + \ln \eta')} \right] d\eta' \\ & \approx \ln \left[\frac{\Omega_3(X)}{\Omega_2(X)} \right] + \frac{\gamma'}{2} \left[\frac{1}{\Omega_2^2(X)} - \frac{1}{\Omega_3^2(X)} \right] \end{aligned} \quad (10.129)$$

Also

$$\begin{aligned} & \int_0^\infty \left[\frac{1}{2(\Omega_0 - \ln 2) - \ln \eta(1 + \eta)} \right. \\ & \quad \left. - \frac{1}{2(\Omega_0 - \ln 2) + i2\pi - \ln \eta(1 + \eta)} \right] \frac{e^{i2kX(1+\eta)}}{1 + \eta} d\eta \\ & \approx i \frac{e^{i2kX}}{2kX} \left[\frac{1}{\Omega_2(X)} - \frac{1}{\Omega_3(X)} \right] \end{aligned} \quad (10.130)$$

The substitution of (10.124), (10.128), and (10.129) leads to the final explicit result of $S(X)$ as given in (10.137). $T(X)$, $U(X)$, and $M(X)$ are derivable in the same fashion.

10.7 Summary of Results and Their Restrictions

In Secs. 10.5 and 10.6, formulas have been obtained to describe the characteristics of a center-driven dipole antenna. These equations are applicable for antennas which are thin and long. This is because the conditions 1' and 2' and 1'' and 2'' are valid approximations for the exact conditions 1 and 2 only if the antenna is long. The antenna has to be thin, because of the approximation discussed in Secs. 10.2 and 10.6. Numerical computation shows that the results are valid for

$$a \leq 0.01\lambda \quad \text{and} \quad h \geq \frac{\lambda}{2} \quad (10.131)$$

The results are summarized as follows:

a. Current distribution:

$$\begin{aligned} g(z) = \frac{iV}{4\pi\zeta_0} [\sin kz U(z) - 2 \cos kz S(z) + (\cos kz + \mathcal{C} \sin kz)S(h+z) \\ + (\cos kz - \mathcal{C} \sin kz)S(h-z) - \frac{1}{2}(\sin kz - \mathcal{C} \cos kz)U(h+z) \\ + \frac{1}{2}(\sin kz + \mathcal{C} \cos kz)U(h-z)] \end{aligned} \quad (10.132)$$

b. Charge distribution:

$$\begin{aligned} q(z) = \frac{V\epsilon_0}{4\pi} \left\{ \frac{2\pi}{k} (\sin kh + \mathcal{C} \cos kh)[M(h+z) - M(h-z)] \right. \\ + \frac{1}{2}(\cos kz - \mathcal{C} \sin kz)U(h-z) - \frac{1}{2}(\cos kz + \mathcal{C} \sin kz)U(h+z) \\ - (\sin kz + \mathcal{C} \cos kz)S(h-z) - (\sin kz - \mathcal{C} \cos kz)S(h+z) \\ \left. + 2 \sin kz S(z) + \cos kz U(z) \right\} \end{aligned} \quad (10.133)$$

c. Input admittance:

$$Y = \frac{i}{4\pi\zeta_0} [2S(h) + \mathcal{C}U(h)] \quad (10.134)$$

d. Far-field pattern:

$$\begin{aligned} E(\theta) = \frac{V}{4} \frac{\sin \theta}{\Omega_1 - \ln \sin \theta} \left\{ \mathcal{C} \frac{\sin [kh(1 - \cos \theta)]}{1 - \cos \theta} + \mathcal{C} \frac{\sin [kh(1 + \cos \theta)]}{1 + \cos \theta} \right. \\ \left. + \frac{1 - \cos [kh(1 - \cos \theta)]}{1 - \cos \theta} + \frac{1 - \cos [kh(1 + \cos \theta)]}{1 + \cos \theta} \right\} \end{aligned} \quad (10.135)$$

where the constant \mathcal{C} is

$$\mathcal{C} = - \frac{\sin kh [2T(h) - T(2h)] - \cos kh [2S(h) - S(2h)]}{\sin kh S(2h) + \cos kh T(2h)} \quad (10.136)$$

All these equations are expressed in terms of four functions $S(X)$, $T(X)$, $U(X)$, and $M(X)$. For large kX , these functions can be written explicitly⁵

$$\begin{aligned} \frac{1}{2\pi} S(X) = & -\ln \left(1 + \frac{\pi i}{\Omega_0 - \ln 2} \right) \\ & - \frac{\pi^2}{12} \left[\frac{1}{(\Omega_0 - 2 \ln 2)^2} - \frac{1}{(\Omega_0 - 2 \ln 2 + \pi i)^2} \right] + \ln \left[\frac{\Omega_3(X)}{\Omega_2(X)} \right] \\ & + \frac{\gamma'}{2} \left[\frac{1}{\Omega_2^2(X)} - \frac{1}{\Omega_3^2(X)} \right] - \frac{i}{2kX} e^{i2kX} \left[\frac{1}{\Omega_2(X)} - \frac{1}{\Omega_3(X)} \right] \end{aligned} \quad (10.137)$$

$$\begin{aligned} -\frac{i}{2\pi} T(X) = & -\ln \left(1 + \frac{\pi i}{\Omega_0 - \ln 2} \right) \\ & - \frac{\pi^2}{12} \left[\frac{1}{(\Omega_0 - 2 \ln 2)^2} - \frac{1}{(\Omega_0 - 2 \ln 2 + \pi i)^2} \right] - \ln \left[\frac{\Omega_3(X)}{\Omega_2(X)} \right] \\ & - \frac{\gamma'}{2} \left[\frac{1}{\Omega_2^2(X)} - \frac{1}{\Omega_3^2(X)} \right] - \frac{i}{2kX} e^{i2kX} \left[\frac{1}{\Omega_2(X)} - \frac{1}{\Omega_3(X)} \right] \end{aligned} \quad (10.138)$$

$$\begin{aligned} \frac{i}{4\pi} U(X) = & \ln \left[\frac{\Omega_3(X)}{\Omega_2(X)} \right] + \frac{\gamma'}{2} \left[\frac{1}{\Omega_2^2(X)} - \frac{1}{\Omega_3^2(X)} \right] \\ & + \frac{i}{2kX} e^{i2kX} \left[\frac{1}{\Omega_2(X)} - \frac{1}{\Omega_3(X)} \right] \end{aligned} \quad (10.139)$$

$$M(X) = \frac{i2}{X} e^{ikX} \left[\frac{1}{\Omega_2(X)} - \frac{1}{\Omega_3(X)} \right] \quad (10.140)$$

In (10.137) to (10.140) the following symbols have been used:

$$\Omega_0 = \ln \left(\frac{2}{ka} \right) - \gamma \quad (10.141)$$

$$\Omega_1 = \Omega_0 + i\frac{\pi}{2} \quad (10.142)$$

$$\Omega_2(X) = 2(\Omega_0 - \ln 2) + \ln(2kX) + \gamma - i\frac{\pi}{2} \quad (10.143)$$

$$\Omega_3(X) = 2(\Omega_0 - \ln 2) + \ln(2kX) + \gamma + i\frac{3\pi}{2} \quad (10.144)$$

$$\gamma' = \Gamma''(1) - \gamma^2 \approx 1.6449 \quad (10.145)$$

Among the quantities determined, the value of \mathcal{C} is based on the conditions 1' and 2' and is therefore the most accurate one. Equations (10.132) to (10.135) are calculated from the conditions 1'' and 2'', which are less accurate. Therefore, (10.132) and (10.133) are the accurate descriptions for the current and charge distributions only for points not close to the ends, $|z| < h - \lambda/4$. If these equations are used in conjunction with (10.137) to (10.140), which are valid for large kX only, then they are not valid for $0 < |z| < \lambda/4$ either. How-

ever, Y , and therefore $g(0)$, is accurately determined by (10.134) with (10.137) and (10.139), and we do know that $g(\pm h) = 0$, the current distribution in the regions close to the driving point and to the ends, can be estimated.

The error due to (1'') and (2'') has little effect on the far-field pattern, which is insensitive to the detailed structure of the current distribution. All these results are valid for both lossless media (k real) and dissipative media (k complex).

We remark that the meaning of the field pattern is somewhat different in the lossless and the dissipative cases. Let f be a field quantity and (R, θ, ϕ) be a spherical coordinate system. With respect to this particular coordinate system, we define the field pattern f_1 for f by

$$f_1(\theta, \phi) = \lim_{R \rightarrow \infty} f(R, \theta, \phi) R e^{-ikR} \quad (10.146)$$

Suppose we displace the spherical coordinate system by

$$\mathbf{R} = \mathbf{R}_0 + \mathbf{R}' \quad (10.147)$$

without rotation. This gives a second spherical coordinate system (R', θ', ϕ') such that, if R is large, $\theta \approx \theta'$, $\phi \approx \phi'$. With respect to this second spherical coordinate system, we can define a second field pattern f'_1 for the same f :

$$f'_1(\theta, \phi) = \lim_{R' \rightarrow \infty} f(R', \theta', \phi') R' e^{-ikR'} \quad (10.148)$$

What is the relation between f_1 and f'_1 ? Let $\hat{\mathbf{r}}$ be the unit vector in the direction (θ, ϕ) , then it follows from (10.146) to (10.148) that

$$f'_1(\theta, \phi) = f_1(\theta, \phi) \exp ik\hat{\mathbf{r}} \cdot \mathbf{R}_0 \quad (10.149)$$

In particular, if the medium is lossless, i.e., if k is real, then,

$$|f'_1(\theta, \phi)| = |f_1(\theta, \phi)| \quad (10.150)$$

In other words, in the lossless case, the absolute value of the field pattern has a meaning independent of the coordinate system. When k is not real, it follows from (10.149) that (10.150) is false in general. Thus in this case we can only define the field pattern with respect to a particular coordinate system. In (10.135) the field pattern refers to the particular one with the origin of the coordinate system at the center of the dipole antenna.

The same technique can be used to investigate the properties of the long, unloaded, receiving dipole antenna. In particular, the back-scattering cross

section σ_B , the current $g_s(z)$, and the charge distribution $q_s(z)$, with broadside incident waves of 1 volt/m at the axis of the dipole, are given as follows:

$$\sigma_B = \frac{4\pi}{|\Omega_1|^2} \left| h + \frac{C_s}{k} \sin kh \right|^2 \quad (10.151)$$

$$g_s(z) = \frac{i\lambda}{4\pi^2\zeta_0} \left\{ \frac{4\pi^2}{\Omega_1} - \frac{i2\pi}{k} [M(h+z) + M(h-z)] \right. \\ \left. + \frac{C_s}{2} \cos kz [U(h+z) + U(h-z)] \right. \\ \left. + C_s \sin kz [S(h+z) - S(h-z)] \right\} \quad (10.152)$$

$$q_s(z) = -\frac{\epsilon_0\lambda}{8\pi^3} \left\{ (1 + C_s \cos kh) \frac{2\pi}{k} [M(h-z) - M(h+z)] \right. \\ \left. + \frac{C_s}{2} \cos kz [S(h+z) - S(h-z)] \right. \\ \left. + \frac{C_s}{2} \sin kz [U(h-z) + U(h+z)] \right\} \quad (10.153)$$

where C_s is given by

$$C_s = -\frac{V_1(2h)\bar{L}_-(-k)}{\cos kh T(2h) + \sin kh S(2h)} \quad (10.154)$$

The function $V_1(X)$ is defined by

$$V_1(X) = \int_{c_0} \bar{L}_-(\zeta) d\zeta \int_0^\infty [H(X-z) - e^{-ikz}] e^{ikz} dz \quad (10.155)$$

and for large kX , $V_1(X)\bar{L}_-(-k)$ is approximately

$$V_1(X)\bar{L}_-(-k) \approx \frac{4\pi^2}{\Omega_1} - i \frac{2\pi}{k} M(X) \quad (10.156)$$

This approximation (10.156) can be somewhat improved by using numerical integration.²³

It should be remarked that the two-wire transmission line and the dielectric-coated dipole antenna can also be treated in the same fashion. For details the reader is referred to the original work.⁵

10.8 Discussion

By far the most extensive calculation is that for the input admittance of the dipole antennas in lossless or dissipative media.²⁴ Some results are shown in Fig. 10.5. In order to ascertain the range of validity of the present theory, we note that the King-Middleton solution and (10.134) are in excellent agreement in the range of $\pi < kh < 2\pi$ and $a/\lambda \leq 0.01$. Since this theory is more accurate for longer antennas, this leads to (10.131).

The numerical computation of the current and charge distribution based on (10.132) and (10.133) has also been carried out. The results agree well with the experimental data.^{23,25} Two typical curves are shown in Fig. 10.6 and Fig. 10.7.

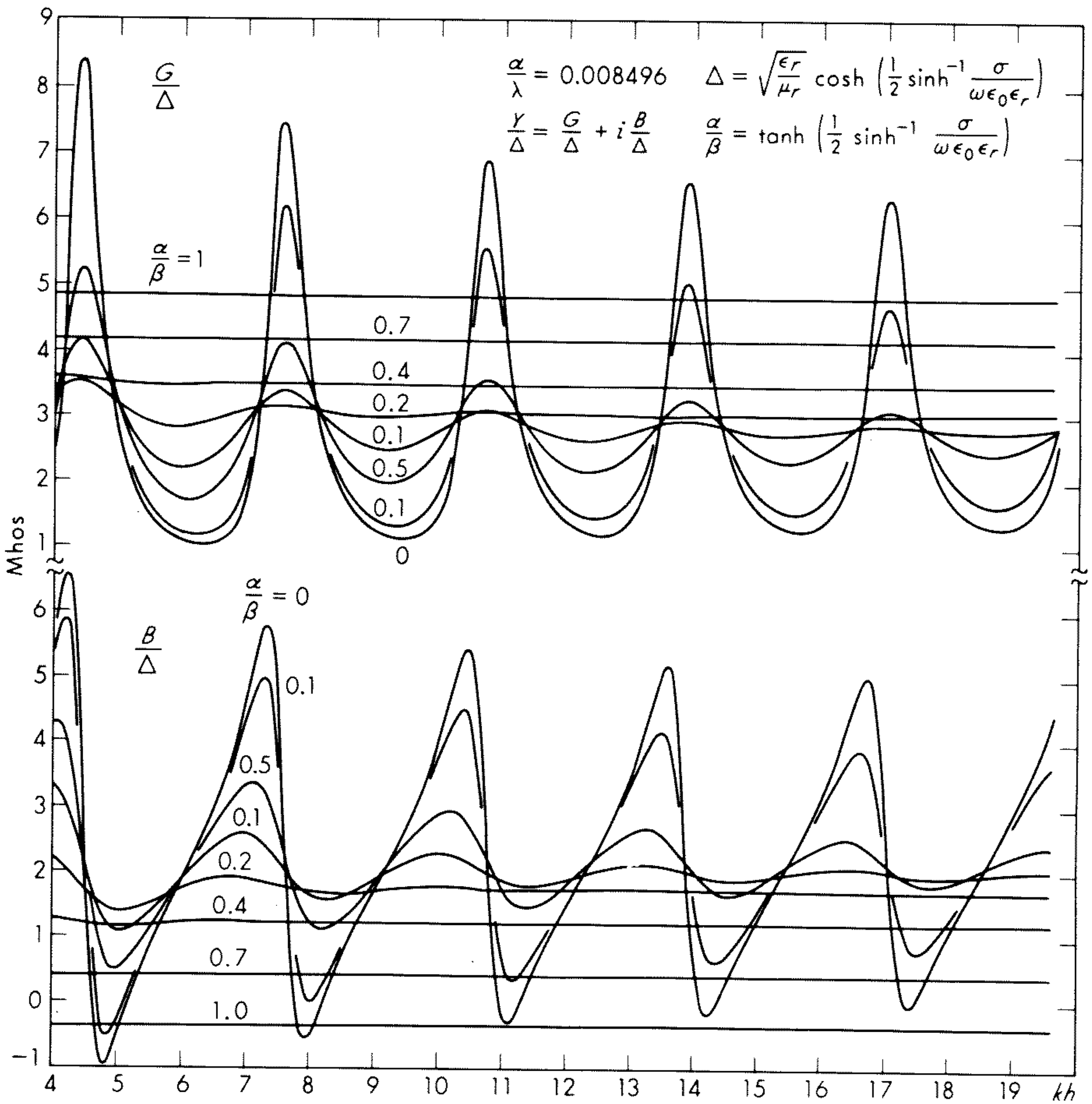


Fig. 10.5 Normalized admittance of dipole antennas in air and in dissipative media.

It is interesting to note that both the maxima and minima decrease toward the end of the antenna, except the last few maxima and minima.

The field pattern, as given by (10.135), differs from the usual zero-order field pattern only in the appearance of the factor $1/(\Omega_1 - \ln \sin \theta)$ when \mathcal{C} is chosen in a sufficiently simple way. For a long dipole, this factor has the effect of reducing the end-firing major lobes. It is also interesting to note the double bumps near the minima as shown in Fig. 10.8. This is because only the absolute value of $E(\theta)$ is of interest and the interference of the real and imaginary parts is most apparent there.

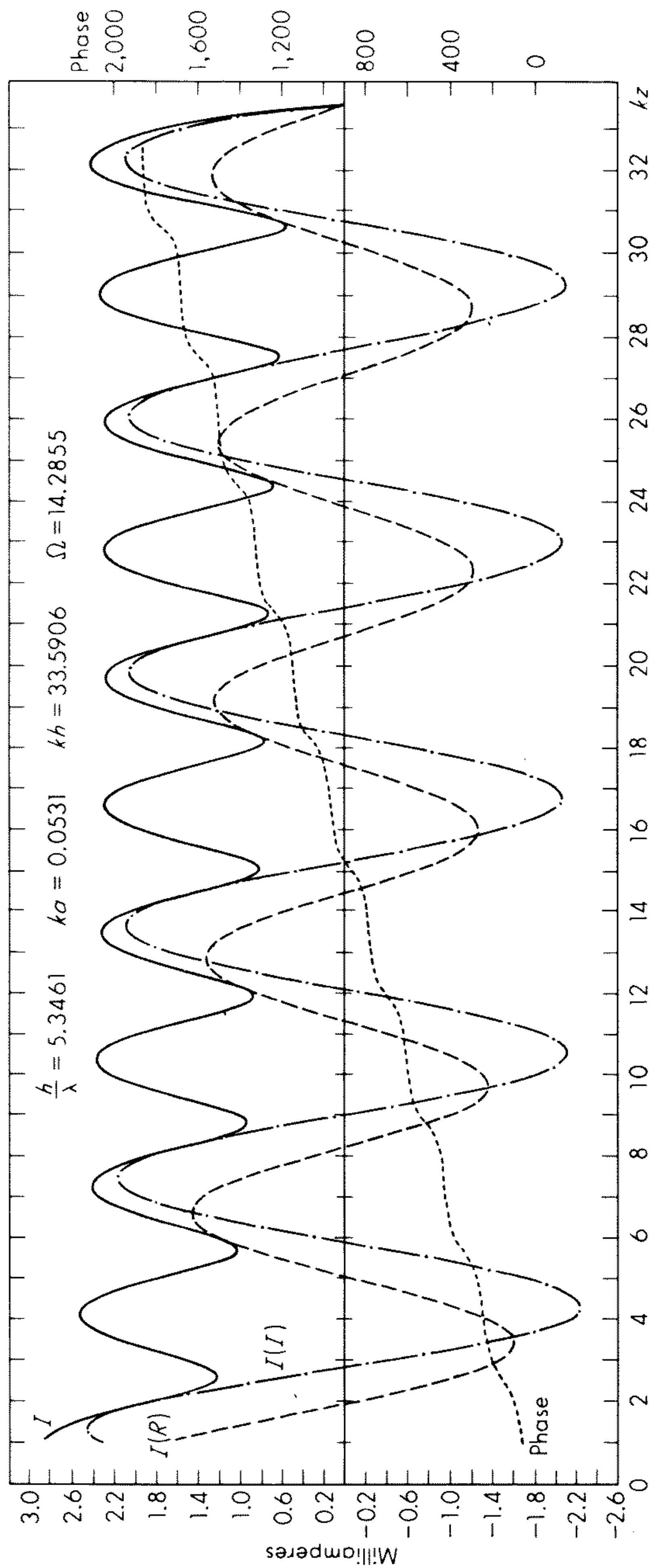


Fig. 10.6 Theoretical current distribution along a center-driven antenna ($ka = 0.0531$, $kh = 33.5906$).

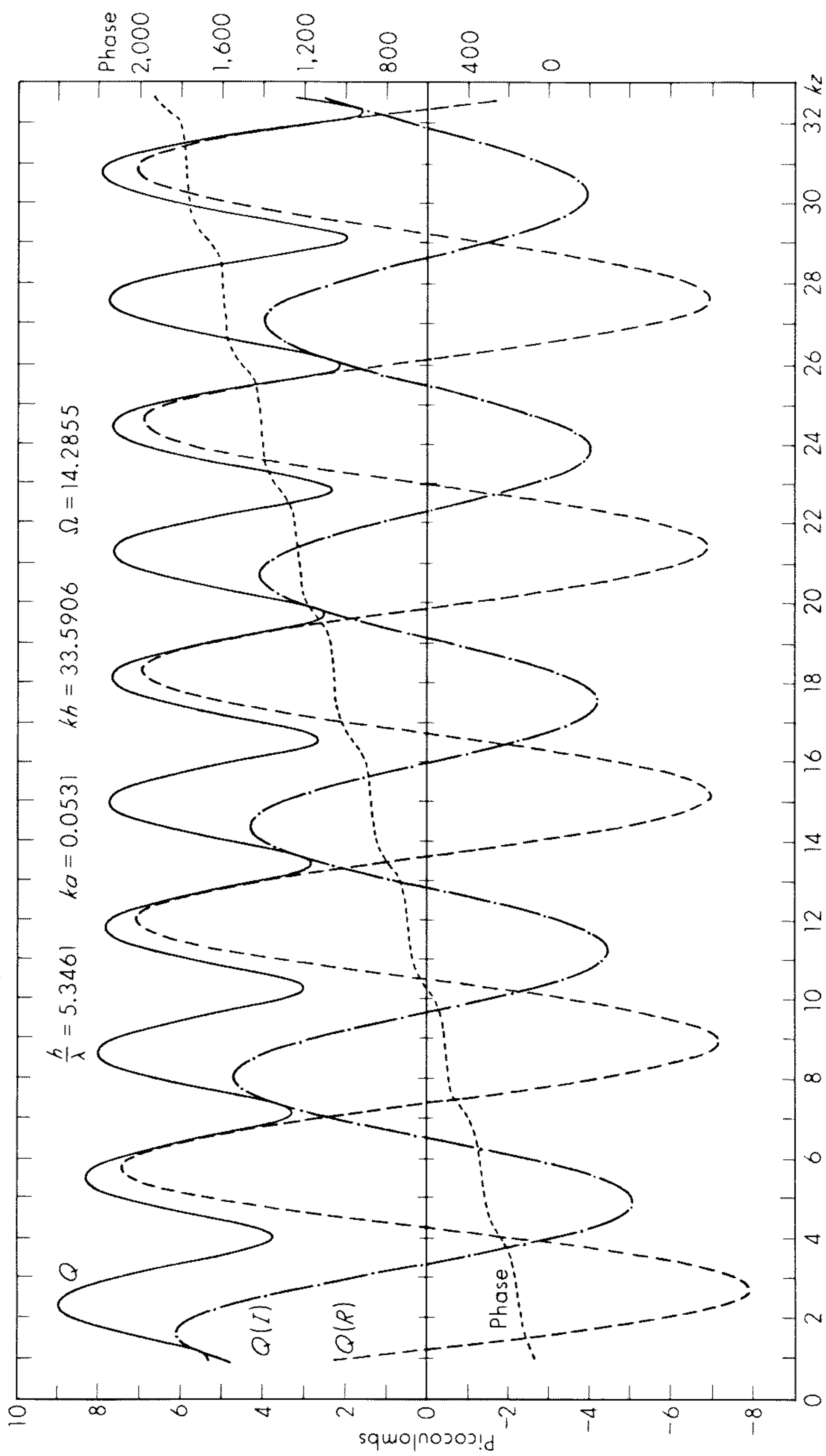


Fig. 10.7 Theoretical charge distribution along a center-driven antenna ($ka = 0.0531$, $kh = 33.5906$).

The back-scattering cross section of a receiving dipole has been obtained for $a/\lambda = 0.0035$ by using (10.151). The theoretical results,[†] together with the experimental data of Sevick²⁶ and Ås and Schmitt,²⁷ are shown in Fig. 10.9. In the theoretical computation, numerical technique is used to evaluate

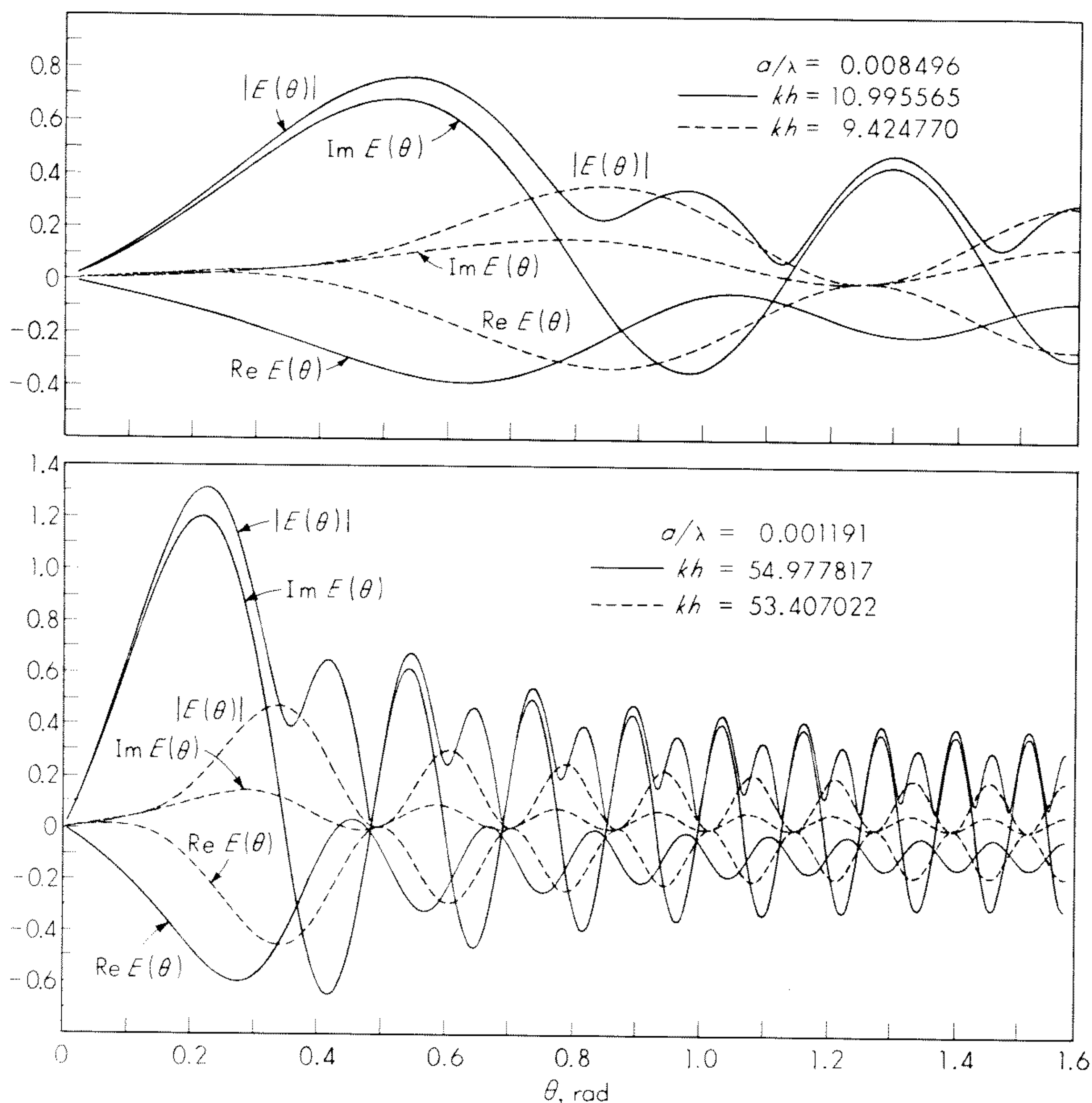


Fig. 10.8 Field patterns of center-driven dipoles ($a/\lambda = 0.008496$, $kh = 3\pi$; and $a/\lambda = 0.001191$, $kh = 17\pi$ and 17.5π).

$V_1(2h)\bar{L}_-(-k)$, instead of the approximation (10.156). It is noted that when the dipole is not too short, the theoretical results are in fair agreement with the experimental data. When there is strong interference between the resonant and nonresonant current, as described by Chu,[†] some discrepancy occurs both between the theoretical results and the experimental data and between the two sets of experimental data. The large discrepancy with Sevick's data for rela-

[†]Figure 7 of Ref. 5 is incorrect.

[†]L. J. Chu, private communication.

tively large values of kh may be traced to an inadequacy in his experimental setup; namely, the transmitter was not sufficiently far away from the scattering dipole.

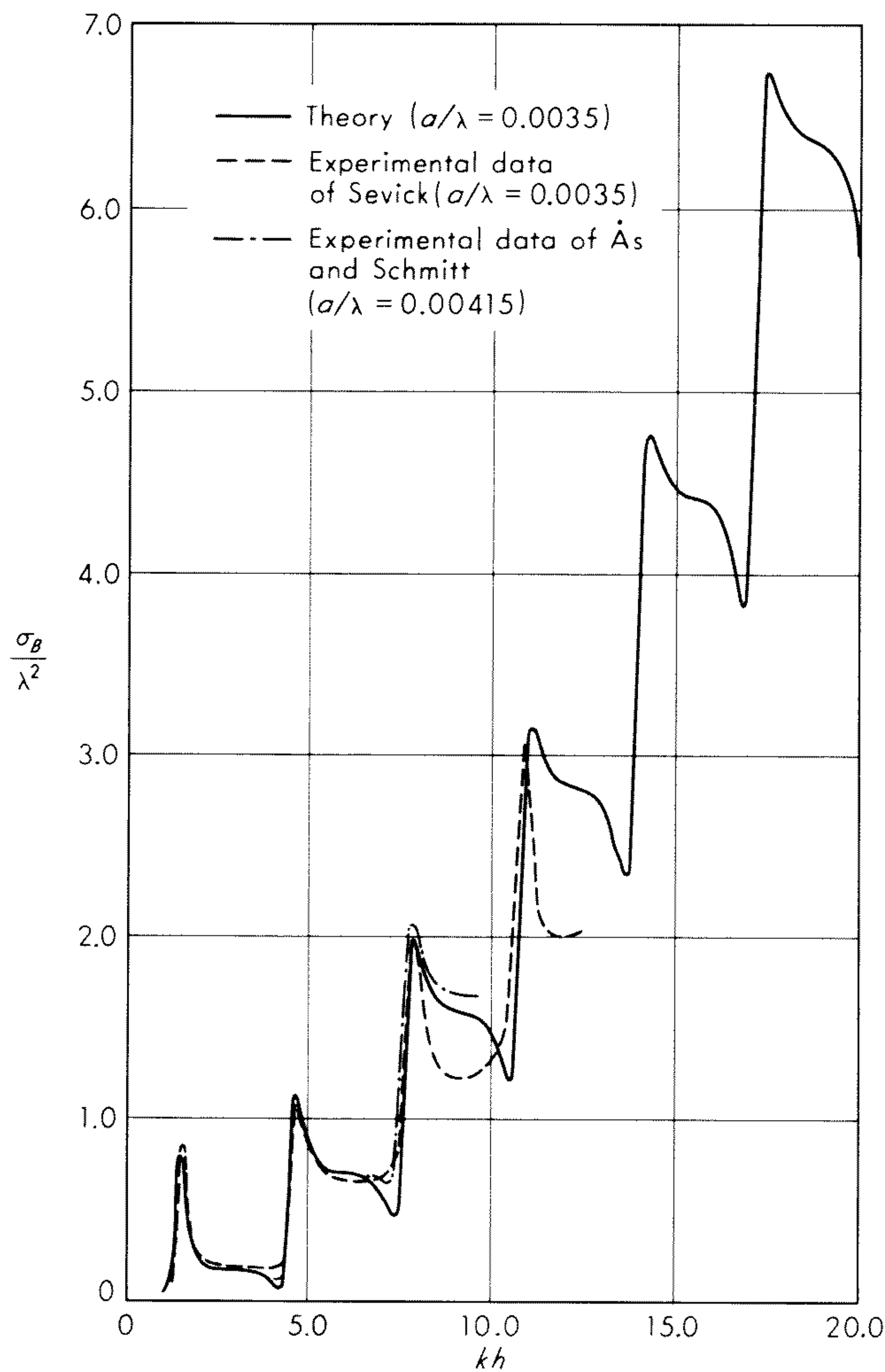


Fig. 10.9 Back-scattering cross section.

Figure 10.10 shows the theoretical results of the current distribution along a long receiving dipole antenna. As far as the authors are aware, there are no experimental data available for comparison.

As previously mentioned, one of the principal interests in the present theory is its application to the transient behavior of a finite dipole antenna. Knowing

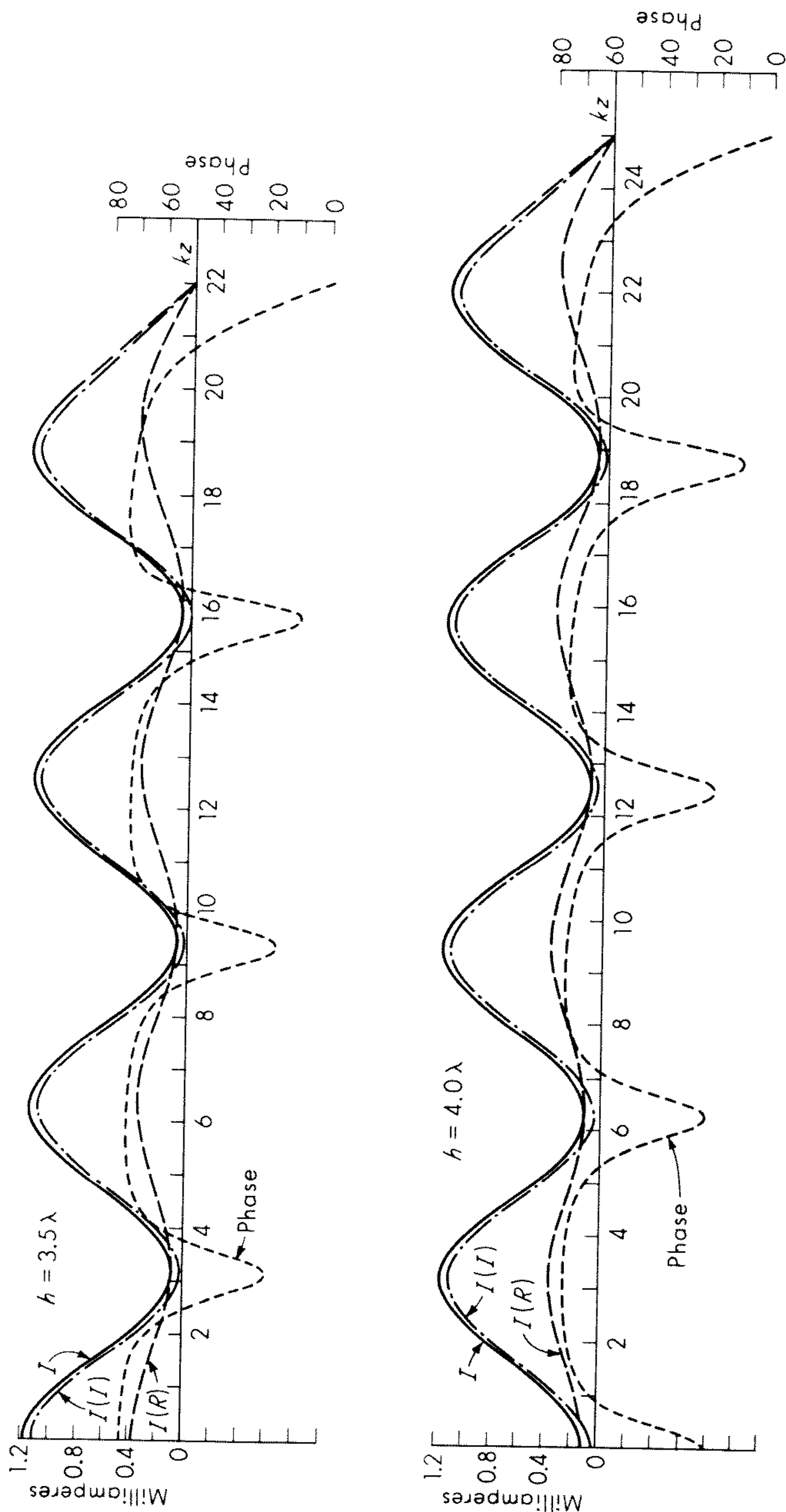


Fig. 10.10 Current distribution along a receiving dipole ($kh = 7\pi, 8\pi$).

which is consistent with the asymptotic behavior of the current distribution along an infinitely long dipole antenna.³⁰⁻³²

Similarly, as $h \rightarrow \infty$, (10.134) becomes

$$Y \approx \frac{1}{\zeta_0} \left\{ \frac{\pi^3(\Omega_0 - 2 \ln 2)}{6[(\Omega_0 - 2 \ln 2)^2 + \pi^2]^2} + \tan^{-1} \frac{\pi}{\Omega_0 - \ln 2} \right\} \\ - \frac{i}{2\zeta_0} \left\{ \ln \left[1 + \frac{\pi^2}{(\Omega_0 - \ln 2)^2} \right] + \frac{[3(\Omega_0 - 2 \ln 2)^2 + \pi^2]\pi^4}{6(\Omega_0 - 2 \ln 2)^2[(\Omega_0 - 2 \ln 2)^2 + \pi^2]^2} \right\} \\ + O\left[\frac{1}{(\ln kh)^2}\right] \quad (10.158)$$

This result has been confirmed experimentally by King and Schmitt⁴ in their study of the transient response of the dipole antenna. It is also noted that, for $ka \ll 1$, the leading term of the conductance as given by (10.158) is essentially the same as that derived by Papas.³⁰

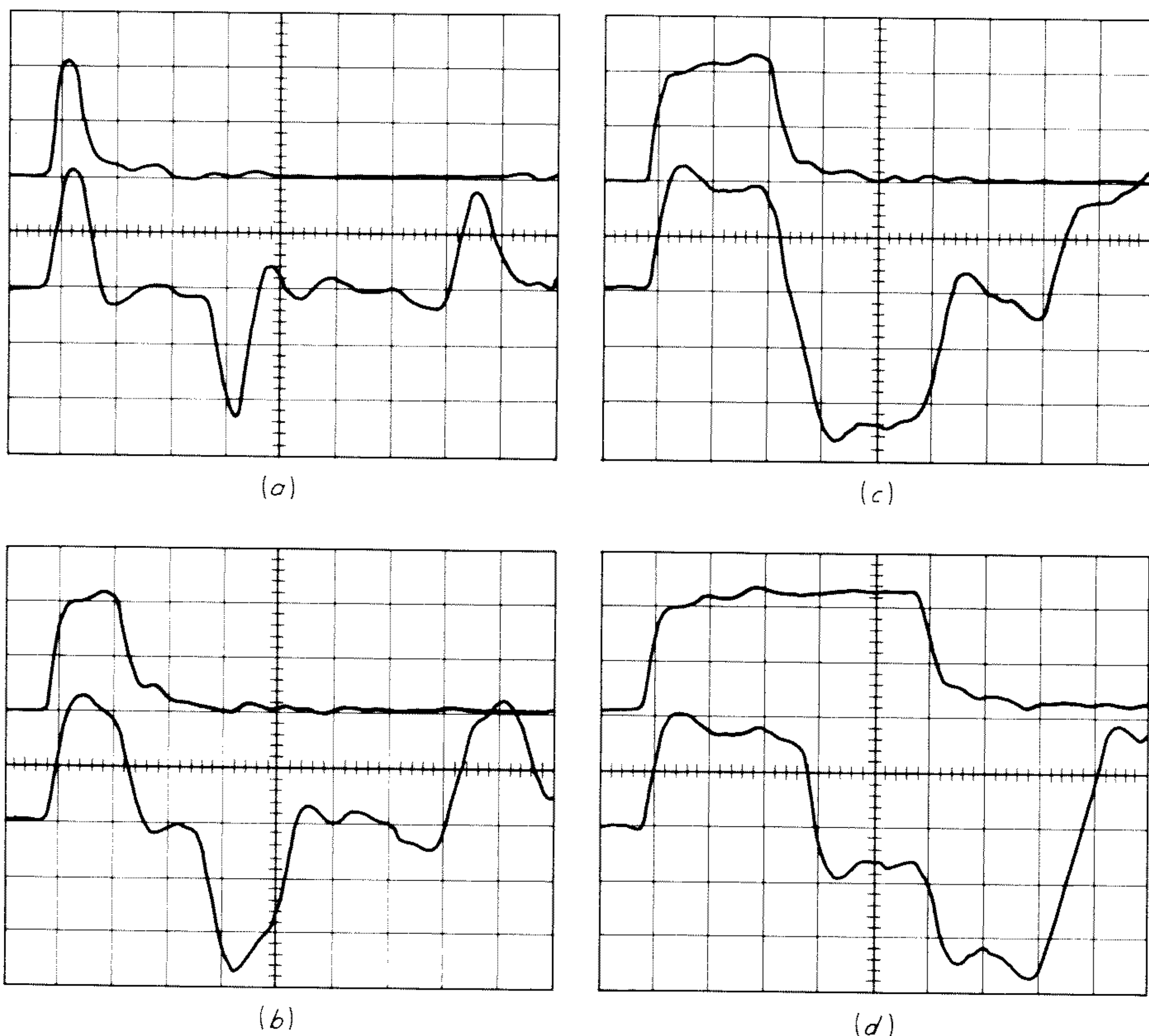


Fig. 10.12 The time history of the measured radiation field $e^{\text{rad}}(t)$ V/m along the ground plane (lower traces) for the excitation $v_g(t)$ shown in the upper traces for $Z_g(f) = Z_g = 50$ ohms, for $h/a = 904$, for $(c/h)t_1 = 0.05$, and for $h = 0.85$ m. Time scale: 1.25 nsec/division. (a) $(c/h)T = 0.2$; (b) $(c/h)T = 0.5$; (c) $(c/h)T = 1.0$; (d) $(c/h)T = 2.0$. (From Schmitt, Harrison, and Williams.²⁹)

In this chapter we have presented in detail a theory for dipole antennas which are electrically thin, long, and perfectly conducting. We conclude with a discussion of an academic question about the possible upper limits on the length of the antenna. We see from (10.157) that the current on an exceedingly long, perfectly conducting dipole antenna decays slowly as $1/\ln |kz|$. Thus, if the antenna is made of copper, for example, the total ohmic loss on such a long antenna may be appreciable. Indeed, for an infinitely long dipole antenna, it has been found³³ that the ohmic loss behaves like $1/\ln (\zeta_0/|z^i|)$ for small internal impedance z^i . This means that, for a given small z^i , the effect of the ohmic loss of the antenna conductor cannot be obtained by any straightforward perturbation theory when the antenna is sufficiently long. However, since the conductivity of copper is quite high, this difficulty does not appear except for extremely long antennas. The technological usefulness of such a thin but extremely long dipole antenna seems to be rather remote. Accordingly, for all practical purposes, we have now a quite complete and accurate description of the highly conducting thin dipole antenna. However, as discussed in Chap. 8, the investigation of electrically thick dipole antennas is very much in its infancy.

REFERENCES

1. King, R. W. P.: "The Theory of Linear Antennas," Harvard University Press, Cambridge, Mass., 1956.
2. Wu, T. T.: Input Admittance of Infinitely Long Dipole Antennas Driven from Coaxial Lines, *J. Math. Phys.*, vol. 3, pp. 1298–1301, 1962.
3. Schmitt, H. J.: Transients in Cylindrical Antennas, *Proc. Inst. Elec. Engrs. (London)*, part C, *Monograph 377E*, 1960.
4. King, R. W. P., and H. J. Schmitt: The Transient Response of Linear Antennas and Loops, *IRE Trans. Antennas Propagation*, vol. AP-10, pp. 222–228, 1962.
5. Wu, T. T.: Theory of the Dipole Antenna and Two-wire Transmission Line, *J. Math. Phys.*, vol. 2, pp. 550–574, 1961.
6. Wu, T. T.: Input Admittance of Linear Antennas Driven from a Coaxial Line, *J. Res. Natl. Bur. Std. (U.S.)*, vol. 67D, pp. 83–89, 1963.
7. King, R. W. P.: "Transmission Line Theory," McGraw-Hill Book Company, New York, 1955.
8. Storer, J. E.: Variational Solution to the Problem of Symmetrical Cylindrical Antennas, *Cruft Lab. Tech. Rept. 101*, Harvard University, 1951.
9. Tai, C. T.: A Variational Solution to the Problem of Cylindrical Antennas, *Stanford Res. Inst. Tech. Rept. 12*, *SRI Project 188*, Stanford, Calif., 1950.
10. Hurd, R. A.: Variational Solution for the Admittance of a Long Cylindrical Antenna, *Radio Sci.*, vol. 68D, pp. 311–316, 1964.
11. Zuhrt, H.: Eine Strenge Berchung der Dipolantennas mit Rohrformigen Querschnitt, *Frequenz*, vol. 4, p. 135, 1950.
12. Storm, B.: Investigation into Modern Aerial Theory and a New Solution of Hallen's Integral Equation for a Cylindrical Aerial, doctoral dissertation, Imperial College, London, 1953; summary in *Wireless Engr.*, July, 1953.
13. Duncan, R. H., and F. A. Hinchey: Cylindrical Antenna Theory, *J. Res. Natl. Bur. Std. (U.S.)*, vol. 64D, pp. 569–584, 1960.

14. King, R. W. P.: Linear Arrays: Currents, Impedances, and Fields, I, *IRE Trans. Antennas Propagation*, vol. AP-7, spec. suppl., p. S440, 1959, and Chap. 9 of this book.
15. Chen, C. L.: Theory of the Balanced Helical Wire Antenna, *Radio Sci.*, vol. 2, pp. 167–190, 1967.
16. Wu, T. T.: Theory of the Thin Circular Loop Antenna, *J. Math. Phys.*, vol. 3, pp. 1301–1304, 1962.
17. Mei, K. K.: Integral Equations of Thin Wire Antennas, *IEEE Trans. Antennas Propagation*, vol. AP-13, p. 374, 1965.
18. Chang, D. C.: On the Thick Cylindrical Antenna, *Cruft Lab. Tech. Rept.* 509, Harvard University, 1966.
19. See Chap. 8 of this book.
20. Morse, P. M., and H. Feshbach: "Methods of Theoretical Physics," McGraw-Hill Book Company, New York, 1953.
21. Klein, M. G.: Integral Equation on a Half-line with Kernel Depending upon the Difference of the Arguments, *Usp. Mat. Nauk (N.S.)*, vol. 13, 1958, *Am. Math. Soc. Trans. Ser. 2*, vol. 22, 1962.
22. King, R. W. P.: "Fundamental Electromagnetic Theory," Dover Publications, Inc., New York, 1963.
23. Chen, C. L.: Theoretical and Experimental Studies on the Long Dipole Antenna, *Cruft Lab. Tech. Rept.* 541, Harvard University, 1967; On the Scattering of Electromagnetic Waves from a Long Wire, *Radio Sci.*, vol. 3, pp. 585–598, 1968.
24. Gooch, D. W., C. W. Harrison, Jr., R. W. P. King, and T. T. Wu: Impedance and Admittance of Long Antennas in Air and in Dissipative Media with Tables of the Functions $f(p) \pm ig(p) = \sqrt{1 \pm ip}$, *Cruft Lab. Tech. Rept.* 353, Harvard University, 1962.
25. Altschuler, E. E.: The Traveling-wave Antenna, *Cruft Lab. Sci. Rept.* 7 (Ser. 2), Harvard University, 1960.
26. Sevick, J.: Experimental and Theoretical Results on the Back-scattering Cross Section of Coupled Antennas, *Cruft Lab. Tech. Rept.* 150, Harvard University, 1952.
27. Ås, B. O., and H. J. Schmitt: Back-scattering Cross Section of Reactively Loaded Cylindrical Antennas, *Cruft Lab. Sci. Rept.* 18 (Ser. 1), Harvard University, 1958.
28. Harrison, C. W., Jr., and C. S. Williams, Jr.: Transients in Wide Angle Conical Antennas, *IEEE Trans. Antennas Propagation*, vol. AP-13, pp. 236–246, 1965.
29. Schmitt, H. J., C. W. Harrison, Jr., and C. S. Williams, Jr.: Calculated and Experimental Responses of Thin Cylindrical Antennas to Pulse Excitation, *IEEE Trans. Antennas Propagation*, vol. AP-14, pp. 120–127, 1966.
30. Papas, C. H.: On the Infinitely Long Cylindrical Antenna, *J. Appl. Phys.*, vol. 20, pp. 437–440, 1949.
31. Kuehl, H. H.: Current on an Infinitely Long Cylindrical Antenna, *J. Math. Phys.*, vol. 39, pp. 121–125, 1960.
32. Kunz, K. S.: Asymptotic Behavior of Current on an Infinite Cylindrical Antenna, *J. Res. Natl. Bur. Std. (U.S.)*, vol. 67D, pp. 417–431, 1963.
33. Shen, L. C., and T. T. Wu: Radiated Power and Ohmic Loss of the Infinitely Long Cylindrical Antenna, *Gordon McKay Lab. Sci. Rept.* 6 (NsG-579), Harvard University, 1966.

CHAPTER 11

THE LOOP ANTENNA FOR TRANSMISSION AND RECEPTION

Ronold W. P. King

11.1 Description and Application of the Loop

The loop antenna consists of one or more turns of highly conducting wire around a frame that may have any shape but is usually circular, square, or rectangular. Although useful as a transmitting antenna, its most important application is for reception. In particular, when the loop is electrically small, the sharp null in its field pattern makes it a valuable tool in direction finding. Another very important application of the small loop is as a probe for measuring magnetic fields and distributions of current. Both when used in direction finding and when used as a probe, it is often enclosed in a slotted metal shield.

In this chapter the general problem of determining the current distribution, the admittance, and the radiation field of a single-turn circular loop is considered in detail when the loop is driven by a δ -function generator and is immersed in an arbitrary homogeneous and isotropic medium characterized by the complex permittivity $\epsilon = \epsilon - j\sigma/\omega$ and the permeability μ . The current in a loaded receiving loop is also studied, and the effective length of the loop is determined. The electrically small transmitting and receiving loops are then examined in detail. The shielded loop and the loop as a probe are considered.

From the analytical point of view the loop antenna is considerably more complicated than the linear antenna. On the other hand, owing to the symmetry of the circular loop, an expansion of the current in an even Fourier series is useful for the loop, whereas it is not adequate for the cylindrical antenna.

11.2 Integral Equation for the Circular Transmitting Loop and Its Solution

The loop to be analyzed is illustrated in Fig. 11.1. It consists of a circular ring of perfectly conducting wire with a δ -function generator $V_0\delta(\phi)$ at $\phi = 0$. The radius of the ring is b , that of the wire a . It is assumed that the latter is very small compared with both the radius of the loop and the wavelength in the medium, so that

$$a^2 \ll b^2 \quad |ka| \ll 1 \quad (11.1)$$

The complex propagation constant of the medium is $k = \beta - j\alpha$. When the medium is air, $\alpha = 0$, $\beta = \omega\sqrt{\mu_0\epsilon_0} = 2\pi/\lambda_0$. For simplicity the analysis will be

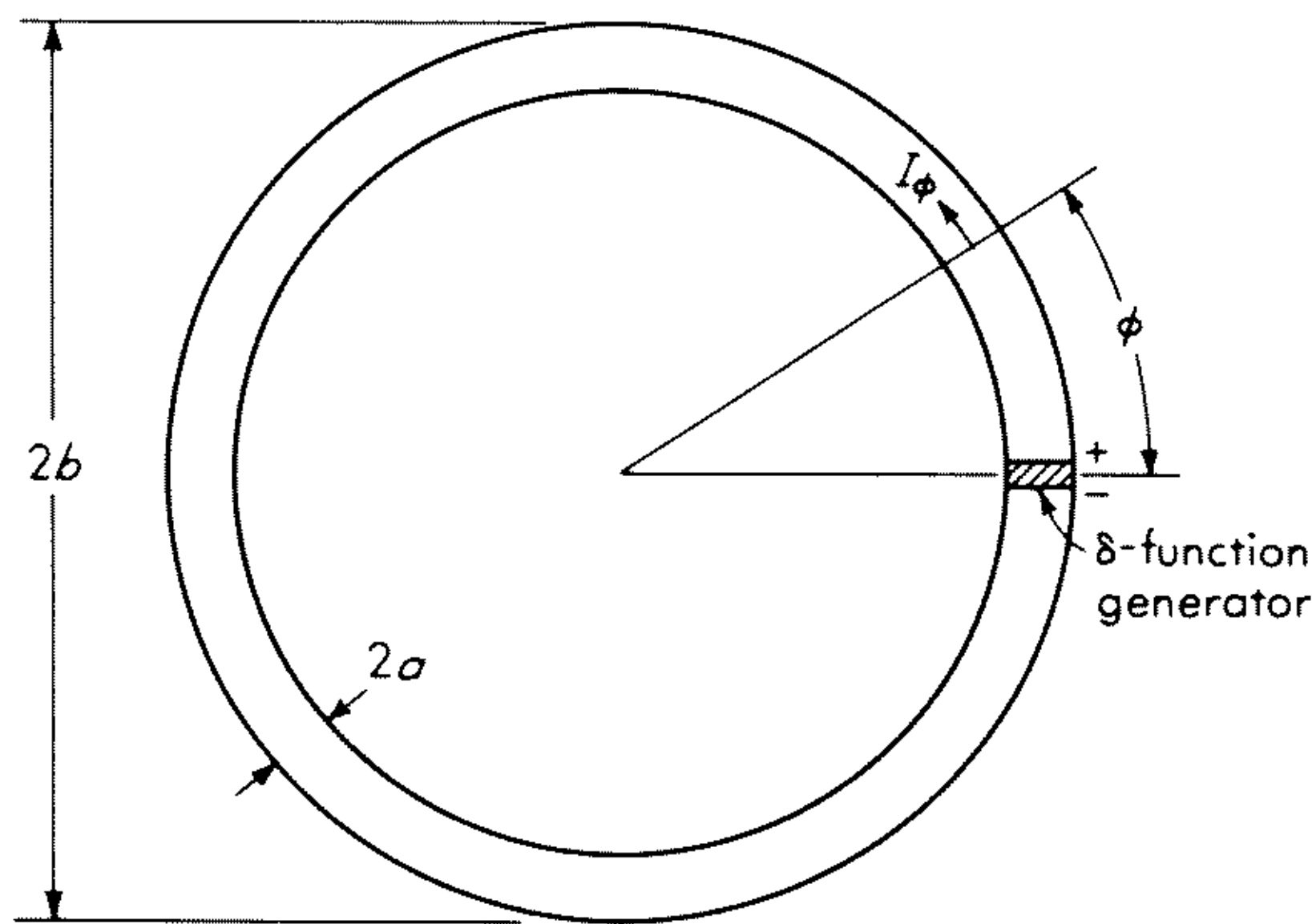


Fig. 11.1 Circular loop antenna.

carried out for air. The subsequent substitution of ϵ for ϵ_0 , k for k_0 is sufficient to generalize the results to an imperfectly conducting medium.

The integral equation for the current $I(\phi)$ can be derived from the boundary condition $E_\phi = -V_0^e \delta(\phi)/b$ on the surface of the loop. This requires that $E_\phi = 0$ except at $\phi = 0$, where it becomes infinite but in such a manner that

$$\int_{-\pi}^{\pi} E_\phi b d\phi = -V_0^e$$

It follows from the defining relation $-\nabla\Phi = \mathbf{E} + j\omega\mathbf{A}$ for the scalar potential that on the surface of the loop

$$\frac{V_0^e \delta(\phi)}{b} = \frac{1}{r} \frac{\partial \Phi}{\partial \phi} + j\omega A_\phi \quad (11.2)$$

The scalar and vector potentials at the element $ds = b d\phi$ are given by the following integrals:

$$\Phi = \frac{1}{4\pi\epsilon_0} \int_{-\pi}^{\pi} q(\phi') W(\phi - \phi') d\phi' \quad (11.3a)$$

$$A_\phi = \frac{\mu_0}{4\pi} \int_{-\pi}^{\pi} I(\phi') W(\phi - \phi') \cos(\phi - \phi') d\phi' \quad (11.3b)$$

where the kernel is

$$W(\phi - \phi') = \frac{1}{2\pi} \int_{-\pi}^{\pi} \frac{e^{-jk_0 b R}}{R} d\psi \quad (11.4a)$$

$$\text{with} \quad R = \sqrt{4 \sin^2 \frac{(\phi - \phi')}{2} + \frac{A^2}{b^2}} \quad A = 2a \sin \frac{\psi}{2} \quad (11.4b)$$

The total current and charge per unit length are $I(\phi) = 2\pi a K_\phi(\phi)$ and $q(\phi) = 2\pi a \eta(\phi)$, where $K_\phi(\phi)$ and $\eta(\phi)$ are the surface densities of current and charge.

If use is made of the equation of continuity, $\partial I(\phi)/b \partial \phi + j\omega q(\phi) = 0$, to eliminate $q(\phi)$ in (11.3a), the expression for $\partial \Phi(\phi)/\partial \phi$ can be integrated by parts with the aid of the condition $\partial W/\partial \phi = -\partial W/\partial \phi'$. If this is used in (11.2) together with (11.3b), the result is the following integral equation for the current in the loop:

$$V_0 e \delta(\phi) = \frac{j\zeta_0}{4\pi} \int_{-\pi}^{\pi} M(\phi - \phi') I(\phi') d\phi' \quad (11.5)$$

where the new kernel is

$$M(\phi - \phi') = \left[k_0 b \cos(\phi - \phi') + \frac{1}{k_0 b} \frac{\partial^2}{\partial \phi^2} \right] W(\phi - \phi') \quad (11.6)$$

and $\zeta_0 = \omega\mu_0/k_0 = \sqrt{\mu_0/\epsilon_0}$.

A solution of the integral equation (11.5) can be obtained in the form of a series expansion. This is derived by expanding both the kernel $W(\phi - \phi')$ and the current in Fourier series. Thus, let

$$W(\phi - \phi') = \sum_{-\infty}^{\infty} K_m e^{-jm(\phi - \phi')} \quad (11.7)$$

$$I(\phi') = \sum_{-\infty}^{\infty} I_n e^{-jn\phi'} \quad (11.8)$$

where the coefficients K_m and I_n must be evaluated. The latter are given by

$$I_n = \frac{1}{2\pi} \int_{-\pi}^{\pi} I(\phi') e^{jn\phi'} d\phi' \quad (11.9)$$

The former are easily obtained if (11.7) is multiplied on both sides by $e^{jn\phi}$ and integrated with respect to ϕ from $-\pi$ to π . Since in the sum over m only the term $m = n$ contributes to the integral (all others vanish), the result is

$$K_n = \frac{1}{2\pi} \int_{-\pi}^{\pi} W(\phi - \phi') e^{jn(\phi - \phi')} d\phi = K_{-n} \quad (11.10)$$

The substitution of (11.7) in (11.6) at once leads to

$$M(\phi - \phi') = \sum_{-\infty}^{\infty} a_n e^{-jn(\phi - \phi')} \quad (11.11)$$

where the coefficients are

$$a_n = \frac{k_0 b}{2} (K_{n+1} + K_{n-1}) - \frac{n^2}{k_0 b} K_n = a_{-n} \quad (11.12)$$

Exercise 11.1 Carry out the steps to obtain (11.12).

The substitution of (11.10) in (11.5) leaves the integral equation in the form

$$V_0 e \delta(\phi) = \frac{j\zeta_0}{4\pi} \sum_{-\infty}^{\infty} a_n \int_{-\pi}^{\pi} e^{-jn(\phi - \phi')} I(\phi') d\phi' \quad (11.13)$$

With (11.9) it follows directly that (11.13) may be expressed in the form

$$V_0^e \delta(\phi) = \frac{j\zeta_0}{2} \sum_{-\infty}^{\infty} a_n I_n e^{-jn\phi} \quad (11.14)$$

This is a Fourier series with the coefficients $j\zeta_0 a_n I_n / 2$. They may be evaluated in the usual manner, but the properties of the δ function yield a very simple result. It is

$$\frac{j\zeta_0 a_n I_n}{2} = \frac{1}{2\pi} \int_{-\pi}^{\pi} V_0^e \delta(\phi) e^{jn\phi} d\phi = \frac{V_0^e}{2\pi} \quad (11.15a)$$

Hence,
$$I_n = \frac{-jV_0^e}{\zeta_0 \pi a_n} \quad (11.15b)$$

so that the desired series for the current in the loop as defined in (11.8) is

$$I(\phi) = \frac{-jV_0^e}{\zeta_0 \pi} \left(\frac{1}{a_0} + 2 \sum_1^{\infty} \frac{\cos n\phi}{a_n} \right) \quad (11.16)$$

The associated admittance is

$$Y = \frac{I(0)}{V_0^e} = \frac{-j}{\zeta_0 \pi} \left(\frac{1}{a_0} + 2 \sum_1^{\infty} \frac{1}{a_n} \right) \quad (11.17)$$

The impedance is $Z = 1/Y$.

11.3 Evaluation of Coefficients

The coefficients a_n that occur in (11.16) and (11.17) must be determined from (11.12), which depends on the evaluation of (11.10). With (11.4a,b) this has the explicit form:

$$K_n = \frac{1}{4\pi^2} \int_{-\pi}^{\pi} d\psi \int_{-\pi}^{\pi} e^{jn\theta} e^{-jk_0 b R(\theta)} \frac{d\theta}{R(\theta)} \quad (11.18)$$

where $\theta = \phi - \phi'$, $R(\theta) = [4 \sin^2 (\theta/2) + A^2/b^2]^{1/2}$, and $A = 2a \sin (\psi/2)$. The evaluation of the K_n has been a major difficulty in the solution of the problem of the loop antenna. Both in the early work of Hallén¹ and a more recent investigation by Storer,² singular or very large values were obtained when the index n came close to a certain large number that is determined by b and a . Wu³ has devised a procedure that avoids this difficulty by making use of approximations that are valid over a greater range of the parameters involved.

The first steps in the evaluation of (11.18) are to interchange the order of integration and substitute A for ψ as the variable of integration. The result is

$$K_n = \frac{2}{\pi} \int_0^{2a} \bar{K}_n(A) \frac{dA}{\sqrt{4a^2 - A^2}} \quad (11.19a)$$

where, for $n \geq 0$,
$$\bar{K}_n(A) = \frac{1}{2\pi} \int_{-\pi}^{\pi} e^{jn\theta} e^{-jk_0 b R(\theta)} \frac{d\theta}{R(\theta)} \quad (11.19b)$$

The method introduced by Wu³ for the evaluation of the \bar{K}_n is one of comparison with a similar known integral. This is

$$N_n(A) = \frac{1}{2\pi} \int_{-\pi}^{\pi} e^{jn\theta} e^{-jk_0 b r(\theta)} \frac{d\theta}{r(\theta)} \tag{11.20}$$

where $r(\theta) = \sqrt{\theta^2 + A^2/b^2}$. At least for n not too large the difference between \bar{K}_n and N_n is approximately independent of A . That is, $\bar{K}_n(A) - N_n(A)$ is not a function of A in first approximation. The integral (11.20) is readily reduced to the form

$$N_n(A) = \frac{1}{2\pi} \int_{-\infty}^{\infty - j\pi} \exp(jAB \sinh v) dv = \frac{1}{\pi} \mathcal{K}_0(AB) \tag{11.21}$$

by changes in variable that include $\theta = (A/b) \sinh t$. In (11.21) $B = (n/b)^2 - k_0^2$ and $\mathcal{K}_0(AB)$ is the modified Bessel function of the second kind. (Since K_0 is used for the $n = 0$ term in the expansion of the kernel W , a script letter is used for the Bessel function.)

Since the difference between $\bar{K}_n(A)$ and $N_n(A)$ is approximately independent of A , it may be evaluated when A is sufficiently small to satisfy the inequality $A \ll b/n$. In this case $R(\theta)$ in (11.19b) may be approximated by $R(\theta) \doteq 2 \sin(\theta/2)$ and the integral expressed as follows:

$$\bar{K}_n(A) = \frac{1}{\pi} \ln \frac{8b}{a} - \frac{2}{\pi} \sum_{m=0}^{n-1} \frac{1}{2m+1} - \frac{1}{2} \int_0^{2k_0 b} [\Omega_{2n}(x) + jJ_{2n}(x)] dx \tag{11.22}$$

where Ω is the Lommel-Weber function

$$\Omega_m(x) = \frac{1}{\pi} \int_0^{\pi} \sin(x \sin \theta - m\theta) d\theta \tag{11.23}$$

and J_{2n} is the Bessel function.

Since

$$\ln \frac{8b}{a} = \frac{1}{2} \ln \left(1 - \frac{k_0^2 b^2}{\pi} \right) - \ln \frac{A}{2} \sqrt{\frac{n^2}{b^2} - k_0^2} + \ln(4n) \tag{11.24}$$

and, for small arguments,

$$N_n(A) = \frac{1}{\pi} \mathcal{K}_0 \left(A \sqrt{\frac{n^2}{b^2} - k_0^2} \right) \doteq -\frac{1}{\pi} \left[\gamma + \ln \frac{A}{2} \sqrt{\frac{n^2}{b^2} - k_0^2} \right] \tag{11.25}$$

where $\gamma = 0.5772 \dots$ is Euler's constant, it follows that

$$\bar{K}_n(A) - N_n(A) = \frac{1}{2\pi} \left\{ \ln \left(1 - \frac{k_0^2 b^2}{\pi} \right) + 2C_n - \pi \int_0^{2k_0 b} [\Omega_{2n}(x) + jJ_{2n}(x)] dx \right\} \tag{11.26}$$

where

$$C_n = \gamma - 2 \sum_{m=0}^{n-1} (2m+1)^{-1} + \ln(4n) \tag{11.27}$$

If the difference $\bar{K}_n(A) - N_n(A)$, which has been evaluated subject to $A \ll nb$ and which is independent of A , is assumed to apply for all values of A , then

$$\bar{K}_n(A) = \frac{1}{2\pi} \left\{ 2\mathcal{K}_0 \left(A \sqrt{\frac{n^2}{b^2} - k_0^2} \right) + \ln \left(1 - \frac{k_0^2 b^2}{\pi} \right) + 2C_n - \pi \int_0^{2k_0 b} [\Omega_{2n}(x) + jJ_{2n}(x)] dx \right\} \quad (11.28)$$

Since A is small, the approximation

$$\mathcal{K}_0 \left(A \sqrt{\frac{n^2}{b^2} - k_0^2} \right) \doteq \mathcal{K}_0 \left(\frac{nA}{b} \right) - \frac{1}{2} \ln \left(1 - \frac{k_0^2 b^2}{n^2} \right) \quad (11.29)$$

may be made, so that the final formula for $\bar{K}_n(A)$ is

$$\bar{K}_n(A) \doteq \frac{1}{2\pi} \left\{ 2\mathcal{K}_0 \left(\frac{nA}{b} \right) + 2C_n - \pi \int_0^{2k_0 b} [\Omega_{2n}(x) + jJ_{2n}(x)] dx \right\} \quad (11.30)$$

If this expression is substituted in the integral (11.19a), the coefficients K_n can be obtained directly. The integration of the constant terms is elementary. The integral

$$\frac{2}{\pi} \int_0^{\pi/2} \mathcal{K}_0(2z \sin \theta) d\theta = \mathcal{G}_0(z) \mathcal{K}_0(z)$$

is derived in Watson.⁴ The results are

$$K_0 = \frac{1}{\pi} \ln \frac{8b}{a} - \frac{1}{2} \int_0^{2k_0 b} [\Omega_0(x) + jJ_0(x)] dx \quad (11.31a)$$

$$K_{-n} = K_n = \frac{1}{\pi} \left[\mathcal{K}_0 \left(\frac{na}{b} \right) \mathcal{G}_0 \left(\frac{na}{b} \right) + C_n \right] - \frac{1}{2} \int_0^{2k_0 b} [\Omega_{2n}(x) + jJ_{2n}(x)] dx \quad (11.31b)$$

where $\mathcal{G}_0(na/b)$ is the modified Bessel function of the first kind. Note that since the product $\mathcal{K}_0(na/b) \mathcal{G}_0(na/b)$ approaches $(\pi b/2na)$ as $n \rightarrow \infty$, whereas both C_n and the integral are of the order of magnitude $1/n^2$, the product remains the dominant term. Clearly, (11.31b) is valid for all values of n . When (11.31a,b) are substituted in (11.12), the coefficients a_n can be evaluated and the Fourier series (11.16) for the current and (11.17) for the admittance determined. Curves of the complex coefficients a_0^{-1} , a_1^{-1} , and a_2^{-1} are in Fig. 11.2.

11.4 The Admittance of and Current in a Circular Loop in Air and in a Dissipative Medium

When a loop antenna is immersed in a dissipative medium, the formulas derived in the preceding sections apply but with $\epsilon = \epsilon - j\sigma/\omega$ substituted for ϵ_0 and μ for μ_0 . The complex wave number that replaces k_0 is

$$k = \beta - j\alpha = \omega \sqrt{\mu\epsilon} \sqrt{1 - jp} \quad (11.32)$$

where $p = \sigma/\omega\epsilon$ is the loss tangent. The complex quantity $(1 - jp)^{1/2}$ is readily separated into real and imaginary parts by means of the functions $f(p)$ and $g(p)$ which satisfy the equation

$$\sqrt{1 \pm jp} = f(p) \pm jg(p) \tag{11.33}$$

and are given by

$$f(p) = \cosh \left(\frac{1}{2} \sinh^{-1} p \right) \qquad g(p) = \sinh \left(\frac{1}{2} \sinh^{-1} p \right) \tag{11.34}$$

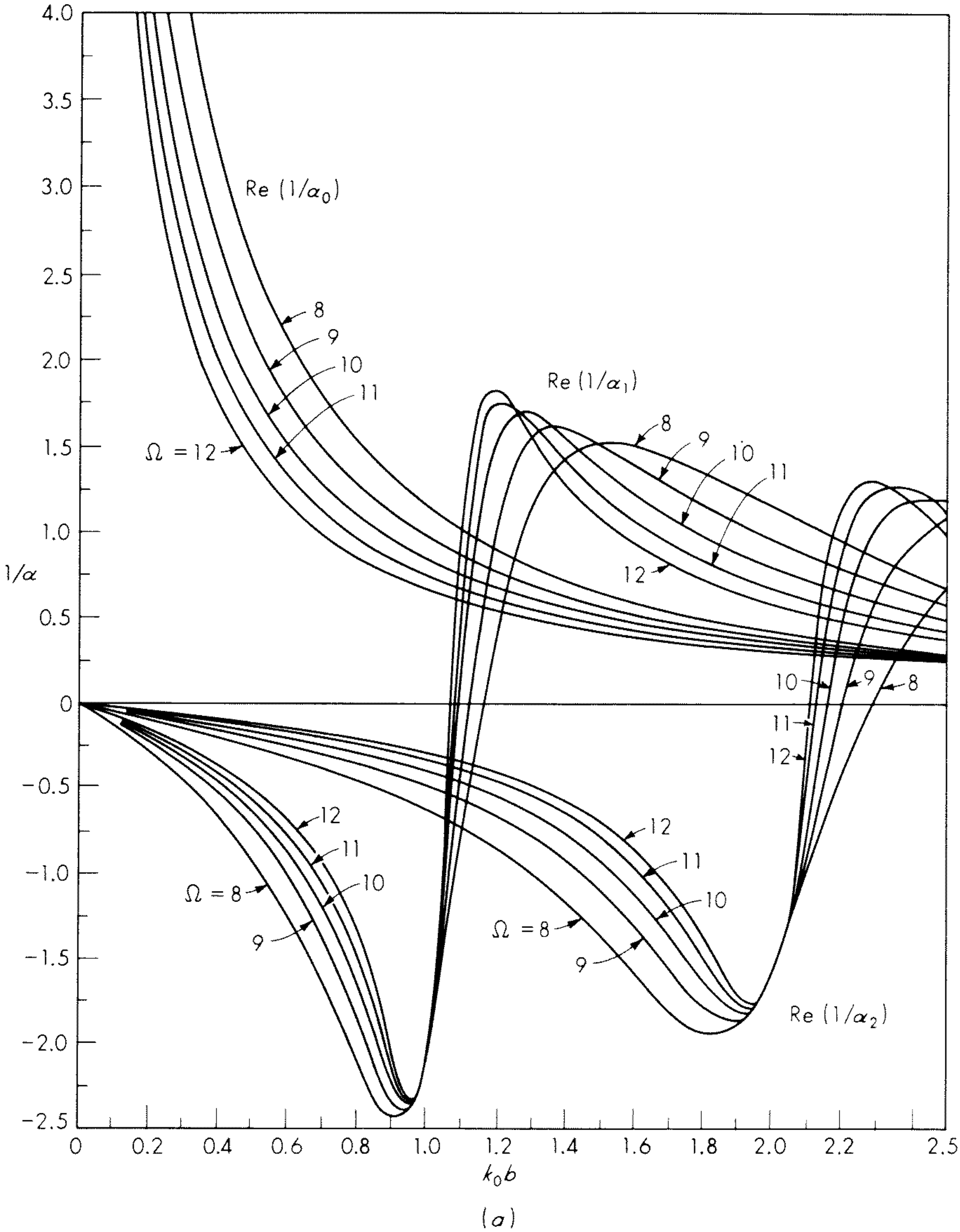


Fig. 11.2 (a) Real parts of the functions $1/\alpha_0$, $1/\alpha_1$, $1/\alpha_2$; (b) imaginary parts of the functions $1/\alpha_0$, $1/\alpha_1$, $1/\alpha_2$.

The functions $f(p)$ and $g(p)$ are extensively tabulated.⁵ Clearly,

$$\beta = \omega\sqrt{\mu\epsilon}f(p) \quad \alpha = \omega\sqrt{\mu\epsilon}g(p) \quad (11.35)$$

When $p^2 \ll 1$,

$$\beta \doteq \omega\sqrt{\mu\epsilon} \quad \alpha \doteq \frac{\sigma}{2}\sqrt{\frac{\mu}{\epsilon}} \quad (11.36)$$

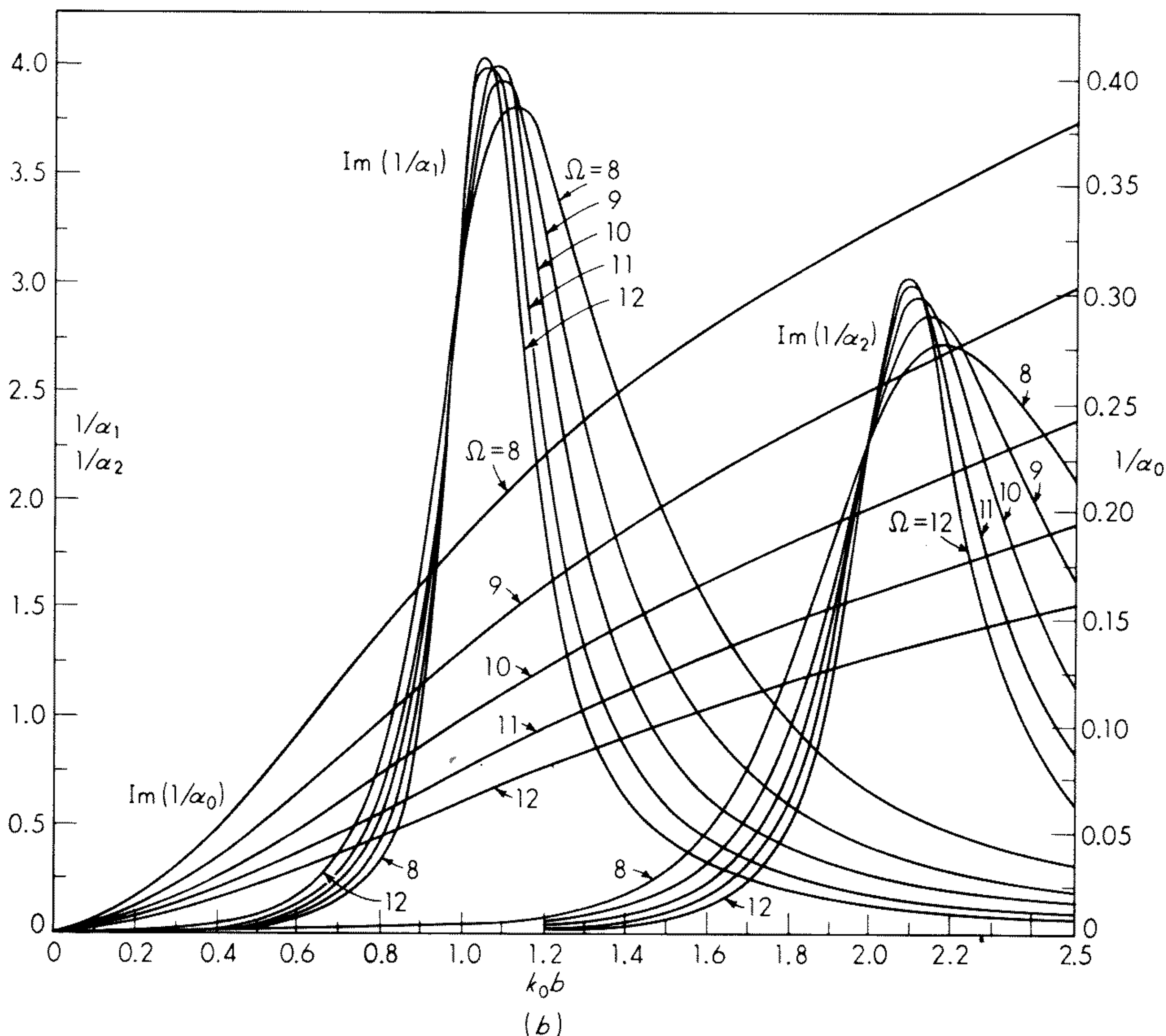
If the normalizing factor

$$\Delta = \sqrt{\frac{\epsilon_r}{\mu_r}}f(p) \quad (11.37)$$

is introduced, where $\epsilon_r = \epsilon/\epsilon_0$, $\mu_r = \mu/\mu_0$, the normalized admittance corresponding to (11.17) is

$$\frac{Y}{\Delta} = \frac{-j(1 - j\alpha/\beta)}{\pi\zeta_0} \left(\frac{1}{a_0} + 2 \sum_1^\infty \frac{1}{a_n} \right) \quad (11.38)$$

where the a_n are given by (11.12) with the associated K 's defined by (11.31a) and (11.31b) with k substituted for k_0 . The integrals with complex k in the



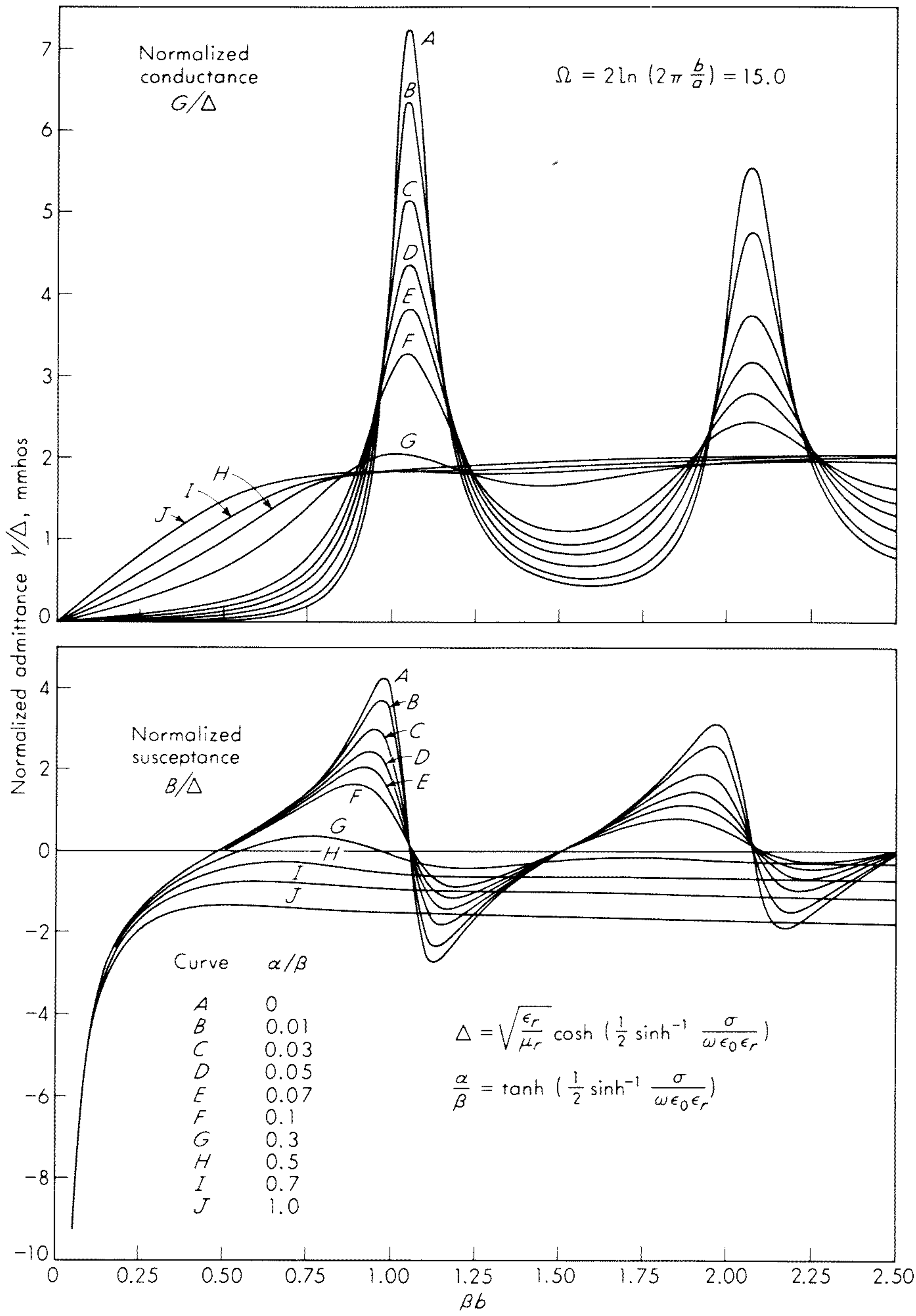


Fig. 11.3 Normalized admittance of circular loop antenna in a dissipative medium: Wu's theory, $\Omega = 15$.

TABLE 11.1 NORMALIZED ADMITTANCE Y/Δ IN MILLIMHOS OF LOOP ANTENNAS IN DISSIPATIVE MEDIA, $\Omega = 12$

βb	$\alpha/\beta = 0.00$		$\alpha/\beta = 0.01$		$\alpha/\beta = 0.05$		$\alpha/\beta = 0.10$		$\alpha/\beta = 0.30$		$\alpha/\beta = 1.00$	
	Y/Δ		Y/Δ		Y/Δ		Y/Δ		Y/Δ		Y/Δ	
0.05	0.0002	-12.3838	0.0026	-12.3839	0.0124	-12.3842	0.0246	-12.3851	0.0734	-12.3951	0.2433	-12.5069
0.10	0.0008	-6.0079	0.0057	-6.0079	0.0254	-6.0086	0.0500	-6.0107	0.1482	-6.0312	0.4857	-6.2596
0.15	0.0019	-3.7985	0.0094	-3.7986	0.0393	-3.7998	0.0767	-3.8031	0.2256	-3.8356	0.7265	-4.1891
0.20	0.0036	-2.6282	0.0137	-2.6284	0.0545	-2.6302	0.1053	-2.6349	0.3066	-2.6814	0.9644	-3.1724
0.25	0.0060	-1.8703	0.0191	-1.8706	0.0713	-1.8732	0.1364	-1.8799	0.3929	-1.9431	1.1973	-2.5867
0.30	0.0095	-1.3150	0.0258	-1.3154	0.0905	-1.3192	0.1710	-1.3283	0.4860	-1.4125	1.4220	-2.2256
0.35	0.0146	-0.8711	0.0343	-0.8717	0.1128	-0.8771	0.2103	-0.8895	0.5877	-1.0005	1.6350	-2.0003
0.40	0.0218	-0.4917	0.0455	-0.4928	0.1396	-0.5005	0.2561	-0.5175	0.7003	-0.6632	1.8323	-1.8652
0.45	0.0323	-0.1495	0.0605	-0.1511	0.1726	-0.1622	0.3105	-0.1858	0.8262	-0.3774	2.0105	-1.7931
0.50	0.0474	0.1742	0.0811	0.1716	0.2142	0.1554	0.3770	0.1224	0.9680	-0.1304	2.1670	-1.7652
0.55	0.0698	0.4934	0.1100	0.4893	0.2683	0.4652	0.4599	0.4184	1.1283	0.0835	2.3008	-1.7675
0.60	0.1033	0.8207	0.1516	0.8142	0.3407	0.7777	0.5660	0.7100	1.3092	0.2652	2.4126	-1.7890
0.65	0.1544	1.1692	0.2131	1.1587	0.4403	1.1020	0.7047	1.0025	1.5114	0.4119	2.5043	-1.8214
0.70	0.2347	1.5538	0.3068	1.5363	0.5814	1.4463	0.8897	1.2971	1.7328	0.5174	2.5789	-1.8585
0.75	0.3646	1.9931	0.4544	1.9631	0.7871	1.8161	1.1403	1.5888	1.9670	0.5739	2.6398	-1.8962
0.80	0.5833	2.5099	0.6961	2.4564	1.0952	2.2094	1.4814	1.8602	2.2021	0.5746	2.6903	-1.9322
0.85	0.9693	3.1257	1.1088	3.0265	1.5639	2.6016	1.9387	2.0703	2.4203	0.5172	2.7332	-1.9653
0.90	1.6821	3.8294	1.8378	3.6393	2.2692	2.9111	2.5192	2.1430	2.6016	0.4083	2.7709	-1.9953
0.95	3.0140	4.4372	3.1124	4.0862	3.2489	2.9404	3.1671	1.9724	2.7293	0.2644	2.8051	-2.0225
1.00	5.1747	4.1923	4.9896	3.7064	4.3203	2.3893	3.7210	1.4915	2.7960	0.1090	2.8369	-2.0471
1.05	6.9797	1.9691	6.4182	1.7662	4.9408	1.2056	3.9720	0.7912	2.8065	-0.0341	2.8671	-2.0699
1.10	6.3872	-0.7830	5.9627	-0.5402	4.7283	-0.0478	3.8479	0.1131	2.7747	-0.1480	2.8961	-2.0913
1.15	4.6500	-1.9270	4.5259	-1.6197	3.9992	-0.8072	3.4768	-0.3481	2.7184	-0.2245	2.9242	-2.1117
1.20	3.2716	-1.9702	3.2919	-1.7477	3.2274	-1.0562	3.0383	-0.5602	2.6537	-0.2641	2.9514	-2.1313
1.25	2.3889	-1.6551	2.4583	-1.5089	2.6099	-1.0065	2.6421	-0.5859	2.5928	-0.2721	2.9779	-2.1505
1.30	1.8314	-1.2655	1.9157	-1.1693	2.1616	-0.8194	2.3258	-0.4980	2.5435	-0.2559	3.0035	-2.1693
1.35	1.4688	-0.8811	1.5575	-0.8168	1.8473	-0.5770	2.0906	-0.3481	2.5095	-0.2232	3.0283	-2.1878
1.40	1.2260	-0.5180	1.3170	-0.4750	1.6321	-0.3156	1.9261	-0.1669	2.4921	-0.1809	3.0523	-2.2060
1.45	1.0616	-0.1741	1.1555	-0.1464	1.4909	-0.0495	1.8213	0.0286	2.4909	-0.1347	3.0755	-2.2241
1.50	0.9530	0.1578	1.0514	0.1730	1.4079	0.2164	1.7673	0.2287	2.5043	-0.0892	3.0979	-2.2419

limits are defined by analytic continuation. For the loop in air, $\sigma = 0$, $p = 0$, $\Delta = 1$.

As with a dipole antenna when center driven by a δ -function generator, the admittance Y_0 strictly does not exist, since its susceptance is infinite owing to the knife-edge terminals with zero separation that characterize the generator. However, as shown for the dipole,^{6,7} the representation of the current by continuous functions, combined with the extreme localization of the part of the current that is associated with the knife-edges of the generator, effectively omits the latter for thin wires unless a very large number of terms is taken in the Fourier series. If the infinite sum in (11.38) is replaced by a finite one, the

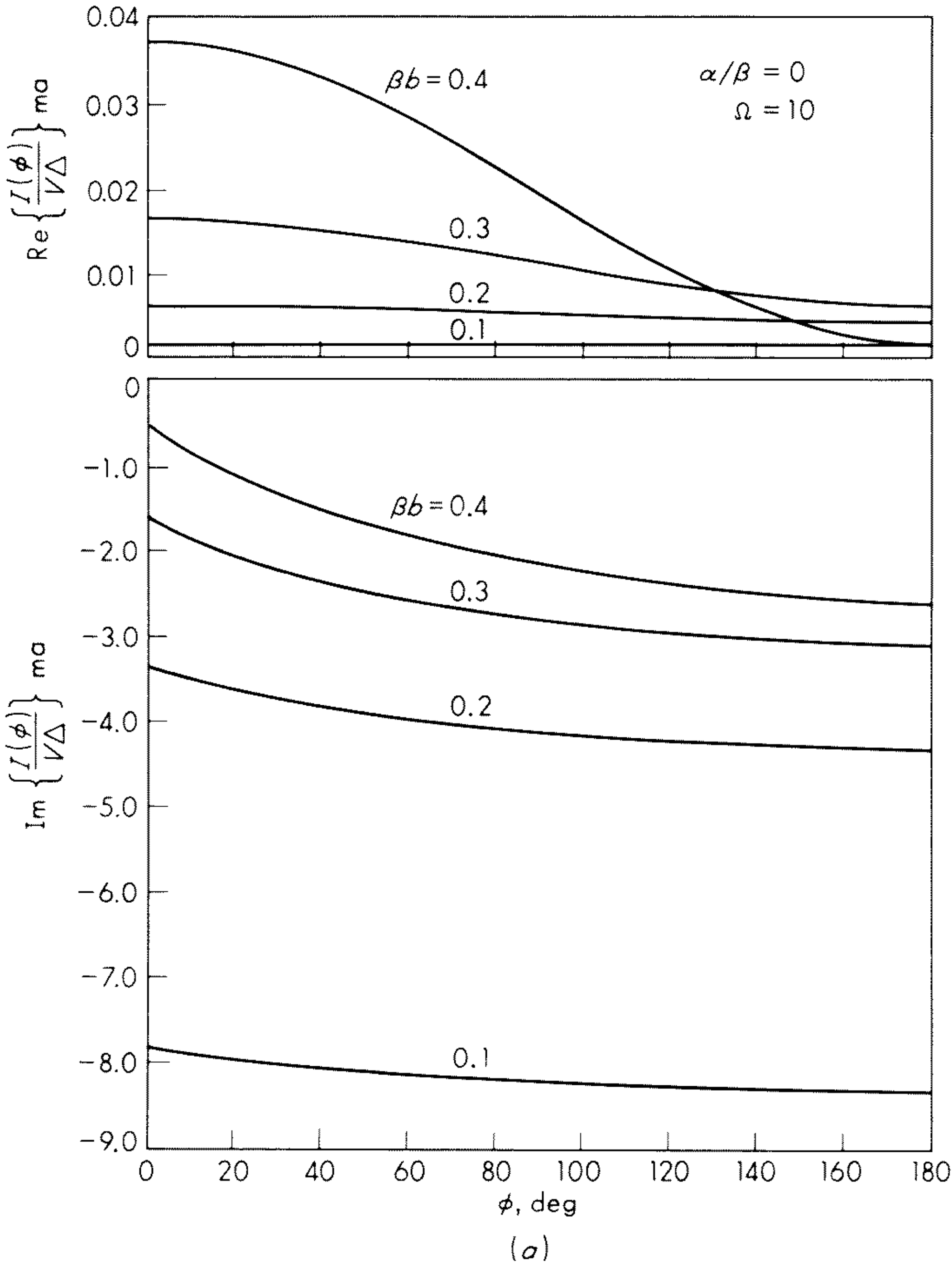
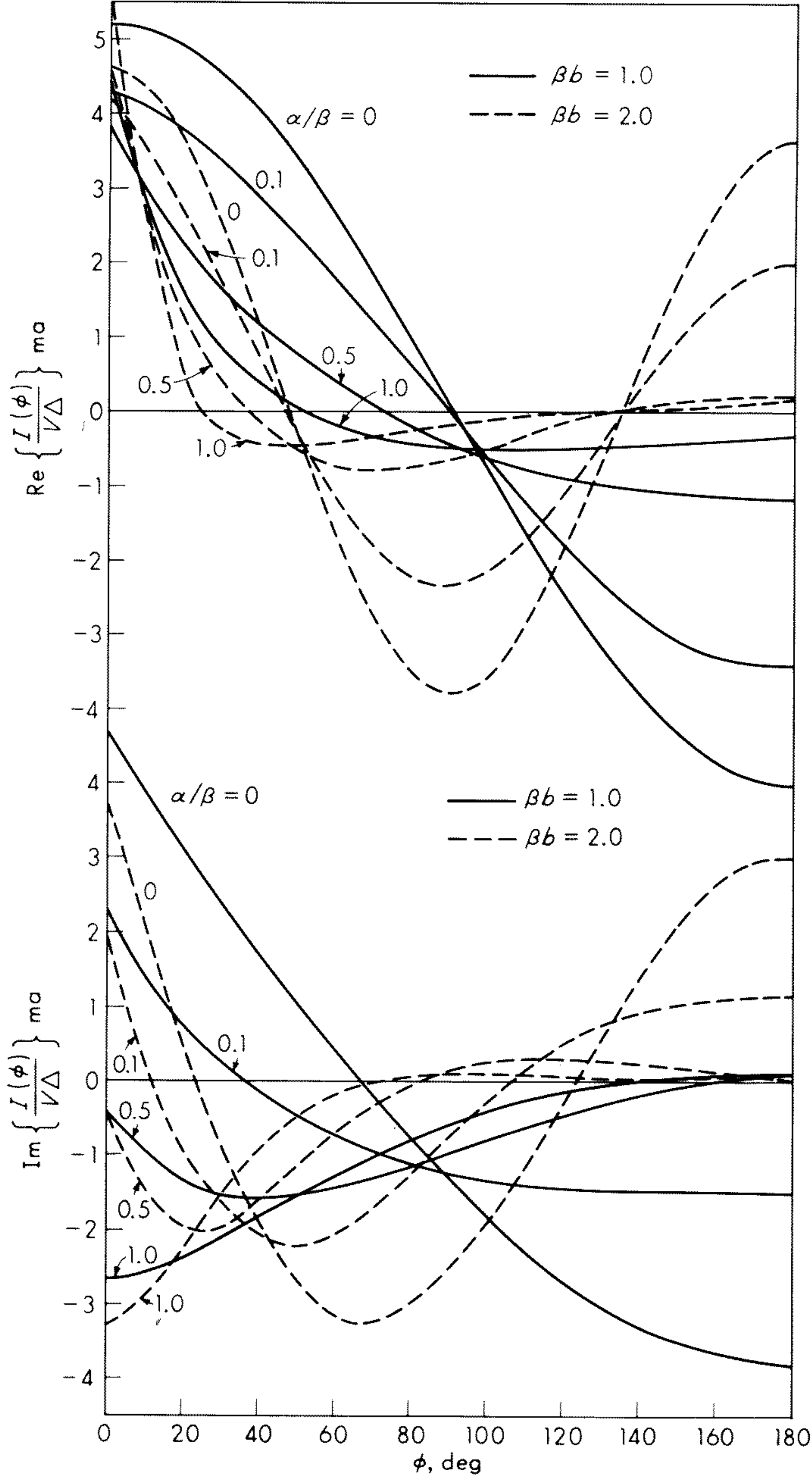


Fig. 11.4 (a) Real and imaginary components of the normalized current in a circular loop antenna in air, $\alpha/\beta = 0$; $\Omega = 10$; $\beta b = 0.1, 0.2, 0.3, 0.4$. (b) Real and imaginary components of the normalized current in a circular loop antenna in dissipative media; $\Omega = 10$; $\beta b = 1.0, 2.0$.



(b)

approximate formula that is obtained is a good measure of the admittance of the antenna for use with a practical method of driving when combined with a suitable terminal-zone network.

The formula (11.38) was evaluated with a high-speed computer using successively 8, 9, 10, 18, 19, and 20 terms. A study of the convergence of this formula⁸ has shown that 20 terms yield satisfactory values of the admittance of thin-wire loops [$\Omega = 2 \ln (2\pi b/a) \geq 10$] that are not too large ($\beta b \leq 2.5$) when in air or in an arbitrary dissipative medium. The approximation is excellent for the conductance, somewhat less accurate for the susceptance. Extensive tables and graphs of the normalized admittance Y/Δ are in the literature.⁸ A short sample is in Table 11.1 and in Fig. 11.3. In the latter the parameter α/β of the surrounding medium ranges from zero (air) to 1 (salt water). It is noteworthy how insensitive to the size of the loop the admittance becomes as α/β approaches unity. This is true in particular of loops near antiresonance that have a high driving-point impedance. Such an insensitivity merely indicates that most of the current is in the surrounding medium and not in the loop.

The normalized distribution of current $I(\phi) = I''(\phi) + jI'(\phi) = |I(\phi)| \exp \theta_I$ in the loop when this is immersed in a dissipative medium is given by

$$\frac{I(\phi)}{\Delta V_0^e} = \frac{-j(1 - j\alpha/\beta)}{\pi\zeta_0} \left(\frac{1}{a_0} + 2 \sum_1^{\infty} \frac{\cos n\phi}{a_n} \right) \quad (11.39)$$

Curves showing typical distributions are in Fig. 12.4a and b.

11.5 The Radiation Field of a Loop Antenna

The electromagnetic field at a point P at a great distance from a loop antenna may be evaluated from the vector potential at that point. The x and y components of the vector potential at P due to the current $I(\phi)$ are readily shown to be

$$A_x^r = -\frac{b\mu_0}{4\pi} \frac{e^{-jk_0 r_0}}{r_0} \int_0^{2\pi} I(\phi') e^{jk_0 b \sin \theta \cos(\phi - \phi')} \sin \phi' d\phi' \quad (11.40)$$

$$A_y^r = \frac{b\mu_0}{4\pi} \frac{e^{-jk_0 r_0}}{r_0} \int_0^{2\pi} I(\phi') e^{jk_0 b \sin \theta \cos(\phi - \phi')} \cos \phi' d\phi' \quad (11.41)$$

where $I(\phi')$ is given by (11.16) or, alternatively, by

$$I(\phi) = \frac{-jV_0^e}{\pi\zeta_0} \sum_{-\infty}^{\infty} \frac{e^{jn\phi}}{a_n} \quad (11.42)$$

Exercise 11.2 Derive A_x^r and A_y^r as given in (11.40) and (11.41).

We assume that the medium is air. If (11.42) is substituted in (11.40) and

(11.41), the resulting integrals for the n th term are easily arranged in the form

$$A_{xn}^r = \frac{jG}{2a_n}(K_1 - K_2) \quad A_{yn}^r = \frac{G}{2a_n}(K_1 + K_2) \quad (11.43)$$

where

$$K_1 = \int_0^{2\pi} e^{j(n+1)\phi'} e^{jk_0 b \sin \theta \cos(\phi - \phi')} d\phi' = \frac{2\pi j^{n+1}}{a_n} e^{j(n+1)\phi} J_{n+1}(k_0 b \sin \theta) \quad (11.44a)$$

$$K_2 = \int_0^{2\pi} e^{j(n-1)\phi'} e^{jk_0 b \sin \theta \cos(\phi - \phi')} d\phi' = \frac{2\pi j^{n-1}}{a_n} e^{j(n-1)\phi} J_{n-1}(k_0 b \sin \theta) \quad (11.44b)$$

$J_n(x)$ is the Bessel function of the first kind and

$$G = \frac{-jV_0 \epsilon \mu_0 b e^{-jk_0 r_0}}{4\pi^2 \zeta_0 r_0} \quad (11.45)$$

In (11.45) r_0 is the distance from P to the center of the loop. The components of the vector potential in the spherical coordinates r_0, θ, ϕ may be obtained from the x and y components with the formulas

$$A_{\theta n}^r = (A_{xn}^r \cos \phi + A_{yn}^r \sin \phi) \cos \theta \quad (11.46a)$$

$$A_{\phi n}^r = -A_{xn}^r \sin \phi + A_{yn}^r \cos \phi \quad (11.46b)$$

They are shown in Fig. 11.5 and are given by

$$A_{\theta n}^r = \frac{-2\pi G}{a_n} e^{jn(\phi + \pi/2)} \frac{n J'_n(k_0 b \sin \theta)}{k_0 b \sin \theta} \cos \theta \quad (11.47a)$$

$$A_{\phi n}^r = \frac{-j2\pi G}{a_n} e^{jn(\phi + \pi/2)} J_n(k_0 b \sin \theta) \quad (11.47b)$$

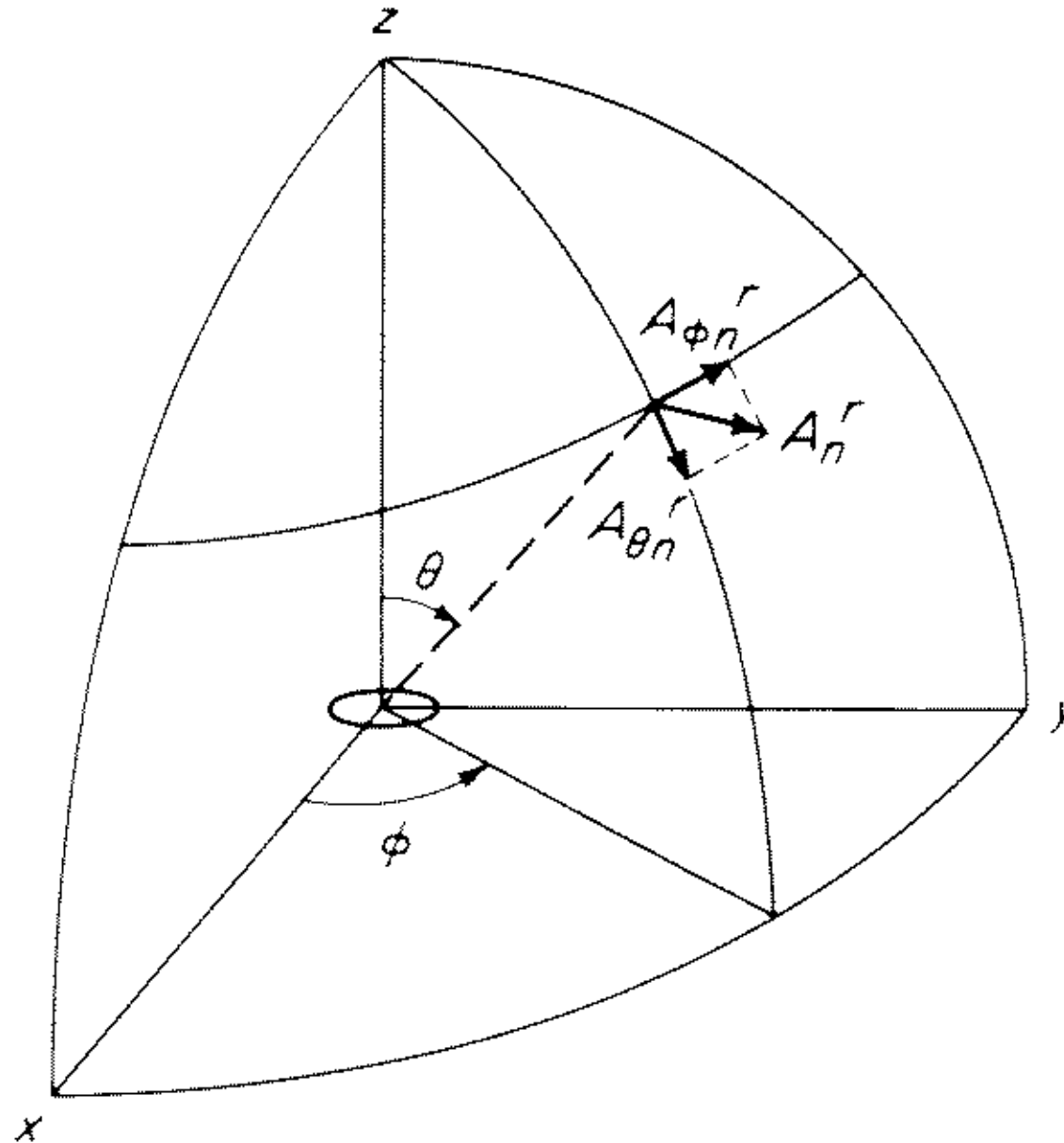


Fig. 11.5 Spherical components $A_{\theta n}^r$ and $A_{\phi n}^r$ of the far-zone vector potential $\mathbf{A}_n^r = \hat{\mathbf{x}}A_{xn}^r + \hat{\mathbf{y}}A_{yn}^r$.

where $J'_n(k_0 b \sin \theta)$ is the derivative of $J_n(b_0 k \sin \theta)$ with respect to the argument.

Exercise 11.3 Derive (11.46a,b).

The resultant vector potential is the sum of all contributions from the terms in the series. Hence

$$A_{\theta}^r = -2\pi G \sum_{-\infty}^{\infty} \frac{e^{jn(\phi+\pi/2)}}{a_n} \frac{n}{k_0 b} \frac{J_n(k_0 b \sin \theta)}{\sin \theta} \cos \theta \quad (11.48a)$$

$$A_{\phi}^r = -j2\pi G \sum_{-\infty}^{\infty} \frac{e^{jn(\phi+\pi/2)}}{a_n} J'_n(k_0 b \sin \theta) \quad (11.48b)$$

The associated electromagnetic field is defined by

$$\mathbf{E}^r = j\omega \hat{\mathbf{r}}_0 \times (\hat{\mathbf{r}}_0 \times \mathbf{A}^r) = -j\omega(\hat{\boldsymbol{\theta}} A_{\theta}^r + \hat{\boldsymbol{\phi}} A_{\phi}^r) \quad (11.49a)$$

$$\mathbf{B}^r = -jk_0 \hat{\mathbf{r}}_0 \times \mathbf{A}^r = -jk_0(\hat{\boldsymbol{\phi}} A_{\theta}^r - \hat{\boldsymbol{\theta}} A_{\phi}^r) \quad (11.49b)$$

It is seen that in general \mathbf{E}^r and \mathbf{B}^r consist of both $\hat{\boldsymbol{\theta}}$ and $\hat{\boldsymbol{\phi}}$ components and that each component is the sum of an infinite number of terms. Fortunately, for loops of small or even moderate size the coefficients $1/a_n$ decrease sufficiently rapidly that only relatively few terms are needed in the sum. In particular, if $k_0 b \leq 1$, two terms are adequate for far-field determinations. If $k_0 b \leq 0.2$, one term is enough. The components of the vector potential, electric, and magnetic fields for the first two terms in the series are

$$n = 0: \quad A_{\theta 0}^r = 0 \quad A_{\phi 0}^r = \frac{j2\pi G}{a_0} J_1(k_0 b \sin \theta) \quad (11.50a)$$

$$E_{\theta 0}^r = 0 \quad B_{\phi 0}^r = 0 \quad E_{\phi 0}^r = \frac{-\omega}{k_0} B_{\theta 0}^r = \frac{2\pi\omega G}{a_0} J_1(k_0 b \sin \theta) \quad (11.50b)$$

$$n = 1: \quad A_{\theta 1}^r = \frac{4\pi G}{a_1} \frac{J_1(k_0 b \sin \theta)}{k_0 b \sin \theta} \cos \theta \sin \phi \quad (11.51a)$$

$$A_{\phi 1}^r = \frac{4\pi G}{a_1} J'_1(k_0 b \sin \theta) \cos \phi \quad (11.51b)$$

$$E_{\theta 1}^r = \frac{-\omega}{k_0} B_{\phi 1}^r = \frac{-j4\pi\omega G}{a_1} \frac{J_1(k_0 b \sin \theta)}{k_0 b \sin \theta} \cos \theta \sin \phi \quad (11.51c)$$

$$E_{\phi 1}^r = \frac{\omega}{k_0} B_{\theta 1}^r = \frac{-j4\pi\omega G}{a_1} J'_1(k_0 b \sin \theta) \cos \phi \quad (11.51d)$$

11.6 The Electrically Small Transmitting Loop

When $k_0 b < 1$, the current in the loop is approximately

$$I(\phi) \doteq I_0 + I_1(\phi) \quad (11.52a)$$

with
$$I_0 = \frac{-jV_0^e}{\zeta_0 \pi a_0} \quad I_1(\phi) = \frac{-j2V_0^e}{\zeta_0 \pi a_1} \cos \phi \quad (11.52b)$$

The current I_0 is independent of ϕ and unidirectional around the loop. On the other hand, $I_1(\phi)$ vanishes at $\phi = \pm\pi/2$, where it reverses direction, so that the currents in the range $-\pi/2 \leq \phi \leq \pi/2$ are always counterclockwise when the currents in the range $\pi/2 \leq \phi \leq 3\pi/2$ are clockwise. For the circulatory "zero" mode there are no accumulations of charges anywhere around the loop. The current is everywhere clockwise for a half cycle, then everywhere counterclockwise. For the dipole "first" mode, $q(\phi) \approx \sin \phi$, so that the loop is oppositely charged at $\phi = \pi/2$ and $\phi = -\pi/2$ and the current oscillates in synchronism on the two halves much as in two parallel dipoles that are driven in phase.

The admittance of the loop is that of two circuits in parallel. Thus

$$Y = Y_0 + Y_1 \quad Z = \frac{Z_0 Z_1}{Z_0 + Z_1} \quad (11.53)$$

where

$$Y_0^{-1} = Z_0 = R_0 + j\omega L_0 = j\zeta_0 \pi a_0 \quad (11.54a)$$

$$Y_1^{-1} = Z_1 = R_1 - \frac{j}{\omega C_1} = \frac{j\zeta_0 \pi a_1}{2} \quad (11.54b)$$

If only the leading terms with small arguments in the formula (11.12) for a_0 and a_1 are retained, it can be shown that

$$R_0 \doteq \frac{\pi\zeta_0}{6} k_0^4 b^4 \quad R_1 = \frac{\pi\zeta_0}{6} k_0^2 b^2 \quad (11.55)$$

$$L_0 \doteq \mu_0 b \left(\ln \frac{8b}{a} - 2 \right) \quad C_1 = 2\epsilon_0 b \left(\ln \frac{8b}{a} - 2 \right)^{-1} \quad (11.56)$$

The resistances R_0 and R_1 associated with the two modes of oscillation have different orders of magnitude, R_1 being the larger. Nevertheless, since R_1 is in series with the very small capacitance C_1 , whereas R_0 is in series with the small inductance L_0 , it follows that $|I_0|$ is much greater than $|I_1|$. This means that for $k_0 b$ very small, the radiated power $|I_0|^2 R_0$ exceeds $|I_1|^2 R_1$. On the other hand, when $k_0 b > 0.35$, $|I_1|^2 R_1 > |I_0|^2 R_0$. The dipole mode is significant when $k_0 b \geq 0.1$.

The far-zone fields for the two modes are readily obtained from (11.50b), (11.51c,d) with $k_0 b < 1$, so that $J_1(u) \doteq u/2$, $J'_1(u) = J_0(u) - J_1(u)/u \doteq 1/2$. They are

$$n = 0: \quad E_{\phi 0^r} = -\frac{\omega}{k_0} B_{\theta 0^r} = \frac{\pi G \omega}{a_0} k_0 b \sin \theta \quad (11.57)$$

$$n = 1: \quad E_{\theta 1^r} = \frac{\omega}{k_0} B_{\phi 1^r} = \frac{-j2\pi G \omega}{a_1} \cos \theta \sin \phi \quad (11.58a)$$

$$E_{\phi 1^r} = -\frac{\omega}{k_0} B_{\theta 1^r} = \frac{-j2\pi G \omega}{a_1} \cos \phi \quad (11.58b)$$

The resultant field is

$$\mathbf{E} = \hat{\theta} E_{\theta 1^r} + \hat{\phi} (E_{\phi 0^r} + E_{\phi 1^r}) \quad \mathbf{B} = \hat{\theta} (B_{\theta 0^r} + B_{\theta 1^r}) + \hat{\phi} B_{\phi 1^r} \quad (11.59)$$

When $k_0 b < 0.1$, only the "zero" mode is significant and the entire field is given by (11.57). Note that

$$G = \frac{-jV_0^e \mu_0}{4\pi^2 \zeta_0} \frac{b e^{-jk_0 r_0}}{r_0} \quad (11.60)$$

where r_0 is measured to the center of the loop.

The far field of the loop shown in Fig. 11.5 is given by (11.59) when $k_0 b < 1$. At a point r_0, θ, ϕ the electric and magnetic fields are mutually perpendicular and perpendicular to r_0 . The component of the magnetic field in a direction s that makes an angle ψ with the plane that contains r_0 and the z axis is $B_s = B_\phi \sin \psi - B_\theta \cos \psi$. With (11.59) and (11.60),

$$B_s = B_0 F(\theta, \psi) \quad (11.61)$$

where

$$B_0 = \frac{j\mu_0 I(0)}{2\pi} \frac{e^{-jk_0 r_0}}{r_0} \quad (11.62)$$

and $F(\theta, \phi, \psi)$

$$= \frac{\pi k_0 b}{2[1 + 2(a_0/a_1)]} \left[jk_0 b \sin \theta \cos \psi + \frac{2a_0}{a_1} (\cos \phi \cos \psi + \cos \theta \sin \phi \sin \psi) \right] \quad (11.63)$$

The associated electric field is in the direction $\hat{\mathbf{t}} \perp \hat{\mathbf{s}}$ with

$$E_t = \frac{\omega}{k_0} B_s \quad (11.64)$$

11.7 The Electrically Small Receiving Loop

The most important applications of loop antennas are for reception. Usually the antennas are electrically small, especially when used as probes for measuring magnetic fields. For many purposes it is sufficient to determine the current in the load Z_L connected in series with the circular loop at $\phi = 0$ when a plane electromagnetic wave is incident from an arbitrary direction as shown in Fig. 11.6a and b. In these figures the loop (radius b , wire radius a) lies in the xy plane. The incident plane wave originates at a great (infinite) distance away along the line R_0 that joins the distant transmitter to the center of the loop. The electric and magnetic vectors ($\mathbf{E}^i, \mathbf{B}^i$) of the incident field are perpendicular to each other and to R_0 . The electric vector may be represented as a wave traveling in the R direction in the form $\mathbf{E}^i(\mathbf{R}) = \mathbf{E}_0^i e^{-j\beta R}$ where $\beta = \omega/c$ is the wave number and c is the velocity of light. \mathbf{E}_0^i is the amplitude at the center of the loop where $R = 0$. As indicated in Fig. 11.6a the vector \mathbf{E}_0^i may be resolved into a component $E_0^i \cos \psi$ in the xy plane and a component $E_0^i \sin \psi$, where the angle ψ is measured in the plane of the wave front. Since the normal to the wave front makes an angle θ with the z axis, the component $E_0^i \sin \psi$ is not perpendicular to the xy plane but has the component $E_0^i \sin \psi \sin \theta$ in the xy plane perpendicular to the component $E_0^i \cos \psi$ as shown in the plane view in Fig. 11.6b.

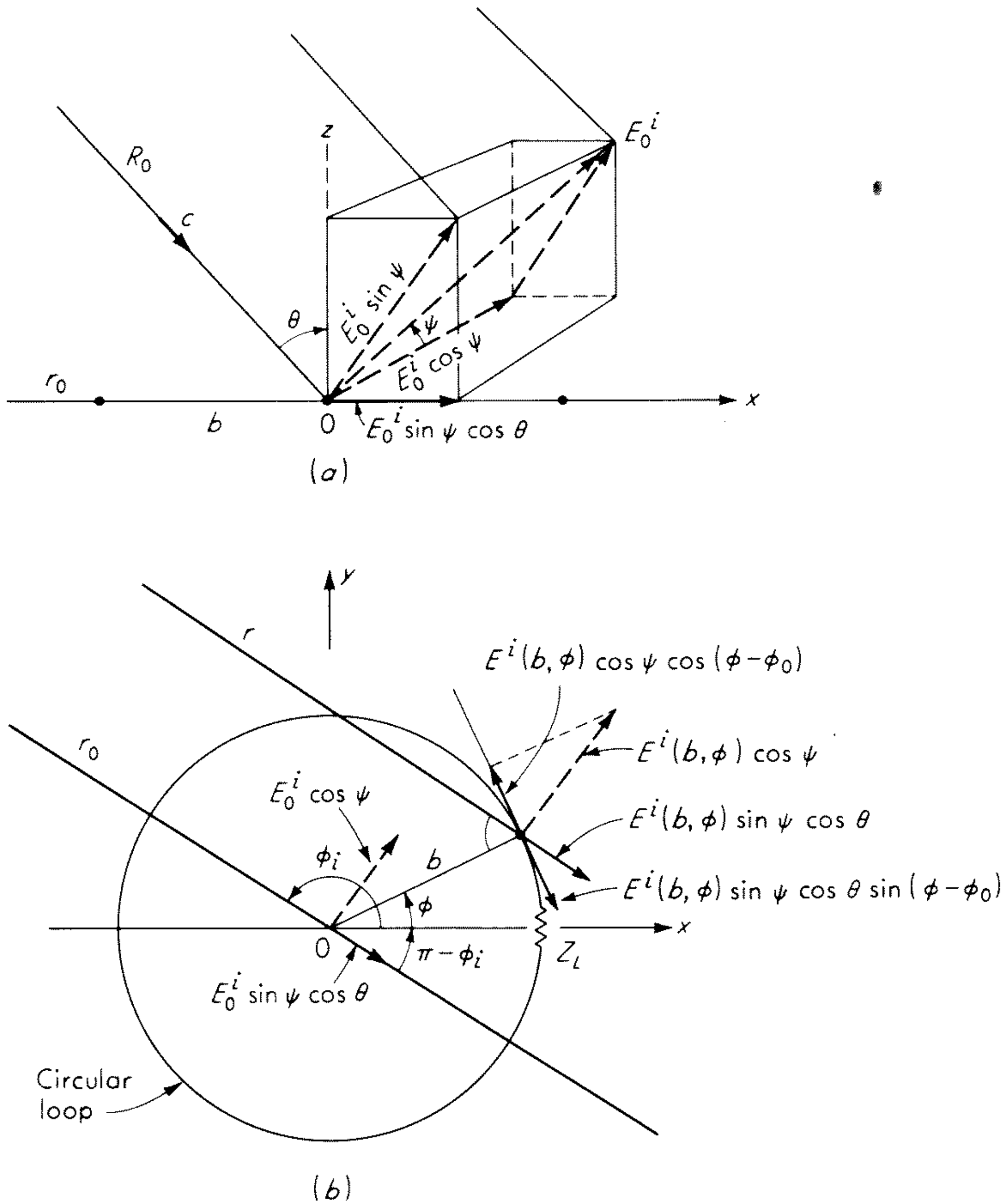


Fig. 11.6 (a) Plane wave incident on circular loop with center at 0. (b) Projection of (a) onto plane of loop.

The incident electric vector $\mathbf{E}^i(b, \phi)$ at the point ϕ on the surface of the loop referred to the vector at the center is

$$\mathbf{E}^i(b, \phi) = \mathbf{E}_0^i e^{j\beta b \sin \theta \cos(\phi - \phi_i)} \quad (11.65)$$

where ϕ_i is the angle from the positive x axis to the direction of origin of the incident wave as shown in Fig. 11.6b. The supplement of this angle, $\phi_0 = \pi - \phi_i$, is convenient. The ϕ component of this vector is

$$E_\phi^i(b, \phi) = E_0^i F(\phi_i, \phi, \psi, \theta) \quad (11.66)$$

where

$$F(\phi, \phi_i, \psi, \theta) = -[\cos \psi \cos(\phi - \phi_i) - \sin \psi \cos \theta \sin(\phi - \phi_i)] e^{j\beta b \sin \theta \cos(\phi - \phi_i)} \quad (11.67)$$

It is this component of the electric field that, acting tangent to the surface of the loop, induces a current in it.

In order to make use of this field in the integral equation for the current, it is convenient to expand it in a Fourier series. Since the load Z_L is at $\phi = 0$ and only even functions of ϕ can lead to components of current that maintain a potential difference across Z_L , it is sufficient to expand $F(\phi, \phi_i, \psi, \theta)$ in a cosine series. [Odd currents in ϕ are excited, but they may be ignored if interest is limited to $I(0)$.] Specifically, for the even part $f_{-n} = f_n$, so that

$$F_{\text{even}}(\phi, \phi_i, \psi, \theta) = \sum_{-\infty}^{\infty} f_n e^{-jn\phi} = f_0 + 2 \sum_1^{\infty} f_n \cos n\phi \quad (11.68)$$

where $f_{-n} = f_n$. The coefficients f_n are readily evaluated from

$$f_n = \frac{2}{\pi} \int_0^{\pi} F(\phi) \cos n\phi d\phi \quad (11.69)$$

to be

$$f_n = j^{n-1} \left[\cos \psi \cos n\phi_i J'_n(\beta b \sin \theta) + \sin \psi \cos \theta \sin n\phi_i \frac{nJ_n(\beta b \sin \theta)}{\beta b \sin \theta} \right]$$

For the electrically small loops for which $\beta b < 1$, $J'_0(x) = -J_1(x) \doteq -x/2$, $J'_1(x) \doteq J_0(x) - J_1(x)/x \doteq 1/2$,

$$f_0 \doteq j \frac{\beta b}{2} \sin \theta \cos \psi \quad (11.70a)$$

$$f_1 \doteq 1/2 (\cos \theta \sin \phi_i \sin \psi + \cos \phi_i \cos \psi) \quad (11.70b)$$

The current $I(0)$ in the load Z_L is now quickly obtained from (11.14) if the left side, which is the value of $bE_{\phi}(b, \phi)$ along the perfectly conducting transmitting loop, is replaced by $bE_{\phi}^i(b, \phi) - I(0)Z_L\delta(\phi)$. In the first term $E_{\phi}^i(b, \phi)$ is the component of the incident field along the loop; in the second term $-I(0)Z_L$ is the voltage drop across the lumped load Z_L at $\phi = 0$. The resulting equation is

$$bE^i(b, \phi) - I(0)Z_L\delta(\phi) = \frac{j\zeta_0}{2} \sum a_n I_n e^{-jn\phi} \quad (11.71)$$

If (11.66) and (11.67) with (11.68) are used in (11.71), the coefficients ($a_n I_n$) of the Fourier series are readily evaluated just as with (11.14). The results are

$$I_n = \frac{-j}{\pi\zeta_0} \left[\frac{2\pi b E_0^i f_n - I(0)Z_L}{a_n} \right] \quad (11.72)$$

It follows that the current, as defined in (11.8), is given by

$$I(\phi) = -[2\pi b E_0^i u(\phi) + I(0)Z_L v(\phi)] \quad (11.73)$$

where
$$u(\phi) = \frac{j}{\pi\zeta_0} \left(\frac{f_0}{a_0} + 2 \sum_1^{\infty} \frac{f_n \cos n\phi}{a_n} \right) \quad (11.74a)$$

$$v(\phi) = \frac{-j}{\pi\zeta_0} \left(\frac{1}{a_0} + 2 \sum_1^{\infty} \frac{\cos n\phi}{a_n} \right) \quad (11.74b)$$

The current in the load is readily obtained from (11.73) with $\phi = 0$. It is

$$I(0) = -\frac{2\pi b E_0^i Z u(0)}{Z + Z_L} \quad (11.75)$$

The impedance Z of the loop is the reciprocal of the admittance $Y = v(0)$. Note that $-2\pi b E_0^i u(0)$ is the current $I(0)$ at $\phi = 0$ when $Z_L = 0$ and that $-2\pi b E_0^i u(0)Z$ is the open-circuit voltage $V(Z_L = \infty)$. Evidently, (11.75) is the current in a circuit in which $V(Z_L = \infty)$, Z_L , and Z are connected in series.

By analogy with the dipole antenna, the complex effective length of the loop may be defined to be the coefficient of $-E_0^i$ in the expression for the open-circuit voltage $V(Z_L = \infty)$. That is,

$$(VZ_L = \infty) = -E_0^i h_e(\theta, \phi_i, \psi) \quad (11.76)$$

It follows with (11.74a,b) and $Z = v^{-1}(0)$ that

$$h_e(\theta, \phi_i, \psi) = 2\pi b Z u(0) = 2\pi b \frac{f_0 a_0^{-1} + 2 \sum_1^{\infty} f_n a^{-n}}{a_0^{-1} + 2 \sum_1^{\infty} a^{-n}} \quad (11.77)$$

For the electrically small loop for which two terms are a sufficiently good approximation, the electrical effective length is

$$\beta h_e(\theta, \psi, \phi_i) \doteq \frac{1}{1 + 2a_0 a_1^{-1}} \left[j\pi b^2 \beta^2 \sin \theta \cos \psi + \frac{2\pi b \beta a_0}{a_1} (\cos \theta \sin \phi_i \sin \psi + \cos \phi_i \cos \psi) \right] \quad (11.78)$$

For the extremely small loop for which $\beta b \ll 1$ and $2a_0 \ll \beta b a_1$,

$$\beta h_e(\theta, \psi) \doteq j\pi b^2 \beta^2 \sin \theta \cos \psi \quad (11.79)$$

This is independent of the direction ϕ_i of the incident plane wave with respect to the location of the load at $\phi = 0$, since only the rotationally symmetrical current is significant. Note that the first term in (11.78) is proportional to the area of the loop and the second term proportional to its circumference.

The maximum open-circuit voltage in the zero or circulating mode is obtained when the loop is oriented to have the incident electric vector in the plane of the loop or the incident magnetic vector perpendicular to the plane of the loop. This means that $\psi = 0$ and $\theta = \pi/2$. Under these conditions (11.78) gives

$$\beta h_e\left(\frac{\pi}{2}, 0, \phi_i\right) = \frac{1}{1 + 2a_0 a_1^{-1}} \left(j\pi b^2 \beta^2 + \frac{2\pi b \beta a_0}{a_1} \cos \phi_i \right) \quad (11.80)$$

If the loop is now turned around its axis like a wheel until $\phi_i = \pi/2$, that part of the current which is oscillating in the dipole mode will have a node at Z_L and will maintain no current through it or voltage across it. This means that

relatively larger loops may be used and the response interpreted in terms of the currents in the circulating mode — as when measuring magnetic fields that link with the loop — without correction due to dipole-mode currents. These may exist with significant amplitude, but they can maintain no voltage across Z_L when $\phi_i = 0$.

Exercise 11.4 With the aid of a diagram show physically why the dipole-mode currents may be ignored in determining $I(0)$ when $\phi_i = \pi/2$.

If the loop is oriented to be in the plane of the wave front ($\theta = 0, \psi = \pi/2$), the effective length is

$$\beta h_e \left(0, \frac{\pi}{2}, \phi_i \right) = \frac{2\pi b \beta a_1}{a_1 + 2a_0} \sin \phi_i \quad (11.81)$$

Note that only dipole-mode currents now contribute to the open-circuit voltage.

Exercise 11.5 Show with a diagram the orientation of the loop when (11.81) is satisfied. Determine βh_e for a loop with $\beta b = 0.3$.

11.8 The Shielded Loop

It is shown in the preceding section that the dipole mode can be ignored insofar as the current in or voltage across the load is concerned when the loop is oriented to maximize the open-circuit voltage and the load is so located that $\phi_i = \pi/2$ as in Fig. 11.7a. A convenient way of connecting an end-loaded transmission line to a circular loop antenna is internally, as indicated in Fig. 11.7b. The shield of the coaxial line is sufficiently highly conducting that the tangential component of the total electric field along its surface is vanishingly small. In addition, the shield is very thick compared to the skin depth. As a

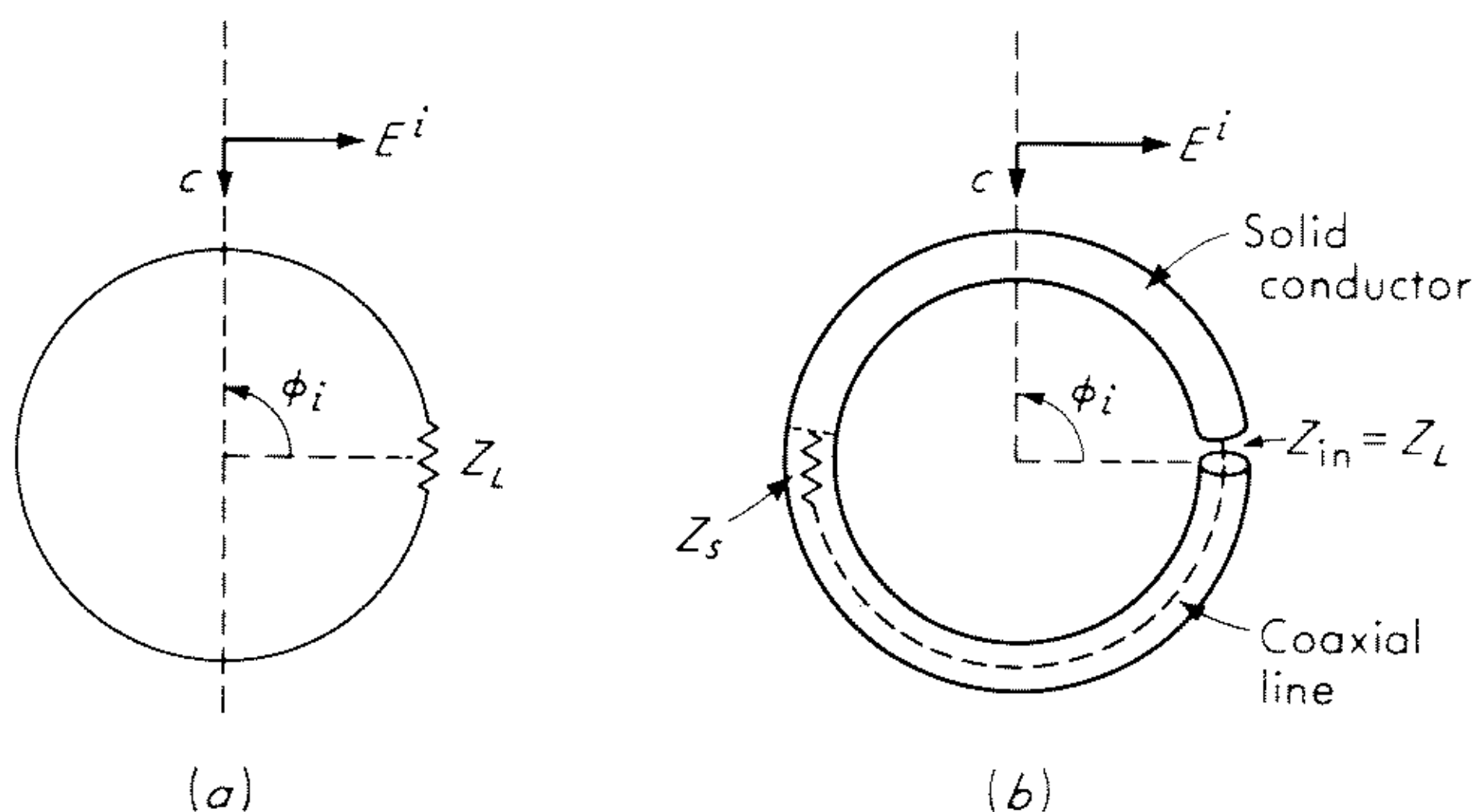


Fig. 11.7 Circular loop loaded with (a) lumped Z_L and (b) Z_L consisting of Z_{in} of end-loaded coaxial line.

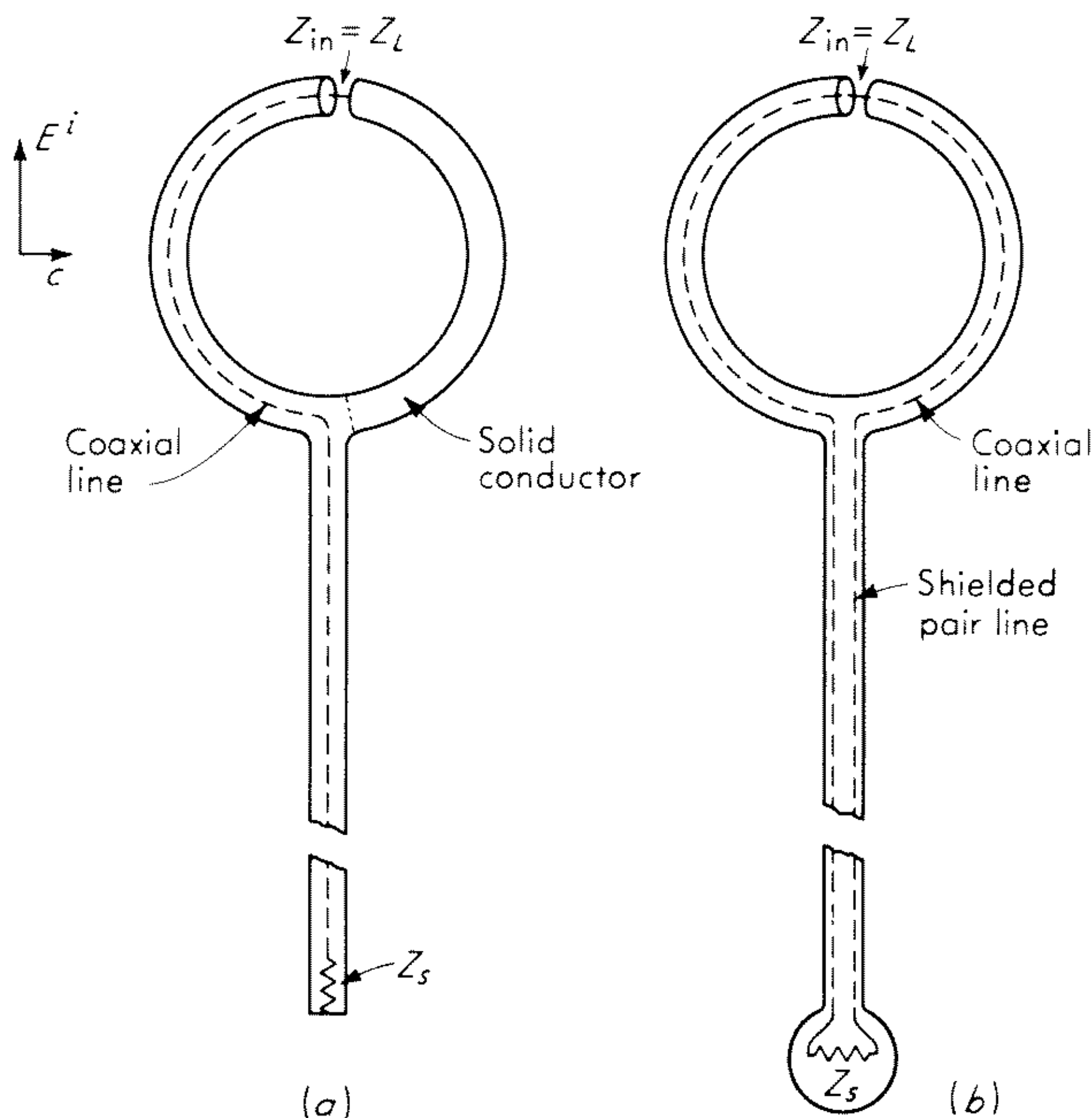


Fig. 11.8 (a) Shielded loop with coaxial transmission line to load. (b) Shielded loop with shielded pair line to load.

result, the inner and outer surfaces of the coaxial line are completely uncoupled except at the gap where the coaxial line (inner conductor, inner surface of outer conductor) is connected to the loop antenna (outer surface of outer conductor). The input impedance of the coaxial line constitutes the load Z_L for the circular loop antenna.

The arrangement in Fig. 11.7b or the equivalent one in Fig. 11.8 is usually called a shielded loop antenna. Actually, the antenna is not shielded, since it consists of the outer surface of the conductor. The conductor inside the shield is the inner conductor of the coaxial line leading to the load; it is not a part of the receiving antenna proper.

An important application of the loop antenna is as a direction finder. The sharp null in the field pattern at $\theta = 0, \pi$ is conveniently used for this purpose. Note, however, that when $\theta = 0, \pi$ and $\psi = 0$, the contribution to the field by the dipole mode is independent of θ and given by (11.78) to be

$$\beta h_e(0,0,\phi_i) = \frac{2\pi b\beta}{a_1 + 2a_0} \cos \phi_i \quad (11.82a)$$

Instead of a null, the observed current in the load has a magnitude that is proportional to $\beta h_e(0,0,\phi_i)$. Unless the load is so located that $\phi_i = \pi/2$, a significant error may result. Since the electric field of a distant transmitter transmitting in directions parallel to the surface of the earth tends to be perpendicular to that surface near the earth, the location of the load at the top

or bottom of the antenna is desirable as in Fig. 11.8*a* and *b*. In the circuits shown in these figures, the dipole mode is likely to have much greater amplitudes than if determined by the size of the loop alone. In these cases it is excited on the full length of the vertical shield. The analysis of the multiturn loop, both unshielded and shielded, has been made with the aid of the method of symmetrical components.⁹

11.9 Loop Antennas Coupled to Open-wire Lines

An interesting and useful arrangement for exciting loop antennas in the dipole mode is readily achieved with an adaptation of the method described in Secs. 9.14 to 9.18 for dipoles. It consists simply in locating the loops — they may be square or circular — as shown in Fig. 11.9 with a two- or four-wire line

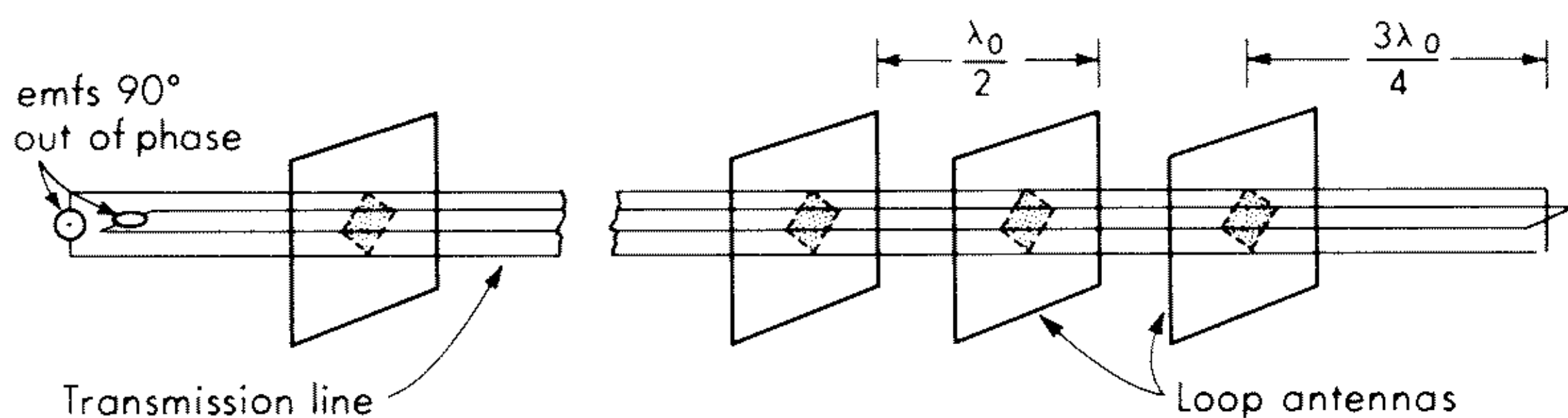


Fig. 11.9 End-fire array of loops coupled to a four-wire line.

extended parallel to the common axis. Each two-wire line excites the loops in a dipole mode as shown in Fig. 11.10. The induced current has a maximum when the loop is resonant with a circumference near a wavelength. Near resonance the distribution of current in a square loop with side $2h = \lambda_0/4$ is quite well approximated by the zero-order value

$$[I_{1x}(x)]_0 = [I_{2x}(x)]_0 = C \cos k_0 x \quad (11.82b)$$

$$[I_{2y}(y)]_0 = -[I_{4y}(y)]_0 = C \sin k_0 y \quad (11.82c)$$

where the amplitude C is a fairly complicated function of the dimension of the loop and the size of the wire.¹⁰ The relative amplitude of the current induced in a square loop as a function of the length of its side in radius $2k_0 h$ is shown in Fig. 11.11 for both the zero-order theory and a first-order theory.¹⁰ Agreement with experiment is seen to be reasonably good.

When the loop is coupled to a four-wire line in the manner shown in Fig. 11.9 and the two mutually perpendicular lines are driven with their currents 90° out of phase, the induced current has the simple zero-order form

$$[I_s(s)]_0 = C e^{jk_0 s} \quad (11.83)$$

where s is measured around the loop.

The field maintained by an array of loops arranged as in Fig. 11.9 has an end-fire pattern. When the loops are excited by a two-wire line, the field is circularly polarized; when excited by a four-wire line with the currents in the

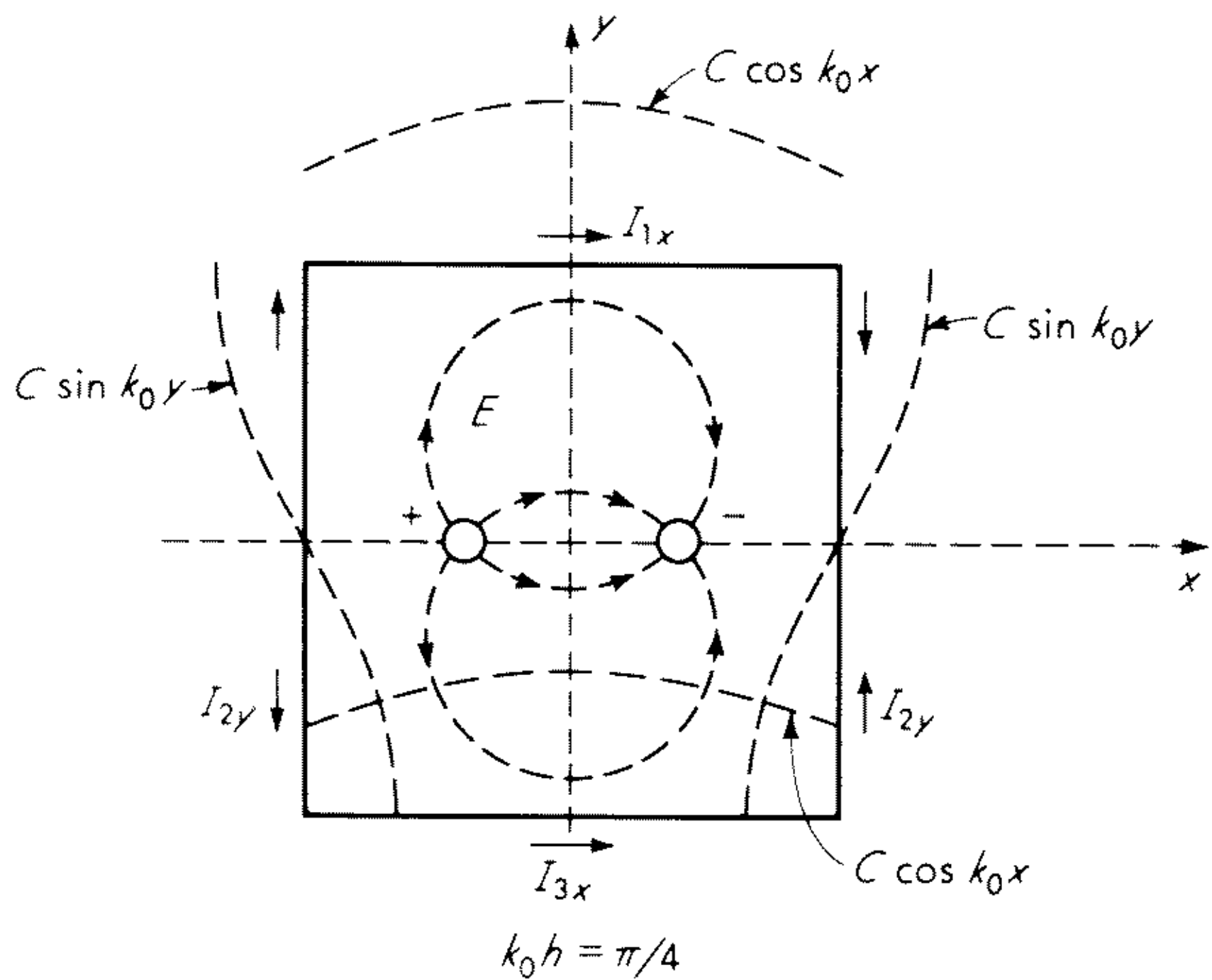


Fig. 11.10 Currents excited in square loop by currents and charges in two-wire line.

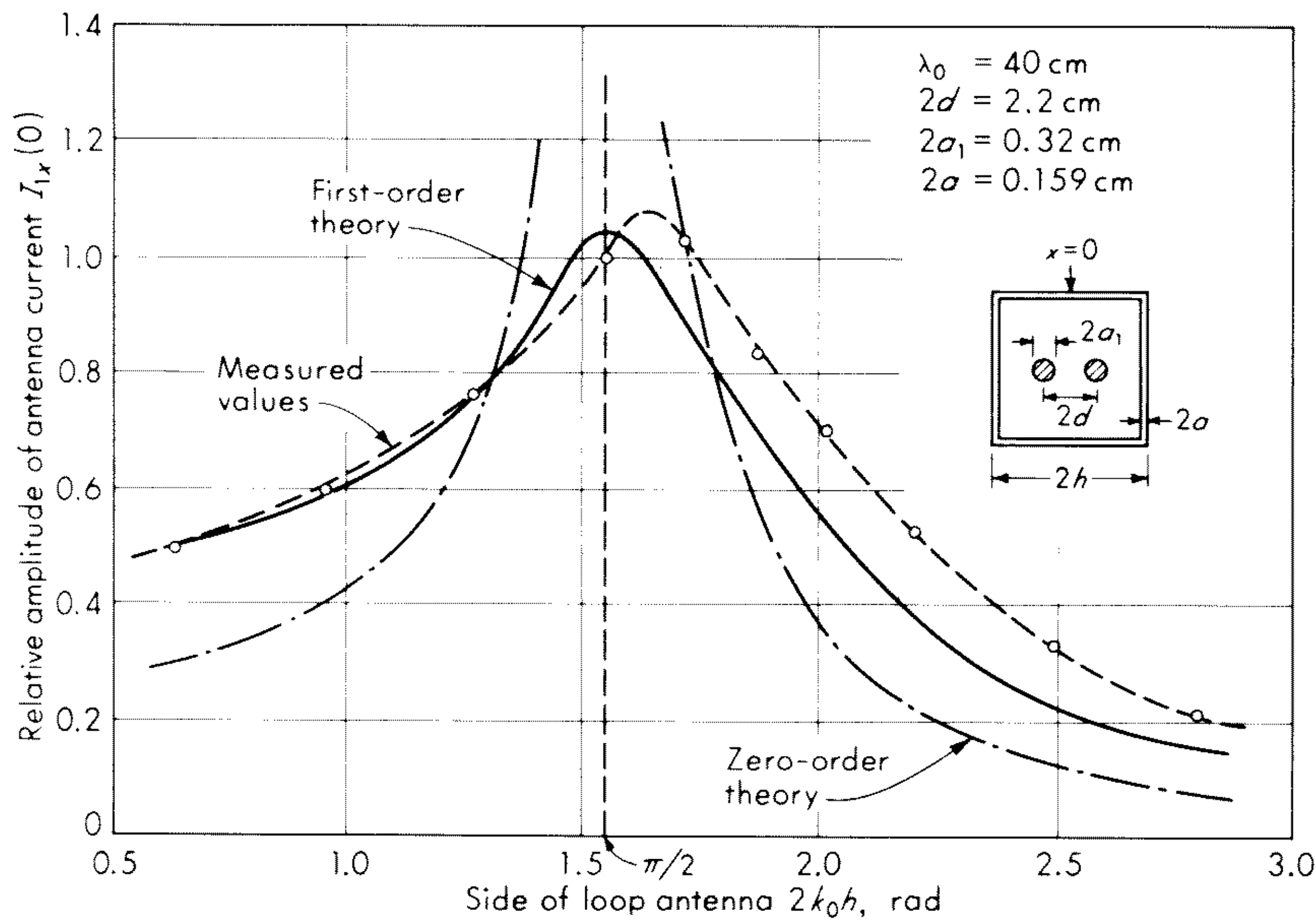


Fig. 11.11 Antenna current at $x = 0$ as a function of antenna size.

diagonally opposite pairs 90° out of phase, the field is circularly polarized in the forward direction.

PROBLEMS

11.1 Carry out all the steps to obtain (11.2) with (11.3a) to (11.4b). Note that $x' = (b - a + a \cos \psi') \cos \phi'$, $x = b \cos \phi$, $z = 0$, $z' = a \sin \psi'$, $y = b \sin \phi$, $y' = (b - a + a \cos \psi') \sin \phi'$.

- 11.2 Carry out the steps leading to (11.22) beginning with (11.19b) and the approximation $R(\theta) = \sin(\theta/2)$.
- 11.3 Determine the normalized far-zone field of a loop with $k_0 b = 1$, neglecting contributions from terms with $n > 1$. Sketch the current in the loop.
- 11.4 Determine the impedance of a loop with $k_0 b = 0.3$.
- 11.5 Construct the field pattern for a loop with $k_0 b = 0.3$.
- 11.6 Determine the effective length for a loop with $\beta b = 0.3$, $\Omega = 12$ when immersed in air and in a dissipative medium for which $\alpha/\beta = 0.05$ and 0.3 . Sketch curves that show the directional properties of the loop.
- 11.7 The operation of the shielded loop antenna in the form shown in Fig. 11.8b is sometimes explained by treating the inner conductor of the coaxial line as the antenna and stating that it is shielded from the electric field but not from the magnetic field. Show that this is incorrect.

REFERENCES

1. Hallén, E.: Theoretical Investigations into the Transmitting and Receiving Qualities of Antennae, *Nova Acta Regiae Soc. Sci. Upsalensis*, vol. 11, no. 4, 1938.
2. Storer, J. E.: Impedance of Thin Wire Antennas, *Trans. AIEE*, vol. 75, pp. 606–619, 1956.
3. Wu, T. T.: Theory of the Thin Circular Antenna, *J. Math. Phys.*, vol. 3, pp. 1301–1304, 1962.
4. Watson, G. N.: "Theory of Bessel Functions," p. 444, The Macmillan Company, New York, 1945.
5. See, for example, R. W. P. King, "Fundamental Electromagnetic Theory," Appendix II, Dover Publications, Inc., New York, 1963.
6. Wu, T. T., and R. W. P. King: Driving Point and Input Admittance of Linear Antennas, *J. Appl. Phys.*, vol. 30, pp. 74–76, 1959.
7. Duncan, R. H., and F. H. Hinchey: Cylindrical Antenna Theory, *J. Res. Natl. Bur. Std.*, vol. 64D, pp. 569–584, 1960.
8. King, R. W. P., C. W. Harrison, Jr., and D. G. Tingley: The Admittance of Bare Circular Loop Antennas in a Dissipative Medium, *IEEE Trans. Antennas Propagation*, vol. AP-12, pp. 434–438, 1964. More extensive tables are in *Cruft Lab. Tech. Rept.* 419, Harvard University, August, 1963.
9. Padhi, T.: Theory of Coil Antennas, *Cruft Lab. Tech. Rept.* 442, Harvard University, July, 1964.
10. Chen, K. M., and R. W. P. King: A Loop Antenna Coupled to a Four-wire Line, *Inst. Elec. Engrs. (London) Monograph* 462E, July, 1961, published in *Proc. Inst. Elec. Engrs. (London)*, vol. 109, part C, pp. 55–62, 1962.

CHAPTER 12

ELECTROMAGNETIC RADIATION FROM CONICAL STRUCTURES

James R. Wait

12.1 Introduction

An important class of boundary-value problems involves conically shaped regions. The best known of these is the symmetrically excited biconical antenna which is surrounded by free space. Notable contributions to this problem have been made by Schelkunoff,^{1,2} Papas,^{3,4} Smith,⁵ and Tai.⁶⁻⁸ In this chapter, some of this work is reviewed and some recent extensions to the theory are discussed. More recent work dealing with conical plasma sheaths is also described.

We consider, mainly, problems which have symmetry about a polar axis. Furthermore, we shall restrict attention to waves which are purely transverse magnetic (TM). In this case, the fields may be derived entirely from an electric Hertz vector which has only a radial component of magnitude rU . Thus, for a homogeneous region with dielectric constant ϵ and permeability μ , the non-vanishing field components in spherical coordinates (r, θ, ϕ) are to be obtained from

$$E_r = \frac{1}{j\epsilon\omega} \left(k^2 + \frac{\partial^2}{\partial r^2} \right) U \quad (12.1)$$

$$E_\theta = \frac{1}{j\epsilon\omega r} \frac{\partial^2 U}{\partial r \partial \theta} \quad (12.2)$$

$$H_\phi = -\frac{1}{r} \frac{\partial U}{\partial \theta} \quad (12.3)$$

where the time factor has been taken as $\exp(j\omega t)$. The scalar quantity U is often described in the literature as a Debye potential. In a source-free homogeneous region, it satisfies

$$(\nabla^2 + k^2) \left(\frac{U}{r} \right) = 0 \quad (12.4)$$

where $k = (\epsilon\mu)^{1/2}\omega$.

Following the well-known separation-of-variables scheme, we write

$$U = R(r)T(\theta) \quad (12.5)$$

where R and T are functions of r and θ , respectively. Thus, it is evident from (12.4) that

$$\frac{d^2 R}{dr^2} + \left[k^2 - \frac{\nu(\nu + 1)}{r^2} \right] R = 0 \quad (12.6)$$

and
$$\sin \theta \frac{d^2 T}{d\theta^2} + \cos \theta \frac{dT}{d\theta} + \nu(\nu + 1) (\sin \theta) T = 0 \quad (12.7)$$

where $\nu(\nu + 1)$ is a separation constant.

Solutions of (12.6) are conveniently written

$$R = A_\nu \hat{J}_\nu(kr) + B_\nu \hat{H}_\nu(kr) \quad (12.8)$$

where \hat{J}_ν and \hat{H}_ν are spherical-type Bessel and Hankel functions, respectively. The latter are defined by

$$\hat{J}_\nu(x) = \left(\frac{\pi x}{2} \right)^{1/2} J_{\nu+1/2}(x) \quad (12.9)$$

and
$$\hat{H}_\nu(x) = \left(\frac{\pi x}{2} \right)^{1/2} H_{\nu+1/2}^{(2)}(x) \quad (12.10)$$

where $J_{\nu+1/2}(x)$ and $H_{\nu+1/2}^{(2)}(x)$ are the Bessel function and the Hankel function (of the second kind) as conventionally defined.

When ν is not an integer, we may write solutions of (12.7) in the following form:

$$T = C_\nu P_\nu(\cos \theta) + D_\nu P_\nu(-\cos \theta) \quad (12.11)$$

where P_ν is the Legendre function of order ν . It might be mentioned that $P_\nu(\cos \theta)$ is unity for $\theta = 0$, whereas $P_\nu(-\cos \theta)$ is logarithmically infinite there.

12.2 General Equations for Biconical Structures

To be specific, we now consider a symmetrical biconical antenna, as indicated in Fig. 12.1. The perfectly conducting antenna is defined by the conical

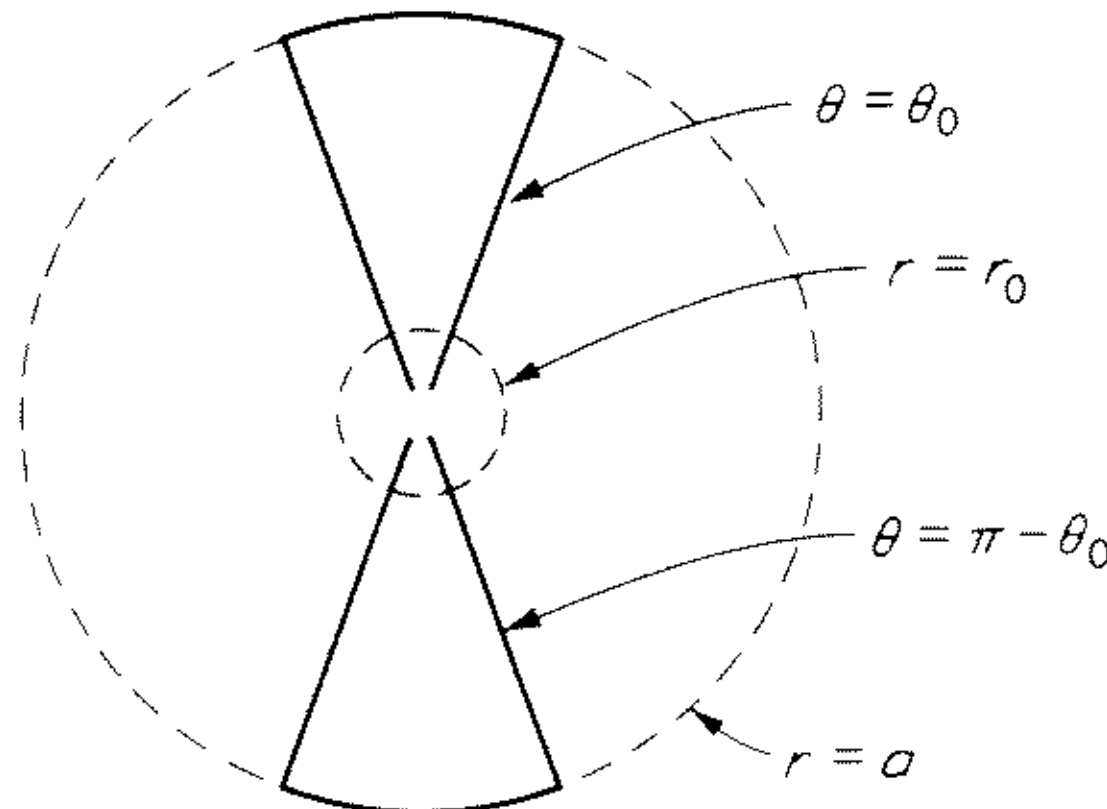


Fig. 12.1 Biconical structure showing divisions between input, antenna, and output regions.

surfaces $\theta = \theta_0$ and $\theta = \pi - \theta_0$, and the spherical end surfaces are at $r = a$. The antenna is to be fed in the apex region which is contained within $r < r_0$. The precise manner in which the generator is connected to the antenna need not be stated. Suffice it to say that E_θ is to be specified at the boundary $r = r_0$ of the "input region."

To construct the appropriate form of the solution in the "antenna region" $r_0 < r < a$, we draw on some useful analogies with transmission line theory. From (12.2) we note that

$$rE_\theta = -\frac{\partial\Phi}{\partial\theta} \quad (12.12)$$

where Φ is a scalar potential related to U by

$$\Phi = -\frac{1}{j\epsilon\omega} \frac{\partial U}{\partial r} \quad (12.13)$$

It is now readily verified that Φ and U satisfy the following coupled equations:

$$\frac{\partial\Phi}{\partial r} = -\left[j\mu\omega + \frac{\nu(\nu+1)}{j\epsilon\omega r^2}\right]U \quad (12.14)$$

and
$$\frac{\partial U}{\partial r} = -j\epsilon\omega\Phi \quad (12.15)$$

It is evident that Φ and U are analogous to the voltage v and current i , respectively, on a transmission line of series impedance Z per unit length and shunt admittance Y per unit length. Thus (12.14) and (12.15) are equivalent to the pair

$$\frac{\partial v}{\partial r} = -Zi \quad (12.16)$$

and
$$\frac{\partial i}{\partial r} = -Yv \quad (12.17)$$

if
$$Z = j\mu\omega + \frac{\nu(\nu+1)}{j\epsilon\omega r^2} \quad (12.18)$$

and
$$Y = j\epsilon\omega \quad (12.19)$$

The fields associated with (12.14) and (12.15) are transverse magnetic waves, in general. However, if $\nu = 0$, the waves are purely transverse electromagnetic (TEM). In the latter case, it is evident from (12.6) and (12.7) that

$$U = R_0 T_0 \quad (12.20)$$

where
$$R_0 = A_0 e^{-jkr} + B_0 e^{jkr} \quad (12.21)$$

and
$$T_0 = C \ln\left(\cot\frac{\theta}{2}\right) + D \quad (12.22)$$

where A_0 , B_0 , C , and D are constants. The voltage $V(r)$ is now defined as

$$V(r) = -\int_{\pi-\theta_0}^{\theta_0} E_{0,\theta} r d\theta \quad (12.23)$$

where
$$E_{0,\theta} = -\frac{1}{r} \frac{\partial \Phi_0}{\partial \theta} \quad \text{and} \quad \Phi_0 = -\frac{1}{j\epsilon\omega} \frac{\partial}{\partial r} (R_0 T_0) \quad (12.24)$$

On the other hand, the antenna current $I(r)$ is to be obtained from

$$I(r) = 2\pi r \sin \theta_0 H_\phi(r, \theta_0) \quad (12.25)$$

This is written as the sum of two parts in the manner

$$I(r) = I_0(r) + \tilde{I}(r) \quad (12.26)$$

where $I_0(r)$ is associated with the TEM waves and $\tilde{I}(r)$ is the contribution from the additional TM waves excited on the antenna structure.

If we define a terminating admittance Y_t by

$$Y_t = \frac{I_0(a)}{V(a)} \quad (12.27)$$

it is now a very straightforward matter to show that

$$KI_0(r) = V(a)[j \sin k(a-r) + KY_t \cos k(a-r)] \quad (12.28)$$

$$V(r) = V(a)[\cos k(a-r) + jKY_t \sin k(a-r)] \quad (12.29)$$

where
$$K = (\zeta/\pi) \ln \cot \frac{\theta_0}{2} \quad \text{and} \quad \zeta = \left(\frac{\mu}{\epsilon}\right)^{1/2} \quad (12.30)$$

The quantity K is the characteristic impedance of the biconical structure for the TEM mode.

If the impressed field E_θ at $r = r_0$ is an even function of θ , it is evident from (12.2) that the combination T , given by (12.11), must be an odd function of θ . Thus, we choose

$$T = T_\nu(\cos \theta) = \frac{1}{2}[P_\nu(\cos \theta) - P_\nu(-\cos \theta)] \quad (12.31)$$

which has the required property.

The total fields in the antenna region $r_0 < r < a$ may now be written

$$r^2 E_r = -\frac{1}{2\pi j\epsilon\omega} \sum_\nu A_\nu \frac{\hat{R}_\nu(kr)}{\hat{R}_\nu(ka)} T_\nu(\cos \theta) \quad (12.32)$$

$$r E_\theta = \frac{\zeta V(r)}{2\pi K \sin \theta} + j \frac{\zeta}{2\pi} \sum_\nu \frac{A_\nu}{\nu(\nu+1)} \frac{\hat{R}'_\nu(kr)}{\hat{R}_\nu(ka)} \frac{d}{d\theta} T_\nu(\cos \theta) \quad (12.33)$$

$$r H_\phi = \frac{I_0(r)}{2\pi \sin \theta} + \frac{1}{2\pi} \sum_\nu \frac{A_\nu}{\nu(\nu+1)} \frac{\hat{R}_\nu(kr)}{\hat{R}_\nu(ka)} \frac{d}{d\theta} T_\nu(\cos \theta) \quad (12.34)$$

where $\hat{R}_\nu(x) = \hat{J}_\nu(x) + (B_\nu/A_\nu)\hat{H}_\nu(x)$ and $\hat{R}'_\nu(x) = d\hat{R}_\nu(x)/dx$. The boundary condition $E_r = 0$ on $\theta = \theta_0$ and $\theta = \pi - \theta_0$ leads to the condition

$$T_\nu(\cos \theta_0) = 0 \quad (12.35)$$

which determines an infinite sequence of discrete values of ν . The summation

sign in (12.32) to (12.34) indicates that contributions from all these roots must be included in the formulation. Of course, as indicated, the TEM wave corresponding to the first term in (12.33) and (12.34) must also be included.

It is important to note that the transverse voltage $V(r)$ defined above by (12.23) is also given by

$$V(r) = - \int_{\pi-\theta_0}^{\theta_0} r E_\theta d\theta \quad (12.36)$$

for $r_0 < r < a$, where E_θ is given by (12.33). In other words, only the principal or TEM mode contributes to the transverse voltage. This is a consequence of the boundary condition (12.35), which means that

$$\int_{\pi-\theta_0}^{\theta_0} (E_\theta - E_{0,\theta}) d\theta = 0 \quad (12.37)$$

On the other hand, as indicated by (12.26), the total current has a contribution I_0 both from the TEM mode and from the “complementary” modes. From (12.25) and (12.34) it is evident that

$$\tilde{I}(r) = \sin \theta_0 \sum_{\nu} \frac{A_{\nu}}{\nu(\nu+1)} \frac{\hat{R}_{\nu}(kr)}{\hat{R}_{\nu}(ka)} \left[\frac{d}{d\theta} T_{\nu}(\cos \theta) \right]_{\theta=\theta_0} \quad (12.38)$$

The input admittance Y_i of the antenna is now defined by

$$Y_i = \frac{I(r_0)}{V(r_0)} = \frac{I_0(r_0)}{V(r_0)} + \frac{\tilde{I}(r_0)}{V(r_0)} \quad (12.39)$$

When the radius r_0 of the input region approaches zero, it follows, in view of the required finiteness of $\tilde{I}(r_0)$, that $\hat{R}_{\nu}(kr)$ must also remain finite. Clearly, this means that $B_{\nu} = 0$ in (12.8). Thus, the \hat{R}_{ν} functions are to be replaced by \hat{J}_{ν} in (12.32), (12.33), (12.34), and (12.38) when the dimensions of the input region are vanishingly small. In most of what follows, we shall tacitly assume this to be the case.

In the region external to the antenna (that is, $r > a$), the fields are also of the TM type. However, here the angular functions must be periodic and finite for all values of θ from 0 to 2π . Thus, the solution of (12.7) is of the form $T = P_{\nu}(\cos \theta)$, where $\nu = n$ is an odd integer.[†] Furthermore, the radial function which is a solution of (12.6) must be of the type

$$R = \hat{H}_n(kr)$$

which has the required property that

$$R \rightarrow e^{-jkr} \quad \text{for} \quad r \rightarrow \infty$$

[†]As indicated later on, the even integers will be present in the summation when the biconical structure is asymmetrical.

In the region external to the antenna, we have a set of field expressions analogous to (12.32) to (12.34). Thus,

$$r^2 E_r = -\frac{1}{2\pi j \epsilon \omega} \sum_{n=1,3,5,\dots} a_n \frac{\hat{H}_n(kr)}{\hat{H}_n(ka)} P_n(\cos \theta) \quad (12.40)$$

$$r E_\theta = j \frac{\zeta}{2\pi} \sum_{n=1,3,5,\dots} \frac{a_n}{n(n+1)} \frac{\hat{H}'_n(kr)}{\hat{H}_n(ka)} \frac{d}{d\theta} P_n(\cos \theta) \quad (12.41)$$

$$r H_\phi = \frac{1}{2\pi} \sum_{n=1,3,5,\dots} \frac{a_n}{n(n+1)} \frac{\hat{H}_n(kr)}{\hat{H}_n(ka)} \frac{d}{d\theta} P_n(\cos \theta) \quad (12.42)$$

Of course, there is no TEM mode in the external region.

12.3 The Formal Solution of the Biconical Antenna Problem

The coefficients A_ν and a_n are not yet known. Their determination is a relatively difficult task, because the ranges of orthogonality are different for the two regions $r < a$ and $r > a$. However, formally, we may proceed as follows. First, we note that, at $r = a$, (12.34) may be written

$$r H_\phi(a, \theta) = \frac{Y_t V(a)}{2\pi \sin \theta} + \frac{1}{2\pi} \sum_\nu \frac{A_\nu}{\nu(\nu+1)} \frac{d}{d\theta} T_\nu(\cos \theta) \quad (12.43)$$

Both sides of this equation are now multiplied by $\sin \theta (d/d\theta) T_{\nu'}(\cos \theta)$, and then they are integrated over θ from θ_0 to $\pi - \theta_0$. It then follows readily that

$$A_\nu = \frac{2\pi \nu(\nu+1)}{N_\nu} \int_{\theta_0}^{\pi-\theta_0} a H_\phi(a, \theta) \sin \theta \frac{d}{d\theta} T_\nu(\cos \theta) d\theta \quad (12.44)$$

where we have used the fact that

$$\int_{\theta_0}^{\pi-\theta_0} \sin \theta \left[\frac{d}{d\theta} T_\nu(\cos \theta) \right] \left[\frac{d}{d\theta} T_{\nu'}(\cos \theta) \right] d\theta = \begin{cases} 0 & \text{if } \nu \neq \nu' \\ N_\nu & \text{if } \nu = \nu' \end{cases}$$

But, according to (12.41),

$$a H_\phi(a, \theta) = \frac{1}{2\pi} \sum_{n=1,3,5,\dots} \frac{a_n}{n(n+1)} \frac{d}{d\theta} P_n(\cos \theta) \quad (12.45)$$

Inserting (12.45) into (12.44), it readily follows that the result is an infinite system of linear equations of the form

$$A_\nu = \sum_{n=1,3,5,\dots} \alpha_{\nu,n} a_n \quad (12.46)$$

where

$$\alpha_{\nu,n} = \frac{\nu(\nu+1)}{n(n+1)} \frac{1}{N_\nu} \int_{\theta_0}^{\pi-\theta_0} \sin \theta \left[\frac{d}{d\theta} T_\nu(\cos \theta) \right] \left[\frac{d}{d\theta} P_n(\cos \theta) \right] d\theta \quad (12.47)$$

This expression may be simplified by integrating by parts and noting that, for any θ ,

$$\frac{d}{d\theta} \sin \theta \frac{dT_\nu}{d\theta} = -\nu(\nu + 1) \sin \theta T_\nu \quad (12.48)$$

and
$$\frac{d}{d\theta} \sin \theta \frac{dP_n}{d\theta} = -n(n + 1) \sin \theta P_n \quad (12.49)$$

while for $\theta = \theta_0$,

$$T_\nu(\cos \theta_0) = T_\nu(-\cos \theta_0) = 0 \quad (12.50)$$

Thus,

$$\alpha_{\nu,n} = \frac{\nu(\nu + 1)}{N_\nu} \int_{\theta_0}^{\pi-\theta_0} T_\nu(\cos \theta) P_n(\cos \theta) \sin \theta d\theta \quad (12.51)$$

Now, for any θ it may be also readily verified from (12.48) and (12.49) that

$$\begin{aligned} [\nu(\nu + 1) - n(n + 1)] \int T_\nu(\cos \theta) P_n(\cos \theta) \sin \theta d\theta \\ = \sin \theta \left(T_\nu \frac{d}{d\theta} P_n - P_n \frac{d}{d\theta} T_\nu \right) \end{aligned} \quad (12.52)$$

Then, of course, we also have

$$\begin{aligned} [\nu(\nu + 1) - \nu'(\nu' + 1)] \int T_\nu(\cos \theta) T_{\nu'}(\cos \theta) \sin \theta d\theta \\ = \sin \theta \left(T_\nu \frac{d}{d\theta} T_{\nu'} - T_{\nu'} \frac{d}{d\theta} T_\nu \right) \end{aligned} \quad (12.53)$$

Letting $\nu \rightarrow \nu'$, the preceding result, along with (12.48), is used to show that

$$\begin{aligned} \int \left[\frac{d}{d\theta} T_\nu(\cos \theta) \right]^2 \sin \theta d\theta &= \nu(\nu + 1) \int [T_\nu(\cos \theta)]^2 \sin \theta d\theta \\ &= \sin \theta \frac{\nu(\nu + 1)}{2\nu + 1} \left[\frac{\partial T_\nu}{\partial \theta} \frac{\partial T_\nu}{\partial \nu} - T_\nu \frac{\partial^2 T_\nu}{\partial \theta \partial \nu} \right] \end{aligned} \quad (12.54)$$

Using (12.52) and (12.53), the coefficient $\alpha_{\nu,n}$, given by (12.51), is now

$$\alpha_{\nu,n} = \frac{2\nu + 1}{n(n + 1) - \nu(\nu + 1)} \frac{P_n(\cos \theta_0)}{\partial T_\nu(\cos \theta_0) / \partial \nu} \quad (12.55)$$

which is the coefficient for the system (12.46). Another system of equations connecting the coefficients is obtained by working with the E_θ component in the aperture surface $r = a$.

From (12.33) it is evident that $aE_\theta(a, \theta) = 0$ for $0 < \theta < \theta_0$ and $\pi - \theta_0 < \theta < \pi$, and

$$aE_\theta(a, \theta) = \frac{jV(a)}{2\pi K \sin \theta} - \frac{1}{2\pi} \sum_\nu \frac{A_\nu}{\nu(\nu + 1)} Z_\nu^- \frac{d}{d\theta} T_\nu(\cos \theta) \quad (12.56)$$

for $\pi - \theta_0 > \theta > \theta_0$, where

$$Z_\nu^- = -j\zeta \frac{\hat{R}'_\nu(ka)}{\hat{R}_\nu(ka)} \quad (12.57)$$

is an inward-looking radial wave impedance. On the other hand, from (12.41), it follows that

$$aE_\theta(a, \theta) = \frac{1}{2\pi} \sum_{n=1,3,5,\dots} \frac{a_n}{n(n+1)} Z_n^+ \frac{d}{d\theta} P_n(\cos \theta) \quad (12.58)$$

for $0 \leq \theta \leq \pi$, where

$$Z_n^+ = j\zeta \frac{\hat{H}'_n(ka)}{\hat{H}_n(ka)} \quad (12.59)$$

is an outward-looking radial wave impedance at the aperture surface.

Using the orthogonality relationship that

$$\int_0^\pi \frac{d}{d\theta} P_n(\cos \theta) \frac{d}{d\theta} P_{n'}(\cos \theta) \sin \theta d\theta = \begin{cases} \frac{2n+1}{2n(n+1)} & \text{for } n = n' \\ 0 & \text{for } n \neq n' \end{cases} \quad (12.60)$$

it readily follows that

$$a_n = \frac{(2n+1)\pi a}{Z_n^+} \int_0^\pi E_\theta(a, \theta) \frac{d}{d\theta} P_n(\cos \theta) d\theta \quad (12.61)$$

Substituting $E_\theta(a, \theta)$ as given by (12.56) into (12.61), it is found that

$$Z_n^+ a_n = -\frac{(2n+1)\zeta V(a)}{K} P_n(\cos \theta_0) + \sum_\nu Z_\nu^- \beta_{\nu,n} A_\nu \quad (12.62)$$

where
$$\beta_{\nu,n} = \frac{n(n+1)}{\nu(\nu+1)} \frac{(2n+1) \sin \theta_0 P_n(\cos \theta_0) dT_\nu(\cos \theta_0)/d\theta_0}{n(n+1) - \nu(\nu+1)} \quad (12.63)$$

In principle, the problem is solvable, since the coefficients a_n and A_ν may be determined by the linear systems of equations given by (12.46) and (12.62). As indicated in the appendix, this final step is a very difficult task; fortunately, however, some simplifications are possible in special cases. These will be discussed below after we make some further general remarks about the formulas for the admittance.

As indicated by (12.28) and (12.29), the terminating admittance Y_t plays a fundamental role. In fact, these two equations show that (12.39) for the antenna admittance Y_i may be expressed in the form

$$Y_i = \frac{\tilde{I}(r_0)}{V(r_0)} + \frac{KY_t \cos k(a - r_0) + j \sin k(a - r_0)}{\cos k(a - r_0) + jKY_t \sin k(a - r_0)} \quad (12.64)$$

When the radius r_0 of the input region is vanishingly small, we have

$$Y_i = \frac{KY_t \cos ka + j \sin ka}{\cos ka + jKY_t \sin ka}$$

A convenient parameter, often used in the theory, is the *inverse radiation impedance* Z_v , which is the impedance seen looking outward at a distance $\lambda/4$ from the end of the line. Thus,

$$Z_v = K^2 Y_t$$

and, therefore,
$$Y_i = \frac{1}{K} \frac{K \cos ka + jZ_v \sin ka}{Z_v \cos ka + jK \sin ka} \quad (12.65)$$

which expresses the antenna input admittance in terms of the inverse radiation impedance.

From (12.43) we readily find that

$$Z_v = K^2 Y_i = \frac{\zeta K a}{V(a)} \int_{\theta_0}^{\pi-\theta_0} H_\phi(a, \theta) d\theta \quad (12.66)$$

and then using (12.45), the above is easily expressed in the form

$$Z_v = -\frac{\zeta K}{\pi V(a)} \sum_{n=1,3,5,\dots} \frac{a_n}{n(n+1)} P_n(\cos \theta_0) \quad (12.67)$$

This is a convenient formula for calculating Z_v once the coefficients a_n have been determined.

12.4 Spherical Antenna as a Limiting Case

An important limiting case is when the cone angle θ_0 approaches $\pi/2$. In this case, we have a symmetrical spherical antenna excited by a narrow equatorial gap. To discuss this case we introduce some approximate formulas for the Legendre functions which have been given by Schelkunoff.¹ Provided θ_0 is not near 0 or π ,

$$P_\nu(\cos \theta_0) \approx \frac{\cos(q\theta_0 - \pi/4)}{[(\pi/2)p \sin \theta_0]^{1/2}} \quad (12.68a)$$

and
$$P_\nu(-\cos \theta_0) \approx \frac{\cos(q\pi - q\theta_0 - \pi/4)}{[(\pi/2)p \sin \theta_0]^{1/2}} \quad (12.68b)$$

where $p = [\nu(\nu + 1)]^{1/2}$ and $q = [(\nu + 1/2)^2 + 1/4]^{1/2}$

Thus,

$$T_\nu(\cos \theta_0) \approx \frac{\sin(q\pi/2 - \pi/2) \sin q(\pi/2 - \theta_0)}{[(\pi/2)p \sin \theta_0]^{1/2}} \quad (12.69)$$

The roots of the equation $T_\nu(\cos \theta_0) = 0$ are thus obtained approximately from

$$q = \frac{2m\pi}{\pi - 2\theta_0} \quad m = 1, 2, 3, \dots \quad (12.70)$$

or
$$\nu = -1/2 + (q^2 - 1/4)^{1/2} = -1/2 + q - \frac{1}{8q} - \frac{1}{128q^3}$$

These roots approach infinity as $\theta_0 \rightarrow \pi/2$.

In terms of the gap width s , we see that

$$q = \frac{2m\pi a}{s}$$

and the roots are

$$\nu \approx \frac{2m\pi a}{s} - \frac{1}{2} - \frac{s}{16m\pi a} - \dots$$

Thus, for small gap widths

$$Z_{\nu}^{-} = -j\zeta \frac{\hat{J}'_{\nu}(ka)}{\hat{J}_{\nu}(ka)} \approx \frac{j\zeta(\nu + 1)}{ka} = \frac{2m\pi}{j\epsilon\omega s} + \frac{1}{j\epsilon\omega a} + \dots \quad (12.71)$$

From this equation, it is evident that the summation on the right-hand side of (12.62) converges very rapidly in this limiting case. In fact, as a first approximation we may neglect the summation altogether, and thus

$$a_n = \frac{-(2n + 1)\zeta V(a)}{KZ_n^{+}} P_n(\cos \theta_0) \quad (12.72)$$

Then, according to (12.67), we find that

$$Z_v = K^2 Y_t = \frac{\zeta^2}{\pi} \sum_{n=1,3,5,\dots} \frac{2n + 1}{n(n + 1)} [P_n(\cos \theta_0)]^2 \frac{1}{Z_n^{+}} \quad (12.73)$$

which corresponds to the situation in which only the principal or TEM mode is retained in the antenna region while all the external modes are used.

For a homogeneous external medium, the reciprocal of the radial wave impedance may be written in the normalized form

$$\frac{\zeta}{Z_n^{+}} = \zeta K_n^{+} = \frac{-j\hat{H}_n(ka)}{\hat{H}'_n(ka)} = \zeta G_n + j\zeta B_n$$

The normalized conductance and susceptance, ζG_n and ζB_n , respectively, are shown plotted in Fig. 12.2 as a function of the radian distance ka for various values of the mode number n . It is evident from these curves that, for small values of ka , only a few modes are needed to secure convergence in (12.73).

Equation (12.73) must be refined if θ_0 is actually allowed to approach $\pi/2$. In this case, Schelkunoff² shows that

$$Y_t = j\omega C_t + \frac{4\pi}{(s/a)^2} \sum_{n=1,3,5,\dots} \frac{2n + 1}{n(n + 1)} \left\{ \frac{(n/2)!}{[(n - 1)/2]!} \right\}^2 \left(\frac{1}{Z_n^{+}} - \frac{j\epsilon\omega a}{k} \right) \quad (12.74)$$

where

$$C_t = 2\epsilon a \left(\ln \frac{a}{s} + 0.52 \right)$$

is the capacitance formed by the hemispheres. The real part of Y_t , as given by (12.73) and (12.74), may be used to calculate the radiation conductance of the symmetrical spherical antenna.

12.5 Thin Wire Antenna as a Limiting Case

Another important limiting case is the vanishingly thin biconical antenna. For example, if $\theta_0 \rightarrow 0$, we see that $K \rightarrow \infty$. In this case, the current distribution is sinusoidal with nodes at the ends. Thus,

$$I(r) \approx jK^{-1}V(a) \sin [k(a - r)] = I_0 \sin [k(a - r)] \quad (12.75)$$

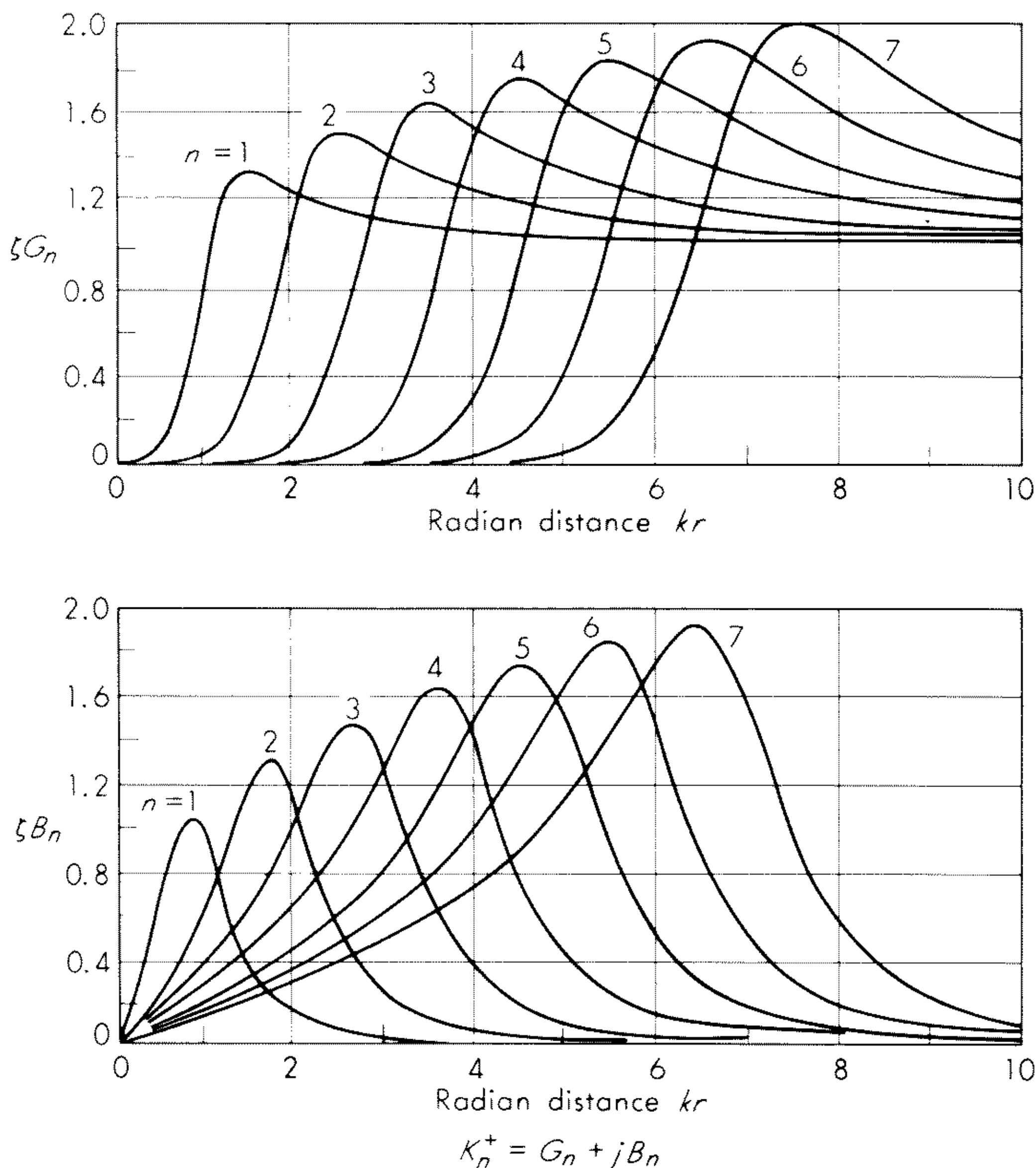


Fig. 12.2 Characteristic wave admittance for outward propagating spherical waves of order n .

The fields produced by this filamental current distribution are well known. Schelkunoff¹ uses this fact to show that, for the infinitesimally thin biconical antenna (that is, $\theta_0 \rightarrow 0$),

$$Ka_n \rightarrow -V(a)(2n + 1)\hat{J}_n(ka)\hat{H}_n(ka) \quad (12.76)$$

Thus, the limiting form of (12.67) for $\theta_0 \rightarrow 0$ is†

$$Z_v = \frac{\zeta}{\pi} \sum_{n=1,3,5,\dots} \frac{2n+1}{n(n+1)} \hat{J}_n(ka)\hat{H}_n(ka) \quad (12.77)$$

An alternative form of this series is well known from the theory of infinitesimally thin antennas. Thus, $Z_v = R_v + jX_v$, where

$$R_v = 60(C + \ln 2L - \text{Ci } 2L) + 30(C + \ln L - 2 \text{Ci } 2L + \text{Ci } 4L) \cos 2L \\ + 30(\text{Si } 4L - 2 \text{Si } 2L) \sin 2L \quad (12.78)$$

and

$$X_v = 60 \text{Si } 2L + 30(\text{Ci } 4L - \ln L - C) \sin 2L - 30 \text{Si } 4L \cos 2L \quad (12.79)$$

†This result also follows immediately from (A-12.9) of the Appendix.

and where

$$L = ka \quad C = 0.5773$$

$$\text{Ci } x = -\int_x^\infty \frac{\cos t}{t} dt \quad \text{Si } x = \int_0^x \frac{\sin t}{t} dt$$

The resistance and reactance functions R_v and X_v are plotted in Fig. 12.3 as a function of the radian length of the cone (that is, ka).

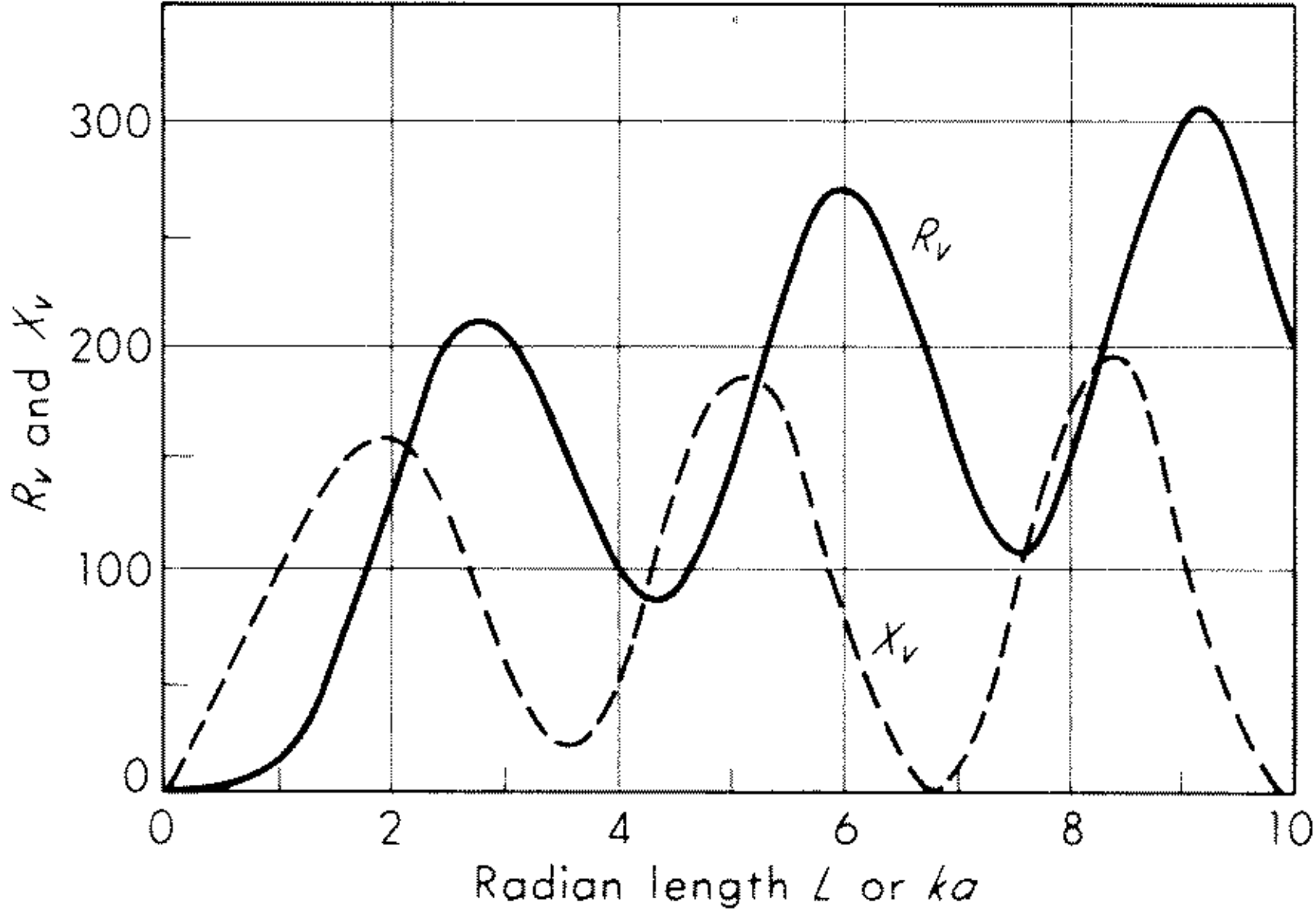


Fig. 12.3 Resistive and reactive parts of the inverse radiation impedance for an infinitesimally thin biconical antenna.

12.6 Variational Treatment of Biconical Antennas

A significant development in the theory of biconical antennas is due to Tai.⁸ He employed a variational method which was originally devised by (Nobel laureate) Julian Schwinger.⁹

The key point in the variational approach is the stationary property of the electric field E_θ in the antenna aperture surface. Thus, instead of determining the terminating admittance Y_t directly, we shall devise an integral equation for E_θ . Then, using this integral equation, we express Y_t in a form which is stationary with respect to small variations of the aperture field.†

The desired variational form is obtained by noting that, for $r = a$, we may write

$$\begin{aligned} \frac{-j\zeta}{2\pi a} \sum_{n=1,3,5,\dots} \frac{a_n}{n(n+1)} M_n P'_n(\theta) \\ = \begin{cases} E_a(\theta) & \text{for } \theta_0 \leq \theta \leq \pi - \theta_0 \\ 0 & \text{for } 0 \leq \theta \leq \theta_0 \text{ and } \pi - \theta_0 \leq \theta \leq \pi \end{cases} \end{aligned} \quad (12.80)$$

or

$$\begin{aligned} \frac{-j\zeta I_0}{2\pi a \sin \theta} - \frac{j\zeta}{2\pi a} \sum_\nu \frac{A_\nu}{\nu(\nu+1)} N_\nu T'_\nu(\theta) \\ = E_a(\theta) \quad \text{for } \theta_0 \leq \theta \leq \pi - \theta_0 \end{aligned} \quad (12.81)$$

†An alternative method is discussed in the Appendix.

where the following abbreviations are employed:

$$\begin{aligned} P'_n(\theta) &= \frac{\partial P_n(\cos \theta)}{\partial \theta} & I_0 &= \frac{V(a)}{K} \\ T'_\nu(\theta) &= \frac{\partial T_\nu(\cos \theta)}{\partial \theta} & E_a(\theta) &= E_\theta(a, \theta) \\ M_n &= \frac{\hat{H}'_n(ka)}{\hat{H}_n(ka)} & \text{and} & N_\nu = \frac{\hat{R}'_\nu(ka)}{\hat{R}_\nu(ka)} \end{aligned}$$

Note that the N_ν used in this section is not the same as that introduced in (12.44). Multiplying (12.80) by $P'_m(\theta) \sin \theta$ and integrating with respect to θ from 0 to π , we find

$$-\frac{j\zeta}{2\pi a} a_m M_m I_{mm} = \int_{\theta_0}^{\pi-\theta_0} E_a(\theta) P'_m(\theta) \sin \theta d\theta \quad (12.82)$$

$$\text{where} \quad I_{mm} = \int_0^\pi P_m^2(\theta) \sin \theta d\theta = \frac{2}{2m+1} \quad m = 1, 3, 5, \dots \quad (12.83)$$

On the other hand, integrating directly both sides of (12.81) with respect to θ from θ_0 to $\pi - \theta_0$ leads to

$$I_0 = \frac{ja}{K} \int_{\theta_0}^{\pi-\theta_0} E_a(\theta) d\theta \quad (12.84)$$

Then, multiplying (12.81) by $T'_\mu(\theta) \sin \theta$ and integrating over the same range, gives

$$A_\mu = \frac{j2\pi a}{\zeta} \frac{1}{N_\mu I_{\mu\mu}} \int_{\theta_0}^{\pi-\theta_0} E_a(\theta) T'_\mu(\theta) \sin \theta d\theta \quad (12.85)$$

$$\text{where} \quad I_{\mu\mu} = \int_{\theta_0}^{\pi-\theta_0} T_\mu^2(\theta) \sin \theta d\theta \quad \mu = \mu_1, \mu_2, \dots \quad (12.86)$$

Here, μ are roots of $T_\mu(\theta_0) = 0$.

We now use the fact that the magnetic field is continuous across the aperture surface $r = a$. This means that

$$\frac{-jKY_t I_0}{2\pi a \sin \theta} - \frac{1}{2\pi a} \sum_\nu \frac{A_\nu}{\nu(\nu+1)} T'_\nu(\theta) = -\frac{1}{2\pi a} \sum_{n=1,3,5,\dots} \frac{a_n}{n(n+1)} P'_n(\theta) \quad (12.87)$$

for $\theta_0 \leq \theta \leq \pi - \theta_0$. Inserting the expressions (12.82), (12.84), and (12.85), for a_n , I_0 , and A_ν , into (12.87), we find that

$$\begin{aligned} \frac{Y_t}{2\pi \sin \theta} \int_{\theta_0}^{\pi-\theta_0} E_a(\theta) d\theta - \frac{j}{\zeta} \sum_\nu \frac{T'_\nu(\theta)}{\nu(\nu+1)N_\nu I_{\nu\nu}} \int_{\theta_0}^{\pi-\theta_0} E_a(\theta) T'_\nu(\theta) \sin \theta d\theta \\ = -\frac{j}{\zeta} \sum_{n=1,3,5,\dots} \frac{P'_n(\theta)}{n(n+1)M_n I_{nn}} \int_{\theta_0}^{\pi-\theta_0} E_a(\theta) P'_n(\theta) \sin \theta d\theta \end{aligned} \quad (12.88)$$

This is the desired integral equation for $E_a(\theta)$. Multiplying it by $\sin \theta E_a(\theta)$, integrating over θ from θ_0 to $\pi - \theta_0$, and, finally, dividing by

$$\left[\int_{\theta_0}^{\pi-\theta_0} E_a(\theta) d\theta \right]^2$$

we obtain

$$Y_t = \frac{j2\pi}{\zeta} \left[\int_{\theta_0}^{\pi-\theta_0} E_a(\theta) d\theta \right]^{-2} \left\{ \sum_{\nu} \frac{1}{\nu(\nu+1)N_{\nu}I_{\nu\nu}} \left[\int_{\theta_0}^{\pi-\theta_0} E_a(\theta) T'_{\nu}(\theta) \sin \theta d\theta \right]^2 - \sum_{n=1,3,5,\dots} \frac{1}{n(n+1)M_n I_{nn}} \left[\int_{\theta_0}^{\pi-\theta_0} E_a(\theta) P'_n(\theta) \sin \theta d\theta \right]^2 \right\} \quad (12.89)$$

The expression for Y_t given above is stationary for small changes of the aperture field E_a . In this sense, it is analogous to the equivalent susceptance in the variational treatment of the discontinuity when two rectangular waveguides of different cross sections are joined. An excellent discussion of waveguide discontinuity problems is found in Collin's book.¹⁰

In Tai's⁸ approach to the variational solution for the biconical antenna, the aperture field $E_a(\theta)$ is written in the form

$$E_a(\theta) = \text{constant} \times \left[\frac{-1}{\sin \theta} + \sum_{\nu} p_{\nu} T'_{\nu}(\theta) \right] \quad (12.90)$$

where p_{ν} are unknown coefficients. This, of course, is the same form as (12.33), but here we need not be concerned with the magnitude of the constant factor, because it cancels out in the evaluation of the admittance function Y_t . Thus, inserting this into (12.89), it is found that

$$Y_t = Y_{t0} + 2 \sum_{\nu} s_{\nu} p_{\nu} + \sum_{\mu} t_{\mu} p_{\mu}^2 + \sum_{\nu} \sum_{\mu} \gamma_{\nu\mu} p_{\nu} p_{\mu} \quad (12.91)$$

where

$$Y_{t0} = \frac{-j\zeta}{\pi K^2} \sum_{n=1,3,5,\dots} \frac{2P_n^2(\cos \theta_0)}{n(n+1)I_{nn}M_n} \quad (12.92)$$

$$s_{\nu} = \frac{-j\zeta}{\pi K^2} \sum_{n=1,3,5,\dots} \frac{P_n(\cos \theta_0) I_{\nu n}}{I_{nn}M_n} \quad (12.93)$$

$$t_{\nu} = \frac{j\zeta}{2\pi K^2} \frac{\nu(\nu+1)I_{\nu\nu}}{N_{\nu}} \quad (12.94)$$

$$\gamma_{\nu\mu} = \gamma_{\mu\nu} = \frac{-j\zeta}{2\pi K^2} \sum_{n=1,3,5,\dots} \frac{n(n+1)I_{\nu n}I_{\mu n}}{I_{nn}M_n} \quad (12.95)$$

$$I_{\nu n} = \int_{\theta_0}^{\pi-\theta_0} P_n(\cos \theta) T_{\nu}(\cos \theta) \sin \theta d\theta \quad (12.96)$$

Now, because Y_t is stationary with respect to the variation $E_a(\theta)$, the coefficients p_{ν} are determined by noting that

$$\frac{\partial Y_t}{\partial p_{\nu}} = 0$$

which gives

$$s_{\nu} + t_{\nu} p_{\nu} + \sum_{\mu} \gamma_{\nu\mu} p_{\mu} = 0 \quad (12.97)$$

When this is combined with (12.91), we find that

$$Y_t = Y_{t0} + \sum_{\nu} s_{\nu} p_{\nu} \quad (12.98)$$

We note that Y_{t0} as given by (12.92) may also be written in the form

$$Y_{t0} = \frac{-j\zeta}{\pi K^2} \sum_{n=1,3,5,\dots} \frac{(2n+1)P_n^2(\cos \theta_0)}{n(n+1)} \frac{\hat{H}_n(ka)}{\hat{H}'_n(ka)} \quad (12.99)$$

which is the expression for the terminating admittance derived on the basis of assuming that the complementary waves in the antenna may be neglected. This is the formula first derived by Smith.⁵ Thus, Y_{t0} is the admittance contributed by the interaction between the principal or TEM wave and all the exterior modes of order $n = 3, 5, 7, \dots$. It is then possible to interpret $s_\nu p_\nu$, in the summation term in (12.98), as an admittance contributed by the interaction between the ν th-order interior mode and all the exterior modes.

Tai,⁸ in a very illuminating development, has shown how the series solution in (12.98) converges to the exact solution for the special case of vanishingly thin cones. In this limit (that is, $\theta_0 \rightarrow 0$) it follows from (12.77) that

$$Y_t = \frac{-j\zeta}{\pi K^2} \sum_{n=1,3,5,\dots} \frac{2n+1}{n(n+1)} \frac{1}{M_n - N_n} \quad (12.100)$$

which is exact. On the other hand, according to the "zero-order" solution indicated by (12.99), we would have

$$Y_{t0} = \frac{-j\zeta}{\pi K^2} \sum_{n=1,3,5,\dots} \frac{2n+1}{n(n+1)} \frac{1}{M_n} \quad (12.101)$$

The "correction terms" for this case are given by

$$\sum_\nu s_\nu p_\nu = \frac{-j\zeta}{\pi K^2} \sum_{n=1,3,5,\dots}^r \frac{2n+1}{n(n+1)} \frac{N_n}{M_n(M_n - N_n)} \quad (12.102)$$

where r is infinite, strictly speaking. For the vanishingly thin cone, the value of r actually corresponds to the order of the solution. For example, in the first-order solution, we take $r = 1$ and there is only one term on the right-hand side of (12.102). On the other hand, the second-order solution amounts to the choice $r = 3$, whence the summation is replaced by only two terms. Similarly, for the third-order solutions $r = 5$ and three terms are included. The manner in which the r th-order solution $Y_t^{(r)}$ converges to the exact solution Y_t is shown in Fig. 12.4, where the real and imaginary parts of $K^2 Y_t^{(r)}$ are plotted for $r = 0, 1, 2$, and 3 along with the exact solution. The abscissa is ka , while the ordinates are $R_\nu = K^2 \operatorname{Re} Y_t^{(r)}$ and $X_\nu = K^2 \operatorname{Im} Y_t^{(r)}$. It is certainly evident here that the zero-order solution is very poor. On the other hand, the first-order solution, which corresponds to the inclusion of only one interior complementary wave, gives a marked improvement.

Application of Tai's variational method⁸ to biconical antennas of arbitrary cone angle is quite straightforward. However, the goodness of the successive approximations can be estimated only from the rate of convergence of the series solution. Furthermore, because of the difficulties in evaluating the fractional-order Bessel functions, only low-order solutions are really feasible. For ex-

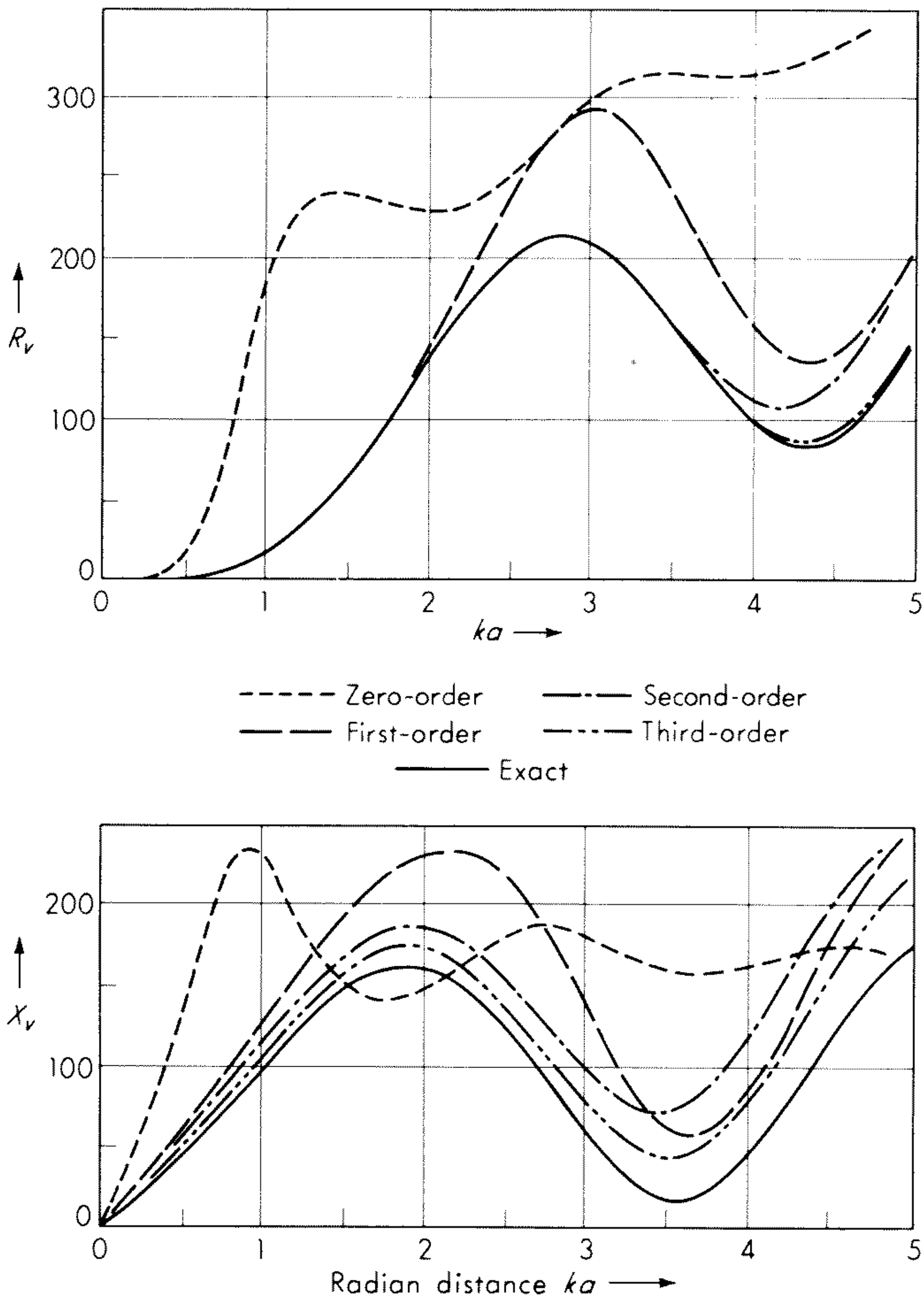


Fig. 12.4 Resistive and reactive parts of the inverse radiation impedance for thin biconical antennas for various orders of approximation. (After Tai.⁸)

ample, the explicit form of the first-order solution applicable to a biconical antenna of any angle is obtained by retaining only one term in the summation over μ in (12.97). Thus, for the first complementary interior mode (denoted $\nu = \nu_1$), we see that

$$p_{\nu_1} = -\frac{s_{\nu_1}}{t_{\nu_1} + \gamma_{\nu_1\nu_1}} \tag{12.103}$$

and thus, to within the same approximation, (12.98) becomes

$$Y_t = Y_{t0} - \frac{(s_{\nu_1})^2}{t_{\nu_1} + \gamma_{\nu_1\nu_1}} \tag{12.104}$$

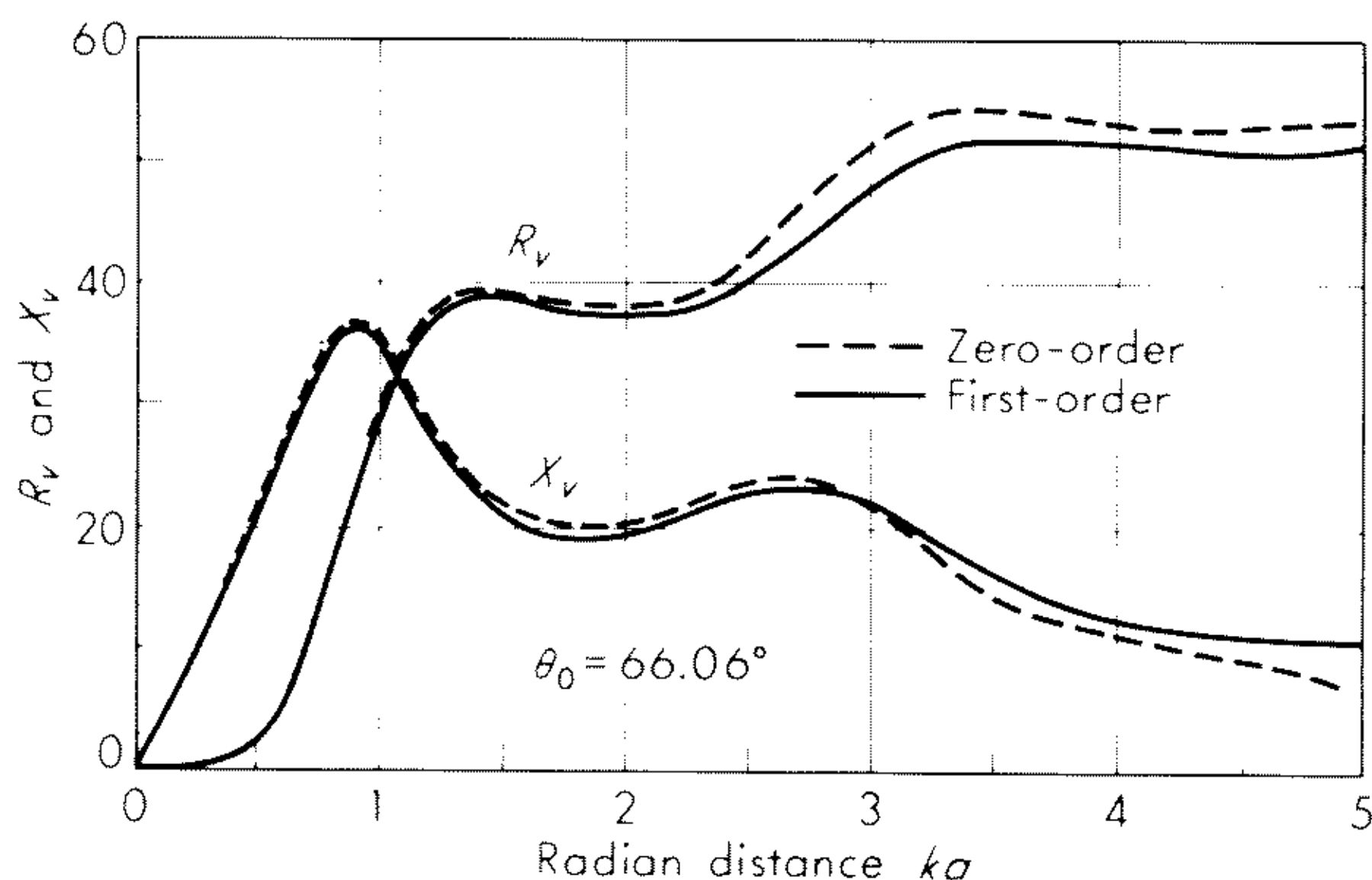


Fig. 12.5 Resistive and reactive parts of the inverse radiation impedance for a wide-angle biconical antenna.

Using this result, curves of R_v and X_v are plotted in Fig. 12.5 as a function of ka for a cone angle θ_0 of 66.06° . In this case, the value of ν_1 is exactly 7. The zero-order solution corresponds to just using $Y_i = Y_{i0}$, while the first-order solution includes the correction term on the right-hand side of (12.104). Some additional first-order results for wide-angle conical dipoles are also given by Tai.⁸

12.7 Some Extensions of Biconical Antenna Theory

In an interesting paper, Galejs¹¹ extends Tai's analysis to biconical structures with spherical cores of lossy dielectric. Galejs, using essentially the first-order variational solution, also presents calculations for biconical antennas half buried in a perfectly conducting ground plane.

The generalization of the biconical antenna theory to a concentrically stratified exterior medium is quite straightforward. In this case, it is only necessary to replace the outward looking radial wave impedances as given by (12.59) by their forms appropriate for a radially stratified medium.¹² The extension to a radially stratified compressible plasma is also not difficult.¹³ Some of these extensions and generalizations are outlined in the following sections.

12.8 General Formulation for Biconical Antenna in Inhomogeneous Dissipative Media

As an example of a useful extension we shall consider a biconical antenna which is immersed in a radially stratified dissipative medium. The situation is illustrated in Fig. 12.6. The perfectly conducting biconical antenna of length $2a$ and cone angle θ_0 is surrounded by a sheath whose inner and outer radii are a and b , respectively. This sheath has conductivity σ_1 , dielectric constant ϵ_1 , and magnetic permeability μ_1 . The infinite medium external to the sheath is taken

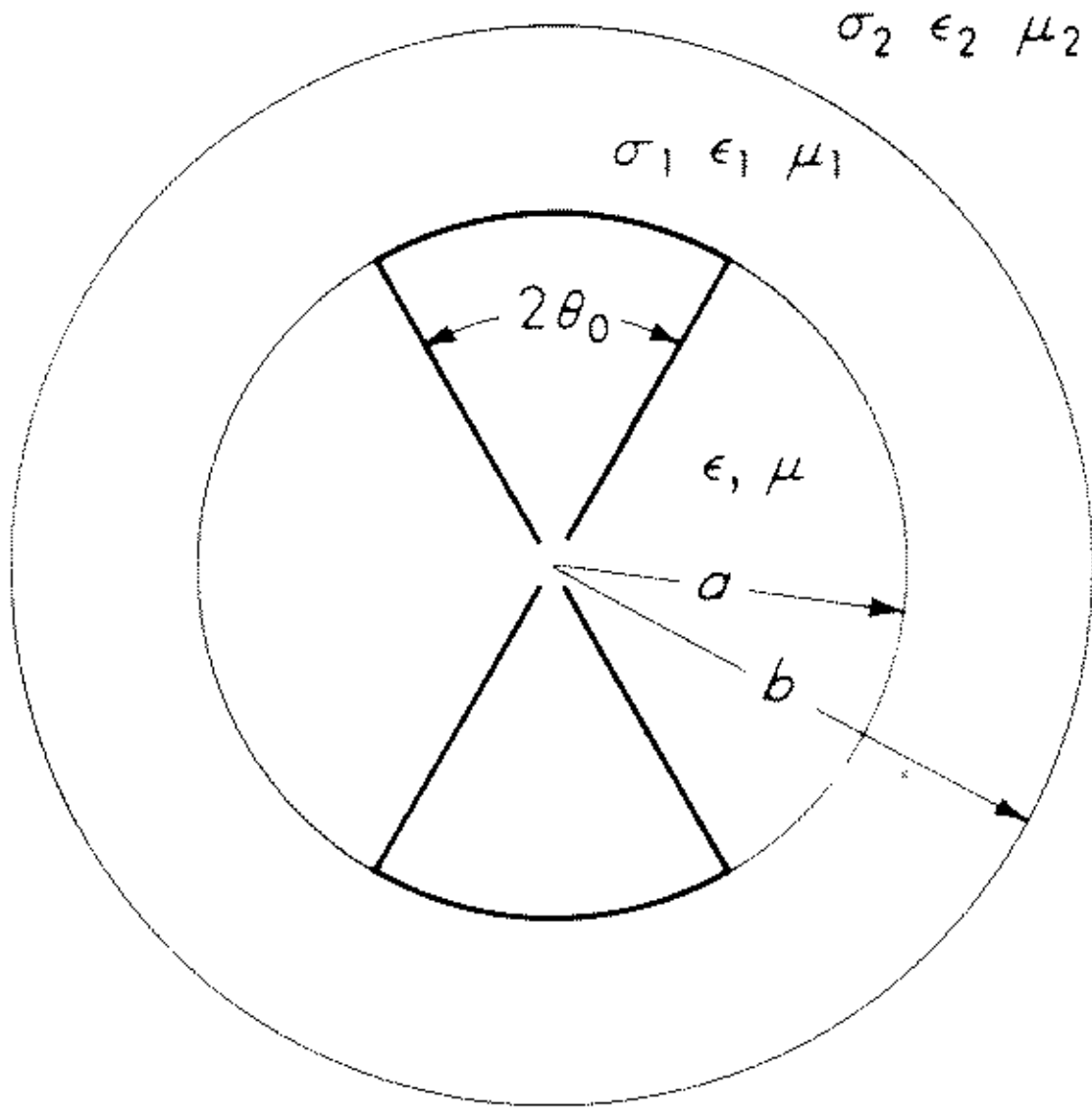


Fig. 12.6 Biconical antenna located in a spherically stratified medium.

to have corresponding properties σ_2, ϵ_2 , and μ_2 . Within the antenna region (that is, $r < a$), the medium is taken for convenience to be a lossless dielectric with properties ϵ and μ .

The formulation of the present problem is very similar to that for the biconical antenna located in free space. The major modification is in the choice of the radial wave functions for each of the homogeneous regions. Using a straightforward boundary-matching technique, the final solution is easily derived, because there are sufficient boundary conditions to solve for the unknown coefficients. The classical approach is rather tedious, and the book-keeping is complicated. Furthermore, to extend the solution to additional layers requires that the algebra be repeated. As a desirable alternative we shall exploit the analogy with nonuniform transmission line theory as expounded by Schelkunoff¹⁴ for similar problems of this kind.

The outward-looking impedance at $r = a$ for TM waves is defined by

$$Z_n^+ = \frac{E_{\theta,n}}{H_{\phi,n}} \Big|_{r=a} \tag{12.105}$$

for spherical modes of integer order n . Now, the characteristic impedance on the equivalent nonuniform transmission line from $r = a$ to b is

$$M(r) = -\zeta_1 \frac{\hat{K}'_n(\gamma_1 r)}{\hat{K}_n(\gamma_1 r)} \tag{12.106}$$

where \hat{K}_n is a modified spherical Bessel function of order n defined by

$$\hat{K}_n(z) = \left(\frac{2z}{\pi}\right)^{1/2} K_{n+1/2}(z)$$

in terms of the modified (cylindrical) Bessel function $K_{n+1/2}$ of order $n + 1/2$. In the above,

$$\zeta_1 = \left(\frac{j\mu_1\omega}{\sigma_1 + j\epsilon_1\omega}\right)^{1/2} \quad \text{and} \quad \gamma_1 = [j\mu_1\omega(\sigma_1 + j\epsilon_1\omega)]^{1/2}$$

are the intrinsic properties of the homogeneous dissipative sheath.

In a similar fashion, the characteristic impedance of the line looking inward is

$$N(r) = \zeta_1 \frac{\hat{I}'_n(\gamma_1 r)}{\hat{I}_n(\gamma_1 r)} \quad (12.107)$$

where

$$\hat{I}_n(z) = \left(\frac{\pi z}{2}\right)^{1/2} I_{n+1/2}(z)$$

The line is now considered to be terminated by an impedance

$$P(b) = -\zeta_2 \frac{\hat{K}'_n(\gamma_2 b)}{\hat{K}_n(\gamma_2 b)} \quad (12.108)$$

where, of course,

$$\zeta_2 = \left(\frac{j\mu_2\omega}{\sigma_2 + j\epsilon_2\omega}\right)^{1/2} \quad \text{and} \quad \gamma_2 = [j\mu_2\omega(\sigma_2 + j\epsilon_2\omega)]^{1/2}$$

are intrinsic properties of the external homogeneous region.

Using nonuniform transmission line theory and with the information given above, we can immediately write down the answer.¹² Thus,

$$Z_n^+ = M(a) \frac{1 + q_e A_e B_e}{1 + q_h A_h B_h} \quad (12.109)$$

where the q 's are reflection coefficients at $r = b$ and the A 's and B 's are transmission factors. The subscripts e and h are to indicate that the quantities pertain to the electric or magnetic fields, respectively. The explicit forms of the relevant quantities are

$$q_e = \frac{1/P(b) - 1/M(b)}{1/P(b) + 1/M(b)} \quad (12.110)$$

$$q_h = \frac{P(b) - M(b)}{P(b) + M(b)} \quad (12.111)$$

$$A_e = \frac{a\hat{K}'_n(\gamma_1 b)}{b\hat{K}'_n(\gamma_1 a)} \quad (12.112)$$

$$B_e = \frac{b\hat{I}'_n(\gamma_1 a)}{a\hat{I}'_n(\gamma_1 b)} \quad (12.113)$$

$$A_h = \frac{a\hat{K}_n(\gamma_1 b)}{b\hat{K}_n(\gamma_1 a)} \quad (12.114)$$

$$B_h = \frac{b\hat{I}_n(\gamma_1 a)}{a\hat{I}_n(\gamma_1 b)} \quad (12.115)$$

For wide-angle cones the inverse impedance Z_v , for the structure, is given by (12.73), with Z_n^+ now given by (12.109) above.

In the case of thin cones (i.e., where $\theta_0 \rightarrow 0$), it is not difficult to see that Z_v , given by (12.77), is to be replaced by

$$Z_v = K^2 Y_t = \frac{-j\zeta}{\pi} \sum_{n=1,3,5,\dots} \frac{2n+1}{n(n+1)} \frac{1}{\bar{M}_n - N_n} \quad (12.116)$$

$$\text{where} \quad \bar{M}_n = \frac{j\zeta_1}{\zeta} \frac{\hat{K}'_n(\gamma_1 a)}{\hat{K}_n(\gamma_1 a)} \frac{1 + q_e A_e B_e}{1 + q_h A_h B_h} \quad (12.117)$$

$$\text{and} \quad N_n = \frac{\hat{J}'_n(ka)}{\hat{J}_n(ka)} \quad \text{with} \quad \zeta = \left(\frac{\mu}{\epsilon}\right)^{1/2} \quad \text{and} \quad k = (\epsilon\mu)^{1/2}\omega \quad (12.118)$$

In the limiting case, when the medium external to $r = a$ is a homogeneous and lossless dielectric, the above formula for \overline{M}_n reduces to

$$\overline{M}_n = \frac{\zeta_1}{\zeta} \frac{\hat{H}'_n(k_1 a)}{\hat{H}_n(k_1 a)} \quad \text{with } \zeta_1 = \left(\frac{\mu_1}{\epsilon_1}\right)^{1/2} \quad \text{and } k_1 = (\epsilon_1 \mu_1)^{1/2} \omega \quad (12.119)$$

12.9 Biconical Antenna with Dielectric Loading

An interesting application of biconical antenna theory was carried out by Polk.¹⁵ He considered the case of the small-angle biconical antenna which was fully loaded with dielectric or ferromagnetic material within the antenna region. This corresponds to the special case considered by (12.119) above if we regard the exterior medium as free space. Explicitly,

$$Z_v = K^2 Y_t = -j120 \sum_{n=1,3,5,\dots} \frac{2n+1}{n(n+1)} \left[\frac{\hat{H}'_n(k_0 a)}{\hat{H}_n(k_0 a)} - \frac{(\mu/\mu_0)^{1/2} \hat{J}'_n(ka)}{(\epsilon/\epsilon_0)^{1/2} \hat{J}_n(ka)} \right]^{-1} \quad (12.120)$$

where k_0 is the wave number for free space and μ/μ_0 and ϵ/ϵ_0 are the relative permeability and dielectric constant, respectively, of the loading material. We also note that $ka = (\mu/\mu_0)^{1/2}(\epsilon/\epsilon_0)^{1/2}k_0 a$ may become quite large even if $k_0 a$ is small if we choose suitable ferromagnetic or ferroelectric materials.

The radiation pattern is to be computed from

$$rE_\theta = a \sum_{n=1,3,5,\dots} f_n \hat{H}'_n(k_0 r) \frac{d}{d\theta} P_n(\cos \theta) \quad (12.121)$$

$$\text{where } f_n = \frac{2n+1}{n(n+1)} \frac{1}{\hat{H}_n(ka)} \left[\frac{(\epsilon/\epsilon_0)^{1/2} \hat{H}'_n(k_0 a)}{(\mu/\mu_0)^{1/2} \hat{H}_n(k_0 a)} - \frac{\hat{J}'_n(ka)}{\hat{J}_n(ka)} \right]^{-1} \quad (12.122)$$

Now, if both $k_0 a$ and $ka \ll 1$, it is not difficult to show that $|f_{n+2}/f_n| < 1$ for n an odd integer. Thus, for biconical antennas which are electrically small in this restrictive sense, the pattern is proportional to $dP_1/d\theta$ or simply to $\sin \theta$. However, if ka is unrestricted while $k_0 a$ is still much less than unity, this inequality may not be correct. For example, in this latter case, it is not difficult to show that

$$f_1 \approx \frac{3}{2} \left[-\left(\frac{\epsilon\mu_0}{\epsilon_0\mu}\right)^{1/2} \frac{1}{k_0 a} - \frac{y^2 \sin y + y \cos y - \sin y}{y(\sin y - y \cos y)} \right]^{-1} \quad (12.123)$$

and

$$f_3 \approx \frac{7}{12} \left[-\left(\frac{\epsilon\mu_0}{\epsilon_0\mu}\right)^{1/2} \frac{3}{k_0 a} + \frac{y^4 \sin y + 6y^3 \cos y - 21y^2 \sin y - 45y \cos y + 45 \sin y}{y(y^3 \cos y - 6y^2 \sin y - 15y \cos y + 15 \sin y)} \right]^{-1} \quad (12.124)$$

where $y = ka$. Then, if $y \gg 1$, while still keeping $k_0 a \ll 1$, it follows that

$$\left| \frac{f_3}{f_1} \right| \approx \frac{14}{36} \left| \frac{\left(\frac{\epsilon\mu_0}{\epsilon_0\mu}\right)^{1/2} \frac{3}{k_0 a} + \frac{y \sin y + \cos y}{\sin y - y \cos y}}{\left(\frac{\epsilon\mu_0}{\epsilon_0\mu}\right)^{1/2} \frac{3}{k_0 a} - \frac{y \sin y + 6 \cos y}{y \cos y - 6 \sin y}} \right| \quad (12.125)$$

which becomes infinitely large if $\tan y = y$ or if

$$\left(\frac{\epsilon\mu_0}{\epsilon_0\mu}\right)^{1/2} \frac{3}{k_0a} = \frac{y \sin y + 6 \cos y}{y \cos y - 6 \sin y} \quad (12.126)$$

Actually, $|f_3/f_1|$ is finite at these “resonances” if (12.123) and (12.124) are used to compute the ratio. Nevertheless, the fact remains that, under certain conditions, $|f_3|$ may become much larger than $|f_1|$. In this situation, the pattern has a multilobe structure described by $dP_3/d\theta$ even though the overall dimension of the antenna is small compared with a free space wavelength. This supergain effect is achieved only at the expense of high antenna Q , which is quite large near one of these critical or resonant frequencies. For example, for a thin, loaded biconical antenna (that is, $\theta_0 = 2^\circ$) with $k_0a = 0.15$ and $\mu/\mu_0 = \epsilon/\epsilon_0 = 10$ the Q is of the order of 4,000.

12.10 Dielectric-loaded Biconical Antenna Immersed in a Conducting Medium

Among Tai's basic investigations of biconical antennas was a numerical study of radiating systems in a dissipative medium.¹⁶ The special case he considered, many years ago, was a small-angle biconical structure which was insulated in the sense that the antenna region (that is, $r < a$) was an insulating dielectric which he chose to have properties ϵ_0 and μ_0 identical with those of free space. The external medium (that is, $r > a$) was a homogeneous dissipative medium with electrical constants ϵ_1 , σ_1 , and μ_0 .

The appropriate formula for the effective terminating admittance Y_t is again determined as a special case of (12.116). Thus,

$$K^2 Y_t = K^2 (G_t + jB_t) = -j120 \sum_{n=1,3,5,\dots} \frac{2n+1}{n(n+1)} \left[\frac{j\zeta_1}{120\pi} \frac{\hat{K}'_n(Z)}{\hat{K}_n(Z)} - \frac{\hat{J}'_n(k_0a)}{\hat{J}_n(k_0a)} \right]^{-1} \quad (12.127)$$

where $Z = \gamma_1 a = [j(\sigma_1 + j\epsilon_1\omega)\mu_0\omega]^{1/2}$, $\zeta_1 = [j\mu_0\omega/(\sigma_1 + j\epsilon_1\omega)]^{1/2}$, $k_0 = (\epsilon_0\mu_0)^{1/2}\omega$, and $K = 120 \ln \cot(\theta_0/2)$.

For applications to seawater and highly conducting rocks or soils, it is often permissible to neglect displacement currents in the external region. Thus, for $\epsilon_1\omega \ll \sigma_1$, we see that

$$Z \approx (j\sigma_1\mu_0\omega)^{1/2}a \approx |Z| \exp(j\pi/4)$$

and $\zeta_1 \approx (j\mu_0\omega/\sigma_1)^{1/2} \approx |\zeta_1| \exp(j\pi/4)$. The behavior of Y_t in the present situation is controlled, in a large measure, by the function $\hat{K}'_n(Z)/\hat{K}_n(Z)$. The real and imaginary parts of this function are sketched in Figs. 12.7a and b, respectively. The abscissa is δ , which is related to Z by $Z = 1.8(1+j)\delta$. In the case of seawater (that is, $\sigma_1 = 3.6$ mho/m) and for a frequency of 1 MHz (that is, $\omega/2\pi = 10^6$), we see that

$$\delta = 100(k_0a)$$

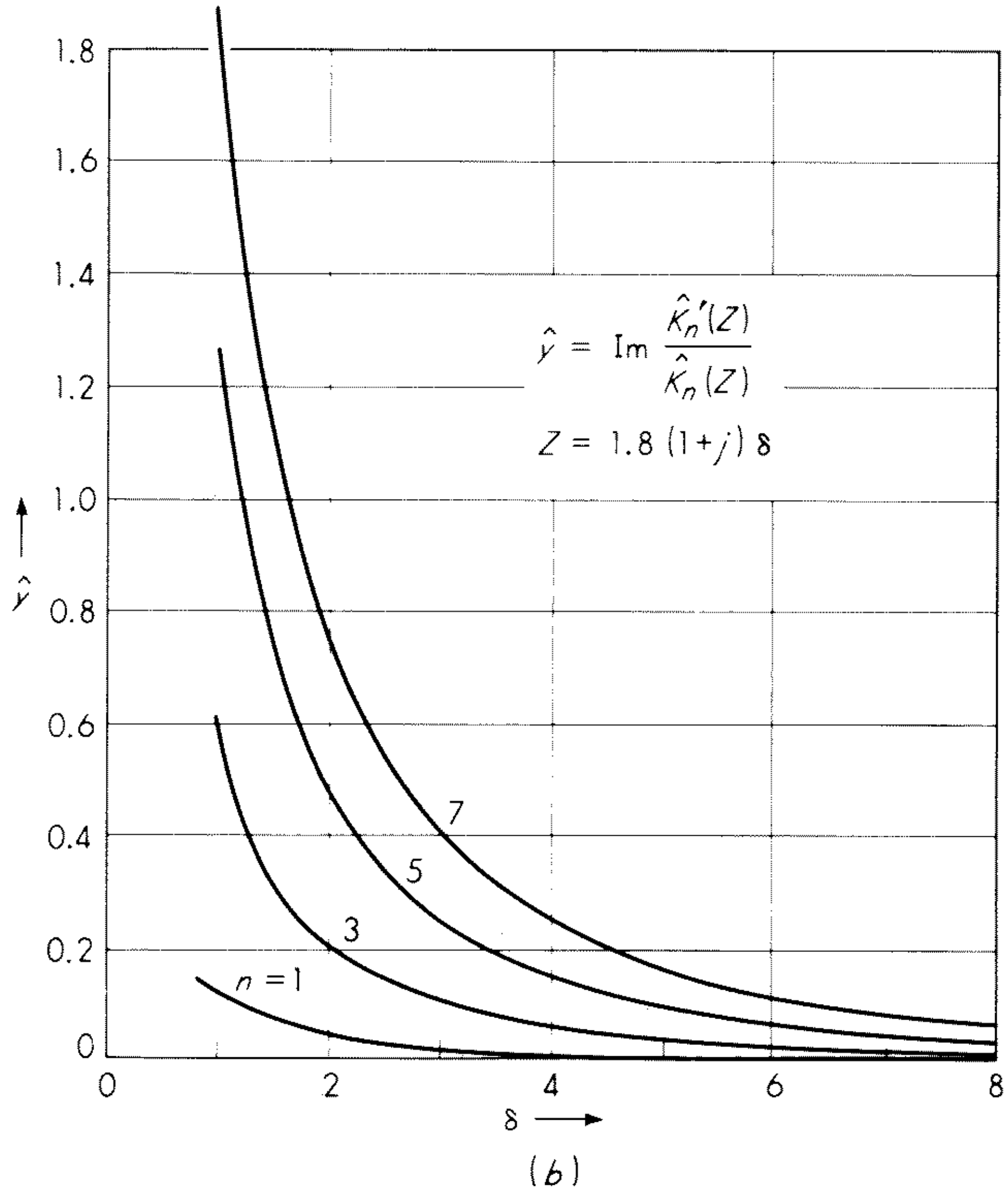
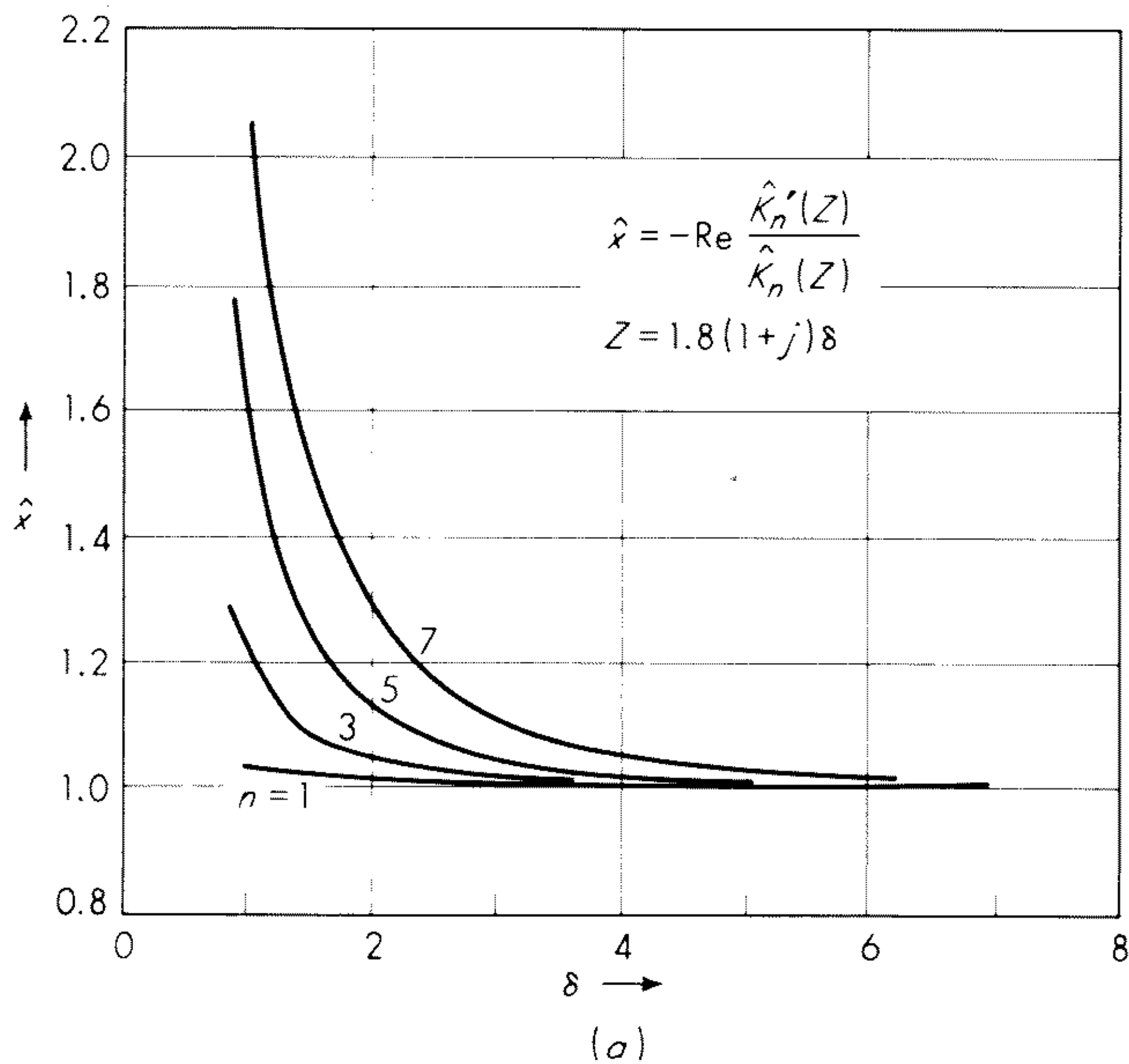


Fig. 12.7 The function $\hat{K}_n'(Z)/\hat{K}_n(Z) = -\hat{x} + j\hat{y}$ plotted as a function of δ .

It is evident that, for small values of k_0a , the terminating conductance G_t may be very small. However, for larger values of k_0a , certain resonances may occur when the square bracket term in (12.127) has a minimum.

An excellent example of the resonant behavior of the structure is shown in Fig. 12.8, where K^2G_t and K^2B_t are plotted as a function of k_0a for the above stated conditions. The system has a behavior akin to that of a cavity resonator. In this particular situation, the waves in the antenna region are very poorly matched to the external conducting medium except, of course, at the resonances. At the first resonance, where $k_0a \approx 2.75$, $K^2G_t \approx K^2B_t \approx 32,400$ ohms, while at the second resonance, where $k_0a \approx 4.92$, $K^2G_t \approx K^2B_t \approx 12,600$ ohms.

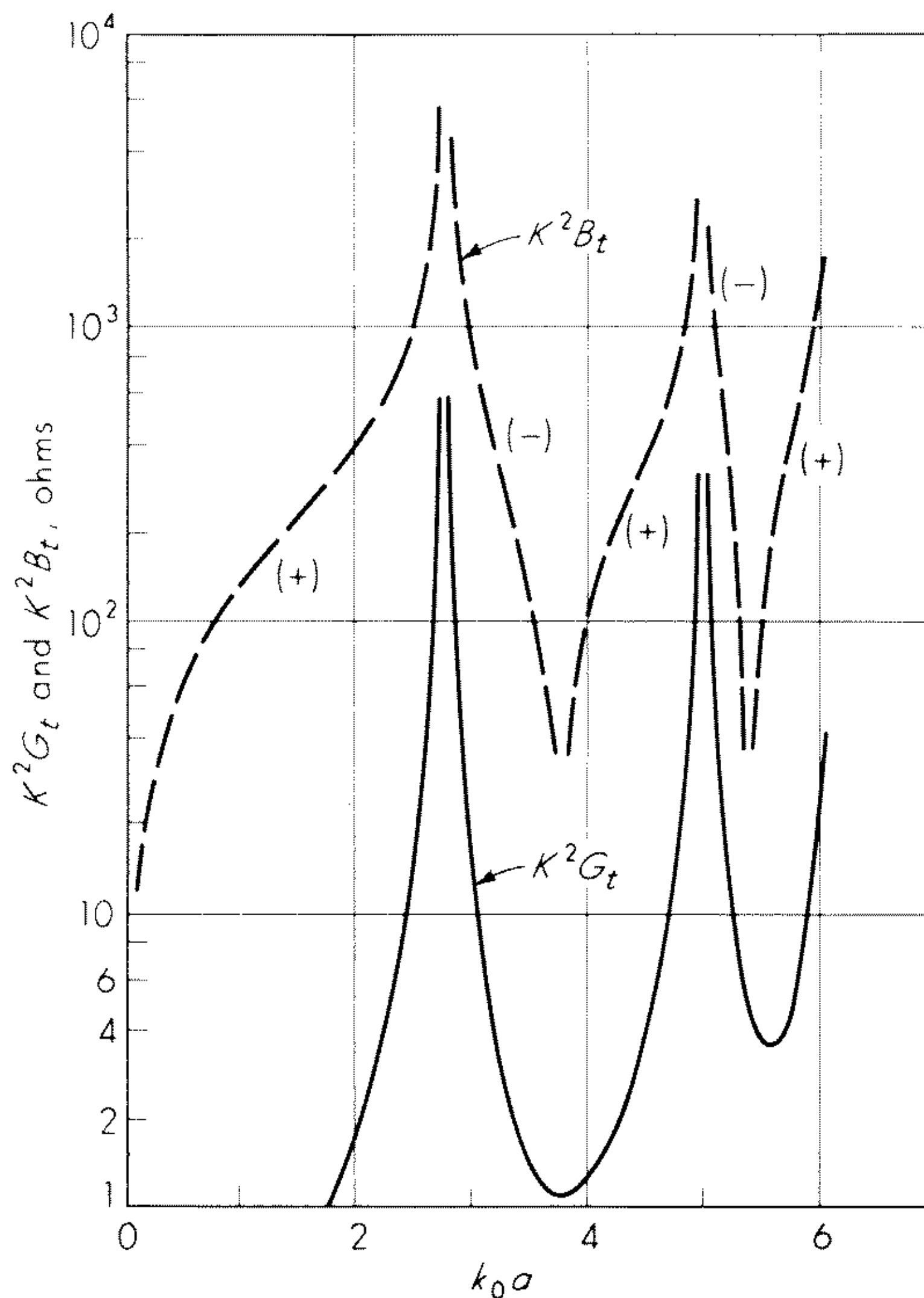


Fig. 12.8 Effective terminating impedance for a biconical antenna immersed in a conducting medium. (After Tai.¹⁶)

It would be interesting to examine the behavior of a biconical structure with an insulating shell surrounding the antenna. The spherical end caps of the antenna would not be in direct contact with the dissipative medium. For example, the medium between $a < r < b$, in Fig. 12.6, might be taken as an insulator, while the external medium for $r > b$ is the homogeneous conductor. Equations (12.116) and (12.117) are applicable directly to this case.

12.11 Dielectric-loaded Biconical Antenna Immersed in a Plasma

Radiation from a biconical antenna immersed in a plasma may be treated straightforwardly in a number of cases. For example, if the medium external to $r = b$ in Fig. 12.6 is a homogeneous cold isotropic plasma, we may simply use the formula given by (12.116) for the terminating impedance as well as the defining equations given by (12.110) to (12.115). However, $M(b)$, as defined by (12.108), is the appropriate radial wave impedance for the electron plasma. Thus,

$$M(b) = Z_c = -\zeta_e \frac{\hat{K}'_n(\gamma_e b)}{\hat{K}_n(\gamma_e b)} \quad (12.128)$$

where $\zeta_e = \frac{j\mu_0\omega}{\gamma_e}$ and $\gamma_e = \frac{j\omega}{c} \left[1 + \frac{\omega_0^2}{j\omega(\nu + j\omega)} \right]^{1/2}$

Here, ω_0 is the (angular) plasma frequency and ν is the effective collision frequency.

For a warm isotropic plasma, the appropriate expression for the radial wave impedance becomes¹⁷

$$M(b) = Z_c(1 - \delta_n) \quad (12.129)$$

where Z_c is as given above and

$$\delta_n = \frac{jn(n+1)\omega_0^2}{\omega(\nu + j\omega)(\gamma_e b)(\gamma_p b)} \frac{\hat{K}_n(\gamma_e b)}{\hat{K}'_n(\gamma_e b)} \frac{\hat{K}_n(\gamma_p b)}{\hat{K}'_n(\gamma_p b) - \hat{K}_n(\gamma_p b)/\gamma_p b} \quad (12.130)$$

in which $\gamma_p = \frac{j}{u} [(\omega^2 - \omega_0^2) - j\omega\nu]^{1/2}$

and u is the velocity of sound in the electron gas.

The above formula for the radial wave impedance of a compressible (i.e., warm) plasma was derived on the basis of the hydrodynamic description of the plasma.¹⁷ It was also assumed in the derivation that the normal component of the mean electron velocity vanishes at the surface $r = b$. (This topic is also discussed in Chap. 25.)

In the limiting case of a cold plasma (that is, $u \rightarrow \infty$), the parameter $|\gamma_p b|$ becomes infinite and δ_n vanishes. Some calculations have been carried out recently to show the effect of the finite temperature on the input impedance^{18,19} of a slotted spherical antenna. This corresponds to the biconical antenna in the limit when $\theta_0 \rightarrow \pi/2$.

12.12 Asymmetric Biconical Structures

In all our discussions up to this point, we have been considering symmetrical biconical structures with a cone angle θ_0 . Most practical radiating systems are symmetrical or, if not, they are operated against a ground plane which effectively produces an image of the actual cone. However, there are some interesting cases in which symmetry no longer prevails. Some examples are indicated

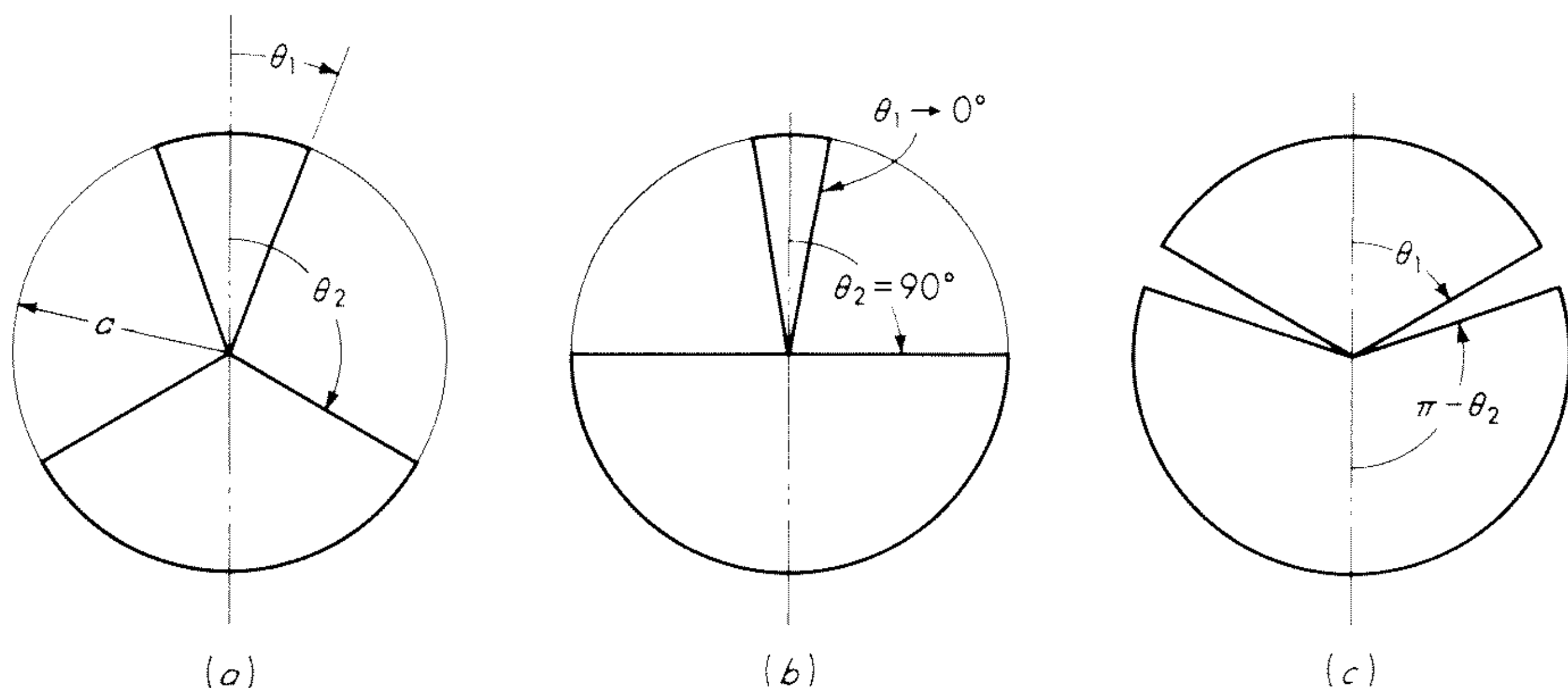


Fig. 12.9 Various asymmetric biconical structures.

in Fig. 12.9. In (a) we have a general asymmetric biconical structure in which the cone angles are $\theta = \theta_1$ and θ_2 and the spherical caps are the surfaces $r = a$. Two limiting forms are shown also in Fig. 12.9. In (b) we have a monopole of height a erected over a hemispherical ground plane, while in (c) we have an asymmetric spherical antenna with a circumferential slot excited by a biconical transmission line.

The formulation for the asymmetrical biconical antenna is very similar to that discussed in some detail above for the symmetrical structure. Therefore, only a bare outline need be given. The key point of departure is the choice of the angular wave functions. In place of $T_\nu(\cos \theta)$, we must choose, instead, the asymmetric function

$$T_\nu^a(\cos \theta) = P_\nu(\cos \theta)P_\nu(-\cos \theta_1) - P_\nu(\cos \theta_1)P_\nu(-\cos \theta) \quad (12.131)$$

which vanishes at $\theta = \theta_1$. Because T_ν^a should also vanish at $\theta = \theta_2$, we have the following modal equation

$$T_\nu^a(\cos \theta_2) = 0 \quad (12.132)$$

which determines the permissible values of ν . Within the antenna region (that is, $r < a$) we now have, in place of (12.33) and (12.34), an identical set except that $dT_\nu/d\theta$ is replaced by $dT_\nu^a/d\theta$, and now the TEM characteristic impedance is given by

$$K = \frac{\zeta}{\pi} \frac{1}{2} \ln \left(\cot \frac{\theta_1}{2} \tan \frac{\theta_2}{2} \right)$$

The field expression in the external region has the same form as (12.40) to (12.42), except that now the summation index includes both even and odd integers (that is, $n = 1, 2, 3, \dots$). In particular, for the magnetic field, we have, for $r \geq a$,

$$rH_\phi = \frac{1}{2\pi} \sum_{n=1,2,3,\dots} \frac{a_n}{n(n+1)} \frac{\hat{H}_n(kr)}{\hat{H}_n(ka)} \frac{d}{d\theta} P_n(\cos \theta) \quad (12.133)$$

By following the same boundary-matching procedure, we arrive at Schelkunoff's² formula for the coefficients a_n

$$Z_n^+ a_n = \frac{(2n+1)\zeta V(a)}{2K} [P_n(\cos \theta_2) - P_n(\cos \theta_1)] - \sum_{n'} Z_{n,n'}^- a_{n'} \quad (12.134)$$

where $Z_{n,n'}^-$ is an infinite matrix which has the same form as (A-12.7) in the Appendix. For the first-order approximation, it may be shown, using the line of reasoning given in the Appendix, that the summation term may be replaced by $Z_n^- a_n$ for narrow-angle cones (that is, $\theta_1 \rightarrow 0$ and $\pi - \theta_2 \rightarrow 0$). On the other hand, for wide-angle cones chosen such that $(\pi - \theta_1 - \theta_2) \rightarrow 0$, the summation term may be neglected altogether.

12.13 Radiation from a Single Infinite Cone

The formulation of radiation from sources in the presence of a single cone is not very different from that involving biconical structures. The central point is that a single cone will not support a TEM mode. Thus, the antenna region, in this case, contains only complementary waves.

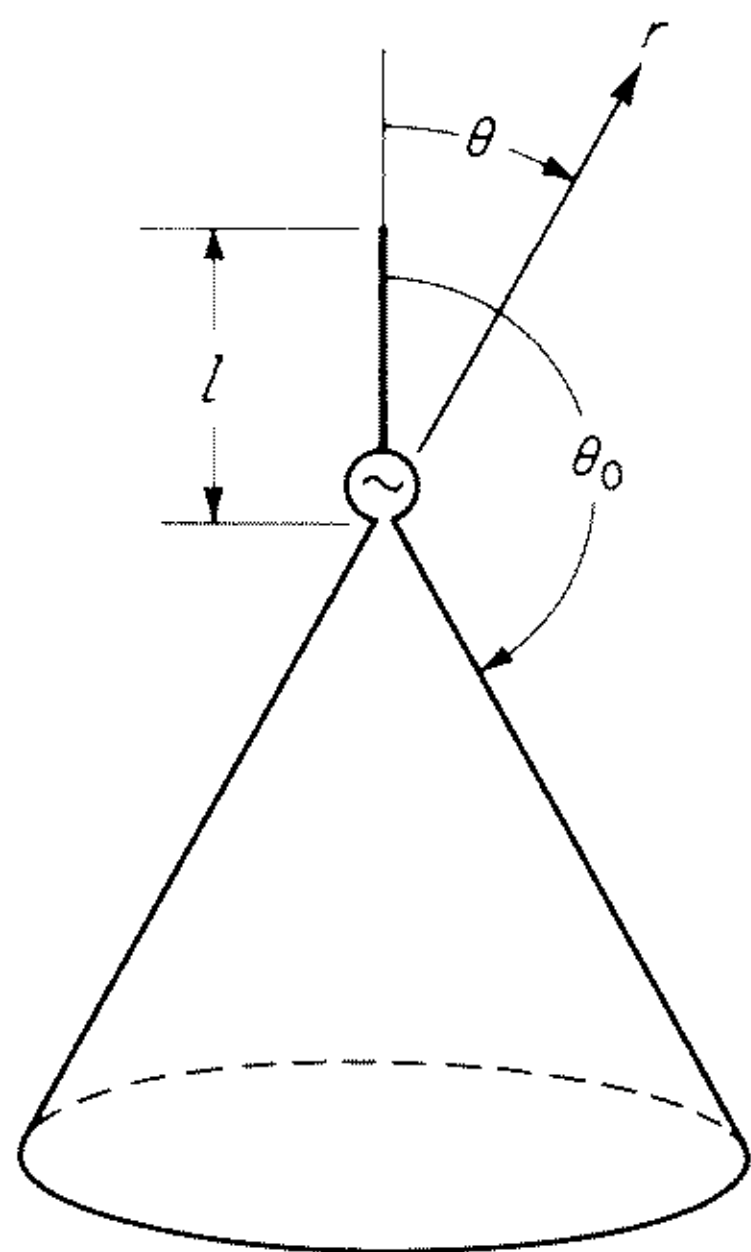


Fig. 12.10 Conical structure excited by a linear current filament.

An interesting configuration involving a single cone was treated by Adachi, et al.²⁰ The configuration, indicated in Fig. 12.10, consists of a perfectly conducting semi-infinite cone excited by a linear antenna with an assumed sinusoidal current distribution. Using a Green's function developed by Felsen,²¹ he showed that the radiation field is given by

$$E_\theta \approx \frac{\zeta I_0 e^{-jkr}}{4r} \sum_q \exp\left(\frac{j\pi q}{2}\right) (2q+1) Q_q(kl) \times \frac{P_q(-\cos \theta_0)}{\sin q\pi \left[\frac{\partial}{\partial q'} P_{q'}(\cos \theta_0) \right] \Big|_{q'=q}} \frac{\partial}{\partial \theta} P_q(\cos \theta) \quad (12.135)$$

where

$$Q_q(kl) = \frac{1}{k} \int_0^l \frac{\sin k(l-z)}{z^2} \hat{J}_q(kz) dz \quad (12.136)$$

The roots q are solutions of the equation

$$P_q(\cos \theta_0) = 0 \quad (12.137)$$

Equation (12.135), given above, is exact for the semi-infinite conical structure excited by the specified filamental distribution. Using this result, Adachi, et al.²⁰ then estimate the effect of truncating the bottom of the cone. The key point of their argument is that the current distribution on the finite cone is approximately the same as if the cone were infinite. The method appears to work well provided the cone length (i.e., from tip to base) is large compared with the wavelength.

It is tempting to suggest that the finite conical structure considered by Adachi, et al.²⁰ could be considered as an asymmetrical biconical structure. It is anticipated, however, that such a formulation would lead to numerical difficulties because of the relatively poor convergence of the modal series when the structure is large compared with the wavelength.

Semi-infinite single conical structures with nonsymmetrical excitation have been treated by various investigators. For example, a very thorough study was carried out by Bailin and Silver.²² They found that the field external to the cone could be expanded in terms of an infinite set of TM and TE modes. The solutions for the Debye potentials U and V had the form

$$\frac{U}{V} = Z_\nu(kr) P_\nu^m(\cos \theta) \exp(jm\phi) \quad (12.138)$$

where Z_ν behaved as an outgoing spherical wave at infinity and where P_n^m is an associated Legendre function. Here the ν 's are the nonintegral eigenvalues so chosen that tangential E vanishes at the cone surface $\theta = \theta_0$. For the TM set, this requires that

$$P_\nu^m(\cos \theta_0) = 0 \quad (12.139)$$

while for the TE set,

$$\frac{\partial P_\nu^m(\cos \theta_0)}{\partial \theta_0} = 0 \quad (12.140)$$

Bailin and Silver²² develop an important "tip condition" for problems of this kind. They show that, when the source is not at the tip of the cone, U and V must vary as r^ν near the tip with $\nu > 0$. This condition is a consequence of the fact that, while the fields may be singular at the tip, the energy in the neighborhood of the tip must be finite (see Sec. 1.7).

A special case of the analysis by Bailin and Silver²² is the semi-infinite cone excited by a circumferential slot a distance r_0 from the tip. Thus, for this case, they find that the field is expressed as a sum of axially symmetric TM modes. It has the form

$$U \approx \frac{1}{r} \sum_{\nu=\nu_i} \frac{2\nu_i + 1}{\nu_i(\nu_i + 1)} \frac{P_{\nu_i}(\cos \theta)}{[\partial P_\nu / \partial \nu]_{\theta=\theta_0}} \hat{J}_{\nu_i}(kr_0) \hat{H}_{\nu_i}(kr) \quad (12.141)$$

where $r > r_0$ and ν_i are the roots which satisfy

$$P_\nu(\cos \theta_0) = 0 \quad (12.142)$$

The radiation field is obtained from

$$H_\phi = -j\epsilon\omega \frac{\partial U}{\partial \theta} \quad \text{for } kr \rightarrow \infty \quad (12.143)$$

The magnitude of H_ϕ as a function of θ is shown schematically in Fig. 12.11, for $r_0 = 2.5\lambda$, using the data given in the Bailin and Silver paper.²² It is evident that the direct field from the slot and the scattered field from the tip interfere with one another to give a rather complicated lobe structure. It is also interesting to note that the field directed back along the cone surface (i.e., away from the tip) has a maximum.

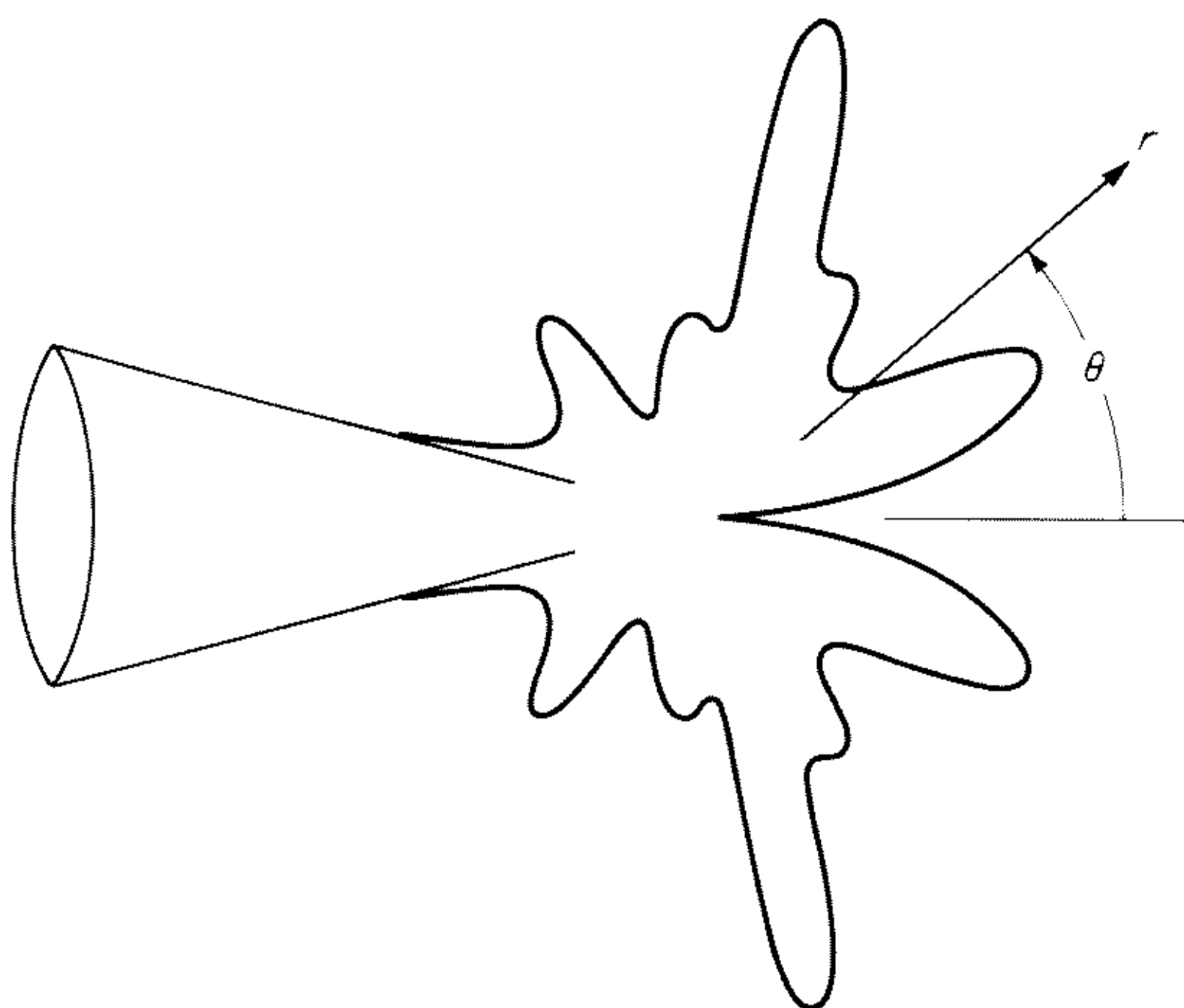


Fig. 12.11 Radiation field pattern (linear scale) for circumferentially slotted cone. (After Bailin and Silver.²²)

12.14 Radiation from a Dielectric-coated Conical Structure

In recent years it has become painfully evident that communication from a reentry vehicle in the upper atmosphere is degraded by a plasma sheath surrounding the antenna. This sheath is a highly conducting layer of ionized material which is produced by the shock wave, which is more or less in the form of a cone.

A very notable contribution to the conical sheath problem was made by Yeh.²³ He was able to utilize effectively the very interesting properties of Sommerfeld's complex-order wave functions. A very brief outline of Yeh's analysis is given here.

The situation is illustrated in Fig. 12.12, where the surface of the perfectly conducting cone is defined by $\theta = \theta_0$ with respect to a spherical coordinate

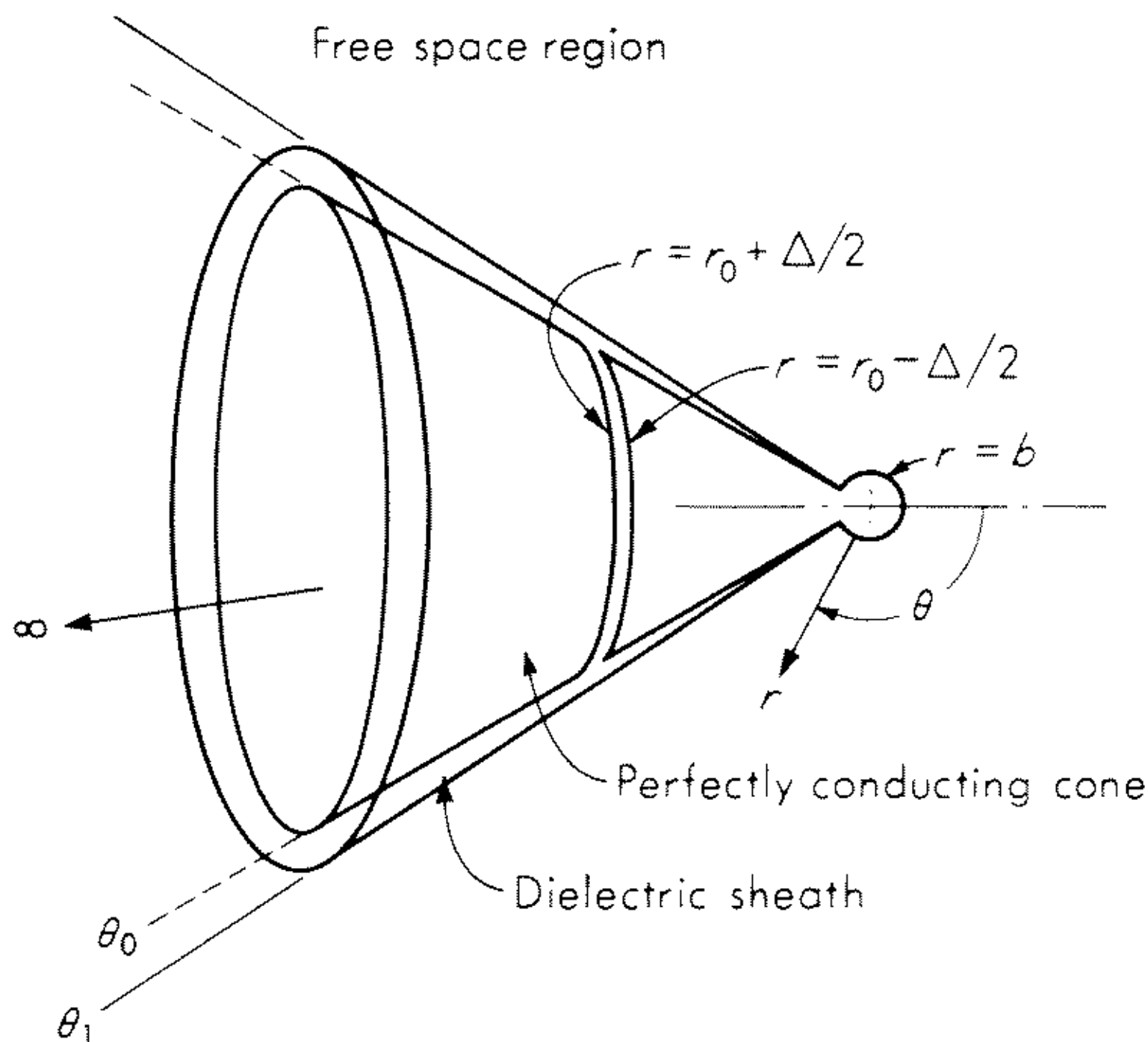


Fig. 12.12 Circumferentially slotted cone with spherical tip and dielectric sheath.

system (r, θ, ϕ) . For reasons which are evident from below, the cone has a small perfectly conducting boss of radius b at the tip. Now, the sheath is regarded as a lossless dielectric which occupies the space $\theta_1 < \theta < \theta_0$ and $b < r < \infty$. The dielectric constant of the sheath is ϵ_1 and the permeability is μ_0 . The medium exterior to the sheath is free space with electrical constants ϵ_0 and μ_0 . The cone structure is excited at $r = r_0$ by a thin circumferential slot of width Δ . The voltage is applied uniformly around the slot.

For the conical configuration as described, the radiated fields are obviously symmetrical with respect to ϕ . The magnetic field has only a ϕ component, and, in the usual manner, it may be determined from a scalar function U . Thus, for the region within the dielectric sheath,

$$H_\phi = -j\epsilon_1\omega \frac{\partial U_1}{\partial \theta} \quad (12.144)$$

where U_1 satisfies

$$(\nabla^2 + k_1^2)U_1 = 0 \quad (12.145)$$

with $k_1^2 = \epsilon_1\mu_0\omega^2$. Outside the sheath (that is, $\theta < \theta_1$),

$$H_\phi = -j\epsilon_0\omega \frac{\partial U_0}{\partial \theta} \quad (12.146)$$

where U_0 satisfies

$$(\nabla^2 + k_0^2)U_0 = 0 \quad (12.147)$$

with $k_0^2 = \epsilon_0\mu_0\omega^2$.

The appropriate forms of the solutions inside and outside the sheath are

$$U_1 = \sum_{\nu} h_{\nu}(k_1 r) [A_{\nu} P_{\nu}(\cos \theta) + B_{\nu} Q_{\nu}(\cos \theta)] \quad (12.148)$$

$$\text{and } U_0 = \sum_{\mu} h_{\mu}(k_0 r) G_{\mu} P_{\mu}(\cos \theta) \quad (12.149)$$

respectively. Here, the spherical Hankel function is defined by

$$xh_\nu(x) = \hat{H}_\nu(x) = \left(\frac{\pi x}{2}\right)^{1/2} H_{\nu+1/2}^{(2)}(x)$$

where ν is the order which is not yet specified. P_ν and Q_ν are Legendre functions of the first and second kind. The summation in (12.148) and (12.149) is over the eigenvalues ν and μ , which are to be determined by the boundary conditions. The coefficients A_ν , B_ν , and G_μ are also yet to be determined.

The eigenvalues are actually obtained by noting that the tangential electric field on the spherical tip must be zero. This leads to

$$\frac{\partial}{\partial r} [rh_\nu(k_1 r)]|_{r=b} = 0 \quad (12.150)$$

and
$$\frac{\partial}{\partial r} [rh_\mu(k_0 r)]|_{r=b} = 0 \quad (12.151)$$

Now, as shown by Sommerfeld,²⁴ $h_\nu(x)$ is orthogonal over the range $x = x_0$ to ∞ for a boundary condition of the kind $\partial(xh_\nu)/\partial x = 0$ at $x = x_0$. Thus, we find, for the sheath region,

$$\int_{k_1 b}^{\infty} h_\nu(k_1 r) h_{\nu'}(k_1 r) d(k_1 r) = \begin{cases} N_\nu(k_1 b) & \text{if } \nu = \nu' \\ 0 & \text{if } \nu \neq \nu' \end{cases} \quad (12.152)$$

where
$$N_\nu(k_1 b) = \int_{k_1 b}^{\infty} [h_\nu(k_1 r)]^2 d(k_1 r) \\ = \frac{1}{2\nu + 1} \left[k_1 b h_\nu(k_1 b) \frac{\partial^2}{\partial(k_1 b) \partial \nu} [k_1 b h_\nu(k_1 b)] \right] \quad (12.153)$$

and ν and ν' are two sets of eigenvalues which satisfy (12.150). In a similar manner, we find for the free space region

$$\int_{k_0 b}^{\infty} h_\mu(k_0 r) h_{\mu'}(k_0 r) d(k_0 r) = \begin{cases} N_\mu(k_0 b) & \text{if } \mu = \mu' \\ 0 & \text{if } \mu \neq \mu' \end{cases} \quad (12.154)$$

where $N_\mu(k_0 b)$ is the same as (12.153) with ν replaced by μ and $k_1 b$ replaced by $k_0 b$.

The boundary conditions require the continuity of the tangential electric and magnetic fields at the conical surface $\theta = \theta_1$. To facilitate the matching, we use the expansion

$$h_\nu(k_1 r) = \sum_{\mu} \Gamma_{\nu, \mu} h_\mu(k_0 r) \quad (12.155)$$

where
$$\Gamma_{\nu, \mu} = \frac{1}{N_\mu(k_0 b)} \int_{k_0 b}^{\infty} h_\nu(k_1 r) h_\mu(k_0 r) d(k_0 r) \quad (12.156)$$

Terms of order μ may now be matched individually. This leads to the two sets of equations

$$\frac{\epsilon_0}{\epsilon_1} G_\mu P'_\mu = \sum_{\nu} (A_\nu P'_\nu + B_\nu Q'_\nu) \Gamma_{\nu, \mu} \quad (12.157)$$

and
$$G_\mu \mu(\mu + 1) P_\mu = \sum_{\nu} (A_\nu P_\nu + B_\nu Q_\nu) \nu(\nu + 1) \Gamma_{\nu, \mu} \quad (12.158)$$

where the arguments of the Legendre functions are $\cos \theta_1$ and a prime indicates differentiation with respect to θ_1 .

A further relation between the coefficients is obtained by noting that the field, on the surface of the perfectly conducting cone, is zero everywhere except at the slot where the field is E_0 . Thus,

$$\begin{aligned} E_r|_{\theta=\theta_0} &= \frac{1}{r} \sum_{\nu} \nu(\nu+1) [A_{\nu} P_{\nu}(\cos \theta_0) + B_{\nu} Q_{\nu}(\cos \theta_0)] h_{\nu}(k_1 r) \\ &= E_0 \quad \text{for } r_0 - \frac{\Delta}{2} < r < r_0 + \frac{\Delta}{2} \\ &= 0 \quad \text{for } 0 < r < r_0 - \frac{\Delta}{2} \quad \text{and} \quad r_0 + \frac{\Delta}{2} < r < \infty \end{aligned} \quad (12.159)$$

From orthogonality, we find that

$$\begin{aligned} A_{\nu} P_{\nu}(\cos \theta_0) + B_{\nu} Q_{\nu}(\cos \theta_0) &= \frac{1}{\nu(\nu+1)} \frac{1}{N_{\nu}(k_1 b)} \int_{r_0-\Delta/2}^{r_0+\Delta/2} E_0 r h_{\nu}(k_1 r) d(k_1 r) \\ &\approx \frac{E_0 r_0 h_{\nu}(k_1 r_0) k_1 \Delta}{\nu(\nu+1) N_{\nu}(k_1 b)} \end{aligned} \quad (12.160)$$

The latter approximation for the integral is valid provided Δ is sufficiently small.

The infinite set of equations (12.157), (12.158), and (12.160) may be solved, in principle, for the coefficients A_{ν} , B_{ν} , and G_{μ} . In practice, the system is truncated in a manner analogous to that for biconical antennas.

The radiation field in the region $\theta < \theta_1$ is then obtained finally from

$$H_{\phi} = -j\epsilon_0\omega \frac{e^{-jk_0 r}}{k_0 r} \sum_{\nu} G_{\nu} \exp \left[-j(\nu+1) \frac{\pi}{2} \right] \frac{\partial}{\partial \theta} P_{\nu}(\cos \theta) \quad (12.161)$$

Yeh,²³ in his paper, discusses the determination of the roots of ν and the evaluation of the function $\Gamma_{\nu,\mu}$. He also gives some numerical results for the radiation pattern. An example is shown in Fig. 12.13, which is a plot of the magnitude of H_{ϕ} as a function of θ for a sheath model in which the relative dielectric constant, ϵ_1/ϵ_0 , is equal to 2. The location of the slot and the radius of the spherical tip are such that $k_0 r_0 = \pi$ and $k_0 b = 0.1$. The cone surface is $\theta_0 = 165^\circ$ and the sheath edge is at $\theta_1 = 160^\circ$.

It is evident for the pattern shown in Fig. 12.13 and in others given by Yeh²³ that the sheath does not have a significant effect on the radiation in the forward direction. However, there is some tendency to enhance the radiation in the backward direction, particularly for angles near the surface of the sheath.

12.15 Radiation from a Dipole with a Conical Sheath

The conical sheath problem has also been considered by Baños et al.²⁵ They consider an electric dipole centrally located inside a thin conducting conical

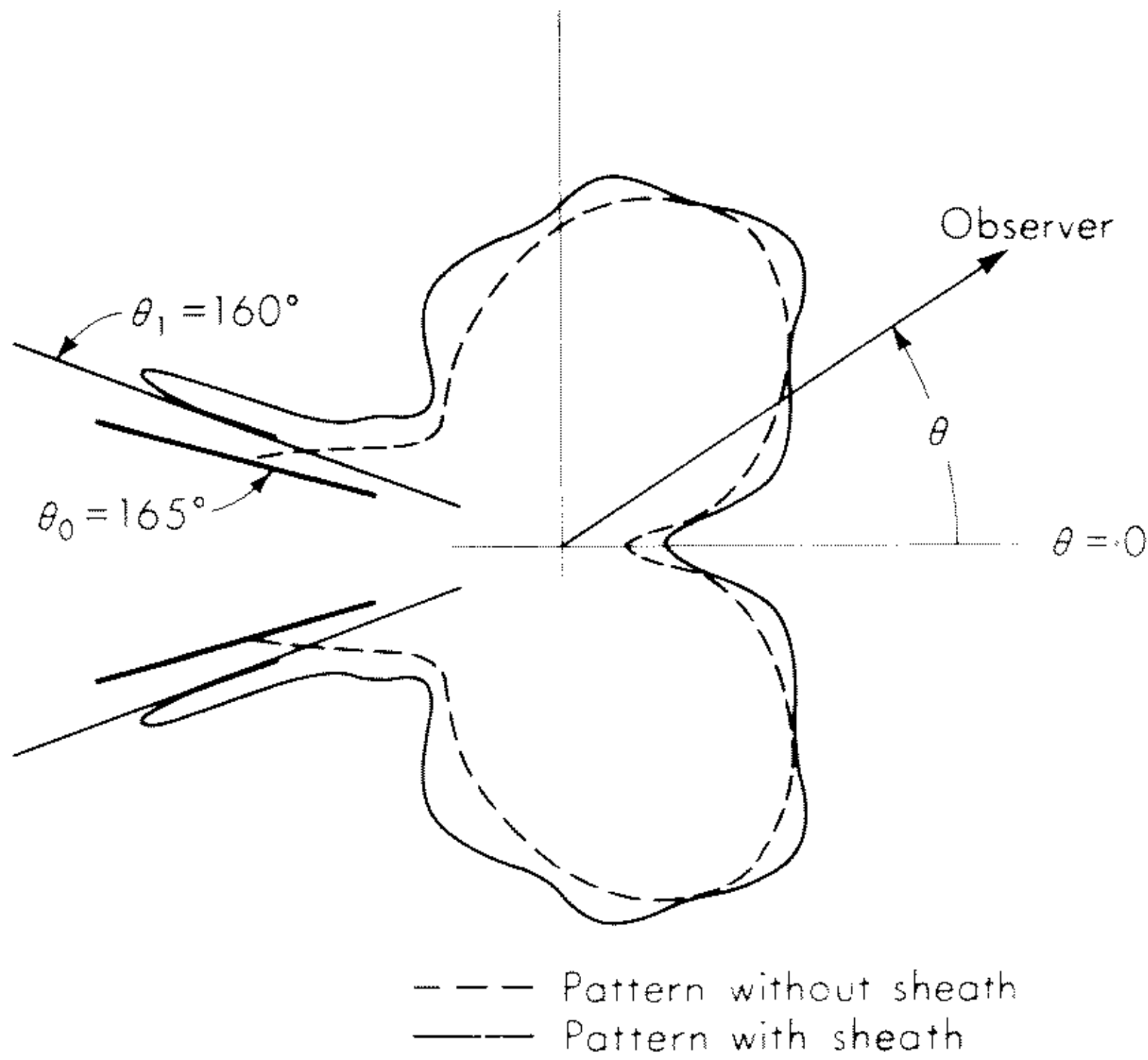


Fig. 12.13 Radiation pattern of circumferentially slotted cone showing effect of dielectric sheath ($\epsilon_1/\epsilon_0 = 2$, $k_0b = 0.1$, $k_0r_0 = \pi$). (After Yeh.²³)

sheath as indicated in Fig. 12.14. The free space regions inside and outside the cone are designated (1) and (2), respectively. A corresponding subscript is added to the field quantities when appropriate.

Because of the axial symmetry, the fields in regions 1 and 2 are again derivable from a Debye potential U in the manner

$$E_r = \left(k_0^2 + \frac{\partial^2}{\partial r^2}\right)(rU) = -\frac{1}{r \sin \theta} \frac{\partial}{\partial \theta} \left(\sin \theta \frac{\partial U}{\partial \theta}\right) \tag{12.162}$$

$$E_\theta = \frac{1}{r} \frac{\partial^2}{\partial \theta \partial r} (rU) \tag{12.163}$$

and
$$H_\phi = -j\epsilon_0\omega \frac{\partial U}{\partial \theta} \tag{12.164}$$

It is now assumed that the sheath may be characterized by the following boundary conditions:²⁶

$$E_{1r} = E_{2r} \quad \text{at } \theta = \theta_0 \tag{12.165}$$

$$H_{1\phi} - H_{2\phi} = -\frac{E_{2r}}{Z_s} \quad \text{at } \theta = \theta_0 \tag{12.166}$$

where
$$Z_s = j\left(\frac{\mu_0}{\epsilon_0}\right)^{1/2} \frac{c(\omega + j\nu)}{\omega_0^2 d} \tag{12.167}$$

Here ω_0 is the plasma frequency, ν is the collision frequency, and d is the sheath thickness.

The type of boundary condition described above is valid if the thickness d is small compared with the wavelength in both free space and the plasma. This,

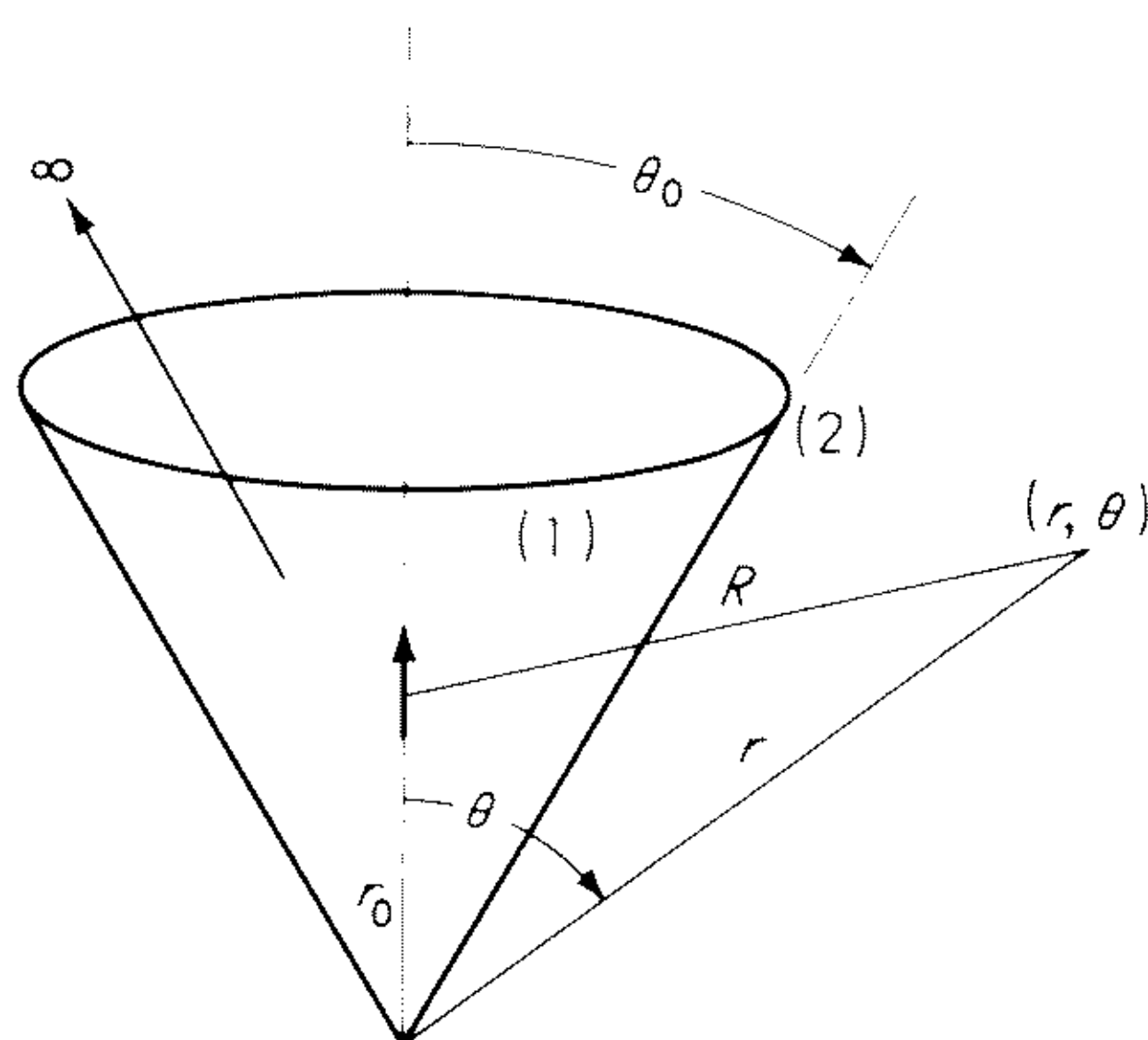


Fig. 12.14 Centrally located electric dipole inside a conical sheath of infinite extent.

in effect, means that only the radial component of the current with the conical sheath conductor need be considered.

As a consequence of (12.165) and (12.166), it follows from (12.162) and (12.164) that

$$U_1 = U_2 \quad (12.168)$$

and

$$\frac{\partial}{\partial \theta} (U_1 - U_2) = \frac{2g}{\pi \sin^2 \theta} \frac{\partial}{\partial \theta} \left(\sin \theta \frac{\partial U_2}{\partial \theta} \right) \Bigg|_{\theta=\theta_0} \quad (12.169)$$

where

$$g = j \left(\frac{\mu_0}{\epsilon_0} \right)^{1/2} \frac{\pi}{2} \sin \theta_0 \frac{c}{\omega r} \frac{1}{Z_s}$$

Now, the key point in the analysis by Baños et al.²⁵ is the assumption that g is independent of r . Thus, the equivalent impedance Z_s of the sheath must be proportional to $1/r$, where, of course, r is the distance from the tip of the cone. This assumption greatly simplifies the analysis, since, as we shall see, the radial eigenmodes for regions 1 and 2 *individually* satisfy the boundary conditions at the sheath. This is in contrast to the treatment of a similar problem by Yeh,²³ which was discussed above.

The formal solution for the problem is now constructed in a fairly straightforward manner. We first note that the primary Debye potential U_p in region 1 is given by (apart from a constant factor),

$$U_p = \frac{e^{-jk_0 R}}{R} \quad (12.170)$$

where $R = (r_0^2 + r^2 - 2r_0 r \cos \theta)^{1/2}$ and r_0 is the radial coordinate of the source dipole. By using a well-known addition theorem,²⁷ we may rewrite (12.170) in the series form

$$U_p = -jk_0 \sum_{n=0}^{\infty} (2n+1) P_n(\cos \theta) f_n(r, r_0) \quad (12.171)$$

where

$$f_n(r, r_0) = \begin{cases} j_n(k_0 r) h_n(k_0 r_0) & 0 < r < r_0 \\ j_n(k_0 r_0) h_n(k_0 r) & r_0 < r < \infty \end{cases}$$

and where j_n and h_n are spherical Bessel and Hankel functions, respectively. Following Watson's²⁷ procedure, U_p is now written as a contour integral

$$U_p = k_0 \int_{C_0} \frac{\nu d\nu}{\cos \nu\pi} P_{\nu-\frac{1}{2}}(-\cos \theta) f_{\nu-\frac{1}{2}}(r, r_0) \quad (12.172)$$

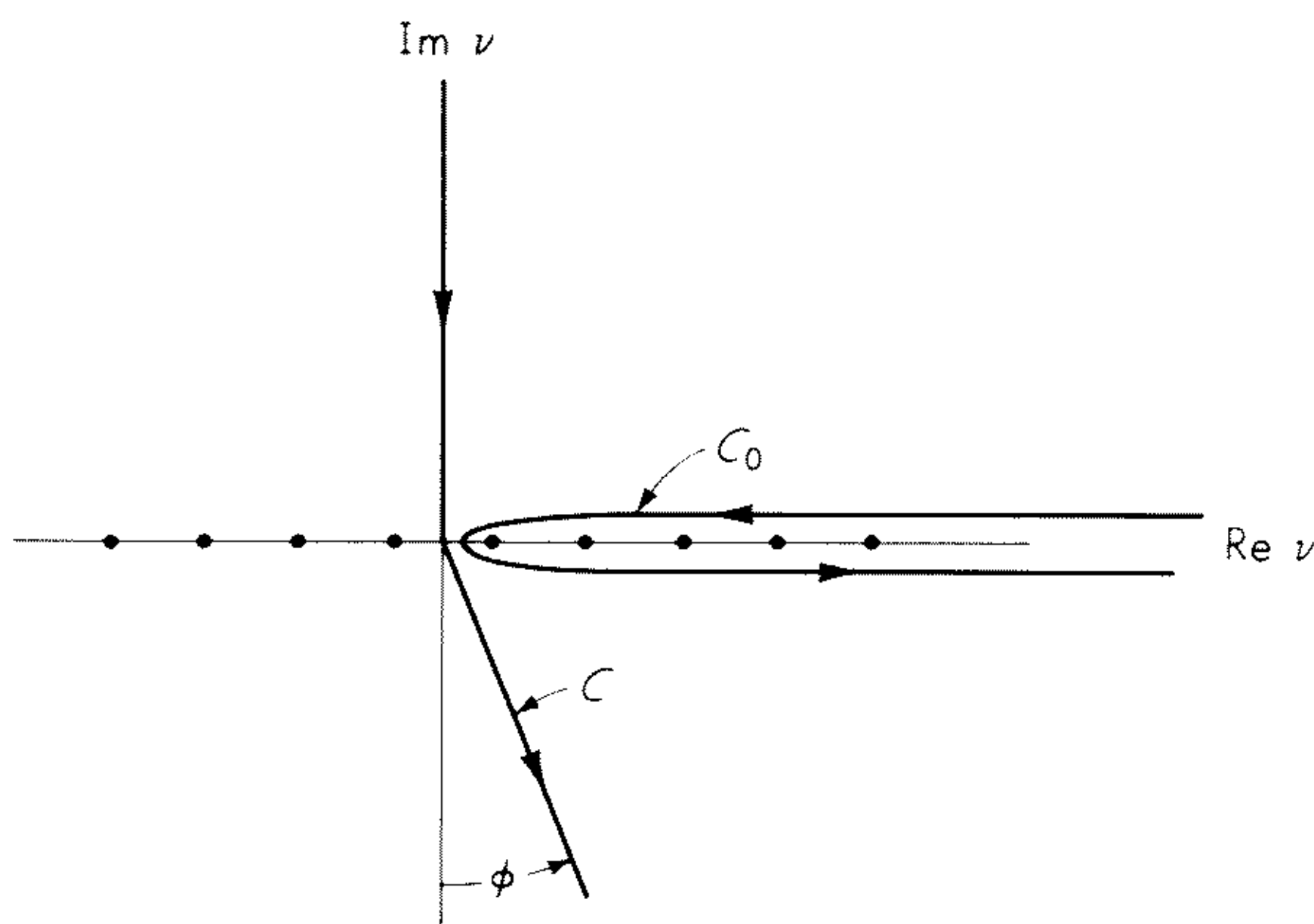


Fig. 12.15 The complex ν plane indicating the contours C and C_0 and the zeroes of $\cos \nu\pi$ on the real axis.

where C_0 is a "hairpin" contour which encloses the positive real axis in an anti-clockwise direction. It may be verified without difficulty that $2\pi j$ times the sum of the residues of the poles of the integrand of (12.172) is the series in (12.171). For reasons which are evident below, the contour C_0 is now deformed into the contour C as indicated in Fig. 12.15, where ϕ is a small but finite angle. By an application of Jordan's lemma it may be proved, without difficulty, that the value of the resultant integral is unchanged.

A suitable integral representation for the total Debye potential in region 1 is now given by

$$U_1 = k_0 \int_C \frac{\nu d\nu}{\cos \nu\pi} [P_{\nu-\frac{1}{2}}(-\cos \theta) + F(\nu)P_{\nu-\frac{1}{2}}(\cos \theta)] f_{\nu-\frac{1}{2}}(r, r_0) \quad (12.173)$$

where $F(\nu)$ is an unknown function of ν which may be regarded as the influence of the conical sheath. In a similar manner, the representation for the external region 2 is chosen to be

$$U_2 = k_0 \int_C \frac{\nu d\nu}{\cos \nu\pi} G(\nu)P_{\nu-\frac{1}{2}}(-\cos \theta) f_{\nu-\frac{1}{2}}(r, r_0) \quad (12.174)$$

where $G(\nu)$ is also unknown. Loosely speaking, $F(\nu)$ and $G(\nu)$ may be described as reflection and transmission coefficients, respectively. In the absence of the sheath, $F \rightarrow 0$, while $G \rightarrow 1$.

The boundary conditions (12.168) and (12.169) are now applied to (12.173)

and (12.174). This leads to two algebraic equations for F and G which are readily solved to give

$$F(\nu) = \left[\frac{\cos \nu \pi}{D(\nu)} - 1 \right] \frac{P_{\nu-\frac{1}{2}}(-x)}{P_{\nu-\frac{1}{2}}(x)} \quad (12.175)$$

and
$$G(\nu) = \frac{\cos \nu \pi}{D(\nu)} \quad (12.176)$$

where $x = \cos \theta_0$ and

$$D(\nu) = \cos \nu \pi + g(\nu^2 - \frac{1}{4})P_{\nu-\frac{1}{2}}(x)P_{\nu-\frac{1}{2}}(-x) \quad (12.177)$$

Here, we have made use of the wronskian condition

$$P_{\nu-\frac{1}{2}}(x) \frac{d}{dx} P_{\nu-\frac{1}{2}}(-x) - P_{\nu-\frac{1}{2}}(-x) \frac{d}{dx} P_{\nu-\frac{1}{2}}(x) = \frac{2}{\pi} \frac{\cos \nu \pi}{1 - x^2} \quad (12.178)$$

On inserting the expressions for F and G , given by (12.175) and (12.176), into (12.173) and (12.174), we have the exact formal solution of the problem. It is important to remember, however, that the g , the sheath parameter, must be independent of r .

Residue series representations for the Debye potentials are obtained by closing the contour C about the complex poles in the right-hand portion of the ν plane. Thus, we arrive at the final results as given by Baños et al.²⁵

$$U_1 = \sum_{s=0}^{\infty} \frac{2\pi j k_0 \nu_s}{D'(\nu_s)} \frac{P_{\nu_s-\frac{1}{2}}(-\cos \theta_0)}{P_{\nu_s-\frac{1}{2}}(\cos \theta_0)} P_{\nu_s-\frac{1}{2}}(\cos \theta) f_{\nu_s-\frac{1}{2}}(r, r_0) \quad (12.179)$$

and
$$U_2 = \sum_{s=0}^{\infty} \frac{2\pi j k_0 \nu_s}{D'(\nu_s)} P_{\nu_s-\frac{1}{2}}(-\cos \theta) f_{\nu_s-\frac{1}{2}}(r, r_0) \quad (12.180)$$

where
$$D'(\nu_s) = \left[\frac{\partial D(\nu)}{\partial \nu} \right]_{\nu=\nu_s} \quad (12.181)$$

and ν_s are the solutions of

$$D(\nu) = 0 \quad (12.182)$$

for $s = 0, 1, 2, 3, \dots$

It should be mentioned that the residues occurring at the zeros of $\cos \nu \pi$ do not appear in the final results, because they cancel each other out identically. Baños et al.²⁵ show that, for any complex value of g , all but two of the zeros of $D(\nu)$ are in a one-to-one correspondence with the zeros of $\cos \nu \pi$. They also show that as g goes to zero, all but two of the roots approach unique zeros of $\cos \nu \pi$. The extra pair of roots approach infinity in opposite directions along the imaginary axis, so that, in the limit, they make a vanishing contribution to the radiated field.

In the general case where the collision frequency is finite, it is seen from (12.167) that both $\text{Re } g$ and $\text{Im } g > 0$. For this case, the roots of $D(\nu)$ lie in the first and third quadrants of the ν plane. Of course, only those in the first quadrant are needed for the residue series representation for U_1 and U_2 .

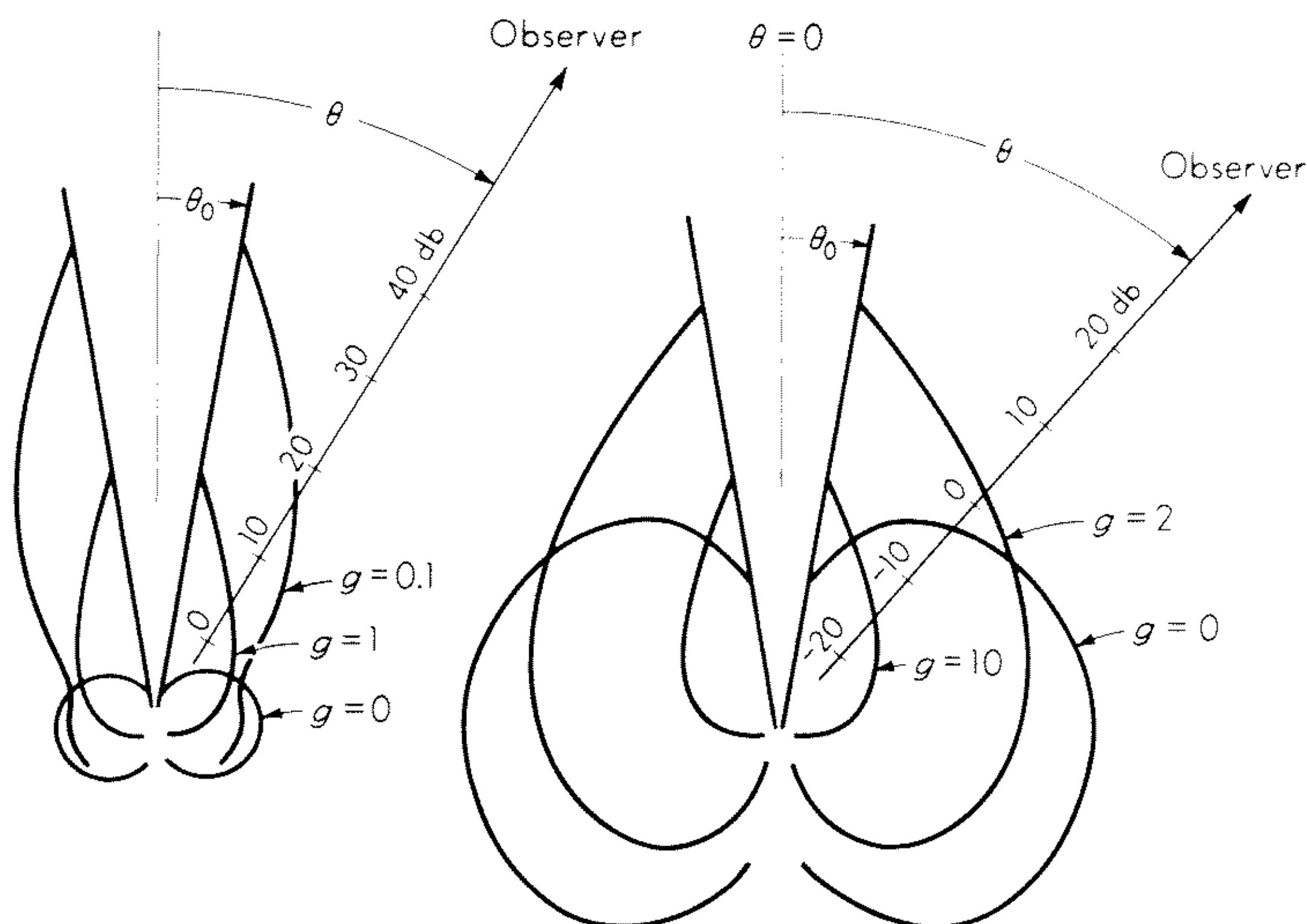


Fig. 12.16 Radiation pattern (log scale) for configuration of Fig. 12.14. (After Baños *et al.*²⁵)

The radiation patterns for a number of representative cases are shown in Fig. 12.16, where $k_0 r_0 = 1$ and $\theta_0 = 10^\circ$. The values of g , which are real, are indicated on the curves. The radiation coordinate in this case is proportional to $20 \log_{10} |H_\phi|$, and it is assumed, of course, that $k_0 r \gg 1$. The scale is normalized, so that the free space pattern (that is, $g = 0$) is 0 db. It is interesting to note that, for certain values of g of the order of 0.1, the field is greatly enhanced in directions away from the tip. Presumably, this may be attributed to the influence of surface waves which may propagate along the cone surface. In fact, the root ν_0 has a surface-wave character, and it appears that this term in the residue series dominates the field pattern for angles near θ_0 .

It should be stressed that the analysis outlined above and the resulting patterns in Fig. 12.16 refer to a dipole source whose current moment is kept constant. In an actual situation, one must also consider the influence of the sheath on the input impedance of the source. The fact that much of the radiated power is directed back along the cone surface would mean that a smaller fraction of the total power available is radiated in the forward directions. This may have important consequences in connection with "communication black-out" during the reentry phase when a space vehicle is returning to the earth.

It is interesting to note that an axially oriented magnetic dipole, located in the conical sheath, does *not* excite a surface wave on the cone surface. Unfortunately, the method used here for the electric dipole is not applicable. However, some results for a sheath with a magnetic dipole excitation have been obtained by Pridmore-Brown²⁸ by using a perturbation method.

In discussing conical sheaths, we have consistently considered that the structure is infinite. It must be stressed that the results and conclusions given here

apply only to this case. Very recently, Pridmore-Brown²⁹ has treated a conical sheath of finite slant height. The radiation pattern for an axially located electric dipole was calculated by using both a modified Wiener-Hopf technique and a perturbation method.

APPENDIX

A Modified Iterative Approach for a Biconical Antenna

As indicated above, the system of equations given by (12.46) and (12.62) constitute the exact formal solution of the biconical antenna problem. While approximate or limiting forms may be obtained without actually solving the system, it is desirable to examine them more carefully.

First of all, we note that the A_ν 's may be eliminated from (12.46) and (12.62) to give the single system

$$a_n Z_n^+ = -\frac{(2n+1)\zeta V(a)}{K} P_n(\cos \theta_0) + \sum_{\nu} \sum_{n'=1,3,5,\dots} Z_{\nu}^- \beta_{\nu,n} \alpha_{\nu,n'} a_{n'} \quad (\text{A-12.1})$$

We now observe that

$$T_{\nu}(\cos \theta_0) = 0 \quad (\text{A-12.2})$$

and thus

$$\frac{\partial T_{\nu}}{\partial \theta_0} d\theta_0 + \frac{\partial T_{\nu}}{\partial \nu} d\nu = 0 \quad (\text{A-12.3})$$

which indicates that

$$\frac{\partial T_{\nu}/\partial \theta_0}{\partial T_{\nu}/\partial \nu} = -\frac{d\nu}{d\theta_0} \quad (\text{A-12.4})$$

Then, on using (12.55) and (12.63), we have

$$\beta_{\nu,n} \alpha_{\nu,n'} = \frac{n(n+1)(2n+1)(2\nu+1) \sin \theta_0 P_n(\cos \theta_0) P_{n'}(\cos \theta_0)}{\nu(\nu+1)(n+\nu+1)(n'+n+1)(n-\nu)(n'-\nu)} \frac{d\nu}{d\theta_0} \quad (\text{A-12.5})$$

This suggests that we write (A-12.1) in the form

$$a_n Z_n^+ = -\frac{2n+1}{K} \zeta V(a) P_n(\cos \theta_0) - \sum_{n'=1,3,5,\dots} Z_{n,n'}^- a_{n'} \quad (\text{A-12.6})$$

where

$$Z_{n,n'}^- = -\sum_{\nu} Z_{\nu}^- \beta_{\nu,n} \alpha_{\nu,n'} \quad (\text{A-12.7})$$

An equivalent form of (A-12.6) which has the main diagonal on the left is

$$(Z_n^+ + Z_{nn}^-) a_n = -\frac{2n+1}{K} \zeta V(a) P_n(\cos \theta_0) - \sum'_{n'=1,3,5,\dots} Z_{n,n'}^- a_{n'} \quad (\text{A-12.8})$$

where the prime over the summation index indicates that the term $n' = n$ is omitted.

The first approximation in the present approach consists of neglecting all the off-diagonal terms. This is equivalent to neglecting the summation term in (A-12.8). Thus, to within this approximation,

$$a_n = a_n^{(1)} = -\frac{(2n+1)\zeta V(a) P_n(\cos \theta_0)}{K(Z_n^+ + Z_{nn}^-)} \quad (\text{A-12.9})$$

Now, from (12.70), it is evident that, provided θ_0 is not too small,

$$\begin{aligned} \nu &= -\frac{1}{2} + \left[\left(\frac{2m\pi}{\pi - 2\theta_0} \right)^2 - \frac{1}{4} \right]^{\frac{1}{2}} \quad m = 1, 2, 3, \dots \\ &\approx \frac{2m\pi}{\pi - 2\theta_0} - \frac{1}{2} - \frac{\pi - 2\theta_0}{16m\pi} - \frac{(\pi - 2\theta_0)^3}{1,024m^3\pi^3} - \dots \end{aligned} \quad (\text{A-12.10})$$

and

$$\frac{\partial \nu}{\partial \theta_0} \approx \frac{4m\pi}{(\pi - 2\theta_0)^2} + \frac{1}{8m\pi} + \dots \quad (\text{A-12.11})$$

Thus, we see from (A-12.5) that Z_{nn}^- vanishes as θ_0 approaches $\pi/2$. The resulting formula for a_n then corresponds to (12.72), as it must. The other limiting case corresponds to θ_0 tending to zero when $\beta_{\nu,n}\alpha_{\nu,n'}$ becomes -1 for $n = n'$ and zero otherwise. Then $Z_{n,n}^-$ in (A-12.9) is replaced by Z_n^- , which is equivalent to (12.76) or the equivalent form indicated in (12.100).

Schelkunoff³⁰ suggests that (A-12.8) may be iterated to obtain an m th-order approximation. Thus, following his prescription, we write the solution in the form

$$a_n = a_n^{(1)} + a_n^{(2)} + a_n^{(3)} + \dots \quad (\text{A-12.12})$$

where $a_n^{(1)}$ is given by (A-12.9)

and

$$a_n^{(m+1)} = - \frac{\sum_{n'} Z_{n,n'}^- a_n^{(m)}}{Z_n^+ + Z_{nn}^-} \quad (\text{A-12.13})$$

The effectiveness of this iterative approach is a consequence of the dominance of the coefficients in the principal diagonal of the infinite matrix given by (A-12.8).

Interesting discussion of the iterative method of solution of (A-12.1) has been given by King³¹ in his comprehensive treatise, and related matters were considered by Robin and Pereira-Gomes,³² Plonus,³³ and Fikioris.³⁴

REFERENCES

1. Schelkunoff, S. A.: Theory of Antennas of Arbitrary Size and Shape, *Proc. IRE*, vol. 29, pp. 493–521, 1941.
2. Schelkunoff, S. A.: Principal and Complementary Waves in Antennas, *Proc. IRE*, vol. 34, pp. 23–32, 1946.
3. Papas, C. H.: Input Impedance of Wide-angle Conical Antennas, *Cruft Lab. Tech. Rept. 52*, Harvard University, 1948.
4. Papas, C. H.: A Theoretical Investigation of Spherically Capped Antennas, doctoral dissertation, Harvard University, 1948.
5. Smith, P. D. P.: The Conical Dipole of Wide Angle, *J. Appl. Phys.*, vol. 19, pp. 11–23, 1948.
6. Tai, C. T.: On the Theory of Biconical Antennas, *J. Appl. Phys.*, vol. 19, pp. 1155–1160, 1948.
7. Tai, C. T.: A Study of the E.M.F. Method, *J. Appl. Phys.*, vol. 20, pp. 717–723, 1949.
8. Tai, C. T.: Application of a Variational Principle to Biconical Antennas, *J. Appl. Phys.*, vol. 20, pp. 1076–1084, 1949.

9. Schwinger, J.: Discontinuities in Waveguides, M.I.T. lecture notes (edited by D. S. Saxon), 1945.
10. Collin, R. E.: "Field Theory of Guided Waves" (chap. 8), McGraw-Hill Book Company, New York, 1960.
11. Galejs, J.: Capacitor-type Biconical Antennas, *Radio Sci. J. Res. Natl. Bur. Std. (U.S.)*, vol. 68D, pp. 165–172, February, 1964.
12. Wait, J. R.: "Electromagnetic Waves in Stratified Media," p. 318, Pergamon Press, Oxford, 1962.
13. Wait, J. R.: Theory of a Slotted-sphere Antenna Immersed in a Compressible Plasma, Part I, *Radio Sci. J. Res. Natl. Bur. Std. (U.S.)/USNC-URSI*, vol. 68D, no. 10, pp. 1127–1136, October, 1964.
14. Schelkunoff, S. A.: "Electromagnetic Waves," D. Van Nostrand Company, Inc., Princeton, N.J., 1943.
15. Polk, C.: Resonance and Super Gain Effects in Small Ferromagnetically or Dielectrically Loaded Biconical Antennas, *IRE Trans. Antennas Propagation*, vol. AP-7, pp. S414–S423, December, 1959.
16. Tai, C. T.: On Radiation and Radiating Systems in the Presence of a Dissipative Medium, *Cruft Lab. Tech. Rept. 77*, Harvard University, May 10, 1949.
17. Wait, J. R.: Theory of a Slotted-sphere Antenna Immersed in a Compressible Plasma, Part II, *Radio Sci. J. Res. Natl. Bur. Std. (U.S.)/USNC-URSI*, vol. 68D, no. 10, pp. 1137–1143, October, 1964.
18. Wait, J. R., and K. P. Spies: Theory of a Slotted-sphere Antenna Immersed in a Compressible Plasma, Part III, *Radio Sci.*, vol. 1 (new series), no. 1, pp. 21–26, January, 1966.
19. Wait, J. R.: Radiation from a Spherical Aperture Antenna Immersed in a Compressible Plasma, *IEEE Trans. Antennas Propagation*, vol. AP-14, pp. 360–368, 1966.
20. Adachi, S., R. G. Kouyoumjian, and R. G. Van Sickle: The Finite Conical Antenna, *IRE Trans. Antennas Propagation*, vol. AP-7, pp. S406–S411, December, 1959.
21. Felsen, L. B.: Back Scattering from Wide Angle and Narrow Angle Cones, *J. Appl. Phys.*, vol. 26, pp. 138–151, February, 1955.
22. Bailin, L., and S. Silver: Exterior Electromagnetic Boundary Value Problems for Spheres and Cones, *IRE Trans. Antennas Propagation*, vol. AP-4, pp. 6–16, January, 1956. For correction see *IRE Trans. Antennas Propagation*, vol. AP-5, p. 313, 1957.
23. Yeh, C.: An Application of Sommerfeld's Complex-order Wave Functions to an Antenna Problem, *J. Math. Phys.*, vol. 5, pp. 344–350, 1964.
24. Sommerfeld, A. N.: "Partial Differential Equations," Academic Press Inc., New York, 1949.
25. Baños, A., R. H. Huddleston, D. C. Pridmore-Brown, and E. C. Taylor: The Radiation Field of an Electric Dipole Antenna in a Conical Sheath, *J. Math. Phys.*, vol. 44, no. 3, pp. 189–213, September, 1965.
26. Wait, J. R.: The Electromagnetic Fields of a Dipole in the Presence of a Thin Plasma Sheet, *Appl. Sci. Res.*, vol. 8, sec. B, pp. 397–417, 1960.
27. Watson, G. N.: The Diffraction of Electric Waves by the Earth, *Proc. Roy. Soc. (London)*, vol. A95, pp. 83–99, 1918.
28. Pridmore-Brown, D. C.: The Radiation Field of a Magnetic Dipole Antenna in a Conical Sheath, *J. Math. Phys.*, vol. 43, no. 3, pp. 199–217, 1964.
29. Pridmore-Brown, D. C.: Electric Dipole Radiation through a Finite Conical Plasma Sheath, *IEEE Trans. Antennas Propagation*, vol. AP-14, pp. 428–433, 1966.
30. Schelkunoff, S. A.: "Advanced Antenna Theory," D. Van Nostrand Company, Inc., Princeton, N.J., 1952.
31. King, R. W. P.: "Theory of Linear Antennas," chap. VIII, Harvard University Press, Cambridge, Mass., 1956.

32. Robin, L., and A. Pereira-Gomes, L'Antenne Biconique, Symetrique, d'Angle Quelconque, *Ann. Telecommuni.*, vol. 8, p. 382, 1953.
33. Plonus, M. A.: Application of Selective Mode Coupling in the Solution to Biconical Antennas, in E. C. Jordan (ed.), "Electromagnetic Theory and Antennas," pp. 1155–1166, Pergamon Press, Oxford, 1963.
34. Fikioris, J. G.: The Biconical Antenna in a Radially Stratified Medium, *IEEE Trans. Antennas Propagation*, vol. AP-13, pp. 289–302, 1965.

ADDITIONAL REFERENCES

- Adachi, S.: A Theoretical Analysis of Semi-infinite Conical Antennas, *IRE Trans. Antennas Propagation*, vol. AP-8, pp. 534–547, November, 1960. Contains an extension of Tai's variational method to a semi-infinite biconical antenna which, of course, is a limiting case of a general biconical antenna.
- Borgnis, F. E., and C. H. Papas: "Randwertprobleme der Microwellenphysik," Springer-Verlag OHG, Berlin, 1955. Chapter 16 deals with the conical antenna problem and includes a comparison between theoretical and measured radiation patterns.
- Fahmy, M. N. I.: On the Theory of Electromagnetic Wave Propagation in Layered Media and Applications to Antenna Theory, communicated to *U.R.S.I. Sympo. of Electromagnetic Theory*, Delft, Holland, September, 1965. This paper deals with an iterative method of calculating transmission through arbitrarily stratified media with application to the mode theory of antennas. The paper is based in part on a 1964 doctoral dissertation, Manchester University.
- Felsen, L. B.: Radiation from Ring Sources in the Presence of a Semi-infinite Cone, *IRE Trans. Antennas Propagation*, vol. AP-7, pp. 168–180, April, 1959. Includes a derivation for wide and narrow azimuthal slots on a cone which reduces the exact solution to a quasi-optic form. Actually, this is much more convenient than the Bailin-Silver method unless, of course, the slot is near the tip. Felsen's quasi-optic formulas also include transition effects which take place in regions near the edges of the shadow zones.
- : Electromagnetic Properties of Wedge and Cone Surfaces with a Linearly varying surface Impedance, *IRE Trans. Antennas Propagation*, vol. AP-7, pp. S231–S243 (special suppl.), December, 1959. Felsen gives an exact solution for radiation from a ring source on or near the cone which has a surface impedance varying inversely as the distance to the tip. He also gives the excitation coefficients for the surface wave and discusses the far-field effects.
- Tai, C. T.: The Input Impedance of a Thin Biconical Antenna Immersed in a Dissipative and an Ionized Medium, *Antenna Lab. Rept.* 1021–14, Ohio State University Research Foundation Mar. 1, 1962. Gives numerical results for a thin biconical antenna in direct contact with both dissipative and ionized media.

CHAPTER 13

ELECTROMAGNETIC RADIATION FROM SPHEROIDAL STRUCTURES

James R. Wait

13.1 Introduction

As indicated by Schelkunoff,¹ the prolate spheroidal model of the radiating structure maintains mathematical rigor and allows one to consider end effects in a systematic manner. Furthermore, if the spheroid becomes sufficiently thin, it is possible to show in a convincing manner that the sinusoidal current assumption is indeed valid.²⁻⁴ Also, of course, when the major and minor axes are equal, the spheroidal model becomes a spherical antenna excited by an annular slot. The limiting case of an oblate spheroid of vanishing thickness (i.e., a disk) is also of interest.

In this chapter we shall present an exposition of the antenna theory for a spheroidal model. Also, some attention is given to the complexities which arise when the surrounding medium is no longer homogeneous. For the sake of completeness and to facilitate the explanation of notation, the first part of the chapter will be a brief introduction to the theory of prolate spheroidal wave functions. As we shall indicate, much of the theory for oblate spheroidal wave functions then follows if a simple change of variable is made.

13.2 Prolate Spheroid Coordinates

The spheroidal coordinate system (u, v, ϕ) used here is related to the cartesian system (x, y, z) as follows:

$$x = l[(1 - v^2)(u^2 - 1)]^{1/2} \cos \phi \quad (13.1)$$

$$y = l[(1 - v^2)(u^2 - 1)]^{1/2} \sin \phi \quad (13.2)$$

$$z = luv \quad (13.3)$$

where l is the semifocal distance.

For the prolate system considered here,

$$1 \leq u < \infty \quad \text{and} \quad -1 \leq v \leq +1$$

As indicated in Fig. 13.1, u is a radial coordinate, whereas v is an angular coordinate. It is also worth noting that, for l finite, the surfaces $u = \text{constant}$

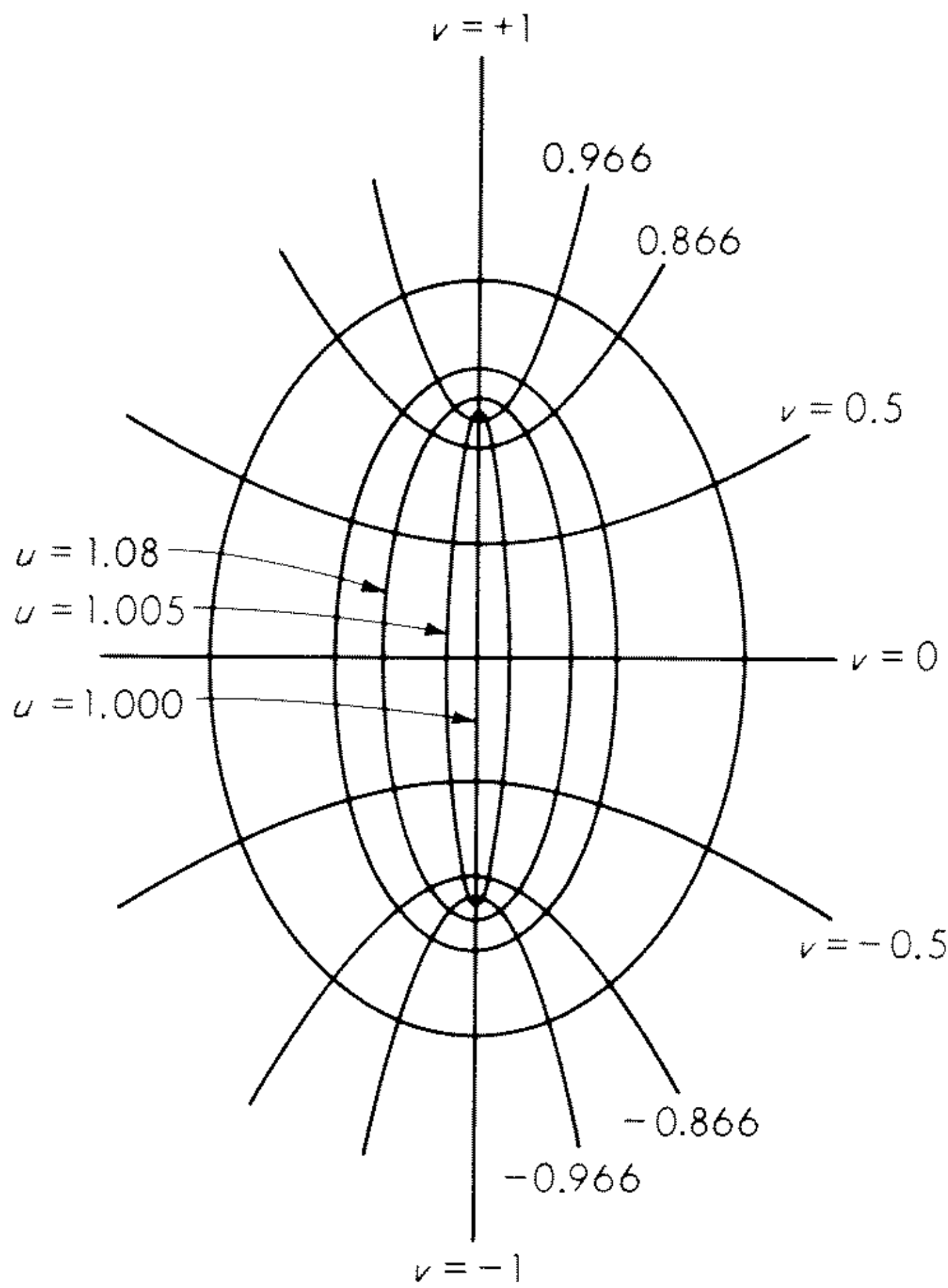


Fig. 13.1 Prolate spheroidal coordinate system.

become spherical as $u \rightarrow \infty$. For example, in this limiting case, it is seen readily that

$$lu \rightarrow r \quad v \rightarrow \cos \theta$$

where r and θ are the usual spherical coordinates.

To express Maxwell's equations in prolate spheroidal coordinates, it is necessary to employ appropriate forms for the metrical coefficients h_u , h_v , and h_ϕ . In terms of an element of length, these are defined by

$$(ds)^2 = (dx)^2 + (dy)^2 + (dz)^2 = h_u^2 du^2 + h_v^2 dv^2 + h_\phi^2 d\phi^2$$

where

$$h_u = l \left(\frac{u^2 - v^2}{u^2 - 1} \right)^{1/2} \quad h_v = l \left(\frac{u^2 - v^2}{1 - v^2} \right)^{1/2}$$

and

$$h_\phi = l[(1 - v^2)(u^2 - 1)]^{1/2}$$

By using well-known expressions for scalar and vector operators in curvilinear coordinates, explicit expressions for the gradient, divergence, curl, and Laplacian are readily obtained. For future reference, we record some of these here (where V is a scalar and \mathbf{F} is a vector):

$$\nabla_u V = \frac{1}{h_u} \frac{\partial V}{\partial u} \quad \nabla_v V = \frac{1}{h_v} \frac{\partial V}{\partial v} \quad \nabla_\phi V = \frac{1}{h_\phi} \frac{\partial V}{\partial \phi} \quad (13.4)$$

$$\nabla \cdot \mathbf{F} = \frac{1}{h_u h_v h_\phi} \left[\frac{\partial}{\partial u} (h_v h_\phi F_u) + \frac{\partial}{\partial v} (h_u h_\phi F_v) + \frac{\partial}{\partial \phi} (h_u h_v F_\phi) \right] \quad (13.5)$$

$$[\nabla \times \mathbf{F}]_u = \frac{1}{h_v h_\phi} \left[\frac{\partial}{\partial v} (h_\phi F_\phi) - \frac{\partial}{\partial \phi} (h_v F_v) \right] \quad (13.6)$$

and

$$\nabla^2 V = \frac{1}{h_u h_v h_\phi} \left[\frac{\partial}{\partial u} \left(\frac{h_v h_\phi}{h_u} \frac{\partial}{\partial u} V \right) + \frac{\partial}{\partial v} \left(\frac{h_\phi h_u}{h_v} \frac{\partial}{\partial v} V \right) + \frac{\partial}{\partial \phi} \left(\frac{h_u h_v}{h_\phi} \frac{\partial}{\partial \phi} V \right) \right] \quad (13.7)$$

13.3 Prolate Spheroidal Wave Functions

The scalar wave equation

$$(\nabla^2 + k^2)V = 0 \quad (13.8)$$

where k is a wave number, has the explicit form

$$\left[\frac{\partial}{\partial u} (u^2 - 1) \frac{\partial}{\partial u} + \frac{\partial}{\partial v} (1 - v^2) \frac{\partial}{\partial v} + \frac{u^2 - v^2}{(u^2 - 1)(1 - v^2)} \frac{\partial^2}{\partial \phi^2} + q^2(u^2 - v^2) \right] V = 0 \quad (13.9)$$

where $q = kl$. In regions where q does not depend on the coordinates, the above equation is separable. Thus, following the notation of Flammer,⁵ we write the basic solutions in the form

$$V_{m,n} = S_{m,n}(q, v) R_{m,n}(q, u) \frac{\cos}{\sin} m\phi \quad (13.10)$$

where $R_{m,n}$ and $S_{m,n}$ satisfy

$$\frac{d}{du} \left[(u^2 - 1) \frac{d}{du} R_{m,n} \right] - \left(\lambda_{m,n} - q^2 u^2 + \frac{m^2}{u^2 - 1} \right) R_{m,n} = 0 \quad (13.11)$$

$$\text{and} \quad \frac{d}{dv} \left[(1 - v^2) \frac{d}{dv} S_{m,n} \right] + \left(\lambda_{m,n} - q^2 v^2 - \frac{m^2}{1 - v^2} \right) S_{m,n} = 0 \quad (13.12)$$

Here, m and n may be taken as integers, since the solutions are to be periodic in both $\arccos v$ and ϕ . Also, it should be noted that $\lambda_{m,n}$ is a separation constant which is a function of q .

Those values of $\lambda_{m,n}(q)$ for which the differential equation (13.12) admits solutions at $v = \pm 1$ are the desired eigenvalues. Thus, in accordance with Flammer,⁵ this leads to the representation

$$S_{m,n}(q, v) = \sum'_{r=0,1,2,\dots} d_r^{m,n}(q) P_{m+r}^m(v) \quad (13.13)$$

The prime over the summation indicates that the summation is over (only) even values when $n - m$ is even and over (only) odd values when $n - m$ is odd. The associated Legendre functions employed here are defined by

$$P_n^m(v) = (1 - v^2)^{m/2} \frac{d^m P_n(v)}{dv^m} \quad (13.14)$$

for $-1 \leq v \leq 1$, where $P_n(v)$ is a Legendre polynomial of order n . The angle functions are normalized such that

$$S_{m,n}(q, 0) = P_n^m(0) \quad (13.15)$$

and, furthermore,

$$\lambda_{m,n}(0) = n(n+1) \quad n \geq m \quad (13.16)$$

From the general theory of Sturm-Liouville differential equations, it follows from (13.12) that the functions $S_{m,n}(q,v)$ form an orthogonal set on the interval $-1 \leq v \leq +1$. Thus,

$$\int_{-1}^{+1} S_{m,n}(q,v) S_{m,n'}(q,v) dv = \begin{cases} N_{m,n} & \text{if } n = n' \\ 0 & \text{if } n \neq n' \end{cases} \quad (13.17)$$

where $N_{m,n}$ is easily found with the use of the normalization factor of the associated Legendre function. To be explicit,

$$N_{m,n} = 2 \sum_{r=0,1,2,\dots}^{\infty'} \frac{(r+2m)!(d_r^{m,n})^2}{(2r+2m+1)r!} \quad (13.18)$$

where $d_r^{m,n}$ is the same coefficient which enters into (13.13). (In what follows, we shall not show the prime in summations over r . Thus, in these cases, we can regard the summation to extend over all values of r , but $d_r^{m,n}$ is zero for even (odd) values of r when $n-m$ is odd (even).)

The radial functions $R_{m,n}(q,u)$ are normalized such that, for $qu \rightarrow \infty$, they have the form

$$R_{m,n}^{(1)} \rightarrow \frac{1}{qu} \cos [qu - \frac{1}{2}(n+1)\pi] \quad (13.19)$$

$$R_{m,n}^{(2)} \rightarrow \frac{1}{qu} \sin [qu - \frac{1}{2}(n+1)\pi] \quad (13.20)$$

$$R_{m,n}^{(3)} \rightarrow \frac{1}{qu} \exp j[qu - \frac{1}{2}(n+1)\pi] \quad (13.21)$$

$$R_{m,n}^{(4)} \rightarrow \frac{1}{qu} \exp -j[qu - \frac{1}{2}(n+1)\pi] \quad (13.22)$$

where the superscript indicates which of the four types is being referred to. The appropriate expansions in terms of spherical Bessel functions are⁵

$$\left. \begin{aligned} R_{m,n}^{(1)}(q,u) \\ R_{m,n}^{(2)}(q,u) \end{aligned} \right\} = \frac{1}{\sum_{r=0,1,\dots}^{\infty} d_r^{m,n}(q) \frac{(2m+r)!}{r!} \left(\frac{u^2-1}{u^2} \right)^{m/2}} \times \sum_{r=0,1,\dots}^{\infty} j^{r+m-n} d_r^{m,n}(q) \frac{(2m+r)!}{r!} \begin{cases} j_{m+r}(qu) \\ y_{m+r}(qu) \end{cases} \quad (13.23)$$

$$\text{where} \quad j_n(z) = \left(\frac{\pi}{2z} \right)^{1/2} J_{n+1/2}(z) \quad (13.24)$$

$$\text{and} \quad y_n(z) = \left(\frac{\pi}{2z} \right)^{1/2} Y_{n+1/2}(z) \quad (13.25)$$

are related to the conventional cylindrical Bessel functions as indicated.

The radial functions of the third and fourth types are obtained from

$$R_{m,n}^{(3)} = R_{m,n}^{(1)} + jR_{m,n}^{(2)} \quad (13.26)$$

and
$$R_{m,n}^{(4)} = R_{m,n}^{(1)} - jR_{m,n}^{(2)} \quad (13.27)$$

The wronskian relationships for the radial functions may be found from (13.11) in the usual manner. Thus, for example,

$$R_{m,n}^{(1)} \frac{dR_{m,n}^{(2)}}{du} - R_{m,n}^{(2)} \frac{dR_{m,n}^{(1)}}{du} = \frac{1}{q(u^2 - 1)} \quad (13.28)$$

Many other useful relationships for the angle and radial functions are to be found in the comprehensive texts by Flammer,⁵ Stratton et al.,^{6,7} and Meixner and Schafke.⁸

13.4 Prolate Spheroidal Antenna in Free Space

A convenient introductory problem is to derive the expressions for the fields of a perfectly conducting prolate spheroid which is excited by a specified field over an aperture on its surface. To simplify the situation, it is assumed that symmetry prevails about the axial direction and, in addition, the medium exterior to the spheroid is taken to be free space.

The semimajor and the semiminor axes of the spheroid are designated by a and b , while the interfocal distance is $2l$. Designating the surface of the spheroid by $u = u_0$, it then follows that

$$u_0 = \frac{a}{l} = a(a^2 - b^2)^{-1/2} \quad (13.29)$$

For the symmetrical situation (that is, $\partial/\partial\phi = 0$), Maxwell's equations, relating \mathbf{E} and \mathbf{H} , take the form

$$h_v E_u = \frac{1}{j\epsilon_0\omega\rho} \frac{\partial(\rho H_\phi)}{\partial v} \quad (13.30)$$

$$h_u E_v = -\frac{1}{j\epsilon_0\omega\rho} \frac{\partial(\rho H_\phi)}{\partial u} \quad (13.31)$$

$$\frac{\partial(h_v E_v)}{\partial u} - \frac{\partial(h_u E_u)}{\partial v} = -j\mu_0\omega h_u h_v H_\phi \quad (13.32)$$

$$h_v H_u = -\frac{1}{j\mu_0\omega\rho} \frac{\partial(\rho E_\phi)}{\partial v} \quad (13.33)$$

$$h_u H_v = \frac{1}{j\mu_0\omega\rho} \frac{\partial(\rho E_\phi)}{\partial u} \quad (13.34)$$

$$\frac{\partial(h_v H_v)}{\partial u} - \frac{\partial(h_u H_u)}{\partial v} = j\epsilon_0\omega h_u h_v E_\phi \quad (13.35)$$

where $\rho = l[(1 - v^2)(u^2 - 1)]^{1/2}$ and where ϵ_0 and μ_0 are the dielectric constant and permeability of the exterior medium (i.e., free space). It is clear from the

above that the problem may be split into two parts. If the applied field on the aperture has only an E_v component, then, obviously, the excited magnetic field has only the H_ϕ component and, at the same time, $E_\phi = 0$. In a similar fashion it follows that, if the applied field, in the aperture, has only an E_ϕ component, the excited electric field has only an E_ϕ component and, at the same time, $H_\phi = 0$.

For the time being, we shall assume that the applied field has only an E_v component. Then, following Schelkunoff,¹ we set

$$H_\phi = \frac{A}{\rho} \quad (13.36)$$

where A is an auxiliary scalar wave function. Thus,

$$E_u = \frac{1}{j\epsilon_0\omega l^2} \frac{1}{[(u^2 - 1)(u^2 - v^2)]^{1/2}} \frac{\partial A}{\partial v} \quad (13.37)$$

and
$$E_v = -\frac{1}{j\epsilon_0\omega l^2} \frac{1}{[(1 - v^2)(u^2 - v^2)]^{1/2}} \frac{\partial A}{\partial u} \quad (13.38)$$

By inserting (13.36), (13.37), and (13.38) into (13.32) it readily follows that A satisfies

$$(u^2 - 1) \frac{\partial^2 A}{\partial u^2} + (1 - v^2) \frac{\partial^2 A}{\partial v^2} + q^2(u^2 - v^2)A = 0 \quad (13.39)$$

where $q = k_0 l$, $k_0 = (\epsilon_0 \mu_0)^{1/2} \omega$. It is interesting to observe that the total antenna current $I(v)$ is related to A by

$$I(v) = 2\pi\rho H_\phi|_{u=u_0} = 2\pi A(u_0, v) \quad (13.40)$$

Substituting

$$A = U_n(u) V_n(v) \quad (13.41)$$

into (13.39) leads readily to the pair

$$(u^2 - 1) \frac{d^2 U_n}{du^2} + (q^2 u^2 - \lambda_{1,n}) U_n = 0 \quad (13.42)$$

$$(1 - v^2) \frac{d^2 V_n}{dv^2} + (\lambda_{1,n} - q^2 v^2) V_n = 0 \quad (13.43)$$

where $\lambda_{1,n}$ is a separation constant. On comparing (13.42) and (13.43) with (13.11) and (13.12) for $m = 1$, it is readily seen that

$$U_n = (u^2 - 1)^{1/2} R_{1,n}^{(4)}(q, u) \quad (13.44)$$

and
$$V_n = (1 - v^2)^{1/2} S_{1,n}(q, v) \quad (13.45)$$

The radial function of the fourth kind has been chosen here, since the physical nature of the problem dictates that only outgoing waves will be present for $qu \rightarrow \infty$. The angle functions $S_{1,n}(q, v)$ or $V_n(v)/(1 - v^2)^{1/2}$ occur frequently in the theory which follows. Therefore, for the convenience of the reader, this

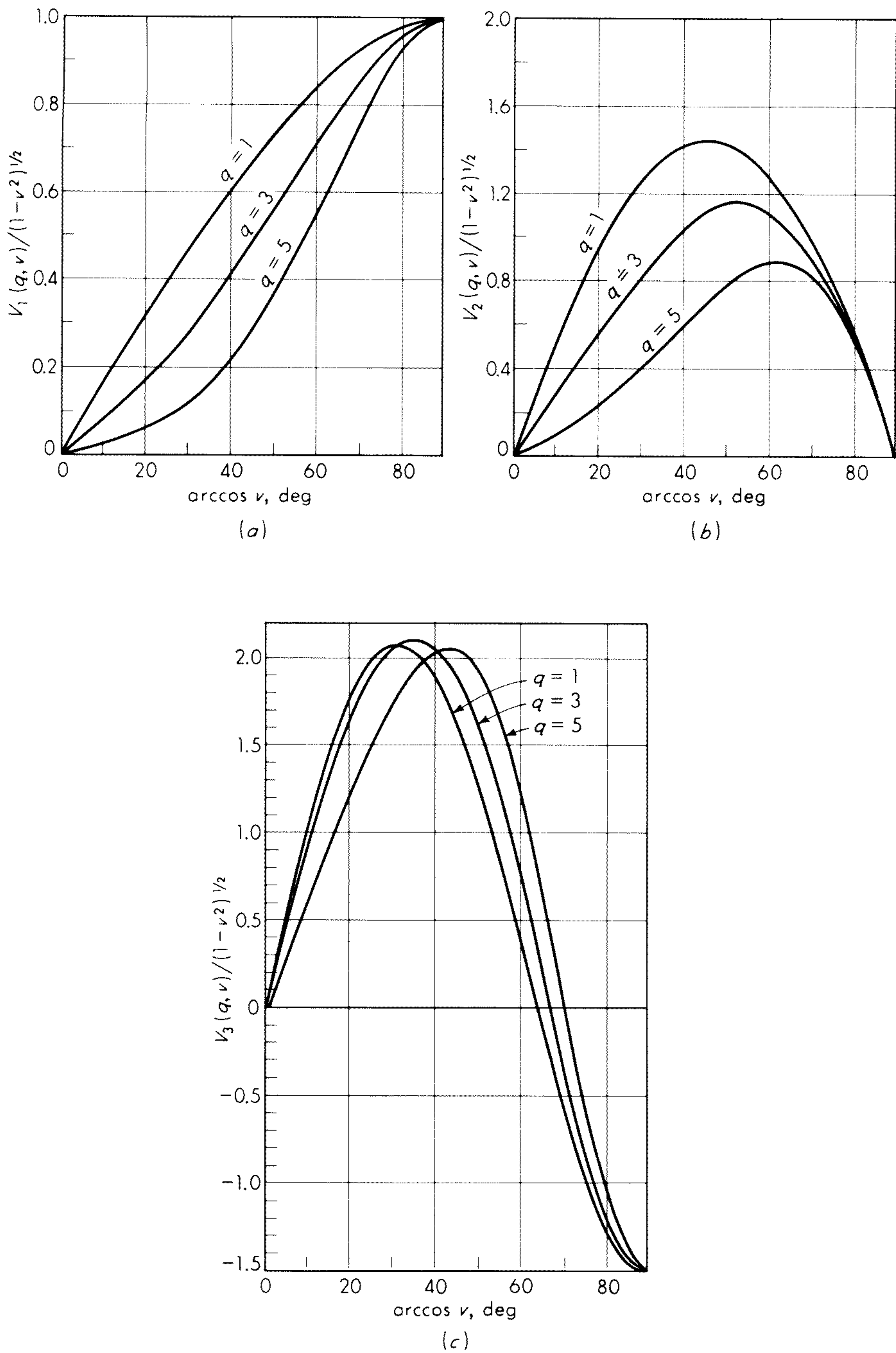


Fig. 13.2 (a) Angle function of order 1; (b) angle function of order 2; (c) angle function of order 3.

function is plotted in Fig. 13.2*a*, *b*, and *c* as a function of $\arccos v$ for various values of q .

The orthogonality condition stated by (13.17) for $m = 1$ is readily seen to be equivalent to

$$\int_{-1}^{+1} (1 - v^2)^{-1} V_n(v) V_{n'}(v) dv = \begin{cases} N_{1,n} & \text{if } n = n' \\ 0 & \text{if } n \neq n' \end{cases} \quad (13.46)$$

Now, for the exterior region (that is, $u > u_0$), we write

$$A = \sum_{n=1,2,\dots}^{\infty} a_n U_n(u) V_n(v) \quad (13.47)$$

where the coefficients a_n are to be determined from the conditions on the spheroid. Explicitly, it is required that

$$E_v(u_0, v) = E_v^a(u_0, v)$$

Thus, by making use of (13.38) and (13.47), an equivalent statement is

$$E_v^a(u_0, v) = -\frac{1}{j\epsilon_0\omega l^2} \frac{1}{[(1 - v^2)(u_0^2 - v^2)]^{1/2}} \sum_{n=1,2,\dots}^{\infty} a_n U'_n(u_0) V_n(v) \quad (13.48)$$

where

$$U'_n(u_0) = \left. \frac{d}{du} U_n(u) \right|_{u=u_0}$$

By multiplying both sides of (13.48) by $(1 - v^2)^{-1/2} V_{n'}(v)$ and then integrating v from -1 to $+1$, we find readily that

$$a_n = -\frac{j\epsilon_0\omega l^2}{N_{1,n} U'_n(u_0)} \int_{-1}^{+1} E_v^a(u_0, v) \left(\frac{u_0^2 - v^2}{1 - v^2} \right)^{1/2} V_n(v) dv \quad (13.49)$$

On inserting this expression into (13.47), a formal solution of the problem results. It may be written in the form

$$A = \sum_{n=1,2,\dots}^{\infty} \frac{j\epsilon_0\omega l}{N_{1,n}} \frac{U_n(u)}{U'_n(u_0)} \bar{V}_n V_n(v_0) V_n(v) \quad (13.50)$$

where

$$\bar{V}_n = -\int_{-1}^{+1} E_v^a(u_0, v) \frac{V_n(v)}{V_n(v_0)} l \left(\frac{u_0^2 - v^2}{1 - v^2} \right)^{1/2} dv \quad (13.51)$$

and v_0 is some fixed angular coordinate. The quantity \bar{V}_n is a generalized voltage. In the case of the so-called delta slot, E_v^a is zero everywhere on the spheroid except at some infinitesimally thin ring at (u_0, v_0) , as indicated in Fig. 13.3. Then, in this limiting case,

$$\begin{aligned} \bar{V}_n &= \lim_{\Delta v_0 \rightarrow 0} - \int_{v_0 - \Delta v_0}^{v_0 + \Delta v_0} E_v^a(u_0, v) h_v dv \\ &= \bar{V} \quad \text{the voltage across the slot} \end{aligned} \quad (13.52)$$

Actually, this is an adequate approximation for a thin annular slot of finite width, provided a large number of terms in the series are not needed.

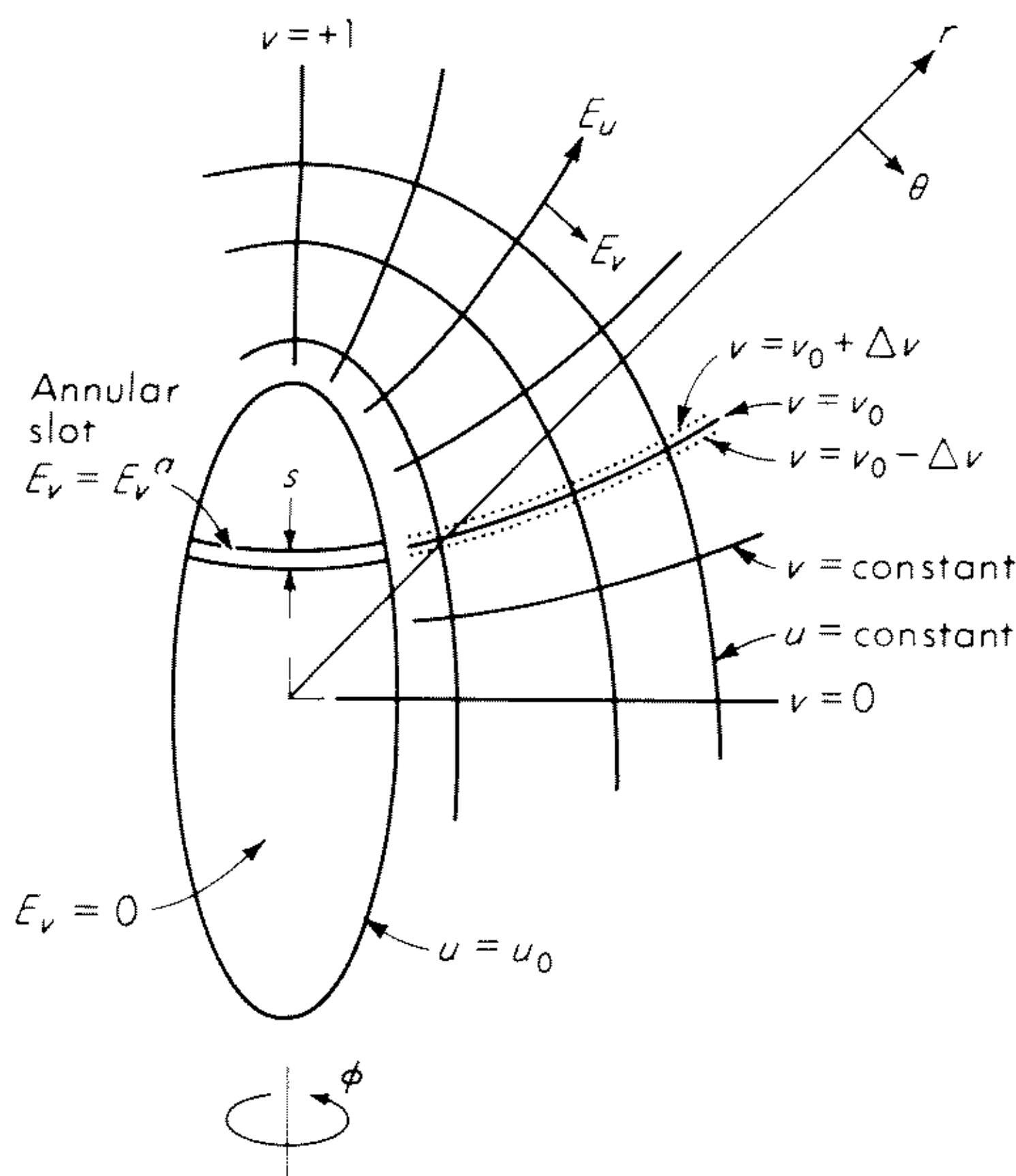


Fig. 13.3 Prolate spheroid model of an antenna with a circumferential slot uniformly excited by an electric field E_v^a .

An explicit expression for the magnetic field at large distances from the spheroid is readily obtained from (13.36) and (13.50) under the condition that $u \rightarrow \infty$. Thus,

$$H_\phi \approx -\epsilon_0 \omega \frac{e^{-jk_0 r}}{k_0 r \sin \theta} \sum_{n=1,2,\dots}^{\infty} \frac{\bar{V}_n V_n(v_0) e^{jn\pi/2} V_n(\cos \theta)}{N_{1,n} U'_n(u_0)} \quad (13.53)$$

and

$$E_\theta \approx \left(\frac{\mu_0}{\epsilon_0} \right)^{1/2} H_\phi$$

where r, θ are spherical coordinates. Equation (13.53) is in a form which lends itself readily to pattern synthesis. For example, if it be required that the radiation field has the form

$$H_\phi \approx -\epsilon_0 \omega \frac{e^{-jk_0 r}}{k_0 r} F(\theta) \quad (13.54)$$

where $F(\theta)$ is the desired pattern function, the required excitation function \bar{V}_n is readily determined. Explicitly, the procedure is to equate the right-hand sides of (13.53) and (13.54) and then multiply each one by $V_{n'}(\cos \theta)$ before integrating θ from 0 to π . As a result of the orthogonality relation,

$$\int_0^\pi V_n(\cos \theta) V_{n'}(\cos \theta) (\sin \theta)^{-1} d\theta = \begin{cases} N_{1,n} & \text{if } n = n' \\ 0 & \text{if } n \neq n' \end{cases} \quad (13.55)$$

it readily follows that

$$\bar{V}_n V_n(v_0) = U'_n(u_0) e^{-jn\pi/2} \int_0^\pi F(\theta) V_n(\cos \theta) d\theta \quad (13.56)$$

Noting that

$$\bar{V}_n V_n(v_0) = - \int_{-1}^{+1} E_v^a(u_0, v) V_n(v) l \left(\frac{u_0^2 - v^2}{1 - v^2} \right)^{1/2} dv \quad (13.57)$$

we may express

$$E_v^a(u_0, v) = \frac{-1}{l[(u_0^2 - v^2)(1 - v^2)]^{1/2}} \sum_{n=1,2,\dots}^{\infty} G_n V_n(v) \quad (13.58)$$

whence it readily follows that

$$G_n = U'_n(u_0) \frac{e^{-jn\pi/2}}{N_{1,n}} \int_0^\pi F(\theta) V_n(\cos \theta) d\theta \quad (13.59)$$

Therefore, we have an explicit formula to calculate the applied field E_v^a on the spheroid in order to produce a desired pattern $F(\theta)$ in the far field.

The result given by (13.50) may be applied directly to calculate the admittance of the spheroidal antenna in the general case. However, in order to simplify the discussion, we shall assume that the antenna is fed in such a manner that a uniform field is applied at a thin gap of width s in the equatorial plane of the spheroid. Thus, the slot extends from $v = -\Delta v$ to $+\Delta v$, where $\Delta v = s/(2lu_0)$ is small compared with unity. For this case, the admittance is obtained from

$$Y = \frac{I(\Delta v)}{V_0} \approx - \frac{j\pi\epsilon_0\omega l}{\Delta v} \sum_n \frac{U_n(u_0)}{U'_n(u_0)} \frac{V_n(\Delta v)}{N_{1,n}} \int_{-\Delta v}^{\Delta v} V_n(v) dv \quad (13.60)$$

where V_0 is the actual voltage across the gap. Using essentially this formula, Chu and Stratton² have given numerical data for the conductance and susceptance for thin spheroids, where $2l/\lambda_0$ varies from 0.2 to 0.8. Their results show that, in this range, the contribution from the first mode (that is, $n = 1$) is by far the most significant provided a/b is somewhat greater than about 10. Physically, the reason for this behavior is that the first mode is resonant when $2l/\lambda_0 = 0.5$, and the admittance behaves as a series resonant circuit in this region. For the same reason, resonances can be expected for the higher modes when $2l$ is an odd multiple of $\lambda_0/2$.

Actually, the characteristics of the modes at a resonance are easy to calculate because the differential equation (13.43), for V_n , has a simple form when $\lambda_{1,n} = q^2$. In this case,

$$\frac{d^2 V_n}{dv^2} + q^2 V_n = 0 \quad (13.61)$$

A solution which is even and which vanishes at $v = \pm 1$ is simply

$$V_n = \cos \left[\frac{(2n-1)\pi v}{2} \right] \times \text{constant} \quad (13.62)$$

For the same condition, we also see from (13.42) that the “radial” solution corresponding to outgoing waves is

$$U_n = \exp \left[\frac{-j(2n-1)\pi u}{2} \right] \times \text{constant} \quad (13.63)$$

From (13.60) we then see that the admittance Y_n of a mode at resonance is given by

$$Y_n = -j \left(\frac{\epsilon_0}{\mu_0} \right)^{1/2} \frac{(2n-1)\pi^2 U_n(u_0)}{N_{1,n} U'_n(u_0)} = \frac{2\pi}{\zeta_0 N_{1,n}} \quad (13.64)$$

where

$$\begin{aligned} N_{1,n} &= \int_{-1}^{+1} V_n^2 (1-v^2)^{-1} dv = \int_0^1 \frac{1 + \cos(2n-1)\pi v}{1-v^2} dv \\ &= \frac{1}{2} \int_0^{2(2n-1)\pi} \frac{1 - \cos x}{x} dx \end{aligned} \quad (13.65)$$

Thus, the admittance is purely real and the corresponding resistance R_n of a mode n at its resonance is given by

$$R_n = \frac{\zeta_0}{4\pi} \int_0^{2\pi(2n-1)} \frac{1 - \cos x}{x} dx \quad (13.66)$$

Numerical values of R_n may be readily obtained from tabulations of the cosine integral. For example, for the first mode and taking the antenna to be in free space

$$R_1 = 73.13 \text{ ohms}$$

It is rather interesting that this value is independent of the ratio a/b for the spheroid provided that $2l/\lambda_0 = 0.5$. Of course, one should remember that for the fatter spheroids (for example, $a/b < 20$), the contributions from the higher modes will be significant.

It also is not difficult to see that, for mode 1, the magnetic field of the slot-excited spheroid is

$$H_\phi \Big|_{n=1} = \text{constant} \times \frac{e^{-jqv}}{lu(1-v^2)^{1/2}} \cos(qv) \quad (13.67)$$

In the far field, $lu \rightarrow r$ and $v \rightarrow \cos \theta$, we have

$$H_\phi \Big|_{n=1} \approx \text{constant} \times \frac{e^{-jk_0 r}}{r} \frac{\cos[(\pi/2) \cos \theta]}{\sin \theta} \quad (13.68)$$

which has the classical form for the radiation field of an infinitesimally thin center-fed “half-wave” antenna. In this case, the result is exact for the first mode when the spheroid is resonant.

13.5 Prolate Spheroidal Antenna with a Confocal Sheath

An interesting situation arises when the medium surrounding the antenna is inhomogeneous. For example, it is known that, when a space vehicle enters the

atmosphere, an ionized sheath is formed in the vicinity of the antenna. One approach to study this problem is to assume that the sheath may be represented by a confocal region extending from $u = u_1$ to u_2 , as indicated in Fig. 13.4. The dielectric constant of the three homogeneous regions adjacent to the antenna surface (that is, $u = u_0$) are ϵ_0 , ϵ_1 , and ϵ . On the other hand, the magnetic permeability is taken to be μ_0 throughout, which is a simplifying rather than a necessary restriction.

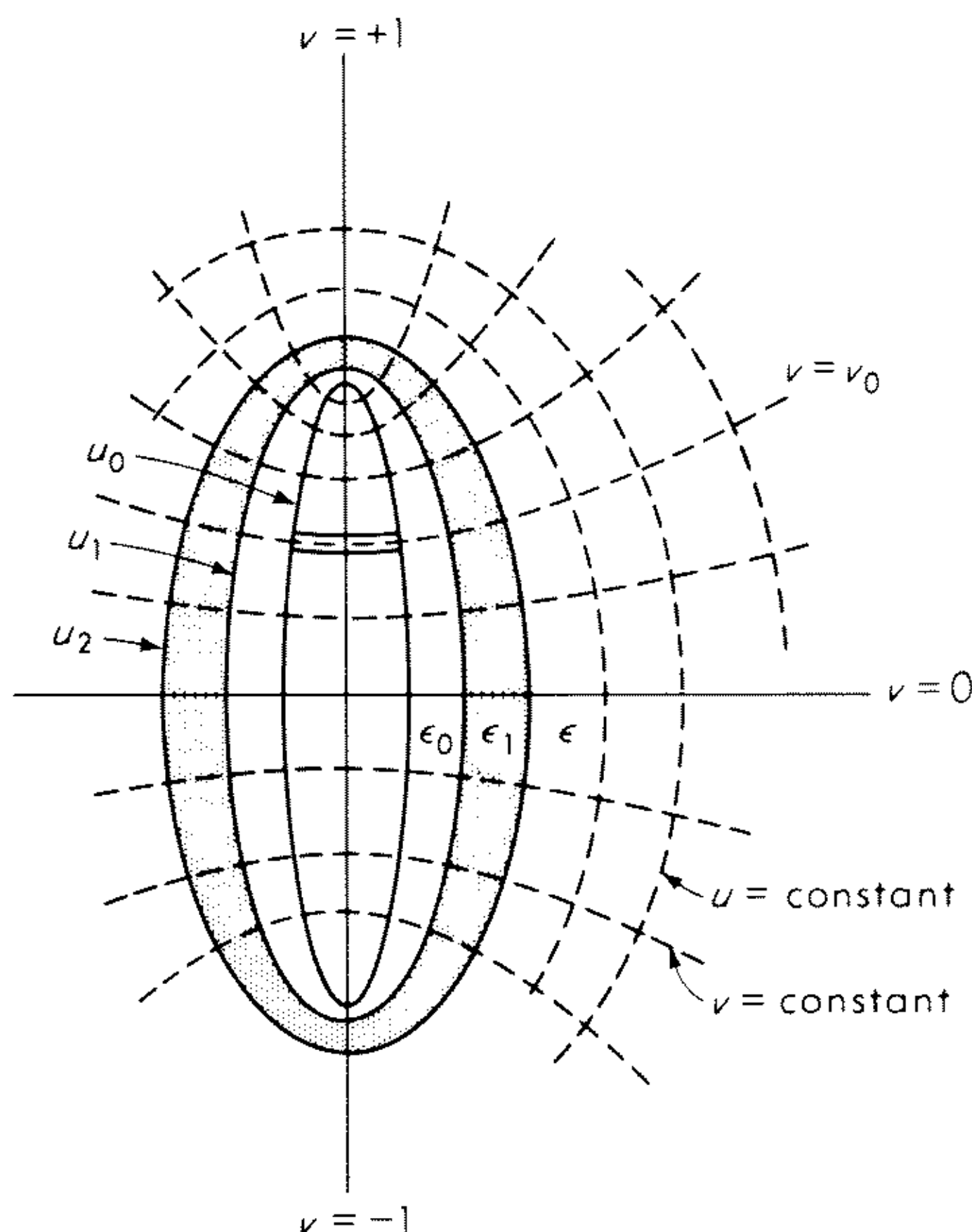


Fig. 13.4 Prolate spheroidal antenna with a confocal sheath.

The solution is obtained by employing a straightforward boundary-matching technique. However, a complication arises. It is not present in spherical geometry,⁹ nor does it arise in the quasi-static solutions^{10,11} for matching solutions on the two sides of a spheroidal boundary. Simply stated, the difficulty is that the angle spheroidal functions depend on the properties of the medium. However, in the spherical geometry, or in the static limit, the angle functions $S_{m,n}(q,v)$ pass over to $P_m^n(v)$, which are not dependent on q .

We shall first turn our attention to the form which the solution should take in the confocal region immediately adjacent to the antenna surface (that is, $u_0 < u < u_1$). As in the preceding section, we may express the tangential fields in the following form:

$$H_\phi^0 = \frac{A_0}{l[(u^2 - 1)(1 - v^2)]^{1/2}} \quad (13.69)$$

$$E_v^0 = -\frac{1}{j\epsilon_0\omega l^2} \frac{1}{[(1 - v^2)(u^2 - v^2)]^{1/2}} \frac{\partial A_0}{\partial u} \quad (13.70)$$

where A_0 satisfies (13.39) with q replaced by q_0 . However, here we must allow the existence of both "ingoing" and "outgoing" radial solutions. Thus, for a general solution, we have linear combinations of $U_n(q_0, u)$ and $T_n(q_0, u)$, where U_n is defined by (13.44) and

$$T_n(q_0, u) = (u^2 - 1)^{1/2} R_{1,n}^{(3)}(q_0, u) \quad (13.71)$$

where $R_{1,n}^{(3)}$ is Flammer's⁵ radial function for $m = 1$. In the present case $q_0 = (\epsilon_0 \mu_0)^{1/2} \omega l$, where, as usual, l is the semifocal distance for the spheroid.

For the region $u_0 < u < u_1$, it is evident that the solution is of the form

$$A_0 = \sum_n [M_n^0 U_n(q_0, u) + N_n^0 T_n(q_0, u)] V_n(q_0, v) \quad (13.72)$$

where M_n^0 and N_n^0 are coefficients and

$$V_n(q_0, v) = (1 - v^2)^{1/2} S_{1,n}(q_0, v) \quad (13.73)$$

(For the remainder of this chapter, the summation \sum_n will mean summation

over n from 1 through integers to ∞ , unless stated otherwise.)

A relation between M_n^0 and N_n^0 can be immediately obtained by expressing the field E_v^a on the surface of the antenna in the form

$$E_v \Big|_{u=u_0} = E_v^a = \frac{-1}{j\epsilon_0 \omega l^2} \frac{1}{[(1 - v^2)(u_0^2 - v^2)]^{1/2}} \sum_n p_n V_n(q_0, v) \quad (13.74)$$

The coefficients p_n may be calculated from

$$p_n = -\frac{j\epsilon_0 \omega l^2}{N_{1,n}(q_0)} \int_{-1}^{+1} E_v^a \left(\frac{u_0^2 - v^2}{1 - v^2} \right)^{1/2} V_n(q_0, v) dv \quad (13.75)$$

which in the case of a thin slot is given by

$$p_n \approx -\frac{j\epsilon_0 \omega l}{N_{1,n}(q_0)} V_n(q_0, v_0) \bar{V} \quad (13.76)$$

where \bar{V} is the applied voltage across the slot.

It now follows from (13.70), (13.72), and (13.74) that the appropriate representation for A_0 is given by

$$A_0 = \sum_n \left[M_n^0 U_n(q_0, u) + \frac{p_n - M_n^0 U'_n(q_0, u_0)}{T'_n(q_0, u_0)} T_n(q_0, u) \right] V_n(q_0, v) \quad (13.77)$$

On the other hand, for the region $u_1 < u < u_2$, it follows that

$$A_1 = \sum_p [M_p^1 U_p(q_1, u) + N_p^1 T_p(q_1, u)] V_p(q_1, v) \quad (13.78)$$

where M_p^1 and N_p^1 are coefficients. Finally, in the outermost region, $u_2 < u$, we use the form

$$A = \sum_s [M_s U_s(q, u)] V_s(q, v) \quad (13.79)$$

where the T radial functions are not permitted because the field must have an outgoing character as $u \rightarrow \infty$.

The boundary conditions, which require the continuity of the tangential fields, may be stated in the equivalent form

$$A_0 = A_1 \qquad u = u_1 \tag{13.80}$$

$$\frac{1}{\epsilon_0} \frac{\partial A_0}{\partial u} = \frac{1}{\epsilon_1} \frac{\partial A_1}{\partial u} \qquad u = u_1 \tag{13.81}$$

and $A_1 = A \qquad u = u_2 \tag{13.82}$

$$\frac{1}{\epsilon_1} \frac{\partial A_1}{\partial u} = \frac{1}{\epsilon} \frac{\partial A}{\partial u} \qquad u = u_2 \tag{13.83}$$

The difficulty of satisfying these conditions is immediately evident because the individual terms in the series (13.77), (13.78), and (13.79) cannot be matched term by term. Of course, a “brute force” approach might be adopted which would, in essence, require that (13.80) to (13.83) be satisfied at a finite number of angular points of v from -1 to $+1$. Presumably, the accuracy could be improved by choosing a smaller interval, but the ultimate convergence of such a process is very difficult to establish.

A more logical approach is to replace the angle functions in (13.77), (13.78), and (13.79) by the series in terms of Legendre functions. For example,

$$V_n(q_0,v) = \sum_{r=0,1,2,\dots}^{\infty} (1 - v^2)^{1/2} d_{r-1}^{1,n}(q_0) P_{1+r}^1(v) \tag{13.84a}$$

$$= \sum_r (1 - v^2)^{1/2} d_{r-1}^{1,n}(q_0) P_r^1(v) \tag{13.84b}$$

The representations (13.77), (13.78), and (13.79) are now written in the respective forms

$$A_0 = (1 - v^2)^{1/2} \sum_r P_r^1(v) \sum_n d_{r-1}^{1,n}(q_0) [\cdots] \tag{13.85}$$

$$A_1 = (1 - v^2)^{1/2} \sum_r P_r^1(v) \sum_p d_{r-1}^{1,p}(q_1) [\cdots] \tag{13.86}$$

$$A = (1 - v^2)^{1/2} \sum_r P_r^1(v) \sum_s d_{r-1}^{1,s}(q) [\cdots] \tag{13.87}$$

where the square brackets in (13.85), (13.86), and (13.87) are identical with those in (13.77), (13.78), and (13.79), respectively. Inserting these expressions into the boundary conditions (13.80) to (13.83) leads readily to the system

$$\begin{aligned} \sum_n d_{r-1}^{1,n}(q_0) \left[M_n^0 U_n(q_0,u_1) + \frac{p_n - M_n^0 U'_n(q_0,u_0)}{T'_n(q_0,u_0)} T_n(q_0,u_1) \right] \\ = \sum_p d_{r-1}^{1,p}(q_1) [M_p^1 U_p(q_1,u) + N_p^1 T_p(q_1,u_1)] \end{aligned} \tag{13.88}$$

$$\begin{aligned} \frac{1}{\epsilon_0} \sum_n d_{r-1}^{1,n}(q_0) \left[M_n^0 U'_n(q_0,u_1) + \frac{p_n - M_n^0 U'_n(q_0,u_0)}{T'_n(q_0,u_0)} T'_n(q_0,u_1) \right] \\ = \frac{1}{\epsilon_1} \sum_p d_{r-1}^{1,p}(q_1) [M_p^1 U'_p(q_1,u_1) + N_p^1 T'_p(q_1,u_1)] \end{aligned} \tag{13.89}$$

$$\begin{aligned} \sum_p d_{r-1}^{1,p}(q_1) [M_p^1 U_p(q_1,u_2) + N_p^1 T_p(q_1,u_2)] \\ = \sum_s d_{r-1}^{1,s}(q) M_s U_s(q,u_2) \end{aligned} \tag{13.90}$$

$$\frac{1}{\epsilon_1} \sum_p d_{r-1}^{1,p}(q_1) [M_p^1 U'_p(q_1, u_2) + N_p^1 T'_p(q_1, u_2)] = \frac{1}{\epsilon} \sum_s d_{r-1}^{1,s}(q) M_s U'_s(q, u_2) \quad (13.91)$$

The equations (13.88) to (13.91) must be solved for the unknown coefficients M_n^0 , M_p^1 , N_p^1 , and M_s . These equations are valid for each value of r , so that, by taking r sufficiently large, an adequate number of relations between the unknown coefficients is generated. Strictly speaking, an infinite set is required, since n , p , and s are integers from 1 to ∞ . However, the fact that the coefficients $d_{r-1}^{1,p}$ peak rather sharply about the value $d_{p-1}^{1,p}$ means that only a finite set of equations is actually needed. Thus, in effect, the coupling between the equations of different order is small. Furthermore, it is also worth noting that the equations involving even-ordered functions are completely decoupled from those of odd order and this, of course, reduces the labor needed to solve the system.

In principle, the problem of the spheroid with a confocal sheath has been solved. Once the coefficients M_s are obtained, the radiation field (that is, $u \rightarrow \infty$) may be calculated from the expression

$$H_\phi \approx \frac{e^{-jkr}}{krl} \sum_s e^{j(\pi/2)(s+1)} M_s \frac{V_s(q, \cos \theta)}{\sin \theta} \quad (13.92)$$

A special case of the sheath model discussed above is when the inner layer becomes of vanishing thickness (that is, $u_1 = u_0$). The four sets of equations (13.88) to (13.91) then reduce to two sets. Of course, the coupling between equations of different orders still applies, but the complexity is not quite so great. In fact, some explicit solutions have actually been obtained by Weeks.¹² Undoubtedly, the success of the method is due to the fact that the representation of the angular functions such as given by (13.84b) is dominated by the term where $r = n$, provided the q value is not too large (i.e., say, $q < 10$).

Some far-field radiation patterns for the coated spheroid are shown in Fig. 13.5a and b, using data from the report by Weeks¹² mentioned above. The parameters are chosen such that $u_0 = u_1 = 1.077$, $u_2 = 1.100$, $\epsilon_1/\epsilon = (8/5)^{1/2}$, and $q = 5$, and various values of the slot location $v = v_0$ are indicated. The corresponding patterns for the same spheroid (that is, $u_0 = 1.077$) with no coating are also shown for comparison. It is evident that the coating has the general effect of increasing the magnitude of the lobes.

It is worth mentioning that another method of handling the boundary-value problem of the sheathed spheroid was pointed out by Yeh.¹³ While he showed explicitly results for a single dielectric coating, the method is amenable to any number of confocal dielectric regions. We shall indicate the approach to the model of Fig. 13.4.

The basic idea is to represent the angle functions in two of the dielectric regions as expansions of the natural angle functions of the third region. For example, we write

$$V_n(q_0, v) = \sum_s L_s^{(n)} V_s(q, v) \quad (13.93)$$

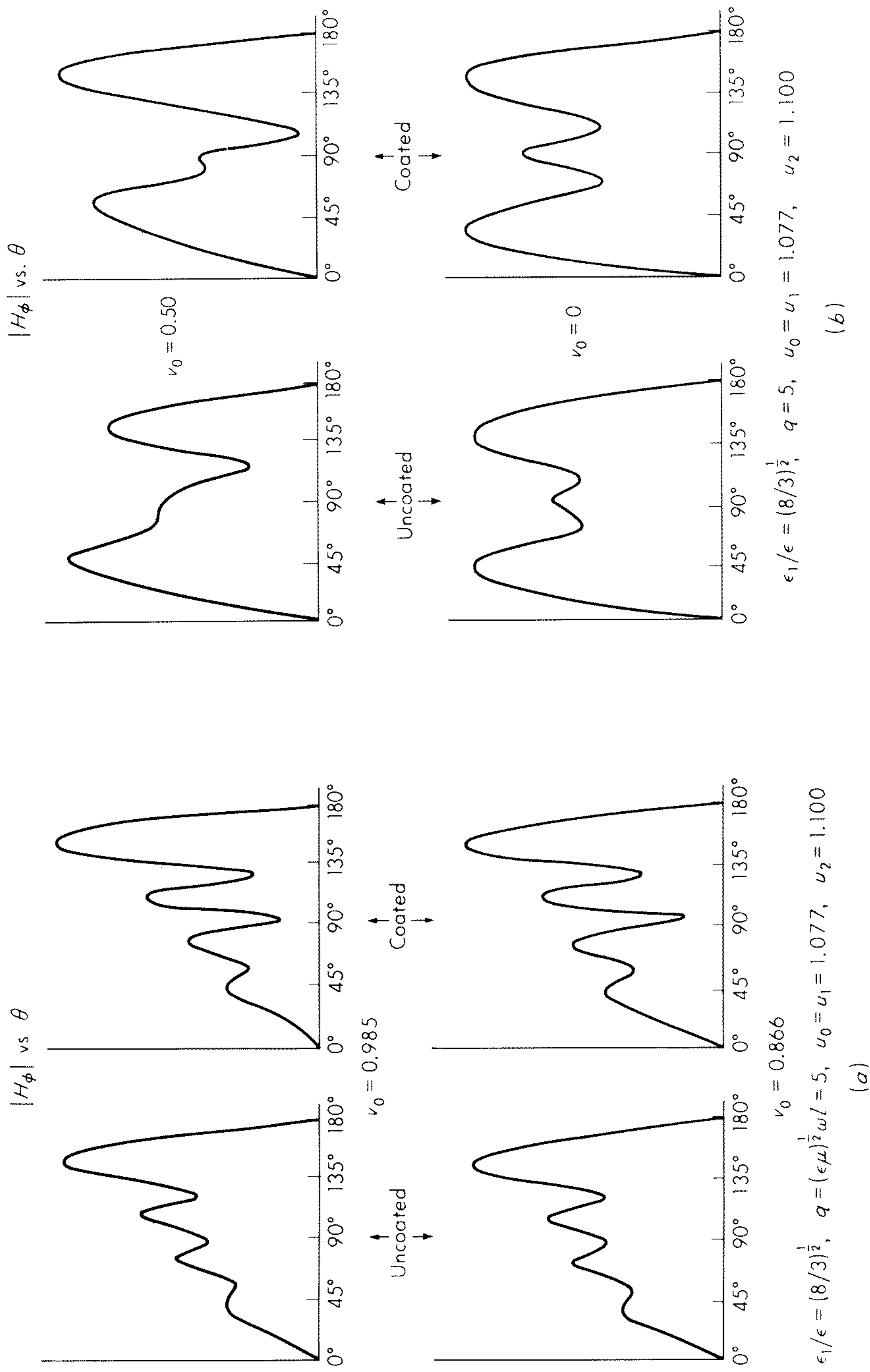


Fig. 13.5 (a) *E*-plane patterns of prolate spheroid antennas with circumferential slot at $v = v_0$; (b) *E*-plane patterns of prolate spheroid antennas with circumferential slot at $v = v_0$. (After Weeks.¹²)

where, as a result of orthogonality,

$$\begin{aligned} L_s^{(n)} &= \frac{1}{N_{1,s}(q)} \int_{-1}^{+1} (1-v^2)^{-1} V_n(q_0, v) V_s(q, v) dv \\ &= \frac{1}{N_{1,s}(q)} \sum_r d_{r-1}^{1,n}(q_0) d_{r-1}^{1,s}(q) \int_{-1}^{+1} [P_r^1(v)]^2 dv \\ &= \frac{1}{N_{1,s}(q)} \sum_r d_{r-1}^{1,n}(q_0) d_{r-1}^{1,s}(q) \frac{2r(r+1)}{2r+1} \end{aligned} \quad (13.94)$$

where the normalization factor $N_{1,s}(q)$ and the coefficients $d_{r-1}^{1,n}$ and $d_{r-1}^{1,s}$ are defined and tabulated by Flammer.⁵ In a similar manner, we find that

$$V_p(q_1, v) = \sum_s L_s^{(p)} V_s(q, v) \quad (13.95)$$

where
$$L_s^{(p)} = \frac{1}{N_{1,s}(q)} \sum_r d_{r-1}^{1,p}(q_1) d_{r-1}^{1,s}(q) \frac{2r(r+1)}{2r+1} \quad (13.96)$$

Expressions for the A functions which are analogous to (13.85), (13.86), and (13.87) are readily seen to be

$$A_0 = \sum_s V_s(q, v) \sum_n L_s^{(n)} [\cdots] \quad (13.97)$$

$$A_1 = \sum_s V_s(q, v) \sum_p L_s^{(p)} [\cdots] \quad (13.98)$$

$$A = \sum_s V_s(q, v) [M_s U_s(q, u)] \quad (13.99)$$

where the square brackets in (13.97) and (13.98) are the same as those in (13.77) and (13.78), respectively. Matching boundary conditions at the two surfaces now leads to a system of equations of the form

$$\sum_n L_s^{(n)} [\cdots] = \sum_p L_s^{(p)} [\cdots] \quad (13.100)$$

$$\frac{1}{\epsilon_0} \sum_n L_s^{(n)} [\cdots] = \frac{1}{\epsilon_1} \sum_p L_s^{(p)} [\cdots] \quad (13.101)$$

$$\sum_p L_s^{(p)} [\cdots] = M_s U_s(q, u_2) \quad (13.102)$$

$$\frac{1}{\epsilon_1} \sum_p L_s^{(p)} [\cdots] = \frac{1}{\epsilon} M_s U'_s(q, u_2) \quad (13.103)$$

where the square brackets in (13.100) to (13.103) are identical with those in (13.88) to (13.91).

Again, when treating the single coating (such that $u_0 = u_1$), the system of four sets of equations given above reduces to two sets. The formal solution thus obtained is identical with the result quoted by Yeh,¹³ who suggested that the further reduction could be carried out by matrix analysis. However, to obtain numerical answers by using Yeh's approach would require that the resulting infinite matrices be truncated or trimmed. This, in effect, means that only a finite number of equations are being used as an approximation for the infinite

set given above. The relative advantage of Yeh's¹³ approach over that used by Weeks¹² remains to be investigated. Presumably, when various dielectric regions are nearly identical in their electrical properties, expansions of the angle functions in one region in terms of those in another region should be highly convergent. This should be the case even for electrically large spheroids, in which case the expansion of the various angle functions in terms of Legendre functions would be very poorly convergent.

13.6 A Note on the Spheroid Excited by an Azimuthally Directed Electric Field

The excitation of the conducting prolate spheroid by an azimuthal field E_ϕ^a on its surface $u = u_0$ is really a straightforward extension of the analysis in Sec. 13.4. For example, if we assume the spheroid is surrounded by free space and azimuthal symmetry prevails, (13.33) to (13.35) are relevant. By direct analogy with (13.36) to (13.38), we now write instead

$$E_\phi = \frac{B}{\rho} \quad (13.104)$$

where B is an auxiliary scalar wave function satisfying (13.39). Then, from (13.33) and (13.34), it follows that

$$H_u = -\frac{1}{j\mu_0\omega l^2} \frac{1}{[(u^2 - 1)(u^2 - v^2)]^{1/2}} \frac{\partial B}{\partial v} \quad (13.105)$$

and
$$H_v = \frac{1}{j\mu_0\omega l^2} \frac{1}{[(1 - v^2)(u^2 - v^2)]^{1/2}} \frac{\partial B}{\partial u} \quad (13.106)$$

The appropriate form of the solution is

$$B = \sum_{n=1,2,\dots}^{\infty} b_n U_n(u) V_n(v) \quad (13.107)$$

or
$$E_\phi = \frac{1}{l[(u^2 - 1)(1 - v^2)]^{1/2}} \sum_{n=1,2,\dots}^{\infty} b_n U_n(u) V_n(v) \quad (13.108)$$

If the field at $u = u_0$ is specified to be E_ϕ^a , we readily deduce that

$$b_n = \frac{1}{N_{1,n} U_n(u_0)} \int_{-1}^{+1} E_\phi^a V_n(v) \left(\frac{u_0^2 - 1}{1 - v^2} \right)^{1/2} l dv \quad (13.109)$$

13.7 Excitation of Spheroid by External Sources

In some situations, the source of the electromagnetic field is external to the spheroid. A case of particular interest is when a spheroid is placed on the axis of a circular loop of electric current. To place the problem in a slightly more general context we shall imagine that a prolate spheroid at $u = u_0$ is confocal with a current-carrying shell at $u = u_a$ where $u_a > u_0$. This situation is illus-

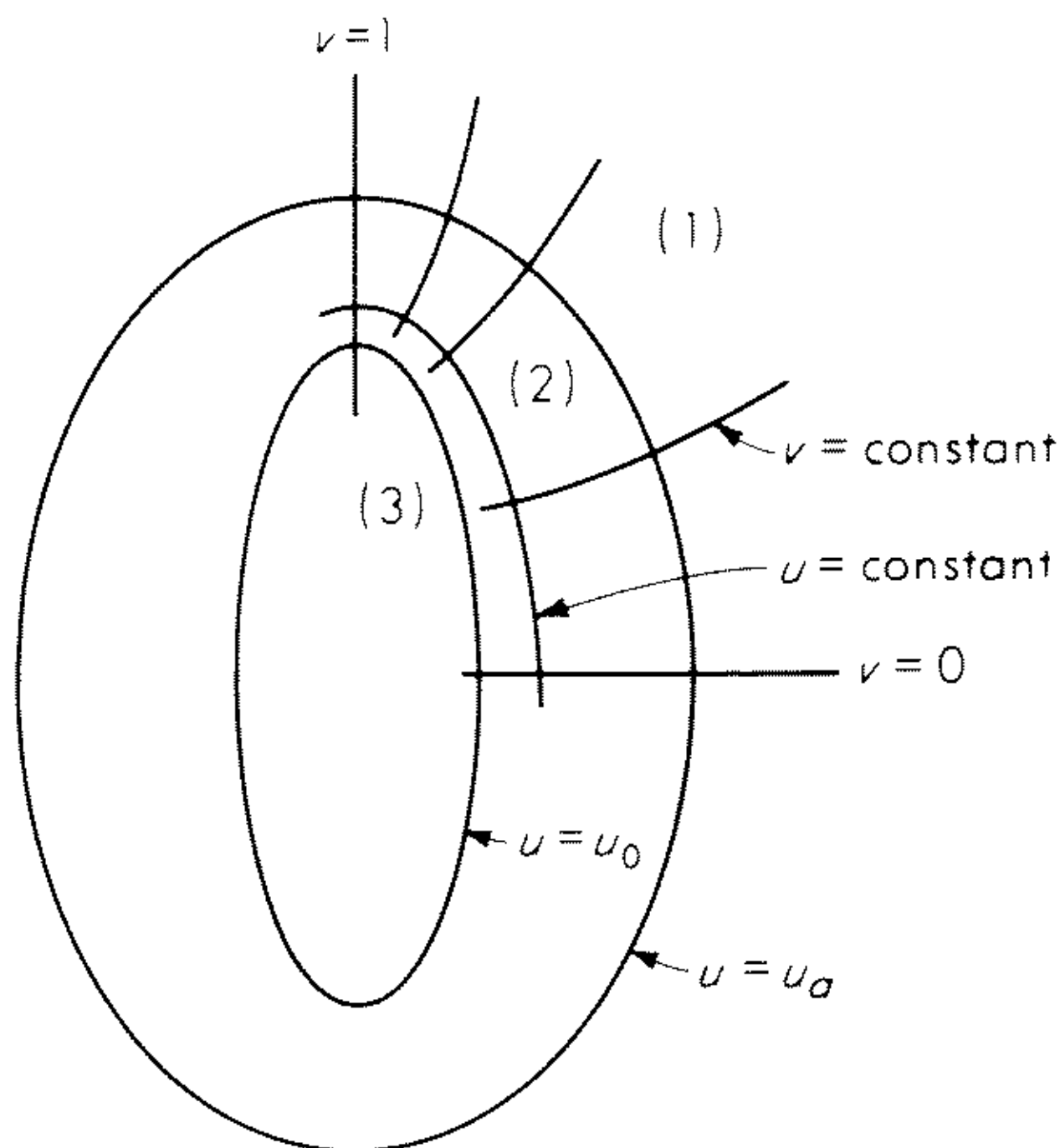


Fig. 13.6 Coordinate system and three confocal spheroidal regions.

trated in Fig. 13.6. It is assumed again that azimuthal symmetry prevails, and thus $\partial/\partial\phi = 0$. Furthermore, the electric current in the shell is taken to have only a ϕ component. Its density is $J_\phi(v)$ amp per unit of length in the v direction [for example, $J_\phi(v)h_v dv$ amp for the interval dv].

For the problem as stated, it is convenient to divide the homogeneous space, with parameters ϵ, μ , external to the spheroid into two regions denoted 1 and 2 as indicated in Fig. 13.6. The nature of the spheroid itself is not yet specified.

The fields may be derived again from a scalar function B as indicated by (13.104) to (13.106). However, now we shall add a subscript 1 or 2 when reference is being made to region 1 or 2, respectively. It is evident that suitable forms for B_1 and B_2 are

$$B_1 = \sum_n \alpha_n U_n(u) V_n(v) \quad (13.110)$$

$$\text{and} \quad B_2 = \sum_n [\beta_n U_n(u) + \gamma_n T_n(u)] V_n(v) \quad (13.111)$$

$$\text{where} \quad T_n(u) = (u^2 - 1)^{1/2} R_{1,n}^{(3)}(q, u) \quad (13.112)$$

$$\text{and} \quad q = kl = (\epsilon\mu)^{1/2} \omega l$$

The q dependence of the functions U_n and V_n is also understood. The coefficients α_n , β_n , and γ_n are to be determined from the source function $J_\phi(v)$ on the shell $u = u_a$ and the boundary conditions at $u = u_0$.

From Ampere's law, we may write immediately that

$$(H_{1v} - H_{2v}) \Big|_{u=u_a} = J_\phi(v) = \frac{1}{j\mu\omega l^2} \frac{1}{[(1 - v^2)(u_a^2 - v^2)]^{1/2}} \sum_n j_n V_n(v) \quad (13.113)$$

$$\text{whereas} \quad (E_{1\phi} - E_{2\phi}) \Big|_{u=u_a} = 0 \quad (13.114)$$

Using (13.104) and (13.106) in conjunction with (13.110) and (13.111), it is evident that

$$(\alpha_n - \beta_n)U'_n(u_a) - \gamma_n T'_n(u_a) = j_n \quad (13.115a)$$

$$\text{and} \quad (\alpha_n - \beta_n)U_n(u_a) - \gamma_n T_n(u_a) = 0 \quad (13.115b)$$

These equations may be solved for α_n to yield

$$\alpha_n = \left[\left(\frac{\beta_n}{\gamma_n} \right) U_n(u_a) + T_n(u_a) \right] \left(\frac{j q}{2} \right) j_n \quad (13.116)$$

where we have used the wronskian relation

$$U'_n(u)T_n(u) - U_n(u)T'_n(u) = \frac{-j^2}{q} \quad (13.117)$$

which follows immediately from (13.28). Now, as we indicated before, the ratio β_n/γ_n may be determined by the boundary condition at $u = u_0$ and, therefore, (13.116) is the formal solution of the problem. Explicit expressions for the fields in region 1 are obtained by inserting the expression for α_n into (13.110) with subsequent operations according to (13.104) to (13.106). For example, the electric field in region 1 is given explicitly by

$$E_\phi = \frac{j q}{2 \rho} \sum_n \left[\frac{\beta_n}{\gamma_n} U_n(u_a) + T_n(u_a) \right] j_n U_n(u) V_n(v) \quad (13.118)$$

which, in the far field (that is, $u \rightarrow \infty$), passes over to

$$E_\phi = F(\theta) \frac{e^{-j k r}}{r} \quad (13.119)$$

where

$$F(\theta) = -\frac{1}{2 \sin \theta} \sum_n \exp \left(j \frac{\pi}{2} n \right) j_n \left[\frac{\beta_n}{\gamma_n} U_n(u_a) + T_n(u_a) \right] V_n(\cos \theta) \quad (13.120)$$

in which, by virtue of (13.113),

$$j_n = \frac{j \mu \omega l}{N_{1,n}} \int_{-1}^{+1} J_\phi(v) V_n(v) h_v dv \quad (13.121)$$

If the current is confined to a filamental loop at $v = v_a$, it is evident from (13.121) that

$$j_n = \frac{j \mu \omega l}{N_{1,n}} V_n(v_a) I \quad (13.122)$$

where I is the total current in the loop.

In passing, it is worth mentioning that the form of (13.120) may be used to derive a synthesis procedure. For example, if $F(\theta)$ is specified, we obtain j_n from

$$\int_{-1}^{+1} \frac{F(\theta)}{\sin \theta} V_n(\cos \theta) d(\cos \theta) = -\frac{e^{j(\pi/2)n}}{2} j_n \left[\frac{\beta_n}{\gamma_n} U_n(u_a) + T_n(u_a) \right] N_{1,n} \quad (13.123)$$

where we have used the result

$$\int_{-1}^{+1} \frac{[V_n(\cos \theta)]^2}{\sin^2 \theta} d(\cos \theta) = N_{1,n}$$

Then the required form of $J_\phi(v)$, to yield the pattern $F(\theta)$, is given by

$$J_\phi(v) = \frac{1}{j\mu\omega l^2} \frac{1}{[(1-v^2)(u_a^2-v^2)]^{1/2}} \sum_n j_n V_n(v) \quad (13.124)$$

We mentioned above that the ratio β_n/γ_n was to be determined by the conditions imposed on the spheroid at $u = u_0$. For example, if the spheroid were *perfectly conducting*, the condition would be $E_\phi = 0$ at $u = u_0$. Thus, using (13.104) and (13.111), it is evident that

$$\frac{\beta_n}{\gamma_n} = -\frac{T_n(u_0)}{U_n(u_0)} \quad (13.125)$$

where the q dependence of the functions U_n and T_n is understood.

The next order of complexity is to allow the spheroid to have a surface admittance defined by

$$H_{2v} = \frac{k}{\mu\omega} y(v) E_{2\phi} \quad \text{at} \quad u = u_0 \quad (13.126)$$

where $y(v)$ is a normalized admittance which is allowed to be a function of v but not of ϕ . Imposition of this condition leads readily to the relation

$$\sum_n \left\{ \left[\left(\frac{\beta_n}{\gamma_n} \right) U'_n(u_0) + T'_n(u_0) \right] - jkly(v) \left(\frac{u_0^2 - v^2}{u_0^2 - 1} \right)^{1/2} \left[\left(\frac{\beta_n}{\gamma_n} \right) U_n(u_0) + T_n(u_0) \right] \right\} \gamma_n V_n(v) = 0 \quad (13.127)$$

Now, immediately we see that if $y(v)$ is chosen to have the special variation according to

$$y(v) = \left(\frac{u_0^2 - 1}{u_0^2 - v^2} \right)^{1/2} y_0 \quad y_0 = \text{constant} \quad (13.128)$$

(13.127) is satisfied if the term in braces is zero for each value of n (i.e., no mode coupling). For this case,

$$\frac{\beta_n}{\gamma_n} = -\frac{T'_n(u_0) - jqy_0 T_n(u_0)}{U'_n(u_0) - jqy_0 U_n(u_0)} \quad (13.129)$$

The interesting thing about this result is that β_n/γ_n may have a strong maximum for a certain value of n when y_0 is purely imaginary (i.e., a reactive surface). The resonance condition corresponds to

$$|U'_n(u_0) - jqly_0 U_n(u_0)| \text{ is a minimum} \quad (13.130)$$

This is approximately satisfied if

$$y_0 = -\frac{j}{q} \frac{\frac{d}{du_0} [\sqrt{u_0^2 - 1} R_{1,n}^{(2)}(q, u_0)]}{\sqrt{u_0^2 - 1} R_{1,n}^{(2)}(q, u_0)} \\ = -\frac{j}{q} \left[\frac{R_{1,n}^{(2)'}(q, u_0)}{R_{1,n}^{(2)}(q, u_0)} + \frac{u_0}{u_0^2 - 1} \right] \quad (13.131)$$

For example, if $q = 3$ and $u_0 = 1.077$, this calculates out to be $y_0 = j0.26$ for $n = 2$ and $y_0 = j1.12$ for $n = 3$. The corresponding (normalized) admittance variation is then given by (13.128) with these particular values of y_0 . Under such a resonance condition, practically all the power is being radiated in one mode, and thus the far-field pattern is closely given by $V_n(\cos \theta)/\sin \theta$ and is quite insensitive to the location of the source. Of course, for more detailed information, one should make a numerical evaluation of the complete mode sum given by (13.120). The concept of resonance excitation of a prolate spheroid with an admittance boundary condition is closely related to earlier investigations dealing with strips,¹⁴ circular cylinders,^{15,16} elliptic cylinders,¹⁷ and spheres.¹⁸ Much more recently, the idea has been expounded by Markov et al.¹⁹, in the U.S.S.R.

Another case of some interest is when the spheroid (whose surface is $u = u_0$) is a homogeneous medium with, say, electrical properties ϵ_c and μ_c which themselves may be complex. Denoting the fields in region $u < u_0$ by (3), it is thus evident that the interior fields are to be derived from

$$E_\phi = \frac{B_3}{l[(1 - v^2)(u^2 - 1)]^{1/2}} \quad (13.132)$$

$$H_v = \frac{1}{j\mu_c\omega l^2} \frac{1}{[(1 - v^2)(u^2 - v^2)]^{1/2}} \frac{\partial B_3}{\partial u} \quad (13.133)$$

$$H_u = \frac{-1}{j\mu_c\omega l^2} \frac{1}{[(u^2 - 1)(u^2 - v^2)]^{1/2}} \frac{\partial B_3}{\partial v} \quad (13.134)$$

for a source current density $J_\phi(v)$ in the external shell at $u = u_a$.

A suitable representation for the auxiliary function B_3 is

$$B_3 = \sum_p \delta_p J_p(q_c, u) V_p(q_c, v) \quad (13.135)$$

$$\text{where} \quad J_p(q_c, u) = (u^2 - 1)^{1/2} R_{1,p}^{(1)}(q_c, u) \quad (13.136)$$

$$V_p(q_c, v) = (1 - v^2)^{1/2} S_{1,p}(q_c, v) \quad (13.137)$$

$q_c = (\epsilon_c \mu_c)^{1/2} \omega l$, and δ_p is an undetermined coefficient. The radial function $R_{1,p}^{(1)}$ of the first kind is chosen, since the fields are to be finite at the center of the spheroid.

The boundary conditions which require that the tangential fields E_ϕ and H_v be continuous at $u = u_0$ are equivalent to

$$B_2 = B_3 \quad u = u_0 \quad (13.138)$$

$$\text{and} \quad \frac{1}{\mu} \frac{\partial B_2}{\partial u} = \frac{1}{\mu_c} \frac{\partial B_3}{\partial u} \quad u = u_0 \quad (13.139)$$

Thus, on using (13.111) and (13.135), we require that

$$\sum_n [\beta_n U_n(q, u_0) + \gamma_n T_n(q, u_0)] V_n(q, v) = \sum_p \delta_p J_p(q_c, u_0) V_p(q_c, v) \quad (13.140)$$

and

$$\frac{1}{\mu} \sum_n [\beta_n U'_n(q, u_0) + \gamma_n T'_n(q, u_0)] V_n(q, v) = \frac{1}{\mu_c} \sum_p \delta_p J'_p(q_c, u_0) V_p(q_c, v) \quad (13.141)$$

where we have explicitly indicated the q dependences of the terms on the left-hand sides of these equations. This system may be simplified slightly by expanding the V_p 's in terms of the V_n 's. Thus, in a similar fashion to that used in Sec. 13.5, we find that

$$(\beta_n U_n + \gamma_n T_n) = \sum_p \delta_p J_p L_p^{(n)} \quad (13.142)$$

$$\text{and} \quad \frac{1}{\mu} [\beta_n U'_n + \gamma_n T'_n] = \frac{1}{\mu_c} \sum_p \delta_p J'_p L_p^{(n)} \quad (13.143)$$

$$\text{where} \quad L_p^{(n)} = \frac{1}{N_{1,n}(q)} \int_{-1}^{+1} (1 - v^2)^{-1} V_n(q, v) V_p(q_c, v) dv \quad (13.144)$$

is the same quantity as given by (13.94).

13.8 Excitation of Spheroid System by a Ring Magnetic Current

The development of the field expressions for a spheroid excited by an azimuthal *electric* current of density $J_\phi(v)$ is identical with the corresponding derivation for a spheroid excited by an azimuthal *magnetic* current of density $J_{m\phi}(v)$. In this case, we need make only the following transformations in the equations (13.110) to (13.144).

$$\begin{aligned} J_\phi(v) &\rightarrow -J_{m\phi}(v) \\ E_\phi &\rightarrow H_\phi \\ H_v &\rightarrow -E_v \\ H_u &\rightarrow -E_u \\ \mu &\rightarrow \epsilon \\ \epsilon &\rightarrow \mu \\ B_i &\rightarrow A_i \quad (\text{for } i = 1, 2, \text{ and } 3) \end{aligned}$$

For example, in analogy to (13.119) and (13.120), the far field of the spheroid at $u = u_0$ excited by a loop of magnetic current I_m at $u = u_a$ and $v = v_a$ is

$$H_\phi = \hat{F}(\theta) \frac{e^{-jkr}}{r} \quad (13.145)$$

where the pattern is

$$\hat{F}(\theta) = -\frac{1}{2 \sin \theta} \sum_n \exp \left(j \frac{\pi}{2} n \right) k_n \left[\frac{\hat{\beta}_n}{\hat{\gamma}_n} U_n(u_a) + T_n(u_a) \right] V_n(\cos \theta) \quad (13.146)$$

and k_n is given by

$$k_n = \frac{j\epsilon\omega l}{N_{1,n}} V_n(v_a) I_m \quad (13.147)$$

In this case, $\hat{\beta}_n/\hat{\gamma}_n$ is directly analogous to β_n/γ_n if the above transformations are kept in mind. In particular, if the spheroid is a perfect electric conductor, it is evident that

$$\frac{\hat{\beta}_n}{\hat{\gamma}_n} = -\frac{T'_n(u_0)}{U'_n(u_0)} \quad (13.148)$$

Then, if the magnetic current loop is allowed to approach the spheroid (that is, $u_a \rightarrow u_0$), we find that (13.146) reduces to

$$\hat{F}(\theta) = \frac{j}{q \sin \theta} \sum_n \exp\left(j \frac{\pi}{2} n\right) k_n \frac{V_n(\cos \theta)}{U'_n(u_0)} \quad (13.149)$$

or

$$\hat{F}(\theta) = -\frac{\epsilon\omega I_m}{k \sin \theta} \sum_n \exp\left(j \frac{\pi}{2} n\right) \frac{V_n(v_a) V_n(\cos \theta)}{N_{1,n} U'_n(u_0)} \quad (13.150)$$

It is rather interesting to note that in the limiting case, where $v_a \rightarrow 1$, (13.150) may be written in the form

$$\hat{F}(\theta) = \frac{j(I ds)}{\pi k l^2 (u_0^2 - 1)} \sum_n \frac{\exp[j(\pi/2)n]}{N_{1,n}} \frac{\sigma_{1,n} V_n(\cos \theta)}{U'_n(u_0) \sin \theta} \quad (13.151)$$

where

$$\begin{aligned} \sigma_{1,n} &= \lim_{v_a \rightarrow 1} \left[\frac{V_n(v_a)}{1 - v_a^2} \right] = \lim_{v_a \rightarrow 1} \left[\frac{S_{1,n}(q, v_a)}{(1 - v_a^2)^{1/2}} \right] \\ &= \frac{1}{2} \sum_{r=0,1,\dots}^{\infty} d_r^{1,n}(q) (r+2)(r+1) \end{aligned} \quad (13.152)$$

Here, $I ds$ is the equivalent electric dipole moment related to I_m by

$$j\epsilon\omega I_m (dA)_e = -(I ds) \quad (13.153)$$

where

$$(dA)_e \approx \pi l^2 [(1 - v_a^2)(u_0^2 - 1)]$$

is the area of the magnetic current loop.

If we write the far field in the form

$$H_\phi = \frac{I ds}{4\pi r} k e^{-jkr} V(\theta) \quad (13.154)$$

we see, on comparing (13.145) and (13.154), that

$$V(\theta) = \frac{4j}{q^2(u_0^2 - 1)} \sum_n \frac{\exp[j(\pi/2)n] \sigma_{1,n} V_n(\cos \theta)}{N_{1,n} U'_n(u_0) \sin \theta} \quad (13.155)$$

This formula for $V(\theta)$ is identical with that given by Belkina,^{20a} who derived it by assuming initially that the electric dipole was located on the tip of a perfectly conducting prolate spheroid.† By definition, the radiation pattern is

†To establish the equivalence with Belkina's result, it is necessary to change her gaussian units to mks, change her time factor $\exp(-j\omega t)$ to $\exp(+j\omega t)$, and, finally, change her notation for the spheroidal functions to that used here.

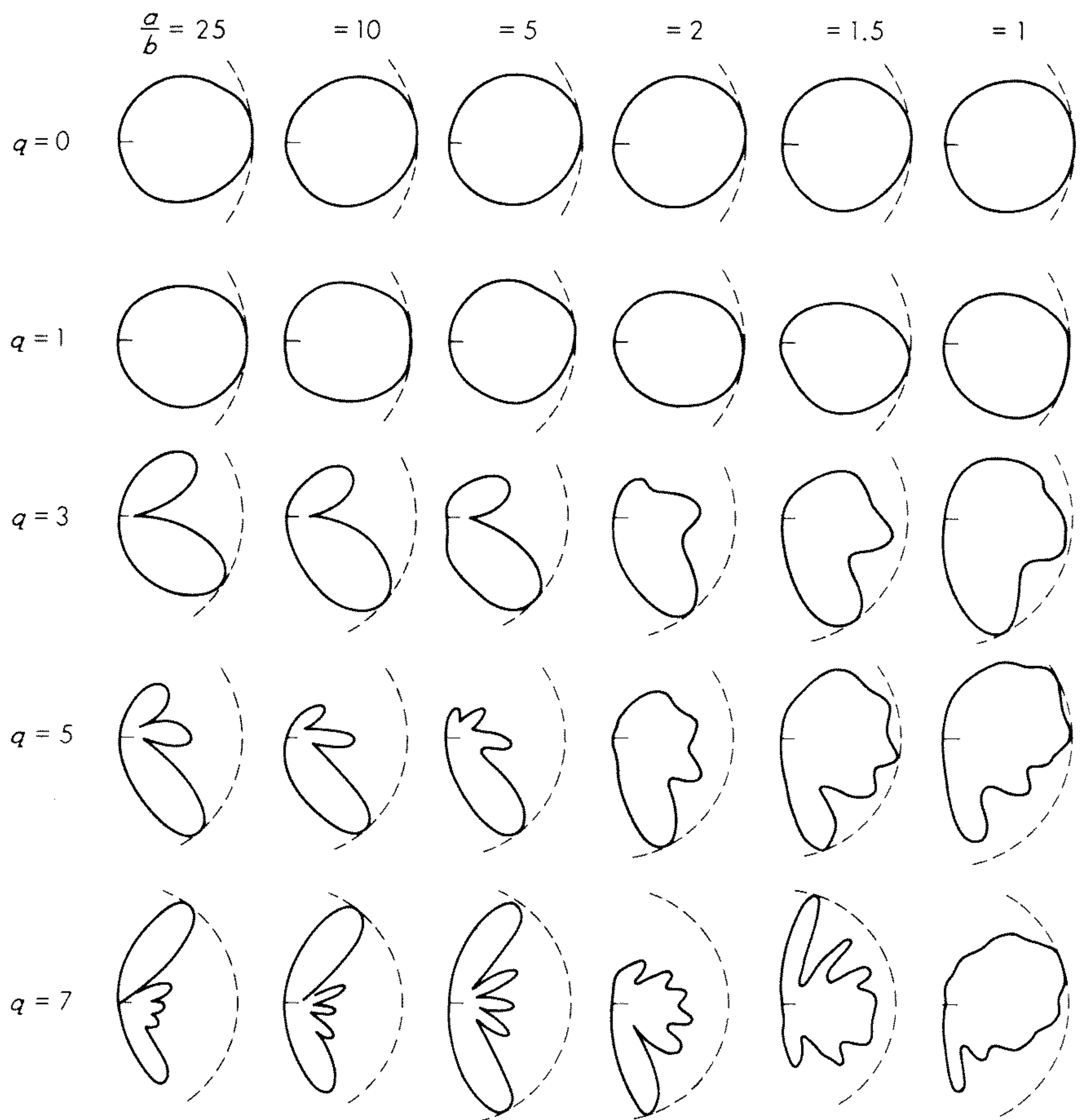


Fig. 13.7 *E*-plane patterns of an electric dipole at the tip (i.e., the top) of a metallic prolate spheroid. (After Belkina.^{20a})

<i>a/b</i> :	25		10		5		1.5		1.0		
<i>u</i> ₀ :	1.000801		1.005037		1.020000		1.154700		1.341641		∞
<i>q</i>	<i>ka</i>	<i>kb</i>	<i>ka</i>	<i>kb</i>	<i>ka</i>	<i>kb</i>	<i>ka</i>	<i>kb</i>	<i>ka</i>	<i>kb</i>	<i>kr</i> ₀
0	0	0	0	0	0	0	0	0	0	0	0
1	0.98	0.04	0.99	0.10	1.00	0.20	1.13	0.57	1.31	0.88	0.59
3	3.00	0.12	3.01	0.30	3.06	0.60	3.46	1.73	4.02	2.68	1.79
5	5.00	0.20	5.02	0.50	5.10	1.00	5.77	2.89	6.71	4.47	2.97
7	7.01	0.28	7.03	0.70	7.14	1.41	8.08	4.04	9.39	6.26	4.18

a plot of $|V(\theta)|$ as a function of θ from 0 to 180° . Using Belkina's numerical data for $V(\theta)$, we sketch in Fig. 13.7 the radiation pattern for a number of representative prolate spheroids. The ratio of major axes and the values of q or kl are indicated in the figure. In addition, we add the accompanying table in order that the reader may see the related parameters. The patterns in the right-hand column are based on the limiting case where $a \rightarrow b \rightarrow r_0$ (i.e., a sphere). The radius of curvature r_0 of the sphere is so chosen that it matches the radius of curvature (that is, b^2/a) at the tip of the spheroid used in the preceding column. Thus, $kr_0 = (kb)_2/ka = kb/1.15$. It is evident that, at least for angles $\theta < \text{about } 100^\circ$, there is some similarity between the patterns in the last two columns of Fig. 13.7. This is a consequence of the dominating influence of the local radius of curvature on which the radiator is mounted. The concept has been expounded at length by V. A. Fock²¹ and his collaborators in the U.S.S.R.

13.9 The Green's Function in Spheroidal Coordinates

In various problems dealing with sources in the presence of spheroidal bodies, it is convenient to start with an expansion of a spherical wave in terms of spheroidal wave functions. For example, the free space Green's function $G_0(\mathbf{r}|\mathbf{r}')$ is defined by

$$G_0(\mathbf{r}|\mathbf{r}') = \frac{\exp(-jk_0|\mathbf{r} - \mathbf{r}'|)}{4\pi|\mathbf{r} - \mathbf{r}'|} \quad (13.156)$$

where \mathbf{r} and \mathbf{r}' are position vectors from the origin to the observer and source, respectively. The right-hand side of (13.156) is an outgoing spherical wave for our adopted time factor $\exp(j\omega t)$. Now, G_0 satisfies the inhomogeneous Helmholtz equation

$$(\nabla^2 + k_0^2)G_0(\mathbf{r}|\mathbf{r}') = -\delta(\mathbf{r} - \mathbf{r}') \quad (13.157)$$

where

$$\delta(\mathbf{r} - \mathbf{r}') = \frac{1}{h_u h_v h_\phi} \delta(u - u') \delta(v - v') \delta(\phi - \phi') \quad (13.158)$$

is the three-dimensional Dirac function. The coordinates of the source point and the observer are (u', v', ϕ') and (u, v, ϕ) in the spheroidal coordinate system.

From symmetry considerations, we now write

$$G_0(\mathbf{r}|\mathbf{r}') = \sum_{m=0}^{\infty} \sum_{n=m}^{\infty} A_{m,n} S_{m,n}(q, v) S_{m,n}(q, v') \\ \times \cos m(\phi - \phi') \begin{cases} R_{m,n}^{(1)}(q, u) R_{m,n}^{(4)}(q, u') & u < u' \\ R_{m,n}^{(1)}(q, u') R_{m,n}^{(4)}(q, u) & u > u' \end{cases} \quad (13.159)$$

where the summations are over integer values of m and n and where $A_{m,n}$ is a coefficient yet to be determined. We note that (13.159) has the required finiteness at $v = \pm 1$ and at $u = 1$. Also, it has the required outgoing wave character as $u \rightarrow \infty$.

Both sides of (13.157) are now multiplied by $l^2(u^2 - v^2)$, and we then integrate with respect to u over a small interval about u' . We then find that

$$(u^2 - 1) \frac{\partial}{\partial u} G_0 \Big|_{u=u'-0}^{u=u'+0} = -\frac{1}{l} \delta(v - v') \delta(\phi - \phi') \quad (13.160)$$

which, on using (13.159), is transformed to

$$\sum_m \sum_n A_{m,n} S_{m,n}(q, v) S_{m,n}(q, v') \cos m(\phi - \phi') = -jk_0 \delta(v - v') \delta(\phi - \phi') \quad (13.161)$$

By orthogonality, it is a simple matter to show that

$$A_{m,n} = \frac{-jk_0 \epsilon_m}{2\pi N_{m,n}} \quad (13.162)$$

where
$$\epsilon_m = \begin{cases} 1 & \text{for } m = 0 \\ 2 & \text{for } m = 1, 2, 3, \dots \end{cases}$$

The desired representation is thus given by (13.158) with the above value for the coefficient $A_{m,n}$.

In some scalar boundary-value problems, such as acoustic scattering^{22,23} from spheroids, the fields may be derived from a scalar Green's function $G(\mathbf{r}|\mathbf{r}')$ which satisfies (13.157) but, in addition, has a boundary condition of the form

$$\frac{\partial G}{\partial u} = \Gamma G \quad \text{at} \quad u = u_0 \quad (13.163)$$

where Γ is an impedance parameter. It is understood here that the radial coordinate u' of the source is such that $u' > u_0$. When the surface of the spheroid is rigid, $\Gamma = 0$, which is a special case of the general impedance boundary condition. The perfectly "soft" spheroid corresponds to setting $\Gamma = \infty$.

It is an interesting exercise for the reader to show that the appropriate form of the Green's function which satisfies (13.163), for $u < u'$, is

$$G(\mathbf{r}|\mathbf{r}') = -\frac{jk_0}{2\pi} \sum_{m=0}^{\infty} \sum_{n=m}^{\infty} \frac{\epsilon_m}{N_{m,n}} S_{m,n}(q, v) S_{m,n}(q, v') \times f_{m,n}(q, u_0, u, u') \cos m(\phi - \phi') \quad (13.164)$$

where

$$f_{m,n}(q, u_0, u, u') = R_{m,n}^{(4)}(q, u') \left[R_{m,n}^{(1)}(q, u) - \frac{R_{m,n}^{(1)'}(q, u_0) - \Gamma R_{m,n}^{(1)}(q, u_0)}{R_{m,n}^{(4)'}(q, u_0) - \Gamma R_{m,n}^{(4)}(q, u_0)} R_{m,n}^{(4)}(q, u) \right] \quad (13.165)$$

The primes here indicate differentiation with respect to u_0 and, as usual, $q = k_0 l$. The corresponding representation valid for $u > u'$ is obtained by simply interchanging u and u' in (13.164) and (13.165). This fact follows from the required symmetry of the problem.

The limiting cases for $\Gamma = 0$ and $\Gamma = \infty$ were given by Flammer,⁵ who, however, inadvertently omitted the factor $\cos m(\phi - \phi')$.

13.10 Application of Scalar Green's Function to Dipole Scattering

While the application of the scalar Green's function to acoustic scattering is very straightforward, this is not the case for electromagnetic problems. The vector nature of the electromagnetic field is the source of considerable difficulty. Fortunately, however, there are classes of symmetric electromagnetic problems in which the solutions become tractable.

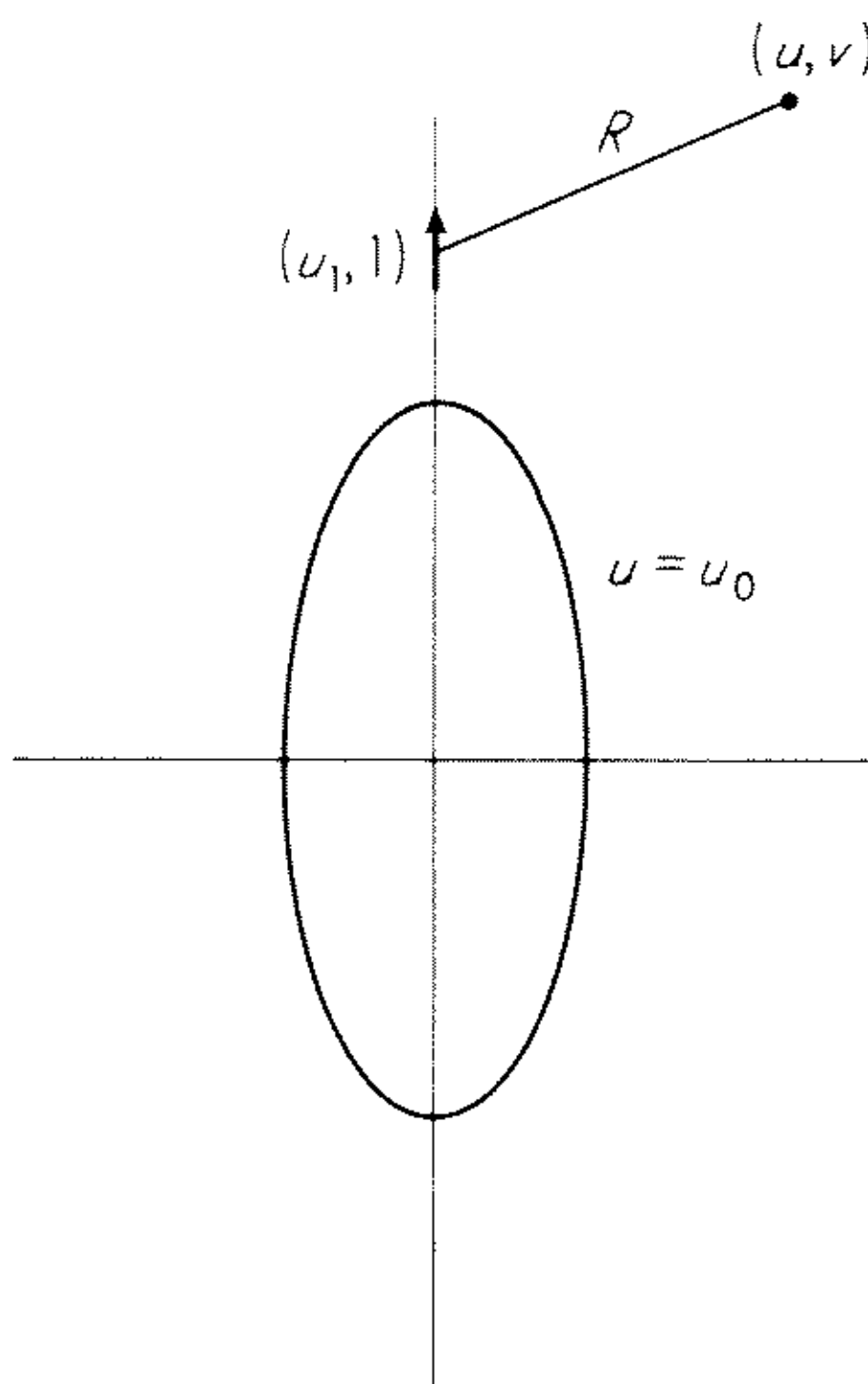


Fig. 13.8 Electric dipole located outside perfectly conducting spheroid.

We consider the example of an electric dipole located outside but on the axis of a perfectly conducting spheroid. The situation is illustrated in Fig. 13.8, where the surface of the spheroid is $u = u_0$ and the source is located at $u = u_1$ and $v = +1$. Because of the symmetry, the magnetic field has only a ϕ component. It is convenient to write this as the sum of a primary field H_ϕ^p and a secondary field H_ϕ^s . Thus,

$$H_\phi = H_\phi^p + H_\phi^s$$

where

$$H_\phi^p = p \frac{e^{-jk_0 R}}{R} \left(1 + \frac{1}{jk_0 R} \right) \frac{\rho}{R} = \frac{jp}{k_0} \frac{\partial}{\partial \rho} \frac{e^{-jk_0 R}}{R} \quad (13.166)$$

Here R is the distance between the observer at (u, v) and the source at $(u_1, 1)$ and p is the dipole moment.

The key step is now to use the expansion for the free space Green's function as

given by (13.159) to enable H_ϕ^p to be expressed in terms of spheroidal wave functions. Then, after some simplification, we find that for $u > u_1$,

$$H_\phi^p = -\frac{4p}{l(u_1^2 - 1)^{1/2}} \sum_{n=1}^{\infty} \frac{\sigma_{1,n}}{N_{1,n}} R_{1,n}^{(1)}(q, u) R_{1,n}^{(4)}(q, u) S_{1,n}(q, v) \quad (13.167)$$

where
$$\sigma_{1,n} = \lim_{v \rightarrow 1} \frac{S_{1,n}(q, v)}{(1 - v^2)^{1/2}}$$

In order that this result be valid for $u < u_1$, we merely interchange u and u_1 .

The secondary field is now so constructed that the boundary condition

$$E_v = \frac{1}{jq(u^2 - v^2)^{1/2}} \frac{\partial}{\partial u} [(u^2 - 1)^{1/2} H_\phi] = 0 \quad (13.168)$$

is satisfied at $u = u_0$. After some consideration, we find that

$$H_\phi^s = \frac{4p}{l(u_1^2 - 1)^{1/2}} \sum_{n=1}^{\infty} \frac{\sigma_{1,n}}{N_{1,n}} r_n R_{1,n}^{(4)}(q, u_1) R_{1,n}^{(4)}(q, u) S_{1,n}(q, v) \quad (13.169)$$

where
$$r_n = \frac{\frac{d}{du} [(u^2 - 1)^{1/2} R_{1,n}^{(1)}(q, u)]}{\frac{d}{du} [(u^2 - 1)^{1/2} R_{1,n}^{(4)}(q, u)]} \Big|_{u=u_0}$$

which is valid for $u \geq u_0$. This is the result given by Belkina.^{20a} If we now allow the source to approach the spheroid (that is, $u_1 \rightarrow u_0$) and then employ the wronskian condition (13.28), we obtain for the total field

$$H_\phi = \frac{4jp}{ql(u_0^2 - 1)} \sum_{n=1}^{\infty} \frac{\sigma_{1,n} R_{1,n}^{(4)}(q, u) S_{1,n}(q, v)}{N_{1,n} U'_n(u_0)} \quad (13.170)$$

where
$$U'_n(u_0) = \frac{d}{du} (u^2 - 1)^{1/2} R_{1,n}^{(4)}(q, u) \Big|_{u=u_0} \quad (13.171)$$

Using the asymptotic approximation for $R_{1,n}^{(4)}(q, u)$, we find, in the limit of $lu \rightarrow \infty$, that

$$H_\phi \approx -p \frac{e^{-jk_0 r}}{r} V(\theta) \quad (13.172)$$

where $V(\theta)$ is, by definition, the radiation pattern.

13.11 Extension to Oblate Spheroid

In all our discussion up to this point, we have been considering prolate spheroidal geometry. Actually, the theory of oblate spheroidal wave functions and many of the connecting formulas are formally equivalent to their counterparts in the prolate system. To demonstrate this, we define oblate spheroidal coordinates (in terms of the cartesian coordinates) as follows:

$$x = l[(u^2 + 1)(1 - v^2)]^{1/2} \cos \phi \quad (13.173)$$

$$y = l[(u^2 + 1)(1 - v^2)]^{1/2} \sin \phi \quad (13.174)$$

$$z = luv \quad (13.175)$$

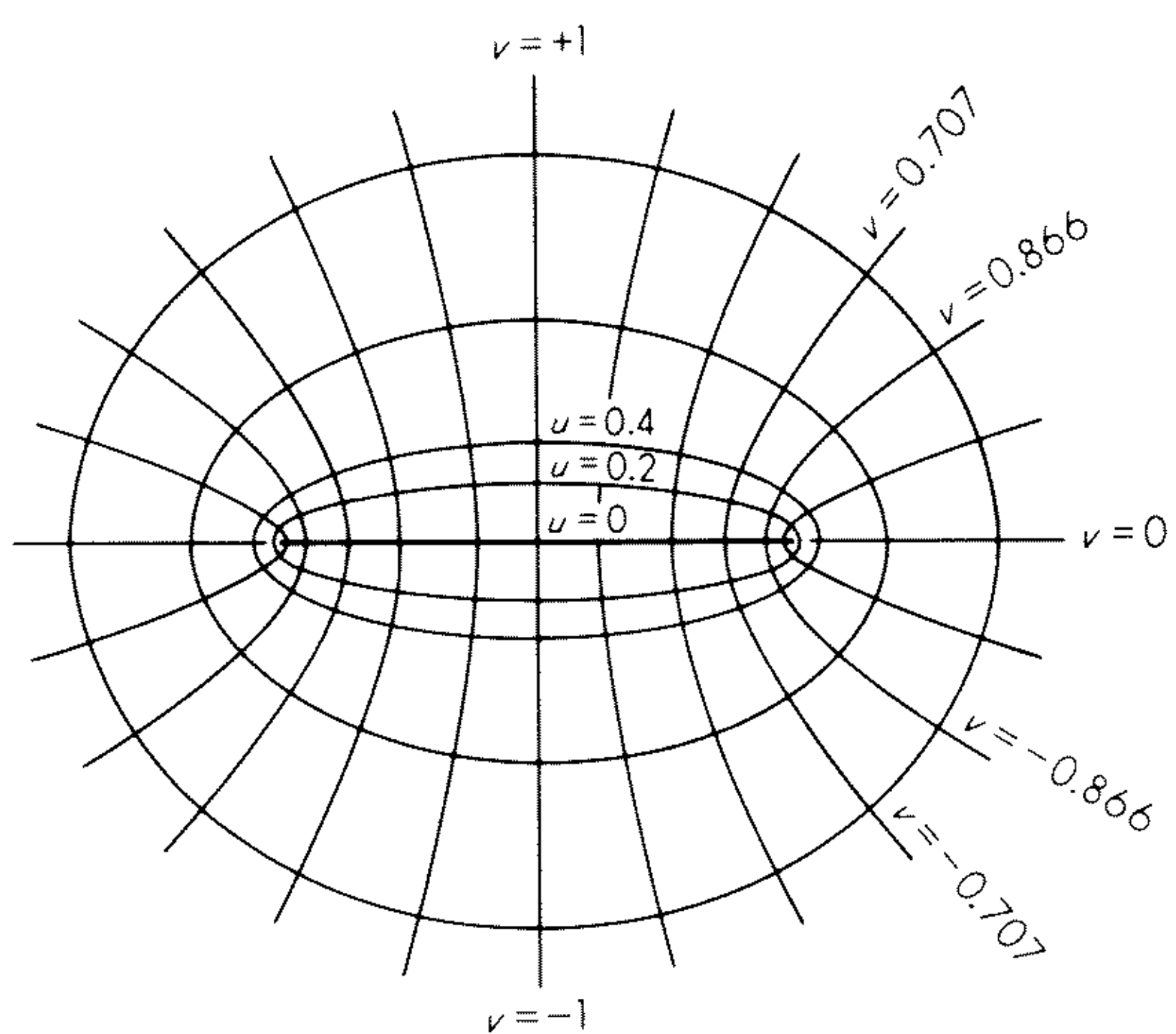


Fig. 13.9 Oblate spheroidal coordinates.

where l is the semifocal distance. It is evident that these are obtained from (13.1) to (13.3) by replacing u and l with $\pm ju$ and $\mp jl$, respectively.

For the oblate coordinate system, which is sketched in Fig. 13.9,

$$0 \leq u \leq \infty \quad \text{and} \quad -1 \leq v \leq +1$$

As in the prolate system, u is a radial coordinate and v is an angular coordinate. Also, as before, when l is finite, the surfaces $u = \text{constant}$ become spherical as $u \rightarrow \infty$. In this same limit, $v \rightarrow \cos \theta$, where θ is the actual spherical angle coordinate.

The metrical coefficients for the oblate system are

$$h_u = l \left(\frac{u^2 + v^2}{u^2 + 1} \right)^{1/2} \quad h_v = l \left(\frac{u^2 + v^2}{1 - v^2} \right)^{1/2} \tag{13.176}$$

and
$$h_\phi = l[(1 - v^2)(u^2 + 1)]^{1/2}$$

Then the scalar wave equation (13.8) has the form

$$\left[\frac{\partial}{\partial v} (1 - v^2) \frac{\partial}{\partial v} + \frac{\partial}{\partial u} (u^2 + 1) \frac{\partial}{\partial u} + \frac{u^2 + v^2}{(u^2 + 1)(1 - v^2)} \frac{\partial^2}{\partial \phi^2} + q^2(u^2 - v^2) \right] V = 0 \tag{13.177}$$

Solutions in Flammer's⁵ notation are

$$V_{m,n} = S_{m,n}(-jq,v)R_{m,n}(-jq,ju) \frac{\cos}{\sin} m\phi \tag{13.178}$$

This may be obtained formally by replacing q and u in (13.10) by $-jq$ and ju , respectively.

Using the transformations indicated, nearly all the formal derivations in the preceding sections may be carried over to the corresponding oblate configura-

tion. The exceptions include the limiting form of the prolate spheroid radial function when $q = m\pi/2$. In the oblate geometry, simplified expressions do not exist for this case. However, it is rather interesting to note that certain simplifications, which occur for a flattened oblate spheroid (i.e., a disk), do not appear to have a meaningful physical counterpart in the prolate system.

13.12 Excitation of Oblate Spheroid by Axial Dipole

An important configuration which may be treated by the transformation technique is the perfectly conducting oblate spheroid which is excited by a centrally located electric dipole. To be specific, the oblate spheroid is defined by $u = u_0$ and the dipole is located at $u = u_1$ and $v = +1$. Expressions for the field of the dipole may be obtained directly from the results already derived for the prolate spheroid. The applicable formula in this case is obtained from (13.169) if we simply make the substitutions $-jq$ in place of q and ju in place of u . In the limit when the dipole is located on the surface of the spheroid, (13.170) applies if the same substitutions are made. In this case, the explicit form for the far field is

$$H_\phi \approx -p \frac{e^{-jk_0 r}}{r} V(\theta) \quad (13.179)$$

where, in analogy to (13.155),

$$V(\theta) = -\frac{4j}{q^2(u_0^2 + 1)} \sum_n \frac{\exp [j(\pi/2)n] \sigma_{1,n} V_n(\cos \theta)}{N_{1,n} U'_n(u_0) \sin \theta} \quad (13.180)$$

with
$$\frac{V_n(\cos \theta)}{\sin \theta} = S_{1,n}(-jq, \cos \theta)$$

$$N_{1,n} = \int_{-1}^{+1} [S_{1,n}(-jq, v)]^2 dv$$

$$\sigma_{1,n} = \lim_{v \rightarrow 0} \frac{S_{1,n}(-jq, v)}{(1 - v^2)^{1/2}} = \frac{1}{2} \sum_{r=0,1,2,\dots}^{\infty} d_r^{1,n}(-jq)(r+2)(r+1)$$

and
$$U'_n(u_0) = \frac{d}{du} [(u^2 + 1)^{1/2} R_{1,n}^{(4)}(-jq, ju)] \Big|_{u=u_0}$$

The oblate coefficients $d_r^{1,n}(-jq)$ have been tabulated by Flammer.⁵

In the limit of a vanishingly thin oblate spheroid, $u_0 \rightarrow 0$ and then l is simply the radius of the disk. The pattern function $V(\theta)$, as given by (13.180), is now written

$$V(\theta) = \frac{4j}{q^2} \sum_{n=1}^{\infty} \frac{\exp (j\pi n/2) \sigma_{1,n} S_{1,n}(-jq, \cos \theta)}{N_{1,n} \frac{d}{du} R_{1,n}^{(4)}(-jq, ju_0)} \quad (13.181)$$

The magnitude of $V(\theta)$ is shown in Fig. 13.10 on a polar plot for $q = 1, 3$, and 5 . For the broadside direction, $\theta = \pi/2$, it turns out that V is unity. (This is a consequence of the fact that the disk currents do not radiate in the plane of the

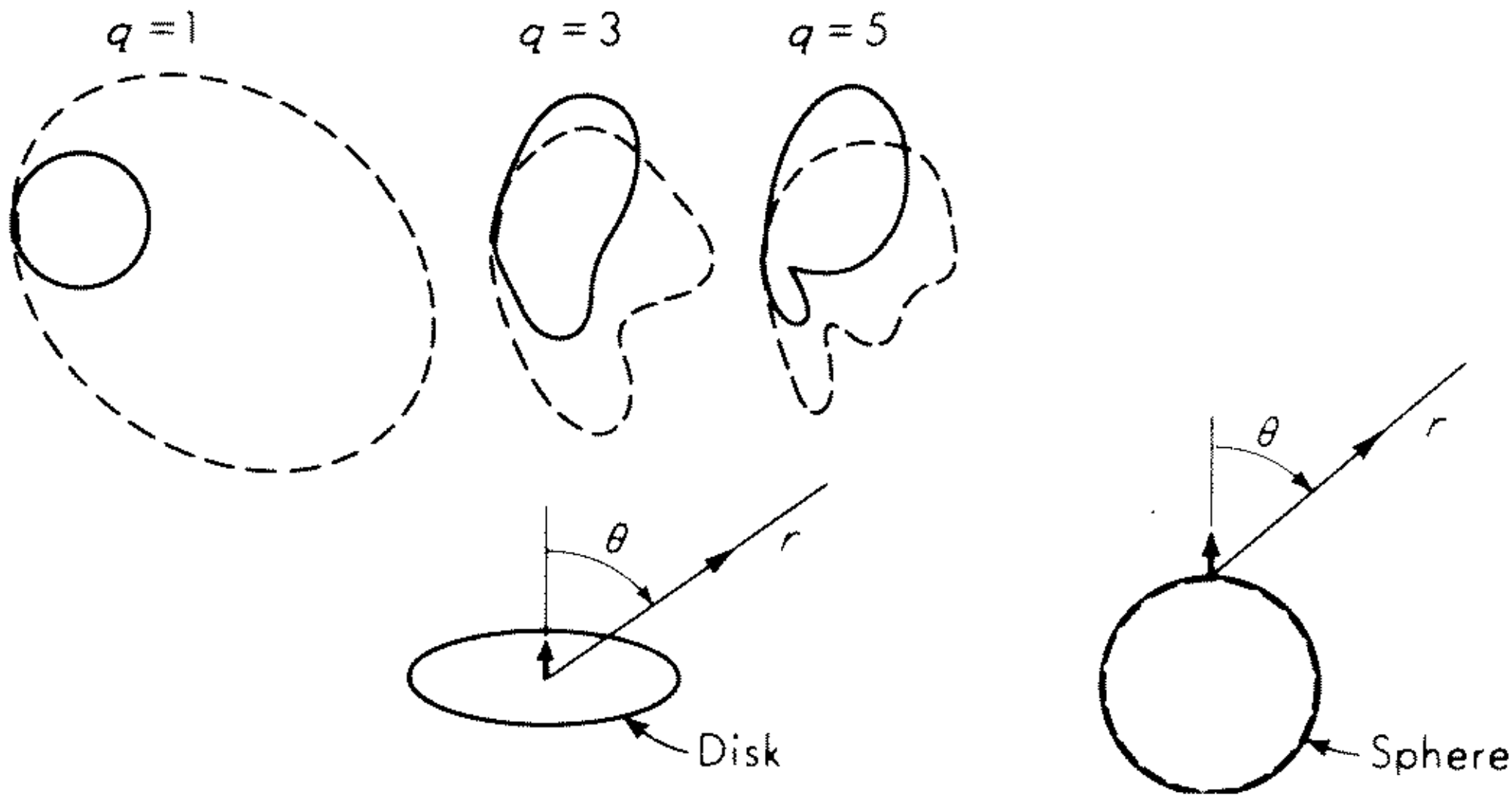


Fig. 13.10 Radiation patterns of electric dipole on metallic circular disk (solid curves) and sphere (dashed curves).

disk.) Also shown, for comparison in Fig. 13.10, are the corresponding patterns for a radial electric dipole on the surface of a perfectly conducting sphere whose radius is the same as that of the disk. It is evident that the disk and the sphere produce mutilations of the free space pattern which bear little resemblance to one another. Some similar patterns were calculated by Leitner and Spence,²⁴ who also gave numerical results for the current distribution on the disk.

The low-frequency limit of the pattern for the dipole on the surface of the oblate spheroid is obtained from (13.180) by letting $q \rightarrow 0$. We then obtain Belkina's^{20b} result, which is given by

$$V(\theta) \approx \frac{\sin \theta}{(u_0^2 + 1)(1 - u_0 \operatorname{arccot} u_0)} \quad (13.182)$$

which, apart from a factor, is the same as the dipole in free space. In the disk limit (that is, $u_0 \rightarrow 0$), we have simply

$$V(\theta) \approx \sin \theta$$

which states that an electrically small disk has a negligible effect on the radiation from an electric dipole.

13.13 Fields of a Horizontal Dipole over a Disk

An interesting oblate-spheroidal configuration was considered by Kocherzhevskii.²⁵ He was concerned specifically with the radiation from a magnetic dipole which was located at the surface of a perfectly conducting disk. Such a radiator is equivalent to an infinitesimally short slot radiating from one side of a vanishingly thin oblate spheroid. It is interesting to note that attempts to solve this problem for the oblate spheroid of finite thickness (that is, $u_0 > 0$) have not been successful. The difficulty lies in the inability to express the electromagnetic field in terms of two scalar functions which are

related to two components of a Hertz vector in the general spheroidal system. However, when the spheroid degenerates into a disk, the currents produce a Hertz vector which does not have a component normal to the disk. This appears to be the reason that certain vector electromagnetic problems associated with perfectly conducting disks are solvable. Meixner,²⁶ Flammer,²⁷ and Belkina^{20b} have exploited this fact in obtaining solutions for dipoles in the presence of disks and apertures. As mentioned above, Kocherzhevskii's result is a limiting case when the dipole (magnetic type) is centrally located and directed along a diameter of the disk.

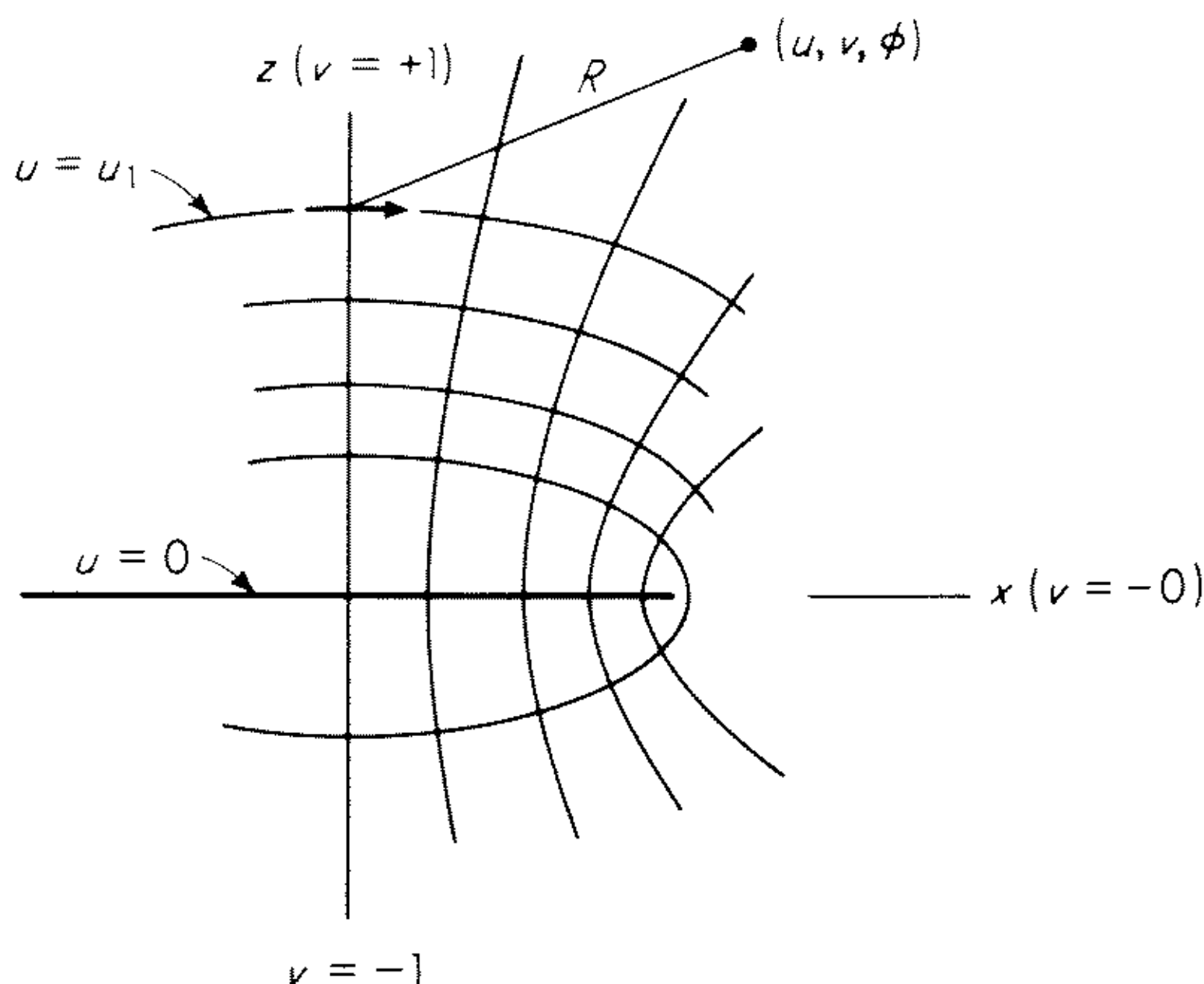


Fig. 13.11 Horizontal magnetic dipole over a perfectly conducting circular disk of radius l .

We shall very briefly outline Belkina's^{20b} derivation for the horizontal magnetic dipole located on the axis of the disk. The situation is illustrated by Fig. 13.11. The circular disk is located at $u = 0$ with respect to the oblate spheroidal coordinate system, which is chosen to have its semifocal distance l equal to the radius of the disk. The magnetic dipole of moment M is located on the axis of the disk at a distance lu . It is oriented in the x direction (that is, $\phi = 0$). The observer at (u, v, ϕ) is a distance R from the source dipole.

As it turns out, the boundary conditions for the present problem can all be satisfied if it is assumed that the resultant magnetic Hertz vector $\mathbf{\Pi}^*$ has only an x and z component. The fields are then to be derived from

$$\mathbf{E} = -j\epsilon_0\omega \text{curl } \mathbf{\Pi}^* \quad (13.183)$$

$$\text{and} \quad \mathbf{H} = (k_0^2 + \text{grad div})\mathbf{\Pi}^* \quad (13.184)$$

In cylindrical coordinates, the components of the magnetic Hertz vector have the following form:

$$\Pi_\rho^* = \Phi(\rho, z) \cos \phi \quad \Pi_\phi^* = -\Phi(\rho, z) \sin \phi \quad \text{and} \quad \Pi_z^* = \psi(\rho, z) \cos \phi$$

where Φ and ψ are two scalar functions which do not depend on ϕ . The boundary conditions

$$\begin{aligned} E_\rho = E_\phi = 0 \quad \text{for } z = 0, \rho < l \\ \text{lead to} \quad \frac{\partial \Phi}{\partial z} = \frac{1}{\rho} \psi \\ \frac{\partial \Phi}{\partial z} = \frac{\partial \psi}{\partial \rho} \quad \rho < l, z = 0 \end{aligned} \tag{13.185}$$

Therefore, on the disk, we must have

$$\frac{\partial \psi}{\partial \rho} = \frac{1}{\rho} \psi \tag{13.186}$$

which may be integrated to give

$$\begin{aligned} \frac{\partial \Phi}{\partial z} &= C \\ \psi &= C\rho \end{aligned} \quad \rho < l, z = 0 \tag{13.187}$$

where C is a constant yet to be determined.

We now write

$$\Phi = \Phi^p + \Phi^s$$

where Φ^p is the potential due to the primary field of the dipole and Φ^s is the secondary influence. At the same time, we note that, in the absence of the disk, $\psi = 0$. We are now led to express Φ^s and ψ as expansions in oblate spheroidal wave functions. In order to match boundary conditions, they must have the form

$$\Phi^s = \sum_{n=0}^{\infty} A_n R_{0,n}^{(4)}(-jq, ju) S_{0,n}(-jq, v) \tag{13.188}$$

$$\psi = \sum_{n=0}^{\infty} B_n R_{1,n}^{(4)}(-jq, ju) S_{1,n}(-jq, v) \tag{13.189}$$

where A_n and B_n are yet to be determined. Using (13.159), with a suitable change to the oblate system, we may express the primary potential as follows:

$$\begin{aligned} \Phi^p &= \frac{M e^{-jk_0 R}}{R} \\ &= -2jk_0 M \sum_{n=0}^{\infty} \frac{S_{0,n}(-jq, 1)}{N_{0,n}(-jq)} R_{0,n}^{(4)}(-jq, ju_1) R_{0,n}^{(1)}(-jq, ju) S_{0,n}(-jq, v) \end{aligned} \tag{13.190}$$

which is valid for $u < u_1$. In order that this apply to $u > u_1$, we merely interchange u and u_1 .

The boundary conditions (13.187), written in the form,

$$\frac{\partial}{\partial u} (\Phi^p + \Phi^s) = Clv \quad u = 0$$

and
$$\psi = Cl(1 - v^2)^{1/2} \quad u = 0$$

may be used to solve for the coefficients A_n and B_n . On the other hand, the constant C is determined by imposing the condition that the radial current at the edge of the disk should be zero. This condition is equivalent to

$$\lim_{\delta \rightarrow 0} \{ H_\phi \Big|_{\substack{v=0 \\ u=-\delta}} - H_\phi \Big|_{\substack{v=0 \\ u=+\delta}} \} = 0$$

Explicit expressions for the coefficients as well as representative radiation patterns have been given by Belkina^{20b} and Kocherzhevskii.²⁵ Their papers should be referred to for further details. The extensive and comprehensive analysis report on this subject by Flammer²⁷ is also to be recommended.

REFERENCES

1. Schelkunoff, S. A.: "Advanced Antenna Theory," John Wiley & Sons, Inc., New York, 1962.
2. Chu, L. J., and J. A. Stratton: Forced Oscillations of a Prolate Spheroid, *J. Appl. Phys.*, vol. 12, pp. 241-248, March, 1941.
3. Page, L.: The Electrical Oscillations of a Prolate Spheroid, Parts II and III, *Phys. Rev.*, vol. 65, pp. 98-117, February, 1947.
4. Ryder, R. M.: The Electrical Oscillations of a Perfectly Conducting Prolate Spheroid, *J. Appl. Phys.*, vol. 13, pp. 327-343, May, 1942.
5. Flammer, C.: "Spheroidal Wave Functions," Stanford University Press, Stanford, Calif., 1957.
6. Stratton, J. A., P. M. Morse, L. J. Chu, and R. A. Hutner: "Elliptic Cylinder and Spheroidal Wave Functions," John Wiley & Sons, Inc., New York, 1941.
7. Stratton, J. A., P. M. Morse, L. J. Chu, D. C. Little, and F. J. Corbato: "Spheroidal Wave Functions," John Wiley & Sons, New York, 1956.
8. Meixner, J., and F. W. Schafke: "Mathieusche Funktionen und Sphäroidfunktionen," Springer-Verlag OHG, Berlin, 1954.
9. Marini, J. W.: Radiation and Admittance of an Insulated Slotted-sphere Antenna Surrounded by a Strongly Ionized Plasma Sheath, *J. Res. Natl. Bur. Std. (U.S.)*, vol. 64D, pp. 525-532; September-October, 1960.
10. Wait, J. R.: Receiving Properties of a Wire Loop with Spheroidal Core, *Can. J. Tech.*, vol. 31, pp. 9-14, January, 1953.
11. Wait, J. R.: The Receiving Loop with a Hollow Prolate Spheroidal Core, *Can. J. Tech.*, vol. 31, pp. 132-139, June, 1953.
12. Weeks, W. L.: Dielectric Coated Spheroidal Radiators, *Univ. Illinois Antenna Lab. Tech. Rept. 34*, Urbana, Ill., Sept. 12, 1958. See also W. L. Weeks, "Electromagnetic Theory for Engineering Applications," pp. 577-590, John Wiley & Sons, Inc., New York, 1964.
13. Yeh, C. W. H.: On the Dielectric-coated Prolate Spheroidal Antenna, *J. Math. Phys.*, vol. 42, pp. 68-77, March, 1963.
14. Wait, J. R.: Scattering of Electromagnetic Waves from a Lossy Strip on a Conducting Plane, *Can. J. Phys.*, vol. 33, pp. 383-390, April, 1955.
15. Cullen, A. L.: Surface Wave Resonance Effect in a Reactive Cylindrical Structure

- Excited by an Axial Line Source, *J. Res. Natl. Bur. Std. (U.S.)*, vol. 64D, no. 1, pp. 13–19, January–February, 1960.
16. Wait, J. R., and A. M. Conda: Resonance Characteristics of a Corrugated Cylinder Excited by a Magnetic Dipole, *IRE Trans. Antennas Propagation*, vol. AP-9, no. 4, pp. 330–333, July, 1961.
 17. Wait, J. R., and A. M. Conda: On the Resonance Excitation of a Corrugated Cylinder Antenna, *Proc. Inst. Elec. Engrs. (London)*, Part C, vol. 107, pp. 362–366, June, 1960.
 18. Wait, J. R., and C. M. Jackson: Resonant Characteristics of a Corrugated Sphere, *J. Res. Natl. Bur. Std. (U.S.)*, vol. 67D (Radio Prop.), no. 3, pp. 347–353, May–June, 1963.
 19. Markov, G. T., D. A. Duplenkov, and N. F. Osipovich: The Radiation of an Elongated Spheroidal Impedance Antenna, *Izve. Vysshikh Uchebn. Zavedenii (Radiofiz.)*, vol. 8, no. 1, pp. 142–152, 1965.
 - 20a. Belkina, M. G.: Radiation Characteristics of a Rotary Ellipsoid, in V. A. Fock, L. A. Weinstein, and M. G. Belkina (eds.), “Diffraction of Electromagnetic Waves on Certain Bodies of Rotation,” pp. 126–147, Soviet Radio Press (Sovetskoye Radio), Moscow, 1957.
 - 20b. Belkina, M. G.: Diffraction of Electromagnetic Waves by a Disk, in V. A. Fock, L. A. Weinstein, and M. G. Belkina (eds.), “Diffraction of Electromagnetic Waves on Certain Bodies of Rotation,” pp. 148–174, Soviet Radio Press (Sovetskoye Radio), Moscow, 1957.
 21. Fock, V. A.: “Electromagnetic Diffraction and Propagation Problems,” Pergamon Press, Oxford, 1965.
 22. Kazarinoff, N. D., and R. K. Ritt: On the Theory of Scalar Diffraction and its Application to the Prolate Spheroid, *Ann. Phys. (N.Y.)*, vol. 6, pp. 277–299, March, 1959.
 23. Senior, T. B. A.: Scalar Diffraction by a Prolate Spheroid at Low Frequencies, *Can. J. Phys.*, vol. 38, pp. 1632–1641, December, 1960.
 24. Leitner, A., and R. D. Spence: Effect of a Circular Ground Plane on Antenna Radiation, *J. Appl. Phys.*, vol. 21, no. 11, pp. 1001–1006, 1950.
 25. Kocherzhevskii, G. N.: Radiation from a Slot Which Has Been Cut in an Ideally Conducting Circular Disk, *Radiotekhn.*, vol. 10, no. 4, p. 48, 1955.
 26. Meixner, J.: Theorie der Beugung Electromagnetischer Wellen an der Vollkommen Leitenden Kreisscheibe und Verwandte Probleme, *Ann. Physik*, vol. 12, ser. 6, pp. 227–236, 1953.
 27. Flammer, C.: Radiation from Electric and Magnetic Dipoles in the Presence of a Conducting Circular Disk, *Stanford Res. Inst. Tech. Rept.* 49, Stanford, Calif., 1955.

ADDITIONAL REFERENCES

- Crispin, J. W., K. M. Siegel, and F. B. Sleator: The Resonance Region, in S. Silver (ed.), “Radio Waves and Circuits,” pp. 11–37, Elsevier Publishing Company, Amsterdam, 1963. Contains a critical discussion of current theories on vector scattering from spheroids including itemized corrections for the article by Levy and Keller, 1960.
- Goodrich, R. F., and N. D. Kazarinoff: Scalar Diffraction by Prolate Spheroids Whose Eccentricities Are Almost One, *Proc. Cambridge Phil. Soc.*, vol. 59, pp. 167–183, 1963.
- Hunter, H. E., D. B. Kirk, T. B. A. Senior, and E. R. Wittenberg: “Tables of Spheroidal Functions for $m = 0$ (i.e., order zero),” vols. I and II, Radiation Laboratory, University of Michigan, Ann Arbor, Mich., 1965.
- Infeld, L.: The Influence of the Width of the Gap upon the Theory of Antennas, *Quart. Appl. Math.*, vol. 5, pp. 113–132, July, 1947.
- Islam, M. A.: A Theoretical Treatment of Low Frequency Loop Antennas with Permeable Cores, *IEEE Trans. Antennas Propagation*, vol. AP-11, pp. 162–169, March, 1963.

- Kennaugh, E. M., and D. L. Moffatt: Axial Echo Area of the Prolate Spheroid, *Proc. Inst. Elec. Engrs. (London)* (correspondence), vol. 52, pp. 1252–1253, October, 1964.
- King, R. W. P.: "Theory of Linear Antennas," chap. VIII, Harvard University Press, Cambridge, Mass., 1956.
- Levy, B. R., and J. B. Keller: Diffraction by a Spheroid, *Can. J. Phys.*, vol. 38, pp. 128–144, January, 1960.
- Lord Rayleigh (J. W. Strutt): On the Incidence of Aerial and Electric Waves upon Small Obstacles in the Form of Ellipsoids or Elliptic Cylinders and on the Passage of Electric Waves through a Circular Aperture in a Conducting Screen, *Phil. Mag.*, vol. 43, pp. 28–52, 1897.
- Siegel, K. M.: Far Field Scattering from Bodies of Revolution, *Appl. Sci. Res.*, vol. 7B, pp. 293–328, 1958.
- Siegel, K. M., B. H. Gere, I. Marx, and F. B. Sleator: The Numerical Determination of the Radar Cross Section of a Prolate Spheroid, *Univ. Michigan Radiation Lab. Rept. UMM-126*, Ann Arbor, Mich., December, 1953.
- Sleator, F. B.: Studies in Radar Cross Sections, *Univ. Michigan Radiation Lab. Rept. 47*, part III, Ann Arbor, Mich., February, 1964.
- Wait, J. R.: Some Solutions for Electromagnetic Problems Involving Spheroidal, Spherical, and Cylindrical Bodies, *J. Res. Natl. Bur. Std. (U.S.)*, vol. 64B, pp. 15–32, January–March, 1960.
- : Comments on A Theoretical Treatment of Low Frequency Loop Antennas with Permeable Cores, *IEEE Trans. Antennas Propagation*, vol. AP-11, p. 592, September, 1963.
- : Theories of Prolate Spheroidal Antennas, *Radio Sci.*, vol. 1 (new series), no. 4, April, 1966. This paper contains material on compressible and anisotropic spheroidal sheaths.

CHAPTER 14

SLOT ANTENNAS

R. T. Compton, Jr. and R. E. Collin

14.1 Introduction

In this chapter we consider slot antennas. Specifically, we shall study a slot in a ground plane, a slot on a cylinder, a slot on a sphere, and waveguide slot arrays. The radiation patterns and some of the impedance properties of these antennas will be discussed.

Our approach in this chapter will be to assume that the aperture electric fields are known and to calculate everything else from them. This approach, although only approximate, gives reasonably good results for most engineering purposes. Furthermore, in most cases, it is the only method by which theoretical calculations of patterns and impedances can be made at all. The configuration of most slot antennas is such that an exact theoretical treatment is impossible. An exception to this is the open-ended parallel-plate waveguide, which can be treated exactly by the Wiener-Hopf method. This problem will be discussed in Chap. 15.

Space does not permit a discussion of the properties of slots on wedges, elliptic cylinders, and other structures of a similar nature. The reader is referred to Wait's book for a treatment of some of them.¹⁴

14.2 The Slot Antenna in a Ground Plane

First we consider a half-wavelength slot in an infinite ground plane as shown in Fig. 14.1. A slot occupying the region $|x| \leq a$, $|y| \leq b$ is cut in a perfectly conducting screen of infinite size. The region $z > 0$ is free space, and the slot radiates into this half space.

Such a slot can be excited in a number of ways. For example, a coaxial line from the rf source may be connected across the center of the slot, as shown in Fig. 14.2. Or the slot may be fed from a waveguide, with the slot as an opening in one of the walls. The slot could be either in a sidewall or across the end of the waveguide as shown in Fig. 14.3. The arrangement in Fig. 14.3 is sometimes called an endwall slot. Another possible feeding arrangement is a cavity behind the slot instead of a waveguide. The cavity itself may be fed by a probe and a coax line, as shown in Fig. 14.4.

With any of these feeding arrangements, the tangential electric field in the aperture will be assumed to be given by

$$\mathbf{E}_a = \hat{\mathbf{x}}E_0 \cos \frac{\pi y}{2b} \quad |x| \leq a, |y| \leq b \quad (14.1)$$

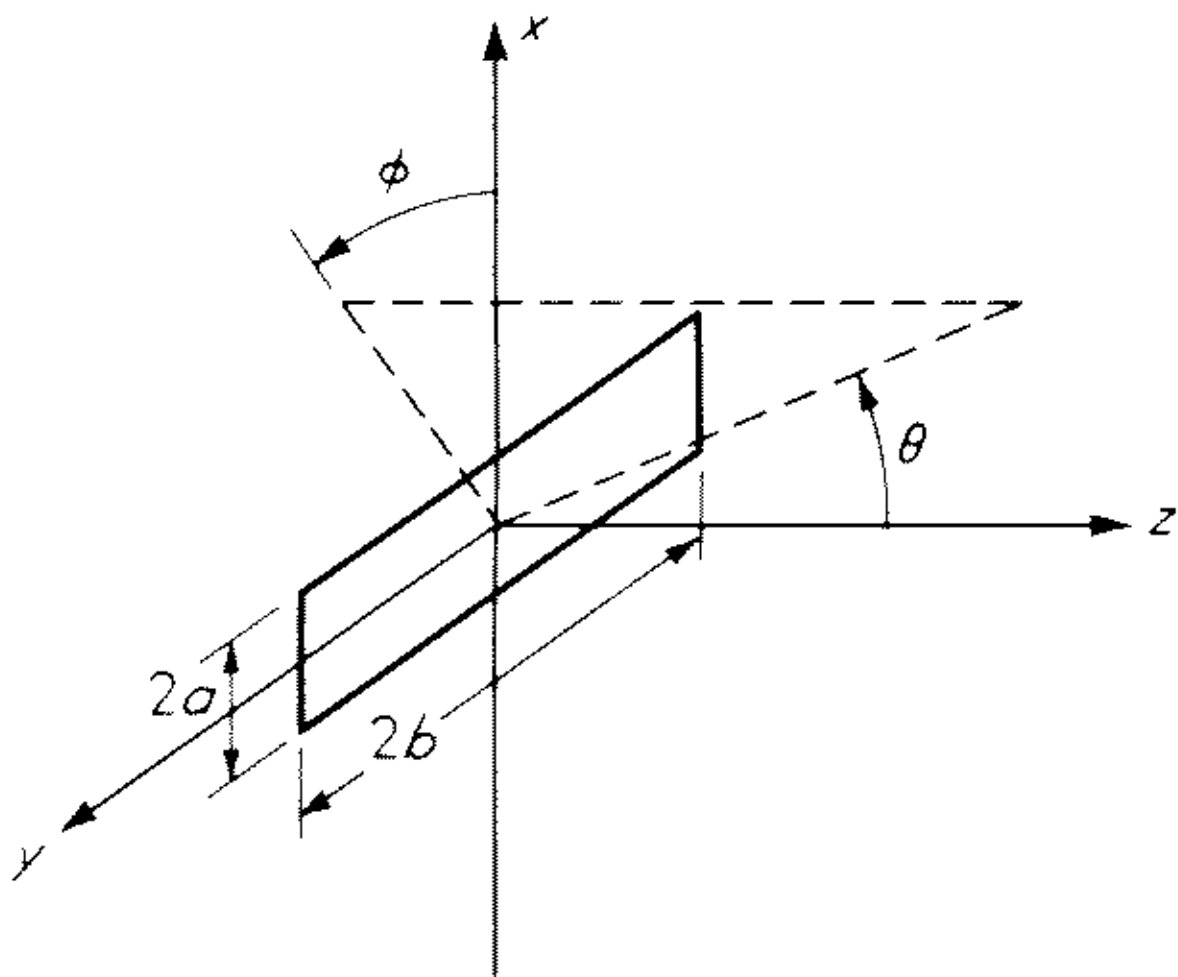


Fig. 14.1 Slot in a ground plane.

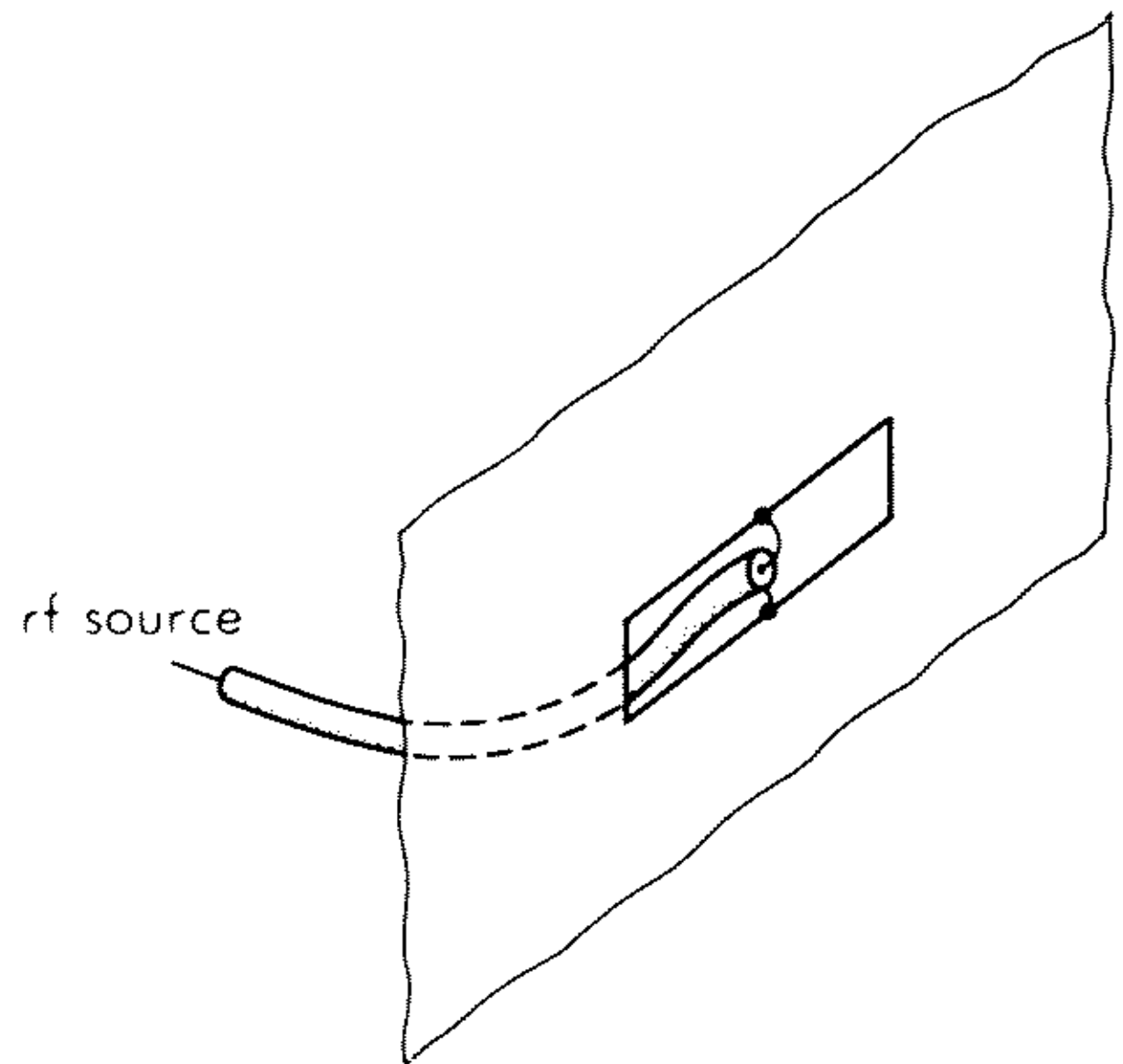


Fig. 14.2 Coax-fed slot.

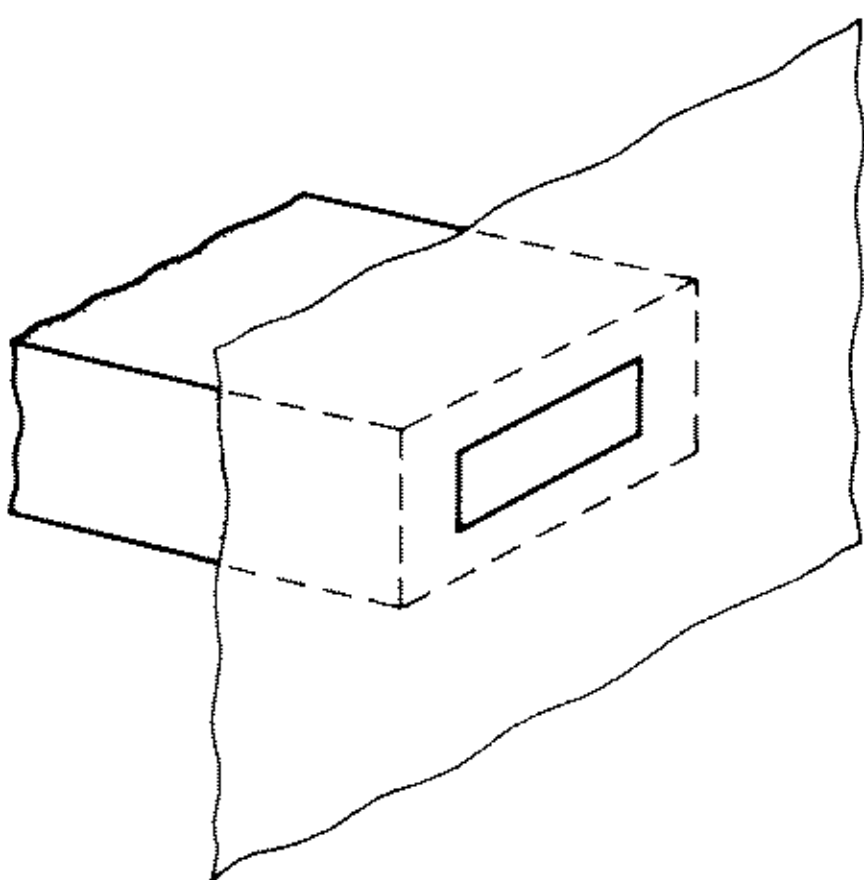


Fig. 14.3 Endwall slot.

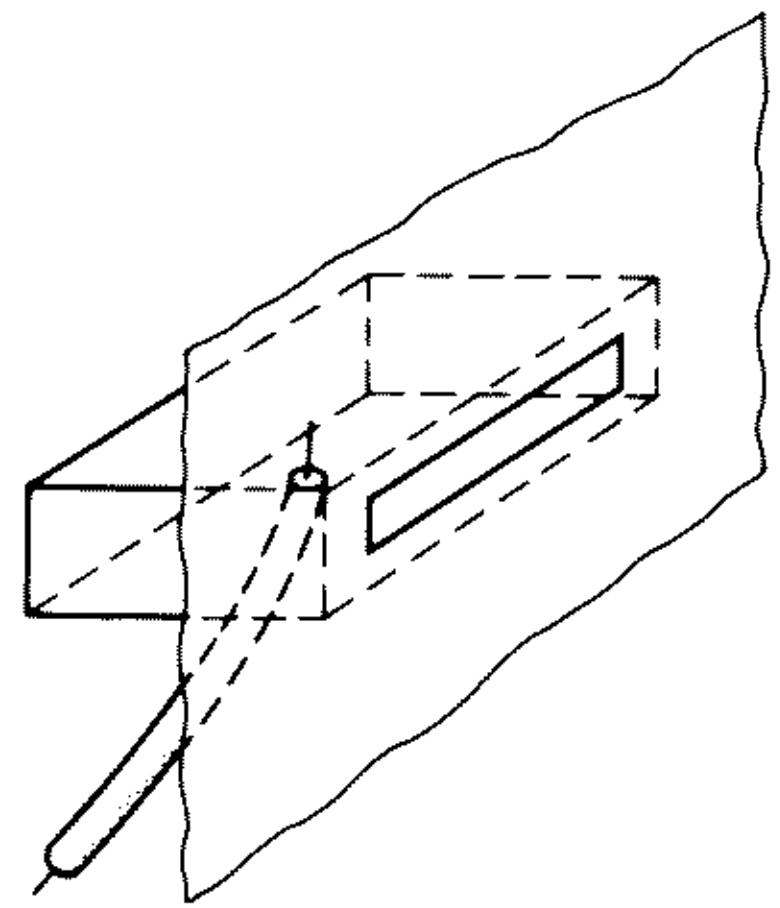


Fig. 14.4 Cavity-fed slot.

The tangential electric field in the xy plane outside the aperture is zero, because the ground plane is perfectly conducting. This assumed aperture field is reasonable, in view of the method of excitation. For the endwall slot of Fig. 14.3, for example, the dominant TE_{10} mode in the waveguide has the same distribution across the waveguide as that given by (14.1). A coax-fed slot and a cavity-fed slot, if the cavity is excited primarily in its fundamental mode, would also generate an aperture distribution that is maximum at the center and tapers to zero at the edges.

The fields in the region $z > 0$ resulting from this aperture distribution are easily found by using (3.1) to (3.14) of Chap. 3. With $\mathbf{E}_a(x, y)$ as the tangential field in the aperture, the transform $\mathbf{f}_t(k_x, k_y)$ is given by

$$\mathbf{f}_t(k_x, k_y) = \int_{x=-a}^a \int_{y=-b}^b \mathbf{E}_a(x, y) e^{j(k_x x + k_y y)} dx dy \quad (14.2)$$

and then the field at any point in space is

$$\mathbf{E}(x, y, z) = \frac{1}{4\pi^2} \int_{k_x=-\infty}^{\infty} \int_{k_y=-\infty}^{\infty} \mathbf{f}(k_x, k_y) \exp(-j\mathbf{k} \cdot \mathbf{r}) dk_x dk_y \quad (14.3)$$

In the far field, (14.3) simplifies to

$$\mathbf{E}(x, y, z) = jk_0 \frac{e^{-jk_0 r}}{2\pi r} [\hat{\phi}(f_y \cos \phi - f_x \sin \phi) \cos \theta + \hat{\theta}(f_x \cos \phi + f_y \sin \phi)] \quad (14.4)$$

where f_x and f_y are evaluated at $k_x = k_0 \cos \phi \sin \theta$ and $k_y = k_0 \sin \phi \sin \theta$ and the angles θ and ϕ are defined in Fig. 14.1.

When these formulas are applied to the aperture distribution given in (14.1), it is found that

$$\mathbf{f}_t(k_x, k_y) = \hat{\mathbf{x}} \left[-\frac{2E_0\pi}{b} \frac{\sin k_x a}{k_x} \frac{\cos k_y b}{k_y^2 - (\pi/2b)^2} \right] \quad (14.5)$$

so

$$\begin{aligned} f_x(k_0 \cos \phi \sin \theta, k_0 \sin \phi \sin \theta) \\ = -\frac{2E_0\pi}{b} \frac{\sin(k_0 a \cos \phi \sin \theta)}{k_0 \cos \phi \sin \theta} \frac{\cos(k_0 b \sin \phi \sin \theta)}{(k_0 \sin \phi \sin \theta)^2 - (\pi/2b)^2} \end{aligned} \quad (14.6)$$

and thus in the far field,

$$\begin{aligned} E_\phi = jk_0 E_0 ab \frac{e^{-jk_0 r}}{r} \sin \phi \cos \theta \frac{\sin(k_0 a \cos \phi \sin \theta)}{k_0 a \cos \phi \sin \theta} \\ \times \frac{\cos(k_0 b \sin \phi \sin \theta)}{(k_0 b \sin \phi \sin \theta)^2 - (\pi/2)^2} \end{aligned} \quad (14.7)$$

$$\begin{aligned} E_\theta = -jk_0 E_0 ab \frac{e^{-jk_0 r}}{r} \cos \phi \frac{\sin(k_0 a \cos \phi \sin \theta)}{k_0 a \cos \phi \sin \theta} \\ \times \frac{\cos(k_0 b \sin \phi \sin \theta)}{(k_0 b \sin \phi \sin \theta)^2 - (\pi/2)^2} \end{aligned} \quad (14.8)$$

If the height of the opening is small, so $k_0 a \ll 1$, and the opening is a half-wavelength long, so $k_0 b = \pi/2$, the pattern expressions become

$$E_\phi = -j \frac{V_0}{\pi} \frac{e^{-jk_0 r}}{r} \sin \phi \cos \theta \frac{\cos\left(\frac{\pi}{2} \sin \phi \sin \theta\right)}{1 - \sin^2 \phi \sin^2 \theta} \quad (14.9)$$

$$E_\theta = j \frac{V_0}{\pi} \frac{e^{-jk_0 r}}{r} \cos \phi \frac{\cos\left(\frac{\pi}{2} \sin \phi \sin \theta\right)}{1 - \sin^2 \phi \sin^2 \theta} \quad (14.10)$$

where we have defined $V_0 = 2aE_0$ as the voltage across the slot.

In the $\phi = 0$ ($y = 0$) plane, E_ϕ is zero and E_θ is constant, so the pattern in this plane is omnidirectional. This result is a consequence of the assumption that a is small. In the $\phi = \pi/2$ ($x = 0$) plane, E_θ is zero and

$$E_\phi = -j \frac{V_0}{\pi} \frac{e^{-jk_0 r}}{r} \frac{\cos\left(\frac{\pi}{2} \sin \theta\right)}{\cos \theta} \quad (14.11)$$

which is shown in polar form in Fig. 14.5.

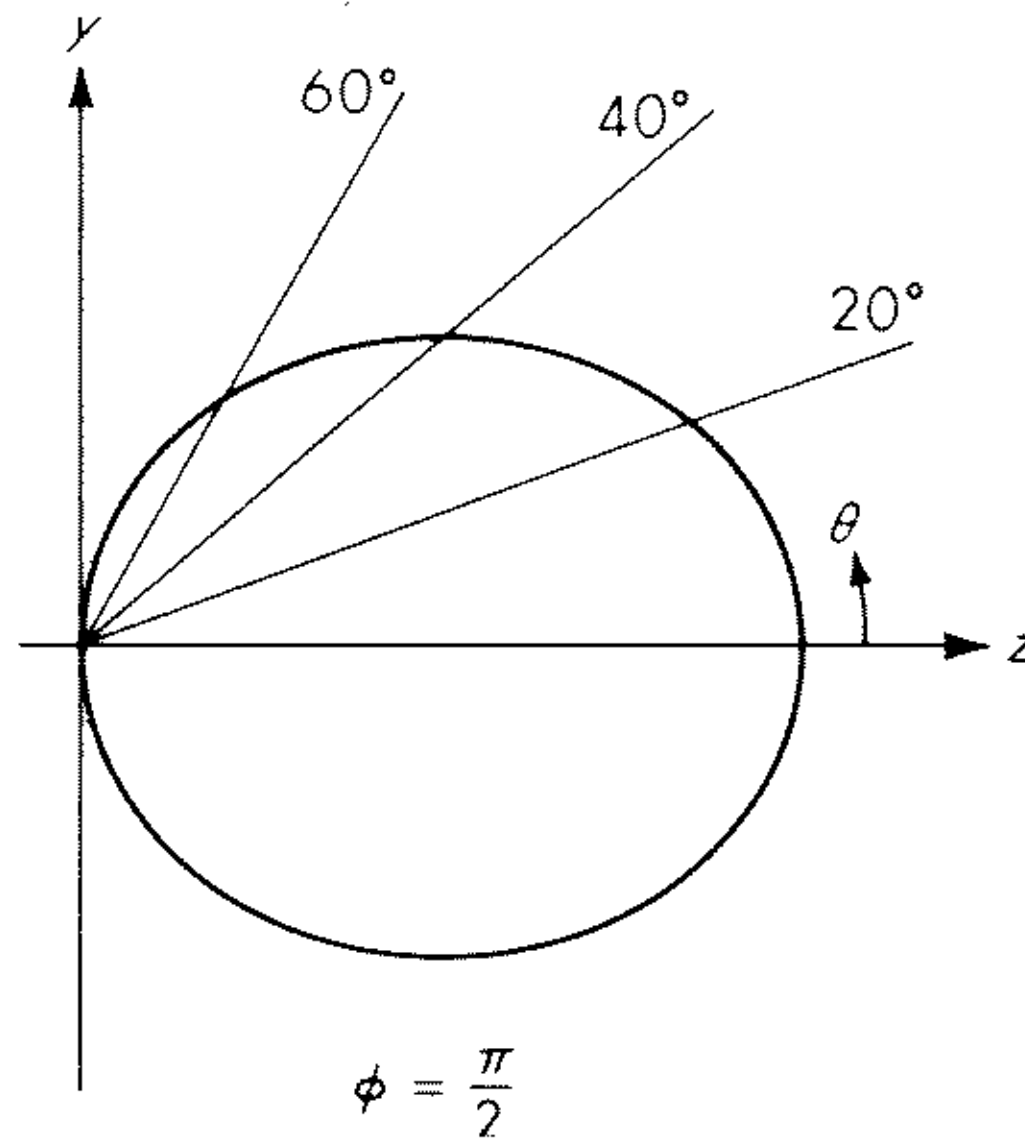


Fig. 14.5 Electric field E_ϕ vs. θ in $\phi = \pi/2$ plane.

This pattern has the same dependence on θ as that of a half-wavelength electric dipole oriented along the y axis. In fact, the aperture treated here produces exactly the same fields as a magnetic dipole with magnetic current

$$I_m = -4aE_0 \cos\left(\frac{\pi y}{2b}\right)\hat{y} \quad |y| \leq b \quad (14.12)$$

radiating in free space, i.e., with no ground plane. Thus the slot is just the dual of an electric dipole. If we interchange electric and magnetic quantities, according to duality theory,¹ (14.11) gives the formula for H_ϕ for an electric dipole. More will be said about this below, in connection with Babinet's principle.

To determine the total power radiated by this aperture, we may integrate the real part of the Poynting vector over a hemisphere of large radius centered on the aperture. In the far field,

$$\mathbf{H} = \zeta_0^{-1}\hat{\mathbf{r}} \times \mathbf{E} \quad (14.13)$$

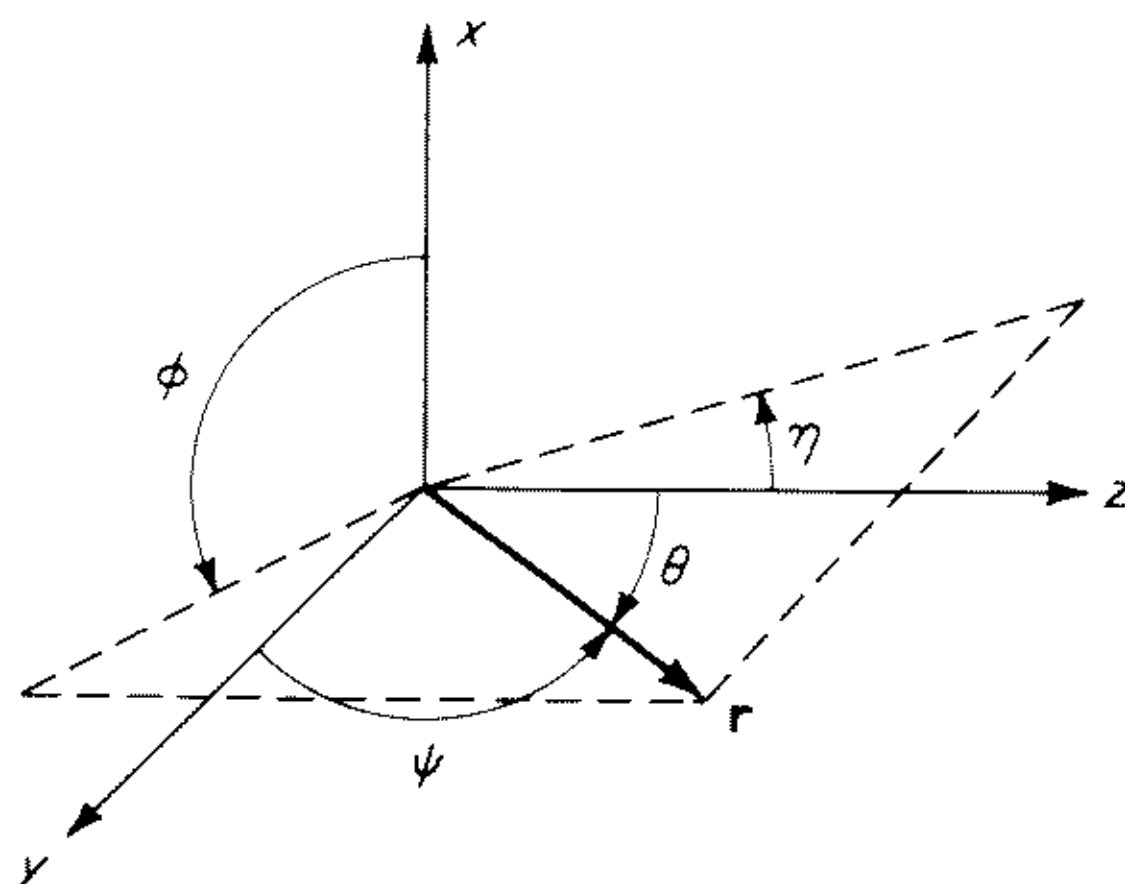
$$\mathbf{E} \times \mathbf{H}^* = \mathbf{E} \times (\zeta_0^{-1}\hat{\mathbf{r}} \times \mathbf{E}^*) = \zeta_0^{-1}(\mathbf{E} \cdot \mathbf{E}^*)\hat{\mathbf{r}} \quad (14.14)$$

and thus $\frac{1}{2} \text{Re} (\mathbf{E} \times \mathbf{H}^*) = \frac{1}{2}\zeta_0^{-1}(E_\theta E_\theta^* + E_\phi E_\phi^*)\hat{\mathbf{r}} \quad (14.15)$

Therefore the total power P radiated by the aperture is

$$\begin{aligned} P &= \int_{\theta=0}^{\pi/2} \int_{\phi=0}^{2\pi} \frac{\zeta_0^{-1}}{2} \frac{V_0^2}{\pi^2 r^2} (\sin^2 \phi \cos^2 \theta + \cos^2 \phi) \\ &\quad \times \frac{\cos^2 [(\pi/2) \sin \phi \sin \theta]}{(1 - \sin^2 \phi \sin^2 \theta)^2} r^2 \sin \theta d\theta d\phi \\ &= \frac{\zeta_0^{-1}}{2} \frac{V_0^2}{\pi^2} \int_{\theta=0}^{\pi/2} \int_{\phi=0}^{2\pi} \frac{\cos^2 [(\pi/2) \sin \phi \sin \theta]}{(1 - \sin^2 \phi \sin^2 \theta)^2} \sin \theta d\theta d\phi \end{aligned} \quad (14.16)$$

This integral may be evaluated by first making a change of coordinates to a spherical coordinate system having the y axis as its polar axis. In Fig. 14.6 is shown the new coordinate system with polar angle ψ and azimuth angle η . For

Fig. 14.6 The angles ψ and η .

a given vector \mathbf{r} , ψ is the angle between \mathbf{r} and the y axis and η is the angle made by the projection of \mathbf{r} in the xz plane with the z axis. It may be seen by writing out the y component of \mathbf{r} in both coordinate systems that

$$\sin \theta \sin \phi = \cos \psi \quad (14.17)$$

and hence

$$P = \frac{\zeta_0^{-1}}{2} \frac{V_0^2}{\pi^2} \int_{\psi=0}^{\pi} \int_{\eta=-\pi/2}^{\pi/2} \frac{\cos^2 [(\pi/2) \cos \psi]}{\sin^2 \psi} \sin \psi d\psi d\eta \quad (14.18)$$

where we do not transform $\sin \theta d\theta d\phi$ directly but merely replace it with $\sin \psi d\psi d\eta$, the appropriate incremental solid angle for the new coordinate system.

The η integration in (14.18) may be done immediately, and then the remaining ψ integral is of exactly the same form as the integral previously considered in (2.46) if $k_0 l$ is set equal to $\pi/2$ in that equation. Hence we find

$$P = \frac{\zeta_0^{-1} V_0^2}{4\pi} (\ln 2\pi\gamma - \text{Ci } 2\pi) = 2.436 \frac{\zeta_0^{-1} V_0^2}{4\pi} \quad (14.19)$$

Since V_0 is the voltage across the center of the slot, we may define a *radiation conductance* G_r as the conductance that, if placed across the voltage V_0 , would dissipate the same power as that radiated by the slot, that is,

$$\frac{1}{2} V_0^2 G_r = P \quad (14.20)$$

$$\text{or} \quad G_r = 2.436 \frac{\zeta_0^{-1}}{2\pi} \approx 1.03 \times 10^{-3} \text{ mhos} \quad (14.21)$$

It may be remarked that, since the narrow half-wavelength slot considered here is the dual of the half-wavelength electric dipole, it is naturally not surprising that the integral needed to evaluate the radiated power is the same as the one that occurred with the electric dipole. Also, the radiation conductance of a slot having length other than a half wavelength may be calculated in the same way as above, and the integral needed will be the same as the one in (2.46) for an electric dipole of arbitrary length.

Babinet's Principle

The duality between this slot and an electric dipole is related to a more general statement known as Babinet's principle.² Consider a source S that radiates behind an infinite electric conducting screen in which there is an aperture S_a , as shown in Fig. 14.7a. Let the fields which result from S on the right side of the screen be denoted by $\mathbf{E}_e, \mathbf{H}_e$. Next consider the same source S radiating in the presence of a perfect magnetic conductor, shown in Fig. 14.7b, whose shape and position are exactly the same as those of the aperture S_a . Let the fields which result to the right of the conductor in this case be denoted by $\mathbf{E}_m, \mathbf{H}_m$. Then Babinet's principle states that

$$\mathbf{E}_e + \mathbf{E}_m = \mathbf{E}_i \quad \mathbf{H}_e + \mathbf{H}_m = \mathbf{H}_i \quad (14.22)$$

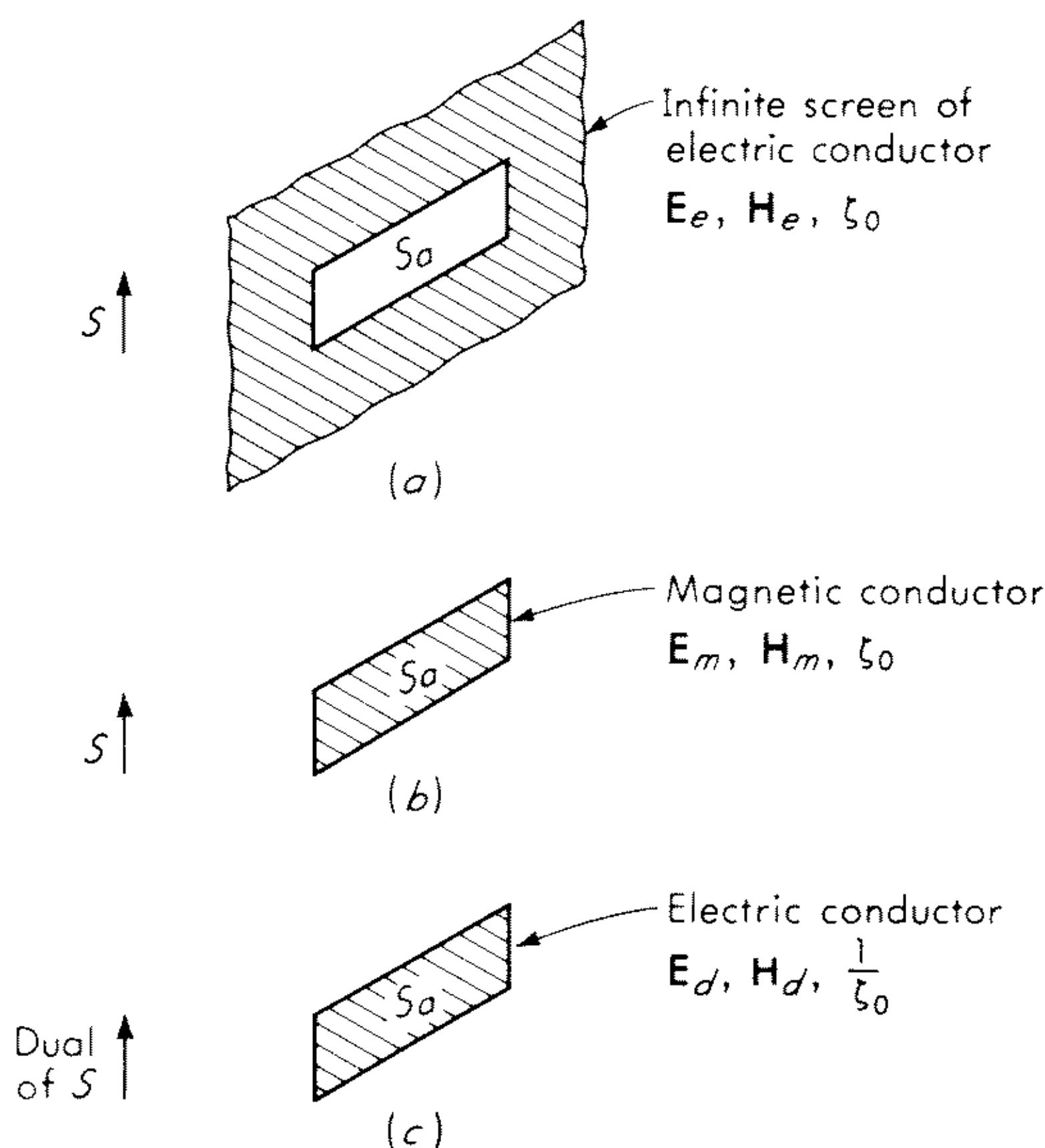


Fig. 14.7 Illustration for Babinet's principle.

where $\mathbf{E}_i, \mathbf{H}_i$ are the fields that would result if the source S were to radiate in empty space, with no conductors present at all. The electric screen and the magnetic screen are usually referred to as *complementary structures*, because the two structures, if fitted together, completely fill the infinite plane with no overlap. A proof of Babinet's principle is given by Harrington.³

A more useful statement of Babinet's principle may be obtained by taking the dual of the situation shown in Fig. 14.7b. Suppose a source that is the dual of S radiates in the presence of an *electric* conductor having shape S_a , as shown in Fig. 14.7c, and the medium surrounding the source and the conductor has characteristic impedance ζ_0^{-1} , where ζ_0 is the characteristic impedance of the medium in Fig. 14.7a and b. Then the problem in Fig. 14.7c is the dual of that

in Fig. 14.7*b*. Let the fields in Fig. 14.7*c* be denoted by $\mathbf{E}_d, \mathbf{H}_d$. Then, from duality, the values of \mathbf{E}_d and \mathbf{H}_d may be obtained from \mathbf{E}_m and \mathbf{H}_m by replacing \mathbf{E}_m by \mathbf{H}_d and \mathbf{H}_m by $-\mathbf{E}_d$. Equations (14.22) then become

$$\mathbf{E}_e + \mathbf{H}_d = \mathbf{E}_i \quad \mathbf{H}_e - \mathbf{E}_d = \mathbf{H}_i \quad (14.23)$$

The situation shown in Fig. 14.7*c* is a more useful complement to that in Fig. 14.7*a*, because both involve electric conductors.

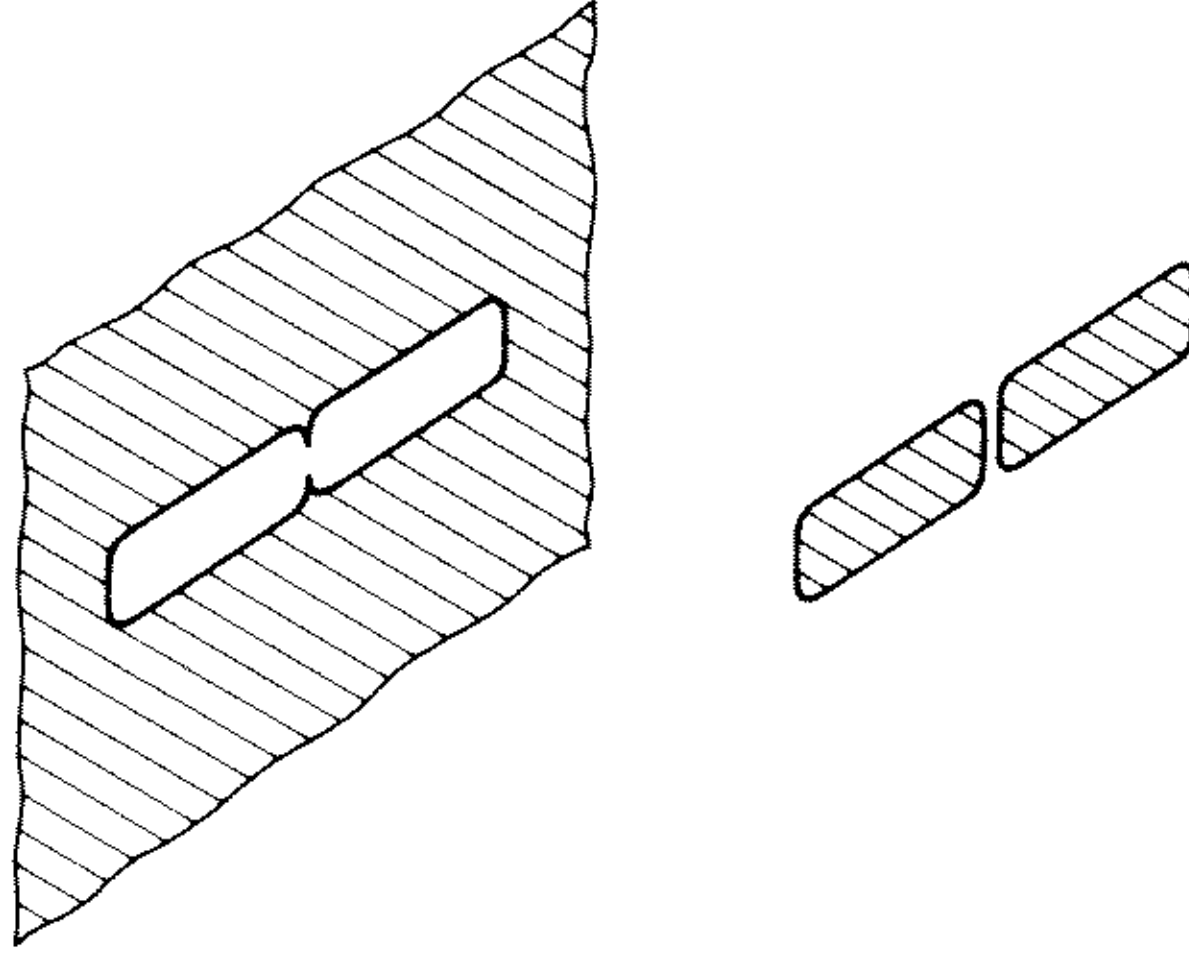


Fig. 14.8 Complementary structures with terminals.

Babinet's principle can also be used to derive a relationship between impedances of complementary structures. If the complementary structures are so shaped that voltages and currents can be defined, as in Fig. 14.8, then it is found that

$$Z_e Z_d = \frac{\zeta_0^2}{4} \quad (14.24)$$

where Z_e is the impedance of the aperture in the conducting screen, Z_d is the impedance of the complementary antenna, and ζ_0 is the wave impedance of free space.

It is interesting to note that the radiation conductance of the slot in Fig. 14.1 could have been calculated directly from Babinet's principle and the fact that the radiation resistance of a half-wave dipole is 73Ω . Since the slot and the dipole are complementary,

$$Z_{\text{aperture}} Z_{\text{dipole}} = \frac{\zeta_0^2}{4} \quad (14.25)$$

Hence (the slot and dipole are assumed resonant, so the reactive components of impedance are zero)

$$\frac{1}{Y_{\text{aperture}}} = \frac{\zeta_0^2}{4Z_{\text{dipole}}} = \frac{377^2}{4(73)} = 486 \quad (14.26)$$

or
$$Y_{\text{aperture}} = 2.06 \times 10^{-3} \text{ mhos} \quad (14.27)$$

The aperture that is used in Babinet's principle would radiate on both sides of

the screen. Since the slot of Fig. 14.1 is understood to radiate on only one side of the screen, it will radiate only one-half as much power as the aperture in Babinet's principle, and hence

$$G_r = \frac{Y_{\text{aperture}}}{2} = 1.03 \times 10^{-3} \text{ mhos} \quad (14.28)$$

which checks the result (14.21).

14.3 Slots on Cylinders — Formal Solution

In this section we consider small slot antennas on conducting cylinders. The circular cylinder is the simplest geometry involving a curved surface, and an antenna on a cylinder is the least difficult problem of this type to treat. Furthermore, the analytical results can be reduced to numerical calculations (at least for small cylinders) because the functions appropriate for this geometry, the Bessel functions, are well tabulated. Hence, this type of antenna is a fruitful one to study.

Consider the cylinder shown in Fig. 14.9. The axis of the cylinder is the z axis of an xyz coordinate system, and a cylindrical coordinate system r, ϕ is also defined. The cylinder has radius a and is infinitely conducting.

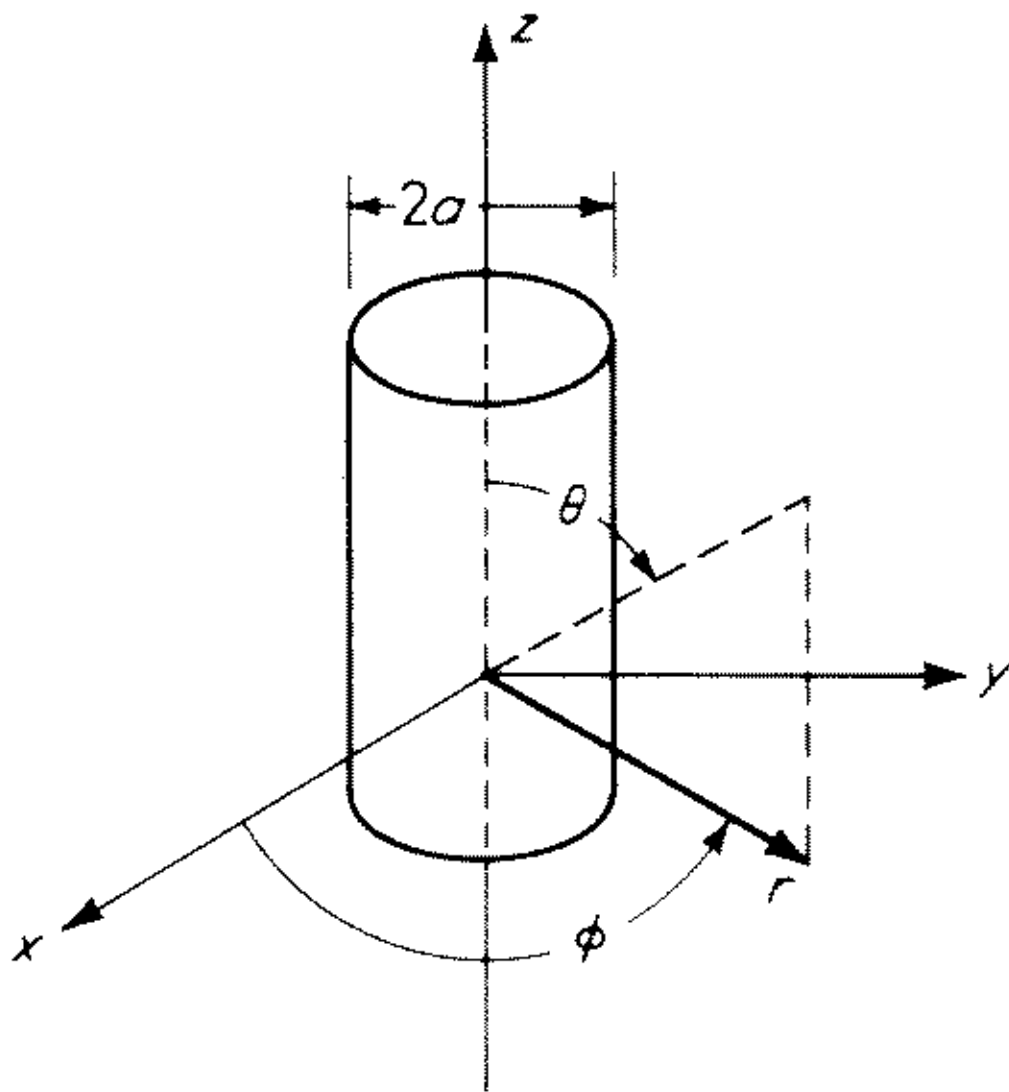


Fig. 14.9 A conducting cylinder with coordinate system.

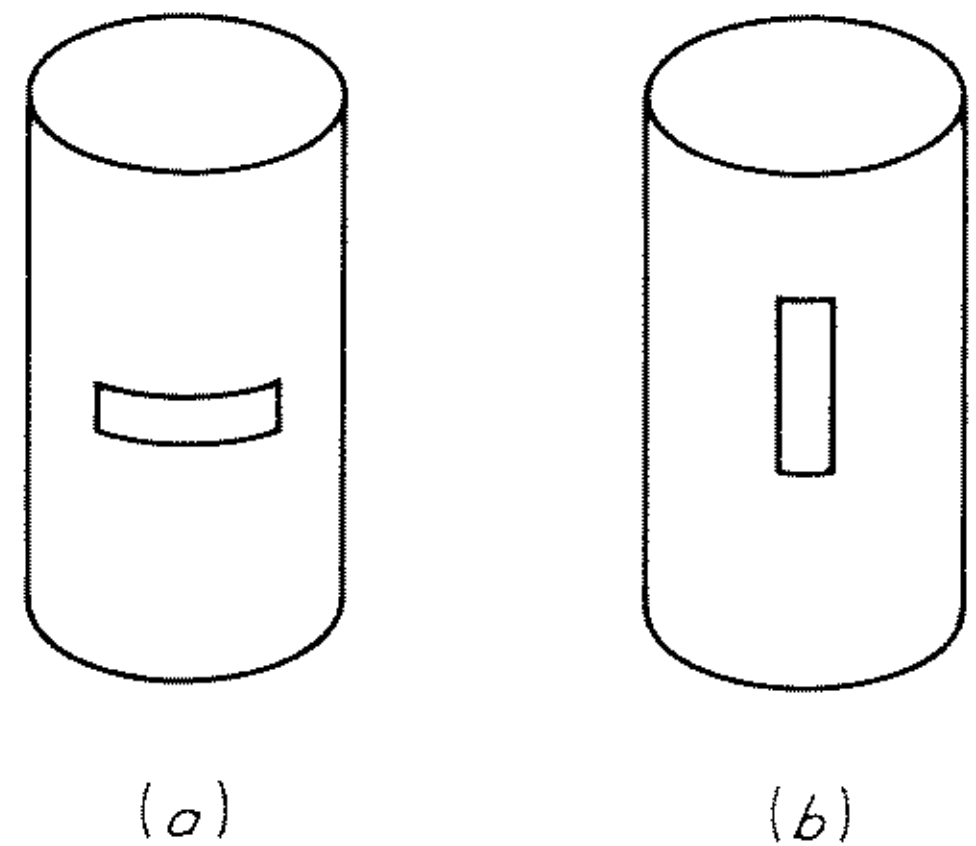


Fig. 14.10 Slots on a cylinder. (a) Circumferential slot; (b) axial slot.

Two types of slot antennas will be considered: The circumferential slot and the axial slot. A circumferential slot is one with a narrow height in the z direction and a large width in the ϕ direction, possibly even the entire circumference. A circumferential slot is shown in Fig. 14.10a. An axial slot is one that is narrow in the ϕ direction and long in the z direction, as shown in Fig. 14.10b. As with the slot in a ground plane, we assume the aperture field to be known and then calculate the fields outside the cylinder.

The properties of such slots have been studied by quite a few authors.

Sinclair discussed the pattern of an infinite axial slot having only a ϕ component of electric field.⁴ He showed radiation patterns for various values of k_0a ($k_0 = 2\pi/\lambda_0$, where λ_0 is the free space wavelength) between 0.0318 and 0.2865 and between 0.5 and 8. Some patterns for an array of two slots were also given. Papas discussed the far fields for a circumferential slot completely around the cylinder with a uniform axial component of electric field.⁵ He also treated the finite circumferential slot with a cosinusoidal aperture distribution.⁶ Silver and Saunders have formulated the general expressions for the far fields for an aperture of arbitrary shape, and they have used their results to study the case of a rectangular aperture of finite width in both the z and ϕ directions excited by both a ϕ component and a z component of electric field.^{7,8} They apply their general results to the specific case of a narrow axial slot one-half wavelength high having a cosinusoidal distribution of E_ϕ , and they give tabular data from which patterns of an axial slot may be computed for two sizes of cylinder, $k_0a = 0.8$ and $k_0a = 2.5$. Wait and Kahana have given extensive calculations of the patterns,⁹ both magnitude and phase, for the case of a half-wavelength circumferential slot on cylinders with $k_0a = 2, 3, 5$. They show both the direct and the cross-polarized component of the far field, and they give calculations for several values of the polar coordinate (see Fig. 14.9). Bailin¹⁰ has given extensive calculations of both components of the far field for the half-wave circumferential slot and for the half-wave axial slot for cylinder sizes $k_0a = 9$ and $k_0a = 12$. Wait^{11,12} has given extensive data on the half-wavelength axial slot for values of k_0a from 0.1 to 21, and Wait and Kates¹³ have given results for the half-wavelength circumferential slot for values of k_0a between 3 and 21. A large bibliography and a review of many of these results have been given by Wait.¹⁴

In our discussion of this problem, we shall follow the derivation given by Silver and Saunders.^{7,8} Consider an infinite conducting cylinder of radius a with cylindrical and spherical coordinate systems defined as shown in Fig. 14.11. A rectangular aperture cut in the surface of the cylinder occupies the

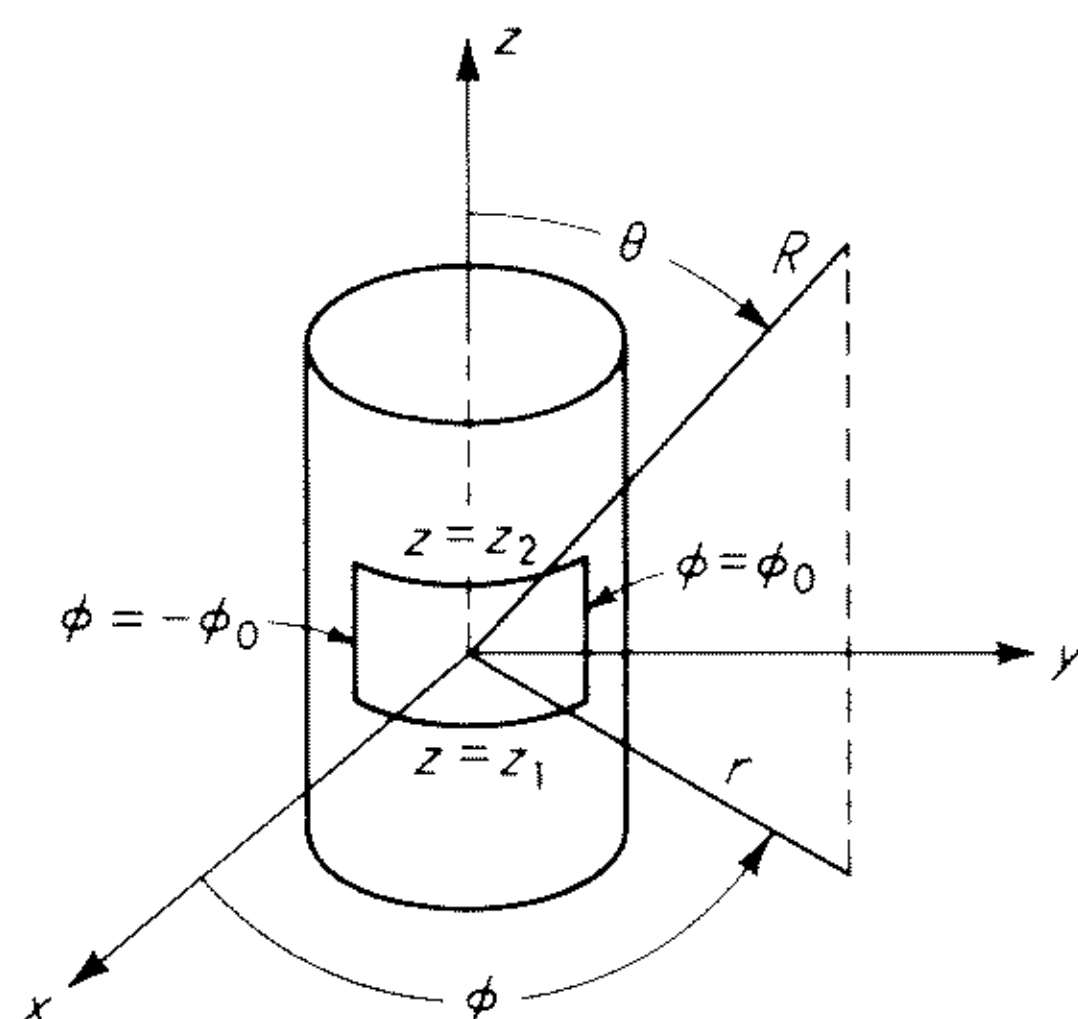


Fig. 14.11 An aperture on an infinite cylinder.

region $z_1 \leq z \leq z_2$ and $-\phi_0 \leq \phi \leq \phi_0$. The electric field in the aperture is assumed to be known and to be given by

$$E_\phi(a, \phi, z) = F_1(\phi)G_1(z) \quad (14.29a)$$

$$E_z(a, \phi, z) = F_2(\phi)G_2(z) \quad (14.29b)$$

To find the fields in the region outside the cylinder, we write general expressions for an arbitrary field in a cylindrical coordinate system and then evaluate the unknown coefficients in the general expression by setting the general expression equal to the assumed fields on the surface of the cylinder. The general expression for an electromagnetic field in cylindrical coordinates may be obtained from the wave equation by the method of separation of variables. If it is assumed the fields are periodic in ϕ , with period 2π , an arbitrary field may be written

$$E_\alpha(r, \phi, z) = \int_{-\infty}^{\infty} \mathcal{E}_\alpha(r, \phi, h) dh \quad (14.30a)$$

$$H_\alpha(r, \phi, z) = \int_{-\infty}^{\infty} \mathcal{H}_\alpha(r, \phi, h) dh \quad (14.30b)$$

where α stands for one of the subscripts r , ϕ , or z , and where

$$\mathcal{E}_r = \left\{ \sum_{n=-\infty}^{\infty} \left[-jha_n \frac{\partial H_n(\Lambda r)}{\partial r} - \frac{n\omega\mu_0}{r} b_n H_n(\Lambda r) \right] e^{-jn\phi} \right\} e^{-jhz} \quad (14.31a)$$

$$\mathcal{E}_\phi = \left\{ \sum_{n=-\infty}^{\infty} \left[-\frac{nh}{r} a_n H_n(\Lambda r) + j\omega\mu_0 b_n \frac{\partial H_n(\Lambda r)}{\partial r} \right] e^{-jn\phi} \right\} e^{-jhz} \quad (14.31b)$$

$$\mathcal{E}_z = \left\{ \sum_{n=-\infty}^{\infty} [(k_0^2 - h^2) a_n H_n(\Lambda r)] e^{-jn\phi} \right\} e^{-jhz} \quad (14.31c)$$

$$\mathcal{H}_r = \left\{ \sum_{n=-\infty}^{\infty} \left[\frac{nk_0^2}{\mu_0\omega r} a_n H_n(\Lambda r) - jhb_n \frac{\partial H_n(\Lambda r)}{\partial r} \right] e^{-jn\phi} \right\} e^{-jhz} \quad (14.31d)$$

$$\mathcal{H}_\phi = \left\{ \sum_{n=-\infty}^{\infty} \left[-j \frac{k_0^2}{\mu_0\omega} a_n \frac{\partial H_n(\Lambda r)}{\partial r} - \frac{nh}{r} b_n H_n(\Lambda r) \right] e^{-jn\phi} \right\} e^{-jhz} \quad (14.31e)$$

$$H_z = \left\{ \sum_{n=-\infty}^{\infty} [(k_0^2 - h^2) b_n H_n(\Lambda r)] e^{-jn\phi} \right\} e^{-jhz} \quad (14.31f)$$

In these formulas, a_n and b_n are arbitrary coefficients to be adjusted to make the formulas for E_ϕ and E_z in the aperture match the known values given in (14.29). $H_n(z)$ is the Hankel function of the second kind of order n and argument z . (Since only the Hankel function of the second kind is used, we have dropped the superscript 2.) The function Λ is given by

$$\Lambda = \sqrt{k_0^2 - h^2} \quad (14.32)$$

where Λ is chosen as that root for which

$$\text{Re}(\Lambda) \geq 0 \quad \text{Im}(\Lambda) \leq 0 \quad (14.33)$$

corresponding to outward radial propagation.

Equations (14.30) to (14.33) are completely general formulas that may be used to represent any electromagnetic field, assuming only that the field is propagating outward. The derivation of these equations is given, for example, in Stratton.¹⁵ As mentioned above, it is assumed in the derivation of these formulas that all fields are periodic in ϕ , so the separation constant for ϕ is an integer n . Actually, it is not necessary to make this assumption, because only the range $0 \leq \phi \leq 2\pi$ is of interest and there is really no requirement of periodicity. Other representations of the fields can be obtained by dropping this assumption.

To determine the coefficients a_n and b_n in this expression we compare the tangential electric field computed from these formulas at $r = a$ with the assumed field on the surface of the cylinder, viz., zero everywhere except in the aperture, where it is given by (14.29). This aperture field may be written as a Fourier series in ϕ and a Fourier integral in z :

$$E_\phi(a, \phi, z) = \frac{1}{4\pi^2} \sum_{n=-\infty}^{\infty} e^{-jn\phi} \int_{-\infty}^{\infty} dh \int_{z_1}^{z_2} G_1(\xi) e^{-jh(z-\xi)} d\xi \int_{\beta=-\phi_0}^{\phi_0} F_1(\beta) e^{jn\beta} d\beta \quad (14.34a)$$

$$E_z(a, \phi, z) = \frac{1}{4\pi^2} \sum_{n=-\infty}^{\infty} e^{-jn\phi} \int_{-\infty}^{\infty} dh \int_{-\infty}^{\infty} G_2(\xi) e^{-jh(z-\xi)} d\xi \int_{\beta=-\phi_0}^{\phi_0} F_2(\beta) e^{jn\beta} d\beta \quad (14.34b)$$

Equations (14.30a) and (14.31b-c), when applied at $r = a$, give

$$E_\phi(a, \phi, z) = \sum_{n=-\infty}^{\infty} e^{-jn\phi} \int_{-\infty}^{\infty} \left[-\frac{nh}{a} a_n H_n(\Lambda a) + j\omega\mu_0 b_n \frac{\partial H_n(\Lambda a)}{\partial a} \right] e^{-jh z} dh \quad (14.35a)$$

$$E_z(a, \phi, z) = \sum_{n=-\infty}^{\infty} e^{-jn\phi} \int_{-\infty}^{\infty} (k_0^2 - h^2) a_n H_n(\Lambda a) e^{-jh z} dh \quad (14.35b)$$

Comparing (14.35) with (14.34) gives

$$\left[-\frac{nh}{a} H_n(\Lambda a) \right] a_n + \left[j\omega\mu_0 \frac{\partial H_n(\Lambda a)}{\partial a} \right] b_n = I_1(h) C_1(n) \quad (14.36a)$$

$$[(k_0^2 - h^2) H_n(\Lambda a)] a_n = I_2(h) C(n) \quad (14.36b)$$

where

$$I_i(h) = \frac{1}{2\pi} \int_{z_1}^{z_2} G_i(\xi) e^{jh\xi} d\xi \quad (14.37a)$$

$$C_i(n) = \frac{1}{2\pi} \int_{-\phi_0}^{\phi_0} F_i(\beta) e^{jn\beta} d\beta \quad (14.37b)$$

The above equations are easily solved for a_n and b_n , with the result

$$a_n = \frac{I_2(h) C_2(n)}{(k_0^2 - h^2) H_n(\Lambda a)} \quad (14.38a)$$

$$b_n = \frac{-jnh I_2(h) C_2(h)}{\omega\mu_0 a (k_0^2 - h^2) [\partial H_n(\Lambda a) / \partial a]} + \frac{j I_1(h) C_1(h)}{\omega\mu_0 [\partial H_n(\Lambda a) / \partial a]} \quad (14.38b)$$

These coefficients, when substituted in (14.31), give the formal solution for the electromagnetic fields outside the cylinder. This solution, however, is too cumbersome for calculating field patterns. In the far field a simple approximation for the fields may be derived by using the saddle-point method to evaluate the integrals in (14.30). The procedure for doing this is as follows. We first describe the far fields in terms of spherical coordinates R, θ, ϕ (shown in Fig. 14.11) by substituting

$$r = R \sin \theta \quad z = R \cos \theta \quad (14.39)$$

in the expressions for the fields. Next we assume that the quantity $R \sin \theta$ is quite large, i.e., that the point where we calculate the fields is at a great distance from the antenna and not too near the surface of the cylinder. Then we replace the Hankel function $H_n(\Lambda R \sin \theta)$ by its asymptotic form:¹⁶

$$H_n(\Lambda R \sin \theta) = \left(\frac{2}{\pi \Lambda R \sin \theta} \right)^{1/2} e^{-j\Lambda R \sin \theta} e^{j(2n+1)\pi/4} \quad (14.40)$$

in (14.31).† When this is done, and (14.31) is substituted into (14.30), the order of integration and summation may be reversed and it is found that the expression for any one of the field components is of the form

$$\sum_{n=-\infty}^{\infty} e^{-jn\phi} \left[C_1(n) \int_{-\infty}^{\infty} K_1(h, R, \theta, n) I_1(h) e^{-jR(\Lambda \sin \theta + h \cos \theta)} dh \right. \\ \left. + C_2(n) \int_{-\infty}^{\infty} K_2(h, R, \theta, n) I_2(h) e^{-jR(\Lambda \sin \theta + h \cos \theta)} dh \right] \quad (14.41)$$

For example, for the field component E_ϕ ,

$$K_1(h, R, \theta, n) = \left(\frac{2\Lambda}{\pi R \sin \theta} \right)^{1/2} \frac{e^{j(2n-1)\pi/4}}{\partial H_n(\Lambda a)/\partial a} \quad (14.42a)$$

$$K_2(h, R, \theta, n) = \left(\frac{2\Lambda}{\pi R \sin \theta} \right)^{1/2} \frac{n h e^{j(2n-1)\pi/4}}{a(k_0^2 - h^2) \partial H_n(\Lambda a)/\partial a} \quad (14.42b)$$

where all terms decaying faster than $1/R^{1/2}$ have been neglected.

The integrals given in (14.41) are of the form

$$\int_{-\infty}^{\infty} F(h) e^{R\Phi(h)} dh \quad (14.43)$$

†In practice it is found that approximately $2k_0 a$ terms are required for convergence of the series in (14.31). The fact that the approximation

$$H_n(x) = \left(\frac{2}{\pi x} \right)^{1/2} \exp \left[-j \left(x - \frac{2n+1}{4} \pi \right) \right]$$

is valid only for $|x| \gg n$ does not impose any restriction, because for cylinders up to moderate size the series converges before this limitation comes into effect. For very large cylinders, an alternative representation is used, as explained later on.

where

$$F(h) = \begin{cases} K_1(h,R,\theta,n)I_1(h) \\ K_2(h,R,\theta,n)I_2(h) \end{cases} \tag{14.44}$$

and

$$\Phi(h) = -j(\Lambda \sin \theta + h \cos \theta) \tag{14.45}$$

The integration is carried out along the real axis in the complex h plane, with the contour indented below the branch point at $h = -k_0$ and above the branch point at $h = +k_0$ to ensure the proper behavior of the integral at infinity. The saddle-point method of integration consists in deforming the contour of integration so that it passes through the saddle point, defined by

$$\left. \frac{d\Phi(h)}{dh} \right|_{h=h_0} = 0 \tag{14.46}$$

in such a way that the contour follows the path of steepest descent. This path may be determined from the equation

$$\text{Im} [\Phi(h)] = \text{Im} [\Phi(h_0)] \tag{14.47}$$

which holds at every point along the path. It is easily shown, by using (14.45) in (14.46), that the saddle point occurs at

$$h_0 = k_0 \cos \theta \tag{14.48}$$

and the steepest descent path is as sketched in Fig. 14.12.

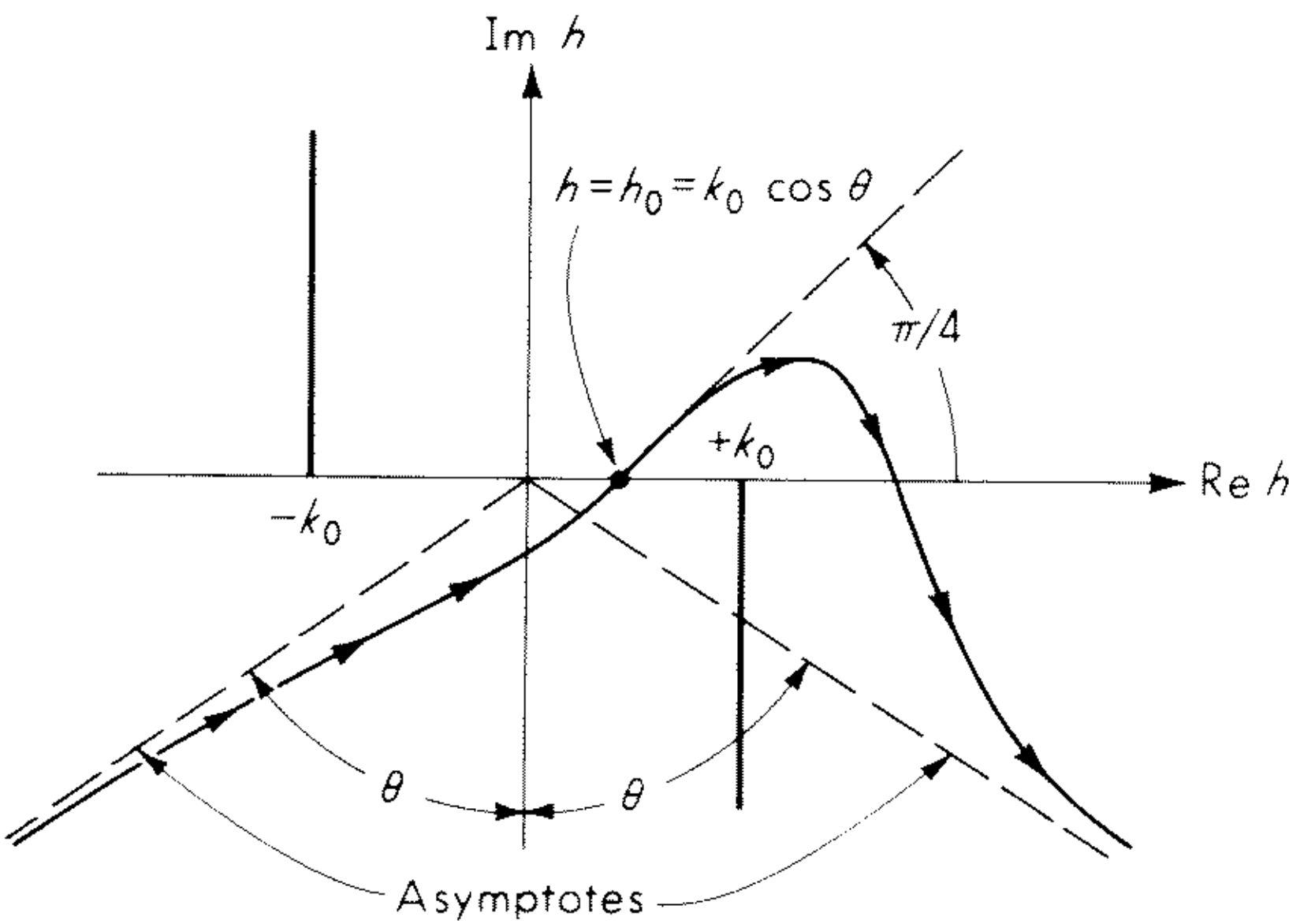


Fig. 14.12 The steepest descent path.

With the sign of Λ defined as in (14.33), it can be shown that the integral along an infinite semicircle connecting the original path and the steepest descent path vanishes. Hence, both paths of integration give the same result. The saddle-point integral is easily evaluated by taking advantage of the fact that the main contribution to the integral occurs in the vicinity of the saddle-

point. Also, in this region $F(h)$ is slowly varying compared with the exponential term, so we may write approximately

$$\begin{aligned}
 \int_{-\infty}^{\infty} F(h) e^{R\Phi(h)} dh &\approx F(h_0) e^{[R\Phi(h_0) + j\pi/4]} \int_{-\epsilon}^{\epsilon} e^{j^{1/2}\Phi''(h_0)u^2} du \\
 &= F(k_0 \cos \theta) e^{-j(k_0 R - \pi/4)} \int_{-\epsilon}^{\epsilon} e^{-Ru^2/(2k_0 \sin^2 \theta)} du \\
 &\approx F(k_0 \cos \theta) e^{-j(k_0 R - \pi/2)} \left(\frac{2k_0 \sin^2 \theta}{R} \right)^{1/2} \int_{-\infty}^{\infty} e^{-\tau^2} d\tau \\
 &= \left(\frac{2\pi k_0}{R} \right)^{1/2} \sin \theta F(k_0 \cos \theta) e^{-jk_0 R} e^{j\pi/4}
 \end{aligned} \tag{14.49}$$

When this result is used in (14.41) and the preceding equations for the fields, it is found that the significant components in the far field are given by

$$E_{\theta} = -2 \frac{e^{-jk_0 R}}{R} \sum_{n=-\infty}^{\infty} \frac{j^{n+1} e^{-jn\phi} C_2(n) I_2(k_0 \cos \theta)}{\sin \theta H_n(k_0 a \sin \theta)} \tag{14.50a}$$

$$\begin{aligned}
 E_{\phi} = 2 \frac{e^{-jk_0 R}}{R} \sum_{n=-\infty}^{\infty} \frac{j^n e^{-jn\phi}}{H'_n(k_0 a \sin \theta)} &\left[C_1(n) I_1(k_0 \cos \theta) \right. \\
 &\left. + \frac{n \cot \theta}{k_0 a \sin \theta} C_2(n) I_2(k_0 \cos \theta) \right]
 \end{aligned} \tag{14.50b}$$

$$\zeta_0 H_{\theta} = -E_{\phi} \tag{14.50c}$$

$$\zeta_0 H_{\phi} = E_{\theta} \tag{14.50d}$$

Both E_r and H_r are negligible compared with the other components. These formulas will now be applied to several specific types of slots.

14.4 The Uniformly Excited Circumferential Slot

Consider a circumferential slot which goes all the way around the cylinder. Suppose the tangential electric field in the slot has only an axial component which is independent of ϕ , that is, assume that in (14.29)

$$F_1(\phi) = G_1(z) = 0 \tag{14.51a}$$

$$F_2(\phi) = 1 \tag{14.51b}$$

$$G_2(z) = \begin{cases} \frac{V}{2w} & |z| \leq w \\ 0 & |z| > w \end{cases} \tag{14.51c}$$

Here V represents the voltage across the slot. An aperture distribution of this form might be excited, for example, by a radial transmission line inside the cylinder, as shown in Fig. 14.13. It is readily found that

$$C_2(n) = \begin{cases} 1 & n = 0 \\ 0 & n \neq 0 \end{cases} \tag{14.52a}$$

and
$$I_2(h) = \frac{V}{2\pi} \frac{\sin hw}{hw} \tag{14.52b}$$

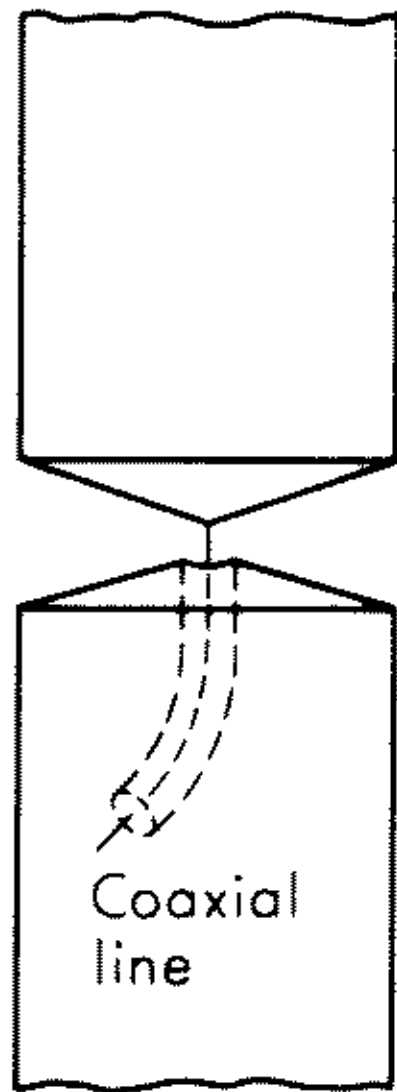


Fig. 14.13 A method of exciting a uniform circumferential slot.

and hence the far field, from (14.50), has only a θ component of \mathbf{E} and a ϕ component of \mathbf{H} :

$$E_{\theta} = -\frac{e^{-jk_0R}}{\pi R} \frac{jV}{\sin \theta H_0(k_0a \sin \theta)} \frac{\sin(k_0w \cos \theta)}{k_0w \cos \theta} \quad (14.53a)$$

$$H_{\phi} = -\sqrt{\frac{\epsilon_0}{\mu_0}} \frac{e^{-jk_0R}}{\pi R} \frac{jV}{\sin \theta H_0(k_0a \sin \theta)} \frac{\sin(k_0w \cos \theta)}{k_0w \cos \theta} \quad (14.53b)$$

If the slot dimension is very small, so that $|k_0w \cos \theta| \ll 1$, then these formulas simplify to

$$E_{\theta} = -\frac{e^{-jk_0R}}{\pi R} \frac{jV}{\sin \theta H_0(k_0a \sin \theta)} \quad (14.54)$$

and similarly for H_{ϕ} . Equations (14.53), or the simplified version (14.54), can easily be used to calculate the pattern for a specific value of k_0a .

14.5 The Circumferential Slot of Finite Width

In this section a circumferential slot that extends only part way around the cylinder, as shown in Fig. 14.14, will be discussed. This model might be used, for example, to study the radiation from a waveguide opening through the side of a rocket body or aircraft wing.

The electric field in the aperture will be assumed to have the same form as that of the dominant TE_{10} mode in a rectangular waveguide, namely,

$$F_1(\phi) \equiv G_1(z) = 0 \quad (14.55a)$$

$$F_2(\phi) = \begin{cases} \cos\left(\frac{\pi\phi}{2\phi_0}\right) & |\phi| \leq \phi_0 \\ 0 & |\phi| > \phi_0 \end{cases} \quad (14.55b)$$

$$G_2(z) = \begin{cases} E_0 & |z| \leq w \\ 0 & |z| > w \end{cases} \quad (14.55c)$$

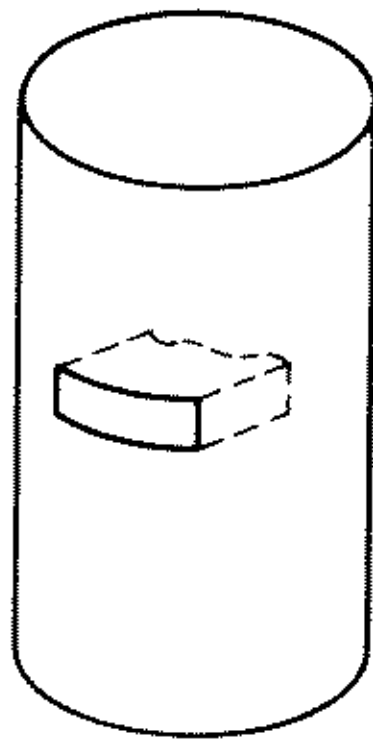


Fig. 14.14 The finite circumferential slot.

On substituting these in (14.37), one finds that

$$I_2(h) = \frac{wE_0}{\pi} \frac{\sin hw}{hw} \quad (14.56a)$$

$$C_2(n) = \frac{1}{(\pi/2\phi_0)^2 - n^2} \frac{\cos n\phi_0}{2\phi_0} \quad (14.56b)$$

and hence the resulting far fields are given by ($\epsilon_n = 1$ for $n = 0$ and $= 2$ otherwise)

$$E_\theta = -\frac{e^{-jk_0R}}{R} \frac{wE_0}{\pi\phi_0} \frac{\sin(k_0w \cos \theta)}{k_0w \cos \theta \sin \theta} \sum_{n=0}^{\infty} \frac{j^{n+1}\epsilon_n \cos n\phi \cos n\phi_0}{H_n(k_0a \sin \theta)[(\pi/2\phi_0)^2 - n^2]} \quad (14.57a)$$

$$E_\phi = -2j \frac{e^{-jk_0R}}{R} \frac{\cot \theta}{k_0a \sin \theta} \frac{wE_0}{\pi} \frac{\sin(k_0w \cos \theta)}{k_0w \cos \theta} \sum_{n=1}^{\infty} \frac{j^n n \sin n\phi \cos n\phi_0}{\phi_0[(\pi/2\phi_0)^2 - n^2]H'_n(k_0a \sin \theta)} \quad (14.57b)$$

$$\zeta_0 H_\theta = -E_\phi \quad (14.57c)$$

$$\zeta_0 H_\phi = E_\theta \quad (14.57d)$$

Several authors have used (14.57) for computing far-field patterns of a circumferential slot whose long dimension is exactly one half wavelength, i.e., for the case where

$$\phi_0 = \frac{\pi}{2k_0a} \quad (14.58)$$

Papas⁶ has given a calculated pattern of the magnitude of E_θ in the plane $\theta = \pi/2$ for $k_0a = 5$. Bailin¹⁰ has given extensive data, both tabulated and in curves, for $k_0a = 8$ and $k_0a = 12$. He gives both E_θ and E_ϕ , magnitude and phase, and his data can be used over the region of space defined by $30^\circ \leq \theta \leq 150^\circ$ and $0^\circ \leq \phi \leq 360^\circ$. Wait and Kahana⁹ give similar data, both magnitude and phase of E_θ and E_ϕ , for $k_0a = 2, 3$, and 5 . Finally, Wait and Kates¹³ have given curves for $|E_\theta|$ in the plane $\theta = \pi/2$ for values of $k_0a = 3, 5, 8, 12, 15, 18, 21$. Tabular data are also given in this paper for an array of two diametrically opposed slots, fed both in phase and out of phase,

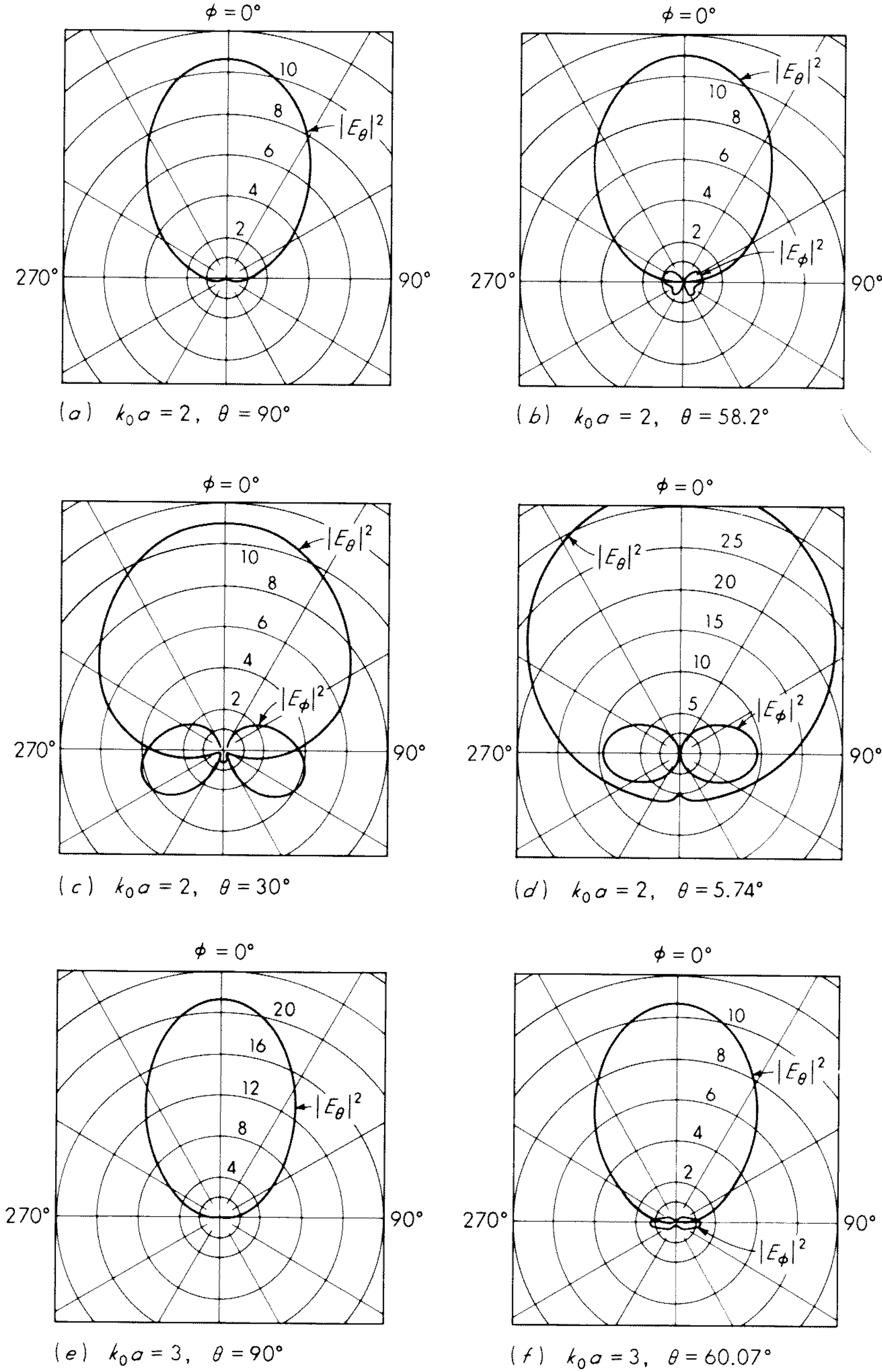
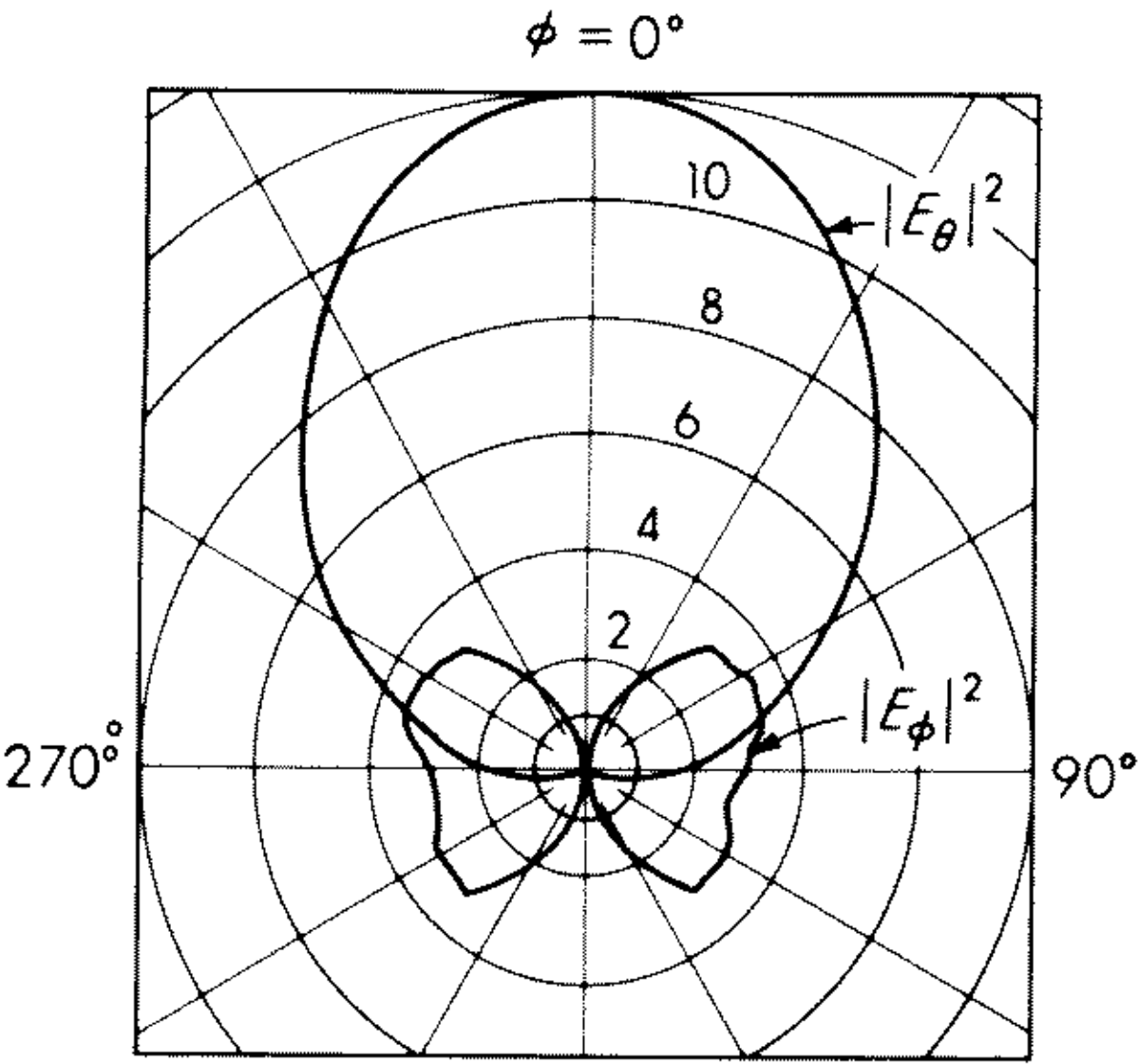
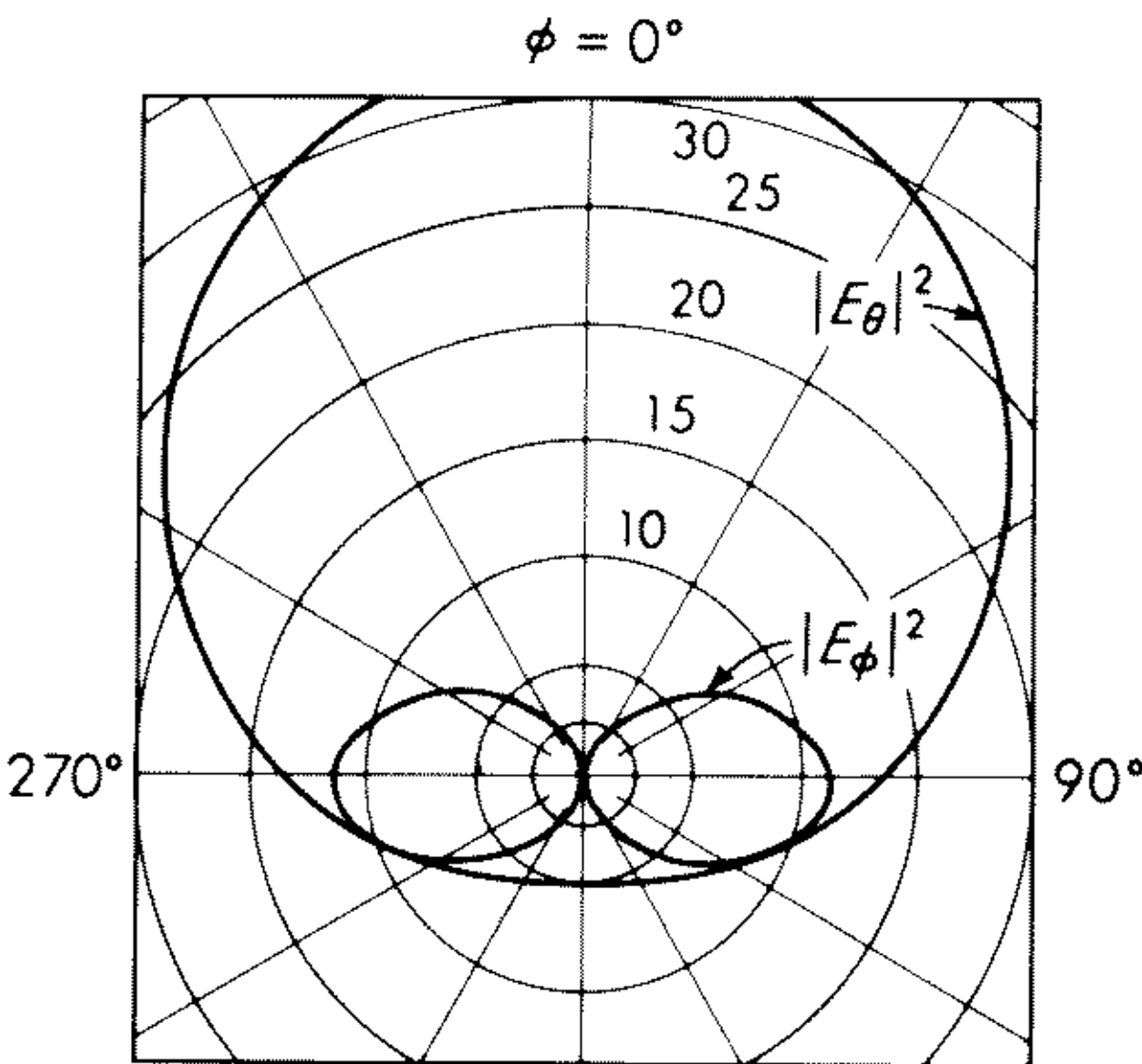


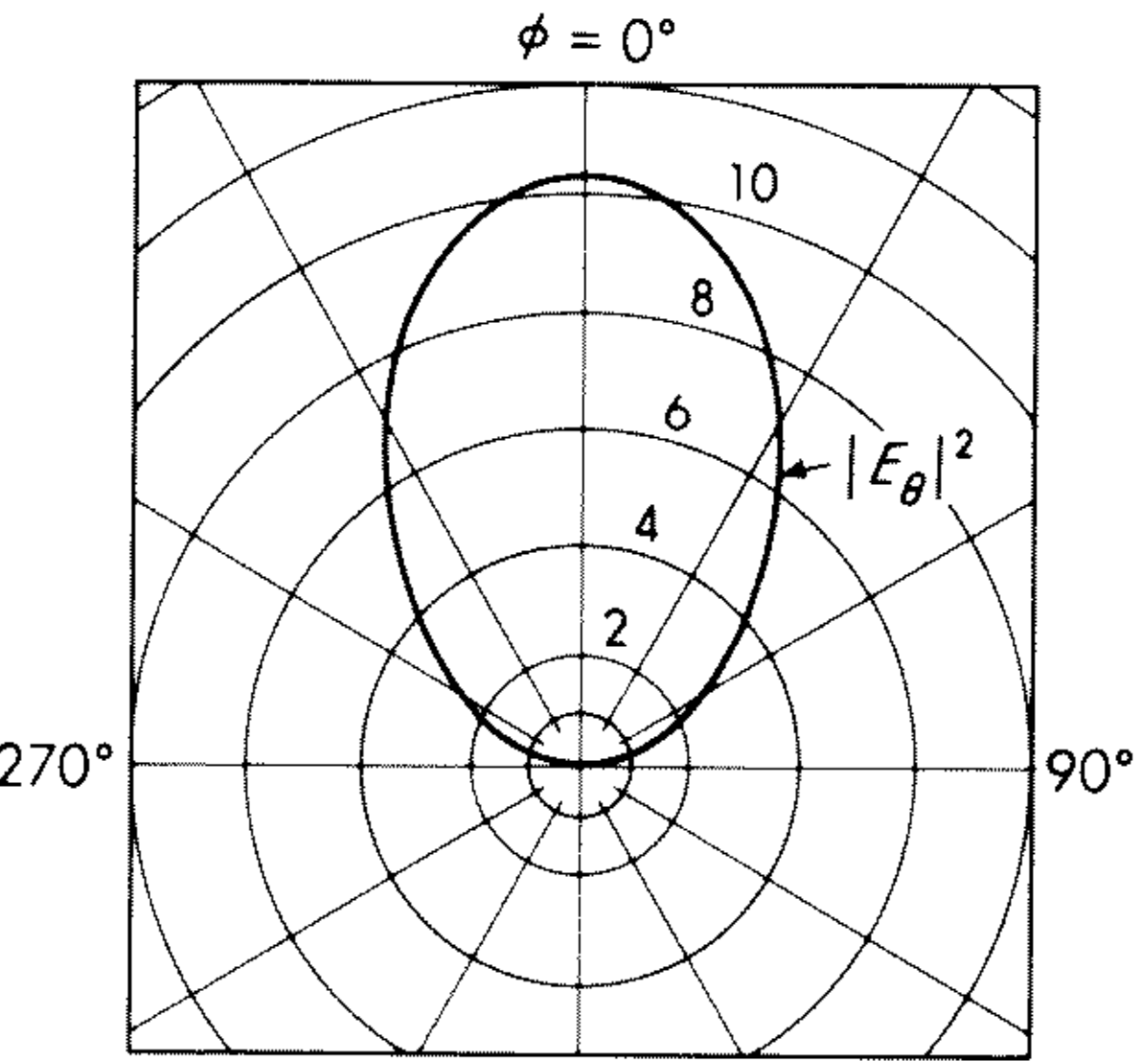
Fig. 14.15 Radiation power patterns (relative values) as functions of ϕ and θ for a finite-width circumferential slot with $2a\phi_0 = \lambda_0/2$. (From Wait and Kahana.⁹ Reproduced by permission of the National Research Council of Canada, Can. J. Tech., Figs. 2-12, vol. 33, pp. 87-92, January, 1955.)



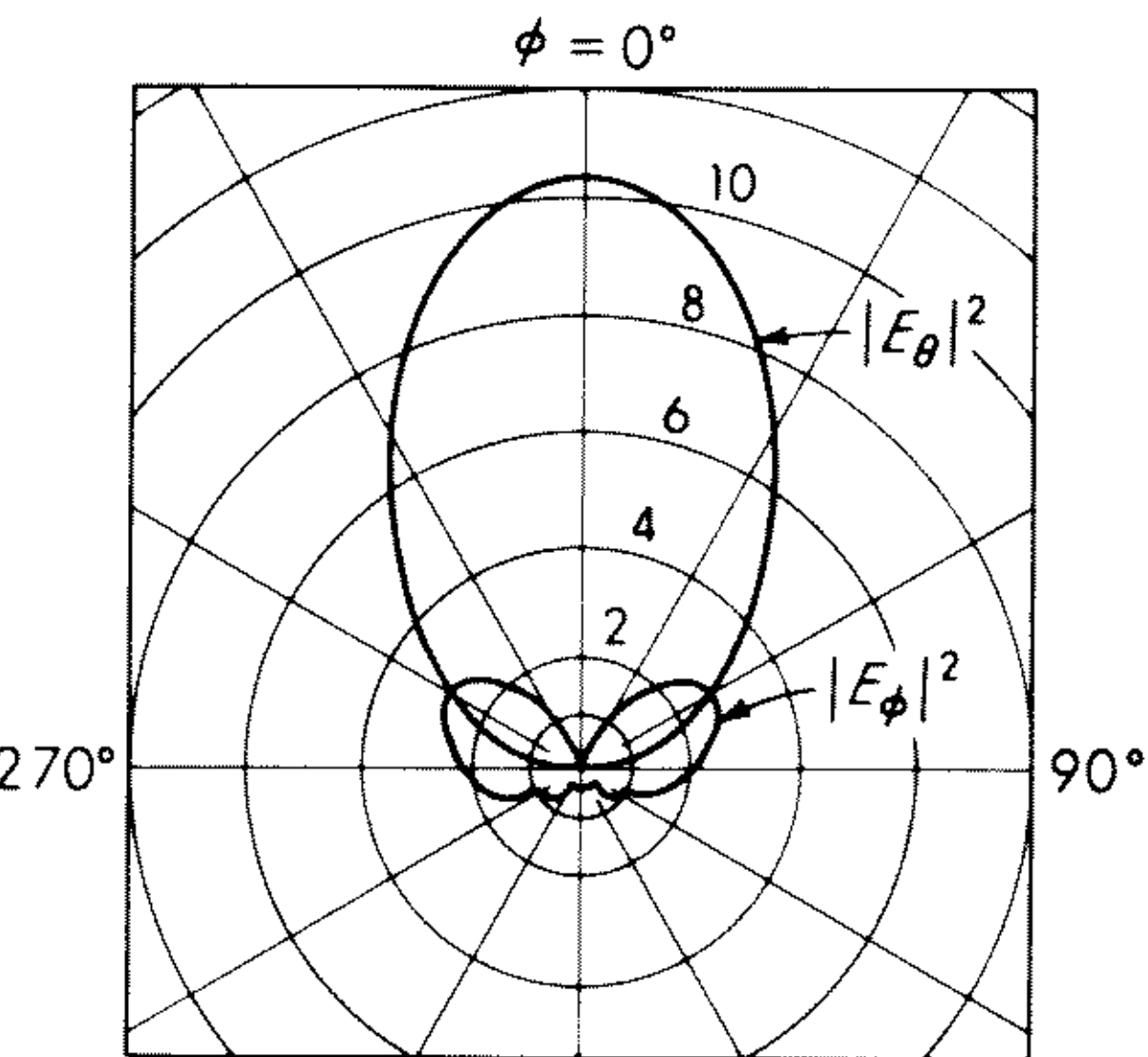
(g) $k_0 a = 3, \theta = 30^\circ$



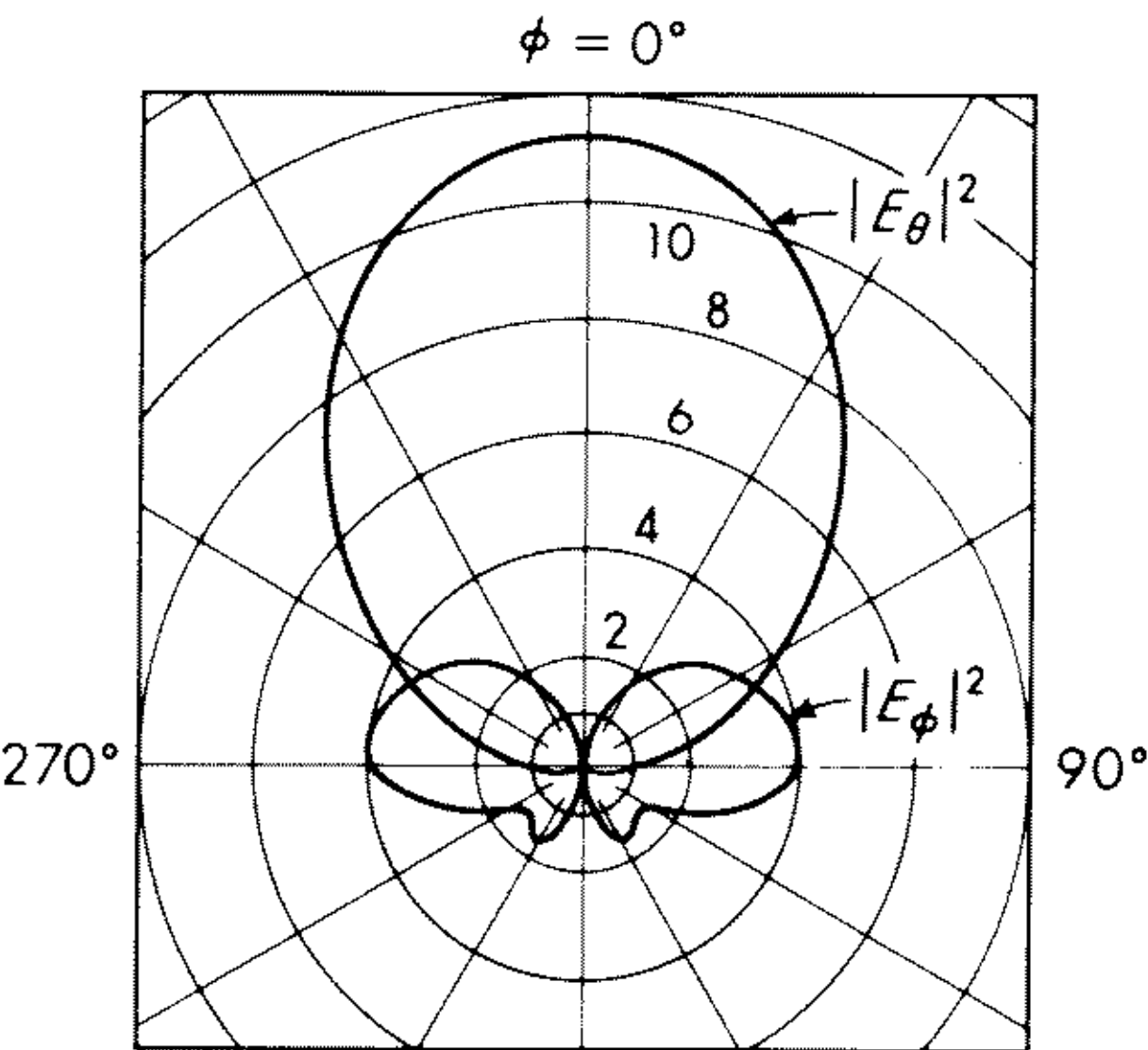
(h) $k_0 a = 3, \theta = 3.82^\circ$



(i) $k_0 a = 5, \theta = 90^\circ$



(j) $k_0 a = 5, \theta = 66.93^\circ$



(k) $k_0 a = 5, \theta = 30^\circ$

which could be used for determining the phase of E_θ in the plane $\theta = \pi/2$ as well.

An example of these calculations is given in Fig. 14.15. Figures 14.15a to 14.15d show $|E_\theta|^2$ and $|E_\phi|^2$ as functions of ϕ , for several values of θ , and for $k_0a = 2$. Figures 14.15e to 14.15h show the same results for $k_0a = 3$, and Figs. 14.15i to 14.15k for $k_0a = 5$. Note that in the $\theta = \pi/2$ plane the field is linearly polarized, but in other planes it is elliptically polarized.

The Residue Series

The series solutions for E_θ and E_ϕ given by (14.57) are not the only possible solutions that can be found. Before going on to another type of slot, we shall consider an alternative solution for E_θ and E_ϕ . The series given in (14.57), although formally correct for any size of cylinder, are found to converge very slowly for large cylinders. It turns out that approximately $2k_0a$ terms must be included in the summation for good accuracy. Hence for large cylinders, these results are practically useless, and for this reason it is helpful to have alternative solutions that converge more rapidly for the case of k_0a large.

The series given in (14.57) is usually referred to as the "harmonic series solution." An alternative representation for the fields that converges more quickly for large k_0a may be obtained by converting the harmonic series into another form known as the *residue series*. The procedure for doing this was originally due to Watson,¹⁷ who used it to study the diffraction of radio waves by the earth, and hence it is frequently called the "Watson transformation."

Consider the harmonic series for E_θ given by (14.57). Assume, to simplify the algebra, that the height of the slot is small, $k_0w \ll 1$, so

$$\frac{\sin(k_0w \cos \theta)}{k_0w \cos \theta} \approx 1 \quad (14.59)$$

Also, assume the slot is a half wavelength long so ϕ_0 is given as in (14.58). Then

$$E_\theta = -\frac{e^{-jk_0R}}{R} \frac{Vk_0a}{\pi^2 \sin \theta} \sum_{n=0}^{\infty} \frac{j^{n+1} \epsilon_n \cos n\phi \cos(n\pi/2k_0a)}{[(k_0a)^2 - n^2] H_n(k_0a \sin \theta)} \quad (14.60)$$

where $V = 2wE_0$ is the "voltage" across the slot. Let the summation in (14.60) be denoted by $M(\phi)$:

$$\begin{aligned} M(\phi) &= \sum_{n=0}^{\infty} \frac{j^{n+1} \epsilon_n \cos n\phi \cos(n\pi/2k_0a)}{[(k_0a)^2 - n^2] H_n(k_0a \sin \theta)} \\ &= \sum_{n=-\infty}^{\infty} \frac{e^{j(n+1)\pi/2} e^{-jn\phi} \cos(n\pi/2k_0a)}{[(k_0a)^2 - n^2] H_n(k_0a \sin \theta)} \end{aligned} \quad (14.61)$$

$M(\phi)$ can be written as a contour integral

$$M(\phi) = \frac{1}{2\pi j} \int_{C_0} \frac{e^{j(\nu+1)\pi/2} e^{-j\nu\phi} \cos(\nu\pi/2k_0a)}{[(k_0a)^2 - \nu^2] H_\nu(k_0a \sin \theta)} \frac{e^{j\nu\pi}}{\sin \nu\pi} d\nu \quad (14.62)$$

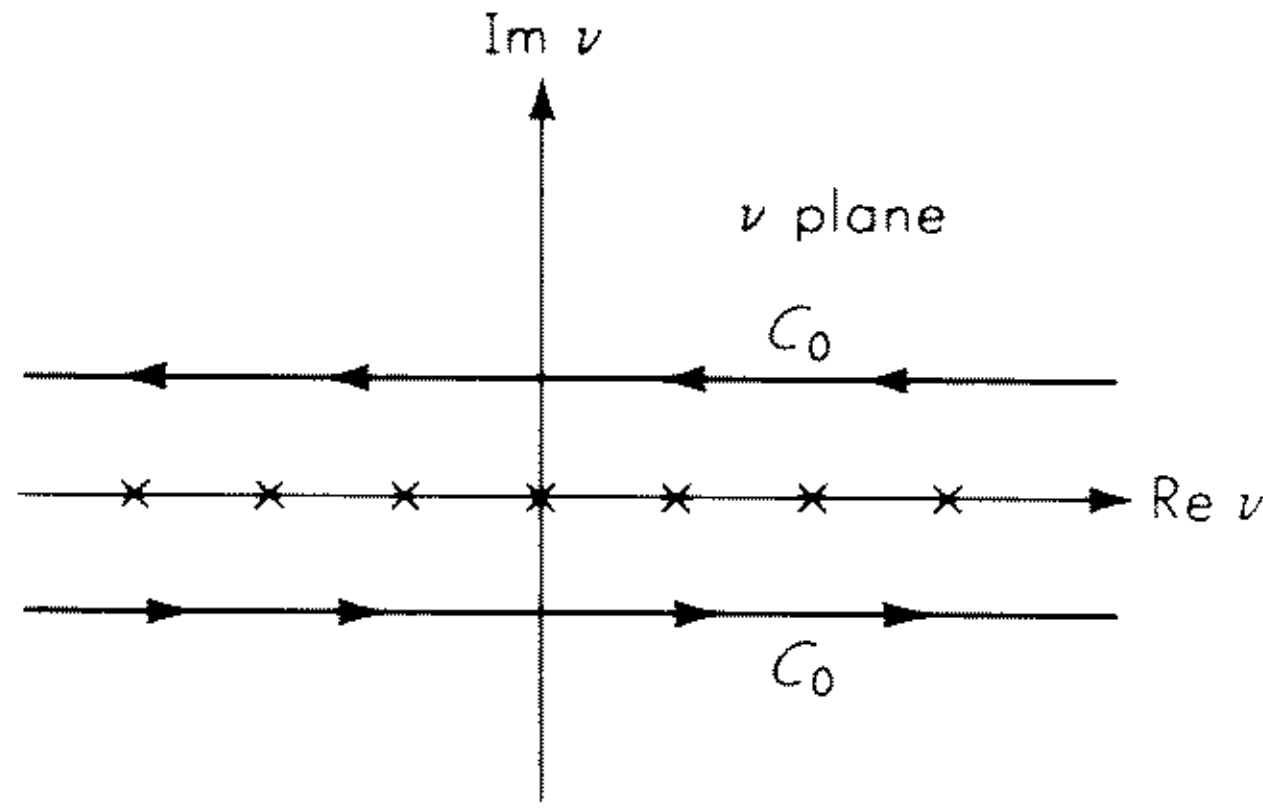


Fig. 14.16 The contour of integration for Eq. (14.62).

where C_0 is the contour shown in Fig. 14.16. The fact that this contour integral is equal to the original sum is easily seen from the fact that the function

$$\frac{e^{j\nu\pi}\pi}{\sin \nu\pi}$$

has simple poles, all of residue 1, at $\nu = 0, \pm 1, \pm 2, \dots$. The contour C_0 is understood to go from $-\infty$ to $+\infty$ just below the real ν axis, cross to just above the real axis at $\nu = +\infty$, go back to $-\infty$ above the real axis, and then cross to just below the real axis at $-\infty$. In this way it encircles all poles on the real ν axis. Since the original harmonic series is convergent, the residues in the poles at $\nu = \pm n$ become arbitrarily small as $n \rightarrow \infty$, and it can be shown that the contribution from the end pieces at $\nu = \pm\infty$ is negligible. Thus the summation in (14.61) is equal to the sum of the two contour integrals shown in Fig. 14.16, one just above the real ν axis and one just below.

An examination of the integrand in (14.62) shows that the integrand also has poles in the complex ν plane at the values of ν for which

$$H_\nu(k_0 a \sin \theta) = 0 \quad (14.63)$$

Denoting these values as ν_m , $m = \pm 1, \pm 2, \dots$, it is found that these poles lie in the second and fourth quadrants of the ν plane, as shown in Fig. 14.17. It is easily shown that if ν_m is a root of

$$H_\nu(x) = 0$$

then $-\nu_m$ is also a root. In Fig. 14.17 the roots are so numbered that

$$\nu_{-m} = -\nu_m \quad (14.64)$$

We now evaluate the integral in (14.62) by deforming the contour C_0 into the pair of contours C_1 surrounding the poles ν_m , $m = \pm 1, \pm 2, \dots$, as shown in Fig. 14.17.

Thus the contour C_0 lying just below the real ν axis is evaluated as the contour C_1 in the lower half ν plane by means of the residue theorem applied to the poles at $\nu = \nu_m$, $m = 1, 2, \dots$. The contour C_0 lying just above the real ν axis is evaluated as the contour C_1 in the upper half plane encircling the poles at

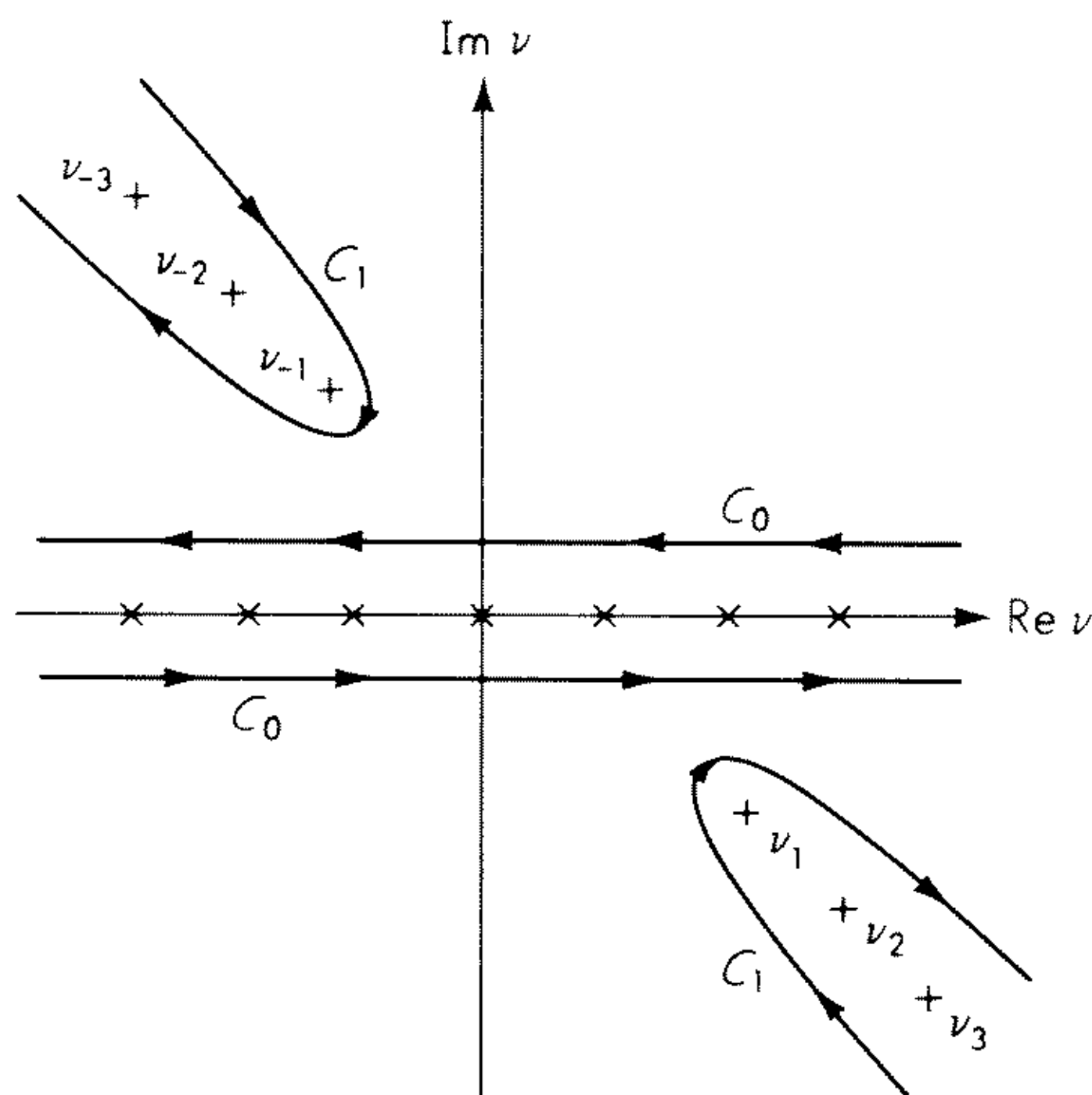


Fig. 14.17 The poles of the integrand in Eq. (14.62).

$\nu = -\nu_m$, $m = 1, 2, \dots$. This deformation of the contour is possible because the contours C_0 and C_1 may be joined by a contour lying on an infinite semi-circle, and it can be shown that the integral on this contour vanishes.¹⁸

Thus, by making use of residue theory, it is found that

$$M(\phi) = -2j \sum_{m=1}^{\infty} \frac{e^{j\nu_m\pi/2} \cos(\nu_m\pi/2k_0a) \cos[\nu_m(\phi - \pi)]}{[(k_0a)^2 - \nu_m^2][\partial H_\nu(k_0a \sin \theta)/\partial \nu]_{\nu=\nu_m} \sin \nu_m\pi} \quad (14.65)$$

and hence

$$E_\theta = 2j \frac{e^{-jk_0R}}{R} \frac{Vk_0a}{\pi^2 \sin \theta} \sum_{m=1}^{\infty} \frac{e^{j\nu_m\pi/2} \cos(\nu_m\pi/2k_0a) \cos[\nu_m(\phi - \pi)]}{[(k_0a)^2 - \nu_m^2][\partial H_\nu(k_0a \sin \theta)/\partial \nu]_{\nu=\nu_m} \sin \nu_m\pi} \quad (14.66)$$

This alternative series representation for E_θ is called the “residue series,” because of the way it was obtained. It is found that this series converges if $\pi/2 < \phi < 3\pi/2$, i.e., in the “shadow region” behind the cylinder. The series converges more quickly the higher the value of k_0a .

To make use of the summation in (14.66) it is necessary to know the positions of the roots at $\nu = \nu_{\pm m}$, and also to know the values of

$$\left[\frac{\partial H_\nu(x)}{\partial \nu} \right]_{\nu=\nu_{\pm m}}$$

Evaluating these numbers is difficult to do exactly, but it can be done by approximate means with adequate accuracy for most purposes. For the details of these calculations, the reader is referred to the works of Wait¹⁹ and Sensiper.²⁰

Figure 14.18 shows a comparison between the patterns computed from the harmonic series and from the residue series for a half-wavelength slot. The curve shows $|E_\theta|$ in the shadow region, $90^\circ < \phi < 150^\circ$ for $\theta = \pi/2$ and

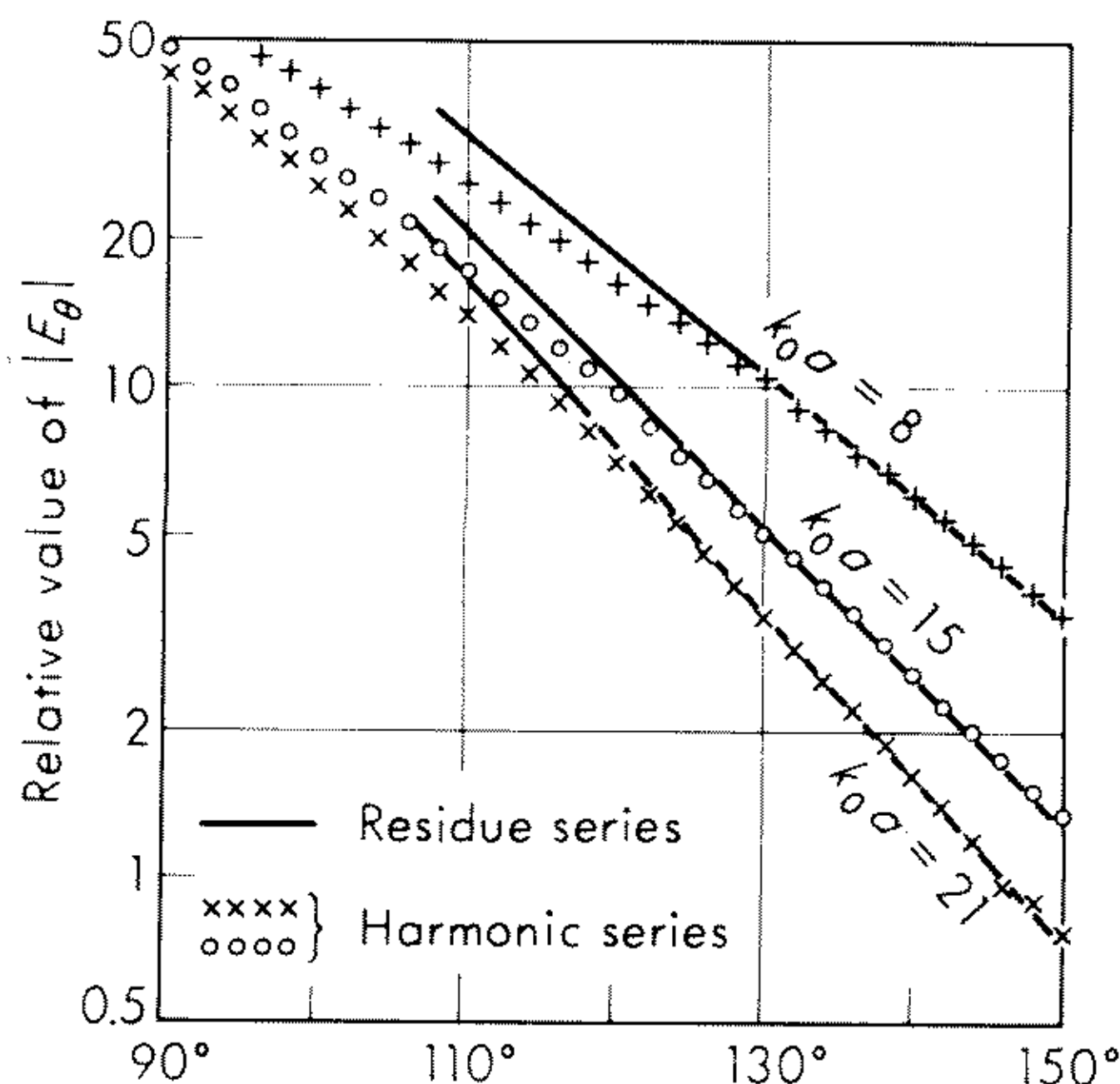


Fig. 14.18 Comparison of patterns obtained from the harmonic series and residue series, for $k_0 a = 8, 15, 21$, in the $\theta = \pi/2$ plane. (From Wait and Kates.¹³)

$k_0 a = 8, 15, 21$. In addition to the harmonic series and the residue series, still other representations for the fields that are valid under various conditions may be found. Some of these are discussed, for example, by Sensiper.²⁰

14.6 Half-wave Axial Slot

We shall now consider the half-wave axial slot, shown in Fig. 14.10b. Assume the slot is excited by an electric field having only a ϕ component with a cosinusoidal distribution in the z direction. In (14.29), we let

$$F_1(\phi) = \begin{cases} \frac{V}{2a\phi_0} & |\phi| \leq \phi_0 \\ 0 & |\phi| > \phi_0 \end{cases} \quad (14.67a)$$

$$G_1(z) = \begin{cases} \cos \frac{\pi z}{l} & |z| \leq \frac{l}{2} \\ 0 & |z| > \frac{l}{2} \end{cases} \quad (14.67b)$$

$$F_2(\phi) = G_2(z) \equiv 0 \quad (14.67c)$$

Then from (14.37),

$$I_1(h) = -\frac{\cos(hl/2)}{l[h^2 - (\pi/l)^2]} \quad (14.68)$$

or, assuming $l = \frac{\lambda_0}{2}$,

$$I_1(k_0 \cos \theta) = \frac{\lambda_0}{2\pi^2} \frac{\cos[(\pi/2) \cos \theta]}{\sin^2 \theta} \quad (14.69a)$$

$$C_1(n) = \frac{V}{2\pi a} \frac{\sin n\phi_0}{n\phi_0} \quad (14.69b)$$

$$I_2(h) = C_2(n) \equiv 0 \quad (14.69c)$$

and thus the fields are found from (14.50) to be

$$E_\theta = 0 \quad (14.70a)$$

$$E_\phi = \frac{\lambda_0}{2\pi^3} \frac{V_0}{a} \frac{e^{-jk_0 R}}{R} \frac{\cos [(\pi/2) \cos \theta]}{\sin \theta} \sum_{n=0}^{\infty} \frac{\epsilon_n j^n \cos n\phi}{\sin \theta H'_n(k_0 a \sin \theta)} \frac{\sin n\phi_0}{n\phi_0} \quad (14.70b)$$

$$\text{and} \quad H_\phi = 0 \quad (14.70c)$$

$$\zeta_0 H_\theta = -E_\phi \quad (14.70d)$$

If it is assumed that the slot is narrow, so ϕ_0 is small, the factor

$$\frac{\sin n\phi_0}{n\phi_0}$$

may be dropped from the summation. It is interesting to note that in (14.70b) the factor

$$\frac{\cos [(\pi/2) \cos \theta]}{\sin \theta}$$

is just the pattern associated with a half-wave vertical dipole, and the summation, which indicates the effect of the cylinder on the pattern, is just the pattern of an infinite axial slot on a cylinder.^{4,7} In this sense it may be said that the pattern is "factorable."

Equation (14.70b) has been used by several authors to calculate patterns for various values of $k_0 a$. Silver and Saunders⁸ give some calculated data (and also some experimental data) for $k_0 a = 0.8$ and $k_0 a = 2.5$. They show polar plots of $|E_\phi|$ in the plane $\phi = 0, \pi$, in the plane $\phi = \pm\pi/2$, and in the plane $\theta = \pi/2$. Bailin¹⁰ gives extensive tabular data for both the magnitude and phase of E_ϕ over the range $30^\circ < \theta < 150^\circ$ and $0 < \phi < 360^\circ$ for both $k_0 a = 8$ and $k_0 a = 12$. Wait¹¹ gives calculated data in graphical form for the summation in (14.70b), which he calls $M(x, \phi)$ (he has a slightly different normalizing constant):

$$M(x, \phi) = \frac{1}{\pi^2 x} \sum_{n=0}^{\infty} \frac{\epsilon_n j^n \cos n\phi}{H'_n(x)} \frac{\sin n\phi_0}{n\phi_0} \quad (14.71a)$$

$$= |M(x, \phi)| e^{j\alpha(x, \phi)} \quad (14.71b)$$

$$\text{where} \quad x = k_0 a \sin \theta \quad (14.71c)$$

He gives curves of both $|M(x, \phi)|$ and $\alpha(x, \phi)$ for the following values of x : 0.1, 0.32, 0.4, 0.64, 0.8, 1, 1.5, 2, 3, 4, 6, 8, 10, 12, 15, 18, and 21. His curves are actually plotted for infinitesimal slot width, i.e., for

$$\frac{\sin n\phi_0}{n\phi_0} \approx 1 \quad (14.72)$$

He also discusses the effect this assumption has on the accuracy of his calculations.

An example of these calculations is shown in Fig. 14.19. This figure shows the pattern of $|E_\phi|$ vs. θ for $k_0 a = 0.8$. Figure 14.19a shows the pattern in the

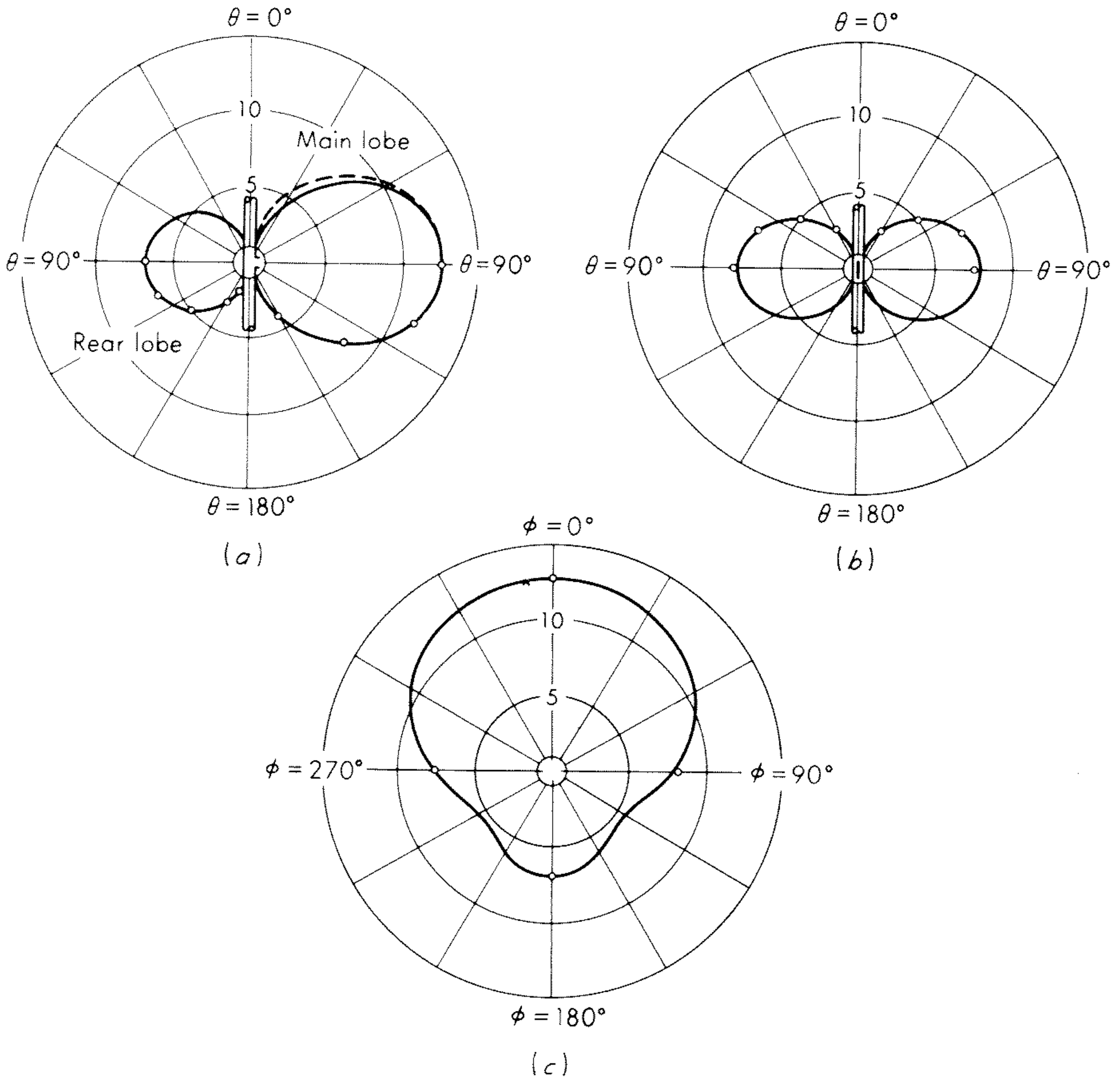


Fig. 14.19 Radiation pattern of a narrow half-wave slot. (a) $|E_\phi|$ vs. θ for $\phi = 0, \pi$; (b) $|E_\phi|$ vs. θ for $\phi = \pm \pi/2$; (c) $|E_\phi|$ vs. ϕ for $\theta = \pi/2$. (From Silver and Saunders.⁸)

plane $\phi = 0, \pi$, and Fig. 14.19b in the plane $\phi = \pm \pi/2$. Figure 14.19c shows $|E_\phi|$ vs. ϕ for $\theta = \pi/2$.

As with the circumferential slot, it is found that the series given in (14.70b), the harmonic series, converges poorly when the cylinder is large. An alternative representation can again be obtained by means of the Watson transformation. The details of this transformation are similar to those given above for the circumferential slot. The reader is referred to Wait²¹ for a detailed discussion. The residue series for this problem is found to be

$$E_\phi = \left(\frac{2}{\pi k_0 R \sin \theta} \right)^{1/2} e^{-j(k_0 R \sin \theta - \pi/4)} \frac{V k_0}{4} M_0(x, \phi) \quad (14.73a)$$

where

$$M_0(x, \phi) = -\frac{4}{x} \sum_{m=1}^{\infty} \frac{\cos \nu_m (\pi - \phi)}{Q_m} \quad (14.73b)$$

$$Q_m = \frac{j \sin \nu_m \pi}{e^{j\nu_m \pi/2}} \left[\frac{\partial H'_\nu(x)}{\partial \nu} \right]_{\nu=\nu_m} \quad (14.73c)$$

and $x = k_0 a \sin \theta$. ν_m , $m = 1, 2, 3, \dots$, are the roots of the equation

$$\frac{\partial H_\nu(x)}{\partial x} = 0$$

having positive real part in the complex ν plane. Approximate methods of finding the values of ν_m are discussed by Sensiper²⁰ and Wait.²¹

As with the circumferential slot, it is found that the residue series representation is useful for $\pi/2 < \phi < 3\pi/2$ and for large values of $k_0 a$. In addition, other representations for E_ϕ can be found.

14.7 Slots on Spheres

This section considers the problem of an aperture on a perfectly conducting sphere. This problem has been studied by Mushiake and Webster,²² and the treatment given here closely follows their work. As with the cylinder problems in the preceding section, only the exterior problem is discussed. Consider the sphere shown in Fig. 14.20. Assume that the sphere has radius a and the aperture is defined by the region $\theta_1 - \alpha \leq \theta \leq \theta_1 + \alpha$ and $-\phi_0 \leq \phi \leq \phi_0$. Furthermore, assume the aperture electric field is polarized in the θ direction and is given by

$$E_\theta = \sum_{m=0}^{\infty} E_m \cos m\phi: \begin{array}{l} \theta_1 - \alpha \leq \theta \leq \theta_1 + \alpha \\ -\phi_0 \leq \phi \leq \phi_0 \end{array} \quad (14.74)$$

and is an even function of ϕ about $\phi = 0$ and is constant as a function of θ over the aperture.

The resulting fields outside the aperture may be written as a sum of spherical mode functions chosen to satisfy the radiation condition at infinity and to have the proper symmetry. The correct form is

$$\mathbf{E} = \sum_{m=0}^{\infty} \mathbf{E}^m \quad (14.75a)$$

$$\mathbf{H} = \sum_{m=0}^{\infty} \mathbf{H}^m \quad (14.75b)$$

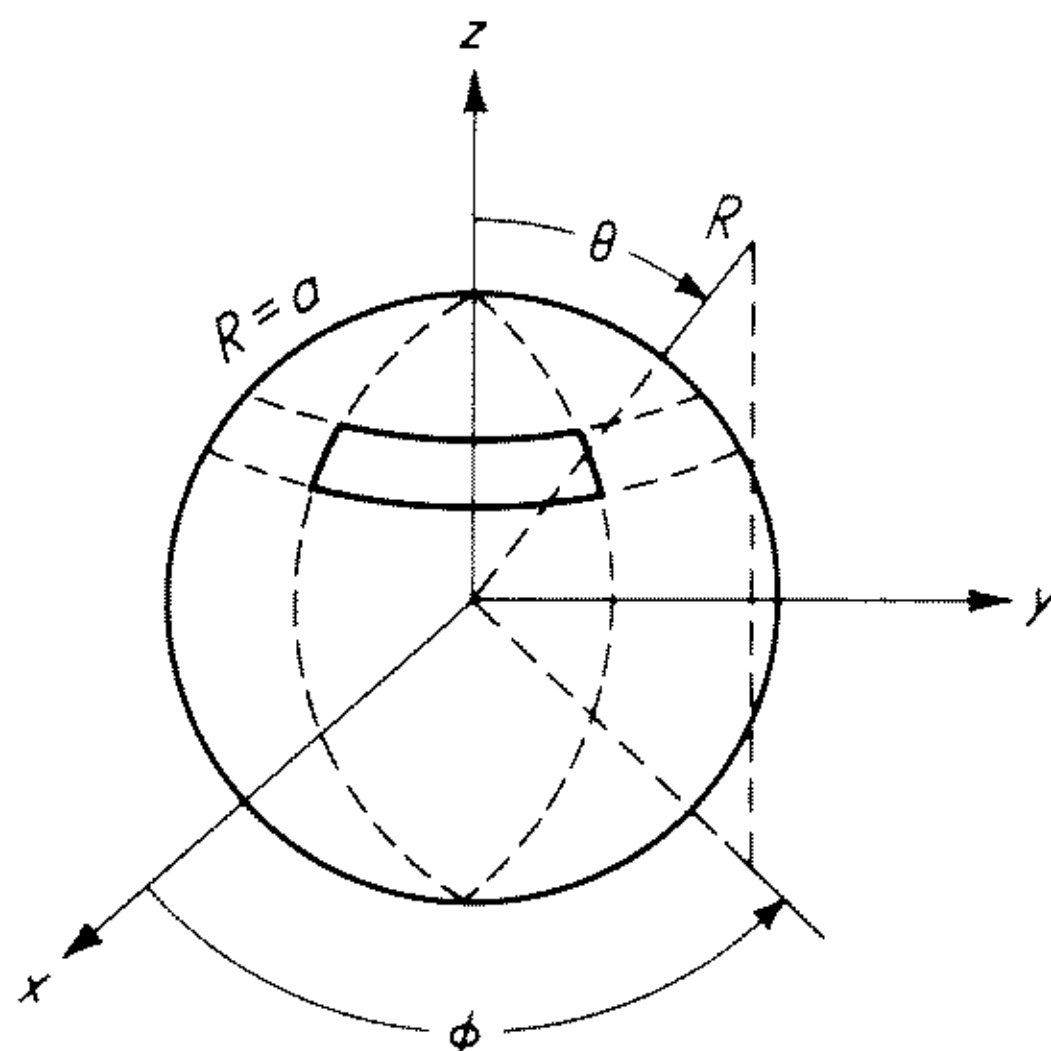


Fig. 14.20 A slot on a sphere.

where the components of \mathbf{E}^m are

$$E_R^m = -E_m \cos m\phi \sum_{n=m}^{\infty} B_n^m \frac{n(n+1)}{k_0 R} \frac{k_0 a h_n(k_0 R)}{[k_0 a h_n(k_0 a)]'} P_n^m(\cos \theta) \quad (14.76a)$$

$$E_\theta^m = -E_m \cos m\phi \sum_{n=m}^{\infty} \left\{ A_n^m \frac{h_n(k_0 R)}{h_n(k_0 a)} \frac{m P_n^m}{\sin \theta} + B_n^m \frac{a}{R} \frac{[k_0 R h_n(k_0 R)]'}{[k_0 a h_n(k_0 a)]'} \frac{dP_n^m}{d\theta} \right\} \quad (14.76b)$$

$$E_\phi^m = E_m \sin m\phi \sum_{n=m}^{\infty} \left\{ A_n^m \frac{h_n(k_0 R)}{h_n(k_0 a)} \frac{dP_n^m}{d\theta} + B_n^m \frac{a}{R} \frac{[k_0 R h_n(k_0 R)]'}{[k_0 a h_n(k_0 a)]'} \frac{m P_n^m}{\sin \theta} \right\} \quad (14.76c)$$

and the components of \mathbf{H}^m are

$$H_R^m = -j \sqrt{\frac{\epsilon_0}{\mu_0}} E_m \sin m\phi \sum_{n=m}^{\infty} A_n^m \frac{n(n+1)}{k_0 R} \frac{h_n(k_0 R)}{h_n(k_0 a)} P_n^m(\cos \theta) \quad (14.77a)$$

$$H_\theta^m = -j \sqrt{\frac{\epsilon_0}{\mu_0}} E_m \sin m\phi \sum_{n=m}^{\infty} \left\{ A_n^m \frac{[k_0 R h_n(k_0 R)]'}{k_0 R h_n(k_0 a)} \frac{dP_n^m}{d\theta} - B_n^m \frac{k_0 a h_n(k_0 R)}{[k_0 a h_n(k_0 a)]'} \frac{m P_n^m}{\sin \theta} \right\} \quad (14.77b)$$

$$H_\phi^m = -j \sqrt{\frac{\epsilon_0}{\mu_0}} E_m \cos m\phi \sum_{n=m}^{\infty} \left\{ A_n^m \frac{[k_0 R h_n(k_0 R)]'}{k_0 R h_n(k_0 a)} \frac{m P_n^m}{\sin \theta} - B_n^m \frac{k_0 a h_n(k_0 R)}{[k_0 a h_n(k_0 a)]'} \frac{dP_n^m}{d\theta} \right\} \quad (14.77c)$$

For a given aperture field, the coefficients E_m are found by expanding the field in a Fourier series as in (14.74). $h_n(k_0 R)$ is the spherical Hankel function of the second kind of order n

$$[k_0 R h_n(k_0 R)]' = \frac{\partial}{\partial(k_0 R)} [k_0 R h_n(k_0 R)] \quad (14.78)$$

and $P_n^m(\cos \theta)$ is the associated Legendre function of the first kind, of degree n and order m . The coefficients A_n^m and B_n^m are found from the orthogonality property of the Legendre functions to be given by

$$A_n^m = -\frac{2n+1}{2n(n+1)} \frac{(n-m)!}{(n+m)!} \int_{\theta_1-\alpha}^{\theta_1+\alpha} m P_n^m d\theta \quad (14.79a)$$

$$B_n^m = -\frac{2n+1}{2n(n+1)} \frac{(n-m)!}{(n+m)!} \int_{\theta_1-\alpha}^{\theta_1+\alpha} \frac{dP_n^m}{d\theta} \sin \theta d\theta \quad (14.79b)$$

To cast (14.76) and (14.77) into a more useful form, the Hankel functions may be replaced by their asymptotic form to obtain a formula that is valid in the far field. The result is

$$E_R^m \approx 0 \quad (14.80a)$$

$$E_\theta^m \approx \frac{e^{-jk_0 R}}{R} \frac{2\alpha E_m}{k_0} D_m \cos m\phi \quad (14.80b)$$

$$E_\phi^m \approx \frac{e^{-jk_0 R}}{R} \frac{2\alpha E_m}{k_0} \sin m\phi \sum_{n=m}^{\infty} (j)^n \left\{ j \frac{A_n^m}{2\alpha} \frac{1}{h_n(k_0 a)} \frac{dP_n^m}{d\theta} + \frac{B_n^m}{2} \frac{k_0 a}{[k_0 a h_n(k_0 a)]'} \frac{m P_n^m}{\sin \theta} \right\} \quad (14.80c)$$

$$H_R^m \approx 0 \quad (14.81a)$$

$$\zeta_0 H_\theta^m \approx -E_\phi \quad (14.81b)$$

$$\zeta_0 H_\phi^m = E_\theta \quad (14.81c)$$

where

$$D_m = - \sum_{n=m}^{\infty} (j)^n \left\{ j \frac{A_n^m}{2\alpha} \frac{1}{h_n(k_0 a)} \frac{m P_n^m}{\sin \theta} - \frac{B_n^m}{2\alpha} \frac{k_0 a}{[k_0 a h_n(k_0 a)]'} \frac{dP_n^m}{d\theta} \right\} \quad (14.82)$$

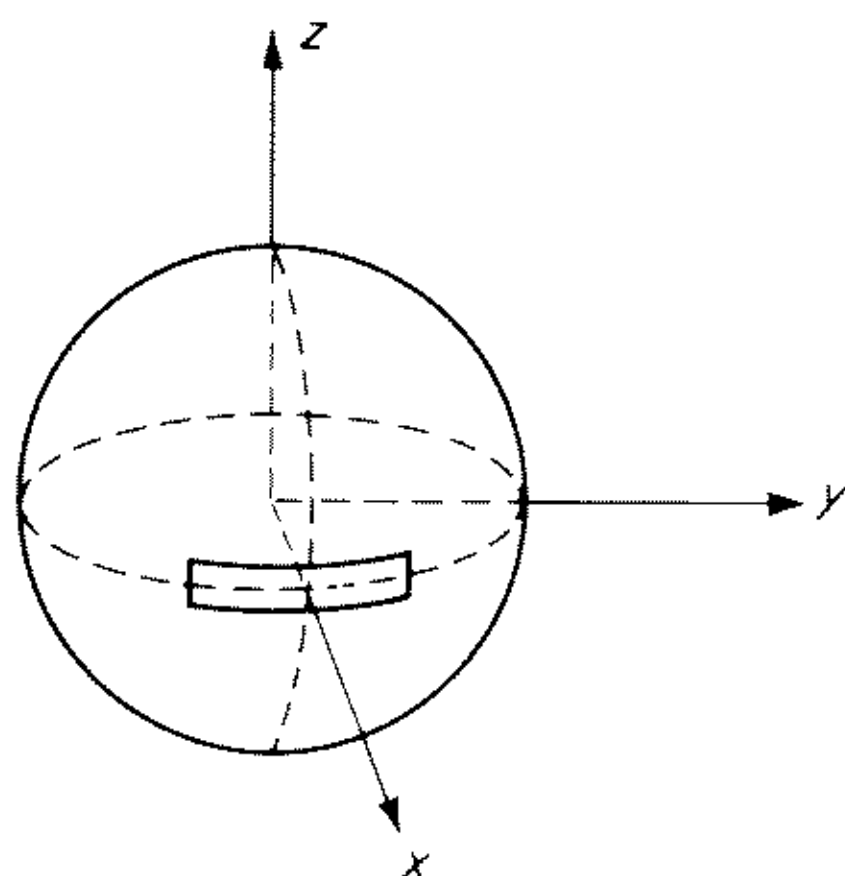


Fig. 14.21 A half-wave equatorial slot.

As an example of this type of problem consider the case of a half-wave aperture located along the equator of the sphere, as shown in Fig. 14.21. Assume the aperture has a narrow dimension in the θ direction and an amplitude distribution which tapers sinusoidally to zero at the ends of the slot:

$$E_\theta(\phi) = \begin{cases} \frac{V}{2a\alpha} \sin \left[\frac{2\pi}{\lambda_0} (l - a|\phi|) \right] & |a\phi| \leq l \\ 0 & |a\phi| > l \end{cases} \quad (14.83)$$

When this is expanded in a Fourier series, as in (14.74), the result is

$$E_m = \begin{cases} \frac{V}{2\pi k_0 a^2 \alpha} (1 - \cos k_0 a) & m = 0 \\ \frac{V}{\pi a \alpha} \frac{2k_0 a}{(k_0 a)^2 - m^2} \left[\cos \left(m \frac{l}{a} \right) - \cos k_0 l \right] & m \neq k_0 a \\ & m \neq 0 \\ \frac{V}{2\pi a \alpha} \frac{l}{a} \sin k_0 l & m = k_0 a \end{cases} \quad (14.84)$$

When these values for the coefficients are substituted into (14.80) and (14.81), the far-field patterns from such a slot may be calculated. The results of such a

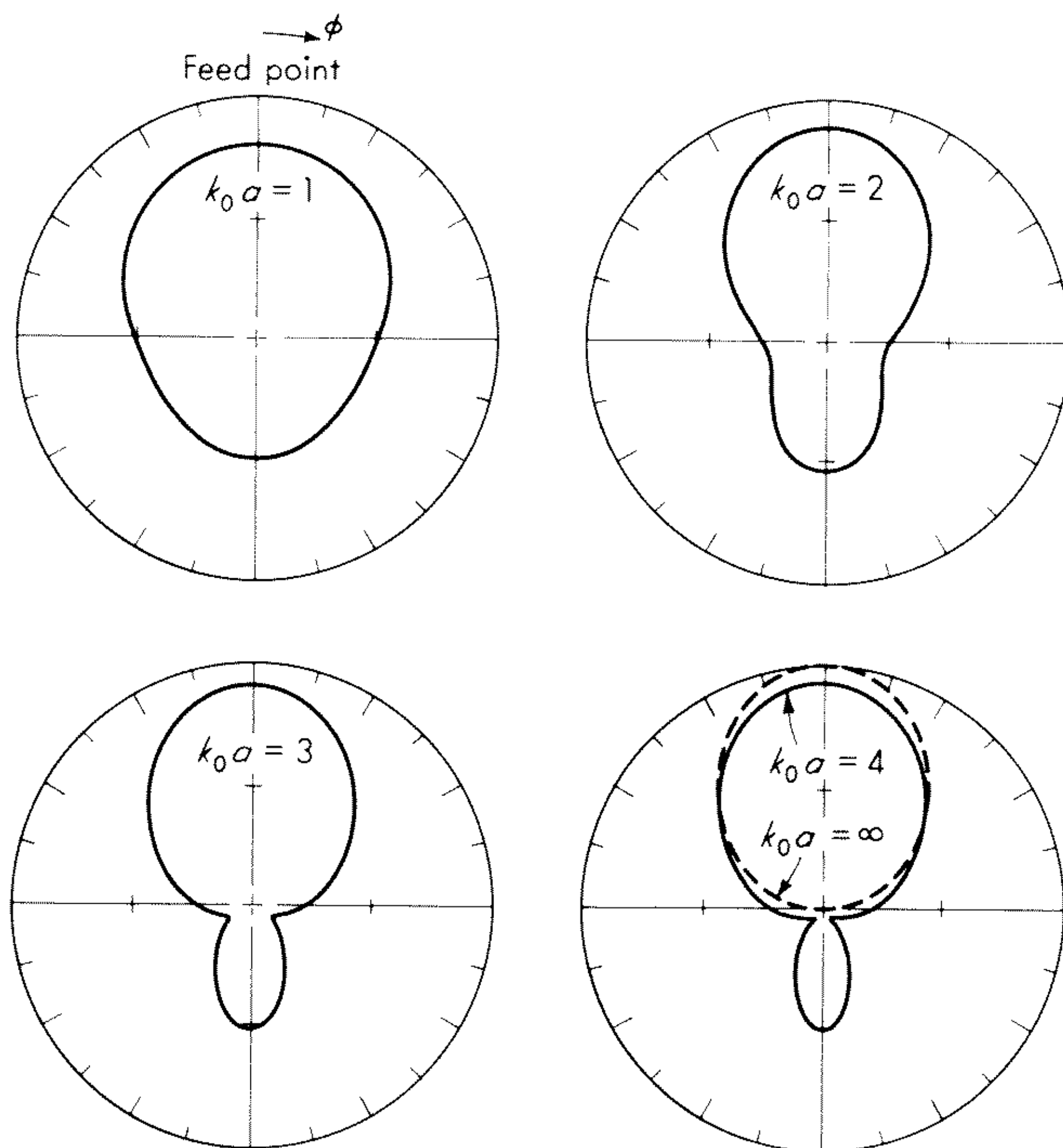


Fig. 14.22 $|E_\theta|$ vs. ϕ in the $\theta = \pi/2$ plane for a half-wave equatorial slot on a sphere. (From Mushiake and Webster.²²)

calculation are shown in Fig. 14.22 for spheres with radii $k_0 a = 1, 2, 3$, and 4 . The patterns show equatorial plane ($\theta = \pi/2$) values of $|E_\theta|$ plotted as a function of ϕ . It is clear that the gain of the antenna in the direction $\theta = \pi/2$, $\phi = 0$ increases as the size of the sphere increases. A number of other patterns for slots on spheres are given in the paper by Mushiake and Webster.²²

14.8 Slotted Waveguide Arrays

The preceding sections have dealt with the properties of a single slot as a radiator. These elemental radiators may obviously be used as the basic radiating elements in an array to obtain much higher directivity and lower side lobes than are obtainable from a single slot. In order to optimize the array it is necessary to have control over the excitation level of each slot in the array. Also, suitable means of feeding the slots is required. Fortunately, both of these conditions can be met by cutting the slots in a waveguide wall with the array axis extending along the length of the waveguide. A common form of slotted waveguide array is one consisting of slots cut in the broadwall of a rectangular guide. The design of this type of array is discussed below.

Figure 14.23 shows a longitudinal slot cut in the broadwall of a rectangular

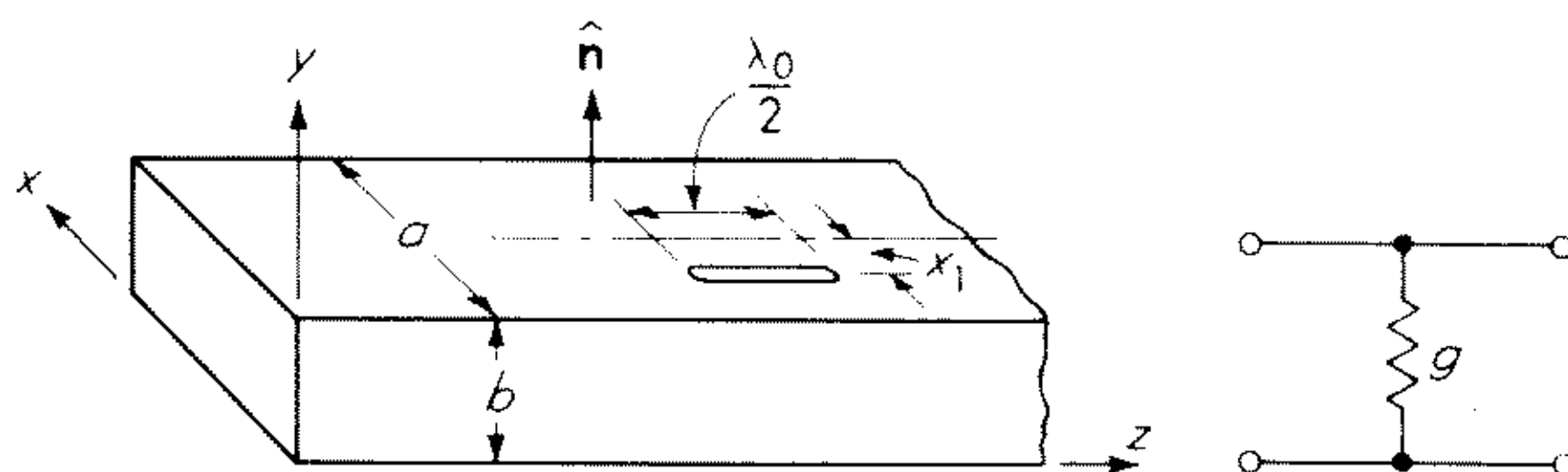


Fig. 14.23 A longitudinal resonant slot in the broadwall of a rectangular waveguide and its equivalent circuit.

guide. If the guide is excited in the dominant TE_{10} mode, the current flowing on the upper wall is proportional to

$$\mathbf{J}_s \propto \hat{\mathbf{x}} \cos \frac{\pi x}{a} - j \frac{\beta a}{\pi} \hat{\mathbf{z}} \sin \frac{\pi x}{a}$$

At the center, where $x = a/2$, the current is entirely in the z direction. Consequently a narrow centered longitudinal slot does not intercept any current flow lines and is not excited. By offsetting the slot from the center, current flow lines are intercepted, and the excitation of the slot increases with the distance it is offset from the center. A detailed analysis, which is presented in the next section, shows that the narrow longitudinal slot acts as a shunt conductance across the waveguide at its resonant frequency. The normalized conductance is given by

$$g = 2.09 \frac{\lambda_g}{\lambda_0} \frac{a}{b} \cos^2 \frac{\pi \lambda_0}{2\lambda_g} \sin^2 \frac{\pi x_1}{a} \quad (14.85)$$

where λ_g is the guide wavelength, λ_0 is the free space wavelength, and x_1 is the offset as shown in Fig. 14.23. The guide width and height are a and b , respectively. Experimentally it is found that the resonant length of the slot is very nearly $\lambda_0/2$.

If the voltage across the equivalent transmission line is V , the power radiated by the slot will be $|V|^2 g/2$. Hence the excitation of the slot is proportional to g and, from (14.85), is seen to vary with offset according to $\sin(\pi x_1/a)$. Thus, varying the offset distance x_1 is a convenient and practical way to control the excitation level of individual slots.

Resonant Array

There are two basic types of slotted waveguide arrays: the resonant array and the nonresonant array. The resonant array is designed for broadside operation and uses a slot spacing of $\lambda_g/2$, while the nonresonant array can be designed to have the main lobe at any angle with respect to the normal to the broadwall of the guide but in the plane containing the array axis and the normal $\hat{\mathbf{n}}$. We shall consider the resonant array first.

To obtain broadside radiation all the slots must be excited in phase. This can be achieved by spacing the slots one guide wavelength λ_g apart. However, in order to avoid more than one main lobe in visible space the spacing must be

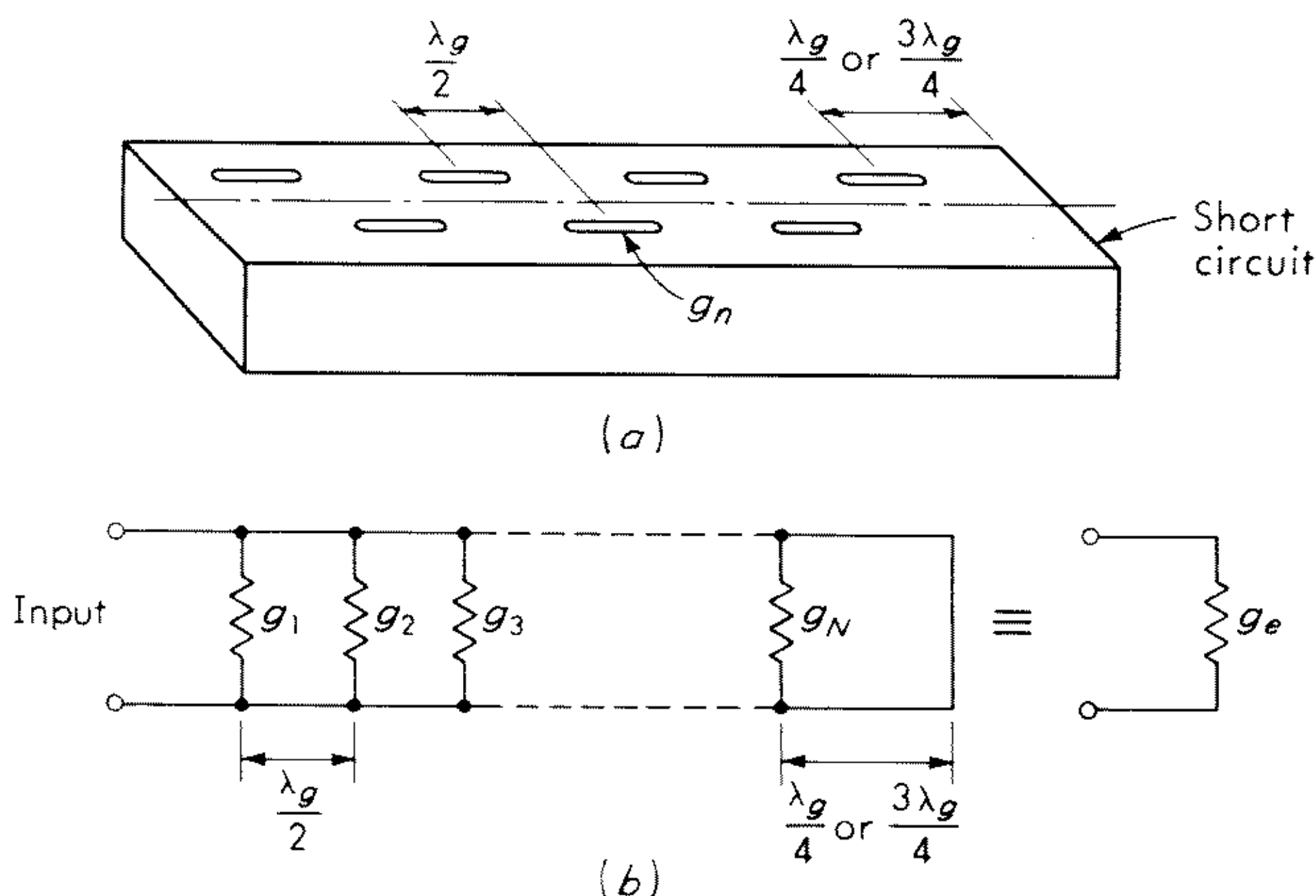


Fig. 14.24 The resonant array and its equivalent circuit.

less than λ_0 for a broadside array. In a conventional unloaded waveguide $\lambda_g > \lambda_0$, so spacing the slots by a distance λ_g will not yield a satisfactory array. The difficulty is overcome by noting that the surface current in the x direction is of opposite sign on adjacent sides of the centerline. Therefore, the slot excitation is reversed in sign by offsetting it on the adjacent side of the centerline. Consequently, a slot spacing of $\lambda_g/2$ may be used with the additional 180° change in phase between adjacent slots obtained by offsetting every other slot on the opposite side of the centerline. An array of this type is illustrated in Fig. 14.24, along with its equivalent circuit. Since the slots are assumed to be resonant and spaced $\lambda_g/2$ apart, the equivalent circuit reduces to a single equivalent shunt conductance

$$g_e = \sum_{n=1}^N g_n \quad (14.86)$$

The guide is terminated in an open circuit at the position of the last slot, i.e., a short circuit a distance $\lambda_g/4$ from the last slot.

Let a_n be the desired excitation coefficient for the n th element in the array (these may be chosen to give a Chebyshev or other form of array as discussed in Chap. 5). The conductances g_n are then given by

$$g_n = K a_n^2 \quad (14.87)$$

where the constant K is so chosen that $g_e = 1$, that is,

$$K \sum_{n=1}^N a_n^2 = 1 \quad (14.88)$$

in order for the array to be matched to the input waveguide for maximum radiated power. The slot offset may be found from (14.85) once the g_n have been specified.

The resonant broadside array is a narrow-band antenna, and the performance deteriorates rapidly with a change in frequency away from the design frequency. One major reason for the rapid deterioration in performance with frequency is that the short circuit spaced $\lambda_0/4$ from the last slot and used to simulate an open-circuit termination reflects a wave with appreciable amplitude. With a small change in frequency the incident and reflected waves rapidly become out of phase with distance along the array toward the input, and this gives rise to large phase differences in the excitation of individual slots. Also, the $\lambda_0/2$ slot spacing results in all of the partial reflected waves from each slot adding in phase at each slot only at the resonant frequency. It is this property that has given rise to the terminology "resonant array."

Nonresonant Array — Second-order Beam Suppression

We shall now consider the basic features of nonresonant arrays designed for other than broadside operation. Again we shall assume that the array consists of resonant longitudinal broadwall slots. The inclination of the main lobe away from the normal is given by the angle ψ with ψ positive if the lobe points in the forward direction as shown in Fig. 14.25a. The waveguide is assumed terminated in a normalized load Y_L so that the equivalent circuit of the array is that shown in Fig. 14.25b.

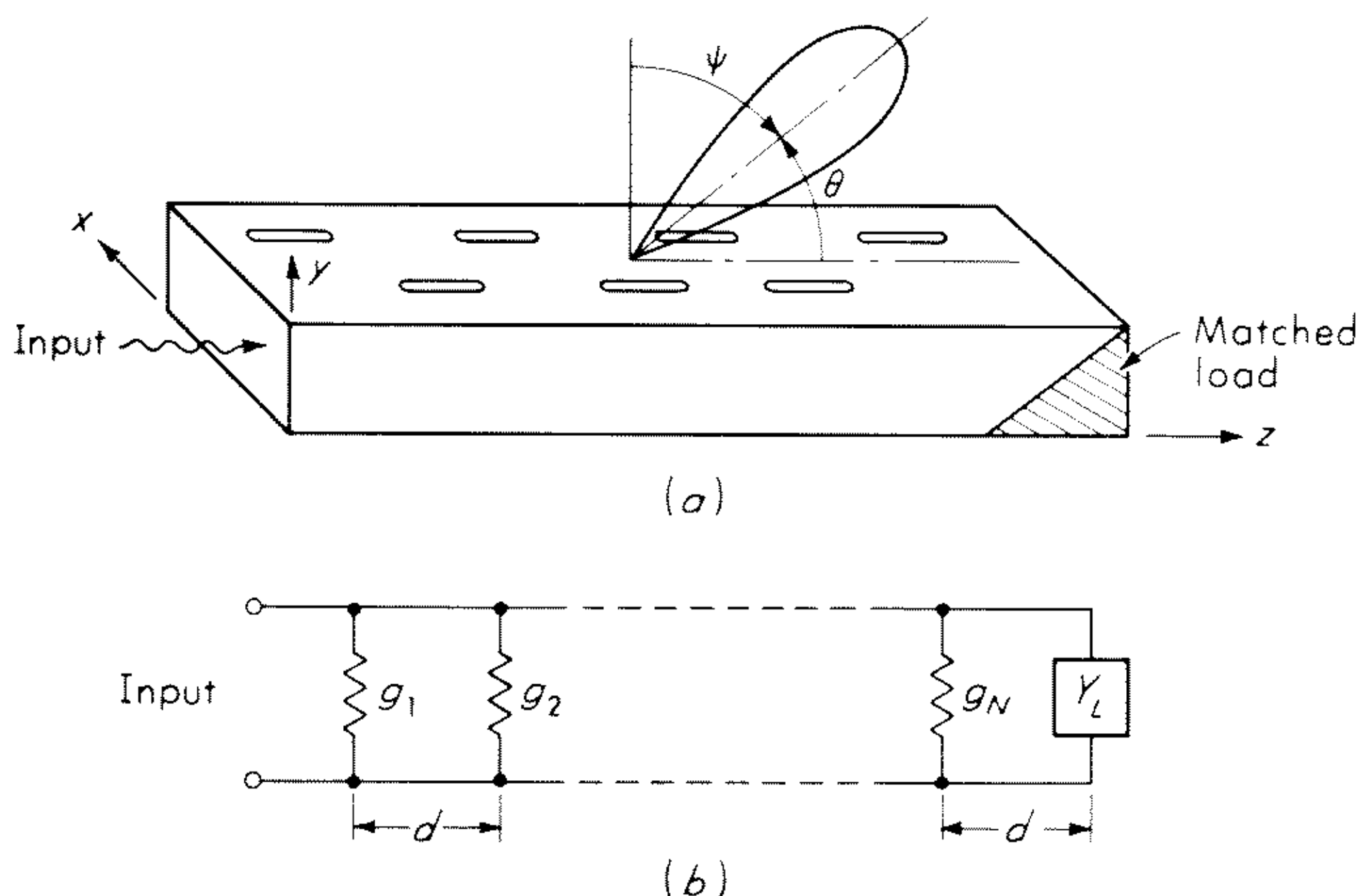


Fig. 14.25 The nonresonant array and its equivalent circuit.

The location of the center of the n th slot is given by

$$\mathbf{r}_n = nd\hat{\mathbf{z}} + x_n\hat{\mathbf{x}}$$

where d is the slot spacing and x_n is the offset measured from the centerline $x = a/2$. If the excitation of the n th slot is a_n (not including the possible 180° phase change due to offset on the opposite side of center) the array factor is of the form

$$f = \sum_{n=1}^N a_n \exp(jk_0\hat{\mathbf{r}} \cdot \mathbf{r}_n - j\beta nd) \quad (14.89a)$$

if the slots are all offset on one side and

$$f = \sum_{n=1}^N a_n \exp(jk_0 \hat{\mathbf{r}} \cdot \mathbf{r}_n + jn\pi - j\beta nd) \quad (14.89b)$$

if every other slot is displaced on adjacent sides of the center. In these expressions $\beta = 2\pi/\lambda_g$. The unit vector $\hat{\mathbf{r}}$ equals $\hat{\mathbf{x}} \sin \theta \cos \phi + \hat{\mathbf{y}} \sin \theta \sin \phi + \hat{\mathbf{z}} \cos \theta$, where θ is the polar angle measured from the z axis and ϕ is the azimuthal angle measured from the x axis. Note that $\psi = \pi/2 - \theta$ in the $\phi = \pi/2$ plane.

In order for all slots to radiate in phase in the direction $\phi = \pi/2, \theta = \pi/2 - \psi$ it is necessary that

$$k_0 d \sin \psi - \beta d = 2m\pi \quad (14.90a)$$

in the case of (14.89a) and

$$k_0 d \sin \psi - \beta d + \pi = 2m\pi \quad (14.90b)$$

for (14.89b), where m is an integer. From (14.90a) we obtain

$$d = \frac{m\lambda_0\lambda_g}{\lambda_g \sin \psi - \lambda_0} \quad (14.91a)$$

while (14.90b) gives

$$d = \frac{(2m - 1)\lambda_0\lambda_g}{2(\lambda_g \sin \psi - \lambda_0)} \quad (14.91b)$$

The required solution for d must be such that only one main lobe occurs in visible space, i.e., second-order beams must not occur. In order to visualize the relations (14.91a) and (14.91b) it is helpful to sketch d as a function of ψ for various values of m . Such sketches are given in Fig. 14.26a and b for (14.91a) and (14.91b), respectively. A special case arises in connection with (14.91a) when $\psi = \sin^{-1} \lambda_0/\lambda_g$. If m is chosen equal to zero, then any value of d will result in a main lobe in the direction $\psi = \sin^{-1} \lambda_0/\lambda_g$. Physically this corresponds to the same angle that the TEM waves making up the TE_{10} mode propagate relative to the guide axis and hence matches the phase velocity of the waveguide mode with the radiated field in the z direction. To avoid a second main lobe it is clear from Fig. 14.26a that d must be restricted to less than $\lambda_0\lambda_g/(\lambda_0 + \lambda_g)$. For other angles of radiation $m = 0$ does not yield a solution for d .

Various solutions for d are possible depending on the relative value of λ_g/λ_0 . It is desirable to keep $\lambda_g < 2\lambda_0$ so that the guide will not be too frequency-dispersive. (A highly dispersive guide leads to large changes in the direction of radiation with small changes in frequency.) If $\lambda_g < 2\lambda_0$, then the points A and B are lower than point C in Fig. 14.26a. Also, as long as $\lambda_g < 3\lambda_0$, the point D is lower than point C . In this case a solution for d yielding an angle of radiation greater than $\sin^{-1}(\lambda_0/\lambda_g)$ will also result in another main lobe at an angle less than $\sin^{-1}(\lambda_0/\lambda_g)$. Thus for $\lambda_g < 2\lambda_0$ the value of d must be so chosen that

$$\frac{\lambda_0\lambda_g}{\lambda_0 + \lambda_g} < d < \frac{2\lambda_0\lambda_g}{\lambda_0 + \lambda_g} \quad (14.92)$$

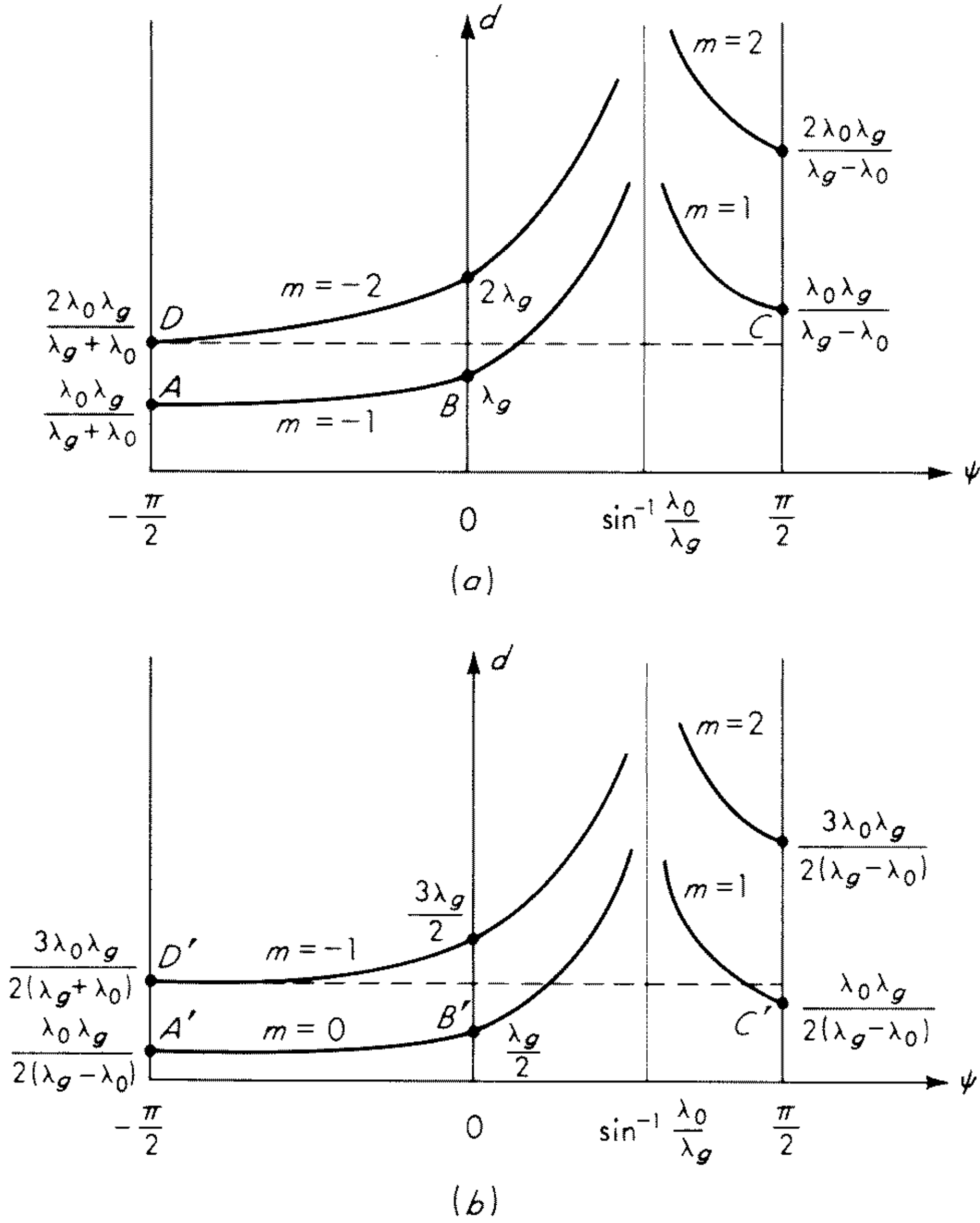


Fig. 14.26 (a) d vs. ψ for Eq. (14.91a); (b) d vs. ψ for Eq. (14.91b).

and

$$\sin \psi = \frac{\lambda_0}{\lambda_g} - \frac{\lambda_0}{d} \quad (14.93)$$

This will give a single main lobe in any direction between $-\pi/2$ to $\sin^{-1}[(2\lambda_0 - \lambda_g)/\lambda_g]$ with all of the slots offset on one side.

If alternate slots are offset on opposite sides, the curves in Fig. 14.26b apply. These curves are the same as those in Fig. 14.26a except for a change in the vertical scale. Hence if we again choose $\lambda_g < 2\lambda_0$, it will be required that

$$\frac{\lambda_0 \lambda_g}{\lambda_0 + \lambda_g} < 2d < \frac{3\lambda_0 \lambda_g}{\lambda_0 + \lambda_g} \quad (14.94)$$

and

$$\sin \psi = \frac{\lambda_0}{\lambda_g} - \frac{\lambda_0}{2d} \quad (14.95)$$

The possible angle of radiation is now limited to the range $-\pi/2$ to $\sin^{-1}[(2\lambda_0 - \lambda_g)/3\lambda_g]$.

It is not possible to get a single lobe in the forward direction at angles greater than the angle given above without at the same time having another main

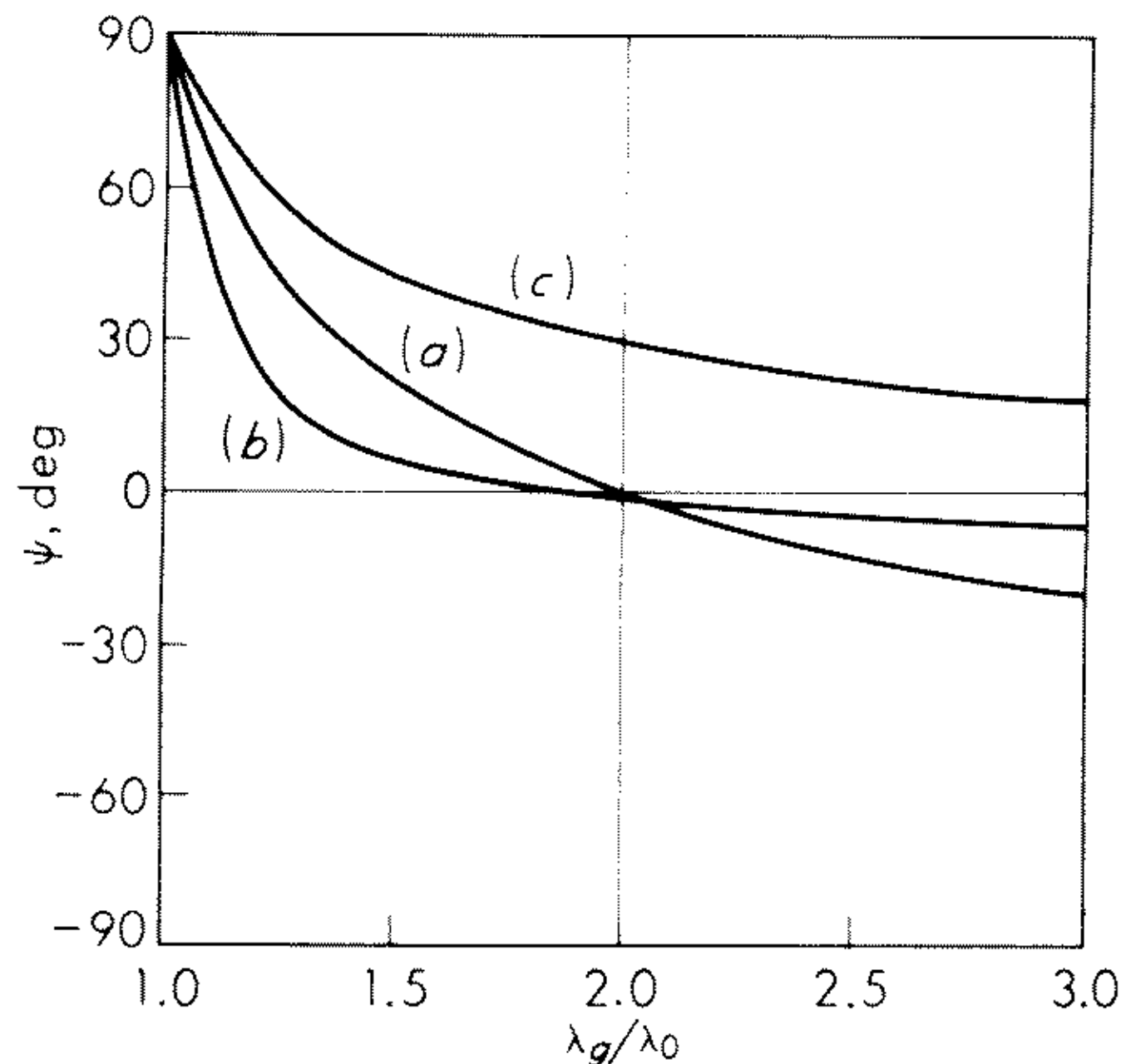


Fig. 14.27 Available main-lobe directions as a function of λ_g/λ_0 . (a) Slots offset on one side only; (b) alternate slots offset on opposite sides; (c) $m = 0$ solution of Eq. (14.91a), $d < \lambda_0\lambda_g/(\lambda_0 + \lambda_g)$, ψ equals the plotted value as a function of λ_0/λ_g only.

lobe appearing at some other angle. This is obvious, since points C , C' can never be lower than points A , A' in Fig. 14.26 because $\lambda_g - \lambda_0 < \lambda_g + \lambda_0$. If $2\lambda_0 < \lambda_g < 3\lambda_0$, then point C is lower than point B but still higher than point D . In this case the direction of the main lobe is confined to the backward direction. In fact, for all values of $\lambda_g > 2\lambda_0$ the condition for a single lobe forces the direction of this lobe to be in the backward direction. The greatest angle in the forward direction is obtained by making λ_g close to λ_0 and choosing d according to (14.92). The range of available angles as a function of λ_g/λ_0 is shown in Fig. 14.27.

The fact that the direction of the main lobe depends on the relative value of λ_g/λ_0 for a given value of d is often made use of in scanning the lobe by changing the frequency. For frequency scanning a highly dispersive waveguide is desirable. This has led to the use of waveguides bent into a sinusoidal shape to increase the electrical length between slots.²³

It is, of course, not necessary to restrict λ_g to be greater than λ_0 . By loading the guide with dielectric it is possible to have λ_g less than λ_0 , in which case some of the restrictions on beam angle given in the above analysis may be lifted. For a detailed discussion the paper by Dion may be consulted.²⁴

If the slots are alternatively offset on opposite sides of the centerline, the overall array is equivalent to two arrays with a separation along the x direction which can be taken as the average value of the slot offset on one side. If x_0 is the average offset, then the array factor (14.89b) may be written

$$f = - \sum_{n=1,3,5} a_n e^{jk_0(x_0 \sin \theta \cos \phi + nd \cos \theta) - j\beta n d} + \sum_{n=2,4,\dots} a_n e^{jk_0(-x_0 \sin \theta \cos \phi + nd \cos \theta) - j\beta n d}$$

For simplicity we now assume that $a_n = a_{n+1}$ and an even number of elements. The array factor may then be written as

$$\begin{aligned}
 f &= \sum_{n=2,4,\dots}^{N/2} a_n e^{jk_0 n d \cos \theta - j\beta n d} (e^{-jk_0 x_0 \sin \theta \cos \phi} - e^{jk_0 x_0 \sin \theta \cos \phi - jk_0 d \cos \theta + j\beta d}) \\
 &= 2j e^{-j(k_0 d/2) \cos \theta + j(\beta d/2)} \sin \left(\frac{k_0 d}{2} \cos \theta - \frac{\beta d}{2} - k_0 x_0 \sin \theta \cos \phi \right) \\
 &\quad \sum_{n=1,2,\dots}^{N/2} a_{2n} e^{j2nd(k_0 \cos \theta - j\beta)} \quad (14.96)
 \end{aligned}$$

This result is seen to be equivalent to an array with slots offset on one side only but with spacing $2d$ and modified by the two-element-group factor

$$\sin \left(\frac{k_0 d}{2} \cos \theta - \frac{\beta d}{2} - k_0 x_0 \sin \theta \cos \phi \right)$$

The overall effect of this is to make the suppression of second-order beams more difficult. The problem has been analyzed in detail by Gruenberg²⁵ and for two-dimensional arrays also by Kurtz and Yu²⁶ and McCormick.^{27,28}

In the principal plane $\phi = \pi/2$ no second-order beams will occur if $2d$ is restricted by the same condition as (14.92), that is,

$$\frac{\lambda_0 \lambda_g}{\lambda_0 + \lambda_g} < 2d < \frac{2\lambda_0 \lambda_g}{\lambda_0 + \lambda_g} \quad (14.97)$$

This condition is seen to be more restrictive than (14.94). However, it may be relaxed to some extent depending on the influence of the two-element-group factor. In the principal plane this factor will permit $2d$ to be increased from $2\lambda_0 \lambda_g / (\lambda_0 + \lambda_g)$ to the value $3\lambda_0 \lambda_g / (\lambda_0 + \lambda_g)$ given by (14.94), since at the smaller value the two-element-group factor is zero and increases to unity at the upper value. In planes other than the principal plane the factor $\sin [(k_0 d \cos \theta)/2 - \beta d/2 - k_0 x_0 \sin \theta \cos \phi]$ will not suppress the second-order beam if $2d$ is greater than the maximum value specified by (14.97). For example, if $2d = 3\lambda_0 \lambda_g / (\lambda_0 + \lambda_g)$, we obtain in phase addition from the array factor at $\cos \theta_1 = \lambda_0 / \lambda_g$, $\cos \theta_2 = (2\lambda_0 - \lambda_g) / 3\lambda_g$, $\cos \theta_3 = (\lambda_0 - \lambda_g) / 3\lambda_g$, and $\cos \theta_4 = -1$. The first and third of these are suppressed in the principal plane by the two-element-group factor, and the last is the appearance of the first second-order beam at $\theta = \pi$. If we consider the plane $\phi = \pi/4$, and θ given by the above expressions, the two-element-group factor has the values

$$\sin \left(\frac{\pi x_0}{\sqrt{2} \lambda_0} \sin \theta_1 \right) \quad \text{and} \quad \sin \left(\frac{\pi x_0}{\sqrt{2} \lambda_0} \sin \theta_3 \right)$$

at the location of the second-order beams, which are suppressed in the principal plane. It is apparent that these lobes are not suppressed in planes other than the principal one, and hence for arrays with slots offset on both sides of the

center line it is necessary to increase the restriction on the spacing d to that given by (14.97). For arrays designed for very low side-lobe levels it is important to pay attention to the possibility of second-order beams appearing in planes other than the principal plane if the overall design objectives are to be met. It should also be kept in mind that the element factor reduces the radiation field to zero in directions coinciding with the axis of the slot.

There are other ways to suppress second-order beams arising from slot offset. These fall into two general categories: (1) the use of flared sheets on either side of the waveguide to establish a new aperture, or some other form of horn arrangement,²⁹ and (2) the use of centered slots with the excitation controlled by obstacles inserted into the guide to control the asymmetry of the field at the position of the slot.^{30,31}

Nonresonant Array Design

We shall now consider the problem of specifying the slot conductances for the nonresonant array. Initially we present a simplified approach along the lines of that used by Dion,²⁴ and then we give the more exact method which was worked out by Kaminow and Stegen.³² In the method used by Dion it is assumed that a large number of slots are used with each slot radiating only a small amount of the incident power. Thus, reflections from the slots are negligible and the incident wave in the guide can be considered to leak out at a rate determined by the smoothed conductance distribution along the guide. Also, it is assumed that the waveguide losses are negligible. The conductance per unit length is first determined to yield the required line source aperture distribution. The individual slot conductances are then chosen to be the same as the conductance for the continuous line source at the position corresponding to the location of the center of the slot. The waveguide is also assumed terminated in a matched load, so the input standing-wave ratio is essentially unity in view of the small reflections produced by the individual slots and the fact that the slot spacing does not equal $\lambda_g/2$, with the result that there is no in-phase addition of the reflected waves (nonresonant array condition).

Since the slot conductance that can be conveniently obtained is limited, it is necessary to have a reasonable fraction (10 to 40 percent) of the incident power available at the position of the last slot in the array. Since this slot will radiate only a portion of the available power, the remainder is dissipated in the matched load. Consequently, the efficiency of the array is less than unity. The loss in efficiency associated with the nonresonant array is the penalty paid for a broader-band antenna as compared with the resonant array.

Let the required amplitude distribution along the equivalent continuous array be $\sqrt{P(z)}$. This distribution must be so chosen as to yield the required beam width and side-lobe level. If a Chebyshev array is desired, then the Taylor line source distribution is used² (see also Sec. 7.8). The direction of the main lobe is determined by the spacing as discussed earlier. Let the input

power to the waveguide be unity and let $g(z)$ be the shunt conductance per unit length at z . The available power at z is then given by

$$\frac{1}{2}|V_a(z)|^2 = P_a(z) = 1 - \int_0^z \frac{|V(z)|^2}{2} g(z) dz \quad (14.98)$$

where $V(z)$ is the equivalent voltage so defined that $|V|^2 g/2$ is the radiated power per unit length. But the radiated power per unit length is also given by $\frac{1}{2}|V_a(z)|^2 g(z)$ and gives an aperture distribution $V_a(z)[g(z)/2]^{1/2}$, which must be proportional to the specified distribution $\sqrt{P(z)}$. Thus we have

$$g(z) = \frac{2KP(z)}{|V_a(z)|^2} = \frac{KP(z)}{P_a(z)} \quad (14.99)$$

where K is a constant to be determined. At the end of the array where $z = L$ a fraction r of the incident power is available to be dissipated in the load. Hence the total power radiated is given by

$$\begin{aligned} 1 - r &= \int_0^L \frac{|V_a(z)|^2}{2} g(z) dz \\ &= K \int_0^L P(z) dz \end{aligned}$$

so
$$K = \frac{1 - r}{\int_0^L P(z) dz} \quad (14.100)$$

Combining this with (14.98) and (14.99) now yields

$$g(z) = \frac{KP(z)}{1 - K \int_0^z P(z) dz} = \frac{(1 - r)P(z)}{\int_0^L P(z) dz - (1 - r) \int_0^z P(z) dz} \quad (14.101)$$

for the normalized shunt conductance per unit length. The conductance of the n th discrete slot in the slotted array is chosen to be

$$g_n = dg(nd) \quad (14.102)$$

where d is the slot spacing. Curves giving the normalized slot conductance for a Taylor distribution for arrays with 20-, 25-, and 30-db side-lobe levels and various array efficiencies are given in the paper by Dion.²⁴

An analysis similar to the above may also be carried out by treating each slot as a discrete element. Let the incident power in the waveguide be unity and let r be the fraction delivered to the matched termination. Let the power to be radiated by the n th slot be denoted by P_n . Thus the power incident at slot N is $r + P_N$. The equivalent voltage at this slot is such that $|V_N|^2/2 = r + P_N$, since the reflected wave is negligible. The power radiated is therefore also given by $(r + P_N)g_N$ and equals P_N . Hence we obtain

$$g_N = \frac{P_N}{r + P_N} \quad (14.103a)$$

The power incident at slot $N - 1$ is $r + P_N + P_{N-1}$, and the radiated power is P_{N-1} , which also equals $(r + P_N + P_{N-1})g_{N-1}$, so

$$g_{N-1} = \frac{P_{N-1}}{r + P_N + P_{N-1}} \quad (14.103b)$$

By continuing this analysis it is readily found that

$$\begin{aligned} g_n &= \frac{P_n}{r + \sum_{i=n}^N P_i} \\ &= \frac{P_n}{1 - \sum_{i=1}^{n-1} P_i} \end{aligned} \quad (14.103c)$$

since r plus the sum of all radiated powers equals unity. This expression corresponds to (14.17) with K chosen equal to unity, that is, $P(z)$ is normalized so that

$$\int_0^L P(z) dz = 1 - r$$

Dion has built an array based on the above simplified design procedure with a design objective of side lobes 30 db down and a beam direction 30° from the normal in the forward direction. A slot spacing of $2\lambda_0/3$ and a guide wavelength equal to $2\lambda_0$ were used.²⁴ The measured radiation pattern agreed quite well with the theoretical predictions. The side-lobe level remained below 30 db, although the far-out side lobes were larger than those predicted from the Taylor distribution.

In general the machining tolerances on slot size and spacing is such that some degradation in performance from the design specification will result. This is particularly noticeable as regards side-lobe level, so it is customary to overdesign the array with regard to the side-lobe level, e.g., a 50-db side-lobe level might be used in a design calling ultimately for side lobes 40 db below the main lobe.

The above equations do not specify any definite criterion for the value of r , the fraction of the power to be dissipated in the load. The essential restriction on r is that it must lead to values of g_n that do not exceed some specified maximum value g_{\max} for two reasons: (1) the maximum value of conductance that can be obtained is limited and (2) the theory neglects reflections from each slot and therefore would not be applicable if the conductances were large. A reasonable upper limit for g_{\max} is 0.2. A slot with this conductance would produce a reflection coefficient of 0.1, which corresponds to 1 percent reflected power. With the above considerations we can give a criterion for determining r . Let the known distribution $P(z)$ be normalized so that

$$\int_0^L P(z) dz = 1$$

From (14.101) we can write

$$\frac{g_{\max}}{d} > \frac{(1-r)P}{1 - (1-r) \int_0^z P dz}$$

$$\text{or} \quad 1-r < \frac{g_{\max}}{Pd + g_{\max} \int_0^z P dz} \quad (14.104)$$

The maximum value of the right-hand side occurs when $dP/dz + g_{\max}P/d = 0$. A graphical, numerical, or analytical solution of this equation may be used to determine r .

As an example consider a triangular distribution

$$P(z) = \frac{2}{L} \left(1 - \left| \frac{2z}{L} - 1 \right| \right)$$

We then find that

$$\frac{dP}{dz} + \frac{g_{\max}}{d} P = -\frac{4}{L^2} + \frac{g_{\max}}{d} P = 0$$

yields $z = L - d/g_{\max}$. Thus we obtain

$$1-r < \frac{g_{\max}}{dP(L - d/g_{\max}) + g_{\max} \int_0^{L-d/g_{\max}} P(z) dz} = \frac{1}{1 + 2(d/Lg_{\max})^2}$$

If we choose $g_{\max} = 0.2$ and a 10-element array for which $L = 10d$, we see that we should have $1-r < 2/3$, which requires about 35 percent of the power to be dissipated in the load. For an array of 20 elements we find that we require $1-r < 8/9$, so now only about 11 percent of the incident power needs to be dissipated in the termination. In general, longer arrays can be made more efficient.

In a nonresonant array it is necessary to use a load termination that has a low VSWR, because the reflected wave will produce a beam on the opposite side of the array normal to the desired direction of the main lobe. If this spurious beam is to be kept below the side-lobe level specified, the amplitude of the reflected wave must be small. For example, if 45 percent of the power is dissipated in the termination and side lobes 30 db below the main lobe are specified, then the VSWR of the termination must not exceed 1.1. For other conditions see the paper by Dion.²⁴

The design procedure used by Kaminow and Stegen is exact in that it takes into account the reflections from each slot as well as waveguide losses. Waveguide losses are easily incorporated into the simplified design procedure given above (see Probs. 14.2 and 14.3), so the main correction to be obtained in the analysis below is the effect of interaction between slots. The analysis will be based on the equivalent circuit given in Fig. 14.25 but with the g_n replaced by

complex admittances Y_n . We shall let $\gamma = \alpha + j\beta$ be the complex propagation constant for the waveguide. The following symbols are also introduced:

$Y_n = g_n + jb_n$ = complex admittance of n th slot

$\Gamma_n = \frac{1 - Y_n^-}{1 + Y_n^-}$ = reflection coefficient on the generator side of the n th slot

$Y_n^+ = g_n^+ + jb_n^+$ = admittance looking toward the load from the load side of slot n

$Y_n^- = g_n^- + jb_n^- = Y_n + Y_n^+$ = admittance looking toward the load from the generator side of slot n

P_n = power radiated by n th slot

P_n^+ = available power on load side of slot n

$P_n^- = P_n + P_n^+$ = available power on generator side of slot n

Let V_n be the voltage at the position of the n th slot. The power radiated by the n th slot is then $\frac{1}{2}|V_n|^2 g_n = P_n$, and the power transmitted toward the load will be $\frac{1}{2}|V_n|^2 g_n^+ = P_n^+$. Hence

$$g_n = \frac{P_n}{P_n^+} g_n^+ \quad (14.105)$$

In Sec. 14.9 it is shown that the phase of the electric field across the slot is the same as that of $jV_n Y_n$. But the phase of the n th slot excitation must be the same as that associated with the factor $e^{-j\beta(n-N)d}$ relative to that of the N th slot. Hence

$$\angle \frac{jV_n Y_n}{jV_N Y_N} = \angle e^{-j\beta(n-N)d}$$

Consequently

$$\begin{aligned} \tan^{-1} \frac{b_n}{g_n} &= \tan^{-1} \frac{b_N}{g_N} + \angle \frac{V_1}{V_n} - \beta(n - N)d \\ &= \tan^{-1} \frac{b_{n+1}}{g_{n+1}} + \beta d + \angle \frac{V_{n+1}}{V_n} \end{aligned} \quad (14.106)$$

If V_L is the voltage at the load, then

$$P_L = \frac{1}{2}|V_L|^2 g_L \quad (14.107)$$

By using transmission line theory the voltage at slot N is found to be

$$V_N = V_L (\cosh \gamma d + Y_L \sinh \gamma d) \quad (14.108a)$$

At slot $N - 1$ the voltage will be

$$V_{N-1} = V_N (\cosh \gamma d + Y_N^- \sinh \gamma d)$$

If we replace Y_N^- by $Y_N + Y_N^+$ and note that

$$Y_N^+ = \frac{Y_L + \tanh \gamma d}{1 + Y_L \tanh \gamma d}$$

and
$$\frac{V_N}{V_L} = \cosh \gamma d (1 + Y_L \tanh \gamma d)$$

we find that we can write

$$V_{N-1} = V_N (2 \cosh \gamma d + Y_n \sinh \gamma d) - V_L \quad (14.108b)$$

Similarly, we find in general that

$$V_n = V_{n+1} (2 \cosh \gamma d + Y_{n+1} \sinh \gamma d) - V_{n+2} \quad (14.108c)$$

The available power on the load side of slot n is P_n^+ . This power consists of that associated with forward and reflected waves, which we denote by $P_{n,f}^+$ and $P_{n,r}^+$, respectively. Thus

$$P_n^+ = P_{n,f}^+ - P_{n,r}^+$$

and similarly we can write

$$P_{n+1}^- = P_{n+1,f}^- - P_{n+1,r}^-$$

But we also have

$$P_{n+1,f}^- = e^{-2\alpha d} P_{n,f}^+ \quad P_{n+1,r}^- = e^{2\alpha d} P_{n,r}^+ = |\Gamma_{n+1}|^2 P_{n+1,f}^-$$

so
$$P_n^+ = e^{2\alpha d} P_{n+1,f}^- - |\Gamma_{n+1}|^2 e^{-2\alpha d} P_{n+1,f}^-$$

$$= (1 - |\Gamma_{n+1}|^2) e^{2\alpha d} P_{n+1,f}^- + 2|\Gamma_{n+1}|^2 P_{n+1,f}^- \sinh 2\alpha d$$

We now use the relation $P_{n+1}^- = (1 - |\Gamma_{n+1}|^2) P_{n+1,f}^-$ to finally obtain

$$P_n^+ = P_{n+1}^- \left(e^{2\alpha d} + \frac{2|\Gamma_{n+1}|^2}{1 - |\Gamma_{n+1}|^2} \sinh 2\alpha d \right) \quad (14.109)$$

where $\Gamma_{n+1} = (1 - Y_n^-)/(1 + Y_n^+)$.

The design procedure based on the above equations proceeds as follows:

1. Determine the powers P_n to be radiated by each slot in order to achieve the desired aperture distribution. The P_n are proportional to the square of the magnitude of the slot excitation coefficients.
2. The simplest load to use is a matched termination. A priori it is not known what fraction of the incident power must be dissipated in the load in order to keep all of the conductances g_n within a range that can be obtained. Initially an estimate for P_L may be made by taking

$$P_L = r \sum_{n=1}^N P_n$$

and using (14.104) to calculate r based on a smoothed distribution for P_n and neglecting waveguide losses. Usually for long arrays (20 or more elements) a value of P_L about 10 percent of the input or total radiated power is suitable. If the calculated values of the conductances turn out to be too large, it will be

necessary to repeat the calculations with a larger value of P_L . The input VSWR automatically turns out to be small because the reflections from individual slots are small and do not add up in phase for a nonresonant array.

3. With P_L known and if a matched termination is used, $V_L = \sqrt{2P_L}$. From (14.109) we obtain $P_N^+ = P_L e^{2\alpha d}$ for a load placed a distance d beyond the last slot. From (14.105) $g_N = P_N/P_N^+$, since $g_N^+ = 1$. The voltage V_N is given by (14.108a), where the phase of V_L may be taken as zero. The susceptance b_N is found from (14.106), i.e.,

$$\tan^{-1} \frac{b_N}{g_N} = \beta d + \angle \frac{V_L}{V_N}$$

The susceptance b_N can be chosen equal to zero, since only the relative phasing between slots is important.

4. Next calculate the parameters for slot $N - 1$. The conductance is given by (14.105) with P_{N-1} specified, P_{N-1}^+ calculated from (14.109) with $P_N^- = P_N + P_N^+$, and g_{N-1}^+ determined from

$$g_{N-1}^+ + jb_{N-1}^+ = \frac{Y_N^- + \tanh \gamma d}{1 + Y_N^- \tanh \gamma d}$$

where $Y_N^- = Y_N + Y_N^+$. The voltage V_{N-1} is found from (14.108c) in terms of quantities already evaluated. The susceptance b_{N-1} is then determined by (14.106).

5. The steps in (4) are repeated for each additional slot in sequence. When the calculations are completed, the slot conductances and susceptances are known, and this determines the slot lengths and offsets. Admittance data for a variety of slot displacements, frequency, etc. are given in the "Antenna Engineering Handbook" and will not be repeated here.³³

The discussion above has concentrated on waveguide arrays using longitudinal slots in the broadwall of a rectangular guide in order to illustrate the essential features of the design. A variety of other slot arrangements are possible, including inclined slots cut in the broadwall or sidewall of the guide. For a discussion of these other types of arrays as well as for further details on the longitudinal slot arrays the reader is referred to the books by Jasik,³³ Silver,²⁹ Hansen,²³ and Watson³⁴ (see also Refs. 26, 27, and 35 to 44).

A simplifying feature associated with the longitudinal slot arrays is the negligible mutual impedance between adjacent slots because of their end-to-end disposition. For other slot arrangements it is necessary to take into account mutual impedance effects.⁴⁵⁻⁴⁹ The design data are best obtained by measuring the incremental admittance added to the total input admittance by each additional slot as it is added to the array.⁴⁸ The experimental data are quite limited, although some useful results are available in the references cited.

14.9 Impedance of Slots in Rectangular Waveguides

Introduction

Figure 14.28 illustrates a typical slot in the broadwall of a rectangular guide. For the purpose of discussion a coordinate system x_0, y_0, z_0 is introduced for describing the field in the slot. Although we have pictured the slot in the broadwall, the discussion to follow applies equally well to a slot cut in the sidewall of a guide. The slot is of length l and width w and is cut in a wall of thickness t . The slot is excited by having the dominant TE_{10} mode incident upon it in the waveguide.

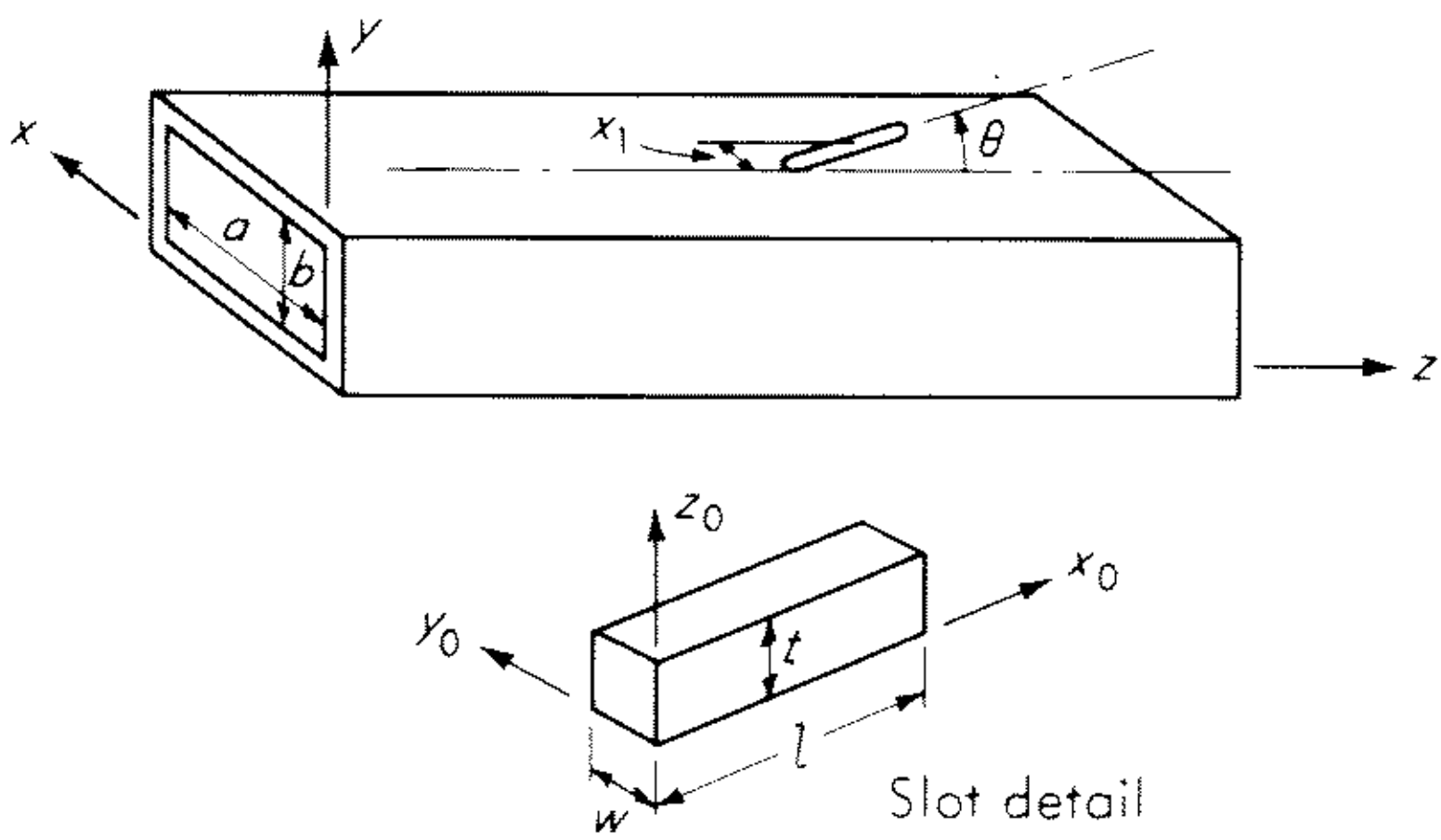


Fig. 14.28 A slot in the broadwall of a rectangular waveguide.

An exact theory of the impedance properties of a slot as described above is not available. Various approximate theories that have been developed give useful results and insight into the general impedance properties of a slot, but they do not yield numerical results for conductance and susceptance parameters accurate to better than a few percent. We shall review these theories in the following sections but make no attempt to carry out detailed and extensive analysis.

The slot may be conveniently viewed as a short section of waveguide which couples the interior of the guide to the exterior free space region. For ease in construction the slot is usually made with rounded ends, but we shall consider it to have square ends for the purpose of examining the nature of the field in the slot.

The dominant mode in the slot, viewed as a waveguide, is the TE_{10} mode, and it has an electric field given by

$$\mathbf{E} = E_0 \hat{y}_0 \sin \frac{\pi x_0}{l} e^{-j\beta_0 z_0}$$

where $\beta_0 = (k_0^2 - \pi^2/l^2)^{1/2}$. The aperture electric field associated with this mode is sinusoidal over both the inner aperture at $z_0 = 0$ and the outer aperture at $z_0 = t$, but it differs in phase at the two apertures (unless $\beta_0 = 0$). The

next mode closest to propagating is the TE_{20} mode with an electric field given by

$$\mathbf{E} = E_0 \hat{\mathbf{y}}_0 \sin \frac{2\pi x_0}{l} e^{-\Gamma_{20} z_0}$$

where $\Gamma_{20} = (4\pi^2/l^2 - k_0^2)^{1/2}$. For a typical slot $l \approx \lambda_0/2$, so $\Gamma_{20} = \sqrt{3}k_0$. The width w is usually approximately equal to the thickness t . For X-band guide $t = 0.05$ in. and λ_0 is around 1.25 in., so as an estimate for typical values of $\Gamma_{20}t$ we have $\Gamma_{20}t = \sqrt{3}\pi/12.5 = 0.43$. Thus this mode is not greatly attenuated in the distance corresponding to the slot thickness t and will strongly couple the electric field of the TE_{20} slot mode between the inner and outer apertures.

The other TE_{30} , TE_{40} , TE_{11} , and TM_{11} slot modes have propagation constants Γ_{30} , Γ_{40} , and Γ_{11} such that, as an estimate based on the above-assumed dimensions, $\Gamma_{30}t = 0.7$, $\Gamma_{40}t = 0.96$, $\Gamma_{11}t = \pi$. From these estimates it is apparent that the first few TE_{n0} modes excited in the slot by the incident waveguide mode will couple effectively to the outside region but that all TE_{nm} , $m > 0$, and TM_{nm} modes produce only weak coupling between the interior and exterior regions.

As a first approximation it is commonly assumed that only the TE_{10} mode is excited with significant amplitude in the slot. With this assumption the slot aperture field is known to within a constant and the field in the waveguide is easily evaluated to within a constant amplitude factor. The exterior radiated field is difficult to calculate because the slot radiates in the presence of a rectangular guide. The problem usually considered is the one with an infinite plane baffle (conducting plane) placed parallel to and coincident with the waveguide wall on which the slot is located. The field radiated by the slot into this half space is readily found. Experimentally it is found that the slot is resonant for a length l very nearly equal to $\lambda_0/2$. By assuming a resonant condition, the amplitude of the field in the slot aperture can be fixed by requiring conservation of incident, reflected, and radiated power. This leads directly to a value for the slot conductance or resistance and forms the basis of Stevenson's theory of slots in waveguides.^{4,8}

Stevenson's theory requires a knowledge of the total radiated power, which can be expressed in the form

$$P_r = \frac{1}{2} V^2 G_r$$

where $V = wE_0$ is the equivalent voltage across the center of the slot and G_r is the radiation conductance of the slot. The radiation conductance for a slot radiating into a half space is related to the radiation resistance of a half-wave dipole antenna by duality (Babinet's principle). The evaluation of G_r is given in Sec. 14.2, and its value is given by $G_r = 1.03 \times 10^{-3}$ mhos. In practice the infinite baffle is not normally used, and consequently the actual value of G_r is not that given above. As an indication of the error involved we show in Fig. 14.29 the radiation conductance of an axial slot on a circular cylinder of radius

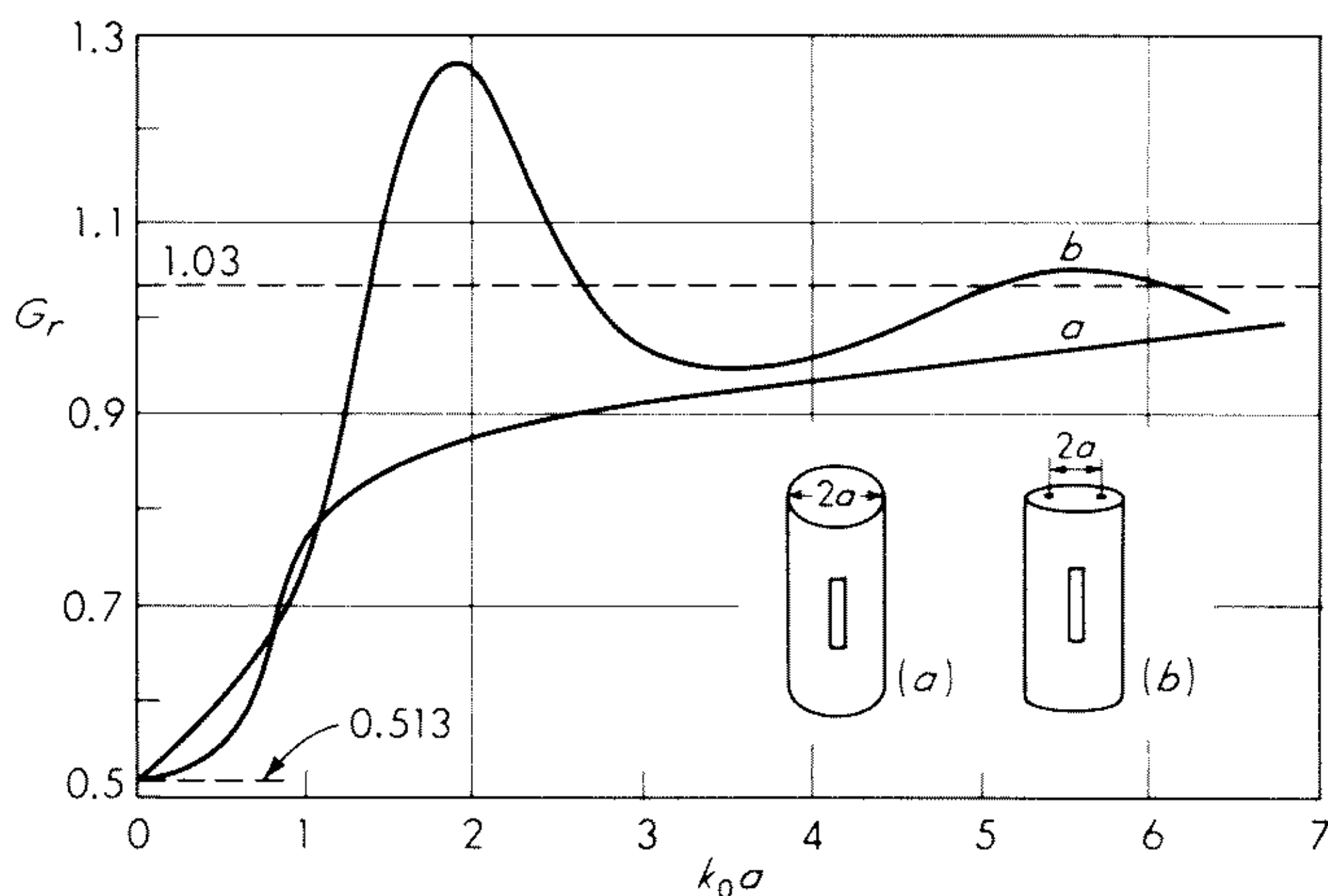


Fig. 14.29 Radiation conductance G_r for axial slots on a circular and elliptical cylinder. (Based on figs. 10 and 36 of Wait.¹⁴)

a and that of a centered axial slot of an elliptical cylinder with foci separation of $2a$. These curves are based on figures 10 and 36 of Wait.¹⁴ For small values of $k_0 a$ the limiting value of G_r is 0.517 mmhos, while for large values of $k_0 a$ it approaches 1.03 mmhos. The small $k_0 a$ value corresponds to the conductance of a slot radiating into free space, while the large $k_0 a$ value is the conductance of a slot radiating into a half space. A notable feature is that G_r is within 10 percent of the large $k_0 a$ limiting value for $k_0 a \geq 2.5$. To the extent that a rectangular guide can be approximated by an elliptical guide it thus seems a reasonable approximation to take $G_r = 1.03$ mmhos for centered or nearly centered axial slots in the broadwall of a rectangular guide.

For slots near a corner, slots cut in the narrow wall, or inclined slots near a corner, G_r could be expected to differ significantly from the value 1.03 mmhos. For example, an axial slot very near a corner of a rectangular guide would be expected to behave similarly to a corner slot radiating into three-quarter space for which the radiation conductance $G_r = \frac{4}{3} \times 0.517 = 0.69$ mmhos. Consequently, as the axial slot is offset toward a corner the radiation conductance would be expected to decrease significantly. Wait has made calculations on the radiation conductance of slots located on a thin ribbon and on a right-angled wedge.⁵⁰ For the slot on a right-angled wedge the conductance has a value of 0.69 mmhos when the slot is at the corner, increases to a maximum value of 1.1 mmhos for a slot a distance $\lambda_0/4$ from the corner, becomes equal to the infinite-baffle value of 1.03 mmhos for a slot offset of about $0.4\lambda_0$, and then oscillates with decreasing amplitude about this value as the slot is moved farther away from the corner.

Transverse slots would be expected to have a radiation conductance more nearly equal to the half-space value 1.03 mmhos, because a slot radiates zero field along its axis and the lack of an infinite baffle would not produce as much

of a perturbation. Of course, there are situations when the guide is located in a large conducting cylinder such as a missile or aircraft or is one of several guides in an array for which the environment may approximate very closely that of an infinite baffle.

The susceptance or reactance of a slot is proportional to the time-average difference in the reactive magnetic and electric energy stored in the evanescent waveguide modes and the near-zone radiated field, i.e., proportional to $W_m - W_e$. When $W_m = W_e$, the slot is resonant. For slots not too close to a waveguide corner the near-zone radiated field is not critically dependent on slot position or orientation, so the radiation susceptance jB_r is relatively insensitive to slot location. However, the amplitudes of the higher-order waveguide modes which are excited do depend quite strongly on slot position and orientation, and as a result the resonant length varies with slot location and orientation. This effect is borne out experimentally.

In the next section we shall present Stevenson's theory for slot conductance, and in the following section we shall outline the variational approach used by Oliner to evaluate the slot impedance.⁵¹⁻⁵³ Felsen has also examined the equivalent circuit of a waveguide-fed slot.⁵⁴ His approach is based on treating the half space into which the slot radiates as a system of spherical transmission lines similar to the scheme utilized in Sec. 4.9 to treat the scattering properties of an antenna.⁵⁵ As an approximation two spherical transmission lines are used; they correspond to the dominant spherical modes excited by a magnetic dipole and an electric dipole. The latter correspond to symmetrical slot excitation by the TE_{10} slot mode and antisymmetrical slot excitation by the TE_{20} slot mode. An equivalent circuit is then derived for this four-port network (two waveguide ports and two spherical transmission line ports), but the evaluation of the network parameters is based on Oliner's variational formulation. By choosing incident dominant modes in the waveguide appropriately, it is possible to ensure that the field excited in the slot is either symmetrical or antisymmetrical, and this permits the problem to be reduced to two simpler two-port network problems corresponding to open-circuit and short-circuit bisections of the four-port network. The general form of equivalent circuit used by Felsen is shown in Fig. 14.30.

Conductance of Slots in Rectangular Waveguides

With reference to Fig. 14.31 let a slot be located in a waveguide between reference planes at z_1 and z_2 . The field in the slot will be assumed to be given by

$$\mathbf{E} = E_0 \hat{\mathbf{y}}_0 \sin \frac{\pi x_0}{l}$$

Let the incident field be a dominant TE_{10} mode from the region $z < z_1$. Because of the slot, an infinite number of waveguide modes are excited. The field in the guide in the two regions $z \leq z_1$ and $z \geq z_2$ can be expanded in terms of

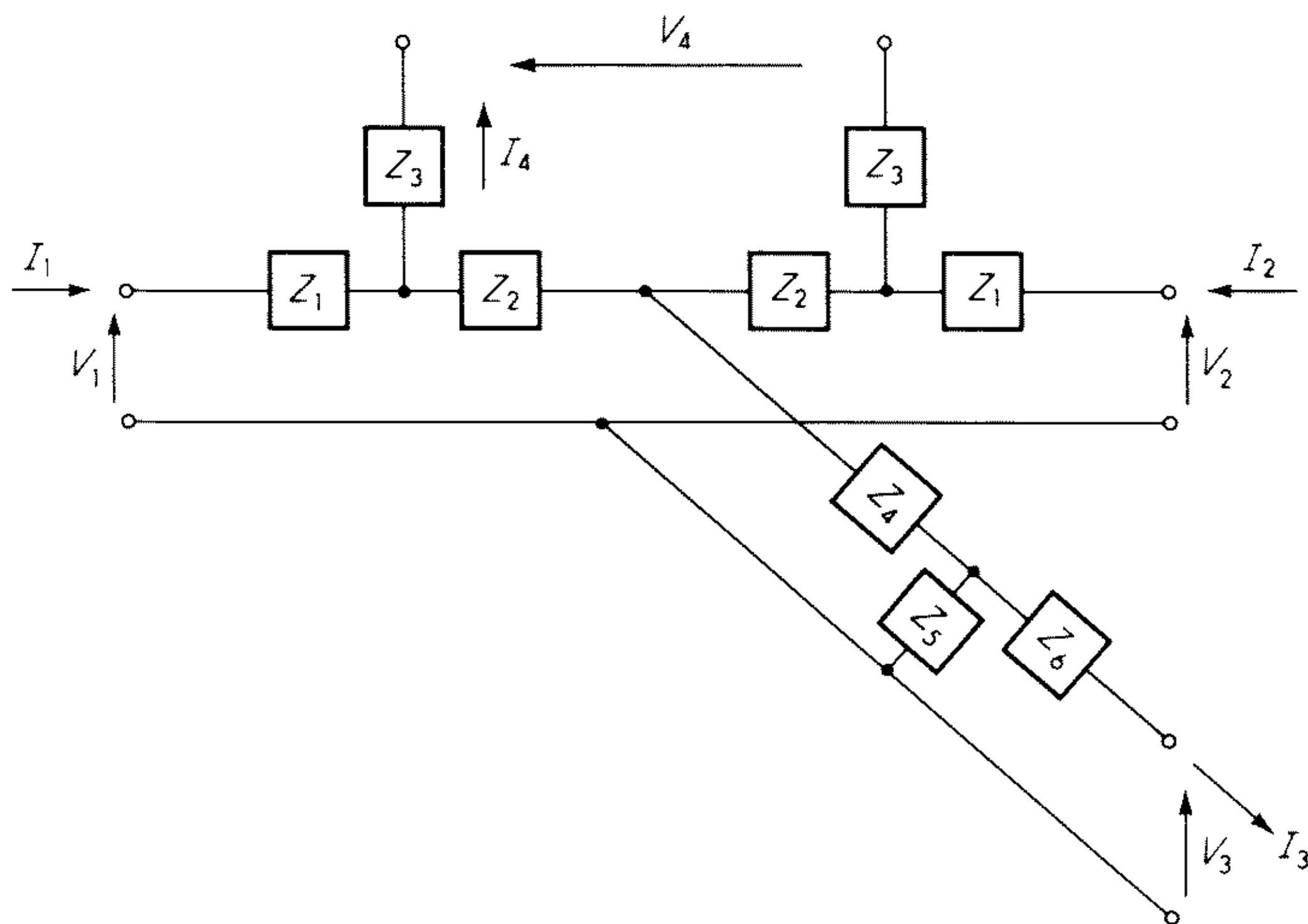


Fig. 14.30 Equivalent circuit of waveguide slot coupling to two spherical modes in a half space.

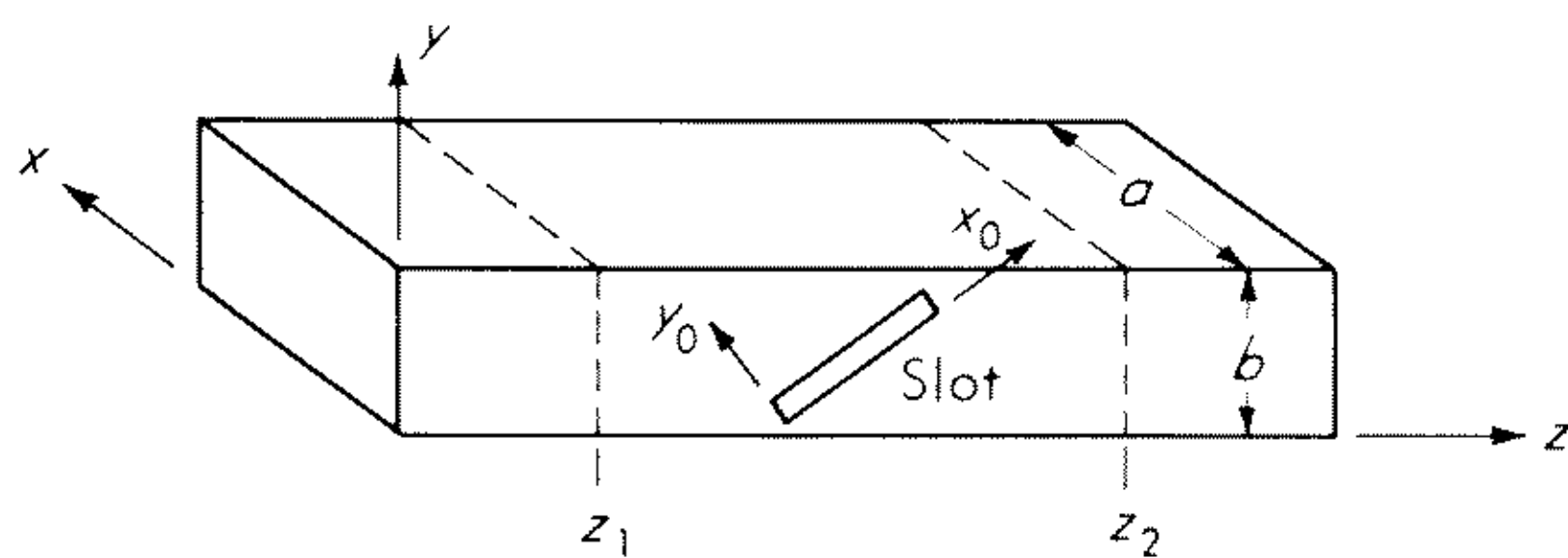


Fig. 14.31 A slot in a rectangular waveguide.

the normal modes for the waveguide in the form (the notation and procedure being used here are described in greater detail elsewhere⁵⁶)

$$\begin{aligned} \mathbf{E} &= C_1 \mathbf{E}_1^+ + \Gamma C_1 \mathbf{E}_1^- + \sum_n' C_n \mathbf{E}_n^- & z \leq z_1 \\ &= TC_1 \mathbf{E}_1^+ + \sum_n' D_n \mathbf{E}_n^+ & z \geq z_2 \end{aligned} \tag{14.110a}$$

$$\begin{aligned} \mathbf{H} &= C_1 \mathbf{H}_1^+ + \Gamma C_1 \mathbf{H}_1^- + \sum_n' C_n \mathbf{H}_n^- & z \leq z_1 \\ &= TC_1 \mathbf{H}_1^+ + \sum_n' D_n \mathbf{H}_n^+ & z \geq z_2 \end{aligned} \tag{14.110b}$$

where the prime on the summation means exclusion of the dominant mode, Γ is the reflection coefficient, T is the transmission coefficient, and the C_n 's and D_n 's are unknown amplitude constants. It is assumed that the guide is terminated in a matched load at some point $z > z_2$, so no incident wave on the slot exists in the region $z \geq z_2$. The field multiplied by C_1 is the incident mode, while the

remaining terms give the modes excited by the slot. The normal mode functions are of the form

$$\mathbf{E}_n^\pm = [\mathbf{e}_n(x, y) \pm \mathbf{e}_{zn}(x, y)]e^{\mp\gamma_n z} \quad (14.111a)$$

$$\begin{aligned} \mathbf{H}_n^\pm &= [\pm \mathbf{h}_n(x, y) + \mathbf{h}_{zn}(x, y)]e^{\mp\gamma_n z} \\ &= [\pm Y_n \hat{\mathbf{z}} \times \mathbf{e}_n + \mathbf{h}_{zn}]e^{\mp\gamma_n z} \end{aligned} \quad (14.111b)$$

where \mathbf{e}_n and \mathbf{h}_n denote the x and y components, Y_n is the mode wave admittance, γ_n is the propagation constant, and n is a general summation index signifying a summation over the complete set of E and H modes. The modes are orthogonal, so that

$$\int_{S_0} \mathbf{e}_n \times \mathbf{h}_m \cdot \hat{\mathbf{z}} dS = 0 \quad n \neq m \quad (14.112a)$$

and are assumed normalized such that

$$\int_{S_0} \mathbf{e}_n \times \mathbf{h}_n \cdot \hat{\mathbf{z}} dS = 1 \quad (14.112b)$$

where the integration is over the guide cross section S_0 .

The Lorentz reciprocity theorem given in Chap. 1 may be applied to the total field in the waveguide and one of the normal modes to yield ($\hat{\mathbf{n}}$ is a unit outward normal)

$$\oint_S \mathbf{E} \times \mathbf{H}_n^+ \cdot \hat{\mathbf{n}} dS = \oint_S \mathbf{E}_n^+ \times \mathbf{H} \cdot \hat{\mathbf{n}} dS \quad (14.113)$$

where S is a closed surface consisting of the perfectly conducting interior waveguide surface, the aperture surface S_a of the slot, and cross section surfaces S_0 at $z = z_1$ and z_2 . On the waveguide walls $\hat{\mathbf{n}} \times \mathbf{E}$ and $\hat{\mathbf{n}} \times \mathbf{E}_n^+$ vanish, while on S_a we have $\hat{\mathbf{n}} \times \mathbf{E}_n^+ = 0$ but

$$\hat{\mathbf{n}} \times \mathbf{E} = \hat{\mathbf{n}} \times \hat{\mathbf{y}}_0 E_0 \sin \frac{\pi x_0}{l}$$

On the surface S_0 the total waveguide field is given by (14.110a) and (14.110b). If the orthogonality and normalization properties of the modes as given by (14.112) are used, it is readily found that (14.113) yields

$$C_n = \frac{E_0}{2} \int_{S_a} \hat{\mathbf{n}} \times \hat{\mathbf{y}}_0 \cdot \mathbf{H}_n^+ \sin \frac{\pi x_0}{l} dS \quad (14.114a)$$

In a similar way, by using the mode \mathbf{E}_n^- , \mathbf{H}_n^- in (14.113), we get

$$D_n = \frac{E_0}{2} \int_{S_a} \hat{\mathbf{n}} \times \hat{\mathbf{y}}_0 \cdot \mathbf{H}_n^- \sin \frac{\pi x_0}{l} dS \quad (14.114b)$$

The quantity $\hat{\mathbf{n}} \times \hat{\mathbf{y}}_0 E_0 \sin (\pi x_0 / l)$ is the equivalent magnetic current in the slot aperture and is directed along the slot, since $\hat{\mathbf{n}} = \hat{\mathbf{z}}_0$, so $\hat{\mathbf{z}}_0 \times \hat{\mathbf{y}}_0 = -\hat{\mathbf{x}}_0$. The expansion formulas (14.114) show that only those modes having a tangential magnetic field along the slot are excited. For an axial slot only TE

modes are excited, and since \mathbf{H}_n^+ and \mathbf{H}_n^- have an axial magnetic field with the same sign, $C_n = D_n$ and the slot behaves like a shunt element. (The transverse electric field is continuous across the plane of the slot.) For a transverse slot, $C_n = -D_n$ and the slot acts like a series element. (The transverse magnetic field is now continuous across the plane of the slot.)

The reflection coefficient Γ is clearly given by

$$\Gamma = \frac{-E_0}{2C_1} \int_{s_a} \hat{\mathbf{x}}_0 \cdot \mathbf{H}_1^+ \sin \frac{\pi x_0}{l} dS \quad (14.115a)$$

and the transmission coefficient T is found to be given by

$$T = 1 - \frac{E_0}{2C_1} \int_{s_a} \hat{\mathbf{x}}_0 \cdot \mathbf{H}_1^- \sin \frac{\pi x_0}{l} dS \quad (14.115b)$$

Exercise 14.1 Carry out the details leading to the results (14.114) and (14.115) for C_n and D_n and to the expressions for Γ and T .

If a resonant slot is assumed, then the radiated power equals $\frac{1}{2}G_r|E_0w|^2$ from the definition of G_r . The incident power minus the reflected power in the waveguide is $\frac{1}{2}|C_1|^2(1 - |\Gamma|^2)$ and must equal the radiated power plus the power transmitted past the slot. Thus we have

$$|C_1|^2(1 - |\Gamma|^2) = G_r|E_0w|^2 + |TC_1|^2 \quad (14.116)$$

This equation determines E_0 in terms of the arbitrary amplitude C_1 of the incident mode. The power in a waveguide mode is given by one-half of the amplitude squared because of the mode normalization (14.112b) which is employed here. When the slot acts like a shunt normalized conductance g in the guide, the reflected power it would produce is given by $\frac{1}{2}[g/(2 + g)]^2|C_1|^2$ and the power absorbed in g , which equals the radiated power, is given by

$$\frac{1}{2} \left(\frac{2}{2 + g} \right)^2 |C_1|^2 g = \frac{1}{2} |E_0w|^2 G_r \quad (14.117)$$

Exercise 14.2 For a normalized shunt conductance g across a transmission line terminated in a matched load show that the power absorbed in g is given by (14.117).

For a series slot with normalized resistance r the formula corresponding to (14.117) is

$$\left(\frac{2}{2 + r} \right)^2 |C_1|^2 r = |E_0w|^2 G_r \quad (14.118)$$

These latter two relations permit the normalized values of slot conductance or resistance to be found provided an assumption is made as regards the value of the radiation conductance G_r .

Broadwall Longitudinal Shunt Slot

Figure 14.32 illustrates a longitudinal slot in the broadwall of a rectangular guide. The slot is offset by an amount x_1 , is of length $\lambda_0/2$, and is assumed to be resonant. The width w is assumed to be very small.

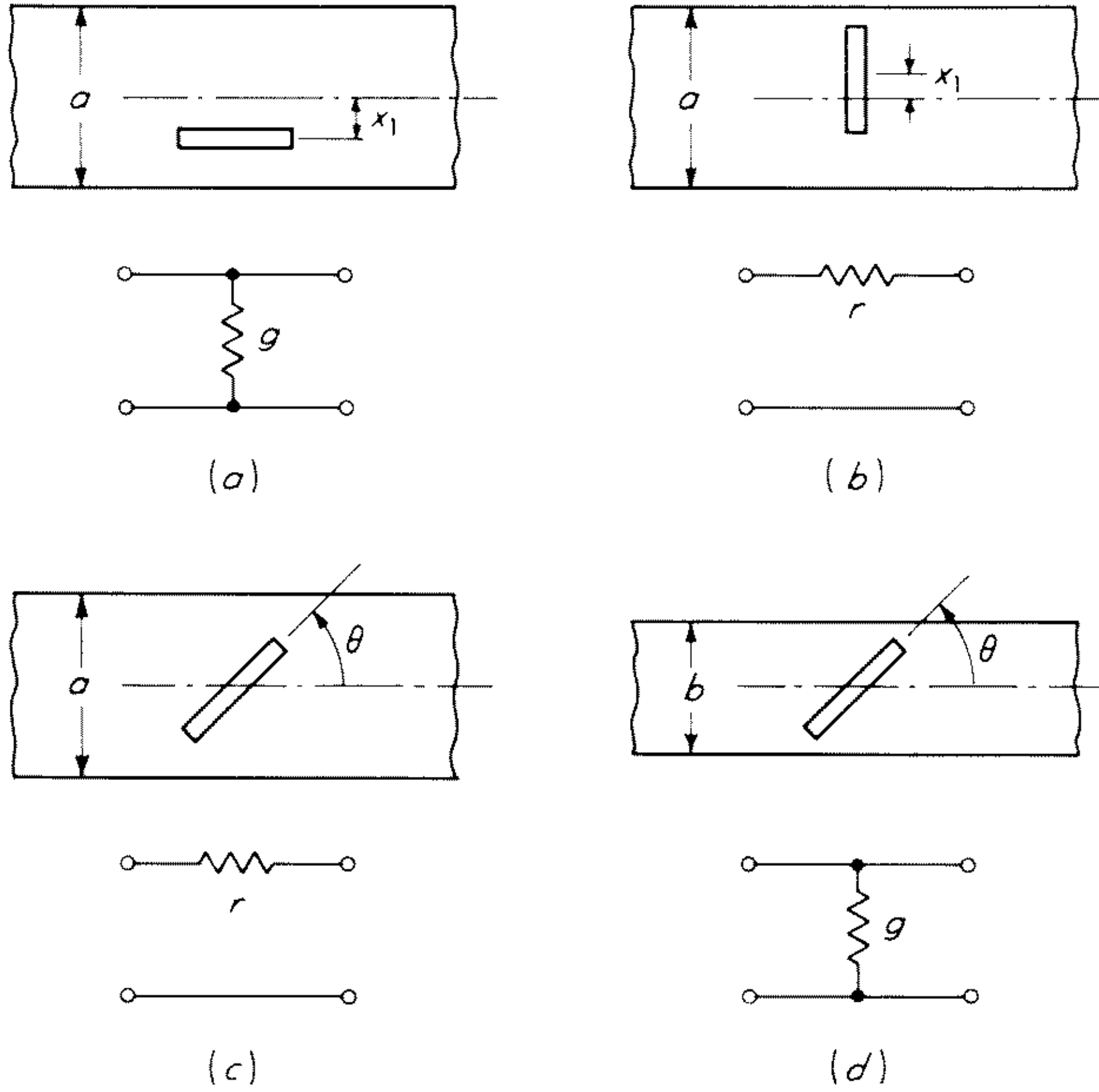


Fig. 14.32 Slots in a waveguide and their equivalent circuit at resonance. (a)–(c) Broadwall slots; (d) sidewall slot.

The fields for the normalized TE_{10} mode are

$$e_y = \frac{k_0 \zeta_0}{\beta} \sqrt{\frac{2\beta}{k_0 \zeta_0 ab}} \sin \frac{\pi x}{a} \quad (14.119a)$$

$$h_x = -\sqrt{\frac{2\beta}{k_0 \zeta_0 ab}} \sin \frac{\pi x}{a} \quad (14.119b)$$

$$h_z = \frac{j\pi}{a} \left(\frac{ab}{2} k_0 \beta \zeta_0 \right)^{-1/2} \cos \frac{\pi x}{a} \quad (14.119c)$$

where $\beta^2 = k_0^2 - (\pi/a)^2$. From (14.115) we find that $T = 1 + \Gamma$, so the slot acts as a shunt conductance g at resonance. Also from (14.115a) we obtain

$$\begin{aligned} \Gamma &= -\frac{E_0 w}{2C_1} \int_{-\lambda_0/4}^{\lambda_0/4} \frac{j\pi}{a} \left(\frac{ab}{2} k_0 \beta \zeta_0 \right)^{-1/2} \cos \frac{\pi}{a} \left(\frac{a}{2} - x_1 \right) e^{-j\beta z} \cos \frac{2\pi z}{\lambda_0} dz \\ &= -\frac{jE_0 w}{C_1} \frac{k_0 a}{\pi} \left(\frac{ab}{2} k_0 \beta \zeta_0 \right)^{-1/2} \sin \frac{\pi x_1}{a} \cos \frac{\pi}{2} \frac{\lambda_0}{\lambda_g} = -\frac{jE_0 w}{C_1} K \end{aligned} \quad (14.120)$$

where K is defined by this equation. From the equivalent circuit we get $\Gamma = -g/(1 + g)$, so Γ is real and negative. It is, therefore, apparent that

$wE_0 = -j|\Gamma|C_1/K$, which shows that the slot field is 90° out of phase with the equivalent voltage in the waveguide, the latter being proportional to $(1 + \Gamma)C_1$. This is the phase relationship which was used in Sec. 14.8. If the slot is offset on the other side of the centerline, wE_0 changes sign.

The conservation of power relation (14.116) gives

$$2A^2G_r = -2A^2K + 2AK$$

$$A = \frac{2K}{G_r + 2K^2} = \frac{2K/\sqrt{G_r}}{\sqrt{G_r}(1 + 2K^2/G_r)} \quad (14.121)$$

where $A = jwE_0/C_1$. From (14.117) we also obtain

$$A = \frac{2\sqrt{g}}{\sqrt{G_r}(2 + g)} \frac{2(1/\sqrt{g})}{\sqrt{G_r}(1 + 2/g)} = \frac{2(\sqrt{g}/2)}{\sqrt{G_r}(1 + 2g/4)} \quad (14.122)$$

By comparing (14.121) and (14.122), we see that there are two possible solutions for g , namely, $g = G_r/K^2$ and $g = 4K^2/G_r$. Only the second solution is physically acceptable, since g must vanish when K equals zero. From (14.120) it is now readily found that

$$g = \frac{480}{73.13\pi} \frac{\lambda_g a}{\lambda_0 b} \sin^2 \frac{\pi x_1}{a} \cos^2 \frac{\pi \lambda_0}{2\lambda_g} \quad (14.123)$$

where we have chosen $G_r = 2 \times 73.13/\zeta_0^2 = 1.03$ mmhos.

In a similar manner the resonant conductance or resistance of the other slot configurations given in Fig. 14.32 can be evaluated. The final results are given below.

Offset Transverse Broadwall Slot

$$r = 0.523 \left(\frac{\lambda_g}{\lambda_0} \right)^3 \frac{\lambda_0^2}{ab} \cos^2 \frac{\pi \lambda_0}{4a} \cos^2 \frac{\pi x_1}{a} \quad (14.124)$$

Centered Broadwall Slot

$$r = 0.131 \frac{\lambda_0^3}{\lambda_g ab} \left[F_1(\theta) \sin \theta + \frac{\lambda_g}{2a} F_2(\theta) \cos \theta \right]^2 \quad (14.125)$$

where

$$\left. \begin{matrix} F_1 \\ F_2 \end{matrix} \right\} = \frac{\cos (\pi \xi / 2)}{1 - \xi^2} \pm \frac{\cos (\pi \eta / 2)}{1 - \eta^2}$$

$$\left. \begin{matrix} \xi \\ \eta \end{matrix} \right\} = \frac{\lambda_0}{\lambda_g} \cos \theta \mp \frac{\lambda_0}{2a} \sin \theta$$

Centered Inclined Sidewall Slot

$$g = 0.13 \frac{\lambda_g \lambda_0^3}{a^3 b} \left\{ \frac{\sin \theta \cos [(\pi \lambda_0 / 2 \lambda_g) \sin \theta]}{1 - [(\lambda_0 / \lambda_g) \sin \theta]^2} \right\}^2 \quad (14.126)$$

14.10 Variational Method for Slot Impedance

In this section we shall formulate the variational method for evaluating the impedance of a radiating slot located in a rectangular guide in which only the dominant TE_{10} mode can propagate. The procedure used is similar to that discussed in Refs. 51 to 53.

In order to formulate the variational expressions for slot impedance we require the Green's dyadic giving the magnetic field radiated by a unit magnetic current source. Note that an aperture electric field \mathbf{E}_a can be regarded as an equivalent magnetic current $-\hat{\mathbf{n}} \times \mathbf{E}_a$, where $\hat{\mathbf{n}}$ points into the region of interest.

With reference to Fig. 14.28 let \mathbf{G}^i be so defined that

$$\mathbf{H}(\mathbf{r}) = \int_S \mathbf{G}^i(\mathbf{r}|\mathbf{r}') \cdot \mathbf{J}_{ms}(\mathbf{r}') dS' \quad (14.127)$$

is the magnetic field radiated into the waveguide by the magnetic current \mathbf{J}_{ms} . If $\mathbf{J}_{ms} = \hat{\mathbf{a}}\delta(x - x')\delta(y - y')\delta(z - z')$, we get $\mathbf{H}(\mathbf{r}) = \mathbf{G}^i \cdot \hat{\mathbf{a}}$. But this field is also given by the expansion (14.110b), so we can write

$$\mathbf{H} = \begin{cases} \sum_n C_n \mathbf{H}_n^- & z < z' \\ \sum_n D_n \mathbf{H}_n^+ & z > z' \end{cases}$$

where, from (14.114),

$$\begin{aligned} C_n &= \frac{1}{2} \mathbf{H}_n^+(x', y', z') \cdot \hat{\mathbf{a}} \\ D_n &= \frac{1}{2} \mathbf{H}_n^-(x', y', z') \cdot \hat{\mathbf{a}} \end{aligned}$$

Thus we have

$$\mathbf{G}^i \cdot \hat{\mathbf{a}} = \begin{cases} \frac{1}{2} \sum_n \mathbf{H}_n^-(\mathbf{r}) \mathbf{H}_n^+(\mathbf{r}') \cdot \hat{\mathbf{a}} & z < z' \\ \frac{1}{2} \sum_n \mathbf{H}_n^+(\mathbf{r}) \mathbf{H}_n^-(\mathbf{r}') \cdot \hat{\mathbf{a}} & z > z' \end{cases}$$

Since $\hat{\mathbf{a}}$ is arbitrary, we see that the required Green's dyadic for the interior of the waveguide is given by

$$\mathbf{G}^i(\mathbf{r}|\mathbf{r}') = \begin{cases} \frac{1}{2} \sum_n \mathbf{H}_n^-(\mathbf{r}) \mathbf{H}_n^+(\mathbf{r}') & z < z' \\ \frac{1}{2} \sum_n \mathbf{H}_n^+(\mathbf{r}) \mathbf{H}_n^-(\mathbf{r}') & z > z' \end{cases} \quad (14.128)$$

For the exterior region we shall assume that an infinite perfectly conducting baffle is placed in the aperture plane outside the region occupied by the slot. Thus we require the half-space Green's dyadic \mathbf{G}^e for the exterior region. By definition

$$\mathbf{H} = \int_S \mathbf{G}^e \cdot \mathbf{J}_{ms} dS'$$

gives the magnetic field in the external region. But by image theory we have

$$\mathbf{H} = \int_S \mathbf{G} \cdot (2\mathbf{J}_{ms}) dS'$$

where \mathbf{G} is the free space dyadic for the magnetic field, and hence $\mathbf{G}^e = 2\mathbf{G}$. In terms of the magnetic vector potential we can write, from (1.61b),

$$\mathbf{H} = -j\omega\mathbf{A}_m + \frac{\nabla\nabla \cdot \mathbf{A}_m}{j\omega\mu_0\epsilon_0}$$

where, by (1.62a),

$$\nabla^2\mathbf{A}_m + k_0^2\mathbf{A}_m = -\epsilon_0\mathbf{J}_m$$

By comparing (1.60b) and (1.58) and using the analogy with (2.35) giving the electric field Green's dyadic, we see that

$$\mathbf{G}^e = -j\omega\epsilon_0 2 \left(\mathbf{I} + \frac{\nabla\nabla}{k_0^2} \right) \frac{e^{-jk_0R}}{4\pi R} \quad (14.129)$$

For a slot in a rectangular guide as shown in Fig. 14.28 let the incident dominant mode fields be

$$\mathbf{E}_{\text{inc}} = V_1^+ Y_1 \mathbf{e}_1 e^{-j\beta z} + V_2^+ Y_1 \mathbf{e}_1 e^{j\beta z} \quad (14.130a)$$

$$\mathbf{H}_{\text{inc}} = I_1^+ (\mathbf{h}_1 + \mathbf{h}_{z1}) e^{-j\beta z} + I_2^+ (-\mathbf{h}_1 + \mathbf{h}_{z1}) e^{j\beta z} \quad (14.130b)$$

where the dominant mode functions are given by (14.119). The fields proportional to I_1^+ and V_1^+ are incident from $z < z_1$, while those proportional to I_2^+ and V_2^+ come from the region $z > z_2$. The presence of the slot will give rise to the following additional scattered dominant mode fields:

$$\mathbf{E}_s = \begin{cases} V_{1s}^- Y_1 \mathbf{e}_1 e^{j\beta z} & z < z_1 \\ V_{2s}^- Y_1 \mathbf{e}_1 e^{-j\beta z} & z > z_2 \end{cases} \quad (14.131a)$$

$$\mathbf{H}_s = \begin{cases} I_{1s}^- (-\mathbf{h}_1 + \mathbf{h}_{z1}) e^{j\beta z} & z < z_1 \\ I_{2s}^- (\mathbf{h}_1 + \mathbf{h}_{z1}) e^{-j\beta z} & z > z_1 \end{cases} \quad (14.131b)$$

In view of the mode definitions and normalization employed [see (14.111)], the voltage and current amplitudes satisfy the relations

$$\begin{aligned} I_i^\pm &= Y_1 V_i^\pm \\ I_{is}^- &= Y_1 V_{is}^- \end{aligned} \quad i = 1, 2, \dots \quad (14.132)$$

where the mode admittance $Y_1 = \beta/k_0\zeta_0$. The positive sense of current flow has been chosen toward the slot on both sides of the slot.

It is readily verified from the above relations that the total dominant mode magnetic field may be expressed in the form

$$\begin{aligned} \mathbf{H}_1 &= \mathbf{h}_1 (I_1 \cos \beta z - jV_1 Y_1 \sin \beta z) \\ &\quad + \mathbf{h}_{z1} (V_1 Y_1 \cos \beta z - jI_1 \sin \beta z) \quad z < z_1 \end{aligned} \quad (14.133a)$$

$$\begin{aligned} \mathbf{H}_1 &= -\mathbf{h}_1 (I_2 \cos \beta z + jV_2 Y_1 \sin \beta z) \\ &\quad + \mathbf{h}_{z1} (V_2 Y_1 \cos \beta z + jI_2 \sin \beta z) \quad z > z_2 \end{aligned} \quad (14.133b)$$

where the total current and voltage amplitudes are given by $V_1 = V_1^+ + V_2^+ + V_{1s}^-$, $V_2 = V_1^+ + V_2^+ + V_{2s}^-$, $I_1 = I_1^+ - I_2^+ - I_{1s}^-$, and $I_2 = I_2^+ - I_1^+ - I_{2s}^-$.

Let the aperture electric field at the interior aperture surface of the slot be \mathbf{E}_a^i . The scattered magnetic field is then given by

$$\mathbf{H}_s = \int_S \mathbf{G}^i(\mathbf{r}|\mathbf{r}') \cdot \hat{\mathbf{y}}_0 \times \mathbf{E}_a^i(\mathbf{r}') dS' \quad (14.134)$$

It will be convenient to split \mathbf{G}^i into a resistive part and a reactive part. The resistive part comes only from the dominant-mode terms. The Green's dyadic satisfies the reciprocity relation

$$\mathbf{G}^i(\mathbf{r}|\mathbf{r}') = \mathbf{G}_t^i(\mathbf{r}'|\mathbf{r})$$

and the symmetry relation

$$\mathbf{G}^i(\mathbf{r}'|\mathbf{r}) = \mathbf{G}_t^i(\mathbf{r}|\mathbf{r}')$$

where the subscript t denotes the transposed dyadic. If we use the above relations, we can write the dominant-mode term of the Green's dyadic as the sum of a symmetrical and antisymmetrical dyadic. By using the definition (14.128), the reader can readily verify that the dominant-mode term can be expressed as

$$-\frac{1}{2}[\mathcal{H}_1(\mathbf{r})\mathcal{H}_1(\mathbf{r}') + \mathcal{H}_2(\mathbf{r})\mathcal{H}_2(\mathbf{r}')] + \frac{j}{2}sg(z - z')[\mathcal{H}_2(\mathbf{r})\mathcal{H}_1(\mathbf{r}') - \mathcal{H}_1(\mathbf{r})\mathcal{H}_2(\mathbf{r}')] \quad (14.135)$$

where the new modal functions are given by

$$\mathcal{H}_1(\mathbf{r}) = \mathbf{h}_1 \cos \beta z - j\mathbf{h}_{z1} \sin \beta z \quad (14.136a)$$

$$\mathcal{H}_2(\mathbf{r}) = \mathbf{h}_1 \sin \beta z + j\mathbf{h}_{z1} \cos \beta z \quad (14.136b)$$

and $sg(z - z') = -1$ for $z < z'$ and equals $+1$ for $z > z'$. The relationship between the new and old modal functions are as follows:

$$\begin{aligned} \mathcal{H}_1 &= \frac{1}{2}(\mathbf{H}_1^+ - \mathbf{H}_1^-) \\ \mathcal{H}_2 &= \frac{j}{2}(\mathbf{H}_1^+ + \mathbf{H}_1^-) \\ \mathbf{H}_1^+ &= \mathcal{H}_1 - j\mathcal{H}_2 \\ \mathbf{H}_1^- &= -(\mathcal{H}_1 + j\mathcal{H}_2) \end{aligned} \quad (14.137)$$

Since \mathbf{h}_{z1} is pure imaginary, both \mathcal{H}_1 and \mathcal{H}_2 are real. Thus the first term in (14.135) is real and symmetric and the second term is imaginary and anti-symmetric. The first term is the resistive part of the Green's dyadic.⁵⁷ We now let

$$j\mathbf{G}_R^i = \mathbf{G}^i + \frac{1}{2}(\mathcal{H}_1\mathcal{H}_1 + \mathcal{H}_2\mathcal{H}_2) \quad (14.138)$$

which defines the reactive part of the Green's dyadic.

By using (14.128), we find that the scattered dominant mode magnetic field is

$$\mathbf{H}_{1s}^- = \frac{1}{2}\mathbf{H}_1^-(\mathbf{r}) \int_S \mathbf{H}_1^+(\mathbf{r}') \cdot \hat{\mathbf{y}}_0 \times \mathbf{E}_a^i(\mathbf{r}') dS' \quad z < z_1 \quad (14.139a)$$

$$\mathbf{H}_{1s}^+ = \frac{1}{2}\mathbf{H}_1^+(\mathbf{r}) \int_S \mathbf{H}_1^-(\mathbf{r}') \cdot \hat{\mathbf{y}}_0 \times \mathbf{E}_a^i(\mathbf{r}') dS' \quad z > z_2 \quad (14.139b)$$

and hence

$$I_{1s}^- = \frac{1}{2} \int_S \mathbf{H}_1^+(\mathbf{r}') \cdot \hat{\mathbf{y}}_0 \times \mathbf{E}_a^i(\mathbf{r}') dS' \quad (14.140a)$$

$$I_{2s}^- = \frac{1}{2} \int_S \mathbf{H}_1^-(\mathbf{r}') \cdot \hat{\mathbf{y}}_0 \times \mathbf{E}_a^i(\mathbf{r}') dS' \quad (14.140b)$$

where the integration is over the slot aperture. Also from (14.134) and by using (14.135) and (14.138) we can write

$$\begin{aligned} & -\frac{1}{2}\mathfrak{H}_1(\mathbf{r}) \int_S \mathfrak{H}_1(\mathbf{r}') \cdot \hat{\mathbf{y}}_0 \times \mathbf{E}_a^i dS' - \frac{1}{2}\mathfrak{H}_2(\mathbf{r}) \int_S \mathfrak{H}_2(\mathbf{r}') \cdot \hat{\mathbf{y}}_0 \times \mathbf{E}_a^i dS' \\ & \quad + j \int_S \mathbf{G}_R^i \cdot \hat{\mathbf{y}}_0 \times \mathbf{E}_a^i dS' \end{aligned}$$

for the total scattered magnetic field. If we now eliminate \mathfrak{H}_1 and \mathfrak{H}_2 by using (14.137), introduce I_{1s}^- and I_{2s}^- from (14.140), and include the incident magnetic field also, we find that the total magnetic field in the guide can be expressed in the form

$$\begin{aligned} & \frac{1}{2}\mathbf{h}_1(I_1 \cos \beta z - jV_1Y_1 \sin \beta z - I_2 \cos \beta z - jV_2Y_1 \sin \beta z) \\ & \quad + \frac{1}{2}\mathbf{h}_{21}(V_1Y_1 \cos \beta z - jI_1 \sin \beta z + V_2Y_1 \cos \beta z + jI_2 \sin \beta z) \\ & \quad + j \int_S \mathbf{G}_R^i \cdot \hat{\mathbf{y}}_0 \times \mathbf{E}_a^i dS' \\ & = \frac{1}{2}(I_1 - I_2)\mathfrak{H}_1 - \frac{j}{2}Y_1(V_1 + V_2)\mathfrak{H}_2 + j \int_S \mathbf{G}_R^i \cdot \hat{\mathbf{y}}_0 \times \mathbf{E}_a^i dS' \quad (14.141) \end{aligned}$$

$$\text{because } -\frac{1}{2} \int_S (\mathfrak{H}_1\mathfrak{H}_2 + \mathfrak{H}_2\mathfrak{H}_1) \cdot \hat{\mathbf{y}}_0 \times \mathbf{E}_a^i dS' = \frac{1}{2}I_{1s}^-\mathbf{H}_1^- + \frac{1}{2}I_{2s}^-\mathbf{H}_1^+$$

as is readily shown by using (14.137). The last form in (14.141) is obtained by expressing \mathbf{H}_1^\pm in terms of \mathfrak{H}_1 and \mathfrak{H}_2 .

For a guide with an infinitely thin wall the external aperture field $\mathbf{E}_a^e = \mathbf{E}_a^i = \mathbf{E}_a$ and the external magnetic field is given by

$$\int_S \mathbf{G}^e \cdot (-\hat{\mathbf{y}}_0) \times \mathbf{E}_a dS'$$

By imposing the continuity condition for the magnetic field in the aperture, we obtain

$$\frac{1}{2}(I_1 - I_2)\mathfrak{H}_1 - \frac{j}{2}Y_1(V_1 + V_2)\mathfrak{H}_2 = - \int_S (j\mathbf{G}_R^i + \mathbf{G}^e) \cdot \hat{\mathbf{y}}_0 \times \mathbf{E}_a dS' \quad (14.142)$$

which is the basic integral equation for the aperture field. This relation is also the starting point for the variational formulas given by Oliner.

If we have a longitudinal slot which acts as a shunt element, we can choose $V_1 = V_2 = V$, and then $I_1 = I_2 = I$ from symmetry considerations. Thus we get

$$jY_1V\mathfrak{K}_2 = \int_S (j\mathbf{G}_{R^i} + \mathbf{G}^e) \cdot \hat{\mathbf{y}}_0 \times \mathbf{E}_a dS' \quad (14.143)$$

Before proceeding further, we must obtain an expression for the total current I . For $z \rightarrow \infty$ the total dominant mode field is given by (14.133b). By comparing with (14.141), we see that the dominant-mode reactive part of the Green's dyadic, as given by the second term in (14.135), must yield the result

$$\begin{aligned} \frac{j}{2} \int_S (\mathfrak{K}_2\mathfrak{K}_1 - \mathfrak{K}_1\mathfrak{K}_2) \cdot \hat{\mathbf{y}}_0 \times \mathbf{E}_a dS' &= \frac{1}{2}I_{2s}^-\mathbf{H}_1^+ - \frac{1}{2}I_{1s}^-\mathbf{H}_1^- \\ &= -\frac{1}{2}I_1\mathfrak{K}_1 + \frac{j}{2}Y_1V_1\mathfrak{K}_2 - \frac{1}{2}I_2\mathfrak{K}_1 - \frac{j}{2}Y_1V_2\mathfrak{K}_2 \end{aligned} \quad (14.144)$$

Note that the first two terms on the right cancel the terms multiplied by I_1 and V_1 in (14.141) and the last two terms are equal to one-half of the field given by (14.133b). When we equate the coefficients multiplying the $\cos \beta z$ and $\sin \beta z$ terms on both sides of (14.144), we obtain the following fundamental results, which were first given by Marcuvitz and Schwinger.⁵⁷

$$I_1 + I_2 = j \int_S \mathfrak{K}_2 \cdot \hat{\mathbf{y}}_0 \times \mathbf{E}_a dS' \quad (14.145a)$$

$$(V_1 + V_2)Y_1 = \int_S \mathfrak{K}_1 \cdot \hat{\mathbf{y}}_0 \times \mathbf{E}_a dS' \quad (14.145b)$$

For a shunt slot we have $I_1 = I_2 = I$, and thus

$$2I = j \int_S \mathfrak{K}_2 \cdot \hat{\mathbf{y}}_0 \times \mathbf{E}_a dS' \quad (14.146)$$

If we divide both sides of (14.143) by

$$\left(\int_S \mathfrak{K}_2 \cdot \hat{\mathbf{y}}_0 \times \mathbf{E}_a dS' \right)^2$$

introduce the current I from (14.146), and also scalar-multiply the numerator by $\hat{\mathbf{y}}_0 \times \mathbf{E}_a$ and integrate over the aperture, we obtain

$$\frac{V}{2I} = R + jX = - \frac{\int_S \int_S \hat{\mathbf{y}}_0 \times \mathbf{E}_a \cdot (j\mathbf{G}_{R^i} + \mathbf{G}^e) \cdot \hat{\mathbf{y}}_0 \times \mathbf{E}_a dS' dS}{Y_1 \left(\int_S \mathfrak{K}_2 \cdot \hat{\mathbf{y}}_0 \times \mathbf{E}_a dS \right)^2} \quad (14.147)$$

This is the required variational expression for the impedance of a longitudinal i.e., a shunt, slot. A first-order approximation to the aperture field \mathbf{E}_a will yield a second-order approximation for the impedance $R + jX$. The way in which (14.147) is employed in practice is the same as for the calculation of antenna impedance by variational methods as described in Sec. 2.9.

For the case of a series slot we choose $V_1 = -V_2 = V$ and by symmetry $I_1 = -I_2 = I$. By using (14.142) and (14.145) it is readily found that

$$\frac{I}{2V} = G + jB = -Y_1 \frac{\int_S \int_S \hat{\mathbf{y}}_0 \times \mathbf{E}_a \cdot (j\mathbf{G}_R^i + \mathbf{G}^e) \cdot \hat{\mathbf{y}}_0 \times \mathbf{E}_a dS' dS}{\left(\int_S \mathfrak{K}_1 \cdot \hat{\mathbf{y}}_0 \times \mathbf{E}_a dS \right)^2} \quad (14.148)$$

is a variational expression for the impedance of a series slot.

When the slot thickness cannot be neglected, $\mathbf{E}_a^i \neq \mathbf{E}_a^e$. The slot field may be expressed in terms of the waveguide modes in the slot; i.e., let

$$\mathbf{E}_a^i = \hat{\mathbf{y}}_0 \sum_m a_m \sin \frac{m\pi y_0}{l} \quad z_0 = 0$$

$$\mathbf{H}_a^i = \hat{\mathbf{x}}_0 \sum_m b_m \sin \frac{m\pi y_0}{l} \quad z_0 = 0$$

then by transmission line theory

$$\begin{aligned} \mathbf{E}_a^e &= \hat{\mathbf{y}}_0 \sum_m \left(a_m \cosh \Gamma_m t + j \frac{\omega\mu_0}{\Gamma_m} b_m \sinh \Gamma_m t \right) \sin \frac{m\pi y_0}{l} \\ \mathbf{H}_a^e &= \hat{\mathbf{x}}_0 \sum_m \left(-\frac{j\Gamma_m}{\omega\mu_0} a_m \sinh \Gamma_m t + b_m \cosh \Gamma_m t \right) \sin \frac{m\pi y_0}{l} \end{aligned}$$

and is the tangential aperture fields at $z_0 = t$. In the above we have assumed that the aperture fields are predominantly TE_{m0} modes, since they are the only modes which strongly couple the interior and exterior regions as discussed at the beginning of Sec. 14.9. The basic integral equation (14.142) must now be replaced by the following:

$$\frac{1}{2}(I_1 - I_2)\mathfrak{K}_1 - \frac{j}{2}Y_1(V_1 + V_2)\mathfrak{K}_2 + j \int_S \mathbf{G}_R^i \cdot \hat{\mathbf{y}}_0 \times \mathbf{E}_a^i dS' = \mathbf{H}_a^i \quad (14.149a)$$

$$- \int_S \mathbf{G}^e \cdot \hat{\mathbf{y}}_0 \times \mathbf{E}_a^e dS' = \mathbf{H}_a^e \quad (14.149b)$$

The above variational expressions for slot impedance have not, by any means, been fully exploited. A number of calculations have been made by the group at Brooklyn Polytechnic Institute, but the details and results are too lengthy for inclusion here. (See Ref. 53 for a summary of the main results obtained.)

PROBLEMS

14.1 Carry out the details leading to the residue series for E_ϕ given by (14.73).

14.2 Consider the simplified nonresonant array design procedure given in Sec. 14.8, but assume that the waveguide is lossy with an attenuation of α nepers/m. Show that in place of (14.101) the normalized conductance is given by

$$g(z) = \frac{(1 - re^{2\alpha L})P(z)e^{2\alpha z}}{\int_0^L P(z)e^{2\alpha z} dz - (1 - re^{2\alpha L}) \int_0^z P(z)e^{2\alpha z} dz}$$

Hint: The rate of loss of available power is given by

$$\frac{dP_a}{dz} = -gP_a - 2\alpha P_a$$

which may be written as

$$\frac{d}{dz} (P_a e^{2\alpha z}) = -gP_a$$

The solution of this equation is $P_a e^{2\alpha z} = 1 - \int_0^z P_a g dz$, where the available power at $z = 0$ is unity. At $z = L$ the available power for the termination is r . Also $P_a g = KP$, where K may be found from the condition $P_a(L) = r$. By replacing $P_a g$ in the integral for P_a by KP and using this in the expression for g , the desired result is obtained.

14.3 Show that for discrete elements in a lossy waveguide the results corresponding to (14.103) for the slot conductances g_n are

$$\begin{aligned} g_n &= \frac{P_n}{\sum_{i=n}^N P_i e^{2\alpha d(i-n)} + r e^{2(N-n+1)\alpha d}} \\ &= \frac{e^{2\alpha(n-1)d} P_n}{1 - \sum_{i=1}^{n-1} P_i e^{2\alpha d(i-1)}} \end{aligned}$$

where the incident power at the first slot is unity and r is the power dissipated in the termination a distance d beyond the last slot.

14.4 Design a five-element longitudinal slot array with a beam angle of 30° in the forward direction. A Chebyshev aperture distribution with 20-db side lobes is called for. The frequency of operation is 9,600 MHz. Specify the waveguide width, slot spacing, and slot susceptance. Assume a matched termination which dissipates an amount of power equal to 25 percent of the radiated power. Use the design procedure based on (14.105) to (14.109), but assume zero waveguide loss, i.e., $\alpha = 0$. What is the input VSWR to the array and the efficiency?

14.5 Determine the slot conductance required to yield a triangular aperture distribution for a 10-element array. Use the simplified design procedure based on (14.103). Specify the fraction r of the power to be dissipated in the load in order that the largest conductance does not exceed 0.3. Choose the $\sqrt{P_n}$ proportional to the numbers in the sequence, 1,2,3,4,5,5,4,3,2,1.

14.6 Fill in the details leading to Eqs. (14.133), (14.135), and (14.141).

14.7 Show that a variation $\delta \mathbf{E}_a$ in \mathbf{E}_a produces no first-order change in $R + jX$ as given by (14.147), and thus verify that this is a variational or stationary expression for the impedance. Hint: In the proof you will need to use the property

$$j\mathbf{G}_R^i(\mathbf{r}|\mathbf{r}') + \mathbf{G}^e(\mathbf{r}|\mathbf{r}') = j\mathbf{G}_{Rt}^i(\mathbf{r}'|\mathbf{r}) + \mathbf{G}_t^e(\mathbf{r}'|\mathbf{r})$$

REFERENCES

1. Harrington, R. F.: "Time-harmonic Electromagnetic Fields," pp. 98ff., McGraw-Hill Book Company, New York, 1961.
2. Booker, H. G.: Slot Aerials and Their Relation to Complementary Wire Aerials

- (Babinet's Principle), *J. Inst. Elec. Engrs. (London)*, part IIIA, vol. 93, pp. 620–626, 1946.
3. Harrington, R. F.: Ref. 1, p. 365.
 4. G. Sinclair, The Patterns of Slotted-cylinder Antennas, *Proc. IRE*, vol. 36, pp. 1487–1492, December, 1948.
 5. Papas, C. H.: On the Infinitely Long Cylindrical Antenna, *J. Appl. Phys.*, vol. 20, pp. 437–440, May, 1949.
 6. Papas, C. H.: Radiation from a Transverse Slot in an Infinite Cylinder, *J. Math. Phys.*, vol. 28, pp. 227–236, January, 1950.
 7. Silver, S., and W. K. Saunders: The External Field Produced by a Slot in an Infinite Circular Cylinder, *J. Appl. Phys.*, vol. 21, pp. 153–158, February, 1950.
 8. Silver, S., and W. K. Saunders: The Radiation from a Transverse Rectangular Slot in a Circular Cylinder, *J. Appl. Phys.*, vol. 21, pp. 745–749, August, 1950.
 9. Wait, J. R., and S. Kahana: Calculated Patterns of Circumferential Slots on a Circular Conducting Cylinder, *Can. J. Tech.*, vol. 33, pp. 77–79, January, 1955.
 10. Bailin, L. L.: The Radiation Field Produced by a Slot in a Large Circular Cylinder, *IRE Trans. Antennas Propagation*, vol. AP-3, pp. 128–137, July, 1955.
 11. Wait, J. R.: Radiation Characteristics of Axial Slots on a Conducting Cylinder, *Wireless Engr.*, vol. 32, pp. 316–323, December, 1955.
 12. Wait, J. R.: Pattern of a Flush-mounted Microwave Antenna, *J. Res. Natl. Bur. Std. (U.S.)*, vol. 59, pp. 255–259, October, 1957.
 13. Wait, J. R., and J. Kates: Radiation Patterns of Circumferential Slots on Moderately Large Conducting Cylinders, *Proc. Inst. Elec. Engrs. (London)*, vol. 103, part C, (monograph 167R, republished), pp. 289–296, September, 1956.
 14. Wait, J. R.: "Electromagnetic Radiation from Cylindrical Structures," Pergamon Press, New York, 1959.
 15. Stratton, J. A.: "Electromagnetic Theory," chap. VI, McGraw-Hill Book Company, New York, 1941.
 16. Stratton, J. A.: Ref. 15, p. 359.
 17. Watson, G. N.: The Diffraction of Electric Waves by the Earth, *Proc. Roy. Soc. London*, vol. A95, pp. 83–99, 1918; The Transmission of Electric Waves around the Earth, *ibid.*, vol. A96, pp. 546–563, 1919.
 18. The proof of this for an infinite axial slot is given in Ref. 14, chap. 8.
 19. Ref. 14, Chap. 8. See also Ref. 13.
 20. Sensiper, S.: Cylindrical Radio Waves, *Hughes Aircraft Tech. Mem.* 310, June 15, 1953. See also, S. Sensiper, Cylindrical Radio Waves, *IRE Trans. Antennas Propagation*, vol. AP-5, pp. 56–70, January, 1957.
 21. See Ref. 14, chap. 8.
 22. Mushiake, Y., and R. E. Webster: Radiation Characteristics with Power Gain for Slots on a Sphere, *IRE Trans. Antennas Propagation*, vol. AP-5, pp. 47–55, January, 1957.
 23. Hansen, R. C.: "Microwave Scanning Antennas," vol. III, Academic Press Inc., New York, 1966.
 24. Dion, A.: Nonresonant Slotted Arrays, *IRE Trans. Antennas Propagation*, vol. AP-6, pp. 360–365, October, 1958.
 25. Gruenberg, H.: Second Order Beams of Slotted Waveguide Arrays, *Can. J. Phys.*, vol. 31, pp. 55–69, January, 1953.
 26. Kurtz, L. A., and Yu, J. S.: Second-order Beams of Two-dimensional Slot Arrays, *IRE Trans. Antennas Propagation*, vol. AP-5, pp. 356–362, October, 1957.
 27. McCormick, G. C.: A Two-dimensional Slotted Array, *IRE Trans. Antennas Propagation*, vol. AP-6, pp. 26–35, January, 1958.
 28. McCormick, G. C.: The Effect of the Size of a Two-dimensional Array on Second-order Beams, *IRE Trans. Antennas Propagation*, vol. AP-6, pp. 297–298, July, 1958.

29. Silver, S.: "Microwave Antenna Theory and Design," McGraw-Hill Book Company, New York, 1949.
30. Tang, R.: A Slot with Variable Coupling and Its Application to a Linear Array, *IRE Trans. Antennas Propagation*, vol. AP-8, pp. 97-101, January, 1960.
31. Dudley, D. G., Jr.: An Iris-excited Slot Radiator in the Narrow Wall of Rectangular Waveguide, *IRE Trans. Antennas Propagation*, vol. AP-9, pp. 361-364, July, 1961.
32. Kaminow, I. P., and R. J. Stegen: Waveguide Slot Array Design, *Hughes Aircraft Tech Mem.* 348, Culver City, Calif., July 1, 1954.
33. Jasik, H. (ed.): "Antenna Engineering Handbook," chap. 9, McGraw-Hill Book Company, New York, 1961.
34. Watson, W. H.: "Waveguide Transmission and Antenna Systems," Oxford University Press, New York, 1947.
35. Cullen, A. L., and F. K. Goward: The Design of a Waveguide-fed Array of Slots to Give a Specified Radiation Pattern, *J. Inst. Elec. Engrs. (London)*, vol. 93, pp. 683-692, 1946.
36. Gruenberg, H.: A Waveguide Array for Solar Noise Studies, *IRE Trans. Antennas Propagation*, vol. AP-3, pp. 147-152, October, 1954.
37. Miller, J. R., and R. J. Forman: A Planar Slot Array with Four Independent Beams, *IEEE Trans. Antennas Propagation*, vol. AP-14, pp. 560-566, September, 1966.
38. Simmons, A. J., O. M. Giddings, M. Diamond, and J. Gindsberg: A Multiple-beam Two-dimensional Waveguide Slot Array, *IEEE Intern. Conv. Record*, part 1, pp. 56-69, 1963.
39. Goebels, F. J., and T. S. Fong: Four Independent Beams from a Single Linear Array, *IEEE Trans. Antennas Propagation*, vol. AP-13, pp. 683-691, September, 1965.
40. Coe, R. J., and G. Held: A Parasitic Slot Array, *IEEE Trans. Antennas Propagation*, vol. AP-12, pp. 10-16, January, 1964.
41. Goodrich, R. F., et al.: Radiation from Slot Arrays on Cones, *IRE Trans. Antennas Propagation*, vol. AP-7, pp. 213-222, July, 1959.
42. Hu, A. Y., and C. D. Lunden: Snake-feed Microstrip Slot Array, *Microwave J.*, vol. 6, pp. 70-73, December, 1963.
43. Hu, A. Y., and C. D. Lunden: Rectangular-ridge Waveguide Slot Array, *IRE Trans. Antennas Propagation*, vol. AP-9, pp. 102-105, January, 1961.
44. Ramsay, J. F., and B. V. Popovich: Series-slotted Waveguide Array Antennas, *IEEE Intern. Conv. Record*, part 1, pp. 30-55, 1963.
45. Ehrlich, J. J., and J. Short: Mutual Coupling Considerations in Linear Slot Array Design, *Proc. IRE*, vol. 42, pp. 956-961, June, 1954.
46. Edelberg, S., and A. A. Oliner: Mutual Coupling Effects in Large Antenna Arrays, Part I. Slot Arrays, *IRE Trans. Antennas Propagation*, vol. AP-8, pp. 286-297, May, 1960. Part II. Compensation Effects, *ibid.*, pp. 360-367, July, 1960.
47. Kay, A. F., and A. J. Simmons: Mutual Coupling of Shunt Slots, *IRE Trans. Antennas Propagation*, vol. AP-8, pp. 389-400, July, 1960.
48. Stevenson, A. F.: Theory of Slots in Rectangular Waveguides, *J. Appl. Phys.*, vol. 19, pp. 24-38, January, 1948.
49. Gruenberg, H.: Theory of Wave-guide Fed Slots Radiating into Parallel-plate Regions, *J. Appl. Phys.*, vol. 23, pp. 733-737, July, 1952.
50. Wait, J. R.: On the Conductance of Slots, *IRE Trans. Antennas Propagation*, vol. AP-4, pp. 124-127, April, 1956. This paper contains several references to other, related work.
51. Oliner, A. A.: Equivalent Circuits for Slots in Rectangular Waveguide, *Microwave Res. Inst. Rept.*, Contract AF19(122)-3, Polytechnic Institute of Brooklyn, August, 1951.
52. Oliner, A. A.: Theoretical and Experimental Investigations in Electromagnetic Diffraction and Microwave Networks, *Final Rept. R-347-53, PIB-281*, Contract No.

AF19(122)-3, Polytechnic Institute of Brooklyn, Nov. 20, 1953. This report summarizes the extensive work on slots carried out by the group at the Microwave Research Institute.

53. Oliner, A. A.: The Impedance Properties of Narrow Radiating Slots in the Broad Face of Rectangular Waveguide, *IRE Trans. Antennas Propagation*, vol. AP-5, pp. 1-20, January, 1957.
54. Felsen, L. B.: Analysis of a Terminated-waveguide Slot Antenna by an Equivalent Circuit Method, *Rept. R-400-54, PIB-333*, Polytechnic Institute of Brooklyn, September, 1954.
55. Felsen, L. B., and N. Marcuvitz: Slot Coupling of Rectangular and Spherical Waveguides, *J. Appl. Phys.*, vol. 24, pp. 755-770, June, 1953.
56. Collin, R. E.: "Field Theory of Guided Waves," sec. 5.6, McGraw-Hill Book Company, New York, 1960.
57. Marcuvitz, N., and J. Schwinger: On the Representation of the Electric and Magnetic Fields Produced by Currents and Discontinuities in Wave Guides, *J. Appl. Phys.*, vol. 22, pp. 806-819, June, 1951.

CHAPTER 15

OPEN WAVEGUIDES AND SMALL HORNS

R. T. Compton, Jr. and R. E. Collin

15.1 Introduction

Open waveguides and small horns are often used for antennas when a simple structure having modest gain is required. In particular, waveguide radiators and small horns are extensively used as primary antennas to illuminate reflectors and lenses. A small horn is essentially a waveguide with one end flared to increase the aperture area and hence the gain. The flaring also provides a smoother transition between the guide and free space and consequently a better match. Horns and waveguides are relatively broad-band antennas and are preferred from this point of view over dipole radiators excited by slotted coaxial line feeds.

The radiation from open waveguides may be calculated exactly by the Wiener-Hopf method provided certain realistic assumptions such as (1) semi-infinitely long guide, (2) infinitely thin waveguide walls, (3) cross sections that coincide with a single constant-coordinate curve, e.g., circular guide, and (4) infinite conductivity, are made. Condition (4) can be relaxed by using a surface impedance to account for finite conductivity, but the additional complications in the analysis probably do not warrant this refinement.

Exact solutions for radiation from horns are not available, so the usual approach is based on an assumed aperture field. In the next section we derive the exact solution for radiation from a parallel-plate guide in order to illustrate the significant features of the Wiener-Hopf technique. This is followed by a presentation of the results which have been obtained for circular guides. The remaining sections deal with radiation from horns.

15.2 Radiation from a Parallel-plate Guide

Perpendicular Polarization

The problem of radiation from a parallel-plate waveguide was solved by Heins in 1948 and independently in Russia in the same year by Vajnshtejn.^{1,2} An account of the theory, as well as a detailed discussion of the Wiener-Hopf method along with many other applications, may be found in Noble's book.³

Figure 15.1 illustrates a parallel-plate waveguide consisting of perfectly conducting, infinitely thin plates extending from $-\infty \leq y \leq \infty$, $-\infty \leq x \leq 0$,

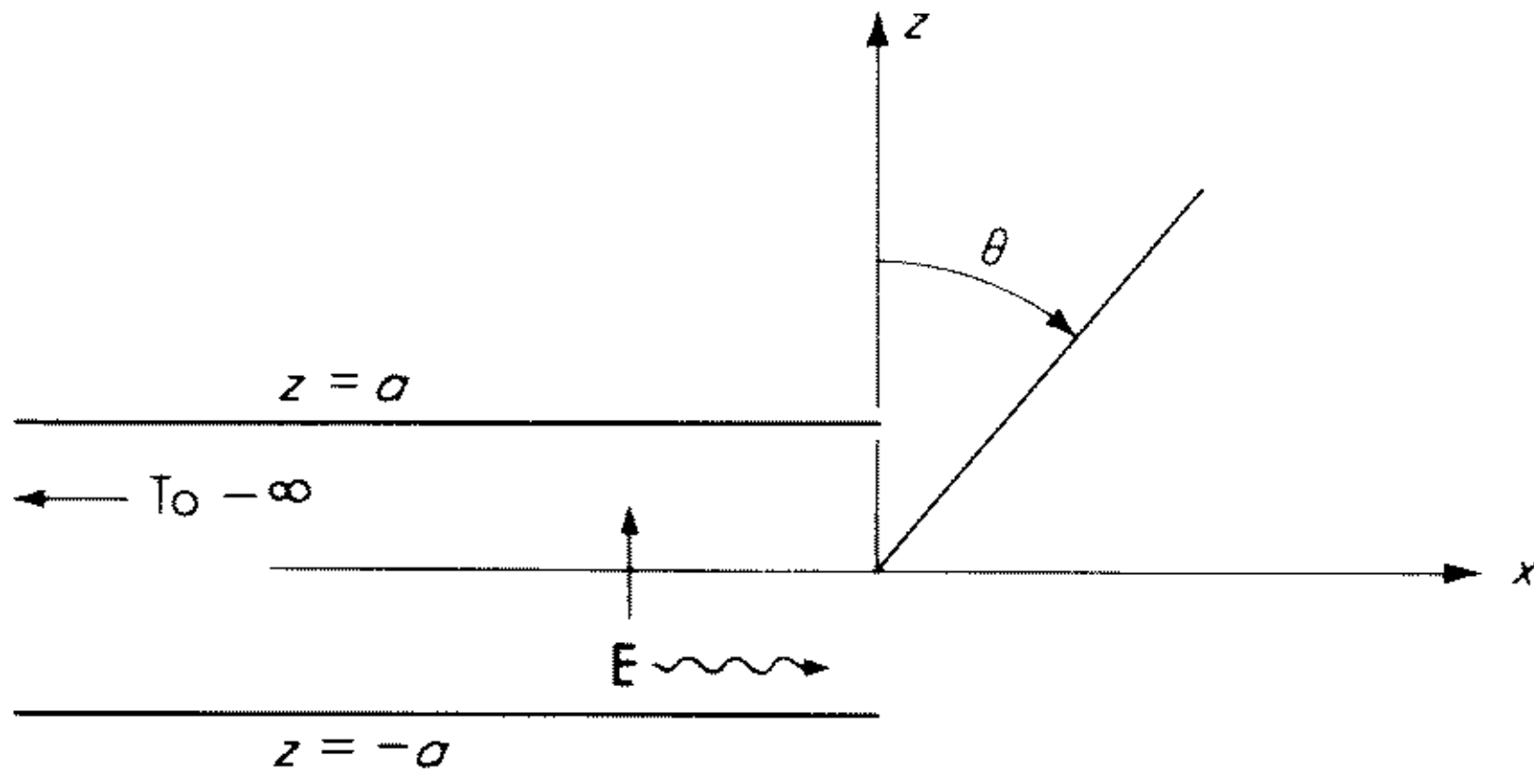


Fig. 15.1 A parallel-plate waveguide with open end.

along $z = \pm a$. We assume that a dominant TEM mode is incident from the region $x < 0$ with fields given by

$$E_z = -\zeta_0 A e^{-jk_0 x} \quad (15.1a)$$

$$H_y = A e^{-jk_0 x} \quad (15.1b)$$

Since the guide is uniform along y and the incident field is independent of y , the scattered field will also be independent of y . Thus the scattered field has only a y component of magnetic field from which the remaining electric field components may be found by means of the relations

$$j\omega\epsilon_0 E_x = -\frac{\partial H_y}{\partial z} \quad (15.2a)$$

$$j\omega\epsilon_0 E_z = \frac{\partial H_y}{\partial x} \quad (15.2b)$$

The induced currents on the plates flow in the x direction only and are independent of y . The current $J(x)$ must satisfy the edge condition, which requires that it vanish as $x^{1/2}$ as the edge is approached. This edge condition will be required in the analysis in order to obtain a unique solution.

An integral equation for determining the current is readily set up and is of the Wiener-Hopf type. We shall follow a somewhat modified procedure and construct the solution in the form of a Fourier transform. Both approaches lead to essentially the same factorization problem which is the key feature of the Wiener-Hopf method.

We shall let $\psi(x, z)$ be the total magnetic field, which is a solution of

$$\frac{\partial^2 \psi}{\partial x^2} + \frac{\partial^2 \psi}{\partial z^2} + k^2 \psi = 0 \quad (15.3)$$

where $k = k' - jk''$; that is, we assume a medium with small loss. At the end of the analysis we shall put k equal to k_0 . The boundary conditions for ψ are:

1. $\frac{\partial \psi}{\partial z} = 0$, $z = \pm a$, $-\infty \leq x \leq 0$ since E_x vanishes on the plates.
2. $\frac{\partial \psi}{\partial z}$ is continuous at $z = \pm a$, all x .

3. The current $J(x) = J_-(x) = \psi(x, a_-) - \psi(x, a_+)$ is identically zero for $x > 0$ and is of order $x^{1/2}$ as $x \rightarrow 0$ from the region $x < 0$.
4. $\psi(x, z)$ is an even function of z because of the symmetry and the symmetrical excitation.
5. $\psi(x, z)$ must satisfy the radiation condition.

A general solution for ψ that satisfies conditions 2, 4, and 5 is readily seen to be given by the Fourier transform

$$\psi(x, z) = \int_{-\infty}^{\infty} e^{-jwx} f(w) \cos \lambda z dw \quad -a < z < a \quad (15.4a)$$

$$\psi(x, z) = \int_{-\infty}^{\infty} -je^{-jwx} e^{-j\lambda(z-a)} \sin \lambda a f(w) dw \quad z > a \quad (15.4b)$$

where $\lambda = \sqrt{k^2 - w^2}$. If we can find the unknown function $f(w)$, we shall be able to determine ψ .

For any finite value of z greater than a we know that ψ is of order $e^{-k''|x|}$ as $|x| \rightarrow \infty$. Therefore, $e^{-j\lambda(z-a)} \sin \lambda a f(w)$ is analytic in the strip $-k'' < v < k''$ where $w = u + jv$. For $-\infty \leq x \leq 0$, $-a < z < a$, the field is an incident TEM mode, a reflected TEM mode, plus higher-order TM modes, and thus is of the form

$$\psi = Ae^{-jkx} - \Gamma A e^{jkx} + \sum_{n=1}^{\infty} A_n \cos \frac{n\pi z}{a} e^{\gamma_n x} \quad (15.5)$$

where Γ is the reflection coefficient and $\gamma_n = [(n\pi/a)^2 - k^2]^{1/2}$. We shall assume that $\pi/a > k$ so only the TEM mode propagates.

The incident field can be represented by

$$\psi_i = Ae^{-jkx} = \frac{1}{2\pi j} \int_C \frac{Ae^{-jwx}}{w - k} dw \quad (15.6)$$

where C is the contour shown in Fig. 15.2. For $x > 0$ we can close C in the lower half plane (lhp); and since the pole is not enclosed, we get zero for the value of the integral. For $x < 0$ we can close C in the upper half plane (uhp), and by the residue theorem we obtain the incident field.

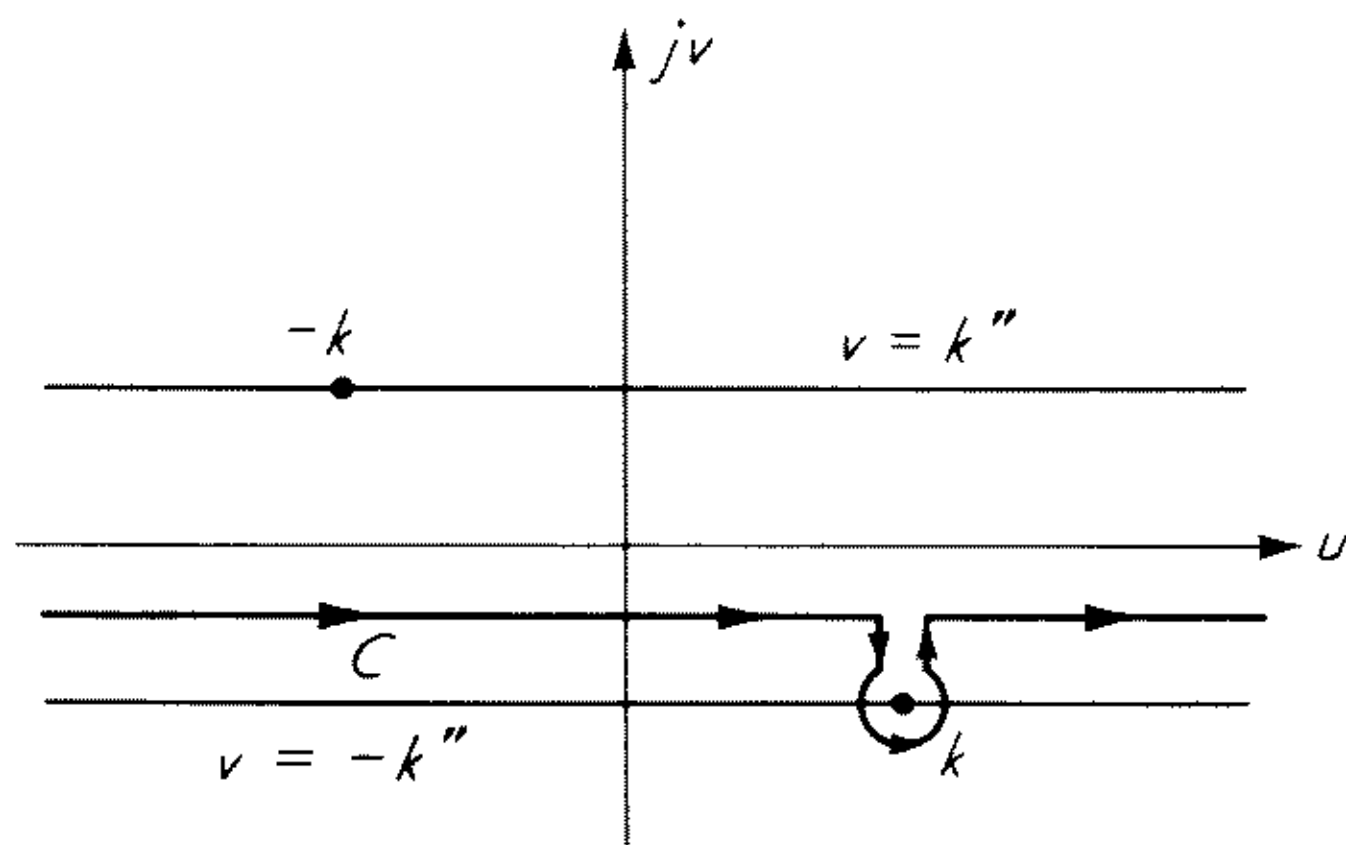


Fig. 15.2 Contour C for evaluating magnetic field.

For $-a < z < a$, all x , the scattered field $\psi_s = \psi - \psi_i$ is of order $e^{-k''|x|}$ as $|x| \rightarrow \infty$. Therefore, for $-a < z < a$, all x , we can write

$$\begin{aligned}\psi_s &= \int_{-\infty}^{\infty} e^{-jwx} f(w) \cos \lambda z dw - \psi_i \\ &= \int_C e^{-jwx} \left[f(w) \cos \lambda z - \frac{A}{2\pi j(w - k)} \right] dw\end{aligned}$$

and because of the asymptotic behavior of ψ_s we have that

$$f(w) \cos \lambda z - \frac{A}{2\pi j(w - k)}$$

is analytic in the strip $-k'' < v < k''$.

The total field for $-a < z < a$ arises from the inversion of $f(w) \cos \lambda z$, so this function must have poles at $w = \pm k$, $w = j\gamma_n$, $n = 1, 2, 3, \dots$ in order to give the form (15.5). These poles, with the exception of the pole at $w = k$, lie in the uhp and are enclosed when the contour is closed in the uhp, which can be done for $x < 0$. To obtain the incident wave the contour C is located in the strip $-k'' < v < k''$ except for the encirclement of the pole at $w = k$ as shown in Fig. 15.2.

We may obtain further conditions on $f(w)$ from the boundary conditions 1 and 3. Condition 1 yields

$$\int_C \lambda \sin \lambda a f(w) e^{-jwx} dw = 0 \quad x \leq 0$$

Since we can close C in the uhp for $x < 0$, we must have $\lambda \sin \lambda a f(w)$ analytic in the upper half plane in order for the integral to vanish. Note that $\lambda \sin \lambda a = 0$ for $w = \pm k, j\gamma_n$, so that the postulated poles of $f(w)$ are canceled by $\lambda \sin \lambda a$ in the uhp. The integral

$$\int_C \lambda \sin \lambda a f(w) e^{-jwx} dw = j\omega\epsilon_0 E_x$$

and since by the edge condition E_x is of order $x^{-1/2}$ as $x \rightarrow 0$ from $x > 0$, the final-value theorem shows that $\lambda \sin \lambda a f(w)$ is of order $w^{-1/2}$ as $|w| \rightarrow \infty$.

The current J_1 flowing on the inside of the plate at $z = a$, $x \leq 0$, is given by

$$J_1 = \int_C e^{-jwx} f(w) \cos \lambda a dw \quad x \leq 0 \quad (15.7)$$

Since $x < 0$, we can close C in the uhp and must obtain a form similar to (15.5). Hence $f(w) \cos \lambda a$ has poles at $w = \pm k_0, j\gamma_n$ and no other singularities in the upper half plane. The current J_2 flowing on the outside of the plate at $z = a$ is given by

$$J_2 = \int_C j e^{-jwx} f(w) \sin \lambda a dw \quad x \leq 0 \quad (15.8)$$

Since C can be closed in the uhp and we must obtain a nonzero value for J_2 , the

function $f(w) \sin \lambda a$ will have a branch cut singularity in the uhp. The total current is given by

$$J(x) = J_-(x) = J_1 + J_2 = \int_C e^{-jwx} e^{j\lambda a} f(w) dw \quad (15.9)$$

and vanishes for $x > 0$. Hence since we can close C in the lhp for $x > 0$, we must have $f(w)e^{j\lambda a}$ analytic in the lhp below C . By the edge condition, J_- is of order $x^{1/2}$ as $x \rightarrow 0$ from $x < 0$, and consequently $f(w)e^{j\lambda a}$ is of order $w^{-3/2}$ as $|w| \rightarrow \infty$.

We now have the following conditions to be satisfied by $f(w)$:

1. $e^{j\lambda a} f(w) = Ow^{-3/2}$ as $|w| \rightarrow \infty$ in lhp.
2. $\lambda \sin \lambda a f(w)$ analytic in uhp above C .
3. $f(w)e^{j\lambda a}$ analytic in lhp below C .
4. $f(w)$ has simple poles at $w = \pm k_0, j\gamma_n$.
5. $\lambda \sin \lambda a f(w) = Ow^{-1/2}$ as $|w| \rightarrow \infty$. (This condition includes condition 1, since $\lambda \rightarrow jw$ as $w \rightarrow \infty$.)

To give decaying waves at infinity, $\sqrt{k^2 - w^2} = \lambda = -j\sqrt{w^2 - k^2}$, that is, the branch with negative imaginary part is chosen (or positive real part when λ is real).

From (3) we can write $e^{j\lambda a} f(w) = L_-(w)$, where L_- is an unknown function that is analytic in the lhp and has poles at $w = \pm k, j\gamma_n$ and is of order $w^{-3/2}$ as w goes to infinity. From (2) we now get $\lambda \sin \lambda a e^{-j\lambda a} L_-(w) = L_+(w)$, where L_+ is a function analytic in the upper half plane. We can express $\lambda \sin \lambda a$ as an infinite product in the form

$$\lambda^2 a \frac{\sin \lambda a}{\lambda a} = \lambda^2 a \prod_{n=-\infty}^{\infty} \left(1 - \frac{\lambda a}{n\pi} \right) e^{\lambda a/n\pi}$$

Now assume also that we can factor $e^{-j\lambda a}$ into the form $S_+(w)S_-(w)$. Then

$$L_-(w) = \frac{L_+}{S_+ S_-} \frac{1}{\lambda^2 a \prod_{n=-\infty}^{\infty} (1 - \lambda a/n\pi) e^{\lambda a/n\pi}} \quad (15.10)$$

For L_- to satisfy the prescribed conditions it is necessary to choose L_+ such that it cancels the factor S_+ and the zeros of $\lambda \sin \lambda a$ in the lower half plane and in addition gives L_- algebraic growth according to $L_- = Ow^{-3/2}$ as $|w| \rightarrow \infty$. Thus we let

$$L_+ = S_+ \prod_{n=1}^{\infty} \left(1 + \frac{\lambda a}{n\pi} \right) e^{\lambda a/n\pi} I(w)$$

where $I(w)$ is to be chosen to give L_- the correct algebraic behavior at infinity. Note that I must be an integral function in the lhp to give L_- this property. The constant to be associated with I is fixed by the requirement that the inci-

dent wave arising from the residue at $w = k$ must equal A . For later convenience we shall choose L_- of the following form

$$L_- = \frac{I(w)}{S_-(w)(w^2 - k^2) \prod_{n=1}^{\infty} (1 - w/j\gamma_n)e^{wa/n\pi j}} \quad (15.11)$$

which is permissible, since we have not specified I as yet. Note that $\gamma_n \rightarrow n\pi/a$ as $n \rightarrow \infty$, and so we can choose $e^{wa/jn\pi}$ as convergence factors in the infinite-product term.

Let $e^{-j\lambda a} = S_+ S_-$. Then $\ln e^{-j\lambda a} = \ln S_+ + \ln S_- = -j\lambda a = j(w^2 - k^2)a(k^2 - w^2)^{-1/2}$. The function $w^2 - k^2$ is analytic everywhere, so we shall factor $(k^2 - w^2)^{-1/2}$ into the form $q_+ + q_-$. Let $q_+ - q_- = g(w)$ so that

$$q_- = \frac{1}{2}(k^2 - w^2)^{-1/2} - g(w)$$

We can express $g(w)$ in the form

$$g(w) = \frac{1}{\pi j} P \int_{-\infty}^{\infty} \frac{d\zeta}{(\zeta - w)\sqrt{k^2 - \zeta^2}}$$

(The general factorization procedure is described in Sec. 10.5 and also in Sec. 1.3 of Noble's book.³) The integral can be evaluated to give

$$g(w) = \frac{1}{\pi\sqrt{w^2 - k^2}} \ln \frac{-w + \sqrt{w^2 - k^2}}{w + \sqrt{w^2 - k^2}}$$

We now obtain

$$q_- = \frac{1}{2\sqrt{k^2 - w^2}} - \frac{1}{2\pi\sqrt{w^2 - k^2}} \ln \frac{-w + \sqrt{w^2 - k^2}}{w + \sqrt{w^2 - k^2}}$$

and thus
$$\ln S_- = j\sqrt{w^2 - k^2} \frac{a}{2\pi} \left[j\pi - \ln \frac{-w + \sqrt{w^2 - k^2}}{w + \sqrt{w^2 - k^2}} \right]$$

or

$$S_- = \exp \left(-\sqrt{w^2 - k^2} \frac{a}{2} \right) \exp \left(-j\sqrt{w^2 - k^2} \frac{a}{2\pi} \ln \frac{-w + \sqrt{w^2 - k^2}}{w + \sqrt{w^2 - k^2}} \right) \quad (15.12)$$

As $w \rightarrow \infty$ in the lower half plane, S_- is asymptotic to

$$\exp \left(jw \frac{a}{\pi} \ln \frac{2w}{k} \right)$$

Note that

$$\ln \frac{-w + \sqrt{w^2 - k^2}}{w + \sqrt{w^2 - k^2}} = \ln \frac{w - \sqrt{w^2 - k^2}}{w + \sqrt{w^2 - k^2}} + \ln(-1) \quad \text{and} \quad \ln(-1) = \pi j$$

so that
$$S_- = \exp \left(-j\sqrt{w^2 - k^2} \frac{a}{2\pi} \ln \frac{w - \sqrt{w^2 - k^2}}{w + \sqrt{w^2 - k^2}} \right)$$

also. If we replace $\sqrt{w^2 - k^2}$ by $-\sqrt{w^2 - k^2}$, S_- does not change value, which must be the case since S_- is analytic in the lhp.

The term

$$\frac{1}{\prod_1^{\infty} \left(1 + \frac{j\omega}{\gamma_n}\right) e^{-j\omega a/n\pi}}$$

differs from

$$\prod_1^{\infty} \left(1 + \frac{j\omega a}{n\pi}\right) e^{-j\omega a/n\pi} = \frac{j\omega a}{\pi} e^{j\gamma\omega a/\pi} \Gamma(j\omega a/\pi)$$

where $\Gamma(z)$ is the gamma function and $\gamma = 0.57722$ is Euler's constant, by only a constant when $w \rightarrow \infty$. Therefore, its asymptotic value can be found by using the result

$$\Gamma(z) \rightarrow \sqrt{2\pi} e^z \ln z z^{-1/2} e^{-z+1} \quad \text{as} \quad |z| \rightarrow \infty$$

Apart from a constant, we thus find that

$$L_-(w) \sim \frac{I(w) w e^{j\gamma\omega a/\pi}}{w^2 e^{(j\omega a/\pi) \ln(2w/k)}} e^{(j\omega a/\pi) \ln(j\omega a/\pi)} w^{-1/2} e^{-j\omega a/\pi} \quad \text{as } w \rightarrow \infty$$

For L_- to be of order $w^{-3/2}$ we must choose $I(w)$ as follows:

$$\begin{aligned} I(w) &= C e^{-j(\gamma-1)\omega a/\pi} e^{(j\omega a/\pi) [\ln(2w/k) - \ln(j\omega a/\pi)]} \\ &= C e^{j(1-\gamma)\omega a/\pi} e^{\omega a/2} e^{(-j\omega a/\pi) \ln(ka/2\pi)} \end{aligned} \quad (15.13)$$

where C is a constant. We now have

$$L_- = e^{j\lambda a} f(w)$$

$$\begin{aligned} &= \frac{C \exp \left[j(1-\gamma) \frac{\omega a}{\pi} + \frac{\omega a}{2} - j \frac{\omega a}{\pi} \ln \frac{ka}{2\pi} \right]}{(w^2 - k^2) \prod_1^{\infty} \left(1 + \frac{jw}{\gamma_n}\right) e^{-j(\omega a/n\pi)} \exp \left(-j \sqrt{w^2 - k^2} \frac{a}{2\pi} \ln \frac{w - \sqrt{w^2 - k^2}}{w + \sqrt{w^2 - k^2}} \right)} \end{aligned} \quad (15.14)$$

From (15.7) we see that $J_1(x) = -\int_C e^{-jwx} L_-(w) e^{j\lambda a} \cos \lambda a dw$. The residue at $w = k$ gives the incident wave, while that at $w = -k$ gives the reflected wave. Hence the reflection coefficient is given by

$$\begin{aligned} \Gamma &= -\frac{\lim_{w \rightarrow -k} L_-(w)(w+k)}{\lim_{w \rightarrow k} L_-(w)(w-k)} = \frac{e^{-j(1-\gamma)k_0 a/\pi} e^{-k_0 a/2}}{e^{j(1-\gamma)k_0 a/\pi} e^{k_0 a/2}} \\ &= \frac{e^{(jk_0 a/\pi) \ln(ka/2\pi)} \prod_1^{\infty} (1 + jk_0/\gamma_n) e^{-jk_0 a/n\pi}}{e^{(-jk_0 a/\pi) \ln(ka/2\pi)} \prod_1^{\infty} (1 - jk_0/\gamma_n) e^{jk_0 a/n\pi}} \\ &= e^{-k_0 a} e^{(j2k_0 a/\pi) [-1+\gamma + \ln(ka/2\pi)]} \prod_1^{\infty} \frac{\gamma_n + jk_0}{\gamma_n - jk_0} e^{-j2k_0 a/n\pi} \end{aligned} \quad (15.15)$$

where we have put $k = k_0$. Since all γ_n are real, we find that

$$|\Gamma| = e^{-k_0 a} \quad (15.16a)$$

$$\text{Phase } \Gamma = \frac{2k_0 a}{\pi} \left(\gamma - 1 + \ln \frac{k_0 a}{2\pi} \right) + 2 \sum_{n=1}^{\infty} \left[\tan^{-1} \left(\frac{k_0}{\gamma_n} \right) - \frac{k_0 a}{n\pi} \right] \quad (15.16b)$$

The series converges rapidly, since $\tan^{-1} (k_0/\gamma_n)$ rapidly approaches $k_0 a/n\pi$ for large n .

To obtain the radiation pattern we use (15.2) together with (15.4b) to obtain

$$\mathbf{E} = \frac{j\zeta_0}{k_0} \int_{-\infty}^{\infty} e^{-jk_x x - jk_z(z-a)} f(k_x) (-\hat{\mathbf{x}}k_z \sin k_z a + \hat{\mathbf{z}}k_x \sin k_z a) dk_x \quad (15.17)$$

upon putting $w = k_x$, $\lambda = k_z$. The asymptotic form of this integral is given by (3.15f), so the radiation field is

$$\mathbf{E} \sim \frac{j\zeta_0}{k_0} \sqrt{\frac{2\pi j}{k_0 r}} e^{-jk_0 r} k_0 \cos \theta [-\hat{\mathbf{x}}k_0 \cos \theta \sin (k_0 a \cos \theta) + \hat{\mathbf{z}}k_0 \sin \theta \sin (k_0 a \cos \theta)] f(k_0 \sin \theta) \quad (15.18)$$

This result gives $E_r = 0$ and

$$E_{\theta} = -j\zeta_0 \sqrt{\frac{2\pi j}{k_0 r}} e^{-jk_0 r} k_0 \cos \theta \sin (k_0 a \cos \theta) f(k_0 \sin \theta) \quad (15.19)$$

for the far-zone field. Note that θ is the angle measured from the z axis. Apart from irrelevant constants, which we replace by K , the radiation pattern is given by

$$|E_{\theta}| = K k_0 \cos \theta \sin (k_0 a \cos \theta) |f(k_0 \sin \theta)|$$

By using (15.14) we find that

$$|f(k_0 \sin \theta)| = \frac{C e^{(k_0 a/2) \sin \theta}}{k_0^2 \cos^2 \theta \left[\prod_{n=1}^{\infty} [1 + (k_0^2 \sin^2 \theta / \gamma_n^2)] \right]^{1/2}}$$

If we note the following infinite product expansion

$$\begin{aligned} \frac{\sin \sqrt{k_0^2 - w^2} a}{\sqrt{k_0^2 - w^2} a} &= \prod_{n=-\infty}^{\infty} \left(1 + \frac{jw}{\gamma_n} \right) e^{-jw a / n\pi} \\ &= \prod_{n=1}^{\infty} \left(1 + \frac{w^2}{\gamma_n^2} \right) \end{aligned}$$

we readily see that $|f(k_0 \sin \theta)|$ can be written in closed form. Thus the normalized radiation pattern is given by

$$|E_{\theta}| = e^{(k_0 a/2)(\sin \theta - 1)} \left[\frac{\sin (k_0 a \cos \theta)}{k_0 a \cos \theta} \right]^{1/2} \quad (15.20)$$

Note that this expression is valid only for $2a < \lambda_0$.

It is instructive to compare (15.20) with the pattern obtained by assuming a constant-aperture field $E_0 \hat{z}$ over the region $-a < z < a$ and zero for $|z| > a$. By using (3.15c) and (3.15f), we obtain

$$E_\theta \sim E_0 k_0 a \sqrt{\frac{j}{2\pi k_0 r}} e^{-jk_0 r} \frac{\sin(k_0 a \cos \theta)}{k_0 a \cos \theta} \quad (15.21)$$

for the far-zone radiation field. If Kirchhoff's formula (3.48b) or the two-dimensional form of (3.25) as given in Prob. 3.9 is used an extra factor, $\frac{1}{2}(1 + \sin \theta)$, is obtained.

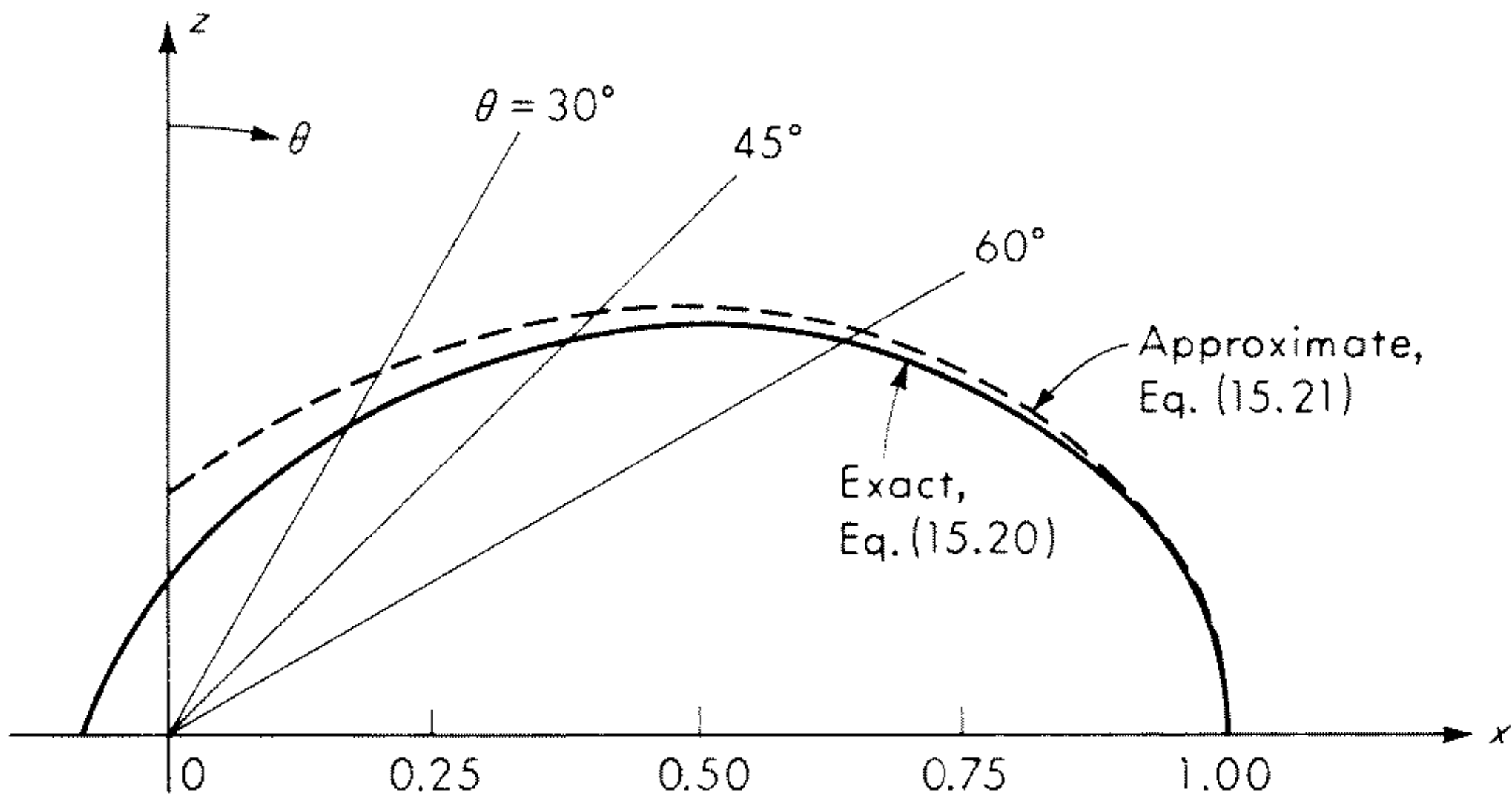


Fig. 15.3 Comparison of exact and approximate radiation patterns from a parallel-plate waveguide for excitation by a TEM mode, $2a = 0.8\lambda_0$.

The two normalized patterns are plotted in Fig. 15.3 and are seen to be in remarkably good agreement for $0 < \theta < \pi/2$. This example shows that the aperture field method of calculating the radiation pattern gives good results, for apertures of the order of a wavelength in size, even though only a rough estimate of the actual aperture field is known. Note that the aperture field method as given in Sec. 3.4 is based on the use of field equivalence methods and gives the field only in the half space $x > 0$. However, Kirchhoff's formula can be applied to the surface consisting of the aperture $-a \leq z \leq a$ and the waveguide walls at $z = \pm a$ and thus gives an approximation to the field everywhere outside the guide (see Prob. 15.1).

Parallel Polarization

If the incident field is chosen as a TE_{10} mode with E_y proportional to $\cos(\pi z/2a)$ and a is so chosen that only the TE_{10} mode propagates, that is, $2a < 1.5\lambda_0$, a similar analysis shows that the exact normalized radiation pattern is given by¹⁻³

$$|E_y| = e^{-(k_0 a/2)(1-\sin \theta)} \left(\frac{1 + \sin \theta}{2} \right)^{1/2} \left[\frac{\cos(k_0 a \cos \theta)}{1 - (4a/\lambda_0)^2 \cos^2 \theta} \right]^{1/2} \quad (15.22)$$

If we use (3.15c) and (3.15f) and assume an aperture field

$$|E_y| = \begin{cases} E_0 \cos \frac{\pi z}{2a} & |z| \leq a \\ 0 & |z| > a \end{cases}$$

we find that the far-zone normalized electric field pattern is given by

$$E_y = \frac{\sin \theta \cos (k_0 a \cos \theta)}{1 - (4a/\lambda_0)^2 \cos^2 \theta} \quad (15.23)$$

The exact and approximate patterns are shown in Fig. 15.4. Again the agreement is seen to be quite good.

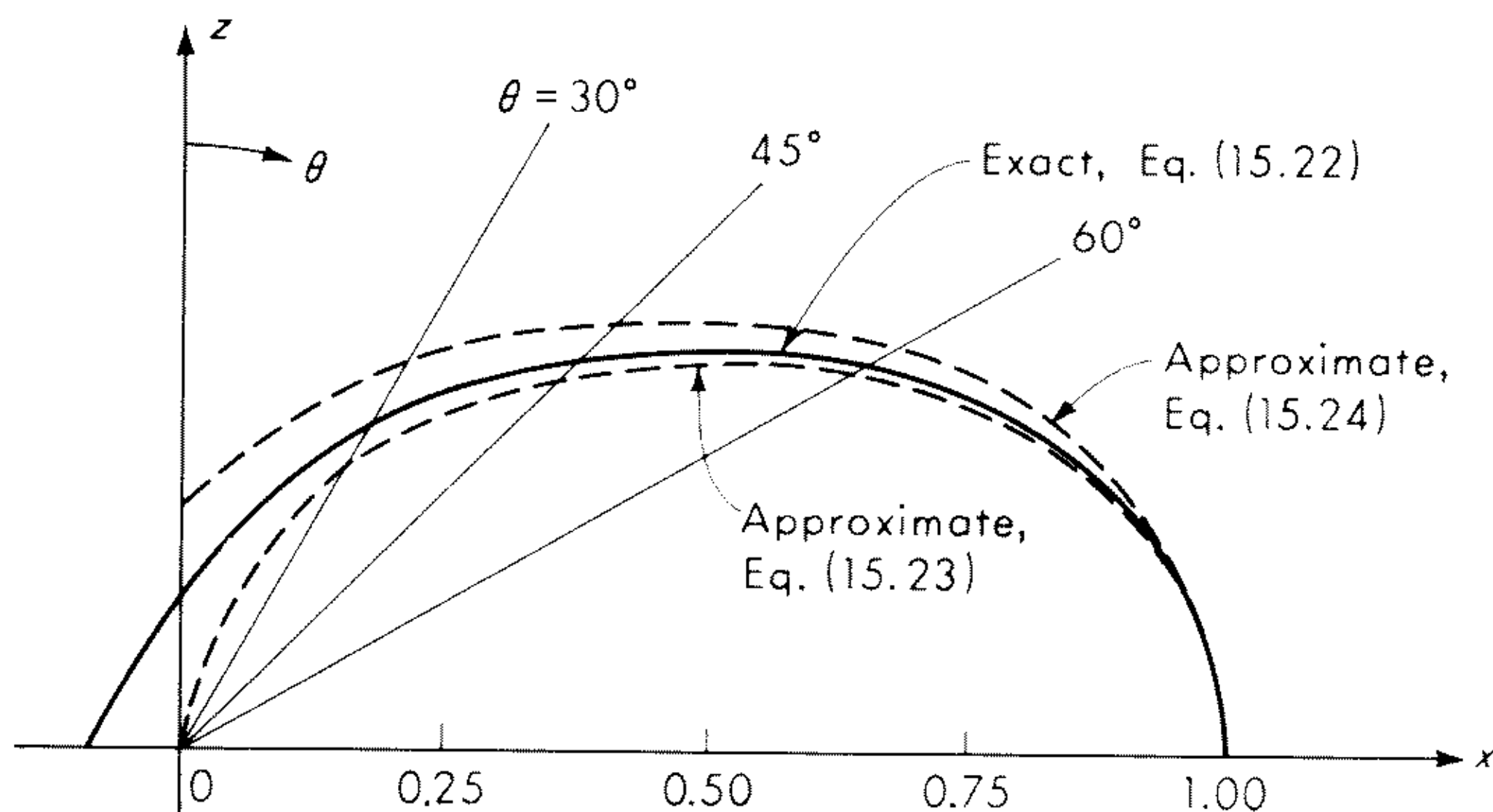


Fig. 15.4 Comparison of exact and approximate radiation patterns for a parallel-plate guide excited by a TE_{10} mode, $2a = 0.8\lambda_0$.

As an alternative to (15.23) we can evaluate the radiation field from an assumed electric and magnetic field aperture distribution. If we choose the incident TE_{10} mode fields for the aperture field, that is,

$$E_y = E_0 \cos \frac{\pi z}{2a} \quad H_z = \frac{\beta E_0}{k_0 \zeta_0} \cos \frac{\pi z}{2a}$$

where $\beta = (k_0^2 - \pi^2/4a^2)^{1/2}$, the far-zone electric field may be found by using the results of Prob. 3.9. It is readily found that the normalized field pattern is given by

$$E_y = \frac{\beta + k_0 \sin \theta}{\beta + k_0} \frac{\cos (k_0 a \cos \theta)}{1 - (4a/\lambda_0)^2 \cos^2 \theta} \quad (15.24)$$

The radiation pattern according to this expression is also shown in Fig. 15.4. This pattern deviates from the exact pattern in a way opposite to that in which the pattern given by (15.23) does. However, it is also a good approximation to the exact result.

15.3 Radiation from Circular Waveguides

The theoretical evaluation of the radiation patterns from circular and rectangular waveguides has been carried out by Chu⁴ by using the aperture field method. The results, although only approximate, do agree reasonably well with measured patterns given by Southworth and King for circular guides and conical horns⁵ and the measured patterns given by Barrow and Greene for rectangular guides.⁶ A summary of Chu's work is given in Silver's book, so it will not be reproduced here.⁷

The exact calculation of the radiation from a circular waveguide has been carried out by Vajnshtejn.^{8,9} (These papers are reproduced in the report EM-63 listed in Ref. 2.) A related problem, the diffraction of a plane wave by a circular guide, has been solved by Pearson.¹⁰ A similar acoustic problem, i.e., sound radiation from a circular guide, has been solved by Levine and Schwinger¹¹ and also by Vajnshtejn.¹² The radiation of electromagnetic waves from circular waveguides was also analyzed exactly with the Wiener-Hopf method by Schwinger and coworkers at the Massachusetts Institute of Technology Radiation Laboratory during World War II. An excellent summary of this work along with all relevant formulas and calculated radiation patterns for circular waveguides excited by the TE₀₁ and TM₀₁ modes is given by Marcuvitz in the "Waveguide Handbook."¹³ Marcuvitz also gives radiation patterns for the parallel-plate waveguide and the aperture equivalent circuit for evaluating the reflection coefficient in all cases. Since these results are readily available, we shall not give a detailed treatment.

Chu's method uses the general formulas (3.44) applied to the surface consisting of the open waveguide aperture and the outer surface of the guide plus the surface of a sphere of infinite radius. The surface at infinity does not contribute, and on the outer waveguide surface it is assumed that the tangential fields are zero. Thus only the fields on the waveguide aperture contribute, and the formulas (3.44) reduce to (3.25). The aperture field is chosen as that of the incident mode. A straightforward calculation then shows that for the TE₁₁ mode the radiated electric field is given by

$$E_{\theta} = jk_0\zeta_0 \frac{e^{-jk_0r}}{2r} \left[\left(1 + \frac{\beta_{11}}{k_0} \cos \theta \right) J_1(p'_{11}) \frac{J_1(k_0a \sin \theta)}{\sin \theta} \sin \phi \right] \quad (15.25a)$$

$$E_{\phi} = jk_0a\zeta_0 \frac{e^{-jk_0r}}{2r} \left[\left(\frac{\beta_{11}}{k_0} + \cos \theta \right) \frac{J_1(p'_{11})J'_1(k_0a \sin \theta)}{1 - [(k_0a \sin \theta)/p'_{11}]^2} \cos \phi \right] \quad (15.25b)$$

where $\beta_{11} = [k_0^2 - (p'_{11}/a)^2]^{1/2}$, $J'_1(x) = dJ_1(x)/dx$, p'_{11} is the first root of $J'_1(x) = 0$, that is, $p'_{11} = 1.841$, and a is the guide radius. The angle θ is measured from the guide axis. From these expressions the half-power E - and H -plane beam widths for $a < \lambda_0$ are found to be given very closely by

$$\Theta_E = 14.7^\circ \frac{\lambda_0}{a} \quad (15.26a)$$

$$\Theta_H = 18.6^\circ \frac{\lambda_0}{a} \quad (15.26b)$$

The directivity is given approximately by

$$D = 10.5 \frac{\pi a^2}{\lambda_0^2} \tag{15.27}$$

Figure 15.5 shows the radiation pattern from a circular guide excited by the TE_{11} mode. The solid curves give the exact results presented by Vajnshtejn,⁹ and the broken curve gives Chu’s approximate results as obtained by the aperture field method. The two patterns agree quite well, especially in the E plane (note that k_0a is not quite the same for both). Even the back lobe is surprisingly well predicted by the aperture field method.

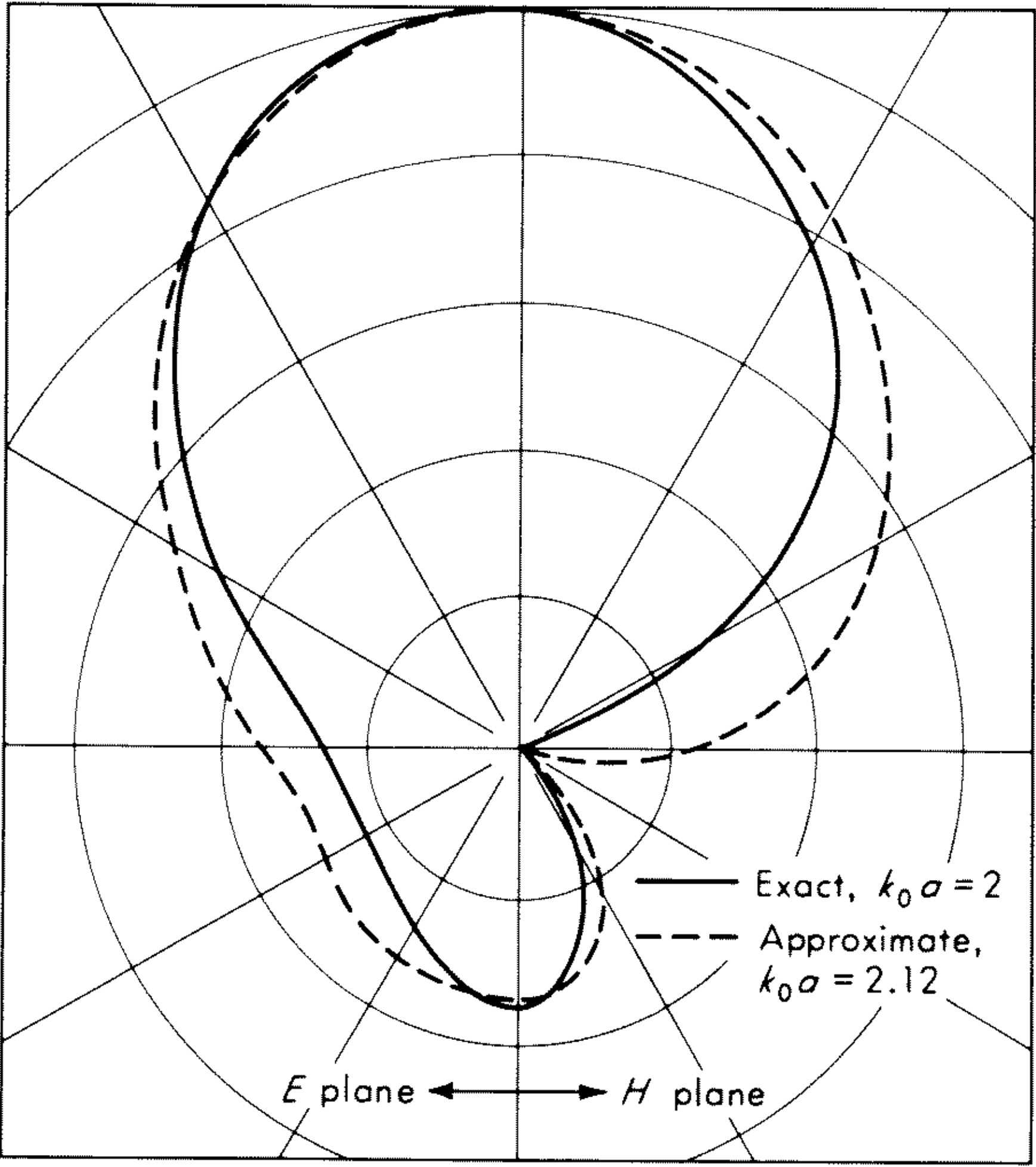


Fig. 15.5 Comparison of exact and approximate radiation patterns for a circular guide excited by the TE_{11} mode.

Circular guides excited by the axially symmetric modes, such as the TE_{01} and TM_{01} modes, are not of much practical interest because they produce a null in the radiation pattern along the axis or forward direction. Typical patterns are given by Marcuvitz.¹³

15.4 Horn Antennas

In this section, we discuss the radiation patterns of four types of horns: the H -plane sectoral horn, the E -plane sectoral horn, the pyramidal horn, and the conical horn. Figure 15.6 shows these types of horns.

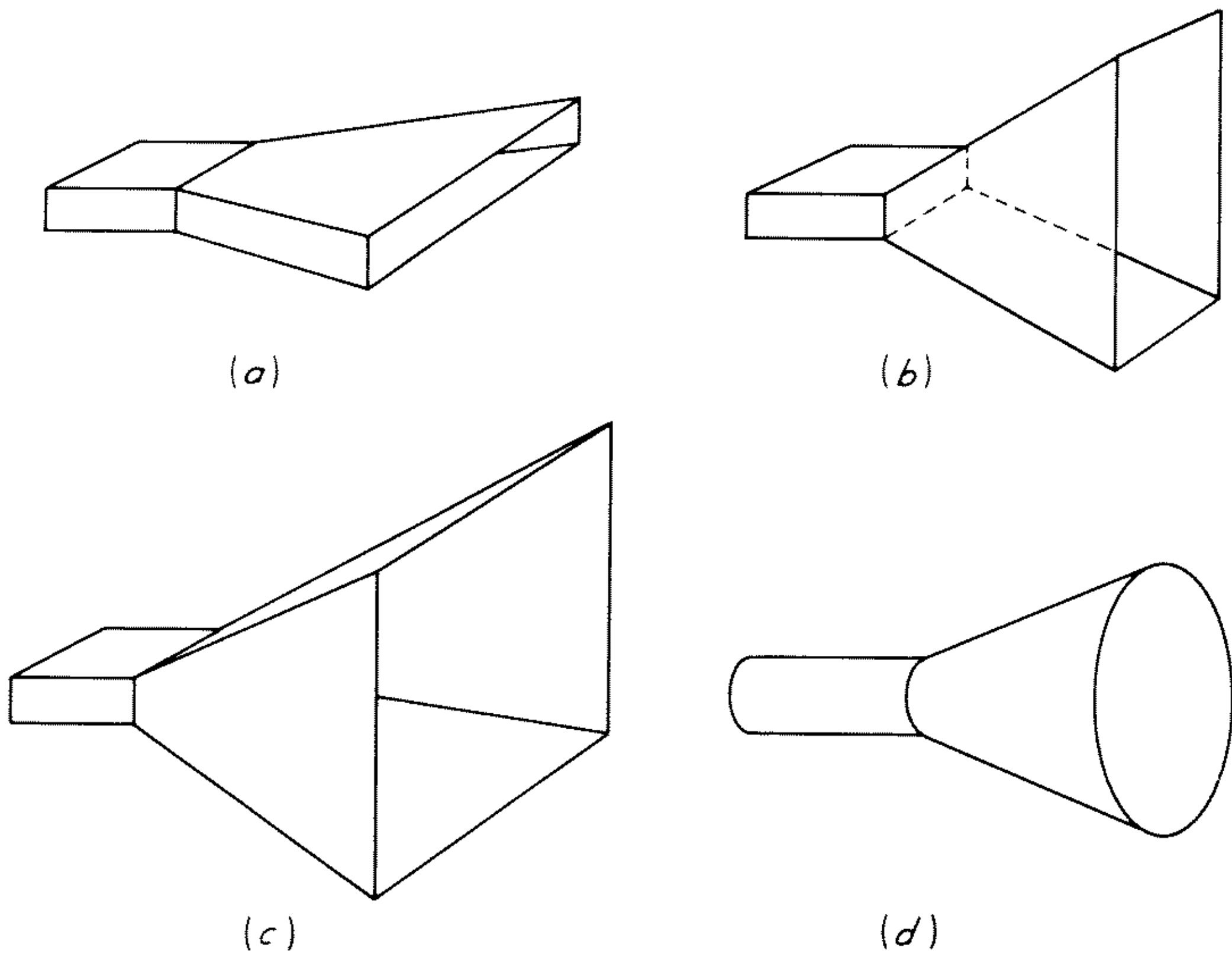


Fig. 15.6 Four types of horns. (a) *H*-plane sectoral; (b) *E*-plane sectoral; (c) pyramidal; (d) conical.

H-plane Sectoral Horn

A sectoral horn is a horn whose walls are flared in one dimension but not in the other. An expanded view of an *H*-plane sectoral horn is shown in Fig. 15.7. The horn is fed by a rectangular waveguide carrying the fundamental TE_{10} mode with the \mathbf{E} and \mathbf{H} vectors oriented as shown. The horn is flared in the plane containing the \mathbf{H} field, and this is the reason for its name. To find the far-field pattern of this antenna, an approximate expression for the fields in the aperture will be found, and then the formulas (3.25) will be used to find the far fields.

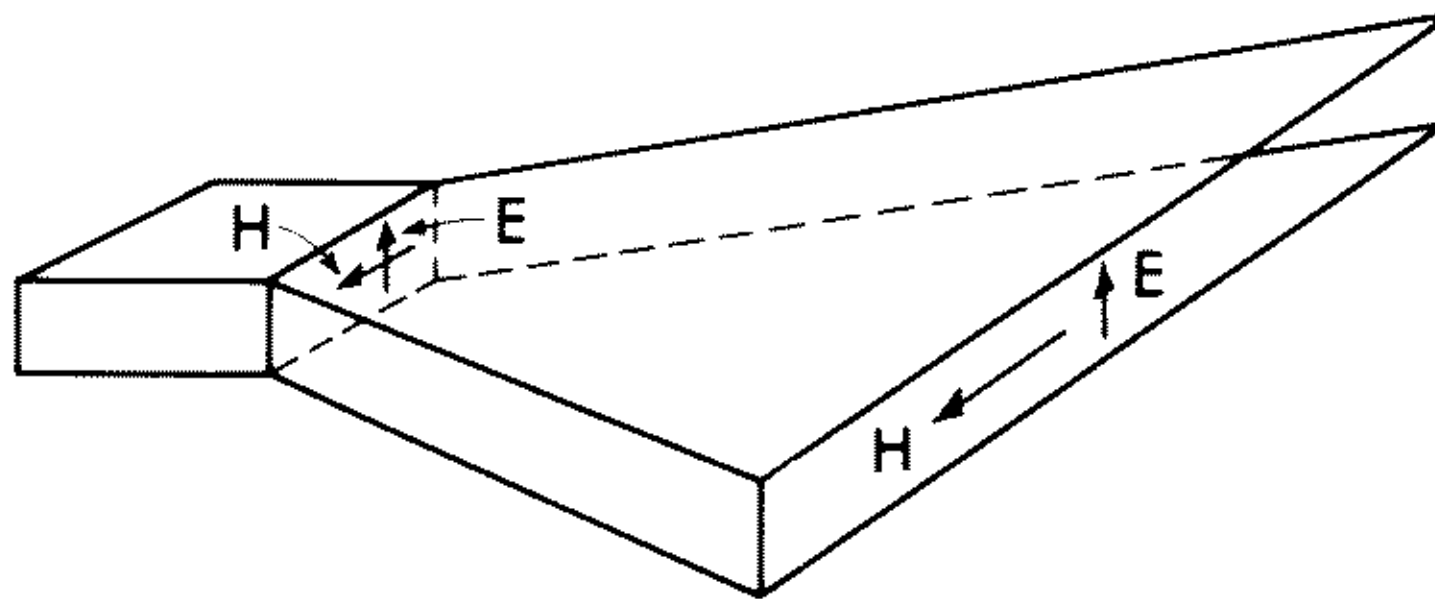


Fig. 15.7 *H*-plane sectoral horn.

To find the aperture fields, we first consider the sectoral portion of the antenna by itself. A cylindrical coordinate system ρ, ϕ, x that can be used to describe the region inside the horn is shown in Fig. 15.8. Let the angular width of the horn be ϕ_0 and the height be b , as shown.

To determine the aperture fields, we first consider a sectoral horn which extends to infinity in the ρ direction. Inside such a horn, Maxwell's equations

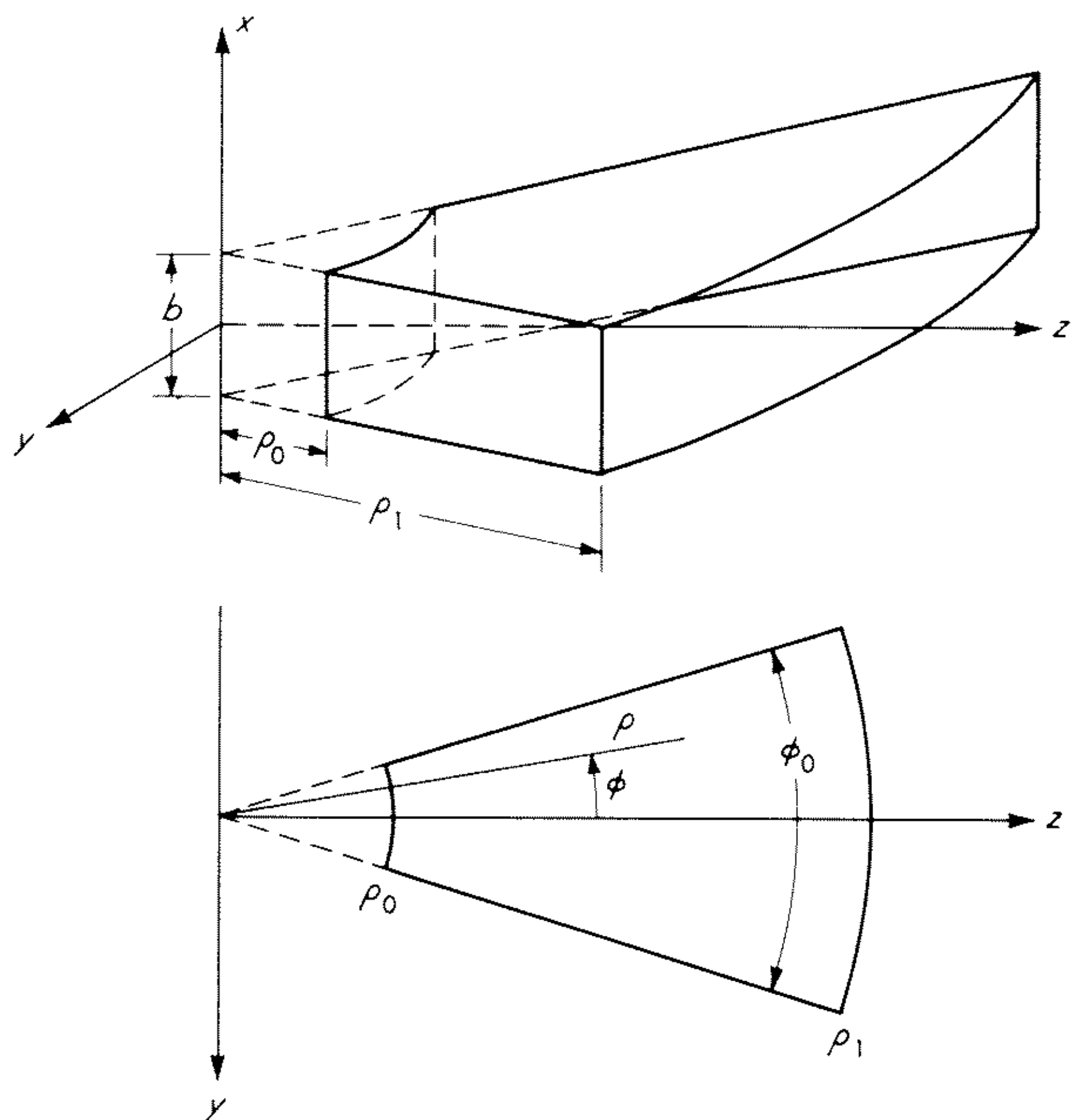


Fig. 15.8 Coordinates for the sectoral *H*-plane horn.

may be solved in cylindrical coordinates, subject to the boundary conditions that $E_\phi = E_\rho = 0$ on the top and bottom surfaces and $E_x = E_\rho = 0$ on the sidewalls. It is found, in the same way as for a rectangular waveguide, that this geometry will support an infinite number of modes. The modes can be divided into TE modes, having no radial component of electric field, and TM modes, having no radial component of magnetic field. For the case when the sectoral horn is excited by a rectangular waveguide supporting the dominant TE₁₀ mode, as shown in Fig. 15.7, an examination of the various modes in the sectoral horn shows that the modes that are excited by this feeding arrangement are the TE_{0m} modes having field components E_x , H_ρ , and H_ϕ . For these modes the fields are given by¹⁴

$$E_x = A \cos \frac{m\pi\phi}{\phi_0} H_{\nu_m}(k_0\rho) \tag{15.28a}$$

$$H_\rho = -jA \frac{m\pi}{k_0\zeta_0\phi_0\rho} \sin \frac{m\pi\phi}{\phi_0} H_{\nu_m}(k_0\rho) \tag{15.28b}$$

$$H_\phi = -jA\zeta_0^{-1} \cos \frac{m\pi\phi}{\phi_0} H'_{\nu_m}(k_0\rho) \tag{15.28c}$$

where $H'_{\nu_m}(x) = dH_{\nu_m}(x)/dx$, $\nu_m = m\pi/\phi_0$, m is an integer indicating the order of the mode, and H_{ν_m} is the Hankel function of the second kind.

For each mode, we can define a propagation constant associated with the radial propagation. As with a rectangular waveguide, it is found that each mode can propagate freely as long as the width of the horn is greater than a

certain minimum size associated with that mode. In other words, for a given flare angle ϕ_0 , there is a certain radius ρ below which the horn becomes cutoff and the mode highly attenuated. Although the transition between the cutoff case and the non-cutoff case is not as distinct as with a rectangular waveguide, the cutoff phenomenon still exists. The higher the order m of the mode, the larger the minimum radius ρ must be to support the mode.

Since the sectoral horn will be driven by a rectangular waveguide with the TE_{10} mode, it turns out that the minimum dimension of the horn, $\rho_0\phi_0$, is just sufficient to support the $m = 1$ sectoral horn mode, but not sufficient for the $m = 2$ mode.¹⁴ Thus as a first approximation, we can assume that the field inside the sectoral horn is given by the first mode alone:

$$E_x = A \cos \frac{\pi\phi}{\phi_0} H_{\nu_1}(k_0\rho) \quad (15.29a)$$

$$H_\rho = -jA \frac{\pi}{k_0\zeta_0\phi_0\rho} \sin \frac{\pi\phi}{\phi_0} H_{\nu_1}(k_0\rho) \quad (15.29b)$$

$$H_\phi = -jA\zeta_0^{-1} \cos \frac{\pi\phi}{\phi_0} H'_{\nu_1}(k_0\rho) \quad (15.29c)$$

To solve for the radiation fields which result from a finite sectoral horn, we shall assume that the fields in the aperture of the finite horn are the same as would exist at the same place in an infinite horn. We shall then use these assumed aperture fields to compute the far-field radiation pattern. Thus, we are making two important approximations in this method. We are neglecting the effect of currents on the outside walls of the horn, and we are neglecting the effect of higher-order modes in the aperture.

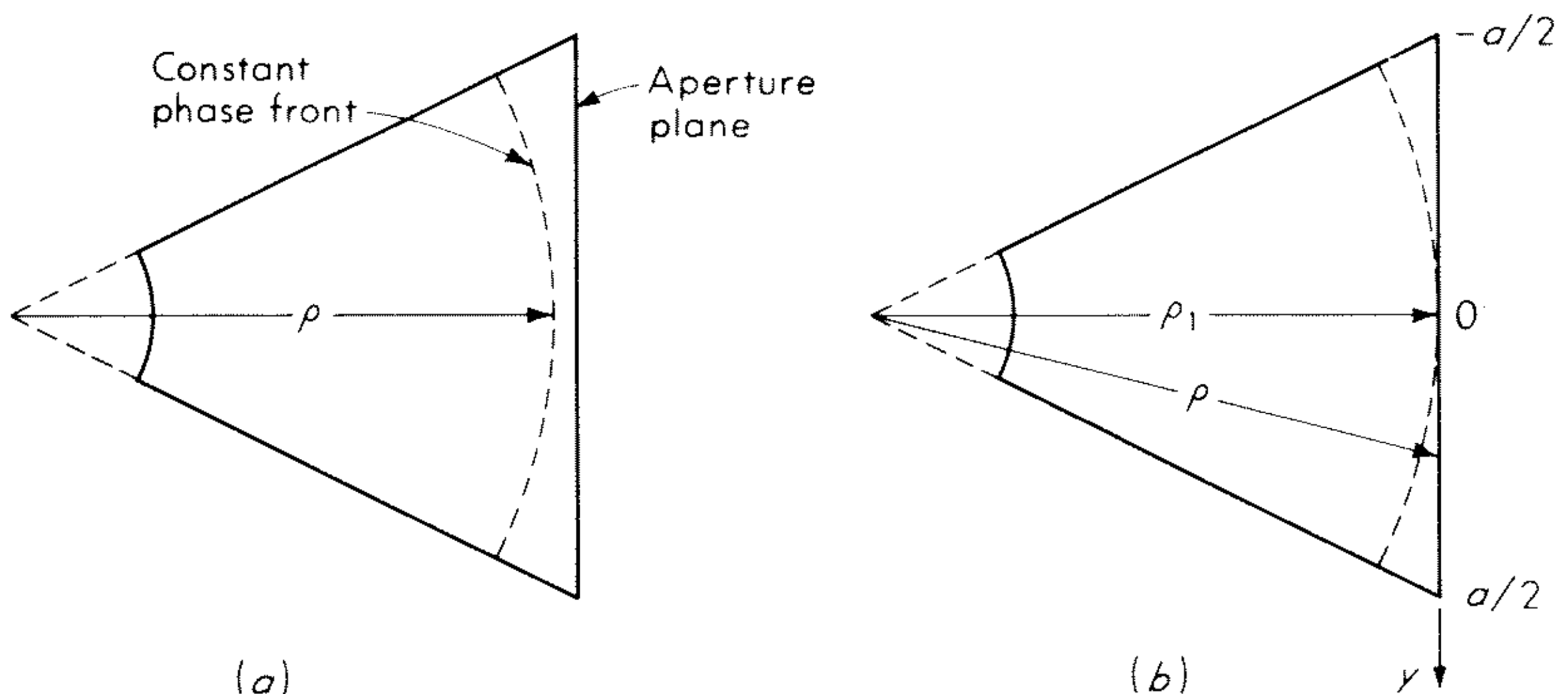


Fig. 15.9 Relation between a constant-phase front and the aperture plane.

Consider the fields given by (15.29a-c). Inside the sectoral horn, the surfaces of constant phase are the surfaces $\rho = \text{constant}$. Thus a constant-phase front has the appearance shown in Fig. 15.9a. The front aperture surface of the antenna does not fall on a surface of constant phase. Hence, the phase of

the field in the aperture is not constant but varies across the aperture. If we approximate the Hankel function by its asymptotic form

$$H_{\nu_1}(k_0\rho) = \sqrt{\frac{2}{\pi k_0\rho}} \exp \left[-j \left(k_0\rho - \frac{2\pi - \phi_0}{4\phi_0} \pi \right) \right] \quad (15.30)$$

we see that the phase propagation of the mode is described by the factor

$$e^{-jk_0\rho}$$

By using the y coordinate to describe position along the face of the aperture, as shown in Fig. 15.9*b*, it may be seen that the phase at point y lags the phase at $y = 0$ by an angle $k_0(\sqrt{\rho_1^2 + y^2} - \rho_1)$. If we assume that the horn aperture is not too large, we may approximate this relation by

$$\Delta(y) = \text{phase at point } y \text{ relative to } y = 0 = -k_0(\sqrt{\rho_1^2 + y^2} - \rho_1) \approx -\frac{k_0 y^2}{2\rho_1} \quad (15.31)$$

Also, we shall assume the amplitude of the electric field across the aperture is not affected appreciably by the fact that the aperture is not exactly on a wave front. Hence we assume the aperture electric field is given by

$$E_x(x,y) = A \cos \frac{\pi y}{a} e^{-jk_0 y^2/2\rho_1} \quad (15.32)$$

We shall also assume that $k_0\rho_1$ is large enough that H_ϕ can be approximated by

$$H_\phi(x,y) = -\frac{E_x}{\zeta_0} \quad (15.33)$$

In other words, we regard the mouth of the sectoral horn as having approximately a plane wave field distribution with a quadratic phase error. Note that (15.33) is valid whenever $\pi/a \ll k_0$, which we assume to be the case.

The far-field radiation pattern resulting from this aperture is easily found by using (3.24) and (3.25). We regard the aperture for our sectoral horn as lying in the xy plane, in the region $|x| \leq b/2$, $|y| \leq a/2$, as shown in Fig. 15.10. The angle ϕ used here is not the same as that used earlier to describe the field in the

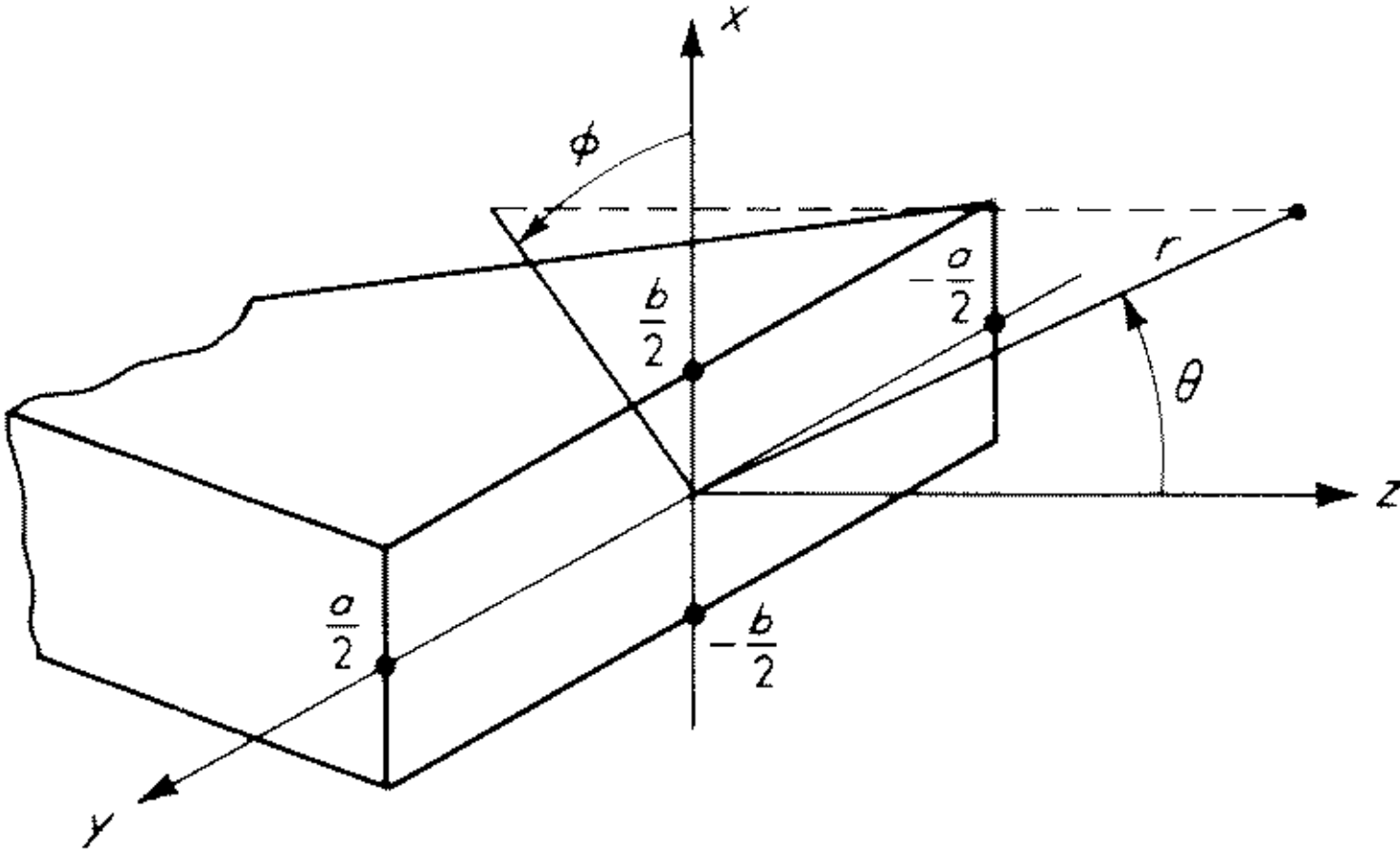


Fig. 15.10 Aperture plane of horn.

horn. For the assumed aperture fields, (3.24) gives $\zeta_0 g_\nu = f_x$, and thus (3.25) yields the following result for the radiated electric field:

$$\mathbf{E} = jk_0 \frac{e^{-jk_0 r}}{4\pi r} (1 + \cos \theta)(\hat{\theta} \cos \phi - \hat{\phi} \sin \phi) f_x \quad (15.34)$$

where

$$f_x = A \frac{\sin [(k_0 b/2) \cos \phi \sin \theta]}{k_0 \cos \phi \sin \theta} I$$

$$I = \sqrt{\frac{\pi \rho_1}{k_0}} \left\{ \left[\exp j \frac{(k_0 \sin \phi \sin \theta + \pi/a)^2 \rho_1}{2k_0} \right] [C(t_2) - jS(t_2) - C(t_1) + jS(t_1)] \right. \\ \left. + \left[\exp j \frac{(k_0 \sin \phi \sin \theta - \pi/a)^2 \rho_1}{2k_0} \right] [C(t_4) - jS(t_4) - C(t_3) + jS(t_3)] \right\}$$

The t_i are given by

$$t_i = \sqrt{\frac{1}{\pi k_0 \rho_1}} \left[(-1)^i \frac{k_0 a}{2} - k_0 \rho_1 \sin \phi \sin \theta + \alpha_i \frac{\pi \rho_1}{a} \right]$$

with $i = 1, 2, 3, 4$ in turn and $\alpha_i = -1$, $i = 1, 2$; $\alpha_i = 1$, $i = 3, 4$; and the $C(t)$, $S(t)$ are the Fresnel integrals

$$C(t) = \int_0^t \cos \left(\frac{\pi}{2} t^2 \right) dt$$

$$S(t) = \int_0^t \sin \left(\frac{\pi}{2} t^2 \right) dt$$

This result is essentially equivalent to that derived by Chu⁴ and Barrow and Chu.¹⁴

Typical computed patterns have been given by Chu and Barrow¹⁵ and are shown in Fig. 15.11. The top row of patterns shows the effect of horn length on the beam width, all of these being for a horn with a flare angle $\phi_0 = 30^\circ$. The patterns are shown for horn lengths

$$6 \leq \frac{\rho_1}{\lambda_0} \leq 50$$

It may be seen that increasing the horn length decreases the beam width up to a point, beyond which there is little sharpening. The bottom row shows the effect of varying the flare angle ϕ_0 for a horn of constant length, in this case $\rho_1/\lambda_0 = 12$. It is seen that as ϕ_0 increases, the beam width at first decreases and then increases again. Thus for a given length there is an optimum flare angle giving minimum beam width. The reason for this type of behavior may be appreciated by considering the behavior of the field distribution in the aperture of the horn. In general, we would expect that the wider the aperture, the narrower the beam. The fact that the behavior differs from this for wide flare angles is due to the fact that the phase is not constant across the aperture, but has the quadratic dependence

$$e^{-jk_0 y^2/2\rho_1}$$

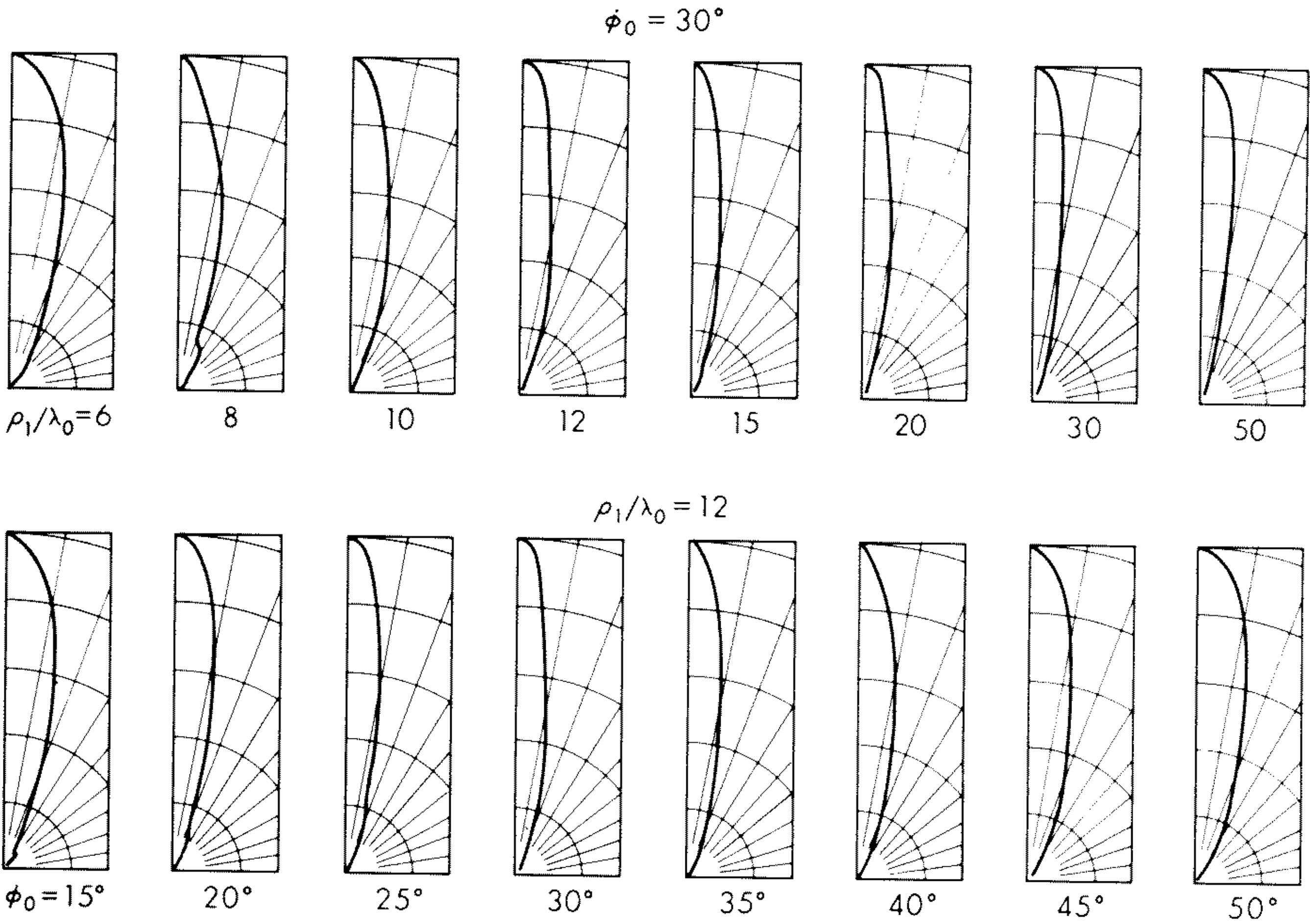


Fig. 15.11 Typical radiation patterns for the *H*-plane sectoral horn. Upper series for a constant flare angle of 30° ; lower series for a constant slant length of $12\lambda_0$ and variable flare angle. (From Chu and Barrow.¹⁵)

For small flare angles, the phase front illustrated in Fig. 15.9 will not differ much from the aperture plane itself, so the phase will be almost constant across the aperture. This is the reason that, for small values of ϕ_0 , the beam width decreases and the gain increases as ϕ_0 is increased. However, for large values of ϕ_0 , the phase front is significantly different from the aperture plane, so there is a marked phase variation across the aperture. In this case the field at the sides of the horn will be out of phase with the field in the center, so that the contribution to the far field tends to cancel that from the center. Hence any further increase in ϕ_0 tends to decrease the gain of the antenna.

Other useful information has also been given by Barrow and Chu¹⁵ and is shown here in Fig. 15.12. This figure shows the beam width of the pattern versus the flare angle ϕ_0 of the horn for several values of horn length ρ_1 . Also shown is the asymptotic curve for an infinite length horn. Based on these curves, Barrow and Chu have drawn the following main conclusions:

1. For a constant flare angle, the beam width decreases with an increase of the length.
2. For a constant flare angle, there is a corresponding length beyond which the beam angle does not decrease appreciably with further increase in length.
3. For a constant length, there is always an optimum flare angle for which the beam angle is a minimum.

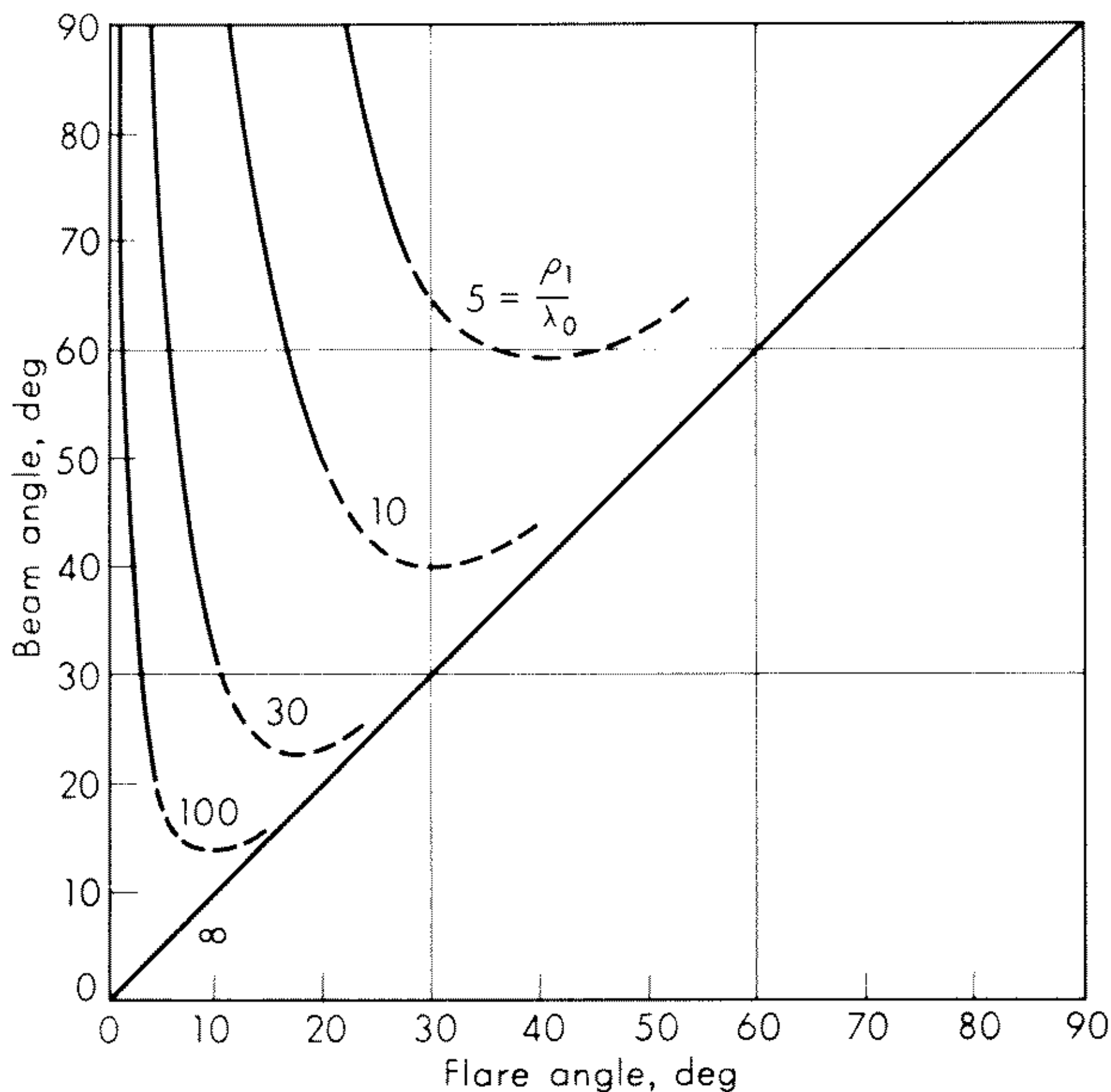


Fig. 15.12 Beam angle versus flare angle for H -plane sectoral horn. (From Barrow and Chu.¹⁴)

4. The optimum flare angle decreases with increasing length, as does the corresponding minimum beam angle.
5. For a constant aperture, the beam angle decreases with decreasing flare angle and is a minimum for zero flare angle.

These general conclusions, which are based on theoretical study, have been well corroborated by experimental data on sectoral horns. For some representative experimental data, the reader is referred to the papers by Barrow and Lewis¹⁶ and Rhodes.¹⁷

The directivity of an H -plane sectoral horn has been computed by Schelkunoff.¹⁸ The directivity is given by

$$D = \frac{4\pi b \rho_1}{\lambda_0 a} \{ [C(u) - C(v)]^2 + [S(u) - S(v)]^2 \} \quad (15.35)$$

where

$$u = \frac{1}{\sqrt{2}} \left(\frac{\sqrt{\lambda_0 \rho_1}}{a} + \frac{a}{\sqrt{\lambda_0 \rho_1}} \right) \quad v = \frac{1}{\sqrt{2}} \left(\frac{\sqrt{\lambda_0 \rho_1}}{a} - \frac{a}{\sqrt{\lambda_0 \rho_1}} \right)$$

Based upon this equation, the gain of the horn is found to depend on the horn dimensions as shown in Fig. 15.13. These curves illustrate clearly that, for a given horn length, there is an optimum aperture width giving maximum gain, and they have been widely used in the design of H -plane horns.†

†Although these curves are based strictly on simplified theoretical calculations, they have been found to be quite accurate in practice. For some comments related to this, see the paper by Jakes.²⁰

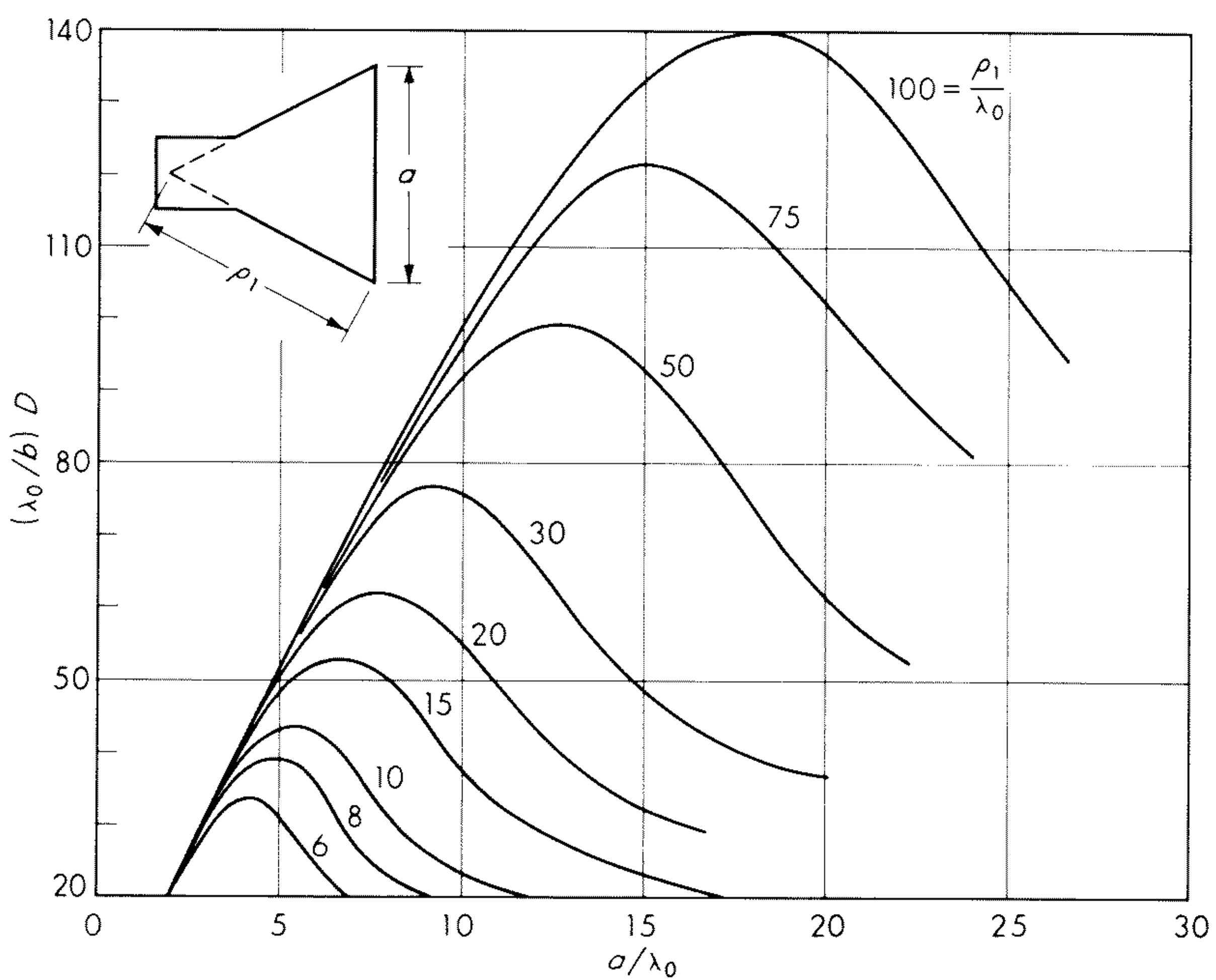


Fig. 15.13 Directivity of *H*-plane horns of width *a* and height *b*. (Based on fig. 16.3 of Schelkunoff and Friis.¹⁹)

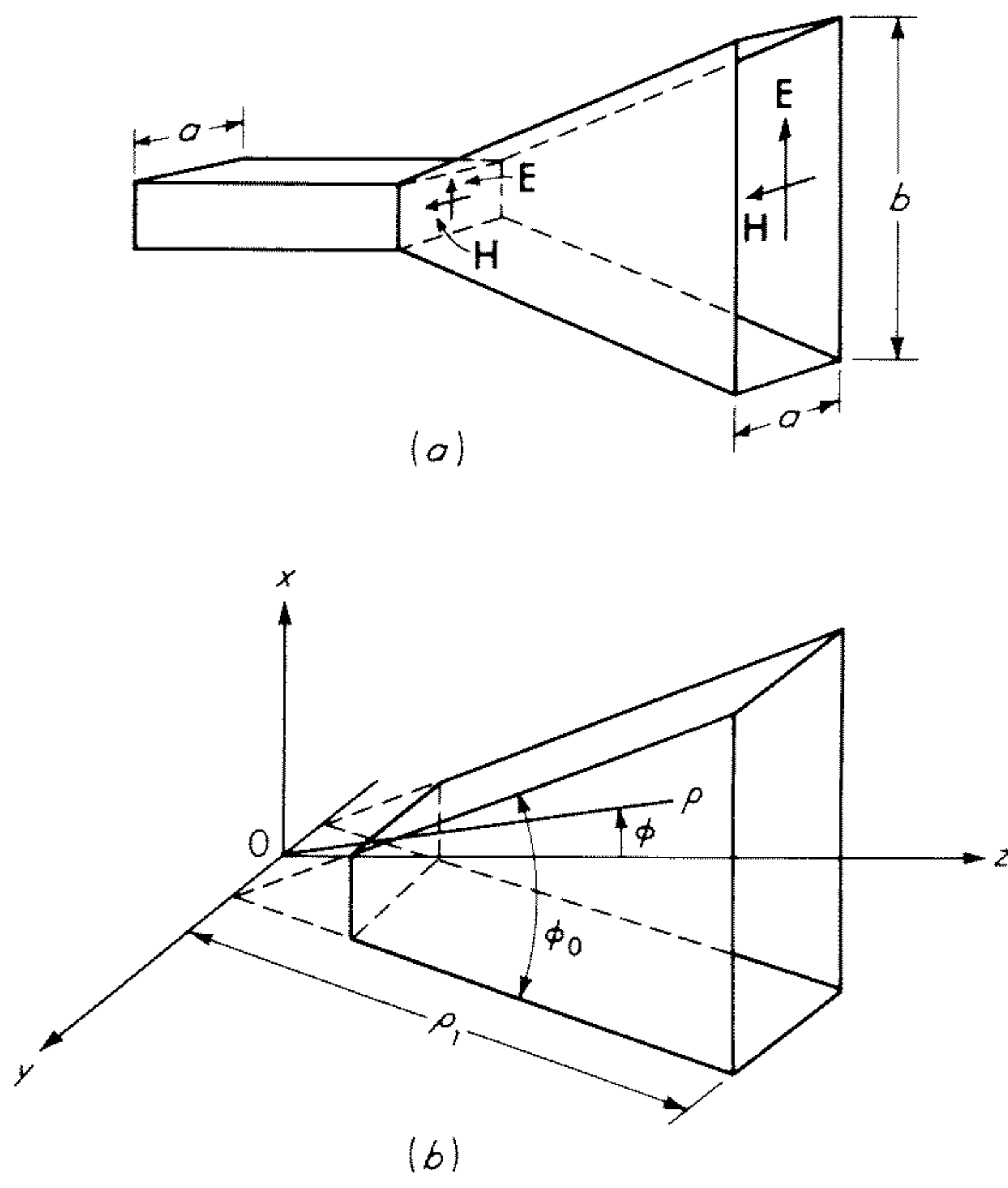


Fig. 15.14 The *E*-plane sectoral horn.

Finally, for a comprehensive discussion of all design aspects for sectoral horns, we refer the reader to the article by Chu and Barrow.¹⁵ It should be noted that the limitation on maximum flare angle for a given horn length, because of the aperture phase error introduced, may be removed by using a lens in the aperture. A discussion of lens-corrected horns is given in Sec. 15.5.

E-plane Sectoral Horn

The *E*-plane horn is different from the *H*-plane horn only in that the aperture distribution has the quadratic phase variation associated with the uniformly illuminated axis rather than the sinusoidally illuminated axis. Figure 15.14 shows an expanded view of an *E*-plane sectoral horn.

Inside the sectoral horn, we may solve Maxwell's equations subject to the boundary conditions that $E_y = E_\rho = 0$ on the top and bottom flared walls and $E_\rho = E_\phi = 0$ on the front and back walls. As before, we find that the modes are divided into TE and TM types, and the modes that are excited by the rectangular waveguide are the TE_{n0} modes having components E_ϕ , H_y , H_ρ , given by

$$E_\phi = B \cos\left(\frac{n\pi}{a} y\right) H_1(\gamma_n \rho) \quad (15.36a)$$

$$H_y = -B \frac{\gamma_n}{j\omega\mu_0} \cos\left(\frac{n\pi}{a} y\right) H_0(\gamma_n \rho) \quad (15.36b)$$

$$H_\rho = -B \frac{n\pi}{j\omega\mu_0 a \rho} \sin\left(\frac{n\pi}{a} y\right) H_1(\gamma_n \rho) \quad (15.36c)$$

where
$$\gamma_n = \sqrt{k_0^2 - \left(\frac{n\pi}{a}\right)^2} \quad \text{and} \quad n = 1, 2, \dots$$

The transmission properties of the TE_{n0} mode depend mainly on the dimension a . For a given n , when a is large enough, γ_n becomes real and the n th mode propagates. For small a , γ_n and hence the argument of the Hankel function become imaginary, and the mode is cut off.

Since the *E*-plane sectoral horn will be normally fed by a TE_{10} waveguide as shown in Fig. 15.14, the usual case is that the dimension a is large enough to support the lowest-order mode, $n = 1$, but not large enough to support any higher-order modes. Hence we can approximate the field in the horn by the first-order mode; thus

$$E_\phi = B \cos\left(\frac{\pi y}{a}\right) H_1(\gamma_1 \rho) \quad (15.37a)$$

$$H_y = -B \frac{\gamma}{j\omega\mu_0} \cos\left(\frac{\pi y}{a}\right) H_0(\gamma_1 \rho) \quad (15.37b)$$

$$H_\rho = -B \frac{\pi}{j\omega\mu_0 a \rho} \sin\left(\frac{\pi y}{a}\right) H_1(\gamma_1 \rho) \quad (15.37c)$$

where
$$\gamma_1 = \sqrt{k_0^2 - \left(\frac{\pi}{a}\right)^2}$$

For the finite horn, we assume the aperture distribution to be given by (15.37) evaluated in the aperture. Aside from unimportant constants, this gives for E_x in the aperture

$$E_x = B \cos \frac{\pi y}{a} e^{-jk_0 x^2/2\rho_1} \tag{15.38}$$

This is almost the same as for an H -plane horn, except now the quadratic phase term is associated with the x axis, the axis in which the amplitude distribution is uniform, instead of the y axis, where the amplitude is sinusoidal.

The far-field pattern is easily calculated by using (3.24) and (3.25). The integration will again involve the use of Fresnel integrals because of the quadratic phase term. The results are given in Prob. 15.4.

When patterns for the far field are computed for the E -plane horn, it is found that the dependence of the pattern on the parameters is similar to that of the H -plane horn. The main difference between the two cases is that with the E -plane horn the side lobes in the plane of the horn are considerably higher. This is due, of course, to the fact that the aperture distribution in this plane is uniform for the E -plane horn. The sinusoidal distribution for the H -plane horn makes the side lobes for that horn much lower. It also lowers the gain and increases the beam width slightly, however.

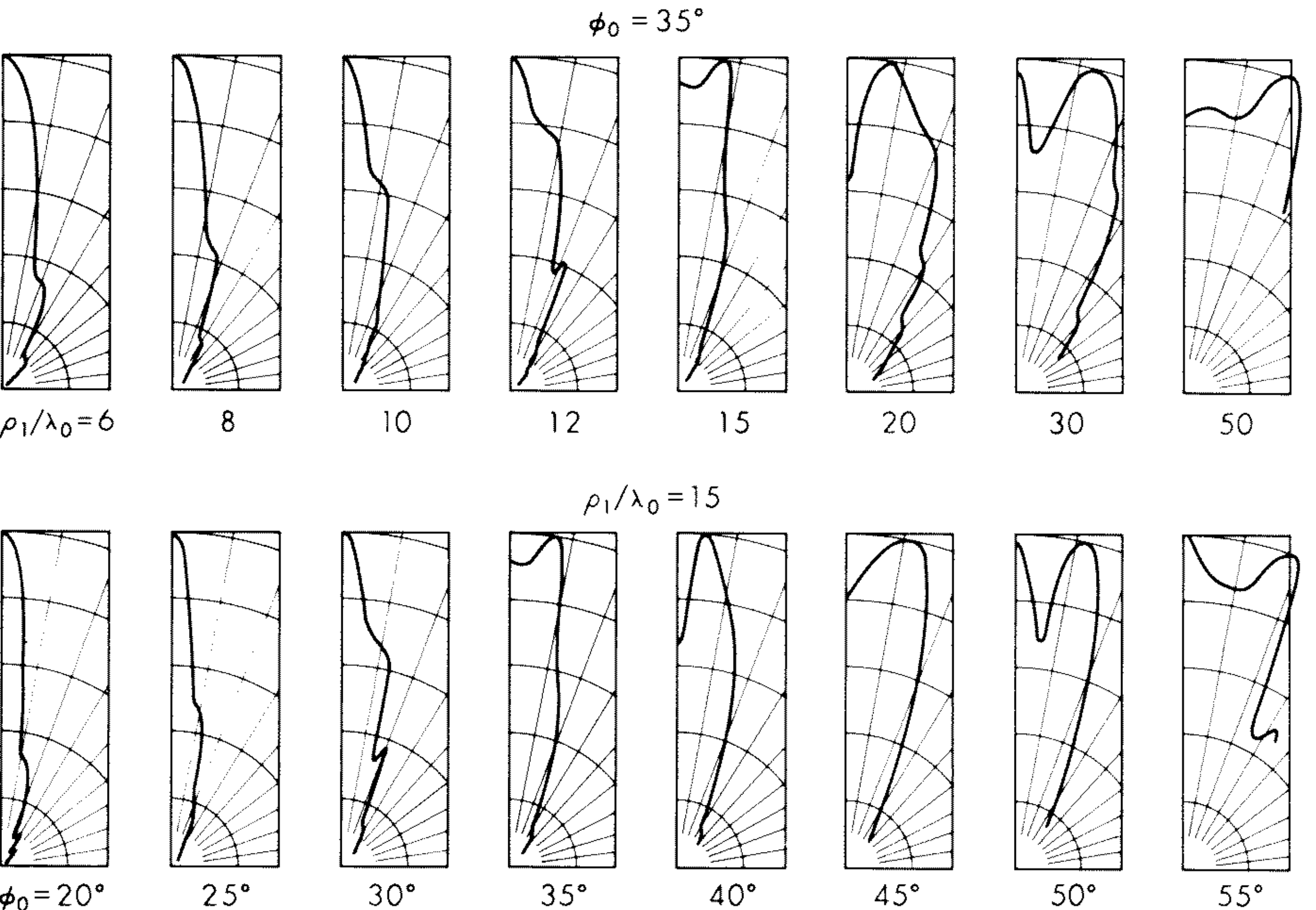


Fig. 15.15 Typical radiation patterns for an E -plane sectoral horn. Upper series for a constant flare angle of 35° ; lower series for a fixed slant length of $15\lambda_0$ and variable flare angle. (From Chu and Barrow.¹⁵)

Figure 15.15 shows calculated patterns for E -plane horns. The top row shows the patterns for a constant flare angle $\phi_0 = 35^\circ$ as a function of the length of the horn, and the bottom row shows the effect of varying the flare angle for a horn of length $\rho_1/\lambda_0 = 15$. It is seen that, although the general trends observed with the H -plane horn also occur here, the patterns for this case are much more irregular because of the presence of the high secondary lobes.

The directivity of an E -plane horn has been computed by Schelkunoff, and the result is²¹

$$D = \frac{64a\rho_1}{\pi\lambda_0 b} \left[C^2 \left(\frac{b}{\sqrt{2\lambda_0\rho_1}} \right) + S^2 \left(\frac{b}{\sqrt{2\lambda_0\rho_1}} \right) \right] \quad (15.39)$$

Figure 15.16 shows the directivity of an E -plane horn as a function of the length of the horn and the aperture dimensions. As with the H -plane horn, it is seen that as the aperture size is increased, the gain increases up to a point, reaches a maximum, and then drops. This phenomenon is again due to the quadratic phase variation across the aperture.

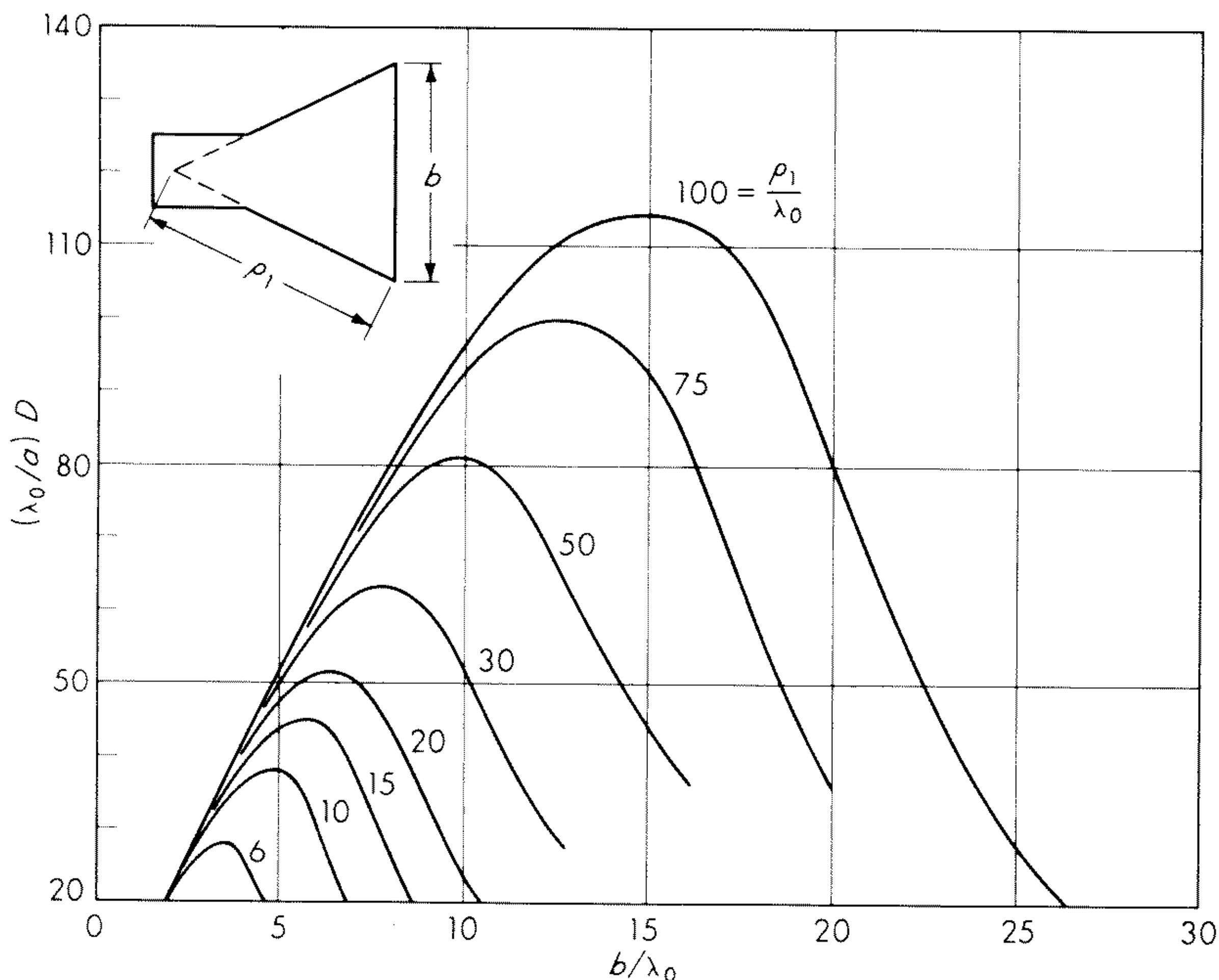


Fig. 15.16 Directivity of E -plane sectoral horns with aperture height b and width a . (Based on fig. 16.4 of Schelkunoff and Friis.¹⁹)

Design data for the E -plane sectoral horn have also been given in the article by Chu and Barrow.¹⁵

Pyramidal Horns

A pyramidal horn is one that is flared in both the E and H planes, as shown in Fig. 15.17. The flare angles for the E -plane flare and the H -plane flare are independent and can be separately adjusted. The E - and H -plane sectoral horns have a sharp beam in one plane but a wide beam width in the other plane. For applications where it is necessary to have directivity in both planes, the pyramidal horn can be used. Because the horn is flared along both axes, the beam is sharp in both planes.

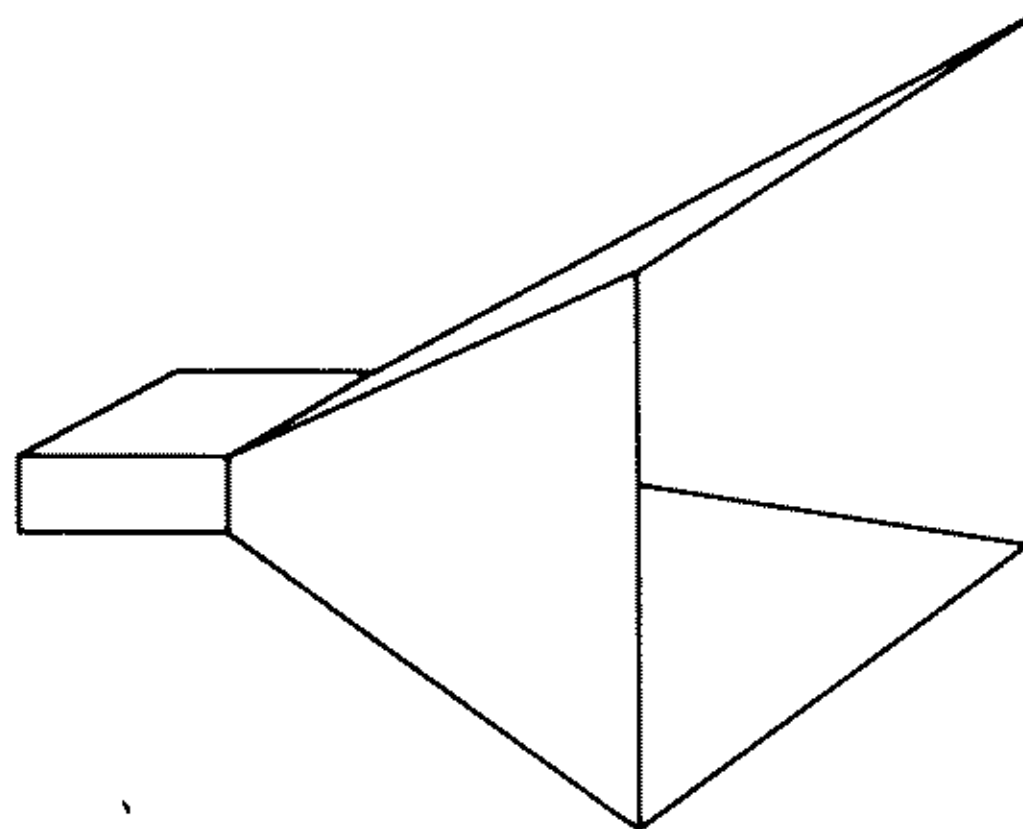


Fig. 15.17 The pyramidal horn.

The usual procedure for treating the pyramidal horn is to combine the results that were obtained for the E -plane sectoral horn and the H -plane sectoral horn. The geometry of a pyramidal horn is such that the walls of the horn do not fit the coordinate surfaces of any separable coordinate system. Hence it is not possible to solve explicitly for the modes associated with this geometry. Instead, the usual practice is to assume that the aperture distribution in the E plane is the same as that of an E -plane sectoral horn, and the aperture distribution in the H plane is the same as that of an H -plane sectoral horn. If the procedure described earlier is used to calculate the pattern, one naturally finds that the E -plane pattern is the same as that of an E -plane sectoral horn and the H -plane pattern is the same as that of an H -plane horn. Thus the E -plane parameters for a pyramidal horn may be chosen by using the E -plane sectoral horn data and the H -plane parameters may be chosen by using H -plane sectoral horn data. Although it would be nice to have a more precise mathematical formulation for the pyramidal horn, in practice it does not seem to matter much, because the above procedure appears to give good results.

Conical Horns

A conical horn is a horn with a circular cross section, as shown in Fig. 15.6*d*. It is essentially the same in performance as a pyramidal horn. A conical horn is normally used when the feed is a circular waveguide, whereas a pyramidal horn is used when the feed is a rectangular waveguide.

Unlike a pyramidal horn, the normal modes associated with the conical horn can be found by associating a spherical coordinate system with the horn. If one chooses the axis of the conical section as the polar axis of a spherical coordinate system, then the cone surface is a surface of constant polar angle, and hence the modes can be solved for. Because of the nature of the functions involved (spherical Bessel functions and Legendre polynomials) the analysis is

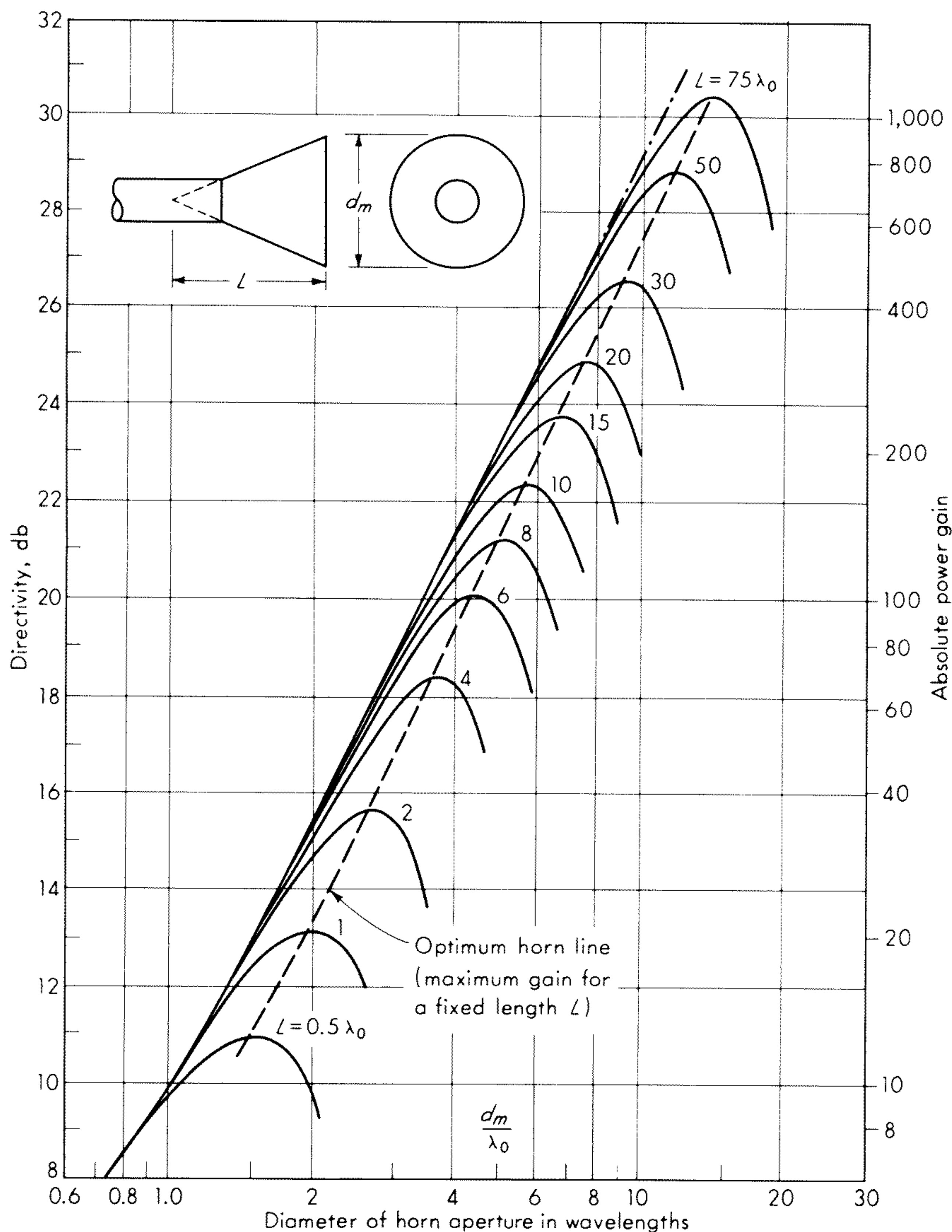


Fig. 15.18 The directivity of a conical horn as a function of axial length and aperture diameter d_m in wavelengths. (From King.²³)

somewhat involved and will not be given here. The reader is referred to the article by Schorr and Beck for the details of the analysis.²²

A conical horn behaves in essentially the same way as a pyramidal horn, and its performance is easily understood from the discussion given above for the sectoral and pyramidal horns. Thus, as the aperture size increases, the gain at first increases and then decreases as the quadratic phase variation begins to become significant. Figure 15.18 shows the gain of a conical horn as a function of horn diameter and length. Excellent design data for conical horns have been given by King,²³ and the reader is referred to his article for a number of useful design curves and performance data.

15.5 Lens-corrected Horns

Large-aperture horns must be very long, since the maximum flare angle is limited by the amount of quadratic phase error in the aperture field that can be tolerated before the directivity falls off. This results in undesirably large and unwieldy structures. Much larger flare angles, and hence a shorter horn length for a given aperture area, can be used if a lens is mounted in the horn aperture to correct the phase distribution of the aperture field. The design of such phase-correction lenses follows the general procedures discussed in Chap. 18. We shall examine only the lens-corrected H -plane horn in detail, but the same principles can be applied to the E -plane, pyramidal, and conical horns. The lens-corrected H -plane sectoral horn has been investigated by Cummins^{24,25} and Jones, Morita, and Cohn.²⁶ The material presented here is based on Cummins' work.²⁴

Figure 15.19 shows a lens-corrected H -plane sectoral horn. The front surface of the lens is plane, and the back surface is hyperbolic. If the field in the horn is assumed to be an expanding cylindrical wave described by the Hankel func-

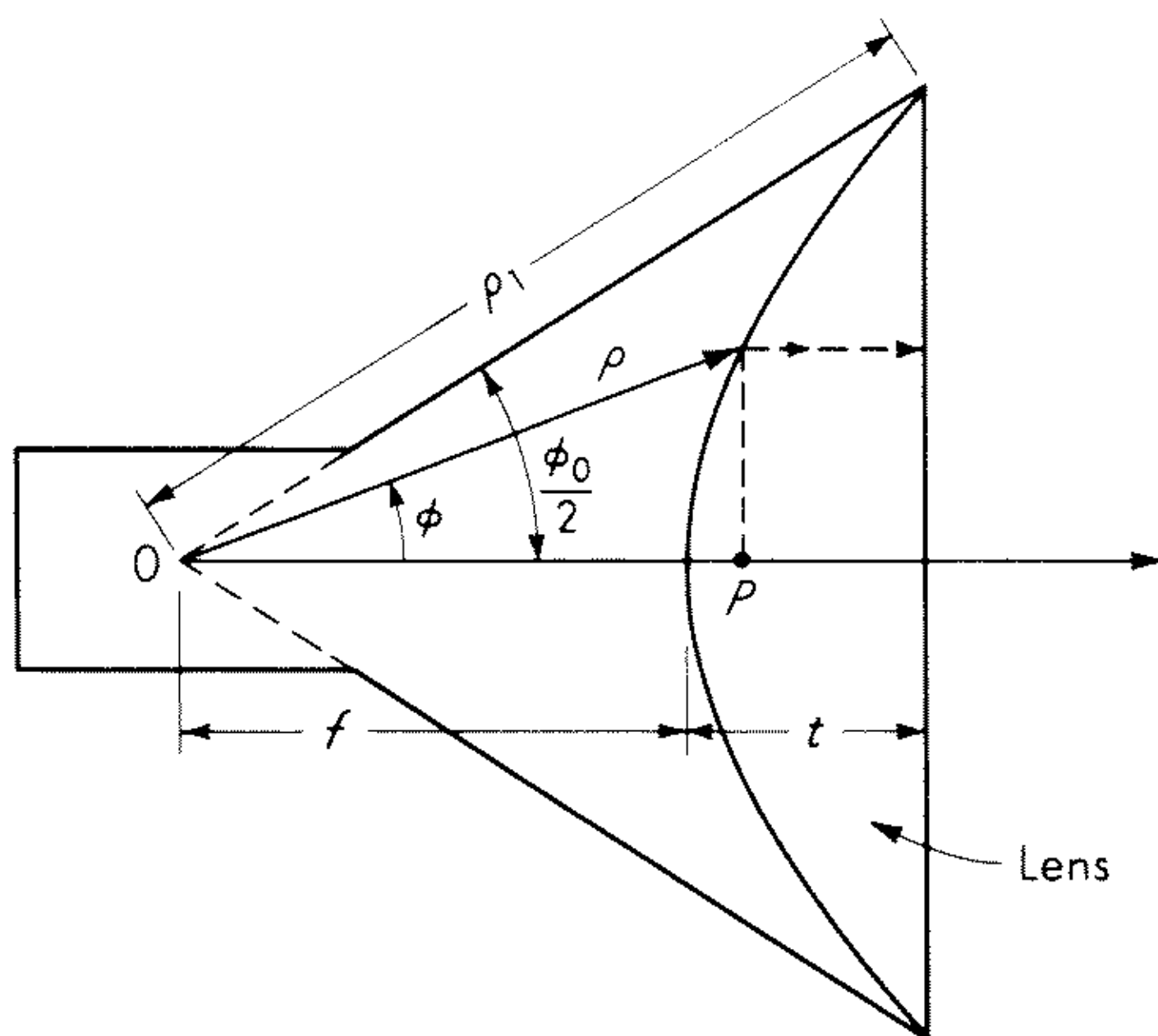


Fig. 15.19 The lens-corrected H -plane horn.

tion of the second kind, the lens contour may be determined by imposing the condition that all ray paths from the vertex 0 to the front lens surface must be equal. From the figure it is easily seen that the back surface of the lens is then determined by the condition

$$\rho = f + n(\overline{OP} - f) = (1 - n)f + n\rho \cos \phi$$

$$\text{or} \quad \rho = \frac{(n - 1)f}{n \cos \phi - 1} \quad (15.40)$$

where $n = \sqrt{\kappa}$ is the index of refraction. The equation for the lens contour is that of a hyperbola in polar coordinates.

The performance of a lens-corrected horn is less than ideal unless the surfaces of the lens are matched to reduce reflections. Reflections from the two surfaces result in interference effects which cause a periodic-like variation in both the amplitude and phase of the aperture field. In addition, multiple reflections from the lens and the horn walls appear to be very significant in increasing the side-lobe level. Techniques for matching the lens surfaces will be described later. For now we shall assume that the lens is matched for the purpose of obtaining the effect of the lens on the aperture field taper.

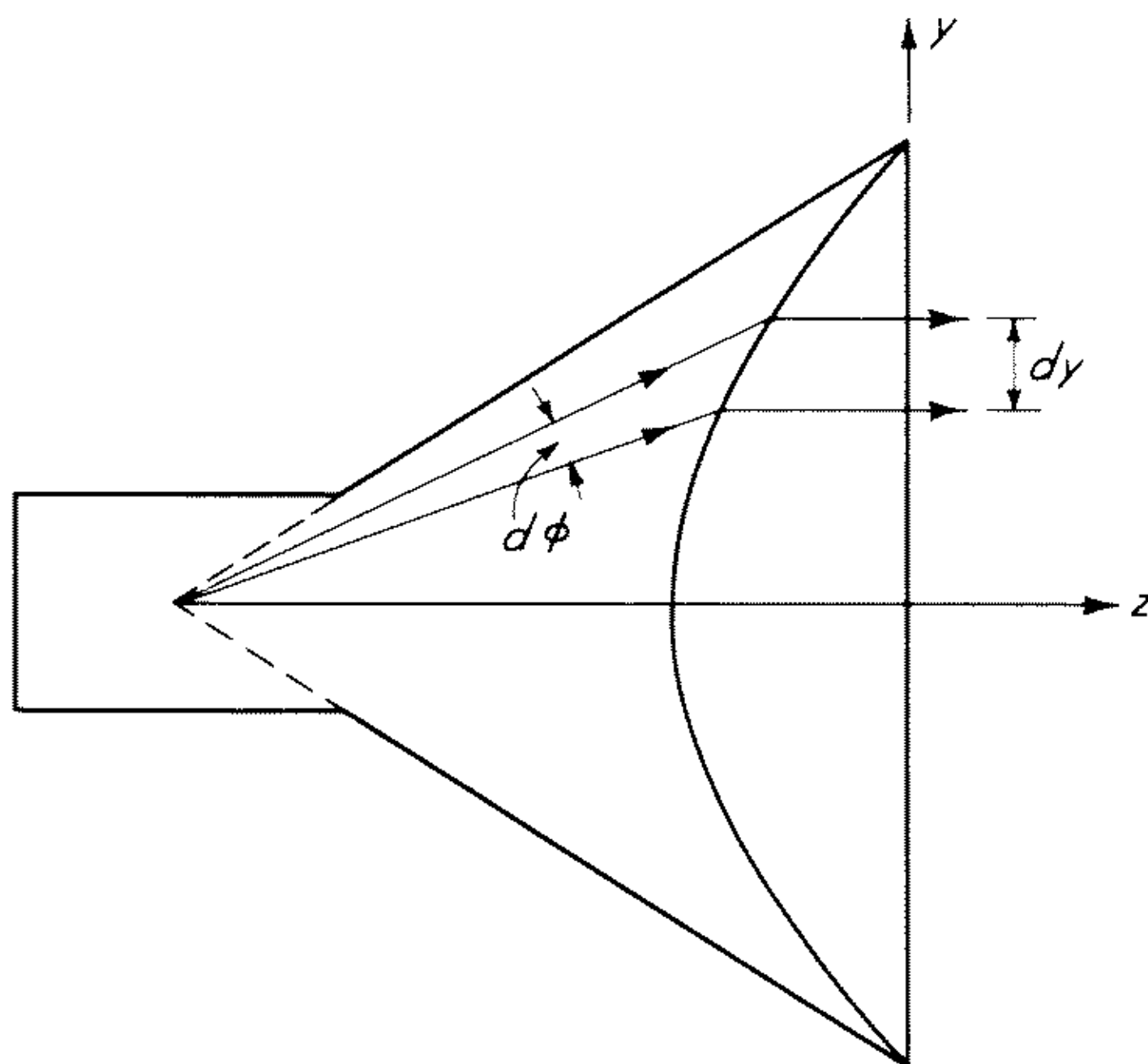


Fig. 15.20 Illustration for the effect of a lens on the aperture field taper.

The power incident on the lens in a wedge of angular width $d\phi$ is refracted into a strip of width dy as shown in Fig. 15.20. If the incident power angular distribution is $P(\phi)$, then the power distribution $P(y)$ along the aperture surface is given by

$$P(y) = P(\phi) \frac{\rho d\phi}{dy}$$

The incident power varies as E_x^2 or $\rho^{-1} \cos^2 (\pi\phi/\phi_0)$, as reference to (15.29a)

shows. Hence the normalized aperture field distribution is proportional to

$$\begin{aligned} \frac{E_x(y)}{E_x(0)} &= \cos \frac{\pi\phi}{\phi_0} \left(\frac{d\phi}{dy} \right)^{\frac{1}{2}} \\ &= \frac{n \cos \phi - 1}{\sqrt{(n - \cos \phi)(n - 1)}} \cos \frac{\pi\phi}{\phi_0} \end{aligned} \quad (15.41)$$

upon evaluating the derivative by using (15.40). To evaluate $E_x(y)$ it is necessary to express ϕ as a function of y . The resultant expression is too complicated for the purpose of evaluating the radiation field. Cummins overcame this difficulty by expanding (15.41) into a Fourier series of the form

$$\frac{E_x(y)}{E_x(0)} = \sum_m C_m \cos \frac{2m\pi y}{a}$$

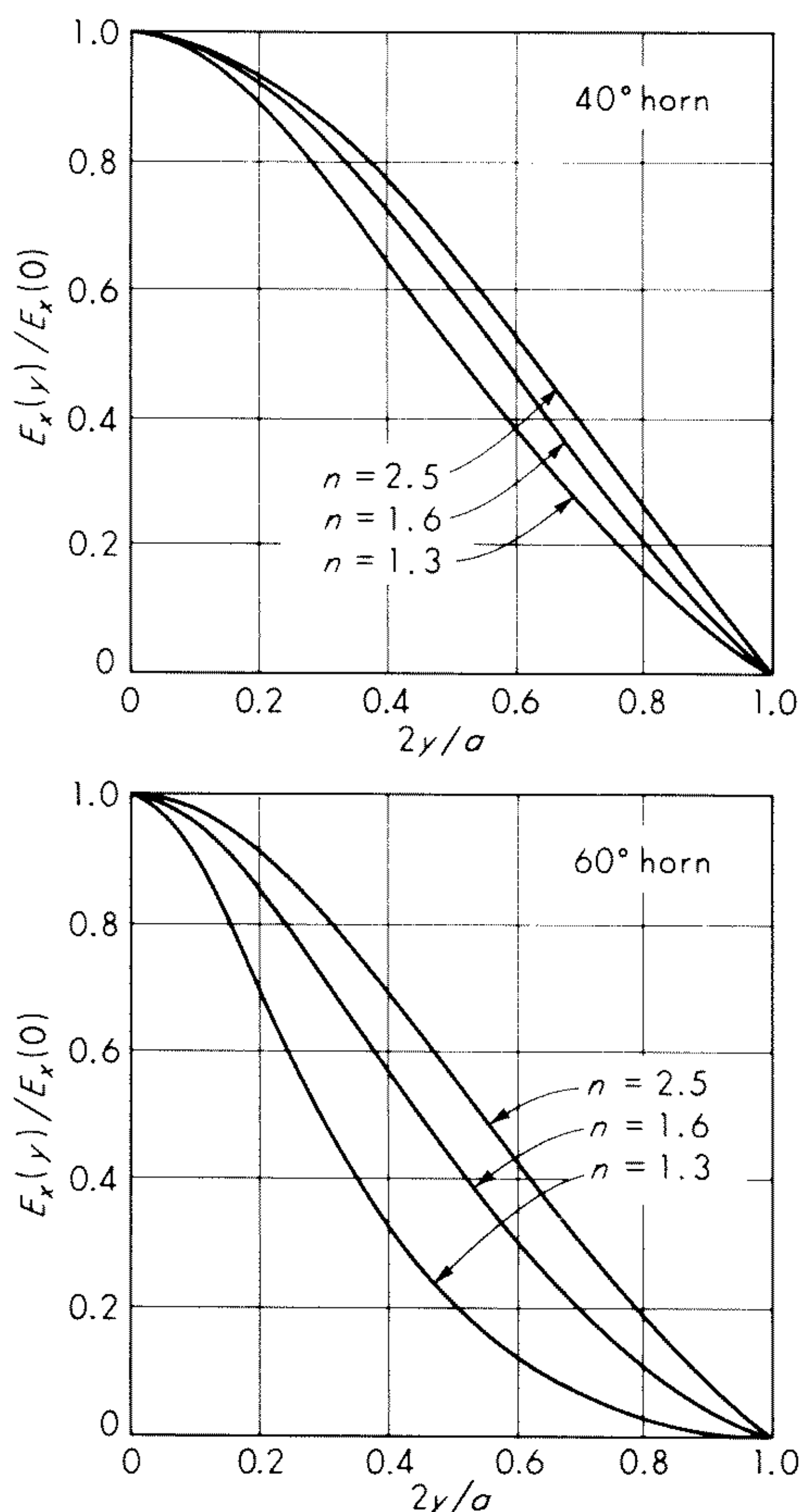


Fig. 15.21 Normalized aperture field distribution in an H -plane horn with a matched lens. (From Cummins.²⁴)

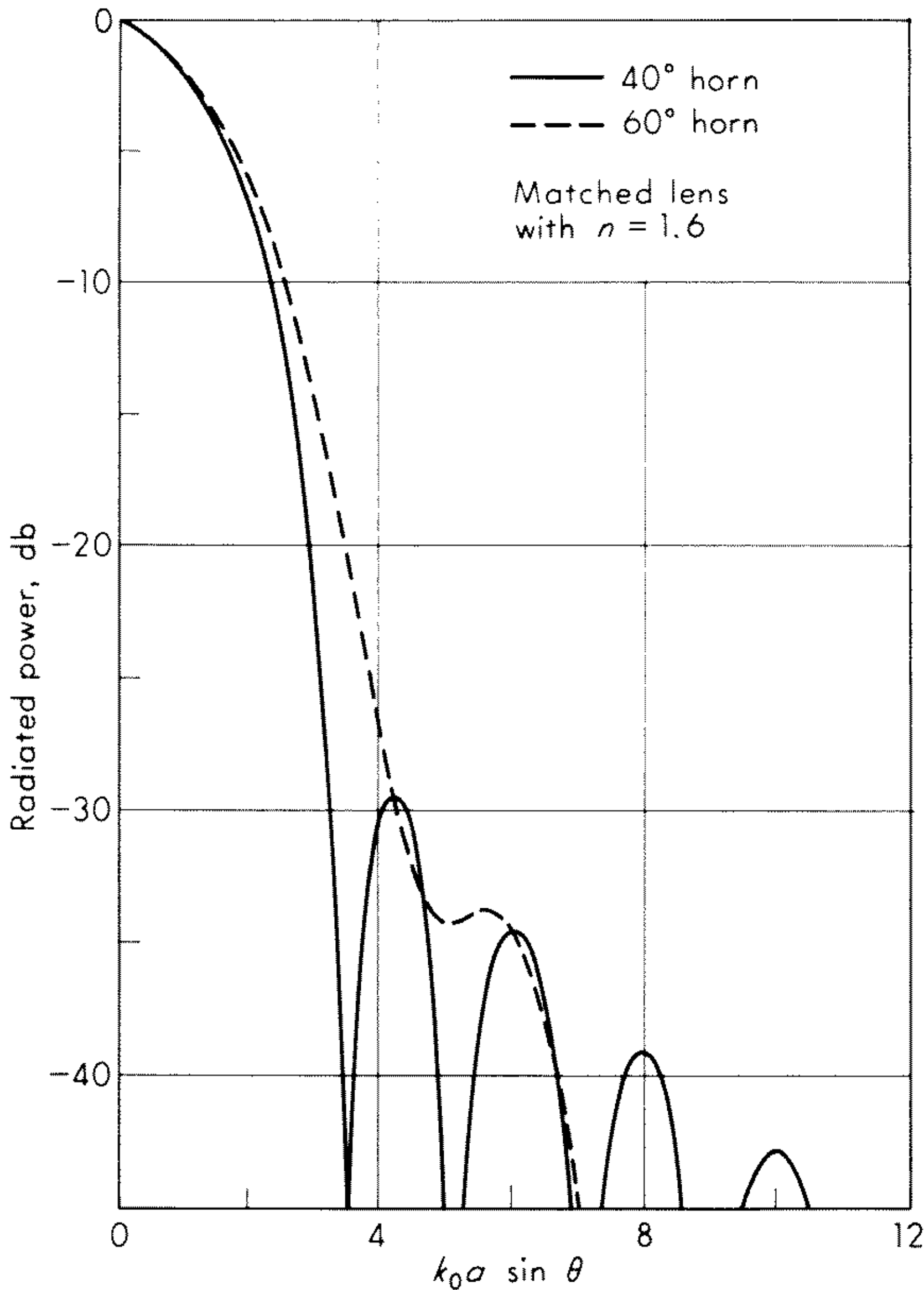


Fig. 15.22 Theoretical radiation patterns from 40 and 60° *H*-plane horns with matched lenses. (From Cummins.²⁴)

where a denotes the aperture width. The results of these computations are shown in Fig. 15.21 for 40 and 60° horns and three different indices of refraction. Note particularly that a high index of refraction results in a smaller-amplitude taper and is therefore preferable.

Using the amplitude distributions given in Fig. 15.21, Cummins calculated the theoretical radiation patterns in the *H* plane with the formula

$$f(\theta) = \int_{-a/2}^{a/2} \frac{E_x(y)}{E_x(0)} e^{jk_0 y \sin \theta} dy$$

These theoretical patterns are shown in Fig. 15.22 for a horn with a matched lens with $n = 1.6$. Cummins gives patterns for $n = 1.3$ and 2.5 also.²⁴ In Fig. 15.23 we show the measured patterns for a lens-corrected 60° horn with and without lens surface matching. Note that for an unmatched lens the side lobes are as much as 12 db higher. Similar results were also obtained by Jones, Morita, and Cohn.²⁶ Cummins has also measured the pattern for a 60° horn with an unmatched lens but with the inside narrow walls of the horn lined with absorbent material. This pattern was essentially as good as the one for a

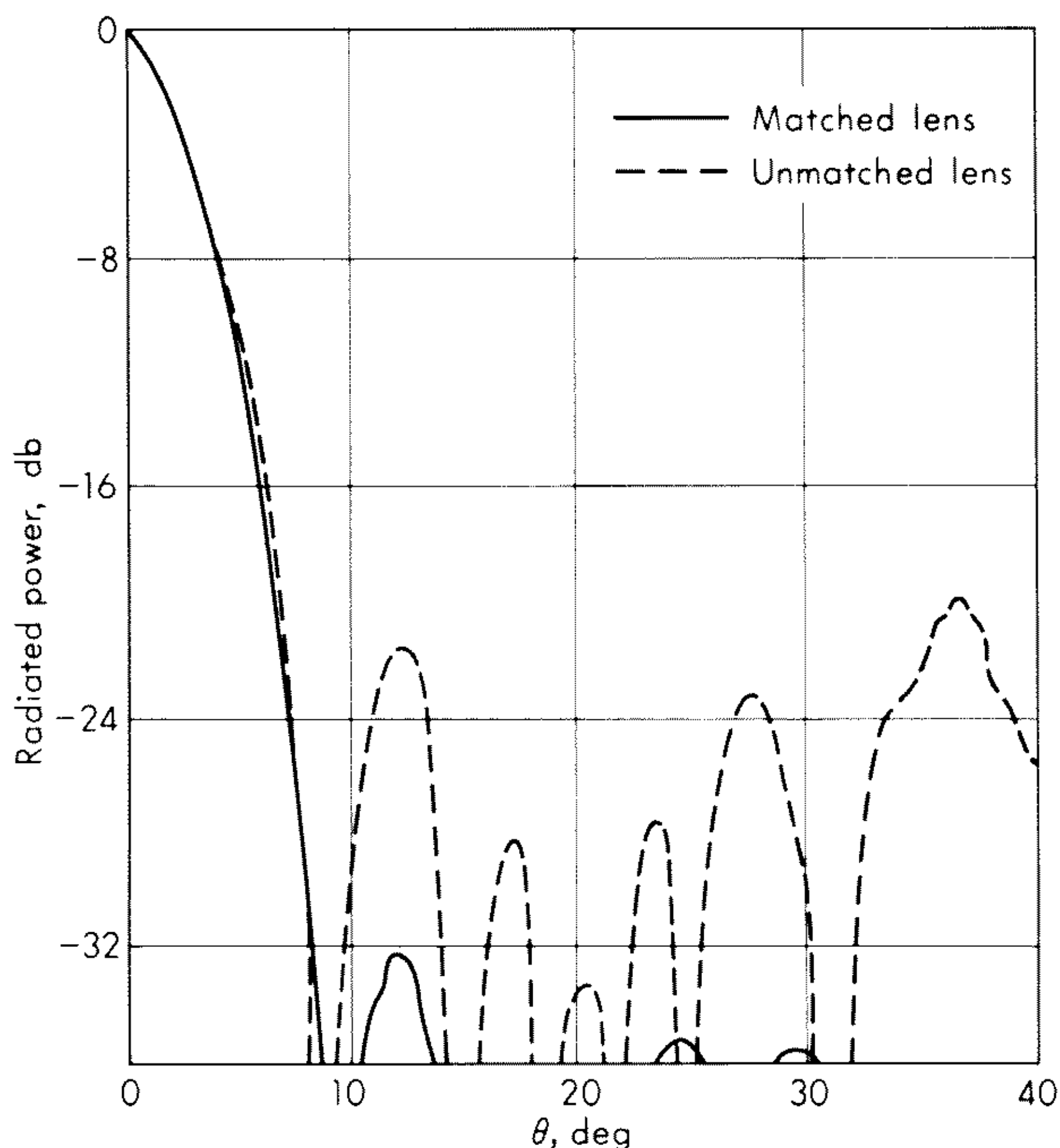


Fig. 15.23 Experimental pattern of a 60° lens-corrected horn, $a = 6$ in., $f = 35$ GHz. (From Cummins.²⁴)

matched lens. The results of this measurement indicate that it is the multiple reflections between the lens and the horn walls that cause the pattern to deteriorate.

Surface Matching of Lenses

The reflections from the surface of a dielectric lens may be reduced to a very small value by the use of impedance-matching techniques adapted from transmission line theory. One method of matching the wave impedance of the lens to that of free space is to locate a row of metallic obstacles, such as round disks, at an appropriate distance from the surface and inside the lens. The metallic obstacles act as a shunt susceptance, and by choosing the parameters correctly, the surface reflections are canceled.^{27,28} A more convenient technique is to construct an equivalent quarter-wave matching layer by cutting slots of appropriate depth and thickness in the surface of the lens.²⁷⁻²⁹ The properties of slotted dielectric interfaces have been examined in detail by Collin and Brown²⁹ and Collin.³⁰

Consider the lens shown in Fig. 15.24a on which a layer of solid dielectric with dielectric constant κ_e has been placed. The lens has a dielectric constant κ . Let a plane wave which is perpendicularly polarized be incident at the point P at an angle θ_i relative to the interface normal. The wave impedance of the incoming wave is³¹

$$Z_0 = \zeta_0 \sec \theta_i$$

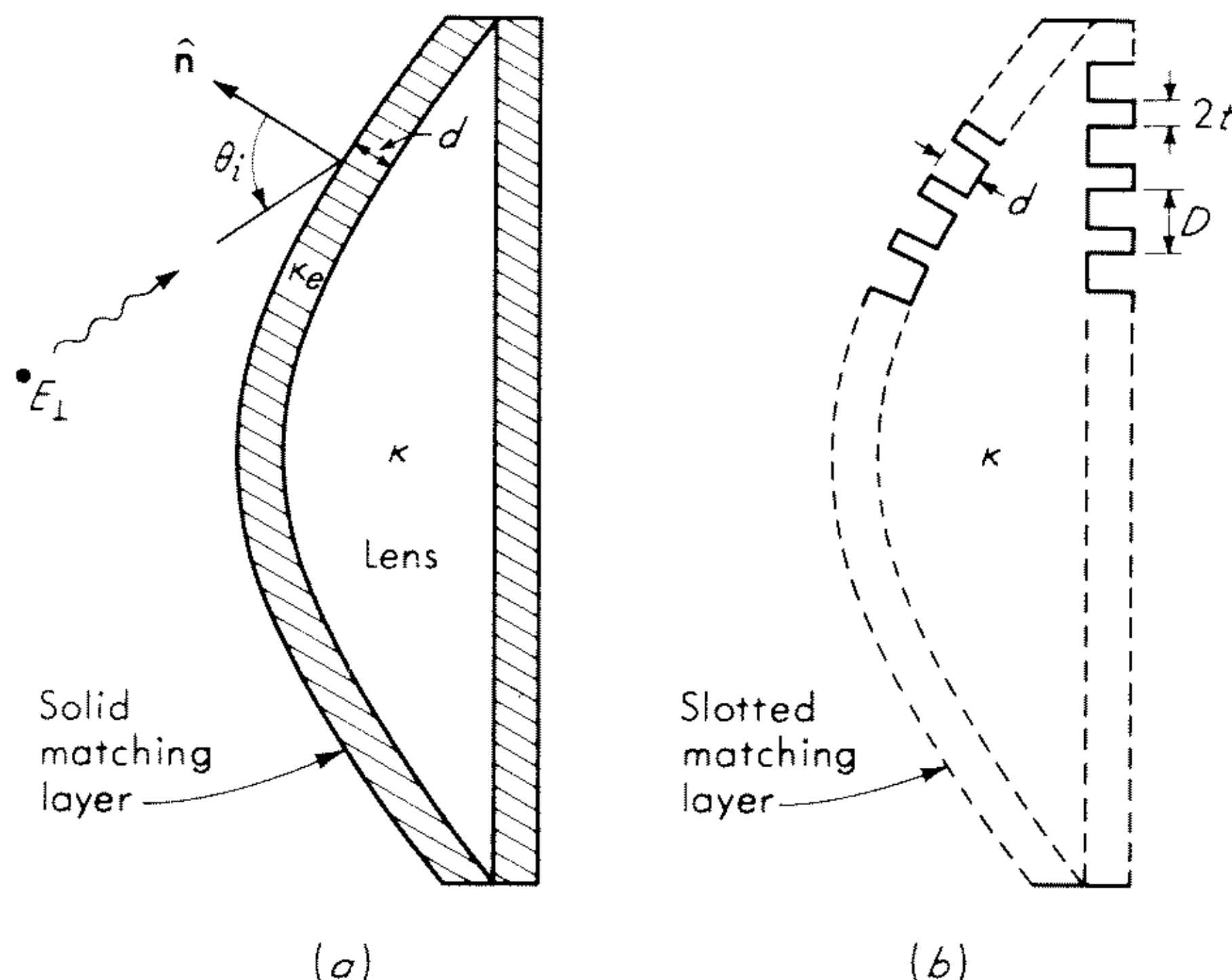


Fig. 15.24 A lens matched with a quarter-wave transformer. (a) Solid layer; (b) slotted layer.

The wave impedances for this plane wave in the two dielectric media are respectively

$$Z_1 = \zeta_0(\kappa_e - \sin^2 \theta_i)^{-1/2} \quad Z_2 = \zeta_0(\kappa - \sin^2 \theta_i)^{-1/2}$$

The wavelength in the medium with dielectric constant κ_e , in the direction perpendicular to the interface, is³¹

$$\lambda_g = \frac{\lambda_0}{\sqrt{\kappa_e - \sin^2 \theta_i}}$$

A quarter-wave transformer that will match the lens to free space without reflection is obtained if κ_e is so chosen that $Z_1 Z_2 = Z_0^2$ and the depth d of the layer equals $\lambda_g/4$. Here it is assumed that the radius of curvature of the lens is large compared with the free-space wavelength λ_0 , so that each portion of the surface may be regarded locally as part of an infinite flat sheet. This assumption is usually quite good in practice. From the above requirements we find that the dielectric constant κ_e is given by

$$\kappa_e = \sin^2 \theta_i + \cos \theta_i \sqrt{\kappa - \sin^2 \theta_i} \quad (15.42)$$

and the depth d is given by

$$d = \frac{\lambda_g}{4} = \frac{\lambda_0}{4\sqrt{\kappa_e - \sin^2 \theta_i}} \quad (15.43)$$

From (15.42) it is apparent that κ_e must be a function of the angle of incidence θ_i , and practically this means that a uniform homogeneous dielectric layer cannot be used.

If slots of thickness $2t$ and spacing D as shown in Fig. 15.24b are cut in the lens surface, the effect is to reduce the effective dielectric constant. By a

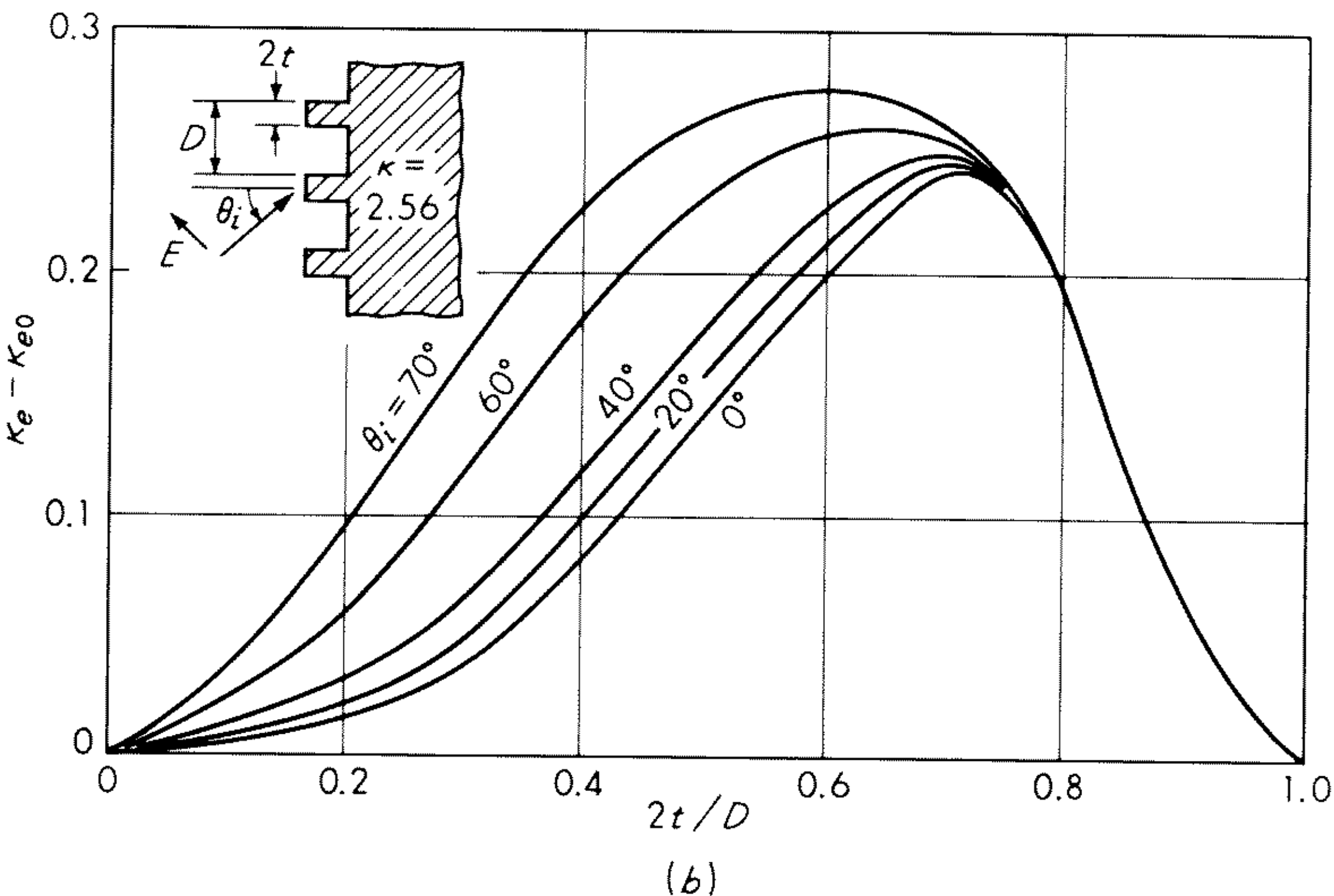
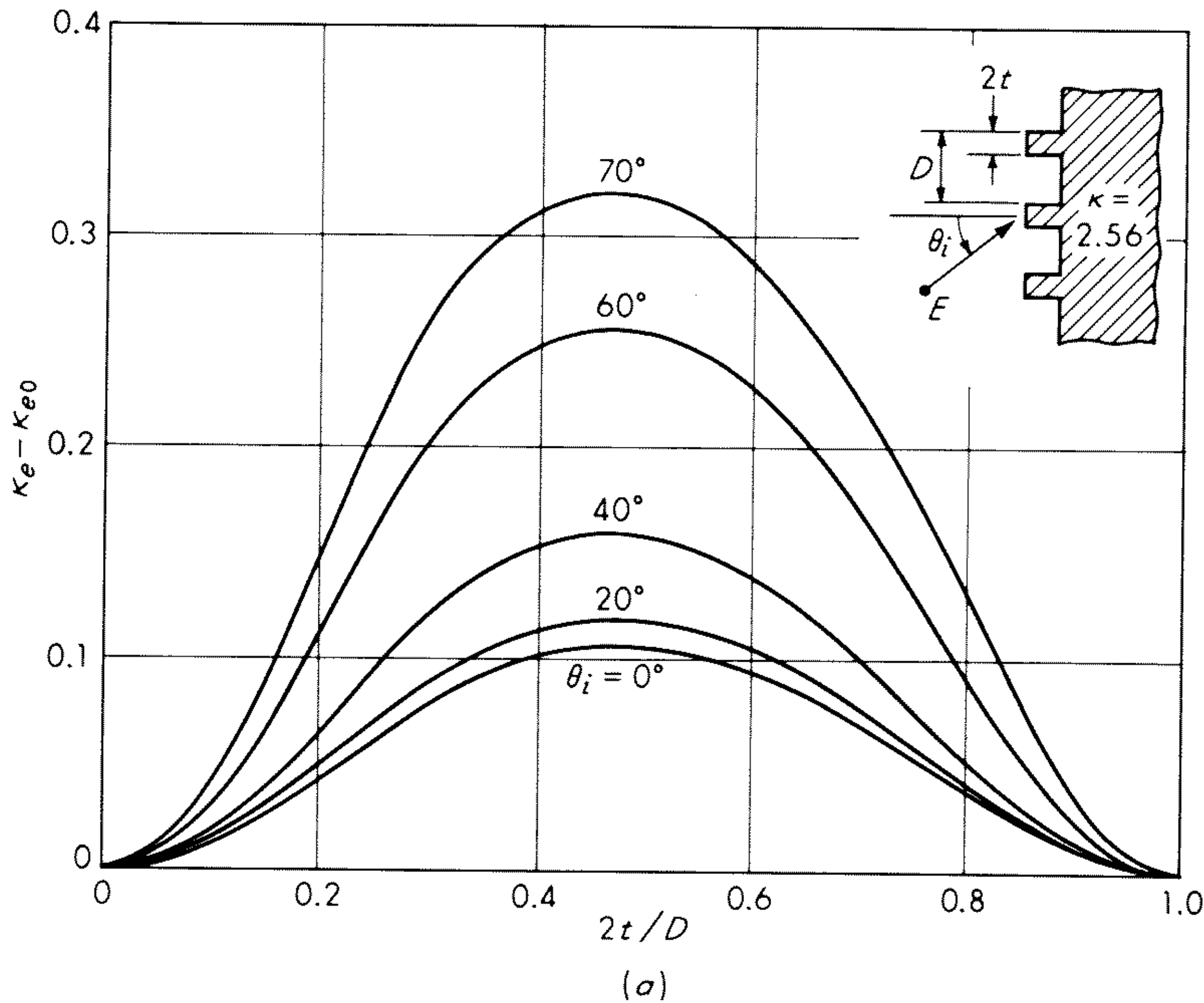


Fig. 15.25 Corrections to static dielectric constants given by (15.44) for $\kappa = 2.56$, $D\sqrt{\kappa} = 0.75\lambda_0$. (a) Perpendicular polarization with electric field parallel to slots; (b) parallel polarization with electric field perpendicular to slots. (From Cummins.²⁴)

proper choice of the ratio $2t/D$, any value of κ_e between unity and κ can be obtained. Hence this is a practical way to provide a varying dielectric constant in a matching layer for the case when the angle of incidence of the incoming wave varies from point to point along the lens surface. If D is very small com-

pared to λ_0 , the effective dielectric constant κ_e is given by the static values

$$\kappa_{e0} = 1 + \frac{(\kappa - 1)2t}{D} \quad \text{perpendicular polarization} \quad (15.44a)$$

$$\kappa_{e0} = \frac{1}{1 - \frac{(\kappa - 1)2t}{\kappa D}} \quad \text{parallel polarization} \quad (15.44b)$$

To reduce the number of slots which must be cut it is desirable to use large values of the spacing D . However, the spacing D must satisfy the relation

$$D < \frac{\lambda_0}{\sqrt{\kappa} + \sin \theta_i} \quad (15.45)$$

to avoid exciting higher-order grating modes in the lens. For a value of D approaching the upper limit the effective dielectric constant κ_e is a few percent larger than the static values given by (15.44) and also depends on the angle θ_i . Cummins has calculated the difference $\kappa_e - \kappa_{e0}$ for values of κ equal to 1.96, 2.56, and 3.24, and 4, with $D = 0.75 \lambda_0 / \sqrt{\kappa}$ (see Ref. 24). His calculations are based on the formulas given by Collin.³⁰ The results for $\kappa = 2.56$ are shown in Fig. 15.25.

A spacing $D = 0.75 \lambda_0 / \sqrt{\kappa}$ satisfies the condition (15.45) for angles of incidence up to 31° only. In the 60° lens-corrected horn the maximum angle of incidence is 64° , so (15.45) is violated. However, this spacing was still used in the design of the matching layer and no serious degradation in performance was found, as the radiation pattern given in Fig. 15.23 shows. Thus it is safe to assume that even though the condition for a higher mode of propagation is violated near the outer edge of the lens, such a mode is, at most, only very weakly excited.

From the above results we can conclude that H -plane horns with flare angles up to at least 60° perform very well if a matched lens is used to correct the aperture field phase distribution. An uncompensated H -plane horn is limited to a maximum flare angle of around 14° for an aperture width of about $18\lambda_0$ if optimum directivity is to be obtained (see Fig. 15.13). Such a horn would be about four times as long as the 60° lens-corrected horn described above, which had an aperture width of $17.7\lambda_0$.

PROBLEMS

15.1 Apply the results of Prob. 3.9 and assume aperture fields $\mathbf{E}_a = E_0 \hat{\mathbf{z}}$, $\mathbf{H}_a = -\zeta_0^{-1} E_0 \hat{\mathbf{y}}$ to show that the resultant radiation pattern differs from (15.21) by a factor $(1 + \sin \theta)/2$. Repeat by using Kirchhoff's formula (3.48b) applied to the surface consisting of the aperture $-a \leq z \leq a$ and the waveguide walls. Since this is a two-dimensional problem, use the asymptotic form of $-(j/4)H_0^2(k_0 R)$ for G_0 . Assume $\mathbf{E} = E_0 \hat{\mathbf{z}}$ on the aperture and zero elsewhere, and note that

$$\frac{\partial \mathbf{E}_a}{\partial n} = -jk_0 \mathbf{E}_a \quad \text{and} \quad \frac{\partial G_0}{\partial n} = \frac{\partial G_0}{\partial x'}$$

Kirchhoff's method gives the result (15.21) multiplied by the factor $(1 + \sin \theta)/2$ for E_z , and this points out one of its shortcomings, since the far-zone field must have a zero radial component.

15.2 Derive the expression (15.25) for the far-zone field radiated by a TE_{11} mode in a circular guide.

15.3 Complete the steps leading to the result (15.34).

15.4 For the E -plane sectoral horn assume an aperture electric field E_z given by (15.38) and an aperture magnetic field $H_y = \zeta_0^{-1} E_z$. Thus show that the far-zone radiation field is given by (15.34) but with

$$f_z = \frac{2B\pi a \cos(k_y a/2)}{\pi^2 - k_y^2 a^2} \sqrt{\frac{\pi \rho_1}{k_0}} e^{jk_x^2 \rho_1/2k_0} [C(t_2) - jS(t_2) - C(t_1) + jS(t_1)]$$

where $k_x = k_0 \cos \phi \sin \theta$, $k_y = k_0 \sin \phi \sin \theta$, and

$$t_i = \sqrt{\frac{1}{\pi k_0 \rho_1}} \left[(-1)^i k_0 \frac{a}{2} - k_x \rho_1 \right] \quad \text{for } i = 1, 2$$

REFERENCES

1. Heins, A. E.: The Radiation and Transmission Properties of a Pair of Semi-infinite Parallel Plates, *Quart. Appl. Math.*, vol. 6, part. I, pp. 157–166, part II, pp. 215–220, 1948.
2. Vajnshtejn, L. A.: Rigorous Solution of the Problem of an Open-ended Parallel-plate Waveguide, *Izv. Akad. Nauk, Ser. Fiz.*, vol. 12, pp. 144–165, 1948. This paper, as well as five others dealing with radiation from waveguides, has been translated into English by J. Shmoys and published as Report EM-63, 1954, by the Institute of Mathematical Sciences, Division of Electromagnetic Research, New York University.
3. Noble, B.: "Methods Based on the Wiener-Hopf Technique," Pergamon Press, New York, 1958.
4. Chu, L. J.: Calculation of the Radiation Properties of Hollow Pipes and Horns, *J. Appl. Phys.*, vol. 11, pp. 603–610, 1940.
5. Southworth, G. C., and A. P. King: Metal Horns as Directive Receivers of Ultra-short Waves, *Proc. IRE*, vol. 27, pp. 95–102, 1939.
6. Barrow, W. L., and F. M. Greene: Rectangular Hollow Pipe Radiator, *Proc. IRE*, vol. 26, pp. 1498–1519, 1938.
7. Silver, S.: "Microwave Antenna Theory and Design," M.I.T. Radiation Laboratory Series, vol. 12, McGraw-Hill Book Company, New York, 1949.
8. Vajnshtejn, L. A.: Theory of Symmetric Waves in a Cylindrical Waveguide with an Open End, *Zh. Tekhn. Fiz.*, vol. 18, pp. 1543–1564, 1948.
9. Vajnshtejn, L. A.: Radiation of Asymmetric Electromagnetic Waves from the Open End of a Circular Waveguide, *Dokl. Akad. Nauk.*, vol. 74, pp. 485–488, 1950.
10. Pearson, J. D.: Diffraction of Electromagnetic Waves by a Semi-infinite Circular Waveguide, *Proc. Cambridge Phil. Soc.*, vol. 49, pp. 659–667, 1953.
11. Levine, H., and J. Schwinger: On the Radiation of Sound from an Unflanged Circular Pipe, *Phys. Rev.*, vol. 73, pp. 383–406, 1948.
12. Vajnshtejn, L. A.: The Theory of Sound Waves in Open Tubes, *Zh. Tekhn. Fiz.*, vol. 19, pp. 911–930, 1949.
13. Marcuvitz, N. (ed.): "Waveguide Handbook," chap. 4, McGraw-Hill Book Company, New York, 1951.
14. Barrow, W. L., and L. J. Chu: Theory of the Electromagnetic Horn, *Proc. IRE*, vol. 27, pp. 51–64, January, 1939.

15. Chu, L. J., and W. L. Barrow: Electromagnetic Horn Design, *Trans. AIEE*, vol. 58, pp. 333–338, July, 1939.
16. Barrow, W. L., and F. D. Lewis: The Sectoral Electromagnetic Horn, *Proc. IRE*, vol. 27, pp. 41–50, January, 1939.
17. Rhodes, D. R.: An Experimental Investigation of the Radiation Patterns of Electromagnetic Horn Antennas, *Proc. IRE*, vol. 36, pp. 1101–1105, September, 1948.
18. Schelkunoff, S. A.: "Electromagnetic Waves," p. 364, D. Van Nostrand Company, Inc., New York, 1943.
19. Schelkunoff, S. A., and H. T. Friis: "Antennas, Theory and Practice," pp. 528 and 529, John Wiley & Sons, Inc., 1952.
20. Jakes, W. C., Jr.: Gain of Electromagnetic Horns, *Proc. IRE*, vol. 39, pp. 160–162, February, 1951.
21. Schelkunoff, S. A.: Ref. 19, p. 362.
22. Schorr, M. G., and F. J. Beck, Jr.: Electromagnetic Field of the Conical Horn, *J. Appl. Phys.*, vol. 21, pp. 795–801, August, 1950.
23. King, A. P.: The Radiation Characteristics of Conical Horn Antennas, *Proc. IRE*, vol. 38, pp. 249–251, March, 1950.
24. Cummins, J. A.: Side Lobe Reduction in the Radiation Field of Lens Corrected *H*-plane Horns, *master of science thesis*, Laval University, August, 1960.
25. Cummins, J. A.: Two Methods of Improving the Performance of Lens Corrected *H*-plane Horns, *IRE Can. Conv. Record*, pp. 232–239, 1958.
26. Jones, E. M. J., T. Morita, and S. B. Cohn: Measured Performance of Matched Dielectric Lenses, *IRE Trans. Antennas Propagation*, vol. AP-4, pp. 31–33, January, 1956.
27. Morita, T., and S. B. Cohn: Microwave Lens Matching by Simulated Quarter-wave Transformers, *IRE Trans. Antennas Propagation*, vol. AP-4, pp. 33–39, January, 1956.
28. Jones, E. M. J., and S. B. Cohn: Surface Matching of Dielectric Lenses, *J. Appl. Phys.*, vol. 26, pp. 452–457, April, 1955.
29. Collin, R. E., and J. Brown: The Design of Quarter-wave Matching Layers for Dielectric Surfaces, *Proc. Inst. Elec. Engrs. (London)*, vol. 103, part C, pp. 153–158, September, 1955.
30. Collin, R. E.: Properties of Slotted Dielectric Interfaces, *IRE Trans. Antennas Propagation*, vol. AP-7, pp. 62–73, January, 1959.
31. Collin, R. E.: "Field Theory of Guided Waves," sec. 3.5, McGraw-Hill Book Company, New York, 1960.

BIBLIOGRAPHY

- Aharoni, J.: "Antennae — An Introduction to Their Theory," Clarendon Press, Oxford, 1946.
- Blake, L. J.: "Antennas," John Wiley & Sons, Inc., New York, 1966.
- Brown, J.: "Microwave Lenses," Methuen & Co., Ltd., London, 1953.
- Fradin, A. Z.: "Microwave Antennas," Pergamon Press, New York, 1961.
- Fry, D. W., and F. K. Goward: "Aerials for Centimetre Wavelengths," Cambridge University Press, New York, 1950.
- Hansen, R. C. (ed.): "Microwave Scanning Antennas," Academic Press Inc., New York, vol. I, 1964, vols. II and III, 1966.
- Harper, A. E.: "Rhombic Antenna Design," D. Van Nostrand Company, Inc., Princeton, N.J., 1941.
- Jasik, H. (ed.): "Antenna Engineering Handbook," McGraw-Hill Book Company, New York, 1961.
- Jordan, E. C.: "Electromagnetic Waves and Radiating Systems," Prentice-Hall, Inc., Englewood Cliffs, N.J., 1950.
- Kiely, D. G.: "Dielectric Aerials," Methuen & Co., Ltd., London, 1953.
- Kraus, J. D.: "Antennas," McGraw-Hill Book Company, New York, 1950.
- Laport, E. A.: "Radio Antenna Engineering," McGraw-Hill Book Company, New York, 1952.
- Moullin, E. B.: "Radio Aerials," Oxford University Press, Fair Lawn, N.J., 1949.
- Page, K. G.: "Principles of Aerial Design," D. Van Nostrand Company, Inc., Princeton, N.J., 1966.
- Rumsey, V. H.: "Frequency Independent Antennas," Academic Press Inc., New York, 1966.
- Schelkunoff, S. A.: "Advanced Antenna Theory," John Wiley & Sons, Inc., New York, 1952.
- and H. T. Friis: "Antennas: Theory and Practice," John Wiley & Sons, Inc., New York, 1952.
- Silver, S.: "Microwave Antenna Theory and Design," McGraw-Hill Book Company, New York, 1949.
- Smith, R. A.: "Aerials for Metre and Decimetre Wavelengths," Cambridge University Press, New York, 1949.
- Thourel, T.: "The Antenna," John Wiley & Sons, Inc., New York, 1960.
- Wait, J. R.: "Electromagnetic Radiation from Cylindrical Structures," Pergamon Press, New York, 1959.
- Walter, C. H.: "Traveling Wave Antennas," McGraw-Hill Book Company, New York, 1965.
- Weeks, W. L.: "Antenna Engineering," McGraw-Hill Book Company, New York, 1968.
- Williams, H. P.: "Antenna Theory and Design," 2 vols., Sir Isaac Pitman & Sons, Ltd., London, 1950 (reprinted in 1966).
- Wolff, E. A.: "Antenna Analysis," John Wiley & Sons, Inc., New York, 1966.

INDEX

- Analytic signal, 110–111
 for polychromatic wave, 109–111
- Anisotropic media, constitutive relations for, 4, 5
- Antenna:
 receiving, 93–94
 coherence matrix for, 113
 cross section of, 100–103
 for polarized waves, 103–109
 directional properties of, 98–100
 loop, 474–478
 mutual coherence matrix for, 116
 noise in, 119–123
 for partially polarized waves, 103–109
 reciprocity for, 94–98
 scattering properties of, 123–133
 Stokes' parameters for, 107
 scattering from, 123–133
 minimum scattering, 131–133
 scattering matrix for, 126–127
- Antenna effective length, 105
 of cylindrical dipole, 378, 379
 of loop, 477, 478
- Antenna Q , definition of, 237
- Aperture, focused, 86–89
 field of, 87–89
- Aperture antenna:
 definition of, 61
 directivity of, 78, 79
 equivalent array, 246–248
 far-zone radiation field for, 65–68
 and field equivalence principle, 69–71
 and Fourier transforms, 62–69
 radiation from, 61–79
 (*See also* Pattern synthesis)
- Array:
 of arrays, 172, 173
 binomial, 175, 176
 Chebyshev, 186–194, 260, 261
 circular, 163–172
- Array:
 circular: array factor for, 163–165
 continuous, 165–168
 of dipoles, 384–387
 (*See also* Cylindrical antenna)
 directive, 171, 172
 omnidirectional, 168–171
 synthesis of, 248–250
 (*See also* Pattern synthesis)
 of dipoles, 379–384
 directivity of, 143–145
 element factor for, 140, 141
 and equivalence with aperture, 246–248
 excitation of, 176–184
 factor (*see* Array factor)
 factorization for, 140–142
 gain of, 143–145
 idling current on, 179
 impedance matrix for, 176, 177
 mutual radiation resistance for, 183
 nonuniform, 207–210
 density tapering for, 207
 deterministic, 212–219
 statistical, 219–225
 dynamic programming method for, 211–212
 missing elements in, effect of, 225–227
 synthesis of, 265–270
 (*See also* Pattern synthesis)
 optimization of performance indices for, 194–201
 and traveling-wave theorems, 196–198
 pattern multiplication for, 173
 pattern synthesis for, 184–193
 Dolph-Chebyshev method, 186–194
 Schelkunoff's method, 185–186
 (*See also* Pattern synthesis)
 radiation from, 139–142

Array:

- random errors in, 227–233
 - effect on directivity, 233
 - effect on side lobes, 231, 232
- rectangular, pattern synthesis for, 238–244
- with tapered current distribution, 158–163
 - and Schelkunoff's polynomial, 158–160
 - and Z transforms, 160–163
- terminal quantities for parameters of, 181–184
- types of, 172
- with uniform current distribution, 145–147
 - directivity of, 151–157
 - pattern of, 147–151
- (*See also* Cylindrical antenna; Loop antenna; Pattern synthesis; Waveguide slot array)

Array factor, 140

- for binomial array, 175, 176
- for triangular current distribution, 174, 175
- for uniform current distribution, 145–151

Babinet's principle, 565–567

Bernstein polynomial (*see* Pattern synthesis)

Biconical antenna:

- admittance of, 490, 491
- asymmetric, 506–508
 - dielectric-coated, 510–513
 - with single cone, 508–510
- with dielectric loading, 502, 503
 - in conducting media, 503, 505
 - in plasma, 506
- and dipole in conical sheath, 513–519
- formal solution for, 488–491
- in inhomogeneous dissipative media, 499–502
- limiting cases of: spherical antenna, 491, 492
 - admittance of, 492
 - thin wire, 492–494
- variational solution for impedance of, 494–499

Binomial array, 175, 176

Boundary conditions:

- at conductor edge, 18, 19
- for cylindrical antenna, 353
- for imperfect conductor, 18
- at infinity, 20, 21, 309–311
- for interface between two media, 16, 17
- for perfect conductor, 17

Brightness of radio source, 116

Chebyshev array, 186–194, 260–261

Chebyshev polynomial, 187, 260

Circular array, 163–172

- of cylindrical antennas, 384–387
- driven, 387–392
- phase sequence currents for, 384
- synthesis of, 248–250
- (*See also* Array; Cylindrical antenna; Pattern synthesis)

Coherence matrix:

- for antenna, 113
- mutual: for antenna, 116
 - for partially polarized waves, 115
 - for partially polarized waves, 112

Constitutive parameters, properties of, 8–10

Continuity equation, 3, 306

Current element:

- radiation from, 29–32
- radiation resistance of, 36

Cylindrical antenna:

- admittance of, 360–366
- boundary conditions for, 353
- center-loaded: charge on, 374–378
 - current on, 374–378
- charge distribution on, 360–362
- circular array of, 384–387
 - current on, 338–392
 - driven, 387–392
 - impedance of, 389–392
 - phase sequence currents for, 384
 - radiation field of, 389–392
- collinear array of, 409, 410
- curtain array of, 392–402
 - admittance for, 397–399
 - currents on, 395, 396
 - radiation field for, 399–402

Cylindrical antenna:

- current distribution on, 360–362
- dipole: arrays of, 417–419
 - field from, 418, 419
- conductance of, 417
- coupled to open-wire line, 410–417
- integral equation for current on, 413–416
- vector potential for, 412, 413
- directivity of, 378, 379
- effective length of, 378, 379
- integral equation for current on, 356–360
- log-periodic array of, 407–409
- near zone fields for, 367–371
- parallel array of, 379–384
- parasitic array of, 402–406
 - admittance of driven elements for, 404, 405
 - current on, 403, 404
 - horizontal field from, 404, 406
- radiation field of, 371–374
- scattering from, near zone field, 379–381
- staggered array of, 409, 410
- vector potential for, 352–356
- (*See also* Dipole antenna; Linear antenna)

Diffraction:

- formulas for, 79–85
- and Kirchhoff's formula for, 85, 86

Dipole antenna:

- finite length: admittance of, 441
- charge on, 441, 449, 450
- cross section of, backscattering, 451, 452
- current on, 441, 449, 450
- radiation field of, 441, 447, 448
- horizontal, above disk, 554–557
- long: driven by coaxial line, 421–430
- Green's function for, 423, 424
- integral equation for electric field of, 425
- thin, input admittance of, 427, 428
- Wiener-Hopf solution for, 432–438

Dipole antenna:

- transient behavior of, 453–455
- (*See also* Cylindrical antenna; Linear antenna)

Dirac delta function, 1

Directivity:

- of antenna, 33
- of aperture, 78, 79
- of current element, 34
- of uniform array, 151–157

Dispersion relation for plane waves, 12

Effective length of antenna (*see* Antenna effective length)

Element factor for array, 140, 141

EMF method for antenna impedance, 48–51

Energy, electromagnetic: and antenna impedance, 35

- in dispersive media, 8

- time average, 6–8

- velocity of, 14–16

Errors, random, in arrays, 227–233
(*See also* Array)

Field equivalence principle, 69–71

- Love's, 70

- modification of, 70

Filled array, 209

Gain of antenna, 34

Green's function:

- for dipole antenna, 423, 424
- dyadic: for electric field in free space, 42, 43
- for slot in waveguide, 611–613
- for vector potential, 41
- scalar: for Helmholtz' equation, 42
- in spheroidal coordinates, 548–550
- for wave equation, 309–311

Group velocity, 13, 14

Hallen's integral equation for linear antenna, 311, 312

- Hansen-Woodyard condition, 156, 157
- Helmholtz' equation, 11
- Horn antenna:
- conical, 644–646
 - E*-plane sectoral, 641–643
 - directivity of, 643
 - pattern of, 642, 643
 - H*-plane sectoral, 633–641
 - directivity of, 639, 640
 - lens corrected, 646–653
 - aperture field for, 647, 648
 - pattern of, 649, 650
 - pattern of, 637, 638
 - radiation field of, 636, 637
 - pyramidal, 644
- Idling current on array, 179
- Impedance of antenna, 35
 - EMF method for, 48–51
 - of thin wire antenna, 50, 51
 - variational method for, 51–57, 431
 - (*See also* Biconical antenna; Cylindrical antenna; Linear antenna)
- Impedance of waveguide slot, 602–616
 - approximate theory for, 602–610
 - broadwall, 609, 610
 - inclined sidewall, 610
 - variational method for, 611–616
- Kirchhoff's formula, 85, 86
- Krönig-Kramers relations, 10
- Lens for *H*-plane sectoral horn, 646–653
 - and aperture field, 647, 648
 - surface matching of, 650–653
- Linear antenna:
- with azimuthal dependent fields, 339–345
 - circular tubular, 314–319
 - field from, 318, 333
 - input conductance for, 319
 - integral equation for current on, 320–324, 335–339
 - iterative solution of, 324–332
 - integral equation for, 311, 312
 - Linear antenna:
 - transient response of, 347–350
 - (*See also* Dipole antenna)
 - Loop antenna, 458
 - coupled to open-wire line, 480, 481
 - in dissipative media, 463–470
 - admittance of, 465–468
 - current on, 468–470
 - integral equation for, 458–460
 - solution of, 460–463
 - radiation field of, 470–472
 - receiving, small, 474–478
 - current on, 476, 477
 - effective length of, 477, 478
 - shielded, 478–480
 - transmitting, small, 472–474
 - admittance of, 473
 - current on, 472, 473
 - radiation field from, 473, 474
 - Lorentz condition, 23, 307
 - Lorentz reciprocity theorem, 24, 25
 - and antennas, 94–98
 - Magnetic dipole:
 - radiation from, 36, 37
 - radiation resistance of, 37
 - Magnetic ring source for cylindrical antenna, 52
 - Maxwell's equations:
 - with magnetic sources, 3
 - time dependent, 2, 306, 307
 - for time harmonic fields, 3, 308, 309
 - Noise in receiving antenna, 119–123
 - Noise temperature, 117–123
 - Nyquist's formula, 121
 - Parasitic array, 402–406
 - (*See also* Cylindrical antenna)
 - Pattern multiplication, 173–176
 - Pattern synthesis, 235–238
 - and antenna *Q*, 237
 - aperture and array equivalence in, 246–248

Pattern synthesis:

- for circular aperture, gaussian error, 250–257
 - for circular array, gaussian error, 248–250
 - with derivative control, 289
 - and derived sector beams, 291, 292
 - gaussian or minimum mean square error for, 236
 - for line source, Chebyshev error, 262–264
 - for linear array, Chebyshev error, 186–194, 260, 261
 - maximally flat, 289
 - with mini-max error, 293–297
 - for nonuniform array, 265–270
 - Anger function method, 267, 268
 - grating plateau method, 268–270
 - and source position function, 265–267
 - with phase constraint, 270–288
 - Gibbs phenomena: Bernstein polynomial method, 285–288
 - reduction of, 283–288
 - weighting method, 283, 284
 - pattern logarithm method for, 273–276
 - variational method for, 276–282
 - quadrature method for, 297, 299
 - for rectangular aperture, gaussian error, 248–250
 - for rectangular array: gaussian error, 238–244
 - with phase constraint, 292, 293
- (*See also* Array)

Plane wave:

- dispersion relation for, 12
- solution for, 11, 12

Poincaré sphere and Stokes' parameters, 107–109

Polarization:

- electric, 4, 5
- magnetic, 5
- of wave, 34, 35

Polarization mismatch for receiving antenna, 106

Polarized wave, reception of, 103–109

Power, 7

Power-pattern synthesis (*see* Pattern synthesis, with phase constraint)

Poynting vector, complex, 7

Radiation:

- from aperture fields, 61–79
 - and directivity, 78, 79
 - with linear phase, 77, 78
 - tapered, 76, 77
 - uniform, 74, 75
- from arbitrary current, 37–41
- from current element, 29–32
- from current loop, 36, 37
- from open waveguide: circular, 631, 632
 - parallel-plate, 621–630
 - radiation field for, 629, 630
 - Wiener-Hopf solution for, 621–630

from thin wire antenna, 43–48

from traveling-wave source, 47, 48

Radiation condition, 20, 21, 309–311

Radiation pattern of current element, 32, 33

Radiation resistance:

- of current element, 36
- of current loop, 37
- of thin wire antenna, 46, 47

Receiving cross section of antenna, 100–103

for distributed sources, 116

for partially polarized waves, 112

for polarized waves, 106

Reciprocity for antennas, 94–98

Reciprocity theorem:

- Lorentz form, 24, 25
- Rayleigh-Carson form, 24, 25

Residue series for slot on cylinder, 578–581, 583, 584

Resonant array (*see* Waveguide slot array)

Scalar potential, 22–24, 307

Schelkunoff's polynomial for arrays, 158–160

Stokes' parameters:

- for antenna, 107
- and coherence matrix, 113, 114
- for partially polarized waves, 112
- for polarized waves, 108

Singularity of field at conductor edge,
18, 19

Slot antenna:

- on cylinder, 567–573
 - circumferential slot, 573, 574
 - residue series for, 578–581
- half-wave axial, 581–584
 - residue series for, 583, 584
- in ground plane, 560–567
 - and Babinet's principle, 565–567
 - radiated power from, 563, 564
 - radiation conductance for, 564, 566, 567
 - radiation field from, 561–563
- on sphere, 584–587
- in waveguide (*see* Waveguide slot array)

Spheroidal antenna:

- oblate: excitation by axial dipole, 553, 554
 - and horizontal dipole above disk, 554–557
- prolate: with confocal sheath, 533–540
 - excitation of: by azimuthal electric field, 540
 - by external source, 540–545
 - by magnetic current ring, 545–548
- in free space, 527–533
- Green's function for, 548–550
 - and dipole scattering, 550, 551

Spheroidal coordinates:

- oblate, 551, 552
- prolate, 523, 524

Spheroidal wave functions, 525–527, 552

Super-gain array, 194, 244

Supergain ratio, 257

Taylor line source, 263, 264

Thinned array, 209

Transient response of linear antenna,
347–350

Traveling-wave theorems for arrays,
196–198

Van Atta array, 180

Variational method:

- for antenna impedance, 51–57, 431
- for biconical antenna, 494–499
- for power-pattern synthesis, 276–282
- for slot in waveguide, 611–616

Vector potential, 22–24, 307

magnetic-type, 23, 24

Wave equation, 10, 11

Waveguide slot array, 587, 588

impedance of (*see* Impedance of waveguide slot)

nonresonant: design of, 595–601

second-order beam suppression for,
590–595

resonant, 588–590

Z transform and array factor, 160–163